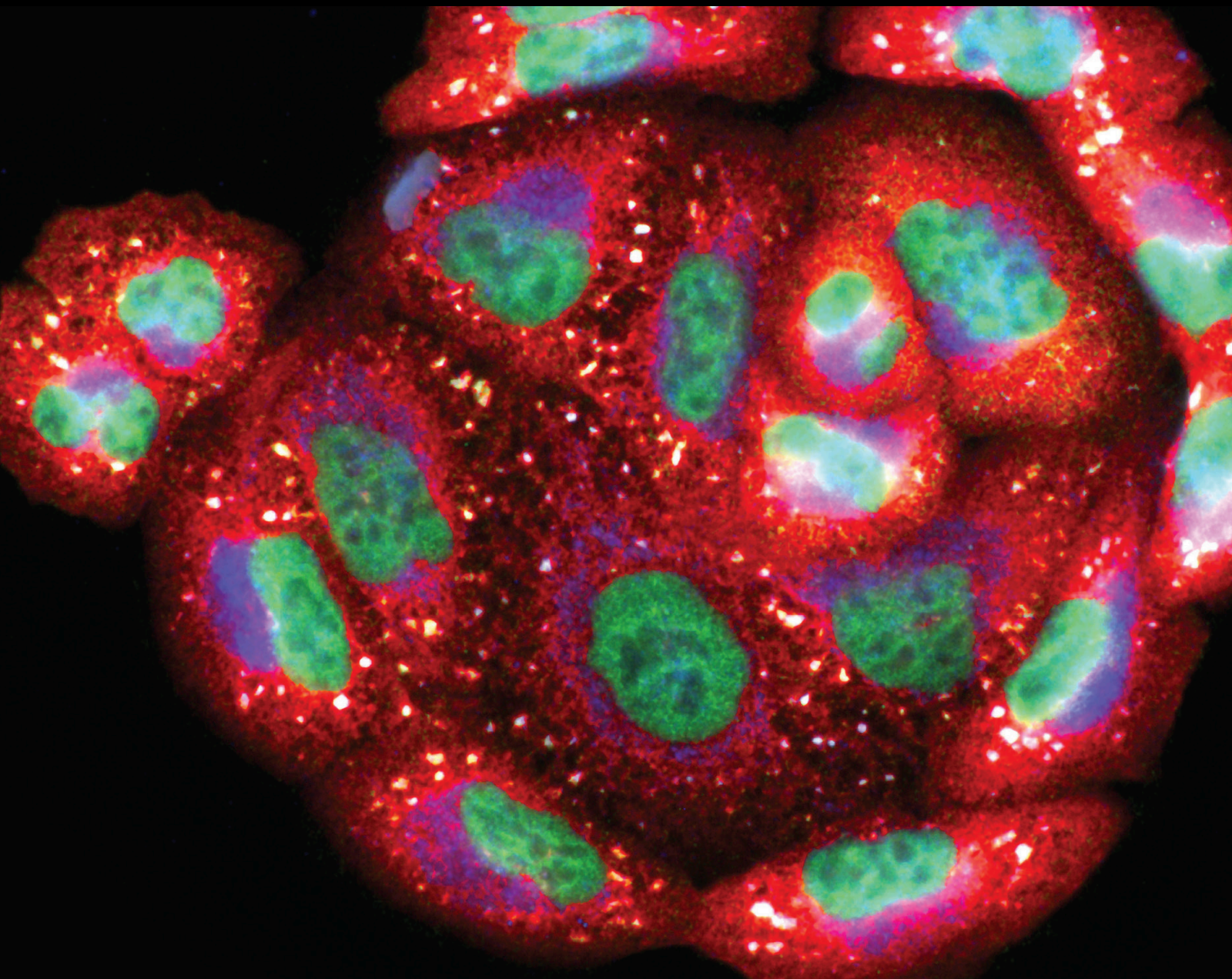


Pharmaceutical and Pharmacological Aspects of Modulation of Oxidative Stress 2020

Special Issue Editor in Chief: Luciano Saso

Guest Editors: Sasanka Chakrabarti and Elzbieta Dorota Miller





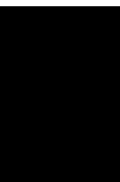
**Pharmaceutical and Pharmacological Aspects
of Modulation of Oxidative Stress 2020**

Oxidative Medicine and Cellular Longevity

**Pharmaceutical and Pharmacological
Aspects of Modulation of Oxidative
Stress 2020**

Special Issue Editor in Chief: Luciano Saso

Guest Editors: Sasanka Chakrabarti and Elzbieta
Dorota Miller



Copyright © 2022 Hindawi Limited. All rights reserved.

This is a special issue published in "Oxidative Medicine and Cellular Longevity" All articles are open access articles distributed under the Creative Commons Attribution License, which permits unrestricted use, distribution, and reproduction in any medium, provided the original work is properly cited.

Chief Editor

Jeannette Vasquez-Vivar, USA

Editorial Board

Ivanov Alexander, Russia
Fabio Altieri, Italy
Silvia Alvarez, Argentina
Fernanda Amicarelli, Italy
José P. Andrade, Portugal
Cristina Angeloni, Italy
Sandro Argüelles, Spain
Antonio Ayala, Spain
Elena Azzini, Italy
Peter Backx, Canada
Damian Bailey, United Kingdom
Jiaolin Bao, China
George E. Barreto, Colombia
Sander Bekeschus, Germany
Ji C. Bihl, USA
Consuelo Borrás, Spain
Nady Braidy, Australia
Ralf Braun, Austria
Laura Bravo, Spain
Matt Brody, USA
Amadou Camara, USA
Gianluca Carnevale, Italy
Roberto Carnevale, Italy
Marcio Caroch, Portugal
Angel Catalá, Argentina
Peter Celec, Slovakia
Giulio Ceolotto, Italy
Shao-Yu Chen, USA
Deepak Chhangani, USA
Ferdinando Chiaradonna, Italy
Zhao Zhong Chong, USA
Xinxin Ci, China
Fabio Ciccarone, Italy
Alin Ciobica, Romania
Ana Cipak Gasparovic, Croatia
Giuseppe Cirillo, Italy
Maria R. Ciriolo, Italy
Massimo Collino, Italy
Graziamaria Corbi, Italy
Manuela Corte-Real, Portugal
Mark Crabtree, United Kingdom
Manuela Curcio, Italy
Andreas Daiber, Germany
Felipe Dal Pizzol, Brazil

Francesca Danesi, Italy
Domenico D'Arca, Italy
Sergio Davinelli, Italy
Claudio de Lucia, Italy
Damião de Sousa, Brazil
Enrico Desideri, Italy
Francesca Diomedea, Italy
Cinzia Domenicotti, Italy
Raul Dominguez-Perles, Spain
Dimitrios Draganidis, Greece
Joël R. Drevet, France
Grégory Durand, France
Alessandra Durazzo, Italy
Anne Eckert, Switzerland
Javier Egea, Spain
Pablo A. Evelson, Argentina
Stefano Falone, Italy
Ioannis G. Fatouros, Greece
Qingping Feng, Canada
Gianna Ferretti, Italy
Giuseppe Filomeni, Italy
Omidreza Firuzi, Iran
Swaran J. S. Flora, India
Teresa I. Fortoul, Mexico
Anna Fracassi, USA
Rodrigo Franco, USA
Joaquin Gadea, Spain
Juan Gambini, Spain
José Luís García-Giménez, Spain
Gerardo García-Rivas, Mexico
Janusz Gebicki, Australia
Alexandros Georgakilas, Greece
Husam Ghanim, USA
Jayeeta Ghose, USA
Rajeshwary Ghosh, USA
Lucia Gimeno-Mallench, Spain
Eloisa Gitto, Italy
Anna M. Giudetti, Italy
Daniela Giustarini, Italy
José Rodrigo Godoy, USA
Saeid Golbidi, Canada
Aldrin V. Gomes, USA
Arantxa González, Spain
Tilman Grune, Germany

Chi Gu, China, China
Nicoletta Guaragnella, Italy
Solomon Habtemariam, United Kingdom
Ying Han, China
Eva-Maria Hanschmann, Germany
Md Saquib Hasnain, India
Md Hassan, India
Tim Hofer, Norway
John D. Horowitz, Australia
Silvana Hrelia, Italy
Dragan Hrcic, Serbia
Juan Huang, China
Zebo Huang, China
Tarique Hussain, Pakistan
Stephan Immenschuh, Germany
Maria Isagulians, Latvia
Luigi Iuliano, Italy
FRANCO J. L, Brazil
Vladimir Jakovljevic, Serbia
Jason Karch, USA
Peeter Karihtala, Finland
Kum Kum Khanna, Australia
Neelam Khaper, Canada
Thomas Kietzmann, Finland
Ramoji Kosuru, USA
Demetrios Kouretas, Greece
Andrey V. Kozlov, Austria
Esra Küpeli Akkol, Turkey
Daniele La Russa, Italy
Jean-Claude Lavoie, Canada
Wing-Kee Lee, Germany
Simon Lees, Canada
Xin-Feng Li, China
Qiangqiang Li, China
Gaocai Li, China
Jialiang Liang, China
Christopher Horst Lillig, Germany
Paloma B. Liton, USA
Ana Lloret, Spain
Lorenzo Loffredo, Italy
Camilo López-Alarcón, Chile
Daniel Lopez-Malo, Spain
Antonello Lorenzini, Italy
Hai-Chun Ma, China
Mateusz Maciejczyk, Poland
Nageswara Madamanchi, USA
Kenneth Maiese, USA




Marco Malaguti, Italy
Tullia Maraldi, Italy
Reiko Matsui, USA
Juan C. Mayo, Spain
Steven McAnulty, USA
Antonio Desmond McCarthy, Argentina
Sonia Medina-Escudero, Spain
Pedro Mena, Italy
Víctor M. Mendoza-Núñez, Mexico
Lidija Milkovic, Croatia
Alexandra Miller, USA
Sanjay Misra, USA
Premysl Mladenka, Czech Republic
Raffaella Molteni, Italy
Maria U. Moreno, Spain
Sandra Moreno, Italy
Trevor A. Mori, Australia
Ryuichi Morishita, Japan
Fabiana Morroni, Italy
Ange Mouithys-Mickalad, Belgium
Iordanis Mourouzis, Greece
Danina Muntean, Romania
Colin Murdoch, United Kingdom
Ryoji Nagai, Japan
Amit Kumar Nayak, India
David Nieman, USA
Cristina Nocella, Italy
Susana Novella, Spain
Hassan Obied, Australia
Julio J. Ochoa, Spain
Pál Pacher, USA
Pasquale Pagliaro, Italy
DR DILIPKUMAR PAL, India
Valentina Pallottini, Italy
Rosalba Parenti, Italy
Mayur Parmar, USA
Vassilis Paschalis, Greece
Visweswara Rao Pasupuleti, Malaysia
Daniela Pellegrino, Italy
Ilaria Peluso, Italy
Claudia Penna, Italy
Serafina Perrone, Italy
Tiziana Persichini, Italy
Shazib Pervaiz, Singapore
Vincent Pialoux, France
Alessandro Poggi, Italy
Ada Popolo, Italy

Aijuan Qu, China
José L. Quiles, Spain
Walid Rachidi, France
Zsolt Radak, Hungary
Sachchida Rai, India
Namakkal Soorappan Rajasekaran, USA
Dario C. Ramirez, Argentina
Erika Ramos-Tovar, Mexico
Abdur Rauf Rauf, Pakistan
Sid D. Ray, USA
Hamid Reza Rezvani, France
Alessandra Ricelli, Italy
Francisco J. Romero, Spain
Mariana G. Rosca, USA
Joan Roselló-Catafau, Spain
Esther Roselló-Lletí, Spain
Josep V. Rubert, The Netherlands
H. P. Vasantha Rupasinghe, Canada
Sumbal Saba, Brazil
Kunihiro Sakuma, Japan
Gabriele Saretzki, United Kingdom
Ajinkya S. Sase, USA
Luciano Saso, Italy
Nadja Schroder, Brazil
Sebastiano Sciarretta, Italy
Ratanesh K. Seth, USA
Anwen Shao, China
Xiaolei Shi, China
Cinzia Signorini, Italy
Mithun Sinha, USA
Giulia Sita, Italy
Eduardo Sobarzo-Sánchez, Chile
Adrian Sturza, Romania
Yi-Rui Sun, China
Eisa Tahmasbpour Marzouni, Iran
Carla Tatone, Italy
Shane Thomas, Australia
Carlo Gabriele Tocchetti, Italy
Angela Trovato Salinaro, Italy
Paolo Tucci, Italy
Rosa Tundis, Italy
Giuseppe Valacchi, Italy
Daniele Vergara, Italy
Victor M. Victor, Spain
László Virág, Hungary
Min-qi Wang, China
Kai Wang, China

Natalie Ward, Australia
Grzegorz Wegrzyn, Poland
Philip Wenzel, Germany
Qiongming Xu, China
Sho-ichi Yamagishi, Japan
Liang-Jun Yan, USA
Guillermo Zalba, Spain
Junmin Zhang, China
Ziwei Zhang, China
Jia Zhang, First Affiliated Hospital of Xi'an
Jiaotong University, Xi'an, Shaanxi Province,
China, China
Yong Zhou, China
Mario Zoratti, Italy



Contents

Pharmaceutical and Pharmacological Aspects of Modulation of Oxidative Stress 2020

Luciano Saso , Sasanka Chakrabarti , and Elzbieta Miller 

Editorial (2 pages), Article ID 9842198, Volume 2022 (2022)

Oxidative Stress, Neuroinflammation, and NADPH Oxidase: Implications in the Pathogenesis and Treatment of Alzheimer's Disease

Upasana Ganguly , Upinder Kaur , Sankha Shubhra Chakrabarti , Priyanka Sharma , Bimal

Kumar Agrawal , Luciano Saso , and Sasanka Chakrabarti 

Review Article (19 pages), Article ID 7086512, Volume 2021 (2021)

Pleiotropic Properties of Amphiphilic Dihydropyridines, Dihydropyridones, and Aminovinylcarbonyl Compounds

Martins Rucins , Rufus Smits , Anda Sipola , Brigita Vigante , Ilona Domracheva , Baiba

Turovska , Ruslan Muhamadejev , Karlis Pajuste , Mara Plotniece , Arkadij Sobolev , Gunars

Duburs , and Aiva Plotniece 





Research Article (17 pages), Article ID 8413713, Volume 2020 (2020)

Hyaluronic Acid Improves Hydrogen Peroxide Modulatory Effects on Calcium Channel and Sodium-Potassium Pump in 4T1 Breast Cancer Cell Line

Ardeshir Abbasi , Nafiseh Pakravan , and Zuhair Mohammad Hassan 

Research Article (9 pages), Article ID 8681349, Volume 2020 (2020)

Azelaic Acid Exerts Antileukemia Effects against Acute Myeloid Leukemia by Regulating the Prdxs/ROS Signaling Pathway





Dongdong Zhang , Ziyi Luo , Yanxia Jin, Yanling Chen, Tian Yang, Qian Yang , Balu Wu , Yufeng

Shang, Xiaoyan Liu , Yongchang Wei , and Fuling Zhou 

Research Article (16 pages), Article ID 1295984, Volume 2020 (2020)




Mitochondrial-Protective Effects of R-Phenibut after Experimental Traumatic Brain Injury

Einars Kupats , Gundega Stelfa , Baiba Zvejniece , Solveiga Grinberga , Edijs Vavers , Marina

Makrecka-Kuka , Baiba Svalbe , Liga Zvejniece , and Maija Dambrova 

Research Article (12 pages), Article ID 9364598, Volume 2020 (2020)

Monoclonal Antibody to CD14, TLR4, or CD11b: Impact of Epitope and Isotype Specificity on ROS Generation by Human Granulocytes and Monocytes

Dmitry S. Kabanov , Sergey V. Grachev , and Isabella R. Prokhorenko 







Review Article (20 pages), Article ID 5708692, Volume 2020 (2020)

Transcriptome Investigation and In Vitro Verification of Curcumin-Induced HO-1 as a Feature of Ferroptosis in Breast Cancer Cells

Ruihua Li, Jing Zhang, Yongfeng Zhou, Qi Gao, Rui Wang, Yurong Fu, Lianwen Zheng , and Hao Yu 



Research Article (18 pages), Article ID 3469840, Volume 2020 (2020)

Oxidative Stress in Amyotrophic Lateral Sclerosis: Pathophysiology and Opportunities for Pharmacological Intervention

Teresa Cunha-Oliveira , Liliana Montezinho , Catarina Mendes, Omidreza Firuzi , Luciano Saso , Paulo J. Oliveira , and Filomena S. G. Silva 



Review Article (29 pages), Article ID 5021694, Volume 2020 (2020)

Dexmedetomidine Alleviates Lipopolysaccharide-Induced Acute Kidney Injury by Inhibiting p75NTR-Mediated Oxidative Stress and Apoptosis

Zhe Wang , Jiali Wu, Zhaolan Hu, Cong Luo, Pengfei Wang, Yanling Zhang, and Hui Li 


Research Article (13 pages), Article ID 5454210, Volume 2020 (2020)

Cranberry for Bacteriuria in Individuals with Spinal Cord Injury: A Systematic Review and Meta-Analysis

Anna Raguzzini, Elisabetta Toti, Tommaso Sciarra , Anna Lucia Fedullo, and Ilaria Peluso 




Research Article (12 pages), Article ID 9869851, Volume 2020 (2020)

Ameliorating Effect of Klotho Protein on Rat Heart during I/R Injury

Agnieszka Olejnik, Anna Krzywonos-Zawadzka, Marta Banaszekiewicz, and Iwona Bil-Lula 







Research Article (11 pages), Article ID 6427284, Volume 2020 (2020)

Bardoxolone Methyl Displays Detrimental Effects on Endothelial Bioenergetics, Suppresses Endothelial ET-1 Release, and Increases Endothelial Permeability in Human Microvascular Endothelium

Ewa Szczesny-Malysiak , Marta Stojak, Roberto Campagna, Marek Grosicki, Marek Jamrozik, Patrycja Kaczara , and Stefan Chlopicki 



Research Article (16 pages), Article ID 4678252, Volume 2020 (2020)

Decoding Aging: Understanding the Complex Relationship among Aging, Free Radicals, and GSH

María E. López-Navarro , Mariana Jarquín-Martínez , Luis A. Sánchez-Labastida , Daniel Ramírez-Rosales, Marycarmen Godínez-Victoria , Laura Itzel Quintas-Granados , and José Guadalupe Trujillo-Ferrara 



Research Article (11 pages), Article ID 3970860, Volume 2020 (2020)

Lupeol Counteracts the Proinflammatory Signalling Triggered in Macrophages by 7-Keto-Cholesterol: New Perspectives in the Therapy of Atherosclerosis

Sarmistha Saha, Elisabetta Profumo, Anna Rita Togna, Rachele Riganò, Luciano Saso , and Brigitta Buttari 

Research Article (12 pages), Article ID 1232816, Volume 2020 (2020)



New 2-Acetyl-3-aminophenyl-1,4-naphthoquinones: Synthesis and In Vitro Antiproliferative Activities on Breast and Prostate Human Cancer Cells

David Ríos , Jaime A. Valderrama, Miriam Cautin, Milko Tapia, Felipe Salas, Angélica Guerrero-Castilla, Giulio G. Muccioli, Pedro Buc Calderón, and Julio Benites 

Research Article (11 pages), Article ID 8939716, Volume 2020 (2020)

Contents

Mechanistic Insights into the Oxidized Low-Density Lipoprotein-Induced Atherosclerosis

Chainika Khatana, Neeraj K. Saini, Sasanka Chakrabarti, Vipin Saini, Anil Sharma, Reena V. Saini , and Adesh K. Saini 

Review Article (14 pages), Article ID 5245308, Volume 2020 (2020)

Hydrogen: A Novel Option in Human Disease Treatment

Mengling Yang , Yinmiao Dong , Qingnan He , Ping Zhu , Quan Zhuang , Jie Shen , Xueyan Zhang , and Mingyi Zhao 


Review Article (17 pages), Article ID 8384742, Volume 2020 (2020)

Blueberry Extracts as a Novel Approach to Prevent Ozone-Induced Cutaneous Inflammation Activation

Erika Pambianchi, Francesca Ferrara, Alessandra Pecorelli, Brittany Woodby, Mary Grace, Jean-Philippe Therrien, Mary Ann Lila , and Giuseppe Valacchi 




Research Article (15 pages), Article ID 9571490, Volume 2020 (2020)

Increased Serum Levels of IFN- γ , IL-1 β , and IL-6 in Patients with Alopecia Areata and Nonsegmental Vitiligo

Katarzyna Tomaszewska , Magdalena Kozłowska, Andrzej Kaszuba, Aleksandra Lesiak, Joanna Narbutt, and Anna Zalewska-Janowska







Research Article (5 pages), Article ID 5693572, Volume 2020 (2020)

Ellagic Acid-Derived Urolithins as Modulators of Oxidative Stress

Jasmina Djedjibegovic , Aleksandra Marjanovic, Emiliano Panieri , and Luciano Saso 


Review Article (15 pages), Article ID 5194508, Volume 2020 (2020)

Sitagliptin Mitigates Total Body Irradiation-Induced Hematopoietic Injury in Mice

Meifang Wang , Yinping Dong, Jing Wu , Hongyan Li, Junling Zhang, Lu Lu, Yuanyang Zhang , Zewei Zhou, Saijun Fan , Deguan Li , and Aimin Meng 

Research Article (11 pages), Article ID 8308616, Volume 2020 (2020)

Hexachloronaphthalene Induces Mitochondrial-Dependent Neurotoxicity via a Mechanism of Enhanced Production of Reactive Oxygen Species

Malwina Lisek , Joanna Stragierowicz , Feng Guo, Philipp P. Prosseda, Magdalena Wiktorska, Bożena Ferenc, Anna Kilanowicz, Ludmila Zylinska , and Tomasz Boczek 




Research Article (17 pages), Article ID 2479234, Volume 2020 (2020)

A Stereological Study of the Toxic Effects of Cerium Oxide during Pregnancy on Kidney Tissues in Neonatal NMRI Mice

Afsaneh Nemati, Vahideh Assadollahi, Ilaria Peluso , Abolfazl Abbaszadeh, Mandana Beigi-boroujeni, Zahra Khanipur, and Mohammadreza Gholami 



Research Article (11 pages), Article ID 9132724, Volume 2020 (2020)

Oxidative Damage of Blood Platelets Correlates with the Degree of Psychophysical Disability in Secondary Progressive Multiple Sclerosis

Angela Dziedzic , Agnieszka Morel , Elzbieta Miller , Michal Bijak , Tomasz Sliwinski , Ewelina Synowiec , Michal Ceremuga , and Joanna Saluk-Bijak 



Research Article (12 pages), Article ID 2868014, Volume 2020 (2020)

Proteome and Transcriptome Analysis of the Antioxidant Mechanism in Chicken Regulated by Eucalyptus Leaf Polyphenols Extract

Wei Li, Ze-qi He, Xiao-Ying Zhang, Yun-Jiao Chen , Jian-Jun Zuo, and Yong Cao 



Research Article (14 pages), Article ID 1384907, Volume 2020 (2020)

Enhanced Efficacy of Direct-Acting Antivirals in Hepatitis C Patients by Coadministration of Black Cumin and Ascorbate as Antioxidant Adjuvants

Sarfraz Ahmed, Adeela Zahoor, Muhammad Ibrahim, Muhammad Younus , Sadia Nawaz, Rahat Naseer, Qaiser Akram, Cun-Liang Deng, and Suvash Chandra Ojha 




Research Article (10 pages), Article ID 7087921, Volume 2020 (2020)

Zinc Oxide Nanoparticle Synergizes Sorafenib Anticancer Efficacy with Minimizing Its Cytotoxicity

Ahmed Nabil , Mohamed M. Elshemy, Medhat Asem, Marwa Abdel-Motaal, Heba F. Gomaa, Faten Zahran, Koichiro Uto, and Mitsuhiro Ebara 

Research Article (11 pages), Article ID 1362104, Volume 2020 (2020)

Metformin Ameliorates A β Pathology by Insulin-Degrading Enzyme in a Transgenic Mouse Model of Alzheimer's Disease

Xin-Yi Lu , Shun Huang , Qu-Bo Chen, Dapeng Zhang, Wanyan Li, Ran Ao, Feona Chung-Yin Leung, Zhimin Zhang, Jisheng Huang , Ying Tang , and Shi-Jie Zhang 

Research Article (10 pages), Article ID 2315106, Volume 2020 (2020)

TBHQ Attenuates Neurotoxicity Induced by Methamphetamine in the VTA through the Nrf2/HO-1 and PI3K/AKT Signaling Pathways

Xianyi Meng , Chenghong Zhang , Yu Guo, Ying Han, Chunyang Wang, Haiying Chu , Li Kong, and Haiying Ma 

Research Article (13 pages), Article ID 8787156, Volume 2020 (2020)

Editorial

Pharmaceutical and Pharmacological Aspects of Modulation of Oxidative Stress 2020

Luciano Saso ¹, Sasanka Chakrabarti ² and Elzbieta Miller ³

¹Department of Physiology and Pharmacology “Vittorio Erspamer”, Sapienza University of Rome, 00161 Rome, Italy

²Department of Biochemistry, Maharishi Markandeshwar Institute of Medical Sciences and Research, Mullana, Haryana, India

³Department of Neurological Rehabilitation, Medical University of Lodz, Poland

Correspondence should be addressed to Luciano Saso; luciano.saso@uniroma1.it

Received 5 January 2022; Accepted 5 January 2022; Published 27 January 2022

Copyright © 2022 Luciano Saso et al. This is an open access article distributed under the Creative Commons Attribution License, which permits unrestricted use, distribution, and reproduction in any medium, provided the original work is properly cited.

Oxidative stress, though not really on the driver’s seat, continues to play key roles within the pathogenic spectrum of many diseases especially cancer, inflammatory, and degenerative diseases. Thus, reactive oxygen species- (ROS-) mediated tissue injury and redox signaling are intensely investigated in disease conditions and model systems for a better understanding of the pathogenesis and identification of new drug targets.

The special issue contains 29 articles which describe the involvement of oxidative stress in various clinical conditions and experimental models of diseases, drug actions, and environmental injuries. We can summarize some of the important concepts and results that have emerged from these studies. In the pathogenesis of AD, a body of evidence links the process of neuroinflammation with the increased production of ROS by microglial NADPH oxidase, and this suggests a potential role of NADPH oxidase inhibitors as disease-modifying agents for Alzheimer’s disease. U. Ganguly et al., in their review succinctly evaluated the current state of research on NADPH oxidase inhibitors [1]. The important role of oxidative stress and mitochondrial dysfunction in ALS and positive effects of antioxidants in preclinical trials of this disease have been reviewed by T. Cunha-Oliveira et al.; the authors suggested that oxidative stress-related damage mechanisms could be different in different subtypes of ALS having defined mutations, and thus, specific and targeted antioxidant therapy would be needed for different subtypes of ALS for novel and effective therapeutic interventions [2]. In an exhaustive review on the complex mechanisms of atherogenesis, C. Khatana and coauthors highlighted the special role of oxidized-LDL and the crucial

involvement of antioxidant enzymes in this process [3]. The authors also discussed the various therapeutic options including the use of antioxidants and life-style management to combat the problem of atherosclerosis and its complications. A rather unusual but elaborate review on the molecular hydrogen as a multipotential therapeutic agent for a variety of diseases including COVID-19 has been presented by M. Yang et al., with a load of direct and indirect experimental evidence of hydrogen acting as an antioxidative or anti-inflammatory agent or a modulator of mitochondrial functions, cell death pathways, and many other biological processes [4].

The research articles contained in this special issue examined a wide range of interesting questions related to redox pathophysiology, and we may mention a few of them here just to indicate the diverse nature of these studies. A. Abbasi and others showed how oxidative stress could be detrimental to cancer cells by causing a loss of ionic homeostasis through alterations in the activities of pumps and channels; hyaluronic acid apparently can be used to optimize and target the cytotoxic effects of oxidative stress on cancer cells [5]. The poor prognosis of acute myeloid leukemia (AML) has been attributed to enhanced ROS production; D. Zhang et al., showed using cell-based and animal studies that azelaic acid could impact against AML by upregulating the peroxiredoxins (Prdxs2/Prdx3) with consequent scavenging of ROS [6]. Likewise, the protection of LPS-induced acute kidney injury and ischemia/reperfusion mediated cardiac damage by dexmedetomidine and Klotho protein, respectively, indicated the therapeutic potentials of these molecules which were partly attributable to their

antioxidative functions [7,8]. An interesting clinical study by S. Ahmed et al. indicated the potentiation of antiviral therapy in patients of hepatitis C by cotreatment with black cumin and ascorbate which decreased the oxidative stress and viral load and improved several clinical parameters [9]. Nrf-2 activators have been under scanner for quite some time as potential drugs for a variety of disease conditions where oxidative stress and inflammation are involved. A significant research paper in this issue attempted to explore the reasons for unexpected toxic side effects of a potent Nrf-2 activator called bardoxolone methyl, and the authors showed that the drug caused severe mitochondrial bioenergetic impairment along with apoptosis and necrosis of endothelial cells in a dose-dependent manner which could be related to its toxicity [10]. There are many other interesting articles in this issue which we would not discuss individually, but together, they send out two important messages. Firstly, oxidative stress affects specific aspects of different diseases or environmental toxicities which could be identified by studies in different experimental models. Secondly, attempts should be continued to develop new drugs targeting oxidative stress which should be safe and of higher efficacy or bioavailability, but in most cases, such drugs, though clinically relevant, would be a part of an add-on or adjunct therapy for a disease condition.

Conflicts of Interest

The guest editors declare that there are no conflict of interests regarding the publication of this special issue.

*Luciano Saso
Sasanka Chakrabarti
Elzbieta Miller*

Review Article

Oxidative Stress, Neuroinflammation, and NADPH Oxidase: Implications in the Pathogenesis and Treatment of Alzheimer's Disease

Upasana Ganguly ¹, Upinder Kaur ², Sankha Shubhra Chakrabarti ³,
Priyanka Sharma ¹, Bimal Kumar Agrawal ⁴, Luciano Saso ⁵,
and Sasanka Chakrabarti ¹

¹Department of Biochemistry, MM Institute of Medical Sciences & Research, Maharishi Markandeshwar Deemed University, Mullana, Ambala, Haryana, India

²Department of Pharmacology, Institute of Medical Sciences, Banaras Hindu University, Varanasi, India

³Department of Geriatric Medicine, Institute of Medical Sciences, Banaras Hindu University, Varanasi, India

⁴Department of General Medicine, MM Institute of Medical Sciences & Research, Maharishi Markandeshwar Deemed University, Mullana, Ambala, Haryana, India

⁵Department of Physiology and Pharmacology "Vittorio Ersparmer", Sapienza University of Rome, Rome, Italy

Correspondence should be addressed to Sasanka Chakrabarti; profschakrabarti95@gmail.com

Received 23 July 2020; Revised 17 March 2021; Accepted 3 April 2021; Published 17 April 2021

Academic Editor: Jos L. Quiles

Copyright © 2021 Upasana Ganguly et al. This is an open access article distributed under the Creative Commons Attribution License, which permits unrestricted use, distribution, and reproduction in any medium, provided the original work is properly cited.

NADPH oxidase as an important source of intracellular reactive oxygen species (ROS) has gained enormous importance over the years, and the detailed structures of all the isoenzymes of the NADPH oxidase family and their regulation have been well explored. The enzyme has been implicated in a variety of diseases including neurodegenerative diseases. The present brief review examines the body of evidence that links NADPH oxidase with the genesis and progression of Alzheimer's disease (AD). In short, evidence suggests that microglial activation and inflammatory response in the AD brain is associated with increased production of ROS by microglial NADPH oxidase. Along with other inflammatory mediators, ROS take part in neuronal degeneration and enhance the microglial activation process. The review also evaluates the current state of NADPH oxidase inhibitors as potential disease-modifying agents for AD.

1. Introduction

A review on oxidative stress and disease mechanisms and therapeutic use of antioxidants is usually not greeted with much enthusiasm, and reasons are not difficult to surmise. The story of oxidative stress and its involvement in multiple disease mechanisms and aging is quite old, spanning many decades [1]. However, a definitive evidence of oxidative stress as a driving mechanism of disease pathogenesis is still lacking. Likewise, inconsistent results of multiple clinical trials of antioxidants in various diseases, especially in neurodegenerative diseases, have been a cause for great disappointment to the advocates of free radical hypothesis of diseases [2–4].

On the other hand, there is a considerable body of experimental evidence that suggests the involvement of reactive oxygen species (ROS) and reactive nitrogen species (RNS), generally free radicals of oxygen and nitrogen, in the pathophysiology of many diseases and aging [4–6]. Thus, the free radical biology in health and disease has grown gradually over the years from the identification of various species of ROS and RNS in living systems and the elucidation of the chemistry and kinetics of their interactions to the identification of their toxic effects on different biomolecules and cell organelles [7, 8]. Further, the enzymatic or nonenzymatic antioxidant defense system of the body and the redox-signalling pathways regulating physiological and pathological

processes within the cells have been identified [7, 9, 10]. The redox-signalling pathways play important roles in cell growth, differentiation, and death as evidenced from a plethora of experimental studies [10–12].

The antioxidant defense of the body generally counterbalances the various ROS and RNS in the normal physiological condition, but in pathological conditions when the free radicals overpower the antioxidant defense, a state of oxidative stress develops. It is presumable that direct damage to biomolecules within the cells by ROS and RNS and aberrant redox-signalling pathways together are involved in many diseases including neurodegenerative disorders [5, 6, 13, 14]. The new technique of redox proteomics with the availability of antibodies against redox-modified proteins has strengthened our understanding of oxidative stress-induced mechanisms in diseases [15]. On the other hand, the identification of new antioxidants from natural sources or synthesis of novel, multifunctional, and organelle-targeted antioxidants has provided a new impetus in therapeutic applications of antioxidants [16–19]. So far, antioxidants have been developed with the precise aim of scavenging the free radicals of oxygen to prevent the deleterious effects of oxidative stress. Much less attempt has been made to prevent the generation of ROS at the source presumably because ROS are generated in most cases as a by-product of important metabolic pathways like the electron transport chain (ETC) of mitochondria which precludes the option of inhibiting the generation of ROS at the source. However, NADPH oxidase (NOX) is one enzyme whose sole function is the production of reactive oxygen species like superoxide radical ($O_2^{\bullet-}$) and hydrogen peroxide, and therefore, inhibition of NOX could be an important rescue avenue against oxidative stress in tissues in different disease conditions. Thus, the therapeutic potential of NOX inhibitors should be explored thoroughly by experimental and clinical research.

2. ROS and NADPH Oxidase

2.1. Sources of ROS. The sources of ROS within the cells are varied, but they predominantly occur as a by-product of enzymatic reactions in different metabolic pathways. The ETC of mitochondria is a major contributor of intracellular ROS, but many other enzyme complexes in mitochondria like pyruvate dehydrogenase, α -ketoglutarate dehydrogenase, *cis*-aconitase, glycerophosphate dehydrogenase, and dihydroorotate dehydrogenase are also responsible for ROS production [20–22]. Of the various complexes of ETC, complex I and complex III are the major sites of ROS production. The enzymes like cyclooxygenase, lipoxygenase, xanthine oxidase, and cytochrome P450-dependent oxygenases also contribute to ROS production [22]. Nonenzymatic or enzymatic oxidation of catecholamines and autoxidation of hemoglobin can also produce ROS under physiological conditions. However, another major source of ROS production is NOX, which was initially identified in neutrophils as the enzyme responsible for the production of superoxide radicals during a “respiratory burst” [23]. Since then, the biochemistry of NOX has been extensively studied, and this enzyme (in various isoforms) is present in a variety of tissues including

the brain as well as in multiple cell lines. The NOX family of enzymes is comprised of 7 isoenzymes named as NOX1–5 and dual oxidases DUOX1 and DUOX2. NOX is responsible for the production of superoxide radicals ($O_2^{\bullet-}$) by the transfer of electrons to molecular oxygen from NADPH via FAD and two heme residues of the enzyme. The $O_2^{\bullet-}$ radicals in turn undergo dismutation to produce H_2O_2 , but it has been suggested that the isoenzymes NOX4, DUOX1, and DUOX2, could directly produce H_2O_2 [23, 24].

2.2. NADPH Oxidase: Structure and Isozymes. Each of the seven members of the NOX family has a catalytic subunit comprised of a transmembrane domain of 6 α -helical segments containing two heme units liganded to histidine residues and a cytosolic segment which contains FAD and NADPH binding sites [23, 24]. Additional structural features of the catalytic subunit are seen in some of the isoenzymes such as the EF-calcium-binding domains of NOX5, DUOX1, and DUOX2 and peroxidase domains of DUOX enzymes [24, 25]. This large membrane-bound (plasma membrane and membranes of some organelles) subunit of NOX is associated with another membrane-bound protein called p22^{phox} in some of the isoenzymes like NOX1, NOX2, NOX3, and NOX4, and the large heterodimer thus formed is called flavocytochrome b558. Likewise, the catalytic subunit of DUOX1 or DUOX2 is associated with another membrane-embedded protein called DUOXA1 or DUOXA2, respectively [24]. In addition, the NOX family of enzymes requires several other regulatory cytosolic proteins for activation, stability, or full function, and these additional interaction proteins are different for different isoenzymes [23, 24]. NOX2, which was the first isoenzyme to be identified in phagocytic cells, has been studied most, and its activation process may be taken as the prototype for other NOX family of enzymes. The catalytic subunit of NOX2 is known as gp91^{phox} which remains in association with a membrane-embedded protein called p22^{phox} which confers stability to the complex. During agonist activation, the cytosolic protein p47^{phox} is phosphorylated, which in association with some other cytosolic proteins called p67^{phox} and p40^{phox} and GTP-binding proteins like Rac2 and Rap1A translocates to the membrane to interact with the heterodimer of gp91^{phox} and p22^{phox} forming a fully functional enzyme. The interaction of src-homology domain 3 (SH3) of p47^{phox} with the C-terminal segment of p22^{phox}, at a proline-rich sequence, is important in this assembly [23–25]. The detailed molecular interactions of these proteins during NOX2 activation and the functions of individual proteins have been identified. For example, p47^{phox} is considered as an organizer protein without any catalytic property, while the activator protein p67^{phox} increases the catalytic activity of NOX2. For some other NOX isoenzymes like NOX1, NOX3, and NOX4, a similar pattern of activation with some variations is seen with the aid of multiple regulatory proteins (activators or organizers) like NOXO1, NOXA1, PDI, and Poldip2, as well several GTP-binding proteins [25, 26]. NOX5, DUOX1, and DUOX2, however, do not need any such assistance from other proteins, and they are presumably activated by the binding of Ca^{2+} ions at their cytosolic EF-calcium-binding domains [25, 26].

2.3. NADPH Oxidase: Physiological Role and Pathological Implications. In contrast to other sources, NOX is distinctive

in producing ROS through a highly regulated complex enzymatic process and not as a by-product of a main reaction. Thus, the physiological role of NOX-dependent ROS production needs to be carefully analysed. In general, NOX-dependent ROS takes part in redox-signalling pathways through redox-responsive signalling molecules (transcription factors, soluble or receptor-kinases, etc.), and the process regulates various aspects of cell growth, differentiation, survival, and metabolism with broad implications in immunity and inflammation, aging, cancer, and cardiovascular function and malfunctions [23, 24, 27–29]. For example, multiple studies have shown that vascular endothelial function and migration, angiogenesis, expression of cell adhesion molecules, vascular smooth muscle cell proliferation, etc. are regulated by multiple agonists like angiotensin II, growth factors, and cytokines through modulation of NADPH-dependent ROS production [28–30]. NOX-dependent ROS signalling is also involved in regulating cardiac remodelling, cardiomyocyte hypertrophy, and interstitial fibrosis after myocardial infarction or during chronic cardiac stress from hypertension [31]. The NOX4 isozyme, expressed in the mitochondria of cardiomyocytes, is particularly important in this context as has been shown in an experimental study; in heart-specific NOX4 knock-out mice, cardiac hypertrophy, interstitial fibrosis, mitochondrial dysfunction, and apoptosis of cardiomyocytes following pressure overload are significantly prevented compared to that in wild-type mice [32]. In cardiac-specific human NOX4 transgenic mice (hNOX4), a significant overexpression of NOX4 was observed with a high level of ROS production and associated myocardial fibrosis under basal condition when compared to littermate controls negative for hNOX4 [33]. This study further demonstrated that treatment with angiotensin II caused cardiac hypertrophy and myocardial fibrosis along with NOX4 upregulation and ROS production in control mice, and all these changes were much more aggravated in hNOX4 [33]. NOX4 in cardiomyocytes has been shown to be regulated by a tyrosine kinase belonging to Src-family [34].

NOX-generated ROS play an important role in tumor cell proliferation, metabolism, and progress. A systematic review has shown the association of lung cancer with increased expression and activity of NOX in tumor tissue and that inhibition of NOX could prevent tumor progression during *in vitro* experiments [35]. Similarly, overexpression of NOX2 has been reported in a significant number of human gastric carcinoma cases along with increased expression of EGFR and VEGF suggesting a biomarker potential of the former in this cancer [36]. Another study demonstrated a dysregulation of the expression of the NOX family of isoenzymes in human gastric cancer with overexpression of NOX2 indicating better prognosis and elevated NOX4 and decreased DUOX1 associated with worse outcome [37]. In other studies with human cancer tissue or cancer cell lines, the NOX family of isoenzymes is expressed differentially that probably has implications in tumor growth and invasion [38]. It is still debatable how exactly NOX regulates tumor growth and progression, but genomic instability caused by ROS, inactivation of p53 function, alterations in the functions of cell signalling kinases and phosphatases, and modu-

lation of the functions of the *ras* oncogene may all be contributing to this process [39, 40]. Another important function of NOX-mediated ROS is to modulate innate immunity and the inflammatory response. The role of NOX is well established in the respiratory burst of neutrophils, which is a component of innate immunity and a first-line defense against invading microbes. The other components of innate immunity involve pattern recognition receptors like membrane-bound toll-like receptors (TLRs) and several cytosolic receptors. These pattern recognition receptors respond to specific patterns in the bacterial proteins, DNA, peptidoglycan, lipopolysaccharide (LPS) etc. or DNA or RNA viruses and initiate multiple signalling mechanisms for host defense [41, 42]. The involvement of NOX-derived ROS has been shown to be necessary for TLR-2-dependent innate immune response against *Mycobacterium tuberculosis* [43]. Similarly, NOX-dependent ROS generation is necessary for RIG-I-mediated activation of the transcription factor IRF-3 leading to antiviral gene expression [44]. The transcription factor NF- κ B is involved in the expression of multiple genes related to innate immunity, and bacterial LPS-induced activation of NF- κ B through TLR-4 requires NOX-dependent ROS production [45]. Although NOX-mediated ROS production is important for host defense against microbial invasion, the role of NOX is possibly more complex. For example, influenza-A-induced lung damage is aggravated by NOX2 isoenzymes, while DUOX2 isoenzymes are apparently protective [46]. Apart from influenza virus, other respiratory viruses like human respiratory syncytial virus and human rhinovirus may also cause increased ROS production by different isoenzymes of NOX, and despite the important role of NOX in host defense, NOX-derived ROS could aggravate lung inflammation and damage in many cases. Under such circumstances, the use of NOX inhibitors may become a potential therapeutic option [46, 47].

The role of oxidative damage in aging has been suggested many decades ago, and the original concept of progressive accumulation of oxidatively damaged biomolecules within cells with functional deterioration of tissues was quite straightforward [48, 49]. Thus, oxidative damage markers have been shown to accumulate in different tissues of aged animals in multiple studies, and ROS derived from mitochondrial metabolism and NOX have been both implicated in this process [48, 50–52]. The precise role of NOX in age-related oxidative damage in brain has been shown using NOX2 knock-out mice or transgenic mice overexpressing NOX2 [53]. Age-dependent increase in NOX activity has been shown in the aged brain of rodents which is modulated by dietary manipulations [54, 55]. Likewise, NOX4 upregulation has been implicated in aging of heart [56]. However, most of these studies indicating a relationship of oxidative stress and aging in mammals are actually correlative in nature and do not necessarily identify a causal relationship. Moreover, this simple concept of generalized and indiscriminate ROS-mediated damage to tissues as a pivotal mechanism of aging seemed contradictory when genetic manipulation studies overexpressing or knocking out antioxidant enzyme genes or environmental modifications in nematodes, flies, yeast, and other organisms revealed that complex interactions of

ROS with life span extension genes instead of direct oxidative damage to tissue components are involved in aging and alteration of the life span of these species [57–61]. Both mitochondrial- and NOX-derived ROS at moderate levels are involved in actually increasing the longevity of these organisms by redox-signalling pathways, while presumably at higher levels of ROS, both oxidative damage and shortening of life span occur [59, 62–64]. However, the results of such life span alteration experiments on mammals by knocking out antioxidant enzyme genes or NOX have remained controversial, failing to show clearly the link between oxidative stress and longevity [65–68]. The redox-signalling pathways comprised of various redox-sensitive transcription factors and cell signalling kinases and their downstream components have also been identified and explored in detail in mammalian cells, but their precise role in mammalian aging at the organismal level has not been elucidated yet [10, 49, 69].

2.4. NADPH Oxidase in the Brain. The vulnerability of the brain to oxidative damage is a well-accepted fact based on high oxygen consumption of the organ, availability of transition metals and autooxidizable catecholamines, abundance of polyunsaturated fatty acids, and the presence of a relatively weak antioxidant defense [13, 70]. Oxidative stress is implicated in many diseases of the central nervous system (CNS); thus, NOX has been studied in a variety of pathological conditions of the brain [71, 72]. The four NOX isoenzymes (NOX1, NOX2, NOX3, and NOX4) in the brain have been well explored in the context of brain development, aging and pathological conditions like ischemic or traumatic injury of the brain, neurodegenerative diseases, and different types of psychosis, but less information is available on NOX5 or the DUOX enzymes [72–76]. Although several early studies identified NOX2 in microglia, the inflammatory cells of the brain, many studies subsequently demonstrated the involvement of neuronal, astrocytic, or brain endothelial NOX in different conditions [72, 74, 75, 77]. NOX4 mRNA was shown to be overexpressed in neurons and newly formed capillaries in the brain in an experimental mouse model of ischemia, which persisted up to one month after the onset of ischemia [78]. Using a luminometric enzyme assay, NOX was also shown to be elevated in aged rat brain associated with increased accumulation of proinflammatory cytokines [55]. The age-dependent increase in ROS production and loss of neurons and capillaries in the brain of aged rats compared to young animals were shown to be significantly decreased in NOX2 knock-out rats [53]. In patients dying of traumatic brain injury (TBI), a selective increase in NOX2 was observed in parvalbumin-positive interneurons, but not in microglia, of postmortem brain without much changes in NOX1 and NOX4 isoenzymes as studied by immunohistochemistry [79].

NOX is also expressed in various primary cultures of neurons or neural stem cells or neural cell lines, and these have been manipulated genetically or pharmacologically to gain insight into normal or toxic functions of NOX-derived ROS in neurons. Thus, in primary culture of cerebellar granule cells, NOX is overexpressed in growth cones and filopodia with NOX-derived ROS involved in neuronal maturation [80]. Similarly, in primary culture of rat hippocampal neu-

rons, genetic or pharmacological inactivation of NOX has been shown to cause altered neuronal polarization and inhibition of axonal growth [81]. In neural stem cells derived from mouse embryonic hippocampus, NOX inhibitors or ROS scavengers can inhibit cellular proliferation [82]. In neural crest stem cells, neuronal differentiation induced by bone morphogenetic protein 2 (BMP-2) in culture is regulated by NOX4 isoenzymes [83]. Likewise, nerve growth factor-induced differentiation of PC12 cells to a neuronal phenotype requires the presence of NADPH-dependent ROS [84]. Furthermore, NOX-dependent ROS have been suggested to play a crucial signalling role in long-term potentiation (LTP) and synaptic plasticity in several studies using pharmacological inhibition of NOX or by employing transgenic mice without functional NOX activity [85]. On the other hand, apoptosis of sympathetic neurons in culture under condition of nerve growth factor deprivation could be prevented by the inhibitor of NOX, suggesting a role of ROS in programmed cell death [86]. Overall, these studies indicate that ROS derived from NADPH oxidase are implicated in a multitude of signalling functions within neurons in normal conditions while their deleterious effects could be important in diseased conditions.

2.5. Oxidative Stress, NADPH Oxidase, and Neurodegenerative Diseases. Oxidative stress is an important element in the pathogenesis of many neurodegenerative diseases, where the deleterious actions of ROS on critical cellular components like proteins, phospholipids, and DNA could lead to the disruption and dysfunction of cell physiology which could be important in the genesis or progression of the disease [87–89]. The direct damage to cellular components by ROS has been extensively studied *in vitro*, and the pathways and end-products of proteins, phospholipids, and DNA oxidation have been elaborately identified forming a vast mass of literature on free radical biology [90–92]. The end-products of such oxidative damage pathways often accumulate in high amounts in many pathological conditions in the tissues and body fluids, which are measured as oxidative damage markers, and this is generally thought to be indicative of oxidative stress in pathological conditions. Thus, accumulation of phospholipid damage markers like malondialdehyde (MDA) or 4-hydroxynonenal (HNE) or F2 isoprostanes; protein damage markers like protein carbonyls and HNE protein adducts; or DNA damage markers like 8-hydroxydeoxyguanosine (8-OHdG) have been demonstrated in the brain, cerebrospinal fluid (CSF), and blood in many neurodegenerative diseases [93–97]. In contrast to such indiscriminate damage to cellular components by ROS, a regulated cell death process called ferroptosis has recently been identified, which is iron-dependent and requires ROS and lipid peroxidation products [98]. The morphological and biochemical characteristics of ferroptosis have been worked out, which appear to be different from apoptosis and necroptosis, and the process is triggered by a diverse group of molecules like erastin, sulphasalazine, BSO, DP12, DP17, cisplatin, and glutamate, many of which deplete the intracellular level of reduced glutathione (GSH) or inhibit glutathione peroxidase 4 (GPX4) [98, 99]. The biochemical features include increased production of ROS, accumulation of lipid

peroxidation products, elevated intracellular level of iron, decreased glutathione level, and inhibition by iron-chelators and lipid-soluble antioxidants like α -tocopherol, ferrostatin-1, and liproxstatin-1. The most characteristic morphological feature is the presence of deformed, shrunken mitochondria with loss of cristae and ruptured outer membrane and an intact nucleus [98–100]. The process of ferroptosis has been implicated in several pathological conditions like acute kidney injury, ischemia-reperfusion injury, cancer, and several neurodegenerative diseases [98, 100]. In addition to these mechanisms, ROS have been shown to be involved both in apoptosis and regulated necrosis (necroptosis) in many experimental conditions, and this could be important in the context of neuronal death which is a hallmark feature of most neurodegenerative diseases [101–103].

Though the involvement of ROS in various cell death pathways is complex, contextual, and probably interrelated, it may be presumed that as a major contributor to intracellular ROS production, NOX would play an important role in cellular death pathways. Thus, enhanced NADPH oxidase activity has been reported in apoptosis and necroptosis in a variety of experimental models involving cardiomyocytes, pancreatic acinar cells, human aortic smooth muscle cells, endothelial cells, and fibroblasts [104–108]. In the context of neuronal death in AD, we will discuss the role of NOX separately, but there is scattered evidence of NOX activation in other neurodegenerative diseases as well. Thus, postmortem brain studies have revealed high levels of NOX2 in the substantia nigra of sporadic Parkinson's disease (PD) patients, localizing with the microglial marker CD68 as evidenced by immunostaining [109]. In the same study, high levels of NOX2 in reactive microglia associated with dopaminergic neuronal loss have been observed in 1-methyl-4-phenyl-1,2,3,6-tetrahydropyridine- (MPTP-) induced experimental models of PD, and interestingly, much less dopaminergic neuronal loss is noticed in mice lacking NOX2 suggesting a clear link between neuronal death and NOX2 activation [109]. In another study of a 6-hydroxydopamine-based model of PD neurodegeneration in rats, increased expression levels of NOX1 and Rac1 (a component of the NOX1 complex) have been observed in dopaminergic neurons of the substantia nigra along with oxidative DNA damage and neuronal death which could be prevented significantly by knocking down the expression of NOX1 [110]. Oxidative stress and NOX have been implicated in the pathogenesis of another devastating neurodegenerative disease—amyotrophic lateral sclerosis (ALS)—in which progressive loss of motor neurons accompanied by gliosis occurs. In spinal cords of genetic mouse models of ALS, an increased expression of NOX2 has been demonstrated, and a similar increase has been observed in microglial NOX2 in postmortem spinal cord samples of ALS patients [111]. This study, however, has failed to show any improvement in the survival of ALS mouse models upon treatment with NOX inhibitors [111]. In an earlier study, mutant SOD1, as present in the familial type of ALS, expressed in human cell lines, was shown to activate NOX directly through the Rac1 regulator protein [112]. The aggregation and accumulation within neurons of mutant ATXN7 because of polyglutamine (poly-Q) expansion has

been held responsible for the inherited neurodegenerative disease spinocerebellar ataxia type 7 (SCA7). In a cell-based model of this disease, the expression of mutant ATXN7 is accompanied by increased ROS production, aggregation of ATXN7, and cytotoxicity, which are preventable by a NOX inhibitor [113].

2.6. Alzheimer's Disease, Oxidative Stress, and NOX

2.6.1. Oxidative Stress in AD. Alzheimer's disease (AD) is characterized by a diffuse loss of neurons in the hippocampus, entorhinal cortex, amygdala, and different regions of the neocortex with extracellular deposition of oligomerized amyloid beta peptide ($A\beta_{42}$) called amyloid plaques and intraneuronal neurofibrillary tangles composed of phosphorylated tau protein [13]. The disease causes progressive dementia and loss of multiple cognitive domains in a devastating form leading to death within 3–9 years of diagnosis. The accumulation of oxidative damage markers of lipids, proteins, and nucleic acids has been shown in multiple studies in CSF or postmortem brain tissue in AD, and the topic is reviewed extensively [13, 87, 88, 93, 94, 114–117]. Such oxidative damage in the brain is also detectable in AD transgenic animals along with the deposition of amyloid plaques [118, 119]. In addition, the accumulation of transition metals like Fe and Cu in the AD brain has been shown in many postmortem studies using histochemical and magnetic resonance spectroscopic methods, but a meta-analysis subsequently has challenged this notion and suggested significant citation bias [120–123]. Antemortem imaging studies have also indicated iron accumulation in AD brains in several areas, but more extensive in vivo studies are necessary [124, 125]. Although ROS can interact with any biomolecule within neurons, oxidative damage to proteins in particular could be important in AD pathogenesis through disruption of neuronal energy metabolism and proteostasis and aberrant redox signalling through activation of stress-activated protein kinases (JNK, p38, and ERK 1/2) or oxidative modifications of redox-sensitive transcription factors [126–128].

Most reviews dealing with oxidative damage in AD have discussed the reasons for enhanced ROS formation in the AD brain. In general, transition metal-catalysed ROS formation, especially with the metal liganded with $A\beta$, could be an important contributor, and in addition, increased ROS formation can take place from dysfunctional mitochondria which is characteristic of AD [128–131]. On the other hand, the release of ROS from activated microglia as a part of the inflammatory response in the AD brain is also important, and NOX could be playing a crucial role in this process.

2.6.2. NADPH Oxidase and AD. NADPH oxidase activation has been strongly implicated in the pathogenesis of AD as evident from postmortem studies showing the translocation of NOX2 subunits p47^{phox} and p67^{phox} from cytosol to membrane, and this activation presumably takes place in activated microglia [132]. In another study, subjects were grouped on the basis of antemortem behavioural testing and postmortem histopathological assessment as no cognitive impairment (NCI), preclinical AD, mild cognitive impairment (MCI),

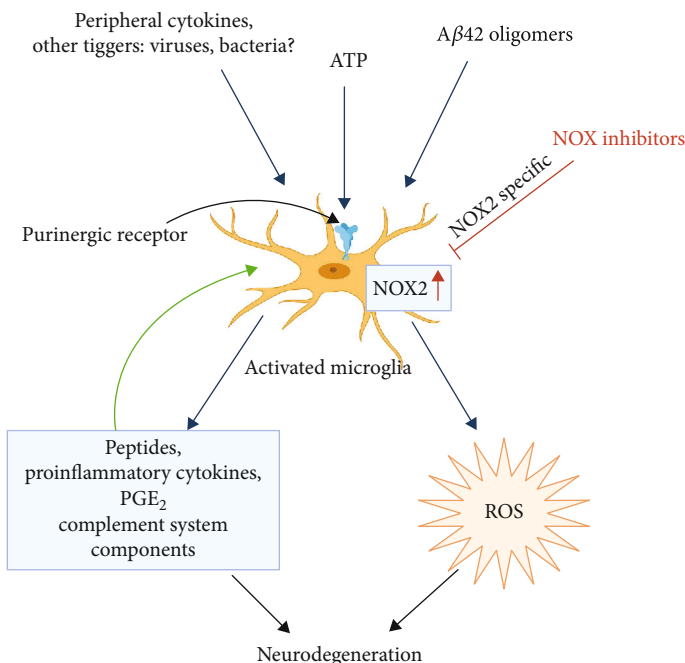


FIGURE 1: NOX activation in brain microglia in Alzheimer's disease. The microglial NOX2 is upregulated through multiple triggers including A β 42. Proinflammatory cytokines, chemokines, and NOX2-derived ROS act in concert to cause further activation of microglia and also neuronal damage linking inflammation and oxidative damage in AD pathology. The potential beneficial effects of NOX2 inhibitors have been indicated (image was created using BioRender).

and early to moderate AD; NOX activity was measured luminometrically, and protein expression levels of NOX2 subunits were assessed by immunoblotting [133]. The NOX enzyme activity was elevated in MCI, and different grades of AD compared to that in NCI. NOX2 subunit (p47^{phox}, p67^{phox}, and p40^{phox}) levels also remained high in different grades of AD, and in addition, a strong inverse correlation was observed with increased NOX activity associated with decreased cognitive functions [133]. In another longitudinal follow-up study of control subjects and patients of preclinical AD, MCI, and advanced AD, increased NOX activity was seen in the temporal cortex of MCI patients but not in those of preclinical AD or advanced AD subjects; immunohistochemical and immunoblotting analyses showed increased levels of gp91^{phox} and p47^{phox} in the MCI group [134]. Further, this study showed that gp91^{phox} was expressed in microglial cells as well as in neurons, and the toxic action of soluble oligomeric A β 42 on neurons in culture were diminished by the NOX inhibitor apocynin [134]. The enhanced activity of NOX2 in AD may be caused by the activation of microglia by A β which releases ATP which in turn leads to NOX2 activation and ROS production; the process is mediated through the activation of the purinergic receptor P2X7 and requires Ca²⁺ influx [135]. Another earlier study showed that microglia in primary culture stimulated by ATP acting through the purinergic receptor P2X7 release superoxide radical (O₂^{•-}), and this process is mediated by NOX activation [136]. Furthermore, such activated microglia can lead to neuronal death in coculture suggesting a clear link among neuroinflammation, NOX activation, oxidative stress, and neurodegeneration [136]. Intracerebrovascular injection of LPS or A β oligomers causes an inflammatory response through the

activation of microglia, but this response is inhibited in NOX-deficient (p47^{phox} or gp91^{phox} deficient or apocynin treated) mice where the microglia attain the alternative phenotype (M2) responsible for tissue healing and repair [137]. Likewise, neuroblastoma cells with an overexpression of APP (wild-type or containing multiple mutations of familial AD) degenerate when cocultured with microglial cells because of ROS production by NOX, and this is expectedly attenuated by the NOX inhibitor DPI or radical scavengers [138].

In addition to NOX2, high levels of NOX1 and NOX3 mRNA have been observed in the frontal lobe of AD patients (early stages), indicating the contribution of other NOX isoforms in AD neuropathology [139]. The activity of NOX and the expression of the NOX4 subunit are also consistently elevated in the brain of APPxPS1 knock-in mice with a significant linear correlation between NOX activity and the age-dependent accumulation of A β with cognitive dysfunction [140]. On the other hand, transgenic mice (Tg2576) carrying human APP with the Swedish mutation and lacking in the catalytic subunit of NOX2 fail to develop oxidative damage, neurovascular dysfunction, and cognitive deficits at 12-15 months of age unlike Tg2576 mice with intact NOX2, though the brain amyloid beta burden in both the groups were similar [141]. Thus, a mounting body of evidence demonstrates NOX activation and ROS generation in the AD brain and primarily implicates microglial response as the trigger for increased ROS production. In the AD brain, soluble oligomers of amyloid beta peptide and other inflammatory triggers activate the microglia to M1 state with changes in morphology and exhibition of many inflammatory surface markers [128, 142, 143]. The microglia proliferate and assemble near the amyloid plaques releasing many

TABLE 1: Drug trials of NOX inhibitors in Alzheimer's disease and its precursor conditions.

Country, trial code, reference if published	Sponsor	Phase	Diagnosis	Study design	Sample size and age	Treatment	Outcome	Duration	Results and status
Germany NCT00951834	Charité University, Berlin	2, 3	Early stage AD	Randomized, placebo controlled	N = 21, ≥60 years	EGCG (200-800 mg) as an add-on to donepezil	(1) ADASCog score (2) Safety, MMSE, brain atrophy, time to hospitalization, time to death, and others	18 months	Results not posted
Spain NCT03978052	Parc de Salut Mar	NA	Apo E4 carriers with SCD	Randomized, double blind, personalized, placebo controlled, four-arm trial	N = 200, 60-80 years	Multimodal intervention (diet, physical activity and cognitive activity) and EGCG (5-6 mg/kg up to 520 mg/day)	(1) ADCS-PACC-like score (2) Changes in functional neuronal connectivity tested by fMRI, changes in structural connectivity networks	12 months of treatment; 24 months total study duration	Ongoing
Spain NCT01699711 [153]	Parc de Salut Mar	2	DS neurological disease	Randomized, double blind, placebo controlled	N = 87, 14-29 years	EGCG (9 mg/kg) and cognitive training	(1) Change in cognitive evaluation and amyloidosis biomarkers (2) Change in DYRK1A activity biomarkers, lipid oxidation biomarkers, neurophysiology, neuroimaging, and others	12 months	EGCG better than placebo in improving visual recognition memory, inhibitory control and adaptive behaviour
US NCT01504854 [154]	ADCS, National Institute on Aging	2	Mild-moderate AD	Randomized, double blind, placebo controlled	N = 119, ≥50 years	Oral resveratrol (500 mg/day; increased up to maximum 2 g/day)	(1) Number of adverse events, volumetric MRI brain changes from baseline (2) Change in ADCS-ADL, CSF-Aβ40 levels	52 weeks	Nausea, diarrhoea, weight loss common with resveratrol. CSF and plasma Aβ declined more in placebo group. Brain volume loss and ventricular volume increase more in resveratrol group.
US NCT00678431 [155]	US Dept. of Veterans Affairs	3	Probable AD patients with MMSE 12-26	Randomized, double blind, placebo controlled	N = 27, 50-90 years	Oral liquid resveratrol, glucose and malate	(1) ADASCog (2) ADCS-CGIC	12 months	All outcome scores showed less deterioration in treatment group; however, statistically insignificant

TABLE 1: Continued.

Country, trial code, reference if published	Sponsor	Phase	Diagnosis	Study design	Sample size and age	Treatment	Outcome	Duration	Results and status
US NCT02502253	Johns Hopkins University, Icahn School of Medicine at Mount Sinai	1	Amnesic MCI; impaired fasting glucose or clinically stable type 2 diabetes	Randomized	N = 48, 50-90 years	BDPP, low-, moderate-, high-dose study	Adverse events and serious adverse events, CSF penetration of BDPP, effect on mood, and effect on cognition	4 months	Recruiting
Turkey NCT04044131	Istanbul Medipol University Hospital, ScandiBio Therapeutics AB, and others	2	Mild to moderate AD (ADASCog \geq 12 and CDR \leq 2)	Randomized, double blind, placebo controlled	N = 60, >50 years	Mixture of NAC, carnitine, nicotinamide riboside, and serine (metabolic cofactors)	(1) MMSE, ADASCog, ADCS-ADL (2) Volumetric brain MRI, resting state fMRI, NPI, MOCA, serum omics, microbiota, adverse events, and biochemical monitoring	3 months	Recruiting
US NCT01320527 [156, 157]	University of Massachusetts, Worcester	2	AD and MCI	Randomized, double blind, placebo controlled	N = 106, \geq 40 years	NF having folic acid 400 μ g, vitamin B12 6 μ g, vitamin E 30 IU, SAM 400 mg, NAC 600 mg, acetyl-L-carnitine 500 mg	(1) Cognitive improvement by CLOX-1 and DRS (2) Improvement in NPI and ADL	12 months; first assessment at 3 months	Statistically significant improvement in the NF group versus placebo in cognitive assessment by CLOX-1 and DRS. Nonsignificant improvement in NPI and ADL. Continuation as open-label in 24 patients and evaluated at 12 months; participants maintained baseline cognitive performance and BPSD.
US NCT01370954	Pamlab, Inc. and InfoMedics, Inc.	NA	Early memory loss, MCI, AD, and VD	Prospective observational	N = 204, 50-80 years	Medical food CerefolinNAC® having NAC 600 mg, methyl cobalamin 2 mg, L-methyl folate calcium 6 mg	(1) QOL-AD measure of quality of life (2) Overall patient satisfaction	3 months	Results not posted

TABLE 1: Continued.

Country, trial code, reference if published	Sponsor	Phase	Diagnosis	Study design	Sample size and age	Treatment	Outcome	Duration	Results and status
US NCT02033941	Hillel Grossman, NCCIH	2	Probable AD with MMSE score of 12-26	Randomized, double blind, placebo controlled	N = 20, all ages	Grape seed polyphenolic extract	(1) Pharmacokinetic analysis, CSF tau and phosphorylated tau protein, adverse events (2) A β in plasma and CSF, scores on ADASCog, ADCS-CGIC, MMSE, ADL	22 months	Recruiting
China NCT03221894	Dongzhimen Hospital, Beijing	NA	AD (mild-severe on MMSE)	Observational study	N = 90, 50-85 years	GRAPE granules (having herbal medicines such as ginseng, <i>Curcuma</i> , <i>Acorus</i> , <i>Polygala</i> , and berberine)	(1) MMSE (2) ADL, NPI, and CDR	12 months	Results not posted, status as of 2017 was recruiting
South Korea NCT00391833	Seoul National University Hospital	1, 2	AD	Observational randomized, open label	N = 97, 40-83 years	<i>Panax ginseng</i> powder 4.5 g/day	MMSE and ADASCog scores	12 weeks therapy; assessment at 12 weeks and after 12 weeks of discontinuation of therapy	Statistically significant improvement in MMSE and ADASCog scores between the groups at 12 weeks. Improvement dissipated at 24 weeks (after 12 weeks of ginseng discontinuation) and adverse events were seen in 12% of patients treated with ginseng and 15% of the control group. Dizziness, headache, diarrhoea, and anorexia were the common adverse events seen in both groups.
Hong Kong NCT00164749	Chinese University of Hong Kong, BUPA Foundation, Kwong Wah Hospital	1, 2	AD	Randomized, double blind, placebo controlled	N = 34, ≥ 50 years	Curcumin powder or capsule (4 g or 1 g) along with standard treatment of ginkgo leaf extract 120 mg/d in all groups (including placebo)	(1) Plasmalipostanes, serum A β ₄₀ (2) Change in cognitive function (MMSE score), curcumin and metabolites in plasma	6 months (some variables at 1 month)	Cognitive scores did not improve with curcumin. Vitamin E increased over 1 month with curcumin. Serum A β ₄₀ did not change.

TABLE 1: Continued.

Country, trial code, reference if published	Sponsor	Phase	Diagnosis	Study design	Sample size and age	Treatment	Outcome	Duration	Results and status
India NCT01001637	Jaslok Hospital and Research Center, others	2	AD, MMSE score of 5-20	Randomized, double blind, placebo controlled	N = 26, 50-80 years	Solid lipid curcumin particle (SLCP) formulation	(1) Mental capacity (based on tests) (2) Blood concentration of A β	2 months	Results not posted
US NCT00099710 [158]	John Douglas French Foundation	Phase 2	Mild-moderate AD	Randomized, double blind, placebo controlled for 6 months followed by open label for next 6 months	N = 30, ≥ 50 years	Curcumin C3 complex (2 g or 4 g daily)	(1) Adverse events, ADASCog, changes in clinical laboratory tests (2) NPI, ADCS-ADL, plasma A β , CSF isoprostanes, t-tau, p-tau, and A β	6 months	No difference in clinical efficacy or biomarkers. Clinically insignificant increase in blood glucose and decrease in hematocrit in curcumin group. GI symptoms occurred in 12.5% patients of curcumin group leading to withdrawal from study.
US NCT01811381	Veterans Affairs Office of Research and Development	2	MCI, MMSE > 24	Randomized, double blind	N = 80, 50-90 years	Curcumin; aerobic and anaerobic yoga/exercises	(1) Blood biomarkers: TNF α , N-terminal BNP, IL-6, IL-1 β , VCAM-1, ApoE, etc. (2) NPI, adverse events, 18-FDG-PET, FAQ	12 months	Active, not recruiting
US NCT01716637	Life Extension Foundation Inc.	1	AD (NINCDS-ADRDA criteria)	Open label, crossover	N = 12, 60-85 years	Perispinal etanercept injection subcutaneously and dietary supplements having curcumin, quercetin, resveratrol, ω -3 fatty acids	(1) MMSE score (2) ADASCog score, MOCA score	16 weeks	Results not posted
France NCT00814346	Ipsen	2	Three groups: mild AD; cognitively normal elderly; cognitively impaired elderly (MMSE-20-28 for AD)	Randomized double blind, placebo controlled followed by open label	N = 49, ≥ 65 years	EGb761® Ginkgo (120 mg twice daily)	(1) Change in brain glucose metabolism (18-FDG-PET) at 1 month (2) CDR, MMSE, GDS, MMSE, adverse events in memory complaint/normal group	18 months	(1) Not reported (2) Falls occurred in 12%; constipation, insomnia, and depression occurred in 7.3% each; gastroesophageal reflux, vertigo, and dyspnoea occurred in 4.8% each, in the open phase

TABLE 1: Continued.

Country, trial code, reference if published	Sponsor	Phase	Diagnosis	Study design	Sample size and age	Treatment	Outcome	Duration	Results and status
China NCT03090516	The First Affiliated Hospital with Nanjing Medical University	2, 3	Mild-moderate AD	Randomized	N = 240, 50-85 years	Donepezil versus donepezil plus ginkgo versus ginkgo	MMSE score, EEG, MRI, ADASCog score, LFT, RFT, NPI, and ADL	3 months	Recruiting as of August 2019
US NCT00010803 [159-161]	NCCIH, others	3	Normal cognition and MCI patients	Randomized, double blind, placebo controlled	N = 3069, ≥75 years	Ginkgo (EGb761®) 120 mg twice daily	(1) All cause dementia including AD (2) CVD events or mortality, progression of cognitive decline	8 years	Ginkgo had no effect on decreasing dementia, cognitive decline, and cardiovascular events. More PVD events were seen in placebo group.
France NCT00276510 [162]	Ipsen	3b/4	Patients with memory complaints	Randomized, double blind, placebo controlled	N = 2854, ≥70 years	Ginkgo (EGb761®) 120 mg BD	(1) Conversion to AD (2) Concomitant diseases, safety, rate of cognitive abilities decline	5 years	Ginkgo had no effect on decreasing AD, overall deaths and stroke. No difference in safety profile.
US NCT00042172	University of Iowa, National Institute of Mental Health	4	Patients with MCI and subjective memory complaints	Randomized	N = 40, ≥65 years	Donepezil versus placebo for 6 months then donepezil plus ginkgo versus donepezil alone for next 6 months	Brain blood flow using PET	12 months	Results not posted
US NCT01009476	Janssen-Cilag G.m.b.H	NA	Mild to moderate AD/mixed dementia	Prospective observational, noninterventional	N = 1134, ≥50 years	Galantamine or nootropics (<i>Ginkgo</i> , piracetam, nicergoline, etc.)	Cognitive decline, safety, vital functions, caregiver's burden, etc.	12 months	Results not posted
US, Israel, UK NCT00940589	Neurim Pharmaceuticals Ltd.	2	Mild-moderate AD (MMSE score > 15)	Randomized, double blind, placebo controlled	N = 73, 50-85 years	AChase inhibitor and melatonin (prolonged release) 2 mg versus AChase inhibitor and placebo	(1) ADASCog change (2) iADL change, MMSE change	6 months	Nonsignificant change in ADASCog between the groups. iADL improved significantly ($P < 0.05$) in placebo compared to melatonin (1.62 versus 0.77). MMSE declined less in the melatonin group (-0.3 versus -1.9). Adverse events: gastrointestinal seen in

TABLE 1: Continued.

Country, trial code, reference if published	Sponsor	Phase	Diagnosis	Study design	Sample size and age	Treatment	Outcome	Duration	Results and status
US NCT00000171 [163]	National Institute on Aging (NIA)	3	AD, MMSE \leq 26, dyssomnia	Randomized, double blind, placebo controlled	N = 157, \geq 55 years	Melatonin 2.5 mg SR, melatonin 10 mg IR	(1) Change in nocturnal sleep time (2) Awake period, daytime agitation, change in ADASCog, MMSE, HAM-D	8 weeks	28.2% of the melatonin group versus 14.7% of the control group; respiratory disorders seen in 20.5% of the melatonin group versus 11.7% of the control group. Angina, falls seen only in the melatonin group (7.7% each); increased blood sugar in the melatonin group (5%) versus the control group (2.9%). Neuropsychiatric disorders common in the melatonin group (17.9%) versus the control group (14.7%).
US NCT03954899	NazanAksan, University of Iowa	NA	MCI, MOCA score \geq 18	Randomized, double blind, placebo-controlled study assessing disease-modifying role of melatonin	N = 230, 60-80 years	Melatonin 5 mg	(1) Episodic memory (2) Overall cognitive function, CSF-p-tau, t-tau, A β 42, sleep efficiency, and others	44 weeks	Recruiting

Abbreviations: AChase = acetylcholine esterase; AD = Alzheimer's disease; ADASCog = Alzheimer's Disease Assessment Scale—cognitive subscale; ADCS = Alzheimer's Disease Cooperative Study; ADCS-CGIC = Alzheimer's Disease Cooperative Study—Clinical Global Impression of Change; ADCS-PACC = Alzheimer's Disease Cooperative Study—Preclinical Alzheimer Cognitive Composite; ADL = activities of daily living; Apo E = apolipoprotein E; A β 40 = amyloid beta 40; BDPP = bioactive dietary polyphenol preparation (has grape seed polyphenolic extract and resveratrol); BNP = brain-type natriuretic peptide; BPSD = behavioural and psychological symptoms in dementia; CDR = clinical dementia rating; CVD = cerebrospinal fluid; CVD = cardiovascular disease; DRS = Dementia Rating Scale; DS = Down's syndrome; DYRK1A = dual-specificity tyrosine phosphorylation-regulated kinase-1A; EEG = electroencephalogram; EGGG = epigallocatechin gallate; FAQ = Functional Activities Questionnaire; FDG = fluorodeoxyglucose; fMRI = functional magnetic resonance imaging; GDS = Geriatric Depression Scale; HAM-D = Hamilton Depression Rating Scale; iADL = instrumental activities of daily living; IL = interleukin; LFT = liver function test; MCI = mild cognitive impairment; MMSE = Mini Mental State Examination; MOCA = Montreal Cognitive Assessment; NA = not applicable; NAC = N-acetyl cysteine; NCCIH = National Center for Complementary and Integrative Health; NINCDS-ADRDA = National Institute of Neurological and Communicative Disorders and Stroke-Alzheimer's Disease and Related Disorders Association; NPI = neuropsychiatric inventory; NF = nutraceutical formulation; PET = positron emission tomography; p-tau = phosphorylated tau protein; PVD = peripheral vascular disease; QOL = quality of life; RFT = renal function test; SCD = subjective cognitive decline; TNF α = tumor necrosis factor α ; t-tau = total tau protein; VCAM-1 = vascular cell adhesion molecule-1; VD = vascular dementia.

peptides, proinflammatory cytokines, chemokines, prostaglandins like PGE₂, components of the complement system, and ROS, and thus a strong inflammatory response is generated which is partly responsible for neuronal and synaptic degeneration [128, 142–144]. The increased ROS production in reactive microglia occurs from activation of NOX2; ROS can cause degeneration of neurons and through redox-signalling pathways enhance the formation and release of proinflammatory cytokines from the microglia [145]. This suggests an overlap of oxidative damage pathways, redox-signalling mechanisms, and inflammatory response in AD brain. Figure 1 summarizes the mechanistic processes linked to NOX activation in microglia and the potential benefits of NOX2 inhibitors.

3. NADPH Oxidase Inhibitors in AD

It is apparent from the discussion above that NOX inhibitors will have substantial effects on the pathogenesis of AD, attenuating both oxidative stress and neuroinflammation in the brain; thus, they are potential candidates as disease-modifying agents in AD. Furthermore, NOX2, present predominantly in microglia, appears to be the most important isoenzyme involved in AD pathogenesis; thus, a specific inhibitor of NOX2 instead of a general NOX inhibitor could be even more effective. The NOX inhibitors are comprised of a heterogeneous group of molecules that include both peptide inhibitors and small molecule inhibitors. The peptide inhibitors are designed to prevent the binding of cytosolic accessory proteins to the membrane-bound catalytic portion of NOX; thus, they act as specific inhibitors of different isoenzymes of NOX (NOX2-ds-TAT and Nox-A1ds are specific for NOX2 and NOX1, respectively) [146]. Many small-molecule inhibitors of NOX are currently available for research applications, and some of them are also being tested in clinical trials [146–148].

The classification of NOX inhibitors is complex. The older generation of small molecule NOX inhibitors include diphenylene iodonium (DPI) and apocynin, and the relatively less tested 4-(2-aminoethyl)-benzenesulphonyl fluoride (AEBSF) or plumbagin, while the more recently introduced compounds are GLX351322 and GSK2795039. A major issue with these drugs is the presence of additional actions such as direct ROS-scavenging properties, rho kinase inhibition, flavoprotein inhibition, and serine kinase inhibition. Many of them do not directly inhibit NOX but instead act on upstream triggers and downstream pathways of NOX [26, 148]. Many of these drugs are not specific for any particular isoenzyme of NOX, but GKT137831 and GKT36901 are claimed to be specific for NOX1 and NOX4 [148]. This not only makes it difficult to judge how much their actual therapeutic benefits may be ascribed to NOX inhibition but also results in off-target effects, making clinical use difficult [26, 148]. One drug that has been prominently tested, especially in a variety of cardiovascular disease states in animal models and some clinical trials is apocynin. It is a phenolic compound which is derived from the medicinal plant *Jatropha multifida* [149]. It has been also suggested that apocynin, which mainly inhibits NOX2, may have a benefi-

cial role in Alzheimer's disease. A study investigating apocynin at an oral dose of 10 mg/kg daily in a hAPP (751) SL transgenic mouse model of AD found a significant reduction of plaque size within the cortex and hippocampus and a reduction of microglia number in the cortex [150]. In another experiment, male Wistar rats treated with scopolamine to induce an AD phenotype showed improvement in cognitive test performance when administered apocynin. This was accompanied by a decline in amyloid β concentration in the rat hippocampi and a decrease in superoxide anion concentration [151]. Apart from the traditional small molecule inhibitors, several new agents such as GKT136901 and GKT137831; ML171; VAS2870 and VAS3947; S17834; Fulvene-5; the triphenylmethane derivative dyes, namely, imipramine blue, brilliant green, and Gentian violet; grindelic acid; ebselen; perhexiline; and Shionogi I and II have been proposed to have NOX-specific inhibitory activity based on experimental studies [26, 152]. Most of these agents, however, have not made it to the clinical trial stage, at least in neurodegenerative disorders. The focus of clinical studies in Alzheimer's disease thus remains on naturally obtained compounds with not only NOX inhibitory but also other beneficial effects. These include berberine, blueberry-derived polyphenols, relatively NOX-specific celastrol, EGCG derived from green tea, *Ginkgo biloba*, resveratrol, and others. Table 1 summarizes several human studies of these agents in patients with Alzheimer's disease and its precursor states such as mild cognitive impairment [153–163]. It is evident that the results are quite variable, and hence, further studies are warranted to evaluate their role in AD therapeutics. It is also to be understood that NOX-generated ROS take part in redox signalling under physiological conditions in the brain; thus, inhibition of NOX as a therapeutic measure may be fraught with additional problems.

4. Conclusion

The complexity of AD pathogenesis especially in sporadic cases precludes any “magic bullet” approach towards the therapy of this disease. Multiple disease-modifying drugs and multitargeted drugs could become important in the coming days to combat AD. To that extent, NOX inhibitors may provide an “add-on” therapy to maximize clinical benefit in AD treatment. However, a molecule specifically and directly inhibiting NOX2 without “off-target” effects would be necessary, and in addition, its bioavailability in the CNS and long-term toxicity have to be carefully evaluated.

Data Availability

This being a review article, no data was generated during the preparation of this manuscript.

Conflicts of Interest

The authors declare that there is no conflict of interest.

Acknowledgments

SC and SSC want to thank the Indian Council of Medical Research, New Delhi, for their continued research support related to neurodegenerative diseases. SC and UG want to acknowledge the management of Maharishi Markandeshwar Deemed University for research and administrative support.

References

- [1] D. Harman, "Free radical theory of aging: the "free radical" diseases," *Age*, vol. 7, no. 4, pp. 111–131, 1984.
- [2] K. Goszcz, S. J. Deakin, G. G. Duthie, D. Stewart, S. J. Leslie, and I. L. Megson, "Antioxidants in cardiovascular therapy: panacea or false hope?," *Frontiers in cardiovascular medicine*, vol. 2, p. 29, 2015.
- [3] M. Polidori and G. Nelles, "Antioxidant clinical trials in mild cognitive impairment and Alzheimer's disease—challenges and perspectives," *Current Pharmaceutical Design*, vol. 20, no. 18, pp. 3083–3092, 2014.
- [4] G. H. Kim, J. E. Kim, S. J. Rhie, and S. Yoon, "The role of oxidative stress in neurodegenerative diseases," *Experimental Neurobiology*, vol. 24, no. 4, pp. 325–340, 2015.
- [5] I. Liguori, G. Russo, F. Curcio et al., "Oxidative stress, aging, and diseases," *Clinical Interventions in Aging*, vol. 13, pp. 757–772, 2018.
- [6] R. D'Oria, R. Schipani, A. Leonardini et al., "The role of oxidative stress in cardiac disease: from physiological response to injury factor," *Oxidative Medicine and Cellular Longevity*, vol. 2020, Article ID 5732956, 29 pages, 2020.
- [7] B. Halliwell and J. M. Gutteridge, "Oxygen toxicity, oxygen radicals, transition metals and disease," *Biochemical Journal*, vol. 219, no. 1, pp. 1–14, 1984.
- [8] H. Sies, C. Berndt, and D. P. Jones, "Oxidative stress," *Annual Review of Biochemistry*, vol. 86, no. 1, pp. 715–748, 2017.
- [9] N. T. Moldogazieva, I. M. Mokhosoev, N. B. Feldman, and S. V. Lutsenko, "ROS and RNS signalling: adaptive redox switches through oxidative/nitrosative protein modifications," *Free Radical Research*, vol. 52, no. 5, pp. 507–543, 2018.
- [10] M. Schieber and N. S. Chandel, "ROS function in redox signaling and oxidative stress," *Current Biology*, vol. 24, no. 10, pp. R453–R462, 2014.
- [11] E. H. Sarsour, M. G. Kumar, L. Chaudhuri, A. L. Kalen, and P. C. Goswami, "Redox control of the cell cycle in health and disease," *Antioxidants & Redox Signaling*, vol. 11, no. 12, pp. 2985–3011, 2009.
- [12] B. W. L. Lee, P. Ghode, and D. S. T. Ong, "Redox regulation of cell state and fate," *Redox Biology*, vol. 25, 2019.
- [13] S. Chakrabarti, M. Sinha, I. Thakurta, P. Banerjee, and M. Chattopadhyay, "Oxidative stress and amyloid beta toxicity in Alzheimer's disease: intervention in a complex relationship by antioxidants," *Current Medicinal Chemistry*, vol. 20, no. 37, pp. 4648–4664, 2013.
- [14] A. H. K. Tsang and K. K. K. Chung, "Oxidative and nitrosative stress in Parkinson's disease," *Biochimica et Biophysica Acta-Molecular Basis of Disease*, vol. 1792, no. 7, pp. 643–650, 2009.
- [15] D. Allan Butterfield and I. Dalle-Donne, "Redox proteomics," *Antioxidants & Redox Signaling*, vol. 17, no. 11, pp. 1487–1489, 2012.
- [16] D.-P. Xu, Y. Li, X. Meng et al., "Natural antioxidants in foods and medicinal plants: extraction, assessment and resources," *International Journal of Molecular Sciences*, vol. 18, no. 1, p. 96, 2017.
- [17] I. I. Severina, F. F. Severin, G. A. Korshunova et al., "In search of novel highly active mitochondria-targeted antioxidants: thymoquinone and its cationic derivatives," *FEBS Letters*, vol. 583, no. 13, pp. 2018–2024, 2013.
- [18] H. H. Szeto, "Mitochondria-targeted peptide antioxidants: novel neuroprotective agents," *The AAPS Journal*, vol. 8, pp. 521–531, 2006.
- [19] J. Wu, J. Ren, S. Yao et al., "Novel antioxidants' synthesis and their anti-oxidative activity through activating Nrf2 signaling pathway," *Bioorganic & Medicinal Chemistry Letters*, vol. 27, no. 7, pp. 1616–1619, 2017.
- [20] A. A. Starkov, "The role of mitochondria in reactive oxygen species metabolism and signaling," *Annals of the New York Academy of Sciences*, vol. 1147, no. 1, pp. 37–52, 2008.
- [21] M. P. Murphy, "How mitochondria produce reactive oxygen species," *Biochemical Journal*, vol. 417, no. 1, pp. 1–13, 2008.
- [22] N. Speed and I. A. Blair, "Cyclooxygenase- and lipoxygenase-mediated DNA damage," *Cancer and Metastasis Reviews*, vol. 30, no. 3–4, pp. 437–447, 2011.
- [23] A. Panday, M. K. Sahoo, D. Osorio, and S. Batra, "NADPH oxidases: an overview from structure to innate immunity-associated pathologies," *Cellular & Molecular Immunology*, vol. 12, no. 1, pp. 5–23, 2015.
- [24] J. L. Meitzler, S. Antony, Y. Wu et al., "NADPH oxidases: a perspective on reactive oxygen species production in tumor biology," *Antioxidants & Redox Signaling*, vol. 20, no. 17, pp. 2873–2889, 2014.
- [25] W. M. Nauseef, "Biological Roles for the NOX Family NADPH Oxidases," *Journal of Biological Chemistry*, vol. 283, no. 25, pp. 16961–16965, 2008.
- [26] S. Altenhöfer, K. A. Radermacher, P. W. M. Kleikers, K. Winkler, and H. H. H. W. Schmidt, "Evolution of NADPH oxidase inhibitors: selectivity and mechanisms for target engagement," *Antioxidants & Redox Signaling*, vol. 23, no. 5, pp. 406–427, 2015.
- [27] I. Lorenzen, L. Mullen, S. Bekeschus, and E. M. Hanschmann, "Redox regulation of inflammatory processes is enzymatically controlled," *Oxidative Medicine and Cellular Longevity*, vol. 2017, Article ID 8459402, 23 pages, 2017.
- [28] R. S. Frey, M. Ushio-Fukai, and A. B. Malik, "NADPH oxidase-dependent signaling in endothelial cells: role in physiology and pathophysiology," *Antioxidants & Redox Signaling*, vol. 11, no. 4, pp. 791–810, 2009.
- [29] R. Prieto-Bermejo and A. Hernández-Hernández, "The importance of NADPH oxidases and redox signaling in angiogenesis," *Antioxidants*, vol. 6, no. 2, 2017.
- [30] A. Konior, A. Schramm, M. Czesnikiewicz-Guzik, and T. J. Guzik, "NADPH oxidases in vascular pathology," *Antioxidants & Redox Signaling*, vol. 20, no. 17, pp. 2794–2814, 2014.
- [31] C. E. Murdoch, M. Zhang, A. C. Cave, and A. M. Shah, "NADPH oxidase-dependent redox signalling in cardiac hypertrophy, remodelling and failure," *Cardiovascular Research*, vol. 71, no. 2, pp. 208–215, 2006.
- [32] J. Kuroda, T. Ago, S. Matsushima, P. Zhai, M. D. Schneider, and J. Sadoshima, "NADPH oxidase 4 (Nox4) is a major source of oxidative stress in the failing heart," *PNAS*, vol. 107, no. 35, pp. 15565–15570, 2010.

- [33] Q. D. Zhao, S. Viswanadhapalli, P. Williams et al., "NADPH oxidase 4 induces cardiac fibrosis and hypertrophy through activating Akt/mTOR and NF κ B signaling pathways," *Circulation*, vol. 131, no. 7, pp. 643–655, 2015.
- [34] S. Matsushima, J. Kuroda, P. Zhai et al., "Tyrosine kinase FYN negatively regulates NOX4 in cardiac remodeling," *The Journal of Clinical Investigation*, vol. 126, no. 9, pp. 3403–3416, 2016.
- [35] M. Han, T. Zhang, L. Yang, Z. Wang, J. Ruan, and X. Chang, "Association between NADPH oxidase (NOX) and lung cancer: a systematic review and meta-analysis," *Journal of Thoracic Disease*, vol. 8, no. 7, pp. 1704–1711, 2016.
- [36] P. Wang, Q. Shi, W. H. Deng et al., "Relationship between expression of NADPH oxidase 2 and invasion and prognosis of human gastric cancer," *World Journal of Gastroenterology*, vol. 21, no. 20, pp. 6271–6279, 2015.
- [37] X. You, M. Ma, G. Hou, Y. Hu, and X. Shi, "Gene expression and prognosis of NOX family members in gastric cancer," *Oncotargets Therapy*, vol. 11, pp. 3065–3074, 2018.
- [38] A. Juhasz, Y. Ge, S. Markel et al., "Expression of NADPH oxidase homologues and accessory genes in human cancer cell lines, tumours and adjacent normal tissues," *Free Radical Research*, vol. 43, no. 6, pp. 523–532, 2009.
- [39] M. Skonieczna, T. Hejmo, A. Poterala-Hejmo, A. Cieslar-Pobuda, and R. J. Buldak, "NADPH oxidases: insights into selected functions and mechanisms of action in cancer and stem cells," *Oxidative Medicine and Cellular Longevity*, vol. 2017, Article ID 9420539, 15 pages, 2017.
- [40] T. Kamata, "Roles of Nox1 and other Nox isoforms in cancer development," *Cancer Science*, vol. 100, no. 8, pp. 1382–1388, 2009.
- [41] O. Takeuchi and S. Akira, "Innate immunity to virus infection," *Immunological Reviews*, vol. 227, no. 1, pp. 75–86, 2009.
- [42] B. Albiger, S. Dahlberg, B. Henriques-Normark, and S. Normark, "Role of the innate immune system in host defence against bacterial infections: focus on the Toll-like receptors," *Journal of Internal Medicine*, vol. 261, no. 6, pp. 511–528, 2007.
- [43] C.-S. Yang, D.-M. Shin, K.-H. Kim et al., "NADPH oxidase 2 interaction with TLR2 is required for efficient innate immune responses to *Mycobacteria* via cathelicidin expression," *The Journal of Immunology*, vol. 182, no. 6, pp. 3696–3705, 2009.
- [44] A. Soucy-Faulkner, E. Mukawera, K. Fink et al., "Requirement of NOX2 and reactive oxygen species for efficient RIG-I-mediated antiviral response through regulation of MAVS expression," *Plos Pathogens*, vol. 6, no. 6, 2010.
- [45] H. S. Park, H. Y. Jung, E. Y. Park, J. Kim, W. J. Lee, and Y. S. Bae, "Cutting edge: direct interaction of TLR4 with NAD(P)H oxidase 4 isozyme is essential for lipopolysaccharide-induced production of reactive oxygen species and activation of NF- κ B," *The Journal of Immunology*, vol. 173, no. 6, pp. 3589–3593, 2004.
- [46] O. Khomich, S. Kochetkov, B. Bartosch, and A. Ivanov, "Redox biology of respiratory viral infections," *Viruses*, vol. 10, no. 8, p. 392, 2018.
- [47] R. Vlahos and S. Selemidis, "NADPH oxidases as novel Pharmacologic targets against influenza A virus infection," *Molecular Pharmacology*, vol. 86, no. 6, pp. 747–759, 2014.
- [48] D. Harman, "The aging process," *PNAS*, vol. 78, no. 11, pp. 7124–7128, 1981.
- [49] K. C. Kregel and H. J. Zhang, "An integrated view of oxidative stress in aging: basic mechanisms, functional effects, and pathological considerations," *American Journal of Physiology-Regulatory, Integrative and Comparative Physiology*, vol. 292, no. 1, pp. R18–R36, 2007.
- [50] K. H. Krause, "Aging: a revisited theory based on free radicals generated by NOX family NADPH oxidases," *Experimental Gerontology*, vol. 42, no. 4, pp. 256–262, 2007.
- [51] Y. Shi, R. Buffenstein, D. A. Puliam, and H. V. Remmen, "Comparative studies of oxidative stress and mitochondrial function in aging," *Integrative & Comparative Biology*, vol. 50, no. 5, pp. 869–879, 2010.
- [52] M. Kasapoglu and T. Ozben, "Alterations of antioxidant enzymes and oxidative stress markers in aging," *Experimental Gerontology*, vol. 36, no. 2, pp. 209–220, 2001.
- [53] L. M. Fan, L. Geng, S. Cahill-Smith et al., "Nox2 contributes to age-related oxidative damage to neurons and the cerebral vasculature," *The Journal of Clinical Investigation*, vol. 129, no. 8, pp. 3374–3386, 2019.
- [54] A. J. Bruce-Keller, C. L. White, S. Gupta et al., "NOX activity in brain aging: exacerbation by high fat diet," *Free Radical Biology and Medicine*, vol. 49, no. 1, pp. 22–30, 2010.
- [55] I. Guha Thakurta, M. Chattopadhyay, A. Ghosh, and S. Chakrabarti, "Dietary supplementation with N-acetyl cysteine, α -tocopherol and α -lipoic acid reduces the extent of oxidative stress and proinflammatory state in aged rat brain," *Biogerontology*, vol. 13, no. 5, pp. 479–488, 2012.
- [56] T. Ago, S. Matsushima, J. Kuroda, D. Zablocki, T. Kitazono, and J. Sadoshima, "The NADPH oxidase Nox4 and aging in the heart," *Aging*, vol. 2, no. 12, pp. 1012–1016, 2010.
- [57] W. C. Orr and R. S. Sohal, "Extension of life-span by overexpression of superoxide dismutase and catalase in *Drosophila melanogaster*," *Science*, vol. 263, no. 5150, pp. 1128–1130, 1994.
- [58] R. J. Mockett, W. C. Orr, J. J. Rahmandar et al., "Overexpression of Mn-Containing Superoxide Dismutase in Transgenic *Drosophila melanogaster*," *Archives of Biochemistry and Biophysics*, vol. 371, no. 2, pp. 260–269, 1999.
- [59] G. N. Landis and J. Tower, "Superoxide dismutase evolution and life span regulation," *Mechanisms of Ageing and Development*, vol. 126, no. 3, pp. 365–379, 2005.
- [60] R. J. Mockett, B. H. Sohal, and R. S. Sohal, "Expression of multiple copies of mitochondrially targeted catalase or genomic Mn superoxide dismutase transgenes does not extend the life span of *Drosophila melanogaster*," *Free Radical Biology and Medicine*, vol. 49, no. 12, pp. 2028–2031, 2010.
- [61] V. M. Labunskyy and V. M. Gladyshev, "Role of reactive oxygen species-mediated signaling in aging," *Antioxidants & Redox Signaling*, vol. 19, no. 12, pp. 1362–1372, 2013.
- [62] A. Sanz, "Mitochondrial reactive oxygen species: do they extend or shorten animal lifespan?," *Biochimica et Biophysica Acta – Bioenergetics*, vol. 1857, no. 8, pp. 1116–1126, 2016.
- [63] H. Sasakura, H. Moribe, M. Nakano, K. Ikemoto, K. Takeuchi, and I. Mori, "Lifespan extension by peroxidase and dual oxidase-mediated ROS signaling through pyrroloquinoline quinone in *C. elegans*," *Journal of Cell Science*, vol. 130, no. 15, pp. 2631–2643, 2017.
- [64] C. Y. Ewald, J. M. Hourihan, M. S. Bland et al., "NADPH oxidase-mediated redox signaling promotes oxidative stress resistance and longevity through *memo-1* in *C. elegans*," *eLife*, vol. 6, article e19493, 2017.

- [65] T. Schrader, C. Reschke, M. Spaeth, S. Wienstroer, S. Wong, and K. Schröder, “NoxO1 knockout promotes longevity in mice,” *Antioxidants*, vol. 9, no. 3, p. 226, 2020.
- [66] F. Rezende, C. Schürmann, S. Schütz et al., “Knock out of the NADPH oxidase Nox4 has no impact on life span in mice,” *Redox Biology*, vol. 11, pp. 312–314, 2017.
- [67] Y. Zhang, Y. Ikeno, W. Qi et al., “Mice deficient in both Mn superoxide dismutase and glutathione peroxidase-1 have increased oxidative damage and a greater incidence of pathology but no reduction in longevity,” *The Journals of Gerontology*, vol. 64A, no. 12, pp. 1212–1220, 2009.
- [68] S. E. Schriener and N. J. Linford, “Extension of mouse lifespan by overexpression of catalase,” *Age*, vol. 28, no. 2, pp. 209–218, 2006.
- [69] P. Davalli, T. Mitic, A. Caporali, A. Lauriola, and D. D’Arca, “ROS, cell senescence, and novel molecular mechanisms in aging and age-related diseases,” *Oxidative Medicine and Cellular Longevity*, vol. 2016, Article ID 3565127, 18 pages, 2016.
- [70] J. N. Cogley, M. L. Fiorello, and D. M. Bailey, “13 reasons why the brain is susceptible to oxidative stress,” *Redox Biology*, vol. 15, pp. 490–503, 2018.
- [71] M. Patel, “Targeting oxidative stress in central nervous system disorders,” *Trends in Pharmacological Sciences*, vol. 37, no. 9, pp. 768–778, 2016.
- [72] Z. Nayernia, V. Jaquet, and K. H. Krause, “New insights on NOX enzymes in the central nervous system,” *Antioxidants & Redox Signaling*, vol. 20, no. 17, pp. 2815–2837, 2014.
- [73] S. J. Cooney, S. L. Bermudez-Sabogal, and K. L. Byrnes, “Cellular and temporal expression of NADPH oxidase (NOX) isoforms after brain injury,” *Journal of Neuroinflammation*, vol. 10, no. 1, 2013.
- [74] C. Angeloni, C. Prata, F. V. D. Segal, R. Piperno, and S. Hrelia, “Traumatic brain injury and NADPH oxidase: a deep relationship,” *Oxidative Medicine and Cellular Longevity*, vol. 2015, Article ID 370312, 10 pages, 2015.
- [75] M. W. Ma, J. Wang, Q. Zhang et al., “NADPH oxidase in brain injury and neurodegenerative disorders,” *Molecular Neurodegeneration*, vol. 12, no. 1, 2017.
- [76] A. Tarafdar and G. Pula, “The role of NADPH oxidases and oxidative stress in neurodegenerative disorders,” *International Journal of Molecular Sciences*, vol. 19, no. 12, p. 3824, 2018.
- [77] S. Sorce and K. H. Krause, “NOX enzymes in the central nervous system: from signaling to disease,” *Antioxidants & Redox Signaling*, vol. 11, no. 10, pp. 2481–2504, 2009.
- [78] P. Vallet, Y. Charnay, K. Steger et al., “Neuronal expression of the NADPH oxidase NOX4, and its regulation in mouse experimental brain ischemia,” *Neuroscience*, vol. 132, no. 2, pp. 233–238, 2005.
- [79] S. Schiavone, M. Neri, L. Trabace, and E. Turillazzi, “The NADPH oxidase NOX2 mediates loss of parvalbumin interneurons in traumatic brain injury: human autoptical immunohistochemical evidence,” *Scientific Reports*, vol. 7, no. 1, p. 8752, 2017.
- [80] M. Olguín-Albuérne and J. Morán, “ROS produced by NOX2 control in vitro development of cerebellar granule neurons development,” *ASN Neuro*, vol. 7, no. 2, p. 175909141557871, 2015.
- [81] C. Wilson, M. Tulio Núñez, and C. González-Billault, “Contribution of NADPH oxidase to the establishment of hippocampal neuronal polarity in culture,” *Journal of Cell Science*, vol. 128, no. 16, pp. 2989–2995, 2015.
- [82] M. Yoneyama, K. Kawada, Y. Gotoh, T. Shiba, and K. Ogita, “Endogenous reactive oxygen species are essential for proliferation of neural stem/progenitor cells,” *Neurochemistry International*, vol. 56, no. 6-7, pp. 74–746, 2010.
- [83] J. E. Lee, K. E. Cho, K. E. Lee, J. Kim, and Y. S. Bae, “Nox4-mediated cell signaling regulates differentiation and survival of neural crest stem cells,” *Molecules and Cells*, vol. 37, no. 12, pp. 907–911, 2014.
- [84] K. Suzukawa, K. Miura, J. Mitsushita et al., “Nerve growth factor-induced neuronal differentiation requires generation of Rac1-regulated reactive oxygen species,” *Journal of Biological Chemistry*, vol. 275, no. 18, pp. 13175–13178, 2000.
- [85] C. A. Massaad and E. Klann, “Reactive oxygen species in the regulation of synaptic plasticity and memory,” *Antioxidants & Redox Signaling*, vol. 14, no. 10, pp. 2013–2054, 2011.
- [86] S. P. Tammariello, M. T. Quinn, and S. Estus, “NADPH oxidase contributes directly to oxidative stress and apoptosis in nerve growth factor-deprived sympathetic neurons,” *Journal of Neuroscience*, vol. 20, no. 1, p. RC53, 2000.
- [87] G. Ganguly, S. Chakrabarti, U. Chatterjee, and L. Saso, “Proteinopathy, oxidative stress and mitochondrial dysfunction: cross talk in Alzheimer’s disease and Parkinson’s disease,” *Drug Design Development and Therapy*, vol. 11, pp. 797–810, 2017.
- [88] A. M. Swomley and D. A. Butterfield, “Oxidative stress in Alzheimer disease and mild cognitive impairment: evidence from human data provided by redox proteomics,” *Archives of Toxicology*, vol. 89, no. 10, pp. 1669–1680, 2015.
- [89] S. C. Barber, R. J. Mead, and P. J. Shaw, “Oxidative stress in ALS: a mechanism of neurodegeneration and a therapeutic target,” *Biochimica et Biophysica Acta (BBA) - Molecular Basis of Disease*, vol. 1762, no. 11-12, pp. 1051–1067, 2006.
- [90] E. Niki, Y. Yoshida, Y. Saito, and N. Noguchi, “Lipid peroxidation: mechanisms, inhibition, and biological effects,” *Biochemical and Biophysical Research Communications*, vol. 338, no. 1, pp. 668–676, 2005.
- [91] I. Marrocco, F. Altieri, and I. Peluso, “Measurement and clinical significance of biomarkers of oxidative stress in humans,” *Oxidative Medicine and Cellular Longevity*, vol. 2017, Article ID 6501046, 32 pages, 2017.
- [92] S. Loft and H. E. Poulsen, “Markers of oxidative damage to DNA: antioxidants and molecular damage,” *Methods in Enzymology*, vol. 300, pp. 166–184, 1999.
- [93] W. R. Markesbery and M. A. Lovell, “Four-Hydroxynonenal, a Product of Lipid Peroxidation, is Increased in the Brain in Alzheimer’s Disease,” *Neurobiology of Aging*, vol. 19, no. 1, pp. 33–36, 1998.
- [94] D. A. Butterfield, M. Perluigi, and R. Sultana, “Oxidative stress in Alzheimer’s disease brain: New insights from redox proteomics,” *European Journal of Pharmacology*, vol. 545, no. 1, pp. 39–50, 2006.
- [95] K. Gmitterová, U. Heinemann, J. Gawinecka et al., “8-OHdG in cerebrospinal fluid as a marker of oxidative stress in various neurodegenerative diseases,” *Neurodegenerative Diseases*, vol. 6, no. 5-6, pp. 263–269, 2009.
- [96] D. T. Dexter, C. J. Carter, F. R. Wells et al., “Basal lipid peroxidation in substantia nigra is increased in Parkinson’s disease,” *Journal of Neurochemistry*, vol. 52, no. 2, pp. 381–389, 1989.

- [97] K. S. Montine, J. F. Quinn, J. Zhang et al., "Isoprostanes and related products of lipid peroxidation in neurodegenerative diseases," *Chemistry and Physics of Lipids*, vol. 128, no. 1-2, pp. 117-124, 2004.
- [98] C. Han, Y. Liu, R. Dai, N. Ismail, W. Su, and B. Li, "Ferroptosis and its potential role in human diseases," *Frontiers in Pharmacology*, vol. 11, no. 239, 2020.
- [99] J. Li, F. Cao, H.-l. Yin et al., "Ferroptosis: past, present and future," *Cell Death & Disease*, vol. 11, no. 2, p. 88, 2020.
- [100] B. R. Stockwell, J. P. F. Angeli, H. Bayir et al., "Ferroptosis: a regulated cell death nexus linking metabolism, redox biology, and disease," *Cell*, vol. 171, no. 2, pp. 273-285, 2017.
- [101] M. Redza-Dutordoir and D. A. Averill-Bates, "Activation of apoptosis signalling pathways by reactive oxygen species," *Biochimica et Biophysica Acta (BBA) - Molecular Cell Research*, vol. 1863, no. 12, pp. 2977-2992, 2016.
- [102] N. Festjens, T. Vanden Berghe, and P. Vandennebeele, "Necrosis, a well-orchestrated form of cell demise: signalling cascades, important mediators and concomitant immune response," *Biochimica et Biophysica Acta (BBA) - Bioenergetics*, vol. 1757, no. 9-10, pp. 1371-1387, 2006.
- [103] M. J. Morgan, Y. S. Kim, and Z. G. Liu, "TNF α and reactive oxygen species in necrotic cell death," *Cell Research*, vol. 18, no. 3, pp. 343-349, 2008.
- [104] Y. Wen, R. Liu, N. Lin et al., "NADPH oxidase hyperactivity contributes to cardiac dysfunction and apoptosis in rats with severe experimental pancreatitis through ROS-mediated MAPK signaling pathway," *Oxidative Medicine and Cellular Longevity*, vol. 2019, Article ID 4578175, 18 pages, 2019.
- [105] J. H. Yu, J. W. Lim, K. H. Kim, T. Morio, and H. Kim, "NADPH oxidase and apoptosis in cerulein-stimulated pancreatic acinar AR42J cells," *Free Radical Biology and Medicine*, vol. 39, no. 5, pp. 590-602, 2005.
- [106] E. Pedruzzi, C. Guichard, V. Ollivier et al., "NAD(P)H oxidase Nox-4 mediates 7-ketocholesterol-induced endoplasmic reticulum stress and apoptosis in human aortic smooth muscle cells," *Molecular and Cellular Biology*, vol. 24, no. 24, pp. 10703-10717, 2004.
- [107] W. Zhao, H. Feng, W. Sun, K. Liu, J. J. Lu, and X. Chen, "tert-Butyl hydroperoxide (t-BHP) induced apoptosis and necrosis in endothelial cells: roles of NOX4 and mitochondrion," *Redox Biology*, vol. 11, pp. 524-534, 2017.
- [108] Y. S. Kim, M. J. Morgan, S. Choksi, and Z. G. Liu, "TNF-induced activation of the Nox1 NADPH oxidase and its role in the induction of necrotic cell death," *Molecular Cell*, vol. 26, no. 5, pp. 675-687, 2007.
- [109] D.-C. Wu, P. Teismann, K. Tieu et al., "NADPH oxidase mediates oxidative stress in the 1-methyl-4-phenyl-1,2,3,6-tetrahydropyridine model of Parkinson's disease," *Proceedings of the National Academy of Sciences*, vol. 100, no. 10, pp. 6145-6150, 2003.
- [110] D. H. Choi, A. C. Cristóvão, S. Guhathakurta et al., "NADPH oxidase 1-mediated oxidative stress leads to dopamine neuron death in Parkinson's disease," *Antioxidants & Redox Signaling*, vol. 16, no. 10, pp. 1033-1045, 2012.
- [111] T. Seredenina, Z. Nayernia, S. Sorce et al., "Evaluation of NADPH oxidases as drug targets in a mouse model of familial amyotrophic lateral sclerosis," *Free Radical Biology and Medicine*, vol. 97, pp. 95-108, 2016.
- [112] S. Boillée and D. W. Cleveland, "Revisiting oxidative damage in ALS: microglia, Nox, and mutant SOD1," *The Journal of Clinical Investigation*, vol. 118, no. 2, pp. 474-478, 2008.
- [113] A. Ajayi, X. Yu, S. Lindberg, Ü. Langel, and A.-L. Ström, "Expanded ataxin-7 cause toxicity by inducing ROS production from NADPH oxidase complexes in a stable inducible spinocerebellar ataxia type 7 (SCA7) model," *BMC Neuroscience*, vol. 13, no. 1, p. 86, 2012.
- [114] N. Y. Calingasan, K. Uchida, and G. E. Gibson, "Protein-bound acrolein: a novel marker of oxidative stress in Alzheimer's disease," *Journal of Neurochemistry*, vol. 72, no. 2, pp. 751-756, 1999.
- [115] D. Galasko and T. J. Montine, "Biomarkers of oxidative damage and inflammation in Alzheimer's disease," *Biomarkers in Medicine*, vol. 4, no. 1, pp. 27-36, 2010.
- [116] M. A. Smith, C. A. Rottkamp, A. Nunomura, A. K. Raina, and G. Perry, "Oxidative stress in Alzheimer's disease," *Biochimica et Biophysica Acta - Molecular Basis of Disease*, vol. 1502, no. 1, pp. 139-144, 2000.
- [117] A. Nunomura, G. Perry, G. Aliev et al., "Oxidative damage is the earliest event in Alzheimer disease," *Journal of Neuropathology & Experimental Neurology*, vol. 60, no. 8, pp. 759-767, 2001.
- [118] M. A. Smith, K. Hirai, K. Hsiao et al., "Amyloid-beta deposition in Alzheimer transgenic mice is associated with oxidative stress," *Journal of Neurochemistry*, vol. 70, no. 5, pp. 2212-2215, 1998.
- [119] Y. Matsuoka, M. Picciano, J. L. Francois, and K. Duff, "Fibrillar β -amyloid evokes oxidative damage in a transgenic mouse model of Alzheimer's disease," *Neuroscience*, vol. 104, no. 3, pp. 609-613, 2001.
- [120] M. A. Smith, P. L. R. Harris, L. M. Sayre, and G. Perry, "Iron accumulation in Alzheimer disease is a source of redox-generated free radicals," *PNAS*, vol. 94, no. 18, pp. 9866-9868, 1997.
- [121] S. van Duijn, M. Bulk, S. G. van Duinen et al., "Cortical iron reflects severity of Alzheimer's disease," *Journal of Alzheimer's Disease*, vol. 60, no. 4, pp. 1533-1545, 2017.
- [122] M. Schrag, C. Mueller, U. Oyoyo, M. A. Smith, and W. M. Kirsch, "Iron, zinc and copper in the Alzheimer's disease brain: a quantitative meta-analysis. Some insight on the influence of citation bias on scientific opinion," *Progress in Neurobiology*, vol. 94, no. 3, pp. 296-306, 2011.
- [123] J. F. Schenck, E. A. Zimmerman, Z. Li et al., "High-field magnetic resonance imaging of brain iron in Alzheimer disease," *Topics in Magnetic Resonance Imaging*, vol. 17, no. 1, pp. 41-50, 2006.
- [124] G. Bartzokis, D. Sultzer, J. Cummings et al., "In vivo evaluation of brain iron in Alzheimer disease using magnetic resonance imaging," *JAMA Psychiatry*, vol. 57, no. 1, pp. 47-53, 2000.
- [125] E. P. Raven, P. H. Lu, T. A. Tishler, P. Heydari, and G. Bartzokis, "Increased iron levels and decreased tissue integrity in hippocampus of Alzheimer's disease detected in vivo with magnetic resonance imaging," *Journal of Alzheimer's Disease*, vol. 37, no. 1, pp. 127-136, 2013.
- [126] D. A. Butterfield, F. Di Domenico, A. M. Swomley, E. Head, and M. Perluigi, "Redox proteomics analysis to decipher the neurobiology of Alzheimer-like neurodegeneration: overlaps in Down's syndrome and Alzheimer's disease brain," *Biochemical Journal*, vol. 463, no. 2, pp. 177-189, 2014.

- [127] B. Su, X. Wang, A. Nunomura et al., "Oxidative stress signaling in Alzheimer's disease," *Current Alzheimer Research*, vol. 5, no. 6, pp. 525–532, 2008.
- [128] U. Kaur, P. Banerjee, A. Bir, M. Sinha, A. Biswas, and S. Chakrabarti, "Reactive oxygen species, redox signaling and neuroinflammation in Alzheimer's disease: the NF- κ B connection," *Current Topics in Medicinal Chemistry*, vol. 15, no. 5, pp. 446–457, 2015.
- [129] C. Cheignon, M. Tomas, D. Bonnefont-Rousselot, P. Faller, C. Hureau, and F. Collin, "Oxidative stress and the amyloid beta peptide in Alzheimer's disease," *Redox Biology*, vol. 14, pp. 450–464, 2018.
- [130] X. Wang, W. Wang, L. Li, G. Perry, H.-g. Lee, and X. Zhu, "Oxidative stress and mitochondrial dysfunction in Alzheimer's disease," *Biochimica et Biophysica Acta-Molecular Basis of Disease*, vol. 1842, no. 8, pp. 1240–1247, 2014.
- [131] P. I. Moreira, C. Carvalho, X. Zhu, M. A. Smith, and G. Perry, "Mitochondrial dysfunction is a trigger of Alzheimer's disease pathophysiology," *Biochimica et Biophysica Acta-Molecular Basis of Disease*, vol. 1802, no. 1, pp. 2–10, 2010.
- [132] S. Shimohama, H. Tanino, N. Kawakami et al., "Activation of NADPH oxidase in Alzheimer's disease brains," *Biochemical and Biophysical Research Communications*, vol. 273, no. 1, pp. 5–9, 2000.
- [133] M. A. Ansari and S. W. Scheff, "NADPH-oxidase activation and cognition in Alzheimer disease progression," *Free Radical Biology and Medicine*, vol. 51, no. 1, pp. 171–178, 2011.
- [134] A. J. Bruce-Keller, S. Gupta, T. E. Parrino et al., "NOX activity is increased in mild cognitive impairment," *Antioxidants & Redox Signaling*, vol. 12, no. 12, pp. 1371–1382, 2010.
- [135] S. Y. Kim, J. H. Moon, H. G. Lee, S. U. Kim, and Y. B. Lee, "ATP released from β -amyloid-stimulated microglia induces reactive oxygen species production in an autocrine fashion," *Experimental & Molecular Medicine*, vol. 39, no. 6, pp. 820–827, 2007.
- [136] L. K. Parvathenani, S. Tertyshnikova, C. R. Greco, S. B. Roberts, B. Robertson, and R. Posmantur, "P2X7 mediates superoxide production in primary microglia and is up-regulated in a transgenic mouse model of Alzheimer's disease," *Journal of Biological Chemistry*, vol. 278, no. 15, pp. 13309–13317, 2003.
- [137] S. H. Choi, S. Aid, H. W. Kim, S. H. Jackson, and F. Bosetti, "Inhibition of NADPH oxidase promotes alternative and anti-inflammatory microglial activation during neuroinflammation," *Journal of Neurochemistry*, vol. 120, no. 2, pp. 292–301, 2012.
- [138] B. Qin, L. Cartier, M. Dubois-Dauphin, B. Li, L. Serrander, and K. H. Krause, "A key role for the microglial NADPH oxidase in APP-dependent killing of neurons," *Neurobiology of Aging*, vol. 27, no. 11, pp. 1577–1587, 2006.
- [139] S. M. de la Monte and J. R. Wands, "Molecular indices of oxidative stress and mitochondrial dysfunction occur early and often progress with severity of Alzheimer's disease," *Journal of Alzheimer's Disease*, vol. 9, no. 2, pp. 167–181, 2006.
- [140] A. J. Bruce-Keller, S. Gupta, A. G. Knight et al., "Cognitive impairment in humanized APP \times PS1 mice is linked to A β _{1–42} and NOX activation," *Neurobiology of Disease*, vol. 44, no. 3, pp. 317–326, 2011.
- [141] L. Park, P. Zhou, R. Pitstick et al., "Nox2-derived radicals contribute to neurovascular and behavioral dysfunction in mice overexpressing the amyloid precursor protein," *Proceedings of the National Academy of Sciences*, vol. 105, no. 4, pp. 1347–1352, 2008.
- [142] E. A. Newcombe, J. Camats-Perna, M. L. Silva, N. Valmas, T. J. Huat, and R. Medeiros, "Inflammation: the link between comorbidities, genetics, and Alzheimer's disease," *Journal of Neuroinflammation*, vol. 15, no. 1, p. 276, 2018.
- [143] P. Agostinho, R. A. Cunha, and C. Oliveira, "Neuroinflammation, oxidative stress and the pathogenesis of Alzheimers disease," *Current Pharmaceutical Design*, vol. 16, no. 25, pp. 2766–2778, 2010.
- [144] T. Wyss-Coray and J. Rogers, "Inflammation in Alzheimer disease—a brief review of the basic science and clinical literature," *Cold Spring Harbor Perspectives in Medicine*, vol. 2, no. 1, 2012.
- [145] M. L. Block, "NADPH oxidase as a therapeutic target in Alzheimer's disease," *BMC Neuroscience*, vol. 9, no. S2, 2008Supplement 2, 2008.
- [146] R. P. Brandes, N. Weissman, and K. Schröder, "Nox family NADPH oxidases: molecular mechanisms of activation," *Free Radical Biology in Medicine*, vol. 76, pp. 208–226, 2014.
- [147] S. K. McCann and C. L. Roulston, "NADPH oxidase as a therapeutic target for neuroprotection against ischaemic stroke: future perspectives," *Brain Sciences*, vol. 3, no. 4, pp. 561–598, 2013.
- [148] G. Teixeira, C. Szyndralewicz, S. Molango et al., "Therapeutic potential of NADPH oxidase 1/4 inhibitors," *British Journal of Pharmacology*, vol. 174, no. 12, pp. 1647–1669, 2017.
- [149] B. A. 't Hart, S. Copray, and I. Philippens, "Apocynin, a low molecular oral treatment for neurodegenerative disease," *BioMed Research International*, vol. 2014, Article ID 298020, 6 pages, 2014.
- [150] M. E. Lull, S. Levesque, M. J. Surace, and M. L. Block, "Chronic apocynin treatment attenuates beta amyloid plaque size and microglial number in hAPP(751)_{SL} mice," *PLoS One*, vol. 6, no. 5, article e20153, 2011.
- [151] E. Joseph, D. M. A. Villalobos-Acosta, M. A. Torres-Ramos et al., "Neuroprotective effects of apocynin and galantamine during the chronic administration of scopolamine in an Alzheimer's disease model," *Journal of Molecular Neuroscience*, vol. 70, no. 2, pp. 180–193, 2020.
- [152] S. Barua, J. Y. Kim, M. A. Yenari, and J. E. Lee, "The role of NOX inhibitors in neurodegenerative diseases," *IBRO Reports*, vol. 7, pp. 59–69, 2019.
- [153] R. de la Torre, S. de Sola, G. Hernandez et al., "Safety and efficacy of cognitive training plus epigallocatechin-3-gallate in young adults with Down's syndrome (TESDAD): a double-blind, randomised, placebo-controlled, phase 2 trial," *The Lancet Neurology*, vol. 15, no. 8, pp. 801–810, 2016.
- [154] R. S. Turner, R. G. Thomas, S. Craft et al., "A randomized, double-blind, placebo-controlled trial of resveratrol for Alzheimer disease," *Neurology*, vol. 85, no. 16, pp. 1383–1391, 2015.
- [155] C. W. Zhu, H. Grossman, J. Neugroschl et al., "A randomized, double-blind, placebo-controlled trial of resveratrol with glucose and malate (RGM) to slow the progression of Alzheimer's disease: a pilot study," *Translational Research & Clinical Interventions*, vol. 4, no. 1, pp. 609–616, 2018.
- [156] R. Remington, C. Bechtel, D. Larsen et al., "A phase II randomized clinical trial of a nutritional formulation for cognition and mood in Alzheimer's disease," *Journal of Alzheimer's Disease*, vol. 45, no. 2, pp. 395–405, 2015.

- [157] R. Remington, C. Bechtel, D. Larsen et al., "Maintenance of cognitive performance and mood for individuals with Alzheimer's disease following consumption of a nutraceutical formulation: a one-year, open-label study," *Journal of Alzheimer's Disease*, vol. 51, no. 4, pp. 991–995, 2016.
- [158] J. M. Ringman, S. A. Frautschy, E. Teng et al., "Oral curcumin for Alzheimer's disease: tolerability and efficacy in a 24-week randomized, double blind, placebo-controlled study," *Alzheimer's Research & Therapy*, vol. 4, no. 5, p. 43, 2012.
- [159] S. T. DeKosky, J. D. Williamson, A. L. Fitzpatrick et al., "Ginkgo biloba for prevention of dementia: a randomized controlled trial," *JAMA*, vol. 300, no. 19, pp. 2253–2262, 2008.
- [160] B. E. Snitz, E. S. O'Meara, M. C. Carlson et al., "Ginkgo biloba for preventing cognitive decline in older adults: a randomized trial," *JAMA*, vol. 302, no. 24, pp. 2663–2670, 2009.
- [161] L. H. Kuller, D. G. Ives, A. L. Fitzpatrick et al., "Does Ginkgo biloba reduce the risk of cardiovascular events?," *Circulation: Cardiovascular Quality and Outcomes*, vol. 3, no. 1, pp. 41–47, 2010.
- [162] B. Vellas, N. Coley, P.-J. Ousset et al., "Long-term use of standardised ginkgo biloba extract for the prevention of Alzheimer's disease (GuidAge): a randomised placebo-controlled trial," *The Lancet Neurology*, vol. 11, no. 10, pp. 851–859, 2012.
- [163] C. Singer, R. E. Tractenberg, J. Kaye et al., "A multicenter, placebo-controlled trial of melatonin for sleep disturbance in Alzheimer's disease," *Sleep*, vol. 26, no. 7, pp. 893–901, 2003.

Research Article

Pleiotropic Properties of Amphiphilic Dihydropyridines, Dihydropyridones, and Aminovinylcarbonyl Compounds

Martins Rucins ¹, Rufus Smits ¹, Anda Sipola ¹, Brigita Vigante ¹,
Ilona Domracheva ¹, Baiba Turovska ¹, Ruslan Muhamadejev ¹, Karlis Pajuste ¹,
Mara Plotniece ², Arkadij Sobolev ¹, Gunars Duburs ¹, and Aiva Plotniece ¹

¹Latvian Institute of Organic Synthesis, Aizkraukles 21, Riga LV-1006, Latvia

²Department of Pharmaceutical Chemistry, Faculty of Pharmacy, Riga Stradiņš University, Dzirciema 16, Riga LV-1007, Latvia

Correspondence should be addressed to Gunars Duburs; gduburs@osi.lv and Aiva Plotniece; aiva@osi.lv

Received 23 July 2020; Revised 9 October 2020; Accepted 10 November 2020; Published 31 December 2020

Academic Editor: Sasanka Chakrabarti

Copyright © 2020 Martins Rucins et al. This is an open access article distributed under the Creative Commons Attribution License, which permits unrestricted use, distribution, and reproduction in any medium, provided the original work is properly cited.

Three groups of synthetic lipids are chosen for studies: (1) 1,4-dihydropyridines (1,4-DHPs) containing two cationic moieties and their analogues; (2) 3,4-dihydro-2(1*H*)-pyridones containing a cationic moiety; and (3) acyclic, open-chain analogues, i.e., 2-amino-3-alkoxycarbonylalkylammonium derivatives. 1,4-DHPs possessing dodecyl alkyl chains in the ester groups in positions 3 and 5 and cationic nitrogen-containing groups in positions 2 and 6 have high cytotoxicity in cancer cells HT-1080 (human lung fibrosarcoma) and MH-22A (mouse hepatoma), but low cytotoxicity in the noncancerous NIH3T3 cells (mouse embryonic fibroblast). On the contrary, similar compounds having short (methyl, ethyl, or propoxyethyl) chains in the ester groups in positions 3 and 5 lack cytotoxicity in the cancer cells HT-1080 and MH-22A even at high doses. Inclusion of fluorine atoms in the alkyl chains in positions 3 and 5 of the DHP cycle decreases the cytotoxicity of the mentioned compounds. Structurally related dihydropyridones with a polar head group are substantially more toxic to normal and cancerous cells than the DHP analogues. Open-chain analogues of DHP lipids comprise the same conjugated aminovinylcarbonyl moiety and possess anticancer activity, but they also have high basal cytotoxicity. Electrochemical oxidation data demonstrate that oxidation potentials of selected compounds are in the range of 1.6–1.7 V for cationic 1,4-DHP, 2.0–2.4 V for cationic 3,4-dihydropyridones, and 1.2–1.5 V for 2-amino-3-alkoxycarbonylalkylammonium derivatives. Furthermore, the tested cationic 1,4-DHP amphiphiles possess antiradical activity. Molecular topological polar surface area values for the tested compounds were defined in accordance with the main fragments of compound structures. The determined $\log P$ values were highest for dodecyl ester groups in positions 3 and 5 of the 1,4-DHP and lowest for short alkyl chain-containing amphiphiles.

1. Introduction

For a long time, liposomes have been considered to have a role in the encapsulation of toxic drugs (mainly anticancer drugs) into liposomal drug delivery systems which are supposed to be inert, having no pharmacological or chemotherapeutic activity *per se* [1]. The properties of liposomes are mainly dependent on the characteristics of their constituent lipids.

Lipids and liposomal agents as liposome-forming building blocks depending on their physicochemical properties can influence the immune system. For the development of

new liposomal systems, it is important to perform analysis on the liposome-forming lipid properties with an emphasis on toxicity to healthy tissues and immune responses [2]. Synthetic cationic amphiphilic bilayers can act as gene, vaccine, or drug carriers; at the same time, they can interact with negatively charged prokaryotic or eukaryotic cells, causing cell adhesion and loss of cell viability. Lipids and liposomes deserve to be investigated as potential drugs [3]. Cytotoxicity of cationic liposomes is a significant property to be checked [4].

Liposomes may induce oxidative damage to normal tissues [5]. Reactive oxygen species (ROS) and lipid peroxidation

products not only are cytotoxic but may also perform and modulate signal transduction in cells [6]. It was demonstrated that the levels of ROS and the activity of scavenging/antioxidant enzymes in drug-resistant cancer cells are typically increased compared to nonresistant cancer and normal cells. Thereby, multidrug-resistant (MDR) cancer cells may be more susceptible to alterations in ROS levels. Numerous studies suggest that compounds modulating cellular ROS levels can enhance MDR cancer cell death and sensitize MDR cancer cells to certain chemotherapeutic drugs [7]. It was concluded that unspecific elimination of ROS by use of low molecular mass antioxidants was not successful for disease initiation and progression. However, controlling specific ROS-mediated signaling pathways by selective targeting offers a perspective for more refined redox medicine in the future [8]. Additional antioxidant activity (antiradical activity) could be beneficial as it would protect cells and organisms in case of oxidative stress or, in general, be involved in the process of redox regulation and master switch systems [9]. In this way, 1,4-dihydropyridines, being a group of synthetic antioxidants, could be used for the modulation of cellular redox signaling. Lipids reveal cancer cell-selective cytotoxicities—they are less cytotoxic in noncancerous healthy cells [10]. Evaluation of the cytotoxicity of nanoparticles and their components is crucial for the accurate interpretation of pharmacological activities [11]. Nonviral synthetic lipid vectors may interact with biomolecules through functional moieties (biosignature), resulting in biological impacts: intrinsic genomic and nongenomic effects [12].

Our research group has developed liposome-forming cationic 1,4-dihydropyridine (1,4-DHP) amphiphiles capable of transfecting pDNA into different cell lines *in vitro*. To assess the influence of different molecular architectures on gene delivery properties, numerous 1,4-DHP amphiphiles were studied [13–15]. Besides, some of these amphiphilic compounds revealed anticancer activity in HT-1080 and MH-22A cells and antiradical activities (27–40% in DPPH tests) [13, 16]. The remarkable increase of N-H acidity (up to pKa ~7–8) in the DHP cycle is the basis for its buffering activity in these types of gene transfection agents [17].

Recently, it was demonstrated that 4-(N-alkylpyridinium)-1,4-dihydropyridines possess toxicity in Gram-positive and Gram-negative bacteria species and eukaryotic microorganisms [18]. The abovementioned 4-(N-alkylpyridinium)-1,4-dihydropyridines also possess calcium channel-blocking and antioxidant activities [19].

In this work, we chose amphiphilic dihydropyridine derivatives as synthetic lipids and their structural analogues as objects to study pleiotropic activities. The cytotoxic properties of 3 types of amphiphilic compounds in 3 cell lines, namely, normal NIH3T3 (mouse embryonic fibroblast), cancerous HT-1080 (human lung fibrosarcoma), and MH-22A (mouse hepatoma), were evaluated. The studied compounds could be divided into 3 groups according to their structural fragments: (a) 1,4-dihydropyridines containing two cationic moieties as a conjugated cyclic bis(β -carbonylvinyl)amino system and some structurally related compounds; (b) 3,4-dihydro-2(1H)-pyridones containing a cationic moiety as an isomeric 3,4-dihydropyridine structure with an additional

intracyclic carbonyl group—a N- β -carbonylvinylamido system; and (c) 2-amino-3-alkoxycarbonylalkylammonium derivatives as acyclic, open-chain β -aminovinylcarbonyl systems. Lipophilicity of the selected compounds was characterized using logP and molecular topological polar surface area calculations. Evaluation of electrochemical oxidation potentials of the selected compounds was also performed.

2. Materials and Methods

2.1. Chemistry. More detailed descriptions of synthetic procedures and characterization of the original unpublished intermediates and compounds are described in the Supplementary data.

2.1.1. Synthesis of Cationic 1,4-Dihydropyridines 1–26. Briefly, the elaborated synthesis of the cationic 1,4-DHP 1–7, 9–25 involved three sequential steps. The first step was the synthesis of the corresponding 2,6-dimethyl 1,4-DHP derivative in a two-component Hantzsch-type cyclization using 1.0 eq of the corresponding aldehyde, 1.2 eq of an ammonia source, and 2.0 eq of the corresponding acetoacetate for symmetrically substituted 1,4-DHP derivatives or 1 eq of the corresponding acetoacetate and 1.0 eq of the corresponding 3-aminobut-2-enoate for unsymmetrically substituted ones. The second step involved the bromination of the methyl groups of the 2,6-dimethyl-1,4-DHP derivative with N-bromosuccinimide, and the third step was the nucleophilic substitution of bromine of the 2,6-dibromomethylene-1,4-DHP by N-heterocycles or amines yielding the target compounds. The first step for the synthesis of the parent 1,4-dihydropyridine in the case of compound 26 involved the reaction between 1.0 eq of the corresponding aldehyde, 2.4 eq of ammonium acetate, and 4.0 eq of the corresponding acetoacetate. More detailed synthetic procedures and characterization of the original compounds are described in the Supplementary data.

2.1.2. Synthesis of Compound 8 [20]. Briefly, the condensation of ethyl 4-chloroacetoacetate with glyoxylic acid monohydrate in the presence of piperidine/acetate provided (*E,Z*)-2-(2-chloroacetyl)-but-2-enedioic acid 1-ethyl ester, which was used in the next reaction with ethyl 3-amino-4-chlorobut-2-enoate. The obtained 3,5-diethyl 2,6-bis(chloromethyl)-1,4-dihydropyridine-3,4,5-tricarboxylate was esterified with methanol to afford the parent 2,6-dichloromethylene-1,4-DHP. The target compound 8 was obtained *via* nucleophilic substitution of chlorine by pyridine in the presence of potassium iodide.

2.1.3. Synthesis of Cationic Pyridine 27 [14]. Briefly, the corresponding 2,6-dibromomethylene-1,4-DHP was oxidized by HNO₂ followed by nucleophilic substitution of bromine with pyridine to give the target compound 27.

2.1.4. Synthesis of Cationic 3,4-Dihydro-2(1H)-pyridones 28–38. Briefly, 3,4-dihydro-2(1H)-pyridone synthesis employed a four-component reaction using Meldrum's acid by a heterocyclization with the corresponding β -ketoester and the corresponding aldehyde. The obtained 3,4-dihydro-2(1H)-pyridones were treated with bromine giving the respective

6-methylbromides, which in subsequent reaction with pyridine or amine provided the target compounds **28–38**.

2.1.5. Synthesis of 2-Amino-3-alkoxycarbonylalkylammonium Halides 39–48. Briefly, the first step included the transesterification of the commercially available ethyl 4-chloroacetoacetate with a corresponding carbinol without solvent by azeotropic removal of ethanol. The further reaction of the corresponding 4-chloro-3-oxobutanoates with ammonium acetate led to enaminoesters, which were used for quaternization by tertiary amines or heterocycles giving the target compounds **39–48**. Potassium iodide or sodium bromide additives were used for obtaining the corresponding iodides or bromides.

2.2. Experiments for Evaluation of Electrochemical Oxidation Potentials. Cyclic voltammetry experiments were carried out on a PARSTAT 2273 electrochemical system. A stationary glassy carbon disk electrode ($d = 0.5$ mm) served as the working electrode, while the counterelectrode was a Pt wire. The oxidation potentials were measured relative to a Ag/Ag⁺ reference electrode. Acetonitrile was dried over P₂O₅ and distilled; the distillate was stored over CaH₂ and redistilled just before use. Recrystallized tetrabutylammonium tetrafluoroborate (TBABF₄) was used as a supporting electrolyte at 0.1 M concentration.

2.3. Determination of LogP and Molecular Topological Polar Surface Area. LogP and Topological Polar Surface Area (TPSA) values were calculated with the Chem3D Ultra 19 program (PerkinElmer Informatics). For logP calculations, the Molecular Networks module was used on single-molecule compounds (salts were taken as cations).

2.4. Cytotoxicity. Cytotoxicity of the compounds was determined on HT-1080 (human lung fibrosarcoma) and MH-22A (mouse hepatoma) cell lines and on the normal NIH3T3 (mouse embryonic fibroblast) cell line. IC₅₀ is the compound concentration (μg/ml) at which 50% of the cells die. CV is a triarylmethane dye that can bind to ribose-type molecules such as DNA in nuclei. CV staining can be used to quantify the total DNA of the remaining population and thus is used to determine the number of live cells based on the concentration of the dye which remains after staining. MTT is a standard colorimetric assay used to measure cellular proliferation. Yellow MTT (3-(4,5-dimethylthiazol-2-yl)-2,5-diphenyltetrazolium bromide) is reduced to purple formazan in the mitochondria of living cells.

Reduction takes place only when mitochondrial reductase enzymes are active, and therefore, conversion is directly related to the number of viable cells which can be quantified by the absorbance of the solution (between $\lambda = 500$ and 600 nm) using a spectrophotometer.

2.5. Cell Culture and Measurement of Cell Viability. Tumor cell lines HT-1080 (human connective tissue fibrosarcoma, ATCC® CCL-121™) and MH-22A (mouse hepatocarcinoma, ECACC, cat. Nr. 96121721) were used.

HT-1080 and MH-22A cells were seeded in 96-well plates in Dulbecco's modified Eagle's (DMEM) medium containing 10% fetal bovine serum and 4 mM L-glutamine,

without antibiotics, and cultivated for 72 h by exposure to different concentrations of compounds. Cell viability was measured using 3-(4,5-dimethylthiazol-2-yl)-2,5-diphenyltetrazolium bromide (MTT). In brief, after incubating with compounds, the culture medium was removed and fresh medium with 0.2 mg/ml MTT was added in each well of the plate. After incubation (3 h, 37°C, 5% CO₂), the medium with MTT was removed, and 200 μl DMSO was added at once to each sample. The samples were tested at 540 nm on a Tecan Infinite M1000 multiplate reader. The IC₅₀ was calculated using the program GraphPad Prism® 3.0.

For the CV assay, cells were stained with 0.05% crystal violet (Sigma-Aldrich) in 30% methanol for 20 minutes at room temperature. After incubation, the staining solution was removed. The cells were washed 4 times with water. For dye solubilization, 200 μl of a solubilizing solution (0.1 M citrate buffer, pH 4.2 in 50% ethanol; 1:1 v/v) was added. The absorbance of the solution was measured using a Tecan Infinite M1000 multiplate spectrophotometer at a wavelength of 570 nm [21].

2.6. Basal Cytotoxicity Test. The Neutral Red Uptake (NRU) assay was performed according to the standard protocol of Stokes et al. [22] modified by a NICEATM-ECVAM validation study [23]. The NRU cytotoxicity assay procedure is based on the ability of viable cells to incorporate and bind neutral red, a supravital dye.

Balb/c NIH 3T3 (mouse Swiss albino embryo fibroblast, ATCC® CRL-1658™) cells (9000 cells/well) were placed into 96-well plates for 24 h in Dulbecco's modified Eagle's medium (DMEM) containing 5% fetal bovine serum. Then, the cells were exposed to the test compound over a range of seven concentrations (1000, 316, 100, 31, 10, 3, and 1 μg/ml) for 24 h. Untreated cells were used as a control. After 24 h, the medium was removed from all plates. Then, 150 μl of neutral red solution was added (0.05 mg/ml NR in DMEM 24 h pre-incubated at 37°C and then filtered before use through a 0.22 μm syringe filter). Plates were incubated for 3 h, and then, the cells were washed three times with PBS. The dye within viable cells was released by extraction with a mixture of acetic acid, ethanol, and water (1:50:49). The absorbance of neutral red was measured using a spectrophotometer multiplate reader (Tecan Infinite M1000) at 540 nm. The optical density (OD) was calculated using the following formula: OD (treated cells) × 100/OD (control cells). The IC₅₀ values were calculated using the GraphPad Prism® 3.0 program.

2.7. Estimation of LD₅₀ from IC₅₀ Values. Data from the *in vitro* tests were used for estimating the starting dose for acute oral systemic toxicity tests in the rodent. The *in vivo* starting dose is an estimated LD₅₀ value calculated by inserting the *in vitro* IC₅₀ value into a regression formula: $\log LD_{50} \text{ (mM/kg)} = 0.439 \log IC_{50} \text{ (mM)} + 0.621$ [23–25]. The value is recalculated to mg/kg, and compounds are evaluated in accordance with 4 toxicity categories [26]: category 1—LD₅₀ ≤ 5 mg/kg (highly toxic); category 2—5 < LD₅₀ ≤ 50 mg/kg (moderately toxic); category 3—50 < LD₅₀ ≤ 300 mg/kg (slightly toxic); and

category $4-300 < LD_{50} \leq 2000$ mg/kg (practically non-toxic). Using an alternative *in vitro* method allows the comparison between possibly toxic new compounds and selecting compounds for further study vastly reducing the number of animal experiments.

3. Results and Discussion

3.1. Structures of Compounds. The studied compounds could be divided into 3 groups considering structure fragments:

- (1) *1st group*: twenty-five representatives of two cationic moieties containing 1,4-dihydropyridines (compounds **1–25** in Table 1) and, additionally, four cationic moieties containing 1,4-dihydropyridine (compound **26** in Table 1) and one as an oxidized form—two cationic moieties containing pyridine (compound **27** in Table 1)
- (2) *2nd group*: eleven representatives of 3,4-dihydro-2(1*H*)-pyridones containing a cationic moiety as an isomeric 3,4-dihydropyridine structure with an additional intracyclic carbonyl group, i.e., the N- β -carbonylvinylamido system (compounds **28–38** in Table 2)
- (3) *3rd group*: ten representatives of cationic 2-amino-3-alkoxycarbonylalkylammonium derivatives as acyclic, open-chain analogues of cyclic 1,4-DHPs (compounds **39–48** in Table 3)

These three groups were selected after analysis of their structure-activity relationships as synthetic lipid-like amphiphilic compounds. Previously, the 3rd group representatives—(2-amino-3-alkoxycarbonylalkyl)trialkylammonium halides—were synthesized, and their ribonucleic acid (RNS) transfection activity was demonstrated [27]. This group covers synthetic lipid-like compounds on the basis of a β -aminovinylcarbonyl (AVC) moiety: a conjugated pentade system connected with a lipophilic carbon atom chain and a cationic part (alkylammonium or pyridinium type). These compounds are proposed as an open-chain system compared to the cationic 1,4-DHP or pyridone heterocyclic systems. Structurally, the 2nd group molecules—the cationic pyridone derivatives—are heterocycles which comprise a cyclic AVC system and an additional intracyclic carbonyl group and an extracyclic cation. Previously, the 1st group representatives—1,4-DHP derivatives containing pyridinium moieties—were presented as promising tools for delivery of DNA into target cells [13, 14, 20, 28]. It is noteworthy that, due to cross-conjugation of two AVC systems of the 1,4-DHP cycle, its N-H group is influenced by two electron-withdrawing vinylcarbonyls.

3.2. Synthesis of the Amphiphiles. Synthesis of the amphiphiles was performed according to Schemes 1–4.

Previously, 3,5-bis(dodecyloxycarbonyl)-1,4-DHPs containing cationic moieties were elaborated as synthetic lipid-like compounds having promising gene delivery properties for DNA transfection; the basic structure-activity relationships have been verified for the cationic 1,4-DHP derivatives

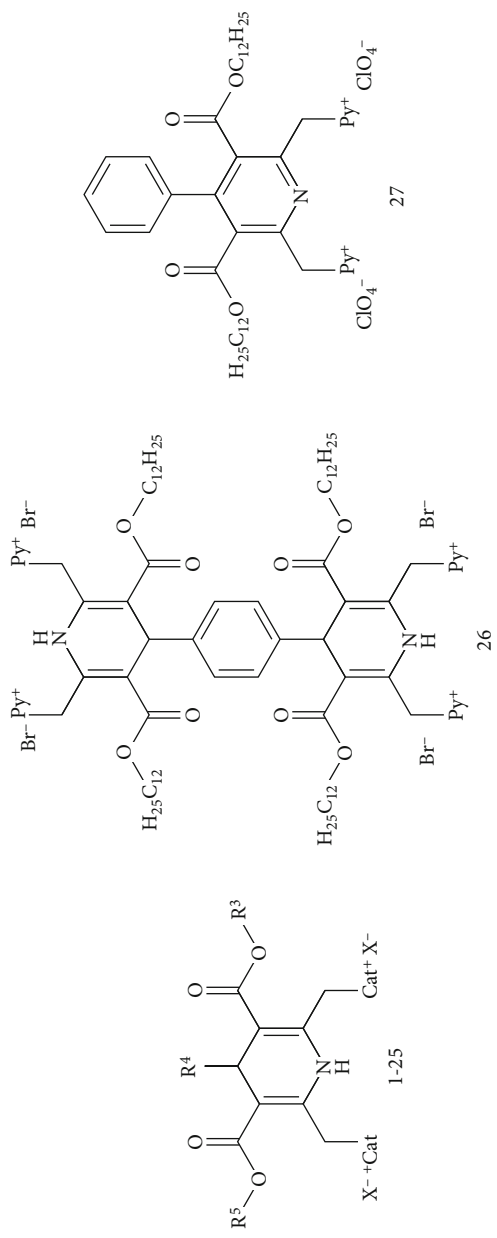
as gene delivery systems, and it has been shown that the molecular structure affected their self-assembling properties, pDNA-binding ability, and properties of the formed 1,4-DHP amphiphile-pDNA complexes [13, 15, 28]. The synthetic procedure for the amphiphilic compounds **1–7**, **9–22**, and **26** is displayed in Scheme 1 via a multistep sequence. The first step was a Hantzsch synthesis of the parent compound 3,5-bis(alkoxycarbonyl)-2,6-dimethyl-4-phenyl-1,4-dihydropyridine. The second step was bromination of the 2,6-methyl groups with N-bromosuccinimide (NBS) [34] resulting in the second parent compound 2,6-di(bromomethyl)-3,5-bis(alkoxycarbonyl)-4-phenyl-1,4-dihydropyridine. The final step was nucleophilic substitution of bromine in the 2,6-di(bromomethyl)-1,4-DHP by N-heterocycles or amines, which is facile and generally takes place in good yields.

Additionally, for studies of targeted changes in the structure of corresponding dicationic compound **10**, which was found to be more active for DNA delivery among the tested 1,4-DHP amphiphiles [13, 15, 28], 1,1',1'',1'''-((1,4-phenylenebis(3,5-bis((dodecyloxy)carbonyl)-1,4-dihydropyridine-4,2,6-triyl))tetrakis(methylene))tetrakis(pyridin-1-ium) tetrabromide (**26**) was synthesized as a double or a “dimeric” molecule of compound **10** and 1,1'-((3,5-bis(dodecyloxycarbonyl)-4-phenylpyridine-2,6-diyl)bis(methylene))-bis(pyridin-1-ium)dibromide (**27**) was prepared in accordance with what was reported in [14] as the oxidized form of compound **10**. For evaluation of the anion influence on cytotoxicity, 1,1'-((3,5-bis((dodecyloxy)carbonyl)-4-phenyl-1,4-dihydropyridine-2,6-diyl)bis(methylene))bis(pyridin-1-ium) ditetrafluoroborate (**11**) was synthesized from compound **10** after treating with NH_4BF_4 .

The unsymmetrical 1,4-DHP amphiphile **23** was designed for analysis of the influence of mixed perfluorinated and alkyl ester moiety substituents on the properties of amphiphiles. The 1,4-DHP **23** molecule contains only one of the two esters as a perfluorinated ester moiety while the other is an alkyl ester—the same as previous compounds. The synthetic procedure (Scheme 2) includes a reaction between an enamine and benzylidene in diglyme with inclusion of n-butylpyridinium chloride as a phase transfer catalyst (PTC) [35] to affording the parent dodecyl 5,5,6,6,7,7,8,8,9,9,10,10,11,11,12,12,12-heptafluorododecyl 1,4-dihydro-2,6-dimethyl-4-phenylpyridine-3,5-dicarboxylate in 43% yield. Without the PTC, the yield was only 25%. Subsequent bromination with NBS formed the corresponding 2,6-dibromomethylene DHP which was used without further purification in nucleophilic substitution with pyridine yielding the unsymmetrical 1,4-DHP **23**.

The 3,4-dihydro-2(1*H*)-pyridones (DHPDO) possess various pharmacological properties as α_1a adrenergic receptor antagonists [36], Rho-kinase inhibitors [37], P_2X_7 receptor antagonists [38], or G-protein-coupled kinase receptor antagonists [39]. Synthesis of 3,4-dihydro-2(1*H*)-pyridone amphiphiles **28–38** was performed according to Scheme 3. In this case, Meldrum's acid was used as the second dicarbonyl component in a Hantzsch-like reaction with heterocyclization, with a corresponding β -ketoester and a corresponding aldehyde in the presence of ammonium acetate in refluxing glacial

TABLE 1: Structure, cytotoxicity, and calculated basal toxicity of 1,4-dihydropyridines containing cationic moieties.



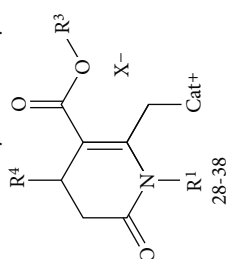
Comp.	Cat ⁺	R ³	R ⁴	R ⁵	X ⁻	HT-1080		MH-22A		NIH3T3		Ref.
						IC ₅₀ (CV) (μg/ml)	IC ₅₀ (MTT) (μg/ml)	IC ₅₀ (CV) (μg/ml)	IC ₅₀ (MTT) (μg/ml)	IC ₅₀ (NR) (μg/ml)	LD ₅₀ (mg/kg)	
1	Py	C ₂ H ₅	Ph	C ₂ H ₅	Br	*	*	*	*	*	>2000	[29]
2	Py-Me-4	C ₂ H ₅	Ph	C ₂ H ₅	Br	*	>740	*	*	*	>3360	[30]
3	Py-NH ₂ -4	C ₂ H ₅	Ph	C ₂ H ₅	Br	nt	441 ± 46	nt	>740	*	>3360	Suppl.
4	Py-NMe ₂ -4	C ₂ H ₅	Ph	C ₂ H ₅	Br	nt	324 ± 29	nt	608 ± 49	*	>3500	Suppl.
5	Py-Me-3	C ₂ H ₅	Ph	C ₂ H ₅	Br	nt	>740	nt	*	*	>3360	Suppl.
6	Py	C ₂ H ₅	C ₆ H ₄ -CF ₃ -2	C ₂ H ₅	Br	*	*	*	*	*	>2000	[20]
7	Py	C ₂ H ₄ OC ₃ H ₇	C ₆ H ₄ -OCHF ₂ -2	C ₂ H ₄ OC ₃ H ₇	Br	*	*	*	*	*	>2000	[20]
8	Py	C ₂ H ₅	COOCH ₃	C ₂ H ₅	I	*	*	*	*	*	>2000	[20]
9	N-Me-morph	CH ₃	C ₆ H ₄ -OCHF ₂ -2	CH ₃	ClO ₄	*	*	*	*	*	>2000	[31]
10	Py	C ₁₂ H ₂₅	Ph	C ₁₂ H ₂₅	Br	3 ± 0.5	3 ± 0.3	6 ± 1	3 ± 0.8	100 ± 6	1482	[13, 28]
11	Py	C ₁₂ H ₂₅	Ph	C ₁₂ H ₂₅	BF ₄	31 ± 4	28 ± 9	30 ± 6	30 ± 9	47 ± 8	1053	Suppl.
12	Py-Me-4	C ₁₂ H ₂₅	Ph	C ₁₂ H ₂₅	Br	10 ± 2	5 ± 1	40 ± 2	29 ± 2	79 ± 11	1431	[13]
13	Py-NMe ₂ -4	C ₁₂ H ₂₅	Ph	C ₁₂ H ₂₅	Br	10 ± 1	3 ± 0.6	6 ± 2	10 ± 3	119 ± 13	1706	[13]
14	Py-C(=O)CH ₃ -3	C ₁₂ H ₂₅	Ph	C ₁₂ H ₂₅	Br	3 ± 0.4	3 ± 0.3	100 ± 13	49 ± 9	922 ± 24	4040	[13]
15	N-Me-morph	C ₁₂ H ₂₅	Ph	C ₁₂ H ₂₅	ClO ₄	13 ± 3	12 ± 3	34 ± 11	27 ± 9	35 ± 13	979	[13]
16	Pyr	C ₁₂ H ₂₅	Ph	C ₁₂ H ₂₅	Br	*	*	*	*	*	>2000	[13]
17	NMe ₂ CyHex	C ₁₂ H ₂₅	Ph	C ₁₂ H ₂₅	Br	35 ± 9	23 ± 3	54 ± 16	35 ± 9	59 ± 12	1274	Suppl.

TABLE 1: Continued.

Comp.	Cat ⁺	R ³	R ⁴	R ⁵	X ⁻	HT-1080		MH-22A		NIH3T3		Ref.
						IC ₅₀ (CV) (μ g/ml)	IC ₅₀ (MTT) (μ g/ml)	IC ₅₀ (CV) (μ g/ml)	IC ₅₀ (MTT) (μ g/ml)	IC ₅₀ (NR) (μ g/ml)	LD ₅₀ (mg/kg)	
18	Py	C ₁₂ H ₂₅	C ₆ H ₄ -OH-4	C ₁₂ H ₂₅	Br	4.3 ± 0.6	10 ± 2	3.4 ± 0.6	16 ± 2	95 ± 7	1479	Suppl
19	Py-CH ₃ -4	C ₁₂ H ₂₅	C ₆ H ₄ -OH-4	C ₁₂ H ₂₅	Br	32 ± 8	22 ± 5	21 ± 3	30 ± 8	44 ± 11	1087	Suppl
20	N-Me ₂ C ₁₂ H ₂₅	C ₁₂ H ₂₅	Ph	C ₁₂ H ₂₅	Br	3 ± 0.3	3 ± 0.4	10 ± 2	10 ± 2	19 ± 6	836	Suppl
21	Py-CF ₃ -4	C ₁₂ H ₂₅	Ph	C ₁₂ H ₂₅	Br	2 ± 0.3	4 ± 0.5	49 ± 8	19 ± 6	12 ± 4	619	[32]
22	Py	C ₁₂ H ₂₄ CF ₃	Ph	C ₁₂ H ₂₄ CF ₃	ClO ₄	18 ± 5	10 ± 2	10 ± 1	19 ± 5	16 ± 3	771	[32]
23	Py	C ₁₂ H ₂₅	Ph	(CH ₂) ₄ (CF ₂) ₇ CF ₃	Br	50 ± 6	47 ± 8	47 ± 2	75 ± 11	477 ± 25	3448	Suppl
24	Py	(CH ₂) ₄ (CF ₂) ₇ CF ₃	Ph	(CH ₂) ₄ (CF ₂) ₇ CF ₃	Br	100 ± 11	100 ± 9	*	*	*	>2000	Suppl
25	Py	(CH ₂) ₁₁ (CF ₂) ₇ CF ₃	Ph	(CH ₂) ₁₁ (CF ₂) ₇ CF ₃	Br	*	*	*	*	*	>2000	Suppl
26		"Dimeric" form of comp. 10			Br	12 ± 4	14 ± 2	27 ± 6	21 ± 4	717 ± 56	5164	Suppl
27		Oxidated form of comp. 10			ClO ₄	3.2 ± 0.8	3.1 ± 0.5	3.0 ± 0.3	3.3 ± 0.4	900 ± 42	3946	[14]

nt: not tested; *: not detected.

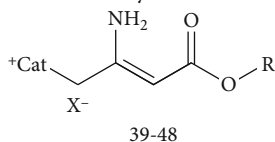
TABLE 2: Structure, cytotoxicity, and calculated basal toxicity of 3,4-dihydro-2(1H)-pyridones containing cationic moiety.



Comp.	R ¹	Cat ⁺	R ³	R ⁴	HT-1080			MH-22A			NIH3T3		Ref.
					X ⁻	IC ₅₀ (CV) (μg/ml)	IC ₅₀ (MITT) (μg/ml)	IC ₅₀ (CV) (μg/ml)	IC ₅₀ (MITT) (μg/ml)	IC ₅₀ (NR) (μg/ml)	LD ₅₀ (mg/kg)		
28	H	Py	CH ₃	C ₆ H ₄ -OCHF ₂ -2	Br	*	*	>100	*	1132 ± 85	>2000	Suppl	
29	PhCH ₂	Py	CH ₃	H	Br	*	*	*	*	972 ± 27	>2000	Suppl	
30	H	PPh ₃	(CH ₂) ₄ (CF ₂) ₇ CF ₃	Ph	Br	10 ± 2	9 ± 2	30 ± 11	39 ± 5	127 ± 11	1779	[33]	
31	H	Py	(CH ₂) ₄ (CF ₂) ₇ CF ₃	Ph	Br	3 ± 0.3	3 ± 0.2	3 ± 1	3 ± 0.6	15 ± 2	604	[33]	
32	H	Py	(CH ₂) ₄ (CF ₂) ₇ CF ₃	Ph	ClO ₄	3 ± 0.3	3 ± 0.5	2 ± 0.3	3 ± 0.2	15 ± 3	618	Suppl	
33	H	N-Me ₂ C ₁₂ H ₂₅	CH ₃	Ph	Br	2 ± 0.4	1 ± 0.2	2 ± 0.1	2 ± 0.6	4 ± 1	269	Suppl	
34	H	N-Me ₂ C ₁₂ H ₂₅	C ₁₂ H ₂₅	Ph	Br	2 ± 0.2	2 ± 0.6	3 ± 0.8	<1	6 ± 2	346	Suppl	
35	H	N-Me ₂ C ₁₂ H ₂₅	(CH ₂) ₄ (CF ₂) ₇ CF ₃	Ph	Br	3 ± 0.3	30 ± 11	26 ± 6	30 ± 8	27 ± 9	898	Suppl	
36	H	N-Me ₂ C ₁₂ H ₂₅	CH ₃	H	Br	2 ± 0.2	1 ± 0.2	18 ± 3	16 ± 3	63 ± 11	831	Suppl	
37	H	N-Me ₂ C ₁₂ H ₂₅	C ₁₂ H ₂₅	H	Br	2 ± 0.5	3 ± 0.4	3 ± 0.6	1 ± 0.2	7 ± 1	369	Suppl	
38	H	N-Me ₂ C ₁₂ H ₂₅	(CH ₂) ₄ (CF ₂) ₇ CF ₃	H	Br	3 ± 0.2	2 ± 0.2	4 ± 0.8	<1	11 ± 3	553	Suppl	

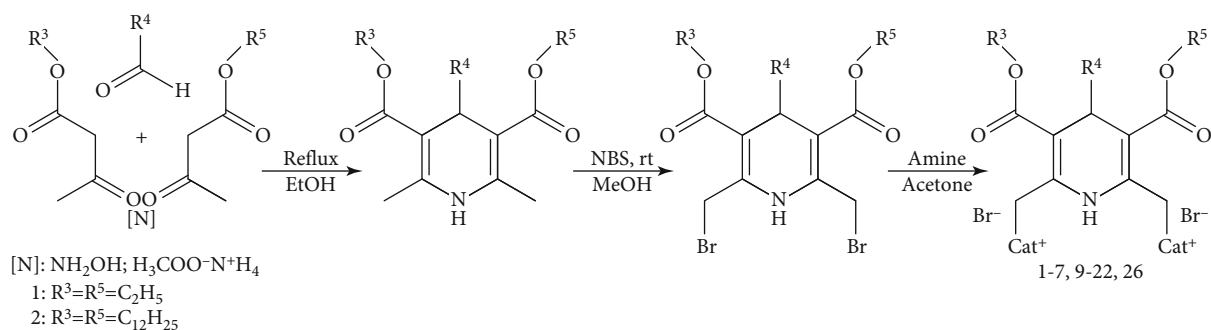
*: not detected.

TABLE 3: Structures, cytotoxicity, and calculated toxicity of 2-amino-3-alkoxycarbonylalkylammonium halides.



Comp.	Cat ⁺	R	X ⁻	HT-1080		MH-22A		NIH3T3		Ref.
				IC ₅₀ (CV) (μg/ml)	IC ₅₀ (MTT) (μg/ml)	IC ₅₀ (CV) (μg/ml)	IC ₅₀ (MTT) (μg/ml)	IC ₅₀ (NR) (μg/ml)	LD ₅₀ (mg/kg)	
39	N-Me ₂ CyHex	C ₁₆ H ₃₃	Cl	0.35 ± 0.06	0.5 ± 0.1	1 ± 0.6	0.2 ± 0.06	0.7 ± 0.1	97	Suppl
40	N-Me(CH ₂) ₄	C ₁₆ H ₃₃	Cl	<1	<1	1 ± 0.2	<1	8 ± 1	312	Suppl
41	N-Me ₂ (CH ₂) ₂ NMe ₂	C ₁₆ H ₃₃	Cl	2 ± 0.3	2 ± 0.6	1 ± 0.3	1 ± 0.2	5 ± 1	286	Suppl
42	N-Me(CH ₂) ₂ N(CH ₂) ₂ Me	C ₁₆ H ₃₃	Cl	2 ± 0.4	2 ± 0.2	1 ± 0.1	2 ± 0.3	4 ± 1	237	Suppl
43	N-Me ₂ C ₆ H ₁₃	C ₁₆ H ₃₃	Cl	3 ± 0.6	2 ± 0.4	2 ± 0.2	1 ± 0.2	21 ± 6	538	Suppl
44	N-Me ₂ C ₁₂ H ₂₅	C ₁₆ H ₃₃	Br	3 ± 0.4	3 ± 0.3	25 ± 3	28 ± 6	31 ± 8	697	Suppl
45	N-Me ₂ C ₁₂ H ₂₅	C ₁₆ H ₃₃	Cl	nt	nt	nt	nt	25 ± 9	573	Suppl
46	N-Me ₂ C ₁₂ H ₂₅	C ₁₆ H ₃₃	I	nt	nt	nt	nt	34 ± 8	637	Suppl
47	Py	C ₁₂ H ₂₅	I	3 ± 0.4	nt	2 ± 0.1	nt	14 ± 9	403	Suppl
48	N-Me ₂ C ₁₂ H ₂₅	C ₁₀ H ₂₁	Cl	3 ± 0.4	nt	2 ± 0.2	nt	17 ± 3	485	Suppl

nt: not tested.



SCHEME 1: Synthesis of 1,4-dihydropyridine (1,4-DHP) amphiphiles 1-7, 9-22, and 26.

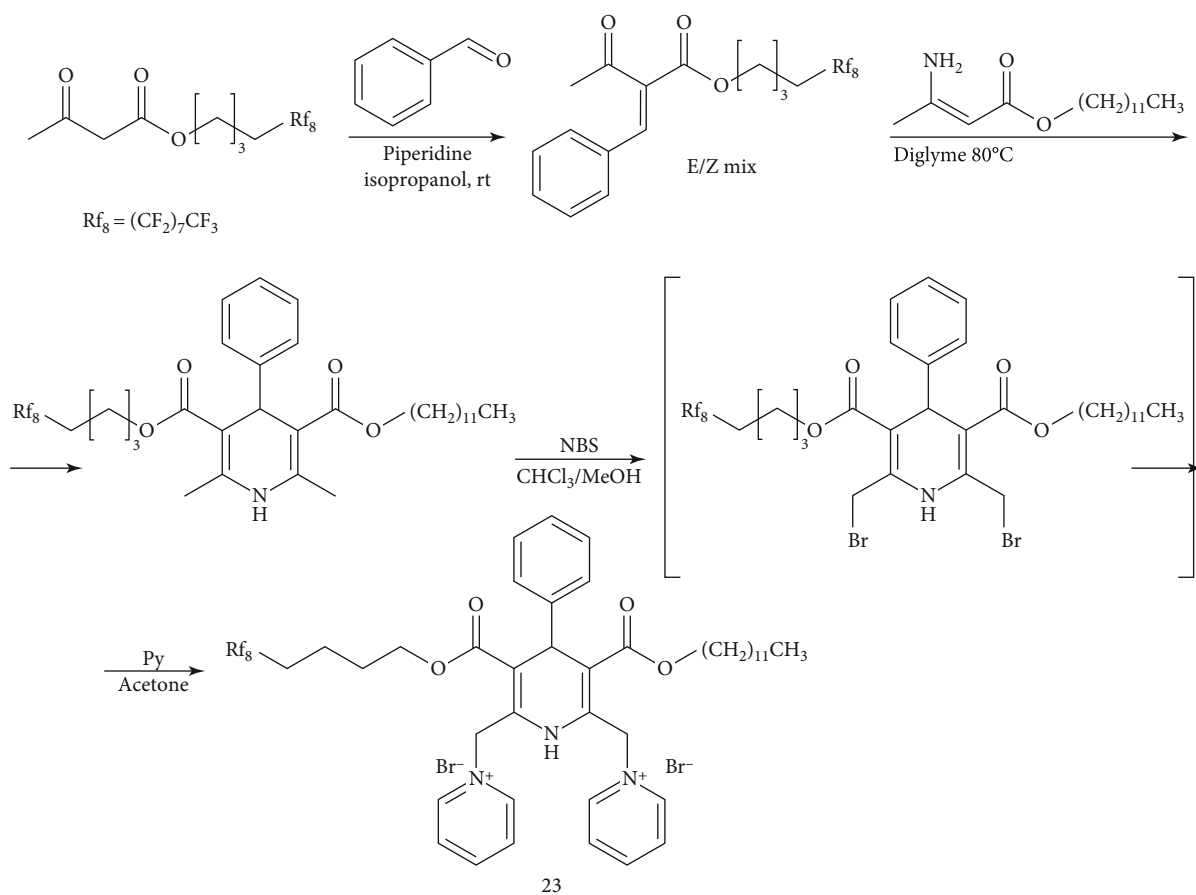
acetic acid [40]. The parent DHPDO solution in chloroform was treated with bromine affording the respective 6-bromo-methyl-DHPDO, which on subsequent reaction with pyridine or N,N-dimethyldodecyl-1-amine in dry acetone yielded the corresponding amphiphilic DHPDO derivatives **28-38**.

Typically, enamines have been studied and used as precursors and enanions for the synthesis of novel heterocyclic systems: pyridines, pyrroles, pyrimidines, dihydropyridines, etc. [41]. Therefore, up to now, most of the research in the field of enamines have been devoted to the elaboration of new strategies and synthetic methods, but lack biological studies [42]. 2-Amino-3-alkoxycarbonylalkylammonium halides with long alkyl chains have appeared as a new class of enaminoesters and were elaborated as a transfection agent for RNS transfection [27]. Also, structure analogues—alkyl acyl carnitine esters—were synthesized and characterized as biocompatible cationic lipids for use in gene delivery [43]. Cationic enaminoesters are stable solid compounds with remarkable solubility in water. The synthetic procedure for 2-amino-3-alkoxycarbonylalkylammonium halides **39-48** is

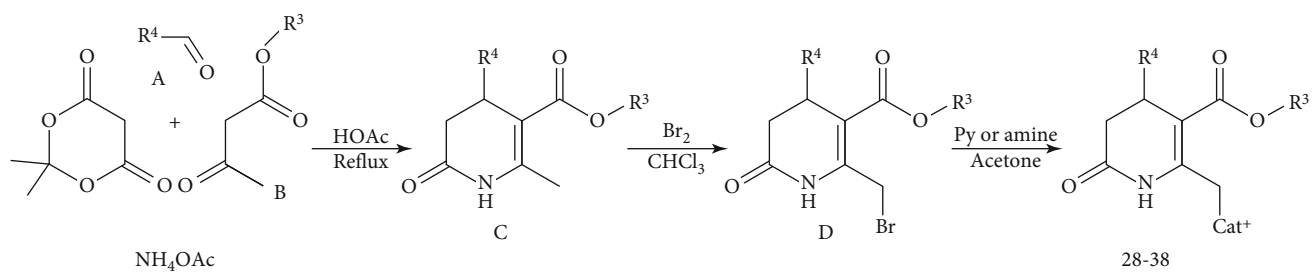
provided in Scheme 4. Briefly, the first step included the transesterification of commercially available ethyl 4-chloroacetoacetate with the corresponding carbinol without solvent by azeotropic removal of ethanol. Further reaction of the corresponding 4-chloro-3-oxobutanoates with ammonium acetate led to the formation of enaminoesters, which were used for quaternization with tertiary amines or heterocycles by extended heating in a dry solvent. Potassium iodide or sodium bromide additives were used for obtaining the corresponding iodides or bromides.

The perchlorates of amphiphiles **9**, **15**, **22**, **27**, and **32** were obtained from the corresponding bromides by treating with excess of conc. HClO₄ according to the procedure elaborated by Turovska et al. [44]. In some cases, the perchlorates were used for obtaining solid salts while the corresponding bromides existed as oils, and it was not possible to isolate them from the reaction mixture.

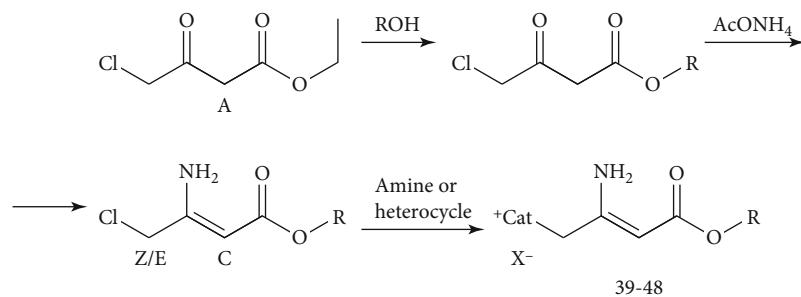
The full description of the synthesis and characterization of the original compounds in detail are given in the Supplementary data. Purity of the studied compounds was at least



SCHEME 2: Synthesis of unsymmetrical 1,4-DHP amphiphile 23.



SCHEME 3: Synthesis of 3,4-dihydro-2(1H)-pyridone (DHPDO) amphiphiles 28-38.



SCHEME 4: Synthesis of 2-amino-3-alkoxycarbonylalkylammonium halides 39-48.

97% according to high-performance liquid chromatography (HPLC) data.

3.3. Estimation of LD_{50} from IC_{50} Values. It has been proposed that the equation from the correlation of IC_{50} (the concentration of a substance that causes 50% toxicity *in vitro*) could be applied to estimate unknown LD_{50} values for a new compound from IC_{50} values measured as basal cytotoxicity *in vitro*. This estimated LD_{50} gives prior information regarding compound properties and would be used to select promising compounds and a starting dose for *in vivo* experiments. The evaluation of cytotoxicity of the abovementioned 3 types of amphiphilic compounds *in vitro* was assessed using the 3-(4,5-dimethylthiazol-2-yl)-2,5-diphenyltetrazolium bromide (MTT) and crystal violet (CV) assays on two monolayer tumor cell lines, namely, HT-1080 (human fibrosarcoma) and MH-22A (mouse hepatoma). Additionally, the compound influence on “normal” mouse fibroblasts (NIH3T3) was estimated for the studies of structure-activity relationships and exploration of the effect of substituents. The results are presented in Tables 1–3. Studies of cytotoxicity of the amphiphilic self-assembling compounds revealed certain regularities.

3.4. Analysis of Structure-Activity Relationships

3.4.1. Two Cationic Moieties Containing 1,4-DHP Amphiphiles (Table 1)

(1) Modification of Ester Alkyl Groups. Compounds possessing short alkyl chains in the ester groups at positions 3 and 5 of the dihydropyridine ring and organic heterocyclic cations in the methylene groups in positions 2 and 6 had very low cytotoxicity in cancer cell lines HT-1080 and MH-22A and high calculated LD_{50} values (comp. 1–9). It means that the compounds were almost inert to the noncancerous cell line NIH3T3 and cancer cell lines HT-1080 and MH-22A. This refers to several groups of the mentioned type of compounds possessing short alkyls in 3,5-ester substituents (methyl, ethyl, and also the more elongated propoxyethyl groups): comp. 9, 1, 6, 8, and 7. Additionally, 3,5-bis(diethyloxycarbonyl)-1,4-DHP amphiphiles comprising substituted pyridinium moieties in positions 2 and 6 (compounds 2–5) have moderate cytotoxicity, around 3300 mg/kg. In most cases, for the 3,5-bis(diethyloxycarbonyl)-1,4-DHP compounds, it was not possible to calculate IC_{50} values for the cancer cell lines HT-1080 and MH-22A due to rather low cytotoxicities; calculated LD_{50} values of compounds 1–9 were >2000 mg/kg (for NIH3T3 cells).

On the contrary, analogues comprising dodecyl chains in the ester groups at positions 3 and 5 and pyridinium moieties in positions 2 and 6 of the dihydropyridine ring (see comp. 10 versus comp. 1, comp. 12 versus comp. 2, comp. 13 versus comp. 4) showed significant cytotoxicity towards cancer cell lines HT-1080 and MH-22A and still very low cytotoxicity in noncancerous NIH3T3 cells. For example, LD_{50} values for compounds 10, 12, and 13 were 1482, 1431, and 1706 mg/kg, respectively, while cytotoxicity towards HT-1080 cells was 3–10 $\mu\text{g/ml}$ and towards

MH-22A cells was 3–40 $\mu\text{g/ml}$. In principle, the obtained data coincide with observations on the impact of dihydropyridine on cell growth, where it was concluded that a long alkyl chain containing 1,4-DHP amphiphiles show promising dual activity—proliferation inhibition on cancer cell lines and proliferation stimulating effect on normal cell lines [31]. It should be noted that the 3,5-bis(dodecyloxycarbonyl)-1,4-DHP amphiphile 14 with an electron-withdrawing acetyl group in the pyridinium moieties in positions 2 and 6 of the 1,4-DHP ring was practically nontoxic on noncancerous NIH3T3 cells and demonstrated selective cytotoxicity toward cancer cells and pronounced cytotoxicity of around 3 $\mu\text{g/ml}$ on HT-1080 cells and of 50–100 $\mu\text{g/ml}$ on MH-22A cells.

Substitution of fluorine for hydrogen atoms in alkyl chains of the 1,4-DHP amphiphiles decreased cytotoxicity of the abovementioned compounds. Thus, substitution of the 3,5-dodecyloxycarbonyl alkyl chain's most distant hydrogen atom by trifluoromethyl groups (comp. 22 versus comp. 10) leads to lower cytotoxicity to cancer cell lines HT-1080 (10–18 $\mu\text{g/ml}$ versus 3 $\mu\text{g/ml}$) and MH-22A (10–19 $\mu\text{g/ml}$ versus 3–6 $\mu\text{g/ml}$) and to higher cytotoxicity to noncancerous cell line NIH3T3 (771 mg/kg versus 1482 mg/kg). In this case, the influence of the anion was not taken into account, but that also could give an effect. Substitution of seven methylene groups of a 3-dodecyloxy moiety by seven difluoromethylene groups leads to the formation of an unsymmetrical 1,4-DHP amphiphile 23, which has lower cytotoxicity to the studied cancer and normal cell lines (comp. 23 versus comp. 10)—a cytotoxicity of around 47–75 $\mu\text{g/ml}$ versus 3–6 $\mu\text{g/ml}$ on cancer cell lines and LD_{50} 3448 mg/kg versus 1482 mg/kg, respectively. Further substitution of the next seven methylene groups by seven difluoromethylene groups (comp. 24) leads to subsequent diminishing of cytotoxicity to cancer cell lines (around 100 $\mu\text{g/ml}$) and also low calculated toxicity to noncancerous cell line NIH3T3 (>2000 mg/kg). In the case of the more extended partially fluorinated 3,5-heptadecafluorononadecyl chains (comp. 25), the compounds revealed undetectable toxicity to the two cancer cell lines and also low toxicity to the noncancerous cell line NIH3T3. So, from the obtained results (Table 1), it is evident that the perfluorinated 1,4-DHP amphiphiles (compounds 23–25) are nontoxic in the tested cell lines.

(2) Modification of Substituents at Position 4 of the 1,4-DHP Ring. Variations of several types of substituents in position 4 of the DHP ring of 3,5-bis(diethyloxycarbonyl)-1,4-DHPs were performed. Compounds with phenyl (comp. 1–5), substituted phenyl (2-difluoromethylphenyl (comp. 7 and 9), trifluoromethyl (comp. 6)), and ethoxycarbonyl (comp. 8) substituents were obtained, but no significant influence on the cytotoxicity of the tested 1,4-DHP amphiphiles was observed. Introducing an HO-substituent in a phenyl moiety in position 4 of the 1,4-DHP ring gives comp. 18 and 19 which are 4-(4'-hydroxyphenyl) analogues of corresponding 4-phenyl-DHPs 10 and 12, respectively. It was demonstrated that the introduction of an HO-substituent does not give a strong influence on the cytotoxicity of the compounds.

(3) *Modification of the Cationic Moieties.* Modification of the cationic moieties in positions 2 and 6 of the 1,4-DHP ring (in the case of 3,5-dodecyloxycarbonyl substituents) may result in substantially different toxicological properties. The insertion of substituents in the pyridinium ring leads to some quantitative modifications of cytotoxicity—mainly to slightly diminished cytotoxicity in the case of 4-methyl and 4-dimethylamino substituents (comp. **12** and comp. **13**)—while introducing a 3-acyl substituent (comp. **14** versus comp. **10**) in the pyridinium moiety did not give any influence on the cytotoxicity in HT-1080 cells (in both cases around 3 $\mu\text{g/ml}$), but decreased cytotoxicity in MH-22A cells (50–100 $\mu\text{g/ml}$ and 3–6 $\mu\text{g/ml}$, respectively) and also decreased cytotoxicity in noncancerous cell line NIH3T3 (4040 mg/kg versus 1482 mg/kg). Comparison of the cytotoxicity of the compounds with 4-methylpyridinium and 4-trifluoromethyl pyridinium moieties (comp. **12** versus comp. **21**) showed that there are no significant changes of cytotoxicity in cancer HT-1080 and MH-22A cells (5–10 $\mu\text{g/ml}$ versus 2–4 $\mu\text{g/ml}$, and 29–40 $\mu\text{g/ml}$ versus 19–49 $\mu\text{g/ml}$, respectively) but a twofold increase of cytotoxicity in noncancerous NIH3T3 cells (1431 mg/kg versus 619 mg/kg). Introduction of a pyrazinium moiety instead of a pyridinium moiety (comp. **16** versus comp. **10**) gave a compound which was practically inert to the studied cancer cell lines HT-1080 and MH-22A and was also nontoxic to normal NIH3T3 cells. Exchange of the heteroaromatic pyridinium moieties to saturated heterocyclic moieties—N-methylmorpholinium fragments (comp. **15**)—led to slightly lower anticancer activity of the compound towards the abovementioned cancer cell lines and comparatively higher cytotoxicity to NIH3T3 cells (979 mg/kg). Also, in this case, the influence of the anion was not taken into account, but it may give an effect (ClO_4^- instead of Br^-). Introducing N,N-dimethylcyclohexylammonium moieties as the cationic part of the amphiphile gave compound **17** with less cytotoxicity (23–54 $\mu\text{g/ml}$) on both tested cancer cell lines and an LD_{50} value of 1274 mg/kg, while the LD_{50} value of compound **18** with the introduced aliphatic N,N-dimethyl-N-dodecylammonium moieties was 836 mg/kg. It was shown that compound **18** with aliphatic ammonium fragments was more cytotoxic. The obtained data is in agreement with conclusions by Lv et al. that among the synthetic cationic delivery systems, quaternary ammonium surfactants are more toxic than their analogues with the cationic charge delocalized in a heterocyclic system [45].

(4) *Change of the Anions.* Insertions of the BF_4^- anion instead of the usual Br^- anion (comp. **11** versus comp. **10**) lead to an increase in basal toxicity—1053 and 1482 mg/kg, respectively—but a decrease in cytotoxicity on HT-1080 (around 30 $\mu\text{g/ml}$ and 3 $\mu\text{g/ml}$, respectively) and MH-22A (30 $\mu\text{g/ml}$ and 3–6 $\mu\text{g/ml}$, respectively) cell lines.

(5) *Change of Dehydrogenation Degree.* Lipid-like pyridine derivative **27**, as the oxidized form of compound **10**, demonstrated very close cytotoxicity data to the corresponding dihydro compound **10**, in all cases around 3 $\mu\text{g/ml}$, while

basal toxicity on noncancerous cell line NIH3T3 is significantly diminished: comp. **27** is not harmful at all (LD_{50} is 3948 mg/kg). In this case also, the influence of the anion was not taken into account, but it may give an effect (ClO_4^- instead of Br^-).

(6) *The Duplication of Moieties.* Synthetic lipid-like compound **26** was obtained as a “dimeric” form of compound **10**, which was proposed as a promising DNA delivery agent. Cytotoxicity data of amphiphiles (comp. **26** versus comp. **10**) demonstrated that this structural modification slightly decreased cytotoxicity of the target compound **26** in both tested cancer HT-1080 and MH-22A cells (12–27 $\mu\text{g/ml}$ versus 3–6 $\mu\text{g/ml}$, respectively) and also considerably decreased the LD_{50} value—5164 mg/kg versus 1482 mg/kg.

3.4.2. Cationic Moiety Containing 3,4-Dihydro-2(1H)-pyridones (Table 2)

(1) *Modification of Ester Alkyl Group.* Same as in the case of 1,4-DHP amphiphiles also, pyridones with a short alkyl chain—the methyl group in the ester moiety and pyridinium in the cationic part of the molecule (comp. **28** and **29**)—were inert to tested cancer cells HT-1080 and MH-22A and demonstrated high calculated LD_{50} values > 2000 mg/kg. In the case of comp. **29**, the influence of the N-substituent in the pyridone and, in the case of comp. **28**, the influence of substituent in the phenyl moiety at position 4 of the pyridone cycle were not taken into account. Two other methyl esters—comp. **33** and **36**—demonstrated significant cytotoxicity on all the tested cell lines. This could be explained by the influence of the cationic moiety in the compound.

Substitution of fluorine for hydrogen atoms in the alkyl chain of the pyridone amphiphiles did not give a strong influence on the cytotoxicity of the compounds, and it seems that this also was dependent on the cationic moiety and other substituents of the compound. So, in the case of 4-unsubstituted pyridones with the N,N-dimethylcyclohexylammonium moiety, comp. **37** with hydrogen atoms in the ester moiety and comp. **38** with fluorine atoms in the ester moiety demonstrated similar cytotoxicity in all of the tested cell lines, while for cytotoxicity of 4-phenyl pyridones with N,N-dimethylcyclohexylammonium moiety, comp. **34** with hydrogen atoms in the ester moiety versus comp. **35** with fluorine atoms in the NIH3T3 cells was two times higher (346 mg/kg versus 898 mg/kg, respectively).

(2) *Modification of Substituents at Position 4 of 3,4-Dihydro-2(1H)-pyridone Ring.* The series of 3,4-dihydro-2(1H)-pyridones with a phenyl substituent at position 4 of the pyridone ring and also the 4-unsubstituted ones were compared. In the case of 4-phenyl pyridone **34** and 4-unsubstituted pyridone **37**, both compounds containing the same N,N-dimethylcyclohexylammonium moiety and hydrogen atoms in the alkyl chain had no significant change of cytotoxicity on the tested cell lines. While in the case of 4-phenyl pyridone **35** and 4-unsubstituted pyridone **38**, both compounds containing the same N,N-

dimethylcyclohexylammonium moiety and fluorine atoms in the alkyl chain, the 4-unsubstituted **38** possessed a slightly higher cytotoxicity—LD₅₀ values were 553 mg/kg for comp. **38** and 898 mg/kg for comp. **35**.

(3) *Change of the Anion.* Change to perchlorate from the usual bromine anion (comp. **32** versus comp. **31**) did not give any influence on cytotoxicity on the tested cell lines.

(4) *Modification of the Cationic Moiety.* It is demonstrated that the dihydropyridone amphiphile **30** with a triphenylphosphonium polar head group was about 3 times less cytotoxic than the analogous dihydropyridone **31** with a pyridinium head group in the NIH3T3 cells, i.e., 1779 mg/kg versus 604 mg/kg. Change of pyridinium to N,N-dimethylcyclohexylammonium moiety as the cationic head group of dihydropyridone—comp. **31** versus comp. **35**—led to a slightly diminished cytotoxicity on cells in the case of comp. **35**. In this case, we observed the opposite relationship as for 1,4-DHP amphiphiles where it was demonstrated that quaternary ammonium surfactants are more toxic than their heterocyclic analogues. Toxicity of cationic lipids may be connected with the structure of their head groups [41].

The obtained data demonstrated that the 3,4-dihydro-2(1*H*)-pyridone amphiphiles (Table 2) with a pyridinium polar head group and introduced fluorine atoms in the ester moiety (comp. **31** and comp. **32**) were substantially more cytotoxic to tested cells than the structurally related 1,4-DHP amphiphiles **23** and **24**.

Most dihydropyridone series cationic amphiphiles show marked cytotoxicity towards cancer cells and medium cytotoxicity towards normal NIH3T3 cells: compounds possessing 1 or 2 long alkyl chains in ester and/or ammonium groups (with or without fluorine atoms on alkyl chains (comp. **31–34** and **36–38**)). There is an exclusion: comp. **30** possessing the triphenylphosphonium cationic group.

The obtained data allows one to choose compounds for putative use depending on their structure. Thus, due to the polyfluorinated alkyl ester groups in the DHP molecule, low toxicity (practically inert) amphiphilic compounds can be obtained (comp. **25**). Inert amphiphilic self-assembling compounds could be used as materials to form gene transfection or drug delivery nanoparticles for transmembrane transport according to the paradigm: pharmacologically inert transport vehicles should be used.

3.4.3. *2-Amino-3-alkoxycarbonylalkylammonium Halides* (Table 3). The last group of delivery systems was formed by a 2-amino-3-alkoxycarbonylalkylammonium cationic moiety containing derivatives **39–48**.

(1) *Modification of the Cationic Moiety.* The cationic moiety was changed for 2-amino-3-hexadecyloxycarbonylammonium derivatives, namely, comp. **39–43**, and **45**. The obtained data demonstrated that N-(2-amino-4-(hexadecyloxy)-4-oxobut-2-en-1-yl)-N,N-dimethylcyclohexylammonium chloride (comp. **39**) shows the highest cytotoxicity in all the tested cell lines with a LD₅₀ value of 97 mg/kg, while alkyl moi-

ety containing compounds—N-(2-amino-4-(hexadecyloxy)-4-oxobut-2-en-1-yl)-N,N-dimethylhexan-1-aminium chloride (comp. **43**) and N-(2-amino-4-(hexadecyloxy)-4-oxobut-2-en-1-yl)-N,N-dimethyldodecan-1-aminium chloride (comp. **45**)—demonstrated lower cytotoxicity in all the tested cell lines with LD₅₀ values of 538 and 573 mg/kg, respectively.

(2) *Modification of the Ester Alkyl Groups.* The influence of the alkyl moiety was compared for two amphiphiles—comp. **48** with decyl ester versus comp. **45** with hexadecyl ester. The obtained LD₅₀ data show that the difference is not large—485 mg/kg versus 573 mg/kg, respectively.

(3) *Change of the Anion.* The anions from the usual bromide comp. **44** were changed to chloride and also to iodide (comp. **45** and comp. **46**). According to IC₅₀ and LD₅₀ data, the change of the anion did not have any influence on the cytotoxicity in NIH3T3 cell lines; IC₅₀ values were around 30 μg/ml.

3.5. *Electrochemical Oxidation.* The electrochemical oxidation of various 1,4-dihydropyridine derivatives has been extensively studied [46–50] including 1,4-DHP derivatives containing cationic moieties [29, 44]. The electrochemical oxidation of the selected compounds studied in this work was performed by cyclic voltammetry on a stationary glassy carbon electrode in dry acetonitrile; the data is presented in Table 4. The perchlorates of the tested amphiphiles were obtained from the corresponding bromides by treating their abs. MeOH solutions with excess of conc. HClO₄ according to the procedure elaborated by Turovska et al. [44].

Now, we have used electrooxidation potentials to characterize electron donor properties of the studied compounds.

Compounds from the 1st group, containing cationic pyridinium methylene groups in positions 2 and 6 in the 1,4-DHP ring, have electrooxidation potentials of 1.57–1.58 V both in the case of 3,5-diethoxycarbonyl- and 3,5-didodecyloxycarbonyl-1,4-DHPs (comp. **1** and comp. **10**). This is also in agreement with our previous results, where the electrochemical oxidation potential of comp. **1** was determined as 1.7 V and electrochemical oxidation of this compound was demonstrated as a two-electron process [29]. Introduction of the CF₃ groups at the β-carbon atom of a dodecyl chain in the ester moieties (comp. **18**) does not change the value of the electrooxidation potential, which is also 1.57 V. On the contrary, the addition of a CF₃ group in the pyridinium moiety in the 2 and 6 positions of the 1,4-DHP cycle (comp. **21**) leads to a slight increase of the electrooxidation potential (1.63 V). Moreover, a change of the 17 terminal H atoms to F atoms in one or both dodecyl chains leads to a further increase of the electrooxidation potential of 1.69–1.70 V (comp. **23** and comp. **24**). It should be noted that the parent compounds—1,4-DHP derivatives without cationic moieties—demonstrated lower electrooxidation potentials. Thus, 4-phenyl-substituted Hantzsch 1,4-dihydropyridine has a 1.08 V potential on a glassy carbon electrode [50] and the other 4-aryl-substituted 1,4-DHPs have 1.11 V potentials [51], but 4-monoalkyl-substituted 1,4-

TABLE 4: Oxidation potentials (E^{ox}) of selected compounds.

Group	Comp.	R ¹	R ³	R ⁴	R ⁵	Cat ⁺	E ^{ox} (V)
1st	1 *	—	C ₂ H ₅	Ph	C ₂ H ₅	Py	1.57
	10 *	—	C ₁₂ H ₂₅	Ph	C ₁₂ H ₂₅	Py	1.58
	21 *	—	C ₁₂ H ₂₅	Ph	C ₁₂ H ₂₅	Py-CF ₃ -4	1.63
	22	—	C ₁₂ H ₂₄ CF ₃	Ph	C ₁₂ H ₂₄ CF ₃	Py	1.57
	23 *	—	C ₁₂ H ₂₅	Ph	(CH ₂) ₄ (CF ₂) ₇ CF ₃	Py	1.70
	24 *	—	(CH ₂) ₄ (CF ₂) ₇ CF ₃	Ph	(CH ₂) ₄ (CF ₂) ₇ CF ₃	Py	1.69
2nd	29 *	PhCH ₂	CH ₃	H	—	Py	2.35
	38 *	H	(CH ₂) ₄ (CF ₂) ₇ CF ₃	Ph	—	Py	2.04
3rd	42 *	—	C ₁₆ H ₃₃	—	—	N-Me(CH ₂) ₂ N(CH ₂) ₂ Me	1.49
	44 #	—	C ₁₆ H ₃₃	—	—	N-Me ₂ C ₁₂ H ₂₅	1.24

*Original compounds—bromide; #original compound—chloride.

dihydropyridines at the same conditions have 1.01–1.03 V oxidation potentials [47].

Compounds from the 2nd group—amphiphilic 3,4-dihydropyridone derivatives with a pyridinium methylene moiety in position 6—have more positive electrooxidation potential. So, the unsubstituted at position 4 pyridone derivative **29** has an electrooxidation potential of 2.35 V. A compound possessing a phenyl substituent at position 4 and a 5-heptadecylfluorododecylcarboxy moiety in position 5 (comp. **38**) has a slightly lower oxidation potential (2.04 V), while the parent 4-unsubstituted or 4-phenyl-substituted 3,4-dihydropyridone derivatives without cationic moiety in position 6 have electrooxidation potentials of 1.52–1.64 V [52].

Compounds from the 3rd group—tested open-chain 2-amino-3-alkoxycarbonylalkylammonium halides **42** and **44**—have oxidation potentials of 1.49 V and 1.24 V, respectively.

Compounds from the 1st group (comp. **1–24**, Table 1) could be considered as analogues of 1,4-dihydropyridine and model compounds of redox coenzyme NAD(P)H. Many 4-aryl-1,4-DHPs possess antioxidant properties, including several Ca²⁺ channel blockers [53]. The antiradical activity (ARA) of two 1,4-DHPs containing cationic moieties was determined by a 1,1-diphenyl-2-picrylhydrazyl (DPPH) radical assay; the results were expressed as a percentage (%) of the DPPH free radical scavenging, and the untreated level of the DPPH radical was designated as 100% [13, 31]. It was demonstrated that 3,5-didodecyloxycarbonyl-4-phenyl-1,4-dihydropyridine derivatives containing pyridinium moieties showed 25–60% radical scavenging activity which are comparable with the ARA of Diludin [54] (40%)—a widely

known antioxidant. Other 1,4-DHP amphiphiles containing saturated heterocyclic moieties—N-methylmorpholinium or N-methylpyrrolidinium derivatives—demonstrated more pronounced ARA, 95% and 54%, respectively. For 1,4-DHP amphiphiles possessing pyridinium moieties, the positive charge is delocalized in the heteroaromatic cycle, causing ARA reduction; for example, the electron donor dimethylamino group as a substituent of pyridinium moiety leads to a lower ARA (27%, comp. **13**) [13].

3.6. Determination of LogP and Molecular Topological Polar Surface Area. The lipophilicity of molecules represents their affinity for a lipophilic environment, and the lipophilicity may be expressed as logP [55, 56]. The molecular polar surface area (PSA) is a very useful parameter for the prediction of drug transport properties, and PSA is defined as a sum of the surfaces of polar atoms [57]. In practice, medicinal chemists use the PSA to quantify the polarity of drug molecules [58]. Data of the calculated topological polar surface area represent the compound's blood-brain barrier permeability [59, 60]. It allows one to plan further activities for the pleiotropic compounds.

Lipid-type compounds could be used as biologically active compounds *per se* or as transport vehicles or additives, so their lipophilicity (logP) and topological polar surface area (TPSA) were calculated, and the data are recorded in Table 5.

LogP values which surpass 5, according to Lipinski's Rule of Five, characterize compounds as lipophilic [61]. According to the obtained data for lipid-like amphiphiles, in some cases, the values of logP were <5, in particular for compounds **1**, **2**, **4**, **6**, **7**, **28**, and **29**. These compounds comprised short alkyl moieties in the ester groups. LogP values close to 5 were

TABLE 5: Log*P* and molecular topological polar surface area (TPSA) of selected compounds.

Comp.	1st group		Comp.	2nd group		Comp.	3rd group	
	Log <i>P</i>	TPSA (Å ²)		Log <i>P</i>	TPSA (Å ²)		Log <i>P</i>	TPSA (Å ²)
1	2.26	70.65	28	1.44	67.64	39	7.52	52.32
2	3.13	70.65	29	1.18	49.62	40	6.25	52.32
4	2.71	77.13	30	14.32	55.40	41	5.63	55.56
6	3.18	70.65	31	9.43	58.41	42	5.44	55.56
7	3.20	98.34	32	9.43	58.41	43	7.98	52.32
10	10.97	70.65	33	6.19	55.40	44	10.65	52.32
12	11.63	70.65	34	10.01	55.40	47	5.40	55.33
13	11.42	77.13	35	14.81	55.40	48	7.98	52.32
17	13.55	64.63	36	4.70	55.40			
20	19.81	64.63	37	8.52	55.40			
21	12.81	70.65	38	13.32	55.40			
22	13.22	70.65						
23	15.77	70.65						
24	18.64	70.65						
25	24.68	70.65						

obtained for compounds **36**, **41**, **42**, and **47**, namely, 4.70, 5.63, 5.44, and 5.40, respectively. Log*P* values for dicationic 1,4-DHP amphiphiles possessing longer alkyl chains or fluorinated alkyl groups in the ester moieties were determined in the 11–24.5 interval, while for long alkyl ester moieties containing 3,4-dihydropyridone amphiphiles, log*P* values were determined in the 6–15 interval. The difference could be due to the number of alkyl groups. Log*P* values for other open-chain compounds were determined in the 6–11 interval.

Nevertheless, TPSA never surpasses 90, so the compounds are prone to permeate cells; additionally, they can penetrate the blood-brain barrier [62]. Among all tested amphiphiles, only for 1,1'-((4-(2-(difluoromethoxy)phenyl)-3,5-bis((propoxymethoxy)carbonyl)-1,4-dihydropyridine-2,6-diyl)bis(methylene))bis(pyridin-1-ium) dibromide (comp. **7**) was the TPSA value higher than 90, i.e., 98.34 Å². This could be explained by the influence of the structure components of the compound. TPSA values for the other compounds were defined in accordance with the main fragments of the compound structures. So, for the other 1st group compounds—dicationic 1,4-DHP amphiphiles—TPSA values were in the 71–77 Å² interval; for the 2nd group compounds—cationic 3,4-dihydropyridone amphiphiles—TPSA values were in the 50–58 Å² interval with the exception of compound **28** which had a TPSA value of 67.64 Å²; and for the 3rd group compounds—open-chain 2-amino-3-alkoxycarbonylalkylammonium cationic moiety containing amphiphiles—the TPSA values were in the 52–56 Å² interval.

4. Conclusions

Polyfunctional self-assembling synthetic lipid-like compounds, such as pharmacological and chemotherapeutical agents, namely, 3,5-dialkoxycarbonyl-1,4-dihydropyridines

(1,4-DHPs) comprising pyridinium or ammonium substituents at the 2 and 6 positions; structurally related compounds, derivatives of 3,4-dihydro-2-oxopyridines as isomeric 3,4-dihydropyridine structures with an additional intracyclic carbonyl group; and the N-β-carbonylvinylamido system, namely, 2-amino-3-alkoxycarbonylalkylammonium halides as open chain analogues of the first type of the abovementioned compounds, were studied. The main properties and major functions of these compounds are their amphiphilic character, liposome-forming ability, RNA transfection (by self-assembling compounds), antiradical and antioxidant properties, growth regulation—both in malignant and non-malignant cell types—anticancer properties due to cytotoxicity, and MDR inhibition [13, 16, 27, 28, 31, 33].

In this work we have demonstrated biological properties of cationic 1,4-dihydropyridine as self-assembling synthetic lipids and dihydropyridones as well as open-chain analogues: their cytotoxicity against cancer cell lines HT-1080 and MH-22A in comparison with cytotoxicity against normal NIH3T3 cells. The obtained data showed that 1,4-DHP derivatives containing cationic moieties in positions 2 and 6 and possessing dodecyl alkyl chains in the ester groups in positions 3 and 5 demonstrated high cytotoxicity on cancer cells HT-1080 and MH-22A, but low cytotoxicity on noncancerous NIH3T3 cells. According to our previous studies, these compounds also demonstrated significant antiradical activity and also gene delivery activity [13], and for some of them, reversal of multidrug resistance in murine lymphoma cells [16]. Together with antiradical activity, cell growth regulation, multidrug resistance inhibition, nucleic acid delivery, and the polyfunctional (pleiotropic) type of properties of the mentioned compounds open new avenues for their studies and use. According to literature data, liposomes could be used not only to transport biologically active compounds but also to have their own specific biological activity, e.g., to protect cells and encapsulated components against oxidative

damage. Liposomes are proposed for the delivery of antioxidants for protection against pathological conditions related to oxidative stress [63]. In our case, liposomes could be used *per se* to protect against oxidative damage.

A calculated degree of lipophilicity and TPSA data can be used to choose compounds according to their permeability through membranes, including the blood-brain barrier, to guide them to the proper location. It was demonstrated that membrane permeability in a variety of systems, including model liposome bilayers, various cells, and epidermal tissue, correlated strongly with data regarding hydrocarbon-water partition coefficients [64]. TPSA values for selected compounds were defined in accordance with the main fragments of compound structures. The determined $\log P$ values were highest for dodecyl ester groups in positions 3 and 5 of the 1,4-DHP and lowest for short alkyl chain containing amphiphiles.

This study also revealed the correlation of the cytotoxic effects of 3 groups of structurally related synthetic cationic lipids according to their molecular structures. The results indicated that among the tested compound groups, amphiphiles based on the 1,4-DHP core demonstrated high cytotoxicity in cancer cells HT-1080 and MH-22A, but low cytotoxicity in the noncancerous NIH3T3 cells.

The obtained results may serve as guidelines for the development of drug formulations to be used in cancer treatment on the basis of these pleiotropic lipid-like 1,4-DHP amphiphiles.

Data Availability

The experimental data used to support the findings of this study are available from the corresponding authors upon request.

Conflicts of Interest

The authors declare that there is no conflict of interest regarding the publication of this paper.

Acknowledgments

This research was supported by the PostDocLatvia Project Nr.1.1.1.2/VIAA/2/18/371 “Bifunctional Amphiphilic Lipid-Like Compounds—Self-Assembling Properties and Biological Activities” (to M. Rucins) and EuroNanoMed2 Project INNOCENT “Innovative Nanopharmaceuticals: Targeting Breast Cancer Stem Cells by a Novel Combination of Epigenetic and Anticancer Drugs with Gene Therapy.”

Supplementary Materials

Scheme S1: synthesis of 1,4-dihydropyridine (1,4-DHP) amphiphiles **1–7**, **9–22**, and **26**. Scheme S2: synthesis of unsymmetrical 1,4-DHP amphiphile **23**. Scheme S3: synthesis of 3,4-dihydro-2(1H)-pyridone (DHPDO) amphiphiles **28–38**. Scheme S4: synthesis of 2-amino-3-alkoxycarbonylalkylammonium halides **39–48**. Physicochemical characterization of new compounds is provided. (*Supplementary Materials*)

References

- [1] T. Olusanya, R. H. Ahmad, D. Ibegbu, J. Smith, and A. Elkordy, “Liposomal drug delivery systems and anticancer drugs,” *Molecules*, vol. 23, no. 4, p. 907, 2018.
- [2] C. T. Inglut, A. J. Sorrin, T. Kuruppu et al., “Immunological and toxicological considerations for the design of liposomes,” *Nanomaterials*, vol. 10, no. 2, p. 190, 2020.
- [3] A. Carmona-Ribeiro, “Bilayer-forming synthetic lipids: drugs or carriers?,” *Current Medicinal Chemistry*, vol. 10, no. 22, pp. 2425–2446, 2003.
- [4] A. Lechanteur, V. Sanna, A. Duchemin, B. Evrard, D. Mottet, and G. Piel, “Cationic liposomes carrying siRNA: impact of lipid composition on physicochemical properties, cytotoxicity and endosomal escape,” *Nanomaterials*, vol. 8, no. 5, p. 270, 2018.
- [5] K. He and M. Tang, “Safety of novel liposomal drugs for cancer treatment: advances and prospects,” *Chemico-Biological Interactions*, vol. 295, pp. 13–19, 2018.
- [6] L. Milkovic, W. Siems, R. Siems, and N. Zarkovic, “Oxidative stress and antioxidants in carcinogenesis and integrative therapy of cancer,” *Current Pharmaceutical Design*, vol. 20, no. 42, pp. 6529–6542, 2014.
- [7] Q. Cui, J.-Q. Wang, Y. G. Assaraf et al., “Modulating ROS to overcome multidrug resistance in cancer,” *Drug Resistance Updates*, vol. 41, pp. 1–25, 2018.
- [8] H. Sies and D. P. Jones, “Reactive oxygen species (ROS) as pleiotropic physiological signalling agents,” *Nature Reviews. Molecular Cell Biology*, vol. 21, no. 7, pp. 363–383, 2020.
- [9] H. Sies, “Oxidative stress: a concept in redox biology and medicine,” *Redox Biology*, vol. 4, pp. 180–183, 2015.
- [10] A. Garu, G. Moku, S. K. Gulla et al., “Examples of tumor growth inhibition properties of liposomal formulations of pH-sensitive histidinylated cationic amphiphiles,” *ACS Biomaterials Science & Engineering*, vol. 1, no. 8, pp. 646–655, 2015.
- [11] Z. Fasili, F. Mehri, H. A. Ebrahimi et al., “Applying nanoparticles in the treatment of viral infections and toxicological considerations,” *Pharmaceutical and Biomedical Research*, vol. 5, no. 4, pp. 1–20, 2019, <http://pbr.mazums.ac.ir/article-1-247-en.html>.
- [12] J. Barar and Y. Omid, “Intrinsic bio-signature of gene delivery nanocarriers may impair gene therapy goals,” *BioImpacts: BI*, vol. 3, no. 3, pp. 105–109, 2013.
- [13] K. Pajuste, Z. Hyvonen, O. Petrichenko et al., “Gene delivery agents possessing antiradical activity: self-assembling cationic amphiphilic 1,4-dihydropyridine derivatives,” *New Journal of Chemistry*, vol. 37, no. 10, pp. 3062–3075, 2013.
- [14] O. Petrichenko, M. Rucins, A. Vezane et al., “Studies of the physicochemical and structural properties of self-assembling cationic pyridine derivatives as gene delivery agents,” *Chemistry and Physics of Lipids*, vol. 191, pp. 25–37, 2015.
- [15] G. Apsite, I. Timofejeva, A. Vezane et al., “Synthesis and comparative evaluation of novel cationic amphiphile C12-Man-Q as an efficient DNA delivery agent in vitro,” *Molecules*, vol. 23, no. 7, p. 1540, 2018.
- [16] M. Cindric, A. Cipak, J. Serly et al., “Reversal of multidrug resistance in murine lymphoma cells by amphiphilic dihydropyridine antioxidant derivative,” *Anticancer Research*, vol. 30, no. 10, pp. 4063–4069, 2010.

- [17] G. Dubur, B. Vigante, A. Plotniece et al., "Dihydropyridine derivatives as bioprotectors," *Chimica Oggi*, vol. 26, no. 2, pp. 68–70, 2008.
- [18] M. Rucins, P. Dimitrijevs, K. Pajuste et al., "Contribution of molecular structure to self-assembling and biological properties of bifunctional lipid-like 4-(N-alkylpyridinium)-1,4-dihydropyridines," *Pharmaceutics*, vol. 11, no. 3, p. 115, 2019.
- [19] M. Rucins, D. Kaldre, K. Pajuste et al., "Synthesis and studies of calcium channel blocking and antioxidant activities of novel 4-pyridinium and/or N-propargyl substituted 1,4-dihydropyridine derivatives," *Comptes Rendus Chimie*, vol. 17, no. 1, pp. 69–80, 2014.
- [20] M. Petrova, R. Muhamadejev, B. Vigante et al., "Intramolecular C-H...O hydrogen bonding in 1,4-dihydropyridine derivatives," *Molecules*, vol. 16, no. 9, pp. 8041–8052, 2011.
- [21] K. Saotome, H. Morita, and M. Umeda, "Cytotoxicity test with simplified crystal violet staining method using microtitre plates and its application to injection drugs," *Toxicology in Vitro*, vol. 3, no. 4, pp. 317–321, 1989.
- [22] W. S. Stokes, S. Casati, J. Strickland, and M. Paris, "Neutral red uptake cytotoxicity tests for estimating starting doses for acute oral toxicity tests," *Current Protocols in Toxicology*, vol. 36, no. 1, 2008.
- [23] Interagency Coordinating Committee on the Validation of Alternative Methods, ICCVAM test method evaluation report (TMER): *in vitro cytotoxicity test methods for estimating starting doses for acute oral systemic toxicity testing*, 2006, NIH Publication No: 07-4519.
- [24] The national toxicology program (NTP) Interagency center for the evaluation of alternative toxicological methods (NICEATM), *Background review document: in vitro cytotoxicity test methods for estimating acute oral systemic toxicity*, vol. 1, 2006 June 2020 https://ntp.niehs.nih.gov/iccvam/docs/acutetox_docs/brd_tmter/brdvol1_nov2006.pdf.
- [25] The national toxicology program (NTP) Interagency center for the evaluation of alternative toxicological methods (NICEATM), *Background review document: in vitro cytotoxicity test methods for estimating acute oral systemic toxicity*, vol. 2, 2006 June 2020 https://ntp.niehs.nih.gov/iccvam/docs/acutetox_docs/brd_tmter/brdvol2_nov2006.pdf.
- [26] EP, *Regulation (EC) No 1272/2008 of the European Parliament and of the Council of 16 December 2008 on classification, labelling and packaging of substances and mixtures, amending and repealing Directives 67/548/EEC and 1999/45/EC, and amending Regulation (EC)*, Publications office of the European Union, 2008, doi:2004R0726 - v.7 of 05.06.2013.
- [27] G. Apsīte, E. Bisenieks, R. Brūvere et al., *Novel biologically active enaminoester derivatives as agents for chemotherapy, LV15347B*, Espacenet, 2019.
- [28] Z. Hyvönen, A. Plotniece, I. Reine, B. Chekavichus, G. Duburs, and A. Urtti, "Novel cationic amphiphilic 1,4-dihydropyridine derivatives for DNA delivery," *Biochimica et Biophysica Acta (BBA) - Biomembranes*, vol. 1509, no. 1-2, pp. 451–466, 2000.
- [29] A. Plotniece, K. Pajuste, D. Kaldre et al., "Oxidation of cationic 1,4-dihydropyridine derivatives as model compounds for putative gene delivery agents," *Tetrahedron*, vol. 65, no. 40, pp. 8344–8349, 2009.
- [30] K. Pajuste, I. Krivicka, M. Plotniece et al., *The synthesis of new cationic 1,4-dihydropyridine derivatives for DNA delivery, Rigas Teh. Univ. Zinat. Raksti, Ser. 1 Materialzinat. Un Lietiska Kim*, vol. 11, pp. 7–10, 2005, July 2020 <https://ortus.rtu.lv/science/lv/publications/6433>.
- [31] I. Bruvere, E. Bisenieks, J. Poikans et al., "Dihydropyridine derivatives as cell growth modulators in vitro," *Oxidative Medicine and Cellular Longevity*, vol. 2017, 15 pages, 2017.
- [32] R. Muhamadejev, M. Petrova, R. Smits et al., "Study of interactions of mononucleotides with 1,4-dihydropyridine vesicles using NMR and ITC techniques," *New Journal of Chemistry*, vol. 42, no. 9, pp. 6942–6948, 2018.
- [33] R. Smits, Y. Goncharenko, I. Vesere et al., "Synthesis and self-assembly of novel fluorous cationic amphiphiles with a 3,4-dihydro-2(1H)-pyridone spacer," *Journal of Fluorine Chemistry*, vol. 132, no. 6, pp. 414–419, 2011.
- [34] M. Rucins, K. Pajuste, A. Sobolev et al., "Data for the synthesis and characterisation of 2,6-di(bromomethyl)-3,5-bis(alkoxycarbonyl)-4-aryl-1,4-dihydropyridines as important intermediates for synthesis of amphiphilic 1,4-dihydropyridines," *Data in Brief*, vol. 30, p. 105532, 2020.
- [35] K. Pajuste, A. Plotniece, K. Kore et al., "Use of pyridinium ionic liquids as catalysts for the synthesis of 3,5-bis(dodecyloxycarbonyl)-1,4-dihydropyridine derivative," *Central European Journal of Chemistry*, vol. 9, no. 1, pp. 143–148, 2011.
- [36] P. G. Nantermet, J. C. Barrow, H. G. Selnick et al., "Selective α 1a adrenergic receptor antagonists based on 4-aryl-3,4-dihydropyridine-2-ones," *Bioorganic & Medicinal Chemistry Letters*, vol. 10, no. 15, pp. 1625–1628, 2000.
- [37] K. B. Goodman, H. Cui, S. E. Dowdell et al., "Development of dihydropyridone indazole amides as selective rho-kinase inhibitors," *Journal of Medicinal Chemistry*, vol. 50, no. 1, pp. 6–9, 2007.
- [38] X. Huang, S. Broadbent, C. Dvorak, and S. H. Zhao, "Pilot-plant preparation of 3,4-dihydropyridin-2-one derivatives, the core structures of P2X7 receptor antagonists," *Organic Process Research and Development*, vol. 14, no. 3, pp. 612–616, 2010.
- [39] K. T. Homan, K. M. Larimore, J. M. Elkins, M. Szklarz, S. Knapp, and J. J. G. Tesmer, "Identification and structure-function analysis of subfamily selective g protein-coupled receptor kinase inhibitors," *ACS Chemical Biology*, vol. 10, no. 1, pp. 310–319, 2014.
- [40] A. Morales, E. Ochoa, M. Suárez et al., "Novel hexahydrofuro[3,4-b]-2(1H)-pyridones from 4-aryl substituted 5-alkoxycarbonyl-6-methyl-3,4-dihydropyridones," *J. Heterocycl. Chem.*, vol. 33, no. 1, pp. 103–107, 1996.
- [41] B. Vigante, A. Plotniece, M. Rucins et al., "An efficient synthesis of multisubstituted 4-nitrobuta-1,3-dien-1-amines and application in cyclisation reactions," *Tetrahedron*, vol. 74, no. 21, pp. 2596–2607, 2018.
- [42] B. Stanovnik, "Enaminone, enaminoesters, and related compounds in the metal-free synthesis of pyridines and fused pyridines," *European J. Org. Chem.*, vol. 2019, no. 31-32, pp. 5120–5132, 2019.
- [43] J. Wang, X. Guo, Y. Xu, L. Barron, and F. C. Szoka, "Synthesis and characterization of long chain alkyl acyl carnitine esters. Potentially biodegradable cationic lipids for use in gene delivery," *Journal of Medicinal Chemistry*, vol. 41, no. 13, pp. 2207–2215, 1998.
- [44] B. Turovska, J. Stradins, I. Turovskis, A. Plotniece, A. Shmidlers, and G. Duburs, "Electrochemical oxidation of compounds containing 1,4-dihydropyridine and pyridinium rings - analogs of gene transfection agents," *Chemistry of Heterocyclic Compounds*, vol. 40, no. 6, pp. 753–758, 2004.

- [45] H. Lv, S. Zhang, B. Wang, S. Cui, and J. Yan, "Toxicity of cationic lipids and cationic polymers in gene delivery," *Journal of Controlled Release*, vol. 114, no. 1, pp. 100–109, 2006.
- [46] L. Baumane, A. Krauze, S. Belyakov et al., "Synthesis, structure, and electrochemical characteristics of 4-aryl-2-carbamoylmethylthio-5-ethoxycarbonyl-1,4-dihydropyridine-3-carboxylic acid nitriles," *Chemistry of Heterocyclic Compounds*, vol. 41, no. 3, pp. 362–373, 2005.
- [47] B. Turovska, I. Goba, I. Turovskis et al., "Electrochemical oxidation of 4-monoalkyl-substituted 1,4-dihydropyridines," *Chemistry of Heterocyclic Compounds*, vol. 44, no. 12, pp. 1483–1490, 2008.
- [48] L. J. Núñez-Vergara, C. López-Alarcón, P. A. Navarrete-Encina, A. M. Atria, C. Camargo, and J. A. Squella, "Electrochemical and EPR characterization of 1,4-dihydropyridines. Reactivity towards alkyl radicals," *Free Radical Research*, vol. 37, no. 1, pp. 109–120, 2009.
- [49] L. J. Núñez-Vergara, R. Salazar, C. Camargo et al., "Oxidation of C4-hydroxyphenyl 1,4-dihydropyridines in dimethylsulfoxide and its reactivity towards alkylperoxyl radicals in aqueous medium," *Bioorganic & Medicinal Chemistry*, vol. 15, no. 12, pp. 4318–4326, 2007.
- [50] V. Pardo-Jiménez, C. Barrientos, K. Pérez-Cruz et al., "Synthesis and electrochemical oxidation of hybrid compounds: dihydropyridine-fused coumarins," *Electrochimica Acta*, vol. 125, pp. 457–464, 2014.
- [51] Y. P. Stradyn, Y. I. Beilis, Y. R. Uldrikis, G. Y. Dubur, A. E. Sausin, and B. S. Chekavichus, "Voltamperometry of 1,4-dihydropyridine derivatives," *Chemistry of Heterocyclic Compounds*, vol. 11, no. 11, pp. 1299–1303, 1975.
- [52] R. Smits, B. Turovska, S. Belyakov, A. Plotniece, and G. Duburs, "Synthesis of 5-carboxy-6-methyl-3,4-dihydro-2(1H)-pyridone derivatives and their electrochemical oxidation to 2-pyridones," *Chemical Physics Letters*, vol. 649, pp. 84–87, 2016.
- [53] A. Augustyniak, G. Bartosz, A. Čipak et al., "Natural and synthetic antioxidants: an updated overview," *Free Radical Research*, vol. 44, no. 10, pp. 1216–1262, 2010.
- [54] G. Tirzitis, D. Tirzite, and Z. Hyvonen, "Antioxidant activity of 2,6-dimethyl-3,5-dialkoxycarbonyl-1,4-dihydropyridines in metal-ion catalyzed lipid peroxidation," *Czech Journal of Food Sciences*, vol. 19, no. 3, pp. 81–84, 2013.
- [55] S. A. Wildman and G. M. Crippen, "Prediction of physicochemical parameters by atomic contributions," *Journal of Chemical Information and Computer Sciences*, vol. 39, no. 5, pp. 868–873, 1999.
- [56] G. H. Goetz and M. Shalaeva, "Leveraging chromatography based physicochemical properties for efficient drug design," *ADMET DMPK*, vol. 6, no. 2, pp. 85–104, 2018.
- [57] P. Ertl, B. Rohde, and P. Selzer, "Fast calculation of molecular polar surface area as a sum of fragment-based contributions and its application to the prediction of drug transport properties," *Journal of Medicinal Chemistry*, vol. 43, no. 20, pp. 3714–3717, 2000.
- [58] G. Caron and G. Ermondi, "Molecular descriptors for polarity: the need for going beyond polar surface area," *Future Medicinal Chemistry*, vol. 8, no. 17, pp. 2013–2016, 2016.
- [59] Z. Wang, H. Yang, Z. Wu et al., "In silico prediction of blood-brain barrier permeability of compounds by machine learning and resampling methods," *ChemMedChem*, vol. 13, no. 20, pp. 2189–2201, 2018.
- [60] S. Benfeito, C. Oliveira, C. Fernandes et al., "Fine-tuning the neuroprotective and blood-brain barrier permeability profile of multi-target agents designed to prevent progressive mitochondrial dysfunction," *European Journal of Medicinal Chemistry*, vol. 167, pp. 525–545, 2019.
- [61] C. A. Lipinski, "Drug-like properties and the causes of poor solubility and poor permeability," *Journal of Pharmacological and Toxicological Methods*, vol. 44, no. 1, pp. 235–249, 2000.
- [62] S. A. Hitchcock and L. D. Pennington, "Structure-brain exposure relationships," *Journal of Medicinal Chemistry*, vol. 49, no. 26, pp. 7559–7583, 2006.
- [63] Z. E. Suntres, "Liposomal antioxidants for protection against oxidant-induced damage," *Journal of Toxicology*, vol. 2011, Article ID 152474, 16 pages, 2011.
- [64] M. R. Naylor, A. M. Ly, M. J. Handford et al., "Lipophilic permeability efficiency reconciles the opposing roles of lipophilicity in membrane permeability and aqueous solubility," *Journal of Medicinal Chemistry*, vol. 61, no. 24, pp. 11169–11182, 2018.

Research Article

Hyaluronic Acid Improves Hydrogen Peroxide Modulatory Effects on Calcium Channel and Sodium-Potassium Pump in 4T1 Breast Cancer Cell Line

Ardeshir Abbasi ¹, Nafiseh Pakravan ², and Zuhair Mohammad Hassan ¹

¹Department of Immunology, Faculty of Medical Sciences, Tarbiat Modares University, Tehran, Iran

²Department of Immunology, Medical School, Alborz University of Medical Sciences, Karaj, Iran

Correspondence should be addressed to Nafiseh Pakravan; n.pakravan@abzums.ac.ir and Zuhair Mohammad Hassan; hasan_zm@modares.ac.ir

Received 19 April 2020; Revised 19 November 2020; Accepted 10 December 2020; Published 30 December 2020

Academic Editor: Sasanka Chakrabarti

Copyright © 2020 Ardeshir Abbasi et al. This is an open access article distributed under the Creative Commons Attribution License, which permits unrestricted use, distribution, and reproduction in any medium, provided the original work is properly cited.

Maintaining homeostasis of ion concentrations is critical in cancer cells. Under hypoxia, the levels of channels and pumps in cancer cells are more active than normal cells suggesting ion channels as a suitable therapeutic target. One of the contemporary ways for cancer therapy is oxidative stress. However, the effective concentration of oxidative stress on tumor cells has been reported to be toxic for normal cells as well. In this study, we benefited from the modifying effects of hyaluronic acid (HA) on H_2O_2 , as a free radical source, to make a gradual release of oxidative stress on cancer cells while preventing/decreasing damage to normal cells under normoxia and hypoxic conditions. To do so, we initially investigated the optimal concentration of HA antioxidant capacity by the DPPH test. In the next step, we found optimum H_2O_2 dose by treating the 4T1 breast cancer cell line with increasing concentrations (0, 10, 20, 50, 100, 200, 500, and 1000 μM) of H_2O_2 alone or H_2O_2 + HA (83%) for 24 hrs. The calcium channel and the sodium-potassium pumps were then evaluated by measuring the levels of calcium, sodium, and potassium ions using an atomic absorption flame spectrophotometer. The results revealed that treatment with H_2O_2 or H_2O_2 + HA led to an intracellular increase of calcium, sodium, and potassium in the normoxic and hypoxic circumstances in a dose-dependent manner. It is noteworthy that H_2O_2 + HA treatment had more favorable and controllable effects compared with H_2O_2 alone. Moreover, HA optimizes the antitumor effect of oxidative stress exerted by H_2O_2 making H_2O_2 + HA suitable for clinical use in cancer treatment along with chemotherapy.

1. Introduction

Nowadays, cancer therapy includes surgery, radiotherapy, chemotherapy, hormone therapy, and cytokine therapies. However, none of the methods present a complete recovery procedure and even can damage healthy cells/tissues of the body. This raises the need to understand more about the cancer biology and its cross-talk with the immune system whose regulation or activation can be manipulated to develop a new anticancer immunotherapy approach such as immune checkpoint blockade [1]. Metastatic cancers, such as breast cancer, are much more resistant to treatment, and despite the current improvement achieved in immunotherapeutic approaches, their treatment still remains a challenge. 4T1 cell

line originates from mice triple-negative breast cancer with a high metastatic capacity to the lung [2].

It is known that a combination of internal and external factors are involved in the initiation, development, and progression of breast tumors [3, 4]. The maintenance of ion homeostasis is crucial for normal cell life. Several pieces of literature have reported that the role of elements such as calcium (Ca^{2+}), sodium (Na^+), and potassium (K^+) in the proliferation, signaling pathways, and metastatic protection of cancer cells is undeniable. On this basis, the homeostasis of these elements is regarded as an important issue in tumor biology. For example, intracellular Ca^{2+} plays a prominent role in cell function involved by enzyme regulation, gene activation, proliferation, apoptosis, cell cycle, and

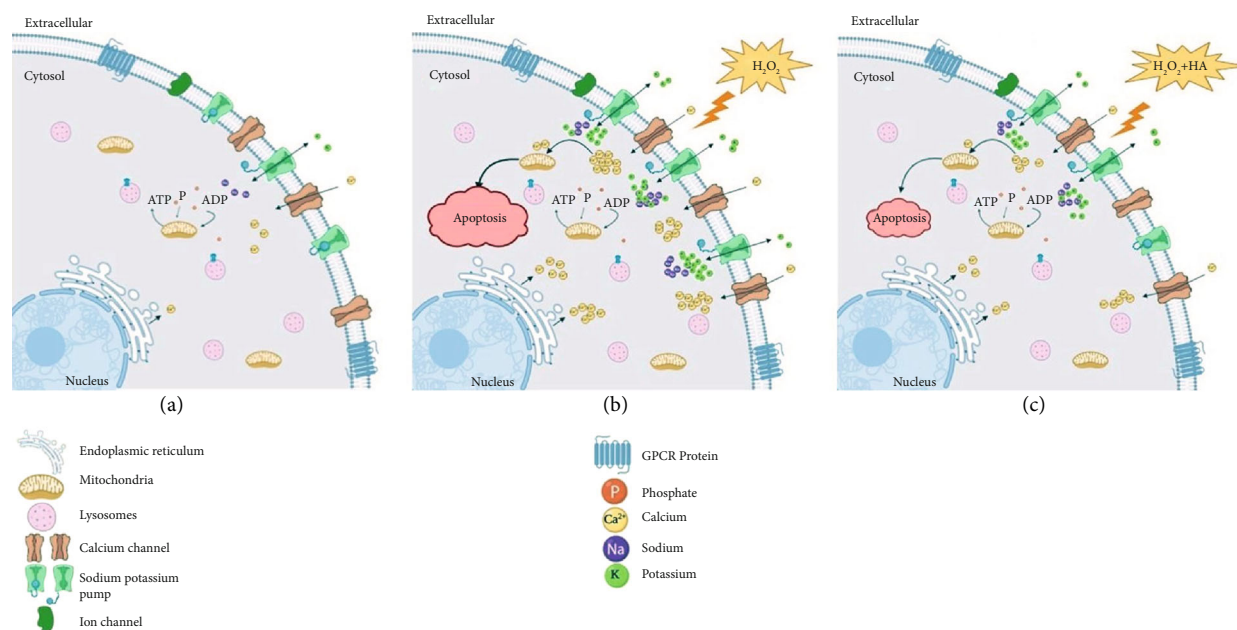


FIGURE 1: Schematic illustration of how H_2O_2 or $\text{H}_2\text{O}_2 + \text{HA}$ functions on 4T1 cell ion channels/pumps. (a) The cell is normal and the channels function well to maintain the homeostasis of cell ions. (b) The membranous channels/pumps of cells exposed to H_2O_2 are disrupted, and the balance of ions is disrupted within the cell causing a severe imbalance due to an increase in intracellular Ca^{2+} , K^+ , and Na^+ . Intracellular Ca^{2+} accumulation induces apoptosis in the cell. (c) HA softens oxidative effects of H_2O_2 , modifies the harsh release of oxidants from H_2O_2 , controls cell proliferation, and gently directs the cell toward apoptosis.

production/performance of transmitters/sensors [5, 6]. Ca^{2+} signaling in cancer is associated with various types of processes in the tumor microenvironment, such as tumorigenesis, proliferation, migration, angiogenesis, and apoptosis escape [7, 8]. It has become evident that Ca^{2+} is required for activities such as cell motility, cell migration, and remodeling of cytoskeleton and extracellular matrix [9]. In addition, the Na^+/K^+ ATPase pump (NKA) as an integrated protein in the cell membrane can maintain the equilibrium Na^+/K^+ between the two sides of the cell membrane. Homeostasis of such an equilibrium is important in metabolic activities of the cell as well as other cellular processes such as proliferation, motility, and apoptosis [10].

There is a piece of considerable evidence demonstrating that the amount of NKA and Ca^{2+} channel is increased to exchange the ions at a higher level than that of the normal cells in cancer cells [11]. Consequently, it can be concluded that the NKA pump and Ca^{2+} channels are good targets for cancer therapy. Given the ability of oxidative stress in disrupting these pumps/channels, oxidative stress can be applied to induce tumor cell death. While ROS regulation at a moderate level is crucial to maintain homeostasis of normal cells to function, higher levels of ROS cause damage to them [12]. One of the most convenient sources of ROS is H_2O_2 . Hydrogen peroxide plays vital roles in pathways which are involved in the regulation of cell proliferation, differentiation, migration, and apoptosis [13, 14]. It follows the importance of precise maintenance of ROS level which affects the flexibility of ion channels/pumps such as Ca^{2+} and Na^+/K^+ [12]. ROS can increase Na^+ level in several ways including (a) changing in the voltage of the Na^+ channel leading to Na^+ accumulation in the cells [15] and (b)

activating the Na^+/H^+ pump promoting Na^+ into the cell [16]. In a simple word, channel disruption causes failure in cell energy production [17] or inhibition of Ca^{2+} extrusion. Additionally, numerous studies have reported dysregulated potassium channel expression in human cancer cases. However, knowledge about the redox modulation of K^+ channel activity is limited. Oxidative stress potentially influences the expression of KV1.5 potassium channel expression in both physiological and pathological conditions [18]. Preclinical studies conducted on the effects of oxidative stress and free radicals on cancer cells have shown that oxidative stress at the administered concentrations might be a possible explanation for the substantial toxicity associated with the clinical management and cancer treatment. Therefore, new approaches are necessitated to target the NKA pump and Ca^{2+} channel using potent agents against cancer with no or least harm for the normal cells. It requires the utilization of reagents mediating the gradual release of free radicals. This would help us to optimize the therapeutic effects of oxidative stress. HA is one candidate to achieve this aim.

To exert and evaluate the effect of oxidative stress on Ca^{2+} , K^+ , and Na^+ concentrations in 4T1 tumor cells, we utilized H_2O_2 along with HA with the aim of suppressing Ca^{2+} channels and NKA pumping and inducing apoptosis tumor cells. HA along with H_2O_2 was used to protect normal cells from oxidative stress damages (see Figure 1).

2. Materials and Methods

2.1. Cell Culture. Mouse breast cancer cell line 4T1 was purchased from the Pasture Institute, Cell Bank of Iran

(NCBI, Tehran, Iran). The cells were cultured in RPMI 1640 medium supplemented with 10% fetal bovine serum (FBS) and 1% glutamine (Sigma Aldrich), 100 IU/ml streptomycin, and 100 IU/ml penicillin at 37°C in 5% CO₂-humidified atmosphere.

2.2. Induction of Normoxic or Hypoxic Condition and Treatments with H₂O₂ and H₂O₂ + HA. Normoxic (18% O₂, 5% CO₂) or hypoxic (1% O₂, 5% CO₂, and 94% N₂) condition was established in two different incubators (Labotec C200, Germany) at 95% humidity. For all tests, 4T1 cancer cells were treated by increasing the concentrations of H₂O₂ (0, 10, 20, 50, 100, 200, 500, and 1000 μM) or H₂O₂ + HA (0.83%) (0, 10, 20, 50, 100, 200, 500, and 1000 μM and HA 0.83%) according to normoxic or hypoxic condition and incubated in two different incubators for 24 hrs.

2.3. Characteristic Hypoxic Model by Anti-PDL-1. To characterize the hypoxic condition, 4T1 cells were seeded in 12-well plates (1 × 10⁵ cells/well) in a regular growth medium and incubated in normoxic (18% O₂, 5% CO₂) and hypoxic (1% O₂, 5% CO₂, and 94% N₂) conditions in two distinct incubators (Labotec C200, Germany) at 95% humidity overnight. Then, cells were collected, washed with phosphate-buffered saline (PBS), and re-suspended in 100 μl PBS. Next, 5 μl anti-PDL-1 mouse antibody conjugated with FITC was added to cells and incubated for 30 minutes at room temperature. Lastly, we added 400 μl flow cytometry staining buffer and performed the flow cytometry, by flow cytometer (BD Biosciences, San Diego, CA, USA). The data were analyzed using FlowJo version 7.6.1.

2.4. Antioxidant Capacity of HA by DPPH Assay. The 2,2-diphenyl-1-picrylhydrazyl (DPPH) radical scavenging assay was performed according to the Blois method with some modifications [19]. Briefly, a 1.0 mM of DPPH radical solution in ethanol was prepared, and then, 1 ml of the solution was mixed with 3 ml of (0, 0.25, 0.5, 0.75, 1%) HA solutions. The absorbance was measured at 517 nm after 30 min. The proportion of DPPH radical scavenging was initially calculated as reported. All experiments were performed three times, and the average values were determined.

Determination of intracellular Ca²⁺, Na⁺, and K⁺ in 4T1 cells was cultured in a six-well in the concentration of 1 × 10⁶ cells/well, incubated for 24 hrs under the normoxic or hypoxic conditions, and treated with H₂O₂ or H₂O₂ + HA for 24 hrs. At the end of the incubation time, the supernatant was discarded and the cells were trypsinized and centrifuged at 1500 rpm for 5 min. 1 × 10⁶ cells were collected and washed twice with Ca²⁺, Na⁺, and K⁺-free wash solution as previously described by Montrose in 1991 [20]. To prepare the solution, 130 mM tetramethylammonium (TMA) chloride (Merck, Germany, no. 822156), 1 mM MgSO₄ (Merck, Germany, no.105886), 2 mM MgCl₂ (Merck, Germany, no.874733), 0.1 mM EGTA (Merck, Germany, no. 99590-86-0), and 10 mM HEPES (Merck, Germany, no. 7365-45-9) were dissolved in ultrapure water, and pH was adjusted at 7.4 using TMA hydroxide (Merck, Germany, no. 75-59-2). Afterward, Ca²⁺, Na⁺, and K⁺ were determined using an

atomic absorption flame spectrophotometer (GBC AA 932). The equipment was calibrated with standard solutions recommended by the manufacturer. All the samples were analyzed in triplicate.

2.5. Statistical Analysis. Statistical difference was determined by one-way and two-way ANOVA analysis of variance using GraphPad Prism 7.0 for Windows (GraphPad Software, Inc., San Diego, CA, USA). **p* < 0.05, ***p* < 0.01, ****p* < 0.001, and *****p* < 0.0001 were considered as significance levels for all analyses performed. Data were presented as mean ± SD in triplicate experiments.

3. Results

3.1. Comparison of PD-L1 Level as Malignancy Marker in Hypoxic and Normoxic Conditions. To determine how hypoxic or normoxic condition affects 4T1 cell line, we used PD-L1 as a marker of malignancy. PD-L1 is one of those markers whose expression is increased under hypoxia conditions and enables tumors to escape from the adaptive immune system [21]. Flow cytometry analysis of 4T1 cells under the normoxic or hypoxic circumstances revealed that the PD-L1 surface expression under the hypoxic conditions significantly increased compared to 4T1 cells under the normoxic condition, as shown in Figure 2.

3.2. Evaluation of Optimizing Effect of HA on H₂O₂. The optimizing effect of HA on H₂O₂ was evaluated using DPPH assay. The results indicated that HA optimized H₂O₂-mediated oxidative stress in a dose-dependent manner. However, HA at concentrations of 1% and 2% did not show a significant difference (see Figure 3). On this basis, effective concentrations were chosen for the subsequent experiments.

3.3. Ca²⁺ Level following Treatment with H₂O₂ or H₂O₂ + HA under Normoxic and Hypoxic Conditions. Intracellular Ca²⁺ level in cancer cells is affected under the influence of micro-environmental conditions and treatments. Treatment with raising concentrations of H₂O₂ increased intracellular Ca²⁺ under normoxic conditions. Accordingly, treatment with H₂O₂ + HA also led to increased intracellular Ca²⁺ content in a dose-dependent manner though the extent of increase was about half that of the treatment with H₂O₂ alone (see Figure 4). Notably, the intracellular Ca²⁺ accumulation in H₂O₂ + HA-exposed cells had a gentler slope in the increment rate than that of the H₂O₂-treated cells in either normoxic or hypoxic conditions. In addition, the intracellular Ca²⁺ accumulation in hypoxic conditions is lower compared to the normoxic condition. This may be due to the adaptation of cancer cells with their specific hypoxic condition of the microenvironment, as demonstrated in Figure 4.

3.4. Treatment with H₂O₂ and H₂O₂ + HA Affects Na⁺ and K⁺ Levels under Normoxia and Hypoxia. In order to investigate the NKA pump function, we examined the changes in intracellular Na⁺ and K⁺ levels. As shown in Figure 5, treatment of cancer cells with increasing concentration of H₂O₂ under normoxic conditions led to increment in intracellular K⁺ and Na⁺ levels as well. However, the rate of increase in K⁺

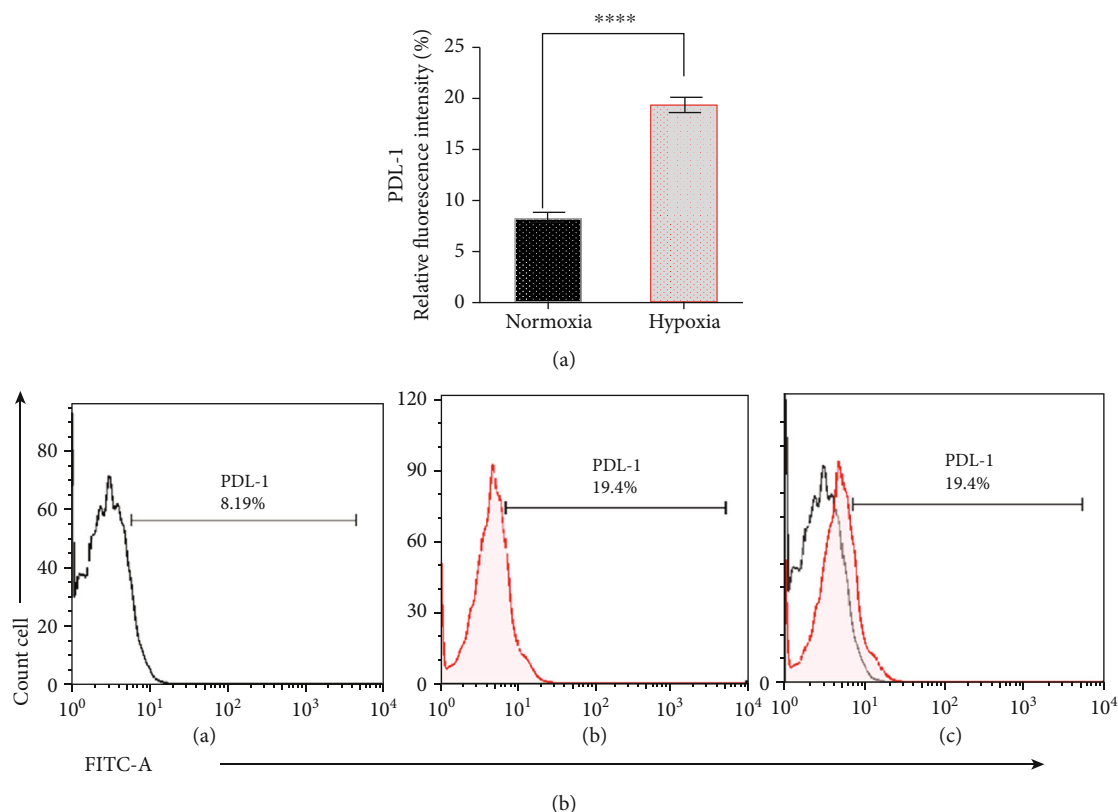


FIGURE 2: Characterization of the hypoxic condition by analysis of PDL-1 expression on 4T1 cancer cell membrane after 24 hrs of incubation (a). Different rate of PDL-1 expression on 4T1 cancer cell membrane under normoxic or hypoxic condition after 24 hrs of incubation (b). (A) Normoxia, (B) hypoxia, and (C) merge of (A) and (B).

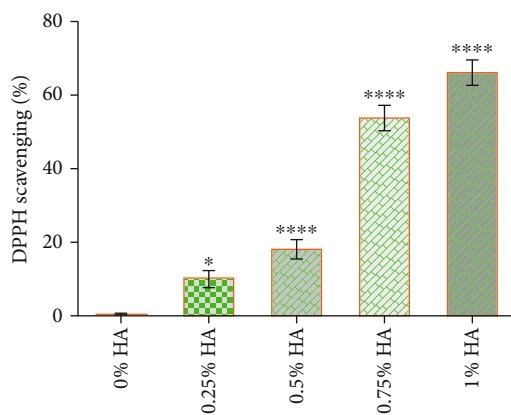


FIGURE 3: Scavenging of DPPH radical by hyaluronic acid: hyaluronic acid was prepared at concentrations of (0, 0.25, 0.5, 0.75, 1%), and then, the modifying capacity of hyaluronic acid on oxidative stress was investigated with the DPPH assay. Data are expressed as mean \pm SD of three independent experiments; undisclosed SDs fall within respective symbols.

was far greater than in Na⁺. Instead, cancer cells treated with H₂O₂ + HA under normoxic conditions had lower intracellular K⁺ and Na⁺ accumulation levels.

The results under hypoxic conditions were similar to those of normoxia. Treatment of cancer cells with H₂O₂ increased the intracellular Na⁺ and K⁺ levels in a dose-

dependent manner. In contrast, treatment of the cells with H₂O₂ + HA caused milder changes compared to the treatment with H₂O₂.

Overall, the comparison of intracellular Na⁺ and K⁺ in cancer cells under hypoxia and normoxia showed that the cells under hypoxia were more resistant to H₂O₂ and H₂O₂ + HA treatment than normoxia (see Figure 5).

4. Discussion

Hypoxia is one of the important features of solid tumors. Several mechanisms are presumed to involve in the development of hypoxic conditions within the tumor foci. They include limited perfusion and/or delivery of O₂ delivery [22]. Tumor cells adapt to persistent hypoxic and harsh conditions and consequently become more invasive and metastatic. This is evidenced by the treatment resistance of tumor cells to a number of anticancer agents. Normal cells typically die in hypoxic conditions while tumor cells adapt to hostile hypoxic microenvironments and remain viable due to hypoxia-mediated proteomic and genomic changes within tumor cells [23].

Despite significant advances toward cancer biology in the last decade, the survival rate of cancer patients has remained insignificant. The approximate failure of the treatment procedure and also the increased cancer cell resistance might be due to several reasons such as (1) hypoxic condition in a cancer microenvironment that plays an essential role in

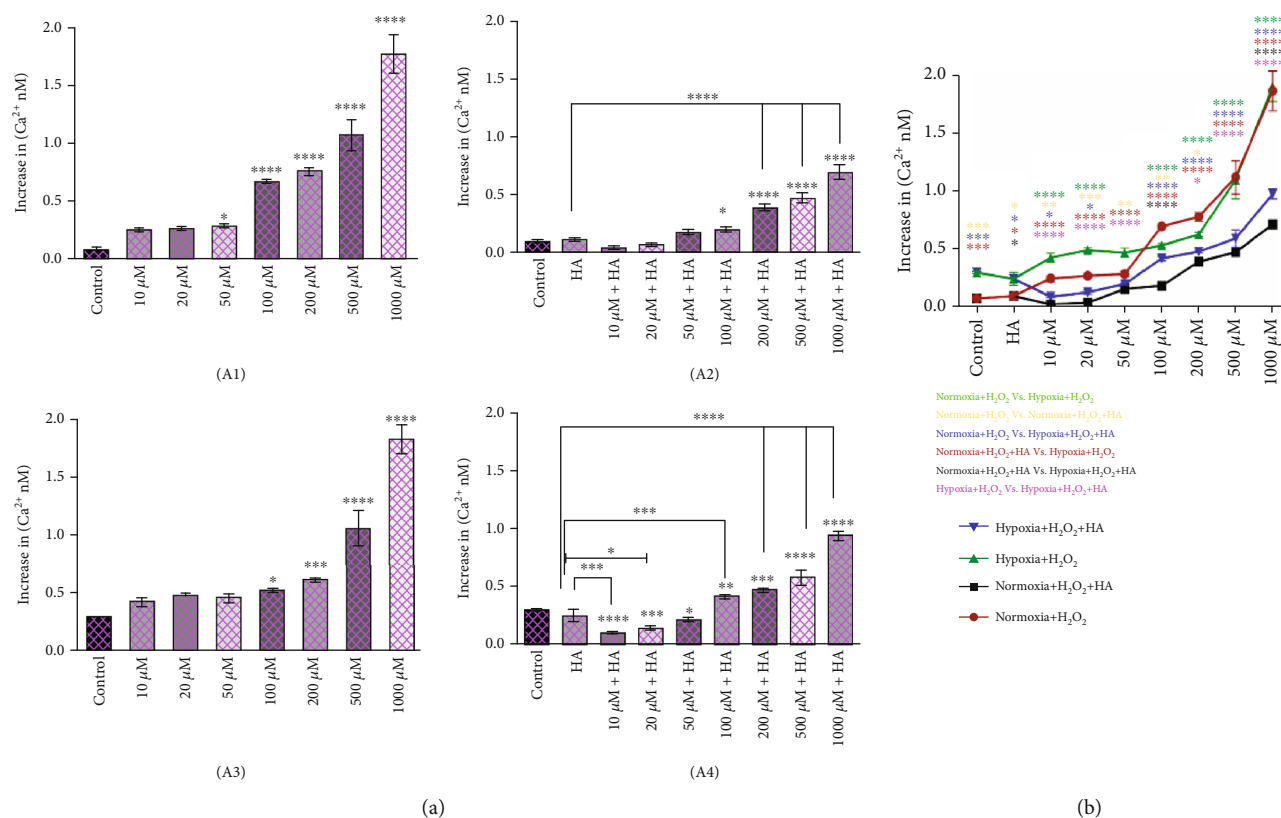


FIGURE 4: Effect of H_2O_2 or $H_2O_2 + HA$ on the intracellular Ca^{2+} levels in breast cancer cells treated under normoxic or hypoxic conditions after 24 hrs of treatment: (a) (a1) Cells under normoxia and treated with H_2O_2 . (a2) Cells under normoxia and treated with $H_2O_2 + HA$. (a3) Cells under hypoxia and treated with H_2O_2 . (a4) Cells under hypoxia and treated with $H_2O_2 + HA$. Data are shown as mean \pm SD ($n = 3$) (* $p < 0.05$, ** $p < 0.01$, *** $p < 0.001$, and **** $p < 0.0001$ vs. respective control). (b) Comparison of intracellular Ca^{2+} levels in 4T1 cancer cells after 24 h of treatments with different concentrations in normoxia and hypoxia conditions determined by scratch assay. Data are shown as mean \pm SD ($n = 3$) (* $p < 0.05$, ** $p < 0.01$, *** $p < 0.001$, and **** $p < 0.0001$ vs. similar concentrations in different conditions. Each index is represented with assigned color in the legend).

tumor survival and resistance, (2) increasing the number of pumps/channels on cancer cells to bypass the apoptotic pathways, and (3) inefficiency of anticancer drugs because of the host condition and side effects. The development, survival, and progression of tumors depend on a combination of internal and external factors of which is the balance of ions [3, 4]. Maintaining the ionic homeostasis and optimal electrical potential is vital for survival in cell biological settings. On this basis, a new approach of drug designation has been developed focusing on ion transport pumps/channels in cell membranes to remove cancer cells. Oxidative stress is one of the novel approaches for cancer therapy. In this regard, many points have not yet been addressed and examined about the pathophysiological effects. This study was based on the premise that ROS kills cancer cells by disrupting the ion transport pumps/channels in cancer cell membranes and eventually induce apoptosis and death in cancer cells.

There are currently therapeutic approaches known as radiotherapy and photodynamic therapy that function based on the production of oxygen radicals within cancer cells [24]. Notably, pretreatment with H_2O_2 in radiotherapy can optimize the cancer microenvironment and improve the efficiency of clinical outcomes [25]. In this approach, ROS production is the mechanism by which apoptosis is induced

in tumour cells [24, 26–29]. Given the point that cancer cells are highly dependent on ROS homeostasis compared to normal cells, they are more sensitive to further variation in their redox homeostasis compared to normal cells. This is because ROS can act as a double-edged sword and affect tumour cells more than normal cells [30]. Presumably, H_2O_2 kills tumour cells via direct induction of ROS production in cancer cells and inhibition of antioxidant machinery as a defence mechanism of cancer cells. The applied concentration of H_2O_2 to kill tumour cells should be optimized depending on the antioxidant potential of cancer cells [31, 32]. Previous studies utilized H_2O_2 as a radiosensitizer material and even H_2O_2 along with sodium hyaluronate have further been used as a radiosensitizer. These approaches are targeted to inactivate cell antioxidant enzymes and produce oxygen from H_2O_2 to decrease hypoxia [33, 34]. Given the important role of oxygen deprivation in tumour adaptation and development, it has been proposed that oxygenation can restore health by destroying cancer cells. Supporters of oxygen therapy claim that low levels of oxygen enable tumour cells to adapt and thrive. Accordingly, oxygenation of tumour cells interferes with their proteomic and genomic changes and destroys them. Hydrogen peroxide is one of the oxygenating agents. The initial idea for the medical use of hydrogen peroxide

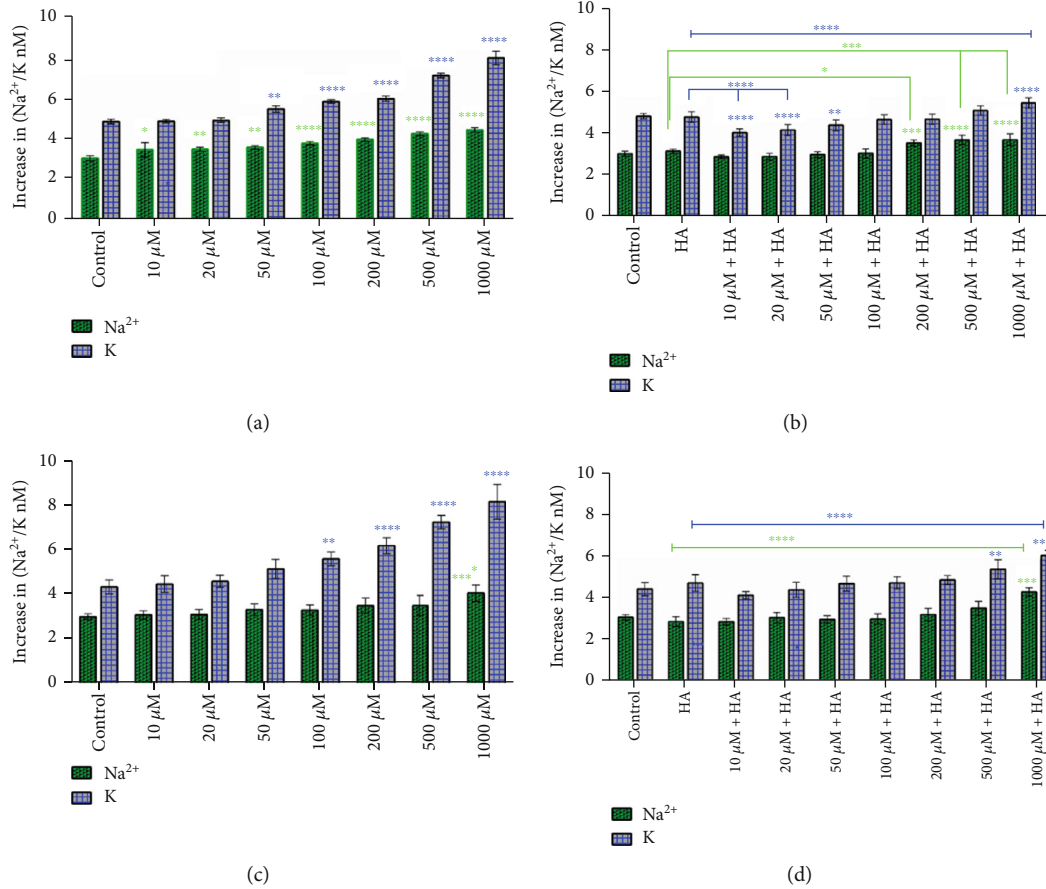


FIGURE 5: Changes in Na^+ and K^+ levels in 4T1 cancer cells treated with different concentrations of H_2O_2 or $\text{H}_2\text{O}_2 + \text{HA}$ under normoxia and hypoxia for 24 hrs. (a) Cells under normoxia and treated with H_2O_2 . (b) Cells under normoxia and treated with $\text{H}_2\text{O}_2 + \text{HA}$. (c) Cells under hypoxia and treated with H_2O_2 . (d) Cells under hypoxia and treated with $\text{H}_2\text{O}_2 + \text{HA}$. Data are expressed as mean \pm SD from three independent experiments (* $p < 0.05$, ** $p < 0.01$, *** $p < 0.001$, and **** $p < 0.0001$ vs. respective control).

dates back to decades ago when antineoplastic hydrogen peroxide was observed [35–38]. However, claims that hydrogen peroxide therapy can increase cellular levels of oxygen have been a matter of debate. Since hydrogen peroxide decomposition and the type of product mainly depend on the micro-environment [39], it may produce OH radical or water and oxygen. On the other hand, HA is one of the chemicals which facilitate the production of oxygen from hydrogen peroxide. Accordingly, it has been shown that hyaluronic acid, commonly used as a drug delivery vehicle [40], is capable of increasing the toxic effects of the oxidative stress mediated by H_2O_2 on tumour cells [41]. This is consistent with the fact that CD44, as major receptor HA, is abundantly expressed on cancer stem cells [42] which facilitates targeting of toxic effects of H_2O_2 on cancer cells. In this study, we utilized hydrogen peroxide along with HA to investigate how it affects 4T1 cell line *in vitro*. H_2O_2 could alternatively be a source of free radicals to exert oxidative stress or could be an oxygen-producing source on cancer cells.

Hydrogen peroxide is one of the inhibitors of PI3K/AKT and the PTEN pathway [18]. Cancer cells adapted themselves to hypoxic conditions to escape from the immune response against cancer. Some of these escape mechanisms include the increase in PDL-1 receptor and elevation of NKA pump

and Ca^{2+} channel levels involved in cellular ion regulation [11]. In this study, the simulation of hypoxic conditions *in vivo* was confirmed in cancer cells by increasing the PDL-1 expression. Previous reports have shown that Ca^{2+} plays a prominent role in tumor proliferation, angiogenesis, invasion, and apoptosis by remodeling of cytoskeleton and extracellular matrix [7, 8, 43]. Ca^{2+} homeostasis is regulated directly and indirectly by different molecules [7, 26, 28]. ROS disrupts these molecules, and subsequently, the membrane channels lose their regulatory function. As a result, disruption of these channels and related molecules changes intracellular Ca^{2+} level, increases Ca^{2+} uptake by mitochondria, and triggers apoptotic pathways leading to cancer cell death. Our results also showed that treatment of cancer cells with H_2O_2 under normoxic and hypoxic conditions increased intracellular Ca^{2+} level suggesting that the Ca^{2+} channels were disrupted. Interestingly, HA softened the H_2O_2 effect and made a gradual release of free radicals under both hypoxic and normoxic conditions.

ROS inhibits and disrupts the NKA pump and increases the Na^+ levels in the cell in several ways including (1) changes the voltage of the NKA pump [15], (2) activates the NKA pump and releases Na^+ into the cell [44], (3) degrades NKA proteasomal complex resulting in reduced expression of the

pump at the membrane surface [45], and (4) activates protein kinase C (PKC) which induces NKA phosphorylation and membrane depolarization [46, 47] all of which lead to cell death. However, knowledge about the redox modulation of the K^+ channel activity is limited. It has been shown that an increase in calcium can alter the K^+ channels and increase K^+ in the cell. Additionally, current data on the effect of oxidative stress on Ca^{2+} -activated K^+ channel (BK_{Ca}) activity in vascular smooth muscle cells suggest that O_2^- and H_2O_2 enhance the BK_{Ca} channel activity [48]. It has also been shown that oxidative stress (O_2^- and H_2O_2) increases the K_{ATP} channel activity in cardiac myocyte vasculature [49]. Moreover, enhanced ATP-dependent K^+ channel activity by H_2O_2 has also been observed in rabbit airway smooth muscle [50]. Our study showed that treatment of cancer cells with H_2O_2 under normoxia or hypoxia led to an increased intracellular Na^+ and K^+ in a dose-dependent manner indicating impaired NKA pumping. In contrast, treatment of cells with $H_2O_2 + HA$ made these changes gradual. This again confirmed the modifying effects of HA on the oxidative stress capacity exerted by H_2O_2 consistent with previous reports in other settings [51]. Unique HA properties include biocompatibility, nontoxicity, and biodegradability which make it suitable to be applied in biomedical applications [52, 53].

Previous studies supported that H_2O_2 increases cell death induced by inhibition of PKC ϵ , PI3K, pAKT, pJAK-2, and pSTAT3 [54]. H_2O_2 also prevents the interaction of AP-1, NF- κ B, and STAT3 transcription factors with DNA [55, 56]. Our results on the effect of H_2O_2 on the NKA pump and Ca^{2+} channels can also be added to the above list as the cause of apoptosis induction by H_2O_2 in cancer cells.

Our results demonstrated that the control cells showed higher K^+ and lower Na^+ concentrations which is supported by previous studies. Increasing evidence suggests that ion channels and pumps not only regulate membrane potential, ion homeostasis, and electric signaling in excitable cells but also play important roles in cell proliferation, migration, apoptosis, and differentiation [57]. In addition, recent analysis has revealed complex interconnections between oncogenic activity, ion channels, hypoxia signaling, and metabolic pathways that are dysregulated in cancerous cells. Normal and tumor cells frequently express distinct pump isoforms. Several changes in the expression of NKA have been observed in cancer cells, such as elevation of activity during the transformation of malignant cells. Roles in cell survival, proliferation, adhesion, and migration have also been described [58–60]. Alterations in K^+ channel subtypes have been confirmed in breast and colon cancer [61]. To maintain the homeostasis of cancer cells, these subunits increase and in some cases decrease; for example, the K2P channel KCNK9 is overexpressed in breast and lung cancer [62]. Recent work has demonstrated that oncogenic stress increases the KCNA1 expression and promotes its relocation from the cytoplasm to the plasma membrane, which is required for oncogene-induced senescence. Ectopic expression of KCNA1 inhibits the RAS-induced transformation, which is related to decreased aggressiveness in breast cancer [63]. In this context, variations in the expression of the different subunits of the enzyme compared to the normal tissues have also been

described. On this basis, cancer has also been named as a channelopathy. Collectively, based on our knowledge, the differences in the expression, function, and activity of ion channels and pumps in cancer cells depend on different factors. These include types of channels, the differences in pump and ion channel isoforms on cancer cells, the type and class of cancer, the metastasis and invasiveness degree, the stage of cancer, and the duration of hypoxia.

We previously evaluated the effect of H_2O_2 or $H_2O_2 + HA$ on 4T1 cancer cells and demonstrated that treatment of 4T1 cells with concentrations higher than 100 μ M of H_2O_2 or 200 μ M of $H_2O_2 + HA$ leads to decreased survival, increased apoptosis, cell cycle disturbance, and decreased expression of MMP2, MMP9, and VEGF genes [26].

Overall, numerous preclinical studies have been done on the effects of oxidative stress on cancer cells with considerations on the dose as oxidative stress at some concentrations may be of higher toxicity and side effects [17]. So finding a way to get this problem under control is essential. In this study, we used HA to overcome toxic and side effects with optimal results. As a result, the effects of H_2O_2 combined with HA may provide us the opportunity to develop and modify cancer treatment using oxidative stress.

5. Conclusion

Our finding suggests considering the inactivation of the NKA pump and Ca^{2+} channels and triggering of cancer cell apoptosis when using chemotherapeutic agents containing oxidative stress. This study also gives an initial image on the rate and ratio of H_2O_2 plus HA usage to put control on our targeted selective and effective oxidative stress therapy.

Data Availability

The data used to support the findings of this study are included within the article.

Conflicts of Interest

The authors declare that they have no conflict of interest.

Acknowledgments

The project is funded by the Tarbiat Modares University.

References


- [1] S. Adams, M. E. Gatti-Mays, K. Kalinsky et al., "Current landscape of immunotherapy in breast cancer," *JAMA Oncology*, vol. 5, no. 8, pp. 1205–1214, 2019.
- [2] P. Lasso, M. Llano Murcia, T. A. Sandoval, C. Urueña, A. Barreto, and S. Fiorentino, "Breast tumor cells highly resistant to drugs are controlled only by the immune response induced in an immunocompetent mouse model," *Integrative Cancer Therapies*, vol. 18, 2019.
- [3] P. Feng, *Zinc inhibits prostate cancer growth: the American society for cell biology 41st annual meeting*, Washington, DC, 2001.

- [4] I. Holcatova and V. Bencko, "Environmental epidemiology of malignancies. The central European perspective," *Central European journal of public health*, vol. 6, no. 1, pp. 13–17, 1998.
- [5] M. D. Bootman, K. Rietdorf, H. Hardy, Y. Dautova, E. Corps, C. Pierro et al., "Calcium signalling and regulation of cell function," *e LS*, 2001.
- [6] L. Munaron, S. Antoniotti, and D. Lovisolo, "Intracellular calcium signals and control of cell proliferation: how many mechanisms?," *Journal of Cellular and Molecular Medicine*, vol. 8, no. 2, pp. 161–168, 2004.
- [7] M. C. Jaramillo and D. D. Zhang, "The emerging role of the Nrf2–Keap1 signaling pathway in cancer," *Genes & Development*, vol. 27, no. 20, pp. 2179–2191, 2013.
- [8] W. Wang, Y. Ren, L. Wang et al., "Orai1 and Stim1 mediate the majority of store-operated calcium entry in multiple myeloma and have strong implications for adverse prognosis," *Cellular Physiology and Biochemistry*, vol. 48, no. 6, pp. 2273–2285, 2018.
- [9] Z. Zhang, C. Sumbilla, D. Lewis, S. Summers, M. G. Klein, and G. Inesi, "Mutational analysis of the peptide segment linking phosphorylation and Ca(2+)-binding domains in the sarcoplasmic reticulum Ca(2+)-ATPase," *Journal of Biological Chemistry*, vol. 270, no. 27, pp. 16283–16290, 1995.
- [10] X. Q. Wang and S. P. Yu, "Novel regulation of Na⁺, K⁺-ATPase by Src tyrosine kinases in cortical neurons," *Journal of Neurochemistry*, vol. 93, no. 6, pp. 1515–1523, 2005.
- [11] M. Baker Bechmann, D. Rotoli, M. Morales et al., "Na, K-ATPase isozymes in colorectal cancer and liver metastases," *Frontiers in physiology*, vol. 7, p. 9, 2016.
- [12] S. A. Castaldo, J. R. Freitas, N. V. Conchinha, and P. A. Madureira, "The tumorigenic roles of the cellular REDOX regulatory systems," *Oxidative Medicine and Cellular Longevity*, vol. 2016, Article ID 8413032, 17 pages, 2016.
- [13] P. A. Madureira, R. Hill, V. A. Miller, C. Giacomantonio, P. W. K. Lee, and D. M. Waisman, "Annexin A2 is a novel cellular redox regulatory protein involved in tumorigenesis," *Oncotarget*, vol. 2, no. 12, pp. 1075–1093, 2011.
- [14] E. A. Veal, A. M. Day, and B. A. Morgan, "Hydrogen peroxide sensing and signaling," *Molecular Cell*, vol. 26, no. 1, pp. 1–14, 2007.
- [15] S. Sossalla, S. Wagner, E. C. Rasenack et al., "Ranolazine improves diastolic dysfunction in isolated myocardium from failing human hearts – role of late sodium current and intracellular ion accumulation," *Journal of Molecular and Cellular Cardiology*, vol. 45, no. 1, pp. 32–43, 2008.
- [16] M. C. Corretti, Y. Koretsune, H. Kusuoka, V. Chacko, J. L. Zweier, and E. Marban, "Glycolytic inhibition and calcium overload as consequences of exogenously generated free radicals in rabbit hearts," *Journal of Clinical Investigation*, vol. 88, no. 3, pp. 1014–1025, 1991.
- [17] N. D. Magnani, L. A. Dada, M. A. Queisser et al., "HIF and HOIL-1L-mediated PKC ζ degradation stabilizes plasma membrane Na, K-ATPase to protect against hypoxia-induced lung injury," *Proceedings of the National Academy of Sciences*, vol. 114, no. 47, pp. E10178–E10186, 2017.
- [18] S. J. Fountain, A. Cheong, J. Li et al., "Kv1.5 potassium channel gene regulation by Sp1 transcription factor and oxidative stress," *American Journal of Physiology-Heart and Circulatory Physiology*, vol. 293, no. 5, pp. H2719–H2725, 2007.
- [19] J. Qu, X. Zhao, Y. Liang, Y. Xu, P. X. Ma, and B. Guo, "Degradable conductive injectable hydrogels as novel antibacterial, anti-oxidant wound dressings for wound healing," *Chemical Engineering Journal*, vol. 362, pp. 548–560, 2019.
- [20] M. Montrose, "Measurement of intracellular sodium and potassium in cultured epithelial cells," *Journal of Tissue Culture Methods*, vol. 13, no. 3, pp. 211–215, 1991.
- [21] H. Onishi, A. Fujimura, Y. Oyama, M. Kawamoto, A. Yamasaki, and T. Morisaki, *Hedgehog Signaling Augments PDL-1 Expression in Cancer Cells under Hypoxic Condition to Inhibit Antitumor Effects by Activated Lymphocytes*, AACR, 2017.
- [22] R. Kumari, D. Sunil, and R. S. Ningthoujam, "Hypoxia-responsive nanoparticle based drug delivery systems in cancer therapy: an up-to-date review," *Journal of Controlled Release*, vol. 319, pp. 135–156, 2020.
- [23] X. Jing, F. Yang, C. Shao et al., "Role of hypoxia in cancer therapy by regulating the tumor microenvironment," *Molecular Cancer*, vol. 18, no. 1, p. 157, 2019.
- [24] C. Ferlini, G. Scambia, M. Marone et al., "Tamoxifen induces oxidative stress and apoptosis in oestrogen receptor-negative human cancer cell lines," *British Journal of Cancer*, vol. 79, no. 2, pp. 257–263, 1999.
- [25] Y. Ogawa, K. Kubota, and M. Tadokoro, "Non-surgical breast-conservation treatment (KORTUC-BCT) using a new image-guided, enzyme-targeted, and breast cancer stem cell targeted radiosensitization treatment (KORTUC II) for patients with stage I or II breast cancer," *Gan no Rinsho*, vol. 57, no. 6, pp. 279–294, 2012.
- [26] A. Abbasi, N. Pakravan, and Z. M. Hassan, "Hyaluronic acid optimises therapeutic effects of hydrogen peroxide-induced oxidative stress on breast cancer," *Journal of Cellular Physiology*, vol. 236, no. 2, pp. 1494–1514, 2021.
- [27] J. Cai, X. Niu, Y. Chen et al., "Emodin-induced generation of reactive oxygen species inhibits RhoA activation to sensitize gastric carcinoma cells to anoikis," *Neoplasia*, vol. 10, no. 1, pp. 41–IN19, 2008.
- [28] Y. Jing, J. Yang, Y. Wang et al., "Alteration of subcellular redox equilibrium and the consequent oxidative modification of nuclear factor κ B are critical for anticancer cytotoxicity by emodin, a reactive oxygen species-producing agent," *Free Radical Biology and Medicine*, vol. 40, no. 12, pp. 2183–2197, 2006.
- [29] A. Yokomizo, M. Ono, H. Nanri et al., "Cellular levels of thiorodoxin associated with drug sensitivity to cisplatin, mitomycin C, doxorubicin, and etoposide," *Cancer Research*, vol. 55, no. 19, pp. 4293–4296, 1995.
- [30] A. V. Snezhkina, A. V. Kudryavtseva, O. L. Kardymon et al., "ROS generation and antioxidant defense systems in normal and malignant cells," *Oxidative Medicine and Cellular Longevity*, vol. 2019, Article ID 6175804, 17 pages, 2019.
- [31] M. S. Alexander, J. G. Wilkes, S. R. Schroeder et al., "Pharmacologic ascorbate reduces radiation-induced normal tissue toxicity and enhances tumor radiosensitization in pancreatic cancer," *Cancer Research*, vol. 78, no. 24, pp. 6838–6851, 2018.
- [32] C. M. Doskey, V. Buranasudja, B. A. Wagner et al., "Tumor cells have decreased ability to metabolize H₂O₂: implications for pharmacological ascorbate in cancer therapy," *Redox Biology*, vol. 10, pp. 274–284, 2016.
- [33] Y. Fang, B. J. Moore, Q. Bai, K. M. Cook, E. J. Herrick, and M. B. Nicholl, "Hydrogen peroxide enhances radiation-induced apoptosis and inhibition of melanoma cell proliferation," *Anticancer Research*, vol. 33, no. 5, pp. 1799–1807, 2013.
- [34] S. Kariya, K. Sawada, T. Kobayashi et al., "Combination treatment of hydrogen peroxide and X-rays induces apoptosis in

- human prostate cancer PC-3 cells,” *International Journal of Radiation Oncology • Biology • Physics*, vol. 75, no. 2, pp. 449–454, 2009.
- [35] C. F. Nathan and Z. A. Cohn, “Antitumor effects of hydrogen peroxide in vivo,” *Journal of Experimental Medicine*, vol. 154, no. 5, pp. 1539–1553, 1981.
- [36] C. F. Nathan, S. C. Silverstein, L. Brukner, and Z. A. Cohn, “Extracellular cytolysis by activated macrophages and granulocytes. II. Hydrogen peroxide as a mediator of cytotoxicity,” *Journal of Experimental Medicine*, vol. 149, no. 1, pp. 100–113, 1979.
- [37] M. K. Samoszuk, C. Rietveld, F. Gidianian, and A. Petersen, “In-vitro sensitivity of Hodgkin's disease to hydrogen peroxide toxicity. Correlation with peroxidase activity,” *Cancer*, vol. 63, no. 11, pp. 2111–2114, 1989.
- [38] H. Sasaki, T. Wakutani, S. Oda, and Y. Yamasaki, “Application of hydrogen peroxide infusion to maxillary cancer,” *Yonago acta medica.*, vol. 11, no. 3, pp. 141–149, 1967.
- [39] H. Sies, “Hydrogen peroxide as a central redox signaling molecule in physiological oxidative stress: oxidative eustress,” *Redox Biology*, vol. 11, pp. 613–619, 2017.
- [40] K. Kim, H. Choi, E. S. Choi, M.-H. Park, and J.-H. Ryu, “Hyaluronic acid-coated nanomedicine for targeted cancer therapy,” *Pharmaceutics*, vol. 11, no. 7, p. 301, 2019.
- [41] R. Akima, Y. Ogawa, S. Morita-Tokuhiro, A. Tsuzuki, and S. Yaogawa, “New enzyme-targeting radiosensitizer (KOR-TUC) containing hydrogen peroxide & sodium hyaluronate for intra-tumoral injection using mice transplanted with SCC VII tumor,” *International Journal of Cancer and Clinical Research*, vol. 3, p. 048, 2016.
- [42] I. Morath, T. Hartmann, and V. Orian-Rousseau, “CD44: more than a mere stem cell marker,” *The International Journal of Biochemistry & Cell Biology*, vol. 81, no. Part A, pp. 166–173, 2016.
- [43] J. Frisch, A. Angenendt, M. Hoth, L. Prates Roma, and A. Lis, “STIM-Orai channels and reactive oxygen species in the tumor microenvironment,” *Cancers*, vol. 11, no. 4, p. 457, 2019.
- [44] A. Sabri, K. L. Byron, A. M. Samarel, J. Bell, and P. A. Lucchesi, “Hydrogen peroxide activates mitogen-activated protein kinases and Na⁺-H⁺ exchange in neonatal rat cardiac myocytes,” *Circulation Research*, vol. 82, no. 10, pp. 1053–1062, 1998.
- [45] F. Thévenod and J. M. Friedmann, “Cadmium-mediated oxidative stress in kidney proximal tubule cells induces degradation of Na⁺/K⁺-ATPase through proteasomal and endo-/lysosomal proteolytic pathways,” *The FASEB Journal*, vol. 13, no. 13, pp. 1751–1761, 1999.
- [46] L. A. Dada, N. S. Chandel, K. M. Ridge, C. Pedemonte, A. M. Bertorello, and J. I. Sznajder, “Hypoxia-induced endocytosis of Na, K-ATPase in alveolar epithelial cells is mediated by mitochondrial reactive oxygen species and PKC- ζ ,” *Journal of Clinical Investigation*, vol. 111, no. 7, pp. 1057–1064, 2003.
- [47] G. A. Gusarova, L. A. Dada, A. M. Kelly et al., “ α 1-AMP-activated protein kinase regulates hypoxia-induced Na, K-ATPase endocytosis via direct phosphorylation of protein kinase C ζ ,” *Molecular and Cellular Biology*, vol. 29, no. 13, pp. 3455–3464, 2009.
- [48] Y. Liu and D. D. Gutterman, “Oxidative stress and potassium channel function,” *Clinical and Experimental Pharmacology and Physiology*, vol. 29, no. 4, pp. 305–311, 2002.
- [49] W. M. Armstead, “Brain injury impairs ATP-sensitive K⁺ channel function in piglet cerebral arteries,” *Stroke*, vol. 28, no. 11, pp. 2273–2280, 1997.
- [50] J. I. Kourie, “Interaction of reactive oxygen species with ion transport mechanisms,” *American Journal of Physiology-Cell Physiology*, vol. 275, no. 1, pp. C1–C24, 1998.
- [51] H. D. Halicka, V. Mitlitski, J. Heeter, E. A. Balazs, and Z. Darzynkiewicz, “Attenuation of the oxidative burst-induced DNA damage in human leukocytes by hyaluronan,” *International Journal of Molecular Medicine*, vol. 23, no. 5, pp. 695–699, 2009.
- [52] P. N. Sudha and M. H. Rose, *Beneficial effects of hyaluronic acid. Advances in food and nutrition research*, vol. 72, Elsevier, 2014.
- [53] E. A. Turley, P. W. Noble, and L. Y. Bourguignon, “Signaling properties of hyaluronan receptors,” *Journal of Biological Chemistry*, vol. 277, no. 7, pp. 4589–4592, 2002.
- [54] N. Khera, M. Singh, and S. Arava, “Immunohistochemical expression of JAK-P, STAT3 & BCL-2 in oral squamous cell carcinoma with and without lymph node metastasis and in verrucous carcinoma”.
- [55] P. Brenneisen, K. Briviba, M. Wlaschek, J. Wenk, and K. Scharfetter-Kochanek, “Hydrogen peroxide (H₂O₂) increases the steady-state mRNA levels of collagenase/MMP-1 in human dermal fibroblasts,” *Free Radical Biology and Medicine*, vol. 22, no. 3, pp. 515–524, 1997.
- [56] G. Martin, R. Andriamanalijaona, M. Mathy-Hartert, Y. Henrotin, and J.-P. Pujol, “Comparative effects of IL-1 β and hydrogen peroxide (H₂O₂) on catabolic and anabolic gene expression in juvenile bovine chondrocytes,” *Osteoarthritis and Cartilage*, vol. 13, no. 10, pp. 915–924, 2005.
- [57] A. Litan and S. A. Langhans, “Cancer as a channelopathy: ion channels and pumps in tumor development and progression,” *Frontiers in Cellular Neuroscience*, vol. 9, p. 86, 2015.
- [58] T. Mijatovic and R. Kiss, “Cardiotonic steroids-mediated Na⁺/K⁺-ATPase targeting could circumvent various chemoresistance pathways,” *Planta Medica*, vol. 79, no. 3/4, pp. 189–198, 2013.
- [59] S. A. Rajasekaran, L. G. Palmer, K. Quan et al., “Na, K-ATPase β -subunit is required for epithelial polarization, suppression of invasion, and cell motility,” *Molecular Biology of the Cell*, vol. 12, no. 2, pp. 279–295, 2001.
- [60] H. Weidemann, “Na/K-ATPase, endogenous digitalis-like compounds and cancer development - A hypothesis,” *Frontiers in Bioscience*, vol. 10, no. 1-3, pp. 2165–2176, 2005.
- [61] N. Comes, J. Bielanska, A. Vallejo-Gracia et al., “The voltage-dependent K⁺ channels Kv1.3 and Kv1.5 in human cancer,” *Frontiers in physiology*, vol. 4, p. 283, 2013.
- [62] D. Mu, L. Chen, X. Zhang et al., “Genomic amplification and oncogenic properties of the *_KCNK9_* potassium channel gene,” *Cancer Cell*, vol. 3, no. 3, pp. 297–302, 2003.
- [63] H. Lallet-Daher, C. Wiel, D. Gitenay et al., “Potassium channel KCNA1 modulates oncogene-induced senescence and transformation,” *Cancer Research*, vol. 73, no. 16, pp. 5253–5265, 2013.

Research Article

Azelaic Acid Exerts Antileukemia Effects against Acute Myeloid Leukemia by Regulating the Prdxs/ROS Signaling Pathway

Dongdong Zhang ^{1,2}, Ziyi Luo ¹, Yanxia Jin,¹ Yanling Chen,¹ Tian Yang,³ Qian Yang ¹, Balu Wu ¹, Yufeng Shang,¹ Xiaoyan Liu ¹, Yongchang Wei ³ and Fuling Zhou ¹

¹Department of Hematology, Zhongnan Hospital, Wuhan University, No. 169 Donghu Road, Wuchang District, Wuhan, 4300071 Hubei Province, China

²Department of Oncology, Xiangyang No. 1 People's Hospital, Hubei University of Medicine, Xiangyang, Hubei 441000, China

³Department of Radiation and Medical Oncology, Zhongnan Hospital, Wuhan University, Wuhan 430071, China

Correspondence should be addressed to Fuling Zhou; zhoufuling@whu.edu.cn

Dongdong Zhang and Ziyi Luo contributed equally to this work.

Received 24 June 2020; Revised 26 November 2020; Accepted 10 December 2020; Published 24 December 2020

Academic Editor: Luciano Saso

Copyright © 2020 Dongdong Zhang et al. This is an open access article distributed under the Creative Commons Attribution License, which permits unrestricted use, distribution, and reproduction in any medium, provided the original work is properly cited.

Acute myeloid leukemia (AML) is a hematological malignancy with a poor prognosis attributed to elevated reactive oxygen species (ROS) levels. Thus, agents that inhibit ROS generation in AML should be exploited. Azelaic acid (AZA), a small molecular compound, can scavenge ROS and other free radicals, exerting antitumor effects on various tumor cells. Herein, this study evaluated the antileukemic activity of AZA against AML via regulation of the ROS signaling pathway. We found that AZA reduced intracellular ROS levels and increased total antioxidant capacity in AML cell lines and AML patient cells. AZA suppressed the proliferation of AML cell lines and AML patient cells, expending minimal cytotoxicity on healthy cells. Laser confocal microscopy showed that AZA-treated AML cells surged and ruptured gradually on microfluidic chips. Additionally, AZA promoted AML cell apoptosis and arrested the cell cycle at the G1 phase. Further analysis demonstrated that peroxiredoxin (Prdx) 2 and Prdx3 were upregulated in AZA-treated AML cells. *In vivo*, AZA prolonged survival and attenuated AML by decreasing CD33⁺ immunophenotyping in the bone marrow of a patient-derived xenograft AML model. Furthermore, mice in the AZA-treated group had an increased antioxidant capacity and Prdx2/Prdx3 upregulation. The findings indicate that AZA may be a potential agent against AML by regulating the Prdxs/ROS signaling pathway.

1. Introduction

Acute myeloid leukemia (AML) is one of the most common hematological malignancies with a rapidly progressive and poor prognosis. Larger numbers of blasts accumulate in the bone marrow and infiltrate other tissues, thus inhibiting hematopoietic functions and inducing subsequent hemorrhage and severe infection. The annual mortality rate is 2.2 per 100,000 [1]. High-dose induction chemotherapy for inhibiting leukemic blast proliferation in the acute stage and consolidation chemotherapy during the remission stage remain the main methods of treating AML; the curative treatment for AML is successful allogeneic stem cell transplantation

after achieving complete remission. However, some patients cannot tolerate the toxic adverse effects of chemotherapeutic drugs and experience chemotherapeutic resistance and severe adverse reactions, such as severe infection, that can lead to treatment failure and result in death.

Reactive oxygen species (ROS) are small short-lived oxygen-containing molecules that regulated many processes, such as cell growth and death, inflammation, stem cell renewal, tumorigenesis, oxygen sensing, angiogenesis, and immune responses [2, 3]. Elevated ROS levels are a major cause of DNA damage and mutation, triggering malignant cell transformation and promoting cancer initiation [4], including the initiation and progression of inherited and

sporadic human leukemias [5]. ROS are frequently elevated in cancer cells [6]. Likewise, AML patients have significantly increased ROS levels and a lower total antioxidant capacity (T-AOC) [7]. Overproduction of NADPH oxidase-derived ROS and Ras-induced ROS can promote the proliferation of AML blasts [8, 9], thus accelerating AML progression [10]. In addition, increased intracellular ROS levels are concomitant with thioredoxin (Trx) and 8-hydroxydeoxyguanosine overexpression, which is associated with AML relapse [7]. Excessive ROS trigger activation of the oncogene, c-Jun activation domain-binding protein 1 (*Jab1*), in AML patient relapse, and the upregulated *Jab1* can regulate Trx by binding to Trx1, which contributes to the poor survival [11]. Additionally, increased ROS levels have been correlated with phenotypic change in hematopoietic stem cells (HSCs) and loss of HSC quiescence, and excessive oxygen limits the lifespan of HSCs by regulating the ROS-p38 MAPK pathway [12].

The roles of ROS depend on their intracellular levels. Low ROS levels are required to initiate and promote tumor growth; moderate ROS levels are involved in the inflammatory response, while high ROS levels contribute to apoptosis and autophagy [13]. Both ROS-elevating and ROS-eliminating strategies have been developed to treat cancer [14]. Over the past several years, ROS-elevating strategies have been predominantly used in clinics, including agents targeting the Prdx2 and Prdx3 to treat AML [15–17]. However, overproduction of ROS induced by chemotherapeutic drugs increases oxidative stress, which can lead to therapeutic resistance and therefore help to drive tumor recurrence [18, 19]. AML patients with FMS-like tyrosine kinase 3 (FLT3) mutations have high relapse rates because FLT3 induces elevated ROS levels [20, 21]. In addition, increased ROS levels accompanied by Trx1 and *Jab1* overexpression are correlated with recurrence and poor survival in AML patients [11]. Furthermore, elevated ROS levels greatly contribute to immunosuppression in the tumor microenvironment [19]. Overproduction of ROS triggers the dysfunction of natural killer and T-cells and inhibits the cytotoxicity of effector cells [22, 23]. Therefore, ROS-eliminating strategies have emerged as a promising approach to treating AML.

Azelaic acid (AZA) is a natural, nontoxic, saturated, nine-carbon dicarboxylic acid that was first recognized as a secondary metabolite in fungal infections with *Malassezia* [24]. AZA, as a competitive inhibitor of tyrosinase [25] and other oxidoreductases, has hypopigmentation and anti-infective properties and is commonly used to treat skin disorders such as melasma and acne [26]. Prior studies demonstrated that AZA can scavenge ROS and inhibit the generation and action of oxygen radicals [27, 28]. AZA can also reversibly inhibit cytochrome-P450 reductase and respiratory chain enzymes [29]. Furthermore, AZA exhibits antitumor effects on several tumor cells, such as lentigo maligna [30], malignant melanoma [31], lymphoma [32], and human T lymphotropic virus 1- (HLTV-1-) infected T-cell leukemia [33], by inhibiting Trx reductase activity, ROS generation, and DNA synthesis in tumor cells [28, 31, 33]. A previous study showed that AZA could suppress AML cell proliferation and sensitize AML cells to chemotherapy [34]. However, the exact mechanism of AZA on AML cells remains unknown. Therefore, in the present

study, we examined the antileukemia activity of AZA and further explored its molecular basis.

2. Materials and Methods

2.1. Materials. DMSO (Cat# D2650) and AZA (Cat# 95054) were purchased from Sigma (USA). PrimeScript™ RT reagent kit with gDNA Eraser was from Takara (Cat# RR047A). Annexin V-FITC Apoptosis Detection Kit was from KeyGEN Biotech (Cat# KGA105-KGA108, China). Cell Cycle Staining Kit was from MultiSciences Biotech (Cat# CCS012, China). Antibodies to the following proteins were used: Prdx3 was from CUSABIO (Cat# CSB-PA003861, China); β -actin (Cat# 14395-1) and Prdx2 (Cat# 10545-2) were from Protein-Tech (USA).

2.2. Cell Culture. AML cell lines U937, HL60, THP-1, and Molm-13 cells were grown in RPMI-1640 medium supplemented with 10% fetal bovine serum and penicillin/streptomycin at 37°C. Different types of AML patient primary cells (AML-PC) according to the FAB classification and healthy peripheral mononuclear cells (PBMCs) were isolated by Ficoll-Hypaque gradient centrifugation followed by the manufacturer's recommendation (TBD sciences, Cat# HY2015, China); the detailed AML patient information can be found in Table S1. Importantly, all subjects were given written informed consent in accordance with the recommendations of the Ethics and Scientific Committee of Zhongnan Hospital of Wuhan University and the Declaration of Helsinki; the Ethics Committee of Wuhan University approval number is 2018278.

2.3. Measurement of ROS. Intracellular ROS levels were measured using the Reactive Oxygen Species Assay Kit (Beyotime, Cat# S0033, China). Briefly, HL60, U937, THP-1, and AML-PC cells were treated with AZA for 24 h, and the collected cells were then washed with serum-free RPMI-1640 and incubated with 2,7-dichlorodihydrofluorescein diacetate (DCF-DA) at the concentration of 5 μ M for 20 minutes at 37°C to assess ROS-mediated oxidation of the fluorescence compound DCF-DA. ROS levels were determined by detecting the fluorescence intensity of the oxidized DCF cytometer, and the flow cytometry analysis results were quantified by using CytExpert2.0 software.

2.4. ROS-Related Index Analysis. HL60, U937, and Molm-13 cells were pretreated with 5 mM AZA for 24 h; cells were collected and washed twice by PBS. Cells were lysed by using the ultrasonic wave breaking, and cell homogenate was centrifuged for 15 minutes at 12,000 rpm at 4°C. Thereafter, supernatant was harvested and stored at -20°C. In vivo experiment, peripheral blood of mice was centrifuged for 15 minutes at 12,000 rpm at 4°C in an anticoagulant tube and the serum was collected from liquid supernatant. The harvested cell supernatant and serum were prepared for the following study. The total antioxidant capacity (T-AOC, Cat# A105), superoxide dismutase (SOD, Cat# A001) activity, glutathione peroxidase (GSH-Px, Cat# A006) content, and malondialdehyde (MDA, Cat# A003) levels were assayed according to the

manufacturer's protocol as described previously (Nanjing Jiancheng Bioengineering Institute, China) [11].

2.5. Analysis of Cell Viability. Cell viability was measured by using a Cell Counting Kit-8 (Dojindo, Cat# JE603, Japan). HL60, THP-1, Molm-13, and different types of AML-PC cells were seeded in a 96-well plate and treated with different concentrations of AZA for 24 h. Thereafter, 10 μ L CCK8 was added to each plate and incubated for additional 2 h. The cell viability was measured by reading the absorbance at 450 nm.

2.6. Cytotoxicity Assays at the Single-Cell Level. To observe the AML cell viability after AZA treatment, THP-1 cells transfected with GFP were used in our study and a DAPI stain was used as a control for indicating all cell numbers in the field. When the GFP⁺-THP-1 cell was dead, the green fluorescence disappeared. The cell viability can be assayed by comparing the green fluorescence intensity between two groups.

To detect the cytotoxic effect of AZA on AML cells, a microfluidic chip was designed to capture the cells and allowing the injection of AZA. The chip size was designed according to the cell size as described previously [35, 36]. Briefly, HL60 cells were injected into the chip and fixed in one inlet, and 5 mM AZA was slowly injected from another inlet. The dynamic changes in the cell morphology after AZA treatment at different time points and fields were observed under microscopy (Nikon).

2.7. Measurement of Mitochondrial Membrane (MMP). Early apoptosis analysis was measured by using the Mitochondrial Membrane Potential Assay Kit with JC-1 (Beyotime, Cat# C2006, China). JC-1 aggregates in the matrix of mitochondria to form a polymer (J-aggregates) and can emit red fluorescence at normal MMP but gets converted to monomer when MMP decreased and then can emit green fluorescence. HL60 cells were treated with 5 mM AZA for 24 h; cells were collected and stained with JC-1 dye. The change in mitochondrial membrane potential was analyzed by flow cytometry.

2.8. Cell Apoptosis and Cell Cycle Assays. The apoptotic rate of U937 cells was detected with the Annexin V/FITC Apoptosis Detection Kit. U937 cells were seeded in 6-well plates and treated with 5 mM AZA for 24 h. The collected cells were washed twice by PBS and stained with 5 μ L Annexin V-FITC and 5 μ L propidium iodide and then incubated for 5 minutes at 25°C. The apoptotic rate was measured by calculating the percentage of FITC and PI-positive cells with flow cytometry.

Cell cycle was measured by using a Cell Cycle Staining Kit. U937 cells were pretreated and collected as above described. Cells were then fixed by 1 mL staining buffer and incubated with 10 μ L propidium iodide for 30 minutes. The number of cells in different phases of the cell cycle was analyzed by flow cytometry. Data were analyzed by using CytExpert2.0 software.

2.9. Protein Mass Spectrometry Analysis (LC-MS). THP-1 cells were treated with 5 mM AZA for 24 h, and total proteins were extracted by RIPA buffer. Then, the peptides from the AZA-treated group and the control group were labeled with isotopomeric dimethyl label. The labeled samples were ana-

lyzed by using a hybrid Quadrupole-TOF Mass Spectrometer as described previously [37] (TripleTOF 5600, AB Sciex Instruments). The raw LC-MS data was accessible on PeptideAtlas, and the direct URL is <http://www.peptideatlas.org/PASS/PASS01499>.

2.10. RNA Isolation, cDNA Preparation, and Quantitative PCR. THP-1 and Molm-13 cells were treated with 5 mM AZA for 24 h. The total RNA was isolated, and the reverse transcription for cDNA was performed by using the Prime-Script[™] RT reagent kit with gDNA Eraser. SYBR-GREEN qPCR was performed to measure the peroxiredoxin 2 (Prdx2) and peroxiredoxin 3 (Prdx3) expression using the SYBR GREEN MIXTURE kit according to the manufacturer's recommendations. The expression level was analyzed using the $2^{-\Delta\Delta CT}$ approach. The primers are listed as follows: GAPDH, sense, 5'-TGATGACATCAAGAAGGTGGTGA-3', antisense, 5'-TCCTTGGAGGCCATG TGGGCCAT-3'; Prdx3, sense, 5'-GCCGCTCTGTGGATGAGACT-3', antisense, 5'-CCAGCTGGGCACACTTCC-3'; Prdx2, sense, 5-GTGTCCCTTCGCCAGATCACT-3', antisense, 5-ACAAAC TTCCCCATGCTCGT-3'.

2.11. Western Blotting Analysis. Molm-13, THP-1, and AML-PC cells were seeded in 6-well plates and treated with 5 mM AZA for 24 h. Total proteins were extracted by RIPA and 10 mM PMSF. Thereafter, protein concentration was determined by the BCA protein assay kit (ThermoFisher, USA). The proteins (20 μ g) were resolved by SDS gel electrophoresis and transferred to PVDF membranes. The membranes were blocked by 5% nonfat milk followed by probing with primary and secondary antibodies.

2.12. Animal Experiment. The B-NSG mice (female, 16-18 g, 5 weeks) were obtained from the Animal Research Center of Wuhan University. AML-PC cells were used to construct the model which were isolated from a hyperleukocytic AML patient sample after undergoing leukapheresis by using a Fresenius COM.TEC machine. Mice were given 1.5 Gy X-ray and injected with 1.0×10^7 human AML cells/per mouse intravenously within 24 h for the development of leukemic disease. The patient-derived xenograft (PDX) AML model was successfully established when AML-PC cells could be observed on the peripheral blood (PB) and bone marrow (BM) smears. Then, mice were randomly divided into two groups with 6 mice in each group. The mice in the AZA group were treated with 10 mg/kg AZA by intraperitoneal injection (200 μ L, every three days, $n = 8$), while the control group ($n = 8$) received saline with the same volume and frequency. At the end of experiments, mice were sacrificed and the tissues were harvested for further study. Importantly, all animal studies were approved by the Institutional Animal Care and Use Committee of Wuhan University (2017048).

2.13. Smear Analysis and Immunohistochemistry. After injecting mice with AML-PC cells for one week, we randomly selected one mouse which was humanly killed, and its PB and BM were harvested. PB and BM smears were stained with Wright's stain and observed microscopically to measure the

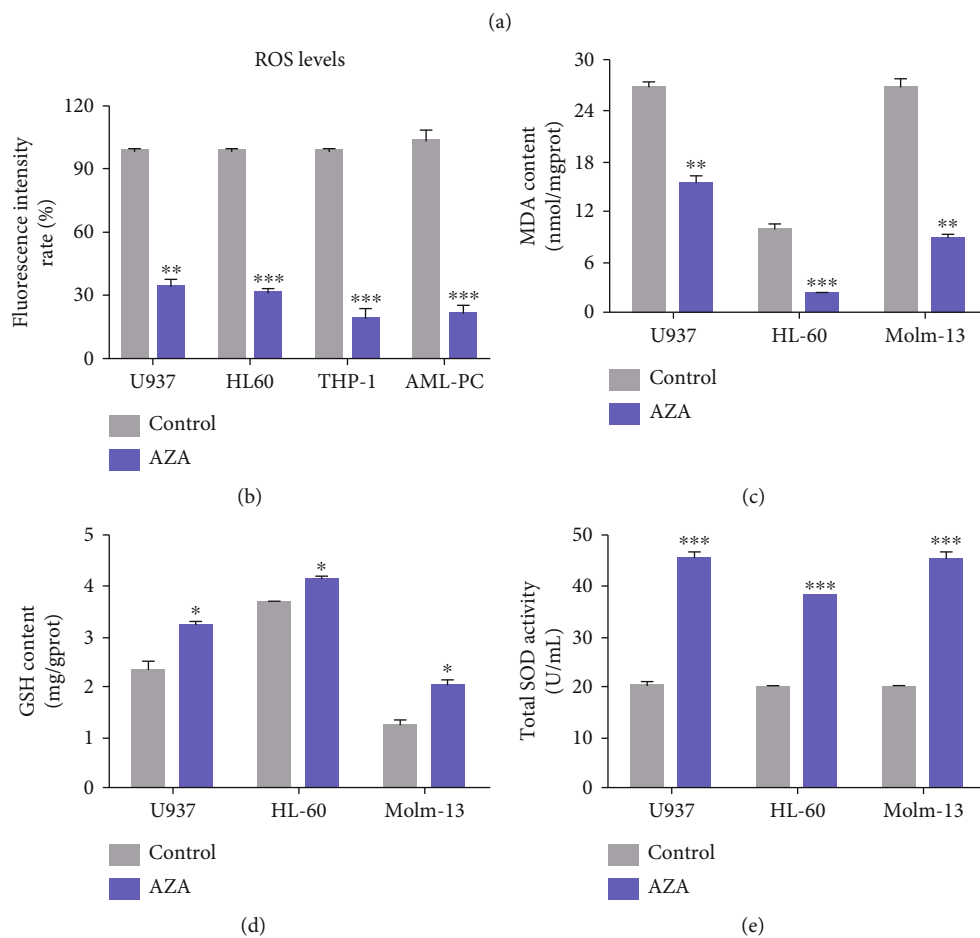
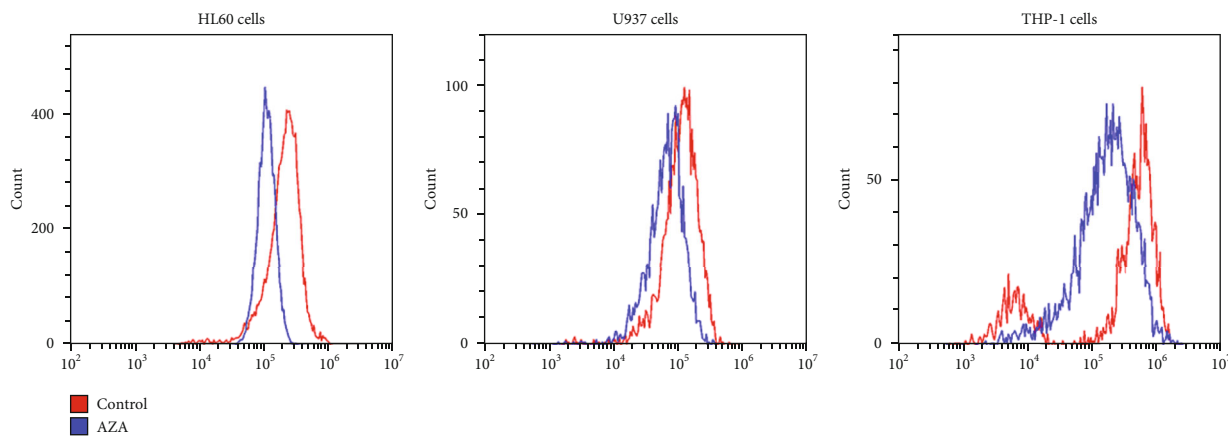


FIGURE 1: Continued.

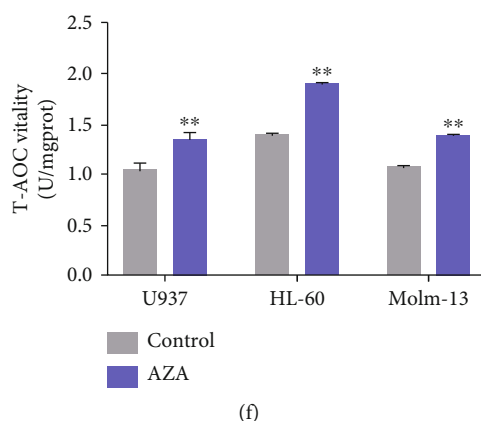


FIGURE 1: AZA decreased intracellular ROS levels and increased the antioxidant capacity. (a) U937, HL60, and THP-1 cells were treated with 5.0 mM c-AZA for 24 h. The collected cells were stained with DCF-DA, and ROS levels were analyzed by flow cytometry. (b) Statistical analysis of the intracellular ROS levels after AML cell lines and AML patient cells were treated with 5 mM AZA for 24 h. (c–f) U937, HL60, and Molm-13 cells were treated with 5.0 mM AZA for 24 h. The cell homogenates were harvested, and ROS-related indices were tested with kits as described in the methods. (c) MDA; (d) GSH; (e) SOD; (f) T-AOC. Each experiment was repeated three times, * $P < 0.05$, ** $P < 0.01$, and *** $P < 0.001$.

proportion of leukemia cells and determine whether the PDX model was constructed successfully [38].

Tissues collected from the mice were fixed, trimmed, processed, dewaxed, and rehydrated, then under pretreated for antigen retrieval in citrate buffer at pH 6.0 at 100°C for 30 minutes. Thereafter, tissues were blocked with primary antibodies (Prdx2 and Prdx3 antibodies, 1:100) overnight, then probed with secondary antibodies. Images were photographed using a Nikon microscope at the Hematology Department, Wuhan University, Zhongnan Hospital, Wuhan, China.

2.14. Bioinformatics and Statistical Analysis. Differentially expressed proteins were identified via LC-MS, annotated by WEGO analysis (<http://wego.genomics.org.cn/>), and analyzed with R code by creating a heat map. The protein-protein interaction networks were analyzed using STRING v11.0 (<https://string-db.org/cgi/network>). Data are presented as the means \pm standard deviations and were analyzed via Student's *t*-test and one-way analysis of variance using GraphPad Prism 7 and IBM SPSS. $P < 0.05$ was considered statistically significant.

3. Results

3.1. AZA Decreased Intracellular ROS Levels and Increased Antioxidant Capacity. Prior studies demonstrated that AML patients had elevated intracellular ROS levels and AZA could scavenge the ROS [28]. We detected the ROS levels and ROS-related indices in HL60, THP-1, and U937 cells and human AML cells after treatment with AZA. As expected, AZA markedly decreased the intracellular ROS levels in the AML cell lines and AML patient cells (Figures 1(a) and 1(b)). Furthermore, in the AZA-treated cell homogenate, the oxidative injury indexes, such as the MDA content (Figure 1(c)), were decreased, while the antioxidant injury indexes, such as the SOD and GSH activity and the total antioxidant capacity, were significantly increased (Figures 1(d)–1(f)).

3.2. AZA Exhibited Cytotoxicity against AML Cells. In our previous study, we have identified that AZA had an antiproliferative effect on different AML cell lines, the IC₅₀ value of AZA for 24 h was ranged from 3.4 to 7.2 mM, and the median IC₅₀ value was approximately 5 mM [34], so we chose the concentration of 2.5, 5.0, and 10.0 mM for our present cytotoxicity assay. AZA markedly suppressed AML cell lines and different types of AML patient cell proliferation dose-independently as described in our previous study (Fig. S1). Additionally, GFP⁺ Molm-13 cells revealed hypofluorescence after treatment with 5 mM AZA for 24 h compared to the control group; this result also indicated AZA could inhibit AML cell viability (Figure 2(a)). However, the same concentration of AZA had little toxicity on PBMC and other healthy cell lines such as 293T, hFOB 1.19, MC3T3-E1, and AML 12 cells (Figure 2(b)). Even so, we believe that more experiments would be required to show that AZA is really more toxic to AML cells compared to hematopoietic stem and progenitor cells.

To observe the cytotoxicity of AZA on AML cells at the single-cell level, we designed a microfluidic chip that can trap cells and injected AZA into the chip from two opposite directions (Figure 2(c)). The HL60 cell morphology became swollen, apoptotic bodies were detected, and the cells ultimately showed lysis after continuous AZA treatment on the microfluidic chips (Figure 2(d)).

3.3. AZA Promoted AML Cell Apoptosis. Loss of MMP is common in the early stages of apoptosis. AZA induced a significant loss of MMP as measured by the percentage of JC-1 monomer cells (Figure 3(a)). AZA markedly increased the percentage of Annexin-V/FITC-positive cells (Figure 3(b)). Furthermore, the cell cycle was arrested at the G₁/G₀ phase after AZA treatment (Figure 3(c)). However, the same AZA concentration had no toxicity on PBMC isolated from healthy people (Figures 3(d) and S2).

3.4. AZA Upregulated Prdx2 and Prdx3 in AML Cells. To understand the molecular basis for the antileukemic activity

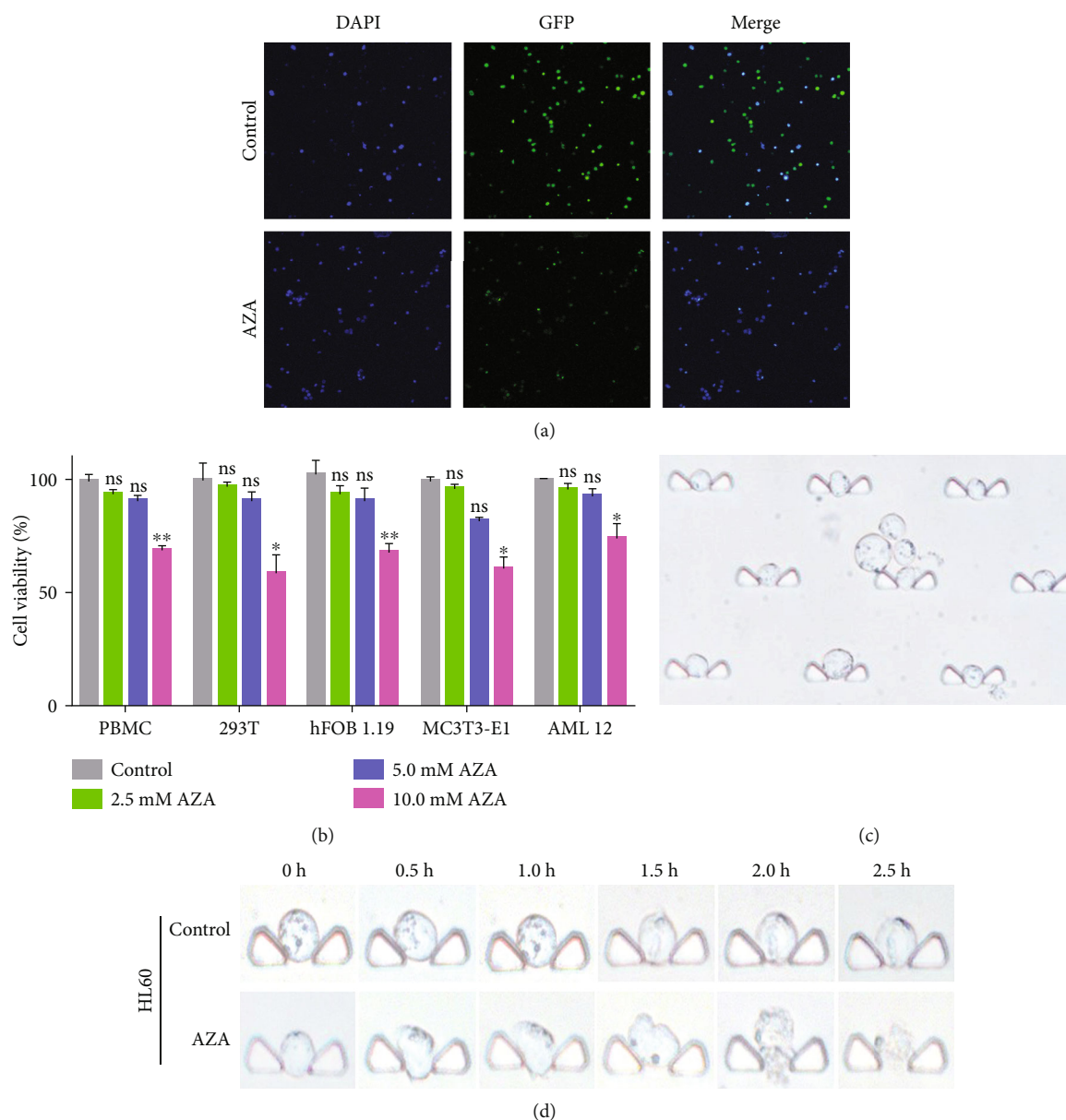


FIGURE 2: AZA inhibited AML cell proliferation and had a little toxic effect on healthy cells. (a) Molm-13 GFP⁺ cells were treated with 5 mM AZA for 24 h and then observed under a fluorescence microscope; DAPI was used as a control. Magnification: $\times 40$. (b) Healthy cell lines such as PBMC, 293T, hBOT 1.19, MC3T3-E1, and alpha mouse live cells were treated with different concentrations of AZA for 24 h. Cell viability was measured by the CCK-8 method. (c) HL60 cells were trapped on a microfluidic chip and observed under a microscope. (d) HL60 cells were treated with 5 mM AZA on the microfluidic chip, and the cell motion morphology was observed at the single-cell level under a microscope. Magnification: $\times 60$. Each experiment was repeated three times, * $P < 0.05$, ** $P < 0.01$, and *** $P < 0.001$.

of AZA, we performed LC-MS analysis. Differentially expressed proteins (DEPs) were identified after AZA treatment. The DEPs were then annotated by WEGO analysis as described previously [38]. Five hundred and twenty-eight DEPs were annotated into three areas: cellular components, molecular functions, and biological processes. The potential DEPs involved in antioxidant activity and immune response were analyzed by a heat map (Figure 4(a)). LC-MS data showed that AZA upregulated Prdx2 and Prdx3 with approximately 2.0-fold higher Prdx3 expression in AZA-treated THP-1 cells than in the control group. The Prdx system played a crucial role in decreasing intracellular ROS levels

and maintaining the redox balance [39]. Prdx2 and Prdx3 were the main ROS-scavenging antioxidant enzymes in the Prdx system. Thus, Prdx3 was selected for further analysis.

We performed quantitative real-time PCR and western blotting to confirm this finding. Consistent with our MS results, AZA induced higher Prdx2 and Prdx3 RNA and protein expressions (Figures 4(b) and 4(d)). Finally, we used STRING to analyze the proteins that interacted with Prdx3 and found that Prdx3 interacted with many antioxidant enzymes, including catalase (CAT) and SOD2 (Figure 4(c)), which were also upregulated after AZA treatment as shown in Figure 4(a). This result was also validated by further

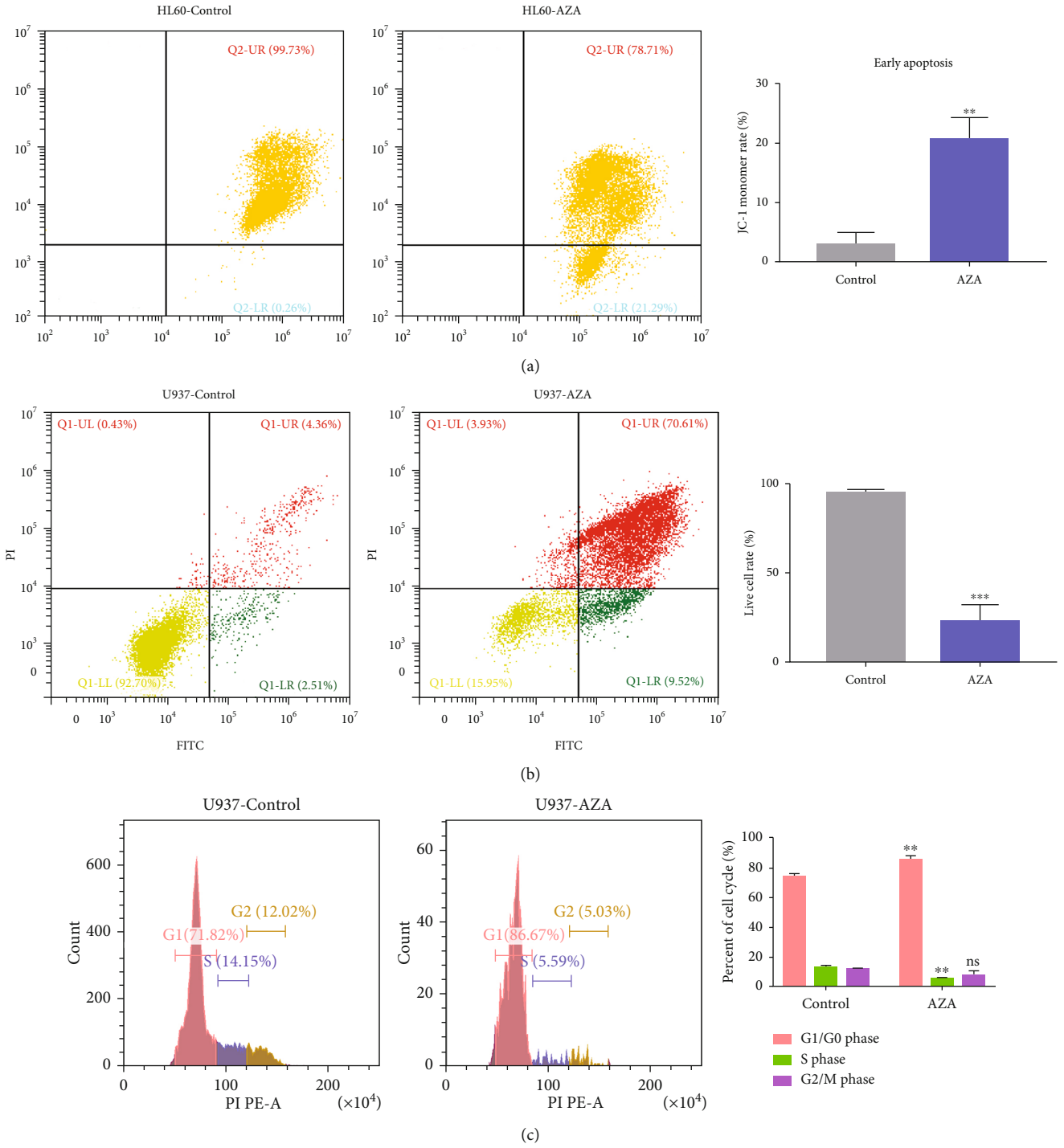


FIGURE 3: Continued.

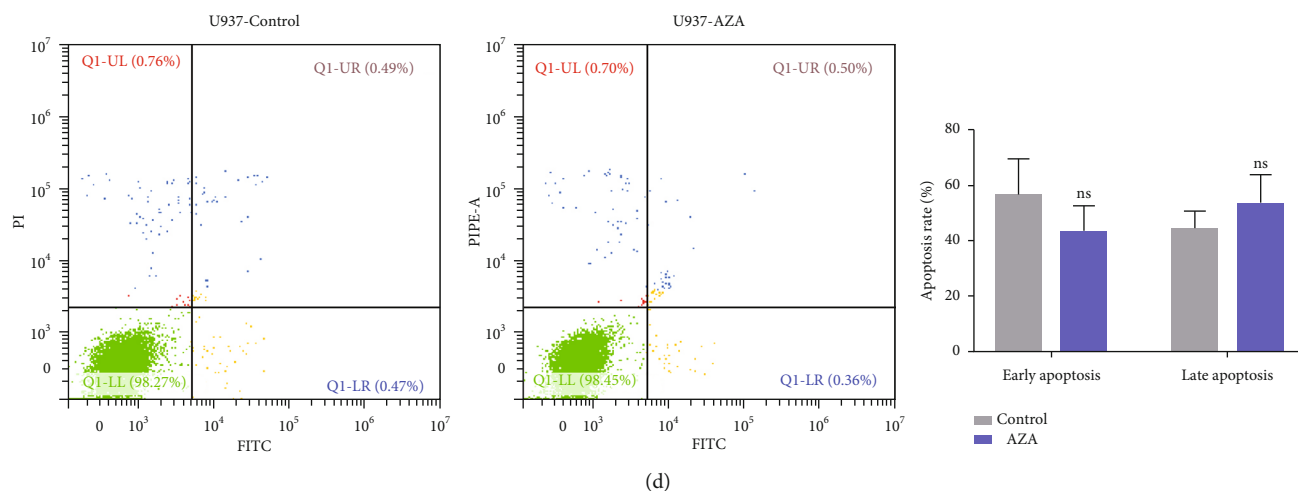


FIGURE 3: AZA promoted AML cell apoptosis. (a) HL60 cells were treated with 5.0 mM AZA for 24 h. The collected cells were stained with JC-1 dye, and the MMP was analyzed by flow cytometry. (b) U937 cells were treated with 5.0 mM AZA for 24 h. The collected cells were stained with Annexin V and PI. Cell apoptosis rate was analyzed by flow cytometry. (c) Cell cycle was analyzed by flow cytometry after U937 cells were treated with 5.0 mM AZA for 24 h. (d) Cell apoptosis rate was analyzed by flow cytometry after healthy PBMCs were treated with 5.0 mM AZA for 24 h. Each experiment was repeated three times, $**P < 0.01$ and $***P < 0.001$. ns: no significance.

analysis by using RT-PCR and WB in Fig. S3. This unexpected finding indicated that the upregulation of SOD2 and CAT caused by AZA may have a synergetic effect with Prdx3 on decreasing intracellular ROS levels. Many nutraceuticals and antioxidants, such as vitamin C, selenium, and lycopene, have been developed for cancer prevention and treatment as they can scavenge ROS [14]; likewise, AZA can exert antileukemic effects by decreasing ROS levels via upregulation of Prdx2 and Prdx3.

3.5. AZA Repressed the Leukemic Growth In Vivo. To test whether AZA could repress leukemia *in vivo*, we constructed a PDX AML model as per a previous report [40]. Briefly, B-NSG mice were intravenously injected with 1.0×10^7 CD33⁺ AML patient primary cells after 1.5 Gy irradiation. When PB and BM smears indicated illness, mice were randomly divided into two groups ($n = 8$). AZA was administered every three days for 2 weeks; saline was administered as a negative control. The PDX AML models progressed rapidly, and most mice died within 18–27 days; thus, all mice were sacrificed on day 21, and their tissues were harvested for further study (Figure 5(a)). AML patient cells could be observed on the PB and BM smears one week after the injection, and the leukemic blasts could be observed on the BM and spleen by hematoxylin and eosin stain, which indicated the development of leukemia disease (Figures 5(b) and S4). Mice in the AZA group lost weight more slowly and survive longer than did mice in the saline group (Figures 5(c) and 5(d)). Additionally, the percentage of CD33⁺ AML cells in the BM was significantly decreased in the AZA group compared with the saline group, suggesting disease remission (Figure 5(e)). Importantly, compared with the saline group, the MDA levels were decreased, while the T-AOC, GSH levels, and SOD activity were increased in the AZA group in the mouse blood plasma (Figure 5(f)). Moreover, higher Prdx2 and Prdx3 expressions occurred in the AZA group than in the saline group on BM biopsies detected via immunohistochemical staining in the PDX AML model

(Figure 5(g)). These results were consistent with the *in vitro* experimental results.

These results suggest that AZA decreases intracellular ROS levels and increases the antioxidant capacity by upregulating Prdx2 and Prdx3, thus maintaining the redox balance and further suppressing AML *in vitro* and *in vivo*.

4. Discussion

AML has a high incidence of relapse and poor prognosis, one of the main reasons is therapeutic resistance. Although emerging targeted drugs and immunotherapies may benefit some patients, they are limited in their applications. Tyrosine kinase inhibitors (TKI) can be used only in patients with FLT-3 mutations and patients who develop resistance [41]. Immune checkpoint inhibitors (ICIs) are effective in malignancies with high mutational burden, but ICIs have little effect on AML because AML patients have the lowest mutational burden [42]. Chimeric antigen receptor T-cell (CAR-T) therapy also has a modest effect on AML because of the lack of leukemia-specific cell surface antigens [43, 44]. Therefore, novel agents and therapeutic approaches should be exploited.

ROS are generated from multiple sources. The main source of intracellular ROS is the mitochondria. Healthy cells control the intracellular ROS balance via the scavenging system [45]. One major scavenging system by which mitochondria neutralize excess ROS is through a dedicated Prdx system comprising Prdx3. Prdx3 is exclusively located in the mitochondria. Prdx3 is the most abundant and efficient H₂O₂-eliminating enzyme involved in detoxifying 90% of H₂O₂ [8]. Deleting of Prdx3 results in H₂O₂ accumulation and elevated ROS levels in the mitochondria [46]. Prdx2 is a cytoplasmic Cys-dependent peroxidase with the highest affinity of H₂O₂ [45]. Early studies showed that Prdx2 inhibited the myeloid cell proliferation by reducing ROS levels and acted as an epigenetically silenced tumor suppressor in AML [47]. In addition, activation of Prdx2 by depletion of cyclin-

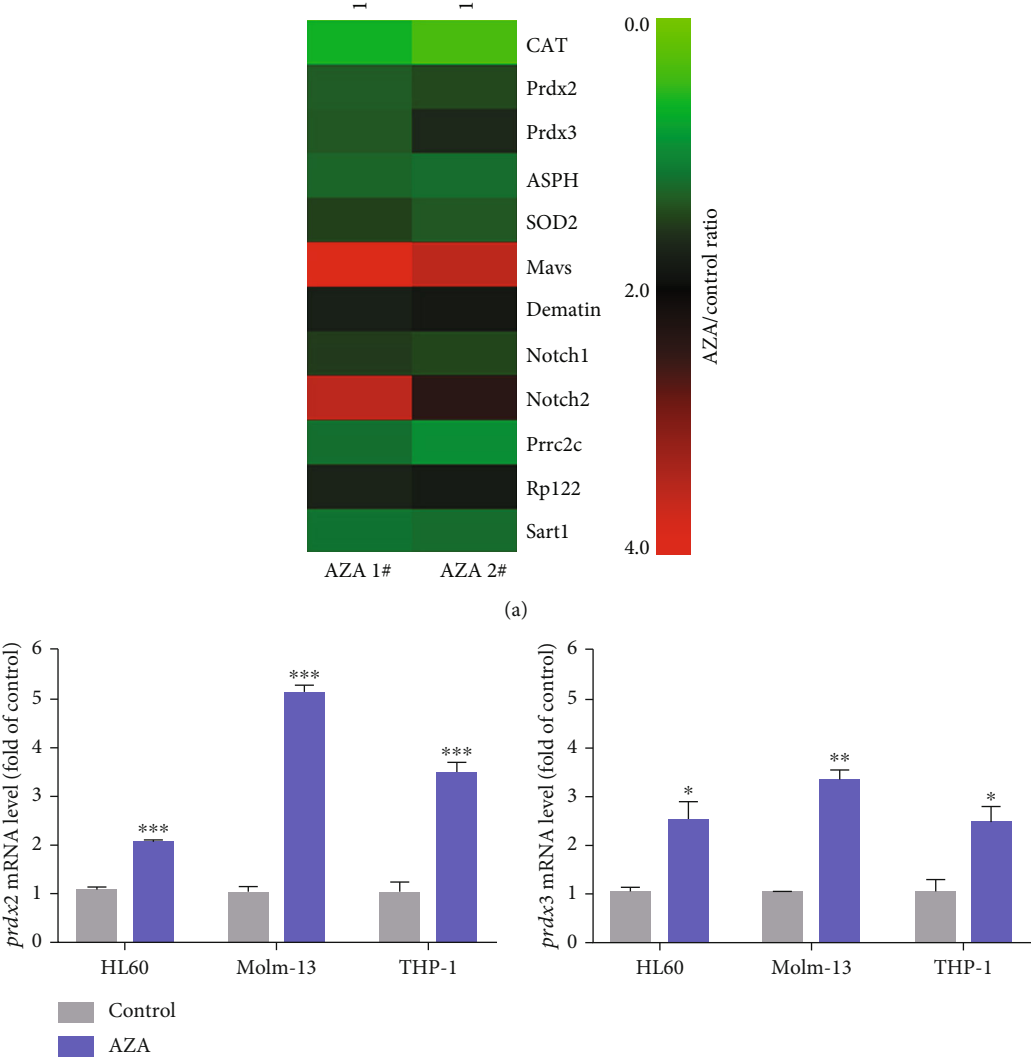


FIGURE 4: Continued.

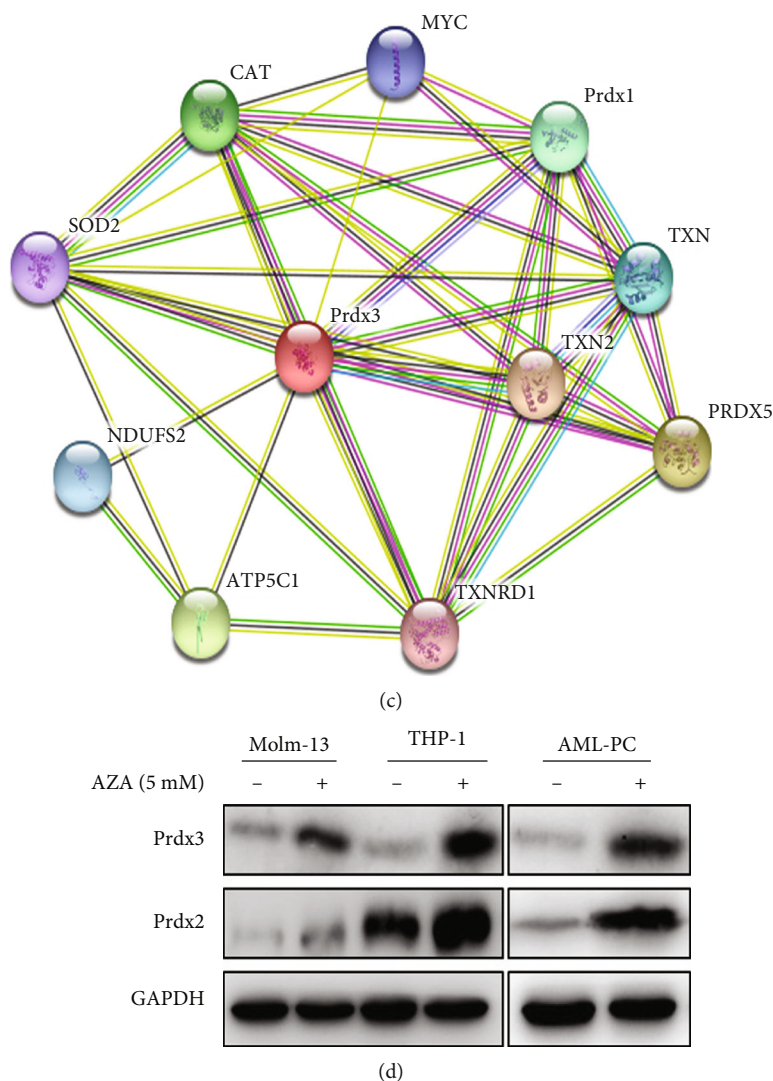


FIGURE 4: AZA upregulated Prdx2 and Prdx3 expression. (a) Differentially expressed proteins (DEPs) were identified by LC-MS/MS after AZA treatment. Then, DEPs were annotated by WEGO analysis; the changes of DEPs involved in antioxidant activity and immune response were shown on a heat map. (b) The RNA expression levels of Prdx2 and Prdx3 in Molm-13 and THP-1 cells after AZA treatment and their detection by qPCR. (c) The interaction between Prdx3 and other proteins was analyzed by STRING. (d) The protein expression levels of Prdx2 and Prdx3 in Molm-13, THP-1, and AML patient primary cells (AML-PC) after AZA treatment and their detection by western blot.

dependent kinase 2 (CDK2) can drive the therapeutic differentiation of AML [48]. Moreover, Prdx3 and Prdx2 have been associated with cancer aggressiveness and patient survival, and higher Prdx2 and Prdx3 expressions were associated with less aggressiveness and longer survival [47, 49]. In our study, we identified that AZA increased Prdx2 and Prdx3 expressions, thus regulating the redox state by decreasing ROS levels to suppress AML growth.

Identifying agents that can decrease intracellular ROS levels is a potential method of treating cancer. Lycopene can suppress the progression of prostate carcinoma by decreasing oxidative DNA damage and scavenging ROS [50, 51]. Some clinical trials showed selenium and vitamin C supplementation could decrease the incidence and mortality of gastric and lung cancer [52, 53]. One study demonstrated selenium exerted antileukemia effect by increasing antioxidant capacity [54]. A previous

study showed that AZA exhibited antitumor effects against melanoma by inhibiting ROS generation and reducing oxidative tissue injury [28]. In the present study, AZA inhibited AML proliferation by decreasing intracellular ROS levels and increasing the antioxidant capacity. Further analysis of the mechanisms by quantitative proteomics, qPCR, western blot, and immunohistochemistry identified that antioxidative Prdx2 and Prdx3 were upregulated after AZA treatment. Accordingly, we concluded that AZA exerts antileukemic effects by regulating the Prdxs/ROS signaling pathway.

AZA exerts antitumor effects at micromole concentration, it was usually topical application in the form of water-miscible or gel for the treatment of skin disorder with only mild additional side effects; however, when it was administered orally or intraperitoneal injection in the form of solution, it could cause noticeable weight loss and acid-base

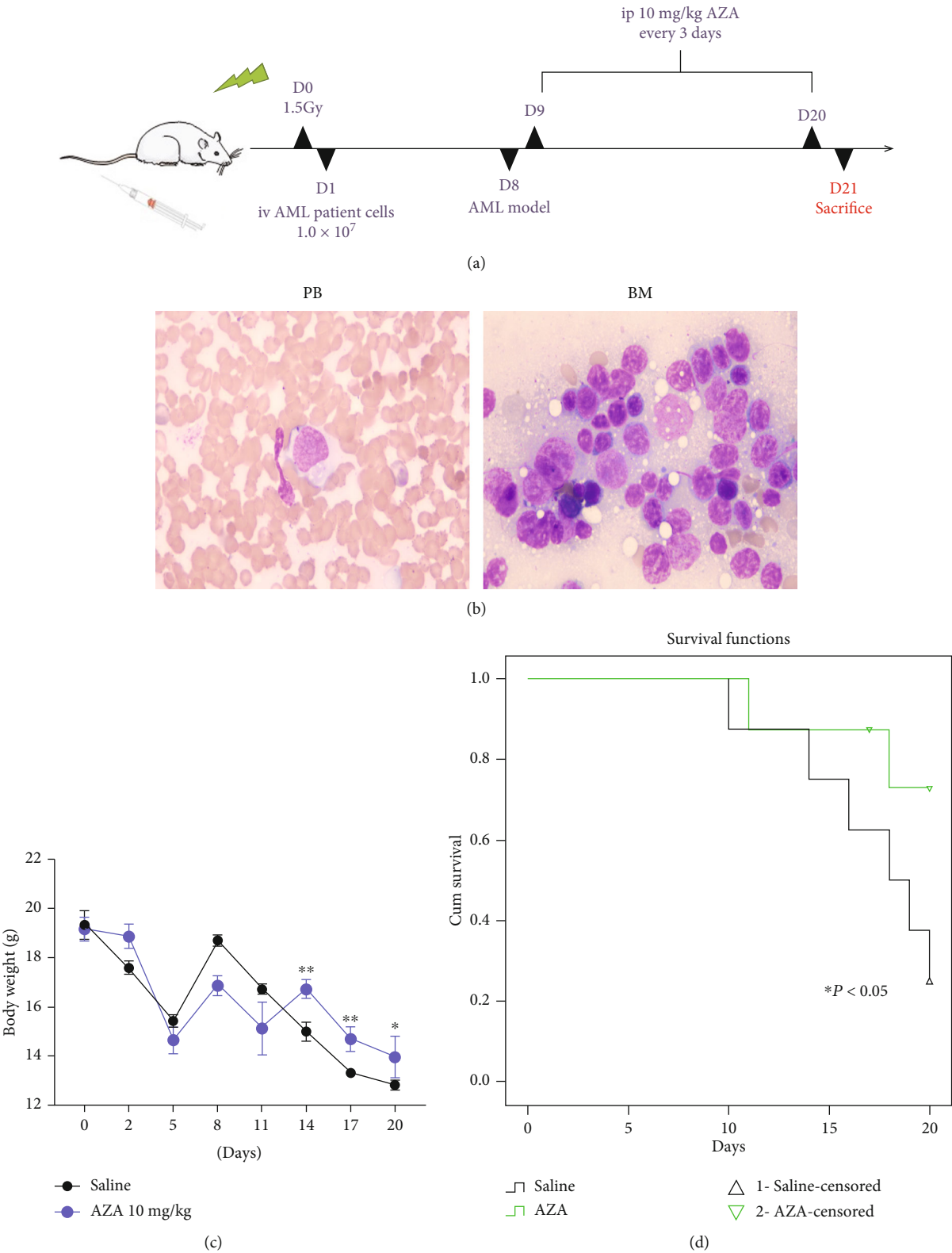
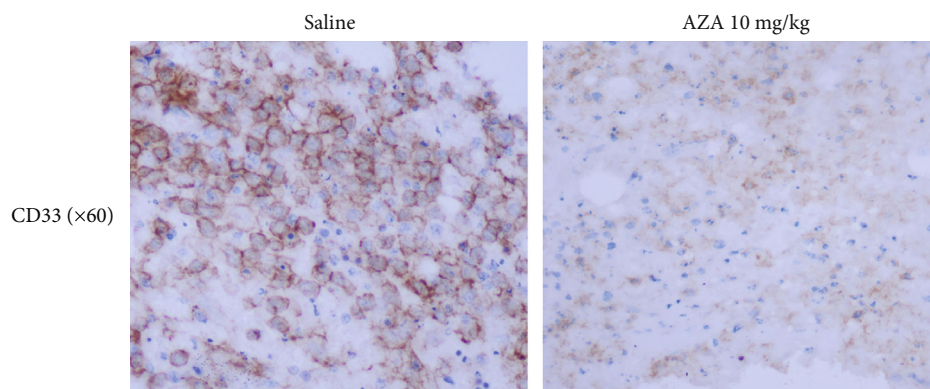
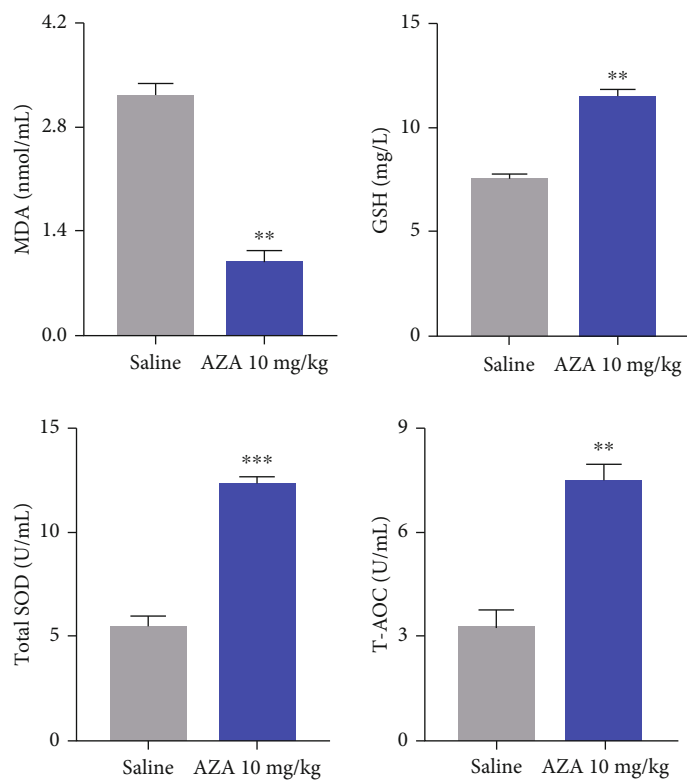


FIGURE 5: Continued.



(e)



(f)

FIGURE 5: Continued.

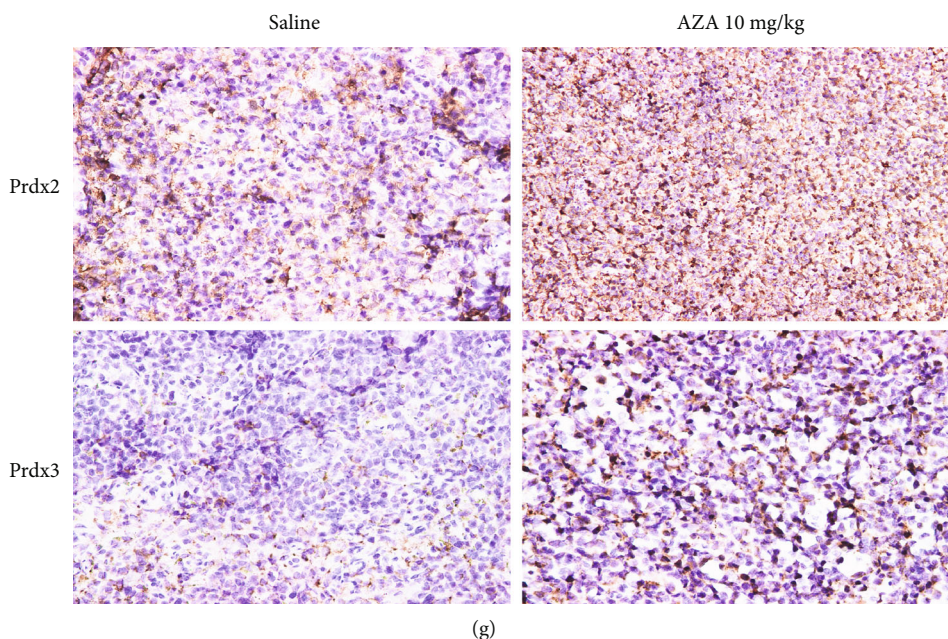


FIGURE 5: AZA suppressed AML tumorigenicity *in vivo*. (a) Flow chart of the PDX animal model construction and treatment. (b) AML patient cells could be observed on the peripheral blood (PB) and bone marrow (BM) smears under a microscope. Magnification: $\times 100$. (c) Body weight change. (d) Survival. There were 8 mice in each group. (e) The expression of CD33 in mice BM after AZA treatment and its detection by immunohistochemistry. Magnification: $\times 40$. (f) The levels of ROS-related indices MDA, SOD, GSH, and T-AOC in blood plasma after AZA treatment. (g) The expression of Prdx2 and Prdx3 in mice spleen after AZA treatment and their detection by immunohistochemistry. Magnification: $\times 40$. * $P < 0.05$, ** $P < 0.01$, and *** $P < 0.001$.

imbalance [55, 56]. Therefore, further research work is still needed to decrease the required concentration so as to minimize side effects.

Our MS detection results showed that AZA upregulated other antioxidant enzymes such as CAT and SOD2. These antioxidant enzymes interact with Prdx3 and Prdx2, but how they act in synergy with Prdxs to maintain intracellular redox equilibrium is being studied. Several immune-related signaling pathways were active after AZA treatment as shown on the heat map; the most obvious was Notch. Notch can maintain low ROS levels to promote cell development and survival [57]. In addition, Notch is an important regulator of immune cell development and function [58]. Our previous study had identified that AZA could activate the Notch signaling pathway and enhance the cytotoxicity of immune effector cells against AML [59]. However, whether AZA can alleviate immunosuppression in the tumor micro-environment via the regulation of Prdxs and Notch requires further study.

In summary, we provided a potential novel agent and therapeutic approach to treating AML by regulating the Prdxs/ROS signaling pathway, which may provide insight into ROS-eliminating strategies.

5. Conclusion

AZA decreased intracellular ROS levels and increased antioxidant capacity by upregulating Prdx2 and Prdx3, which maintained the intracellular redox balance and further suppressed AML *in vitro* and *in vivo*. AZA is a potential agent

for treating AML; ROS-eliminating strategies may be promising strategies for treating AML.

Data Availability

The raw data supporting the conclusions of this manuscript will be made available by the authors.

Conflicts of Interest

The authors declare that they have no competing interests.

Authors' Contributions

FLZ and YXJ provided the direction of the study. DDZ performed the major experiments, analyzed the data, and wrote the manuscript. YXJ guided the experiments. ZYL, YLC, QY, and TY contributed to the cell experiments. YLC, BLW, and ZYL contributed to the animal experiments. XYL helped to analyze the peripheral blood smears, HE, and ICH. YFS, YXJ, and YCW revised the manuscript. All authors read and approved the final manuscript. Dongdong Zhang and Ziyi Luo contributed equally to this work.

Acknowledgments

We appreciate the support from Professor Yi Yang for designing the microfluidic chips and the uncompensated use of laser confocal microscopy at the School of Physics and Technology, Key Laboratory of Artificial Micro/Nano, Wuhan University. This work was supported by the Natural

Science Foundation of China (NSFC) program (grant number 81770179) and the Hong Kong Scholars Program (No. XJ2018060).

Supplementary Materials

Figure S1: AML cell lines and different types of AML patient cells were treated with different concentrations of AZA for 24 h. Cell viability was measured by the CCK-8 method. Figure S2: cell apoptosis rate was analyzed by flow cytometry after healthy PBMCs were treated with 5.0 mM AZA for 24 h. Figure S3: the expression levels of SOD2 and CAT in Molm-13 and THP-1 cells after AZA treatment and their detection by RT-PCR (A) and western blot (B). SOD2 (Cat# 24127-1-AP) and CAT (Cat# 21260-1-AP) used for WB were from ProteinTech (USA). The primers for RT-PCR are as follows: SOD2 (MnSOD): forward 5'-GCC TCC CTG ACC TGC CTT AC-3', reverse 5'-GCA TGA TCT GCG CGT TAA TG-3'; CAT (catalase): forward 5'-CCC AGA AGC CTA AGA ATG CAA-3', reverse 5'-GCT TTT CCC TTG GCA GCT ATG-3. Figure S4: AML patient cells could be observed on the bone marrow (BM) and spleen smears by hematoxylin and eosin stain under a microscope. Magnification: $\times 60$. Table S1: the detailed genetic information of AML patient cells. (*Supplementary Materials*)

References










- [1] O. Beyar-Katz and S. Gill, "Novel approaches to acute myeloid leukemia immunotherapy," *Clinical Cancer Research*, vol. 24, no. 22, pp. 5502–5515, 2018.
- [2] C. Nathan and A. Cunningham-Bussell, "Beyond oxidative stress: an immunologist's guide to reactive oxygen species," *Nature Reviews Immunology*, vol. 13, no. 5, pp. 349–361, 2013.
- [3] H. Sies and D. P. Jones, "Reactive oxygen species (ROS) as pleiotropic physiological signalling agents," *Nature reviews Molecular Cell Biology*, vol. 21, no. 7, pp. 363–383, 2020.
- [4] G. Y. Liou and P. Storz, "Reactive oxygen species in cancer," *Free Radical Research*, vol. 44, no. 5, pp. 479–496, 2010.
- [5] H. D. Popp and S. K. Bohlander, "Genetic instability in inherited and sporadic leukemias," *Genes, Chromosomes & Cancer*, vol. 49, no. 12, pp. 1071–1081, 2010.
- [6] D. Trachootham, J. Alexandre, and P. Huang, "Targeting cancer cells by ROS-mediated mechanisms: a radical therapeutic approach?," *Nature Reviews Drug Discovery*, vol. 8, no. 7, pp. 579–591, 2009.
- [7] F. L. Zhou, W. G. Zhang, Y. C. Wei et al., "Involvement of oxidative stress in the relapse of acute myeloid leukemia," *The Journal of Biological Chemistry*, vol. 285, no. 20, pp. 15010–15015, 2010.
- [8] P. S. Hole, J. Zabkiewicz, C. Munje et al., "Overproduction of NOX-derived ROS in AML promotes proliferation and is associated with defective oxidative stress signaling," *Blood*, vol. 122, no. 19, pp. 3322–3330, 2013.
- [9] P. S. Hole, L. Pearn, A. J. Tonks et al., "Ras-induced reactive oxygen species promote growth factor-independent proliferation in human CD34+ hematopoietic progenitor cells," *Blood*, vol. 115, no. 6, pp. 1238–1246, 2010.
- [10] F. Zhou, Q. Shen, and F. X. Claret, "Novel roles of reactive oxygen species in the pathogenesis of acute myeloid leukemia," *Journal of Leukocyte Biology*, vol. 94, no. 3, pp. 423–429, 2013.
- [11] F. Zhou, Y. Pan, Y. Wei et al., "Jab1/Csn5-thioredoxin signaling in relapsed acute monocytic leukemia under oxidative stress," *Clinical cancer research : an official journal of the American Association for Cancer Research*, vol. 23, no. 15, pp. 4450–4461, 2017.
- [12] K. Ito, A. Hirao, F. Arai et al., "Reactive oxygen species act through p38 MAPK to limit the lifespan of hematopoietic stem cells," *Nature Medicine*, vol. 12, no. 4, pp. 446–451, 2006.
- [13] X. Li, P. Fang, J. Mai, E. T. Choi, H. Wang, and X. F. Yang, "Targeting mitochondrial reactive oxygen species as novel therapy for inflammatory diseases and cancers," *Journal of Hematology & Oncology*, vol. 6, no. 1, p. 19, 2013.
- [14] S. C. Gupta, D. Hevia, S. Patchva, B. Park, W. Koh, and B. B. Aggarwal, "Upsides and downsides of reactive oxygen species for cancer: the roles of reactive oxygen species in tumorigenesis, prevention, and therapy," *Antioxidants & Redox Signaling*, vol. 16, no. 11, pp. 1295–1322, 2012.
- [15] P. E. Vivas-Mejia, B. Ozpolat, X. Chen, and G. Lopez-Berestein, "Downregulation of the c-MYC target gene, peroxiredoxin III, contributes to arsenic trioxide-induced apoptosis in acute promyelocytic leukemia," *International Journal of Cancer*, vol. 125, no. 2, pp. 264–275, 2009.
- [16] R. Bera, M. C. Chiu, Y. J. Huang, D. C. Liang, Y. S. Lee, and L. Y. Shih, "Genetic and epigenetic perturbations by DNMT3A-R882 mutants impaired apoptosis through augmentation of PRDX2 in myeloid leukemia cells," *Neoplasia*, vol. 20, no. 11, pp. 1106–1120, 2018.
- [17] C. X. Liu, Q. Q. Yin, H. C. Zhou et al., "Adenanthin targets peroxiredoxin I and II to induce differentiation of leukemic cells," *Nature Chemical Biology*, vol. 8, no. 5, pp. 486–493, 2012.
- [18] F. Sotgia, U. E. Martinez-Outschoorn, and M. P. Lisanti, "Mitochondrial oxidative stress drives tumor progression and metastasis: should we use antioxidants as a key component of cancer treatment and prevention?," *BMC Medicine*, vol. 9, no. 1, p. 62, 2011.
- [19] G. Bossis, J. E. Sarry, C. Kifagi et al., "The ROS/SUMO axis contributes to the response of acute myeloid leukemia cells to chemotherapeutic drugs," *Cell Reports*, vol. 7, no. 6, pp. 1815–1823, 2014.
- [20] S. Gaballa, R. Saliba, B. Oran et al., "Relapse risk and survival in patients with FLT3 mutated acute myeloid leukemia undergoing stem cell transplantation," *American Journal of Hematology*, vol. 92, no. 4, pp. 331–337, 2017.
- [21] A. Sallmyr, J. Fan, K. Datta et al., "Internal tandem duplication of FLT3 (FLT3/ITD) induces increased ROS production, DNA damage, and misrepair: implications for poor prognosis in AML," *Blood*, vol. 111, no. 6, pp. 3173–3182, 2008.
- [22] D. Sarhan, J. Wang, U. S. Arvindam et al., "Mesenchymal stromal cells shape the MDS microenvironment by inducing suppressive monocytes that dampen NK cell function," *JCI Insight*, vol. 5, no. 5, 2020.
- [23] S. E. Weinberg, L. A. Sena, and N. S. Chandel, "Mitochondria in the regulation of innate and adaptive immunity," *Immunity*, vol. 42, no. 3, pp. 406–417, 2015.
- [24] A. S. Breathnach, E. J. Robins, H. C. Pätzold et al., "Effect of dicarboxylic acids (C6 and C9) on human choroidal melanoma in cell culture," *Investigative Ophthalmology & Visual Science*, vol. 30, no. 3, pp. 491–498, 1989.

- [25] M. Nazzaro-Porro and S. Passi, "Identification of tyrosinase inhibitors in cultures of *Pityrosporum*," *The Journal of Investigative Dermatology*, vol. 71, no. 3, pp. 205–208, 1978.
- [26] K. U. Schallreuter and J. M. Wood, "Azelaic acid as a competitive inhibitor of thioredoxin reductase in human melanoma cells," *Cancer Letters*, vol. 36, no. 3, pp. 297–305, 1987.
- [27] S. Passi, M. Picardo, C. Zompetta, C. De Luca, A. S. Breathnach, and M. Nazzaro-Porro, "The oxyradical-scavenging activity of azelaic acid in biological systems," *Free Radical Research Communications*, vol. 15, no. 1, pp. 17–28, 2009.
- [28] H. Akamatsu, J. Komura, Y. Asada, Y. Miyachi, and Y. Niwa, "Inhibitory effect of azelaic acid on neutrophil functions: a possible cause for its efficacy in treating pathogenetically unrelated diseases," *Archives of Dermatological Research*, vol. 283, no. 3, pp. 162–166, 1991.
- [29] S. Passi, M. Picardo, M. Nazzaro-Porro, A. Breathnach, A. M. Confaloni, and G. Serlupi-Crescenzi, "Antimitochondrial effect of saturated medium chain length (C₈-C₁₃) dicarboxylic acids," *Biochemical Pharmacology*, vol. 33, no. 1, pp. 103–108, 1984.
- [30] M. Nazzaro-Porro, "Azelaic acid," *Journal of the American Academy of Dermatology*, vol. 17, no. 6, pp. 1033–1041, 1987.
- [31] H. Leibl, G. Stingl, H. Pehamberger, H. Korschan, K. Konrad, and K. Wolff, "Inhibition of DNA synthesis of melanoma cells by azelaic acid," *The Journal of Investigative Dermatology*, vol. 85, no. 5, pp. 417–422, 1985.
- [32] M. Picardo, S. Passi, M. C. Sirianni et al., "Activity of azelaic acid on cultures of lymphoma- and leukemia-derived cell lines, normal resting and stimulated lymphocytes and 3T3 fibroblasts," *Biochemical Pharmacology*, vol. 34, no. 10, pp. 1653–1658, 1985.
- [33] Y. Ut, K. Furuke, H. Masutani, H. Nakamura, and J. Yodoi, "Cell cycle inhibition of HTLV-I transformed T cell lines by retinoic acid: the possible therapeutic use of thioredoxin reductase inhibitors," *Oncology Research*, vol. 7, no. 3-4, pp. 183–189, 1995.
- [34] Y. Pan, D. Liu, Y. Wei et al., "Azelaic acid exerts antileukemic activity in acute myeloid leukemia," *Frontiers in Pharmacology*, vol. 8, p. 359, 2017.
- [35] L. Liang, Y. F. Zuo, W. Wu, X. Q. Zhu, and Y. Yang, "Optofluidic restricted imaging, spectroscopy and counting of nanoparticles by evanescent wave using immiscible liquids," *Lab on a Chip*, vol. 16, no. 16, pp. 3007–3014, 2016.
- [36] L. Liang, Y. X. Jin, X. Q. Zhu, F. L. Zhou, and Y. Yang, "Real-time detection and monitoring of the drug resistance of single myeloid leukemia cells by diffused total internal reflection," *Lab on a Chip*, vol. 18, no. 10, pp. 1422–1429, 2018.
- [37] P. J. Boersema, R. Raijmakers, S. Lemeer, S. Mohammed, and A. J. Heck, "Multiplex peptide stable isotope dimethyl labeling for quantitative proteomics," *Nature Protocols*, vol. 4, no. 4, pp. 484–494, 2009.
- [38] Y. Jin, Q. Yang, L. Liang et al., "Compound kushen injection suppresses human acute myeloid leukaemia by regulating the Prdxs/ROS/Trx1 signalling pathway," *Journal of Experimental & Clinical Cancer Research*, vol. 37, no. 1, p. 277, 2018.
- [39] A. Hall, P. A. Karplus, and L. B. Poole, "Typical 2-Cys peroxiredoxins—structures, mechanisms and functions," *The FEBS Journal*, vol. 276, no. 9, pp. 2469–2477, 2009.
- [40] D. Zhang, Y. Liu, Z. Luo et al., "The novel thioredoxin reductase inhibitor A-Z2 triggers intrinsic apoptosis and shows efficacy in the treatment of acute myeloid leukemia," *Free Radical Biology & Medicine*, vol. 146, pp. 275–286, 2020.
- [41] M. Wu, C. Li, and X. Zhu, "FLT3 inhibitors in acute myeloid leukemia," *Journal of Hematology & Oncology*, vol. 11, no. 1, p. 133, 2018.
- [42] L. B. Alexandrov, A. P. C. G. Initiative, S. Nik-Zainal et al., "Signatures of mutational processes in human cancer," *Nature*, vol. 500, no. 7463, pp. 415–421, 2013.
- [43] S. Gill, S. K. Tasian, M. Ruella et al., "Preclinical targeting of human acute myeloid leukemia and myeloablation using chimeric antigen receptor-modified T cells," *Blood*, vol. 123, no. 15, pp. 2343–2354, 2014.
- [44] H. Jetani, I. Garcia-Cadenas, T. Nerretter et al., "CAR T-cells targeting FLT3 have potent activity against FLT3^{ITD} AML and act synergistically with the FLT3-inhibitor crenolanib," *Leukemia*, vol. 32, no. 5, pp. 1168–1179, 2018.
- [45] C. C. Winterbourn, "Reconciling the chemistry and biology of reactive oxygen species," *Nature Chemical Biology*, vol. 4, no. 5, pp. 278–286, 2008.
- [46] T. S. Chang, C. S. Cho, S. Park, S. Yu, S. W. Kang, and S. G. Rhee, "Peroxiredoxin III, a mitochondrion-specific peroxidase, regulates apoptotic signaling by mitochondria," *The Journal of Biological Chemistry*, vol. 279, no. 40, pp. 41975–41984, 2004.
- [47] S. Agrawal-Singh, F. Isken, K. Agelopoulos et al., "Genome-wide analysis of histone H3 acetylation patterns in AML identifies PRDX2 as an epigenetically silenced tumor suppressor gene," *Blood*, vol. 119, no. 10, pp. 2346–2357, 2012.
- [48] M. Ying, X. Shao, H. Jing et al., "Ubiquitin-dependent degradation of CDK2 drives the therapeutic differentiation of AML by targeting PRDX2," *Blood*, vol. 131, no. 24, pp. 2698–2711, 2018.
- [49] S. Luthra, U. Chandran, B. Diergaarde, M. Becich, A. V. Lee, and C. A. Neumann, "Expression of reactive species related genes is associated with patient survival in luminal B breast cancer," *Free Radical Biology & Medicine*, vol. 120, pp. 170–180, 2018.
- [50] L. Chen, M. Stacewicz-Sapuntzakis, C. Duncan et al., "Oxidative DNA damage in prostate cancer patients consuming tomato sauce-based entrees as a whole-food intervention," *Journal of the National Cancer Institute*, vol. 93, no. 24, pp. 1872–1879, 2001.
- [51] H. S. Kim, P. Bowen, L. Chen et al., "Effects of tomato sauce consumption on apoptotic cell death in prostate benign hyperplasia and carcinoma," *Nutrition and Cancer*, vol. 47, no. 1, pp. 40–47, 2003.
- [52] A. J. Duffield-Lillico, M. E. Reid, B. W. Turnbull et al., "Baseline characteristics and the effect of selenium supplementation on cancer incidence in a randomized clinical trial: a summary report of the Nutritional Prevention of Cancer Trial," *Cancer Epidemiology and Prevention Biomarkers*, vol. 11, no. 7, pp. 630–639, 2002.
- [53] W.-Q. Li, J.-Y. Zhang, J.-L. Ma et al., "Effects of *Helicobacter pylori* treatment and vitamin and garlic supplementation on gastric cancer incidence and mortality: follow-up of a randomized intervention trial," *BMJ*, vol. 366, article 15016, 2019.
- [54] Y. Jin, L. Cai, Q. Yang et al., "Anti-leukemia activities of selenium nanoparticles embedded in nanotube consisted of triple-helix β -d-glucan," *Carbohydrate Polymers*, vol. 240, p. 116329, 2020.

- [55] C. Wu, S. H. Hwang, Y. Jia et al., "Olfactory receptor 544 reduces adiposity by steering fuel preference toward fats," *The Journal of Clinical Investigation*, vol. 127, no. 11, pp. 4118–4123, 2017.
- [56] R. A. Bojar, W. J. Cunliffe, and K. T. Holland, "Disruption of the transmembrane pH gradient—a possible mechanism for the antibacterial action of azelaic acid in *Propionibacterium acnes* and *Staphylococcus epidermidis*," *The Journal of Antimicrobial Chemotherapy*, vol. 34, no. 3, pp. 321–330, 1994.
- [57] C. Small, J. Ramroop, M. Otazo, L. H. Huang, S. Saleque, and S. Govind, "An unexpected link between notch signaling and ROS in restricting the differentiation of hematopoietic progenitors in *Drosophila*," *Genetics*, vol. 197, no. 2, pp. 471–483, 2014.
- [58] F. Radtke, H. R. MacDonald, and F. Tacchini-Cottier, "Regulation of innate and adaptive immunity by Notch," *Nature Reviews Immunology*, vol. 13, no. 6, pp. 427–437, 2013.
- [59] Z. Dongdong, Y. Jin, T. Yang et al., "Antiproliferative and immunoregulatory effects of azelaic acid against acute myeloid leukemia via the activation of Notch signaling pathway," *Frontiers in Pharmacology*, vol. 10, p. 1396, 2019.

Research Article

Mitochondrial-Protective Effects of R-Phenibut after Experimental Traumatic Brain Injury

Einars Kupats ^{1,2}, Gundega Stelfa ^{1,3}, Baiba Zvejniece ¹, Solveiga Grinberga ¹,
Edijs Vavers ¹, Marina Makrecka-Kuka ¹, Baiba Svalbe ¹, Liga Zvejniece ¹,
and Maija Dambrova ^{1,4}

¹Latvian Institute of Organic Synthesis, Riga, Latvia

²Department of Neurology and Neurosurgery, Riga Stradins University, Riga, Latvia

³Latvia University of Life Sciences and Technologies, Jelgava, Latvia

⁴Department of Pharmaceutical Chemistry, Riga Stradins University, Riga, Latvia

Correspondence should be addressed to Einars Kupats; einars.kupats@farm.osi.lv

Received 15 July 2020; Revised 24 September 2020; Accepted 3 November 2020; Published 21 November 2020

Academic Editor: Luciano Saso

Copyright © 2020 Einars Kupats et al. This is an open access article distributed under the Creative Commons Attribution License, which permits unrestricted use, distribution, and reproduction in any medium, provided the original work is properly cited.

Altered neuronal Ca^{2+} homeostasis and mitochondrial dysfunction play a central role in the pathogenesis of traumatic brain injury (TBI). R-Phenibut ((3R)-phenyl-4-aminobutyric acid) is an antagonist of the $\alpha_2\delta$ subunit of voltage-dependent calcium channels (VDCC) and an agonist of gamma-aminobutyric acid B (GABA-B) receptors. The aim of this study was to evaluate the potential therapeutic effects of R-phenibut following the lateral fluid percussion injury (latFPI) model of TBI in mice and the impact of R- and S-phenibut on mitochondrial functionality *in vitro*. By determining the bioavailability of R-phenibut in the mouse brain tissue and plasma, we found that R-phenibut (50 mg/kg) reached the brain tissue 15 min after intraperitoneal (i.p.) and peroral (p.o.) injections. The maximal concentration of R-phenibut in the brain tissues was 0.6 $\mu\text{g/g}$ and 0.2 $\mu\text{g/g}$ tissue after i.p. and p.o. administration, respectively. Male Swiss-Webster mice received i.p. injections of R-phenibut at doses of 10 or 50 mg/kg 2 h after TBI and then once daily for 7 days. R-Phenibut treatment at the dose of 50 mg/kg significantly ameliorated functional deficits after TBI on postinjury days 1, 4, and 7. Seven days after TBI, the number of Nissl-stained dark neurons (N-DNs) and interleukin-1beta (IL-1 β) expression in the cerebral neocortex in the area of cortical impact were reduced. Moreover, the addition of R- and S-phenibut at a concentration of 0.5 $\mu\text{g/ml}$ inhibited calcium-induced mitochondrial swelling in the brain homogenate and prevented anoxia-reoxygenation-induced increases in mitochondrial H_2O_2 production and the $\text{H}_2\text{O}_2/\text{O}$ ratio. Taken together, these results suggest that R-phenibut could serve as a neuroprotective agent and promising drug candidate for treating TBI.

1. Introduction

Traumatic brain injury (TBI) is a leading cause of mortality and disability among trauma-related injuries [1]. TBI can result in temporary, long-term, and even life-long physical, cognitive, and behavioural problems [2, 3]. Therefore, there is an increased need for effective pharmacological approaches for treating patients with TBI. Phenibut, a nootropic prescription drug with anxiolytic activity, is used in clinical practice in Eastern European countries for the treatment of anxiety, tics, stuttering, insomnia, dizziness, and alcohol abstinence [4, 5]. R-Phenibut ((3R)-phenyl-4-aminobutyric

acid), which is one of the optical isomers of phenibut, binds to gamma-aminobutyric acid B (GABA-B) receptors and the $\alpha_2\delta$ subunit of voltage-dependent calcium channels (VDCC), while S-phenibut binds only to the $\alpha_2\delta$ subunit of VDCC [6–8]. Our previous studies have shown that R-phenibut treatment significantly decreased the brain infarct size and increased brain-derived neurotrophic factor and vascular endothelial growth factor gene expression in damaged brain tissue in an experimental stroke model [9]. The similarity of the pathogenic mechanisms of TBI and cerebral ischaemia indicate that therapeutic strategies that are successful in treating one may also be beneficial in treating the other [10].

Treatment options for TBI are limited due to its complex pathogenesis and the heterogeneity of its presentation, which includes haematomas, contusions, hypoxia, and vascular, axonal, and other types of central nervous system injuries [11, 12]. Among the processes that impact TBI, the generation of reactive oxygen species (ROS) by mitochondria occurs within the first minutes after TBI and thus leads to the disruption of calcium ion (Ca^{2+}) homeostasis, which is the “final common pathway” for toxic cellular degradation [13, 14]. Maintaining regional neuronal Ca^{2+} homeostasis and mitochondrial function is crucial to prevent secondary neuronal injury [15, 16]. Thus, mitochondrial-targeted drugs and drugs acting on specific intracellular Ca^{2+} signalling pathways or subcellular components show promise as therapeutic interventions for TBI [17, 18]. In fact, upregulation of the neuronal calcium channel $\alpha_2\delta$ subunit modulates the activation of mitochondrial Ca^{2+} buffering in pathological conditions [19]. There is also evidence that GABA-B receptor agonists provide neuroprotection against N-methyl-D-aspartate-induced neurotoxicity mediated by the mitochondrial permeability transition pore [20]. Since both isomers of phenibut bind to the $\alpha_2\delta$ subunit of VDCC and only R-phenibut binds to the GABA-B receptor, these both isomers could be used to specify the possible molecular mechanisms of phenibut in different experimental models.

This is the first investigation of the potential therapeutic effects of R-phenibut following TBI in mice. In addition, to evaluate possible molecular mechanisms underlying the actions of R-phenibut against anoxia-reoxygenation-induced mitochondrial damage, the effects on mitochondrial functionality were evaluated in an *in vitro* model of anoxia-reoxygenation and compared for R- and S-phenibut.

2. Materials and Methods

2.1. Animals and Treatment. Forty-eight Swiss-Webster male mice (25–40 g; Laboratory Animal Centre, University of Tartu, Tartu, Estonia) were used in a lateral fluid percussion injury (latFPI) model of TBI [21, 22]. Additionally, 6 Swiss-Webster male mice were used for the preparation of brain homogenate and the isolation of brain mitochondria for *in vitro* assays. Forty-two ICR male mice (Laboratory Animal Breeding Facility, Riga Stradins University, Latvia) were used in a pharmacokinetic study. All animals were housed under standard conditions (21–23°C, 12 h light-dark cycle) with unlimited access to standard food (Lactamin AB, Mjölby, Sweden) and water in an individually ventilated cage housing system (Allentown Inc., Allentown, New Jersey, USA). Each cage contained bedding consisting of Eco-Pure™ Shavings wood chips (Datesand, Cheshire, UK), nesting material, and wooden blocks from TAPVEI (TAPVEI, Paekna, Estonia). For enrichment, a transparent tinted (red) nontoxic durable polycarbonate safe harbour mouse retreat (AnimaLab, Poznan, Poland) was used. The mice were housed with up to 5 mice per standard cage (38 × 19 × 13 cm). All studies involving animals were reported in accordance with the ARRIVE guidelines [23, 24]. The experimental procedures were performed in accordance with the guidelines reported in the EU Directive 2010/63/EU and in accordance

with local laws and policies; all procedures were approved by the Latvian Animal Protection Ethical Committee of Food and Veterinary Service in Riga, Latvia.

The dose of R-phenibut was selected based on the previous studies, where pharmacological efficacy was observed in dose-range between 10 and 50 mg/kg, while R-phenibut at doses higher than 100 mg/kg showed sedative and coordination inhibitory effects [6, 8, 9]. Mice were randomly assigned to four experimental groups: sham-operated mice, saline-treated latFPI mice, and latFPI mice that received R-phenibut (JSC Olainfarm, Olaine, Latvia) at a dose of 10 mg/kg or 50 mg/kg. Six mice were excluded because of a dural breach that occurred during surgery (4 mice from the sham-operated, 1 mouse from the control, and 1 mouse from the R-phenibut 50 mg/kg groups), and four mice died immediately after latFPI and were excluded from the study (3 mice from the control and 1 mouse from the R-phenibut 50 mg/kg groups). The final number of included animals per group was as follows: sham-operated mice ($n = 8$), saline-treated latFPI mice (control group, $n = 8$), and latFPI mice that received R-phenibut at a dose of 10 mg/kg ($n = 12$) or 50 mg/kg ($n = 10$). R-Phenibut and saline were initially administered intraperitoneally (i.p.) 2 h after injury and then once daily for an additional 7 days for a total treatment period of 1 week. During the treatment period, the animals were weighed at 0, 1, 2, 4, and 7 days after latFPI between 9:00 and 10:00 am. To avoid the influence of subjective factors on the rating process, all experimental procedures were performed in a blinded fashion.

2.2. Determination of R-Phenibut in the Plasma and Brain Tissue after p.o. and i.p. Administration. The concentrations of R-phenibut in the brain tissue extracts and plasma were measured by ultraperformance liquid chromatography-tandem mass spectrometry (UPLC/MS/MS). To determine the concentration of R-phenibut in the plasma and brain, mice received an i.p. and p.o. R-phenibut at a dose of 50 mg/kg 15 and 30 min and 1, 2, 4, 6, and 24 h ($n = 3$ in each time point) before the plasma and brain tissue collection. The blood and brain samples were prepared as described previously [25]. The chromatographic separation was performed using an ACQUITY UPLC system (Waters, USA) on an ACQUITY UPLC BEH Shield RP18 (1.7 μm , 2.1 × 50 mm) (Waters) with a gradient elution from 5 to 98% acetonitrile in 0.1% formic acid aqueous solution at a flow rate of 0.15 ml/min. The analyte was ionized by electrospray ionization in positive ion mode on a Quattro Micro triple quadrupole mass spectrometer (Waters). The mass spectrometer was set up as follows: capillary voltage of 3.3 kV; source and desolvation temperatures of 120 and 400°C, respectively. Cone voltage was 20 V, and collision energy was 18 eV. R-Phenibut analysis was performed in the MRM mode. Precursor to production transition was $m/z/m/z$ 180.0 → 116.1. Data acquisition and processing were performed using the MassLynx V4.1 and QuanLynx V4.1 software (Waters).

2.3. Lateral Fluid Percussion Injury-Induced Brain Trauma. To induce TBI, the latFPI model was generated as previously described [21, 22] with slight modifications. Mice were

anaesthetized with 4% isoflurane contained in a mixture of oxygen and nitrous oxide (70:30, AGA, Riga, Latvia), and anaesthesia with 2% isoflurane (Chemical Point, Deisenhofen, Germany) was maintained during the surgical procedures using a face mask. The depth of anaesthesia was monitored by a toe pinch using tweezers. Before trauma induction, mice received subcutaneous (s.c.) administration of tramadol (KRKA, Novo Mesto, Slovenia) (10 mg/kg). Eye cream was applied to prevent the eyes from drying out. A midline longitudinal scalp incision was made, and the skull was exposed. A craniectomy that was centred at 2 mm posterior to bregma and 2 mm right of midline was performed using a 3 mm outer-diameter trephine. Any animal noted to have a dural breach was euthanized and excluded from the study. A plastic cap was attached over the craniotomy using dental cement (Fullident, Switzerland), and a moderate severity (1.5 ± 0.2 atm) brain injury was induced with a commercially available fluid percussion device (AmScien Instruments, Richmond, USA). Immediately after the injury, apnoea was noted, and when spontaneous breathing returned, anaesthesia was resumed. The cement and cap were removed, and the skin was sutured using resorbable sutures (6-0, silk). The animal was placed in a separate cage to allow full recovery from anaesthesia. Sham-injured animals were subjected to an identical procedure as the latFPI animals except for the induction of trauma.

2.4. Neurological Severity Score (NSS). The neurobehavioural status of mice was obtained by the NSS using the method described previously [26]. The animals were trained on the NSS beams and equipment prior to the baseline measurements. The general neurological state of mice was evaluated at baseline (day before latFPI) and 1, 4, and 7 days postinjury before the next dose of R-phenibut or saline administration. The NSS consisted of 9 individual clinical parameters, including motor function, alertness, and physiological behaviour tasks. The mice were assessed for the following items: presence of paresis; impairment of seeking behaviour; absence of perceptible startle reflex; inability to get down from a rectangle platform (34×27 cm); inability to walk on 3, 2, and 1 cm wide beams; and inability to balance on a vertical beam of 7 mm width and horizontal round stick of 5 mm diameter for 10 sec. If a mouse showed impairment on one of these items, a value of 1 was added to its NSS score. Thus, higher scores on the NSS indicate greater neurological impairment.

2.5. Tissue Preparation for Histological Analysis. The animals used for histological analysis were randomly selected from each group. Seven days after TBI, the mice were anaesthetized using i.p. administration of ketamine (200 mg/kg) and xylazine (15 mg/kg). The depth of anaesthesia was monitored by a toe pinch using tweezers. Animals were transcardially perfused at a rate of 3 ml/minutes with 0.01 M phosphate-buffered saline (PBS, pH = 7.4) for 5 minutes until the blood was completely removed from the tissue. Perfusion was then performed with 4% paraformaldehyde (PFA) fixative solution for 5-7 minutes until stiffening of the mouse body occurred. After perfusion, the brains were carefully dissected

and postfixed in 4% PFA overnight at 4°C. The brains were cryoprotected with a 10-20-30% sucrose-PBS gradient for 72 hours. Coronal sections of the brain (20 μ m) were made using a Leica CM1850 cryostat (Leica Biosystems, Buffalo Grove, IL, United States) and mounted on Superfrost Plus microscope slides (Thermo Scientific, Waltham, MA, United States).

2.6. Cresyl Violet (Nissl) Staining and Interleukin-1beta (IL-1 β) Immunofluorescence Staining. Nissl and IL-1 β staining techniques were used to evaluate neuronal cell damage. Nissl-stained dark neurons (N-DNs) indicated the typical morphological change in injured neurons following TBI [27, 28]. The number of N-DNs and cells expressing IL-1 β in the cerebral neocortex in the cortical impact area were determined at day 7 after latFPI. For Nissl staining, coronal frozen sections (20 μ m) of the mouse brain were used. The sections were incubated in graded ethanol solutions (96% ethanol for 3 minutes and 70% ethanol for 3 minutes). After washing with distilled water for 3 minutes, the sections were stained with 0.01% cresyl violet acetate (ACROS organics) solution for 14 minutes. The sections were then washed with distilled water for 3 minutes and dehydrated in ethanol. The stained sections were coverslipped using DPX mounting medium (Sigma-Aldrich, St. Louis, MO, United States).

For IL-1 β staining, the sections were washed once with PBS containing 0.2% Tween 20 for 5 minutes (on a rotary shaker at 250 rpm). The antigen retrieval procedure was performed with 0.05 M Na citrate (pH = 6.0) containing 0.05% Tween 20 for 30 minutes at 85°C. The sections were then washed with PBS (0.2% Tween 20) 3 times for 5 minutes each. Protein blocking was performed using 5% BSA solution, and the sections were incubated for 1 hour at room temperature. The sections were washed with PBS (0.2% Tween 20) 3 times for 5 minutes each. The slices were incubated with primary antibody against anti-IL-1 β (1:1000; Abcam, Cat# ab9722) for 16 h at +4°C. The antibody was diluted in PBS containing 3% BSA and 0.3% Triton™ X-100. After incubation with the primary antibody, the sections were washed with PBS (0.2% Tween 20) 4 times for 5 minutes each. The sections were subsequently incubated for 1 h at room temperature with goat anti-rabbit IgG H&L (Alexa Fluor® 488, 1:200; Abcam, Cat# ab150077) diluted in PBS containing 5% BSA. The sections were washed with PBS (0.2% Tween 20) 4 times for 5 minutes each. The stained sections were mounted using Fluoromount™ aqueous mounting medium (Sigma-Aldrich, St. Louis, MO, United States, Cat# F4680) and finally coverslipped. Images were obtained with a Nikon Eclipse TE300 microscope (Nikon Instruments, Tokyo, Japan).

N-DNs were defined as hyperbasophilic neurons with a shrunken morphology. The number of N-DNs per field of vision was calculated in three randomly selected sections at the epicentre of the injury. The number of N-DNs and cells expressing IL-1 β per field of vision were calculated using ImageJ software at 10-fold magnification for N-DNs and at 4-fold magnification for IL-1 β . For analysis of expression of IL-1 β , eight-bit images were generated from the pictures and were cropped to contain the regions of interest. Images

for IL-1 β staining were thresholded to select a specific signal over the background, and the stained area for each region was calculated and used for statistical analysis. Three individual measurements were performed for each sample. The schematic illustration of the brain region was created using BioRender software (<https://biorender.com>).

2.7. Mitochondrial Respiration and H₂O₂ Production Measurements. To evaluate mitochondrial functionality, mouse brain homogenate or isolated brain mitochondria were prepared. Briefly, brain tissues were homogenized 1:20 (*w/v*) in a medium containing 320 mM sucrose, 10 mM Tris, and 1 mM EDTA (pH 7.4). The homogenate was centrifuged at 1000 g for 10 min, and the supernatant was centrifuged at 6200 g for 10 min. The mitochondrial pellet obtained was washed once and resuspended in the isolation medium. Mitochondrial respiration and H₂O₂ production measurements were performed at 37°C using Oxygraph-2k (O2k; Oroboros Instruments, Austria) with O2k-Fluo-Modules in MiR05Cr (110 mM sucrose, 60 mM K-lactobionate, 0.5 mM EGTA, 3 mM MgCl₂, 20 mM taurine, 10 mM KH₂PO₄, 20 mM HEPES, pH 7.1, 0.1% BSA essentially fatty acid free, and creatine 20 mM). H₂O₂ flux (ROS flux) was measured simultaneously with respirometry in the O2k-fluorometer using the H₂O₂-sensitive probe Ampliflu™ Red (AmR) [29, 30]. 10 μ M AmR, 1 U/ml horse radish peroxidase (HRP), and 5 U/ml superoxide dismutase (SOD) were added to the chamber. H₂O₂ detection is based on the conversion of AmR into the fluorescent resorufin. Calibrations were performed with H₂O₂ added at 0.1 μ M step. H₂O₂ flux was corrected for background (AmR slope before addition of sample). H₂O₂/O flux ratio (%) was calculated as H₂O₂ flux/(0.5 O₂ flux).

2.8. In Vitro Anoxia-Reoxygenation Model. Mitochondrial functionality after anoxia-reoxygenation was determined in mouse brain tissue homogenate prepared as described previously [31]. To induce anoxia maximal respiration rate, the sample was stimulated by the addition of substrates, pyruvate + malate (5 + 2 mM), succinate (10 mM), and ADP (5 mM), and preparation was left to consume all O₂ in the respiratory chamber (within 10–20 min), thereby entering into an anoxic state [32]. 15 minutes after anoxia, the vehicle or R-phenibut (0.5 μ g/ml) was added to the chamber and O₂ was reintroduced to the chamber by opening the chamber to achieve reoxygenation. After 8 minutes of reoxygenation, the chamber was closed and O₂ flux was monitored for additional 2 minutes. At the end of the experiment, antimycin A (2.5 μ M) was added to determine residual oxygen consumption (ROX).

2.9. Substrate-Uncoupler-Inhibitor Titration (SUIT) Protocol. To determine the effect of R-phenibut on mitochondrial electron transfer system functionality, mitochondria were isolated from mouse brain as described previously, and mitochondrial respiration and H₂O₂ production measurements were performed in the presence or absence of R-phenibut at 0.5 μ g/ml concentration [30]. In addition, effects of S-phenibut (0.5 μ g/ml) were tested to determine whether

the effects of R-phenibut in mitochondria involve the GABA-B receptor or the $\alpha_2\delta$ subunit of VDCC. Pyruvate and malate (5 mM and 2 mM, respectively) were used to determine N-pathway complex I (CI) linked LEAK (L) respiration. ADP was added at 5 mM concentration to determine oxidative phosphorylation-dependent respiration (OXPHOS state, P). Then, glutamate (10 mM) was added as an additional substrate for N-pathway. Succinate (10 mM, complex II (CII) substrate) was added to reconstitute convergent NS-pathway CI&II-linked respiration. Titrations with the uncoupler CCCP (0.5–1 μ M steps) were performed to determine the electron transfer system (ETS) capacity. Rotenone (0.5 μ M, inhibitor of complex I) was added to determine the CII-linked OXPHOS capacity. Then, antimycin A (2.5 μ M, inhibitor of complex III) was added to evaluate residual (non-mitochondrial) oxygen consumption (ROX). Oxygen fluxes were compared after correction for ROX.

2.10. Ca²⁺-Induced Mitochondrial Swelling Measurement. Swelling of isolated brain mitochondria was assessed by measuring changes in absorbance at 540 nm as described previously with slight modifications [33–35]. Mitochondria (0.125 mg/ml) were preincubated with R- or S- phenibut at a concentration of 0.5 μ g/ml for 15 min in a buffer containing 120 mM KCl, 10 mM Tris, 5 mM KH₂PO₄ pH 7.4, and pyruvate (5 mM), malate (2 mM), and ADP (5 mM) as substrates. R- and S-enantiomers of phenibut were used to determine whether the effects of R-phenibut on Ca²⁺-induced mitochondrial swelling involve the GABA-B receptor or the $\alpha_2\delta$ subunit of VDCC. Swelling was induced by the addition of 200 μ M CaCl₂, and changes in absorbance were monitored for 10 min. All experiments were performed at 37°C.

2.11. Statistical Analysis. All results are expressed as the mean \pm S.E.M or S.D. (for mitochondrial studies). Health outcomes, animal behaviour, and Ca²⁺-induced mitochondrial swelling were analysed using two-way repeated-measures analysis of variance (ANOVA). Dunnett's post hoc test was performed when appropriate. The histological data and mitochondrial functionality were evaluated by one-way ANOVA. Whenever the analysis of variance indicated a significant difference, further multiple comparisons were made using Tukey's multiple comparison test as the post hoc test. *p* values less than 0.05 were considered to be significant. The statistical calculations were performed using the GraphPad Prism software package (GraphPad Software, Inc., La Jolla, California, USA).

The sample size calculations for latFPI-induced brain trauma were based on the effects of R-phenibut in our previous experiments. For example, it was calculated that R-phenibut demonstrates a medium effect in the ET-1-induced middle cerebral artery occlusion model [9] and a large effect in the formalin-induced paw-licking test [6]. Through a power calculation (using G-power software) for a two-way ANOVA test (repeated measures), four-group comparison, four measurements per group (0, 1, 4, and 7 days after TBI) with $\alpha = 0.05$, a power of 80%, and a standardized effect size Cohen's *f* = 0.5, a total sample size of 8 mice per group was deemed sufficient. Since TBI-induced

brain trauma can result in death of some animals, our sample size of $n = 12$ would allow identifying smaller differences, with the same statistical power, for the same significance level.

3. Results

3.1. R-Phenibut Crosses the Blood-Brain Barrier. As shown in Figure 1(a), R-phenibut in plasma could be detected 15 min after a single i.p. and p.o. injection. The maximal concentrations of R-phenibut in the plasma were observed 15 min after the i.p. injection and 30 min after the p.o. administration (Figure 1(a)). The maximal concentration of R-phenibut in the plasma after the i.p. injection was $16.8 \mu\text{g/ml}$; at the same time, the maximal concentration of R-phenibut in the plasma after the p.o. injection was $24 \mu\text{g/ml}$ (see Figure 1(a)). R-Phenibut in the plasma was not detected 24 h after both the i.p. and p.o. injections. R-Phenibut in the brain tissue extracts was detected already 15 min after a single i.p. and p.o. injection (Figure 1(b)). The maximal concentrations of R-phenibut in the brain tissues were $0.64 \mu\text{g/g}$ and $0.17 \mu\text{g/g}$ tissue after the i.p. and p.o. injections, respectively (Figure 1(a)). The maximal concentrations of R-phenibut in the brain tissues were observed 15 min after i.p. injection and 60 till 240 min after p.o. administration. 24 h after both the i.p. and p.o. injections, R-phenibut in the brain tissues was $0.02 \mu\text{g/g}$ and $0.012 \mu\text{g/g}$, respectively.

3.2. Health Outcome Monitoring after latFPI. The body weight of the sham group animals was not decreased at 1, 2, 4, and 7 days after TBI. A two-way repeated-measures ANOVA showed a significant interaction between time and treatment ($F_{(12,118)} = 4.6$, $p < 0.0001$) and main effects of time ($F_{(1,4,42.7)} = 25.7$, $p < 0.0001$) and treatment ($F_{(3,34)} = 6.7$, $p = 0.0011$). The control group animals lost significantly more weight after TBI than the sham-operated group animals ($p < 0.05$). Treatment with R-phenibut at both doses had no effect on weight loss compared to weight loss in the control group (Figure 2).

3.3. R-Phenibut Treatment Improved Neurological Status after TBI. TBI induced significant functional deficits in control mice compared with sham-operated mice ($p < 0.0001$). The average NSS in the control group was 6.1 ± 0.4 , 5.3 ± 0.3 , and 5.0 ± 0.6 on postinjury days 1, 4, and 7, respectively. The average NSS score between baseline value and the first day postcraniotomy in the sham-operated group was significantly higher ($p < 0.01$). There was a significant time \times treatment interaction observed between groups (two-way repeated-measures ANOVA: ($F_{(9,102)} = 5.7$, $p < 0.0001$) for time \times treatment interaction; ($F_{(3,34)} = 22.2$, $p < 0.0001$) for treatment; ($F_{(2,7,92)} = 161.8$, $p < 0.0001$) for time; Figure 3). R-Phenibut treatment at a dose of 50 mg/kg significantly ameliorated functional deficits by 28%, 25%, and 30% after TBI on postinjury days 1, 4, and 7, respectively ($p < 0.05$; Figure 3).

3.4. R-Phenibut Treatment Reduced Early Neuronal Cell Death and Neuroinflammation in the Brain Cortex after TBI. To assess histopathological changes in the ipsilateral

brain site, N-DNs and cells expressing IL-1 β (Figure 4) were quantified in the sham-operated, control, and R-phenibut treatment groups 7 days after TBI. N-DNs and IL-1 β -expressing cells were found in the ipsilateral hemisphere of control group animals (Figures 4(a) and 4(b)). Histological analysis showed that R-phenibut treatment at a dose of 50 mg/kg significantly reduced the number of N-DNs and cells expressing IL-1 β in the neocortex after TBI ($p < 0.05$). Significant differences were found in the N-DNs and IL-1 β -positive cell numbers in the ipsilateral cortex around the lesion site between the control group (9.1 ± 6.4 /per field of vision for N-DNs and 379 ± 82 /per field of vision for IL-1 β -expressing cells) and the R-phenibut treatment group at a dose of 50 mg/kg (3.0 ± 1.9 /per field of vision for N-DNs and 246 ± 31 /per field of vision for IL-1 β -expressing cells; $p < 0.05$; Figures 4(d) and 4(e)). There was no statistically significant difference between the control group and the R-phenibut treatment group at the dose of 10 mg/kg. No N-DNs were observed in the sham-operated mice.

3.5. R-Phenibut Protects Brain Mitochondria against Anoxia-Reoxygenation Damage. To determine whether R-phenibut-induced neuroprotection could be a result of the preservation of mitochondrial functionality, ROS production and the mitochondrial respiration rate were assessed after anoxia-reoxygenation *in vitro*. To better mimic the conditions observed *in vivo*, R-phenibut at the concentration of $0.5 \mu\text{g/ml}$ was added to the chamber immediately before reoxygenation. Anoxia-reoxygenation induced 33% and 59% increases in the H_2O_2 production rate and the $\text{H}_2\text{O}_2/\text{O}$ ratio, respectively (Figure 5). R-Phenibut treatment significantly decreased the anoxia-reoxygenation-induced increase in the H_2O_2 production rate and the $\text{H}_2\text{O}_2/\text{O}$ ratio ($p < 0.05$).

3.6. R-Phenibut Reduces ROS Production and Attenuates Ca^{2+} -Induced Mitochondrial Swelling. To determine whether the protective effect of R-phenibut is related to its direct action on mitochondria, measurements of mitochondrial respiration, ROS production, and Ca^{2+} -induced swelling were performed in isolated mouse brain mitochondria in the presence or absence of the compounds. As seen in Figure 6, R-phenibut and S-phenibut at $0.5 \mu\text{g/ml}$ did not induce any changes in the mitochondrial respiration rate (Figure 6(a)), while H_2O_2 production and the $\text{H}_2\text{O}_2/\text{O}$ ratio (Figures 6(b) and 6(c)) were significantly decreased by 31-53% in the LEAK and OXPHOS states. These results show that R-phenibut and S-phenibut reduce ROS production without affecting the mitochondrial electron transfer system capacities, indicating the improvement of mitochondrial coupling. In addition, both R- and S-phenibut attenuated calcium-induced brain mitochondrial swelling (two-way repeated-measures ANOVA: main effect of treatment ($F_{(40,360)} = 4.576$, $p < 0.0001$), time ($F_{(2,611,46.99)} = 104.5$, $p < 0.0001$), and interaction between treatment and time ($F_{(40,360)} = 4.576$, $p < 0.0001$); Figure 6(d)).

Thus, the phenibut treatment-induced protection of mitochondria against anoxia-reoxygenation could be due to a reduction in ROS production and the modulation of Ca^{2+} signalling.

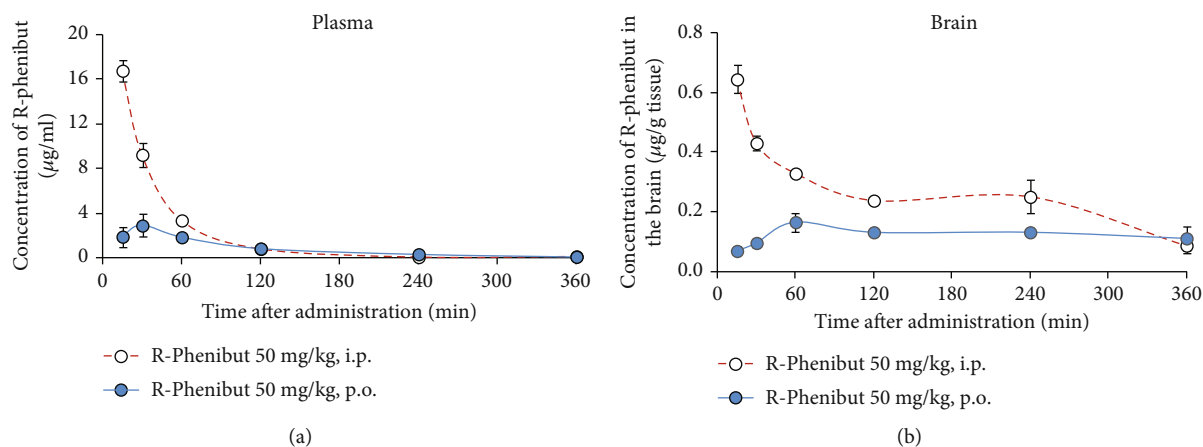


FIGURE 1: The concentration of R-phenibut in the mouse plasma and brain tissue after a single administration. Mice received an i.p. and p.o. injection of R-phenibut at a dose of 50 mg/kg. The amount of compound in the plasma (a) and brain tissue extracts (b) was measured 15 and 30 min and 1, 2, 4, and 6 h after R-phenibut administration ($n = 3$). Values are represented as the mean \pm S.E.M..

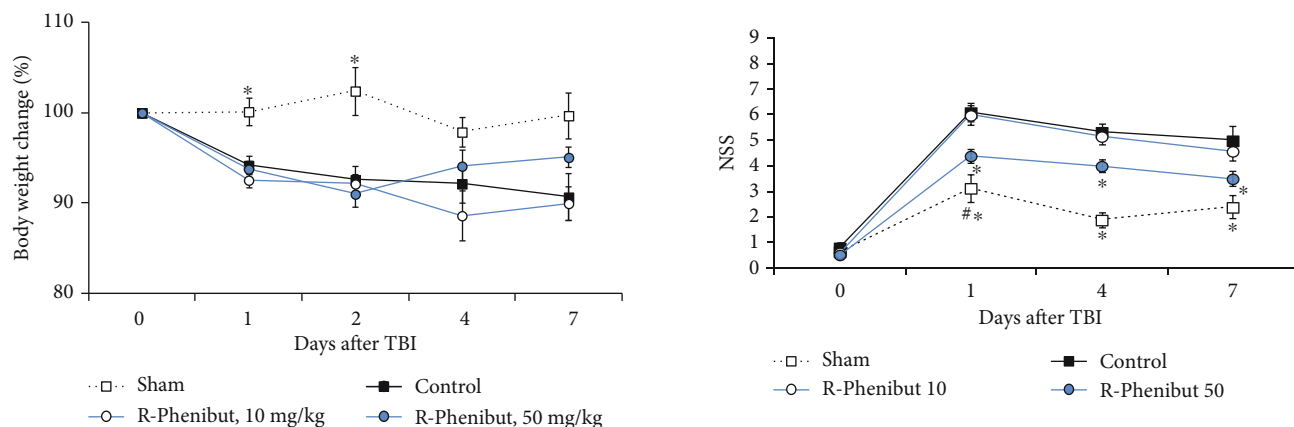


FIGURE 2: Body weight changes of the sham-operated, control, and R-phenibut treatment groups. Mice were weighed before and 1, 2, 4, and 7 days after latFPI. Data are expressed as the percentage change in body weight relative to the initial body weight of each animal (%). Data are shown as the mean \pm S.E.M. ($n = 8 - 12$). *Indicates a significant difference compared to the sham-operated group (two-way repeated-measures ANOVA followed by Dunnett's multiple comparison test; $*P < 0.05$).

4. Discussion

In the current study, we examined the effects of R-phenibut treatment on brain trauma induced by latFPI. For the first time, we showed that R-phenibut could be detected in the mouse brain 15 min after a single p.o. or i.p. injection and found in brain extracts even 24 h after the administration. The present study confirms that R-phenibut, which is an antagonist of the $\alpha_2\delta$ subunit of VDCC and an agonist of GABA-B receptors, improves sensorimotor functional outcomes and significantly ameliorates brain damage and neuronal death in the acute phase after TBI via mechanisms related to Ca^{2+} homeostasis and oxidative stress.

The binding characteristics of R-phenibut were previously investigated using radiolabeled gabapentin that was the first ligand shown to bind to the $\alpha_2\delta_1$ and $\alpha_2\delta_2$ subunits with high affinity ($K_d = 59$ and 153 nM, respectively), while

FIGURE 3: Effects of R-phenibut on the neurological severity score (NSS) after TBI. R-phenibut and saline were initially administered i.p. 2 h after injury and then once daily for an additional 7 days for a total treatment period of 1 week. Data are shown as the mean \pm S.E.M. ($n = 8 - 12$). *Indicates a significant difference compared to the control group; #indicates a significant difference compared to the sham-operated group (two-way repeated-measures ANOVA followed by Dunnett's multiple comparison test; $*P < 0.05$; $\#P < 0.01$).

at the same time demonstrating no binding activity to the $\alpha_2\delta_3$ and $\alpha_2\delta_4$ subunits [36, 37]. The pathologies associated with gene disruption of $\alpha_2\delta_1$ protein include neuropathic pain and cardiac dysfunction, while in case of $\alpha_2\delta_2$ protein, the pathologies are related to epilepsy and cerebellar ataxia [38]. We showed previously that pharmacological activity of R-phenibut is associated with neuropathic pain rather than epilepsy [6]; thus, we could speculate that the effects of R-phenibut are $\alpha_2\delta_1$ protein binding-related.

The $\alpha_2\delta$ subunits of VDCC are widely expressed by excitatory neurons in the cerebral cortex, hippocampus, and other brain regions [39, 40]. Furthermore, the $\alpha_2\delta$ subunits of VDCC have been shown to be involved in processes that are not directly linked to calcium channel function, such as synaptogenesis [41]. Other studies have reported that the administration of VDCC ligands in rodent models of TBI

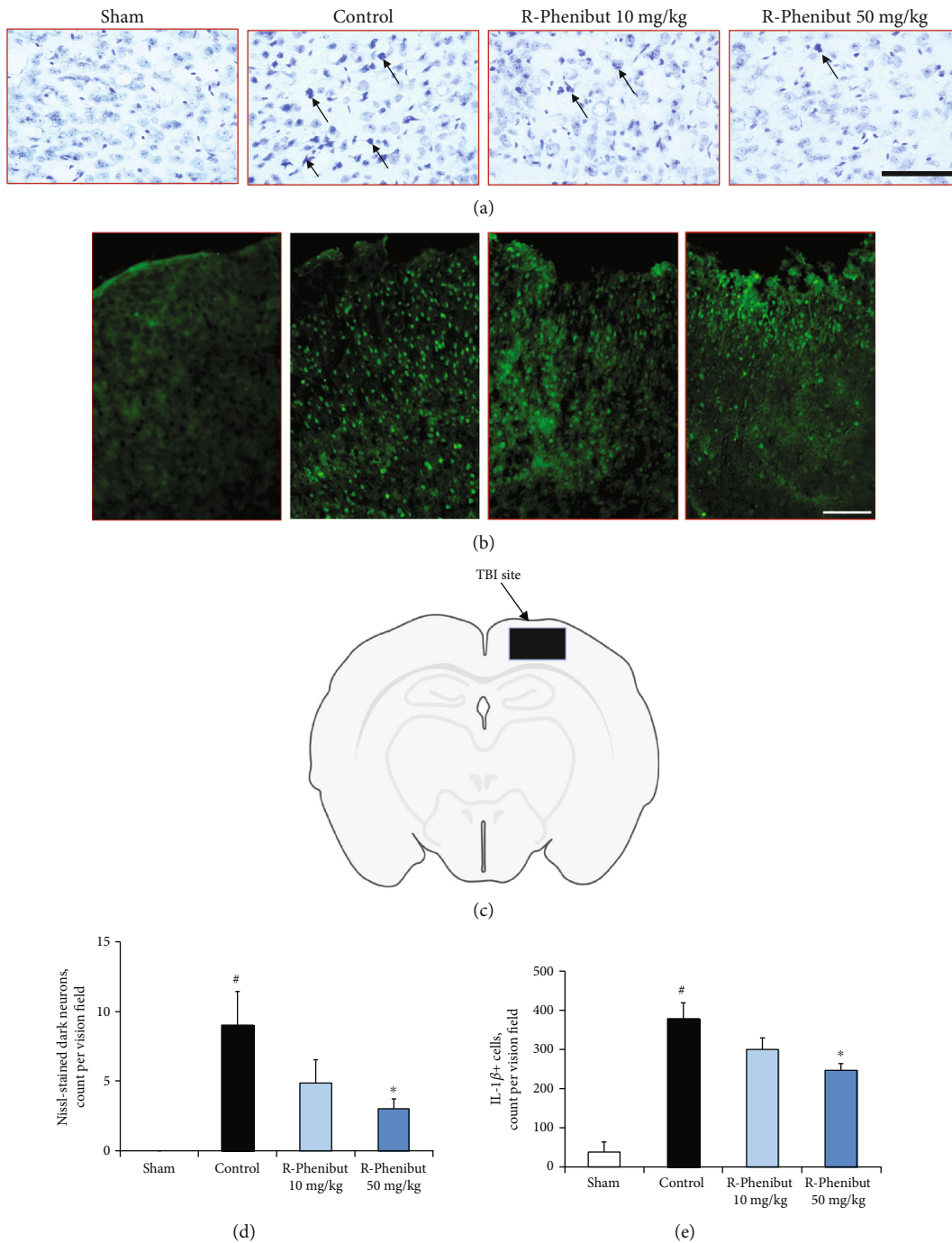


FIGURE 4: Cresyl violet (Nissl) and IL-1 β immunofluorescence staining 7 days post-TBI. (a) Cresyl violet-stained sections of the mouse neocortex ipsilateral to the injury site. R-Phenibut treatment at doses of 10 mg/kg and 50 mg/kg reduced the number of N-DNs. Scale bar = 100 μm . (b) IL-1 β expression based on immunofluorescence staining in the mouse neocortex ipsilateral to the injury site. R-Phenibut treatment at doses of 10 mg/kg and 50 mg/kg reduced the number of IL-1 β -positive cells. Scale bar = 250 μm . (c) Schematic illustration of the brain region indicated in the filled area, which was selected for the quantitative analysis of cell injury. (d) Quantitative assessment of N-DNs in the ipsilateral cortex at postinjury day 7. Data are expressed as the mean \pm S.E.M. ($n = 7$ for the R-phenibut 50 mg/kg group and $n = 6$ for the sham, control, and R-phenibut 10 mg/kg groups). (e) Quantitative assessment of IL-1 β -positive cells in the ipsilateral cortex at postinjury day 7. Data are expressed as the mean \pm S.E.M. ($n = 4$ for the control group and $n = 3$ for the sham, R-phenibut 10 mg/kg, and 50 mg/kg groups). [#]Indicates a significant difference compared to the sham-operated group; ^{*}indicates a significant difference compared to the control group (one-way ANOVA followed by Tukey's multiple comparison test; $*P < 0.05$).

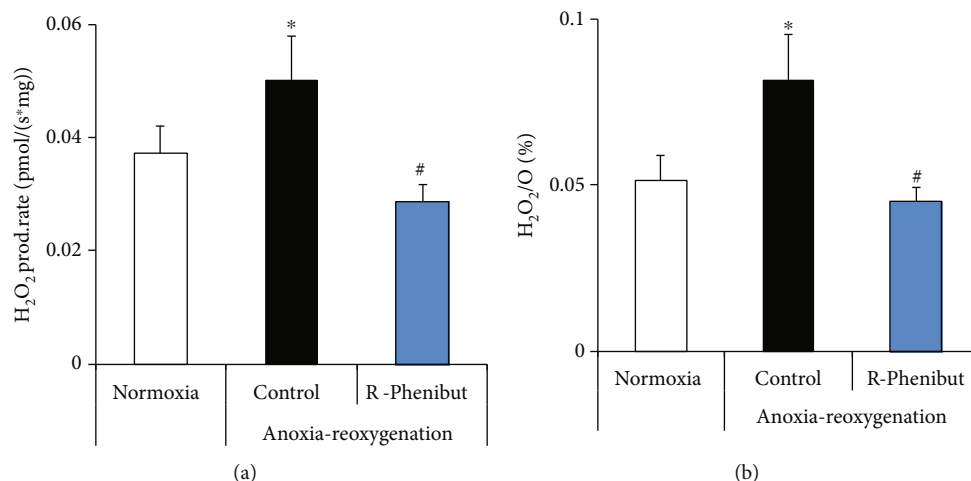


FIGURE 5: The effects of R-phenibut (0.5 $\mu\text{g/ml}$) on ROS production in an *in vitro* anoxia-reoxygenation model. After anoxia-reoxygenation, the H_2O_2 production rate (a) and $\text{H}_2\text{O}_2/\text{O}$ ratio (b) were significantly decreased in the R-phenibut group. The results are presented as the mean \pm S.D. of 6 independent replicates. *Indicates a significant difference compared to normoxia; # indicates a significant difference compared to the anoxia-reoxygenation control group (one-way ANOVA followed by Tukey's multiple comparison test; * $P < 0.05$).

reduced cell death and improved cognitive function [40]. Similar to phenibut, ligands of the $\alpha_2\delta$ subunit of VDCC, such as pregabalin, at a high dose of 60 mg/kg reduce neuronal loss and improve functional outcomes 24 h after trauma in experimental models of TBI [41, 42]. Moreover, pregabalin at a dose of 30 mg/kg has been shown to improve functional recovery and to demonstrate anti-inflammatory and anti-apoptotic effects in a rat model of spinal cord injury [43, 44].

Cytoskeletal protein loss results in altered neuronal morphology after TBI [45, 46]. N-DNs represent a typical pathomorphological change in injured neurons after TBI, showing abnormal basophilia and shrinkage [27, 28]. N-DNs appear in the neocortex immediately after TBI and can be observed even two weeks postinjury [27, 47]. In addition, IL-1 is a major driver of the secondary neuronal injury cascade after TBI [48]. It is involved in the recruitment of other types of immune cells, neuronal apoptosis, and blood-brain barrier disruption after TBI [49–51]. Furthermore, IL-1 β antagonism was shown to be neuroprotective in clinical trials and in rodent models of TBI [52–54]. The present study shows that treatment with R-phenibut at a dose of 50 mg/kg significantly reduced the number of N-DNs and significantly reduced IL-1 β expression in the neocortex after TBI. The histopathological findings of the current study revealed that R-phenibut could attenuate neuronal damage, inflammation, and degeneration.

For the first time, we showed that R-phenibut limits mitochondrial dysfunction in the brain induced by anoxia-reoxygenation. Compared with other types of cells, neurons are endowed with less robust antioxidant defence systems [55]. As mitochondrial dysfunction has been shown to be involved in TBI, perturbations in energy metabolism are likely to contribute to the pathogenesis of TBI [56, 57]. In TBI, oxidative cell damage is caused by an imbalance between the production and accumulation of ROS, in which mitochondria are the major intracellular source of ROS. Accordingly, there is accumulating evidence that antioxidant agents and membrane lipid peroxidation inhibitors, such as tirilazad, U-78517F and U-83836E, are effective in treating

preclinical models of TBI [17]. Mitochondrial-targeted drugs, such as mitoquinone and thymoquinone-containing antioxidants, have been shown to decrease neurological deficits and β -amyloid-induced neurotoxicity after TBI [58, 59]. Meanwhile, the inhibition of ROS production has been shown to inhibit secretion of IL-1 β [60].

Notably, the immunosuppressant drug cyclosporine A, which is an IL-1 β receptor antagonist, has been shown to decrease pathological changes in the brain after TBI by blocking the mitochondrial permeability transition pore [61]. Our results indicate that R-phenibut treatment improves mitochondrial tolerance and thus protects brain energetics against anoxia-reoxygenation damage by reducing ROS production. R-Phenibut treatment reduces ROS production without affecting the mitochondrial electron transfer system capacities, indicating the improvement of mitochondrial coupling. Another study has demonstrated that phenibut has neuroprotective effects *in vitro* but does not possess antioxidant potential [62]. Perfilova et al. recently showed that phenibut can limit heart and brain mitochondrial damage in rats exposed to stress [63].

To determine the molecular mechanisms underlying the actions of R-phenibut against anoxia-reoxygenation-induced mitochondrial damage, the activity of the R- and S-enantiomers of racemic phenibut was compared. We found that both R-phenibut and S-phenibut reduced mitochondrial ROS production and inhibited Ca^{2+} -induced mitochondrial swelling. This suggests that the protective effects of R-phenibut in mitochondria do not involve the GABA-B receptor (in contrast to R-phenibut, S-phenibut does not bind to the GABA-B receptor) and might be mediated by the $\alpha_2\delta_1$ subunit of VDCC. It was shown previously that increased intracellular Ca^{2+} , as a result of increased activity of $\alpha_2\delta_1$, could be rapidly taken up by mitochondria and subsequently released into the cytoplasm avoiding Ca^{2+} accumulation and maintaining intracellular Ca^{2+} signalling [19]. This could explain why, in the presence of R- and S-phenibut, reduced Ca^{2+} -induced mitochondrial swelling was observed. Both R-phenibut and S-phenibut demonstrate mitochondrial-

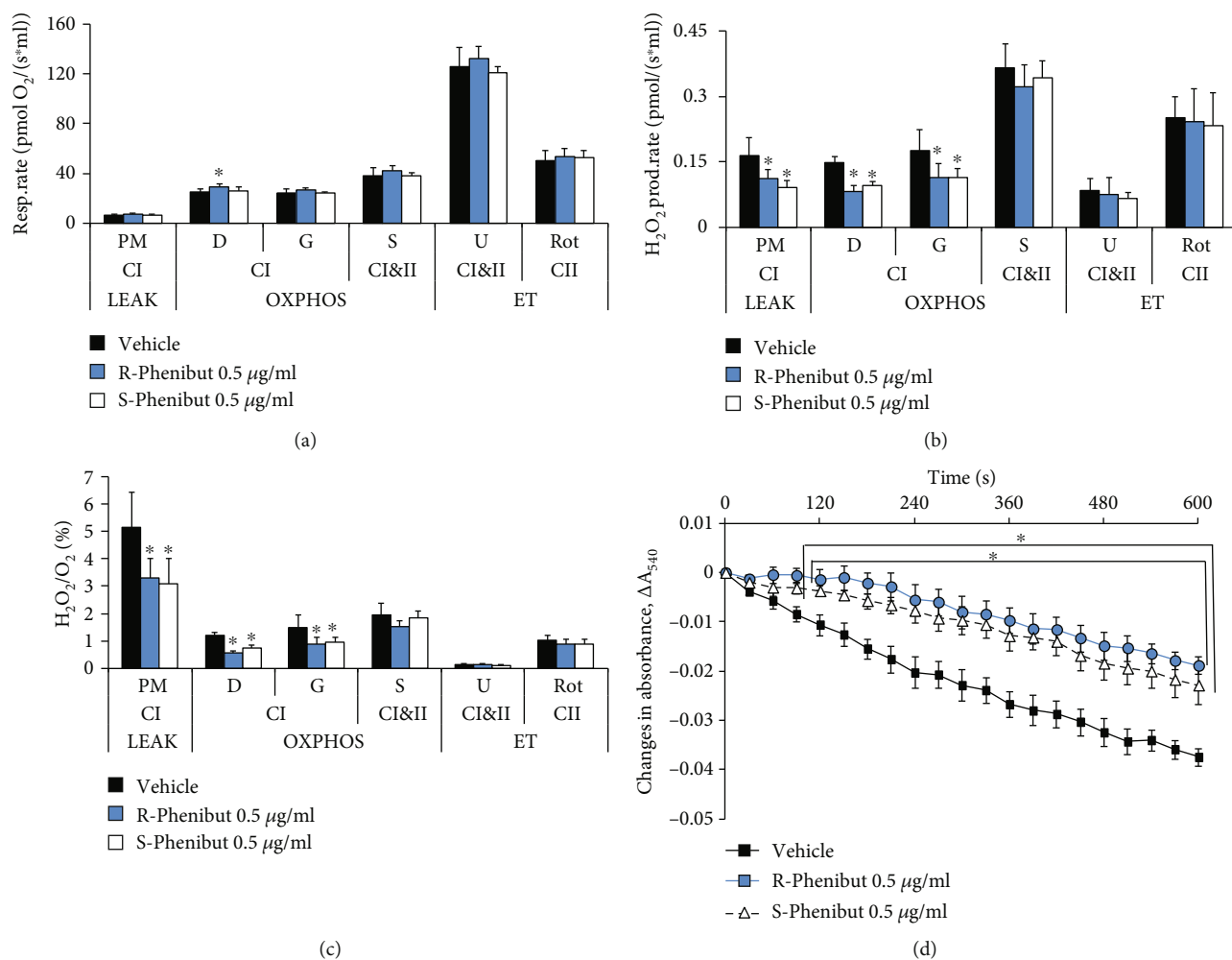


FIGURE 6: The effects of R-phenibut and S-phenibut (0.5 μg/ml) on mitochondrial functionality and Ca²⁺-induced swelling in isolated mouse brain mitochondria. R-Phenibut and S-phenibut did not affect the mitochondrial respiration rate (a) but significantly decreased the H₂O₂ production rate (b) and H₂O₂/O₂ ratio (c). The results are presented as the mean ± S.D. of 5 independent measurements. P: pyruvate; M: malate; D: ADP; G: glutamate; S: succinate; U: uncoupler; Rot: rotenone; CI: complex I; CII: complex II; LEAK: substrate metabolism-dependent state; OXPHOS: oxidative phosphorylation-dependent state; ET: electron transfer capacity state. *Indicates a significant difference compared to the control group (one-way ANOVA followed by Tukey's multiple comparison test, **P* < 0.05). Both R-phenibut and S-phenibut at a concentration of 0.5 μg/ml significantly attenuated Ca²⁺-induced swelling (d). The results are presented as the mean ± S.D. of 7 independent replicates. *Indicates a significant difference compared to the control group (two-way repeated-measures ANOVA followed by Dunnett's multiple comparison test; **P* < 0.05).

protective properties against anoxia-reoxygenation and Ca²⁺-induced stress. Since there is no evidence of α₂δ localization in the mitochondrial membrane, it is possible that compounds could alter Ca²⁺ signalling pathways and protect mitochondria by targeting mitochondrial-specific or mitochondrial-endoplasmic reticulum-associated Ca²⁺ transporters.

Our study has several limitations. One of the limitations of this study is that the level of ROS in mouse brain after treatment of R-phenibut following TBI was not measured. Another limitation is the increase in the NSS score between the baseline value and the first day postcraniotomy in the sham-operated group. The increase of the NSS score in sham-operated mice was reported previously and can be related to the distinct injury caused by craniotomy procedures [64]. Similar to other studies, the NSS score of injured mice showed maximum deficits on postinjury day 1 and

remained elevated at 1, 2, 4, and 7 days after latFPI [64, 65]. A potential limitation of this study is that only male mice were used in experiments.

5. Conclusions

In conclusion, R-phenibut treatment reduces TBI-induced neuronal death and improves functional recovery, suggesting its therapeutic potential. The present study suggests that the neuroprotective properties of phenibut may be mediated by its effects on mitochondrial calcium influx and ROS generation.

Data Availability

The data used to support the findings of this study are available from the corresponding author upon request.

Conflicts of Interest

The authors declare that there is no conflict of interest regarding the publication of this paper.

Acknowledgments

This study was supported by the framework of the EU-ERA-NET NEURON projects TRAINS and CnsAflame.

References

- [1] A. M. Rubiano, N. Carney, R. Chesnut, and J. C. Puyana, "Global neurotrauma research challenges and opportunities," *Nature*, vol. 527, no. 7578, pp. S193–S197, 2015.
- [2] L. J. Carroll, J. D. Cassidy, C. Cancelliere et al., "Systematic review of the prognosis after mild traumatic brain injury in adults: cognitive, psychiatric, and mortality outcomes: results of the international collaboration on mild traumatic brain injury prognosis," *Archives of Physical Medicine and Rehabilitation*, vol. 95, no. 3, pp. S152–S173, 2014.
- [3] M. Majdan, D. Plancikova, A. Brazinova et al., "Epidemiology of traumatic brain injuries in Europe: a cross-sectional analysis," *Lancet Public Health*, vol. 1, no. 2, pp. e76–e83, 2016.
- [4] E. Kupats, J. Vrublevska, B. Zvejniece et al., "Safety and tolerability of the anxiolytic and nootropic drug phenibut: a systematic review of clinical trials and case reports," *Pharmacopsychiatry*, vol. 53, no. 5, pp. 201–208, 2020.
- [5] I. Lapin, "Phenibut (beta-phenyl-GABA): a tranquilizer and nootropic drug," *CNS Drug Reviews*, vol. 7, no. 4, pp. 471–481, 2001.
- [6] L. Zvejniece, E. Vavers, B. Svalbe et al., "R-phenibut binds to the $\alpha 2\text{-}\delta$ subunit of voltage-dependent calcium channels and exerts gabapentin-like anti-nociceptive effects," *Pharmacology, Biochemistry, and Behavior*, vol. 137, pp. 23–29, 2015.
- [7] I. Belozertseva, J. Nagel, B. Valastro, L. Franke, and W. Danysz, "Optical isomers of phenibut inhibit $[\text{H}^3]$ -gabapentin binding in vitro and show activity in animal models of chronic pain," *Pharmacological Reports*, vol. 68, no. 3, pp. 550–554, 2016.
- [8] M. Dambrova, L. Zvejniece, E. Liepinsh et al., "Comparative pharmacological activity of optical isomers of phenibut," *European Journal of Pharmacology*, vol. 583, no. 1, pp. 128–134, 2008.
- [9] E. Vavers, L. Zvejniece, B. Svalbe et al., "The neuroprotective effects of R-phenibut after focal cerebral ischemia," *Pharmacological Research*, vol. 113, pp. 796–801, 2016.
- [10] H. M. Bramlett and W. D. Dietrich, "Pathophysiology of cerebral ischemia and brain trauma: similarities and differences," *Journal of Cerebral Blood Flow & Metabolism*, vol. 24, no. 2, pp. 133–150, 2004.
- [11] Y. Xiong, A. Mahmood, and M. Chopp, "Animal models of traumatic brain injury," *Nature Reviews Neuroscience*, vol. 14, no. 2, pp. 128–142, 2013.
- [12] L. Zvejniece, G. Stelfa, E. Vavers et al., "Skull fractures induce neuroinflammation and worsen outcomes after closed head injury in mice," *Journal of Neurotrauma*, vol. 37, no. 2, pp. 295–304, 2020.
- [13] A. Görlach, K. Bertram, S. Hudcová, and O. Krizanová, "Calcium and ROS: a mutual interplay," *Redox Biology*, vol. 6, pp. 260–271, 2015.
- [14] D. N. Granger and P. R. Kvietys, "Reperfusion injury and reactive oxygen species: the evolution of a concept," *Redox Biology*, vol. 6, pp. 524–551, 2015.
- [15] M. Bains and E. D. Hall, "Antioxidant therapies in traumatic brain and spinal cord injury," *Biochimica et Biophysica Acta*, vol. 1822, no. 5, pp. 675–684, 2012.
- [16] J. T. Weber, "Altered calcium signaling following traumatic brain injury," *Frontiers in Pharmacology*, vol. 3, p. 60, 2012.
- [17] E. D. Hall, R. A. Vaishnav, and A. G. Mustafa, "Antioxidant therapies for traumatic brain injury," *Neurotherapeutics*, vol. 7, no. 1, pp. 51–61, 2010.
- [18] G. Cheng, R. Kong, L. Zhang, and J. Zhang, "Mitochondria in traumatic brain injury and mitochondrial-targeted multipotential therapeutic strategies," *British Journal of Pharmacology*, vol. 167, no. 4, pp. 699–719, 2012.
- [19] M. D'Arco, W. Margas, J. S. Cassidy, and A. C. Dolphin, "The upregulation of $\alpha 2\delta\text{-}1$ subunit modulates activity-dependent Ca^{2+} signals in sensory neurons," *The Journal of Neuroscience*, vol. 35, no. 15, pp. 5891–5903, 2015.
- [20] T. Kinjo, Y. Ashida, H. Higashi et al., "Alleviation by GABAB receptors of neurotoxicity mediated by mitochondrial permeability transition pore in cultured murine cortical neurons exposed to N-methyl-D-aspartate," *Neurochemical Research*, vol. 43, no. 1, pp. 79–88, 2018.
- [21] J. Flygt, K. Ruscher, A. Norberg et al., "Neutralization of interleukin- 1β following diffuse traumatic brain injury in the mouse attenuates the loss of mature oligodendrocytes," *Journal of Neurotrauma*, vol. 35, no. 23, pp. 2837–2849, 2018.
- [22] N. Marklund, "Rodent models of traumatic brain injury: methods and challenges," *Methods in Molecular Biology*, vol. 1462, pp. 29–46, 2016.
- [23] C. Kilkenny, W. Browne, I. C. Cuthill, M. Emerson, D. G. Altman, and NC3Rs Reporting Guidelines Working Group, "Animal research: reporting in vivo experiments: the ARRIVE guidelines," *The Journal of Gene Medicine*, vol. 12, no. 7, pp. 561–563, 2010.
- [24] J. C. McGrath, G. B. Drummond, E. M. McLachlan, C. Kilkenny, and C. L. Wainwright, "Guidelines for reporting experiments involving animals: the ARRIVE guidelines," *British Journal of Pharmacology*, vol. 160, no. 7, pp. 1573–1576, 2010.
- [25] L. Zvejniece, B. Zvejniece, M. Videja et al., "Neuroprotective and anti-inflammatory activity of DAT inhibitor R-phenylpiracetam in experimental models of inflammation in male mice," *Inflammopharmacology*, vol. 28, no. 5, pp. 1283–1292, 2020.
- [26] M. A. Flierl, P. F. Stahel, K. M. Beauchamp, S. J. Morgan, W. R. Smith, and E. Shohami, "Mouse closed head injury model induced by a weight-drop device," *Nature Protocols*, vol. 4, no. 9, pp. 1328–1337, 2009.
- [27] H. Ooigawa, H. Nawashiro, S. Fukui et al., "The fate of Nissl-stained dark neurons following traumatic brain injury in rats: difference between neocortex and hippocampus regarding survival rate," *Acta Neuropathologica*, vol. 112, no. 4, pp. 471–481, 2006.
- [28] R. Hicks, H. Soares, D. Smith, and T. McIntosh, "Temporal and spatial characterization of neuronal injury following lateral fluid-percussion brain injury in the rat," *Acta Neuropathologica*, vol. 91, no. 3, pp. 236–246, 1996.
- [29] M. Makrecka-Kuka, G. Krumschnabel, and E. Gnaiger, "High-resolution respirometry for simultaneous measurement of oxygen and hydrogen peroxide fluxes in permeabilized cells,

- tissue homogenate and isolated mitochondria,” *Biomolecules*, vol. 5, no. 3, pp. 1319–1338, 2015.
- [30] G. Krumschnabel, M. Fontana-Ayoub, Z. Sumbalova et al., “Simultaneous high-resolution measurement of mitochondrial respiration and hydrogen peroxide production,” *Methods in Molecular Biology*, vol. 1264, pp. 245–261, 2015.
- [31] J. Burtscher, L. Zangrandi, C. Schwarzer, and E. Gnaiger, “Differences in mitochondrial function in homogenated samples from healthy and epileptic specific brain tissues revealed by high-resolution respirometry,” *Mitochondrion*, vol. 25, pp. 104–112, 2015.
- [32] M. Makrecka, B. Svalbe, K. Volska et al., “Mildronate, the inhibitor of L-carnitine transport, induces brain mitochondrial uncoupling and protects against anoxia-reoxygenation,” *European Journal of Pharmacology*, vol. 723, pp. 55–61, 2014.
- [33] T. Kristián, J. Gertsch, T. E. Bates, and B. K. Siesjö, “Characteristics of the calcium-triggered mitochondrial permeability transition in nonsynaptic brain mitochondria: effect of cyclosporin A and ubiquinone O,” *Journal of Neurochemistry*, vol. 74, no. 5, pp. 1999–2009, 2000.
- [34] C. P. Baines, R. A. Kaiser, N. H. Purcell et al., “Loss of cyclophilin D reveals a critical role for mitochondrial permeability transition in cell death,” *Nature*, vol. 434, no. 7033, pp. 658–662, 2005.
- [35] T. Kobayashi, S. Kuroda, M. Tada, K. Houkin, Y. Iwasaki, and H. Abe, “Calcium-induced mitochondrial swelling and cytochrome c release in the brain: its biochemical characteristics and implication in ischemic neuronal injury,” *Brain Research*, vol. 960, no. 1-2, pp. 62–70, 2003.
- [36] E. Marais, N. Klugbauer, and F. Hofmann, “Calcium channel $\alpha(2)\delta$ subunits-structure and gabapentin binding,” *Molecular Pharmacology*, vol. 59, no. 5, pp. 1243–1248, 2001.
- [37] N. Qin, S. Yagel, M.-L. Momplaisir, E. E. Codd, and M. R. D’Andrea, “Molecular cloning and characterization of the human voltage-gated calcium channel $\alpha 2\delta$ -4 subunit,” *Molecular Pharmacology*, vol. 62, no. 3, pp. 485–496, 2002.
- [38] A. C. Dolphin, “The $\alpha 2\delta$ subunits of voltage-gated calcium channels,” *Biochimica et Biophysica Acta*, vol. 1828, no. 7, pp. 1541–1549, 2013.
- [39] C. P. Taylor and R. Garrido, “Immunostaining of rat brain, spinal cord, sensory neurons and skeletal muscle for calcium channel $\alpha 2$ -delta ($\alpha 2$ - δ) type 1 protein,” *Neuroscience*, vol. 155, no. 2, pp. 510–521, 2008.
- [40] G. Gurkoff, K. Shahlaie, B. Lyeth, and R. Berman, “Voltage-gated calcium channel antagonists and traumatic brain injury,” *Pharmaceuticals (Basel)*, vol. 6, no. 7, pp. 788–812, 2013.
- [41] C. Calikoglu, H. Aytakin, O. Akgül et al., “Effect of pregabalin in preventing secondary damage in traumatic brain injury: an experimental study,” *Medical Science Monitor*, vol. 21, pp. 813–820, 2015.
- [42] M. Shamsi Meymandi, Z. Soltani, G. Sepehri, S. Amiresmaili, F. Farahani, and M. Moeini Aghaei, “Effects of pregabalin on brain edema, neurologic and histologic outcomes in experimental traumatic brain injury,” *Brain Research Bulletin*, vol. 140, pp. 169–175, 2018.
- [43] K.-Y. Ha, Y.-H. Kim, K.-W. Rhyu, and S.-E. Kwon, “Pregabalin as a neuroprotector after spinal cord injury in rats,” *European Spine Journal*, vol. 17, no. 6, pp. 864–872, 2008.
- [44] K.-Y. Ha, E. Carragee, I. Cheng, S.-E. Kwon, and Y.-H. Kim, “Pregabalin as a neuroprotector after spinal cord injury in rats: biochemical analysis and effect on glial cells,” *Journal of Korean Medical Science*, vol. 26, no. 3, pp. 404–411, 2011.
- [45] J. K. Newcomb, A. Kampfl, R. M. Posmantur et al., “Immunohistochemical study of calpain-mediated breakdown products to alpha-spectrin following controlled cortical impact injury in the rat,” *Journal of Neurotrauma*, vol. 14, no. 6, pp. 369–383, 1997.
- [46] R. M. Posmantur, J. K. Newcomb, A. Kampfl, and R. L. Hayes, “Light and confocal microscopic studies of evolutionary changes in neurofilament proteins following cortical impact injury in the rat,” *Experimental Neurology*, vol. 161, no. 1, pp. 15–26, 2000.
- [47] L. Talley Watts, J. A. Long, J. Chemello et al., “Methylene blue is neuroprotective against mild traumatic brain injury,” *Journal of Neurotrauma*, vol. 31, no. 11, pp. 1063–1071, 2014.
- [48] E. A. Newell, B. P. Todd, J. Mahoney, A. A. Pieper, P. J. Ferguson, and A. G. Bassuk, “Combined blockade of interleukin-1 α and -1 β signaling protects mice from cognitive dysfunction after traumatic brain injury,” *eNeuro*, vol. 5, no. 2, pp. -ENEURO.0385–ENEU17.2018, 2018.
- [49] M. Sun, R. D. Brady, D. K. Wright et al., “Treatment with an interleukin-1 receptor antagonist mitigates neuroinflammation and brain damage after polytrauma,” *Brain, Behavior, and Immunity*, vol. 66, pp. 359–371, 2017.
- [50] N. J. Rothwell and G. N. Luheshi, “Interleukin 1 in the brain: biology, pathology and therapeutic target,” *Trends in Neurosciences*, vol. 23, no. 12, pp. 618–625, 2000.
- [51] K.-T. Lu, Y.-W. Wang, J.-T. Yang, Y.-L. Yang, and H.-I. Chen, “Effect of interleukin-1 on traumatic brain injury-induced damage to hippocampal neurons,” *Journal of Neurotrauma*, vol. 22, no. 8, pp. 885–895, 2005.
- [52] F. Clausen, A. Hånell, M. Björk et al., “Neutralization of interleukin-1 β modifies the inflammatory response and improves histological and cognitive outcome following traumatic brain injury in mice,” *The European Journal of Neuroscience*, vol. 30, no. 3, pp. 385–396, 2009.
- [53] R. Tehranian, S. Andell-Jonsson, S. M. Beni et al., “Improved recovery and delayed cytokine induction after closed head injury in mice with central overexpression of the secreted isoform of the interleukin-1 receptor antagonist,” *Journal of Neurotrauma*, vol. 19, no. 8, pp. 939–951, 2002.
- [54] J. Lazovic, A. Basu, H.-W. Lin et al., “Neuroinflammation and both cytotoxic and vasogenic edema are reduced in interleukin-1 type 1 receptor-deficient mice conferring neuroprotection,” *Stroke*, vol. 36, no. 10, pp. 2226–2231, 2005.
- [55] R. A. Floyd and J. M. Carney, “Free radical damage to protein and DNA: mechanisms involved and relevant observations on brain undergoing oxidative stress,” *Annals of Neurology*, vol. 32, no. S1, pp. S22–S27, 1992.
- [56] C. Werner and K. Engelhard, “Pathophysiology of traumatic brain injury,” *British Journal of Anaesthesia*, vol. 99, no. 1, pp. 4–9, 2007.
- [57] M. Prins, T. Greco, D. Alexander, and C. C. Giza, “The pathophysiology of traumatic brain injury at a glance,” *Disease Models & Mechanisms*, vol. 6, no. 6, pp. 1307–1315, 2013.
- [58] E. E. Genrikhs, E. V. Stelmashook, O. V. Popova et al., “Mitochondria-targeted antioxidant SkQT1 decreases trauma-induced neurological deficit in rat and prevents amyloid- β -induced impairment of long-term potentiation in rat

- hippocampal slices,” *Journal of Drug Targeting*, vol. 23, no. 4, pp. 347–352, 2015.
- [59] J. Zhou, H. Wang, R. Shen et al., “Mitochondrial-targeted antioxidant MitoQ provides neuroprotection and reduces neuronal apoptosis in experimental traumatic brain injury possibly via the Nrf2-ARE pathway,” *American Journal of Translational Research*, vol. 10, no. 6, pp. 1887–1899, 2018.
- [60] R. L. Schmidt and L. L. Lenz, “Distinct licensing of IL-18 and IL-1 β secretion in response to NLRP3 inflammasome activation,” *PLoS One*, vol. 7, no. 9, article e45186, 2012.
- [61] R. L. Veech, C. R. Valeri, and T. B. VanItallie, “The mitochondrial permeability transition pore provides a key to the diagnosis and treatment of traumatic brain injury,” *IUBMB Life*, vol. 64, no. 2, pp. 203–207, 2012.
- [62] D. Huynh, C. S. Wai, A. Liang, T. J. Maher, and A. Pino-Figueroa, “In vitro neuroprotective activity of phenibut,” *The FASEB Journal*, vol. 26, 672.6 pages, 2012.
- [63] V. N. Perfilova, T. A. Popova, I. I. Prokofiev, I. S. Mokrousov, O. V. Ostrovskii, and I. N. Tyurenkov, “Effect of phenibut and glufimet, a novel glutamic acid derivative, on respiration of heart and brain mitochondria from animals exposed to stress against the background of inducible NO-synthase blockade,” *Bulletin of Experimental Biology and Medicine*, vol. 163, no. 2, pp. 226–229, 2017.
- [64] J. T. Cole, A. Yarnell, W. S. Kean et al., “Craniotomy: true sham for traumatic brain injury, or a sham of a sham?,” *Journal of Neurotrauma*, vol. 28, no. 3, pp. 359–369, 2011.
- [65] L. D. Schurman, T. L. Smith, A. J. Morales et al., “Investigation of left and right lateral fluid percussion injury in C57BL6/J mice: in vivo functional consequences,” *Neuroscience Letters*, vol. 653, pp. 31–38, 2017.

Review Article

Monoclonal Antibody to CD14, TLR4, or CD11b: Impact of Epitope and Isotype Specificity on ROS Generation by Human Granulocytes and Monocytes

Dmitry S. Kabanov ¹, Sergey V. Grachev ^{1,2} and Isabella R. Prokhorenko ¹

¹Department of Molecular Biomedicine, Institute of Basic Biological Problems, Federal Research Center “Pushchino Scientific Center for Biological Research of the Russian Academy of Sciences”, Pushchino 142290, Russia

²Department of Human Pathology of the Institute of Clinical Medicine, Federal State Autonomous Educational Institution of Higher Education I. M. Sechenov’s First Moscow State Medical University of Russian Healthcare Ministry (Sechenov University), Moscow 119991, Russia

Correspondence should be addressed to Dmitry S. Kabanov; kabanovd1@rambler.ru

Received 19 July 2020; Revised 24 September 2020; Accepted 10 November 2020; Published 21 November 2020

Academic Editor: Luciano Saso

Copyright © 2020 Dmitry S. Kabanov et al. This is an open access article distributed under the Creative Commons Attribution License, which permits unrestricted use, distribution, and reproduction in any medium, provided the original work is properly cited.

Lipopolysaccharides (LPSs or endotoxins) from Gram-negative bacteria represent pathogen-associated molecular patterns (PAMPs) that are recognized by CD14 and Toll-like receptor 4 (TLR4). Lipopolysaccharides prime polymorphonuclear leukocytes (PMNs) for substantial production of reactive oxygen species (ROS) during its response to secondary stimuli such as chemoattractants or pathogens. The excessive ROS production can damage surrounding host tissues, thereby amplifying the inflammatory reaction caused by pathogens. Today, specific antibodies against CD14, TLR4, and CD11b are being used as the essential tools to elucidate the role of these receptors in acute inflammation and some of these antibodies have advised as therapeutic agents for clinical use. Because each antibody has two antigen-binding arms [F(ab')₂] and one Fc arm, its effect on cellular response is much more complicated rather than simple blockage of target receptor. In fact, IgG antibody, once bound to target receptor, engages Fc receptors γ (Fc γ Rs) and thereby is able to activate the adaptive immune system. The consequences of antibody-dependent binary heterotypic association of CD14, TLR4, or CD11b with Fc γ Rs as well as homotypic one on ROS production are not well elucidated. Moreover, the consequences of antigenic recognition of CD14, TLR4, or CD11b by specific F(ab')₂ fragments are not always investigated. In this review, we will discuss known mechanisms underlying the therapeutic efficiency of CD14, TLR4, and CD11b/CD18 antibodies with a focus on LPS-dependent ROS or cytokine production by PMNs or monocytes. The impacts of F(ab')₂ as well as antibody IgG subclasses (isotypes) in therapeutic efficiency or agonistic potency of known antibodies against abovementioned receptors are presented. We also pay attention to how the efficiency of different IgG antibody subclasses is modulated during LPS-induced inflammation and by production of priming agents such as interferon γ (IFN- γ). Our review reinforces the molecular targets and therapeutic approaches to amelioration of harmful consequences of excessive activation of human pattern recognition receptors.

1. Introduction

Inflammatory and immune diseases affect millions of people worldwide, providing an impetus to develop new anti-inflammatory and immunomodulatory therapies. Over the past two decades, great progress has been made in elucidating the molecular basis of the inflammation process during infec-

tious, autoimmune, and malignant diseases [1–4]. It favors the development of new therapeutic drugs directly targeting cell surface or intracellular molecules involved in the initiation and progression of inflammation. In the case of endotoxemia, the major attention has been on application of LPS analogs with “under-acylated” lipid A structures, synthetic nontoxic lipid A derivatives, monoclonal antibodies to lipid

A or truncated Re-LPS structure, blocking antibodies against both cell surface receptors and cytokines, and to other intracellular small molecule antagonists for therapeutic purposes. Today, a range of specific antibodies against CD14, TLR4, and CD11b are being used as the essential tool to elucidate their role in acute inflammation [1, 5–16]. We have shown earlier that some certain antibodies such as anti-CD11b^{ICRF-44}Fc^{mIgG1} or anti-TLR4^{HTA125}Fc^{mIgG2a} are unable to ameliorate significantly the *N*-formyl-methionyl-leucyl-phenylalanine- (fMLP-) triggered ROS production (luminol) from LPS-primed PMNs [12, 13], while anti-CD14^{UCHM-1}Fc^{mIgG2a} suppresses LPS priming successfully [14]. Molecular mechanisms underlying our observations, however, have not been described. So, in this review, we discuss molecular mechanisms underlying LPS-induced functional responses of human PMNs and monocytes/macrophages such as ROS generation and production of cytokines after cell exposure to mouse IgG (mIgG) antibody to CD14, TLR4, or CD11b.

ROS is a collective term that often includes not only superoxide anion radical ($O_2^{\cdot-}$) but other oxygen radicals such as hydroxyl (OH^{\cdot}), peroxy (RO_2^{\cdot}), alkoxy (RO^{\cdot}), hydroperoxy (HO_2^{\cdot}), and also nonradicals as hydrogen peroxide (H_2O_2), hypochlorous acid (HOCl), singlet oxygen (ΔgO_2), and peroxynitrite ($ONOO^-$) [17]. Among them, H_2O_2 is relatively stable diffusible oxidant acting as a signaling molecule and second messenger in the inflammatory settings. Today, it is known that signaling or damaging actions of ROS are determined by its amount, type, and cellular location. For example, H_2O_2 has been shown to be involved in activation of nuclear factor NF- κ B and probably in MAPK signaling cascades [18–22].

Circulating leukocytes are programmed for distinct functions in human physiology. The three main antimicrobial functions are accepted for PMNs: phagocytosis, degranulation, and the release of nuclear material in the form of PMN extracellular traps. Nowadays, it is recognized that PMNs can produce cytokines, modulate activities of neighboring cells, contribute to the resolution of inflammation, regulate macrophages for long-term immune responses, and even have a role in innate memory [23, 24]. The main function of monocytes is the “processing” and degradation of antigens. Once produced from the bone marrow into the blood, circulating monocytes should be rapidly activated by inflammatory signals and migrate to areas of inflammation where they can differentiate into the proinflammatory (M1) or anti-inflammatory (M2) phenotypes known as tissues macrophages. In the M1 state, the activated monocyte-macrophages undergo a metabolic switch from the oxidative phosphorylation to glycolysis. Inhibition of oxidative phosphorylation increases ROS production which exerts bactericidal activities. During the resolution of inflammation, abundance of anti-inflammatory (M2) monocyte-macrophages with more oxidative phosphorylation phenotype is increased [25]. Classically activated M1 monocyte-macrophages have elevated microbicidal function associated with the ability to secrete high amount of proinflammatory cytokines (TNF- α , IL-1 β , and IL-12) and ROS, while alternatively activated M2 monocyte-macrophages

produce high levels of anti-inflammatory mediators (IL-10 and TGF- β) [26].

A change in redox homeostasis may facilitate differentiation of monocytes into macrophages [26]. In fact, in human myeloid leukemia PLB-985 cells, during VD3-triggered monocyte-to-macrophage differentiation, the expression and translocation of nicotinamide adenine dinucleotide phosphate (NADPH) oxidase components to the plasma membrane coincides with upregulation of surface markers such as CD11b and CD36 [26, 27]. Mitochondrial ROS (mitoROS) contribute to LPS-induced cytokine release by monocyte-macrophages [18, 28]. For example, mitoROS regulate IL-1 β transcription (inflammasome priming), but may also regulate the maturation and secretion of IL-1 β (inflammasome activation) [18, 29].

ROS are by-products of numerous enzymatic reactions in various cell compartments, including the cytoplasm, cell membrane, endoplasmic reticulum, mitochondria, and peroxisome [18]. It has been suggested that peripheral blood monocytes depend on oxidative phosphorylation (ATP synthesis) for their energy supply, whereas PMNs do not. PMNs lose their mitochondrial dependency during maturation from bone marrow mitochondrion-rich precursors into peripheral blood PMNs with relative few mitochondria [30]. As the result, it has been proposed that mitochondria in PMNs (unlike monocyte-macrophages) do not play a role in energy metabolism, but maintain mitochondrial membrane potential for apoptotic signaling [25]. PMNs during phagocytosis use large quantities of molecular O_2 not for mitochondrial respiration, but, rather, to generate $O_2^{\cdot-}$ and other oxidants via a respiratory burst catalyzed by NADPH oxidase [31].

NADPH oxidase is the enzyme responsible for $O_2^{\cdot-}$ production [32]. This multicomponent enzyme system is composed of two transmembrane proteins (p22^{phox} and gp91^{phox}/NOX2 forming cytochrome b_{558}), three cytosolic proteins (p40^{phox}, p47^{phox}, and p67^{phox}), and GTPase (Rac1 or Rac2). These components of NADPH oxidase are assembled at membrane sites upon transition of PMNs to a state of enhanced responsiveness known as priming. Three major events accompany activation of NADPH oxidase: (1) protein phosphorylation, (2) activation of GTPases, and (3) translocation of cytosolic components of NADPH oxidase to plasma membrane or to membrane of intracellular granules. Actually, NADPH oxidase in PMNs exists in different states: resting, primed, activated, or inactivated [33]. It has been demonstrated that $O_2^{\cdot-}$ /ROS derived by NADPH oxidase are critically involved in LPS intracellular signaling leading to PMN priming as well as to maintenance of the resting or nonprimed state [34–37]. The primed PMNs have been identified in humans with infections, rheumatoid arthritis, chronic kidney disease, traumatic injury, and acute respiratory distress syndrome [38].

As known, PMNs express a range of receptors including β_2 integrins (CD11/CD18) and Fc receptors γ (Fc γ Rs) which are capable of initiating complex intracellular signaling events robustly activating NADPH oxidase. In addition, some members of G protein-coupled receptors (GPCRs), especially fMLP receptor FPR1, can directly activate NADPH oxidase, although to a lesser extent than what has been

observed with activated integrins or Fc γ Rs [32]. It is necessary to note that LPS itself does not elicit in PMN significant O₂⁻/ROS production but transforms them into a primed state in which NADPH oxidase is not fully assembled but becomes more susceptible to activation by secondary stimuli [32–34, 39, 40].

2. TLR4 and Their Intracellular Signaling Molecules

LPS in the bloodstream is recognized by LPS-binding protein (LBP) that transfers them to CD14 followed by their presentation to MD-2·TLR4 on the surface of monocytes and PMNs [1, 5, 6, 11, 41–43]. Structural LPS-induced rearrangements in MD-2·TLR4 trigger TLR4 partitioning into lipid rafts where it undergoes homotypic dimerization facilitating signal transduction events. TLR4 operates with the assistance of other cell surface receptors which are assembled in the LPS-induced “receptor cluster” [6]. Besides CD14 and TLR4, other receptors including the β_2 integrin CD11b/CD18 and Fc γ Rs (CD16A, CD32, and CD64) have been also detected as constituents of monocyte LPS-induced “receptor cluster” [41, 42, 44].

MyD88-dependent and MyD88-independent TRIF-dependent signaling pathways have been described in monocytes following TLR4 activation [45, 46]. These signaling pathways are dependent on Toll/interleukin-1 adaptor proteins including MyD88, TIRAP/MAL, TRIF/TICAM-1, and TRAM/TICAM-2 [47–49]. It has been shown that the LPS-caused initiation of MyD88-dependent pathway results in rapid NF- κ B activation and release of proinflammatory cytokines (TNF- α , IL-1 β , and IL-6) and chemokines (MCP-1, MIP-3 α , and IL-8). Moreover, in monocytes, the LPS-caused initiation of the MyD88-independent pathway results in rapid activation of interferon regulatory factor 3 (IRF3) leading to release of beta interferon (IFN- β) and to the second delayed NF- κ B activation [50, 51]. Unlike monocytes, the MyD88-independent signaling pathway cannot be mobilized in PMNs in the response to LPS [52].

An amplified O₂⁻/ROS production from LPS-primed and fMLP-stimulated PMNs is the result at least of two converging intracellular signaling pathways. The first LPS-induced signaling pathway engages in PMNs such adaptor proteins as MyD88, TIRAP/MAL, IRAK, TRAF6, and TAK1. Among them, TAK1 is linked to MAPK signaling cascades [52]. After 20 minutes of PMN exposure to LPS, the MKK3-dependent phosphorylation of p38 MAPK is observed [53]. The p38 MAPK-dependent translocation of cytochrome b₅₅₈ and p47^{phox} but not p67^{phox} or Rac2 to the plasma membrane is also known. fMLP in LPS-primed PMNs causes a rapid and strong translocation of the other cytosolic components of NADPH oxidase to the already mobilized cytochrome b₅₅₈ followed by O₂⁻/ROS production [54].

3. Heterotrimeric G_{i α 2} Proteins and Their Intracellular Signaling Events

The second fMLP-initiated pathway is realized by FPR1 coupled with heterotrimeric G_{i α 2} proteins. The activated

G _{$\beta\gamma$} subunit of G_{i α 2} initiates concomitant activation of phospholipase C (PLC) and PI3K signaling pathways. The activity of p38 MAPK and ERK1/2 kinases is also upregulated during activation of G proteins [55–57]. Activated PLC hydrolyses phosphatidylinositol 4,5-bis-phosphate [PtdIns(4,5)P₂ or PI(4,5)P₂] in the plasma membrane leading to production of inositol 1,4,5-triphosphate [Ins(1,4,5)P₃] that is followed by Ca²⁺ release from intracellular stores and generation of diacylglycerol (DAG), which in turn activates protein kinase C (PKC). The increase in intracellular free Ca²⁺ leads to Ca²⁺ influx into the cell. A rise in Ca²⁺ is an essential step in PMN activation and O₂⁻/ROS generation. Activated PKC induces phosphorylation of several substrates including p47^{phox} of NADPH oxidase. At the same time, activated PI3K produces phosphatidylinositol 3,4,5-triphosphate [PtdIns(3,4,5)P₃ or PI(3,4,5)P₃] from PtdIns(4,5)P₂. The ability of wortmannin to inhibit PI3K and to abolish the fMLP-triggered respiratory burst without any effect on agonist-induced [Ca²⁺]_i flux or PKC-mediated NADPH oxidase activation has provided strong evidence to support a second-messenger role for PtdIns(3,4,5)P₃ in O₂⁻ generation [58].

In monocytes, LPS-induced release of proinflammatory cytokines is mediated by PI3K in both a ROS- and G protein-dependent manner, propagated through NADPH oxidase complex 4 (NOX4). Upregulation of PKB/Akt is completely inhibited by pretreatment of human PBMC with either pertussis toxin (inhibitor of G_{ai}PCRs) or apocynin (inhibitor of NADPH oxidase 4) [21].

4. Human Fc γ Receptors and Their Ligands

Monoclonal antibodies to cell surface receptors such as CD14, TLR4, or CD11b/CD18 have various modes of actions. The simplest mode of their action is mere binding of the antibody to its antigen, thereby interfering or not with receptor activation. On the other hand, the antibody is able to block receptor interaction with their ligand, interfering with a multimerization process or triggering internalization of the receptor. In addition, once bound to antigen, IgG antibodies can engage the adaptive immune system via the interaction of their constant Fc region with Fc γ Rs [59]. The human Fc γ R family contains six known members in three subgroups, including CD64, CD32 (CD32A, B, C), and CD16 (CD16A, B) [60]. CD32A is mainly expressed on monocytes (5 × 10⁴/cell), macrophages, and PMNs (1 – 4 × 10⁴/cell), whereas CD32B is on B cells principally [11, 61–63]. The cytoplasmic domain of CD32A contains the immunoreceptor tyrosine-based activation motif (ITAM), while CD32B the immunoreceptor tyrosine-based inhibitory motif (ITIM) [11]. Human CD64 is abundantly expressed on monocytes (15 – 40 × 10³/cell) while at lower levels on PMNs (1 – 2 × 10³/cell) and macrophages (1 × 10⁵/cell) [61, 62]. Human CD64 could be engaged by human IgG1 or mouse IgG2a (mIgG2a) but not mIgG1 or mIgG2b. Human CD32 appears to be engaged by mIgG1 or mIgG2b preferentially [64–70]. It is becoming increasingly evident that many receptors on myeloid cells do not act in isolation, but rather cooperate with other receptors to

coordinate responses to stimuli. For example, during immune complex (IC) recognition by the cell, CD11b/CD18 cooperates with CD16B ($1 - 3 \times 10^5$ /PMN) to cause Ca^{2+} flux and ROS generation. CD16 and CD11b/CD18 jointly prime CD32 for ROS generation [71, 72]. In human PMNs, both CD32 and CD16B are able to upregulate PI3K activity. Moreover, simultaneously engaged CD32 and CD16B via “inside-out” signaling can recruit and activate CD11b/CD18 on PMNs. Thus, three different types of interaction between Fc γ R and integrins could be realized: (1) a physical interaction on the cell surface, (2) integrin response that occurs because of Fc γ R engagement and “inside-out” signaling, and (3) cellular responses to Fc γ R that occur only after integrin occupation or when both receptors are stimulated simultaneously, i.e., “outside-in” signaling [73].

CD11b is able to regulate PtdIns(4,5) P_2 generation at the cell membrane through an ADP-ribosylation factor (ARF6)-PIP5K pathway. The increase in PtdIns(4,5) P_2 levels causes association of adaptor protein TIRAP/MAL with the plasma membrane, where it is needed to recruit MyD88 to TLR4 [74]. The functional coupling of aggregated CD64 to the PLD- and PKC-dependent activation of NADPH oxidase in IFN- γ -primed and IC-stimulated human monocytic U937 cells has been shown earlier. On the other hand, CD32A is coupled to PLC but is independent of PLD activation [75].

5. CD14-Associated Intracellular Signaling Events

CD14 is the most excessively studied TLR4 gatekeeper. Because CD14 is a glycosylphosphatidylinositol- (GPI-) anchored membrane protein without a transmembrane sequence, it is believed that CD14 has no intrinsic signaling ability during LPS recognition by innate immune cells. However, the LBP-LPS complex initially binds to CD14 and only then LPS is presented to the MD-2-TLR4 complex. CD14 controls the generation of PtdIns(4,5) P_2 that is required for maximal LPS-induced TLR4-dependent proinflammatory signaling [76]. Moreover, CD14 is essential for LPS-dependent activation of phospholipases and MAPKs [77]. All together, these facts indicate CD14 as a promising therapeutic target. The impact of CD14 in TLR4-initiated signaling events has been studied in several works [64, 78–82] including our own [14].

5.1. CD14 in Ca^{2+} Signaling. Targeting CD14 by whole anti-CD14^{Mo2}Fc^{mIgM} antibody is not able to stimulate Ca^{2+} mobilization in human PMNs (CD14 $2 - 4 \times 10^3$ /cell) [83, 84]. However, in human monocytes, targeting CD14 ($10 - 135 \times 10^3$ /cell) by whole anti-CD14^{UCHM-1}Fc^{mIgG2a} antibody (divalent-Fc format) causes a rapid Ca^{2+} mobilization [64, 84]. This rise in intracellular free Ca^{2+} is less marked than that seen in the response to anti-CD32^{CIKM5}Fc^{mIgG1} antibody [64, 78]. Similar to anti-CD14^{Mo2}Fc^{mIgM} antibody, the antigenic recognition of CD14 by anti-CD14^{UCHM-1}F(ab')₂ fragments (divalent Fab₂ format) does not elicit in human monocytes a raise in intracellular free Ca^{2+} [78].

Thus, in monocytes, Ca^{2+} signaling could be induced by antibody-dependent association of CD14 with the high affinity receptor CD64. In addition, antibody-dependent homotypic CD32 association (CD32 \leftarrow anti-CD32^{CIKM5}Fc^{mIgG1} \rightarrow CD32) is also able to induce Ca^{2+} mobilization. However, association of two CD32 is less effective for Ca^{2+} mobilization when compared to heterotypic CD14 association with CD64. When CD64 is saturated, the lower affinity CD32A may also be engaged by mIgG2a antibody (CD14 \leftarrow anti-CD14^{UCHM-1}Fc^{mIgG2a} \rightarrow CD64/CD32). It is necessary to note that anti-CD14^{UCHM-1}Fc^{mIgG2a}-induced Ca^{2+} mobilization is weaker than that caused by fMLP [64]. Thus, G protein-coupled FPR1 appeared to be a more potent inducer of Ca^{2+} signaling than the engagement of CD32 or CD64 (note not clustering).

Unexpectedly, Ca^{2+} mobilization in monocytes exposed to anti-CD14^{UCHM-1}Fc^{mIgG2a} antibody has been not associated with $\text{O}_2^{\cdot-}$ generation (SOD-inhibitable ferricytochrome C reduction) [64]. Although in our settings the anti-CD14^{UCHM-1}Fc^{mIgG2a} antibody caused certain priming effect on fMLP-triggered $\text{O}_2^{\cdot-}$ /ROS production by human PMNs, we did not observe any statistically significant differences [14]. The data from other works have suggested that anti-CD14^{UCHM-1}Fc^{mIgG2a} antibody is able to elicit in monocytes or PMN sufficient signal for phosphoinositide breakdown and Ca^{2+} mobilization but it is not enough to initiate the assembly of NADPH oxidase and $\text{O}_2^{\cdot-}$ /ROS generation [14, 78]. Sufficient mobilization of Ca^{2+} in all monocytes but only in subset of PMN (40%) has been detected only after CD14 crosslinking by anti-CD14^{Mo2}Fc^{mIgM} or anti-CD14^{MEM-18/63D3}Fc^{mIgG1} antibodies followed by secondary F(ab')₂ fragments. The broad homotypic aggregation (crosslinking) of CD14 in the plane of plasma membrane has been suggested to be responsible for the robust increase in H_2O_2 /ROS production in monocytes while less pronounced in PMNs [80, 81]. The higher sensitivity of monocytes to antibody-dependent initiation of Ca^{2+} signaling in comparison to PMNs can be explained by the differences in CD14 levels on their cell surfaces [84].

The Ca^{2+} mobilization induced by CD14 crosslinking is suppressed when PLC or protein tyrosine kinases (PTK) have been inhibited [80]. Thus, only broad CD14 aggregation is able to stimulate substantial rise in intracellular free Ca^{2+} and $\text{O}_2^{\cdot-}$ /ROS production. CD14 in monocytes is physically associated with nonreceptor PTK^{Src}Lyn^{p53/56}. The crosslinking of CD14 leads to ^{Src}Lyn^{p53/56} activation followed by concomitant upregulation of ^{Src}Frg^{p58} and ^{Src}Hck^{p59/61} kinases [85, 86]. Earlier studies have shown that the signaling events triggered by CD14 crosslinking were abolished when the GPI anchor had been replaced by transmembrane sequence, suggesting that the localization to lipid rafts endowed CD14 with signaling ability [79, 80]. As GPI-anchored receptors have high lateral mobility in the plane of cell membrane, they may be more easily aggregated upon interaction with a specific ligand [81]. Thus, CD14 would function to concentrate LPS at the cell surface for their recognition by other LPS-binding proteins and to facilitation of PtdIns(4,5) P_2 generation [87].

6. Epitope Specificity and Effectiveness of Anti-CD14 Antibodies against LPS-Induced Effects

LPS-binding sites on CD14 have been intensively studied, and four regions within the NH₂-terminal 65 amino acid residues are identified. All of these regions (R) are clustered around the hydrophobic pocket of CD14. R1 (D₉DED₁₂) is located close to the wall, whereas R3 (A₃₅VEVE₃₉) is at the bottom of the pocket, while R2 (P₂₂QPD₂₅) and R4 (D₅₇ADPRQY₆₃) are located at the rim of the pocket. Another three regions of CD14, namely, T1 (E₇LDDED₁₃), T2 (L₉₁RVLAYSRLKE₁₀₁), and T3 (P₁₈₅GL), have been proposed to be involved in LPS transfer to MD-2·TLR4 and therefore are responsible for LPS signaling. R1 within CD14 overlaps with T1 region. Therefore, the T1/R1 sequence appears to play a role in both LPS binding and transfer (LPS signaling) to MD-2·TLR4 [88, 89]. The effectiveness of various anti-CD14 antibodies against LPS-induced effects is listed in Table 1.

6.1. Targeting R1 and T1 by 3C10 Antibodies Interferes with LBP·LPS Binding to CD14. Anti-CD14^{3C10}Fc^{mIgG2b} antibody binds to mostly anionic E₇LDDED₁₃ sequence in CD14 that is able to interact with cationic proteins such as serum LBP [106, 111, 112]. Anti-CD14^{3C10} antibody almost completely prevents PMN priming by LBP·LPS for fMLP-triggered O₂⁻/ROS production (luminol) [90]. So, the first antibody-dependent mechanism downregulating LPS deleterious effects is based on the ability of anti-CD14 antibodies to prevent the binding of LBP·LPS to CD14 and to abolish subsequent LPS transfer to MD-2·TLR4 [106, 111].

6.2. Targeting R4 by MEM-18 Antibodies Suppresses LBP·LPS Binding to CD14. Anti-CD14^{MEM-18}Fc^{mIgG1} antibody binds to L₅₁-A₆₄ sequence in R4 region (D₅₇-A₆₄) of CD14. It is able to interfere with entry of lipid A, the hydrophobic region of LPS, into the hydrophobic pocket of CD14 (R4) during CD14 recognition of LBP·LPS, thereby suppressing the harmful effects caused by LPS [113–116]. Thus, despite the differences in isotype, the anti-CD14^{MEM-18}Fc^{mIgG1} antibody, similar to anti-CD14^{3C10}Fc^{mIgG2b} antibody, prevents the binding of LPS to CD14 [113, 117]. As a result, LPS-induced production of both TNF-α from human monocytes [97, 118] or IL-8 from PBMC [119] has been suppressed. The effectiveness of anti-CD14^{MEM-18}Fc^{mIgG1} antibody can be explained also by its supplementary ability to downregulate CD14 and TLR4, but not CD11b/CD18, from the cell surface as has been shown earlier using differentiated monocytic THP-1 cells [113, 120]. Since anti-CD14^{MEM-18} is a mIgG1 antibody and may be recognized by FcγRs (CD14 ← anti-CD14^{MEM-18}Fc^{mIgG1} → CD64/CD32), its mode of action is more complicated [113, 121].

It is necessary to note that LPS-induced IL-8 production has been shown to be suppressed more effectively by anti-CD14^{MEM-18} antibody than anti-TLR4^{HTA125}Fc^{mIgG2a} antibody [119]. The effectiveness of anti-CD14^{UCHM-1}Fc^{mIgG2a} antibody against LPS-induced effects in human monocytes is less evident than that of anti-CD14^{MEM-18}Fc^{mIgG1} antibody [97, 118].

6.3. Targeting R3 by MY4 Antibodies Causes Internalization of CD14 and TLR4. Anti-CD14^{MY4}Fc^{mIgG2b} antibody binds to S₃₄-G₄₄ sequence of CD14 and does not prime human PMNs for fMLP-triggered O₂⁻/ROS production (reduction of ferricytochrome C) [104, 113] but suppresses LBP·LPS-induced CD11b/CD18 mobilization to the cell surface [87]. Moreover, both LPS-induced association of G_{ia2} with PMN plasma membrane and activation of PLD are significantly suppressed by prior cell exposure to anti-CD14^{MY4} antibody [104]. The effectiveness of anti-CD14^{MY4}Fc^{mIgG2b} antibody against LPS-induced effects is associated with its ability to induce downregulation of CD14 and TLR4 from the cell surface. It is interesting to note that LPS-independent internalization of CD14 and TLR4 during cell response to anti-CD14^{MY4}Fc^{mIgG2b} antibody exceeded that of anti-CD14^{MEM-18}Fc^{mIgG1} antibody [100, 104, 113]. Thus, the effectiveness of anti-CD14^{MY4} antibody against LPS-induced effects is based on its ability to block LBP·LPS binding to CD14 and to downregulate CD14 and TLR4 from the cell surface. Why mIgG2b antibodies to CD14 (MY4) or TLR4 (HT4) are internalized better than mIgG1 anti-CD14^{MEM-18} antibody remain to be elucidated.

6.4. Anti-CD14 Antibodies as a Constituent of Therapeutic Medications. CD14 as evidenced from data presented in Table 1 is involved in LPS-dependent PMN priming [103]. The relative weak effectiveness of anti-CD14^{UCHM-1}Fc^{mIgG2a} antibody as a suppressor of LPS-dependent PMN priming for fMLP-triggered O₂⁻/ROS production may be explained by its epitope specificity that blocks CD14 incompletely [14]. However, the inhibitory effectiveness of anti-CD14^{UCHM-1} antibodies may be improved by replacing their mIgG2a isotype with mouse or human IgG1.

The therapeutic relevance of anti-CD14^{28C}Fc^{mIgG1} or anti-CD14^{18E12}Fc^{mIgG1} antibodies against LPS-induced effects has been already studied *in vivo* in INF-γ-sensitized *Macaca fascicularis* [109] and in normal human subjects (anti-CD14^{IC14}Fc^{mIgG1}) [122]. Anti-CD14^{28C/18E12}Fc^{mIgG1} antibodies protect primates from most of the physiologic and proinflammatory consequences of acute endotoxemia. The intravenous treatment of *M. fascicularis* by anti-CD14^{18E12} antibody blocks signaling events without affecting the binding of LPS to CD14 as it has been estimated during LPS-induced production of TNF-α. On the other hand, productions of IL-6 and IL-1β have been inhibited better by another anti-CD14^{28C} antibody that is able to block LBP·LPS binding to CD14 [109]. A beneficial anti-CD14^{IC14}Fc^{mIgG1} antibody attenuates acute LPS-induced clinical symptoms and strongly inhibits LPS-induced production of proinflammatory cytokines, while it only delayed the release of the anti-inflammatory cytokines such as soluble TNF receptor type I and IL-1 receptor antagonist [122].

7. Epitope Specificity and Effectiveness of Anti-TLR4 Antibodies against LPS-Induced Effects

Human TLR4 is linked to a range of diseases, including infectious disease, atherosclerosis, asthma, cardiac disease, liver disease, renal disease, inflammatory bowel disease, obesity,

TABLE 1: The capability of antibodies against CD14 affects the LPS-induced effects (the references are indicated inside the square brackets).

Clone (isotype)	Epitope	Influence on LPS-induced effects		References
		Does	Does not	
3C10 (mIgG2b) Effectiveness decreases when LPS concentration increases	E ₇ -R ₁₄	(1) Suppress CD14 binding to LBP-Re-LPS <i>Salmonella minnesota</i> (1 ng/ml) as well as PMN priming for fMLP-triggered O ₂ ⁻ /ROS		[90–96]
		(2) Whole or F(ab') ₂ suppress O ₂ ⁻ /ROS production in monocytes challenged by Re-LPS <i>Escherichia coli</i> (1 ng/ml, 5% blood serum)		
		(3) Prevent CD11b/CD18 mobilization to the cell surface in PMNs stimulated by Ra/Rb-LPS <i>E. coli</i> K12 (30 ng/ml, without serum)		
biG10 (mIgG1)	D ₉ -F ₁₃	(1) Suppress TNF- α production in whole human blood exposed to LPS <i>Salmonella abortus-equi</i> (10 ng/ml)		[97, 98]
MY4 (mIgG2b)	S ₃₄ -G ₄₄	(1) Suppress CD14 binding to LBP-Re-LPS	(1) Affect fMLP-triggered O ₂ ⁻ /ROS production from unprimed PMNs	[77, 94, 99–104]
		(2) Decrease PMN priming by LPS from <i>E. coli</i> O55:B5 (10 ng/ml, 1% serum) or <i>E. coli</i> O111:B4 (10 ng/ml, 10% serum)		
		(3) Inhibit phosphatidic acid generation in LPS-primed and fMLP-stimulated PMNs		
		(4) Suppress LPS-dependent activation of p38 MAPK in human PMNs		
		(5) Whole or Fab suppress LPS uptake by human monocytes		
60bca (mIgG1)	S ₃₄ -V ₃₈	(1) Prevent LBP-Re-LPS <i>S. minnesota</i> binding to CD14		[90, 105]
		(2) Abolish almost completely PMN priming by LBP-Re-LPS <i>S. minnesota</i> (1 ng/ml) for fMLP-triggered O ₂ ⁻ /ROS		
63D3 (mIgG1)		(1) Whole or F(ab') ₂ suppress weakly LPS-induced ROS production in human monocytes	(1) Prevent LBP-dependent delivery of Re-LPS <i>S. minnesota</i> to CD14	[91, 94, 95, 106–108]
			(2) Suppress LPS-induced TNF- α and IL-8 production	
28C5 (mIgG1)		(1) Suppress LBP-dependent delivery of Re-LPS <i>S. minnesota</i> to CD14		[94, 109]
		(2) Suppress LPS-dependent activation of p38 MAPK		
biG14 (mIgG2a)	E ₃₉ -G ₄₄	(1) Decrease binding of Ra-LPS <i>E. coli</i> to CD14		[97]
UCHM-1 (mIgG2a)		(1) Suppress LPS-induced IL-8 production by human retinal pigment epithelial cells		[14, 110]
		(2) Decrease PMN priming by S- or Re-LPS <i>E. coli</i> (100 ng/ml, 2% serum) for fMLP-triggered O ₂ ⁻ /ROS production		

diabetes (types I and II), rheumatoid arthritis, Alzheimer's disease, Parkinson's disease, and multiple sclerosis [1, 6, 61, 123]. As a result, targeting TLR4 has attracted increasing attention in the context of anti-inflammatory medications for patients with different TLR4-dependent complications [6, 15, 16, 62, 106, 124–129]. The data presented in Table 2 represent TLR4 as a promising therapeutic target for "antibody"-based therapy.

The extracellular region of TLR4 can be divided into N-terminal (L₅₂-P₂₀₂), central (L₂₀₃-L₃₄₈), and C-terminal

(K₃₄₉-F₅₈₂) domains; each of which contains LRRs 1–6, LRRs 7–12, and LRRs 13–22, respectively [1].

7.1. Targeting the N-Terminal Domain of TLR4. Targeting LRR2–LRR7 (D₅₀-I₁₉₀) repeats in TLR4 by anti-TLR4^{HTA125}Fc^{mIgG2a} antibody does not suppress LPS-dependent PMN priming for fMLP-triggered O₂⁻/ROS production (luminol) [12, 132]. The same result has been obtained by Sanui et al. [133]. These authors did not observe pronounced inhibitory effect of anti-TLR4^{HTA125} antibody

on LPS-induced PMN priming. However, Stadlbauer et al. [129] showed that the anti-TLR4^{HTA125} antibody is able to suppress LPS-induced production of ROS (Phagoburst kit) in PMNs.

When LPS-induced production of IL-6 and IL-8 was studied in the human embryonic cell line HEK293, no inhibitory effect of anti-TLR4^{HTA125}Fc^{mIgG2a} was detected [6, 11]. However, in human retinal pigment epithelial cells, anti-TLR4^{HTA125} antibody was almost equally as effective as anti-CD14^{UCHM-1}Fc^{mIgG2a} antibody in suppression of LPS-induced IL-8 production. It is interesting to note that simultaneous use of anti-TLR4^{HTA125} and anti-CD14^{UCHM-1} antibodies did not further potentiate antibody inhibitory effectiveness, suggesting that blockage of initial LPS binding to CD14 was highly effective and not further increased when TLR4 was also targeted [110].

The weak inhibitory effectiveness of anti-TLR4^{HTA125}-Fc^{mIgG2a} antibody could be explained by the epitope specificity. This antibody recognizes an antigenic epitope within D₅₀-I₁₉₀ sequence and binds to TLR4 irrespective of the presence or absence of MD-2 [132]. Thus, it may be suggested that blockage of LRR2-LRR7 (HTA125) is not enough to prevent LPS-MD-2-induced TLR4 dimerization (Table 2).

7.2. Targeting the C-Terminal Domain of TLR4. Anti-TLR4^{HT4}Fc^{mIgG2b} antibody recognizes the nonlinear epitope within the LRR13 repeat of TLR4. This epitope is composed of several amino acid residues (K₃₄₉, K₃₅₁S₃₅₂, G₃₆₄NA, and S₃₆₈E) closely located to the TLR4 dimerization interface created by LRR15-LRR17 repeats of two LPS-MD-2·TLR4 complexes. Based on experimental data, it has been assumed that anti-TLR4^{HT4} antibody is unable to prevent LPS-MD-2 binding to TLR4 but nevertheless inhibits LPS-MD-2-induced TLR4 internalization. The effectiveness of anti-TLR4^{HT4}Fc^{mIgG2b} antibody in suppression of lipid A-induced production of TNF- α , IL-6, and IL-12p40 from human leukocytes is better than that of the anti-TLR4^{HTA125}Fc^{mIgG2a} antibody [1, 5, 6]. Taking these facts into consideration, it could be concluded that targeting the C-terminal domain of TLR4 may lead to a more pronounced therapeutic effect than targeting the N-terminal domain of TLR4 by HTA125^{mIgG2a} or HT52^{mIgG1} antibodies. The effect of anti-TLR4^{HT52}Fc^{mIgG1} (LRR2-LRR7: D₅₀-I₁₉₀ sequence) antibody may be potentiated by simultaneous application with anti-TLR4^{HT4}Fc^{mIgG2b} (LRR13) antibody thus causing double blocking of TLR4 (LRR2-LRR7 and LRR13) [1, 5, 6]. Note that anti-TLR4^{HTA125} antibody recognizes the same antigenic epitope as did anti-TLR4^{HT52} antibody. We assume that double targeting TLR4 by anti-TLR4^{HT4} and anti-TLR4^{HTA125} antibodies would improve the inhibitory effectiveness of the latter.

As has been shown experimentally, the inhibitory effectiveness of anti-TLR4^{HT4}Fc^{mIgG2b} or anti-TLR4^{HT52}Fc^{mIgG1} is not associated with engagement of Fc γ Rs. In fact, the inhibitory effectiveness of anti-TLR4^{HT4}Fc^{mIgG2b} or anti-TLR4^{HT52}Fc^{mIgG1} against lipid A-induced effects was unaffected by prior cell exposure to blocking anti-CD32^{AT-10}Fc^{mIgG1} antibody [1, 5, 6].

7.3. Targeting Both N- and C-Terminal Domains of TLR4. The improved antibody effectiveness seen with double-targeted TLR4 led to the generation of a new anti-TLR4^{15C1}Fc^{mIgG1} antibody recognizing both LRR12 (Y₃₂₈N) and LRR13 (K₃₄₉LK, E₃₆₉VD) sequences [11]. Anti-TLR4^{15C1} antibody blocks TLR4 binding to LPS-MD-2 and TLR4 dimerization as well. In addition, anti-TLR4^{15C1} antibody effectively suppresses LPS-induced IL-6 and IL-8 production analogous to anti-TLR4^{HT4}Fc^{mIgG2b} or anti-TLR4^{HT52}Fc^{mIgG1} antibodies but with stronger effect than anti-TLR4^{HTA125}Fc^{mIgG2a} antibody [6, 11]. Furthermore, anti-TLR4^{15C1} antibody prevents LPS-induced TLR4 partitioning into lipid rafts [61]. As earlier has been shown, the effectiveness of anti-TLR4^{15C1}Fc^{mIgG1} antibody is dependent on the engagement of Fc γ Rs (CD32) [1, 11]. Targeting CD32 by anti-CD32^{IV.3/AT-10}Fc^{mIgG2b} antibodies dramatically reduces the effectiveness of anti-TLR4^{15C1}Fc^{mIgG1} antibody when LPS-induced production of IL-6 was studied. It is necessary to note that LPS-induced IL-6 production had not been significantly affected by isotype-matched control mIgG1. Thus, in addition to engagement of CD32 (TLR4 \leftarrow anti-TLR4^{15C1}Fc^{mIgG1} \rightarrow CD32) and its signaling pathway(s), the therapeutic effect of anti-TLR4^{15C1}Fc^{mIgG1} antibody is based on its ability to prevent LPS-MD-2 binding to TLR4 thereby abolishing TLR4 dimerization and its movement into lipid rafts [1, 11, 134].

7.4. Humanized Anti-TLR4 Antibody and Fc γ Rs. The differences in the affinity of Fc γ Rs for IgG subclasses have been explored in development of new therapeutic antibodies such as Hu15C1. This antibody is the humanized version of anti-TLR4^{15C1}Fc^{mIgG1} antibody [61, 135]. Two substitutions (N₃₂₅ \rightarrow S and L₃₂₈ \rightarrow F) have been introduced into Fc arm of anti-TLR4^{15C1}Fc^{mIgG1} antibody to amplify its inhibitory effectiveness. As a result, the affinity of the new anti-TLR4^{Hu15C1}Fc^{hIgG1} for CD64 is potentiated, while for CD16, it is eliminated. An intermediate affinity of anti-TLR4^{Hu15C1}Fc^{hIgG1} for CD32 was detected. Thus, CD64 (TLR4 \leftarrow anti-TLR4^{Hu15C1}Fc^{hIgG1} \rightarrow CD64/CD32) is viewed as the first contributor to the potent inhibitory effectiveness of anti-TLR4^{Hu15C1}Fc^{hIgG1} antibody. In addition, CD32-initiated ITAMi signaling is expected when CD64 would be not available. The blockage of CD32B does not change significantly the inhibitory effectiveness of anti-TLR4^{Hu15C1} antibody. When anti-TLR4^{Hu15C1} antibody had been compared with the parental anti-TLR4^{15C1}Fc^{mIgG1} antibody, the former antibody was more effective than the latter in inhibition of LPS-induced effects. In addition, it has been shown using neuronal originated HEK293 cells that CD32A is involved in the inhibitory potency of anti-TLR4^{Hu15C1} antibody. It was also discovered that the inhibitory potency of anti-TLR4^{Hu15C1} antibody against LPS-induced effects is much higher in CD32A-positive HEK293 cells than in CD32A-negative ones. Besides engagement of CD64 and CD32, the anti-TLR4^{Hu15C1} antibody is able to interfere with LPS-induced TLR4 dimerization thereby preventing TLR4 partitioning into lipid rafts. Thus, it is postulated that dimerization of TLR4 is a prerequisite for TLR4 clustering [61].

TABLE 2: The capability of antibodies against TLR4 affects the LPS-induced effects (the references are indicated inside the square brackets).

Clone (isotype)	Epitope	Does	Influence on LPS-induced effects	Does not	References
HTA125 (mIgG2a)	Within D ₅₀₋₁₉₀ LRR2-LRR7	(1) Suppress by 30% the intracellular O ₂ ⁻ /ROS production in PMNs stimulated by LPS <i>E. coli</i> O111:B4 (100 ng/ml) (2) Suppress IRAK degradation induced by LPS <i>E. coli</i> O111:B4 (500 ng/ml, 10% FCS) in THP-1 (CD14 ⁺ , CD11b/CD18 ⁺) cells (3) Inhibit by 80% NF-κB activation in monocytes stimulated by O-4' MPLA <i>E. coli</i> (10 μg/ml) (4) Inhibit TNF-α (55%) and IL-10 (85%) production from PBMC stimulated by O-4' MPLA <i>E. coli</i> (10 μg/ml) (5) Suppress TNF-α production from differentiated THP-1 cells stimulated by LOS (1 ng/ml, without serum) from <i>Neisseria meningitidis</i> NMB	(1) Affect O ₂ ⁻ /ROS production caused in PBMC by Ra/Rb-LPS <i>E. coli</i> K12LCD25 (3 ng/ml) (2) Influence on PMN priming by S- or Re-LPS <i>E. coli</i> (100 ng/ml, 2% serum) for fMLP-triggered O ₂ ⁻ /ROS production		[12, 106, 119, 124, 125, 130, 129]
HT52 (mIgG1)	Within D ₅₀₋₁₉₀ LRR2-LRR7	(1) More effectively suppress IL-6 production induced in U373/TLR2 ⁻ cells by LPS <i>E. coli</i> (100 ng/ml) than HTA125 antibody does (2) Suppress TNF-α and IL-6 production in whole human blood stimulated by lipid A <i>E. coli</i> (10 ng/ml) in the same extent as HTA125 antibody does			[1, 5]
15C1 (mIgG1)	Y ₃₂₈ N (LRR12) K ₃₄₉ LK and EVD ₃₆₉ (LRR13)	(1) Suppress IL-6 production in whole blood stimulated by Ra/Rb-LPS <i>E. coli</i> K12LCD25 (4 ng/ml)			[6, 11, 61]
Hu15C1 (hIgG1)	Y ₃₂₈ N (LRR12) K ₃₄₉ LK and EVD ₃₆₉ (LRR13)	(1) Suppress IL-6 production from differentiated U937 cells stimulated by Re-LPS <i>S. minnesota</i> 595 (1 ng/ml)			[61]
HT4 (mIgG2b)	K ₃₄₉ LKS ₃₅₂ and G ₃₆₄ NAFSE ₃₆₉ (LRR13)	(1) Suppress LPS-induced internalization of TLR4 (2) Probably stimulate dimerization of two TLR4	(1) Interfere with transfer of mCD14-LPS to MD-2·TLR4 and LPS-induced TLR4 dimerization as well		[6, 131]
HTA405 (isotype not pointed out)		(1) Suppress production of TNF-α and IL-8 from THP-1/CD14 ⁺ cells stimulated by Re-LPS <i>S. minnesota</i> R595 (10 ng/ml) (2) The same positive effectiveness of HTA405 on TNF-α production has been observed in whole blood stimulated by Ra/Re-LPS <i>S. minnesota</i> or S/Re-LPS <i>E. coli</i> (3) Decrease IL-6 production by 50% or 20% from U373/TLR2 ⁻ cells stimulated by Re-LPS <i>S. minnesota</i> R595 (10 ng/ml) or S-LPS <i>E. coli</i> O111:B4 (100 ng/ml), respectively	(1) Marginally decrease the production of TNF-α and IL-8 from THP-1/CD14 ⁺ cells stimulated by S-LPS <i>E. coli</i> O111:B4 (100 ng/ml, 2% serum)		[108]
HT414 HTA1216 (isotypes not pointed out)		(1) Suppress production of TNF-α and IL-8 from THP-1/CD14 ⁺ cells stimulated by Re-LPS <i>S. minnesota</i> R595 (10 ng/ml)	(1) Marginally suppress the production of TNF-α and IL-8 from THP-1/CD14 ⁺ cells stimulated by S-LPS <i>E. coli</i> O111:B4 (100 ng/ml)		[108]

The therapeutic effectiveness of humanized anti-TLR4^{N1-0101} antibody has been already evaluated *ex vivo* and *in vivo* in the absence or presence of systemic LPS challenge (acute inflammation) [7, 9]. The other effective neutralizing anti-TLR4^{WN1222-5} antibody mimics the site of TLR4, recognizing an inner core structure of LPS from most infectious bacteria regardless of the presence of O-polysaccharide (O-antigen) and prevents LPS binding to target cells in the bloodstream [136].

7.5. Impact of CD32 in Effectiveness of IgG Antibodies. Antigenic recognition of CD32A by anti-CD32^{IV.3} Fab/F(ab')₂ fragments recognizing the F₁₃₂SHLDP₁₃₇ sequence does not cause Ca²⁺ mobilization, upregulation of p38 and ERK MAPK kinases, and intracellular production of H₂O₂/ROS (scopoletin) [137]. The other anti-CD32^{CIKM5} Fab/F(ab')₂ are also unable to induce Ca²⁺ mobilization when crosslinking by secondary F(ab')₂ fragments is omitted [64, 78]. Targeting CD32 by anti-CD32^{AT-10} F(ab')₂ inhibits constitutive and fMLP-triggered O₂⁻/ROS (luminol) production by PMNs [134, 138]. In PMNs, a small rise in intracellular free Ca²⁺ has been induced also by anti-CD32^{CIKM5}Fc^{mIgG1} antibody but it was not associated with O₂⁻ release (SOD-inhibitable reduction of ferricytochrome C) [64, 78]. Antigenic recognition of CD32A by anti-CD32^{AT-10} Fab fragments recognizing an epitope located near or within IgG-binding site fails to activate differentiated monocytic THP-1 cells [134, 138]. Recent findings however have indicated that antigenic CD32 recognition by anti-CD32^{IV.3/AT-10} Fab/F(ab')₂ induced ITAMi signaling [134]. It has been shown that engagement of CD32 by anti-CD32^{AT-10} F(ab')₂ stimulates transient recruitment of tyrosine kinase ^{2SH2}Syk/p72^{Tyr} to cytoplasmic domain of CD32A followed by incomplete phosphorylation of the ITAM leading to the inhibitory ITAMi conformation. As a result, activated ITAMi allows tyrosine phosphorylation of SHP-1 (protein tyrosine phosphatase) followed by inhibition of the major intracellular signaling players of immune cells such as guanine nucleotide exchange factor Vav-1 (RacGEF) and IRAK-1 kinase that are both involved in O₂⁻/ROS and cytokine production. Thus, blockage of Vav-1 in human PMNs can abrogate association of p67^{phox} with NADPH oxidase thereby suppressing O₂⁻/ROS production [134]. This suppressive effect of CD32A and mIgG1 might be reversed by LPS-induced assembly and stabilization of TLR4, CD11b/CD18, and FcγRs in lipid rafts followed by the activation of classical ITAM signaling [11, 41, 44, 79, 139]. Since PMNs express very low levels of CD32B, an impact of its involvement in the inhibitory effectiveness of mIgG1 antibodies should be negligible [140].

Antigenic recognition of CD16 by anti-CD16^{3G8} Fab/F(ab')₂ despite the minor rise in free Ca²⁺ does not cause activation of p38 and ERK MAPK kinases nor actin polymerization and intracellular H₂O₂/ROS production (DHR) [137, 141, 142]. In addition, fMLP-triggered ROS production (luminol) is also not influenced by prior PMN exposure to anti-CD16^{3G8} F(ab')₂ [143]. Thus, it can be concluded that targeting CD16 by anti-CD16^{3G8} Fab/F(ab')₂ is unable to prime or upregulate intracellular O₂⁻/ROS production in

PMNs. By contrast, in monocytes, antibody-dependent association of CD32 with CD16 (CD16 ← anti-CD16^{3G8}Fc^{mIgG1} → CD32) in the plane of plasma membrane is able to initiate intracellular signaling events leading to generation of Ins(1,4,5)P₃, DAG, and Ca²⁺ mobilization but not to calcium influx [64, 78].

Now, the impact of mIgG subclasses in activation of human immune cells has been revealed. It has been shown in PMNs that mIgG2a is unable to induce protein tyrosine phosphorylation and substantial rise in intracellular free Ca²⁺ [70, 144]. When we have used mIgG1 or mIgG2a and unprimed PMNs, only marginal fMLP-triggered O₂⁻/ROS production was observed [12–14]. Neither anti-CD11b^{60.1/44}Fc^{mIgG1} nor anti-CD11b/CD18^{IB4}Fc^{mIgG2a} antibodies are not able to induce Ca²⁺ mobilization in PMNs [70, 145, 146]. Targeting CD11b/CD18 on freshly prepared PMNs by anti-CD11b^{Leu-15}Fc^{mIgG2a} antibody does not stimulate considerable intracellular O₂⁻/ROS production [62, 63, 147]. Anti-CD11b/CD18^{IB4}Fc^{mIgG2a} or anti-CD11b^{44a}Fc^{mIgG1} antibodies cause negligible intracellular H₂O₂/ROS (DHR) production in PMNs and even to a lesser extent than agonistic anti-CD11b^{VIM12}Fc^{mIgG1} antibody [147]. Antibody-dependent association of CD11b/CD18 with CD64/CD32 (CD11b ← anti-CD11b^{Leu-15}Fc^{mIgG2a} → CD64/CD32 or CD11b ← anti-CD11b^{44a}Fc^{mIgG1} → CD32 or CD11b/CD18 ← anti-CD11b/CD18^{IB4}Fc^{mIgG2a} → CD64/CD32) is also unable to stimulate considerable intracellular O₂⁻/ROS production in PMNs. These data, including ours, may suggest that neither mIgG2a nor mIgG1 are able to stimulate substantial rise in intracellular free Ca²⁺ and ROS production in freshly isolated PMNs. It is necessary to note that agonistic anti-CD11b^{VIM12}Fc^{mIgG1} antibody recognizing the CD11b lectin site causes intracellular H₂O₂/ROS production in PMNs to the same extent as fMLP [147].

By contrast, in macrophage-like Mono Mac 6 cells, LPS-induced production of TNF-α and IL-10 has been potentiated by mIgG2a, while production of IL-1β has been suppressed [62]. A line of other data indicates that LPS-induced activation of IRAK and production of TNF-α and IL-8 from differentiated human monocytic THP-1 cells are not influenced by mIgG2a [106, 124, 127].

7.6. Upregulation of PMN Sensitivity to mIgG2a after IFN-γ Priming. IFN-γ is the most potent priming agent released in bloodstream during LPS-induced inflammation [15, 16, 148, 149]. Thus, during inflammation, the expression of CD64 on PMN is upregulated, while CD32 is unaffected or downregulated [62, 63]. As a result, IFN-γ-primed PMNs (20 h) acquire the ability to respond to mIgG2a antibodies such as anti-CD11b^{Leu-15}Fc^{mIgG2a} by marked intracellular O₂⁻/ROS production (DCFDA) (CD11b ← anti-CD11b^{Leu-15}Fc^{mIgG2a} → CD64) [63]. However, IFN-γ does not confer on PMNs the capability to generate O₂⁻/ROS in response to mIgG1 antibodies such as anti-CD11b^{VIM12}Fc^{mIgG1} or anti-CD11b^{5A4.C5}Fc^{mIgG1} (CD11b ← anti-CD11b^{VIM12/5A4.C5}Fc^{mIgG1} → CD32), which is in agreement with IFN-γ-dependent CD32 downregulation [62, 63]. Thus, we concluded that only primed PMNs would be sensitive to

mIgG2a antibodies, while freshly isolated PMNs are marginally responsive to mouse antibodies with IgG2a or IgG1 isotypes (regardless of epitope specificity).

In humans, as it has been revealed *in vivo*, the LPS administration causes an initial rapid decline in the absolute PMN counts at 1 h followed by an increase that reaches a maximum at 6 h and then declines at 22 h to basal levels. In addition, LPS injection induces biphasic CD64 upregulation on circulating PMNs. The first phase has been observed after 1 h of LPS challenge, while the second started at 6 h and reached a maximum at 22 h [148].

By contrast, freshly isolated monocytes constitutively express high levels of surface CD64 [61, 62] and respond to anti-CD11b^{VIM12}Fc^{mIgG1} or anti-CD11b^{Leu-15}Fc^{mIgG2a} antibodies by intracellular ROS production (DCFDA). For example, anti-CD11b^{Leu-15}Fc^{mIgG2a} antibody causes an increase in ROS production in monocytes of all responders, while agonistic anti-CD11b^{VIM12}Fc^{mIgG1} in 60% only. When anti-CD11b^{VIM12}Fc^{mIgG1} antibody has been devoid of the Fc arms, its ability to stimulate ROS (DCFDA) production in freshly isolated monocytes was diminished [63]. Thus, the agonistic activity of anti-CD11b^{VIM12}Fc^{mIgG1} antibody represents the cumulative effect of epitope specificity and capability to engage CD64/CD32 receptors.

The engagement of CD64, and CD32 to a lesser extent, by anti-TLR4^{HTA125}Fc^{mIgG2a} antibody has been already revealed using macrophage-like Mono Mac 6 cells (CD32 > CD64). Mouse IgG2a inhibits most effectively the binding of anti-TLR4^{HTA125}Fc^{mIgG2a} antibody to Mono Mac 6 cells, while mIgG1 or mIgG2b reveals no significant effect. Further, the binding of anti-TLR4^{HTA125} antibody to Mono Mac 6 cells has been most effectively prevented by anti-CD64^{10.1}Fc^{mIgG1} antibody by contrast to anti-CD32^{FL18.26}Fc^{mIgG2b} antibody. Targeting CD16 by anti-CD16^{3G8}Fc^{mIgG1} antibody does not influence significantly on anti-TLR4^{HTA125} binding to Mono Mac 6 cells [62]. Based on these findings, the high affinity of human CD64 and moderate affinity of human CD32 for the constant Fc arm of mIgG2a antibodies can be concluded [62, 63]. These results indicate also that specific Fab or F(ab')₂ fragments against cell surface receptors would be most appropriate and safe for applying in “antibody”-based therapy.

In summary, the major mechanisms underlying the inhibitory effectiveness of anti-TLR4 antibodies follow (1) an interference with TLR4 binding to CD14-LPS and LPS-MD-2, (2) inhibition of ligand- (LPS-) induced conformational changes that are indispensable for TLR4 signaling (HT4, HT52, 15C1, and Hu15C1) [1, 11, 61], (3) prevention of ligand-induced TLR4 partitioning into lipid rafts and its subsequent internalization (HT4, HT52, and Hu15C1) [1], and (4) engagement of FcγRs (CD32/CD64) followed by ITAMi-initiated inhibitory signaling interfering with positive signaling induced by other receptors on the same cell (CD14, MD-2-TLR4, and CD11b/CD18) [61, 134].

8. CD11b/CD18 and Their Signaling Partners

Macrophage-1 antigen (Mac-1, $\alpha_M\beta_2$, or CD11b/CD18) is a complement receptor (CR3). It consists of noncovalently

linked CD11b (integrin α_M) and CD18 (integrin β_2) subunits. Integrins regulate important leukocyte functions including adhesion, migration, proteolysis, phagocytosis, and oxidative (respiratory) burst [150]. In resting PMNs, integrins are maintained in a conformationally inactive state and are unable to bind their ligands [151]. On cell stimulation, “inside-out” signaling originating from nonintegrin cell surface receptors such as FPR1, FcγRs, or TLR4 leads to vast conformational changes in CD11b/CD18, but not directly to receptor clustering (integrin redistribution in the plane of plasma membrane) [42, 52]. Thus, only “inside-out” primed integrins exhibit increased ligand-binding avidity and initiate “outside-in” signaling by themselves. CD11b/CD18 has been detected in the LPS-induced “receptor cluster” on monocytes and can act as a signaling partner for such receptors as FPR1 and CD14 [44, 106, 150, 152, 153]. CD11b/CD18 can be found also in association with FcγRs, but the consequences of these functional interactions are not fully understood. The functional association of the GPI-anchored form of CD16 (^{PMN}CD16^{GPI}) with CD11b/CD18 is mediated by the lectin-binding site of the latter [147, 151, 153–155]. The mechanisms by which CD11b/CD18 regulates leukocyte functions such as respiratory burst are still poorly understood.

Like other β_2 integrins, CD11b consists of a short cytoplasmic tail, single transmembrane domain, and long extracellular domain. The extracellular domain of CD11b is composed of seven repeats. The V to VII repeats are similar to the divalent cation-binding “EF-hand” motif. The II and III repeats are separated by the I (inserted) domain that is known also as $\alpha A/I$ -domain [156]. The effectiveness of anti-CD11b/CD18 antibodies against LPS-induced effects is listed in Table 3.

8.1. Targeting the CD11b $\alpha A/I$ -Domain. Antigenic recognition of CD11b/CD18 by anti-CD11b⁴⁴ Fab recognizing $\alpha A/I$ -domain does not lead to considerable changes in conformation of CD11b/CD18 nor to activation of “outside-in” signaling [161, 162]. However, full anti-CD11b^{44a} or anti-CD11b/CD18^{IB4}Fc^{mIgG2a} antibodies induce epitope exposition by CD11b that is recognized by anti-CD11b^{VIM12}Fc^{mIgG1} antibody [147]. This effect may be explained by antibody-dependent association of CD11b/CD18 with FcγRs. So, 44a or IB4 antibodies are able to induce “outside-in” signaling followed by “inside-out” signaling leading to further conformational changes in CD11b/CD18.

8.2. Targeting the C-Terminal Lectin Domain of CD11b. Antigenic recognition of the C-terminal lectin domain of CD11b (AA_{614–682}) located near the cell membrane by anti-CD11b^{OKM1} Fab or F(ab')₂ does not induce PMN intracellular H₂O₂/ROS (scopoletin) production [137]. In PMNs, neither anti-CD11b^{60.1/44}Fc^{mIgG1} nor anti-CD11b/CD18^{IB4}Fc^{mIgG2a} antibodies cause Ca²⁺ mobilization [70, 145, 146]. The same result was obtained during cell response to anti-CD18^{MHM23}Fc^{mIgG1} or anti-CD11b/CD18^{60.3}Fc^{mIgG2a} antibodies regardless of isotype differences [78, 145]. Further, intracellular H₂O₂/ROS (DHR) triggered in PMNs by antibody-dependent association of CD32 with CD11b/CD18

TABLE 3: The capability of antibodies against CD11b/CD18 affects the LPS-induced effects (the references are indicated inside the square brackets).

Clone (isotype)	Epitope	Influence on LPS-induced effects		References
		Does	Does not	
OKM-1 (mIgG2b)	CD11b AA ₆₁₄₋₆₈₂ (lectin site)	(1) Increase TNF- α production from monocytes stimulated by LPS <i>S. minnesota</i> (1 ng/ml, without serum)	(1) Inhibit binding of LPS <i>E. coli</i> O111:B4 (10 ng/ml, 10% FCS) to human PBMC	[63, 91, 99, 100, 104, 105, 157, 158]
			(2) Inhibit PMN priming by LPS <i>E. coli</i> O55:B5 (100 ng/ml, 1% serum) for fMLP-triggered O ₂ ⁻ /ROS production	
904 (mIgG2b)	CD11b AA ₇₄₋₃₁₆ (α A/I-domain)	(1) Suppress macrophage interaction with bovine erythrocytes opsonized by Re-LPS <i>S. minnesota</i> R595	(3) Inhibit protein (41 and 42 kDa) tyrosine phosphorylation in macrophages stimulated by Re-LPS <i>S. minnesota</i> R595 (1 ng/ml, human serum)	[159, 160]
			(4) Influence on O ₂ ⁻ /ROS production induced by Re-LPS <i>E. coli</i> (1 ng/ml, 5% serum) in human monocytes	
ICRF 44 (mIgG1)	CD11b		(5) Influence on TNF- α production from human PBMC stimulated by LPS <i>E. coli</i> O111:B4 (100 ng/ml, 10% serum)	
IB4 (mIgG2a)	CD11b/CD18	(1) Increase TNF- α production from monocytes stimulated by LPS <i>S. minnesota</i> (1 ng/ml, without serum)	(1) Affect PMN priming by S- or Re-LPS <i>E. coli</i> (100 ng/ml, 2% serum) for fMLP-triggered O ₂ ⁻ /ROS production	[13]
			(2) Influence on activation of p38 MAPK during PMN priming by LPS <i>E. coli</i> O55:B5 (5 ng/ml) for fMLP-triggered O ₂ ⁻ /ROS production	

(CD11b/CD18 \leftarrow anti-CD11b^{44/IB4}Fc^{mIgG1/mIgG2a}) was less pronounced than that in response to agonistic anti-CD11b^{VIM12}Fc^{mIgG1} antibody [147]. Thus, it can be concluded that simple antibody-dependent association of CD11b/CD18 with CD32 (regardless of epitope specificity) is not enough to initiate significant agonistic (activating) signaling events and H₂O₂/ROS production in PMNs, whereas to induce sufficient intracellular signaling by IgG1 antibodies, targeting of a particular epitope on CD11b is required. In fact, when agonistic anti-CD11b^{VIM12}Fc^{mIgG1} antibody recognizing the CD11b lectin site had been employed to PMNs, “outside-in” signaling, clustering of activated CD11b/CD18, upregulation of PI3K and PKB/Akt signaling pathways, Ca²⁺ mobilization, and actin polymerization were all realized, but the Raf \rightarrow MEK1/2 \rightarrow ERK1/2 signaling pathway was not upregulated [163]. Agonistic anti-CD11b^{VIM12}Fc^{mIgG1} antibody prevents association of CD11b/CD18 with CD16B^{GPI} [163] but nevertheless induces PMNs for generation of H₂O₂/ROS (DHR) to the same extent as fMLP. Anti-CD11b^{VIM12}Fc^{mIgG1}-dependent production of H₂O₂/ROS (DHR) exceeds that induced by IB4 or 44a antibodies [147]. Taking these facts into consideration, it may be suggested that CD11b/CD18-dependent “outside-in” signaling would be successfully realized when CD11b lectin domain is docked (thus, CD11b/CD18 is primed) by other appropriate GPI-anchored protein on the same cell. In PMNs, “outside-in” signaling is also initiated by CD11b/CD18 that has been clustered in the response to

anti-CD11b^{2LPM19c}F(ab')₂ recognizing α A/I-domain. The same effect had been observed when whole anti-CD11b^{2LPM19c}Fc^{mIgG1} antibody was used. Unexpectedly, monovalent anti-CD11b^{2LPM19c}Fab is unable to produce such agonistic activity [158]. These results clearly show that agonistic activity of anti-CD11b antibodies is determined by F(ab')₂ epitope specificity. Moreover, F(ab')₂ can potentially bind two targets leading to close proximity of two integrin molecules that mimic receptor crosslinking [164].

In PMNs, generation of H₂O₂/ROS (DHR) induced by anti-CD11b^{VIM12}Fc^{mIgG1} antibody is not diminished by prior cell exposure to anti-CD11b^{44a}Fc^{mIgG1} or anti-CD11b/CD18^{IB4}Fc^{mIgG2a} antibodies. It necessary to note that sequential treatment of PMNs in whole blood by anti-CD11b/CD18^{IB4}Fc^{mIgG2a} and anti-CD11b^{VIM12}Fc^{mIgG1} antibodies led to more pronounced generation of H₂O₂/ROS (DHR) than treatment with anti-CD11b^{44a}Fc^{mIgG1} combined with anti-CD11b^{VIM12}Fc^{mIgG1} antibody [147]. This result may be explained by the fact that anti-CD11b/CD18^{IB4}Fc^{mIgG2a} antibody is able to potentiate the binding of anti-CD11b^{VIM12}Fc^{mIgG1} antibody to CD11b/CD18 in addition to their ability to affect both subunits of CD11b/CD18. Thus, anti-CD11b/CD18^{IB4}Fc^{mIgG2a} antibody, besides binding to CD11b/CD18, can also engage other β_2 integrins via the common CD18 subunits (CD11a/CD18 and CD11c/CD18). Such broad targeting of β_2 integrins could provide sufficient

signals for intracellular H_2O_2 /ROS generation (DHR). This conclusion is supported by the fact that antigenic recognition of CD11b/CD18 by anti-CD11b/CD18^{IB4} F(ab')₂ induces Ca^{2+} mobilization to a similar extent as whole anti-CD11b/CD18^{IB4}Fc^{mIgG2a} antibody [165].

In PMNs, generation of ROS/ H_2O_2 (DHR) induced by anti-CD11b^{VIM12}Fc^{mIgG1} antibody can be blocked almost completely by prior cell exposure to anti-CD32^{IV.3}Fc^{mIgG2b} antibody [160]. Thus, unlike monocytes, CD32 receptor on PMNs is involved in CD11b/CD18-induced generation of ROS/ H_2O_2 (DHR) in the response to anti-CD11b^{VIM12}Fc^{mIgG1} antibody (CD11b/CD18 ← anti-CD11b^{VIM12}Fc^{mIgG1} → CD32). Therefore, it has been supposed that association of CD11b/CD18 with CD32 is required for ROS generation during PMN response to anti-CD11b^{VIM12}Fc^{mIgG1} antibody [147]. Ortiz-Stern and Rosales [73] have shown that CD32 and CD11b/CD18 are uniformly distributed and not colocalized on the surface of unstimulated PMNs. A similar observation has been made for ^{PMN}CD16B^{GPI} which is also uniformly distributed across the cell surface and is not colocalized with CD32 in unstimulated PMNs [73].

By contrast to PMNs, in monocytes, a close spatial proximity between CD11b/CD18 and CD32/CD64 has been suggested by Gadd et al. [63]. These authors have observed that anti-CD11b^{VIM12}Fc^{mIgG1} antibody interferes sterically with anti-CD32^{IV.2}Fc^{mIgG2b} antibody for binding to CD32 on monocytes, but not on PMNs [63]. Interestingly, in their study, anti-CD11b^{VIM12}Fc^{mIgG1} antibody had been unable to induce intracellular ROS (DCFDA) generation in PMNs as they did in monocytes [63, 147].

8.3. Anti-CD11b/CD18 Antibodies in Therapeutic Medications. In the light of data presented here, the effectiveness of anti-CD11b/CD18 antibodies against LPS-induced effects should be discussed. It has been shown that CD11b/CD18 has a site recognizing LPS carbohydrates, namely, N-acetyl-D-glucosamine (GlcNAc) and mannose. In addition, CD11b/CD18 binds truncated LPS glycoforms such as Re-LPS [153–155]. Two putative LPS-binding sites within the CD18 β A region (AA_{216–248}, _{266–318}) had been proposed earlier [166]. It was found that Re-LPS from *Salmonella minnesota* is bound through cationic interactions by the β A_{266–318}-exposed CD18 sequence, while another β A_{216–248} sequence probably utilizes other interactions like hydrophobic ones [166]. Thus, it is not excluded that 3-deoxy-D-manno-octulosonic acid (KDO), the inner core sugar of almost all LPS molecules, may be involved in LPS recognition by CD18 [153, 155, 159, 160]. However, neither LPS binding to PBMC nor LPS-induced PMN priming for fMLP-triggered ROS production has been blocked by anti-CD11b^{OKM1}Fc^{mIgG1} antibody [91, 99, 100, 104]. A similar result has been obtained in our work [13] where we used anti-CD11b^{ICRF44}Fc^{mIgG1} antibody. This antibody binds probably to α A/I-domain of CD11b (AA_{201–217}, _{245–261}) in a manner independent of inactive or active CD11b/CD18 state [158, 162, 167]. Thus, it may be concluded that targeting the α A/I-domain of CD11b by anti-CD11b^{ICRF44}Fc^{mIgG1} or the CD11b lectin site by anti-CD11b^{OKM1}Fc^{mIgG1} antibodies is unable to suppress significantly LPS-dependent PMN prim-

ing for fMLP-triggered $O_2^{\cdot-}$ /ROS production [13, 91, 99, 100, 104]. From the data presented here, we can, however, not exclude that other CD11b/CD18 sites might be involved in LPS recognition. The effectiveness of anti-CD11b⁴⁴Fc^{mIgG1} antibodies as suppressors of LBP·LPS-dependent PMN priming for fMLP-triggered $O_2^{\cdot-}$ /ROS production is less pronounced than that of anti-CD14^{3C10}Fc^{mIgG2b} antibody [90]. Thus, targeting CD14 by appropriate antibodies would be more effective in comparison to targeting CD11b/CD18 or TLR4. Moreover, it has been shown that CD11b/CD18 interacts more avidly with aggregated but not monomeric LPS and this interaction occurs even better in the absence of LBP [106, 168]. Taking these data into consideration, we concluded that CD11b/CD18 is not an appropriate target for “antibody”-based therapy even when anti-CD11b Fab/F(ab')₂ fragments are used.

9. Conclusions

In summary, several conclusions can be drawn. Neither mIgG2a nor mIgG1 are able to stimulate Ca^{2+} mobilization and ROS production in freshly isolated PMNs.

Sufficient signals for phosphoinositide breakdown could be induced in monocytes by CD14 association with CD64. Moreover, this heterotypic CD14 association with CD64/CD32 (anti-CD14^{UCHM-1}Fc^{mIgG2a}) or association of two CD32 receptors together (CD32 ← anti-CD32^{CIKM5}Fc^{mIgG1} → CD32) leads to Ca^{2+} signaling in monocytes. The homotypic CD32 association is less effective in Ca^{2+} signaling than heterotypic association of CD14 with CD64. In spite of this, CD14 association with CD64 is not enough to trigger $O_2^{\cdot-}$ /ROS production in monocytes. Ca^{2+} signaling caused by CD64/CD32 engagement without crosslinking is weaker than that induced by fMLP.

In monocytes not only sufficient production of PI(4,5)P₂ but also robust upregulation of intracellular H_2O_2 /ROS is initiated in response to broad CD14 crosslinking by anti-CD14^{mIgG1} antibodies and secondary F(ab')₂. In PMNs, this effect of CD14 crosslinking is less pronounced. TLR4 crosslinking [anti-TLR4^{76B351.1}Fc^{mIgG2b} plus F(ab')₂] does not have the same effect on PI(4,5)P₂ production as CD14 crosslinking. Thus, PI(4,5)P₂ generation is a specific response to CD14 crosslinking (clustering).

Antigenic recognition of CD32 by anti-CD32^{IV.3/AT-10} Fab/F(ab')₂ is already able to induce ITAMi signaling in PMNs thereby suppressing both constitutive and fMLP-triggered $O_2^{\cdot-}$ /ROS production. Antigenic recognition of CD16 by anti-CD16^{3G8} Fab/F(ab')₂ is unable to prime or activate PMNs for intracellular $O_2^{\cdot-}$ /ROS production.

In most cases in PMNs, targeting CD11b [Fab⁴⁴] causes “outside-in” signaling and generation of intracellular H_2O_2 /ROS [Fab/F(ab')₂^{OKM1}]. Antigenic recognition of both CD11b/CD18 subunits by F(ab')₂^{IB4} stimulates Ca^{2+} mobilization in the similar extent as the whole IB4 antibody. In PMNs, antibody-dependent [anti-CD11b^{mIgG1/mIgG2a}] association of CD11b/CD18 with CD32 or CD64 without crosslinking (clustering) does not induce sufficient Ca^{2+} mobilization and intracellular $O_2^{\cdot-}$ /ROS production. Thus,

nonagonistic targeting CD11b followed by its association with CD32 is not enough to activate PMNs for significant H_2O_2 /ROS generation but it takes place when CD11b will be targeted by agonistic antibody followed by CD32 engagement. A high sensitivity of CD11b/CD18 to environmental stimuli including antibodies and its ability to initiate “inside-out” signaling makes CD11b/CD18 not an appropriate target for “antibody”-based therapy even if anti-CD11b Fab/F(ab')₂ fragments would be used.

By contrast to CD11b/CD18, targeting CD14 by Fab or F(ab')₂ fragments is the most appropriate and safe approach for “antibody”-based therapy for LPS-induced deleterious effects even when innate immune cells are primed by PAMPs or endogenous priming molecules. A similar conclusion can be made accordingly targeting TLR4 by specific Fab/F(ab')₂ fragments. The effectiveness of anti-TLR4 Fab/F(ab')₂ fragments further may be potentiated by simultaneous use with anti-CD14 Fab/F(ab')₂. However, it is necessary to kept in mind that partial TLR4 blockage may cause the better therapeutic effect since certain TLR4 activation is required for development of the adaptive immune responses. Anti-TLR4 antibody is able to interfere with TLR4 binding to LPS-MD-2 thereby preventing TLR4 dimerization in addition to engagement of CD32 and CD64 signaling pathways.

In light of the data presented and based on our own observations [12, 13, 14], we can conclude that only anti-CD14^{UCHM-1}Fc^{mIgG2a} but neither anti-TLR4^{HTA125}Fc^{mIgG2a} nor anti-CD11b^{ICRF44}Fc^{mIgG1} antibodies are able to prevent significantly LPS-induced PMN priming for fMLP-triggered O_2^- /ROS generation. Therefore, we confirm that CD14 is really the main TLR4 gatekeeper. We believe that anti-CD14 Fab/F(ab')₂ fragments will be very suitable for clinical use and could improve outcomes during LPS-initiated inflammation.

Abbreviations

ADP:	Adenosine diphosphate
ARF6:	ADP-ribosylation factor 6
CD14:	Glycosylphosphatidylinositol-anchored protein
DAG:	Diacylglycerol
DAMPs:	Damage-associated molecular patterns
ERK:	Extracellularly regulated kinase
FcγRs:	Fc receptors γ
FPR1:	Formyl peptide receptor 1
fMLP:	<i>N</i> -Formyl-methionyl-leucyl-phenylalanine
GPCRs:	G protein-coupled receptors
GPI:	Glycosylphosphatidylinositol
GTPase:	Guanine nucleotide triphosphatase
IC:	Immune complexes
IL:	Interleukin
INF-γ, β:	Interferon γ, β
Ins(1,4,5)P ₃ :	Inositol 1,4,5-triphosphate
IRAK:	IL-1 receptor-associated kinase
IRF3:	Interferon regulatory factor 3

ITAM:	Immunoreceptor tyrosine-based activation motif
ITIM:	Immunoreceptor tyrosine-based inhibitory motif
LBP:	Lipopolysaccharide-binding protein
LPS:	Lipopolysaccharide (endotoxin)
LRR:	Leucine rich repeat
MAPK:	Mitogen-activated protein kinase
MCP-1:	Monocyte chemoattractant protein 1
MD-2:	Myeloid differentiation factor 2
MEK:	Mitogen-activated ERK-activated kinase (also referred as MAP2K, MAPKK)
MIP-3α:	Macrophage inflammatory protein 3α
MKK3:	Mitogen-activated protein kinase kinase 3 (also referred as MAP2K3, MAPKK3, MEK3, and SAPKK-2)
MyD88:	Myeloid factor of differentiation 88
NADPH oxidase:	Nicotinamide adenine dinucleotide phosphate oxidase
NF-κB:	Nuclear factor κ-light-chain-enhancer of activated B cells
NOX4:	NADPH oxidase complex 4
PAMPs:	Pathogen-associated molecular patterns
PBMC:	Peripheral blood mononuclear cells
PI3K:	Phosphatidylinositol 3-kinase
PIP5K:	Phosphatidylinositol 4-phosphate 5-kinase
PLC:	Phospholipase C
PLD:	Phospholipase D
PtdIns(3,4,5)P ₃ or PI(3,4,5)P ₃ :	Phosphatidylinositol 3,4,5-triphosphate
PtdIns(4,5)P ₂ or PI(4,5)P ₂ :	Phosphatidylinositol 4,5-bis-phosphate
PTK:	Protein tyrosine kinase
PMNs:	Polymorphonuclear leukocytes
PKB/Akt:	Protein kinase B or serine/threonine-specific protein kinase alpha
Raf:	Serine/threonine-protein kinase
ROS:	Reactive oxygen species
SHP-1:	Protein tyrosine phosphatase 1
SOD:	Superoxide dismutase
TAK1:	TGF-β-activated kinase
TGF-β:	Transforming growth factor β
TNF-α:	Tumor necrosis factor α
TICAM-1:	TIR domain-containing adaptor molecule 1
TIR:	Toll/interleukin-1 receptor domain
TIRAP/MAL:	TIR domain-containing adaptor protein also known as MyD88 adaptor-like
TLR:	Toll-like receptor
TRAF6:	TNF-α receptor-associated factor
TRAM:	TRIF-related adaptor molecule
TRIF:	TIR domain-containing adaptor inducing interferon-beta
Vav-1/RacGEF:	Guanine nucleotide exchange factor
VD3:	1α,25-Dihydroxyvitamin D3
DHR:	Dihydrorhodamine 123
DCFDA:	2',7'-Dichlorofluorescein diacetate
O-4' MPLA:	O-4' monophosphorylated lipid A.

Conflicts of Interest

The authors declare no conflict of interest.

Acknowledgments

This study was financially supported by the Mission of the National Government NAAA-A17-117030110138-2 established by the Ministry of Education and Science of the Russian Federation (Minobrnauka).

References

- [1] H. Tsukamoto, K. Fukudome, S. Takao et al., "Multiple potential regulatory sites of TLR4 activation induced by LPS as revealed by novel inhibitory human TLR4 mAbs," *International Immunology*, vol. 24, no. 8, pp. 495–506, 2012.
- [2] W. Gao, Y. Xiong, Q. Li, and H. Yang, "Inhibition of Toll-Like Receptor Signaling as a Promising Therapy for Inflammatory Diseases: A Journey from Molecular to Nano Therapeutics," *Frontiers in Physiology*, vol. 8, 2017.
- [3] N. Kuzmich, K. Sivak, V. Chubarev, Y. Porozov, T. Savateeva-Lyubimova, and F. Peri, "TLR4 Signaling Pathway Modulators as Potential Therapeutics in Inflammation and Sepsis," *Vaccines*, vol. 5, no. 4, p. 34, 2017.
- [4] Q. u. Ain, M. Batool, and S. Choi, "TLR4-Targeting Therapeutics: Structural Basis and Computer-Aided Drug Discovery Approaches," *Molecules*, vol. 25, no. 3, p. 627, 2020.
- [5] H. Tsukamoto, I. Ukai, Y. Yamagata et al., "Leucine-rich repeat 2 of human Toll-like receptor 4 contains the binding site for inhibitory monoclonal antibodies," *Federation of European Biochemical Societies Letters*, vol. 589, no. 24PartB, pp. 3893–3898, 2015.
- [6] H. Tsukamoto, Y. Yamagata, I. Ukai et al., "An inhibitory epitope of human Toll-like receptor 4 resides on leucine-rich repeat 13 and is recognized by a monoclonal antibody," *Federation of European Biochemical Societies Letters*, vol. 591, no. 16, pp. 2406–2416, 2017.
- [7] E. Monnet, G. Lapeyre, E. V. Poelgeest et al., "Evidence of NI-0101 pharmacological activity, an anti-TLR4 antibody, in a randomized phase I dose escalation study in healthy volunteers receiving LPS," *Clinical Pharmacology & Therapeutics*, vol. 101, no. 2, pp. 200–208, 2017.
- [8] D. Wolf, N. Anto-Michel, H. Blankenbach et al., "A ligand-specific blockade of the integrin Mac-1 selectively targets pathologic inflammation while maintaining protective host-defense," *Nature Communications*, vol. 9, no. 1, p. 525, 2018.
- [9] E. Monnet, E. H. Choy, I. McInnes et al., "Efficacy and safety of NI-0101, an anti-toll-like receptor 4 monoclonal antibody, in patients with rheumatoid arthritis after inadequate response to methotrexate: a phase II study," *Annals of the Rheumatic Diseases*, vol. 79, no. 3, pp. 316–323, 2020.
- [10] C. A. Spek, A. Verbon, H. Aberson et al., "Treatment with an anti-CD14 monoclonal antibody delays and inhibits lipopolysaccharide-induced gene expression in humans in vivo," *Journal of Clinical Immunology*, vol. 23, no. 2, pp. 132–140, 2003.
- [11] I. Dunn-Siegrist, O. Leger, B. Daubeuf et al., "Pivotal involvement of Fcγ receptor IIA in the neutralization of lipopolysaccharide signaling via a potent novel anti-TLR4 monoclonal antibody 15C1," *Journal of Biological Chemistry*, vol. 282, no. 48, pp. 34817–34827, 2007.
- [12] D. S. Kabanov and I. R. Prokhorenko, "Involvement of Toll-like receptor 4 and Fc receptors gamma in human neutrophil priming by endotoxins from *Escherichia coli*," *Biochemistry*, vol. 78, no. 2, pp. 185–193, 2013.
- [13] D. S. Kabanov, S. V. Grachev, and I. R. Prokhorenko, "Role of CD11b/CD18 in priming of human leukocytes by endotoxin glycoforms from *Escherichia coli*," *Biochemistry*, vol. 79, no. 8, pp. 812–819, 2014.
- [14] D. S. Kabanov, O. Y. Vvedenskaya, M. A. Fokina, E. M. Morozova, S. V. Grachev, and I. R. Prokhorenko, "Impact of CD14 on reactive oxygen species production from human leukocytes primed by *Escherichia coli* lipopolysaccharides," *Oxidative Medicine and Cellular Longevity*, vol. 2019, Article ID 6043245, 9 pages, 2019.
- [15] D. S. Kabanov, D. A. Serov, S. V. Zubova, S. V. Grachev, and I. R. Prokhorenko, "Dynamics of antagonistic potency of *Rhodobacter capsulatus* PG lipopolysaccharide against endotoxin-induced effects," *Biochemistry*, vol. 81, no. 3, pp. 275–283, 2016.
- [16] D. S. Kabanov, V. A. Rykov, S. V. Prokhorenko, A. N. Murashev, and I. R. Prokhorenko, "In vivo proinflammatory cytokine production by CD-1 mice in response to equipotential doses of *Rhodobacter capsulatus* PG and *Salmonella enterica* lipopolysaccharides," *Biochemistry*, vol. 83, no. 7, pp. 846–854, 2018.
- [17] S. Jin, F. Zhou, F. Katirai, and P.-L. Li, "Lipid raft redox signaling: molecular mechanisms in health and disease," *Antioxidants & Redox Signaling*, vol. 15, no. 4, pp. 1043–1083, 2011.
- [18] S. J. Forrester, D. S. Kikuchi, M. S. Hernandez, Q. Xu, and K. K. Griendling, "Reactive oxygen species in metabolic and inflammatory signaling," *Circulation Research*, vol. 122, no. 6, pp. 877–902, 2018.
- [19] J. Zhang, X. Wang, V. Vikash et al., "ROS and ROS-mediated cellular signaling," *Oxidative Medicine and Cellular Longevity*, vol. 2016, Article ID 4350965, 18 pages, 2016.
- [20] N. Di Marzo, E. Chisci, and R. Giovannoni, "The role of Hydrogen peroxide in redox-dependent signaling: homeostatic and pathological responses in mammalian cells," *Cells*, vol. 7, no. 10, p. 156, 2018.
- [21] A. Ngkelo, K. Meja, M. Yeadon, I. Adcock, and P. A. Kirkham, "LPS induced inflammatory responses in human peripheral blood mononuclear cells is mediated through NOX4 and G_i -alpha dependent PI-3kinase signalling," *Journal of Inflammation*, vol. 9, no. 1, p. 1, 2012.
- [22] H. S. Park, H. Y. Jung, E. Y. Park, J. Kim, W. J. Lee, and Y. S. Bae, "Cutting edge: direct interaction of TLR4 with NAD(P)H oxidase 4 isozyme is essential for lipopolysaccharide-induced production of reactive oxygen species and activation of NF- κ B," *The Journal of Immunology*, vol. 173, no. 6, pp. 3589–3593, 2004.
- [23] M. G. Netea, L. A. B. Joosten, E. Latz et al., "Trained immunity: a program of innate immune memory in health and disease," *Science*, vol. 352, no. 6284, p. aaf1098, 2016.
- [24] C. Rosales, "Neutrophil: A Cell with Many Roles in Inflammation or Several Cell Types?," *Frontiers in Physiology*, vol. 9, 2018.
- [25] P. A. Kramer, S. Ravi, B. Chacko, M. S. Johnson, and V. M. Darley-Usmar, "A review of the mitochondrial and glycolytic metabolism in human platelets and leukocytes: implications for their use as bioenergetic biomarkers," *Redox Biology*, vol. 2, pp. 206–210, 2014.

- [26] H.-Y. Tan, N. Wang, S. Li, M. Hong, X. Wang, and Y. Feng, "The reactive oxygen species in macrophage polarization: reflecting its dual role in progression and treatment of human diseases," *Oxidative Medicine and Cellular Longevity*, vol. 2016, Article ID 2795090, 16 pages, 2016.
- [27] B. Fuhrman, M. Shiner, N. Volkova, and M. Aviram, "Cell-induced copper ion-mediated low density lipoprotein oxidation increases during in vivo monocyte-to-macrophage differentiation," *Free Radical Biology and Medicine*, vol. 37, no. 2, pp. 259–271, 2004.
- [28] A. C. Bulua, A. Simon, R. Maddipati et al., "Mitochondrial reactive oxygen species promote production of proinflammatory cytokines and are elevated in TNFR1-associated periodic syndrome (TRAPS)," *Journal of Experimental Medicine*, vol. 208, no. 3, pp. 519–533, 2011.
- [29] M. G. Netea, A. Simon, F. van de Veerdonk, B.-J. Kullberg, J. W. M. Van der Meer, and L. A. B. Joosten, "IL-1 β Processing in Host Defense: Beyond the Inflammasomes," *PLoS Pathogens*, vol. 6, no. 2, p. e1000661, 2010.
- [30] M. Reiss and D. Roos, "Differences in Oxygen metabolism of phagocytosing monocytes and neutrophils," *The Journal of Clinical Investigation*, vol. 61, no. 2, pp. 480–488, 1978.
- [31] G. Fossati, D. A. Moulding, D. G. Spiller, R. J. Moots, M. R. H. White, and S. W. Edwards, "The mitochondrial network of human neutrophils: role in chemotaxis, phagocytosis, respiratory burst activation, and commitment to apoptosis," *The Journal of Immunology*, vol. 170, no. 4, pp. 1964–1972, 2003.
- [32] G. T. Nguyen, E. R. Green, and J. Meccas, "Neutrophils to the ROScue: mechanisms of NADPH oxidase activation and bacterial resistance," *Frontiers in Cellular and Infection Microbiology*, vol. 7, 2017.
- [33] J. El-Benna, P. M.-C. Dang, and M.-A. Gougerot-Pocidallo, "Priming of the neutrophil NADPH oxidase activation: role of p47^{phox} phosphorylation and NOX2 mobilization to the plasma membrane," *Seminars in Immunopathology*, vol. 30, no. 3, pp. 279–289, 2008.
- [34] J. G. Moreland, A. P. Davis, J. J. Matsuda et al., "Endotoxin priming of neutrophils requires NADPH oxidase-generated oxidants and is regulated by the anion transporter ClC-3," *The Journal of Biological Chemistry*, vol. 282, no. 47, pp. 33958–33967, 2007.
- [35] S. Br  chard, S. Plan  on, and E. J. Tschirhart, "New Insights into the Regulation of Neutrophil NADPH Oxidase Activity in the Phagosome: A Focus on the Role of Lipid and Ca²⁺ Signaling," *Antioxidants & Redox Signaling*, vol. 18, no. 6, pp. 661–676, 2013.
- [36] Y. Mazaki, S. Hashimoto, T. Tsujimura et al., "Neutrophil direction sensing and superoxide production linked by the GTPase-activating protein GIT2," *Nature Immunology*, vol. 7, no. 7, pp. 724–731, 2006.
- [37] J. Schymeinsky, A. M  csai, and B. Walzog, "Neutrophil activation via β 2 integrins (CD11/CD18): Molecular mechanisms and clinical implications," *Thrombosis and Haemostasis*, vol. 98, no. 8, pp. 262–273, 2017.
- [38] I. Miralda, S. M. Uriarte, and K. R. McLeish, "Multiple Phenotypic Changes Define Neutrophil Priming," *Frontiers in Cellular and Infection Microbiology*, vol. 7, 2017.
- [39] F. R. DeLeo, J. Renee, S. McCormick et al., "Neutrophils exposed to bacterial lipopolysaccharide upregulate NADPH oxidase assembly," *The Journal of Clinical Investigation*, vol. 101, no. 2, pp. 455–463, 1998.
- [40] L. R. Prince, M. K. Whyte, I. Sabroe, and L. C. Parker, "The role of TLRs in neutrophil activation," *Current Opinion in Pharmacology*, vol. 11, no. 4, pp. 397–403, 2011.
- [41] A. Pfeiffer, A. B  ttcher, E. Ors   et al., "Lipopolysaccharide and ceramide docking to CD14 provokes ligand-specific receptor clustering in rafts," *European Journal of Immunology*, vol. 31, no. 11, pp. 3153–3164, 2001.
- [42] G. Schmitz and E. Ors  , "CD14 signalling in lipid rafts: new ligands and co-receptors," *Current Opinion in Lipidology*, vol. 13, no. 5, pp. 513–521, 2002.
- [43] D. S. Kabanov, Y. V. Radzyukevich, S. V. Grachev, and I. R. Prokhorenko, "Влияние структуры липида А липополисахаридов на их взаимодействие с ЛПС-связывающим белком сыворотки крови и активацию лейкоцитов," *Biological Membranes (Moscow)*, vol. 35, no. 5, pp. 341–350, 2018.
- [44] A. Pfeiffer, M. Kapinsky, E. Ors   et al., "The Cholesterol Content of the Plasma Membrane as a Regulator of CD14 Dependent Signal Transduction," *Single Molecules*, vol. 2, no. 2, pp. 113–115, 2001.
- [45] K. Miyake, "Innate recognition of lipopolysaccharide by Toll-like receptor 4-MD-2," *Trends in Microbiology*, vol. 12, no. 4, pp. 186–192, 2004.
- [46] H. Oshiumi, M. Sasai, K. Shida, T. Fujita, M. Matsumoto, and T. Seya, "TIR-containing adapter molecule (TICAM)-2, a bridging adapter recruiting to toll-like receptor 4 TICAM-1 that induces interferon-beta," *Journal of Biological Chemistry*, vol. 278, no. 50, pp. 49751–49762, 2003.
- [47] T. Hornig, G. M. Barton, and R. Medzhitov, "TIRAP: an adapter molecule in the Toll signaling pathway," *Nature Immunology*, vol. 2, no. 9, pp. 835–841, 2001.
- [48] M. Yamamoto, "Role of adaptor TRIF in the MyD88-independent toll-like receptor signaling pathway," *Science*, vol. 301, no. 5633, pp. 640–643, 2003.
- [49] M. Yamamoto, S. Sato, H. Hemmi et al., "TRAM is specifically involved in the Toll-like receptor 4-mediated MyD88-independent signaling pathway," *Nature Immunology*, vol. 4, no. 11, pp. 1144–1150, 2003.
- [50] T. Kawai, O. Takeuchi, T. Fujita et al., "Lipopolysaccharide stimulates the MyD88-independent pathway and results in activation of IFN-regulatory factor 3 and the expression of a subset of lipopolysaccharide-inducible genes," *The Journal of Immunology*, vol. 167, no. 10, pp. 5887–5894, 2001.
- [51] S. M. Zughair, S. M. Zimmer, A. Datta, R. W. Carlson, and D. S. Stephens, "Differential induction of the Toll-like receptor 4-MyD88-dependent and -independent signaling pathways by Endotoxins," *Infection and Immunity*, vol. 73, no. 5, pp. 2940–2950, 2005.
- [52] N. Tamassia, V. Le Moigne, F. Calzetti et al., "The MyD88-independent pathway is not mobilized in human neutrophils stimulated via TLR4," *Journal of Immunology*, vol. 178, no. 11, pp. 7344–7356, 2007.
- [53] J. A. Nick, N. J. Avdi, S. K. Young et al., "Selective activation and functional significance of p38 α mitogen-activated protein kinase in lipopolysaccharide-stimulated neutrophils," *Journal of Clinical Investigation*, vol. 103, no. 6, pp. 851–858, 1999.
- [54] J. El-Benna, M. Hurtado-Nedelec, V. Marzaioli, J.-C. Marie, M.-A. Gougerot-Pocidallo, and P. M.-C. Dang, "Priming of the neutrophil respiratory burst: role in host defense and

- inflammation,” *Immunological Reviews*, vol. 273, no. 1, pp. 180–193, 2016.
- [55] K. Futosi, S. Fodor, and A. Mócsai, “Neutrophil cell surface receptors and their intracellular signal transduction pathways,” *International Immunopharmacology*, vol. 17, no. 3, pp. 638–650, 2013.
- [56] J. B. Klein, A. Buridi, P. Y. Coxon et al., “Role of extracellular signal-regulated kinase and phosphatidylinositol-3 kinase in chemoattractant and LPS delay of constitutive neutrophil apoptosis,” *Cellular Signalling*, vol. 13, no. 5, pp. 335–343, 2001.
- [57] D. D. Browning, N. D. Windes, and R. D. Ye, “Activation of p38 mitogen-activated protein kinase by lipopolysaccharide in human neutrophils requires nitric oxide-dependent cGMP accumulation,” *The Journal of Biological Chemistry*, vol. 274, no. 1, pp. 537–542, 1999.
- [58] A. M. Condliffe, E. Kitchen, and E. R. Chilvers, “Neutrophil priming: pathophysiological consequences and underlying mechanisms,” *Clinical Science*, vol. 94, no. 5, pp. 461–471, 1998.
- [59] P. Chames, M. Van Regenmortel, E. Weiss, and D. Baty, “Therapeutic antibodies: successes, limitations and hopes for the future,” *British Journal of Pharmacology*, vol. 157, no. 2, pp. 220–233, 2009.
- [60] F. Nimmerjahn and J. V. Ravetch, “Antibodies, Fc receptors and cancer,” *Current Opinion in Immunology*, vol. 19, no. 2, pp. 239–245, 2007.
- [61] L. Shang, B. Daubeuf, M. Triantafilou et al., “Selective antibody intervention of Toll-like receptor 4 activation through Fc γ receptor tethering,” *The Journal of Biological Chemistry*, vol. 289, no. 22, pp. 15309–15318, 2014.
- [62] R. Wang, J. Stephens, and M. J. Lacy, “Characterization of monoclonal antibody HTA125 with specificity for human TLR4,” *Hybridoma and Hybridomics*, vol. 22, no. 6, pp. 357–365, 2003.
- [63] S. J. Gadd, R. Eher, O. Majdic, and W. Knapp, “Signal transduction via Fc gamma R and Mac-1 alpha-chain in monocytes and polymorphonuclear leucocytes,” *The Journal of Immunology*, vol. 81, no. 4, pp. 611–617, 1994.
- [64] E. A. Macintyre, P. J. Roberts, M. Jones et al., “Activation of human monocytes occurs on cross-linking monocytic antigens to an Fc receptor,” *The Journal of Immunology*, vol. 142, no. 7, pp. 2377–2383, 1989.
- [65] E. van Mirre, W. B. Breunis, J. Geissler et al., “Neutrophil responsiveness to IgG, as determined by fixed ratios of mRNA levels for activating and inhibitory Fc γ RII (CD32), is stable over time and unaffected by cytokines,” *Blood*, vol. 108, no. 2, pp. 584–590, 2006.
- [66] S. Rivas-Fuentes, E. Garcia-Garcia, G. Nieto-Castaneda, and C. Rosales, “Fc γ receptors exhibit different phagocytosis potential in human neutrophils,” *Cellular Immunology*, vol. 263, no. 1, pp. 114–121, 2010.
- [67] J. G. J. van de Winkel and C. L. Anderson, “Biology of human immunoglobulin G Fc receptors,” *Journal of Leukocyte Biology*, vol. 49, no. 5, pp. 511–524, 1991.
- [68] J. G. J. van de Winkel and P. J. A. Capel, “Human IgG Fc receptor heterogeneity: molecular aspects and clinical implications,” *Immunology Today*, vol. 14, no. 5, pp. 215–221, 1993.
- [69] P. M. Guyre, R. F. Graziano, B. A. Vance, P. M. Morganelli, and M. W. Fanger, “Monoclonal antibodies that bind to distinct epitopes on Fc gamma RI are able to trigger receptor function,” *The Journal of Immunology*, vol. 143, no. 5, pp. 1650–1655, 1989.
- [70] B. Walzog, R. Seifert, A. Zakrzewicz, P. Gaehtgens, and K. Ley, “Cross-linking of CD18 in human neutrophils induces an increase of intracellular free Ca²⁺, exocytosis of azurophilic granules, quantitative up-regulation of CD18, shedding of L-selectin, and actin polymerization,” *Journal of Leukocyte Biology*, vol. 56, no. 5, pp. 625–635, 1994.
- [71] T. W. Huizinga, F. van Kemenade, L. Koenderman et al., “The 40-kDa Fc gamma receptor (FcRII) on human neutrophils is essential for the IgG-induced respiratory burst and IgG-induced phagocytosis,” *The Journal of Immunology*, vol. 142, no. 7, pp. 2365–2369, 1989.
- [72] J. C. Edberg and R. P. Kimberly, “Modulation of Fc gamma and complement receptor function by the glycosyl-phosphatidylinositol-anchored form of Fc gamma RIII,” *The Journal of Immunology*, vol. 152, no. 12, pp. 5826–5835, 1994.
- [73] A. Ortiz-Stern and C. Rosales, “Cross-talk between Fc receptors and integrins,” *Immunology Letters*, vol. 90, no. 2-3, pp. 137–143, 2003.
- [74] T. K. Means and A. D. Luster, “Integrins limit the Toll,” *Nature Immunology*, vol. 11, no. 8, pp. 691–693, 2010.
- [75] A. J. Melendez, L. Bruetsch, R. A. Floto, M. M. Harnett, and J. M. Allen, “Functional coupling of Fc γ RI to nicotinamide adenine dinucleotide phosphate (reduced form) oxidative burst and immune complex trafficking requires the activation of phospholipase D1,” *Blood*, vol. 98, no. 12, pp. 3421–3428, 2001.
- [76] A. P. Ociennikowska, M. I. Zdioruk, G. Traczyk, A. Swiatkowska, and K. Kwiatkowska, “LPS-induced clustering of CD14 triggers generation of PI(4,5)P₂,” *Journal of Cell Science*, vol. 128, no. 22, pp. 4096–4111, 2015.
- [77] S. R. Yan, W. Al-Hertani, D. Byers, and R. Bortolussi, “Lipopolysaccharide-binding protein- and CD14-dependent activation of mitogen-activated protein kinase p38 by lipopolysaccharide in human neutrophils is associated with priming of respiratory burst,” *Infection and Immunity*, vol. 70, no. 8, pp. 4068–4074, 2002.
- [78] E. A. MacIntyre, P. J. Roberts, R. Abdul-Gaffar et al., “Mechanism of human monocyte activation via the 40-kDa Fc receptor for IgG,” *The Journal of Immunology*, vol. 141, no. 12, pp. 4333–4343, 1988.
- [79] A. Plociennikowska, A. Hromada-Judycka, K. Borzecka, and K. Kwiatkowska, “Co-operation of TLR4 and raft proteins in LPS-induced pro-inflammatory signaling,” *Cellular and Molecular Life Sciences*, vol. 72, no. 3, pp. 557–581, 2015.
- [80] J. Pugin, V. V. Kravchenko, J.-D. Lee, L. Kline, R. J. Ulevitch, and P. S. Tobias, “Cell activation mediated by glycosylphosphatidylinositol-anchored or transmembrane forms of CD14,” *Infection and Immunity*, vol. 66, no. 3, pp. 1174–1180, 1998.
- [81] F. Lund-Johansen, J. Olweus, A. Aarli, and R. Bjerknes, “Signal transduction in human monocytes and granulocytes through the PI-linked antigen CD14,” *FEBS Letters*, vol. 273, no. 1-2, pp. 55–58, 1990.
- [82] Z. Wu, Z. Zhang, Z. Lei, and P. Lei, “CD14: biology and role in the pathogenesis of disease,” *Cytokine and Growth Factor Reviews*, vol. 48, pp. 24–31, 2019.
- [83] F. Lund-Johansen, J. Olweus, F. W. Symington et al., “Activation of human monocytes and granulocytes by monoclonal

- antibodies to glycosylphosphatidylinositol-anchored antigens," *European Journal of Immunology*, vol. 23, no. 11, pp. 2782–2791, 1993.
- [84] P. Antal-Szalmas, J. A. G. van Strijp, A. J. L. Weersink et al., "Quantitation of surface CD14 on human monocytes and neutrophils," *Journal of Leukocyte Biology*, vol. 61, no. 6, pp. 721–728, 1997.
- [85] I. Stefanova, M. L. Corcoran, E. M. Horak, L. M. Wahl, J. B. Bolen, and I. D. Horak, "Lipopolysaccharide induces activation of CD14-associated protein tyrosine kinase p53/56lyn," *The Journal of Biological Chemistry*, vol. 268, no. 28, pp. 20725–20728, 1993.
- [86] B. Seed, "Initiation of signal transduction by receptor aggregation: role of nonreceptor tyrosine kinases," *Seminars in Immunology*, vol. 7, no. 1, pp. 3–11, 1995.
- [87] E. B. Lynam, S. I. Simon, Y. P. Rochon, and L. A. Sklar, "Lipopolysaccharide enhances CD11b/CD18 function but inhibits neutrophil aggregation," *Blood*, vol. 83, no. 11, pp. 3303–3311, 1994.
- [88] M. D. Cunningham, R. A. Shapiro, C. Seachord, K. Ratcliffe, L. Cassiano, and R. P. Darveau, "CD14 Employs Hydrophilic Regions to "Capture" Lipopolysaccharides," *The Journal of Immunology*, vol. 164, no. 6, pp. 3255–3263, 2000.
- [89] J.-I. Kim, C. J. Lee, M. S. Jin et al., "Crystal structure of CD14 and its implications for lipopolysaccharide signaling," *The Journal of Biological Chemistry*, vol. 280, no. 12, pp. 11347–11351, 2005.
- [90] A. Troelstra, B. N. G. Giepmans, K. P. M. van Kessel, H. S. Lichenstein, J. Verhoef, and J. A. G. van Strijp, "Dual effects of soluble CD14 on LPS priming of neutrophils," *Journal of Leukocyte Biology*, vol. 61, no. 2, pp. 173–178, 1997.
- [91] R. Landmann, F. Scherer, R. Schumann, S. Link, S. Sansano, and W. Zimmerli, "LPS directly induces oxygen radical production in human monocytes via LPS binding protein and CD14," *Journal of Leukocyte Biology*, vol. 57, no. 3, pp. 440–449, 1995.
- [92] R. Weingarten, L. A. Sklar, J. C. Mathison et al., "Interactions of lipopolysaccharide with neutrophils in blood via CD14," *Journal of Leukocyte Biology*, vol. 53, no. 5, pp. 518–524, 1993.
- [93] W. A. Lynn, C. R. H. Raetz, N. Qureshi, and D. T. Golenbock, "Lipopolysaccharide-induced stimulation of CD11b/CD18 expression on neutrophils. Evidence of specific receptor-based response and inhibition by lipid A-based antagonists," *The Journal of Immunology*, vol. 147, no. 9, pp. 3072–3079, 1991.
- [94] P. S. Tobias, K. Soldau, L. Kline et al., "Cross-linking of lipopolysaccharide (LPS) to CD14 on THP-1 cells mediated by LPS-binding protein," *The Journal of Immunology*, vol. 150, no. 7, pp. 3011–3021, 1993.
- [95] R. Landmann, H.-P. Knopf, S. Link, S. Sansano, R. Schumann, and W. Zimmerli, "Human monocyte CD14 is upregulated by lipopolysaccharide," *Infection and Immunity*, vol. 64, no. 5, pp. 1762–1769, 1996.
- [96] A. M. Soler-Rodriguez, H. Zhang, H. S. Lichenstein et al., "Neutrophil activation by bacterial lipoprotein versus lipopolysaccharide: differential requirements for serum and CD14," *The Journal of Immunology*, vol. 164, no. 5, pp. 2674–2683, 2000.
- [97] F. Stelter, M. Bernheiden, R. Menzel et al., "Mutation of amino acids 39–44 of human CD14 Abrogates binding of lipopolysaccharide and Escherichia coli," *European Journal of Biochemistry*, vol. 243, no. 1–2, pp. 100–109, 1997.
- [98] C. Hermann, I. Spreitzer, N. W. J. Schröder et al., "Cytokine induction by purified lipoteichoic acids from various bacterial species – role of LBP, sCD14, CD14 and failure to induce IL-12 and subsequent IFN- γ release," *European Journal of Immunology*, vol. 32, no. 2, pp. 541–551, 2002.
- [99] D. Heumann, P. Gally, C. Barras et al., "Control of lipopolysaccharide (LPS) binding and LPS-induced tumor necrosis factor secretion in human peripheral blood monocytes," *The Journal of Immunology*, vol. 148, no. 11, pp. 3505–3512, 1992.
- [100] K. Yasui, E. L. Becker, and R. I. Sha'afi, "Lipopolysaccharide and serum cause the translocation of G-protein to the membrane and prime neutrophils via CD14," *Biochemical and Biophysical Research Communications*, vol. 183, no. 3, pp. 1280–1286, 1992.
- [101] P. Gally, C. V. Jongeneel, C. Barras et al., "Short time exposure to lipopolysaccharide is sufficient to activate human monocytes," *The Journal of Immunology*, vol. 150, no. 11, pp. 5086–5093, 1993.
- [102] M. Pollack, A. M. Espinoza, G. Guelde, N. L. Koles, L. M. Wahl, and C. A. Ohl, "Lipopolysaccharide (LPS)-specific monoclonal antibodies regulate LPS uptake and LPS-induced tumor necrosis Factor- Responses by human monocytes," *The Journal of Infectious Diseases*, vol. 172, no. 3, pp. 794–804, 1995.
- [103] G. Qing, K. Rajaraman, and R. Bortolussi, "Diminished priming of neonatal polymorphonuclear leukocytes by lipopolysaccharide is associated with reduced CD14 expression," *Infection and Immunity*, vol. 63, no. 1, pp. 248–252, 1995.
- [104] K. Yasui, A. Komiyama, T. F. Molski, and R. I. Sha'afi, "Pentoxifylline and CD14 antibody additively inhibit priming of polymorphonuclear leukocytes for enhanced release of superoxide by lipopolysaccharide: possible mechanism of these actions," *Infection and Immunity*, vol. 62, no. 3, pp. 922–927, 1994.
- [105] S. L. Weinstein, C. H. June, and A. L. DeFranco, "Lipopolysaccharide-induced protein tyrosine phosphorylation in human macrophages is mediated by CD14," *The Journal of Immunology*, vol. 151, no. 7, pp. 3829–3838, 1993.
- [106] S. Noubir, Z. Hmama, and N. E. Reiner, "Dual receptors and distinct pathways mediate interleukin-1 receptor-associated kinase degradation in response to lipopolysaccharide. Involvement of CD14/TLR4, CR3, and phosphatidylinositol 3-kinase," *The Journal of Biological Chemistry*, vol. 279, no. 24, pp. 25189–25195, 2004.
- [107] J. Pugin, D. Heumann, A. Tomasz et al., "CD14 is a pattern recognition receptor," *Immunity*, vol. 1, no. 6, pp. 509–516, 1994.
- [108] R. I. Tapping, S. Akashi, K. Miyake, P. J. Godowski, and P. S. Tobias, "Toll-like receptor 4, but not Toll-like receptor 2, is a signaling receptor for Escherichia and Salmonella lipopolysaccharides," *The Journal of Immunology*, vol. 165, no. 10, pp. 5780–5787, 2000.
- [109] D. J. Leturcq, A. M. Moriarty, G. Talbott, R. K. Winn, T. R. Martin, and R. J. Ulevitch, "Antibodies against CD14 protect primates from endotoxin-induced shock," *The Journal of Clinical Investigation*, vol. 98, no. 7, pp. 1533–1538, 1996.
- [110] S. G. Elner, H. R. Petty, V. M. Elner et al., "TLR4 mediates human retinal pigment epithelial endotoxin binding and

- cytokine expression," *Transactions of the American Ophthalmological Society*, vol. 103, pp. 126–137, 2005.
- [111] D. Iwaki, C. Nishitani, H. Mitsuzawa, N. Hyakushima, H. Sano, and Y. Kuroki, "The CD14 region spanning amino acids 57–64 is critical for interaction with the extracellular Toll-like receptor 2 domain," *Biochemical and Biophysical Research Communications*, vol. 328, no. 1, pp. 173–176, 2005.
- [112] S. Baveye, E. Ellass, D. G. Fernig, C. Blanquart, J. Mazurier, and D. Legrand, "Human lactoferrin interacts with soluble CD14 and inhibits expression of endothelial adhesion molecules, E-selectin and ICAM-1, induced by the CD14-lipopolysaccharide complex," *Infection and Immunity*, vol. 68, no. 12, pp. 6519–6525, 2000.
- [113] D. Kim and J. Y. Kim, "Anti-CD14 antibody reduces LPS responsiveness via TLR4 internalization in human monocytes," *Molecular Immunology*, vol. 57, no. 2, pp. 210–215, 2014.
- [114] T. Nakata, M. Yasuda, M. Fujita et al., "CD14 directly binds to triacylated lipopeptides and facilitates recognition of the lipopeptides by the receptor complex of Toll-like receptors 2 and 1 without binding to the complex," *Cellular Microbiology*, vol. 8, no. 12, pp. 1899–1909, 2006.
- [115] M. Triantafyllou, K. Triantafyllou, and N. Fernandez, "Rough and smooth forms of fluorescein-labelled bacterial endotoxin exhibit CD14/LBP dependent and independent binding that is influenced by endotoxin concentration," *European Journal of Biochemistry*, vol. 267, no. 8, pp. 2218–2226, 2000.
- [116] T. S.-C. Juan, E. Hailman, M. J. Kelley et al., "Identification of a lipopolysaccharide binding domain in CD14 between amino acids 57 and 64," *The Journal of Biological Chemistry*, vol. 270, no. 10, pp. 5219–5224, 1995.
- [117] K. Kuronuma, H. Mitsuzawa, K. Takeda et al., "Anionic pulmonary surfactant phospholipids inhibit inflammatory responses from alveolar macrophages and U937 cells by binding the lipopolysaccharide-interacting proteins CD14 and MD-2," *The Journal of Biological Chemistry*, vol. 284, no. 38, pp. 25488–25500, 2009.
- [118] M. A. Dentener, V. Bazil, E. J. U. von Asmuth, M. Ceska, and W. A. Buurman, "Involvement of CD14 in lipopolysaccharide-induced tumor necrosis factor- α , IL-6 and IL-8 release by human monocytes and alveolar macrophages," *The Journal of Immunology*, vol. 150, no. 7, pp. 2885–2891, 1993.
- [119] A. L. Blomkalns, L. L. Stoll, W. Shaheen et al., "Low level bacterial endotoxin activates two distinct signaling pathways in human peripheral blood mononuclear cells," *Journal of Inflammation*, vol. 8, no. 1, p. 4, 2011.
- [120] A. Kato, T. Ogasawara, T. Homma, H. Saito, and K. Matsumoto, "Lipopolysaccharide-binding protein critically regulates lipopolysaccharide-induced IFN- β signaling pathway in human monocytes," *The Journal of Immunology*, vol. 172, no. 10, pp. 6185–6194, 2004.
- [121] M. Suzuki, C. Kato, and A. Kato, "Therapeutic antibodies: their mechanisms of action and the pathological findings they induce in toxicity studies," *Journal of Toxicologic Pathology*, vol. 28, no. 3, pp. 133–139, 2015.
- [122] A. Verbon, P. E. P. Dekkers, T. ten Hove et al., "IC14, an anti-CD14 antibody, inhibits endotoxin-mediated symptoms and inflammatory responses in humans," *The Journal of Immunology*, vol. 166, no. 5, pp. 3599–3605, 2001.
- [123] L. A. J. O'Neill, C. E. Bryant, and S. L. Doyle, "Therapeutic targeting of Toll-like receptors for infectious and inflammatory diseases and cancer," *Pharmacological Reviews*, vol. 61, no. 2, pp. 177–197, 2009.
- [124] S. Sugawara, S. Yang, K. Iki et al., "Monocytic cell activation by nonendotoxic glycoprotein from *Prevotella intermedia* ATCC 25611 is mediated by Toll-like receptor 2," *Infection and Immunity*, vol. 69, no. 8, pp. 4951–4957, 2001.
- [125] S. M. Zughair, Y.-L. Tzeng, S. M. Zimmer, A. Datta, R. W. Carlson, and D. S. Stephens, "Neisseria meningitidis lipooligosaccharide structure-dependent activation of the macrophage CD14/Toll-like receptor 4 pathway," *Infection and Immunity*, vol. 72, no. 1, pp. 371–380, 2004.
- [126] C. Basak, S. K. Pathak, A. Bhattacharyya, D. Mandal, S. Pathak, and M. Kundu, "NF- κ B- and C/EBP β -driven Interleukin-1 β gene expression and PAK1-mediated caspase-1 activation play essential roles in Interleukin-1 β release from *Helicobacter pylori* Lipopolysaccharide-stimulated macrophages," *The Journal of Biological Chemistry*, vol. 280, no. 6, pp. 4279–4288, 2005.
- [127] M. Martin, J. Katz, S. N. Vogel, and S. M. Michalek, "Differential induction of endotoxin tolerance by lipopolysaccharides derived from *Porphyromonas gingivalis* and *Escherichia coli*," *The Journal of Immunology*, vol. 167, no. 9, pp. 5278–5285, 2001.
- [128] T. Ogawa, Y. Asai, Y. Sakai et al., "Endotoxic and immunobiological activities of a chemically synthesized lipid A of *Helicobacter pylori* strain 206-1," *FEMS Immunology and Medical Microbiology*, vol. 36, no. 1-2, pp. 1–7, 2003.
- [129] V. Stadlbauer, R. P. Mookerjee, G. A. K. Wright et al., "Role of Toll-like receptors 2, 4, and 9 in mediating neutrophil dysfunction in alcoholic hepatitis," *American Journal of Physiology Gastrointestinal and Liver Physiology*, vol. 296, no. 1, pp. G15–G22, 2009.
- [130] M. Martin, S. M. Michalek, and J. Katz, "Role of innate immune factors in the adjuvant activity of monophosphoryl lipid A," *Infection and Immunity*, vol. 71, no. 5, pp. 2498–2507, 2003.
- [131] B. S. Park, D. H. Song, H. M. Kim, B.-S. Choi, H. Lee, and J.-O. Lee, "The structural basis of lipopolysaccharide recognition by the TLR4-MD-2 complex," *Nature*, vol. 458, no. 7242, pp. 1191–1195, 2009.
- [132] R. Shimazu, S. Akashi, H. Ogata et al., "MD-2, a molecule that confers lipopolysaccharide responsiveness on Toll-like receptor 4," *Journal of Experimental Medicine*, vol. 189, no. 11, pp. 1777–1782, 1999.
- [133] T. Sanui, M. Takeshita, T. Fukuda, A. Haraguchi, Y. Aida, and F. Nishimura, "Anti-CD14 antibody-treated neutrophils respond to LPS: possible involvement of CD14 upregulated by anti-CD14 antibody binding," *Immunological Investigations*, vol. 46, no. 2, pp. 190–200, 2016.
- [134] S. B. Mkaddem, G. Hayem, F. Jönsson et al., "Shifting Fc γ RIIA-ITAM from activation to inhibitory configuration ameliorates arthritis," *Journal of Clinical Investigation*, vol. 124, no. 9, pp. 3945–3959, 2014.
- [135] J. Loyau, G. Didelot, P. Malinge et al., "Robust antibody-antigen complexes prediction generated by combining sequence analyses, mutagenesis, in vitro evolution, X-ray crystallography and in silico docking," *Journal of Molecular Biology*, vol. 427, no. 16, pp. 2647–2662, 2015.
- [136] K. Gomery, S. Muller-Loennies, C. L. Brooks et al., "Antibody WN1 222-5 mimics Toll-like receptor 4 binding in the recognition of LPS," in *Proceedings of the National Academy of*

- Sciences of the United States of America (PNAS)*, vol. 109no. 51, pp. 20877–20882, 2012.
- [137] M.-J. Zhou and E. J. Brown, “CR3 (Mac-1, alpha M beta 2, CD11b/CD18) and Fc gamma RIII cooperate in generation of a neutrophil respiratory burst: requirement for Fc gamma RIII and tyrosine phosphorylation,” *The Journal of Cell Biology*, vol. 125, no. 6, pp. 1407–1416, 1994.
- [138] J. Greenman, A. L. Tutt, A. J. T. George, K. A. F. Pulford, G. T. Stevenson, and M. J. Glennie, “Characterization of a new monoclonal anti-Fcγ RII antibody, AT10, and its incorporation into a bispecific F(ab)₂ derivative for recruitment of cytotoxic effectors,” *Molecular Immunology*, vol. 28, no. 11, pp. 1243–1254, 1991.
- [139] S. Bournazos, S. P. Hart, L. H. Chamberlain, M. J. Glennie, and I. Dransfield, “Association of FcγRIIA (CD32A) with lipid rafts regulates ligand binding Activity,” *The Journal of Immunology*, vol. 182, no. 12, pp. 8026–8036, 2009.
- [140] K. Su, H. Yang, X. Li et al., “Expression profile of FcγRIIb on leukocytes and its dysregulation in systemic lupus erythematosus,” *The Journal of Immunology*, vol. 178, no. 5, pp. 3272–3280, 2007.
- [141] M.-J. Zhou, R. F. Todd III, J. G. J. van de Winkel, and H. R. Petty, “Cocapping of the leukoadhesin molecules complement receptor type 3 and lymphocyte function-associated antigen-1 with Fc gamma receptor III on human neutrophils. Possible role of lectin-like interactions,” *The Journal of Immunology*, vol. 150, no. 7, pp. 3030–3041, 1993.
- [142] P. Y. Coxon, M. J. Rane, D. W. Powell, J. B. Klein, and K. R. McLeish, “Differential mitogen-activated protein kinase stimulation by Fcγ receptor IIa and Fcγ receptor IIIb determines the activation phenotype of human neutrophils,” *The Journal of Immunology*, vol. 164, no. 12, pp. 6530–6537, 2000.
- [143] M. Aloulou, S. B. Mkaddem, M. Biarnes-Pelicot et al., “IgG1 and IVIg induce inhibitory ITAM signaling through FcγRIII controlling inflammatory responses,” *Blood*, vol. 119, no. 13, pp. 3084–3096, 2012.
- [144] B. Walzog, S. Offermanns, A. Zakrzewicz, P. Gaetgens, and K. Ley, “β2-integrins mediate protein tyrosine phosphorylation in human neutrophils,” *Journal of Leukocyte Biology*, vol. 59, no. 5, pp. 747–753, 1996.
- [145] M. Petersen, J. D. Williams, and M. B. Hallett, “Cross-linking of CD11b or CD18 signals release of localized Ca²⁺ from intracellular stores in neutrophils,” *Immunology*, vol. 80, no. 1, pp. 157–159, 1993.
- [146] J. NGSIKORSKI, “Calcium signaling capacity of the CD11b/CD18 integrin on human neutrophils 1,” *Experimental Cell Research*, vol. 195, no. 2, pp. 504–508, 1991.
- [147] A. T. L. T. Loi, “Dissociation of the FcγRII/Mac-1 complex on neutrophils changes the functionality of Mac-1 (CD11b/CD18),” in *Phenotypes in COPD Visualized by Changes in Neutrophil Activation*, p. 39, Dissertation, Netherlands, 2014.
- [148] W. van der Meer, P. Pickkers, C. S. Scott, J. G. van der Hoeven, and J. K. Gunnewiek, “Hematological indices, inflammatory markers and neutrophil CD64 expression: comparative trends during experimental human endotoxemia,” *Journal of Endotoxin Research*, vol. 13, no. 2, pp. 94–100, 2016.
- [149] M. A. Cassatella, I. Guasparri, M. Ceska, F. Bazzoni, and F. Rossi, “Interferon-gamma inhibits interleukin-8 production by human polymorphonuclear leucocytes,” *Immunology*, vol. 78, no. 2, pp. 177–184, 1993.
- [150] H. R. Petty, R. G. Worth, and R. F. Todd, “Interactions of integrins with their partner proteins in leukocyte membranes,” *Immunologic Research*, vol. 25, no. 1, pp. 75–96, 2002.
- [151] M. A. Williams and J. S. Solomkin, “Integrin-mediated signaling in human neutrophil functioning,” *Journal of Leukocyte Biology*, vol. 65, no. 6, pp. 725–736, 1999.
- [152] R. Ostuni, I. Zanoni, and F. Granucci, “Deciphering the complexity of Toll-like receptor signaling,” *Cellular and Molecular Life Sciences*, vol. 67, no. 24, pp. 4109–4134, 2010.
- [153] D. M. Zarewych, A. L. Kindzelskii, R. F. Todd III, and H. R. Petty, “LPS induces CD14 association with complement receptor type 3, which is reversed by neutrophil adhesion,” *The Journal of Immunology*, vol. 156, no. 2, pp. 430–433, 1996.
- [154] B. P. Thornton, V. Vetvicka, M. Pitman, R. C. Goldman, and G. D. Ross, “Analysis of the sugar specificity and molecular location of the beta-glucan-binding lectin site of complement receptor type 3 (CD11b/CD18),” *The Journal of Immunology*, vol. 156, no. 3, pp. 1235–1246, 1996.
- [155] S. D. Wright and M. T. Jong, “Adhesion-promoting receptors on human macrophages recognize Escherichia coli by binding to lipopolysaccharide,” *Journal of Experimental Medicine*, vol. 164, no. 6, pp. 1876–1888, 1986.
- [156] L. B. Balsam, T. W. Liang, and C. A. Parkos, “Functional mapping of CD11b/CD18 epitopes important in neutrophil-epithelial interactions: a central role of the I domain,” *The Journal of Immunology*, vol. 160, no. 10, pp. 5058–5065, 1998.
- [157] T. H. Flo, L. Ryan, L. Kilaas et al., “Involvement of CD14 and β₂-integrins in activating cells with soluble and particulate lipopolysaccharides and mannuronic acid polymers,” *Infection and Immunity*, vol. 68, no. 12, pp. 6770–6776, 2000.
- [158] R. Osicka, A. Osickova, S. Hasan, L. Bumba, J. Cerny, and P. Sebo, “Bordetella adenylate cyclase toxin is a unique ligand of the integrin complement receptor 3,” *eLife*, vol. 4, 2015.
- [159] S. M. Violette, J. R. Rusche, S. R. Purdy, J. G. Boyd, J. Cos, and S. Silver, “Differences in the binding of blocking anti-CD11b monoclonal antibodies to the A-domain of CD11b,” *The Journal of Immunology*, vol. 155, no. 6, pp. 3092–3101, 1995.
- [160] R. R. Ingalls, M. A. Arnaout, and D. T. Golenbock, “Outside-in signaling by lipopolysaccharide through a tailless integrin,” *The Journal of Immunology*, vol. 159, no. 1, pp. 433–438, 1997.
- [161] M. H. Faridi, M. M. Altintas, C. Gomez, J. C. Duque, R. I. Vazquez-Padron, and V. Gupta, “Small molecule agonists of integrin CD11b/CD18 do not induce global conformational changes and are significantly better than activating antibodies in reducing vascular injury,” *Biochimica et Biophysica Acta*, vol. 1830, no. 6, pp. 3696–3710, 2013.
- [162] C. T. Lefort, Y.-M. Hyun, J. B. Schultz et al., “Outside-in signal transmission by conformational changes in integrin Mac-1,” *The Journal of Immunology*, vol. 183, no. 10, pp. 6460–6468, 2009.
- [163] J. Stockl, O. Majdic, W. F. Pickl et al., “Granulocyte activation via a binding site near the C-terminal region of complement receptor type 3 α-chain (CD11b) potentially involved in intramembrane complex formation with glycosylphosphatidylinositol-anchored FcγRIIIB (CD16) molecules,” *The Journal of Immunology*, vol. 154, no. 10, pp. 5452–5463, 1995.

- [164] J. Loyau, P. Malinge, B. Daubeuf et al., "Maximizing the potency of an anti-TLR4 monoclonal antibody by exploiting proximity to Fc γ receptors," *MAbs*, vol. 6, no. 6, pp. 1621–1630, 2014.
- [165] C. Hellberg, L. Molony, L. Zheng, and T. Andersson, "Ca²⁺ signalling mechanisms of the β_2 integrin on neutrophils: involvement of phospholipase C $_{\gamma 2}$ and Ins(1,4,5)P₃," *Biochemical Journal*, vol. 317, no. 2, pp. 403–409, 1996.
- [166] K. F. Wong, J. M. Luk, R. H. Cheng, L. B. Klickstein, and S. T. Fan, "Characterization of two novel LPS-binding sites in leukocyte integrin βA domain," *Federation of American Societies for Experimental Biology Journal*, vol. 21, no. 12, pp. 3231–3239, 2007.
- [167] L. Zhang and E. F. Plow, "Amino acid sequences within the α subunit of integrin $\alpha_M\beta_2$ (Mac-1) critical for specific recognition of C3bi," *Biochemistry*, vol. 38, no. 25, pp. 8064–8071, 1999.
- [168] E. A. Medvedev, T. Flo, R. R. Ingals et al., "Involvement of CD14 and complement receptors CR3 and CR4 in nuclear factor-kappaB activation and TNF production induced by lipopolysaccharide and group B streptococcal cell walls," *The Journal of Immunology*, vol. 160, no. 9, pp. 4535–4542, 1998.

Research Article

Transcriptome Investigation and In Vitro Verification of Curcumin-Induced HO-1 as a Feature of Ferroptosis in Breast Cancer Cells

Ruihua Li,¹ Jing Zhang,^{1,2} Yongfeng Zhou,¹ Qi Gao,³ Rui Wang,¹ Yurong Fu,¹ Lianwen Zheng ,⁴ and Hao Yu ¹

¹College of Animal Science, Jilin University, Changchun 130062, China

²Key Laboratory of Zoonosis Research, Ministry of Education, Jilin University, Changchun 130062, China

³Biological Emergency and Clinical POCT Key Laboratory, Beijing 102600, China

⁴Reproductive Medical Center, Department of Obstetrics and Gynecology, The Second Hospital of Jilin University, Changchun 130022, China

Correspondence should be addressed to Lianwen Zheng; zhenglw@jlu.edu.cn and Hao Yu; yu_hao@jlu.edu.cn

Ruihua Li and Jing Zhang contributed equally to this work.

Received 18 June 2020; Revised 7 October 2020; Accepted 29 October 2020; Published 19 November 2020

Academic Editor: Luciano Saso

Copyright © 2020 Ruihua Li et al. This is an open access article distributed under the Creative Commons Attribution License, which permits unrestricted use, distribution, and reproduction in any medium, provided the original work is properly cited.

Ferroptosis is a form of oxidative cell death and has become a chemotherapeutic target for cancer treatment. Curcumin (CUR), a well-known cancer inhibitor, significantly inhibits the viability of breast cancer cells. Through transcriptomic analysis and flow cytometry experiments, it was found that after 48 hours of treatment of breast cancer cells at its half maximal inhibitory concentration (IC₅₀), curcumin suppressed the viability of cancer cells via induction of ferroptotic death. Use of the ferroptosis inhibitor ferrostatin-1 and the iron chelator deferoxamine rescued cell death induced by curcumin. Furthermore, in subsequent cell validation experiments, the results showed that curcumin caused marked accumulation of intracellular iron, reactive oxygen species, lipid peroxides, and malondialdehyde, while glutathione levels were significantly downregulated. These changes are all manifestations of ferroptosis. Curcumin upregulates a variety of ferroptosis target genes related to redox regulation, especially heme oxygenase-1 (HO-1). Using the specific inhibitor zinc protoporphyrin 9 (ZnPP) to confirm the above experimental results showed that compared to the curcumin treatment group, treatment with ZnPP not only significantly improved cell viability but also reduced the accumulation of intracellular iron ions and other ferroptosis-related phenomena. Therefore, these data demonstrate that curcumin triggers the molecular and cytological characteristics of ferroptosis in breast cancer cells, and HO-1 promotes curcumin-induced ferroptosis.

1. Introduction

Breast cancer is the most common invasive cancer in women and the second most common cause of death [1]. Globally, approximately 2.1 million new breast cancer cases were diagnosed in 2018, accounting for one-quarter of cancer cases in women [2]. According to the North American Association of Central Cancer Registries (NAACCR) criteria, the breast cancer subtypes are defined as HR+/HER2-, HR+/HER2+, HR-/HER2+, and HR-/HER2- [3]. Due to the poor prognosis and tumor heterogeneity of breast cancer, no clear molecular

target has been identified, making the recovery of breast cancer patients very challenging [4]. In addition, fewer than 30% of women with metastatic triple negative breast cancer (TNBC) survive 5 years [5]. Therefore, in addition to the known effective molecular targets of classical chemotherapy treatment, the search for new targets among natural drugs with extensive anticancer effects is expected to become a feasible strategy for the safe treatment of breast cancer [6].

Curcumin has been widely and safely consumed for hundreds of years as a natural food color, and preclinical studies have shown its potential applications in both pharmacology

and cancer treatment [7]. Curcumin was first discovered by Vogel and Pelletier in turmeric rhizomes (turmeric) and is chemically referred to as diferuloylmethane [8]. Previous studies have shown that curcumin has antiproliferative and proapoptotic effects in pancreatic cancer cells [9], prostate cancer cells [10], and malignant mesothelioma cell lines [11]. Curcumin not only effectively removes active oxygen but also activates antioxidant response elements to inhibit active oxygen-induced lipid peroxidation [12]. Interestingly, it has been shown that curcumin inhibits the production of reactive oxygen species at low concentrations but induces the production of reactive oxygen species at high concentrations [13]. Depending on the cell type, curcumin may exhibit both antioxidant and prooxidant effects [14]. In addition, numerous studies have shown that curcumin upregulates the expression of HO-1 in a variety of cells. Shi and Li showed that HO-1 expression was upregulated in a dose- and time-dependent manner after treatment of neuroblastoma with curcumin [15]. Recent studies have shown that upregulation of HO-1 promotes the degradation of heme and the synthesis of ferritin, altering the iron distribution in cells. Enhanced HO-1 expression can increase or induce ferroptosis by promoting iron accumulation and reactive oxygen species (ROS) production [16], which means that curcumin is closely related to ferroptosis through its effects on HO-1.

Inducing direct cytotoxicity in cancer cells is one of the main goals of anticancer treatments. In general, apoptosis is considered the major form of cytotoxicity and is through to be required for tumor regression and sustained clinical remission [17]. Ferroptosis is a unique iron-dependent form of non-apoptotic cell death characterized by the accumulation of intracellular iron, which leads to the overproduction of ROS, decreased glutathione (GSH) levels, and lipid peroxidation [18, 19]. Recently, regulating mast cell processes has been used in a chemotherapy-based strategy for cancer treatment, and several drugs have been shown to trigger cell ferroptosis by acting on system X_c^- , glutathione peroxidase 4 (GPX4), and ferritin degradation through autophagy [20, 21]. Interestingly, curcumin can regulate the intracellular redox response and, as explained above, also induces the high HO-1 expression in cells, which may cause changes in intracellular ferritin. Therefore, a discussion of whether the anticancer effects of curcumin are the basis for induction of ferroptosis is worthwhile.

Curcumin affects a variety of molecular targets and signaling pathways, and bioavailability-enhanced curcumin preparations are administered to patients with breast cancer, in whom they have been observed to inhibit systemic inflammation and significantly improve the quality of life in these patients [11]. Therefore, the purpose of this study was to accurately assess the possible gene pathways targeted by curcumin in breast cancer cells using RNA sequencing and bioinformatics analysis and to explore and validate the therapeutic potential of curcumin in representative major breast cancer cell lines.

2. Materials and Methods

2.1. Chemicals and Reagents. Antimycotics (#15240062), fetal bovine serum (FBS, #10091148), RPMI 1640 medium

(#A1049101), and Dulbecco's modified Eagle's high glucose medium (#11965118) were purchased from HyClone (HyClone, Logan, UT, USA). Cell Counting Kit-8 (CCK-8, #CK04) was obtained from Dojindo (Dojindo Laboratories, Kumamoto, Japan). The malondialdehyde (MDA) assay kit (#A003-1-2) and reduced glutathione (GSH) assay kit (#A006-2-1) were purchased from Jiancheng (Jiancheng, Nanjing, China). The DAPI staining solution kit (#MA0127) and zinc protoporphyrin-9 (#MB4231) were purchased from Meilui (Meilui, Dalian, China). Liperfluo (#L248) was purchased from Dojindo (Dojindo Laboratories, Shanghai, China). 2',7'-Dichlorodihydrofluorescein diacetate (DCFH-DA, #S0033S), Annexin V (#C1062M-1), and Propidium Iodide (PI, #C1062M-3) were purchased from Beyotime (Beyotime, Shanghai, China). For western blot analysis, antibodies against HO-1 (#ab13243), GPX4 (#ab40993), Nrf2 (#ab137550), and β -actin (#ab8226) were purchased from Abcam (Abcam, Cambridge, MA). The Iron Assay Kit (#MAK025), dimethyl sulfoxide (DMSO, #D2650), curcumin (#C1386), z-VAD-fmk (#V116), ferrostatin-1 (#SML0583), and deferoxamine (#D9533) were purchased from Sigma (Sigma, St Louis, USA). These compounds were dissolved in DMSO (at final concentrations less than 0.1% (v/v)).

2.2. Cell Culture. The breast cancer cells used in this study were obtained from American type culture collection (ATCC). The human breast adenocarcinoma-derived MCF-7 cell line was cultured in Dulbecco's modified Eagle's high glucose medium supplemented with 10% FBS, 100 UI/mL penicillin, and 100 μ g/mL streptomycin. The human TNBC cell line MDA-MB-231 was cultured in RPMI 1640 medium supplemented with 10% FBS, 100 UI/mL penicillin, 100 μ g/mL streptomycin, and 2 mM glutamine. Cells were maintained in a humidified incubator at 37°C and 5% CO₂. Cultures were tested periodically and confirmed to be mycoplasma-free.

2.3. Treatment Methods for Cells. Curcumin was dissolved in DMSO at a concentration of 50 mM for storage and diluted to specific concentrations in cell culture medium for cell treatments. ZnPP was dissolved in DMSO to a concentration of 6 mM and diluted to 10 μ M in cell culture medium for cell treatments. The final concentration of DMSO in the above-prepared treatment solutions was less than 0.1% (v/v). During treatment, the same volume of DMSO was added to the control groups. The curcumin stock solution was diluted in cell culture medium to concentrations of 5, 10, 20, 40, 60, 80, 100, 120, and 140 μ M, and the same volume of DMSO was added to the control groups. When the confluence of breast cancer cells in the culture dish reached more than 80%, cell viability was tested after 48 hours of treatment with the above concentrations. The IC₂₀ and IC₅₀ values were calculated using GraphPad Prism7.0.

2.4. Treatment Method of Inhibitor. Culture the cells in a 6-well plate, and when the degree of polymerization of the cells in the culture dish reaches 80%, preincubate the breast cancer cells with 50 μ M z-VAD-fmk, 1 μ M ferrostatin-1, and 50 μ M

deferroxamine, respectively, for 2 h. Then, the cells were treated with curcumin at IC₅₀ concentration for 24 h or 48 h.

2.5. Cell Viability Assay. Cell viability was determined by the Cell Counting Kit-8 (CCK-8; Dojindo, Tokyo, Japan). Cells were seeded into 96-well plates at a density of 0.2×10^4 cells per well, and after curcumin treatment of breast cancer cells for 24 h or 48 h, 10 μ L CCK-8 reagent was added to each well. Plates were incubated for 1 hour at 37°C, and the absorbance value (OD) of each well was measured at 450 nm according to the manufacturer's instructions.

2.6. RNA Sequencing. MCF-7 cells were treated with vehicle or 40 μ M curcumin for 48 h, and MCF-MB-231 cells were treated with vehicle or 50 μ M curcumin for 48 h. Breast cancer cells were collected and washed with cold PBS twice. According to the TriPure protocol, total RNA was extracted and resuspended in diethyl pyrocarbonate. After validating its integrity and purity, qualifying RNA was subjected to PCR amplification for the construction of a cDNA library. Raw data were filtered to remove low-quality sequences that might affect data quality and subsequent analysis. The cDNA library was sequenced using an Illumina HiSeq™ 300 platform. Raw sequence data were filtered using HISAT to remove low-quality sequences and adaptor reads. After quality trimming, Bowtie (1.1.2) was used to map pure reads to the *V. vinifera* reference genome using standard mapping parameters. Data that could be mapped to the reference genome were >100 bp in length and contained <2 mismatched reads. SAM tools and BamIndexStats were used to calculate the gene expression and reads per kilobase per million (RPKM). Gene expression annotation was performed using the Cufflinks software, and all the parameters were set to default values. The BioProject accession of this study is PRJNA613560.

2.7. K-Means Heat Map Clustering and Pathway Enrichment Analyses. K-Means heat map clustering was performed using the IDEP website (<http://bioinformatics.sdstate.edu/idep/>). KEGG pathway enrichment analyses were performed to determine upregulated and downregulated genes in each comparison group from the heat map cluster using the ClusterProfiler package [22].

2.8. Gene Set Enrichment Analysis (GSEA) and PPI Network Diagrams. GSEA analysis was based on NetworkAnalyst, an integrative approach for protein-protein interaction network analysis and visual exploration, and the GSEA results were used to correlate the gene signature with the effects of curcumin. The normalized enrichment score (NES) is the primary statistic for examining gene set enrichment analysis results, and the nominal *P* value estimates the significance of the enrichment score. A gene set with a nominal $P \leq 0.05$ was considered to be significantly enriched in the genes identified. PPI network diagrams were generated using the Cytoscape 3.7.2 software for visualization and analysis of biological networks.

2.9. Staining with Annexin V and PI. Ferroptosis was assessed following the method described by Chen et al. [23]. After

treatments, cells were collected and stained with Annexin V-FITC reagent and PI followed by analysis by flow cytometry. The percentage of dead cells was quantified using the FlowJo 10.5 software.

2.10. Fluorescence Measurements of Intracellular Oxidants. DCFH-DA was used to detect ROS production in cells. The fluorescence of each labelled penetrant significantly increased after oxidation in cells. DCFH-DA was dissolved in dimethyl sulfoxide (DMSO) and stored at -20°C in a 10 mM stock solution. MCF-7 cells and MDA-MB-231 cells were cultured with curcumin for 48 h, incubated with 10 μ M DCFH-DA for 30 minutes, washed 3 times with PBS, and immediately observed and imaged using a fluorescence microscope.

2.11. Measurement of MDA, Total Iron, and GSH Content. The cellular MDA, total iron, and GSH contents were determined using commercial kits. The MDA level is expressed as nmol/mg protein in relation to the cellular protein concentration. The GSH level is expressed as μ mol/gprot protein in relation to the cellular protein concentration.

2.12. Cell Morphology Observation. FITC fluorescent substance-labeled phalloidin specifically binds to F-actin in eukaryotic cells, thereby showing the distribution of the microfilament skeleton in the cell. Three days before being stained, cells were cultured on sterile glass coverslips. The coverslips were fixed with a 4% formaldehyde solution for 10 minutes, permeabilized with a 0.5% Triton X-100 solution for 5 minutes, and then incubated with FITC-labeled phalloidin in the dark for 30 minutes at room temperature. Cells were washed 3 times with PBS, and then, nuclei were counterstained for 30 seconds using a 100 nM DAPI solution, washed with PBS, inverted on a glass slide containing a drop of a Fluoromount-GTM water-soluble sealing solution, and permanently sealed with nail polish. Fluorescence was observed under a fluorescence microscope.

2.13. Detection of Lipid Peroxides in Cells. The Spy-LHP analogue Liperfluo was used for lipid peroxide detection. In organic solvents, such as ethanol, the specific oxidation of lipid peroxides causes intense fluorescence emission. The oxidized form shows little fluorescence in aqueous solution but produces strong fluorescence in fat-soluble fractions, such as cell membranes. Therefore, Liperfluo can be used for fluorescence imaging of lipid peroxides in living cells. First, 60 μ L DMSO was added to a test tube containing 50 μ g Liperfluo and uniformly mixed to prepare a Liperfluo solution at a concentration of 1 mmol/L. Then, 2 μ L of the Liperfluo solution was added to each well of a six-well plate and incubated for 30 minutes at 37°C in the dark. Cells were examined using a fluorescence microscope.

2.14. RNA Isolation and Quantitative Real-Time PCR. MCF-7 cells were randomly divided into two groups: the control and 40 μ M curcumin-treated groups. MDA-MB-231 cells were randomly divided into two groups: the control and 50 μ M curcumin-treated groups. Tested according to the methods of this laboratory, total RNA was isolated using

TriPure isolation reagent (Roche, Mannheim, Germany), and DNA was removed from samples using DNase I (TaKaRa, Shiga, Japan). The purity of the isolated RNA was determined using a Nanodrop-2000 system (Thermo). RNA samples were used to prepare cDNA using a reverse transcriptase kit. Ten microliters of cDNA was analyzed using the SYBR Green PCR kit and a real-time fluorescence quantifier. The list of primers used for sequence validation is presented in the Supplement File (for the details of the primers used for sequence verification, please refer to Table 1 in the supplementary document). The primer pairs and probes were designed using the Primer3 software according to the recommendations described therein, and their specificity was determined with the Primer-BLAST program. Three analyses were performed for each sample. PCR was performed under the following conditions: 95°C for 10 minutes, 35 cycles at 95°C for 15 s, 60°C for 20 s, and 72°C for 30 s. Melting curve analysis confirmed the specificity of the amplification. The fold change of the target gene expression was normalized by the 2-fold abundance of β -actin mRNA^{- $\Delta\Delta C_t$} method.

2.15. Western Blot Analysis. Cells were extracted as lysates, and 20 μ g protein from each sample was subjected to 12% sodium dodecyl sulfate polyacrylamide gel electrophoresis (SDS-PAGE). The separated proteins were transferred to a nitrocellulose membrane (NC) filters (Pall, BioTrace NT, USA) and blocked with 5% skim milk in TBST (10 mmol/L Tris-HCl (pH 8.0), 150 mmol/L NaCl, and 0.1% Tween 20) at RT for 2 hours. The membranes were washed one time with TBST buffer and incubated with a suitable primary rabbit antibody (1:1000) specific for HO-1, GPX4, or Nrf2 at 4°C overnight. After washing four times with TBST, the immunoblotted membranes were incubated with a horseradish peroxidase-labeled goat antirabbit IgG-conjugated secondary antibody for 2 hours at room temperature. Finally, using a Pierce ECL substrate (Thermo Scientific, Waltham, Massachusetts, USA), protein bands were imaged on a chemiluminescence imaging analyzer (Tanon 5200, Shanghai, China).

2.16. Statistical Analysis. All experiments were performed independently at least three times, and the data are expressed as the mean \pm standard error of the mean (SEM). The GraphPad PRISM software (Windows 5.02; GraphPad Software, Inc.) was used to test the significance of the data by the independent sample *t*-test, the statistical method for the treatment group using ZnPP used one-way analysis of variance, and $P < 0.05$ was deemed a statistically significant difference.

3. Results

3.1. Breast Cancer Cell Viability Is Inhibited by Curcumin Treatment. We first examined the effect of curcumin on breast cancer cell proliferation. Cell viability was used as a measure of cell proliferation. We treated breast cancer cells with curcumin at the same concentration gradient for 24 h and 48 h. After 24 hours of treatment, the IC₅₀ values of curcumin in MCF-7 and MDA-MB-231 cells were approxi-

mately 101.3 μ M and 87.42 μ M, respectively (Figure 1(a)). After 48 h of treatment, the IC₅₀ values of curcumin in MCF-7 and MDA-MB-231 cells were approximately 41.90 μ M and 53.51 μ M, respectively (Figure 1(b)). The research results of Ali et al. show that the IC₅₀ value of curcumin at 24 h in human normal breast epithelial MCF-10A cells is approximately 190 μ M, and the IC₅₀ value at 48 h is approximately 114 μ M [24]. Therefore, we selected the IC₅₀ value of curcumin after 48 hours of breast cancer cell treatment for subsequent experiments. This choice allowed us to obtain sufficient biological information with less toxicity to and fewer side effects in normal breast epithelial cells, thereby laying a good foundation for studying the clinical anticancer effects of curcumin. Phalloidin staining was used to observe changes in cell morphology after 48 h of curcumin treatment. As shown in Figure 1(c), curcumin treatment caused significant changes in the morphology of breast cancer cells. The cell shape was significantly rounded, and the volume was greatly reduced.

3.2. Transcriptomic Analysis of the Effects of Curcumin on Breast Cancer Cells. To systematically investigate the biological processes underlying the inhibition of breast cancer cell proliferation by curcumin, we sequenced the above curcumin-treated breast cancer cells by transcriptome sequencing. The results of the differential expression analysis revealed that a total of 2740 genes were upregulated, and 3893 genes were downregulated in the MCF-7 cell line, while in the MDA-MB-231 cell line, 4619 genes were upregulated, and 1964 genes were downregulated (Figures 2(a) and 2(b)). To further explore the key pathways shared by the two cell lines, we performed K-means clustering analysis. The results suggested that 3000 differentially expressed genes in the four groups formed three clusters. Cluster A is a specific upregulated gene groups (NC + curcumin) in the MCF-7 cell line, and Cluster C is a specific upregulated gene groups (NC + curcumin) in the MDA-MB-231 cell line. Cluster B is responsible for the genome of curcumin treatment effect (MDA-MB-231-curcumin+MCF7-curcumin). Therefore, we only focused on the signal pathways enriched in Cluster B; among them, the pathway with the highest enrichment ratio is ferroptosis, as shown in Figure 2(c).

3.3. Ferroptosis Network Analysis of Breast Cancer Cells Treated with Curcumin. We generated a GSEA heat map based on analysis of the ferroptotic pathway from the results of the pathway enrichment analysis determined through NetworkAnalyst. As shown in Figure 3(a), we found that after treatment with curcumin at a specified concentration, MCF-7 cells exhibited greater gene activation than MDA-MB-231 cells, and the GSEA plots showed that the ferroptotic pathways in both cell lines were upregulated. Next, 14 curcumin targets were identified in the ferroptotic pathway according to the comparative toxicogenomics database(CTD), and in MCF-7 and MDA-MB-231 cells, these targets presented the same expression trends (Figures 3(b) and 3(c)). We used Cytoscape to construct a target gene interaction network diagram of curcumin in these ferroptotic pathways. Using the STRING database, we found that curcumin

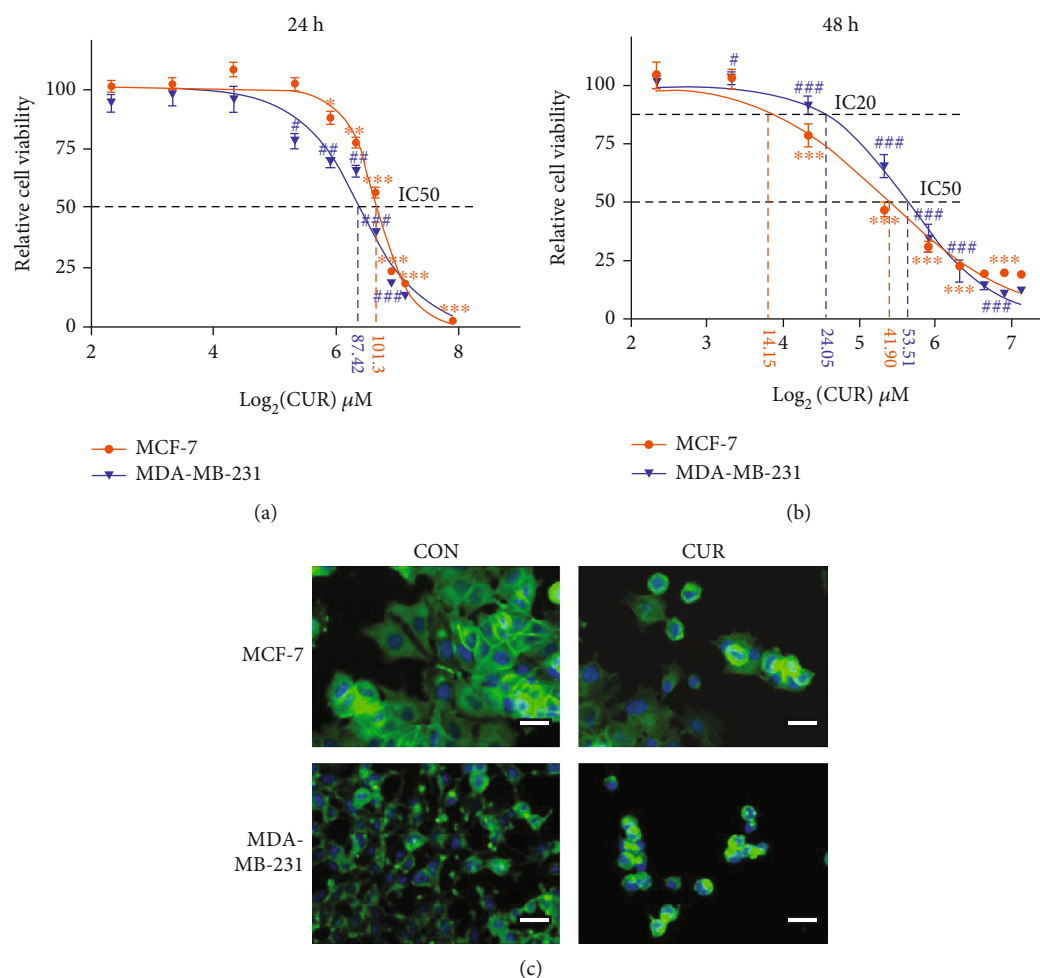


FIGURE 1: Breast cancer cell viability is inhibited by curcumin treatment. (a) Curcumin effectively inhibits the cell viability of cancer cells. Cancer cells were treated with the indicated concentrations of curcumin for 24 h. Cell viability was measured by the CCK-8 assay. Each point represents the mean value of three independent determinations; the error bars represent the SEM. $*P < 0.05$; $**P < 0.01$; $***P < 0.001$, compared to controls (MCF-7 cells). $\#P < 0.05$; $\#\#P < 0.01$; $\#\#\#P < 0.001$, compared to controls (MDA-MB-231 cells). (b) Curcumin effectively inhibits the cell viability of cancer cells. Cancer cells were treated with the indicated concentrations of curcumin for 48 h. Cell viability was measured by the CCK-8 assay. Each point represents the mean value of three independent determinations; the error bars represent the SEM. $*P < 0.05$; $**P < 0.01$; $***P < 0.001$, compared to controls (MCF-7 cells). $\#P < 0.05$; $\#\#P < 0.01$; $\#\#\#P < 0.001$, compared to controls (MDA-MB-231 cells). (c) MCF-7 cells were treated with $40 \mu\text{M}$ curcumin for 48 h (CUR), and MCF-MB-231 cells were treated with $50 \mu\text{M}$ curcumin for 48 h (CUR), with the control groups (CON) receiving the same volume of DMSO (curcumin solvent) as the treatment groups, and cell morphology was imaged using a fluorescence microscope (scale bar represents $100 \mu\text{m}$). Representative images from three independent experiments are shown. All the CON groups treated above received the same volume of reagent solvent as the treatment groups.

not only directly activates HO-1 but also upregulates its expression by activating nuclear factor-E2-related factor 2 (Nrf2). In addition, Nrf2 inhibits the expression of GPX4 (Figure 3(d)). The KEGG pathway analysis results indicated that the upregulation of HO-1 and downregulation of GPX4 directly trigger ROS production and that ferroptosis depends on the cytotoxicity induced by ROS (Figure 3(e)).

3.4. Curcumin Causes Iron Accumulation in Breast Cancer Cells to Induce Ferroptosis. To confirm the validity of ferroptosis as the main cause of cell death, various pharmacological inhibitors of apoptosis (z-VAD-fmk) and ferroptosis (ferrostatin-1 and deferoxamine) were used to define the type of cell death induced by curcumin. As shown in Figure 4(a), when

cells were treated with curcumin at the IC50 concentration, cell death induced by curcumin was significantly reduced in the presence of ferrostatin-1 and deferoxamine, but z-VAD-fmk had no such effect. At the same time, when the IC20 concentration of curcumin was used to treat cells, none of the pharmacological inhibitors had a significant effect on cell death induced by curcumin. Cell death was also determined by Annexin V/PI and analyzed by flow cytometry [23]. As shown in Figures 4(b) and 4(c), curcumin significantly increased the PI positive cell population but had little effect on Annexin V staining. The addition of ferrostatin-1 and deferoxamine effectively suppressed curcumin-induced cell death. Next, we used the intracellular iron detection kit to further assess the changes in the total iron

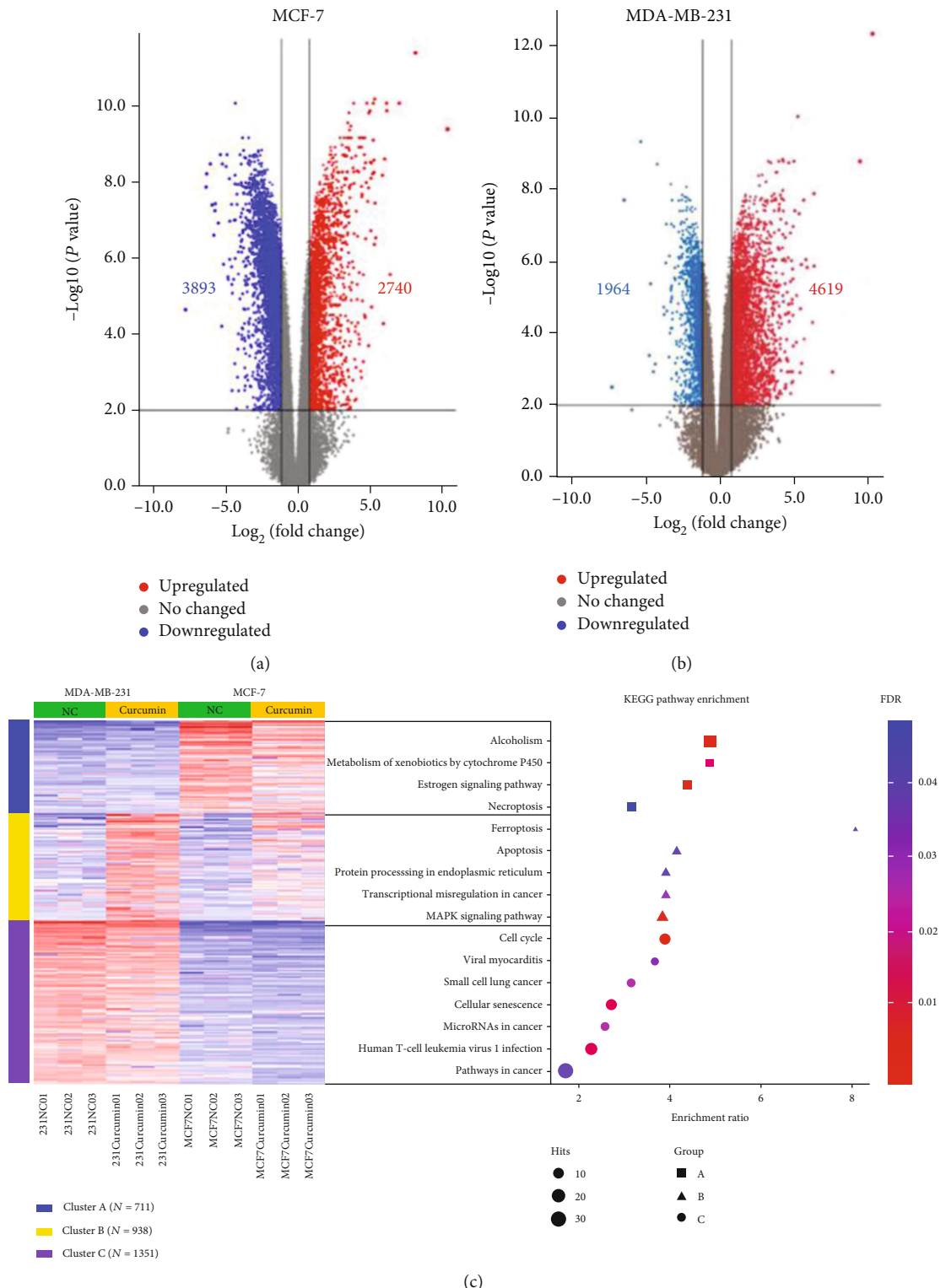
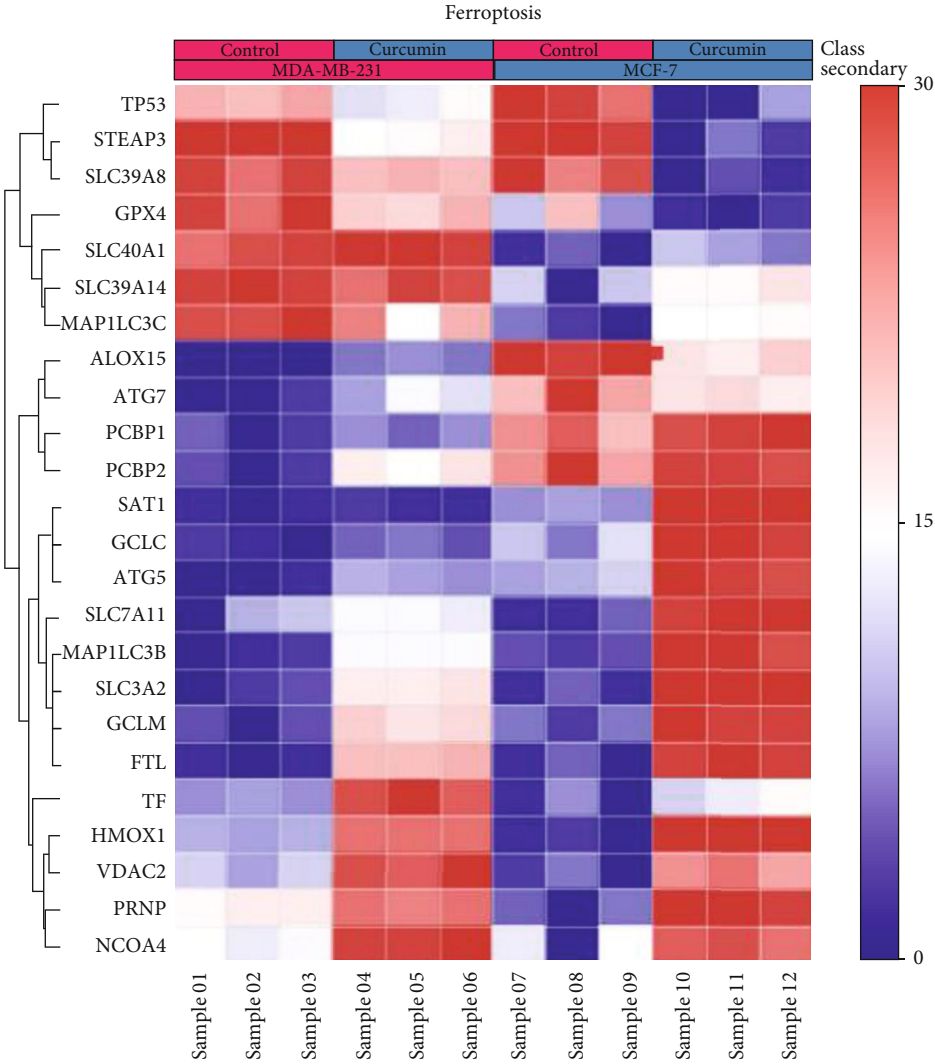
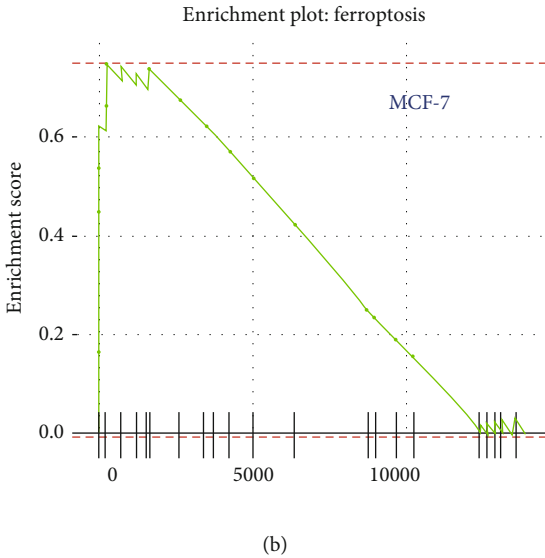


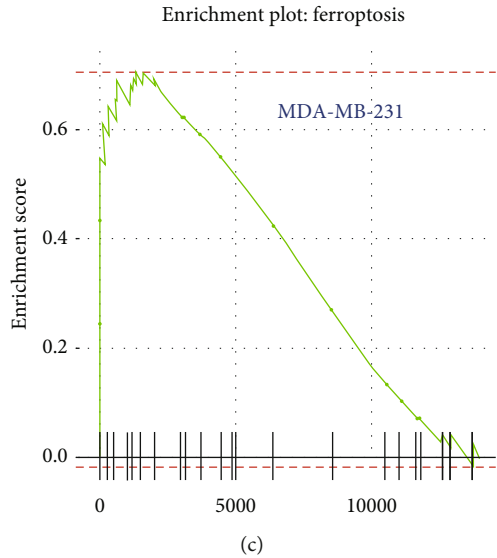
FIGURE 2: Differential expression and heat map hierarchical clustering analysis. (a, b) Volcano plots of the transcription levels of genes in control and 40 μM curcumin-treated MCF-7 cells. Volcano plots of the transcription levels of genes in control and 50 μM curcumin-treated MDA-MB-231 cells. (c) Differentially upregulated genes are defined by their fold change ($\log_2\text{fold change} > 1$) and FDR ($-\log_{10}\text{FDR} > 1$). (c) K-Means heat map hierarchical clustering and KEGG pathway enrichment analysis of the top 3000 DEGs among the 4 groups. The sequence of the enriched pathways represents the degree of enrichment. The area of each spot represents the number of genes contained in the pathway.



(a)



(b)



(c)

FIGURE 3: Continued.

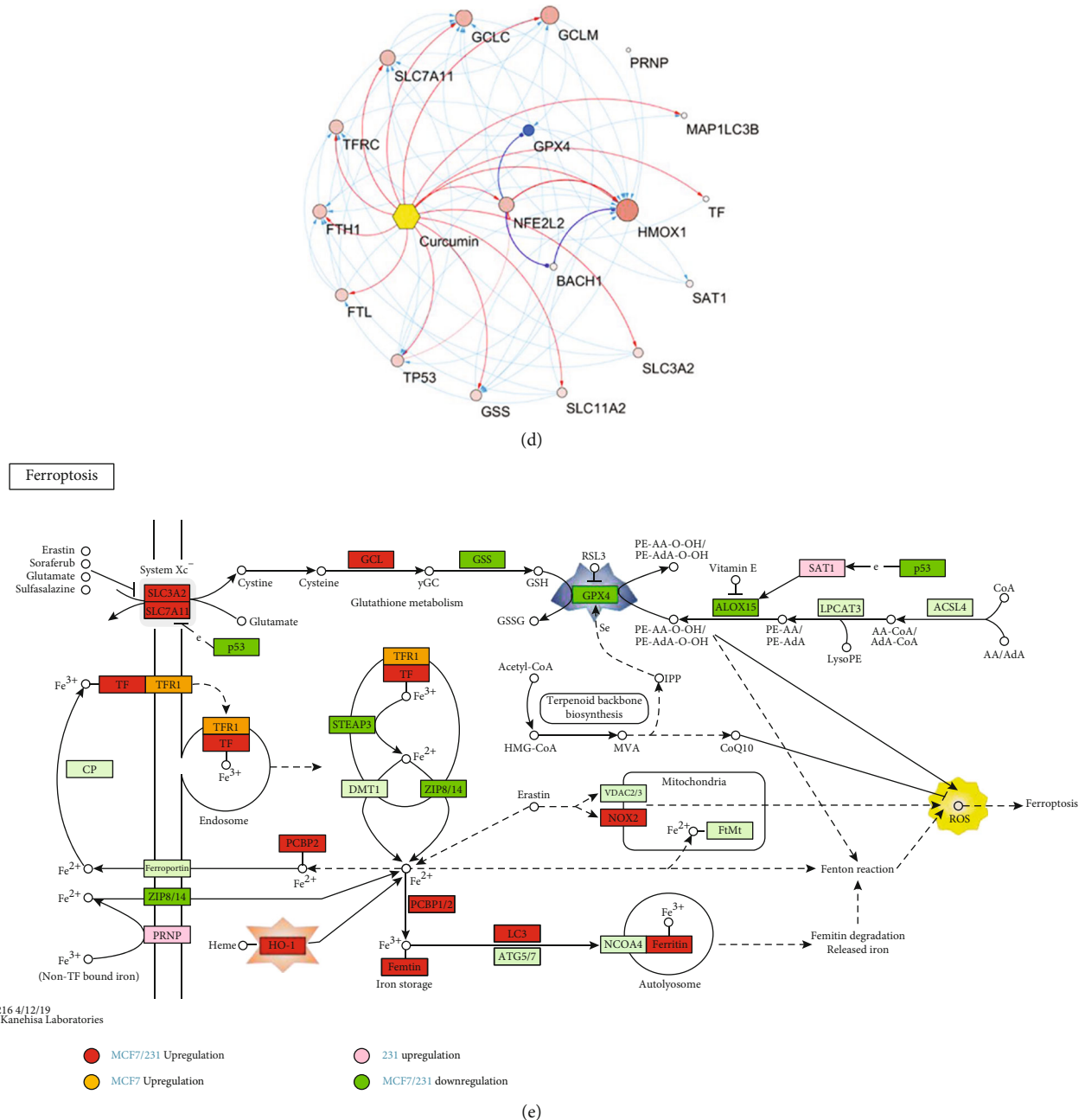


FIGURE 3: Ferroptosis network analysis of breast cancer cells treated with curcumin. (a) GSEA heat map analysis showing the ferroptotic pathway. Interactive heat map (GSEA) analysis was provided by NetworkAnalyst (<https://www.networkanalyst.ca/NetworkAnalyst/home.xhtml>). The value of 0-30 on the color scale bar of the heat map does not represent the relative fold change degree; each value is ranked on DE method used; the minimum value is 0, and the maximum value is 30, which has been explained by the literature provided by the official website [25]. (b, c) GSEA results based on KEGG pathways with enriched genes, indicating that the ferroptotic signaling pathway was upregulated by curcumin in both cell lines. (d) Cytoscape was used to construct a target gene interaction network diagram showing the ferroptotic pathways affected by curcumin according to the STRING database. (e) The ferroptotic pathway model was obtained from the KEGG pathway analysis results. The green boxes indicate genes that were downregulated by curcumin treatment. The red boxes indicate genes that were upregulated by curcumin treatment.

concentration in breast cancer cells after curcumin treatment. As shown in Figure 4(d), after 48 h of treatment with curcumin at the IC50 concentration, the total iron content of the cells was significantly increased, but there was no significant change at the IC20 concentration. These results indicate that the primary form of cell death caused by treatment

of cells with the IC50 concentration of curcumin for 48 h can be attributed to ferroptosis.

3.5. RT-qPCR and Western Blotting Results Validate the RNA and Redox Proteins Related to the Ferroptotic Pathway. We next examined the gene expression associated with cellular

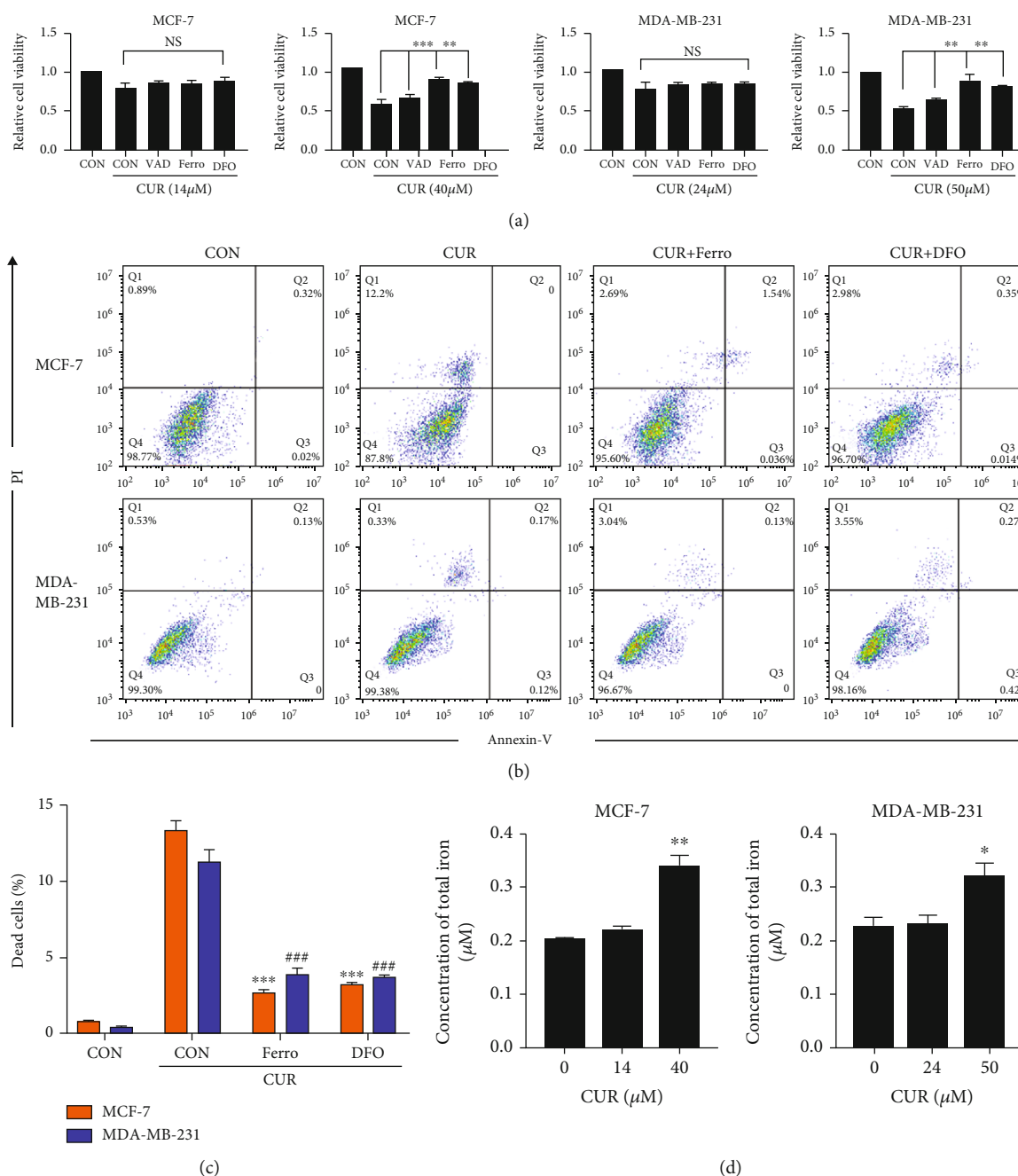


FIGURE 4: Curcumin causes iron accumulation in breast cancer cells to induce ferroptosis. (a) Cancer cells were preincubated with various inhibitors, *z*-VAD-fmk (VAD, 50 μ M), ferrostatin-1 (Ferro, 1 μ M), or deferoxamine (DFO, 50 μ M), for 2 h followed by curcumin (IC50) treatment for 48 h. Cell viability was assessed by the CCK-8 assay. All values are the mean \pm SEM of three independent experiments. ** P < 0.01; *** P < 0.001, compared to CUR (curcumin) alone. NS: no significant difference compared to CUR (curcumin) alone. (b) Cancer cells were preincubated with various inhibitors, ferrostatin-1 (Ferro, 1 μ M), or deferoxamine (DFO, 50 μ M), for 2 h followed by curcumin (MCF-7: 40 μ M, MDA-MB-231: 50 μ M) treatment for 48 h. Cell death was assessed by Annexin V/PI staining. For Annexin V/PI staining, cells were collected, and the proportion of PI positive cells (dead) was determined by flow cytometry. Q1: nonapoptotic or ferroptotic cells (Annexin V negative/PI positive); Q2: late apoptotic and early necrotic cells (Annexin V positive/PI positive); Q3: early apoptotic cells (Annexin V positive/PI negative); Q4: viable cells (Annexin V negative/PI negative). (c) Use the FlowJo 10.5 software to perform statistical analysis on the experimental results of (b). All values are the mean \pm SEM of three independent experiments. *** P < 0.001, compared to CUR (curcumin) alone (MCF-7 cells). ### P < 0.001, compared to CUR (curcumin) alone (MDA-MB-231 cells). (d) After treating both cell lines with the IC20 (MCF-7: 14 μ M, MDA-MB-231: 24 μ M) and IC50 concentrations of curcumin for 48 h, the changes in the intracellular iron levels were measured according to the instructions of the kit. All the values are the mean \pm SEM of three independent experiments. * P < 0.05; ** P < 0.01, compared to CON (control) alone. All the CON (control) groups treated above received the same volume of reagent solvent as the treatment groups.

redox reactions, intracellular iron homeostasis, autophagy, and endoplasmic reticulum stress, as shown in Figures 5(a) and 5(b), which have been shown to respond to ferroptotic agents. Curcumin upregulates genes involved in oxidative stress and ER stress, including HO-1, heat shock 70 kDa protein 5 (HSPA5), activating transcription factor 4 (ATF4), and DNA damage inducible transcript 3 (DDIT3). Curcumin also induced transcription factors, including BTB domain and CNC homolog 1 (BACH1), v-rel reticuloendotheliosis viral oncogene homolog A (RELA), upstream transcription factor 1 (USF1), NFE2-related factor 2 (NFE2L2), and the autophagy-related gene beclin 1 (BECN1). Cellular redox regulation and autophagy pathways were also responsive to curcumin, including glutamate-cysteine ligase catalytic subunit (GCLC), sequestosome 1 (SQSTM1), and X-box binding protein 1 (XBP1). At the same time, curcumin treatment caused a decrease in the GPX4 gene expression in both cells. The intracellular iron content is affected by the transferrin receptor and iron transporter. Studies have shown that the amount of intracellular transferrin is positively correlated with the degree of ferroptosis [26]. Curcumin upregulated FTL (encoding ferritin light chain), FTH1 (encoding ferritin heavy chain), and TFRC (encoding transferrin receptor) in MDA-MB-231 cells (Figure 5(b)). In MCF-7 cells, FTH1 and FTL were upregulated (Figure 5(a)).

Next, we used western blotting to determine the expression levels of GPX4, HO-1, and Nrf2 in both cell lines in response to curcumin treatment for 48 hours. The results showed that GPX4 was significantly downregulated compared its level in the control group (Figures 5(c) and 5(d)). HO-1 and Nrf2 were significantly upregulated compared with their levels in the control group (Figures 5(c)–5(f)), and Figures 5(c)–5(e) show that HO-1 in MCF-7 cells was upregulated to a greater extent than in MDA-MB-231 cells.

3.6. Curcumin Induces ROS Production in the Breast Cancer Cells. Ferroptosis cytotoxicity depends on ROS. To investigate whether upregulation of the HO-1 expression and downregulation of the GPX4 expression cause inevitable ROS generation in the ferroptotic pathway, using DCFH-DA staining, we examined the intracellular ROS content after 48 hours of curcumin treatment. As shown in Figures 6(a) and 6(b), the ROS content in MCF-7 and MDA-MB-231 cells was significantly increased in response to curcumin treatment compared to the control group. At the same time, ZnPP treatment significantly prevented the increase in ROS levels caused by curcumin.

3.7. Marked Upregulation of HO-1 Is the Primary Factor for Curcumin-Induced Ferroptosis. To determine whether HO-1 is a key gene for curcumin-induced ferroptosis, we used a specific inhibitor of HO-1. The use of ZnPP to verify the role of HO-1 in cell ferroptosis has proven very effective [27]. Treatment with ZnPP effectively alleviated curcumin-induced cancer cell death, as shown in Figure 7(a). ZnPP also significantly reduced the intracellular iron accumulation induced by curcumin (Figure 7(b)). In addition, for live cell imaging, we used Liperfluo (L248), which reduces lipid hydrogen peroxide to its hydroxyl homologues, producing

fluorescent products. Liperfluo fluorescence reliably reflects intracellular sites of lipid hydroperoxide accumulation [28]. We found that breast cancer cells accumulated lipid-reactive lipid hydrogen peroxide for 48 hours after curcumin treatment. The accumulation of lipid hydroperoxide, as shown in these cells, is considered the primary feature of ferroptosis. Subsequently, accumulation of lipid hydroperoxide was partially inhibited by ZnPP (Figures 7(c) and 7(d)). GSH is an important reducing agent involved in cellular redox reactions and participates in the ferroptotic pathway. Treatment with curcumin caused significant inhibition of the intracellular GSH levels, but treatment with ZnPP reversed this phenomenon (Figure 7(e)). Free radicals induce lipid peroxidation, and the final oxidation product is malonaldehyde, which is cytotoxic. After curcumin treatment of breast cancer cells for 48 hours, the intracellular MDA content was significantly increased, and compared to the curcumin treatment group, ZnPP treatment significantly reduced the MDA content (Figure 7(f)). Taken together, these results indicate that in response to ZnPP inhibition of HO-1, curcumin-induced breast cancer cell death and cell lipid peroxidation are significantly attenuated, and the intracellular glutathione levels are increased. Therefore, HO-1 plays a significant role in promoting curcumin-induced breast cancer cell ferroptosis.

4. Discussion

In general, the consumption of curcumin is considered safe and healthy. As per JECFA (The Joint FAO/WHO Expert Committee on Food Additives) and EFSA (European Food Safety Authority) reports, the adequate daily intake value of curcumin is from 0–3 mg·kg⁻¹ [29, 30]. According to the results of Ramachandran et al., MCF-7 cells are more sensitive to curcumin than normal human breast epithelial cells (MCF-10A). After curcumin treatment, MCF-10A cells break down curcumin and retain relatively little drug in the medium, thereby reducing the cytotoxic effect of MCF-10A cells. Curcumin induced a significantly higher percentage of Annexin V positive apoptotic cells in MCF-7 than in MCF-10A cells. In addition, among the apoptosis-related genes identified by microarray hybridization, curcumin treatment of MCF-7 cells upregulated apoptosis regulatory factors, including Bcl-w, caspase-2 precursor, caspase-3, and caspase-4. However, curcumin-induced gene expression changes were significantly reduced in MCF-10A cells, and the changes were always less than 2-fold [31]. These results indicate that curcumin induces breast cancer cell apoptosis while having relatively few side effects on human normal breast epithelial cells.

In this study, RNA was sequenced and quantified from breast cancer cells with and without curcumin treatment. Bioinformatics analysis after RNA sequencing showed that both the apoptotic and ferroptotic pathways were enriched by KEGG pathway analysis (Figure 2(c)). However, it can be seen in the figure that the degree of enrichment of the ferroptotic pathway was greater than the apoptosis pathway. To further clarify the form of cell death caused by treatment of cells with the IC₅₀ concentration of curcumin for 48 hours,

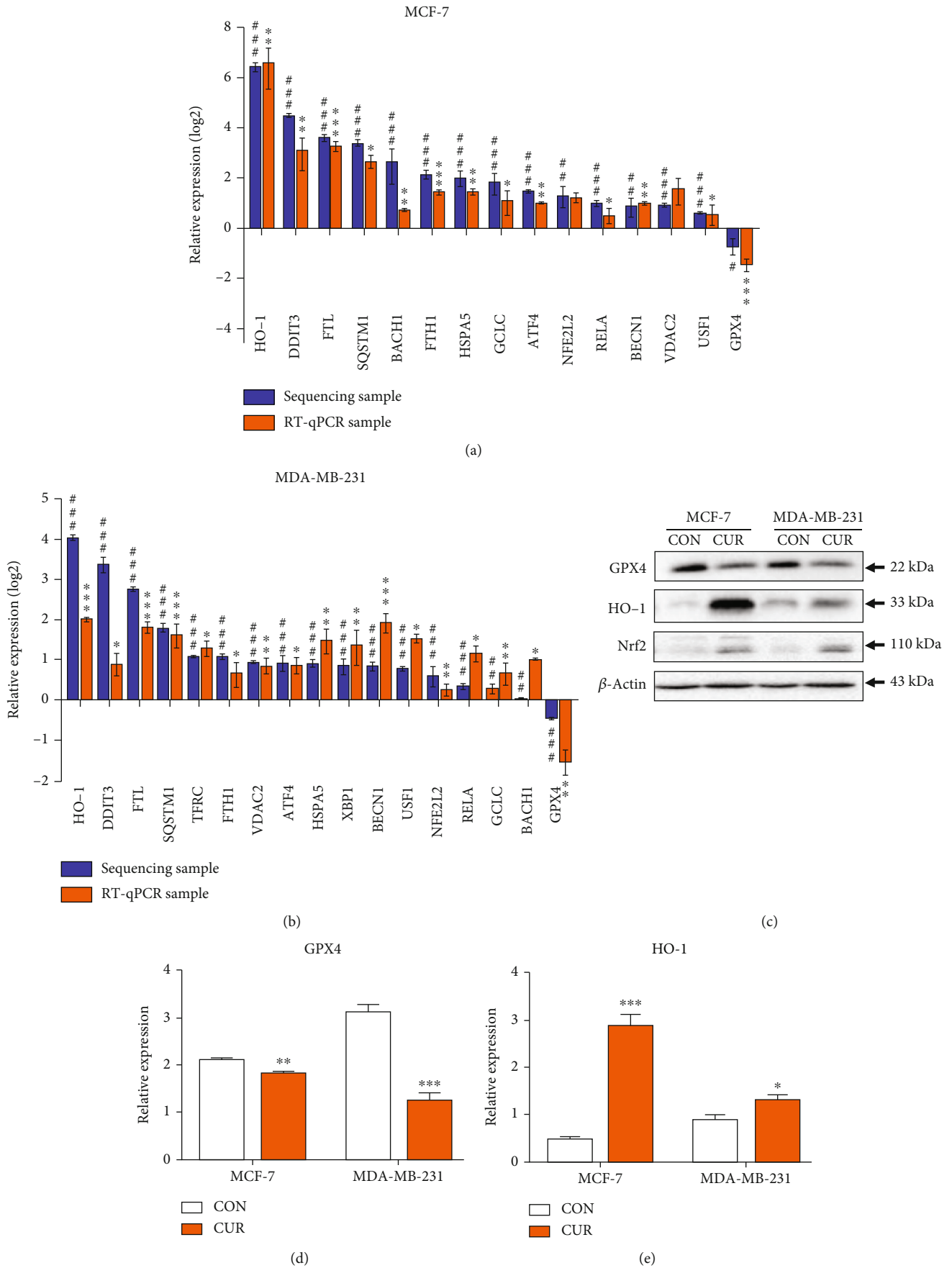


FIGURE 5: Continued.

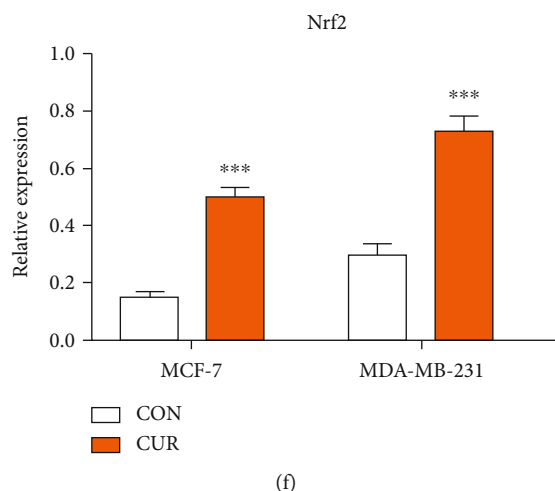


FIGURE 5: RT-qPCR verification of RNA associated with the ferroptotic pathway. (a) Total RNA extracted from MCF-7 cells treated with 40 μM curcumin (CUR) for 48 hours was analyzed by RT-qPCR for gene expression analysis. The expression levels of mRNA were normalized to the level of β -actin. Each reported value represents the mean \pm SEM from three independent experiments. * $P < 0.05$; ** $P < 0.01$; *** $P < 0.001$, compared to CON (control, RT-qPCR samples). # $P < 0.05$; ## $P < 0.01$; ### $P < 0.001$, compared to CON (control, sequencing samples). (b) Total RNA extracted from MDA-MB-231 cells treated with 50 μM curcumin (CUR) for 48 hours was analyzed by RT-qPCR for gene expression analysis. The expression levels of mRNA were normalized to the level of β -actin. Each reported value represents the mean \pm SEM of three independent experiments. * $P < 0.05$; ** $P < 0.01$; *** $P < 0.001$, compared to CON (control, RT-qPCR samples). # $P < 0.05$; ## $P < 0.01$; ### $P < 0.001$, compared to CON (control, sequencing samples). (c) MCF-7 cells were treated with vehicle or 40 μM curcumin for 48 h, and MCF-MB-231 cells were treated with vehicle or 50 μM curcumin for 48 h. Cells were then harvested for the western blot analysis. The representative figure shows one of the three independent experiments. (d) Quantitative results for the GPX4 expression in breast cancer cells as determined from greyscale analysis of (c) using the ImageJ software. The results are expressed as the means \pm SEM of three independent experiments; ** $P < 0.01$; *** $P < 0.001$, compared to CON (control). (e) Quantitative results of the HO-1 expression in breast cancer cells determined by greyscale analysis of (c) using the ImageJ software. The results are expressed as the means \pm SEM of three independent experiments; * $P < 0.05$; *** $P < 0.001$, compared to CON (control). (f) Quantitative results of the Nrf2 expression in breast cancer cells determined by greyscale analysis of (c) using the ImageJ software. The results are expressed as the means \pm SEM of three independent experiments; *** $P < 0.001$, compared to CON (control). All CON (control) groups treated above received the same volume of reagent solvent as the treatment groups.

apoptosis inhibitors and ferroptosis inhibitors were used (Figure 4). The results showed that compared to the curcumin treatment group, the addition of ferroptosis inhibitors significantly improved cell viability and inhibited cell death, while apoptosis inhibitors had no such effect. Based on the above data, it can be inferred that ferroptosis is the primary pathway of death in this experiment. We conducted a series of validation tests and found that cancer cells treated with curcumin for 48 hours showed increased ROS levels and significantly reduced GPX4, cell lipid peroxidation, and iron accumulation levels. Class I ferroptotic inducers (e.g., erastin and sulfasalazine) cause cellular GSH depletion and a redox status imbalance [32]. Class II ferroptotic inducers, especially GPX4 inhibitors (e.g., RSL3 and DPI derivatives), can cause fatal levels of lipid peroxidation [33]. The results of our experiments were consistent with the treatment results of these recognized ferroptotic compounds. Therefore, we can be certain that, in these experiments, curcumin-treated breast cancer cells underwent ferroptosis.

An increasing number of studies have shown that HO-1 plays a key role in ferroptosis and plays a pathogenic role in the development of many diseases [34, 35]. Patients with Alzheimer's disease exhibit increased lipid peroxidation levels, which may be related to increased HO-1 and iron accumulation [36]. Several HO-1 inhibitors have been developed and

widely and effectively used. ZnPP is a heme analog composed of protoporphyrin IX and metal Zn [37]. Due to its similar chemical structure to heme, it is possible to competitively inhibit enzymatic activity by occupying the heme binding site of heme oxygenase. ZnPP has been widely used in studying HO-1 in ferroptosis. In breast cancer cells, ZnPP not only inhibits BAY-induced cell ferroptosis but also significantly prevents the increase of unstable iron pools caused by BAY and h-HO-1 overexpression [27]. The carcinogenic RAS selective lethal small molecule erastin induces ferroptosis. In HT-1080 fibrosarcoma cells, erastin induces the HO-1 expression in a time- and dose-dependent manner, and erastin-induced cellular ferroptosis is inhibited by ZnPP in a manner similar as ferrostatin-1, which has been identified as an inhibitor of ferroptosis [28].

HO-1 is a rate-limiting enzyme in the degradation of heme. Some studies have shown that the induction of HO-1 has antitumor activity. The induction of HO-1 in breast cancer suppressed proliferation and invasion through reducing intracellular ROS [38, 39]. Overexpression of HO-1 in hepatomas reduced cell migration and xenograft tumor growth [40]. In addition, induction of HO-1 by chemopreventive agents such as curcumin and sulforaphane inhibits tumorigenesis via increasing antioxidant response genes [41, 42]. Heme can be degraded into bilirubin, CO, and Fe^{2+} .

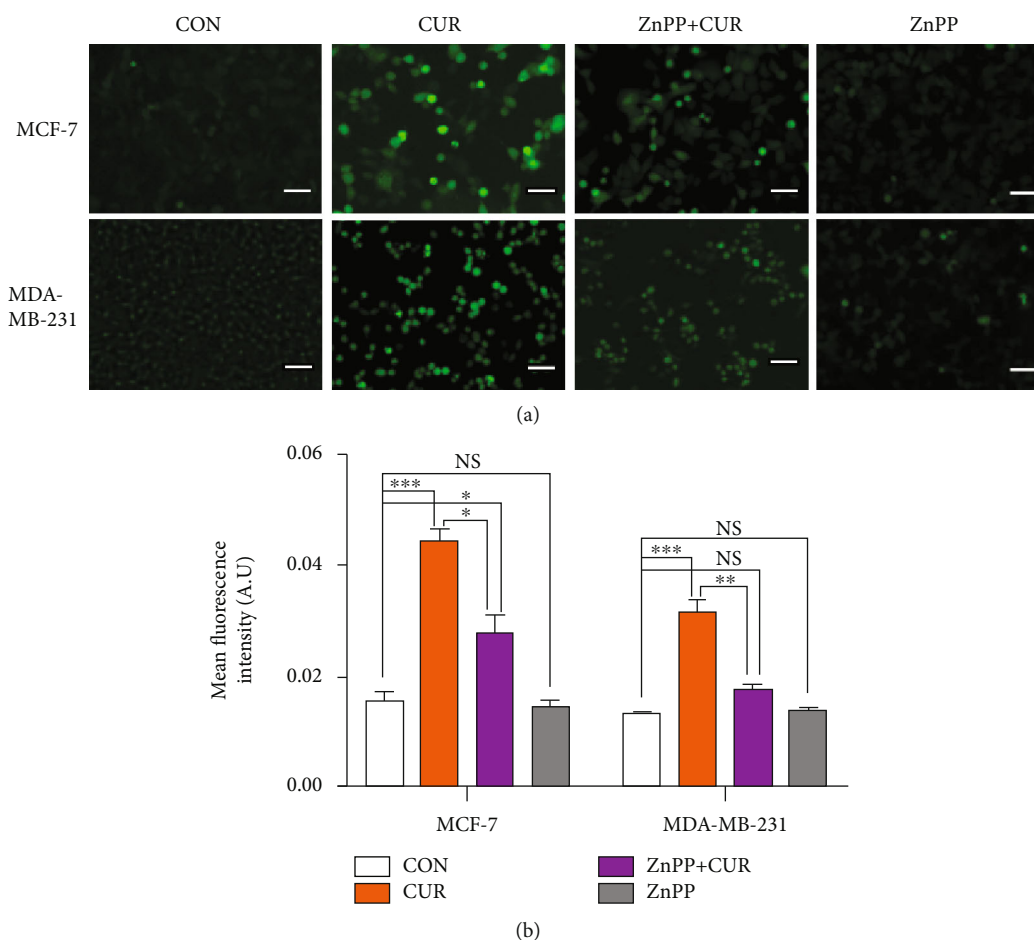


FIGURE 6: Determination of the ROS levels by fluorescence intensity measurements using a fluorescence microscope. (a) MCF-7 cells were treated with vehicle (CON, DMSO), curcumin (CUR, 40 μ M), or a mixture of 40 μ M curcumin and zinc protoporphyrin 9 (ZnPP, 10 μ M) for 48 hours. MDA-MB-231 cells were treated with vehicle (CON, DMSO), curcumin (CUR, 50 μ M), or a mixture of 50 μ M curcumin and zinc protoporphyrin 9 (ZnPP, 10 μ M) for 48 hours. After incubation with 5 μ M DCFH-DA, cells were washed and examined by a fluorescence microscopy (scale bar represents 200 μ m). Representative images from three independent experiments are shown. (b) The results of ROS upregulation in breast cancer cells were determined by fluorescence analysis using the ImageJ software. The results are expressed as the means \pm SEM of three independent experiments; * P < 0.05; ** P < 0.01; *** P < 0.001. NS: no significant difference compared to CON alone. All CON groups treated above received the same volume of reagent solvent as the treatment groups.

Upregulation of HO-1 enhances the degradation of heme and the synthesis of ferritin, altering the intracellular iron distribution [43]. Iron overload can promote Fenton reactions and ROS production. Excessive ROS generation leads to peroxidation and oxidative damage to neighboring lipids, DNA, and proteins, eventually leading to ferroptosis [44]. The metabolism of iron in cells is regulated by related ferritin. When the regulation capacity of ferritin is disturbed by strong oxidative stress, it causes uncontrolled release of large amounts of iron, eventually leading to excessive accumulation of iron in the cell and subsequent lipid peroxidation [45]. Activation of iron metabolism-related proteins promotes the development of ferroptosis [26]. In our study, the gene expression of the transferrin receptor and iron transporter in breast cancer cells was significantly upregulated, and cellular ROS and cellular lipid peroxidation were intensified. It can be concluded that overexpression of HO-1 causes intracellular iron metabolic disorders and cellular lipid peroxidation, leading to ferroptosis. Previous studies have

detailed the dual role of HO-1 in cells, and its role in ferroptosis may be cell type and stimulus specific [46]. In a recent study of kidney damage related to rhabdomyolysis, curcumin was found to inhibit renal tubular cell ferroptosis by activating HO-1 [47]. This finding means that the exact regulatory mechanism of curcumin in ferroptosis needs to be further studied and that the role of HO-1 in ferroptosis still needs to be elaborated. Furthermore, the application of curcumin in cancer chemotherapy needs far more research support.

In addition, GPX4 is an essential regulator of ferroptotic cancer cell death that provides antioxidants to counteract lipid peroxidation and is the only enzyme that reduces lipid hydroperoxides in biofilms [48]. GPX4 is a key factor in maintaining cell redox balance [49]. Analysis of mass spectrometry-based proteomics data from an affinity pull-down experiment ranked GPX4 as the top protein target for (1S,3R)-RSL3 [50]. Friedmann et al. provided direct genetic evidence that knocking out GPX4 leads to cell death in a pathologically related form of ferroptosis [51]. Glyoxalases

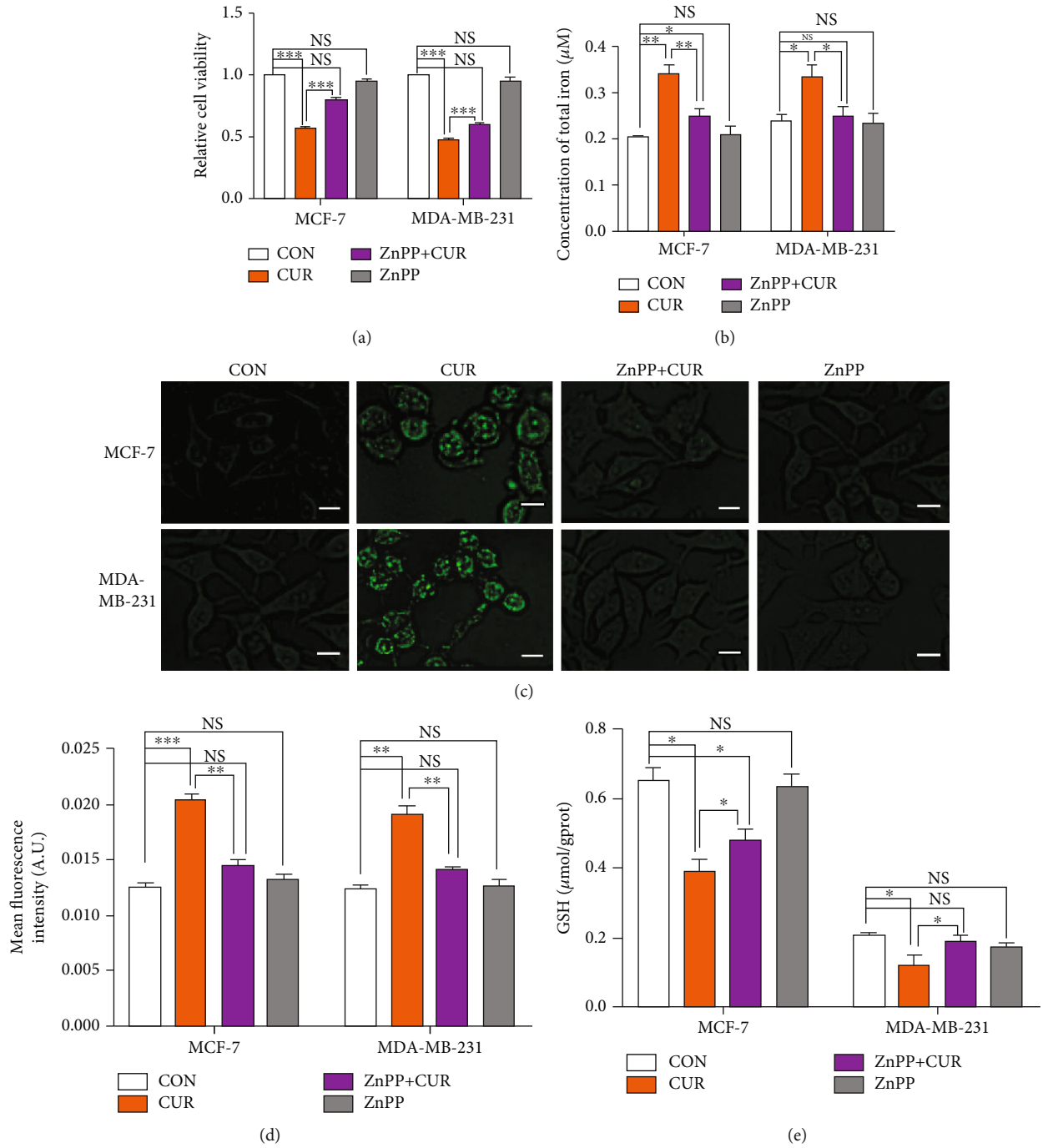


FIGURE 7: Continued.

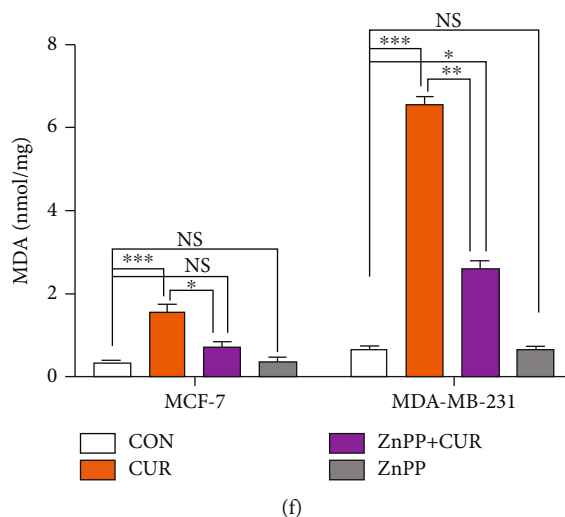


FIGURE 7: Curcumin upregulates the expression of HO-1 in breast cancer cells and triggers ferroptosis, as verified by ZnPP treatment. (a) Cell viability after treatment and under basal conditions (i.e., untreated cells) as measured by the CCK-8 assay. MCF-7 cells were treated with vehicle (CON, DMSO), curcumin (CUR, 40 μ M), or a mixture of 40 μ M curcumin and zinc protoporphyrin 9 (ZnPP, 10 μ M) for 48 hours. MDA-MB-231 cells were treated with vehicle (CON, DMSO), curcumin (CUR, 50 μ M), or a mixture of 50 μ M curcumin and zinc protoporphyrin 9 (ZnPP, 10 μ M) for 48 hours. The results are expressed as the means \pm SEM of three independent experiments. *** P < 0.001. NS: no significant difference compared to CON alone. (b) Iron assay kit to detect changes in the total iron content in cells. The cell treatment method is the same as for (a). The results are expressed as the means \pm SEM of three independent experiments. * P < 0.05 and ** P < 0.01. NS: no significant difference compared to CON alone. (c) Using Liperfluo to detect changes in the lipid peroxide content in cells. The cell treatment method was the same as for (a). After incubation with 2 μ M Liperfluo, cells were washed and examined by a fluorescence microscopy (scale bar represents 50 μ m). Representative images from three independent experiments are shown. (d) The results of lipid peroxide upregulation in breast cancer cells were determined by fluorescence analysis using the ImageJ software. The results are expressed as the means \pm SEM of three independent experiments; ** P < 0.01; *** P < 0.001. NS: no significant difference compared to CON alone. All the CON groups treated above received the same volume of reagent solvent as the treatment group. (e) The GSH detection kit was used to detect changes in the GSH content in cells. The cell treatment method is the same as for (a). The results are expressed as the means \pm SEM of three independent experiments. * P < 0.05; NS: no significant difference compared to CON alone. (f) The MDA detection kit was used to detect changes in the MDA content in cells. The cell treatment method is the same as for (a). The results are expressed as the means \pm SEM of three independent experiments. * P < 0.05; ** P < 0.01; *** P < 0.001. NS: no significant difference compared to CON alone. All CON groups treated above received the same volume of reagent solvent as the treatment group.

(Glo1 and Glo2) are involved in the glycolytic pathway by detoxifying the reactive methylglyoxal (MGO) into d-lactate in a two-step reaction using glutathione (GSH) as cofactor. Inhibitors of glyoxalases are considered anti-inflammatory and antitumor agents. Curcumin inhibits Glo1, resulting in nontolerable levels of MGO and GSH. As a result, various metabolic pathways are disturbed so that, for example, cellular ATP and GSH content are depleted [52]. The depletion of cellular ATP and GSH may in turn decrease cell survival. GPX4 reduces membrane hydroperoxide through GSH, and GPX4 and GSH appear together to become the main determinant of the balance between cell proliferation and death. The inactivation of GPx4 or the depletion of GSH in the cell can lead to a new type of cell death that depends on lipid peroxidation, which is called ferroptosis [53]. Therefore, GPX4 and GSH play an important regulatory role in ferroptosis.

In both the sequencing and RT-qPCR results in our study, curcumin treatment significantly downregulated GPX4 and upregulated HO-1. It is worth noting that 48 hours after curcumin treatment, the upregulation of the HO-1 expression in MCF-7 cells was dramatic. The degree of GPX4 downregulation was similar between the two cell lines, but the degree of ferroptosis in the two cells was different, indicating that GPX4 is not the most important regulator

in the process of curcumin-induced breast cancer cell ferroptosis. Therefore, we believe that GPX4 is a basic effector of curcumin, but HO-1 seems to be more responsible for the difference in the inhibitory effects of curcumin observed in the two cell lines. HO-1 is the limiting factor for curcumin to exert its therapeutic role and thus is the preferred target gene for this study. Although the comparative toxicogenomics database suggests HO-1 as a direct target gene for curcumin, in our opinion, the activation of HO-1 also depends on additional transcription factors, including Nrf2. Nrf2 is a major regulator of cellular antioxidant and electrophilic stress defense responses, and HO-1 is one of its target genes [54]. Due to its binding to the cytoskeleton-related protein Keap1, the inactive form of Nrf2 partially or fully localizes in the cytoplasm. The activation of Nrf2 is considered an important molecular target for many chemopreventive and cytoprotective agents. Nrf2 protects cells against oxidative stress through ARE-directed induction of several phase 2 detoxifying and antioxidant enzymes, particularly HO-1. Some studies have reported that Nrf2 inhibits ferroptosis [55, 56], but the results from study by Cao et al. have shown that even when Nrf2 induces increased intracellular glutathione content, it only weakly protects cells from ferroptosis [57].

5. Conclusions

Based on the evidence that curcumin has a significant inhibitory effect on breast cancer cells, this study analyzed the possible genetic pathways of curcumin targeting breast cancer cells using RNA sequence technology. Ferroptosis, a novel pathogenic mechanism screened from high-throughput data, was verified in our in vitro results. The results of our current study suggest that curcumin triggers the molecular and cytological features of ferroptosis in breast cancer cells by upregulating HO-1 and downregulating GPX4. In subsequent experiments, it was obvious that ferroptosis occurred in response to curcumin treatment. After treatment with the HO-1 specific inhibitor ZnPP, compared to the curcumin-treated group, these phenomena were partially reversed. Therefore, these data highlight that curcumin triggers the molecular and cytological features of ferroptosis in breast cancer cells and that HO-1 potentiates curcumin-induced ferroptosis. Of note, this study only examined the anticancer effects of curcumin on two representative breast cancer cell lines. Whether curcumin can be used as a broad-spectrum antibreast cancer drug remains unknown, and more extensive follow-up investigations are needed. Our study only provides the basis of molecular data for the mechanism of action of curcumin.

Data Availability

The datasets generated for this study can be found in NCBI. The BioProject accession of this study is PRJNA613560.

Conflicts of Interest

The authors declare no conflicts of interest.

Authors' Contributions

RL, JZ, and HY proposed the study protocol. RL, YZ, and RW participated in the experiments. RL, QG, and LZ contributed to the sample preparation and data analysis. RL, JZ, HY, and YF edited and reviewed the final version of the article. All the authors provided constructive comments on the manuscript. Ruihua Li and Jing Zhang contributed equally to this work.

Acknowledgments

This study was financially supported by the Jilin Scientific and Technological Development Program (20170307018NY, 20190301034NY); the Special Project of the Province-University Co-constructing Program of Jilin Province (SXGJXX2017-4); the Open Projects of Northeast Agricultural University/Scientific Observing and Experimental Station of Animal Nutrition and Feed Science in Northeast, Ministry of Agriculture of the People's Republic of China; the Jilin Modern Agricultural Technology Demonstration and Extension Project; the central finance forestry science and technology promotion demonstration fund project; and the National Key Research and Development Program of China Stem Cell and Translational Research (2017YFA0105101).

Supplementary Materials

Table 1: the list of the primers used for sequence validation. (*Supplementary Materials*)

References

- [1] L. A. Torre, F. Bray, R. L. Siegel, J. Ferlay, J. Lortet-Tieulent, and A. Jemal, "Global cancer statistics, 2012," *CA: a Cancer Journal for Clinicians*, vol. 65, no. 2, pp. 87–108, 2015.
- [2] F. Bray, J. Ferlay, I. Soerjomataram, R. L. Siegel, L. A. Torre, and A. Jemal, "Global cancer statistics 2018: GLOBOCAN estimates of incidence and mortality worldwide for 36 cancers in 185 countries," *CA: a Cancer Journal for Clinicians*, vol. 68, no. 6, pp. 394–424, 2018.
- [3] B. Wang, L. Yang, Q. Zhao, and L. Zhu, "Vasohibin 2 as a potential predictor of aggressive behavior of triple-negative breast cancer," *American Journal of Translational Research*, vol. 9, no. 6, pp. 2911–2919, 2017.
- [4] L. T. Steward, F. Gao, M. A. Taylor, and J. A. Margenthaler, "Impact of radiation therapy on survival in patients with triple-negative breast cancer," *Oncology Letters*, vol. 7, no. 2, pp. 548–552, 2014.
- [5] C. Denkert, G. von Minckwitz, S. Darb-Esfahani et al., "Tumour-infiltrating lymphocytes and prognosis in different subtypes of breast cancer: a pooled analysis of 3771 patients treated with neoadjuvant therapy," *The Lancet Oncology*, vol. 19, no. 1, pp. 40–50, 2018.
- [6] Y. Xiang, Z. Guo, P. Zhu, J. Chen, and Y. Huang, "Traditional Chinese medicine as a cancer treatment: modern perspectives of ancient but advanced science," *Cancer Medicine*, vol. 8, no. 5, pp. 1958–1975, 2019.
- [7] S. Prasad, S. C. Gupta, A. K. Tyagi, and B. B. Aggarwal, "Curcumin, a component of golden spice: from bedside to bench and back," *Biotechnology Advances*, vol. 32, no. 6, pp. 1053–1064, 2014.
- [8] S. Prasad, A. K. Tyagi, and B. B. Aggarwal, "Recent developments in delivery, bioavailability, absorption and metabolism of curcumin: the golden pigment from golden Spice," *Cancer Research and Treatment*, vol. 46, no. 1, pp. 2–18, 2014.
- [9] R. P. Sahu, S. Batra, and S. K. Srivastava, "Activation of ATM/Chk1 by curcumin causes cell cycle arrest and apoptosis in human pancreatic cancer cells," *British Journal of Cancer*, vol. 100, no. 9, pp. 1425–1433, 2009.
- [10] T. Dorai, N. Gehani, and A. Katz, "Therapeutic potential of curcumin in human prostate cancer-I. curcumin induces apoptosis in both androgen-dependent and androgen-independent prostate cancer cells," *Prostate Cancer and Prostatic Diseases*, vol. 3, no. 2, pp. 84–93, 2000.
- [11] L. Masuelli, M. Benvenuto, E. D. Stefano et al., "Curcumin blocks autophagy and activates apoptosis of malignant mesothelioma cell lines and increases the survival of mice intraperitoneally transplanted with a malignant mesothelioma cell line," *Oncotarget*, vol. 8, no. 21, pp. 34405–34422, 2017.
- [12] Y.-J. Surh, J. Kundu, and H.-K. Na, "Nrf2 as a master redox switch in turning on the cellular signaling involved in the induction of cytoprotective genes by some chemopreventive phytochemicals," *Planta Medica*, vol. 74, no. 13, pp. 1526–1539, 2008.
- [13] J. Chen, D. Wanming, D. Zhang, Q. Liu, and J. Kang, "Water-soluble antioxidants improve the antioxidant and anticancer

- activity of low concentrations of curcumin in human leukemia cells," *Pharmazie Die*, vol. 60, no. 1, pp. 57–61, 2005.
- [14] A. Kunwar, S. K. Sandur, M. Krishna, and K. I. Priyadarsini, "Curcumin mediates time and concentration dependent regulation of redox homeostasis leading to cytotoxicity in macrophage cells," *European Journal of Pharmacology*, vol. 611, no. 1-3, pp. 8–16, 2009.
- [15] X. Shi and Y. Li, "Curcumin upregulate HO-1 expression but downregulate HO-2 expression in SHSY5Y cell," in *2010 4th International Conference on Bioinformatics and Biomedical Engineering, Chengdu*, pp. 1–4, Chengdu, Sichuan Province, China, 2010.
- [16] K. Jomova and M. Valko, "Advances in metal-induced oxidative stress and human disease," *Toxicology*, vol. 283, no. 2-3, pp. 65–87, 2011.
- [17] D. M. Hockenbery, "Targeting mitochondria for cancer therapy," *Environmental and Molecular Mutagenesis*, vol. 51, no. 5, pp. 476–489, 2010.
- [18] S. J. Dixon and B. R. Stockwell, "The role of iron and reactive oxygen species in cell death," *Nature Chemical Biology*, vol. 10, no. 1, pp. 9–17, 2014.
- [19] W. Yang, R. SriRamaratnam, M. Welsch et al., "Regulation of ferroptotic cancer cell death by GPX4," *Cell*, vol. 156, no. 1-2, pp. 317–331, 2014.
- [20] S. J. Dixon, D. N. Patel, M. Welsch et al., "Pharmacological inhibition of cystine–glutamate exchange induces endoplasmic reticulum stress and ferroptosis," *eLife*, vol. 3, pp. 3–e02523, 2014.
- [21] M. Gao, P. Monian, Q. Pan, W. Zhang, J. Xiang, and X. Jiang, "Ferroptosis is an autophagic cell death process," *Cell Research*, vol. 26, no. 9, pp. 1021–1032, 2016.
- [22] G. Yu, L. G. Wang, Y. Han, and Q. Y. He, "clusterProfiler: an R package for comparing biological themes among gene clusters," *OMICS: A Journal of Integrative Biology*, vol. 16, no. 5, pp. 284–287, 2012.
- [23] D. Chen, I. Y. Eyupoglu, and N. Savaskan, "Ferroptosis and cell death analysis by flow cytometry," *Methods in Molecular Biology*, vol. 1601, pp. 71–77, 2017.
- [24] N. M. Ali, S. K. Yeap, N. Abu et al., "Synthetic curcumin derivative DK1 possessed G2/M arrest and induced apoptosis through accumulation of intracellular ROS in MCF-7 breast cancer cells," *Cancer Cell International*, vol. 17, no. 1, pp. 30–38, 2017.
- [25] J. Zyla, M. Marczyk, J. Weiner, and J. Polanska, "Ranking metrics in gene set enrichment analysis: do they matter?," *BMC Bioinformatics*, vol. 18, no. 1, pp. 256–265, 2017.
- [26] M. Gao, P. Monian, N. Quadri, R. Ramasamy, and X. Jiang, "Glutaminolysis and transferrin regulate ferroptosis," *Molecular Cell*, vol. 59, no. 2, pp. 298–308, 2015.
- [27] L.-C. Chang, S.-K. Chiang, S.-E. Chen, Y.-L. Yu, R.-H. Chou, and W.-C. Chang, "Heme oxygenase-1 mediates BAY 11-7085 induced ferroptosis," *Cancer Letters*, vol. 416, pp. 124–137, 2018.
- [28] E. M. Kenny, E. Fidan, Q. Yang et al., "Ferroptosis contributes to neuronal death and functional outcome after traumatic brain injury," *Critical Care Medicine*, vol. 47, no. 3, pp. 410–418, 2019.
- [29] A. B. Kunnumakkara, D. Bordoloi, G. Padmavathi et al., "Curcumin, the golden nutraceutical: multitargeting for multiple chronic diseases," *British Journal of Pharmacology*, vol. 174, no. 11, pp. 1325–1348, 2017.
- [30] B. Ü. Kocaadam and N. İ. Şanlıer, "Curcumin, an active component of turmeric (*Curcuma longa*), and its effects on health," *Critical Reviews in Food Science and Nutrition*, vol. 57, no. 13, pp. 2889–2895, 2015.
- [31] C. Ramachandran, Z. Khatib, R. Ramachandran et al., "Curcumin-induced differential gene expression identified by microarray hybridization in breast cancer cell lines," *Cancer Research*, vol. 64, no. 7, pp. 880–881, 2004.
- [32] S. Dixon, K. Lemberg, M. Lamprecht et al., "Ferroptosis: an iron-dependent form of nonapoptotic cell death," *Cell*, vol. 149, no. 5, pp. 1060–1072, 2012.
- [33] Y. Xie, W. Hou, X. Song et al., "Ferroptosis: process and function," *Cell Death & Differentiation*, vol. 23, no. 3, pp. 369–379, 2016.
- [34] M. Y. Kwon, E. Park, S. J. Lee, and S. W. Chung, "Heme oxygenase-1 accelerates erastin-induced ferroptotic cell death," *Oncotarget*, vol. 6, no. 27, pp. 24393–24403, 2015.
- [35] A. V. Paez, C. Pallavicini, F. Schuster et al., "Heme oxygenase-1 in the forefront of a multi-molecular network that governs cell–cell contacts and filopodia-induced zippering in prostate cancer," *Cell Death & Disease*, vol. 7, no. 12, p. e2570, 2016.
- [36] N. J. LAMB, G. J. QUINLAN, S. MUMBY, T. W. EVANS, and J. M. C. GUTTERIDGE, "Haem oxygenase shows pro-oxidant activity in microsomal and cellular systems: implications for the release of low-molecular-mass iron," *Biochemical Journal*, vol. 344, no. 1, pp. 153–158, 1999.
- [37] S. Schulz, R. J. Wong, H. J. Vreman, and D. K. Stevenson, "Metalloporphyrins – an update," *Frontiers in Pharmacology*, vol. 3, p. 68, 2012.
- [38] M. Hill, V. Pereira, C. Chauveau et al., "Heme oxygenase-1 inhibits rat and human breast cancer cell proliferation: mutual cross inhibition with indoleamine 2,3-dioxygenase," *FASEB Journal*, vol. 19, no. 14, pp. 1957–1968, 2005.
- [39] C. W. Lin, S. C. Shen, W. C. Hou, L. Y. Yang, and Y. C. Chen, "Heme oxygenase-1 inhibits breast cancer invasion via suppressing the expression of matrix metalloproteinase-9," *Molecular Cancer Therapeutics*, vol. 7, no. 5, pp. 1195–1206, 2008.
- [40] C. Zou, H. Zhang, Q. Li et al., "Heme oxygenase-1: a molecular brake on hepatocellular carcinoma cell migration," *Carcinogenesis*, vol. 32, no. 12, pp. 1840–1848, 2011.
- [41] B. S. Cornblatt, L. Ye, A. T. Dinkova-Kostova et al., "Preclinical and clinical evaluation of sulforaphane for chemoprevention in the breast," *Carcinogenesis*, vol. 28, no. 7, pp. 1485–1490, 2007.
- [42] Y. S. Keum, S. Yu, P. P. J. Chang et al., "Mechanism of action of sulforaphane: inhibition of p38 mitogen-activated protein kinase isoforms contributing to the induction of antioxidant response element-mediated heme oxygenase-1 in human hepatoma HepG2 cells," *Cancer Research*, vol. 66, no. 17, pp. 8804–8813, 2006.
- [43] L. Lanceta, C. Li, A. Choi, and J. W. Eaton, "Haem oxygenase-1 overexpression alters intracellular iron distribution," *Biochemical Journal*, vol. 449, no. 1, pp. 189–194, 2013.
- [44] D. M. Suttner and P. A. Dennery, "Reversal of HO-1 related cytoprotection with increased expression is due to reactive iron," *The FASEB Journal*, vol. 13, no. 13, pp. 1800–1809, 1999.
- [45] W. S. Yang and B. R. Stockwell, "Synthetic lethal screening identifies compounds activating Iron-dependent, nonapoptotic cell death in oncogenic-RAS-harboring cancer cells," *Chemistry & Biology*, vol. 15, no. 3, pp. 234–245, 2008.

- [46] S. K. Chiang, S. E. Chen, and L. C. Chang, "A dual role of heme oxygenase-1 in cancer cells," *International Journal of Molecular Sciences*, vol. 20, no. 1, pp. 39–57, 2019.
- [47] M. Guerrero-Hue, C. García-Caballero, A. Palomino-Antolín et al., "Curcumin reduces renal damage associated with rhabdomyolysis by decreasing ferroptosis-mediated cell death," *FASEB Journal: Official Publication of the Federation of American Societies for Experimental Biology*, vol. 33, no. 8, pp. 8961–8975, 2019.
- [48] A. Wendel, "Glutathione peroxidase," *Methods in Enzymology*, vol. 1830, no. 5, pp. 325–333, 2013.
- [49] G. J. McBean, "The transsulfuration pathway: a source of cysteine for glutathione in astrocytes," *Amino Acids*, vol. 42, no. 1, pp. 199–205, 2012.
- [50] W. S. Yang and B. R. Stockwell, "Ferroptosis: death by lipid peroxidation," *Trends in Cell Biology*, vol. 26, no. 3, pp. 165–176, 2016.
- [51] J. P. Friedmann Angeli, M. Schneider, B. Proneth et al., "Inactivation of the ferroptosis regulator Gpx4 triggers acute renal failure in mice," *Free Radical Biology & Medicine*, vol. 16, no. 12, pp. 1180–1191, 2014.
- [52] T. Santel, G. Pflug, N. Y. A. Hemdan et al., "Correction: Curcumin inhibits glyoxalase 1—a possible link to its anti-inflammatory and anti-tumor activity," *PLoS One*, vol. 6, no. 7, p. e3508, 2011.
- [53] F. Ursini and M. Maiorino, "Lipid peroxidation and ferroptosis: the role of GSH and GPx4," *Free Radical Biology and Medicine*, vol. 152, pp. 175–185, 2020.
- [54] A. L. Furfaro, N. Traverso, C. Domenicotti et al., "The Nrf2/HO-1 axis in cancer cell growth and chemoresistance," *Oxidative Medicine and Cellular Longevity*, vol. 2016, no. 20, Article ID 1958174, pp. 1–14, 2016.
- [55] Z. Fan, A. K. Wirth, D. Chen et al., "Nrf2-Keap1 pathway promotes cell proliferation and diminishes ferroptosis," *Oncogene*, vol. 6, no. 8, p. e371, 2017.
- [56] J. L. Roh, E. H. Kim, H. Jang, and D. Shin, "Nrf2 inhibition reverses the resistance of cisplatin-resistant head and neck cancer cells to artesunate-induced ferroptosis," *Redox Biology*, vol. 11, no. C, pp. 254–262, 2017.
- [57] J. Y. Cao, A. Poddar, L. Magtanong et al., "A genome-wide haploid genetic screen identifies regulators of glutathione abundance and ferroptosis sensitivity," *Cell Reports*, vol. 26, no. 6, pp. 1544–1556.e8, 2019.

Review Article

Oxidative Stress in Amyotrophic Lateral Sclerosis: Pathophysiology and Opportunities for Pharmacological Intervention

Teresa Cunha-Oliveira ¹, **Liliana Montezinho** ^{1,2}, **Catarina Mendes**,^{1,3}
Omidreza Firuzi ⁴, **Luciano Saso** ⁵, **Paulo J. Oliveira** ¹ and **Filomena S. G. Silva** ¹

¹CNC-Center for Neuroscience and Cell Biology, University of Coimbra, UC Biotech Building, Biocant Park, Cantanhede, Portugal

²Center for Investigation Vasco da Gama (CIVG), Escola Universitária Vasco da Gama, Coimbra, Portugal

³Coimbra College of Agriculture, Polytechnic Institute of Coimbra (ESAC, IPC), Bencanta, Coimbra, Portugal

⁴Medicinal and Natural Products Chemistry Research Center, Shiraz University of Medical Sciences, Shiraz, Iran

⁵Department of Physiology and Pharmacology “Vittorio Ersamer”, Sapienza University of Rome, Italy

Correspondence should be addressed to Filomena S. G. Silva; filomena.silva@uc-biotech.pt

Received 24 July 2020; Revised 25 September 2020; Accepted 24 October 2020; Published 16 November 2020

Academic Editor: Jos L. Quiles

Copyright © 2020 Teresa Cunha-Oliveira et al. This is an open access article distributed under the Creative Commons Attribution License, which permits unrestricted use, distribution, and reproduction in any medium, provided the original work is properly cited.

Amyotrophic lateral sclerosis (ALS), also known as Lou Gehrig’s disease or Charcot disease, is a fatal neurodegenerative disease that affects motor neurons (MNs) and leads to death within 2–5 years of diagnosis, without any effective therapy available. Although the pathological mechanisms leading to ALS are still unknown, a wealth of evidence indicates that an excessive reactive oxygen species (ROS) production associated with an inefficient antioxidant defense represents an important pathological feature in ALS. Substantial evidence indicates that oxidative stress (OS) is implicated in the loss of MNs and in mitochondrial dysfunction, contributing decisively to neurodegeneration in ALS. Although the modulation of OS represents a promising approach to protect MNs from degeneration, the fact that several antioxidants with beneficial effects in animal models failed to show any therapeutic benefit in patients raises several questions that should be analyzed. Using specific queries for literature search on PubMed, we review here the role of OS-related mechanisms in ALS, including the involvement of altered mitochondrial function with repercussions in neurodegeneration. We also describe antioxidant compounds that have been mostly tested in preclinical and clinical trials of ALS, also describing their respective mechanisms of action. While the description of OS mechanism in the different mutations identified in ALS has as principal objective to clarify the contribution of OS in ALS, the description of positive and negative outcomes for each antioxidant is aimed at paving the way for novel opportunities for intervention. In conclusion, although antioxidant strategies represent a very promising approach to slow the progression of the disease, it is of utmost need to invest on the characterization of OS profiles representative of each subtype of patient, in order to develop personalized therapies, allowing to understand the characteristics of antioxidants that have beneficial effects on different subtypes of patients.

1. Introduction

Amyotrophic lateral sclerosis (ALS), also known as Lou Gehrig’s disease or Charcot disease, is the most common fatal motor neuron disorder. This neurodegenerative disease is characterized by the progressive loss of upper motor neurons in the cerebral cortex and lower motor neurons in the brain

stem and spinal cord, leading to muscle weakness, and progressing into muscle atrophy and paralysis, which culminates in respiratory failure and death [1, 2]. On average, ALS patients have a survival of about 2-3 years from diagnosis, being estimated that only 5-10% of patients survive more than 10 years after diagnosis [3]. So far, no disease-modifying treatment modality has been found for ALS.

Currently, there are only two drugs approved by the US Food and Drug Administration for ALS treatment, riluzole, which is a neuroprotective agent that only extends the ALS life expectancy about 3 months, and edaravone, which is an antioxidant that only delays ALS development [4] in some patients [5], as detailed in Section 3.9. This fatal neurodegenerative disease has a worldwide prevalence of 4-6 cases in 100,000 and typically has a late-onset with symptoms arising between 55 and 65 years of age, on average [3]. Generally, men present with an earlier age of onset compared to women, and they are more prone to spinal-onset, whereas bulbar-onset is more frequent in women [6]. The most common form of ALS is sporadic (sALS), with no known etiology, accounting for nearly 90-95% of all the cases, while the remaining 5-10% of the cases are inherited (Familial ALS-fALS), and frequently associated with an earlier age of onset [2, 7].

Although the causes of sALS are still unknown, the disease has been associated with different risk factors, including age, smoking, body mass index, level of physical fitness, and occupational and environmental risk factors, such as exposure to chemicals, pesticides, metals, and electromagnetic fields [8]. However, as none of these external parameters are considered as direct factors triggering the development of this disease, it is believed that there are some individual susceptibility factors that coupled to external exposure to environmental factors lead to the development of ALS [9-11]. Over 50 disease-modifying genes have been described in ALS [12]; mutations in chromosome 9 open reading frame 72 (*C9orf72*) [13, 14], Cu²⁺/Zn²⁺ superoxide dismutase type-1 (*SOD1*) [15-18], TAR DNA-Binding (*TARDBP*) [19], and fused in sarcoma (*FUS*) [20, 21] are among the most prevalent ones. As neither the mutations nor the environmental risk factors completely describe the etiopathogenesis of this disease, a gene-time-environment model has arisen to explain the development of this disease, considering the development of ALS as a multistep process in which genetic background is one of the several triggering factors [10, 22].

Although the precise pathological mechanisms of ALS are still unknown, it is assumed that fALS and sALS share at least some pathological mechanisms, since they present similar clinical pictures [3, 23]. Many molecular mechanisms have been suggested, including glutamate excitotoxicity, altered RNA metabolism, defective axonal transport, protein misfolding and aggregation, endoplasmic reticulum stress, disrupted protein trafficking, oxidative stress (OS), inflammation, and mitochondrial dysfunction [3, 24, 25].

In this review, we provide an update on the role of OS in ALS that accelerates mitochondrial dysfunction and cell damage. Considering that OS decisively contributes to neurodegeneration in ALS, we also describe antioxidant-based therapeutic strategies that have been suggested for ALS management. Several antioxidant agents have failed to show any meaningful therapeutic benefit or were not sufficiently examined. In this regard, we try to sum up the evidence on the positive and negative outcomes for each drug with the aim of achieving novel opportunities for intervention.

2. Evidence on the Involvement of Oxidative Stress in ALS

Reactive oxygen species (ROS) are radical or nonradical oxygen species formed by the partial reduction of oxygen, such as superoxide radical anion (O₂^{•-}), hydrogen peroxide (H₂O₂), and hydroxyl radical (HO[•]), which are generated as cellular metabolic by-products through enzymatic and non-enzymatic reactions [26]. Mitochondria are one of the most important sites of intracellular ROS production due to their main role in oxidative ATP production, in which molecular oxygen is reduced to water in the electron transport chain [27, 28]. The O₂^{•-} is produced at a number of sites in mitochondria, including complexes I and III of the electron transport chain [27, 29], pyruvate dehydrogenase [30], and 2-oxoglutarate dehydrogenase [31, 32], all directing ROS towards the mitochondrial matrix (MM), glycerol 3-phosphate dehydrogenase [33] that produces ROS towards the intermembrane mitochondrial space (IMS) [27], and complex III that can leak electrons to oxygen on both sides of the inner mitochondrial membrane (IMM) [34]. Other proteins involved in mitochondrial ROS generation include cytochrome P450 (CYP) enzymes [35], dihydroorotate dehydrogenase [36, 37], complex II [38], and monoamine oxidases [39] which can also contribute to mitochondrial ROS production. Outside mitochondria, several enzymes have also been identified as major sources of ROS, including the nicotinamide adenine dinucleotide phosphate oxidase (NOX), xanthine oxidase, cyclooxygenases, CYP450, and lipoxygenases [40]. Under normal conditions, the production and the clearance of ROS are balanced [41]. OS arises when the capability of the organism to maintain the balance is compromised by an excess amount of ROS or by defective antioxidant defense and can be manifested in multiple ways, including modifications of the redox state of critical proteins, and hence of their activity [42, 43]. The cellular antioxidant defense is composed of enzymatic and nonenzymatic antioxidants [44]. Superoxide dismutases, catalase (CAT), glutathione peroxidase (GPx), glutathione reductase (GR), and thioredoxin (Trx) are the major enzymatic antioxidants with an important role in the catalytic removal of ROS, while nonenzymatic antioxidants include low molecular weight compounds, as glutathione (GSH), vitamins A, C, and E, flavonoids, and proteins (e.g., albumin, ceruloplasmin, and metallothionein) [45]. An excessive ROS production associated with an inefficient antioxidant defense represents an important pathological feature in ALS [46].

A large number of studies have reported increased levels of oxidative damage in proteins, lipids, and DNA of postmortem neuronal tissue [47-49], as well as in cerebrospinal fluid (CSF) [50-53], plasma [54], and urine [55] samples collected from ALS patients, suggesting the involvement of OS mechanisms in the central nervous system (CNS) as well as other tissues. However, it is difficult to determine if oxidative damage represents the primary cause or a secondary consequence of this disease [56, 57] and whether oxidative damage appears early or late in the course of the disease. The impossibility of evaluating OS markers in humans at an early stage of the disease constitutes an obstacle to resolve this riddle, since

the initial phase of the disease progresses in a subclinical manner and thus years can pass before the diagnosis. There is no current way to predict which individuals will develop this neurodegenerative disease. On the other hand, the patients' life expectancy is usually very short, and it is not possible to follow OS markers during a long period of time. Nevertheless, animal models can bring some insights. For example, it was described in mutant SOD1 (mutSOD1) mice that the activation of the nuclear factor erythroid-2-related factor 2 (Nrf2)-antioxidant response element (ARE) OS-responsive system occurred in distal muscles before the disease onset [58], supporting the hypothesis that augmented OS in the muscles is implicated in an initial phase of this disease that eventually leads to axonal "dying back" and culminates with motor neurons (MNs) loss. However, it is noted that the studies with animal models that correlate different OS markers with the disease progression only refer to the mutSOD1 model of the disease, which does not represent the majority of patients. For sALS, which represents the highest number of patients, evidence of oxidative damage includes the increase in protein carbonyls [48, 49, 59, 60], 8-hydroxy-2'-deoxyguanosine (8-OHdG) [48, 61], malondialdehyde-modified proteins [48], 4-hydroxynonenal (4-HNE) protein conjugates [61, 62], and nitrotyrosine products [63–65] in spinal cord tissue. Moreover, in erythrocytes from sALS patients, an increase in lipid peroxidation associated with a decrease in CAT, GR, and glucose-6-phosphate dehydrogenase activities and a decrease in GSH, especially in cases with longer disease duration times were measured [66]. The fact that some of the environmental risk factors of ALS, including exposure to agricultural chemicals, heavy metals, excessive physical exertion, chronic head trauma, and smoking, share OS mechanisms as a possible common factor suggests that the appearance of ALS can be facilitated by any factor that favors the prooxidative state [67]. However, the exact oxidative mechanism involved in ALS progression remains to be determined, as well as the real involvement of mitochondria in this process. To clarify this question, Walczak et al. [68] analyzed different parameters of mitochondrial function and antioxidant enzymes to compare sALS patients with fALS patients and controls. Decreased expression of complexes I, II, III, and IV protein subunits was observed in fibroblasts from practically all sALS patients, which also presented lower mitochondrial membrane potential and decreased protein expression of two different antioxidant enzymes: SOD1 and CAT (Figure 1). Principal component analysis allowed a clear separation between 3 classes, corresponding to controls, sALS, and fALS. Controls were mainly characterized by a high expression of SOD1 protein, whereas sALS samples were characterized by high Ci for complexes I and IV (a coefficient that represents the control of metabolic fluxes by a given enzyme), and fALS samples were characterized by a high rate of maximal respiration with substrates for complexes I and II and a high level of the complex I NDUFB8 subunit. These results suggest distinct mechanisms of mitochondrial dysfunction in sALS patients that can lead to chronic mitochondrial stress [68], which should be further clarified in the future.

2.1. Association of SOD-1 Mutations with Oxidative Stress in ALS. MutSOD1, accounting for approximately 20% of ALS cases, is one of the most studied causes of ALS, involving OS mechanisms and disruption of mitochondrial function observed in cultured cells [69–71] and in animal models [72–74]. SOD1 is a Cu-Zn metalloprotein responsible for the conversion of $O_2^{\bullet-}$ into O_2 and H_2O_2 and is localized mainly in the cytosol, being also present in the nucleus, peroxisomes, and mitochondria. This enzyme plays a key role in the antioxidant defense of the cell [75], also regulating cellular respiration and energy metabolism [76]. In ALS patients, there are more than 180 mutations identified across the coding region of the SOD1 gene as well as several others in the noncoding regions [77, 78]. The influence of these mutations on dismutase activity is considerably variable, and they may be associated with a decrease [52], maintenance [79, 80], or increase [52, 81] in the activity compared to wild-type SOD1. Because SOD1 knockout mice do not develop ALS per se [82], and due to the lack of correlation between SOD1 dismutase activity and aggressiveness of clinical phenotypes [83], it has been suggested that mutSOD1 exerts its deleterious effect by a toxic gain of function rather than by altered SOD1 activity [84].

The mechanism of this toxic gain is currently unknown. A number of hypotheses regarding this toxic property have been proposed, none of them being proven so far: (1) mutSOD1 could act as a peroxidase by using as a substrate the H_2O_2 produced through ordinary dismutase reaction [80, 85]; (2) mutSOD1 could react with peroxyxynitrite to cause tyrosine nitration [42, 86]; and (3) formation of aggregates due to a decrease in the stability of SOD1 monomer/dimers [87]. As a peroxidase, it has been proposed that SOD1 catalyzes the reverse of its normal dismutase reaction or uses the H_2O_2 produced in the dismutation as a substrate to produce HO^{\bullet} through the Fenton reaction [88, 89]. It has also been suggested that mutSOD1 causes elevated oxidative damage through the dissociation of zinc from the enzyme [90] or exposure to toxic copper at the active site, promoting reverse $O_2^{\bullet-}$ production [91]. On the other hand, $O_2^{\bullet-}$ also reacts with nitric oxide which is generated by nitric oxide synthase, more rapidly than it does with native SOD1, producing peroxyxynitrite, with consequent tyrosine nitration of cellular proteins [42, 86] (Figure 2).

Notwithstanding, it has also been proposed that the maturation of SOD1 is a complex multistep process, which easily predisposes SOD1 to misfolding or/and polymerization and aggregation [92–94]. In fact, the SOD1 enzyme can itself be a target for OS, leading to possible folding and aggregation defects [95], which remains controversial in ALS pathogenesis. While a correlation was found between the accumulation of SOD1 aggregates and the disease progression in cervical, thoracic, and lumbar spinal cord tissues of B6-SJL-Tg (SOD1^{G93A}) mice, it was also suggested that an enhanced capacity of drawing the misfolded SOD1 into aggregates may confer resistance against its own toxicity [96]. Similarly, Zhu et al. [92] showed that low molecular weight nonnative SOD1 trimers were cytotoxic in neuroblastoma cells, while SOD1 aggregates did not affect cell viability. Together, these studies suggest that misfolded SOD1

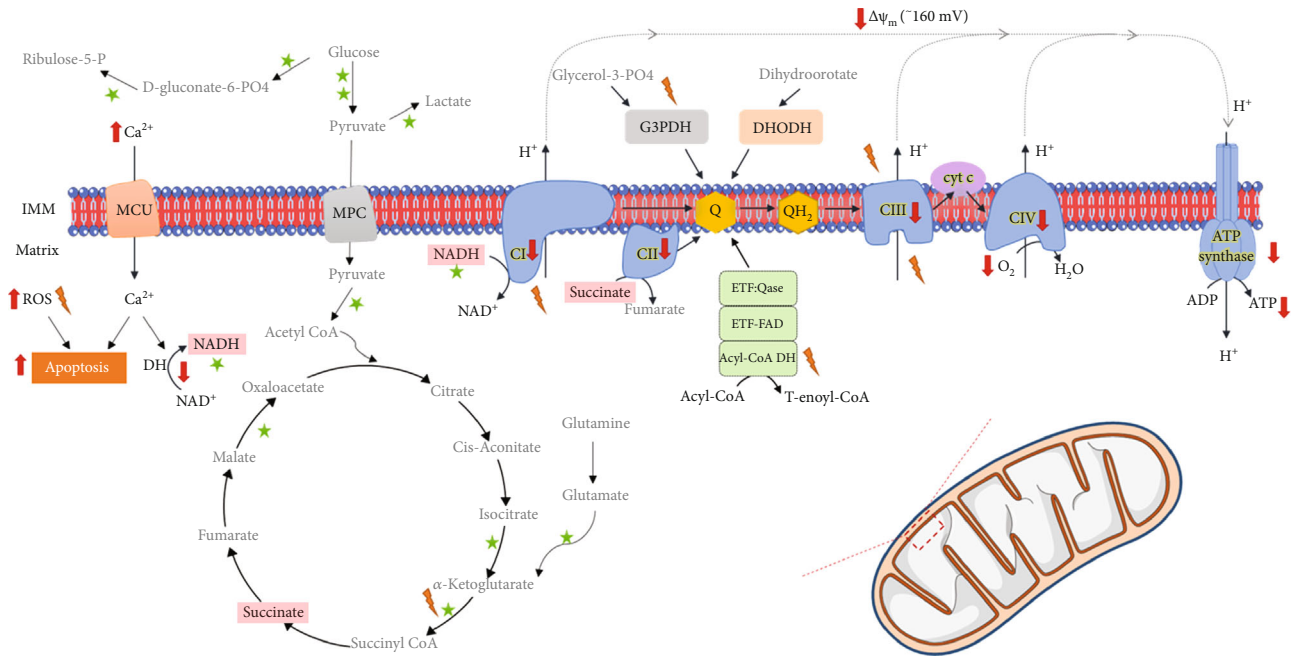


FIGURE 1: Mitochondrial dysfunction in sporadic forms of ALS. Mitochondrial bioenergetics is driven by the oxidation of different substrates and is stimulated by calcium. Flux of electrons through the electron transport chain creates a transmembrane proton gradient of about 160 mV in the resting state (negative inside), which fuels ATP synthesis in the mitochondrial matrix. Leak of electrons in some of the bioenergetic reactions generates reactive oxygen species (ROS) that are involved in important cellular signaling processes but that, when in excess, may also lead to cellular dysfunction and death. Fibroblasts from sALS patients showed markers of mitochondrial dysfunction, compared to control fibroblasts, including decreased activity of metabolic dehydrogenases, increased ROS levels, increased intracellular calcium levels, decreased expression of components of the oxidative phosphorylation system, decreased mitochondrial potential, oxygen consumption, and ATP levels [68]. Abbreviations: NAD: β -Nicotinamide adenine dinucleotide; NADH: β -Nicotinamide adenine dinucleotide 2'-phosphate reduced form; FAD: Flavin Adenine Dinucleotide; CI: Complex I; CII: Complex II; CIII: Complex III; CIV: Complex IV; Cyt c: Cytochrome c; ETF: electron transfer flavoprotein; ROS: reactive oxygen species; DH: dehydrogenase; MCU: mitochondrial calcium uniporter; MPC: mitochondrial pyruvate carrier; $\Delta\Psi_m$: mitochondrial transmembrane electric potential; ATP: adenosine triphosphate; ADP: adenosine diphosphate; IMM: inner mitochondrial membrane

can be a disease driver, especially for the spinal cord, while SOD1 aggregates are considered benign or protective agents against the disease progression. Indeed, misfolded SOD1 identified in spinal cord mitochondria from both SOD1^{G93A} rats and SOD1^{G37R} mice was associated with an increased susceptibility to OS and mitochondrial damage [72]. Moreover, in the mouse motoneuronal NSC-34 cell line, the mut-SOD1 proteins were found to associate with mitochondria due to the oxidation of cysteine residues, which causes mut-SOD1 to accumulate in an oxidized, aggregated state. Consequently, the presence of mutSOD1 leads to the impairment of the respiratory chain and a shift in the mitochondrial redox balance (GSH/GSSG ratio) towards a higher level of OS [69] (Table 1). Similarly, Liying et al. [70] reported reduced levels of GSH and enhanced levels of GSSG in NSC34 motor neuron-like cells and lumbar tissues of the spinal cord of mutant SOD^{G93A} mice, suggesting that the decrease in GSH and a higher oxidative state in cells promote apoptotic cell death that contributes, at least partially, to motor neuron degeneration in ALS. Additionally, it was also found that the expression of mutSOD1 in SH-SY5Y human neuroblastoma cells induces the activation of p66Shc, a protein involved in controlling mitochondrial redox homeostasis in neuronal-like cells [71].

The overexpression of mitochondria-targeted CAT improved mitochondrial antioxidant defenses and mitochondrial function in SOD1^{G93A} astrocyte primary cultures, however SOD1^{G93A} mice treated with this antioxidant did not develop the disease later or survive longer, suggesting that preventing peroxide-mediated mitochondrial damage alone is not sufficient to delay the disease [97]. In mutSOD1 ALS models (H46R/G93A rats and G1H/G1L-G93A mice), certain residual motor neurons showed the overexpression of peroxiredoxin-I and glutathione peroxidase-I (PrxI/GPxI) during their clinical courses, while at the terminal stage of ALS, a disruption of this common PrxI/GPxI-overexpression mechanism was observed in neurons, suggesting that the breakdown of this redox system at the advanced disease stage probably accelerates neuronal degeneration and neuronal death [98] (Table 1). Indeed, decreased GSH levels caused motor neuron degeneration in the SOD1^{wt} mice model [99] and accelerated motor neuron death in SOD1^{G93A} mice, by aggravating mitochondrial pathology [73].

Protein cysteine residues are crucial in the regulation of cellular redox balance, due to their thiol groups that can form covalent disulfide bonds, which are critical for correct protein folding, function, and stability [100]. The tripeptide GSH, which contains cysteine, is the major thiol antioxidant

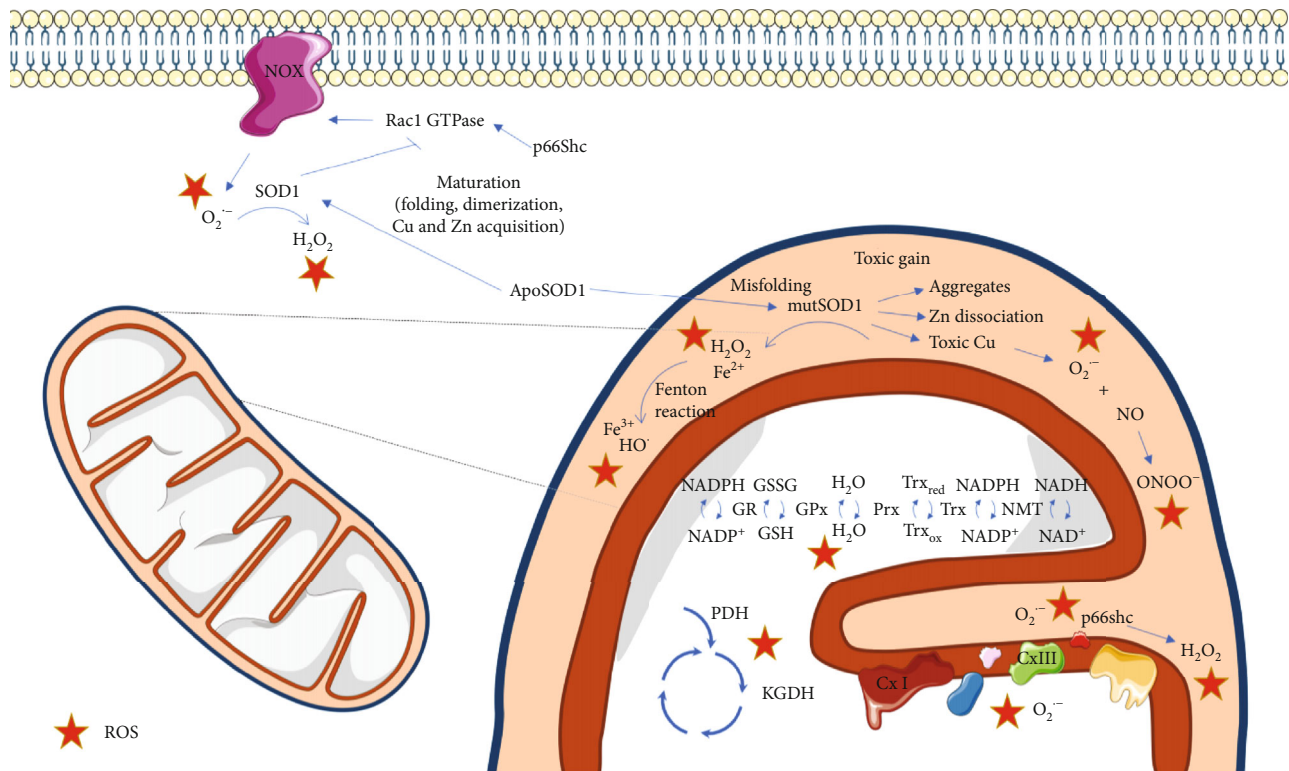


FIGURE 2: Mitochondrial dysfunction associated with SOD1 mutations. Reactive oxygen species (ROS) may be formed in several cellular reactions and are controlled by a network of antioxidant enzymes that include superoxide dismutase 1 (SOD1), a Cu-Zn metalloprotein responsible for the conversion of $O_2^{\bullet-}$ into O_2 and H_2O_2 , which is mainly localized in the cytosol. SOD1 mutations are one of the most studied causes of ALS. Mutant SOD1 (mutSOD1) toxic gain involves its translocation to the mitochondrial intermembrane space, where it aggregates due to lower stability of mutSOD1 monomers/dimers. mutSOD1 may also cause elevated oxidative damage through the dissociation of zinc from the enzyme or exposure to toxic copper at the active site, promoting reverse $O_2^{\bullet-}$ production. $O_2^{\bullet-}$ reacts with nitric oxide generated by nitric oxide synthase, more rapidly than it does with SOD1, producing peroxynitrite, with consequent tyrosine nitration of cellular proteins. mutSOD1 may also act as a peroxidase by using H_2O_2 as a substrate, or the H_2O_2 produced in the dismutation reaction may originate HO^{\bullet} through the Fenton reaction. mutSOD1 may also induce the activation of p66Shc, a protein involved in controlling mitochondrial redox homeostasis. Outside mitochondria, mutSOD1 associates more strongly with Rac1 compared to the wild type form of SOD1, being less sensitive to redox uncoupling, consequently leading to an increase in NADPH oxidase- (NOX-) derived $O_2^{\bullet-}$. ApoSOD1: metal-deficient Cu,Zn-superoxide dismutase; NADP: β -Nicotinamide adenine dinucleotide 2'-phosphate; NADPH: β -Nicotinamide adenine dinucleotide 2'-phosphate reduced form; NAD: β -Nicotinamide adenine dinucleotide; NADH: β -Nicotinamide adenine dinucleotide 2'-phosphate reduced form; GSH: reduced glutathione; GSSG: oxidized glutathione; Trx_{red}: reduced Thioredoxin; Trx_{ox}: oxidized Thioredoxin; Trx: Thioredoxin, NMT: N-myristoyltransferase; Prx: peroxiredoxin; GPx: glutathione peroxidase; GR: glutathione reductase; PDH: pyruvate dehydrogenase; KGDH: alpha-ketoglutarate dehydrogenase; CxI: complex I; CxIII: complex III.

and can act as an electron donor to reduce disulfide bonds in proteins. Cysteine thiols are critical for several cellular functions, including signal transduction and DNA binding of redox-responsive transcription factors, such as Nrf2 and nuclear factor kappa-light-chain-enhancer of activated B cells (NF- κ B) [101]. SOD1 has four cysteine residues (Cys 5, 57, 111, and 146), and its oligomerization may involve covalent disulfide cross-linking mediated by Cys 111, which is relatively exposed on the protein surface [102], with Cys 6 also playing a possible role [103]. However, this cannot completely explain SOD1 aggregation in ALS because all SOD1 cysteine residues have been found to be mutated in ALS and, therefore, are not present in some patients that present SOD1 aggregates [104].

SOD1 has a tight connection with the Nrf2 pathway, which is a major regulator of the phase II antioxidant response and respective antioxidant elements, including GPx, CAT, GR, and enzymes involved in GSH synthesis and nicotinamide adenine dinucleotide phosphate (NADPH)-regenerating enzymes [105–107]. Nrf2 usually resides in the cytosol bound to Keap1 (Kelch ECH-associating protein 1; the cytoplasmic Nrf2 regulator). Oxidative modification of cysteine residues on Keap1 leads to the release of Nrf2, which in turn translocates to the nucleus upregulating the expression of genes with an ARE in their promoter [108, 109]. Nrf2 expression was found to be decreased in NSC-34 cells expressing mutSOD1, in MNs isolated from familial SOD1-associated ALS patients [110], and in primary motor cortex and spinal cord

TABLE 1: Representative studies that demonstrate the association of specific genetic alterations with oxidative stress in ALS.

Altered gene	Genetic alterations	Experimental model	Observed effects on oxidative stress makers	Reference
SOD1	Mutation: G93A	(i) Transgenic mice	(i) Reduced GSH in the spinal cord and motor neuron cells that correlates with apoptosis-inducing factor translocation, caspase 3 activation, and motor neuron degeneration during ALS-like disease onset and progression	[70]
SOD1	Mutations: A4V, G37R, H48Q, H80R, G85R, D90A, G93A, D124V, D125H, E138Δ, S134N, H46R	(i) NSC-34 motor neuron-like cell line	(i) MutSOD1s lowered the GSH/GSSG ratio in mitochondria of cells	[69]
SOD1	Mutations: G1H, G1L, A4V, H46R, G93A, frame-shift 126 mutation	(i) Motor neurons from 40 sALS and 5 mutated SOD1 sALS patients (frame-shift 126 mutation and A4V) (ii) Transgenic rats (H46R/G93A) (iii) Transgenic mice (G1H/G1L-G93A)	(i) The number of motor neurons with negative expression of antioxidant enzymes (PrxII and GPxI) increased with ALS disease (ii) Neurons with higher expression of PrxII and GPxI were less susceptible to oxidative stress	[98]
TDP-43	Mutations: M33V, Q331K	(i) TDP-43Q331K mice (ii) Primary astrocyte cultures from TDP-43Q331K mice (iii) Fibroblasts from pre- and postsymptomatic ALS patient fibroblasts harboring a TDP-43M337V mutation	(i) Increased transcript expression of Nrf2 signaling-related genes (NFE2L2, HMOX1, GCLM, and NQO1) in the spinal cord of transgenic mice (ii) No change in protein expression levels of HO-1, GCLM, GPx1, and NQO1 antioxidant proteins in transgenic mice (impaired protein translation of antioxidants) (iii) Decreased total GSH levels in fibroblasts from pre- and postsymptomatic patients (iv) Decreased total GSH levels in primary astrocytes from transgenic mice	[116]
TDP-43	Mutation: M337V	(i) NSC-34 motor neuron-like cell line	(i) Decreased nuclear translocation of Nrf2, total Nrf2, cytoplasmic Nrf2, and downstream phase II detoxifying enzyme (NQO1) (ii) Increased lipid peroxidation products	[115]
TDP-43	Mutations: Q331K, M337V	(i) NSC-34 motor neuron-like cell line	(i) Mitochondrial dysfunction, oxidative damage, and nuclear accumulation of Nrf2 in cells (ii) Downregulation of HO-1, that could not be restored by sulforaphane (iii) Reduction of LDH and lipid peroxidation products by sulforaphane	[117]
C9orf72	GGGGCC hexanucleotide repeat expansion in noncoding region	(i) iPSC-derived astrocytes from C9orf72-mutated fALS patients and nonaffected donors	(i) Decreased secretion of antioxidant proteins (SOD1, SOD2, and GSH) in mutant C9orf72 astrocytes (ii) Increased ROS levels in mutant C9orf72 astrocytes (iii) Conditioned media of mutant C9orf72 astrocytes increased ROS levels in wild type motor neurons (iv) Oxidative stress was increased in an age-dependent manner (v) poly(GR) in C9orf72 neurons compromises mitochondrial function and causes DNA damage in part by increasing oxidative stress	[129]

TABLE 1: Continued.

Altered gene	Genetic alterations	Experimental model	Observed effects on oxidative stress makers	Reference
C9orf72	GGGGCC hexanucleotide repeat expansion in noncoding region	(i) iPSCs-derived motor neurons isolated from C9orf72-mutated fALS patients (ii) iPSC-derived control neurons expressing (GR)80 and dipeptide repeat (DPR) protein	(i) Increased mitochondrial ROS levels cause DNA damage in both models (ii) Prevention of DNA damage by an antioxidant (Trolox)	[128]
ANG	Human wild type ANG (wANG) and its variant K40I (mANG)	(i) SH-SY5Y neuroblastoma cells and NSC-34 motor neuron-like cell line	(i) wANG prevented cell death under H ₂ O ₂ -induced oxidative stress (ii) Increased hydrogen peroxide-induced cell damage in mutant ANG motor NSC-34 neuron-like cell line	[131]

fALS: familial ALS; GCLM: glutamate-cysteine ligase modifier subunit; GPX1: glutathione peroxidase-1; HMOX1: heme oxygenase-1; iPSC: induced pluripotent stem cell; LDH: lactate dehydrogenase; NQO1: NAD(P)H quinone dehydrogenase 1; PrxII: peroxiredoxin-II; sALS: sporadic ALS.

postmortem tissue samples from ALS patients [111], which suggested that increasing neuronal Nrf2 activity may represent a novel therapeutic target. The endogenous activation of the Nrf2-ARE system during the development of pathology in the SOD1^{G93A} mouse model of ALS showed that the early Nrf2-ARE activation occurs in muscle tissue and that eventually, it progresses in a retrograde manner leading to MN loss [58], as previously described. However, the fact that Nrf2-ARE activation may occur in sALS patients, as well as in those carrying mutSOD1, led these authors to speculate that this pathway is probably independent of mutSOD1 [58].

Nicotinamide adenine dinucleotide phosphate oxidase-dependent redox stress is another mechanism described to be related to mutSOD1. In fact, it has been demonstrated that the deletion of NOX2, and to a lesser extent NOX1, in SOD1^{G93A} transgenic mice, slows down disease progression and improves survival [112, 113]. Accordingly, it was also presumed that SOD1 can regulate NOX2-dependent O₂^{•-} production by binding to Rac1, also known as Ras-related C3 botulinum toxin substrate 1, leading to the inhibition of its GTPase activity [114]. These authors suggested that in physiological conditions, SOD1 efficiently binds to Rac-GTP and inhibits its GTPase activity, increasing NOX2 activity in reducing conditions, whereas the accumulation of H₂O₂ leads to the dissociation of SOD1 from Rac-GTP, promoting the inactivation of Rac through GTP hydrolysis, with consequent NOX2 inactivation and decrease in ROS production. In ALS, mutSOD1 associates more strongly with Rac1 compared to the wild type form of SOD1 (SOD1^{G93A} vs. SOD1^{WT} transgenic mice), being less sensitive to redox uncoupling, consequently leading to the hyperactivation of NOX-derived O₂^{•-} by endomembranes [114] (Figure 2).

2.2. Association of TDP-43 Mutations with Oxidative Stress in ALS. Other less characterized mutated genes linked to ALS have also been associated with OS mechanisms. Mutant TAR DNA-Binding Protein 43 (TDP-43), which has several interactions with the members of the family of heterogeneous nuclear ribonucleoproteins (hnRNPs), has also been reported to affect the Nrf2 pathway [115–117]. Supporting this idea,

Moujalled et al. [116] suggested an association between the TDP-43 protein and Nrf2, mediated by the third partner hnRNP K. The same authors showed that fibroblasts from TDP-43^{M337V} patients and astrocyte cultures from TDP-43^{Q331K} mice both displayed impaired levels of GSH (downstream Nrf2 antioxidant), indicating an increase in OS dependent on a disruption of the Nrf2 pathway. The idea of an impairment in the Nrf2/ARE pathway has also been evidenced in studies with TDP43 mutations in NSC-34 cells [115, 117]. NSC-34 cells overexpressing TDP-43^{M337V} showed increased values of intracellular lipid peroxidation, lower cell viability, nuclear accumulation of Nrf2, and decreased protein expression of NAD(P)H quinone dehydrogenase 1 (NQO1, downstream Nrf2 antioxidant), suggesting that TDP-43^{M337V} weakened cellular antioxidant defenses, which turned the cells more susceptible to the increase of OS [115]. Similar results were also described by Duan et al. [117] in NSC-34 cells overexpressing TDP-43^{M337V/Q331K} that showed nuclear accumulation of Nrf2, as well as decreased heme oxygenase (HO-1) protein levels, which is also a phase II detoxification enzyme regulated by the Nrf2 pathway (Table 1).

Similarly to SOD1, cysteine residues are candidates for the mediation of TDP-43 aggregation, although the mechanisms are still not completely explained [118]. TDP-43 has six cysteine residues, four located in RNA recognition motifs (Cys 173, 175, 198, and 244) and two in the N-terminal domain (Cys 39 and 50) [119], with no mutations found so far in ALS [104]. In fact, oxidation of cysteine residues in the RNA recognition motifs was shown to decrease protein solubility and lead to the formation of intra- and intermolecular disulfide bridges [120, 121].

2.3. Association of FUS Mutations with Oxidative Stress in ALS. Fus, a hnRNP (hnRNP P2) [122], is involved in DNA damage response induced by DNA-double strand breaks [123, 124], among other pathways, although its role has not been completely clarified. Wang et al. [124] showed that the loss of nuclear FUS in fibroblasts obtained from fALS patients with the R521H and P525L FUS mutations, and in

induced pluripotent stem cells (iPSCs)/MNs derived from these fibroblasts, caused the accumulation of unrepaired DNA strand breaks, which culminated in an increased vulnerability to OS, suggesting a protective effect of FUS against OS [124].

2.4. Association of C9orf72 Mutations with Oxidative Stress in ALS. Concerning C9orf72, the most prevalent mutation in ALS, few studies have related this mutation with OS mechanisms. In C9orf72-related ALS, the expansion of GGGGCC (G4C2) hexanucleotide is found repeated in the first intron of the C9orf72 gene at least thirty times [125]. The expression of expanded G4C2 repeats results in the production of 5 dipeptide repeat (DPR) proteins: poly-glycine-alanine (poly-GA), poly-glycine-proline (poly-GP), poly-glycine-arginine (poly-GR), poly-proline-alanine (poly-PA), and poly-proline-arginine (poly-PR), which still have an unknown role in ALS progression and OS mechanisms [126, 127]. C9orf72 motor neurons derived from iPSC presented an overexpression of the poly-GR protein and DNA damage that increased gradually with the time of cell culture, possibly due to poly-GR-induced OS [128]. Additionally, these authors reported that poly-GR preferentially binds to mitochondrial ribosomal proteins, compromising mitochondrial function by increasing mitochondrial membrane potential and ROS production, revealing the importance of mitochondrial OS mechanisms in C9orf72-related ALS [128]. Another study with astrocytes derived from mutant C9orf72 iPSC also reported a reduced secretion of several antioxidant proteins by astrocytes, and wild type MNs exposed to media conditioned by these C9orf72-astrocytes showed increased OS [129], suggesting that dysfunction of C9orf72-astrocytes also leads to OS in MNs, contributing to neurodegeneration (Table 1).

2.5. Association of Other Less Frequent Mutations with Oxidative Stress in ALS. Mutations in angiogenin (ANG) may occur in 1-2% of ALS patients [130], and there is evidence that it may be involved in OS associated with ALS [67, 131, 132] (Table 1). ANG is a secreted ribonuclease that can cleave some tRNAs and modulate protein translation in neurons. A study in murine astrocytes has shown that ANG activates the Nrf-2 pathway in these cells, and the conditioned medium of these astrocytes protects neuronal cells against H₂O₂-induced oxidative damage [133].

Paraoxonases (PONs including PON1, PON-2, and PON-3) are enzymes involved in the neutralization of highly toxic organophosphates, and their polymorphisms have been reported in ALS patients [134–136]. Their antioxidant role has been well studied in cardiovascular diseases [137]; however, PON genetic alterations may also be associated with OS in ALS, especially in the context of organophosphate poisoning, which is one of the well-established ALS risk factors [67].

3. Preclinical and Clinical Studies with Antioxidants

Although evidence of oxidative damage in ALS pathogenesis has been largely described in the literature, all antioxidants

tested in patients have so far failed, remaining unclear whether any antioxidant therapies might be effective for treating ALS. In this section, we describe various preclinical and clinical trials with antioxidants that have already been completed or are ongoing.

3.1. Vitamin E. Vitamin E (alpha-tocopherol) is the most active natural lipophilic antioxidant that protects cell membranes from lipid peroxidation [138, 139] and has been extensively tested in the context of ALS (Figure 3). A preclinical study in SOD1^{G93A} transgenic mice showed that dietary supplementation with vitamin E (200 UI/kg) slowed the disease progression and delayed the onset, but did not affect the survival time [140] (Table 2). Although vitamin E deficiency is not consistently present in ALS patients [141–143], a reduced risk for ALS was described in patients with higher vitamin E levels [141], or in those with low baseline vitamin E levels who were supplemented with vitamin E [144–146]. Despite these positive results, three double-blind, placebo-controlled, clinical trials on ALS patients using oral administration of vitamin E (in a range from 500 mg twice a day to 5000 mg/day) until 18 months of treatment did not affect the quality of life neither the survival of the patients, although ALS progression was slowed [147–149] (Table 2). Although vitamin E did not appear to affect the survival in ALS, patients receiving riluzole plus alpha-tocopherol remained longer in the milder states of ALS, and after 3 months of treatment, they presented an increase in plasma GSH levels and a decrease in plasma thiobarbituric acid reactive species levels [147]. The negative results in human studies may be justified in part by the effect that vitamin E does not readily penetrate the blood-brain barrier (BBB) and does not reach the CNS in sufficient concentration to be efficient. In fact, the mean ventricular CSF concentration of vitamin E was 0.114 μ M after an increased monthly dosage (400, 800, 1,600, 3,200, and 4,000 IU/day) over 5 months [150], while its IC₅₀ (concentration at which a 50% inhibitory effect is observed) in a variety of *in vitro* radical scavenging assays was between 1.5 and 59 μ M [151].

Based on the assumption that supplementation with vitamin E may reduce the risk of ALS and moderately slow ALS progression, a randomized crossover clinical trial in phase III to test the effect of vitamin E on treatment of muscular cramps in ALS patients was initiated in 2006 (NCT00372879); however, the results have not yet been published. A pilot randomized, double-blind, placebo-controlled clinical trial in phase II (NCT04140136) was also initiated in 2019 to investigate the effects of vitamin E mixed tocotrienols in patients with ALS, particularly in delaying disease progression, as well as to assess its safety profile in this group of patients. A Cochrane systematic review found that the evidences on the beneficial effect of vitamin E and other treatment strategies on muscle cramps were not conclusive to support the use of these agents in ALS patients [152].

3.2. N-Acetyl-L-Cysteine (NAC). N-acetyl-L-cysteine (NAC) is a membrane-permeable antioxidant molecule that alleviates free radical damage [153] and replenishes the plasma levels of cysteine, as well as the depleted GSH pools

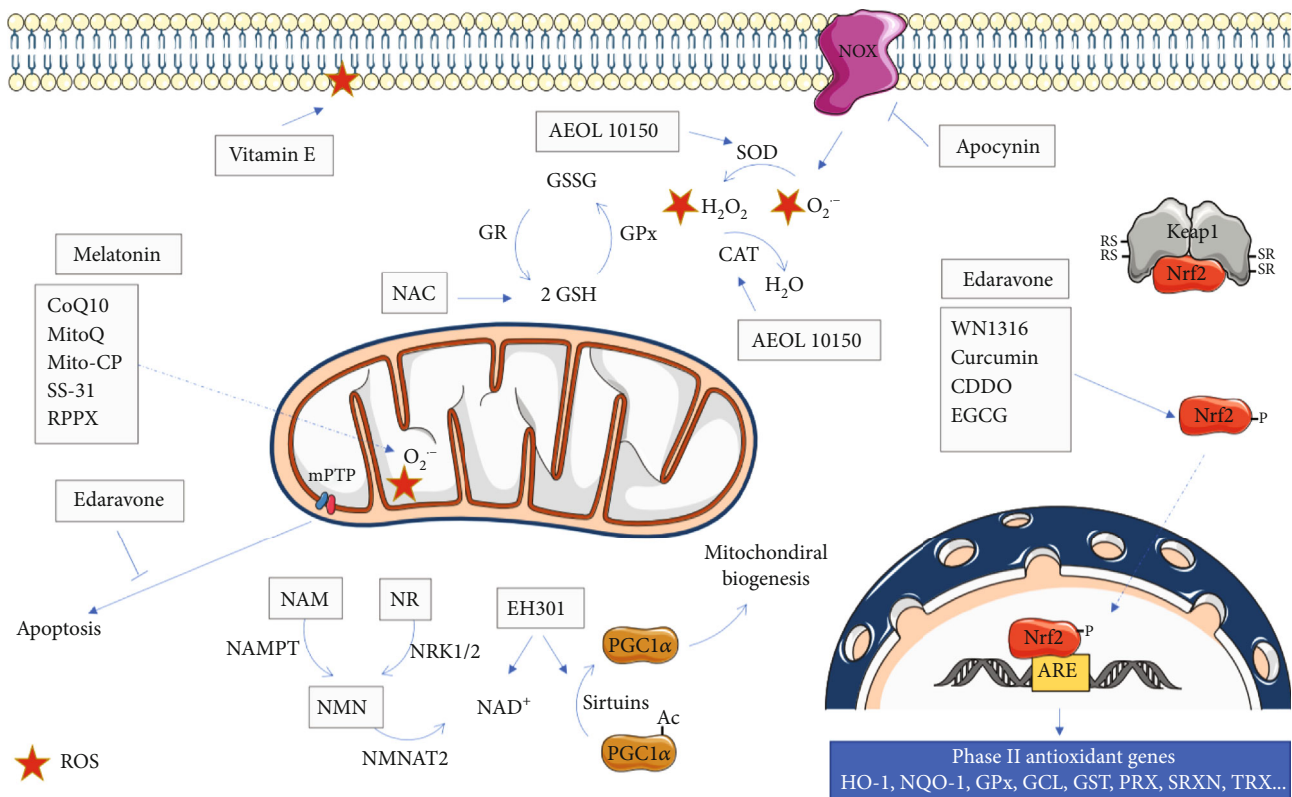


FIGURE 3: Mitochondrial effects of different antioxidant agents in ALS. The scheme represents the main molecular targets of antioxidants used in ALS, as discussed in the main text. HO-1: heme oxygenase 1; NQO-1: NADPH quinone oxidoreductase 1; GPx: glutathione peroxidase; GCL: γ -glutamylcysteine synthetase; GST: glutathione S-transferase; PRX: peroxiredoxin; SRXN: sulfiredoxin; TRX: Thioredoxin; GR: glutathione reductase; CAT: catalase; SOD: superoxide dismutase; NAMPT: nicotinamide phosphoribosyltransferase; NMNAT2: nicotinamide/nicotinic acid mononucleotide adenylyltransferase 2; NRK1/2: nicotinamide riboside kinase 1/2; CoQ10: coenzyme Q10; RPPX: dexrampipexole; NAC: N-acetyl cysteine; CDDO: 2-cyano-3,12-dioxooleana-1,9-dien-28-oic acid; EGCG: epigallocatechin gallate; ROS: reactive oxygen species.

(Figure 3), when administered orally [154]. A preclinical study showed that NAC (1 mM and 24 h) lowered mitochondrial ROS production, returned MTT reduction rate to control levels, and also increased ATP levels in human neuroblastoma SH-SY5Y cell lines carrying G93A SOD1 mutation [155]. Additionally, the administration of NAC (2.0 mg/Kg/day) in SOD1^{G93A} transgenic mice significantly extended survival and improved motor performance [153]. However, in a double-blind placebo-controlled clinical trial on 110 ALS patients, a subcutaneous infusion of NAC (50 mg/kg daily) did not result in a major increase in a 12-month survival or in a reduction of disease progression [156] (Table 2); therefore, the beneficial effects of NAC in ALS remain questionable.

3.3. Coenzyme Q10. Coenzyme Q10 (CoQ10), also known as ubiquinone, is a lipophilic antioxidant, as well as an essential mitochondrial cofactor that mediates electron transfer in the respiratory chain [157, 158]. It has been described that CoQ10 exerts beneficial effects in ALS by scavenging free radicals, protecting against OS (Figure 3). The administration of CoQ10 (200 mg/kg daily) significantly increased the mitochondrial concentrations of coenzyme Q10 in the cerebral cortex and prolonged the survival of SOD1^{G93A} trans-

genic mice when the administration started at 50 days after birth [159]. However, another study showed that the administration of CoQ10 (800 mg/kg/day orally) was unable to prolong the survival of SOD1^{G93A} mice when it started from the onset of disease until death [160]. Controversial results were also found for the serum or plasma CoQ10 concentrations in ALS patients (Table 2). While an increase in the oxidized form of CoQ10 was found in 20 sALS patients compared to controls [161], another study described similar serum concentrations of CoQ10 in 30 ALS patients and controls [162]. CoQ10 has subsequently been shown to be well-tolerated in 31 ALS patients at doses up to 3000 mg/day for 8 months [163]. However, a phase II randomized, placebo-controlled, double-blind, multicenter clinical trial (NCT00243932) with the administration of CoQ10 (2700 mg/day) in ALS patients concluded that the difference between the CoQ10 group and the placebo group was not large enough to justify continuing to a phase III trial [164, 165] (Table 2). The limited pharmacological effect of CoQ10 could be justified by its poor CNS availability after an oral administration [160].

3.4. Nrf2/ARE Modulators. The protective role of Nrf2 against neurodegenerative diseases is well described in the

TABLE 2: Preclinical and clinical studies with different antioxidant therapies for ALS.

Antioxidant	Preclinical animal or cellular model/ clinical trial	Dose/concentration (treatment time)	Effects	Reference
Vitamin E	SOD1 ^{G93A} transgenic mice	200 UI/Kg (starting at 30 days of age)	(i) Slowed disease progression, delayed (ii) Disease onset, did not affect survival time	[140]
	RCT	500 mg twice daily—5000 mg/day (18 months)	(i) Did not affect the quality of life (ii) Did not affect survival time (iii) Slowed ALS progression	[147–149]
N-Acetyl-L-cysteine (NAC)	SH-SY5Y cells with SOD1 ^{G93A}	1 mM (24 h)	(i) Reduction mROS (ii) Increased ATP levels (iii) Increased viability	[155]
	SOD1 ^{G93A} transgenic mice	2 mg/kg/day (from 4-5 weeks of age)	(i) Prolonged the survival time (ii) Improved motor performance	[153]
	RCT	50 mg/kg s.c. infusion (12 months)	(i) Did not affect survival time (ii) Did not affect disease progression	[156]
Coenzyme Q10	SOD1 ^{G93A} transgenic mice	200 mg/kg daily (from 50 days after birth)	(i) Prolonged the survival time	[159]
	SOD1 ^{G93A} transgenic mice	800 mg/kg/daily (from symptom onset)	(i) No effect on survival time	[160]
	RCT, NCT00243932	2700 mg/kg, three times daily (9 months)	(i) No significant differences between treatment and placebo groups	[164, 165]
Nrf2/ARE modulators				
WNI1316	SOD1 ^{H46R} and SOD1 ^{G93A} transgenic mice	1-100 μ g/kg/day (from 21–22 weeks of age)	(i) Improved motor function, prolonged survival time; reduced motor neuron loss, gliosis, and oxidative damage	[170]
Dimethoxy curcumin	NSC-34 cell lines transfected with M337V or Q331K mutant TDP-43	15 μ M (3 days)	(i) Improved mitochondrial dysfunction	[173]
Nanocurcumin (SinaCurcumin)	RCL	80 mg/day (3 months)	(i) Improved the probability of survival time	[174]
Curcumin (Brainoil)	RCL	600 mg/day (6 months)	(i) Slowed disease progression, reduced oxidative stress	[175]
CDDO-EA, CDDO-TFEA	SOD1 ^{G93A} transgenic mice	80 mg/kg/day (starting at 30 days of age or from the onset of the disease)	(i) At presymptomatic age: enhanced motor performance and prolonged survival time (ii) At symptomatic age: slowed disease progression	[178]
S(+9)-apomorphine	Fibroblasts from ALS patients		(i) Reduced oxidative stress, improved survival after oxidative insult	[179]
	SOD1 ^{G93A} transgenic mice	5 mg/kg/day s.c. (from day 21 until end)	(i) Enhanced motor performance, slowed disease progression	[179]
EGCG	Neuronal-differentiated VSC 4.1 cells with SOD1 ^{G93A}	20, 40, 50, 100 μ M (2 h)	(i) Reduced H ₂ O ₂ -induced cell death	[182]

TABLE 2: Continued.

Antioxidant	Preclinical animal or cellular model/ clinical trial	Dose/concentration (treatment time)	Effects	Reference
RPPX	SOD1 ^{G93A} transgenic mice	10 mg/kg/day (from presymptomatic stage) 2.9 μM/g/day	(i) Delayed disease onset and prolonged survival time	[183, 184]
	SOD1 ^{G93A} transgenic mice	100 mg/kg/day, p.o (from day 45)	(i) Enhanced motor performance and prolonged survival time	[187]
	SOD1 ^{G93A} transgenic mice	200 mg/kg/day (from day 55 until 180 days)	(i) No effect was observed on disease progression or survival	[193]
	RCT, phase II	50 mg/day or 300 mg/day (24 weeks)	(i) Beneficial effects on functional decline and survival	[191]
Melatonin	RCT, phase III (NCT01281189)	150 mg/twice daily (12-18 months)	(i) Did not show any efficacy on functional and survival assessment	[192]
	SOD1 ^{G93A} transgenic mice	57–88 mg/kg/day, p.o. (from presymptomatic stage)	(i) Slowed disease progression and prolonged survival time	[54]
	SOD1 ^{G93A} transgenic mice	30 mg/kg/day, i.p. (from six weeks of age)	(i) Delayed disease onset, slowed disease progression, and neurological deterioration and mortality	[198]
	SOD1 ^{G93A} transgenic mice	0.5, 2.5 and 50 mg/kg (from presymptomatic stage)	(i) Increased the motoneuron loss and lipid peroxidation, reduced survival time	[199]
NOX	SOD1 ^{G93A} transgenic mice	Deletion of NOX	(i) Slowed disease progression and prolonged survival time	[112, 113]
	MO59] glial cells and SH-SY neuronal cells overexpressing mutant SOD1	100 μM	(i) Decreased O ₂ ⁻ levels and increased cell viability	[114]
Apocynin	SOD1 ^{G93A} transgenic mice	30, 150, and 300 mg/kg/day (from 2 weeks of age)	(i) Decreased ROS levels, increased neurons in the spinal cord, prolonged survival time, and slowed disease progression	[114]
	SOD1 ^{G93A} transgenic mice	300 mg/kg/day (from 21 days of age)	(i) Failed to significantly prolong survival time	[205]
AEOL10150	Cocultured hESC-derived motor neurons with human primary astrocytes expressing SOD1 ^{G37R}	300 μM (48 h pretreatment)	(i) Prevented motor neuron loss (ii) Decreased ROS levels	[203]
	SOD1 ^{G93A} transgenic mice	Initial dose of 5.0 mg/kg and a maintenance dose of 2.5 mg/kg/day i.p. (from the onset of the disease)	(i) Reduced oxidative stress, enhanced motor performance, prevented motor neuron loss, prolonged survival time	[210]
	SOD1 ^{G93A} transgenic mice	2.5 mg/kg/day i.p. (from the onset of the disease)	(i) Reduced astrogliosis, prevented motor neuron loss, prolonged survival time	[211]
Edaravone	SH-SY5Y cells	25 μM (8 h)	(i) Reduced H ₂ O ₂ -induced cell death	[218]
	SOD1 ^{G93A} transgenic mice	5 mg/kg/day and 15 mg/kg/day i.p. (from the onset of the disease)	(i) Slowed motor decline, prevented motor neuron loss, slowed disease progression	[224]

TABLE 2: Continued.

Antioxidant	Preclinical animal or cellular model/ clinical trial	Dose/concentration (treatment time)	Effects	Reference
	SOD1 ^{H46R} transgenic rats	1.5 or 3.0 mg/kg/h i.v. continuous infusion (1 h per day) for 2 days, followed by a 2-day holiday (y from 18 weeks of age to the day of loss of righting reflex)	(i) Improved motor function	[223]
	Open-label phase II	30 mg or 60 mg/day i.v. (6 months) two weeks of administration followed by a two-week observation period (4 weeks cycle repeated six times)	(i) Slowed disease progression (using ALSFRS-R) (ii) Reduced 3-NT levels in cerebrospinal fluid	[225]
	RCT, phase III, NCT00330681	60 mg/day i.v. during 60 min (24-week treatment)	(i) Did not significantly reduce the ALSFRS-R score. Significant differences observed when analyzing a subgroup of patients (scored of at least 2 points on all 12 items of ALSFRS-R, forced vital capacity of 80% or more, disease duration of 2 years or less)	[213]
	RCT, phase III, NCT01492686	60 mg/day i.v. during 60 min (24-week treatment)	(i) Slowed disease progression (using ALSFRS-R) in a well-defined population of ALS patients	[5]
	Mixed mouse cortical culture	30 or 100 μ M (30 min treatment)	(i) Blocked phorbol 12-myristate	[233]
	Cortical cultures	1-30 μ M (24 h treatment)	(i) Attenuated neuronal death induced by 30 μ M kainate or NMDA, but not that by 100 μ M NMDA (ii) Attenuated nonexcitotoxic oxidative injury induced by exposure to FeCl ₃ in the presence of MK-801 and CNQX	[234]
Riluzole	Rats	21.35 μ mol/kg (every two days, lasting for 4 weeks)	(iii) Reduced Fe ³⁺ -induced lipid peroxidation, and inhibited cytosolic phospholipase A2 (i) Antagonized methylmercury-induced oxidative through elevation of GSH synthesis by activating of glutamate transporters	[235]
	Human SH-SY5Y neuroblastoma cells	1-10 μ M	(i) Counteracted the effects of H ₂ O ₂ exposure (ii) Demonstrated direct antioxidant defense capacities against acute oxidative, but not on nitrosative stress	[236]
	SOD1 ^{G93A} model, the TDP-43 ^{A315T} model, and FUS (1-359) model	22 mg/kg (in drinking water from symptom onset)	(i) Had no significant benefit on lifespan in any of the ALS mouse models tested	[237]
	NAD ⁺ /SIRT1 modulators			

TABLE 2: Continued.

Antioxidant	Preclinical animal or cellular model/ clinical trial	Dose/concentration (treatment time)	Effects	Reference
NMN and NR	SOD1 ^{G93A} mice astrocytes	5 mM (24 h pretreatment)	Increased total and mitochondrial NAD ⁺ content in, increased oxidative resistance and reversal of astrocyte toxicity towards cocultured motor neurons	[248]
NR	SOD1 ^{G93A} transgenic mice	400 mg/kg/day	NR supplementation delayed motor neuron degeneration, decreased markers of neuroinflammation in the spinal cord, modified muscle metabolism, and prolonged survival time	[249]
EH301	RCT, NCT03489200	1200 mg (4 months)	Slowed the progression of ALS (using ALSFRS-R)	[253]
Mitochondria-Targeted Antioxidants				
MitoQ	SOD1 ^{G93A} rat astrocytes	10–100 nM (24 h pretreatment)	Reduced nitrooxidative stress and mitochondrial dysfunction. Restored motor neuron survival in cocultures	[264]
	SOD1 ^{G93A} motor neurons	1–10 pM (48 h pretreatment)	Prevented NGF-induced neuron loss	[268]
	SOD1 ^{G93A} transgenic mice	500 μM (from 90 days of age)	Slowed decline of mitochondrial function, reduced nitrooxidative markers and pathological signs in the spinal cord, neuromuscular junctions were recovered associated with a significant increase in hindlimb strength, prolonged survival time	[265]
Mito-CP	SOD1 ^{G93A} rat astrocytes	10–100 nM (24 h pretreatment)	Reduced nitrooxidative stress and mitochondrial dysfunction. Restored motor neuron survival in cocultures	[264]
	SOD1 ^{G93A} motor neurons	100–1000 pM (48 h pretreatment)	Prevented NGF-induced neuron loss	[268]
	N2a cells overexpressing SOD1 ^{G93A}	1, 10, or 100 μM (6 h pretreatment)	Reduced H ₂ O ₂ -induced cell death	[269]
SS-31	SOD1 ^{G93A} transgenic mice	5 mg/kg/day i.p. (from 30 days of age)	Decreased cell loss, decreased markers of oxidative stress in the lumbar spinal cord, improved motor function, and prolonged survival time	[269]

RTC: double-blind randomized controlled trial; mROS: mitochondrial ROS production; s.c: subcutaneous; p.o: oral; i.p: intraperitoneal; i.v: intravenous; WN1316:2-[methyl(methylamino)-N-(4-(pyridin-2-yl)-1H-imidazol-2-yl) acetamide trihydrochloride; CDDO-EA: 2-cyano-3,12-dioxooleana-1,9-dien-28-oic acid ethylamide; CDDO-TFEA:2-cyano-3,12-dioxooleana-1,9-dien-28-oic acid trifluoroethylamide; EGCG: epigallocatechin-3-gallate; RPPX: dextraprimipexole; NOX: nicotinamide adenine dinucleotide phosphate oxidase; ROS: reactive oxygen species; AEOL10150: manganese [III] tetrakis[N,N'-diethylimidazolium-2-yl]porphyrin; Edaravone: 3-methyl-1-phenyl-2-pyrazolin-5-one; ALSFRS-R: revised ALS functional rating scale; 3-NI: 3-nitrotyrosine; NMDA: N-methyl-D-aspartate; CNQX: 6-cyano-7-nitroquinoxaline-2,3-dione; MK-801: (5R,10S) (+)-5-methyl-10,11-dihydro-5H-dibenzo[ad]cyclohepten-5, 10-imine hydrogen maleate; MitoQ: [10-(4,5-dimethoxy-2-methyl-3,6-dioxo-1,4-cyclohexadien-1-yl)decyl]triphenylphosphonium methane sulfonate; Mito-CP: mitochondria-targeted carboxy-proxyl; SS-31: cell-permeable peptide antioxidant D-ArgDmt-Lys-Phe-NH₂; NMN and NR: nicotinamide mononucleotide and nicotinamide riboside.

literature and may represent a therapeutic target for ALS and other neurological disorders [166]. In fact, the overexpression of Nrf2 in astrocytes in coculture protects motor neurons from SOD1^{G93A} toxicity, increasing the amount of GSH secreted by astrocytes [167]. Crossing SOD1^{G93A} mice with mice overexpressing Nrf2 selectively in astrocytes significantly delayed disease onset and extended survival of SOD1^{G93A} transgenic mice [167], making Nrf2 a possible therapeutic target in ALS. However, contrary to what was expected, Guo et al. [168] reported a slight impact of the Nrf2 knockout on the course of disease in SOD1^{G93A} mice. These authors also demonstrated that the elimination of Nrf2 only affected NQO1, among different Nrf2-regulated phase II enzymes, leaving it an open question whether Nrf2-mediated neuroprotection is a key mechanism to prevent ALS neurodegeneration [168].

Pharmacological targeting of Nrf2/ARE pathways has been proposed as a therapeutic strategy against neurodegenerative disorders, including ALS, since it helps neuronal cells to cope with OS [169]. One example is the case of the novel acylaminoimidazole derivative, 2-[mesityl(methyl)amino]-N-[4-(pyridin-2-yl)-1H-imidazol-2-yl] acetamide trihydrochloride (WN1316) that proved to upregulate Nrf2 and regulate GSH, protecting motor neurons against OS [170] (Figure 3). The oral administration of WN1316 (1-100 µg/kg/day) improved mice motor function and extended the survival of SOD1^{H46R} and SOD1^{G93A} mice [170] (Table 2). Additionally, transgenic mice treated with WN1316 showed reduced oxidative damage to neuronal cells and preserved integrity of the skeletal muscle together with the suppression of astrocytosis and microgliosis in the spinal cord [170]. Although the molecular mechanism of WN1316 is not yet completely understood, the activation of the Nrf2 signaling pathway is thought to take part in this process. Phase I clinical trials of WN1316 (UMIN000015054) were completed in early 2015, but results were not published so far (https://upload.umin.ac.jp/cgi-open-bin/ctr_e/ctr_view.cgi?recptno=R000017516; accessed on 23 July 2020).

Curcumin, a natural and liposoluble dye obtained from turmeric is another compound that modulates the Nrf2 pathway [166] (Figure 3). Curcumin was shown to activate the Nrf2 pathway in primary spinal cord astrocytes, attenuating oxidative damage and mitochondrial dysfunction [171]. Additionally, to these beneficial effects, curcumin was also shown to bind to the prefibrillar aggregates of SOD1 and alter their amyloidogenic pathway, alleviating cytotoxicity [172]. Dimethoxy curcumin improved mitochondrial dysfunction in NSC-34 cell line transfected with human M337V or Q331K mutant TDP-43, suggesting that this compound can be useful to treat neurodegenerative diseases linked with mutated TDP-43 [173]. The oral administration of 80 mg/day nanocurcumin (SinaCurcumin) in a pilot randomized clinical trial using 54 sALS patients during 12 months showed a general improvement in the survival of ALS patients, especially those with bulbar involvement (<https://en.irct.ir/trial/11697>) [174]. Moreover, in a double-blind clinical trial, curcumin oral supplementation (600 mg/day, Brainoil) in 42 ALS patients during 6 months resulted in a decrease in ALS progression,

improvement of aerobic metabolism, and a reduction of oxidative damage [175] (Table 2). Despite these beneficial effects, curcumin chemical instability, low oral bioavailability, and low water solubility constitute an obstacle that has to be overcome during the development of drug delivery systems based on this compound [176, 177].

Adding to the list of Nrf2 modulators, two triterpenoids, CDDO (2-cyano-3, 12-dioxooleana-1,9-dien-28-oic acid) ethylamide (CDDO-EA) and CDDO-trifluoroethylamide (CDDO-TFEA), were also described to activate Nrf2/ARE in SOD1^{G93A} mouse model as well as in a cell culture model of ALS [178]. The treatment of NSC-34 cells with CDDO-TFEA upregulated Nrf2 and resulted in translocation of Nrf2 into the nucleus (Figure 3). The administration of CDDO-EA and CDDO-TFEA at a presymptomatic age enhanced motor performance and extended the survival of SOD1^{G93A} mice, while at a symptomatic age, it only slowed disease progression [178] (Table 2), suggesting that the activation of the Nrf2/ARE signaling pathway may be a useful strategy in the treatment of ALS especially when administered early in the course of the disease.

Another relevant compound is S(+)-apomorphine, a nonselective dopamine agonist and an activator of the Nrf2/ARE pathway, which has shown the capacity to reduce pathological OS and to improve survival following an oxidative insult in fibroblasts from ALS patients [179]. S(+)-apomorphine also attenuated motor dysfunction and slowed disease progression in SOD1^{G93A} mice, when administered at 5 mg/kg/day (Table 2) [179]. Another candidate is the green tea polyphenol epigallocatechin-3-gallate (EGCG), a known Nrf2 inducer [180] (Figure 3), that crosses the BBB [181] and that partially protected a motor neuronal cell line expressing SOD1^{G93A} from H₂O₂-induced cell death [182]. Oral administration of EGCG (2.9-10 mg/Kg/day) from a presymptomatic stage significantly delayed the onset of disease and extended life span in SOD1^{G93A} mice (Table 2) [183, 184].

3.5. Dexpramipexole. Dexpramipexole (RPPX) is the R(+) enantiomer of pramipexole, used in Parkinson's disease, also tested in ALS patients [185, 186]. Dexpramipexole is a lipophilic cation that concentrates into mitochondria, scavenging reactive oxygen and nitrogen species (Figure 3). It was shown to prevent cell death in glutathione-depleted neuroblastoma cells [187, 188] and to block caspase activation in SH-SY5Y neuroblastoma cells treated with methylpyridinium ion (MPP⁺), which induces Parkinson's disease-like neurodegeneration [189]. Treatment with RPPX (100 mg/Kg) in SOD1^{G93A} transgenic mice was shown to prolong survival and preserve motor function [187]. Two-phase I clinical studies in 54 healthy volunteers found that RPPX was safe and well-tolerated in doses up to 150 mg twice a day for 4.5 days [190]. Dexpramipexole (300 mg/day or 50 mg/day for 24 weeks) showed beneficial effects on functional decline and survival in a phase II study in 102 subjects with ALS [191] making it an interesting candidate to include in a multidrug approach for the treatment of ALS. However, in the phase III trial (NCT01281189) with RPPX (150 mg twice daily) in 943 people with ALS, this compound failed to show

any efficacy on functional and survival assessment, when compared with placebo control (Table 2) [192]. Considering the discrepant outcomes, Vieira et al. [193] reassessed the effect of RPPX (200 mg/kg) in SOD1^{G93A} transgenic mice but did not recognize any beneficial effects (Table 2). The authors in the latter study argued the lack of balance for sex, age, and weight could justify the previous discrepant results with the same ALS mice model [193].

3.6. Melatonin. Melatonin (N-acetyl-5-methoxytryptamine) is a neurohormone secreted by the pineal gland, which has ROS scavenging activity, as well as amphiphilic properties that allow its entrance into both lipophilic and hydrophilic cellular environments [194] (Figure 3). Due to melatonin's antioxidant properties, it has been tested as an experimental drug in different neurodegenerative diseases linked to excessive ROS levels [195]. Besides being a potent free radical scavenger, melatonin also enhances cellular antioxidant potential by stimulating the expression of antioxidant enzymes including SOD, GPx, and GR and by augmenting GSH levels [196]. It was also described that melatonin preserves mitochondrial homeostasis, attenuating free radical generation and promoting mitochondrial ATP synthesis by stimulating the activity of complexes I and IV [197].

In SOD1^{G93A}-transgenic mice, the oral administration of melatonin (57–88 mg/kg/day) at a presymptomatic stage delayed disease progression and extended survival [54] (Table 2). The same authors also showed that the rectal administration of 300 mg/day melatonin to 31 sALS patients was well tolerated during an observation period of up to 2 years, reducing circulating serum protein carbonyls, however, without showing any evidences of upregulation of genes encoding antioxidant enzymes [54]. The attenuation of oxidative damage in ALS upon melatonin treatment proved to be safe in humans and suggested the need for further clinical trials to clarify the neuroprotective effect of melatonin in ALS.

More recently, Zhang et al. [198] showed that the administration of melatonin (30 mg/kg) to presymptomatic SOD1^{G93A}-transgenic mice significantly delayed disease onset, neurological deterioration, and mortality, which were associated to the inhibition of the caspase-1/cytochrome *c*/caspase-3 pathways and to the reduction of melatonin receptor 1A protein expression. In contrast, Dardiotis et al. [199] showed that the intraperitoneal administration of melatonin (0.5, 2.5, and 50 mg/kg) to presymptomatic SOD1^{G93A}-transgenic mice reduced their survival. These authors also reported that, compared to untreated animals, mice treated with melatonin presented an increase in motoneuron loss and in the levels of 4-HNE, a marker of lipid peroxidation, as well as an upregulation of SOD1 expression, suggesting that melatonin exacerbates the disease phenotype in the SOD1^{G93A} mouse ALS model (Table 2), by upregulating toxic SOD1, that overrides its antioxidant and antiapoptotic effects [199]. The fact that the upregulation of mutSOD1 in the SOD1^{G93A} ALS mouse model can influence the beneficial effect of melatonin raises the possibility that this animal model may not be ideal for assessing the neuroprotective properties of melatonin or other molecules with complex

antioxidative properties because ALS progression does not always involve SOD1 mutation. Further studies need to be done to understand the mechanisms of action of melatonin and if its antioxidant and antiapoptotic effects can be translated into beneficial effects at the clinical level.

3.7. NOX Inhibition. NOX is one of the most important enzymes that regulate ROS production in the CNS, and increasing evidence is showing that NOX inhibition improves neurological disease conditions [200, 201]. In the particular case of ALS, the inactivation of NOX in SOD1^{G93A} transgenic mice has shown to slow disease progression and improve survival [112, 113]. Pharmacological inhibition of NOX using apocynin, a natural organic compound also known as acetovanillone [202] (Figure 3), decreased O₂^{•-} levels and increased cell viability in MO59J human glioblastoma cells expressing mutSOD1 [114] and decreased ROS levels in primary astrocytes expressing mutSOD1, also restoring motor neuron survival in cocultured hESC-derived motor neurons with human primary astrocytes expressing SOD^{G37R} [203] (Table 2). However, apocynin-mediated NOX inhibition is indirect, involving the presence of myeloperoxidase (MPO) together with H₂O₂. These two elements promote the dimerization of apocynin that consequently oxidizes thiols in NOX, being the formation of apocynin dimers necessary to inhibit NOX activity, and not occurring in cells devoid of MPO [204].

Similar to other neurodegenerative diseases, apocynin has been tested in the ALS animal models. In the SOD1^{G93A} transgenic mice, apocynin (30, 150, and 300 mg/kg/day) blocked ROS production, increased the number of neurons in the spinal cord, and prolonged life span compared to wild-type mice [114]. However, Trumbull et al. [205] showed that the administration of apocynin (300 mg/kg/day) had a limited benefit to SOD1^{G93A} mice (Table 2). Although the reasons for this discrepancy have not been clarified, these authors suggested that it could be due to the interference of antibiotics, gender, or the drift in the genetic background resultant from breeding for multiple generations [205]. However, the fact that the treatments with apocynin in mice frequently led to fatal eye infections [113, 114] points to some safety issues regarding this NOX inhibitor. Treatments with apocynin in humans have not been extensively studied; however, some studies were performed in asthmatics receiving nebulized apocynin [206]. Further studies are needed to clarify the functional specificity of apocynin on NOX isomers and to determine a functional dose for therapeutic use. Taking into consideration that mitochondrial ROS and NOX-derived ROS are interrelated, and that an increase in one might lead to the increase in the other [207], the role of NOX-derived ROS production in neurodegenerative diseases needs to be further explored, as a possible strategy of treatment in ALS.

3.8. AEOL 10150. AEOL 10150 (manganese [III] tetrakis[N-N'-diethylimidazolium-2-yl]porphyrin) is a manganese porphyrin antioxidant developed by US Aeolus Pharmaceuticals that possesses SOD- and CAT-like activity [208] (Figure 3), being capable of neutralizing O₂^{•-}, H₂O₂, and peroxytrinitrite,

and inhibiting lipid peroxidation [209]. The administration of AEOL-10150 at the onset of symptoms markedly prolonged survival in SOD1 transgenic mice [210, 211]. AEOL-10150 decreased 3-nitrotyrosine (3-NT) and malondialdehyde levels in the spinal cord, extended animal survival, provided better preservation of motor neuron architecture, and decreased the level of astrogliosis when administered to ALS mice at symptom onset (at an initial dose of 5.0 mg/kg and a maintenance dose of 2.5 mg/kg/day) [211]. In addition, the use of AEOL-10150 (2.5 mg/kg/day), alone or combined with histone deacetylase inhibitor phenylbutyric acid, was found to significantly enhance motor function and prolong survival [210] (Table 2). Aeolus pharmaceuticals announced that AEOL-10150 was safe and well tolerated in 40 ALS patients and 9 healthy subjects (<https://www.accesswire.com/475614/AEOLUS-AEOL-10150-is-Safe-and-Well-Tolerated-in-Phase-1-Study-in-Healthy-Subjects>, accessed on 23 July 2020). The same pharmaceutical company also reported that multiple doses of AEOL 10150 up to 2 mg/kg/day over a period of 6.5 days were well tolerated by 12 ALS patients with no serious or clinically significant adverse events (<https://www.businesswire.com/news/home/20070322005176/en/Aeolus-Pharmaceuticals-Announces-Successful-Completion-Multiple-Dose>, accessed on 23 July 2020).

3.9. Edaravone. Edaravone, the active ingredient of Radicut®, is a free radical scavenger widely used in the treatment of cerebral ischemia in Japan [212–214]. Edaravone eliminates lipid peroxides and hydroxyl radicals during cerebral ischemia and exerts a protective effect on the neurons of patients [215, 216]. Although the detailed mechanism of edaravone action is not known, it was proposed that besides its radical scavenger effect, edaravone also inhibits the opening of mitochondrial permeability transition pore (mPTP) in the brain (Figure 3), which may contribute to its neuroprotective effect [217]. Other studies also showed that edaravone reversed the cytotoxic effects of H₂O₂ in SH-SY5Y neuroblastoma cells, increasing the expression of Prx2 [218], as an additional neuronal protection mechanism in response to OS. Edaravone also was also shown to promote the antioxidant defense mechanisms by increasing Nrf2, GPx, SOD, HO-1, and NQO1 protein contents (Figure 3), attenuating the effects of traumatic brain injury [219]. In addition, part of the beneficial effects of edaravone can be attributed to its anti-inflammatory capacity [219], which adds to its protective effects in neurons, microglia [220], astrocytes [221], and oligodendrocytes [222].

Preclinical studies demonstrated that edaravone (ranging from 1.5 to 15 mg/kg) improves motor function, slows symptom progression, and attenuates motor neuron degeneration in transgenic SOD1 rodent models of ALS (Table 2) [223, 224].

In an open-label phase II study of 20 patients with ALS, the intravenous administration of edaravone (30 mg or 60 mg/day) was shown to be safe and well-tolerated, slowing disease progression as measured by the revised ALS functional rating scale (ALSFRS-R) score during the six-month treatment period, compared with the six months before the administration of edaravone [225]. Additionally, the same

clinical trial also showed that all patients presented a marked reduction in 3-NT in CSF to almost undetectable values, at the end of the six-month treatment period (Table 2) [225], suggesting that the progression delay may be related to the attenuation of OS in ALS patients. A confirmatory double-blind, placebo-controlled study of edaravone in 206 ALS patients (102 edaravone group and 104 placebo group) demonstrated a nonsignificant reduction of ALSFRS-R score in patients receiving edaravone over a 24-week treatment period, and the efficacy of edaravone for the treatment of ALS was not demonstrated (NCT00330681) [213]. However, when analyzing only a subgroup of ALS patients (137 patients: 68 edaravone group, 66 placebo group) with scores of 2 or more on all items of ALSFRS-R, forced vital capacity of 80% at baseline, and disease duration of 2 years or less, significant differences were observed in the ALSFRS-R score after treatment with edaravone (60 mg intravenous) compared with placebo, suggesting a potential benefit of edaravone in a well-defined subset of ALS patients (NCT01492686, Table 2) [5]. Additionally, in the open-label 24-week extension period, edaravone maintained its beneficial effects throughout 48 weeks in ALS patients, with no new or cumulative safety concerns (NCT01492686) [226].

Currently, edaravone is approved for use as a treatment for ALS in Japan and South Korea, having been also approved by the FDA in May 2017 [227], although its mechanism of action remains unclear. A phase I trial of an oral formulation of edaravone (TW001) developed by the Treeway company has returned positive results, proving to be safe and well-tolerated with the oral formulation (<http://www.cphi-online.com/treeway-announces-positive-data-from-two-separate-news038315.html>, accessed on 23 July 2020). Two recent clinical trials, sponsored by Mitsubishi Tanabe Pharma Development America, Inc., are in progress to evaluate the pharmacokinetics of single doses of edaravone oral suspension in ALS patients with gastrostomy (NCT04254913, phase I), as well as to evaluate the long-term safety and tolerability of oral edaravone in subjects with ALS over 24 and 48 weeks (NCT04165824, phase III).

3.10. Riluzole. Riluzole is a benzothiazole with antiglutamergic properties which has shown a modest survival benefit (about 3 months) in patients at a dosage of 100 mg/day without showing any effect in muscle strength [228, 229]. Although the precise neuroprotective mechanisms of riluzole are not completely understood, it has been proposed that it has multiple effects beyond the inhibition of glutamate release in presynaptic terminals through the blockage of voltage-gated sodium channels [230]. It has been demonstrated that riluzole also affects the chloride, calcium, and potassium channels and interferes with intracellular events that follow transmitter binding at excitatory amino acid receptors [230, 231], which can include OS [232]. However, other studies have also evidenced some antioxidant properties of this compound, mediated by the inhibition of protein kinase C [233] and phospholipase A activities [234] that consequently attenuate a broad spectrum of oxidative damage. Consistent with its antioxidative effects, it is also been shown that riluzole also decreases methylmercury-induced OS by

promoting the elevation of GSH synthesis through the activation of glutamate transporters and the increase of intracellular glutamate levels, which is a GSH precursor [123, 235]. Based on these different studies, it is possible that the beneficial effect of riluzole may be due to a combined action on different targets that still remain largely unclear. Thus, although riluzole treatment prevents cell death and controls increased ROS levels in parental SH-SY5Y cells, it was shown to be ineffective in reversing ROS effects in SH-SY5Y cells carrying the G93A SOD1 mutation [236], suggesting that riluzole is unable to reverse chronic oxidative damage. This situation is in agreement with the fact that this compound does not present significant benefit on lifespan and motor performance in SOD1^{G93A} transgenic mice [237]. The fact the riluzole has a direct antioxidant effect against acute OS, but not against RNS [236], also supports the hypothesis that combined treatment with edaravone may be more effective in treating ALS, since edaravone has the capacity to reduce RNS [225, 238].

3.11. NAD⁺/SIRT1 Modulators. NAD⁺ plays a key role in many redox reactions in the cells, being involved in many processes including signaling pathways, gene expression, DNA repair, and mitochondrial metabolism [239]. NAD⁺ is also a cosubstrate for sirtuins (SIRT's), a family of signaling proteins involved in the regulation of cellular metabolic status, playing a key role in several processes such as mitochondrial function, DNA repair, and also activating metabolic pathways responsible for the detoxification of ROS (e.g., SOD, CAT, and isocitrate dehydrogenase 1) [240]. Sirtuins regulate peroxisome proliferator-activated receptor gamma coactivator 1-alpha (PGC1 α), which affects mitochondrial biogenesis, activity, and dynamics [241, 242] and is considered a promising therapeutic target for ALS [243]. Decreased SIRT1 levels have been found in postmortem tissues from ALS patients [244] and intraperitoneal injection of the SIRT1 activator resveratrol resulted in a significant improvement in both symptoms and survival of SOD1^{G93A} mice [245]. In addition, SIRT3 was reported to protect against mitochondrial fragmentation and neuronal cell death induced by SOD1^{G93A} overexpression in cultured rat spinal cord motor neurons [246].

Therapeutic strategies based on NAD⁺ precursors, including nicotinamide (NAM), nicotinic acid (NA), nicotinamide riboside (NR), and nicotinamide mononucleotide (NMN), [247] have been proposed in ALS [248] (Figure 3). NMN and NR (5 mM for 24 h) were shown to increase total and mitochondrial NAD⁺ content in astrocytes from SOD^{G93A} mice, which was associated with an increase in OS resistance and reversal of astrocyte toxicity towards cocultured motor neurons [248] (Table 2). The effects of modulation of NAD⁺ availability in SOD1^{G93A} mice were also tested, using two strategies: supplementation with NR and ablation of a NAD⁺-consuming enzyme (CD38) [249]. NR was found to delay motor neuron degeneration, whereas CD38 ablation was not protective [249]. The same study also found that the expression of NMNAT2 (nicotinamide mononucleotide adenylyl transferase 2, involved in NAD⁺ synthesis) and SIRT6 was decreased in the spinal cord of ALS

patients, suggesting a deficit of this neuroprotective pathway in humans and highlighting the therapeutic potential of increasing NAD⁺ levels in ALS [249]. Since NAD⁺ supplementation is known to promote neural stem cells/neuronal precursor cells (NSCs/NPCs) pool maintenance, another study wanted to determine if the administration of NR could enhance the proliferation and migration of NSCs/NPCs in ALS [250]. SOD1^{G93A} transgenic and wild-type mice were treated with 400 mg/kg/day, starting at 50 days of age, which was found to improve the adult neurogenesis in the brain of SOD1^{G93A} mice [251]. This was associated with the activation of mitochondrial unfolded protein response (UPR^{mt}) signaling and modulation of mitochondrial proteostasis, which can ameliorate misfolded protein accumulation. Increasing total NAD⁺ content in astrocytes using NMN (5 mM and 24 h) was reported to induce the activation of Nrf2 and upregulation of the antioxidant proteins HO-1 and sulfiredoxin 1 (SRXN1), mediated by SIRT6 [252].

A clinical trial based on modulation of NAD⁺/sirtuins in ALS used EH301, which is a combination of two active compounds (1-(beta-D-ribofuranosyl)nicotinamide chloride and 3,5-dimethoxy-4'-hydroxy-trans-stilbene) from Elysium Health, that were proposed to act synergistically to increase NAD⁺ levels and support SIRT activity [253]. This was a single-center, prospective, double-blind, randomized, placebo-controlled pilot study (NCT03489200), in which the efficacy of EH301 (1200 mg) was tested in ALS patients. The results of this trial showed that EH301 significantly slowed the progression of ALS compared to placebo, also showing improvements in several key outcome measures compared with baseline [253] (Table 2). A phase II clinical trial has been planned to expand the scope of the original trial with EH301, using over-the-counter antioxidants such as CoQ10, vitamin E, NAC, and L-cystine at safe dosages (NCT04244630). This study is expected to be completed in December 2021.

3.12. Mitochondria-Targeted Antioxidants. The mitochondria-targeted antioxidant 10-(60-ubiquinonyl) decyltriphenylphosphonium (MitoQ) comprises a triphenylphosphonium (TPP) functional group conjugated to an ubiquinone antioxidant moiety [254]. MitoQ crosses biological membranes, accumulates inside mitochondria driven by the transmembrane electric potential [255], and effectively prevents mitochondrial oxidative damage [254, 256] (Figure 3). Within mitochondria, the ubiquinone moiety of MitoQ is reduced to its active ubiquinol form, protecting mitochondria against oxidative damage that could be derived from the leakage of electrons [256]. Reactions with a variety of oxidants readily oxidize ubiquinol to ubiquinone, which is quickly reduced back to ubiquinol by the respiratory chain [257] and is thus continually recycled. A protective effect of MitoQ was described in chronic hepatitis C patients, by decreasing liver damage [258], as well as in some neurodegenerative diseases, including Parkinson's [259, 260] and Alzheimer's [261, 262] diseases, by decreasing the oxidative damage. However, very disappointing results were obtained when MitoQ was used in a phase II clinical trial for the treatment of Parkinson's disease (NCT00329056-Antipodean Pharmaceuticals, Inc.)

[263]. Despite these negative results, MitoQ treatment reduced nitroxidative stress and mitochondrial dysfunction in SOD1^{G93A}-expressing astrocytes, reducing the toxicity to motor neurons in cocultures [264]. Also, the administration of MitoQ (500 μ M) improved the ALS phenotype in the SOD1^{G93A} mice, slowing the decline of mitochondrial function in both the spinal cord and quadriceps muscle and increasing the life span of affected animals [265]. Importantly, the same authors also described a marked reduction of nitroxidative markers and pathological signs in the spinal cord of MitoQ-treated animals, as well as the recovering of the neuromuscular junctions associated with a significant increase in hindlimb strength [265] (Table 2). These results, associated to the fact that MitoQ rapidly crosses the BBB [261] and is well-tolerated in both animals and humans [258], with nausea as the most common side effect [266], pointed out mitochondria-directed antioxidants as a possible strategy to delay ALS symptoms, that deserves to be further developed.

Another mitochondria-targeted antioxidant tested in ALS models was the mitochondria-targeted carboxy-proxyl (Mito-CP), which also comprises TPP cation covalently coupled to carboxy-proxyl nitroxide and, similarly to MitoQ, accumulates into the mitochondria [267]. Low doses of Mito-CP (1-10 nM) effectively prevented the death of motor neurons expressing SOD1^{G93A} induced by nerve growth factor (NGF), which involved an increase in mitochondrial O₂^{•-} [268] (Figure 3), and also avoided mitochondrial dysfunction in SOD1^{G93A} astrocytes, decreasing O₂^{•-} levels, and restoring motor neuron survival [264] (Table 2). However, additional studies should be performed with other types of mitochondriotropic compounds, with lower toxicity and higher therapeutic efficacy.

The cell-permeable antioxidant peptide SS31 (D-Arg-Dmt-Lys-Phe-NH₂), which targets the IMM and protects against mitochondrial oxidative damage (Figure 3), was also tested by Petri et al. [269] in *in vitro* and *in vivo* models of ALS associated with SOD1^{G93A} mutations. These authors showed that SS-31 (1 μ M) protected cells against cell death induced by H₂O₂ in N2a mouse neuroblastoma cells transfected either with wild type or mutSOD1. The administration of SS-31 (5 mg/kg/day) to SOD1^{G93A} mice at the presymptomatic stage led to decreases in cell loss, lipid peroxidation and protein nitration (4-HNE and 3-NT) markers in the lumbar spinal cord. Moreover, it significantly improved the survival and motor performance compared to controls [269] (Table 2). The capacity of SS-31 to inhibit the mPTP and cytochrome *c* release induced by the addition of calcium in isolated liver mitochondria [270], and its ability to protect against the loss of mitochondrial potential, and apoptosis induced by tert-butyl hydroperoxide in N2A and SH-SY5Y cells [271], suggests that this antioxidant can be a very interesting therapeutic strategy to treat neuronal damage in ALS, and this needs to be explored in the future.

4. Conclusions

Several studies have been adding strong evidence to the role of OS mechanisms in ALS that culminate in mitochondrial

dysfunction and cell damage and contribute to neurodegeneration. If it is accepted that the excessive ROS production is a common pathological feature in ALS patients, there are doubts whether oxidative damage represents a primary cause or a secondary consequence of this disease and what is the real contribution of OS in ALS progression, considering the different subtypes of patients. Although the mechanisms of OS and mitochondrial dysfunction represent promising therapeutic targets to slow the disease progression, it is of utmost importance to characterize the different OS profiles present in different types of patients (e.g., identify different OS mechanisms associated with different mutations), in order to develop personalized therapies that allow retarding the progression of the disease according to the OS profiles of patients.

Although several antioxidants have shown beneficial effects in ALS animal models, they have failed to show any meaningful therapeutic benefit in ALS patients. There are different reasons for the lack of beneficial effects of antioxidant therapies in ALS patients that should be considered in the future. Some reasons evidenced are the lack of proper blinding measurements, uniform exclusion criteria, or statistical power associated with the use of a small number of samples per group in animal assays that can lead to false-positive results and confounding biological results [272]. These issues should be avoided by following programmed experimental designs based on the guidelines for preclinical animal research in ALS [273]. Moreover, the low CNS bioavailability of some of the antioxidants may limit their pharmacological effects, being necessary to invest more in compounds that can cross the BBB. Another reason may be the fact that most antioxidants have been exclusively tested in mutSOD1 animal models, being the mutSOD1 representative of a small percentage of patients [274, 275]. To overcome this issue, it is necessary to invest more on the development of ALS models that can be representative of the different subtypes of this disease, which can support preclinical trials before proceeding to clinical trials. Preclinical trials using other animal models of the disease should be done in parallel with the common mutSOD1 models, including C9orf72 and TDP-43 mice models that represent the most prevalent mutation in ALS and the formation of ubiquitinated TDP-43 cytoplasmic inclusions that are expressed in the majority of patients, respectively [276, 277]. Although less characterized than the mutSOD1 models and with some construct validity limitations, both C9orf72 and TDP-43 mice models develop many features of ALS [276, 277] that can be of extreme usefulness in the future to complement the experiments with the traditional mutSOD1 models. Complementarily, the use of preclinical assays that are not based on specific mutations models should be considered, as for example the use of iPSCs from sALS and fALS patients (with or without specific mutations) that can be differentiated in MNs, astrocytes, and microglial cells [278] and represent a valuable tool for screening different compounds [279]. Another reason that can also explain this failure is the fact that these compounds have been generally tested in animal models in presymptomatic stages of the disease that do not represent the stage in which patients are diagnosed [274]. It is necessary to establish limits

of the disease progression, based on OS profiles, that allow understanding until what stage of the disease a certain compound may have any beneficial effect.

Among the different antioxidant strategies described in Section 3, there are two that should be explored in the future due to their capacity to control OS mechanisms and improve the mitochondrial function. The first example is the case of NAD⁺/SIRT1 modulators that have shown capacity to increase mitochondrial OS resistance and protect against mitochondrial dysfunction in ALS models, as well as to significantly slow the disease progression in ALS patients, tested in a phase I clinical trial (NCT03489200) [253]. To confirm these results, a clinical trial phase II is already planned, which is expected to be complete by the end of 2021 (NCT04244630). The second strategy of great importance is the development of mitochondria-targeted antioxidants that have shown a capacity to accumulate inside mitochondria, prevent mitochondrial oxidative damage, and attenuate mitochondrial dysfunction. Although the administration of MitoQ has shown very promising results in the SOD1^{G93A} mice by slowing the decline of mitochondrial function in both the spinal cord and quadriceps muscle, by recovering the neuromuscular junctions associated with a significant increase in hindlimb strength, and by increasing the life span of the affected animals [265], its disappointing results in a phase II clinical trial for the treatment of Parkinson's disease (NCT00329056-Antipodean Pharmaceuticals, Inc.) [263] evidenced also the necessity to develop other types of mitochondriotropic compounds, with lower toxicity and higher therapeutic efficacy that may afterwards be tested in ALS models.

Altogether, the present review shows the need to invest on the characterization of OS profiles which are representative of each subtype of patient, permitting the development of personalized therapies based on the differential OS mechanisms that characterize different subtypes of patients. This approach will allow understanding what are the characteristics of certain antioxidants that can have beneficial effects on different subtypes of patients and help to understand what is the disease progression window at which a compound may have beneficial effects.

Abbreviations

AEOL 10150: Manganese [III] tetrakis[N-N'-diethylimidazolium-2-yl]porphyrin
 ALS: Amyotrophic lateral sclerosis
 ALSFRS-R: Revised amyotrophic lateral sclerosis functional rating scale
 ANG: Angiogenin
 ARE: Antioxidant response element
 BBB: Blood-brain barrier
 C9orf72: Chromosome 9 open reading frame 72
 CAT: Catalase
 CD38: Cluster of differentiation 38 (NAD⁺-consuming enzyme)
 CDDO-EA: 2-Cyano-3, 12-dioxooleana-1,9-dien-28-oic acid ethylamide
 CDDO-TFEA: 2-Cyano-3, 12-dioxooleana-1,9-dien-28-oic acid-trifluoroethylamide

CNS: Central nervous system
 CoQ10: Coenzyme Q10
 CSF: Cerebrospinal fluid
 CYP: Cytochrome P450
 DPR: Dipeptide repeat
 EGCG: Epigallocatechin-3-gallate
 fALS: Familial amyotrophic lateral sclerosis
 FUS: Fused in sarcoma
 GPx: Glutathione peroxidase
 GR: Glutathione reductase
 GSH: Glutathione
 Keap1: Kelch ECH-associating protein 1
 H₂O₂: Hydrogen peroxide
 4-HNE: 4-Hydroxynonenal
 HO•: Hydroxyl radical
 HO-1: Heme oxygenase
 hnRs: Heterogeneous nuclear ribonucleoproteins
 IMM: Inner mitochondrial membrane
 IMS: Intermembrane mitochondrial space
 iPSCs: Induced pluripotent stem cells
 Keap1: Kelch ECH-associating protein 1
 MitoQ: 10-(60-Ubiquinonyl) decyltriphenylphosphonium
 Mito-CP: Triphenyl-phosphonium-carboxy-proxyl
 mPTP: Mitochondrial permeability transition pore
 mutSOD1: SOD1 mutation
 MM: Mitochondrial matrix
 MNs: Motor neurons
 MPO: Myeloperoxidase
 MPP⁺: 1-methyl-4-phenylpyridinium
 NA: Nicotinic acid
 NAC: N-Acetyl-L-cysteine
 NADPH: Nicotinamide adenine dinucleotide phosphate
 NAM: Nicotinamide
 NF-κB: Nuclear factor kappa-light-chain-enhancer of activated B cells
 NGF: Nerve growth factor
 NMN: Nicotinamide mononucleotide
 NMNAT2: Nicotinamide mononucleotide adenylyl transferase 2
 NOX: Nicotinamide adenine dinucleotide phosphate oxidase
 NPCs: Neuronal precursor cells
 NQO1: NAD(P)H quinone dehydrogenase 1
 NR: Nicotinamide riboside
 Nrf2: Nuclear factor erythroid -2-related factor 2
 NSCs: Neural stem cells
 3-NT: 3-Nitrotyrosine
 O₂^{•-}: Superoxide radical anion
 8-OHdG: 8-hydroxy-2'-deoxyguanosine
 OS: Oxidative stress
 PGC-1α: Peroxisome proliferator-activated receptor gamma coactivator 1-alpha
 Poly-GA: Poly-glycine-alanine
 Poly-GP: Poly-glycine-proline
 Poly-GR: Poly-glycine-arginine
 Poly-PA: Poly-proline-alanine
 Poly-PR: Poly-proline-arginine

PON:	Paraoxonase
Prxl:	Peroxiredoxin-1
Rac1:	Ras-related C3 botulinum toxin substrate 1
ROS:	Reactive oxygen species
RPPX:	Dexpropiprime
sALS:	Sporadic amyotrophic lateral sclerosis
SIRT:	Sirtuin
SOD1:	Cu ²⁺ /Zn ²⁺ superoxide dismutase type-1
SRXN1:	Sulfiredoxin 1
SS-31:	D-ArgDmt-Lys-Phe-NH ₂
TARDBP:	TAR DNA-Binding
TDP-43:	TAR DNA-Binding Protein 43
TPP:	Triphenylphosphonium
Trx:	Thioredoxin
UBQLN2:	Ubiquilin 2
UPRmt:	Mitochondrial unfolded-protein response
WN1316:	2-[mesityl(methyl)amino]-N-[4-(pyridin-2-yl)-1H-imidazol-2-yl] acetamide trihydrochloride.

Conflicts of Interest

The authors declare no competing financial interest.

Acknowledgments

This work was financed by the European Regional Development Fund (ERDF), through the COMPETE 2020-Operational Programme for Competitiveness and Internationalisation and Portuguese national funds via FCT-Fundação para a Ciência e a Tecnologia, under projects PTDC/MED-FAR/29391/2017, POCI-01-0145-FEDER-029391 (Mito4ALS), PTDC/BTM-SAL/29297/2017, POCI-01-0145-FEDER-029297 (MitoScreening), and UIDB/04539/2020.

References

- [1] F. Tafuri, D. Ronchi, F. Magri, G. P. Comi, and S. Corti, "SOD1 misplacing and mitochondrial dysfunction in amyotrophic lateral sclerosis pathogenesis," *Frontiers in Cellular Neuroscience*, vol. 9, p. 336, 2015.
- [2] S. Zarei, K. Carr, L. Reiley et al., "A comprehensive review of amyotrophic lateral sclerosis," *Surgical Neurology International*, vol. 6, no. 1, p. 171, 2015.
- [3] E. F. Smith, P. J. Shaw, and K. J. De Vos, "The role of mitochondria in amyotrophic lateral sclerosis," *Neuroscience Letters*, vol. 710, article 132933, 2019.
- [4] M. Tanaka, T. Sakata, J. Palumbo, and M. Akimoto, "A 24-week, phase III, double-blind, parallel-group study of edaravone (MCI-186) for treatment of amyotrophic lateral sclerosis (ALS) (P3.189)," *Neurology*, vol. 86, 2016.
- [5] The Writing Group Edaravone (MCI-186) ALS 19 Study Group et al., "Safety and efficacy of edaravone in well defined patients with amyotrophic lateral sclerosis: a randomised, double-blind, placebo-controlled trial," *The Lancet Neurology*, vol. 16, no. 7, pp. 505–512, 2017.
- [6] P. A. McCombe and R. D. Henderson, "Effects of gender in amyotrophic lateral sclerosis," *Gender Medicine*, vol. 7, no. 6, pp. 557–570, 2010.
- [7] P. N. Valdmanis and G. A. Rouleau, "Genetics of familial amyotrophic lateral sclerosis," *Neurology*, vol. 70, no. 2, pp. 144–152, 2008.
- [8] C. Ingre, P. M. Roos, F. Piehl, F. Kamel, and F. Fang, "Risk factors for amyotrophic lateral sclerosis," *Clinical Epidemiology*, vol. 7, pp. 181–193, 2015.
- [9] E. Lacorte, L. Ferrigno, E. Leoncini, M. Corbo, S. Boccia, and N. Vanacore, "Physical activity, and physical activity related to sports, leisure and occupational activity as risk factors for ALS: a systematic review," *Neuroscience and Biobehavioral Reviews*, vol. 66, pp. 61–79, 2016.
- [10] A. Al-Chalabi and O. Hardiman, "The epidemiology of ALS: a conspiracy of genes, environment and time," *Nature Reviews Neurology*, vol. 9, no. 11, pp. 617–628, 2013.
- [11] B. Yu and R. Pamphlett, "Environmental insults: critical triggers for amyotrophic lateral sclerosis," *Translational Neurodegeneration*, vol. 6, no. 1, p. 15, 2017.
- [12] K. Boylan, "Familial amyotrophic lateral sclerosis," *Neurologic Clinics*, vol. 33, no. 4, pp. 807–830, 2015.
- [13] M. DeJesus-Hernandez, I. R. Mackenzie, B. F. Boeve et al., "Expanded GGGGCC hexanucleotide repeat in noncoding region of C9ORF72 causes chromosome 9p-linked FTD and ALS," *Neuron*, vol. 72, no. 2, pp. 245–256, 2011.
- [14] A. E. Renton, E. Majounie, A. Waite et al., "A hexanucleotide repeat expansion in C9ORF72 is the cause of chromosome 9p21-linked ALS-FTD," *Neuron*, vol. 72, no. 2, pp. 257–268, 2011.
- [15] H. X. Deng, A. Hentati, J. A. Tainer et al., "Amyotrophic lateral sclerosis and structural defects in Cu,Zn superoxide dismutase," *Science*, vol. 261, no. 5124, pp. 1047–1051, 1993.
- [16] S. J. Kaur, S. R. McKeown, and S. Rashid, "Mutant SOD1 mediated pathogenesis of amyotrophic lateral sclerosis," *Gene*, vol. 577, no. 2, pp. 109–118, 2016.
- [17] D. R. Rosen, T. Siddique, D. Patterson et al., "Mutations in Cu/Zn superoxide dismutase gene are associated with familial amyotrophic lateral sclerosis," *Nature*, vol. 362, no. 6415, pp. 59–62, 1993.
- [18] M. Synofzik, D. Ronchi, I. Keskin et al., "Mutant superoxide dismutase-1 indistinguishable from wild-type causes ALS," *Human Molecular Genetics*, vol. 21, no. 16, pp. 3568–3574, 2012.
- [19] J. Sreedharan, I. P. Blair, V. B. Tripathi et al., "TDP-43 mutations in familial and sporadic amyotrophic lateral sclerosis," *Science*, vol. 319, no. 5870, pp. 1668–1672, 2008.
- [20] T. J. Kwiatkowski, D. A. Bosco, A. L. LeClerc et al., "Mutations in the FUS/TLS gene on chromosome 16 cause familial amyotrophic lateral sclerosis," *Science*, vol. 323, no. 5918, pp. 1205–1208, 2009.
- [21] C. Vance, B. Rogelj, T. Hortobagyi et al., "Mutations in FUS, an RNA processing protein, cause familial amyotrophic lateral sclerosis type 6," *Science*, vol. 323, no. 5918, pp. 1208–1211, 2009.
- [22] B. Oskarsson, T. F. Gendron, and N. P. Staff, "Amyotrophic lateral sclerosis: an update for 2018," *Mayo Clinic Proceedings*, vol. 93, no. 11, pp. 1617–1628, 2018.
- [23] S. R. Bacman, W. G. Bradley, and C. T. Moraes, "Mitochondrial involvement in amyotrophic lateral sclerosis: trigger or target?," *Molecular Neurobiology*, vol. 33, no. 2, pp. 113–132, 2006.
- [24] H. Lu, W. Dong le, Y. Y. Xie, and X. P. Wang, "Current therapy of drugs in amyotrophic lateral sclerosis," *Current Neuropharmacology*, vol. 14, no. 4, pp. 314–321, 2016.

- [25] E. C. Browne and B. M. Abbott, "Recent progress towards an effective treatment of amyotrophic lateral sclerosis using the SOD1 mouse model in a preclinical setting," *European Journal of Medicinal Chemistry*, vol. 121, pp. 918–925, 2016.
- [26] G. Pizzino, N. Irrera, M. Cucinotta et al., "Oxidative stress: harms and benefits for human health," *Oxidative Medicine and Cellular Longevity*, vol. 2017, Article ID 8416763, 13 pages, 2017.
- [27] M. D. Brand, "The sites and topology of mitochondrial superoxide production," *Experimental Gerontology*, vol. 45, no. 7–8, pp. 466–472, 2010.
- [28] S. Kausar, F. Wang, and H. Cui, "The role of mitochondria in reactive oxygen species generation and its implications for neurodegenerative diseases," *Cells*, vol. 7, no. 12, p. 274, 2018.
- [29] M. P. Murphy, "How mitochondria produce reactive oxygen species," *The Biochemical Journal*, vol. 417, no. 1, pp. 1–13, 2009.
- [30] A. A. Starkov, G. Fiskum, C. Chinopoulos et al., "Mitochondrial alpha-ketoglutarate dehydrogenase complex generates reactive oxygen species," *The Journal of Neuroscience*, vol. 24, no. 36, pp. 7779–7788, 2004.
- [31] L. Tretter and V. Adam-Vizi, "Generation of reactive oxygen species in the reaction catalyzed by -Ketoglutarate Dehydrogenase," *The Journal of Neuroscience*, vol. 24, no. 36, pp. 7771–7778, 2004.
- [32] V. I. Bunik and C. Sievers, "Inactivation of the 2-oxo acid dehydrogenase complexes upon generation of intrinsic radical species," *European Journal of Biochemistry*, vol. 269, no. 20, pp. 5004–5015, 2002.
- [33] A. L. Orr, C. L. Quinlan, I. V. Perevoshchikova, and M. D. Brand, "A refined analysis of superoxide production by mitochondrial sn-glycerol 3-phosphate dehydrogenase," *The Journal of Biological Chemistry*, vol. 287, no. 51, pp. 42921–42935, 2012.
- [34] F. L. Muller, Y. Liu, and H. Van Remmen, "Complex III releases superoxide to both sides of the inner mitochondrial membrane," *The Journal of Biological Chemistry*, vol. 279, no. 47, pp. 49064–49073, 2004.
- [35] T. Omura, "Mitochondrial P450s," *Chemico-Biological Interactions*, vol. 163, no. 1–2, pp. 86–93, 2006.
- [36] H. J. Forman and J. Kennedy, "Dihydroorotate-dependent superoxide production in rat brain and liver. A function of the primary dehydrogenase," *Archives of Biochemistry and Biophysics*, vol. 173, no. 1, pp. 219–224, 1976.
- [37] M. Hey-Mogensen, R. L. S. Goncalves, A. L. Orr, and M. D. Brand, "Production of superoxide/H₂O₂ by dihydroorotate dehydrogenase in rat skeletal muscle mitochondria," *Free Radical Biology & Medicine*, vol. 72, pp. 149–155, 2014.
- [38] C. L. Quinlan, A. L. Orr, I. V. Perevoshchikova, J. R. Treberg, B. A. Ackrell, and M. D. Brand, "Mitochondrial complex II can generate reactive oxygen species at high rates in both the forward and reverse reactions," *The Journal of Biological Chemistry*, vol. 287, no. 32, pp. 27255–27264, 2012.
- [39] N. Kaludercic, J. Mialet-Perez, N. Paolocci, A. Parini, and F. di Lisa, "Monoamine oxidases as sources of oxidants in the heart," *Journal of Molecular and Cellular Cardiology*, vol. 73, pp. 34–42, 2014.
- [40] V. Rani, G. Deep, R. K. Singh, K. Palle, and U. C. S. Yadav, "Oxidative stress and metabolic disorders: pathogenesis and therapeutic strategies," *Life Sciences*, vol. 148, pp. 183–193, 2016.
- [41] E. Birben, U. M. Sahiner, C. Sackesen, S. Erzurum, and O. Kalayci, "Oxidative stress and antioxidant defense," *World Allergy Organization Journal*, vol. 5, no. 1, pp. 9–19, 2012.
- [42] S. C. Barber, R. J. Mead, and P. J. Shaw, "Oxidative stress in ALS: a mechanism of neurodegeneration and a therapeutic target," *Biochimica et Biophysica Acta (BBA) - Molecular Basis of Disease*, vol. 1762, no. 11–12, pp. 1051–1067, 2006.
- [43] G. Bodega, M. Alique, L. Puebla, J. Carracedo, and R. M. Ramirez, "Microvesicles: ROS scavengers and ROS producers," *Journal of Extracellular Vesicles*, vol. 8, no. 1, article 1626654, 2019.
- [44] A. Phaniendra, D. B. Jestadi, and L. Periyasamy, "Free radicals: properties, sources, targets, and their implication in various diseases," *Indian Journal of Clinical Biochemistry*, vol. 30, no. 1, pp. 11–26, 2015.
- [45] E. Niedzielska, I. Smaga, M. Gawlik et al., "Oxidative Stress in Neurodegenerative Diseases," *Molecular Neurobiology*, vol. 53, no. 6, pp. 4094–4125, 2016.
- [46] O. H. Tam, N. V. Rozhkov, R. Shaw et al., "Postmortem Cortex Samples Identify Distinct Molecular Subtypes of ALS: Retrotransposon Activation, Oxidative Stress, and Activated Glia," *Cell Reports*, vol. 29, no. 5, pp. 1164–1177.e5, 2019, e5.
- [47] N. Y. Calingasan, J. Chen, M. Kiaei, and M. F. Beal, "Beta-amyloid 42 accumulation in the lumbar spinal cord motor neurons of amyotrophic lateral sclerosis patients," *Neurobiology of Disease*, vol. 19, no. 1–2, pp. 340–347, 2005.
- [48] R. J. Ferrante, S. E. Browne, L. A. Shinobu et al., "Evidence of increased oxidative damage in both sporadic and familial amyotrophic lateral sclerosis," *Journal of Neurochemistry*, vol. 69, no. 5, pp. 2064–2074, 1997.
- [49] P. J. Shaw, P. G. Ince, G. Falkous, and D. Mantle, "Oxidative damage to protein in sporadic motor neuron disease spinal cord," *Annals of Neurology*, vol. 38, no. 4, pp. 691–695, 1995.
- [50] E. P. Simpson, Y. K. Henry, J. S. Henkel, R. G. Smith, and S. H. Appel, "Increased lipid peroxidation in sera of ALS patients: a potential biomarker of disease burden," *Neurology*, vol. 62, no. 10, pp. 1758–1765, 2004.
- [51] R. G. Smith, Y. K. Henry, M. P. Mattson, and S. H. Appel, "Presence of 4-hydroxynonenal in cerebrospinal fluid of patients with sporadic amyotrophic lateral sclerosis," *Annals of Neurology*, vol. 44, no. 4, pp. 696–699, 1998.
- [52] Y. Ihara, K. Nobukuni, H. Takata, and T. Hayabara, "Oxidative stress and metal content in blood and cerebrospinal fluid of amyotrophic lateral sclerosis patients with and without a Cu, Zn-superoxide dismutase mutation," *Neurological Research*, vol. 27, no. 1, pp. 105–108, 2013.
- [53] H. Tohgi, T. Abe, K. Yamazaki, T. Murata, E. Ishizaki, and C. Isobe, "Remarkable increase in cerebrospinal fluid 3-nitrotyrosine in patients with sporadic amyotrophic lateral sclerosis," *Annals of Neurology*, vol. 46, no. 1, pp. 129–131, 1999.
- [54] J. H. Weishaupt, C. Bartels, E. Pölking et al., "Reduced oxidative damage in ALS by high-dose enteral melatonin treatment," *Journal of Pineal Research*, vol. 41, no. 4, pp. 313–323, 2006.
- [55] H. Mitsumoto, R. M. Santella, X. Liu et al., "Oxidative stress biomarkers in sporadic ALS," *Amyotrophic Lateral Sclerosis*, vol. 9, no. 3, pp. 177–183, 2009.
- [56] J. Agar and H. Durham, "Relevance of oxidative injury in the pathogenesis of motor neuron diseases," *Amyotrophic Lateral*

- Sclerosis and Other Motor Neuron Disorders*, vol. 4, no. 4, pp. 232–242, 2009.
- [57] M. T. Carri, A. Ferri, M. Cozzolino, L. Calabrese, and G. Rotilio, “Neurodegeneration in amyotrophic lateral sclerosis: the role of oxidative stress and altered homeostasis of metals,” *Brain Research Bulletin*, vol. 61, no. 4, pp. 365–374, 2003.
- [58] A. Kraft, J. Resch, D. Johnson, and J. Johnson, “Activation of the Nrf2-ARE pathway in muscle and spinal cord during ALS-like pathology in mice expressing mutant SOD1,” *Experimental Neurology*, vol. 207, no. 1, pp. 107–117, 2007.
- [59] A. C. Bowling, J. B. Schulz, R. H. Brown Jr., and M. F. Beal, “Superoxide dismutase activity, oxidative damage, and mitochondrial energy metabolism in familial and sporadic amyotrophic lateral sclerosis,” *Journal of Neurochemistry*, vol. 61, no. 6, pp. 2322–2325, 1993.
- [60] I. Niebroj-Dobosz, D. Dzielulska, and H. Kwiecinski, “Oxidative damage to proteins in the spinal cord in amyotrophic lateral sclerosis ALS,” *Folia Neuropathologica*, vol. 42, no. 3, pp. 151–156, 2004.
- [61] N. Shibata, R. Nagai, K. Uchida et al., “Morphological evidence for lipid peroxidation and protein glycooxidation in spinal cords from sporadic amyotrophic lateral sclerosis patients,” *Brain Research*, vol. 917, no. 1, pp. 97–104, 2001.
- [62] W. A. Pedersen, W. Fu, J. N. Keller et al., “Protein modification by the lipid peroxidation product 4-hydroxynonenal in the spinal cords of amyotrophic lateral sclerosis patients,” *Annals of Neurology*, vol. 44, no. 5, pp. 819–824, 1998.
- [63] M. F. Beal, R. J. Ferrante, S. E. Browne, R. T. Matthews, N. W. Kowall, and R. H. Brown, “Increased 3-nitrotyrosine in both sporadic and familial amyotrophic lateral sclerosis,” *Annals of Neurology*, vol. 42, no. 4, pp. 644–654, 1997.
- [64] K. Abe, L.-H. Pan, M. Watanabe, H. Konno, T. Kato, and Y. Itoyama, “Upregulation of protein-tyrosine nitration in the anterior horn cells of amyotrophic lateral sclerosis,” *Neurological Research*, vol. 19, no. 2, pp. 124–128, 2016.
- [65] K. Abe, L. H. Pan, M. Watanabe, T. Kato, and Y. Itoyama, “Induction of nitrotyrosine-like immunoreactivity in the lower motor neuron of amyotrophic lateral sclerosis,” *Neuroscience Letters*, vol. 199, no. 2, pp. 152–154, 1995.
- [66] G. N. Babu, A. Kumar, R. Chandra et al., “Oxidant-antioxidant imbalance in the erythrocytes of sporadic amyotrophic lateral sclerosis patients correlates with the progression of disease,” *Neurochemistry International*, vol. 52, no. 6, pp. 1284–1289, 2008.
- [67] E. D’Amico, P. Factor-Litvak, R. M. Santella, and H. Mitsuoto, “Clinical perspective on oxidative stress in sporadic amyotrophic lateral sclerosis,” *Free Radical Biology & Medicine*, vol. 65, pp. 509–527, 2013.
- [68] J. Walczak, G. Dębska-Vielhaber, S. Vielhaber et al., “Distinction of sporadic and familial forms of ALS based on mitochondrial characteristics,” *The FASEB Journal*, vol. 33, no. 3, pp. 4388–4403, 2018.
- [69] A. Ferri, M. Cozzolino, C. Crosio et al., “Familial ALS-superoxide dismutases associate with mitochondria and shift their redox potentials,” *Proceedings of the National Academy of Sciences of the United States of America*, vol. 103, no. 37, pp. 13860–13865, 2006.
- [70] L. Chi, Y. Ke, C. Luo, D. Gozal, and R. Liu, “Depletion of reduced glutathione enhances motor neuron degeneration in vitro and in vivo,” *Neuroscience*, vol. 144, no. 3, pp. 991–1003, 2007.
- [71] M. G. Pesaresi, I. Amori, C. Giorgi et al., “Mitochondrial redox signalling by p66Shc mediates ALS-like disease through Rac1 inactivation,” *Human Molecular Genetics*, vol. 20, no. 21, pp. 4196–4208, 2011.
- [72] S. Pickles, L. Destroismaisons, S. L. Peyrard et al., “Mitochondrial damage revealed by immunoselection for ALS-linked misfolded SOD1,” *Human Molecular Genetics*, vol. 22, no. 19, pp. 3947–3959, 2013.
- [73] M. R. Vargas, D. A. Johnson, and J. A. Johnson, “Decreased glutathione accelerates neurological deficit and mitochondrial pathology in familial ALS-linked hSOD1(G93A) mice model,” *Neurobiology of Disease*, vol. 43, no. 3, pp. 543–551, 2011.
- [74] A. Igoudjil, J. Magrane, L. R. Fischer et al., “In vivo pathogenic role of mutant SOD1 localized in the mitochondrial intermembrane space,” *The Journal of Neuroscience*, vol. 31, no. 44, pp. 15826–15837, 2011.
- [75] J. M. McCord and I. Fridovich, “Superoxide dismutase. An enzymic function for erythrocuprein (hemocuprein),” *The Journal of Biological Chemistry*, vol. 244, no. 22, pp. 6049–6055, 1969.
- [76] A. R. Reddi and V. C. Culotta, “SOD1 integrates signals from oxygen and glucose to repress respiration,” *Cell*, vol. 152, no. 1–2, pp. 224–235, 2013.
- [77] J. Huai and Z. Zhang, “Structural properties and interaction partners of familial ALS-associated SOD1 mutants,” *Frontiers in Neurology*, vol. 10, p. 527, 2019.
- [78] N. Luquin, B. Yu, R. J. Trent, J. M. Morahan, and R. Pamphlett, “An analysis of the entire SOD1 gene in sporadic ALS,” *Neuromuscular Disorders*, vol. 18, no. 7, pp. 545–552, 2008.
- [79] D. R. Borchelt, M. K. Lee, H. S. Slunt et al., “Superoxide dismutase 1 with mutations linked to familial amyotrophic lateral sclerosis possesses significant activity,” *Proceedings of the National Academy of Sciences of United States of America*, vol. 91, no. 17, pp. 8292–8296, 1994.
- [80] M. B. Yim, J. H. Kang, H. S. Yim, H. S. Kwak, P. B. Chock, and E. R. Stadtman, “A gain-of-function of an amyotrophic lateral sclerosis-associated Cu,Zn-superoxide dismutase mutant: An enhancement of free radical formation due to a decrease in K_m for hydrogen peroxide,” *Proceedings of the National Academy of Sciences of United States of America*, vol. 93, no. 12, pp. 5709–5714, 1996.
- [81] A. N. Kokić, Z. Stević, S. Stojanović et al., “Biotransformation of nitric oxide in the cerebrospinal fluid of amyotrophic lateral sclerosis patients,” *Redox Report*, vol. 10, no. 5, pp. 265–270, 2013.
- [82] A. G. Reaume, J. L. Elliott, E. K. Hoffman et al., “Motor neurons in Cu/Zn superoxide dismutase-deficient mice develop normally but exhibit enhanced cell death after axonal injury,” *Nature Genetics*, vol. 13, no. 1, pp. 43–47, 1996.
- [83] T. Ratovitski, L. B. Corson, J. Strain et al., “Variation in the biochemical/biophysical properties of mutant superoxide dismutase 1 enzymes and the rate of disease progression in familial amyotrophic lateral sclerosis kindreds,” *Human Molecular Genetics*, vol. 8, no. 8, pp. 1451–1460, 1999.
- [84] F. M. Menzies, P. G. Ince, and P. J. Shaw, “Mitochondrial involvement in amyotrophic lateral sclerosis,” *Neurochemistry International*, vol. 40, no. 6, pp. 543–551, 2002.

- [85] C. M. J. Higgins, C. Jung, H. Ding, and Z. Xu, "Mutant Cu, Zn superoxide dismutase that causes motoneuron degeneration is present in mitochondria in the CNS," *The Journal of Neuroscience*, vol. 22, no. 6, p. RC215, 2002.
- [86] D. Liu, "The roles of free radicals in amyotrophic lateral sclerosis," *Journal of Molecular Neuroscience*, vol. 7, no. 3, pp. 159–167, 1996.
- [87] J. S. Valentine, P. A. Doucette, and S. Zittin Potter, "Copper-zinc superoxide dismutase and amyotrophic lateral sclerosis," *Annual Review of Biochemistry*, vol. 74, no. 1, pp. 563–593, 2005.
- [88] M. B. Yim, P. B. Chock, and E. R. Stadtman, "Copper, zinc superoxide dismutase catalyzes hydroxyl radical production from hydrogen peroxide," *Proceedings of the National Academy of Sciences of the United States of America*, vol. 87, no. 13, pp. 5006–5010, 1990.
- [89] M. B. Yim, P. B. Chock, and E. R. Stadtman, "Enzyme function of copper, zinc superoxide dismutase as a free radical generator," *The Journal of Biological Chemistry*, vol. 268, no. 6, pp. 4099–4105, 1993.
- [90] J. S. Beckman, A. G. Estévez, J. P. Crow, and L. Barbeito, "Superoxide dismutase and the death of motoneurons in ALS," *Trends in Neurosciences*, vol. 24, no. 11, pp. S15–S20, 2001.
- [91] A. G. Estévez, "Induction of Nitric Oxide – Dependent Apoptosis in Motor Neurons by Zinc-Deficient Superoxide Dismutase," *Science*, vol. 286, no. 5449, pp. 2498–2500, 1999.
- [92] C. Zhu, M. V. Beck, J. D. Griffith, M. Deshmukh, and N. V. Dokholyan, "Large SOD1 aggregates, unlike trimeric SOD1, do not impact cell viability in a model of amyotrophic lateral sclerosis," *Proceedings of the National Academy of Sciences of the United States of America*, vol. 115, no. 18, pp. 4661–4665, 2018.
- [93] X. Chen, H. Shang, X. Qiu et al., "Oxidative modification of cysteine 111 promotes disulfide bond-independent aggregation of SOD1," *Neurochemical Research*, vol. 37, no. 4, pp. 835–845, 2012.
- [94] S. A. Ezzi, M. Urushitani, and J. P. Julien, "Wild-type superoxide dismutase acquires binding and toxic properties of ALS-linked mutant forms through oxidation," *Journal of Neurochemistry*, vol. 102, no. 1, pp. 170–178, 2007.
- [95] D. Petrov, X. Daura, and B. Zagrovic, "Effect of oxidative damage on the stability and dimerization of superoxide dismutase 1," *Biophysical Journal*, vol. 110, no. 7, pp. 1499–1509, 2016.
- [96] M. Neumann, D. M. Sampathu, L. K. Kwong et al., "Ubiquitinated TDP-43 in frontotemporal lobar degeneration and amyotrophic lateral sclerosis," *Science*, vol. 314, no. 5796, pp. 130–133, 2006.
- [97] M. Pehar, G. Beeson, C. C. Beeson, J. A. Johnson, and M. R. Vargas, "Mitochondria-targeted catalase reverts the neurotoxicity of hSOD1G93A astrocytes without extending the survival of ALS-linked mutant hSOD1 mice," *PLoS One*, vol. 9, no. 7, article e103438, 2014.
- [98] S. Kato, M. Kato, Y. Abe et al., "Redox system expression in the motor neurons in amyotrophic lateral sclerosis (ALS): immunohistochemical studies on sporadic ALS, superoxide dismutase 1 (SOD1)-mutated familial ALS, and SOD1-mutated ALS animal models," *Acta Neuropathologica*, vol. 110, no. 2, pp. 101–112, 2005.
- [99] K. M. Killoy, B. A. Harlan, M. Pehar, K. L. Helke, J. A. Johnson, and M. R. Vargas, "Decreased glutathione levels cause overt motor neuron degeneration in hSOD1WT over-expressing mice," *Experimental Neurology*, vol. 302, pp. 129–135, 2018.
- [100] O. B. V. Oka and N. J. Bulleid, "Forming disulfides in the endoplasmic reticulum," *Biochimica et Biophysica Acta*, vol. 1833, no. 11, pp. 2425–2429, 2013.
- [101] C. Espinosa-Diez, V. Miguel, D. Mennerich et al., "Antioxidant responses and cellular adjustments to oxidative stress," *Redox Biology*, vol. 6, pp. 183–197, 2015.
- [102] M. Cozzolino, I. Amori, M. G. Pesaresi, A. Ferri, M. Nencini, and M. T. Carri, "Cysteine 111 affects aggregation and cytotoxicity of mutant Cu,Zn-superoxide dismutase associated with familial amyotrophic lateral sclerosis," *The Journal of Biological Chemistry*, vol. 283, no. 2, pp. 866–874, 2008.
- [103] J. Niwa, S. I. Yamada, S. Ishigaki et al., "Disulfide bond mediates aggregation, toxicity, and ubiquitylation of familial amyotrophic lateral sclerosis-linked mutant SOD1," *The Journal of Biological Chemistry*, vol. 282, no. 38, pp. 28087–28095, 2007.
- [104] C. Valle and M. T. Carri, "Cysteine Modifications in the Pathogenesis of ALS," *Frontiers in Molecular Neuroscience*, vol. 10, p. 5, 2017.
- [105] R. K. Thimmulappa, K. H. Mai, S. Srisuma, T. W. Kensler, M. Yamamoto, and S. Biswal, "Identification of Nrf2-regulated genes induced by the chemopreventive agent sulforaphane by oligonucleotide microarray," *Cancer Research*, vol. 62, no. 18, pp. 5196–5203, 2002.
- [106] J. M. Lee, M. J. Calkins, K. Chan, Y. W. Kan, and J. A. Johnson, "Identification of the NF-E2-related factor-2-dependent genes conferring protection against oxidative stress in primary cortical astrocytes using oligonucleotide microarray analysis," *The Journal of Biological Chemistry*, vol. 278, no. 14, pp. 12029–12038, 2003.
- [107] S. Petri, S. Korner, and M. Kiaei, "Nrf2/ARE signaling pathway: key mediator in oxidative stress and potential therapeutic target in ALS," *Neurology Research International*, vol. 2012, Article ID 878030, 7 pages, 2012.
- [108] T. Nguyen, P. Nioi, and C. B. Pickett, "The Nrf2-antioxidant response element signaling pathway and its activation by oxidative stress," *The Journal of Biological Chemistry*, vol. 284, no. 20, pp. 13291–13295, 2009.
- [109] T. Nguyen, P. J. Sherratt, and C. B. Pickett, "Regulatory mechanisms controlling gene expression mediated by the antioxidant response element," *Annual Review of Pharmacology and Toxicology*, vol. 43, no. 1, pp. 233–260, 2003.
- [110] J. Kirby, E. Halligan, M. J. Baptista et al., "Mutant SOD1 alters the motor neuronal transcriptome: implications for familial ALS," *Brain*, vol. 128, Part 7, pp. 1686–1706, 2005.
- [111] A. Sarlette, K. Krampfl, C. Grothe, N. Neuheff, R. Dengler, and S. Petri, "Nuclear erythroid 2-related factor 2-antioxidative response element signaling pathway in motor cortex and spinal cord in amyotrophic lateral sclerosis," *Journal of Neuropathology and Experimental Neurology*, vol. 67, no. 11, pp. 1055–1062, 2008.
- [112] D. C. Wu, D. B. Re, M. Nagai, H. Ischiropoulos, and S. Przedborski, "The inflammatory NADPH oxidase enzyme modulates motor neuron degeneration in amyotrophic lateral sclerosis mice," *Proceedings of the National Academy of Sciences of the United States of America*, vol. 103, no. 32, pp. 12132–12137, 2006.

- [113] J. J. Marden, M. M. Harraz, A. J. Williams et al., "Redox modifier genes in amyotrophic lateral sclerosis in mice," *The Journal of Clinical Investigation*, vol. 117, no. 10, pp. 2913–2919, 2007.
- [114] M. M. Harraz, J. J. Marden, W. Zhou et al., "SOD1 mutations disrupt redox-sensitive Rac regulation of NADPH oxidase in a familial ALS model," *Journal of Clinical Investigation*, vol. 118, no. 2, pp. 659–670, 2008.
- [115] Y. P. Tian, F. Y. Che, Q. P. Su et al., "Effects of mutant TDP-43 on the Nrf2/ARE pathway and protein expression of MafK and JDP2 in NSC-34 cells," *Genetics and Molecular Research*, vol. 16, no. 2, 2017.
- [116] D. Moujalled, A. Grubman, K. Acevedo et al., "TDP-43 mutations causing amyotrophic lateral sclerosis are associated with altered expression of RNA-binding protein hnRNP K and affect the Nrf2 antioxidant pathway," *Human Molecular Genetics*, vol. 26, no. 9, pp. 1732–1746, 2017.
- [117] W. Duan, X. Li, J. Shi, Y. Guo, Z. Li, and C. Li, "Mutant TAR DNA-binding protein-43 induces oxidative injury in motor neuron-like cell," *Neuroscience*, vol. 169, no. 4, pp. 1621–1629, 2010.
- [118] R. C. Hergesheimer, A. A. Chami, D. R. de Assis et al., "The debated toxic role of aggregated TDP-43 in amyotrophic lateral sclerosis: a resolution in sight?," *Brain*, vol. 142, no. 5, pp. 1176–1194, 2019.
- [119] L. François-Moutal, S. Perez-Miller, D. D. Scott, V. G. Miranda, N. Mollasalehi, and M. Khanna, "Structural insights into TDP-43 and effects of post-translational modifications," *Frontiers in Molecular Neuroscience*, vol. 12, p. 301, 2019.
- [120] T. J. Cohen, A. W. Hwang, T. Unger, J. Q. Trojanowski, and V. M. Y. Lee, "Redox signalling directly regulates TDP-43 via cysteine oxidation and disulphide cross-linking," *The EMBO Journal*, vol. 31, no. 5, pp. 1241–1252, 2012.
- [121] C. K. Chang, M. H. Chiang, E. K. W. Toh, C. F. Chang, and T. H. Huang, "Molecular mechanism of oxidation-induced TDP-43 RRM1 aggregation and loss of function," *FEBS Letters*, vol. 587, no. 6, pp. 575–582, 2013.
- [122] C. Vance, E. L. Scotter, A. L. Nishimura et al., "ALS mutant FUS disrupts nuclear localization and sequesters wild-type FUS within cytoplasmic stress granules," *Human Molecular Genetics*, vol. 22, no. 13, pp. 2676–2688, 2013.
- [123] Q. Deng, C. J. Holler, G. Taylor et al., "FUS is phosphorylated by DNA-PK and accumulates in the cytoplasm after DNA damage," *The Journal of Neuroscience*, vol. 34, no. 23, pp. 7802–7813, 2014.
- [124] H. Wang, W. Guo, J. Mitra et al., "Mutant FUS causes DNA ligation defects to inhibit oxidative damage repair in amyotrophic lateral sclerosis," *Nature Communications*, vol. 9, no. 1, p. 3683, 2018.
- [125] J. D. Lai and J. K. Ichida, "C9ORF72 protein function and immune dysregulation in amyotrophic lateral sclerosis," *Neuroscience Letters*, vol. 713, article 134523, 2019.
- [126] K. Mori, T. Arzberger, F. A. Grässer et al., "Bidirectional transcripts of the expanded C9orf72 hexanucleotide repeat are translated into aggregating dipeptide repeat proteins," *Acta Neuropathologica*, vol. 126, no. 6, pp. 881–893, 2013.
- [127] K. Mori, S. M. Weng, T. Arzberger et al., "The C9orf72 GGGGCC repeat is translated into aggregating dipeptide-repeat proteins in FTL/ALS," *Science*, vol. 339, no. 6125, pp. 1335–1338, 2013.
- [128] R. Lopez-Gonzalez, Y. Lu, T. F. Gendron et al., "Poly(GR) in C9ORF72-related ALS/FTD compromises mitochondrial function and increases oxidative stress and DNA damage in iPSC-derived motor neurons," *Neuron*, vol. 92, no. 2, pp. 383–391, 2016.
- [129] A. Birger, I. Ben-Dor, M. Ottolenghi et al., "Human iPSC-derived astrocytes from ALS patients with mutated C9ORF72 show increased oxidative stress and neurotoxicity," *eBioMedicine*, vol. 50, pp. 274–289, 2019.
- [130] M. Ghasemi and R. H. Brown Jr., "Genetics of amyotrophic lateral sclerosis," *Cold Spring Harbor Perspectives in Medicine*, vol. 8, no. 5, 2018.
- [131] G. W. Cho, B. Y. Kang, and S. H. Kim, "Human angiogenin presents neuroprotective and migration effects in neuroblastoma cells," *Molecular and Cellular Biochemistry*, vol. 340, no. 1–2, pp. 133–141, 2010.
- [132] R. Fernández-Santiago, S. Hoenig, P. Lichtner et al., "Identification of novel angiogenin (ANG) gene missense variants in German patients with amyotrophic lateral sclerosis," *Journal of Neurology*, vol. 256, no. 8, pp. 1337–1342, 2009.
- [133] T. T. Hoang, D. A. Johnson, R. T. Raines, and J. A. Johnson, "Angiogenin activates the astrocytic Nrf2/antioxidant-response element pathway and thereby protects murine neurons from oxidative stress," *The Journal of Biological Chemistry*, vol. 294, no. 41, pp. 15095–15103, 2019.
- [134] A. M. Wills, S. Cronin, A. Slowik et al., "A large-scale international meta-analysis of paraoxonase gene polymorphisms in sporadic ALS," *Neurology*, vol. 73, no. 1, pp. 16–24, 2009.
- [135] P. N. Valdmanis, E. Kabashi, A. Dyck et al., "Association of paraoxonase gene cluster polymorphisms with ALS in France, Quebec, and Sweden," *Neurology*, vol. 71, no. 7, pp. 514–520, 2008.
- [136] M. Saeed, N. Siddique, W. Y. Hung et al., "Paraoxonase cluster polymorphisms are associated with sporadic ALS," *Neurology*, vol. 67, no. 5, pp. 771–776, 2006.
- [137] C. J. Ng, D. J. Wadleigh, A. Gangopadhyay et al., "Paraoxonase-2 is a ubiquitously expressed protein with antioxidant properties and is capable of preventing cell-mediated oxidative modification of low density lipoprotein," *The Journal of Biological Chemistry*, vol. 276, no. 48, pp. 44444–44449, 2001.
- [138] S. Zoccollella, A. Santamato, and P. Lamberti, "Current and emerging treatments for amyotrophic lateral sclerosis," *Neuropsychiatric Disease and Treatment*, vol. 5, pp. 577–595, 2009.
- [139] R. S. Bedlack, B. J. Traynor, and M. E. Cudkowicz, "Emerging disease-modifying therapies for the treatment of motor neuron disease/amyotrophic lateral sclerosis," *Expert Opinion on Emerging Drugs*, vol. 12, no. 2, pp. 229–252, 2007.
- [140] M. E. Gurney, F. B. Cutting, P. Zhai et al., "Benefit of vitamin E, riluzole, and gababapentin in a transgenic model of familial amyotrophic lateral sclerosis," *Annals of Neurology*, vol. 39, no. 2, pp. 147–157, 1996.
- [141] D. Michal Freedman, R. W. Kuncl, S. J. Weinstein, N. Malila, J. Virtamo, and D. Albanes, "Vitamin E serum levels and controlled supplementation and risk of amyotrophic lateral sclerosis," *Amyotrophic Lateral Sclerosis and Frontotemporal Degeneration*, vol. 14, no. 4, pp. 246–251, 2012.
- [142] F. de Bustos, F. J. Jiménez-Jiménez, J. A. Molina et al., "Cerebrospinal fluid levels of alpha-tocopherol in amyotrophic lateral sclerosis," *Journal of Neural Transmission*, vol. 105, no. 6–7, pp. 703–708, 1998.

- [143] Y. Iwasaki, K. Ikeda, and M. Kinoshita, "Vitamin A and E levels are normal in amyotrophic lateral sclerosis," *Journal of the Neurological Sciences*, vol. 132, no. 2, pp. 193–194, 1995.
- [144] H. Wang, E. J. O'Reilly, M. G. Weisskopf et al., "Vitamin E intake and risk of amyotrophic lateral sclerosis: a pooled analysis of data from 5 prospective cohort studies," *American Journal of Epidemiology*, vol. 173, no. 6, pp. 595–602, 2011.
- [145] J. H. Veldink, S. Kalmijn, G.-J. Groeneveld et al., "Intake of polyunsaturated fatty acids and vitamin E reduces the risk of developing amyotrophic lateral sclerosis," *Journal of Neurology, Neurosurgery, and Psychiatry*, vol. 78, no. 4, pp. 367–371, 2006.
- [146] A. Ascherio, M. G. Weisskopf, E. J. O'Reilly et al., "Vitamin E intake and risk of amyotrophic lateral sclerosis," *Annals of Neurology*, vol. 57, no. 1, pp. 104–110, 2005.
- [147] C. Desnuelle, M. Dib, C. Garrel, and A. Favier, "A double-blind, placebo-controlled randomized clinical trial of alpha-tocopherol (vitamin E) in the treatment of amyotrophic lateral sclerosis. ALS riluzole-tocopherol study group," *Amyotrophic Lateral Sclerosis and Other Motor Neuron Disorders*, vol. 2, no. 1, pp. 9–18, 2009.
- [148] A. Galbussera, L. Tremolizzo, L. Brighina et al., "Vitamin E intake and quality of life in amyotrophic lateral sclerosis patients: a follow-up case series study," *Neurological Sciences*, vol. 27, no. 3, pp. 190–193, 2006.
- [149] M. Graf, D. Ecker, R. Horowski et al., "High dose vitamin E therapy in amyotrophic lateral sclerosis as add-on therapy to riluzole: results of a placebo-controlled double-blind study," *Journal of Neural Transmission (Vienna)*, vol. 112, no. 5, pp. 649–660, 2005.
- [150] E. J. Pappert, C. C. Tangney, C. G. Goetz et al., "Alpha-tocopherol in the ventricular cerebrospinal fluid of Parkinson's disease patients: dose-response study and correlations with plasma levels," *Neurology*, vol. 47, no. 4, pp. 1037–1042, 1996.
- [151] R. L. Kraus, R. Pasieczny, K. Lariosa-Willingham, M. S. Turner, A. Jiang, and J. W. Trauger, "Antioxidant properties of minocycline: neuroprotection in an oxidative stress assay and direct radical-scavenging activity," *Journal of Neurochemistry*, vol. 94, no. 3, pp. 819–827, 2005.
- [152] R. Baldinger, H. D. Katzberg, and M. Weber, "Treatment for cramps in amyotrophic lateral sclerosis/motor neuron disease," *Cochrane Database of Systematic Reviews*, no. 4, article Cd004157, 2012.
- [153] O. A. Andreassen, A. Dedeoglu, P. Klivenyi, M. F. Beal, and A. I. Bush, "N-acetyl-L-cysteine improves survival and preserves motor performance in an animal model of familial amyotrophic lateral sclerosis," *Neuroreport*, vol. 11, no. 11, pp. 2491–2493, 2000.
- [154] J. M. Burgunder, A. Varriale, and B. H. Lauterburg, "Effect of N-acetylcysteine on plasma cysteine and glutathione following paracetamol administration," *European Journal of Clinical Pharmacology*, vol. 36, no. 2, pp. 127–131, 1989.
- [155] S. Beretta, G. Sala, L. Mattavelli et al., "Mitochondrial dysfunction due to mutant copper/zinc superoxide dismutase associated with amyotrophic lateral sclerosis is reversed by N-acetylcysteine," *Neurobiology of Disease*, vol. 13, no. 3, pp. 213–221, 2003.
- [156] E. S. Louwse, G. J. Weverling, P. M. M. Bossuyt, F. E. P. Meyjes, and J. M. B. V. de Jong, "Randomized, double-blind, controlled trial of acetylcysteine in amyotrophic lateral sclerosis," *Archives of Neurology*, vol. 52, no. 6, pp. 559–564, 1995.
- [157] N. Bresolin, L. Bet, A. Binda et al., "Clinical and biochemical correlations in mitochondrial myopathies treated with coenzyme Q10," *Neurology*, vol. 38, no. 6, pp. 892–899, 1988.
- [158] T. Q. Do, J. R. Schultz, and C. F. Clarke, "Enhanced sensitivity of ubiquinone-deficient mutants of *Saccharomyces cerevisiae* to products of autoxidized polyunsaturated fatty acids," *Proceedings of the National Academy of Sciences of the United States of America*, vol. 93, no. 15, pp. 7534–7539, 1996.
- [159] R. T. Matthews, L. Yang, S. Browne, M. Baik, and M. F. Beal, "Coenzyme Q10 administration increases brain mitochondrial concentrations and exerts neuroprotective effects," *Proceedings of the National Academy of Sciences of the United States of America*, vol. 95, no. 15, pp. 8892–8897, 1998.
- [160] J. Lucchetti, M. Marino, S. Papa et al., "A mouse model of familial ALS has increased CNS levels of endogenous ubiquinol9/10 and does not benefit from exogenous administration of ubiquinol10," *PLoS One*, vol. 8, no. 7, article e69540, 2013.
- [161] M. Sohmiya, M. Tanaka, Y. Suzuki, Y. Tanino, K. Okamoto, and Y. Yamamoto, "An increase of oxidized coenzyme Q-10 occurs in the plasma of sporadic ALS patients," *Journal of the Neurological Sciences*, vol. 228, no. 1, pp. 49–53, 2005.
- [162] J. A. Molina, F. de Bustos, F. J. Jiménez-Jiménez et al., "Serum levels of coenzyme Q10 in patients with amyotrophic lateral sclerosis," *Journal of Neural Transmission (Vienna)*, vol. 107, no. 8–9, pp. 1021–1026, 2000.
- [163] K. L. Ferrante, J. Shefner, H. Zhang et al., "Tolerance of high-dose (3,000 mg/day) coenzyme Q10 in ALS," *Neurology*, vol. 65, no. 11, pp. 1834–1836, 2005.
- [164] G. Levy, P. Kaufmann, R. Buchsbaum et al., "A two-stage design for a phase II clinical trial of coenzyme Q10 in ALS," *Neurology*, vol. 66, no. 5, pp. 660–663, 2006.
- [165] P. Kaufmann, J. L. P. Thompson, G. Levy et al., "Phase II trial of CoQ10 for ALS finds insufficient evidence to justify phase III," *Annals of Neurology*, vol. 66, no. 2, pp. 235–244, 2009.
- [166] A. Neves Carvalho, O. Firuzi, M. Joao Gama, J. van Horssen, and L. Saso, "Oxidative stress and antioxidants in neurological diseases: is there still hope?," *Current Drug Targets*, vol. 18, no. 6, pp. 705–718, 2017.
- [167] M. R. Vargas, D. A. Johnson, D. W. Sirkis, A. Messing, and J. A. Johnson, "Nrf2 activation in astrocytes protects against neurodegeneration in mouse models of familial amyotrophic lateral sclerosis," *The Journal of Neuroscience*, vol. 28, no. 50, pp. 13574–13581, 2008.
- [168] Y. Guo, Y. Zhang, D. Wen et al., "The modest impact of transcription factor Nrf2 on the course of disease in an ALS animal model," *Laboratory Investigation*, vol. 93, no. 7, pp. 825–833, 2013.
- [169] F. van Muiswinkel and H. Kuiperij, "The Nrf2-ARE signaling pathway: promising drug target to combat oxidative stress in neurodegenerative disorders," *Current Drug Targets. CNS and Neurological Disorders*, vol. 4, no. 3, pp. 267–281, 2005.
- [170] K. Tanaka, T. Kanno, Y. Yanagisawa et al., "A novel acylaminoimidazole derivative, WN1316, alleviates disease progression via suppression of glial inflammation in ALS mouse model," *PLoS One*, vol. 9, no. 1, article e87728, 2014.
- [171] H. Jiang, X. Tian, Y. Guo, W. Duan, H. Bu, and C. Li, "Activation of nuclear factor erythroid 2-related factor 2 cytoprotective signaling by curcumin protect primary spinal cord

- astrocytes against oxidative toxicity," *Biological & Pharmaceutical Bulletin*, vol. 34, no. 8, pp. 1194–1197, 2011.
- [172] N. K. Bhatia, A. Srivastava, N. Katyal et al., "Curcumin binds to the pre-fibrillar aggregates of Cu/Zn superoxide dismutase (SOD1) and alters its amyloidogenic pathway resulting in reduced cytotoxicity," *Biochimica et Biophysica Acta*, vol. 1854, no. 5, pp. 426–436, 2015.
- [173] J. Lu, W. Duan, Y. Guo et al., "Mitochondrial dysfunction in human TDP-43 transfected NSC34 cell lines and the protective effect of dimethoxy curcumin," *Brain Research Bulletin*, vol. 89, no. 5-6, pp. 185–190, 2012.
- [174] M. Ahmadi, E. Agah, S. Nafissi et al., "Safety and efficacy of nanocurcumin as add-on therapy to riluzole in patients with amyotrophic lateral sclerosis: a pilot randomized clinical trial," *Neurotherapeutics*, vol. 15, no. 2, pp. 430–438, 2018.
- [175] L. Chico, E. C. Ienco, C. Bisordi et al., "Amyotrophic lateral sclerosis and oxidative stress: a double-blind therapeutic trial after curcumin supplementation," *CNS & Neurological Disorders Drug Targets*, vol. 17, no. 10, pp. 767–779, 2018.
- [176] M. Rakotoarisoa and A. Angelova, "Amphiphilic nanocarrier systems for curcumin delivery in neurodegenerative disorders," *Medicines*, vol. 5, no. 4, p. 126, 2018.
- [177] G. Tripodo, T. Chlapanidas, S. Perteghella et al., "Mesenchymal stromal cells loading curcumin-INVITE-micelles: a drug delivery system for neurodegenerative diseases," *Colloids and Surfaces, B: Biointerfaces*, vol. 125, pp. 300–308, 2015.
- [178] A. Neymotin, N. Y. Calingasan, E. Wille et al., "Neuroprotective effect of Nrf2/ARE activators, CDDO ethylamide and CDDO trifluoroethylamide, in a mouse model of amyotrophic lateral sclerosis," *Free Radical Biology & Medicine*, vol. 51, no. 1, pp. 88–96, 2011.
- [179] R. J. Mead, A. Higginbottom, S. P. Allen et al., "[S+] Apomorphine is a CNS penetrating activator of the Nrf2-ARE pathway with activity in mouse and patient fibroblast models of amyotrophic lateral sclerosis," *Free Radical Biology & Medicine*, vol. 61, pp. 438–452, 2013.
- [180] H. K. Na and Y. J. Surh, "Modulation of Nrf2-mediated antioxidant and detoxifying enzyme induction by the green tea polyphenol EGCG," *Food and Chemical Toxicology*, vol. 46, no. 4, pp. 1271–1278, 2008.
- [181] M. Pervin, K. Unno, A. Nakagawa et al., "Blood brain barrier permeability of (-)-epigallocatechin gallate, its proliferation-enhancing activity of human neuroblastoma SH-SY5Y cells, and its preventive effect on age-related cognitive dysfunction in mice," *Biochemistry and Biophysics Reports*, vol. 9, pp. 180–186, 2017.
- [182] S. H. Koh, H. Kwon, K. S. Kim et al., "Epigallocatechin gallate prevents oxidative-stress-induced death of mutant Cu/Zn-superoxide dismutase (G93A) motoneuron cells by alteration of cell survival and death signals," *Toxicology*, vol. 202, no. 3, pp. 213–225, 2004.
- [183] S. H. Koh, S. M. Lee, H. Y. Kim et al., "The effect of epigallocatechin gallate on suppressing disease progression of ALS model mice," *Neuroscience Letters*, vol. 395, no. 2, pp. 103–107, 2006.
- [184] Z. Xu, S. Chen, X. Li, G. Luo, L. Li, and W. le, "Neuroprotective effects of (-)-epigallocatechin-3-gallate in a transgenic mouse model of amyotrophic lateral sclerosis," *Neurochemical Research*, vol. 31, no. 10, pp. 1263–1269, 2006.
- [185] G. L. Pattee, G. R. Post, R. E. Gerber, and J. P. Bennett, Jr, "Reduction of oxidative stress in amyotrophic lateral sclerosis following pramipexole treatment," *Amyotrophic Lateral Sclerosis and Other Motor Neuron Disorders*, vol. 4, no. 2, pp. 90–95, 2009.
- [186] M. Cudkowicz, M. E. Bozik, E. W. Ingersoll et al., "The effects of dextramipexole (KNS-760704) in individuals with amyotrophic lateral sclerosis," *Nature Medicine*, vol. 17, no. 12, pp. 1652–1656, 2011.
- [187] R. Danzeisen, B. Schwalenstoecker, F. Gillardon et al., "Targeted antioxidative and neuroprotective properties of the dopamine agonist pramipexole and its nondopaminergic enantiomer SND919CL2x [(+)-2-amino-4,5,6,7-tetrahydro-6-L-propylamino-benzothiazole dihydrochloride]," *The Journal of Pharmacology and Experimental Therapeutics*, vol. 316, no. 1, pp. 189–199, 2005.
- [188] G. Ferrari-Toninelli, G. Maccarinelli, D. Uberti, E. Buerger, and M. Memo, "Mitochondria-targeted antioxidant effects of S(-) and R(+) pramipexole," *BMC Pharmacology*, vol. 10, no. 1, p. 2, 2010.
- [189] N. A. Abramova, D. S. Cassarino, S. M. Khan, T. W. Painter, and J. P. Bennett, "Inhibition by R(+) or S(-) pramipexole of caspase activation and cell death induced by methylpyridinium ion or beta amyloid peptide in SH-SY5Y neuroblastoma," *Journal of Neuroscience Research*, vol. 67, no. 4, pp. 494–500, 2002.
- [190] M. E. Bozik, J. L. Mather, W. G. Kramer, V. K. Gribkoff, and E. W. Ingersoll, "Safety, tolerability, and pharmacokinetics of KNS-760704 (dextramipexole) in healthy adult subjects," *Journal of Clinical Pharmacology*, vol. 51, no. 8, pp. 1177–1185, 2011.
- [191] S. A. Rudnicki, J. D. Berry, E. Ingersoll et al., "Dextramipexole effects on functional decline and survival in subjects with amyotrophic lateral sclerosis in a phase II study: subgroup analysis of demographic and clinical characteristics," *Amyotrophic Lateral Sclerosis and Frontotemporal Degeneration*, vol. 14, no. 1, pp. 44–51, 2013.
- [192] M. E. Cudkowicz, L. H. van den Berg, J. M. Shefner et al., "Dextramipexole versus placebo for patients with amyotrophic lateral sclerosis (EMPOWER): a randomised, double-blind, phase 3 trial," *Lancet Neurology*, vol. 12, no. 11, pp. 1059–1067, 2013.
- [193] F. G. Vieira, E. LaDow, A. Moreno et al., "Dextramipexole is ineffective in two models of ALS related neurodegeneration," *PLoS One*, vol. 9, no. 12, article e91608, 2014.
- [194] D. X. Tan, R. Reiter, L. Manchester et al., "Chemical and physical properties and potential mechanisms: melatonin as a broad spectrum antioxidant and free radical scavenger," *Current Topics in Medicinal Chemistry*, vol. 2, no. 2, pp. 181–197, 2002.
- [195] S. A. Ganie, T. A. Dar, A. H. Bhat et al., "Melatonin: a potential anti-oxidant therapeutic agent for mitochondrial dysfunctions and related disorders," *Rejuvenation Research*, vol. 19, no. 1, pp. 21–40, 2016.
- [196] S. R. Pandi-Perumal, A. S. BaHammam, G. M. Brown et al., "Melatonin antioxidative defense: therapeutical implications for aging and neurodegenerative processes," *Neurotoxicity Research*, vol. 23, no. 3, pp. 267–300, 2013.
- [197] J. Leon, D. Acuna-Castroviejo, G. Escames, D. X. Tan, and R. J. Reiter, "Melatonin mitigates mitochondrial malfunction," *Journal of Pineal Research*, vol. 38, no. 1, pp. 1–9, 2005.
- [198] Y. Zhang, A. Cook, J. Kim et al., "Melatonin inhibits the caspase-1/cytochrome c/caspase-3 cell death pathway, inhibits MT1 receptor loss and delays disease progression in a mouse

- model of amyotrophic lateral sclerosis," *Neurobiology of Disease*, vol. 55, pp. 26–35, 2013.
- [199] E. Dardiotis, E. Panayiotou, M. L. Feldman et al., "Intraperitoneal melatonin is not neuroprotective in the G93ASOD1 transgenic mouse model of familial ALS and may exacerbate neurodegeneration," *Neuroscience Letters*, vol. 548, pp. 170–175, 2013.
- [200] S. Barua, J. Y. Kim, M. A. Yenari, and J. E. Lee, "The role of NOX inhibitors in neurodegenerative diseases," *IBRO Reports*, vol. 7, pp. 59–69, 2019.
- [201] L. Saso and O. Firuzi, "Pharmacological applications of antioxidants: lights and shadows," *Current Drug Targets*, vol. 15, no. 13, pp. 1177–1199, 2014.
- [202] A. Y. Sun, Q. Wang, A. Simonyi, and G. Y. Sun, "Botanical phenolics and brain health," *Neuromolecular Medicine*, vol. 10, no. 4, pp. 259–274, 2008.
- [203] M. C. Marchetto, A. R. Muotri, Y. Mu, A. M. Smith, G. G. Cezar, and F. H. Gage, "Non-cell-autonomous effect of human SOD1 G37R astrocytes on motor neurons derived from human embryonic stem cells," *Cell Stem Cell*, vol. 3, no. 6, pp. 649–657, 2008.
- [204] S. Heumüller, S. Wind, E. Barbosa-Sicard et al., "Apocynin is not an inhibitor of vascular NADPH oxidases but an antioxidant," *Hypertension*, vol. 51, no. 2, pp. 211–217, 2008.
- [205] K. A. Trumbull, D. McAllister, M. M. Gandelman et al., "Diapocynin and apocynin administration fails to significantly extend survival in G93A SOD1 ALS mice," *Neurobiology of Disease*, vol. 45, no. 1, pp. 137–144, 2012.
- [206] J. Stefanska, M. Sokolowska, A. Sarniak et al., "Apocynin decreases hydrogen peroxide and nitrate concentrations in exhaled breath in healthy subjects," *Pulmonary Pharmacology & Therapeutics*, vol. 23, no. 1, pp. 48–54, 2010.
- [207] S. Dikalov, "Cross talk between mitochondria and NADPH oxidases," *Free Radical Biology & Medicine*, vol. 51, no. 7, pp. 1289–1301, 2011.
- [208] X. R. Zhang, W. X. Zhou, and Y. X. Zhang, "Improvements in SOD mimic AEOL-10150, a potent broad-spectrum antioxidant," *Military Medical Research*, vol. 5, no. 1, p. 30, 2018.
- [209] M. Patel and B. J. Day, "Metalloporphyrin class of therapeutic catalytic antioxidants," *Trends in Pharmacological Sciences*, vol. 20, no. 9, pp. 359–364, 1999.
- [210] S. Petri, M. Kiaei, K. Kipiani et al., "Additive neuroprotective effects of a histone deacetylase inhibitor and a catalytic antioxidant in a transgenic mouse model of amyotrophic lateral sclerosis," *Neurobiology of Disease*, vol. 22, no. 1, pp. 40–49, 2006.
- [211] J. P. Crow, N. Y. Calingasan, J. Chen, J. L. Hill, and M. F. Beal, "Manganese porphyrin given at symptom onset markedly extends survival of ALS mice," *Annals of Neurology*, vol. 58, no. 2, pp. 258–265, 2005.
- [212] H. Shichinohe, S. Kuroda, H. Yasuda et al., "Neuroprotective effects of the free radical scavenger Edaravone (MCI-186) in mice permanent focal brain ischemia," *Brain Research*, vol. 1029, no. 2, pp. 200–206, 2004.
- [213] K. Abe, Y. Itoyama, G. Sobue et al., "Confirmatory double-blind, parallel-group, placebo-controlled study of efficacy and safety of edaravone (MCI-186) in amyotrophic lateral sclerosis patients," *Amyotrophic Lateral Sclerosis and Frontotemporal Degeneration*, vol. 15, no. 7-8, pp. 610–617, 2014.
- [214] O. Firuzi, R. Miri, M. Tavakkoli, and L. Saso, "Antioxidant therapy: current status and future prospects," *Current Medicinal Chemistry*, vol. 18, no. 25, pp. 3871–3888, 2011.
- [215] A. Mizuno, K. Umemura, and M. Nakashima, "Inhibitory effect of MCI-186, a free radical scavenger, on cerebral ischemia following rat middle cerebral artery occlusion," *General Pharmacology*, vol. 30, no. 4, pp. 575–578, 1998.
- [216] T. Yamamoto, S. Yuki, T. Watanabe, M. Mitsuka, K. I. Saito, and K. Kogure, "Delayed neuronal death prevented by inhibition of increased hydroxyl radical formation in a transient cerebral ischemia," *Brain Research*, vol. 762, no. 1-2, pp. 240–242, 1997.
- [217] Y. Takayasu, J. Nakaki, T. Kawasaki et al., "Edaravone, a radical scavenger, inhibits mitochondrial permeability transition pore in rat brain," *Journal of Pharmacological Sciences*, vol. 103, no. 4, pp. 434–437, 2007.
- [218] M. S. Jami, Z. Salehi-Najafabadi, F. Ahmadijad et al., "Edaravone leads to proteome changes indicative of neuronal cell protection in response to oxidative stress," *Neurochemistry International*, vol. 90, pp. 134–141, 2015.
- [219] M. Zhang, C. H. Teng, F. F. Wu et al., "Edaravone attenuates traumatic brain injury through anti-inflammatory and antioxidative modulation," *Experimental and Therapeutic Medicine*, vol. 18, no. 1, pp. 467–474, 2019.
- [220] M. Banno, T. Mizuno, H. Kato et al., "The radical scavenger edaravone prevents oxidative neurotoxicity induced by peroxynitrite and activated microglia," *Neuropharmacology*, vol. 48, no. 2, pp. 283–290, 2005.
- [221] Q. Wang, X. Zhang, S. Chen et al., "Prevention of motor neuron degeneration by novel iron chelators in SOD1^{-G93A} transgenic mice of amyotrophic lateral sclerosis," *Neurodegenerative Diseases*, vol. 8, no. 5, pp. 310–321, 2011.
- [222] N. Miyamoto, T. Maki, L. D. D. Pham et al., "Oxidative stress interferes with white matter renewal after prolonged cerebral hypoperfusion in mice," *Stroke*, vol. 44, no. 12, pp. 3516–3521, 2013.
- [223] M. Aoki, H. Warita, H. Mizuno, N. Suzuki, S. Yuki, and Y. Itoyama, "Feasibility study for functional test battery of SOD transgenic rat (H46R) and evaluation of edaravone, a free radical scavenger," *Brain Research*, vol. 1382, pp. 321–325, 2011.
- [224] H. Ito, R. Wate, J. Zhang et al., "Treatment with edaravone, initiated at symptom onset, slows motor decline and decreases SOD1 deposition in ALS mice," *Experimental Neurology*, vol. 213, no. 2, pp. 448–455, 2008.
- [225] H. Yoshino and A. Kimura, "Investigation of the therapeutic effects of edaravone, a free radical scavenger, on amyotrophic lateral sclerosis (Phase II study)," *Amyotrophic Lateral Sclerosis*, vol. 7, no. 4, pp. 241–245, 2006.
- [226] THE WRITING GROUP ON BEHALF OF THE EDARAVONE (MCI-186) ALS 19 STUDY GROUP, "Open-label 24-week extension study of edaravone (MCI-186) in amyotrophic lateral sclerosis," *Amyotrophic Lateral Sclerosis and Frontotemporal Degeneration*, vol. 18, Supplement 1, pp. 55–63, 2017.
- [227] O. Hardiman and L. H. van den Berg, "Edaravone: a new treatment for ALS on the horizon?," *Lancet Neurology*, vol. 16, no. 7, pp. 490–491, 2017.
- [228] G. Bensimon, L. Lacomblez, and V. Meininger, "A controlled trial of riluzole in amyotrophic lateral sclerosis. ALS/Riluzole

- Study Group," *The New England Journal of Medicine*, vol. 330, no. 9, pp. 585–591, 1994.
- [229] R. G. Miller, J. P. Bouchard, P. Duquette et al., "Clinical trials of riluzole in patients with ALS," *Neurology*, vol. 47, no. Issue 4, Supplement 2, pp. 86S–92S, 1996.
- [230] M. Jackson, J. Lladó, and J. D. Rothstein, "Therapeutic developments in the treatment of amyotrophic lateral sclerosis," *Expert Opinion on Investigational Drugs*, vol. 11, no. 10, pp. 1343–1364, 2005.
- [231] M. K. Jaiswal, "Riluzole and edaravone: a tale of two amyotrophic lateral sclerosis drugs," *Medicinal Research Reviews*, vol. 39, no. 2, pp. 733–748, 2019.
- [232] A. C. Rego and C. R. Oliveira, "Mitochondrial dysfunction and reactive oxygen species in excitotoxicity and apoptosis: implications for the pathogenesis of neurodegenerative diseases," *Neurochemical Research*, vol. 28, no. 10, pp. 1563–1574, 2003.
- [233] K. M. Noh, J. Y. Hwang, H. C. Shin, and J. Y. Koh, "A novel neuroprotective mechanism of riluzole: direct inhibition of protein kinase C," *Neurobiology of Disease*, vol. 7, no. 4, pp. 375–383, 2000.
- [234] J. Y. Koh, D. K. Kim, J. Y. Hwang, Y. H. Kim, and J. H. Seo, "Antioxidative and proapoptotic effects of riluzole on cultured cortical neurons," *Journal of Neurochemistry*, vol. 72, no. 2, pp. 716–723, 1999.
- [235] Y. Deng, Z.-F. Xu, W. Liu, B. Xu, H.-B. Yang, and Y.-G. Wei, "Riluzole-triggered GSH synthesis via activation of glutamate transporters to antagonize methylmercury-induced oxidative stress in rat cerebral cortex," *Oxidative Medicine and Cellular Longevity*, vol. 2012, 534712 pages, 2012.
- [236] G. Sala, A. Arosio, E. Conti et al., "Riluzole selective antioxidant effects in cell models expressing amyotrophic lateral sclerosis endophenotypes," *Clinical Psychopharmacology and Neuroscience*, vol. 17, no. 3, pp. 438–442, 2019.
- [237] M. C. Hogg, L. Halang, I. Woods, K. S. Coughlan, and J. H. M. PREHN, "Riluzole does not improve lifespan or motor function in three ALS mouse models," *Amyotrophic Lateral Sclerosis and Frontotemporal Degeneration*, vol. 19, no. 5-6, pp. 438–445, 2018.
- [238] M. Nagase, Y. Yamamoto, Y. Miyazaki, and H. Yoshino, "Increased oxidative stress in patients with amyotrophic lateral sclerosis and the effect of edaravone administration," *Redox Report*, vol. 21, no. 3, pp. 104–112, 2016.
- [239] K. Yaku, K. Okabe, and T. Nakagawa, "NAD metabolism: implications in aging and longevity," *Ageing Research Reviews*, vol. 47, pp. 1–17, 2018.
- [240] A. Salminen, K. Kaarniranta, and A. Kauppinen, "Crosstalk between oxidative stress and SIRT1: impact on the aging process," *International Journal of Molecular Sciences*, vol. 14, no. 2, pp. 3834–3859, 2013.
- [241] S. Austin and J. St-Pierre, "PGC1 and mitochondrial metabolism - emerging concepts and relevance in ageing and neurodegenerative disorders," *Journal of Cell Science*, vol. 125, no. 21, pp. 4963–4971, 2012.
- [242] P. J. Fernandez-Marcos and J. Auwerx, "Regulation of PGC-1 α , a nodal regulator of mitochondrial biogenesis," *The American Journal of Clinical Nutrition*, vol. 93, no. 4, pp. 884S–890S, 2011.
- [243] G. M. Pasinetti, A. E. Bilski, and W. Zhao, "Sirtuins as therapeutic targets of ALS," *Cell Research*, vol. 23, no. 9, pp. 1073–1074, 2013.
- [244] S. Körner, S. Bösel, N. Thau, K. J. Rath, R. Dengler, and S. Petri, "Differential sirtuin expression patterns in amyotrophic lateral sclerosis (ALS) postmortem tissue: neuroprotective or neurotoxic properties of sirtuins in ALS?," *Neurodegenerative Diseases*, vol. 11, no. 3, pp. 141–152, 2013.
- [245] S. Han, J. R. Choi, K. Soon Shin, and S. J. Kang, "Resveratrol upregulated heat shock proteins and extended the survival of G93A-SOD1 mice," *Brain Research*, vol. 1483, pp. 112–117, 2012.
- [246] W. Song, Y. Song, B. Kincaid, B. Bossy, and E. Bossy-Wetzel, "Mutant SOD1G93A triggers mitochondrial fragmentation in spinal cord motor neurons: neuroprotection by SIRT3 and PGC-1 α ," *Neurobiology of Disease*, vol. 51, pp. 72–81, 2013.
- [247] N. Braidy, J. Berg, J. Clement et al., "Role of nicotinamide adenine dinucleotide and related precursors as therapeutic targets for age-related degenerative diseases: rationale, biochemistry, pharmacokinetics, and outcomes," *Antioxidants & Redox Signaling*, vol. 30, no. 2, pp. 251–294, 2019.
- [248] B. A. Harlan, M. Pehar, D. R. Sharma, G. Beeson, C. C. Beeson, and M. R. Vargas, "Enhancing NAD⁺ salvage pathway reverts the toxicity of primary astrocytes expressing amyotrophic lateral sclerosis-linked mutant superoxide dismutase 1 (SOD1)," *The Journal of Biological Chemistry*, vol. 291, no. 20, pp. 10836–10846, 2016.
- [249] B. A. Harlan, K. M. Killoy, M. Pehar, L. Liu, J. Auwerx, and M. R. Vargas, "Evaluation of the NAD(+) biosynthetic pathway in ALS patients and effect of modulating NAD(+) levels in hSOD1-linked ALS mouse models," *Experimental Neurology*, vol. 327, p. 113219, 2020.
- [250] J. Ma, B. Feng, D. Kong et al., "Production and validation of human induced pluripotent stem cell line from sporadic amyotrophic lateral sclerosis (SALS)," *Stem Cell Research*, vol. 44, p. 101760, 2020.
- [251] Q. Zhou, L. Zhu, W. Qiu et al., "Nicotinamide riboside enhances mitochondrial proteostasis and adult neurogenesis through activation of mitochondrial unfolded protein response signaling in the brain of ALS SOD1G93AMice," *International Journal of Biological Sciences*, vol. 16, no. 2, pp. 284–297, 2020.
- [252] B. A. Harlan, M. Pehar, K. M. Killoy, and M. R. Vargas, "Enhanced SIRT6 activity abrogates the neurotoxic phenotype of astrocytes expressing ALS-linked mutant SOD1," *The FASEB Journal*, vol. 33, no. 6, pp. 7084–7091, 2019.
- [253] J. E. de la Rubia, E. Drehmer, J. É. L. Platero et al., "Efficacy and tolerability of EH301 for amyotrophic lateral sclerosis: a randomized, double-blind, placebo-controlled human pilot study," *Amyotrophic Lateral Sclerosis and Frontotemporal Degeneration*, vol. 20, no. 1-2, pp. 115–122, 2019.
- [254] M. P. Murphy and R. A. Smith, "Targeting antioxidants to mitochondria by conjugation to lipophilic cations," *Annual Review of Pharmacology and Toxicology*, vol. 47, no. 1, pp. 629–656, 2007.
- [255] P. G. Finichiu, A. M. James, L. Larsen, R. A. J. Smith, and M. P. Murphy, "Mitochondrial accumulation of a lipophilic cation conjugated to an ionisable group depends on membrane potential, pH gradient and pK(a): implications for the design of mitochondrial probes and therapies," *Journal of Bioenergetics and Biomembranes*, vol. 45, no. 1-2, pp. 165–173, 2013.
- [256] G. F. Kelso, C. M. Porteous, C. V. Coulter et al., "Selective targeting of a redox-active ubiquinone to mitochondria within

- cells: antioxidant and antiapoptotic properties," *The Journal of Biological Chemistry*, vol. 276, no. 7, pp. 4588–4596, 2001.
- [257] H. M. Cochemé, G. F. Kelso, A. M. James et al., "Mitochondrial targeting of quinones: therapeutic implications," *Mitochondrion*, vol. 7, Supplement, pp. S94–102, 2007.
- [258] R. A. Smith and M. P. Murphy, "Animal and human studies with the mitochondria-targeted antioxidant MitoQ," *Annals of the New York Academy of Sciences*, vol. 1201, no. 1, pp. 96–103, 2010.
- [259] M. E. Solesio, T. A. Prime, A. Logan et al., "The mitochondria-targeted anti-oxidant MitoQ reduces aspects of mitochondrial fission in the 6-OHDA cell model of Parkinson's disease," *Biochimica et Biophysica Acta*, vol. 1832, no. 1, pp. 174–182, 2013.
- [260] A. Ghosh, K. Chandran, S. V. Kalivendi et al., "Neuroprotection by a mitochondria-targeted drug in a Parkinson's disease model," *Free Radical Biology & Medicine*, vol. 49, no. 11, pp. 1674–1684, 2010.
- [261] M. J. McManus, M. P. Murphy, and J. L. Franklin, "The mitochondria-targeted antioxidant MitoQ prevents loss of spatial memory retention and early neuropathology in a transgenic mouse model of Alzheimer's disease," *The Journal of Neuroscience*, vol. 31, no. 44, pp. 15703–15715, 2011.
- [262] M. Manczak, P. Mao, M. J. Calkins et al., "Mitochondria-targeted antioxidants protect against amyloid-beta toxicity in Alzheimer's disease neurons," *Journal of Alzheimer's Disease*, vol. 20, Supplement 2, pp. S609–S631, 2010.
- [263] B. J. Snow, F. L. Rolfe, M. M. Lockhart et al., "A double-blind, placebo-controlled study to assess the mitochondria-targeted antioxidant MitoQ as a disease-modifying therapy in Parkinson's disease," *Movement Disorders*, vol. 25, no. 11, pp. 1670–1674, 2010.
- [264] P. Cassina, A. Cassina, M. Pehar et al., "Mitochondrial dysfunction in SOD1G93A-bearing astrocytes promotes motor neuron degeneration: prevention by mitochondrial-targeted antioxidants," *The Journal of Neuroscience*, vol. 28, no. 16, pp. 4115–4122, 2008.
- [265] E. Miquel, A. Cassina, L. Martínez-Palma et al., "Neuroprotective effects of the mitochondria-targeted antioxidant MitoQ in a model of inherited amyotrophic lateral sclerosis," *Free Radical Biology & Medicine*, vol. 70, pp. 204–213, 2014.
- [266] E. J. Gane, F. Weilert, D. W. Orr et al., "The mitochondria-targeted anti-oxidant mitoquinone decreases liver damage in a phase II study of hepatitis C patients," *Liver International*, vol. 30, no. 7, pp. 1019–1026, 2010.
- [267] J. Zielonka, J. Joseph, A. Sikora et al., "Mitochondria-targeted triphenylphosphonium-based compounds: syntheses, mechanisms of action, and therapeutic and diagnostic applications," *Chemical Reviews*, vol. 117, no. 15, pp. 10043–10120, 2017.
- [268] M. Pehar, M. R. Vargas, K. M. Robinson et al., "Mitochondrial superoxide production and nuclear factor erythroid 2-related factor 2 activation in p75 neurotrophin receptor-induced motor neuron apoptosis," *The Journal of Neuroscience*, vol. 27, no. 29, pp. 7777–7785, 2007.
- [269] S. Petri, M. Kiaei, M. Damiano et al., "Cell-permeable peptide antioxidants as a novel therapeutic approach in a mouse model of amyotrophic lateral sclerosis," *Journal of Neurochemistry*, vol. 98, no. 4, pp. 1141–1148, 2006.
- [270] K. Zhao, G. M. Zhao, D. Wu et al., "Cell-permeable peptide antioxidants targeted to inner mitochondrial membrane inhibit mitochondrial swelling, oxidative cell death, and reperfusion injury," *The Journal of Biological Chemistry*, vol. 279, no. 33, pp. 34682–34690, 2004.
- [271] K. Zhao, G. Luo, S. Giannelli, and H. H. Szeto, "Mitochondria-targeted peptide prevents mitochondrial depolarization and apoptosis induced by tert-butyl hydroperoxide in neuronal cell lines," *Biochemical Pharmacology*, vol. 70, no. 12, pp. 1796–1806, 2005.
- [272] S. Scott, J. E. Kranz, J. Cole et al., "Design, power, and interpretation of studies in the standard murine model of ALS," *Amyotrophic Lateral Sclerosis*, vol. 9, no. 1, pp. 4–15, 2009.
- [273] A. C. Ludolph, C. Bendotti, E. Blaugrund et al., "Guidelines for preclinical animal research in ALS/MND: a consensus meeting," *Amyotrophic Lateral Sclerosis*, vol. 11, no. 1-2, pp. 38–45, 2010.
- [274] M. Benatar, "Lost in translation: treatment trials in the SOD1 mouse and in human ALS," *Neurobiology of Disease*, vol. 26, no. 1, pp. 1–13, 2007.
- [275] E. Pollari, G. Goldsteins, G. Å. Bart, J. Koistinaho, and R. Giniatullin, "The role of oxidative stress in degeneration of the neuromuscular junction in amyotrophic lateral sclerosis," *Frontiers in Cellular Neuroscience*, vol. 8, p. 131, 2014.
- [276] J. R. Morrice, C. Y. Gregory-Evans, and C. A. Shaw, "Animal models of amyotrophic lateral sclerosis: a comparison of model validity," *Neural Regeneration Research*, vol. 13, no. 12, pp. 2050–2054, 2018.
- [277] C. Lutz, "Mouse models of ALS: past, present and future," *Brain Research*, vol. 1693, no. Part A, pp. 1–10, 2018.
- [278] P. Bossolasco, F. Sassone, V. Gumina, S. Peverelli, M. Garzo, and V. Silani, "Motor neuron differentiation of iPSCs obtained from peripheral blood of a mutant TARDBP ALS patient," *Stem Cell Research*, vol. 30, pp. 61–68, 2018.
- [279] F. B. Russo, F. R. Cugola, I. R. Fernandes, G. C. Pignatari, and P. C. Beltrão-Braga, "Induced pluripotent stem cells for modeling neurological disorders," *World Journal of Transplantation*, vol. 5, no. 4, pp. 209–221, 2015.

Research Article

Dexmedetomidine Alleviates Lipopolysaccharide-Induced Acute Kidney Injury by Inhibiting p75NTR-Mediated Oxidative Stress and Apoptosis

Zhe Wang¹,^{ORCID} Jiali Wu,² Zhaolan Hu,¹ Cong Luo,¹ Pengfei Wang,¹ Yanling Zhang,¹ and Hui Li¹^{ORCID}

¹Department of Anesthesiology, The Second Xiangya Hospital, Central South University, Changsha, China

²Department of Laboratory Medicine, The First Affiliated Hospital, Sun Yat-sen University, Guangzhou, China

Correspondence should be addressed to Hui Li; lihui_1166@csu.edu.cn

Received 13 May 2020; Revised 22 July 2020; Accepted 7 October 2020; Published 31 October 2020

Academic Editor: Luciano Saso

Copyright © 2020 Zhe Wang et al. This is an open access article distributed under the Creative Commons Attribution License, which permits unrestricted use, distribution, and reproduction in any medium, provided the original work is properly cited.

Oxidative stress and apoptosis play a key role in the pathogenesis of sepsis-associated acute kidney injury (AKI). Dexmedetomidine (DEX) may present renal protective effects in sepsis. Therefore, we studied antioxidant effects and the mechanism of DEX in an inflammatory proximal tubular epithelial cell model and lipopolysaccharide- (LPS-) induced AKI in mice. *Methods.* We assessed renal function (creatinine, urea nitrogen), histopathology, oxidative stress (malondialdehyde (MDA) and superoxide dismutase (SOD)), and apoptosis (TUNEL staining and Cleaved caspase-3) in mice. *In vitro* experiments including Cleaved caspase-3 and p75NTR/p38MAPK/JNK signaling pathways were evaluated using western blot. Reactive oxidative species (ROS) production and apoptosis were determined using flow cytometry. *Results.* DEX significantly improved renal function and kidney injury and also revert the substantially increased level of MDA concentrations as well as the reduction of the SOD enzyme activity found in LPS-induced AKI mice. In parallel, DEX treatment also reduced the apoptosis and Cleaved caspase-3 expression evoked by LPS. The expression of p75NTR was increased in kidney tissues of mice with AKI but decreased after treatment with DEX. In cultured human renal tubular epithelial cell line (HK-2 cells), DEX inhibited LPS-induced apoptosis and generation of ROS, but this was reversed by overexpression of p75NTR. Furthermore, pretreatment with DEX significantly downregulated phosphorylation of JNK and p38MAPK in LPS-stimulated HK-2 cells, and this effect was abolished by overexpression of p75NTR. *Conclusion.* DEX ameliorated AKI in mice with sepsis by partially reducing oxidative stress and apoptosis through regulation of p75NTR/p38MAPK/JNK signaling pathways.

1. Introduction

Sepsis is a complex disease characterized by a maladaptive host response to infection resulting in organ dysfunction and shock [1]. More than 50% of patients with sepsis develop acute kidney injury (AKI), a common complication of sepsis and endotoxemia [2]. Lipopolysaccharide (LPS) is a component of the outer membrane of Gram-negative bacteria, and an injection of LPS is commonly used in a model of experimental sepsis-associated AKI [3]. LPS primarily combines with toll-like receptor 4 (TLR4) to activate an inflammation pathway [4] and simultaneously generate

abundant reactive oxygen species (ROS) [5]. ROS triggers cellular dysfunction, detachment, and apoptotic cell death in proximal tubules [6]. Studies have reported that sepsis-related AKI is principally caused by glomerular or tubular apoptosis, in particular in tubular epithelial cells [7]. Little progress has been made on the pharmacological treatment of AKI associated with sepsis, despite the existing knowledge on the prevention mechanism of oxidative stress and apoptosis in proximal tubular cells which is critical to the management of sepsis-associated AKI.

The α_2 -adrenoreceptors are widely distributed in renal proximal and distal tubules and in peritubular tissues [8].

Dexmedetomidine (DEX) is a potent α_2 -adrenergic agonist, which has been proclaimed to exhibit antioxidant and anti-inflammatory effects [9, 10]. Previous research has demonstrated that DEX mitigates apoptosis; it has been established to protect organs by exhibiting protective effects against ischemia/reperfusion (I/R) injury in the liver, heart, and kidney [11–13]. Intraperitoneal injection of DEX was able to alleviate oxidative stress damage in LPS-induced acute liver injury [14]. Of particular importance is the protective effect of DEX on perioperative AKI revealed in several clinical studies [9, 15]. Experimental studies have demonstrated that DEX remarkably attenuates renal oxidative stress and apoptosis in early LPS-induced AKI [16]. However, the exact effect of DEX on tubular epithelial cells in mice with sepsis-associated AKI has not been fully elucidated.

The p75 neurotrophin receptor (p75NTR) is a multi-functional transmembrane protein with the ability to bind members of the neurotrophin family, including nerve growth factor (NGF), brain-derived neurotrophic factor (BDNF), and their precursors like proNGF and proBDNF [17]. Studies of mice have revealed that p75NTR is crucial for naturally occurring developmental apoptosis within the retina, superior cervical ganglia, spinal cord, and basal forebrain [18–21]. A lipid peroxidation product, 4-hydroxynonenal (HNE), resulted in neurite degeneration and apoptosis, which was reduced in p75NTR^{-/-} mice [22]. Moreover, several types of injury such as seizure, ischemia, and oxidative stress cause upregulation of p75NTR in brain neurons [23, 24]. p75NTR-induced superoxide production and subsequent apoptosis have also been reported in motor neurons [25]. p75NTR has also been reported to participate in kidney development and is distributed in kidney tissues [26]. Strikingly, p75NTR is overexpressed in kidneys under pathological conditions such as renal cell carcinoma [27], diabetic nephropathy [28], and chronic kidney disease [29].

No study has focused on the expression and role of p75NTR in AKI to date. Protective effects of DEX in high glucose-induced apoptosis can be reversed by overexpression of p75NTR in human retinal pigment epithelial cells [30], suggesting that DEX acts on p75NTR in AKI. Therefore, we examined whether DEX can alleviate LPS-induced apoptosis in tubular epithelial cells and AKI and the role of p75NTR.

2. Materials and Methods

2.1. Animals and Treatments. Male C57BL/6 mice (age, 7–8 weeks; weight, 20–22 g) were obtained from the Central South University Animal Service (Changsha, China). Mice were housed under conditions of constant temperature (25°C), 50 ± 10% relative humidity, and 12-hour light-dark cycle, and they had free access to food and water. Mice were randomly divided into the following three groups ($n = 6 - 10$ in each group): (I) control group mice i.p. with saline solution, (II) LPS group mice i.p. with LPS (L2880-25MG, Sigma-Aldrich, St. Louis, CA, USA) at a dose of 10 mg/kg once, and (III) LPS+low dose of DEX group which had mice i.p. injected with 10 μ g/kg of DEX (H20090248, Jiangsu Hengrui Pharmaceutical Co., Ltd., China) 30 minutes before

treatment with LPS, (IV) LPS+DEX group which had mice i.p. with 30 μ g/kg of DEX 30 minutes before treatment with LPS, and (V) LPS+large dose of DEX group which had mice i.p. with 50 μ g/kg of DEX 30 minutes before treatment with LPS. The mice in each group had free access to food and water under pathogen-free conditions. After LPS administration, survival rate was then recorded for the next 120 hours. All experiments were approved by the Hospital Ethics Committee of the Second Xiangya Hospital of Central South University and carried out in accordance with the National Institutes of Health Guide for the Care and Use of Laboratory Animals (NIH Publications No. 8023, revised 1978).

2.2. Cell Culture and Treatments. Human renal tubular epithelial cell line (HK-2 cell) was purchased from the Cell Bank of the Chinese Academy of Sciences and cultured in minimum essential medium (MEM) (Invitrogen, Carlsbad, CA, USA) with 10% fetal bovine serum (FBS) (Invitrogen, Carlsbad, CA, USA) at a temperature of 37°C and 5% CO₂. In the *in vitro* experiments and western blot of the signaling pathway, the dose of LPS and DEX is as follows: LPS: HK-2 cells (density, 1×10^5 cells per well) in 12-well plates were treated with 1 μ g/mL of LPS; LPS+DEX: HK-2 cells were treated with 1 μ g/mL of LPS and 100 μ M of DEX for 24 hours. All groups are treated for 24 hours.

2.3. p75NTR Overexpression Assay. pc/p75, a pcDNA3.1 expression vector inserted in the human p75NTR gene, was purchased from GeneChem (Shanghai, China). pc/C, an empty pcDNA3.1, was also purchased from GeneChem (Shanghai, China) and used as control overexpression vector. HK-2 cells were transfected with pc/p75 or pc/C using Lipofectamine 3000 (Invitrogen, Shanghai, China) according to the manufacturer's method; the effect of p75NTR overexpression was analyzed by western blot assay after transfection.

2.4. Kidney Function Test. Mice were sacrificed at 24 hours after LPS injection, and serum was collected. Whole blood was drawn and immediately anticoagulated with ethylenediaminetetraacetic acid- (EDTA-) 2K. Subsequently, serum creatinine (Cr) and blood urea nitrogen (BUN) were automatically detected using automatic cell analyzers (ARCHITECT c 8000, Abbott Corporation, Chicago, USA).

2.5. Reverse Transcription and Quantitative Real-Time Polymerase Chain Reaction (PCR). Mice were sacrificed at 24 hours after LPS injection; kidney tissues were collected. Total RNA was extracted from kidney tissues as described previously [31]. Complementary DNA (cDNA) was synthesized using RevertAid First-Strand cDNA Synthesis kits (Thermo Scientific, Waltham, USA). Quantitative real-time PCR was performed using Synergy Brands (SYBR) Green (Bio-Rad, Hercules, CA, USA) on CFX96 Touch™ Deep Well Real-Time PCR Detection System (Bio-Rad, Hercules, CA, USA). PCR primers were ACCACCATGGAGAAGGCTGG and CTCAGTGTAGCCCAGGATGC (glyceraldehyde-3-phosphate dehydrogenase (GAPDH)); GACAGCACAGA ATGTTCCAG and TGGCCAGATGTTCTCTATT

(inducible NOS (iNOS)); AGGGCACATACTCAGACGAA and AGATGGAGCAATAGACAGGAAT (p75NTR); ACCAACAATACGCACCAGC and AATAGCCATGCCGA ACTCC (Sortilin); TCATAAGATCCCCCTGGATG and TGCTTCTCAGCTGCCTGAC (tyrosine kinase receptor A (TrkA)); CAACAGGACTCACCGGAGCA and GGCTGC AGGCAAGTCAGCCT (NGF). Quantitative real-time PCR was performed as per the manufacturer's instructions: 95°C for 3 min, 40 cycles of 95°C for 10 sec, and 59°C for 30 s. The experiment was conducted in triplicate. Data were processed using the $2^{-\Delta\Delta Ct}$ method.

2.6. Oxidative Stress Evaluation. Mice were sacrificed at 24 hours after LPS injection; kidney tissues were collected. The kidney tissues were homogenized with phosphate-buffered solution (PBS), and the supernatants were collected. Then, the levels of malondialdehyde (MDA) and superoxide dismutase (SOD) enzyme activity were determined using commercial detection kits (A003-1 and A001-1-1, Nanjing KeyGen Biotech. Co. Ltd., Nanjing, China) according to the manufacturer's instructions. ROS of cells was assessed by flow cytometry using total reactive oxygen species (ROS) assay kit 520 nm (88-5930-74; Invitrogen, Carlsbad, CA, USA). Cells were read on the flow cytometer (Cytek, Fremont, CA, USA), and data were analyzed with the FlowJo vX0.7 software. All the steps were performed according to the manufacturer's instructions.

2.7. Measurement of Apoptosis. Mice were sacrificed at 24 hours after LPS injection; kidney tissues were collected. Kidneys from mice were fixed and made into paraffin sections. Apoptosis in kidney tissues was analyzed using a TUNEL assay kit (Roche Diagnostics, Indianapolis, USA) according to the instructions of the manufacturer. Five high-power fields ($\times 200$) were randomly selected from each slice, the number of apoptotic cells and the total number of cells were counted, and the apoptosis index (AI) = the number of apoptotic cells/the total number of cells $\times 100\%$. The HK-2 cells were assessed by flow cytometry using an Annexin V-FITC/PI kit (556547, Becton Dickinson, USA). All the steps were performed according to the manufacturer's instructions.

2.8. Western Blot. Mice were sacrificed at 24 hours after LPS injection; kidney tissues were collected. Kidney tissues were lysed in a radioimmunoprecipitation assay lysis buffer (CW Biotech, Jiangsu, China) with 1% protease inhibitor cocktails (Sigma-Aldrich, St. Louis, CA, USA) and 1% EDTA solution. Concentration of proteins was evaluated using bicinchoninic acid (BCA) protein assay kit (CW Biotech, Wuhan, China). Proteins were separated using electrophoresis and then transferred onto polyvinylidene fluoride (PVDF) membranes. Proteins were blocked with PBS and 10% fat-free milk for 1 hour followed by incubation overnight at 4°C with the following primary antibodies: anti-proNGF, PA5-77532 (1:5000, Sigma-Aldrich, St. Louis, CA, USA); anti-p75 antibody, ab8874 (1:5000); anti-NGF antibody, ab52918 (1:500, Abcam, Cambridge, United Kingdom); anti-p-JNK, ab124956 (1:2500, Abcam, Cambridge, United Kingdom);

anti-JNK, ab179461 (1:2500, Abcam, Cambridge, United Kingdom); anti-GAPDH antibody, ab8245 (1:5000, Abcam, Cambridge, United Kingdom); anti-Cleaved caspase-3 antibody, #9661 (1:1000, Cell Signaling Technology, Boston, USA); anti-P-p38, #4511 (1:2000, Cell Signaling Technology, Boston, USA); and anti-p38, #8690 (1:2000, Cell Signaling Technology, Boston, USA). Blot was then incubated with horseradish peroxidase-conjugated goat anti-rabbit IgG or goat anti-mouse IgG in Tris-buffered saline (TBS) for 2 hours at room temperature. The PVDF membrane was then exposed to film before development. Western blot band was analyzed using the mean grey value with NIH ImageJ program version 7.0 and standardized to GAPDH.

2.9. Histological Analysis. Mice were sacrificed at 24 hours after LPS injection; kidney tissues were collected. We fixed kidney tissues with 4% paraformaldehyde for 48 hours and subsequently subjected them to paraffin embedding. Mouse kidney was fixed, prepared into paraffin sections, and then stained with either hematoxylin and eosin (H&E) or Periodic Acid-Schiff stain (PAS). All images were viewed under a microscope (Nikon ECLIPSE 80i, Nikon Corporation, Tokyo, Japan) and analyzed using the ImageJ software version 7.0 (Media Cybernetics, Rockville, USA). Two pathologists used the Jablonski semiquantitative score to evaluate the degree of renal tubular damage 0-4 points: 0 points: normal; 1 point: the most mild injury of cortical or medullary outer layer $< 5\%$; 2 points: 5%-25% of leather or medullary outer layer injury; 3 points: 26%-75% of leather or medullary outer layer injury; 4 points: $> 75\%$ of leather or medullary outer layer injury [32].

2.10. Immunohistochemistry (IHC) Analysis. Paraffin-embedded tissues were cut into 4 μm thick sections, followed by antigen unmasking process, and incubated overnight at 4°C with Cleaved caspase-3 antibody (1:1000, #9661, Cell Signaling Technology, Boston, USA). Phosphate-buffered saline replaced the primary antibody as a negative control. The subsequent detection was done with the use of anti-rabbit or mouse immunohistochemistry assay kit (DAKO, Carpinteria, CA, USA) as a chromogen for visualization. Finally, hematoxylin was used to counterstain the nuclei. We chose five 40x magnification fields per tissue section at random, and two independent blinded observers obtained the mean area values of positive signals for final analysis by using the ImageJ software version 7.0 (Media Cybernetics, Rockville, USA).

2.11. Statistical Analysis. Data are expressed as mean \pm standard error of the mean (SEM). Statistical analysis was performed using the paired Student's *t*-test or one-way analysis of variance (ANOVA) followed by Bonferroni analysis where appropriate. Statistical significance was arbitrarily declared at *p* values below 0.05. All analyses were performed using SPSS version 23 (SPSS Inc., Chicago, IL, USA).

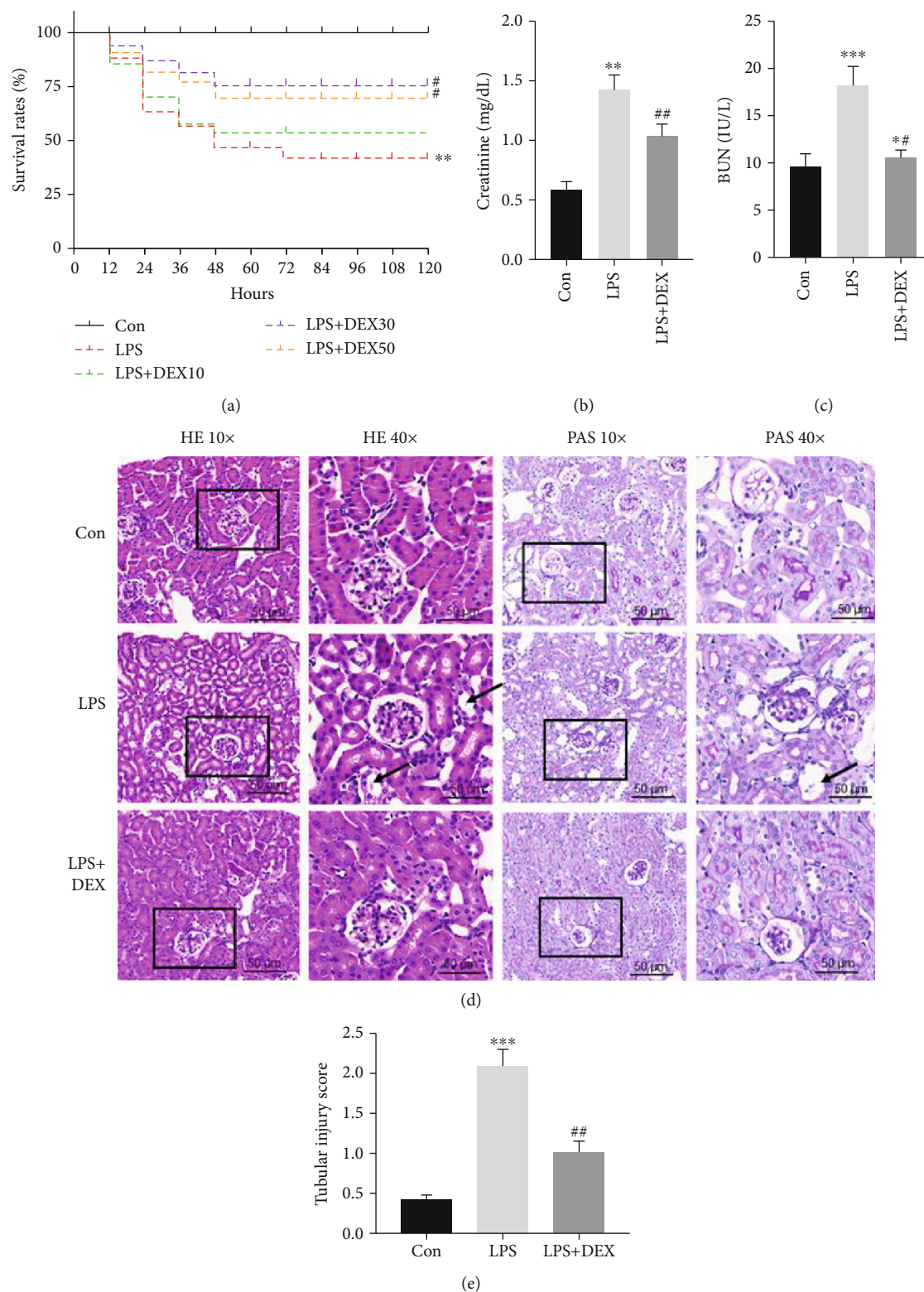


FIGURE 1: DEX improves survival rate and attenuates kidney damage induced by LPS. (a) Survival rates of septic mice, 10, 30, and 50 $\mu\text{g}/\text{kg}$ DEX pretreatment groups (** $p < 0.01$, versus control; # $p < 0.05$ versus LPS, $n = 10$ per group; log-rank (Mantel-Cox) test). (b, c) Cr and BUN levels in serum. (d) Histopathological changes in kidney tissues (scale bar = 50 μm); yellow arrow indicates tubular necrosis and vacuolar degeneration. (e) Tubular injury score (* $p < 0.05$, ** $p < 0.01$, and *** $p < 0.0001$ versus control; ## $p < 0.01$ versus LPS. Data were presented as mean \pm SEM, $n = 6$). H&E: hematoxylin and eosin; PAS: Periodic Acid-Schiff stain.

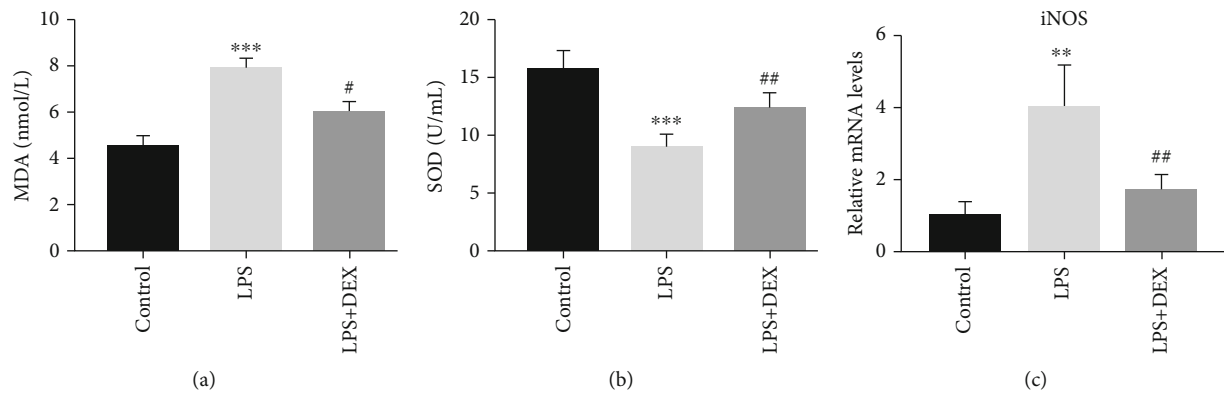


FIGURE 2: Dexmedetomidine alleviates oxidative stress in AKI induced by LPS. (a) MDA assay in kidney tissues of mice. (b) SOD assay in kidney tissues of mice. (c) Real-time PCR of iNOS in kidney tissues of mice (* $p < 0.05$, ** $p < 0.01$, and *** $p < 0.0001$ versus control; # $p < 0.05$ and ## $p < 0.01$ versus LPS. Data were presented as mean \pm SEM, $n = 6$). MDA: malondialdehyde; SOD: superoxide dismutase; iNOS: inducible nitric oxide synthase.

3. Results

3.1. DEX Alleviates LPS-Induced AKI. As shown in Figure 1(a), survival rate dropped about 80% in mice subjected to LPS injection within 12 hours and continued to decline sharply starting from 12 hours after sepsis, reaching almost 42% by 120 hours after LPS injection. Intravenous administration of 30 $\mu\text{g}/\text{kg}$ and 50 $\mu\text{g}/\text{kg}$ DEX extended lifetime and increased survival rate compared with the LPS group ($p = 0.038$ and $p = 0.042$). Kidney function was evaluated based on serum Cr and BUN which are the primary indicators of the severity of kidney damage. Levels of BUN and Cr in mice kidneys were significantly higher in the LPS group than in the control group, whereas treatment with DEX decreased serum Cr and BUN levels compared to the LPS group (Figure 1(b)). Furthermore, histological analysis in HE and PAS revealed that mice treated with LPS exhibited severe renal pathological lesions, indicated by widespread tubular necrosis, tubular degeneration, cellular swelling, and inflammatory cell infiltration in renal tissues, whereas DEX treatment significantly reversed these effects (Figure 1(c)). Kidney histology scores in the LPS group were significantly higher than those in the control group, whereas kidney scores in the DEX+LPS group were significantly lower than those in the LPS group. Our results suggest that treatment with DEX protects mice from acute kidney injury caused by LPS.

3.2. DEX Alleviates Oxidative Stress and Nitrosative Stress in AKI Induced by LPS. AKI induced by LPS breaks intracellular redox balance inducing oxidative stress [16]. MDA concentrations were substantially increased in mice injected with LPS and SOD enzyme activity concentrations were decreased, but treatment with DEX reduced levels of MDA and elevated SOD which had been changed by LPS (Figures 2(a) and 2(b)). Expression levels of mRNA for iNOS in renal tissues were further evaluated. mRNA expression levels for iNOS were considerably upregulated in renal tissues of LPS-treated mice in comparison with the control group. However, DEX remarkably reduced the upregulated

mRNA expression levels for iNOS in renal tissues of LPS-treated mice. Our results suggest that DEX considerably alleviates oxidative and nitrosative stress.

3.3. DEX Reduced Apoptosis and Expression of p75NTR in Mouse Model of AKI. A TUNEL assay was performed to examine the effects of LPS and DEX on cell apoptosis (Figure 3). The number of TUNEL-positive cells was significantly higher in mice injected with LPS than in mice in the control group, and fewer positive cells were recorded in the DEX+LPS group than in the LPS group (Figures 3(a) and 3(b)). Our findings indicate that DEX is capable of suppressing LPS-induced apoptosis in the AKI model.

We analyzed expressions of Cleaved caspase-3, p75NTR, and its upstream molecule proNGF to unravel the signaling pathways associated with protective effects of DEX in LPS-induced renal injury. A few Cleaved caspase-3-positive cells were detected in the control group. Nevertheless, the positive density of Cleaved caspase-3 in mice injected with LPS was significantly higher than that of mice in the control group. Pretreatment with DEX substantially decreased the positive density of Cleaved caspase-3 induced by LPS (Figures 3(c) and 3(d)). Western blot results demonstrated that LPS caused significant increase in the levels of Cleaved caspase-3, p75NTR, proNGF, and NGF in kidney tissues compared to the control group (Figure 3). However, levels of Cleaved caspase-3 and p75NTR in kidney tissues of mice treated with LPS were remarkably reduced after pretreatment with DEX. On the contrary, expression of proNGF and NGF remained unchanged after treatment with DEX. Then, we used PCR to complete western blot analysis; as shown in Figure 3(f), the gene expression of NGF and its receptors Sortilin and TrkA decreased in AKI model but remained unchanged after treatment with DEX. These results imply that p75NTR may be involved in pathophysiological processes related to DEX alleviating effects in AKI apoptosis.

3.4. Suppression of Apoptosis and ROS Generation in LPS-Induced Cells by Dexmedetomidine and Counteraction through Overexpression of p75NTR. In AKI animal model,

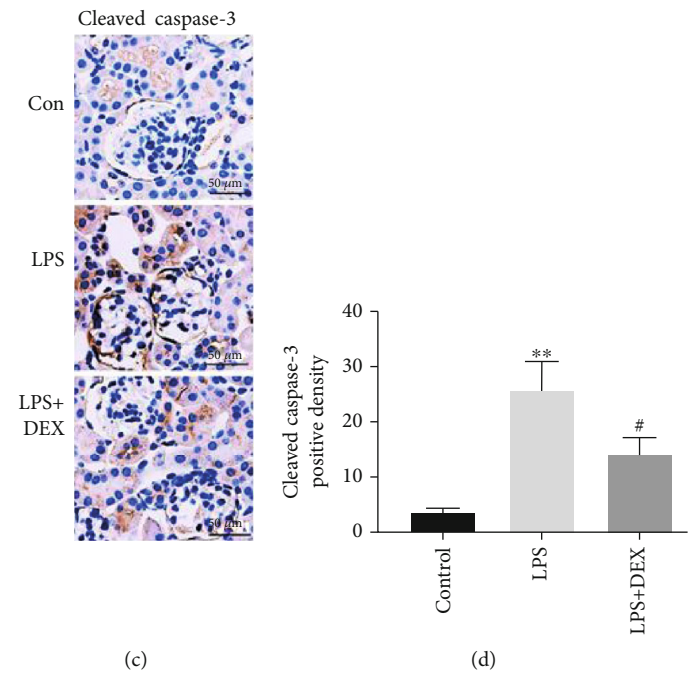
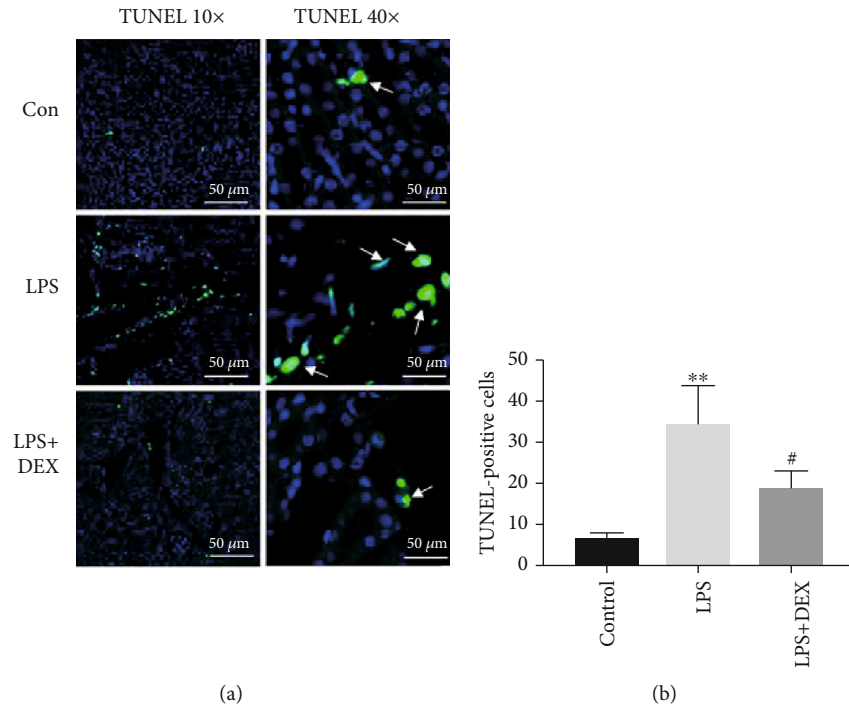


FIGURE 3: Continued.

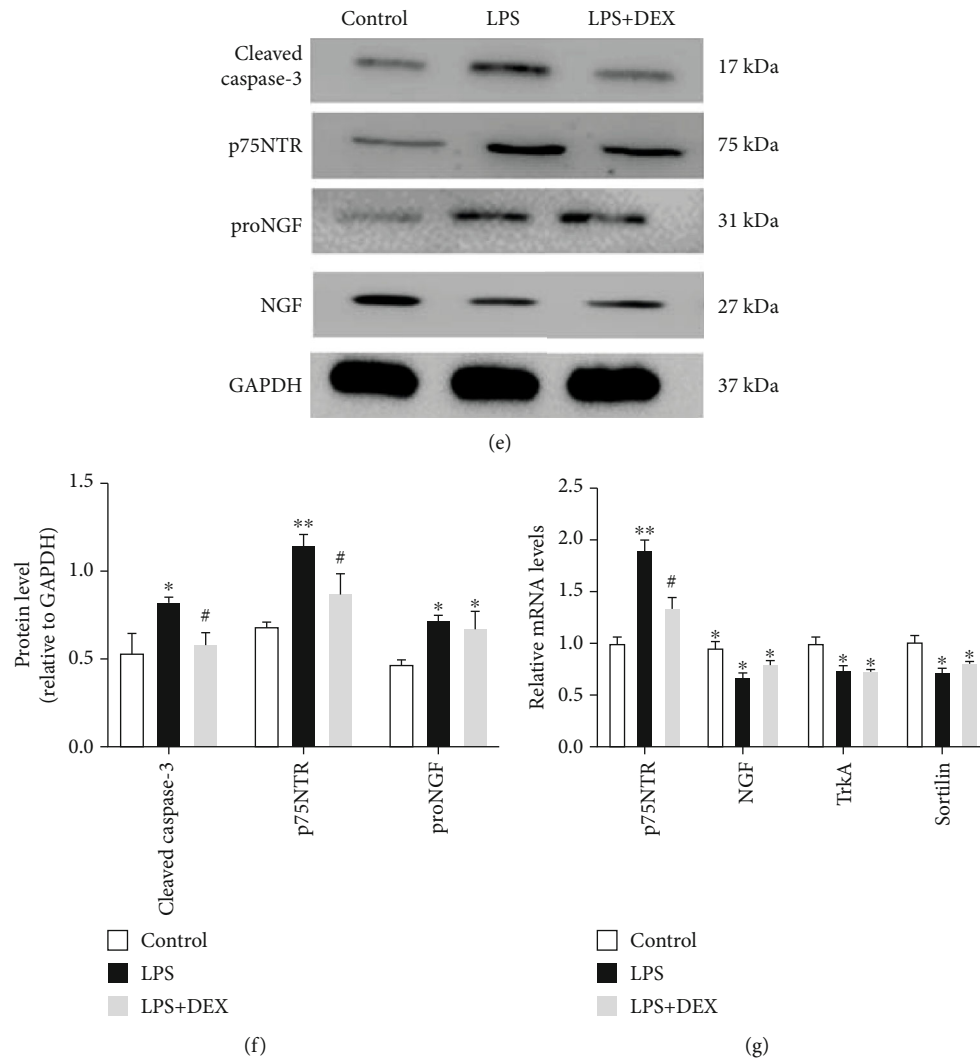


FIGURE 3: Dexmedetomidine suppressed apoptosis in AKI induced by LPS. (a, b) TUNEL staining in kidney sections of mice (scale bar = 50 μ m), white arrows to show TUNEL-positive nuclei and quantitation of TUNEL-positive cells. (c, d) Cleaved caspase-3 staining in kidney sections of mice (scale bar = 50 μ m), and quantitation of Cleaved caspase-3-positive cells. (e, f) Western blot analysis and quantitative data for Cleaved caspase-3, p75NTR, proNGF, and NGF in kidney tissues of mice; GAPDH was used as a loading control. (g) p75NTR, NGF, TrkA, and Sortilin gene expression in the kidney tissues of mice (* $p < 0.05$ and ** $p < 0.01$ versus control; # $p < 0.05$ and ## $p < 0.01$ versus LPS. Data were presented as mean \pm SEM, $n = 6$).

p75NTR protein is upregulated in the kidney tissue and reversed by DEX pretreatment. Consistently, similar alterations of p75NTR expression were observed in HK-2 cells (Figures 4(a) and 4(b)). Then, HK-2 cells were transfected through vector-mediated overexpression of pc/p75 or a controlled vector and assessed using western blot assay. Expression levels of p75NTR were much higher in pc/p75-transfected HK-2 cells than in pc/C-transfected HK-2 cells (Figures 4(c) and 4(d)).

To investigate whether p75NTR can reverse the protective effect of DEX *in vitro*, HK-2 cells were treated with LPS for 24 hours and flow cytometry assays used to analyze ROS production. ROS generation was significantly increased after LPS stimulation, and treatment with 100 μ M of DEX reduced ROS levels which had risen after treatment with LPS. Conversely, ROS levels were considerably higher in pc/p75-transfected cells than in pc/C-transfected cells (Figure 4(h)).

Consequently, results indicated that DEX suppressed ROS generation in cells treated with LPS which was countered by overexpression of p75NTR.

Cell apoptosis was substantially promoted in mice treated with LPS, and injection with 100 μ M of DEX reduced cell apoptosis from 24.6% to 13.28%. However, antiapoptotic effects of DEX were reversed through overexpression of p75NTR. Overexpression of p75NTR reversed the protective effects of DEX on apoptosis induced by LPS in HK-2 cells (Figure 4(g)).

3.5. Inhibition of p38 Mitogen-Activated Protein Kinase (MAPK-) Jun N-Terminal Kinase (JNK) Signaling Pathway by DEX in HK-2 Cells. The increased proNGF mediated p75NTR activation and subsequently induced the activation of p38MAPK and JNK signaling [33]. ROS has been reported to activate proapoptotic signaling pathways such as JNK and

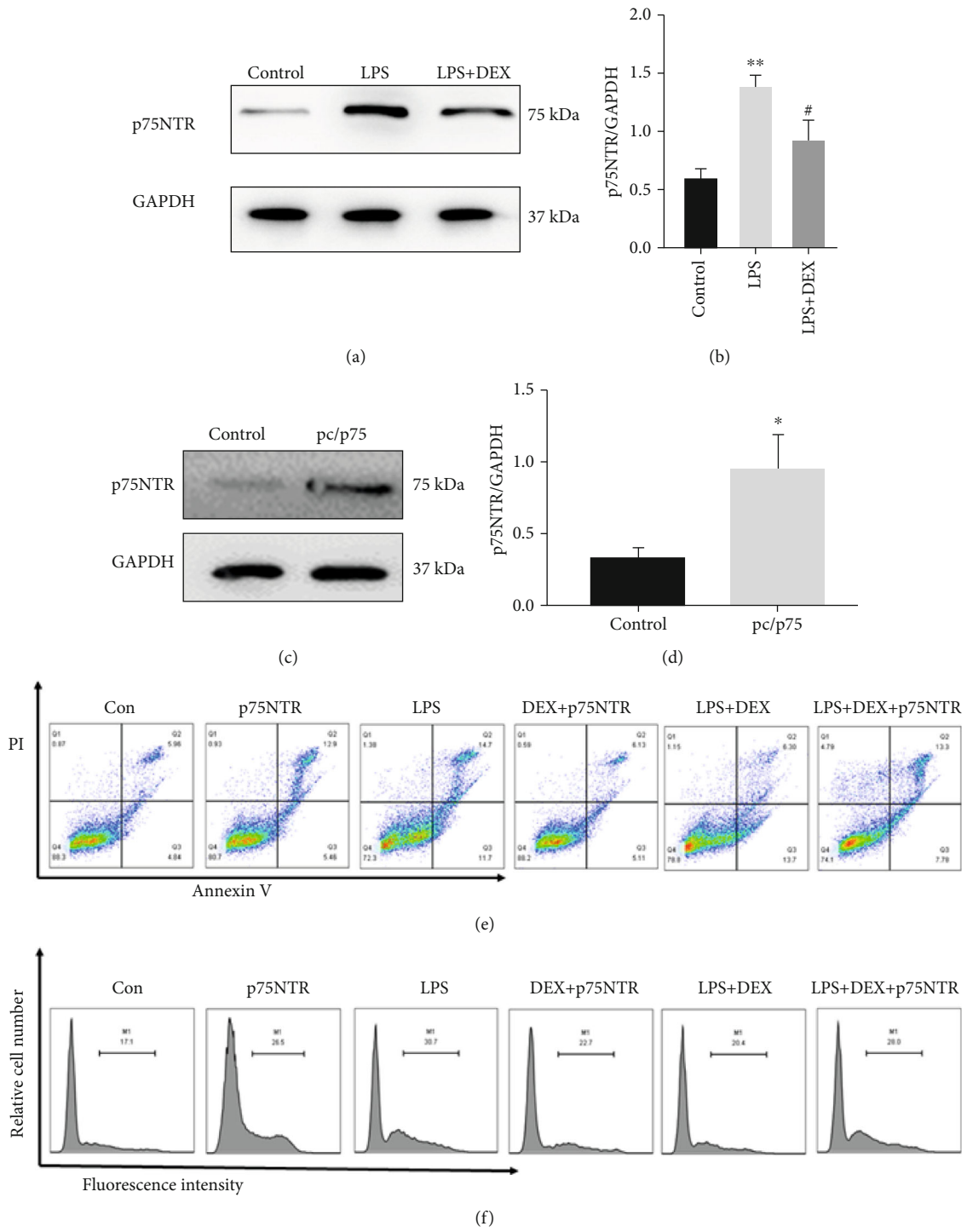


FIGURE 4: Continued.

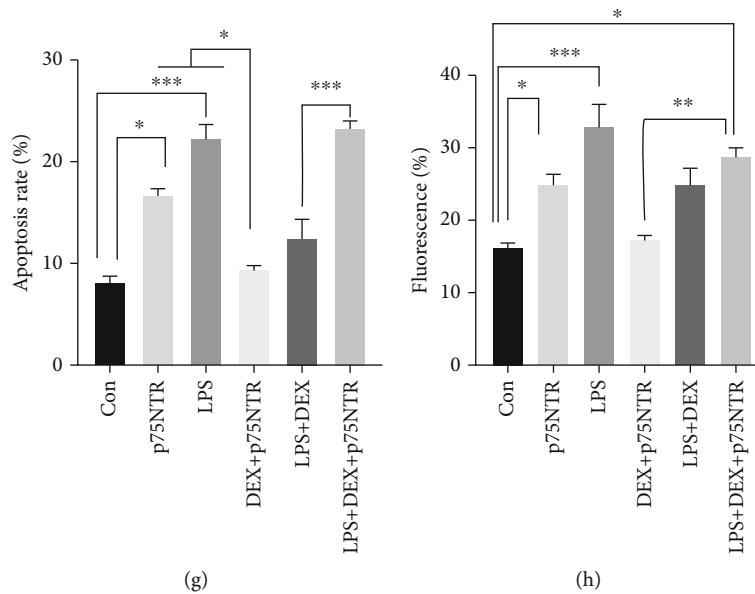


FIGURE 4: Suppression of apoptosis and ROS generation by dexmedetomidine in cells treated with LPS was reversed by overexpression of p75. (a) Western blots and (b) their semiquantitative analyses of p75NTR in the LPS-treated group or the LPS+DEX-treated group; (c) western blots and (d) their semiquantitative analyses of p75NTR in pc/C-transfected group or pc/p75-transfected group; (e) the apoptotic rate of HK-2 cells was determined by flow cytometry; (g) statistical analysis of the apoptotic rate of HK-2 cells; (f) ROS levels of HK-2 cells was determined by flow cytometry; (h) statistical analysis of the ROS fluorescence (* $p < 0.05$ and ** $p < 0.001$ versus control; # $p < 0.05$ and # $p < 0.01$ versus LPS. Data were presented as mean \pm SEM, $n = 6$).

p38MAPK through stimulation of upstream kinases [34]. Western blot analysis revealed that both JNK and p38MAPK pathways were activated by LPS (Figure 5). Incubation of HK-2 cells with DEX 24 hours significantly reduced expression of phosphorylated protein levels in p38MAPK and JNK1/2 pathways. Notably, p75NTR inhibited phosphorylation of JNK and p38MAPK pathways after treatment with DEX. Overall, the p75NTR/JNK/p38MAPK axis is involved in apoptosis associated with LPS.

4. Discussion

Acute kidney injury is one of the most severe complications of sepsis and is a rapid renal dysfunction associated with inflammation and oxidative stress. Intraperitoneal injection of LPS to induce sepsis is a commonly used animal model. LPS is a classic TLR4 agonist which can induce an immediate and robust inflammatory response thus stimulating activation of the innate immune system in human sepsis [3]. The most significant advantage of this model is that the technology used is simple and easy to replicate. Our results revealed that treatment with DEX significantly alleviated LPS-induced oxidative stress and apoptosis which consequently attenuated kidney dysfunction. Overexpression of p75NTR enhanced apoptosis, ROS generation, and phosphorylation of p38MAPK-JNK pathway but eventually reversed the protective effects of DEX in sepsis-associated AKI.

DEX is a class of highly selective α_2 -adrenergic receptor agonists with receptors which are widely distributed in the proximal and distal tubules of the kidney [8]. The protective effects of DEX have been reported against oxidative stress,

apoptosis, and pyroptosis in the brain and peripheral tissues in various *in vitro* and *in vivo* models [35, 36]. Experimental studies of animals have indicated that DEX attenuates LPS-induced renal dysfunction and histological tissue damage in the kidneys [37]. Oxidative stress has been identified as one of the critical contributors of pathogenesis in AKI [6]. Production of free radicals is eliminated by intracellular antioxidant enzymes such as SOD [38], thus maintaining the balance between production and elimination of free radicals. AKI increases superoxide production and inhibits SOD activity. MDA is the end product of lipid peroxidation and its production is increased in kidney tissues after renal I/R injury [38]; MDA contributes to cell apoptosis and is strongly involved in AKI [39]. In addition, we established that DEX reduced markers of oxidative stress including MDA and SOD and apoptosis as indicated by TUNEL and Cleaved caspase-3 analysis. The kidney consists of tubules, renal vesicles, and glomeruli. Studies have reported that sepsis-related AKI is principally caused by glomerular or tubular apoptosis [7]. In support of animal studies, our *in vitro* data firstly demonstrated that DEX alleviated LPS-induced ROS production and apoptosis in the kidney tissue, suggesting that the inhibitory effect of DEX in sepsis-related AKI is partially due to alleviation of oxidative stress and apoptosis in the tubules.

p75NTR is a member of tumor necrosis factor receptor superfamily and a transmembrane receptor that can transduce a “death”—the receptor-mediated apoptotic cascade in several neuronal populations [40]. Several studies have revealed that silencing p75NTR prevents cell death and oxidative stress, therefore alleviating diseases like neurodegenerative disorders and microvascular degeneration [41, 42].

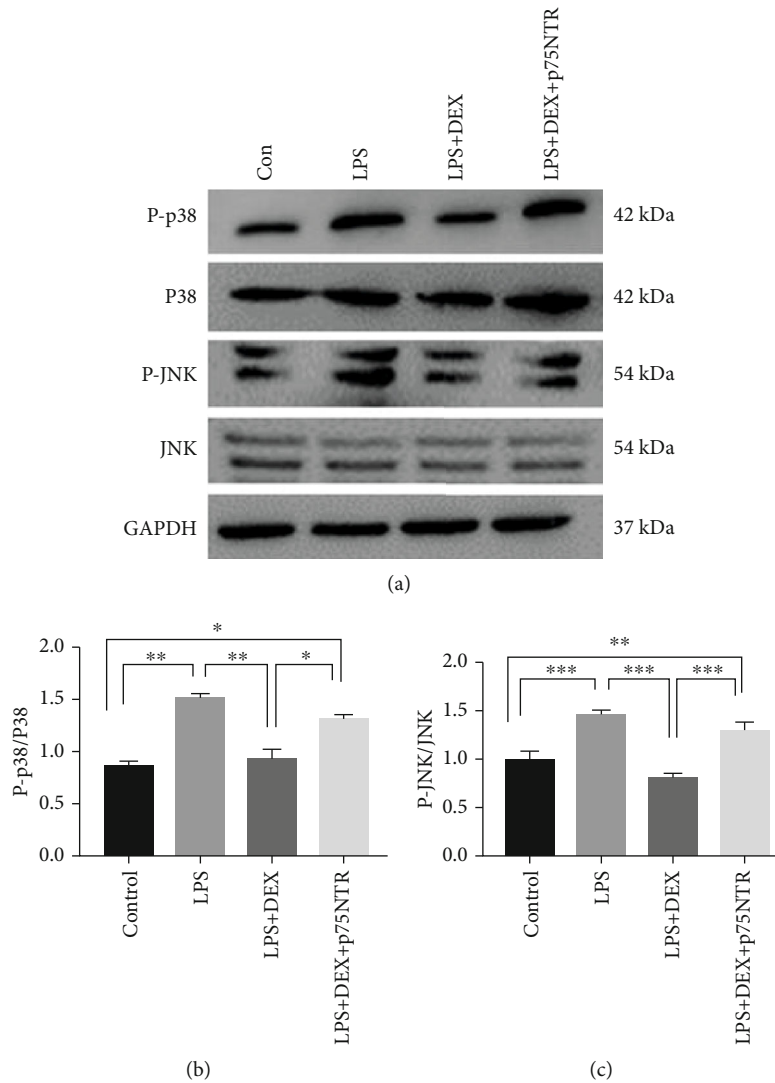


FIGURE 5: Inhibition of the p38MAPK-JNK signaling pathway by dexmedetomidine in HK-2 cells of AKI which was reversed by overexpression of p75NTR. (a) Representative western blots and (b, c) their semiquantitative analyses (* $p < 0.05$ and ** $p < 0.001$ versus control; # $p < 0.05$ and ## $p < 0.01$ versus LPS. Data were presented as mean \pm SEM, $n = 6$).

Other than its abundant expression in the central nervous system, p75NTR can also be expressed in the kidneys [27]. During the kidney development, all the developing glomeruli show a marked increase of p75NTR expression during the differentiation of mesenchymal into podocytes [43]. Previous studies have reported the upregulation of p75NTR in a mouse model with unilateral ischemic reperfusion injury [44]. Strikingly, p75NTR RNA silencing also inhibits human renal cell carcinoma (ACHN) cell migration implying that p75NTR may play an essential role in kidney diseases [45]. Nevertheless, its fundamental role in kidney injury remains unknown. In the present study, p75NTR was considerably expressed in kidney tissues in mice with LPS-induced AKI, accompanied by increased expression of markers of apoptosis and oxidative stress. These results indicate a positive correlation of p75NTR with apoptosis and oxidative stress in sepsis-related AKI. Previous studies [45] have shown that knocking down p75NTR can inhibit the ACHN cell migration and there-

fore attenuate the kidney injury. In our study, DEX decreased ROS production and apoptosis upon LPS treatment in HK-2 cells. However, overexpression of p75NTR can abolish the protective effects of DEX. These findings suggest that the protective effect of DEX is mediated by p75NTR signaling, at least in part.

In the animal studies, we have observed that LPS treatment increased the upregulation of proNGF and p75NTR. The increased ligand can act on the increased p75NTR and mediate the downstream signaling. However, DEX cannot inhibit the upregulated proNGF upon LPS treatment. Therefore, we did not examine the proNGF level in our further studies. Notably, our study cannot identify if the effect of p75NTR is ligand dependent or not. Given that DEX can downregulate the expression of p75NTR, its protective effect may not be related to the proNGF level. However, other ligands including proBDNF and proneurotrophin-3 may be changed after LPS and/or DEX treatment which need to be studied in the future.

Studies have revealed that p75NTR induces apoptosis in a JNK-dependent manner [46] and that p38MAPK and JNK pathways are crucial for amyloid-induced cell death that is mediated by p75NTR [47]. The activity of JNK can be upregulated by neurotrophins such as proNGF and proBDNF under apoptotic conditions with p75NTR [45, 48]. Currently, there is no direct evidence that DEX ameliorates septic AKI via the p38MAPK-JNK signaling pathway. Nonetheless, Walshe et al. [49] reported that DEX protects the kidney and other organs from subsequent I/R damage via p38MAPK-JNK pathway-dependent mechanisms. Targeted inhibition of p38MAPK pathway reduces renal cell apoptosis and improves renal function after I/R injury [50]. Furthermore, several studies have reported that ROS can initiate phosphorylation of JNK and p38MAPK pathways [51]. The p38MAPK-JNK pathway has been proven to have an essential function in determining the fate of renal tubular cells [52]. Our results correspond with previous observations and demonstrate that DEX can protect the kidney from oxidative stress and apoptosis by inhibiting expression of p75NTR and subsequent p38MAPK and JNK signaling pathways in tubular epithelial cells stimulated by LPS.

Over the last 30 years, numerous attempts are under way to improve outcomes for AKI patients, including therapy targeted at hemodynamics, diuretics, and oxidative stress, but little progress has been made [53]. Despite early goal-directed therapy (EGDT) becoming a standard therapy in sepsis shock, recent multicenter trials of EGDT failed to show improved survival, as well as a reduction in AKI or inflammation [54]. New therapies for sepsis-associated AKI are urgently needed. To date, large amounts of preclinical researches have investigated several potential targets to treat AKI, such as statins [55], N-acetyl-cysteine [56], and alkaline phosphatase [57], but none of them have translated into human clinical experiments of AKI. DEX is widely used in patients undergoing mechanic ventilation in ICU and operations because of its analgesic and sedative effect [58, 59]. We and other studies [60] have shown that treatment with DEX markedly attenuates LPS-induced renal dysfunction in mice and reduces injury in tubular epithelial cells. These findings point to a potential treatment strategy of DEX in sepsis-associated AKI. The effects of DEX in clinical patients warranted further study in the future.

In summary, our results demonstrated the following: (1) DEX inhibited LPS-induced ROS production and apoptosis in tubular epithelial cells indicating that the inhibitory effects observed after treatment with DEX in mice with sepsis-related AKI are partially due to alleviation of oxidative stress and apoptosis in the tubules; (2) p75NTR was highly expressed during progression of sepsis-related AKI, and overexpression of p75NTR reversed the protective effects of DEX against ROS production and apoptosis in LPS-treated tubular epithelial cells; (3) DEX reduces oxidative stress and apoptosis possibly by a mechanism that may involve the p75NTR, p38MAPK, and JNK pathways in sepsis-associated AKI. Results of this study elucidate the potential protective and molecular mechanisms of DEX in sepsis-related AKI from a perspective of oxidative stress and provide a theoretical basis for future clinical research.

5. Conclusions

DEX ameliorated AKI in mice with sepsis by practically reducing oxidative stress and apoptosis through the regulation of p75NTR/p38MAPK/JNK signaling pathways.

Data Availability

The data used to support the findings of this study are available from the corresponding author upon request.

Conflicts of Interest

The authors declare no conflict of interest.

Authors' Contributions

Li Hui and Zhe Wang designed the experiments; Zhe Wang, Jiali Wu, Zhaolan Hu, and Pengfei Wang performed the experiments and analyzed the data; Cong Luo and Yanling Zhang interpreted the results of the experiments; Zhe Wang drafted the manuscript; Hui Li edited and revised the manuscript; all authors had a final approval of the manuscript submission.

Acknowledgments

This research was supported by the National Natural Science Foundation of China (NSFC 81873770 to Hui Li).

References

- [1] C. W. Goodman and A. S. Brett, "Gabapentin and Pregabalin for Pain — Is Increased Prescribing a Cause for Concern?," *New England Journal of Medicine*, vol. 377, no. 5, pp. 411–414, 2017.
- [2] H. P. Shum, W. W. Yan, and T. M. Chan, "Recent knowledge on the pathophysiology of septic acute kidney injury: a narrative review," *Journal of Critical Care*, vol. 31, no. 1, pp. 82–89, 2016.
- [3] J. Cohen, "The immunopathogenesis of sepsis," *Nature*, vol. 420, no. 6917, pp. 885–891, 2002.
- [4] H. Yuan, C. N. Perry, C. Huang et al., "LPS-induced autophagy is mediated by oxidative signaling in cardiomyocytes and is associated with cytoprotection," *American Journal of Physiology-Heart and Circulatory Physiology*, vol. 296, no. 2, pp. H470–H479, 2009.
- [5] M. Aragno, J. C. Cutrin, R. Mastrocola et al., "Oxidative stress and kidney dysfunction due to ischemia/reperfusion in rat: attenuation by dehydroepiandrosterone," *Kidney International*, vol. 64, no. 3, pp. 836–843, 2003.
- [6] C. T. Chien, T. C. Chang, C. Y. Tsai, S. K. Shyue, and M. K. Lai, "Adenovirus-mediated bcl-2 gene transfer inhibits renal ischemia/reperfusion induced tubular oxidative stress and apoptosis," *American Journal of Transplantation*, vol. 5, no. 6, pp. 1194–1203, 2005.
- [7] P. Calzavacca, C. N. May, and R. Bellomo, "Glomerular haemodynamics, the renal sympathetic nervous system and sepsis-induced acute kidney injury," *Nephrology Dialysis Transplantation*, vol. 29, no. 12, pp. 2178–2184, 2014.

- [8] J. Gu, P. Sun, H. Zhao et al., "Dexmedetomidine provides renoprotection against ischemia-reperfusion injury in mice," *Critical Care*, vol. 15, no. 3, p. R153, 2011.
- [9] J. S. Cho, J.-K. Shim, S. Soh, M. K. Kim, and Y.-L. Kwak, "Perioperative dexmedetomidine reduces the incidence and severity of acute kidney injury following valvular heart surgery," *Kidney International*, vol. 89, no. 3, pp. 693–700, 2016.
- [10] T. Şahin, Z. Begeç, H. İ. Toprak et al., "The effects of dexmedetomidine on liver ischemia-reperfusion injury in rats," *Journal of Surgical Research*, vol. 183, no. 1, pp. 385–390, 2013.
- [11] M. Arslan, F. M. Comu, B. Isik, L. Ozturk, and E. Kesimci, "Effect of dexmedetomidine on erythrocyte deformability during ischemia-reperfusion injury of liver in diabetic rats," *Bratislava Medical Journal*, vol. 113, no. 12, pp. 687–691, 2012.
- [12] B. Gencer, T. Karaca, H. A. Tufan et al., "The protective effects of dexmedetomidine against apoptosis in retinal ischemia/reperfusion injury in rats," *Cutaneous and Ocular Toxicology*, vol. 33, no. 4, pp. 283–288, 2014.
- [13] G. Kip, A. Çelik, M. Bilge et al., "Dexmedetomidine protects from post-myocardial ischaemia reperfusion lung damage in diabetic rats," *Libyan Journal of Medicine*, vol. 10, no. 1, p. 27828, 2015.
- [14] J. Sha, H. Zhang, Y. Zhao et al., "Dexmedetomidine attenuates lipopolysaccharide-induced liver oxidative stress and cell apoptosis in rats by increasing GSK-3 β /MKP-1/Nrf2 pathway activity via the α 2 adrenergic receptor," *Toxicology and Applied Pharmacology*, vol. 364, pp. 144–152, 2019.
- [15] Y. Song, D. H. Kim, T. D. Kwon et al., "Effect of intraoperative dexmedetomidine on renal function after cytoreductive surgery and hyperthermic intraperitoneal chemotherapy: a randomized, placebo-controlled trial," *International journal of hyperthermia: the official journal of European Society for Hyperthermic Oncology, North American Hyperthermia Group*, vol. 36, no. 1, pp. 1–8, 2019.
- [16] Y. Chen, L. Luan, C. Wang et al., "Dexmedetomidine protects against lipopolysaccharide-induced early acute kidney injury by inhibiting the iNOS/NO signaling pathway in rats," *Nitric Oxide: biology and chemistry*, vol. 85, pp. 1–9, 2019.
- [17] E. Castrén and M. Kojima, "Brain-derived neurotrophic factor in mood disorders and antidepressant treatments," *Neurobiology of Disease*, vol. 97, pp. 119–126, 2017.
- [18] M. Platón-Corchado, P. F. Barcelona, S. Jmaeff et al., "p75NTR antagonists attenuate photoreceptor cell loss in murine models of retinitis pigmentosa," *Cell Death & Disease*, vol. 8, no. 7, article e2922, 2017.
- [19] L. Howard, S. Wyatt, G. Nagappan, and A. M. Davies, "ProNGF promotes neurite growth from a subset of NGF-dependent neurons by a p75NTR-dependent mechanism," *Development*, vol. 140, no. 10, pp. 2108–2117, 2013.
- [20] A. L. M. Scott and M. S. Ramer, "Schwann cell p75NTR prevents spontaneous sensory reinnervation of the adult spinal cord," *Brain: a Journal of Neurology*, vol. 133, no. 2, pp. 421–432, 2010.
- [21] L. Qian, M. R. Milne, S. Shephard, M. L. Rogers, R. Medeiros, and E. J. Coulson, "Removal of p 75 neurotrophin receptor expression from cholinergic basal forebrain neurons reduces amyloid- β plaque deposition and cognitive impairment in aged APP/PS1 mice," *Molecular Neurobiology*, vol. 56, no. 7, pp. 4639–4652, 2019.
- [22] N. Niimi, H. Yako, S. Takaku et al., "A spontaneously immortalized Schwann cell line from aldose reductase-deficient mice as a useful tool for studying polyol pathway and aldehyde metabolism," *Journal of Neurochemistry*, vol. 144, no. 6, pp. 710–722, 2018.
- [23] M. A. Hausburg, K. L. Banton, P. E. Roman et al., "Effects of propofol on ischemia-reperfusion and traumatic brain injury," *Journal of Critical Care*, vol. 56, pp. 281–287, 2020.
- [24] S. Choi and W. J. Friedman, "Interleukin-1 β enhances neuronal vulnerability to proNGF-mediated apoptosis by increasing surface expression of p75NTR and sortilin," *Neuroscience*, vol. 257, pp. 11–19, 2014.
- [25] M. Pehar, M. R. Vargas, K. M. Robinson et al., "Mitochondrial superoxide production and nuclear factor erythroid 2-related factor 2 activation in p 75 neurotrophin receptor-induced motor neuron apoptosis," *The Journal of Neuroscience: the Official Journal of the Society for Neuroscience*, vol. 27, no. 29, pp. 7777–7785, 2007.
- [26] U. M. Saarinen, S. Wikström, O. Koskimies, and H. Sariola, "Percutaneous needle biopsy preceding preoperative chemotherapy in the management of massive renal tumors in children," *Journal of Clinical Oncology: official journal of the American Society of Clinical Oncology*, vol. 9, no. 3, pp. 406–415, 1991.
- [27] M. A. De la Cruz-Morcillo, J. Berger, R. Sánchez-Prieto et al., "p75 neurotrophin receptor and pro-BDNF promote cell survival and migration in clear cell renal cell carcinoma," *Oncotarget*, vol. 7, no. 23, pp. 34480–34497, 2016.
- [28] L. Aloe, S. Rossi, and L. Manni, "Altered expression of nerve growth factor and its receptors in the kidneys of diabetic rats," *Journal of Nephrology*, vol. 24, no. 6, pp. 798–805, 2011.
- [29] Y. Sato and M. Yanagita, "Resident fibroblasts in the kidney: a major driver of fibrosis and inflammation," *Inflammation and Regeneration*, vol. 37, no. 1, 2017.
- [30] R. Liu, X. Li, and X. Zhang, "Dexmedetomidine protects high-glucose induced apoptosis in human retinal pigment epithelial cells through inhibition on p 75 (NTR)," *Biomed Pharmacother*, vol. 106, pp. 466–471, 2018.
- [31] Z. Wang, J. L. Wu, F. Zhong et al., "Upregulation of proBDNF in the mesenteric lymph nodes in septic mice," *Neurotoxicity Research*, vol. 36, no. 3, pp. 540–550, 2019.
- [32] P. Jablonski, B. O. Howden, D. A. Rae, C. S. Birrell, V. C. Marshall, and J. Tange, "An experimental model for assessment of renal recovery from warm ischemia," *Transplantation*, vol. 35, no. 3, pp. 198–204, 1983.
- [33] M. Sycheva, J. Sustarich, Y. Zhang et al., "Pro-nerve growth factor induces activation of RhoA kinase and neuronal cell death," *Brain sciences*, vol. 9, no. 8, p. 204, 2019.
- [34] M. Dhupal, J. M. Oh, D. R. Tripathy, S. K. Kim, S. B. Koh, and K. S. Park, "Immunotoxicity of titanium dioxide nanoparticles via simultaneous induction of apoptosis and multiple toll-like receptors signaling through ROS-dependent SAPK/JNK and p 38 MAPK activation," *International Journal of Nanomedicine*, vol. Volume 13, pp. 6735–6750, 2018.
- [35] Y. B. Sun, H. Zhao, D. L. Mu et al., "Dexmedetomidine inhibits astrocyte pyroptosis and subsequently protects the brain in in vitro and in vivo models of sepsis," *Cell Death & Disease*, vol. 10, no. 3, p. 167, 2019.
- [36] Y. Zhong, Y. P. Li, Y. Q. Yin, B. L. Hu, and H. Gao, "Dexmedetomidine inhibits pyroptosis by down-regulating miR-29b in myocardial ischemia reperfusion injury in rats," *International Immunopharmacology*, vol. 86, article 106768, 2020.

- [37] X. Feng, W. Guan, Y. Zhao et al., “Dexmedetomidine ameliorates lipopolysaccharide-induced acute kidney injury in rats by inhibiting inflammation and oxidative stress via the GSK-3 β /Nrf 2 signaling pathway,” *Journal of Cellular Physiology*, vol. 234, no. 10, pp. 18994–19009, 2019.
- [38] B. D. Sahu, J. M. Kumar, and R. Sistla, “Baicalein, a bioflavonoid, prevents cisplatin-induced acute kidney injury by up-regulating antioxidant defenses and down-regulating the MAPKs and NF- κ B pathways,” *Plos One*, vol. 10, no. 7, p. e0134139, 2015.
- [39] M. H. Ben-Mahdi, P. M. Dang, M. A. Gougerot-Pocidalo, Y. O’Dowd, J. el-Benna, and C. Pasquier, “Xanthine oxidase-derived ROS display a biphasic effect on endothelial cells adhesion and FAK phosphorylation,” *Oxidative Medicine and Cellular Longevity*, vol. 2016, Article ID 9346242, 9 pages, 2016.
- [40] G. L. Barrett, “The p 75 neurotrophin receptor and neuronal apoptosis,” *Progress in Neurobiology*, vol. 61, no. 2, pp. 205–229, 2000.
- [41] B. R. Kraemer, J. P. Snow, P. Vollbrecht et al., “A role for the p 75 neurotrophin receptor in axonal degeneration and apoptosis induced by oxidative stress,” *Journal of Biological Chemistry*, vol. 289, no. 31, pp. 21205–21216, 2014.
- [42] A. Caporali, E. Pani, A. J. Horrovoets et al., “Neurotrophin p 75 receptor (p75NTR) promotes endothelial cell apoptosis and inhibits angiogenesis: implications for diabetes-induced impaired neovascularization in ischemic limb muscles,” *Circulation Research*, vol. 103, no. 2, pp. e15–e26, 2008.
- [43] E. F. Wheeler, H. Gong, R. Grimes, D. Benoit, and L. Vazquez, “p75NTR and Trk receptors are expressed in reciprocal patterns in a wide variety of non-neural tissues during rat embryonic development, indicating independent receptor functions,” *The Journal of Comparative Neurology*, vol. 391, no. 4, pp. 407–428, 1998.
- [44] U. Lönngren, U. Näpänkangas, M. Lafuente et al., “The growth factor response in ischemic rat retina and superior colliculus after brimonidine pre-treatment,” *Brain Research Bulletin*, vol. 71, no. 1-3, pp. 208–218, 2006.
- [45] A. Y. Shanab, B. A. Mysona, S. Matragoon, and A. B. el-Remessy, “Silencing p75NTR prevents proNGF-induced endothelial cell death and development of acellular capillaries in rat retina,” *Molecular Therapy - Methods & Clinical Development*, vol. 2, article 15013, 2015.
- [46] R. S. Aloyz, S. X. Bamji, C. D. Pozniak et al., “p53 is essential for developmental neuron death as regulated by the TrkA and p75 neurotrophin receptors,” *The Journal of Cell Biology*, vol. 143, no. 6, pp. 1691–1703, 1998.
- [47] C. Costantini, F. Rossi, E. Formaggio, R. Bernardoni, D. Cecconi, and V. Della-Bianca, “Characterization of the signaling pathway downstream p 75 neurotrophin receptor involved in beta-amyloid peptide-dependent cell death,” *Journal of Molecular Neuroscience: MN*, vol. 25, no. 2, pp. 141–156, 2005.
- [48] S. Chakraborty, V. Castranova, M. K. Perez, and G. Piedimonte, “Nanoparticles-induced apoptosis of human airway epithelium is mediated by proNGF/p75NTRsignaling,” *Journal of Toxicology and Environmental Health. Part A*, vol. 80, no. 1, pp. 53–68, 2017.
- [49] C. M. Walshe, J. G. Laffey, L. Kevin, and D. O’Toole, “Sepsis protects the myocardium and other organs from subsequent ischaemic/reperfusion injury via a MAPK-dependent mechanism,” *Intensive Care Medicine Experimental*, vol. 3, no. 1, p. 35, 2015.
- [50] M. J. Rane, Y. Song, S. Jin et al., “Interplay between Akt and p 38 MAPK pathways in the regulation of renal tubular cell apoptosis associated with diabetic nephropathy,” *American Journal of Physiology-Renal Physiology*, vol. 298, no. 1, pp. F49–F61, 2010.
- [51] X. Ma, C. Dang, H. Kang et al., “Saikosaponin-D reduces cisplatin-induced nephrotoxicity by repressing ROS-mediated activation of MAPK and NF- κ B signalling pathways,” *International Immunopharmacology*, vol. 28, no. 1, pp. 399–408, 2015.
- [52] J. H. Kim, S. S. Lee, M. H. Jung et al., “N-Acetylcysteine attenuates glycerol-induced acute kidney injury by regulating MAPKs and Bcl-2 family proteins,” *Nephrology Dialysis Transplantation*, vol. 25, no. 5, pp. 1435–1443, 2010.
- [53] A. X. Garg, P. J. Devereaux, S. Yusuf et al., “Kidney function after off-pump or on-pump coronary artery bypass graft Surgery,” *JAMA*, vol. 311, no. 21, pp. 2191–2198, 2014.
- [54] D. C. Angus, A. E. Barnato, D. Bell et al., “A systematic review and meta-analysis of early goal-directed therapy for septic shock: the ARISE, ProCESS and ProMISE Investigators,” *Intensive Care Medicine*, vol. 41, no. 9, pp. 1549–1560, 2015.
- [55] T. Yoshida, M. Yamashita, M. Iwai, and M. Hayashi, “Endothelial Krüppel-like factor 4 mediates the protective effect of statins against ischemic AKI,” *Journal of the American Society of Nephrology*, vol. 27, no. 5, pp. 1379–1388, 2016.
- [56] S. Huang, J. You, K. Wang et al., “N-acetylcysteine attenuates cisplatin-induced acute kidney injury by inhibiting the C5a receptor,” *BioMed Research International*, vol. 2019, Article ID 4805853, 11 pages, 2019.
- [57] C. Beumer, M. Wulferink, W. Raaben, D. Fiechter, R. Brands, and W. Seinen, “Calf intestinal alkaline phosphatase, a novel therapeutic drug for lipopolysaccharide (LPS)-mediated diseases, attenuates LPS toxicity in mice and piglets,” *The Journal of Pharmacology and Experimental Therapeutics*, vol. 307, no. 2, pp. 737–744, 2003.
- [58] X. Liu, G. Xie, K. Zhang et al., “Dexmedetomidine vs propofol sedation reduces delirium in patients after cardiac surgery: a meta-analysis with trial sequential analysis of randomized controlled trials,” *Journal of Critical Care*, vol. 38, pp. 190–196, 2017.
- [59] H. Torbic, S. Papadopoulos, J. Manjourides, and J. W. Devlin, “Impact of a protocol advocating dexmedetomidine over propofol sedation after robotic-assisted direct coronary artery bypass surgery on duration of mechanical ventilation and patient safety,” *The Annals of Pharmacotherapy*, vol. 47, no. 4, pp. 441–446, 2013.
- [60] Y. Liu, Y. Yu, J. Zhang, and C. Wang, “The therapeutic effect of dexmedetomidine on protection from renal failure via inhibiting KDM5A in lipopolysaccharide-induced sepsis of mice,” *Life Sciences*, vol. 239, article 116868, 2019.

Research Article

Cranberry for Bacteriuria in Individuals with Spinal Cord Injury: A Systematic Review and Meta-Analysis

Anna Raguzzini,¹ Elisabetta Toti,¹ Tommaso Sciarra ,² Anna Lucia Fedullo,¹ and Iaria Peluso ¹

¹Research Centre for Food and Nutrition, Council for Agricultural Research and Economics (CREA-AN), Rome, Italy

²Joint Veteran Center, Scientific Department, Army Medical Center, Rome, Italy

Correspondence should be addressed to Tommaso Sciarra; sciarratommaso@hotmail.com and Iaria Peluso; i.peluso@tiscali.it

Received 11 June 2020; Revised 6 August 2020; Accepted 12 October 2020; Published 31 October 2020

Academic Editor: Luciano Saso

Copyright © 2020 Anna Raguzzini et al. This is an open access article distributed under the Creative Commons Attribution License, which permits unrestricted use, distribution, and reproduction in any medium, provided the original work is properly cited.

Background. Urinary tract infection (UTI) is common in individuals with spinal cord injury (SCI) and neurogenic lower urinary tract dysfunction (NLUTD) and in veterans with SCI who use antibiotics improperly for asymptomatic bacteriuria. Cranberry (CB) has been suggested for UTI prevention. **Methods.** We performed a systematic search up to May 2020 in the following databases: AccessMedicine, BioMed Central, CINAHL, Cochrane Library, ProQuest, and PubMed. Quality assessment was performed using a specifically designed quality score. Risk ratio was calculated with both random effect model analysis (DerSimonian-Laird method) and quality effect model analysis (Doi Thalib method). **Results.** Six studies on bacteriuria and SCI were reviewed. From the four studies available for meta-analysis, two of which with individuals taking both CB and control, 477 data from 415 participants were analysed (241 CB and 236 control). No significant differences were detected with meta-analysis. However, bias, limitations, and incompleteness were observed in the reviewed studies. **Conclusion.** Although further studies are needed, we suggest an accurate monitoring of diet and fluid intake, the evaluation of risk for potential food or nutraceutical interactions with drugs, and the inclusion of inflammatory markers among the outcomes in addition to UTI.

1. Introduction

Spinal cord injury (SCI) is a damage to the spinal cord that may result in motor paralysis and sensory loss below the level of the lesion [1]. The highest documented global prevalence of SCI was found in the United States of America (906/million) and the lowest in France (250/million), while the incidence of traumatic SCI was highest in New Zealand (49.1/million) and lowest in Spain (8.0/million) [2]. In Italy, the incidence of traumatic SCI during 2013-2014 was 14.7/million per year, the mean age was 54 years old, and the male to female ratio was 4 : 1 [3]. High incidence was documented in veterans. In a systematic review of 25 articles, the overall incidence rate of war-related SCI varied from 4.3 to 5.6/10,000 person-years [4]. These veterans had predominantly thoracic or lumbar level, complete (American Spinal Injury Association [ASIA] Impairment Scale A) SCI, associated with other bodily injuries in 43.9-78.1% of cases [4].

Moreover, polypharmacy is common in veterans [5, 6], and nutraceutical-drug [5] and food-drug interactions [6] should be considered.

Neurogenic lower urinary tract dysfunction (NLUTD) can be observed in 83% of veterans with SCI and is associated with urinary tract infection (UTI) [7]. Results of routine testing reported that 69% of the urine cultures of veterans with SCI were positive for bacteria, but 87% were asymptomatic bacteriuria cases, of which 36% were treated with antibiotics [8]. Epidemiology of antibiotic resistance in veterans with SCI suggests improving prescribing of appropriate antibiotics [9]. There is a large consensus that antibiotic prophylaxis is not recommended for UTI [10-12] and that asymptomatic bacteriuria should not be treated with antibiotics [13].

Although cranberry (CB) may be effective in preventing UTI recurrence in women [14], data from meta-analyses have reported conflicting results, and it has been suggested that conclusions on cranberry and UTI should consider the

differences among the populations studied [15]. Sappal et al. [16] recently investigated the effect of concentrated proanthocyanidins (PAC) from CB for reduction of bacteriuria in male veterans with SCI and did not find reduction of bacteriuria and pyuria or improvement in subjective urine quality.

1.1. Aim and Objectives. We aimed to evaluate the following hypothesis: CB products (including extracts) are more effective than placebo or no treatment in reducing bacteriuria and/or in the prevention of UTI in individuals with SCI. Furthermore, we aimed to suggest a specific quality assessment for studies with nutraceuticals involving individuals with SCI.

To this aim, we conducted a systematic review and evaluated previous meta-analysis risk of bias assessment [17–19]. Although it was not a meta-analysis, we also considered the systematic review of Navarrete-Opazo et al. [20], because it was focused on individuals with SCI.

2. Materials and Methods

2.1. Study Selection. Figure 1 shows the four-phase diagram of meta-analysis (according to the PRISMA Statement) and the flow of the studies processed in this review. We performed a systematic search in PubMed and in the Discovery Sapienza/medicine pharmacy and psychology including (among others) the following databases: AccessMedicine, BioMed Central, CINAHL, Cochrane Library, and ProQuest, with the search terms spinal cord injury and cranberry, up to May 2020 (Figure 1).

Given that the aim of the present review was specifically SCI, interventions that involved individuals with other health conditions were excluded. In particular, we excluded studies involving subjects with spina bifida, who had higher urinary tumor growth factor β -1 than patients with SCI [21], and children with myelomeningocele [22], being children among the groups where CB products seemed to be more effective (relative risk: RR range -0.33 [18] -0.48 [17]). Moreover, these are two congenital conditions [23], and this review is aimed at evaluating the effect of CB in individuals with traumatic SCI.

All studies that met the following criteria were included in this review: studies that appear in an edited journal (peer-review criterion), published in English (language criterion), and focused on the effect of CB on bacteriuria or UTI versus control (topic criterion), regardless of the CB bioactive compounds' source and dose and the study design (parallel, crossover, controlled, and uncontrolled). First trials were identified through the title or abstract. Then, the full text of the article was obtained. Finally, based on inclusion and exclusion criteria, eligible studies were included (A.R. and E.T.).

2.2. Data Extraction and Quality Assessment. A data extraction form, including quality characteristics, was designed, and selected studies were reviewed by all authors. To ensure uniformity, data extraction was performed independently by two reviewers (A.R. and E.T.), and all data were entered

by these reviewers. Discrepancies were resolved by discussion between the two reviewers, and unresolved disagreement was referred to a third reviewer (I.P.).

Table 1 shows previously reported judgments of studies (Table 1). The previously used (Table 1) assessment of bias tool includes random sequence generation (selection bias), allocation concealment (selection bias), blinding of participants and personnel (performance bias), blinding of outcome assessment (detection bias), incomplete outcome data (attrition bias), selective reporting (reporting bias), and other biases [17], each scored as “high risk,” “low risk,” or “unclear.” Navarrete-Opazo et al. [20] judged studies as unclear risk for reporting bias, because there was no previous registration of the protocols.

In this study, withdrawal was not considered as a bias, being the compliance of volunteers generally due to factors not imputable to researchers [24], according to the quality score previously used for intervention studies with flavonoids [24]. The score (range 0-1) [24] includes proper control (0.3), compliance assessment (0.1), dietary record (food records or food-frequency questionnaires throughout the study, 0.06), food antioxidant intake in subjects' selection criteria (flavonoid-rich food or antioxidant supplement consumption, 0.05), washout and/or run-in period (0.05, washout and/or run-in period for crossover studies only run-in for parallel design), marker of bioavailability (0.05), double blinding (0.05), no funding support (0.03, from profit companies), and no food/supplement donation (0.01).

Intra- and interstudy baseline comparability was removed from the previously suggested score [24] because no mean difference after versus before treatment was calculated, and the corresponding score 0.3 was divided into groups balanced for lesion level/urine collection (0.1), UTI diagnosis after treatment including autonomic dysreflexia (0.1), and comorbidity and drug use specified (0.1).

Discrepancies were resolved through discussions between the two authors who performed the quality assessment (A.R. and T.S.) or through consultation with a third investigator (I.P.).

2.3. Meta-Analysis. Two [16, 25] out of the 6 selected studies [16, 25–29] have been excluded from the meta-analysis since results were provided in the form of figures, but we retained them for discussion, as in the previous meta-analysis [24]. With the definition of UTI being different among the studies, we use bacteriuria as the outcome. Moreover, asymptomatic bacteriuria is often improperly treated with antibiotics [8].

Four studies [26–29] met the inclusion criteria and provided data for the analyses of CB versus control (Figure 1). Dichotomous outcomes (UTI cases in CB and control groups) from each study were collected in order to compute individual-study RR (with 95% confidence intervals). Random effect model analysis (DerSimonian-Laird method) and quality effect model analysis (Doi Thalib method, by using the quality score as the probability modifier) were reported. Number needed to treat (NNT) was estimated. Statistical heterogeneity was assessed by using the Q statistics for quality effect model and by t^2 and prediction interval [30] for the random effect model.

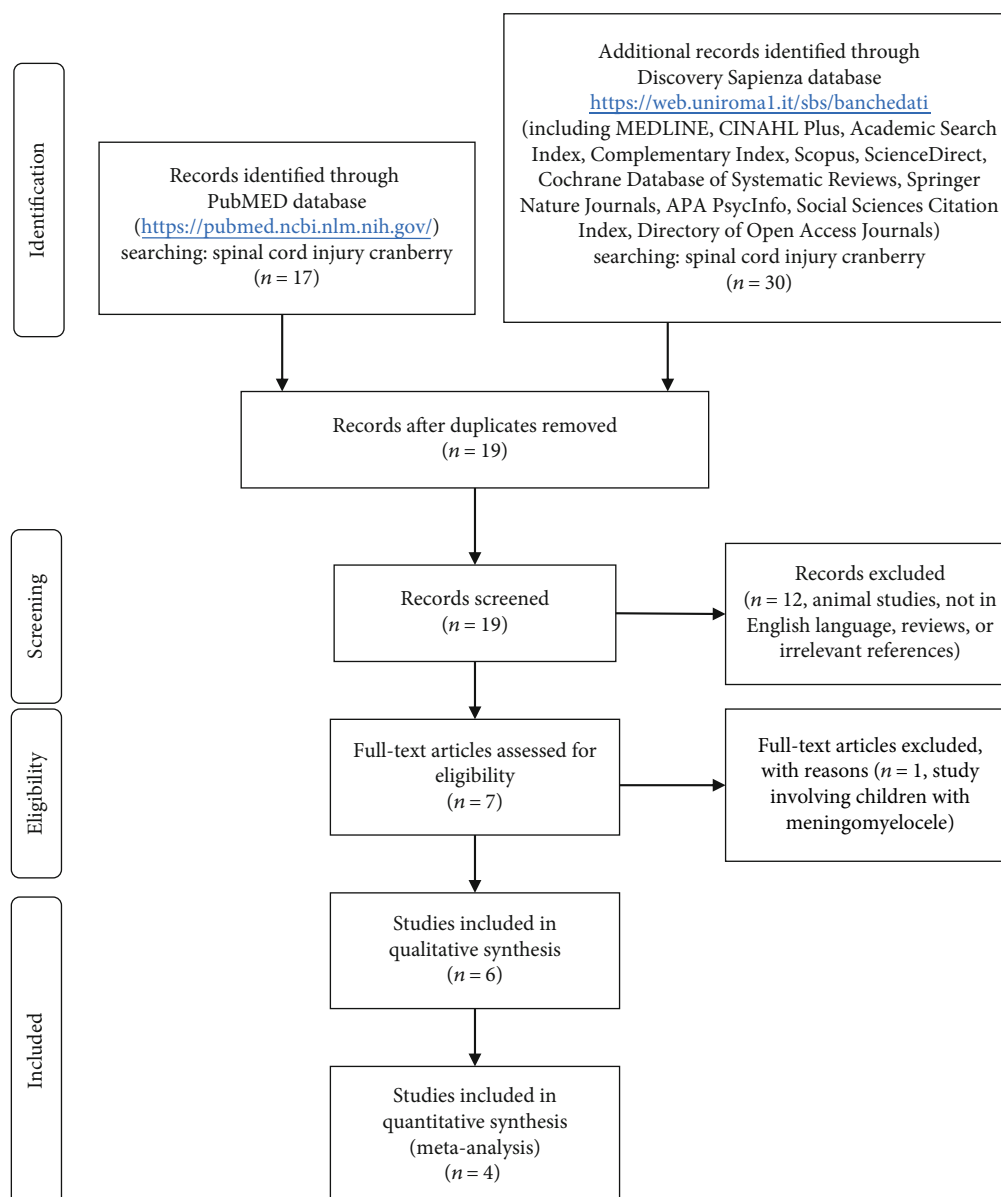


FIGURE 1: Four-phase flow diagram of systematic review and meta-analysis, according to the PRISMA Statement.

In order to detect the presence of publication bias, funnel plot and Egger's weighted regression statistics were used. Symmetry/asymmetry of the funnel plot was defined through visual examination, and trim-and-fill sensitivity analysis was performed. Furthermore, we used the L'Abbe plot [31] in order to visualize the relationship between the effect of treatment and the bacteriuria.

3. Results

3.1. Description of Included Studies. Six studies were retrieved from the systematic search, of which 2 crossover, 3 parallel (two 2 arms and one 4 arms), and 1 longitudinal (water before washout and CB juice), with a total of 449 volunteers.

Characteristics of participants, including and excluding selection criteria, are shown in Table 2. Lesion level and ASIA

classification were very variable among studies and, when reported, among groups within the same study (Table 2). Reported reasons for dropout/loss of follow-up included noncompliance with pill counts [29], developing of urinary stones [29], recurrent UTI [25], abdominal discomfort attributed to CB [25], and personal reasons, including travels [25].

Only 1 study evaluated the effect of CB juice, whereas the others evaluated CB tablets or capsules (Table 3). Treatment range between 1 week and 6 months and 2 out of 3 crossover studies included a washout period between the two periods of intervention (treatment and control), whereas the other studies did not include a run-in period. The 4-arm study also included a methenamine hippurate (MH) group and a CB +MH group. All except for 1 study did not report PAC content in the CB product. Dropout rates range from 0% to 43%

TABLE 1: Risk of bias from previous meta-analyses.

Study name Year	Linsmeyer 2004	Waites 2004	Lee 2007	Hess 2008
Random sequence generation				
Jepson et al. 2012 [17]	Unclear	Unclear	Low	Unclear
Wang et al. 2012 [18]	Not reported	Unclear	Not reported	Unclear
Luis et al. 2017 [19]	Not reported	Unclear	Low	Unclear
Allocation concealment				
Jepson et al. 2012 [17]	Unclear	Unclear	Low	Low
Wang et al. 2012 [18]	Not reported	Unclear	Not reported	Unclear
Luis et al. 2017	Not reported	Low	Low	Unclear
Blinding of participants and personnel				
Jepson et al. 2012 [17]	Low	Low	Low	Low
Wang et al. 2012 [18]	Not reported	Low	Not reported	Low
Luis et al. 2017 [19]	Not reported	Low	Low	Low
Blinding of outcome assessment				
Jepson et al. 2012 [17]	Low	Unclear	Low	Low
Wang et al. 2012 [18]	Not reported	Not reported	Not reported	Not reported
Luis et al. 2017 [19]	Not reported	Low	Low	Low
Incomplete outcome data				
Jepson et al. 2012 [17]	Low	High	Low	High
Wang et al. 2012 [18]	Not reported	High	Not reported	Unclear
Luis et al. 2017 [19]	Not reported	Low	Unclear	Unclear
Selective reporting				
Jepson et al. 2012 [17]	Low	Low	Low	Low
Wang et al. 2012 [18]	Not reported	High	Not reported	High
Luis et al. 2017 [19]	Not reported	Low	Unclear	Low
Other bias				
Jepson et al. 2012 [17]	Unclear	Unclear	Low	Low
Wang et al. 2012 [18]	Not reported	Not reported	Not reported	Not reported
Luis et al. 2017 [19]	Not reported	Low	Low	Low

and different dropout rates were reported for CB (15%), CB+MH (21%), placebo (13%), and MH (23%) in the 4-arm study.

The outcomes of studies were symptomatic UTI, bacteriuria plus pyuria (urinary white blood cells count: WBC), or bacteriuria only (Table 3). Among the studies, only Hess et al. [29] reported a significant effect on symptomatic UTI after consumption of CB tablet (1 g/d for 6 months) compared to placebo. On the other hand, Lee et al. [28] reported bowel dysfunctions (diarrhoea or constipation) in eleven participants, nausea in two, and rash in one, after the treatment with the CB capsule (2 g/d for 6 months).

3.2. Quality of the Included Studies. Disagreement, between the two authors who performed data extraction and quality assessment, occurred for the study of Lee et al. [28], who did not exclude from the follow-up patients who discontinued the intervention and coupled CB and CB+MH groups and placebo and MH groups for the analysis. After the consultation with the third reviewer, the study was included in the quantitative synthesis (Figure 1), due to the great number

of subjects, but with the lower quality score, according with criteria in Table 4.

The most frequent limitations were no comorbidity and drug use specified (all studies), markers of bioavailability (all studies), and no compliance, diet, or antioxidant monitoring (Table 4).

Only 3 studies included autonomic dysfunction in the symptomatic UTI diagnostic criteria, and in 3 studies, the balancing between treatment and control for the lesion level and urinary collection (management of NLUTD) was not properly controlled.

In particular, Waites et al. [27] stated that groups were unbalanced for catheterization and Lee et al. [28] did not furnish information for the 4 arms of treatment, pooling CB and CB+MH in the treatment group and placebo and MH in the control group. This kind of analysis is a bias also for proper control (Table 4).

3.3. Meta-Analysis. Since there were 2 studies with individuals taking both treatment and control, 1 crossover [29] and 1 longitudinal [26], 477 data from 415 participants were

TABLE 2: Study setting, characteristics of volunteers, and missing data.

Study name Year	Reid 2001	Linsenmeyer 2004	Waites 2004	Lee 2007	Hess 2008	Sappal 2018
Country	Canada	USA	USA	Australia	USA	USA
Setting		Urology clinic	Hosp. clinic, community residing	SCI database, community residing	Veterans Admin Hosp.	Veterans Affairs Medical Center
Inclusion criteria	SCI with UTI history	SCI with NLUUD	SCI (≥ 1 year) with NLUUD	SCI with NLUUD	SCI (≥ 1 year) with NLUUD	SCI (≥ 6 -months) requiring catheterization
Lesion level, ASIA class	Paraplegia/tetraplegia not reported	From cervical 4 to cervical 7: 8 From thoracic 4 to thoracic 10: 7 From thoracic 11 to lumbar 1: 6	Paraplegia/tetraplegia 20/6 (treatment) 14/8 (control) complete/incomplete 23/3 (treatment) 17/5 (control)	Paraplegia/tetraplegia 62/91 (treatment) 76/76 (control) Complete/incomplete 67/86 (treatment) 81/71 (control)	ASIA A: 27 ASIA B: 10 ASIA C: 10 Para/tetra: 24/23	Cervical 5: 1; cervical 6: 3; cervical 7: 3; thoracic 1: 1; thoracic 5: 1; thoracic 7: 1; thoracic 9: 1; thoracic 11: 1 ASIA A: 9 ASIA B: 1 ASIA C: 3
Exclusion criteria	High serum creatinine, antibiotics, immunosuppressants, autonomic dysreflexia, cancer, stone, symptomatic UTI	Antimicrobial urinary acidifying agents (within 7 days) fever, chills	Antimicrobial symptomatic-UTI renal or hepatic disease Allergy	Antimicrobial symptomatic-UTI renal or hepatic disease Allergy	Low glomerular filtration rate, immunosuppressant malignancy	Antimicrobial symptomatic UTI (within 2 weeks) Immunocompromising (HIV, steroid, chemotherapy)
Included in UTI definition	White blood cells, symptoms (autonomic dysreflexia)	White blood cells $\geq 10/\mu\text{L}$	White blood cells ≥ 100 high power field Symptoms (autonomic dysreflexia)	White blood cells ≥ 100 high power field Symptoms (autonomic dysreflexia)	White blood cells ≥ 10 high power field Symptoms (autonomic dysreflexia)	White blood cells ≥ 10 high power field
Age (years)	Mean: 42.3	Not specified	Range: 20-73	Range: 16-82	Range: 28-79	Range: 18-65
Gender	Males: 10/15	Males: 16/21	Males: 42/48	Males: 253/305	All men (47)	All men (13)
Number (analysed)	15	21	48	305	47	13
Loss to follow-up	1/16	16/37	26/74	0/305	10/57	0/13
Dropout	1/16 (6%)	16/37 (43%)	26/74 (35%)	CB: 12/78 (15%) CB+MH: 16/75 (21%) Placebo: 10/77 (13%) MH: 17/75 (23%)	10/57 (17%)	0/13

ASIA: American Spinal Injury Association; CB: cranberry; MH: methenamine hippurate; NLUUD: neurogenic lower urinary tract dysfunction; UTI: urinary tract infection.

TABLE 3: Intervention and outcomes.

Study name Year	Reid 2001	Linsensmeyer 2004	Waites 2004	Lee 2007	Hess 2008	Sappal 2018
Study design	Longitudinal	Crossover randomized controlled	Parallel randomized controlled	Parallel (4 groups) randomized controlled	Crossover randomized controlled	Parallel randomized controlled
Intervention Cranberry	Juice 750 mL (3 × 259 mL, mealtimes) PAC content not reported	Tablets 1.2 g/d (3 × 0.4 g) PAC content not reported	Capsule 2.0 g/d PAC content not reported	Tablets 1.6 g/d CB 1.6 g/d + MH 0.2 g/d PAC content not reported	Tablet 1.0 g/d (2 × 0.5 g) PAC content not reported	Capsule PAC content 36 mg
Control	Water 750 mL (3 × 259 mL, mealtimes)	Placebo	Placebo identical (lactose)	Placebo and MH 0.2 g/d	Placebo identical (rice flour)	Placebo
Study duration	1 week each, 2 days washout	4 weeks each, 1 week washout	6 months	6 months	6 months	15 days
Outcomes	Bacteriuria Bacterial biofilm load	Bacteriuria, pyuria	Bacteriuria	Symptomatic UTI	Symptomatic UTI	Bacteriuria, pyuria
Bacteriuria (cut-off)	Not specified	Midstream specimen of urine: $\geq 10^7$ /mL catheter specimen of urine: $> 10^5$ /mL	Catheter specimen of urine: $\geq 10^4$ /mL	$\geq 10^5$ /mL	$\geq 10^4$ /mL	$\geq 10^5$ /mL
Reported effects	Water: 7/15 CB juice: 7/15	Not significant	Treatment: 10/26 Control: 8/22	Treatment (CB and CB+MH): 67/153 Control (placebo and MH): 71/152	Treatment: 6/47 Control: 16/47	Not significant
Adverse effects	Not reported	Not reported	Not reported	Mild and infrequent	Not reported	Not reported

CB: cranberry; MH: methenamine hippurate; PAC: proanthocyanidins; UTI: urinary tract infection.

TABLE 4: Specific risk of bias assessment.

Study name Year	Reid 2001	Linsenmeyer 2004	Waites 2004	Lee 2007	Hess 2008	Sappal 2018
Groups balanced for lesion level/urine collection	Yes 0.1	Yes 0.1	Unbalanced catheterization (treatment/control 65.4/36.3%)	No data for each of the 4 arms	Yes 0.1	Not reported
UTI diagnosis including autonomic dysreflexia	No	Yes 0.1	No	Yes 0.1	Yes 0.1	No
Comorbidity and drug use specified	No	No	No	No	No	No
Proper control	Yes 0.3	Yes 0.3	Yes 0.3	Placebo+MH	Yes 0.3	Yes 0.3
Compliance assessment	No	No	Pills' count 0.1	No	Pills' count 0.1	No
Dietary record	No	No	Only fluid intake 0.03	No	No	No
Food antioxidant intake	Only no CB/vit. C 0.025	Only no CB 0.025	Only no CB 0.025	No	No	Only no CB 0.025
Washout and/or run-in	2d-w/o only	Yes 0.05	No	No	No	No
Marker of bioavailability	No	No	No	No	No	No
Double blinding	No	Yes 0.05	Yes 0.05	Yes 0.05	Yes 0.05	Yes 0.05
No funding support	Yes 0.03 (no conflict)	Yes 0.03	Yes 0.03	Brucia Pharmaceuticals	Yes 0.03	Yes (critical versus sponsor) 0.03
No supplement donation	Yes 0.01	Kessler Pharmacy	AIM This Way	Yes 0.01	Cran-Max Swiss	Yes 0.01
Quality score (range 0–1)	0.465	0.655	0.535	0.16	0.68	0.415

CB: cranberry; MH: methenamine hippurate; UTI: urinary tract infection.

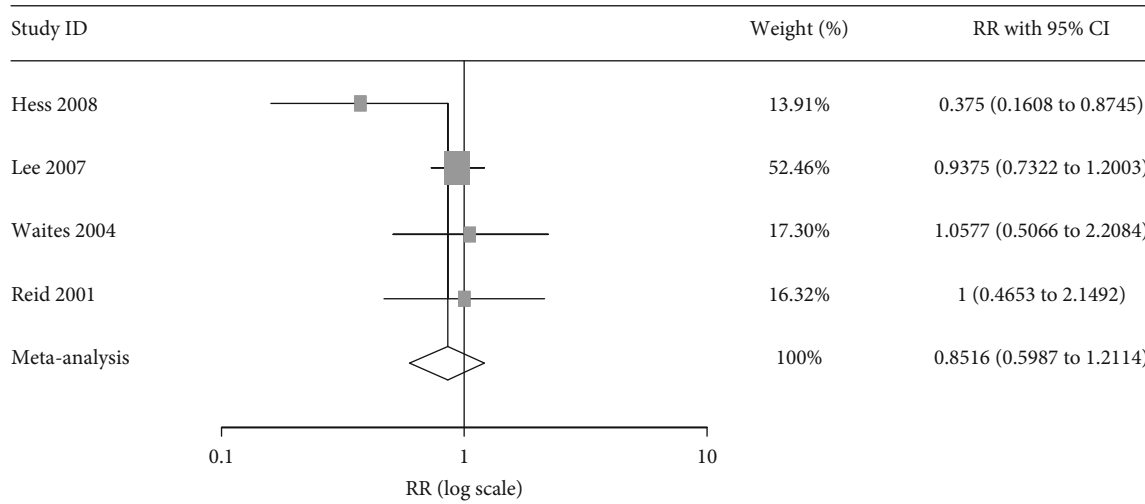
analysed in this meta-analysis. Overall, 241 subjects received CB and 236 control. No significant differences were detected with meta-analysis in random ($p = 0.372$) and quality ($p = 0.415$) effect models (Figure 2). NNT was 17 (95% CI 34.36 to 6.82), and low to high statistical heterogeneity was found for random and quality effect models, respectively (t^2 0.05, Q 75%, Egger intercept -0.880 , $p = 0.568$). However, the 95% prediction interval ranged between 0.3 and 2.1. The funnel plot showed no asymmetric distribution of results (Figure 3(a)) and trim-and-fill analysis did not suggest potential publication bias. On the other hand, the visual inspection of the L'Abbe plot revealed that only half of the participants were at risk of UTI in the control group (Figure 3(b)).

4. Discussion

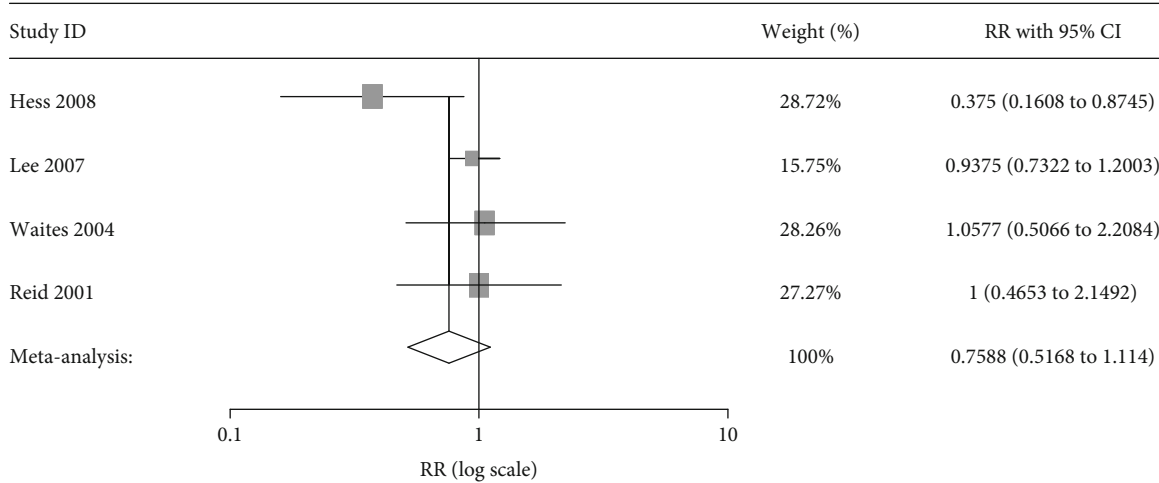
4.1. Summary of Main Results. Six studies were retrieved in the present systematic review, 4 of which reported data suitable for the meta-analysis (Figure 1). Considering that inclusion of low-quality studies may bias the estimated effect, while restriction to high-quality studies can reduce information, a quality score has been assigned and a quality effect model meta-analysis has been performed, in addition to the random effect model meta-analysis. We did not observe significant effect of CB products (Table 3) on bacteriuria in individuals with SCI (Table 2 and Figure 2).

About one in every 17 patients will benefit from the treatment. However, NNT does not account for a patient's baseline risk, probably different due to intra- and interstudy variability (Table 2). Moreover, the NNT of a given treatment will be very different when describing the value versus placebo instead of another active therapy (Tables 3 and 4; Lee et al. [28] did not furnish information for the 4 arms of treatment). Moreover, we observed a broad prediction interval (95% 0.3-2.1), suggesting a range of possible effects in relation to harm and clinical benefit thresholds (1, null effect) and indicating the existence of settings where the treatment has a suboptimal and possibly even harmful effect. None of the studies included in the quantitative synthesis involved the veterans who can be very different from the patients seen in all studies that have been done in the past. Therefore, the prediction interval cannot tell us what we might expect for these patients and specific studies are required to enable more informed clinical decision-making. Moreover, the prediction interval is affected by study bias. If bias exists, as summarized in Table 4, the effect sizes observed in future studies might occur beyond the limits of the prediction interval.

4.2. Completeness, Quality, and Applicability of Evidence. Navarrete-Opazo et al. [20], after a quality assessment across studies, carried out using the Grading of Recommendations Assessment, Development and Evaluation (GRADE),



(a)



(b)

FIGURE 2: Meta-analysis: (a) forest plot of random effect model; (b) forest plot of quality effect model.

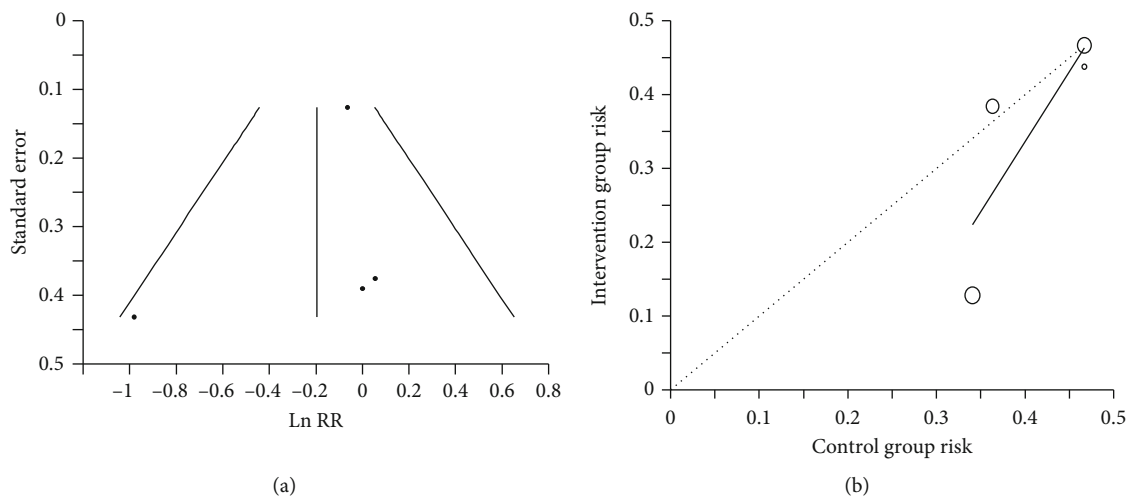


FIGURE 3: (a) Funnel plot. Ln RR: risk ratio logarithm. (b) L'Abbe plot. Dotted line: line of equality.

reported that overall, the studies were rated as moderate-quality evidence and the highest quality was found in the trial by Lee et al. [28]. From that, the authors concluded that the quality of the evidence was strong enough to reasonably conclude that cranberry supplementation is not effective for prevention of UTIs in people with SCI [20]. By using our risk of bias assessment (Table 4), we concluded that the quality of evidence is low due to the bias, limitations, and incompleteness of the reviewed studies.

Intersubjects' variability has been reported for absorption, metabolism, and excretion of CB polyphenols in healthy individuals, partly due to the variation in the gut microbiota [32]. Several studies have reported different intestinal microbiota in individuals with SCI compared to healthy controls [33], and diet is known to influence gut microbiota [33] and to affect UTI risk [34]. Therefore, monitoring food consumption is of great importance in those studies aimed at evaluating the effects of bioactive compounds from plant food. Mobile phone applications for dietary intake monitoring are available in many countries [35, 36], and it has been reported that a 12-hour dietary recall app was in good agreement with the two reference methods (food frequency questionnaire and four dietary records) and useful for categorizing individuals according to their habitual intake of selected food and drink groups [37].

Only few of the reviewed studies included CB-product consumption among exclusion criteria and/or have instructed volunteers to avoid their consumption, whereas none of them have monitored the diet (Table 4).

We could not analyse the effects of different study designs (crossover/parallel), due to the low number of studies. As previously suggested [24], parallel design could lead to ineffective randomization and potential confounding, while the correct washout period in crossover design, in order to prevent a carry-over (or residual) effect, is difficult to establish in absence of bioavailability data, as in the reviewed studies (Table 4).

CB and its bioactive compounds, *in vitro*, inhibited enzymes and transporters involved in drug bioavailability and pharmacokinetics [38, 39]. Although only few cases have been reported [38], probably related to genetic polymorphisms in the enzymes or transporters [40], potential food-drug interactions should be monitored in individuals with SCI under treatment for NLUTD with drugs including oxybutynin and solifenacin [41]. The panel of experts of the "clinical guidelines for the diagnosis and treatment of lower urinary tract dysfunction in patients with SCI" concluded that anticholinergic (oxybutynin) and β 3-adrenoceptor agonist (mirabegron) drugs are recommended for patients at risk of renal damage, with symptomatic UTI or urinary incontinence [10]. However, adverse anticholinergic events can occur in SCI patients, including blurred vision, dry mouth, and constipation [10]. In this context, neurogenic bowel dysfunction (NBD), comorbidity, and polypharmacy and potential nutraceutical-drug interactions should be monitored [33], in particular in aged patients with SCI [42]. With ageing, individuals with SCI have an increased risk of renal stones [42], and the effect of CB on nephrolithiasis is controversial [43, 44].

Despite the large age range of many reviewed studies (Table 2), comorbidity and drug use were not reported (Table 4), and only antimicrobials and drugs acting on the immune system were among the exclusion criteria (Table 2).

Only a study evaluated the effect of CB juice (Table 3) and did not observe differences in bacteriuria compared to water (Table 3 and Figure 2). Reid et al. [26] reported that CB juice ingestion, but not water intake, decreased the adhesion of Gram-negative ($p = 0.054$) and Gram-positive ($p = 0.022$) bacteria from the urinary sample to uroepithelial cells, despite the similar reduction of bacteriuria compared to baseline. In addition to urine culture, the authors suggested that further parameters need to be tested in patients with SCI, since urine alone is a poor indicator of bacterial colonization [26]. Accordingly, CB products do not appear to inhibit bacterial growth or sterilize the urinary tract, and among the suggested mechanisms explaining the preventive effects of CB consumption against UTI, the hypothesis concerning acidification of urine, due to the excretion of the bacteriostatic hippuric acid, has currently been disproved [45].

On the other hand, PAC, especially A-linked PAC, had an antiadhesion effect of P-fimbriated uropathogenic *Escherichia coli* to uroepithelial cells, whereas B-linked PAC, found in green tea, dark chocolate, grapes, and apples, did not have this antiadhesion activity [45]. It has been reported that mucosal production of interleukin-6 (IL-6) was due to an adhesion-dependent interaction of bacteria with the mucosa [46], and it has been suggested that CB may reduce UTI symptoms through anti-inflammatory mechanisms [45]. Despite this, urinary or serum cytokines have not been included among the outcomes in the reviewed studies.

4.3. Agreements and Disagreements with Other Reviews. The presence of mixed treatment groups (CB and CB+MH) and the low risk of incomplete outcome data (Table 1) assigned by Jepson et al. [17] to the study of Lee et al. [28], which included in the analysis also individuals who had discontinued the treatment, are in our opinion a bias in evaluating the efficacy.

As reported in the meta-analysis by Jepson et al. [17] the "gold standard" bacteriological criteria for diagnosis of UTI includes bacteriuria greater than 100,000 bacterial cfu/mL from the midstream specimen of urine, whereas for the catheter specimen of urine, a bacteriuria < 100,000/mL is acceptable. Despite this recommendation, only one of the reviewed studies gave a different bacteriuria threshold for midstream and catheter specimens of urine (Table 2), despite the high variability in NLUTD management, due to the differences in lesion level and completeness among patients (Table 2). Cervical SCI has distinct features compared to other SCI, caused by the impairment of manual dexterity, preventing individuals from carrying out self-catheterization (complete injury above C5 and C6), and it is often accompanied by autonomic dysfunction [10]. The latter develops in patients with high-level SCI (above T6), and bladder and bowel distension are the leading causes of autonomic dysfunction [10]. Autonomic dysfunction (above T6) is among the symptoms suggestive of UTI that can be used for the diagnosis of

symptomatic UTI in conjunction with significant bacteriuria and pyuria [10, 12, 13, 47]. In some of the reviewed studies, symptomatic UTI diagnosis required also autonomic dysfunction in individuals with lesions above T6. However, in some cases, symptomatic UTI was among the exclusion criteria (Table 2). This choice could be a bias for the evaluation of efficacy due to the low risk of UTI in the control group (Figure 3). Previous reviews did not consider these aspects, as well as bias included in the quality score described in Table 4.

5. Conclusion

5.1. Implication for Practice. The low quality of the reviewed studies makes it impossible to recommend or exclude the use of CB for preventing bacteriuria in individuals with SCI. On the other hand, it must be considered that fluid intake (2–2.5 L/day) is part of NBD management [33], and reductions greater than threefold of UTI incidence have been documented when NBD was reduced in individuals with SCI [47]. Therefore, in clinical practice, we suggest the evaluation of comorbidity and accurate diet and fluid intake monitoring. Previously, mobile phone applications were used for fluid and/or food intake recording and monitoring in the management of patients undergoing dialysis [48] or with diabetes [49], age-related macular degeneration [50], and cancer [51]. In addition, a risk evaluation for potential food-drug or nutraceutical-drug interactions, due to treatment for NLUTD and comorbidity, should be performed in a personalized patient-centered approach [6].

5.2. Implication for Research. A possible solution to overcome the observed variability among individuals (Table 2) could be the crossover design and monitoring of total polyphenols or of their metabolites identified in plasma and urine after the consumption of CB juice, including cinnamic, dihydrocinnamic, phenylacetic, benzoic, and hippuric acids; flavonols; benzaldehydes; catechols; valerolactones; and/or pyrogallols [32]. The pentacyclic triterpene ursolic acid has been suggested as the main compound in CB able to inhibit the activity of cyclooxygenase-2, and CB extracts inhibited nuclear factor κ B transcriptional activation in T lymphocytes and suppressed the release of IL-6, IL-1 β , IL-8, and tumor necrosis factor- α (TNF- α) from *Escherichia coli* lipopolysaccharide-stimulated peripheral blood mononuclear cells [45].

Serum levels of inflammatory cytokines, including TNF- α and IL-6, were higher in individuals with SCI, compared to healthy controls, and were further elevated in SCI subjects with UTI [52]. In a pilot study on pregnant women, CB juice consumption reduced urinary IL-6 [53], which has been suggested for differentiating between lower UTI and pyelonephritis [54].

For future research, we suggest crossover design with appropriate washout period in order to overcome variability among subjects and to consider plasma and urinary markers of inflammation as outcomes in addition to symptomatic UTI.

Abbreviations

ASIA:	American Spinal Injury Association
CB:	Cranberry
GRADE:	Grading of Recommendations Assessment, Development and Evaluation
IL:	Interleukin
MH:	Methenamine hippurate
NBD:	Neurogenic bowel dysfunction
NLUTD:	Neurogenic lower urinary tract dysfunction
NNT:	Number needed to treat
PAC:	Proanthocyanidins
RR:	Risk ratio
SCI:	Spinal cord injury
TNF:	Tumor necrosis factor
UTI:	Urinary tract infection.

Data Availability

The data used to support the findings of this study are available from the corresponding author upon request.

Conflicts of Interest

The authors declare no conflict of interest.

Authors' Contributions

I.P. was responsible for the conceptualization; A.R. and E.T. were responsible for the data search; A.R., E.T., and I.P. were responsible for the study selection; A.R., E.T., and I.P. were responsible for the data extraction; A.R., T.S., and I.P. were responsible for quality assessment; A.R., A.L.F., and I.P. were responsible for the formal analysis; I.P. was responsible for writing the manuscript; and T.S., A.L.F., and E.T. were responsible for the review and editing. All authors have read and agreed to the published version of the manuscript.

Acknowledgments

This research was funded by Ministero della Difesa, Italy, Project AMAMP (2019-2021).

References

- [1] Asia and ISIS Committee, "The 2019 revision of the International Standards for Neurological Classification of Spinal Cord Injury (ISNCSCI)—what's new?," *Spinal Cord*, vol. 57, no. 10, pp. 815–817, 2019.
- [2] M. Fehlings, A. Singh, L. Tetreault, S. Kalsi-Ryan, and A. Nouri, "Global prevalence and incidence of traumatic spinal cord injury," *Clinical Epidemiology*, vol. 6, pp. 309–331, 2014.
- [3] for the Italian SCI Study Group, S. Ferro, L. Ceconi et al., "Incidence of traumatic spinal cord injury in Italy during 2013-2014: a population-based study," *Spinal Cord*, vol. 55, no. 12, pp. 1103–1107, 2017.
- [4] J. C. Furlan, S. Gulatingam, and B. C. Craven, "Epidemiology of war-related spinal cord injury among combatants: a systematic review," *Global Spine Journal*, vol. 9, no. 5, pp. 545–558, 2018.

- [5] T. Sciarra, M. Ciccotti, P. Aiello et al., “Polypharmacy and nutraceuticals in veterans: pros and cons,” *Frontiers in Pharmacology*, vol. 10, p. 994, 2019.
- [6] M. Ciccotti, A. Raguzzini, T. Sciarra et al., “Nutraceutical-based integrative medicine: adopting a Mediterranean diet pyramid for attaining healthy ageing in veterans with disabilities,” *Current Pharmaceutical Design*, vol. 24, no. 35, pp. 4186–4196, 2019.
- [7] M. H. Rabadi and C. Aston, “Evaluate the impact of neurogenic bladder in veterans with traumatic spinal cord injury,” *The Journal of Spinal Cord Medicine*, vol. 39, no. 2, pp. 175–179, 2015.
- [8] F. Skelton, L. Grigoryan, S. A. Holmes, I. O. Poon, and B. Trautner, “Routine urine testing at the spinal cord injury annual evaluation leads to unnecessary antibiotic use: a pilot study and future directions,” *Archives of Physical Medicine and Rehabilitation*, vol. 99, no. 2, pp. 219–225, 2018.
- [9] M. A. Fitzpatrick, K. J. Suda, N. Safdar et al., “Changes in bacterial epidemiology and antibiotic resistance among veterans with spinal cord injury/disorder over the past 9 years,” *The Journal of Spinal Cord Medicine*, vol. 41, no. 2, pp. 199–207, 2017.
- [10] N. Sekido, Y. Igawa, H. Kakizaki et al., “Clinical guidelines for the diagnosis and treatment of lower urinary tract dysfunction in patients with spinal cord injury,” *International Journal of Urology*, vol. 27, no. 4, pp. 276–288, 2020.
- [11] J. Pannek, “Prevention of recurrent urinary tract infections in neurourology,” *European Urology Focus*, vol. 6, no. 5, pp. 817–819, 2020.
- [12] L. E. Nicolle, K. Gupta, S. F. Bradley et al., “Clinical practice guideline for the management of asymptomatic bacteriuria: 2019 update by the Infectious Diseases Society of America,” *Clinical Infectious Diseases*, vol. 68, no. 10, pp. e83–e110, 2019.
- [13] S. Compton, L. Trease, C. Cunningham, and D. Hughes, “Australian Institute of Sport and the Australian Paralympic Committee position statement: urinary tract infection in spinal cord injured athletes,” *British Journal of Sports Medicine*, vol. 49, no. 19, pp. 1236–1240, 2015.
- [14] Z. Fu, D. Liska, D. Talan, and M. Chung, “Cranberry reduces the risk of urinary tract infection recurrence in otherwise healthy women: a systematic review and meta-analysis,” *The Journal of Nutrition*, vol. 147, no. 12, pp. 2282–2288, 2017.
- [15] D. J. Liska, H. J. Kern, and K. C. Maki, “Cranberries and urinary tract infections: how can the same evidence lead to conflicting advice?,” *Advances in Nutrition*, vol. 7, no. 3, pp. 498–506, 2016.
- [16] S. Sappal, L. L. Goetz, R. Vince, and A. P. Klausner, “Randomized trial of concentrated proanthocyanidins (PAC) for acute reduction of bacteriuria in male veterans with spinal cord injury utilizing clean intermittent catheterization,” *Spinal Cord Series And Cases*, vol. 4, no. 1, p. 58, 2018.
- [17] R. G. Jepson, G. Williams, and J. C. Craig, “Cranberries for preventing urinary tract infections,” *Cochrane Database of Systematic Reviews*, vol. 10, no. 10, article CD001321, 2012.
- [18] C. H. Wang, C. C. Fang, N. C. Chen et al., “Cranberry-containing products for prevention of urinary tract infections in susceptible populations: a systematic review and meta-analysis of randomized controlled trials,” *Archives of Internal Medicine*, vol. 172, no. 13, pp. 988–996, 2012.
- [19] A. Luis, F. Domingues, and L. Pereira, “Can cranberries contribute to reduce the incidence of urinary tract infections? A systematic review with meta-analysis and trial sequential analysis of clinical trials,” *The Journal of Urology*, vol. 198, no. 3, pp. 614–621, 2017.
- [20] A. Navarrete-Opazo, P. Cuitino, and I. Salas, “Effectiveness of dietary supplements in spinal cord injury subjects,” *Disability and Health Journal*, vol. 10, no. 2, pp. 183–197, 2017.
- [21] C. Richard, C. Bendavid, J. Hascoet et al., “Urinary biomarkers profiles in patients with neurogenic detrusor overactivity according to their neurological condition,” *World Journal of Urology*, vol. 38, no. 9, pp. 2261–2268, 2020.
- [22] H. Mutlu and Z. Ekinici, “Urinary tract infection prophylaxis in children with neurogenic bladder with cranberry capsules: randomized controlled trial,” *International Scholarly Research Notices*, vol. 2012, Article ID 317280, 4 pages, 2012.
- [23] J. Kumar, M. Afsal, and A. Garg, “Imaging spectrum of spinal dysraphism on magnetic resonance: a pictorial review,” *World Journal of Radiology*, vol. 9, no. 4, pp. 178–190, 2017.
- [24] I. Peluso, A. Raguzzini, and M. Serafini, “Effect of flavonoids on circulating levels of TNF- α and IL-6 in humans: a systematic review and meta-analysis,” *Molecular Nutrition & Food Research*, vol. 57, no. 5, pp. 784–801, 2013.
- [25] T. A. Linsenmeyer, B. Harrison, A. Oakley, S. Kirshblum, J. A. Stock, and S. R. Millis, “Evaluation of cranberry supplement for reduction of urinary tract infections in individuals with neurogenic bladders secondary to spinal cord injury. A prospective, double-blinded, placebo-controlled, crossover study,” *The Journal of Spinal Cord Medicine*, vol. 27, no. 1, pp. 29–34, 2016.
- [26] G. Reid, J. Hsiehl, P. Potter et al., “Cranberry juice consumption may reduce biofilms on uroepithelial cells: pilot study in spinal cord injured patients,” *Spinal Cord*, vol. 39, no. 1, pp. 26–30, 2001.
- [27] K. B. Waites, K. C. Canupp, S. Armstrong, and M. J. DeVivo, “Effect of cranberry extract on bacteriuria and pyuria in persons with neurogenic bladder secondary to spinal cord injury,” *The Journal of Spinal Cord Medicine*, vol. 27, no. 1, pp. 35–40, 2004.
- [28] B. B. Lee, M. J. Haran, L. M. Hunt et al., “Spinal-injured neuropathic bladder antisepsis (SINBA) trial,” *Spinal Cord*, vol. 45, no. 8, pp. 542–550, 2007.
- [29] M. J. Hess, P. E. Hess, M. R. Sullivan, M. Nee, and S. V. Yalla, “Evaluation of cranberry tablets for the prevention of urinary tract infections in spinal cord injured patients with neurogenic bladder,” *Spinal Cord*, vol. 46, no. 9, pp. 622–626, 2008.
- [30] J. IntHout, J. P. Ioannidis, M. M. Rovers, and J. J. Goeman, “Plea for routinely presenting prediction intervals in meta-analysis,” *BMJ Open*, vol. 6, no. 7, article e010247, 2016.
- [31] S. A. Bahloul, “Use of L’Abbe plot in meta-analysis,” *British Journal of Anaesthesia*, vol. 107, no. 1, p. 104, 2011.
- [32] R. P. Feliciano, C. Mills, G. Ista, C. Heiss, and A. Rodriguez-Mateos, “Absorption, metabolism and excretion of cranberry (poly)phenols in humans: a dose response study and assessment of inter-individual variability,” *Nutrients*, vol. 9, no. 3, p. 268, 2017.
- [33] M. Bernardi, A. L. Fedullo, E. Bernardi et al., “Diet in neurogenic bowel management: a viewpoint on spinal cord injury,” *World Journal of Gastroenterology*, vol. 26, no. 20, pp. 2479–2497, 2020.
- [34] Y. C. Chen, C. C. Chang, T. H. T. Chiu, M. N. Lin, and C. L. Lin, “The risk of urinary tract infection in vegetarians and

- non-vegetarians: a prospective study,” *Scientific Reports*, vol. 10, no. 1, p. 906, 2020.
- [35] F. Mandracchia, E. Llauro, L. Tarro et al., “Potential use of mobile phone applications for self-monitoring and increasing daily fruit and vegetable consumption: a systematized review,” *Nutrients*, vol. 11, no. 3, p. 686, 2019.
- [36] M. R. Jospe, K. A. Fairbairn, P. Green, and T. L. Perry, “Diet app use by sports dietitians: a survey in five countries,” *JMIR mHealth and uHealth*, vol. 3, no. 1, article e7, 2015.
- [37] L. M. Bejar, O. A. Reyes, and M. D. Garcia-Perea, “Electronic 12-hour dietary recall (e-12HR): comparison of a mobile phone app for dietary intake assessment with a food frequency questionnaire and four dietary records,” *JMIR mHealth and uHealth*, vol. 6, no. 6, article e10409, 2018.
- [38] N. R. Srinivas, “Cranberry juice ingestion and clinical drug-drug interaction potentials; review of case studies and perspectives,” *Journal of Pharmacy & Pharmaceutical Sciences*, vol. 16, no. 2, pp. 289–303, 2013.
- [39] H. Bartikova, I. Bousova, P. Jedlickova, K. Lnenickova, L. Skalova, and B. Szotakova, “Effect of standardized cranberry extract on the activity and expression of selected biotransformation enzymes in rat liver and intestine,” *Molecules*, vol. 19, no. 9, pp. 14948–14960, 2014.
- [40] M. Chen, S. Y. Zhou, E. Fabriaga, P. H. Zhang, and Q. Zhou, “Food-drug interactions precipitated by fruit juices other than grapefruit juice: an update review,” *Journal of Food and Drug Analysis*, vol. 26, no. 2, pp. S61–S71, 2018.
- [41] P. Pasko, T. Rodacki, R. Domagala-Rodacka, and D. Owczarek, “A short review of drug-food interactions of medicines treating overactive bladder syndrome,” *International Journal of Clinical Pharmacy*, vol. 38, no. 6, pp. 1350–1356, 2016.
- [42] L. W. Chan, T. L. Griebing, E. P. Arnold, P. S. Chu, P. W. New, and A. Wagg, “Special considerations in the urological management of the older spinal cord injury patient,” *World Journal of Urology*, vol. 36, no. 10, pp. 1603–1611, 2018.
- [43] E. J. Redmond, C. F. Murphy, J. Leonard et al., “The influence of dietary supplementation with cranberry tablets on the urinary risk factors for nephrolithiasis,” *World Journal of Urology*, vol. 37, no. 3, pp. 561–566, 2019.
- [44] T. McHarg, A. Rodgers, and K. Charlton, “Influence of cranberry juice on the urinary risk factors for calcium oxalate kidney stone formation,” *BJU International*, vol. 92, no. 7, pp. 765–768, 2003.
- [45] I. Vasileiou, A. Katsargyris, S. Theocharis, and C. Giaginis, “Current clinical status on the preventive effects of cranberry consumption against urinary tract infections,” *Nutrition Research*, vol. 33, no. 8, pp. 595–607, 2013.
- [46] P. de Man, C. van Kooten, L. Aarden, I. Engberg, H. Linder, and C. S. Eden, “Interleukin-6 induced at mucosal surfaces by gram-negative bacterial infection,” *Infection and Immunity*, vol. 57, no. 11, pp. 3383–3388, 1989.
- [47] M. Kennelly, N. Thiruchelvam, M. A. Averbeck et al., “Adult neurogenic lower urinary tract dysfunction and intermittent catheterisation in a community setting: risk factors model for urinary tract infections,” *Advances in Urology*, vol. 2019, Article ID 2757862, 13 pages, 2019.
- [48] L. C. S. Pinto, M. C. Andrade, R. O. Chaves et al., “Development and validation of an application for follow-up of patients undergoing dialysis: NefroPortátil,” *Journal of Renal Nutrition*, vol. 30, no. 4, pp. e51–e57, 2020.
- [49] J. Porter, C. E. Huggins, H. Truby, and J. Collins, “The effect of using mobile technology-based methods that record food or nutrient intake on diabetes control and nutrition outcomes: a systematic review,” *Nutrients*, vol. 8, no. 12, p. 815, 2016.
- [50] Z. C. Ali, R. Silvioli, A. Rajai, and T. M. Aslam, “Feasibility of use of a mobile application for nutrition assessment pertinent to age-related macular degeneration (MANAGER2),” *Translational Vision Science & Technology*, vol. 6, no. 1, p. 4, 2017.
- [51] T. Orlemann, D. Reljic, B. Zenker et al., “A novel mobile phone app (OncoFood) to record and optimize the dietary behavior of oncologic patients: pilot study,” *JMIR Cancer*, vol. 4, no. 2, article e10703, 2018.
- [52] A. L. Davies, K. C. Hayes, and G. A. Dekaban, “Clinical correlates of elevated serum concentrations of cytokines and auto-antibodies in patients with spinal cord injury,” *Archives of Physical Medicine and Rehabilitation*, vol. 88, no. 11, pp. 1384–1393, 2007.
- [53] D. A. Wing, P. J. Rumney, S. Y. Leu, and F. Zaldivar, “Comparison of urinary cytokines after ingestion of cranberry juice cocktail in pregnant subjects: a pilot study,” *American Journal of Perinatology*, vol. 27, no. 2, pp. 137–142, 2010.
- [54] N. Nanda and M. Juthani-Mehta, “Novel biomarkers for the diagnosis of urinary tract infection—a systematic review,” *Biomarker Insights*, vol. 4, 2009.

Research Article

Ameliorating Effect of Klotho Protein on Rat Heart during I/R Injury

Agnieszka Olejnik, Anna Krzywonos-Zawadzka, Marta Banaszkiewicz, and Iwona Bil-Lula 

Division of Clinical Chemistry and Laboratory Hematology, Department of Medical Laboratory Diagnostics, Faculty of Pharmacy, Wrocław Medical University, Borowska 211A St., 50-556 Wrocław, Poland

Correspondence should be addressed to Iwona Bil-Lula; iwona.bil-lula@umed.wroc.pl

Received 9 June 2020; Revised 22 September 2020; Accepted 29 September 2020; Published 17 October 2020

Academic Editor: Luciano Saso

Copyright © 2020 Agnieszka Olejnik et al. This is an open access article distributed under the Creative Commons Attribution License, which permits unrestricted use, distribution, and reproduction in any medium, provided the original work is properly cited.

An essential procedure for the treatment of myocardial infarction is restoration of blood flow in the obstructed infarct artery, which may cause ischaemia/reperfusion (I/R) injury. Heart I/R injury manifests in oxidative stress, metabolic and morphological disorders, or cardiac contractile dysfunction. Klotho protein was found to be produced in the heart tissue and participate in antioxidation or ion homeostasis. The aim of this study was to examine an influence of Klotho protein on the heart subjected to I/R injury. Wistar rats served as a surrogate heart model *ex vivo*. Rat hearts perfused using the Langendorff method were subjected to global no-flow ischaemia, and isolated rat cardiomyocytes underwent chemical I/R *in vitro*, with or without recombinant Klotho protein administration. Haemodynamic parameters of heart function, cell contractility, markers of I/R injury and oxidative stress, and the level of contractile proteins such as myosin light chain 1 (MLC1) and troponin I (TnI) were measured. The treatment of hearts subjected to I/R injury with Klotho protein resulted in a recovery of heart mechanical function and ameliorated myocyte contractility. This improvement was associated with decreased tissue injury, enhanced antioxidant capacity, and reduced release of MLC1 and TnI. The present research showed the contribution of Klotho to cardioprotection during I/R. Thus, Klotho protein may support the protection from I/R injury and prevention of contractile dysfunction in the rat heart.

1. Introduction

Restoration of the flow in the obstructed infarct artery is pivotal for the treatment of myocardial infarction. However, revascularization and restoration of the blood flow inflict myocardial ischaemia/reperfusion (I/R) injury. I/R injury can be irreversible, and it manifests itself in increased infarct size and microvascular dysfunctions [1, 2]. It is known that I/R leads to oxidative stress and the subsequent cascade of pathophysiological events in the heart. The important factors contributing to the pathogenesis of I/R injury are the degradation of heart contractile proteins by proteolytic enzymes and necrotic cell death. The proteolytic enzymes like matrix metalloproteinases (MMPs) degrade cardiac troponin, titin, or myosin light chains (MLCs). As a result, numerous meta-

bolic, morphological, and contractile disorders in the myocardium are observed [3]. The approach of regulating oxidative stress in the heart may support the reduction of maladaptive response established during I/R injury. Therefore, searching for new factors contributing to the prevention and treatment of myocardial injury following I/R is needed.

Klotho is an antiaging protein that is bounded to the cell membrane or released into extracellular space and then found in the blood, urine, or cerebrospinal fluid. The main function of Klotho is the regulation of fibroblast growth factor (FGF) signalling and ion homeostasis. There is a lot of evidence for the protective role of Klotho in the kidney, the main organ that produces Klotho protein. The expression of Klotho was observed also in the pituitary gland, placenta, skeletal muscle, urinary bladder, aorta, pancreas, testis,

ovary, colon, or thyroid gland. β Klotho, other Klotho family member, is expressed in the adipose tissues, liver, pancreas, and some part of the brain [4–8]. An intracellular Klotho form in the cytoplasm of mouse kidney and human parathyroid gland cells was also found. Importantly, intracellular Klotho served as an endogenous anti-inflammatory and anti-aging factor [6, 7]. It has been shown that Klotho was involved in the kidney or brain protection by regulation of oxidative stress, inflammation, and apoptosis [5, 9–11]. Moreover, Klotho deficiency correlated with the occurrence and development of atherosclerosis, coronary artery disease, myocardial infarction, and left ventricular hypertrophy [7]. We have reported the expression of Klotho in the cardiomyocytes recently [12]. However, a cell line model does not include the effect of the intercellular interactions and signaling between the cardiomyocytes and other types of cells in the cardiac tissue. For this reason, we decided to examine Klotho influence at the tissue level using Wistar rat hearts. We propose that Klotho may contribute to the protection of the heart against I/R injury in the current research.

This study was aimed at investigating the influence of Klotho protein on the rat hearts subjected to I/R injury.

2. Materials and Methods

2.1. Experimental Animals. Adult male Wistar rats weighing 200–350 grams were obtained from Mossakowski Medical Research Center, Polish Academy of Sciences, Warsaw, Poland. The animals were housed in cages (two rats/cage) and kept at controlled temperature ($22 \pm 2^\circ\text{C}$), humidity ($55 \pm 5\%$), and light/dark (12/12 hours) cycle. An *ad libitum* access to a diet of standard laboratory chow and water was provided. All experimental procedures in the animals were performed following the published Guide of the Polish Ministry of Science and Higher Education for the Care and Use of Experimental Animals. This investigation was approved by the Ethics Committee for Experiments on Animals at the Ludwik Hirsfeld Institute of Immunology and Experimental Therapy Polish Academy of Sciences, Wroclaw, Poland (Resolution 002/2020 of 15th January 2020).

2.2. Isolated Rat Hearts Perfused with the Langendorff Method. Rats were desensitized with buprenorphine (0.05 mg/kg, i.p.) and anesthetized with sodium pentobarbital (0.5 ml/kg i.p.), and the hearts were rapidly excised from animals. The spontaneously beating hearts were then rinsed by immersion in ice-cold Krebs-Henseleit Buffer (118 mmol/L NaCl, 4.7 mmol/L KCl, 1.2 mmol/L KH_2PO_4 , 1.2 mmol/L MgSO_4 , 3.0 mmol/L CaCl_2 , 25 mmol/L NaHCO_3 , 11 mmol/L glucose, and 0.5 mmol/L EDTA, pH 7.4) and cannulated by the aorta on a Langendorff system (EMKA Technologies, Paris, France). The above procedure was completed within 30 sec. Then, hearts were perfused at constant pressure (60 mmHg) with Krebs-Henseleit Buffer (pH 7.4, 37°C) and gassed continuously (5% $\text{CO}_2/95\% \text{O}_2$). A latex balloon was filled with water, and then, it was connected to a pressure transducer (EMKA Technologies, Paris, France). Then, the balloon was introduced into the left ventricle via a mistrial valve. The volume of the balloon was adjusted to achieve a

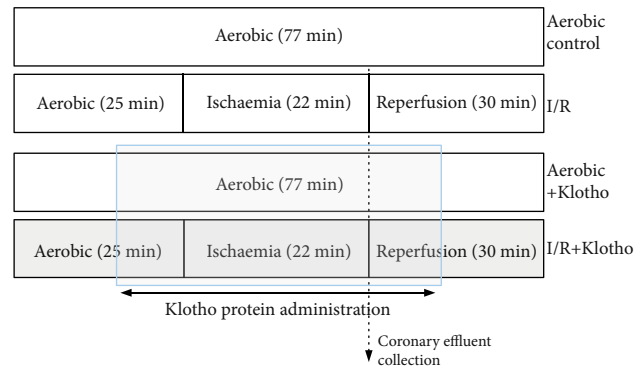


FIGURE 1: Experimental protocol for I/R injury of isolated rat hearts, with and without Klotho administration. Klotho protein was added into the perfusion buffer and administered to isolated hearts during the last 10 min of aerobic stabilization (prior to the global ischaemia) and within the first 10 min of reperfusion after global ischaemia. I/R: ischaemia/reperfusion.

stable left ventricular end-diastolic pressure of 8–10 mmHg during stabilization and reperfusion. The following haemodynamic parameters using an EMKA recording system with IOX2 software (EMKA Technologies, Paris, France) were monitored: coronary flow (CF), heart rate (HR), left ventricular developed pressure (LVDP), left ventricular end-diastolic pressure (PED), and intraventricular pressure (dP/dt). Hearts that showed $\text{CF} > 28 \text{ mL/min}$ or $< 10 \text{ mL/min}$ were excluded from the study.

2.3. Global Ischaemia/Reperfusion Injury of Isolated Rat Hearts. Rat hearts were distributed equally and randomly into 4 groups: aerobic control without Klotho ($n = 12$), aerobic control with Klotho ($n = 3$), acute myocardial I/R injury without ($n = 14$), and with Klotho ($n = 7$). The scheme of the experimental protocol of heart ischaemia/reperfusion injury is shown in Figure 1. No injury of isolated hearts prior to global ischaemia was established in the preliminary experiment by measurement of the activity of LDH released from hearts (a marker of cell injury). There was no difference between groups in LDH activity in coronary effluents collected at 25 minutes of the experiment (data not shown). The isolated hearts from I/R groups underwent 25 min of aerobic stabilization, 22 min of global no-flow ischaemia (by a cessation of the buffer flow), and 30 min of reperfusion (aerobic conditions) [13], in the presence or absence of Klotho protein. The hearts from aerobic groups were perfused aerobically for 77 min, with or without Klotho protein administration. Recombinant Rat α Klotho protein (Cloud-Clone Corp., RPH757Ra01) was diluted to a final concentration of 0.5 ng/mL with Krebs-Henseleit Buffer, immediately before administration. The optimal concentration of Klotho protein was determined experimentally. Klotho was administered with the perfusion buffer into the hearts during the last 10 min of aerobic stabilization and in the first 10 min of reperfusion (after global ischaemia) [13, 14] (Figure 1). To determine cardiac mechanical function, the recovery of rate pressure product (RPP) was expressed as the product of HR and LVPD and evaluated at 25 min of the experiment (the end of aerobic perfusion) and at 77 min (the end of

reperfusion) [13, 14]. After the experimental protocol, isolated hearts were immediately immersed in liquid nitrogen and stored at -80°C for further investigations. 15 mL of coronary effluents was collected at the beginning of reperfusion (47 min of the experiment) (Figure 1). Then, coronary effluents were concentrated (1 mL final volume) using Amicon Ultra-15 Centrifugal Filter Units with Ultracel-10 membrane (EMD Millipore, USA), aliquoted, and frozen at -80°C for further biochemical analysis.

2.4. Heart Perfusion and Isolation of Ventricular Rat Cardiomyocytes. Rats were treated with buprenorphine (0.05 mg/kg, i.p.) and anaesthetized with sodium pentobarbital (0.5 mL/kg i.p.). The hearts were rapidly excised from animals and rinsed immediately after removal by immersion in ice-cold Myocyte Isolation Buffer (MIB) containing 120 nmol/L NaCl, 5 mmol/L KCl, 2 mmol/L NaAc, 2 mmol/L MgCl_2 , 1 mmol/L Na_2HPO_4 , 20 mmol/L NaHCO_3 , 5 mmol/L glucose, 9 mmol/L taurine, and 10 mmol/L CaCl_2 at pH 7.4. The spontaneously beating hearts were suspended on a blunt-end needle by the aorta in a Langendorff system and perfused with MIB containing 1 mmol/L CaCl_2 at 37°C for 5 min. To induce the loss of contractility of cardiomyocytes, the buffer was replaced with MIB containing $5\ \mu\text{mol/L}$ CaCl_2 . Then, the right ventricle was excised after mild swelling of the myocardium in HEPES buffer (120 mM NaCl 140, 5 mM KCl, 2 mM MgCl_2 , 5 mM glucose, 9 mM taurine, and 5 mM HEPES) containing $40\ \mu\text{mol/L}$ CaCl_2 , collagenase, and protease. The ventricle was rinsed with HEPES buffer containing $100\ \mu\text{mol/L}$ CaCl_2 and 150 mg bovine serum albumin and minced into small pieces in the digestion solution (HEPES buffer containing $100\ \mu\text{mol/L}$ CaCl_2 , 150 mg BSA, 15 mg collagenase, and 1 mg protease). The minced tissue was repeatedly digested six times for 20 and 10 min in a water bath (37°C). The 3rd-6th fraction was used for further experiments.

2.5. Chemical Ischaemia/Reperfusion of Isolated Ventricular Rat Cardiomyocytes. Isolated rat cardiomyocytes underwent 15 min of aerobic stabilization in HEPES buffer containing $100\ \mu\text{mol/L}$ CaCl_2 and 150 mg BSA. Then, the ischaemia was induced by covering the cell pellet with HEPES buffer containing 4 mmol/L 2-deoxyglucose (to inhibit glycolysis) and 40 mmol/L sodium cyanide (an inhibitor of cellular respiration) for 3 min (I/R groups). The optimal duration of ischaemia was established in our previous studies [13, 15]. Then, the reperfusion was conducted by removing the buffer containing sodium cyanide by centrifugation (1 min, $1500 \times g$) and incubation of cell pellet for 20 min in a fresh portion of HEPES buffer ($100\ \mu\text{mol/L}$ CaCl_2 , 150 mg BSA). In the I/R+Klotho group, cells were incubated in the appropriate buffers with Recombinant Rat α Klotho protein (Cloud-Clone Corp., RPH757Ra01) during aerobic stabilization, ischaemia, and reperfusion (whole experimental protocol of I/R). The following concentrations of Klotho in the buffers were tested: 100 ng/mL, 5 ng/mL, and 0.5 ng/mL (final concentration). Cells from the aerobic control group were maintained in aerobic conditions and kept exposed to atmospheric air for 38 min in HEPES buffer ($100\ \mu\text{mol/L}$ CaCl_2 , 150 mg BSA).

For contractility measurement, cells were centrifuged at $1500 \times g$ for 5 min and suspended in HEPES buffer ($100\ \mu\text{mol/L}$ CaCl_2 , 150 mg BSA).

2.6. Measurement of Ventricular Rat Cardiomyocyte Contractility. After the protocol of I/R injury, a $100\ \mu\text{L}$ aliquot of cell suspension was placed in the rapid change stimulation chamber of the IonOptix Contractility System (IonOptix, Milton, MA, USA). The cardiomyocytes were stabilized for 3 min and perfused with oxygenated HEPES buffer containing 2 mmol/L CaCl_2 (4 mL/min) at 37°C . The contractility was measured by continuously pacing the cells with 1 Hz and 5 V (MyoPacer, IonOptix) and expressed as a percent of peak shortening in comparison to the length of the diastolic cell. At least an average of six cells per sample and six samples per experimental condition was evaluated.

2.7. Preparation of Heart Homogenates. Frozen hearts were crushed using a mortar and pestle in liquid nitrogen. Then, heart tissue was homogenized mechanically in ice-cold homogenization buffer (50 mmol/L Tris-HCl (pH 7.4), 3.1 mmol/L sucrose, 1 mmol/L dithiothreitol, 10 mg/mL leupeptin, 10 mg/mL soybean trypsin inhibitor, 2 mg/mL aprotinin, and 0.1% Triton X-100). The homogenate was centrifuged ($10\ 000 \times g$ at 4°C for 15 min), and the supernatant was collected and stored at -80°C for further biochemical experiments.

2.8. Assessment of LDH Activity. Lactate dehydrogenase (LDH) activity served as a marker of heart injury. The activity of LDH was assessed with the Lactate Dehydrogenase Activity Assay Kit (Sigma-Aldrich) according to the manufacturer's instruction. LDH is a stable cytosolic enzyme that is released into the extracellular space upon cell membrane damage or permeability. Briefly, LDH interconverts pyruvate and lactate with the reduction of NAD to NADH, which is detected with a colorimetric assay at 450 nm. LDH activity was determined in coronary effluents and normalized to CF.

2.9. Assessment of Cytotoxicity Level in Rat Hearts. To evaluate an influence of I/R injury and Klotho on isolated rat hearts, the cytotoxicity level using the CytoTox-Glo™ Cytotoxicity Assay (Promega, Madison, WI, USA) according to the manufacturer's instruction was assessed. The assay measures the relative number of dead cells based on the extracellular activity of a distinct intracellular protease (dead-cell protease). Dead-cell protease is released from membrane-compromised or damaged cells. Briefly, to measure extracellular dead-cell protease activity, a luminogenic cell-impermeant peptide substrate (alanyl-alanyl-phenylalanyl-aminoluciferin; AAF-aminoluciferin) is used. Dead-cell protease cleaves the luminogenic AAF-aminoluciferin substrate. Then, the Ultra-Glo™ Recombinant Luciferase is used for the measurement of luminescence generated by liberated aminoluciferin product. The intensity of luminescence is proportional to the percentage of cells undergoing cytotoxic stress. The number of dead cells was based on the measurement of the extracellular activity of released dead-cell protease in coronary effluents, normalized to CF, and served as a level of cytotoxicity in isolated hearts.

TABLE 1: An influence of Klotho on cardiac mechanical function of isolated rat hearts.

Parameter	Aero	Aero+Klotho	I/R	I/R+Klotho
dP/dt_{max} (mmHg/s) [†]	1559 ± 93	1407 ± 72	1227 ± 57*	1494 ± 157
PED (mmHg) [†]	9.9 ± 0.9	10.6 ± 0.8	8.6 ± 0.5*	9.1 ± 0.2
LVDP (mmHg) [†]	57.3 ± 2.4	61.0 ± 4.9	40.5 ± 4.8*	66.5 ± 6.2 [#]
RPP (mmHg × min ⁻¹ × 10 ³) [†]	17.8 ± 1.0	19.0 ± 0.8	9.9 ± 1.1*	21.4 ± 1.8 [#]
CF (mL/min) [‡]	12.5 ± 1.6	13.2 ± 1.1	3.4 ± 1.1*	10.6 ± 0.8 [#]

CF: coronary flow; dP/dt_{max} : baseline left ventricular maximal contractility; I/R: ischaemia/reperfusion; LVDP: left ventricular developed pressure; PED: left ventricular end-diastolic pressure; RPP: rate pressure product; mean ± SEM; $n_{aero} = 12$; $n_{aero+Klotho} = 3$; $n_{I/R} = 14$; $n_{I/R+Klotho} = 7$; * $p < 0.05$ vs. Aero; [#] $p < 0.05$ vs. I/R; ANOVA. [†]After I/R (77 min of the experiment); [‡]after ischaemia (first minute of reperfusion).

2.10. Assessment of Oxidative Stress in Rat Hearts. OxiSelect™ In Vitro ROS/RNS Assay Kit (Cell Biolabs, San Diego, USA) was used to document an influence of Klotho on the level of total reactive oxygen and nitrogen species (ROS/RNS) in the rat heart tissue. The assay measures total ROS and RNS, including hydrogen peroxide, nitric oxide, peroxy radical, and peroxy nitrite anion, using a proprietary fluorogenic probe, dichlorodihydrofluorescein DiOxyQ (DCFH-DiOxyQ). The probe is primed with a dequenching reagent to the highly reactive DCFH form. In the presence of ROS and RNS, the DCFH is rapidly oxidized to the highly fluorescent 2', 7'-dichlorodihydrofluorescein (DCF). Fluorescence intensity is proportional to the total ROS/RNS level within the sample. The total ROS/RNS level was assessed in coronary effluents and normalized to CF.

2.11. Measurement of Total Antioxidant Capacity in Rat Hearts. To document an influence of Klotho on oxidative stress resistance during I/R, OxiSelect™ Total Antioxidant Capacity (TAC) Assay Kit (Cell Biolabs, San Diego, USA) was used. Measurement of the total nonenzymatic antioxidant capacity (TAC) is indicative of cells' ability to counteract induced oxidative stress. Briefly, TAC Assay is based on the reduction of copper (II) to copper (I) by the antioxidants present in the sample. Upon reduction, the copper (I) ion further reacts with a coupling chromogenic reagent that produces a color with a maximum absorbance at 490 nm. Absorbance values were proportional to the total reductive capacity in the hearts. TAC level was measured in heart homogenates and normalized to total protein concentration.

2.12. Analysis of MLC1 and TnI Concentration in Coronary Effluents. The concentration of ventricular isoform of myosin light chain 1 (MLC1) in perfusates was determined using Rat Myosin Light Chain 3 ELISA Kit (Bioassay Technology Laboratory, Shanghai, China). Briefly, primary capture antibodies bind MLC1 from the sample. Then, MLC1 is detected with biotinylated anti-MLC1 secondary antibodies and streptavidin-horseradish peroxidase (HRP) complex. The substrate solution is then added, and color develops in proportion to the amount of rat MLC1.

Cardiac troponin I (TnI) in coronary effluents was quantitatively measured using Rat Cardiac Troponin I SimpleStep ELISA Kit (Abcam, Cambridge, UK). Briefly, TnI is tied with antibody specific to rat cardiac muscle TnI and is detected by

biotin-conjugated polyclonal antibody and HRP. Next, TMB Development Solution is used to enable visualization of the reaction. The concentration of MLC1 and TnI in coronary effluents was normalized to CF.

2.13. Determination of Total Protein Concentration. The concentration of total protein in the cardiac tissue and coronary effluents was measured by the Bradford method using Bio-Rad Protein Assay Dye Reagent (Bio-Rad) and Spark multi-mode microplate reader (Tecan Trading AG, Switzerland). BSA (heat shock fraction, ≥98%, Sigma-Aldrich) served as the protein standard.

2.14. Statistical Analysis. Experimental data were analysed using GraphPad Prism 6 software (GraphPad Software, San Diego, CA, USA). The normality of variance changes was calculated with the Shapiro-Wilk normality test or Kolmogorov-Smirnov test. Student's *t*-test or Mann-Whitney *U* tests were used to analyse the data between two groups. The analysis of data in multiple groups was performed with ANOVA or nonparametric test with post hoc tests. Correlations were assessed using Pearson's or Spearman's tests. Results were expressed as mean ± SEM and a value of $p < 0.05$ was regarded as statistically significant.

3. Results

3.1. An Influence of Klotho Protein on Heart Contractility. Subjecting the isolated rat hearts to I/R protocol resulted in a significant decrease in cardiac haemodynamic parameters (Table 1, Figure 2). Cardiac mechanical function was decreased approximately by 40% in hearts subjected to I/R in comparison to aerobically perfused hearts (approximately 100% of recovery), showing heart dysfunction (Figure 2(a)). To check the cytotoxicity of Klotho protein, hearts from the aerobic control group were perfused aerobically with Klotho. Supplementation of aerobically perfused hearts with Klotho protein did not affect any of the measured parameters in comparison to the aero group (Table 1, Figure 2). Perfusion of hearts subjected to I/R with Klotho protein resulted in a full recovery of heart contractility (average recovery 110%) (Figure 2(a)) and in a significant increase in cardiac haemodynamic parameters, such as RPP (Table 1, Figure 2(b)), CF (Table 1, Figure 2(c)), HR (Figure 2(d)), and LVDP (Table 1), in comparison to I/R hearts.

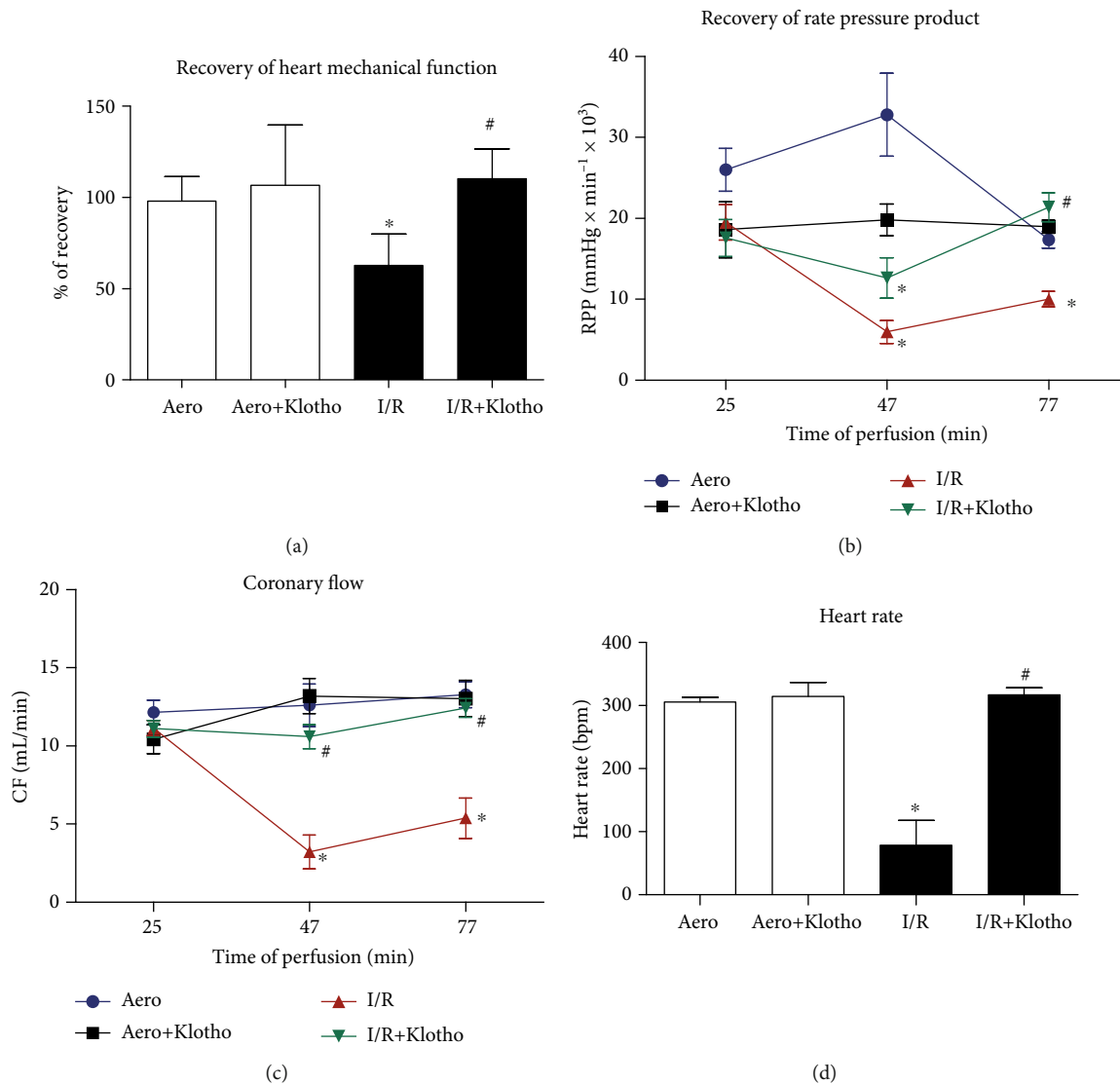


FIGURE 2: An effect of global I/R injury and Klotho protein on heart contractile function: (a) recovery of heart mechanical function. Percent recovery was calculated as a difference between RPP at 25 and 75 min of perfusion protocol; (b) RPP calculated as the product of the heart rate and pressure developed in the left ventricle (intraventricular pressure of left ventricle \times heart rate/1000); (c) coronary flow; (d) heart rate at the end of reperfusion (77 min). Bpm: beats per minute; CF: coronary flow; I/R: ischaemia/reperfusion; RPP: rate pressure product; mean \pm SEM; $n_{aero} = 12$; $n_{aero+Klotho} = 3$; $n_{I/R} = 14$; $n_{I/R+Klotho} = 7$; * $p < 0.05$ vs. Aero; # $p < 0.05$ vs. I/R; ANOVA.

An isolated rat cardiomyocyte contractility, expressed as a peak shortening (% of cell length), was significantly reduced in cells subjected to I/R in comparison to group maintained in aerobic condition (Figure 3). Supplementation of the cardiomyocytes with Klotho protein contributed to the maintenance of cell contractility inversely to Klotho dose. Klotho at the concentration of 0.5 ng/mL supported the increase of contractility, whereas 100 ng/mL represented a subthreshold dose that did not significantly maintain contractile function in the cardiomyocytes subjected to I/R (Figure 3).

3.2. An Influence of Klotho on the Magnitude of Heart I/R Injury. The measurement of the activity of LDH released from hearts and the number of cardiac dead cells (cytotoxicity level) served as a marker of heart injury. The activity of LDH (Figure 4(a)) and the number of cardiac dead cells

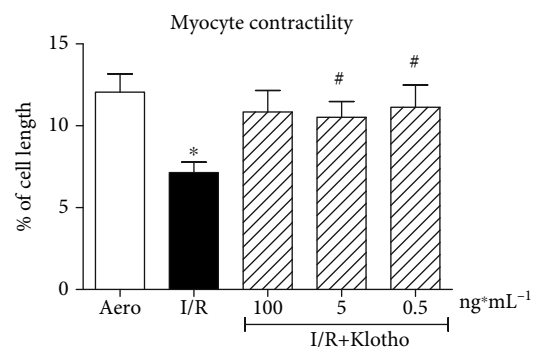


FIGURE 3: An influence of Klotho protein on isolated rat cardiomyocyte contractility. The contractility was expressed as peak shortening (%) in comparison to the length of the diastolic cell. Mean \pm SEM; $n = 6$; * $p < 0.05$ vs. Aero; # $p < 0.05$ vs. I/R; ANOVA.

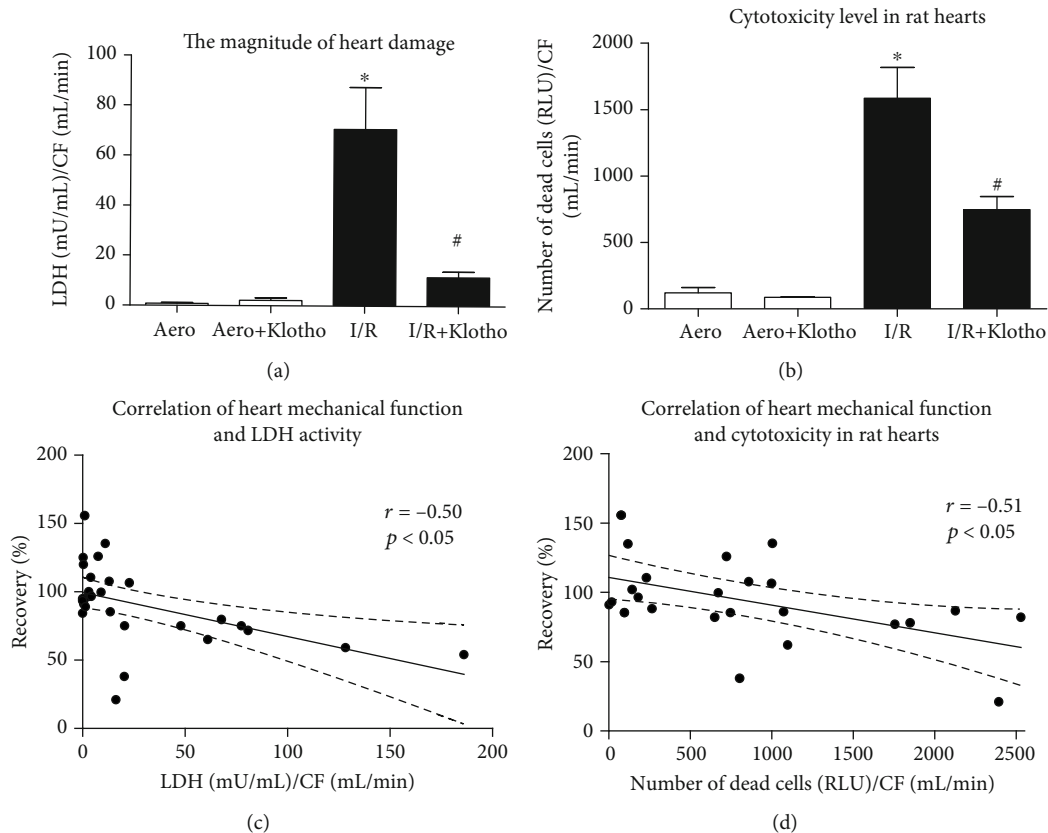


FIGURE 4: An influence of Klotho on the magnitude of heart I/R injury: (a) the activity of LDH in coronary effluents as a marker of heart injury. LDH activity was normalized to CF; (b) the number of dead cells in rat hearts based on the activity of dead cell protease, tested by cytotoxicity assay. The data was expressed in RLU and normalized to CF; (c) correlation of heart mechanical function and LDH activity; (d) correlation of heart mechanical function and cytotoxicity in rat hearts. CF: coronary flow; LDH: lactate dehydrogenase; mU/mL: milli-international enzyme units per millilitre; RLU: relative light units; mean \pm SEM; $n_{\text{aero}} = 9$; $n_{\text{aero+Klotho}} = 3$; $n_{\text{I/R}} = 10$; $n_{\text{I/R+Klotho}} = 7$; * $p < 0.05$ vs. Aero; # $p < 0.05$ vs. I/R; ANOVA.

(Figure 4(b)) were significantly increased in hearts that underwent I/R procedure compared to the aerobic control group. To check the toxicity of Klotho protein on cardiac tissue, hearts from the aerobic control group were treated with Klotho. Aerobic perfusion with recombinant Klotho protein did not cause cell injury (Figures 4(a) and 4(b)). Administration of Klotho protein to hearts subjected to I/R led to almost full protection against injury (Figure 4(a)) and decreased cytotoxicity (Figure 4(b)) in comparison to the I/R group. Heart mechanical function negatively correlated with LDH activity ($r = -0.50$, $p < 0.05$) (Figure 4(c)) and cytotoxicity level ($r = -0.51$, $p < 0.05$) (Figure 4(d)), showing heart contractile dysfunction due to injury.

3.3. Oxidative Status in the Hearts Subjected to I/R Injury. Total ROS/RNS level in rat hearts was significantly higher in the I/R group compared to the aerobic control group, confirming oxidative/nitrosative stress (Figure 5(a)). Administration of Klotho protein slightly reduced the production of ROS/RNS (Figure 5(a)) and significantly enhanced total antioxidant capacity (TAC) in hearts subjected to I/R (Figure 5(b)). ROS/RNS level positively correlated with LDH activity ($r = 0.57$, $p < 0.05$) (Figure 5(c)).

3.4. Release of Contractile Proteins from Hearts during I/R. MLC1 concentration was increased in coronary effluents from hearts subjected to I/R injury compared to aerobic control, showing increased release of MLC1 from the hearts (Figure 6(a)). Administration of Klotho protein to I/R hearts effectively reduced the release of MLC1 (Figure 6(a)). The concentration of MLC1 in coronary effluents negatively correlated with heart mechanical function ($p < 0.05$, $r = -0.49$) (Figure 6(b)) and positively correlated with LDH activity ($p < 0.05$, $r = 0.62$) (Figure 6(c)), confirming the mechanism of I/R injury.

The content of TnI in coronary effluents from hearts subjected to I/R injury was increased compared to aerobic control (Figure 7(a)). Administration of Klotho protein during I/R contributed to reduced release of TnI (Figure 7(a)). The release of TnI positively correlated with LDH activity ($r = 0.79$, $p < 0.05$) (Figure 7(b)).

4. Discussion

Kidneys are considered to be the major site of Klotho expression and primary source of the circulating protein. However, Klotho is also produced in other types of tissue, like the skeletal muscle, adipose tissues, brain, or liver [5, 8]. Recent

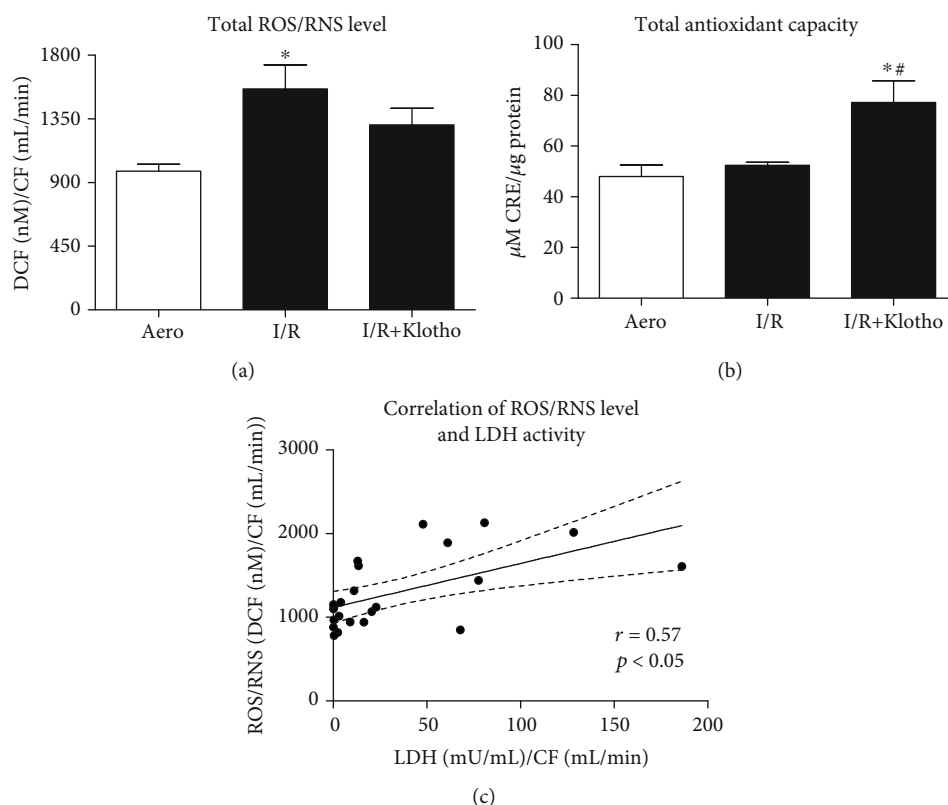


FIGURE 5: Oxidative status in the hearts subjected to I/R injury: (a) total ROS and RNS level expressed as nM of DCF and normalized to coronary flow; (b) total antioxidant capacity of hearts subjected to I/R. TAC was expressed as μM of CRE and normalized to total protein concentration; (c) correlation of ROS/RNS level and LDH activity. CF: coronary flow; CRE: copper reducing equivalents; DCF: 2', 7'-dichlorodihydrofluorescein; LDH: lactate dehydrogenase; mU/mL: milli international enzyme units per millilitre; RNS: reactive nitrogen species; ROS: reactive oxygen species; TAC: total antioxidant capacity; mean \pm SEM; $n_{\text{aero}} = 8$; $n_{\text{I/R}} = 9$; $n_{\text{I/R+Klotho}} = 6$; * $p < 0.05$ vs. Aero; # $p < 0.05$ vs. I/R; ANOVA.

studies have underlined the importance of Klotho in the cardiac muscle too [16]. We had previously reported compensative production of Klotho in the rat hearts to protect cardiac tissue from I/R injury. Enhanced production and release of Klotho into the extracellular space were also proposed as a biomarker of heart damage [12]. Therefore, the main aim of this investigation was to examine the influence of Klotho administration on the rat hearts injured by ischaemia/reperfusion. Our research showed that Klotho protein contributed to the reduction of damage and contractile dysfunction in the heart during I/R. We strongly suggest that Klotho can be valuable as a potential agent that supports cardioprotection/protection in ischaemic heart disorders.

In this study, subjecting the isolated rat hearts to the I/R procedure resulted in a significant decrease in haemodynamic parameters. The administration of Klotho protein during I/R supported the recovery of heart mechanical function and contractility of isolated cardiomyocytes. Our results correspond to the research of Hui et al., where treatment with recombinant Klotho after endotoxemia-induced heart injury improved the haemodynamic parameters and cardiac function in aging mice [17]. It is known that ROS directly influence contractile function by modifying proteins involved in excitation-contraction coupling. The suppression of calcium channels and oxidative interaction with Ca^{2+} ATPase in the

sarcoplasmic reticulum occur. It results in the inhibition of Ca^{2+} uptake. Thus, intracellular and mitochondrial Ca^{2+} overload contributes to cardiac contractile disorders [3, 18]. It was found that membrane-bound Klotho is a coreceptor for fibroblast growth factor 23 (FGF23) and plays a role in ion homeostasis. Soluble Klotho can induce negative phosphate and calcium balance also independently of FGF23 as an endocrine, autocrine, and paracrine hormone [6, 19]. Importantly, stress-induced heart hypertrophy and remodeling were impaired by means of Klotho. Soluble Klotho was recognized as an inhibitor of TRPC6 channel exocytosis in the cardiomyocytes. Thus, Klotho protected the heart during stress conditions by downregulating of Ca^{2+} influx and abnormal Ca^{2+} signalling [6, 20–22]. It was also shown that Klotho acted as an endogenous inhibitor of calcification and mediated between FGF23 and vascular cells [23]. The current research showed that Klotho supported contractility in the injured cardiomyocytes. Taking into account that Klotho influences calcium homeostasis in the heart, it may contribute to the prevention of cardiac mechanical function and contractile disorders. However, further studies are needed to explore the underlying molecular mechanism of the potential effect of Klotho on calcium-dependent heart contractility.

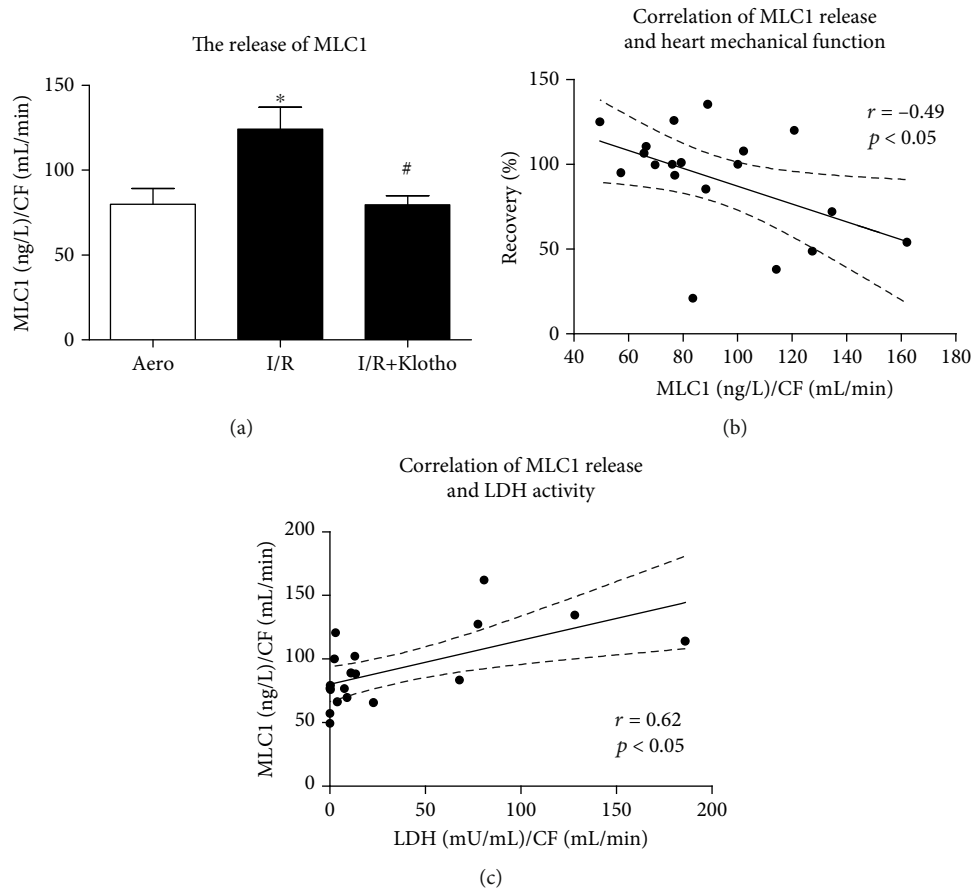


FIGURE 6: An influence of Klotho protein on MLC1 amount in rat hearts: (a) concentration of MLC1 in coronary effluents tested by ELISA and normalized to CF; (b) correlation of MLC1 concentration and heart mechanical function; (c) correlation of MLC1 concentration and LDH activity. CF: coronary flow; GAPDH: glyceraldehyde 3-phosphate dehydrogenase; LDH: lactate dehydrogenase; mU/mL: milli-international enzyme units per millilitre; MLC1: myosin light chain I; mean \pm SEM; $n_{aero} = 7$; $n_{I/R} = 5$; $n_{I/R+Klotho} = 7$; * $p < 0.05$ vs. Aero; # $p < 0.05$ vs. I/R; ANOVA.

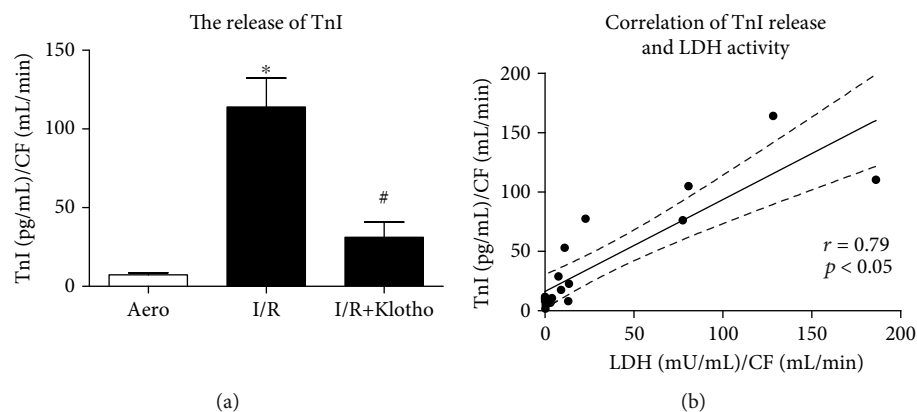


FIGURE 7: An influence of Klotho protein on TnI release in rat hearts: (a) concentration of TnI in coronary effluents tested by ELISA and normalized to CF; (b) correlation of TnI concentration and LDH activity. CF: coronary flow; LDH: lactate dehydrogenase; mU/mL: milli-international enzyme units per millilitre; TnI: troponin I; mean \pm SEM; $n_{aero} = 7$; $n_{I/R} = 5$; $n_{I/R+Klotho} = 7$; * $p < 0.05$ vs. Aero; # $p < 0.05$ vs. I/R; ANOVA.

There are studies showing that Klotho protein has been characterized as a factor in the prevention of oxidative stress, inflammation, fibrosis, and apoptosis [7, 9, 10, 24]. Moreover, Klotho deficiency has been identified in many disorders

such as inflammatory bowel disease, kidney disease, atherosclerosis, cardiac hypertrophy, and remodelling [10, 16, 20, 25–27]. In our previous research, human cardiomyocytes subjected to I/R injury produced Klotho in a compensative

manner to protect from the damage [12]. In the present study, subjecting the rat hearts to I/R caused injury and increased production of ROS/RNS in the cardiac tissue. Heart mechanical function negatively correlated with the markers of injury, showing heart contractile dysfunction due to I/R. There was also a positive correlation of ROS/RNS level and LDH activity, indicating the heart damage due to overproduction of ROS/RNS. Klotho protein contributed to the reduction of cardiac injury and cytotoxicity and supported the production of antioxidants and antioxidant capacity in I/R hearts. However, only a slight decline of ROS/RNS level in the I/R+Klotho group compared to the I/R group does not explain the protective mechanism of Klotho. Further study is needed to clarify this concatenation. Moreover, the magnitude of damage and the number of dead cells were significantly lower after supplementation of the cardiac muscle with Klotho. These data were confirmed in other studies showing that Klotho prevents cell apoptosis and cytotoxic activity after induced oxidative stress in other organs [9, 11, 27–29]. Klotho also reduced the apoptosis in an animal model of I/R kidney injury or in a mouse kidney cell line after exposure to hydrogen peroxide [10, 27, 30]. Similarly, the level of necroptotic markers after renal I/R injury in mice was ameliorated by Klotho due to oxidative stress inhibition [31]. There was also a correlation of the neuroprotection and inhibition of neuropathological changes with the induced expression of Klotho after ischaemic injury in the murine brain [11]. Finally, the apoptosis and heart damage caused by endotoxemia or hyperglycaemia in mice were alleviated by Klotho [17, 32]. Our previous research revealed improved viability and metabolic activity, as well as reduced injury after Klotho administration in human cardiomyocytes subjected to I/R [12]. The current study showed the potential influence of Klotho on cellular defence against oxidative stress, reduction of cell death, and injury at the tissue level in I/R rat hearts. As previously mentioned, Klotho protein was characterized by its antioxidative activity. Klotho had a distinct capacity to inhibit the production of ROS [9, 11, 29, 31–34]. Importantly, it was revealed that Klotho led to enhanced expression of oxidative scavengers like superoxide dismutase (SOD) and antioxidation through the inhibition of phosphatidylinositol-3 kinase (PI3K)/protein kinase B (Akt) signalling pathway [9, 28, 29, 34]. Thus, Klotho may contribute to the promotion of antioxidation and protection against apoptosis during heart I/R.

Based on present knowledge, the main contributors to I/R injury of the heart are increased production of ROS, enhanced expression of nitric oxide synthase (NOS), overproduction of nitric oxide (NO), subsequent activation of MMPs, and proteolytic degradation of cardiac contractile proteins [3, 35–39]. It was found that ROS and RNS contribute to nitration/nitrosylation of heart contractile proteins and activate MMPs, including MMP-2 and MMP-9 [37–39]. It was shown that MMP-2 not only acts in the extracellular matrix but also functions at the cellular level in the cardiomyocytes [40]. Heart contractile proteins like myosin light chains 1 (MLC1) or troponin are nitrated, nitrosylated, and phosphorylated during I/R, which increases their affinity for the proteolytic enzymes. As a result, MLC1 is then

degraded by MMPs. It was confirmed that degradation of MLC1 during I/R injury leads to contractile dysfunction in the cardiac muscle [38, 41]. It was reported that Klotho contributed to decrease in iNOS expression in human endothelial cells during oxidative stress. The expression of MMP-2 and MMP-9 in the kidneys was also reduced by means of Klotho [24, 33, 42–44]. In the present research, the level of MLC1 and TnI in coronary effluents was increased after I/R injury of the rat hearts. The release of MLC1 and TnI positively correlated with the magnitude of heart damage and negatively correlated with heart mechanical function, confirming the mechanism of I/R injury. Importantly, we have previously reported that the administration of inhibitors of NOS, MMP-2, and MLC phosphorylation resulted in cardioprotection of the human cardiomyocytes or isolated rat hearts [13–15, 45, 46]. The current study showed reduced release of MLC1 and TnI during I/R after Klotho administration. For this reason, we hypothesize that Klotho may contribute to the protection of heart contractility throughout limitation of oxidative/nitrosative stress and subsequent reduction of MMP-dependent degradation of MLCs. Thus, the next goal of our investigation is to elucidate the underlying mechanism of Klotho influence in relation to ROS/RNS and MLC1. The analysis of NOS, NO, MMP-2, MMP-9, and tissue inhibitors of metalloproteinases levels will be then performed.

5. Conclusion

In conclusion, the presented research showed that the administration of Klotho protein to the heart during I/R injury enhanced antioxidant capacity and supported the reduction of cell death, toxicity, and release of heart contractile proteins. We are also aware that confirmation of the potential influence and cardioprotection of Klotho in the heart needs further studies.

Data Availability

The data that support the findings of this study are available from the corresponding author upon reasonable request.

Conflicts of Interest

The authors declare that there is no conflict of interest regarding the publication of this paper.

Authors' Contributions

All authors participated in the design, interpretation of the studies, analysis of the data, and review of the manuscript. AO, AKZ, and IBL designed the research study. AO, AKZ, MB, and IBL performed the research. AO and IBL analysed the data. AO wrote the paper. IBL made critical revision of the manuscript.

Acknowledgments

We kindly thank Wrovasc for allowing the Langendorff system apparatus to be rented. This work was supported by the National Science Centre (grant number 2019/33/N/NZ3/01649).




References

- [1] E. M. Antman, D. T. Anbe, P. W. Armstrong et al., "ACC/AHA guidelines for the management of patients with ST-elevation myocardial infarction—executive summary: a report of the American College of Cardiology/American Heart Association Task Force on Practice Guidelines (writing committee to revise the 1999 guidelines for the management of patients with acute myocardial infarction)," *Circulation*, vol. 110, pp. 588–636, 2004.
- [2] G. Heusch and B. J. Gersh, "The pathophysiology of acute myocardial infarction and strategies of protection beyond reperfusion: a continual challenge," *European Heart Journal*, vol. 38, no. 11, pp. 774–784, 2017.
- [3] H. Tsutsui, S. Kinugawa, and S. Matsushima, "Oxidative stress and heart failure," *American Journal of Physiology. Heart and Circulatory Physiology*, vol. 301, no. 6, pp. H2181–H2190, 2011.
- [4] M. Kuro-o, "Klotho as a regulator of fibroblast growth factor signaling and phosphate/calcium metabolism," *Current Opinion in Nephrology and Hypertension*, vol. 15, no. 4, pp. 437–441, 2006.
- [5] M. Kuro-o, Y. Matsumura, H. Aizawa et al., "Mutation of the mouse klotho gene leads to a syndrome resembling ageing," *Nature*, vol. 390, no. 6655, pp. 45–51, 1997.
- [6] J.-H. Kim, K.-H. Hwang, K.-S. Park, I. D. Kong, and S. K. Cha, "Biological role of anti-aging protein Klotho," *Journal of Lifestyle Medicine*, vol. 5, no. 1, pp. 1–6, 2015.
- [7] A. Olejnik, A. Franczak, A. Krzywonos-Zawadzka, M. Kałużna-Oleksy, and I. Bil-Lula, "The biological role of Klotho protein in the development of cardiovascular diseases," *BioMed Research International*, vol. 2018, Article ID 5171945, 17 pages, 2018.
- [8] K. R. Markan, M. C. Naber, S. M. Small, L. Peltekian, R. L. Kessler, and M. J. Potthoff, "FGF21 resistance is not mediated by downregulation of beta-klotho expression in white adipose tissue," *Molecular Metabolism*, vol. 6, no. 6, pp. 602–610, 2017.
- [9] M. Yamamoto, J. D. Clark, J. V. Pastor et al., "Regulation of oxidative stress by the anti-aging hormone klotho," *The Journal of Biological Chemistry*, vol. 280, no. 45, pp. 38029–38034, 2005.
- [10] H. Sugiura, T. Yoshida, K. Tsuchiya et al., "Klotho reduces apoptosis in experimental ischaemic acute renal failure," *Nephrology, Dialysis, Transplantation*, vol. 20, no. 12, pp. 2636–2645, 2005.
- [11] H.-J. Zhou, H. Li, M.-Q. Shi et al., "Protective effect of Klotho against ischemic brain injury is associated with inhibition of RIG-I/NF- κ B signaling," *Frontiers in Pharmacology*, vol. 8, 2018.
- [12] A. Olejnik, A. Krzywonos-Zawadzka, M. Banaszkiwicz, and I. Bil-Lula, "Klotho protein contributes to cardioprotection during ischaemia/reperfusion injury," *Journal of Cellular and Molecular Medicine*, vol. 24, no. 11, pp. 6448–6458, 2020.
- [13] A. Krzywonos-Zawadzka, A. Franczak, A. Olejnik et al., "Cardioprotective effect of MMP-2-inhibitor-NO-donor hybrid against ischaemia/reperfusion injury," *Journal of Cellular and Molecular Medicine*, vol. 23, no. 4, pp. 2836–2848, 2019.
- [14] A. Krzywonos-Zawadzka, M. Wozniak, G. Sawicki, and I. Bil-Lula, "A drug cocktail for protecting against ischemia-reperfusion injury," *Frontiers in Bioscience*, vol. 25, pp. 722–735, 2020.
- [15] I. Bil-Lula, H.-B. Lin, D. Biały et al., "Subthreshold nitric oxide synthase inhibition improves synergistic effects of subthreshold MMP-2/MLCK-mediated cardiomyocyte protection from hypoxic injury," *Journal of Cellular and Molecular Medicine*, vol. 20, no. 6, pp. 1086–1094, 2016.
- [16] G. Corsetti, E. Pasini, T. M. Scarabelli et al., "Decreased expression of Klotho in cardiac atria biopsy samples from patients at higher risk of atherosclerotic cardiovascular disease," *Journal of Geriatric Cardiology*, vol. 13, no. 8, pp. 701–711, 2016.
- [17] H. Hui, Y. Zhai, L. Ao et al., "Klotho suppresses the inflammatory responses and ameliorates cardiac dysfunction in aging endotoxemic mice," *Oncotarget*, vol. 8, no. 9, pp. 15663–15676, 2017.
- [18] A. R. Marks, "Calcium and the heart: a question of life and death," *The Journal of Clinical Investigation*, vol. 111, no. 5, pp. 597–600, 2003.
- [19] H. Kurosu, Y. Ogawa, M. Miyoshi et al., "Regulation of fibroblast growth factor-23 signaling by klotho," *The Journal of Biological Chemistry*, vol. 281, no. 10, pp. 6120–6123, 2006.
- [20] J. Xie, S.-K. Cha, S.-W. An, M. Kuro-o, L. Birnbaumer, and C.-L. Huang, "Cardioprotection by Klotho through downregulation of TRPC6 channels in the mouse heart," *Nature Communications*, vol. 3, no. 1, p. 1238, 2012.
- [21] G. D. Dalton, J. Xie, S.-W. An, and C. L. Huang, "New insights into the mechanism of action of soluble klotho," *Frontiers in Endocrinology*, vol. 8, 2017.
- [22] E. H. P. Leunissen, A. V. Nair, C. Büll et al., "The epithelial calcium channel TRPV5 is regulated differentially by klotho and sialidase," *The Journal of Biological Chemistry*, vol. 288, no. 41, pp. 29238–29246, 2013.
- [23] K. Lim, T.-S. Lu, G. Molostvov et al., "Vascular Klotho deficiency potentiates the development of human artery calcification and mediates resistance to fibroblast growth factor 23," *Circulation*, vol. 125, no. 18, pp. 2243–2255, 2012.
- [24] S. Doi, Y. Zou, O. Togao et al., "Klotho inhibits transforming growth factor- β 1 (TGF- β 1) signaling and suppresses renal fibrosis and cancer metastasis in mice," *The Journal of Biological Chemistry*, vol. 286, no. 10, pp. 8655–8665, 2011.
- [25] R. D. Semba, A. R. Cappola, K. Sun et al., "Plasma klotho and cardiovascular disease in adults," *Journal of the American Geriatrics Society*, vol. 59, no. 9, pp. 1596–1601, 2011.
- [26] Y. Matsumura, H. Aizawa, T. Shiraki-Iida, R. Nagai, M. Kuro-o, and Y. I. Nabeshima, "Identification of the human Klotho gene and its two transcripts encoding membrane and secreted Klotho protein," *Biochemical and Biophysical Research Communications*, vol. 242, no. 3, pp. 626–630, 1998.
- [27] M. Mitobe, T. Yoshida, H. Sugiura, S. Shirota, K. Tsuchiya, and H. Nihei, "Oxidative stress decreases klotho expression in a mouse kidney cell line," *Nephron Experimental Nephrology*, vol. 101, no. 2, pp. e67–e74, 2005.
- [28] S. W. Lim, L. Jin, K. Luo et al., "Klotho enhances FoxO3-mediated manganese superoxide dismutase expression by negatively regulating PI3K/AKT pathway during tacrolimus-induced oxidative stress," *Cell Death & Disease*, vol. 8, no. 8, article e2972, 2017.
- [29] Y. Yao, Y. Wang, Y. Zhang, and C. Liu, "Klotho ameliorates oxidized low density lipoprotein (ox-LDL)-induced oxidative stress via regulating LOX-1 and PI3K/Akt/eNOS pathways," *Lipids in Health and Disease*, vol. 16, no. 1, p. 77, 2017.
- [30] H. Sugiura, T. Yoshida, M. Mitobe et al., "Klotho reduces apoptosis in experimental ischaemic acute kidney injury via HSP-

- 70," *Nephrology, Dialysis, Transplantation*, vol. 25, pp. 60–68, 2009.
- [31] Y. Qian, X. Guo, L. Che et al., "Klotho reduces necroptosis by targeting oxidative stress involved in renal ischemic-reperfusion injury," *Cellular Physiology and Biochemistry*, vol. 45, pp. 2268–2282, 2018.
- [32] Y. Guo, X. Zhuang, Z. Huang et al., "Klotho protects the heart from hyperglycemia-induced injury by inactivating ROS and NF- κ B-mediated inflammation both in vitro and in vivo," *Biochimica et Biophysica Acta - Molecular Basis of Disease*, vol. 1864, no. 1, pp. 238–251, 2018.
- [33] B. Richter, J. Haller, D. Haffner, and M. Leifheit-Nestler, "Klotho modulates FGF23-mediated NO synthesis and oxidative stress in human coronary artery endothelial cells," *Pflügers Archiv*, vol. 468, no. 9, pp. 1621–1635, 2016.
- [34] T. Takenaka, H. Kobori, T. Inoue et al., "[op.4b.02] klotho supplementation attenuates blood pressure and oxidative stress in diabetes," *Journal of Hypertension*, vol. 35, article e38, 2017.
- [35] J. A. Byrne, D. J. Grieve, A. C. Cave, and A. M. Shah, "Oxidative stress and heart failure," *Archives des Maladies du Coeur et des Vaisseaux*, vol. 96, no. 3, pp. 214–221, 2003.
- [36] R. Marfella, C. Di Filippo, K. Esposito et al., "Absence of inducible nitric oxide synthase reduces myocardial damage during ischemia reperfusion in streptozotocin-induced hyperglycemic mice," *Diabetes*, vol. 53, no. 2, pp. 454–462, 2004.
- [37] W. Wang, C. J. Schulze, W. L. Suarez-Pinzon, J. R. B. Dyck, G. Sawicki, and R. Schulz, "Intracellular action of matrix metalloproteinase-2 accounts for acute myocardial ischemia and reperfusion Injury," *Circulation*, vol. 106, no. 12, pp. 1543–1549, 2002.
- [38] G. Sawicki, H. Leon, J. Sawicka et al., "Degradation of myosin light chain in isolated rat hearts subjected to ischemia-reperfusion injury," *Circulation*, vol. 112, no. 4, pp. 544–552, 2005.
- [39] W. Wang, G. Sawicki, and R. Schulz, "Peroxynitrite-induced myocardial injury is mediated through matrix metalloproteinase-2," *Cardiovascular Research*, vol. 53, no. 1, pp. 165–174, 2002.
- [40] J. A. Kwan, C. J. Schulze, W. Wang et al., "Matrix metalloproteinase-2 (MMP-2) is present in the nucleus of cardiac myocytes and is capable of cleaving poly (ADP-ribose) polymerase (PARP) in vitro," *The FASEB Journal*, vol. 18, no. 6, pp. 690–692, 2004.
- [41] V. J. J. Cadete, J. Sawicka, J. S. Jaswal et al., "Ischemia/reperfusion-induced myosin light chain 1 phosphorylation increases its degradation by matrix metalloproteinase 2," *FEBS Journal*, vol. 279, no. 13, pp. 2444–2454, 2012.
- [42] B. Chang, J. Kim, D. Jeong et al., "Klotho inhibits the capacity of cell migration and invasion in cervical cancer," *Oncology Reports*, vol. 28, no. 3, pp. 1022–1028, 2012.
- [43] Y.-L. Wu, J. Xie, S.-W. An et al., "Inhibition of TRPC6 channels ameliorates renal fibrosis and contributes to renal protection by soluble klotho," *Kidney International*, vol. 91, no. 4, pp. 830–841, 2017.
- [44] X. Cheng, Q. Zhou, S. Lin, and R. Wu, "Fosinopril and valsartan intervention in gene expression of Klotho, MMP-9, TIMP-1, and PAI-1 in the kidney of spontaneously hypertensive rats," *Zhong Nan Da Xue Xue Bao. Yi Xue Ban*, vol. 35, no. 10, pp. 1048–1056, 2010.
- [45] A. Krzywonos-Zawadzka, A. Franczak, G. Sawicki, and I. Bil-Lula, "Mixture of MMP-2, MLC, and NOS inhibitors affects NO metabolism and protects heart from cardiac I/R injury," *Cardiology Research and Practice*, vol. 2020, Article ID 1561478, 10 pages, 2020.
- [46] I. Bil-Lula, A. Krzywonos-Zawadzka, J. Sawicka et al., "L-NAME improves doxycycline and ML-7 cardioprotection from oxidative stress," *Frontiers in Bioscience*, vol. 23, pp. 298–309, 2018.

Research Article

Bardoxolone Methyl Displays Detrimental Effects on Endothelial Bioenergetics, Suppresses Endothelial ET-1 Release, and Increases Endothelial Permeability in Human Microvascular Endothelium

Ewa Szczesny-Malysiak ¹, Marta Stojak¹, Roberto Campagna^{1,2}, Marek Grosicki¹,
Marek Jamrozik¹, Patrycja Kaczara ¹, and Stefan Chlopicki ^{1,3}

¹Jagiellonian Centre for Experimental Therapeutics (JCET), Jagiellonian University, Bobrzynskiego 14, 30-348 Krakow, Poland

²Department of Clinical Sciences, Polytechnic University of Marche, Via Ranieri 65, 60131 Ancona, Italy

³Chair of Pharmacology, Jagiellonian University Medical College, Grzegorzeczka 16, Krakow, Poland

Correspondence should be addressed to Stefan Chlopicki; stefan.chlopicki@jcet.eu

Received 23 April 2020; Revised 24 July 2020; Accepted 2 September 2020; Published 15 October 2020

Academic Editor: Luciano Saso

Copyright © 2020 Ewa Szczesny-Malysiak et al. This is an open access article distributed under the Creative Commons Attribution License, which permits unrestricted use, distribution, and reproduction in any medium, provided the original work is properly cited.

Nrf2 is a master regulator of antioxidant cellular defence, and agents activating the Nrf2 pathway have been tested in various diseases. However, unexpected side effects of cardiovascular nature reported for bardoxolone methyl in patients with type 2 diabetes mellitus and stage 4 chronic kidney disease (the BEACON trial) still have not been fully explained. Here, we aimed to characterize the effects of bardoxolone methyl compared with other Nrf2 activators—dimethyl fumarate and L-sulforaphane—on human microvascular endothelium. Endothelial toxicity, bioenergetics, mitochondrial membrane potential, endothelin-1 (ET-1) release, endothelial permeability, Nrf2 expression, and ROS production were assessed in human microvascular endothelial cells (HMEC-1) incubated for 3 and 24 hours with 100 nM–5 μ M of either bardoxolone methyl, dimethyl fumarate, or L-sulforaphane. Three-hour incubation with bardoxolone methyl (100 nM–5 μ M), although not toxic to endothelial cells, significantly affected endothelial bioenergetics by decreasing mitochondrial membrane potential (concentrations $\geq 3 \mu$ M), decreasing spare respiratory capacity (concentrations $\geq 1 \mu$ M), and increasing proton leak (concentrations ≥ 500 nM), while dimethyl fumarate and L-sulforaphane did not exert such actions. Bardoxolone methyl at concentrations $\geq 3 \mu$ M also decreased cellular viability and induced necrosis and apoptosis in the endothelium upon 24-hour incubation. In turn, endothelin-1 decreased permeability in endothelial cells in picomolar range, while bardoxolone methyl decreased ET-1 release and increased endothelial permeability even after short-term (3 hours) incubation. In conclusion, despite that all three Nrf2 activators exerted some beneficial effects on the endothelium, as evidenced by a decrease in ROS production, bardoxolone methyl, the most potent Nrf2 activator among the tested compounds, displayed a distinct endothelial profile of activity comprising detrimental effects on mitochondria and cellular viability and suppression of endothelial ET-1 release possibly interfering with ET-1-dependent local regulation of endothelial permeability.

1. Introduction

Nrf2—nuclear factor (erythroid 2-related factor) 2—is the primary player in the inducible cell defence system that regulates expression of over 600 target genes including detoxification, cytoprotective, and antioxidant enzymes; ABC transporters; and other stress response enzymes and proteins [1, 2]. The plethora of products encoded by these genes

includes antioxidant and cytoprotective genes (e.g. genes related to glutathione synthesis, glutathione S-transferases, thioredoxin, peroxiredoxins, hemoxygenase-1, and ferritin) and many others, i.e., regulators of transcription, growth factors, and proteins responsible for xenobiotic metabolism and clearance (reviewed in Baird and Dinkova-Kostova [3]).

Given the important role of Nrf2 in cellular defence, it was not a surprise that Nrf2^{-/-} mice were more susceptible

to oxidative stress-induced diseases, including acute lung injury, chronic obstructive pulmonary diseases, diabetic nephropathy, heart failure, and cancer [4]. On the other hand, Nrf2 pathway activation exerts a wide range of protective functions. There is a substantial interest in identifying and developing Nrf2 activators that could be exploited therapeutically in conditions related to oxidative stress and inflammation, such as multiple sclerosis and complications of diabetes (e.g., retinopathy and nephropathy), as well as many other diseases including solid tumors, lymphomas, and neurodegenerative diseases [1, 3–9].

L-sulforaphane, an isothiocyanate present in cruciferous vegetables (broccoli), was one of the first studied activators of Nrf2. This compound was tested in a phase 2 clinical study in men with recurrent prostate cancer [10], but the expected therapeutic effects were not achieved. However, in type 2 diabetic patients, L-sulforaphane-rich broccoli sprout powder caused a significant improvement in serum insulin concentration, glucose-to-insulin ratio, and insulin resistance [11].

Another Nrf2 inducer, dimethyl fumarate, is a methyl ester of fumaric acid—a metabolite of the citric acid cycle in mitochondria. Dimethyl fumarate was tested in the treatment of psoriasis where it decreased the number of T-cells via the activation of apoptosis [12] and has been used in the treatment of psoriasis for many years [13]. Importantly, this compound has been shown to be efficacious in the treatment of multiple sclerosis [14]. In a phase 3 clinical study in relapsing-remitting multiple sclerosis patients, dimethyl fumarate was shown to reduce the progression of disability [15], and the compound was approved by FDA in 2013 for the treatment of relapsing-remitting multiple sclerosis [16].

Some of the most promising Nrf2 inducers are the derivatives of oleanolic acid [17]. A semisynthetic triterpenoid derivative named bardoxolone methyl (also known as CDDO-Me) is a potent Nrf2 inducer that stimulates Nrf2-dependent cytoprotective responses in nanomolar concentrations [13, 17]. In multiple preclinical studies, bardoxolone methyl was shown to reduce diabetic complications, cancer, cardiovascular disease, neurodegenerative diseases, and chronic obstructive pulmonary disorder [13, 17] and numerous clinical trials were launched [1, 13, 17]. However, in October 2012, a phase 3 BEACON trial was terminated. This clinical study (Bardoxolone Methyl Evaluation in Patients with Chronic Kidney Disease and Type 2 Diabetes Mellitus: The occurrence of renal events (BEACON)) was a phase 3 randomized, double-blind, placebo-controlled trial designed to determine whether bardoxolone methyl could reduce End-Stage Renal Disease (ESRD) and cardiovascular events [18]. The study was terminated due to safety concerns and a significantly increased risk of heart failure requiring hospitalization, which also increased the composite cardiovascular outcome (nonfatal myocardial infarction, nonfatal stroke, hospitalization for heart failure, or death from cardiovascular causes) in the bardoxolone methyl-treated group compared to placebo [18]. Increased incidence of cardiovascular events in bardoxolone methyl-treated patients in the BEACON trial was attributed to the ability of bardoxolone methyl to modulate the endothelin pathway [18, 19]. An excess rate of

heart failure hospitalization among those assigned to the bardoxolone-treated group was linked to fluid overload in patients at risk [20] and seemed to recapitulate those observed with endothelin receptor antagonists in patients with advanced CKD [19, 21]. Furthermore, preclinical studies demonstrated the suppressive effects of bardoxolone methyl on endothelin signalling in the kidneys by reducing the expression of the ET_A receptor protein, independently of bardoxolone methyl-induced improvement of eGFR and preservation of kidney function [19]. Given the fact that ET-1 plays an important role in the regulation of sodium and water homeostasis [22], it was claimed that bardoxolone methyl may pharmacologically promote acute retention of sodium and water through the modulation of the endothelin pathway [21]. However, this hypothesis could not fully explain the symptoms observed in patients suffering from bardoxolone methyl-induced side effects [23], particularly when post hoc analysis confirmed improved kidney function and eGFR in bardoxolone methyl-treated patients [21]. Furthermore, ET antagonists have different hemodynamic effects from those induced by bardoxolone methyl, and generally, suppression of the endothelin pathway should rather be protective than detrimental against an adverse cardiovascular event [24–26]. Moreover, the manner in which bardoxolone methyl modulates the endothelin pathway in other tissues including the endothelium has yet to be examined, and it is not known whether bardoxolone methyl displays any detrimental effect on endothelial function—in particular the endothelial barrier—that could possibly result in peripheral oedema. Endothelial function determines heart failure progression not only by an NO-dependent action that is known to have prognostic significance in heart failure patients [27] but also by regulating the barrier function in microcirculation. Indeed, changes in endothelial permeability and vascular leakage could contribute to drug-induced progression of heart failure and peripheral oedema, and such detrimental mechanism in diabetic patients was reported for rosiglitazone [28], a peroxisome proliferator-activated receptor- γ (PPAR- γ) agonist, shown to significantly increase the risk of heart failure [29]. Therefore, we aimed to test the hypothesis that the detrimental effects of bardoxolone methyl in the BEACON trial could be, at least partially, explained by bardoxolone-induced effects on endothelial function. For that purpose, in the present work we characterize the effects of bardoxolone methyl on microvascular human endothelium toxicity, mitochondrial function, endothelin-1 release, and endothelial permeability. The effects of bardoxolone methyl were compared with those of two other well-characterized Nrf2 activators used in clinical studies: dimethyl fumarate and L-sulforaphane.

2. Methods

2.1. Cell Culture and Drug Treatment. Human dermal microvascular endothelial cells, HMEC-1 (purchased from ATCC, Cat. No. CRL3243TM), were cultured in MCDB 131 Medium (Thermo Fisher Scientific) supplemented with FBS (10%, Thermo Fisher Scientific), L-glutamine (2 mM, Thermo Fisher Scientific), hydrocortisone (0.05 mg/ml,

Sigma-Aldrich), Epidermal Growth Factor (5 ng/ml), 100 U/ml penicillin, 10 µg/ml streptomycin, and 250 ng/ml amphotericin B (Sigma-Aldrich). HMEC-1 were cultured under standard conditions (37°C, 5% CO₂) and passaged two times a week. In all experiments, cells between the second and tenth passages were used only when they reached full postplating confluency. Bardoxolone methyl (CDDO methyl ester, Cayman Chemical), dimethyl fumarate (Sigma-Aldrich), and L-sulforaphane (Sigma-Aldrich) initially diluted in DMSO were added to the culture medium at final concentrations of 100 nM, 300 nM, 500 nM, 1 µM, 3 µM, and 5 µM in triplicates, if not stated otherwise. Control cells were treated with 0.05% DMSO added to the culture medium. To check for acute toxicity, the cells were incubated with tested agents for 3 hours. Standard toxicity assessment time was set to 24 hours, according to the literature [30].

2.2. Assessment of Nrf2 Nuclear Expression. HMECs were seeded at a density of 1,000,000 per well and grown in 6-well plates until they reached full confluence, then cells were incubated with bardoxolone methyl, dimethyl fumarate, and L-sulforaphane for three hours. To measure Nrf2 expression in the nucleus, a Nuclear Extract Kit (Active Motif) was used to isolate the nuclear and cytoplasmic fractions. Nuclear and cytoplasmic extracts (25 or 30 µg protein/sample) were processed as follows: first, the membranes were scanned for total protein content for further band normalization, and subsequently, they were incubated with primary rabbit polyclonal Anti-Nrf2 Antibody (H-300) (sc-13032, Santa Cruz Biotechnology, lot No. GR197455-1) 1 : 1000 overnight and with goat anti-rabbit secondary antibody (sc-2004, Santa Cruz Biotechnology, lot No. 12314) 1 : 2500 for 45 minutes. After chemiluminescent band detection, membranes were washed and incubated with primary Anti-Lamin A/C Monoclonal Antibody (mab636, Thermo Fisher Scientific, lot No. QF215120) 1 : 1000 overnight and with anti-mouse secondary antibody (sc-516102, Santa Cruz Biotechnology) 1 : 5000 for 1 hour. Bands were again detected with the use of chemiluminescence, measured and normalized to total protein content using Image Lab Software (Bio-Rad).

2.3. Assessment of ROS Production. HMECs were cultured in 96-well plates (seeding density: 15,000 cells per well) and treated with bardoxolone methyl, dimethyl fumarate, and L-sulforaphane for 24 hours and incubated for 15 minutes with the following fluorescent dyes: dihydroethidium DHE (2 µg/ml, Thermo Fisher Scientific) and Hoechst 33342 (0.5 µl/ml, Thermo Fisher Scientific) at 37°C. After washing, images were captured with an Olympus Scan[^]R automated fluorescence microscope (Olympus Corporation) with the use of 20x magnification in two channels: DAPI for nuclei localization (Hoechst 33342, ex/em 346/460 nm) and Texas Red for reactive oxygen species/reactive nitrogen species (ROS/RNS) indication (DHE, ex/em 518/606 nm). Image analysis was performed with the use of a Columbus Image Data Storage and Analysis System (Perkin Elmer), and mean fluorescence intensity was normalized to the number of living cells.

2.4. Assessment of Endothelial Toxicity

2.4.1. MTS Tetrazolium Assay. HMECs were plated into 96-well plates at a density of 15,000 per well in order to produce confluency on the second postplating day. The cells were incubated with bardoxolone methyl, dimethyl fumarate, and L-sulforaphane for 3 and 24 hours. Cell viability was determined with use of a Non-Radioactive Cell Proliferation Assay (Promega) according to the manufacturer's instructions. The absorbance was recorded at 490 nm using a Synergy4 plate reader (BioTek). Cells were then washed with PBS and suspended in Mammalian Protein Extraction Reagent (Thermo Fisher Scientific) containing phosphatase (PhosSTOP, Roche) and protease (cOmplete, Roche) inhibitors and frozen at -20°C. The next day, the samples were thawed and total protein concentration was determined with use of a colorimetric BCA Protein Assay Kit (Thermo Fisher Scientific). Absorbance was recorded at 562 nm. The results of the MTS test were normalized to the protein concentration of the sample and calculated as a percent of control cells.

2.4.2. Annexin V/Propidium Iodide Flow Cytometry Assay. Flow cytometry was used to determine cellular apoptosis and necrosis. HMECs were cultured in 24-well plates (500,000 per well) and incubated for 3 and 24 hours with bardoxolone methyl, dimethyl fumarate, and L-sulforaphane (single wells). After incubation, staining with Annexin V and propidium iodide was performed with the use of a FITC Annexin V Apoptosis Detection Kit (BD Biosciences) according to the manual. The cells were analyzed with an LSR II flow cytometer (Becton Dickinson).

2.4.3. Cell Counting. HMECs were cultured as described above (Section 2.4.1) and treated with bardoxolone methyl (100 nM-10 µM), dimethyl fumarate (500 nM-1 mM), and L-sulforaphane (500 nM-100 µM) for 24 hours. Afterwards, the cells were washed with PBS 1x, fixed with 4% formaldehyde for 10 min at RT, and incubated for 30 minutes at 37°C with the following fluorescent dyes: Hoechst 33258 (1 µg/ml, Sigma-Aldrich) for nucleic acid staining and YO-PRO-1 Iodide (1 : 1000, Thermo Fisher Scientific) for identification of apoptotic cells. Cell imaging was performed with a Confocal Quantitative Image Cytometer CQ1 (Yokogawa Electric Corporation) with the use of 10x magnification at two wavelengths: 405/452 nm (blue) and 488/525 nm (green). Image analysis was performed using a Columbus Image Data Storage and Analysis System (Perkin Elmer).

2.5. Assessment of Mitochondrial Function. Cellular bioenergetics were measured with use of the Seahorse XFe96 Analyzer (Agilent Technologies). Forty-eight hours prior to the start of the experiment, cells were seeded at a density of 19,500 per well into 96-well XF cell culture plates, according to the manufacturer's protocol. Before the start of experiments, cells were washed twice with 200 µl of bicarbonate-free low-buffered assay medium (containing 10 mM glucose, 1 mM pyruvate, and 2 mM glutamine, pH = 7.4) and pre-incubated for 1 hour with bardoxolone methyl, dimethyl fumarate, and L-sulforaphane diluted in assay medium. Changes in cellular respiration were assessed for 2 hours

(total time of incubation with Nrf2 activators was three hours). During the assay, sequential injections of 1 $\mu\text{g/ml}$ oligomycin (an inhibitor of mitochondrial ATPase/ATP synthetase), 0.7 μM FCCP (trifluoromethoxy carbonylcyanide phenylhydrazine—a protonophore and uncoupler of oxidative phosphorylation), and 1 μM rotenone/antimycin A (an inhibitor of mitochondrial electron transport at NADH:ubiquinone oxidoreductase and an inhibitor of electron transfer at complex III) were performed. Results regarding the following parameters—basal respiration, proton leak, maximal respiration, spare respiratory capacity, nonmitochondrial respiration, and ATP production—were obtained with use of a test report generator provided by Agilent Technologies.

Mitochondrial membrane potential was evaluated using JC-1, which is a cationic dye that accumulates inside mitochondria. Depending on the value of the mitochondrial membrane potential, it forms either red fluorescent aggregates or green fluorescent monomers. A decrease in the red/green fluorescence intensity ratio indicates mitochondrial depolarization. HMECs were plated into 96-well plates at a density of 40,000 per well in order to produce confluency on the first postplating day. After 3 hours of incubation with bardoxolone methyl, dimethyl fumarate, and L-sulforaphane, cells were washed with PBS and incubated for 30 minutes at 37°C in the dark with 1 $\mu\text{g/ml}$ JC-1 (Thermo Fisher Scientific). Shortly before JC-1 addition, 100 μM FCCP was added to the cells incubated with culture media to serve as a positive control. Cell imaging was performed with a Confocal Quantitative Image Cytometer CQ1 (Yokogawa Electric Corporation) with the use of 20x magnification at two wavelengths: 561/617 nm (red) and 488/525 nm (green). Image analysis was performed using a Columbus Image Data Storage and Analysis System (Perkin Elmer).

2.6. Assessment of Endothelin-1 Release. HMECs were plated into 96-well plates at a density of 15,000 per well and treated with bardoxolone methyl, dimethyl fumarate, and L-sulforaphane for 3 and 24 hours in duplicates. After the assigned time, cell culture supernatants were collected, centrifuged, and stored at -80°C. Endothelin-1 was quantified with use of an ELISA Kit (R&D Systems). Total protein concentration was determined as described above and the results were normalized.

2.7. Assessment of Endothelial Permeability. To measure changes in endothelial permeability, we used the ECIS methodology based on the measurement of cellular electric potential [31, 32]. HMEC-1 cells were seeded at a density of 30,000 per well into special 96-well plates containing golden electrodes (Applied Biophysics). An ECIS array holder was placed into the incubator, and cells were grown for approximately ten days until they reached full confluence confirmed by ECIS readout (capacitance values: 0.5–1.0 nanoFarads). One day prior to the start of the experiment, fully supplemented culture medium was changed to medium without FBS. Endothelin-1 (100, 300, 500, and 1000 pM), selective antagonists of ET_A and ET_B receptors BQ123 and BQ788 (1 μM), bardoxolone methyl, dimethyl fumarate, and L-

sulforaphane (0.1–5 μM) were added into the wells in quadruplicate and the impedance was measured throughout 24 hours. Control wells were treated with fresh culture medium (no FBS), 0.05% DMSO, 5 μM forskolin, and 10 μM histamine.

2.8. Statistical Analysis. All parameters were expressed as mean \pm standard error of the mean (SEM). The data from each experiment (repeated three times or more) were first processed with the Shapiro-Wilk normality test, and all data were normally distributed. Intergroup differences were assessed by one-way analysis of variance (ANOVA), followed by an adequate post hoc test (Duncan's, Dunnett's, or Dunn's), if appropriate.

3. Results

3.1. Effects of Bardoxolone Methyl, Dimethyl Fumarate, and L-Sulforaphane on Nrf2 Expression in HMECs. To compare the effects of bardoxolone methyl, dimethyl fumarate, and L-sulforaphane on Nrf2 nuclear expression in HMECs, the expression of Nrf2 in the nuclear fractions was assessed by means of Western blots. As shown in Figure 1, bardoxolone methyl at concentrations of 300 nM and 3 μM increased Nrf2 expression in the nuclear fraction of HMECs by 17.5-fold and 45-fold, respectively. L-sulforaphane appeared to be less potent and dimethyl fumarate the least potent activator of Nrf2 because at a concentration of 3 μM , these compounds increased Nrf2 expression in the nuclear fraction of HMECs by 9.3- and 3.1-fold, respectively (Figure 1(a)). In the cytoplasmic fraction, a pronounced increase in the level of Nrf2 was present only after treatment with 3 μM of bardoxolone methyl (Figure 1(b)). Expression of Lamin A/C was detected in the nuclear extracts, while it was absent in the cellular fractions, confirming the nuclear fraction purity (Figure 1(c)).

3.2. Effects of Bardoxolone Methyl, Dimethyl Fumarate, and L-Sulforaphane on Reactive Oxygen Species (ROS) Generation in HMECs. Incubation of HMECs with bardoxolone methyl for twenty four hours at a concentration of 300 nM resulted in a significant decrease in ROS production measured by DHE fluorescence, and this effect was even more pronounced in the cells treated with 5 μM bardoxolone methyl. Under similar experimental conditions, dimethyl fumarate also produced a decrease in the DHE signal, but this effect was clearly visible at the concentration of 5 μM . Similarly, 5 μM of L-sulforaphane significantly lowered the DHE signal in HMECs (Figure 2).

3.3. Endothelial Toxicity of Bardoxolone Methyl, Dimethyl Fumarate, and L-Sulforaphane in HMECs. As shown in Figure 3, bardoxolone methyl, dimethyl fumarate, and L-sulforaphane after a 3-hour-long incubation did not cause any significant changes in cell viability assessed by the MTS reduction assay, with the exception of 1 and 5 μM bardoxolone methyl (Figures 3(a)–3(c)). However, after a 24-hour-long treatment, bardoxolone methyl at a concentration range of 100 nM–1 μM caused an increase in normalized MTS reduction, while higher concentrations caused a substantial

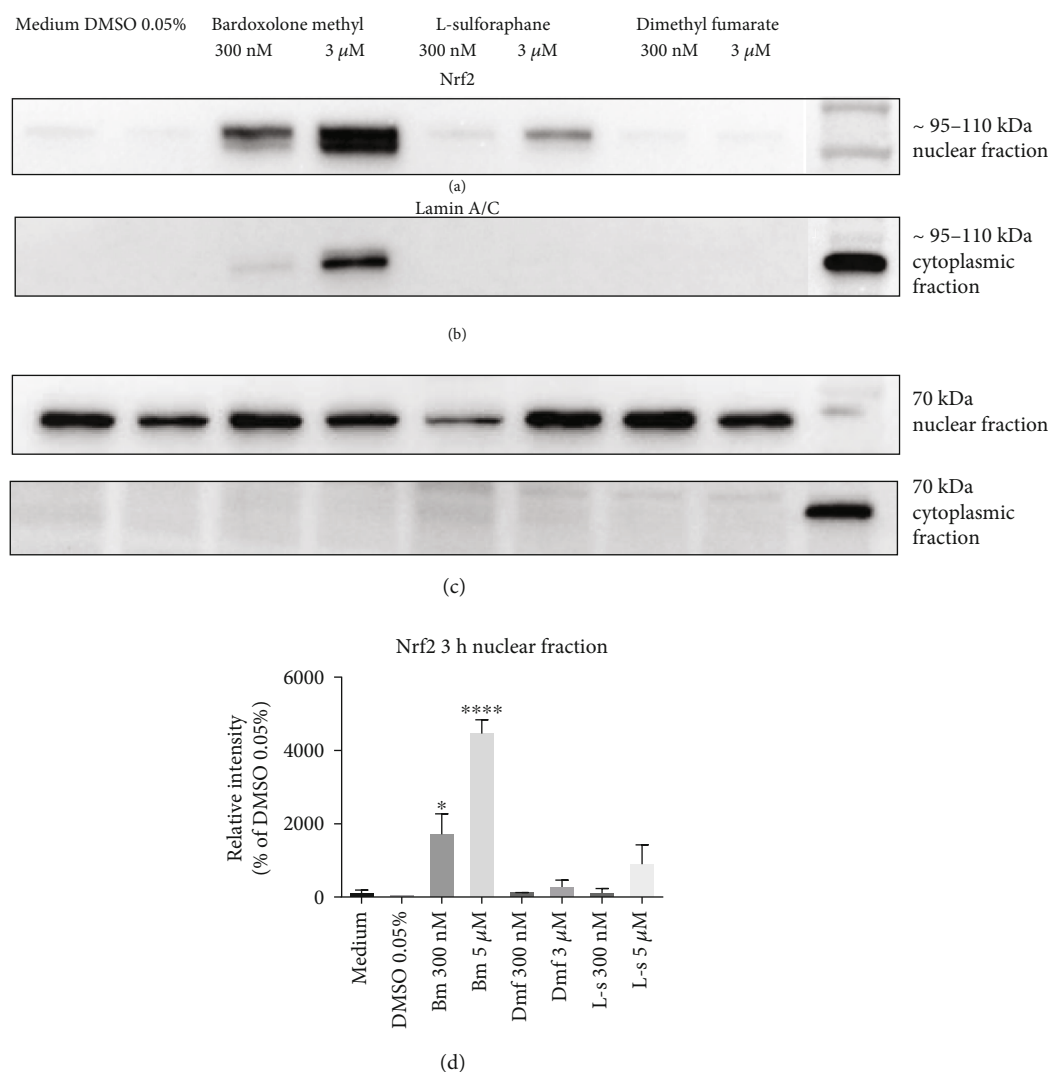


FIGURE 1: Effects of Nrf2 activators on Nrf2 expression in endothelial cells. A representative Western blot analysis of Nrf2 expression in nuclear (a, d) and cytoplasmic (b) fraction lysates obtained from HMEC-1 cells treated for 3 hours with 300 nM and 3 μ M of bardoxolone methyl (Bm), dimethyl fumarate (Dmf), L-sulforaphane (L-s), culture medium alone, or with the addition of 0.05% DMSO. The expression of Lamin A/C was also determined to define fraction purity and serve as loading control (c). The results (d) are presented as a % of control (DMSO 0.05%) \pm SEM, $n = 3$. The significance of the differences between the means was evaluated by one-way analysis of variance (ANOVA) with Dunnett's post hoc test; * $p < 0.05$ and **** $p < 0.0001$ indicate significant difference vs. the control group (DMSO 0.05%). The results were obtained in three independent experiments. In all panels, the first lane on the right contains a protein molecular weight marker.

decrease in the parameter ($IC_{50} = 3.23 \mu\text{M}$) (Figure 3(d)). In the same experimental conditions (24-hour-long drug treatment), dimethyl fumarate given at micromolar concentrations (1–50 μM) caused an increase in MTS reduction (Figure 3(e)). L-sulforaphane increased MTS reduction at the concentration range of 500 nM–10 μM but not at the highest concentrations used (30–50 μM) (Figure 3(f)). To confirm the obtained results, the effects of Nrf2 activators on the cell count was tested using an extended concentration range. Bardoxolone methyl did cause a significant decrease in the number of living cells in the tested concentration range after 24 hours of treatment (Figure 3(g)). Cell counting revealed increasing dose-dependent toxicity of dimethyl fumarate ($IC_{50} = 95.52 \mu\text{M}$) at the concentration range of

500 nM–1 mM (Figure 3(h)). Due to the compound solubility, the highest concentration of L-sulforaphane that could be tested in order to not exceed a 0.05% concentration of DMSO was 100 μM , at the same time being the only toxic concentration. The cells treated with 500 nM–50 μM did not show neither an increase nor a decrease in cellular viability (Figure 3(i)).

To characterize further effects of Nrf2 activators on cellular viability, apoptotic and necrotic cells were quantified by flow cytometry with use of Annexin V and propidium iodide. As shown in Table 1, HMECs treated for 24 hours with bardoxolone methyl (3 and 5 μM) but not with dimethyl fumarate or L-sulforaphane displayed a significantly diminished subpopulation of live cells and increased subpopulations of

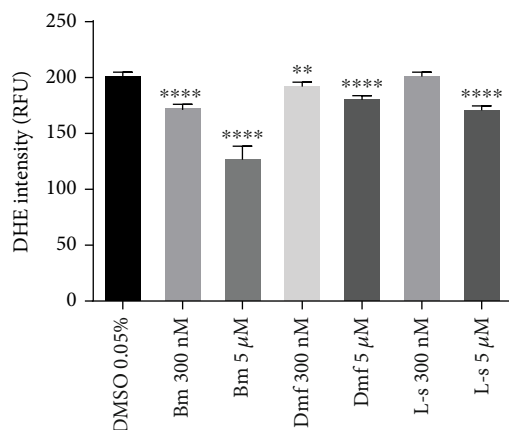


FIGURE 2: Effects of Nrf2 activators on reactive oxygen species production in endothelial cells. HMEC-1 cells were incubated for 24 hours with bardoxolone methyl (Bm), dimethyl fumarate (Dmf), and L-sulforaphane (L-s), (300 nM and 5 μ M). Intensity values of DHE fluorescence are expressed as relative fluorescence units \pm SEM, $n = 3$. The significance of the differences between the means was evaluated by one-way analysis of variance (ANOVA) with Dunnett's post hoc test; ** $p < 0.01$ and **** $p < 0.0001$ indicate significant difference vs. the control group (DMSO 0.05%). The results were obtained in three independent experiments.

necrotic and apoptotic+necrotic cells. There was no significant difference between the control and experimental groups in the composition of the cell population regarding live, apoptotic, necrotic, and apoptotic+necrotic cells.

3.4. Effects of Bardoxolone Methyl, Dimethyl Fumarate, and L-Sulforaphane on Mitochondrial Respiration and Mitochondrial Membrane Potential in HMECs. To characterize the effects of Nrf2 activators on endothelial bioenergetics, a mitochondrial stress assay was performed in HMECs treated with bardoxolone methyl, dimethyl fumarate, or L-sulforaphane for 3 hours. As shown in Figure 4, among all three Nrf2 activators, bardoxolone methyl exerted the most pronounced actions: it significantly increased proton leakage in a concentration-dependent manner (0.5–5 μ M), decreased spare respiratory capacity (3–5 μ M), and showed a tendency to decrease ATP production that, however, did not reach statistical significance (Figure 4(a)). Although low concentrations (100 and 300 nM) of dimethyl fumarate increased basal respiration and showed a tendency to increase spare respiratory capacity and ATP production (Figure 4(b)), there were no other significant effects of dimethyl fumarate on HMEC bioenergetics. L-sulforaphane did not change any of the bioenergetic parameters in a statistically significant fashion (Figure 4(c)).

Detrimental effects of bardoxolone methyl on mitochondria in endothelial cells were confirmed by the demonstration that bardoxolone methyl (3 and 5 μ M) decreased mitochondrial membrane potential as evidenced by a decrease in the red/green fluorescence intensity of the JC-1 aggregate/monomer ratio, while dimethyl fumarate and L-sulforaphane did not have any effect (Figure 5).

3.5. Effects of Bardoxolone Methyl, Dimethyl Fumarate, and L-Sulforaphane on Endothelin-1 Release in HMEC Culture.

Bardoxolone methyl, but not the other Nrf2 activators, caused a decrease in ET-1 concentration in the medium, even upon a short-term, 3-hour-long incubation of HMECs with the compound (Figure 6(a)). The effect of bardoxolone methyl on ET-1 release was more pronounced (and concentration dependent) when the incubation period was prolonged up to 24 hours (Figure 6(b)). Dimethyl fumarate at almost all tested concentrations (0.1–5 μ M) slightly increased ET-1 production in HMECs. L-sulforaphane in the lower concentration range (0.1–0.3 μ M) slightly increased ET-1 production in HMECs, while a higher concentration of L-sulforaphane (3–5 μ M) decreased ET-1 release in HMECs. The inhibitory effect of L-sulforaphane on ET-1 release, however, was much less pronounced compared with that of bardoxolone methyl (Figure 6(b)) and was not observed after a 3-hour-long incubation (Figure 6(a)).

3.6. Effects of Bardoxolone Methyl, Dimethyl Fumarate, and L-Sulforaphane on Endothelial Permeability in HMECs. As shown in Figure 7, histamine (10 μ M) decreased and forskolin (5 μ M) increased impedance, showing an increase and a decrease in endothelial layer permeability, respectively (Figure 7(a)), thus supporting the reliability of our experimental setup to study the endothelial barrier. To link the effects of Nrf2 activators on endothelial permeability in HMECs with ET-1 function, the effect of ET-1 given alone on endothelial permeability was assessed. ET-1 caused a concentration-dependent decrease in permeability (Figures 7(b) and 7(c)), while ET-1 receptor antagonists BQ123 and BQ 788 increased endothelial permeability (Figure 7(d)), as evidenced by increased and decreased impedance, respectively.

Bardoxolone methyl (3 and 5 μ M), even after 3 hours of incubation (that did not cause endothelial toxicity (Figure 3, Table 1) but lowered ET-1 production (Figure 6)), significantly decreased the impedance indicating an increase in the permeability of the endothelial monolayer (Figure 8(a)), while dimethyl fumarate did not disturb endothelial barrier function and L-sulforaphane at the highest concentrations had only minor effects after 3 hours of incubation (Figures 8(b) and 8(c)). After a 24-hour-long period of incubation, a further increase in permeability of endothelial cells was observed in the cells treated with micromolar concentrations of bardoxolone methyl, an effect shared also by L-sulforaphane (Figures 8(d) and 8(f)). In these experimental conditions (24 hour incubation), dimethyl fumarate did not affect endothelial permeability (Figure 8(e)).

4. Discussion

To the best of our knowledge, in the present work, we have demonstrated for the first time that bardoxolone methyl affects mitochondrial function, cellular viability, ET-1 release, and endothelial barrier function in human microvascular endothelium, and those effects are not shared with dimethyl fumarate and L-sulforaphane tested in the same concentration range.

Clearly, the beneficial effect of Nrf2 on vascular endothelial function has been repeatedly reported and evidenced, also in our study by, e.g., a decrease in ROS production. Such

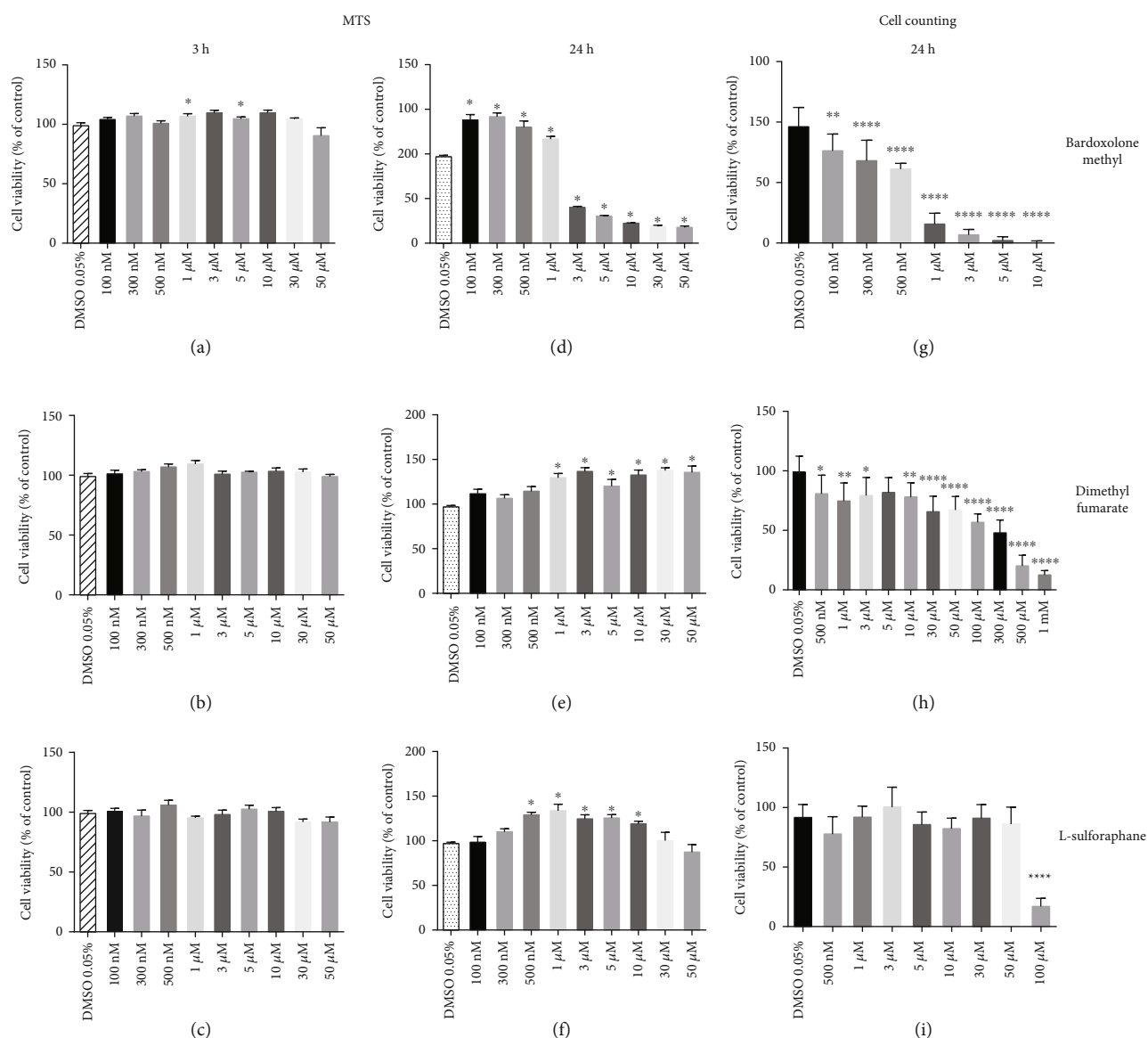


FIGURE 3: Effects of Nrf2 activators on endothelial viability assessed by the MTS test and cell counting. HMEC-1 cells were incubated with bardoxolone methyl, dimethyl fumarate, and L-sulforaphane (100 nM–50 μ M) for 3 (a–c) and 24 (d–f) hours for the MTS test. Concentrations ranging from 100 nM up to 1 mM were applied in the cell counting test (g–i). Results are expressed as a % of control (cells treated with 0.05% DMSO). Values are expressed as mean \pm SEM, $n = 4$. The significance of the differences between the means was evaluated by one-way analysis of variance (ANOVA) with Duncan's (MTS) or Dunnett's (cell counting) post hoc test if appropriate; * $p < 0.05$, ** $p < 0.01$, and **** $p < 0.0001$ indicate significant difference vs. the control group (DMSO 0.05%). The results were obtained in four independent experiments.

effects include not only a decrease in vascular oxidative stress but also a downregulation of endothelial proinflammatory adhesion molecule expression [33] and restoration of endothelial function in hypertension, atherosclerosis, diabetes, or aging [7, 34, 35]. Here, by means of flow cytometry, we detected direct endothelial toxicity for bardoxolone methyl (at concentrations 3–5 μ M), but not for other Nrf2 activators, which was not unequivocally supported by the MTS assay in any of the experimental groups, as the latter assay may show divergent results if mitochondrial activity is altered. Indeed, bardoxolone methyl seems to have a biphasic effect: it sustains cellular metabolism at lower doses and becomes cyto-

toxic in higher concentrations; similarly, dimethyl fumarate increased MTS readouts.

To better understand the mechanisms involved in bardoxolone methyl-induced endothelial toxicity, we analyzed the effects of bardoxolone methyl compared with other Nrf2 activators on cellular bioenergetics and mitochondrial membrane potential. Although the main source of energy in the endothelium is glycolysis [36], mitochondrial activity and redox signalling plays an important role in maintaining endothelial integrity [37]. We showed concentration-dependent effects of bardoxolone methyl on mitochondrial activity comprising proton leak, spare respiratory capacity,

TABLE 1: Quantification of apoptosis and necrosis with the use of an Annexin V/propidium iodide assay for flow cytometry in HMEC-1 cells after a 24-hour-long incubation with bardoxolone methyl, dimethyl fumarate, and L-sulforaphane. Values are expressed as mean % of cell population \pm SEM, $n = 4$. The significance of the differences between the means was evaluated by one-way analysis of variance (ANOVA) with Dunn's post hoc test if appropriate; * $p < 0.05$ and ** $p < 0.01$ indicate significant difference vs. the control group (DMSO 0.05%). The results were obtained in four independent experiments.

Population (mean %)	Bardoxolone methyl				Dimethyl fumarate				L-sulforaphane			
	Necrosis (AV-/PI+)	Apoptosis +necrosis (AV+/PI+)	Live (AV-/PI-)	Apoptosis (AV+/PI-)	Necrosis (AV-/PI+)	Apoptosis +necrosis (AV+/PI+)	Live (AV-/PI-)	Apoptosis (AV+/PI-)	Necrosis (AV-/PI+)	Apoptosis +necrosis (AV+/PI+)	Live (AV-/PI-)	Apoptosis (AV+/PI-)
DMSO 0.05%	0.45 \pm 0.03	1.15 \pm 0.14	90.48 \pm 0.54	7.93 \pm 0.54	0.45 \pm 0.03	1.15 \pm 0.14	90.48 \pm 0.54	7.93 \pm 0.54	0.45 \pm 0.03	1.15 \pm 0.14	90.48 \pm 0.54	7.93 \pm 0.54
100 nM	1.33 \pm 0.39	4.25 \pm 1.71	87.98 \pm 1.28	6.43 \pm 1.96	2.8 \pm 0.80	8.6 \pm 0.80	84.75 \pm 0.05	3.8 \pm 0.00	0.90 \pm 0.12	3.98 \pm 0.48	89.80 \pm 0.29	5.85 \pm 0.40
300 nM	1.40 \pm 0.55	4.43 \pm 2.18	87.35 \pm 1.43	6.85 \pm 1.86	2.85 \pm 0.75	7.3 \pm 2.30	86.4 \pm 3.50	3.4 \pm 0.50	0.95 \pm 0.18	3.42 \pm 0.44	88.60 \pm 0.65	6.47 \pm 0.68
500 nM	1.40 \pm 0.61	4.40 \pm 2.20	86.10 \pm 1.38	8.00 \pm 2.49	1.75 \pm 0.45	7.7 \pm 1.20	86.65 \pm 1.75	3.9 \pm 0.20	1.10 \pm 0.25	3.43 \pm 0.47	89.10 \pm 0.45	6.37 \pm 0.55
1 μ M	2.68 \pm 1.00	8.45 \pm 2.83	83.23 \pm 5.95	6.03 \pm 0.85	2.4 \pm 0.80	9.45 \pm 2.95	84.15 \pm 4.35	3.95 \pm 0.65	1.05 \pm 1.12	4.32 \pm 0.38	88.13 \pm 0.24	6.52 \pm 0.45
3 μ M	11.33 \pm 4.82*	39.80 \pm 11.52*	33.53 \pm 5.64*	15.35 \pm 3.37	2.7 \pm 0.50	7.3 \pm 1.30	86.1 \pm 2.40	3.8 \pm 0.60	1.85 \pm 0.29	6.38 \pm 1.3	83.32 \pm 2.22	8.42 \pm 0.78
5 μ M	18.90 \pm 7.86**	51.18 \pm 11.80**	17.18 \pm 4.58**	12.85 \pm 3.87	2.75 \pm 0.45	7.65 \pm 2.25	85.7 \pm 3.10	3.95 \pm 0.45	1.20 \pm 0.17	4.25 \pm 0.55	87.23 \pm 0.46	7.30 \pm 1.69

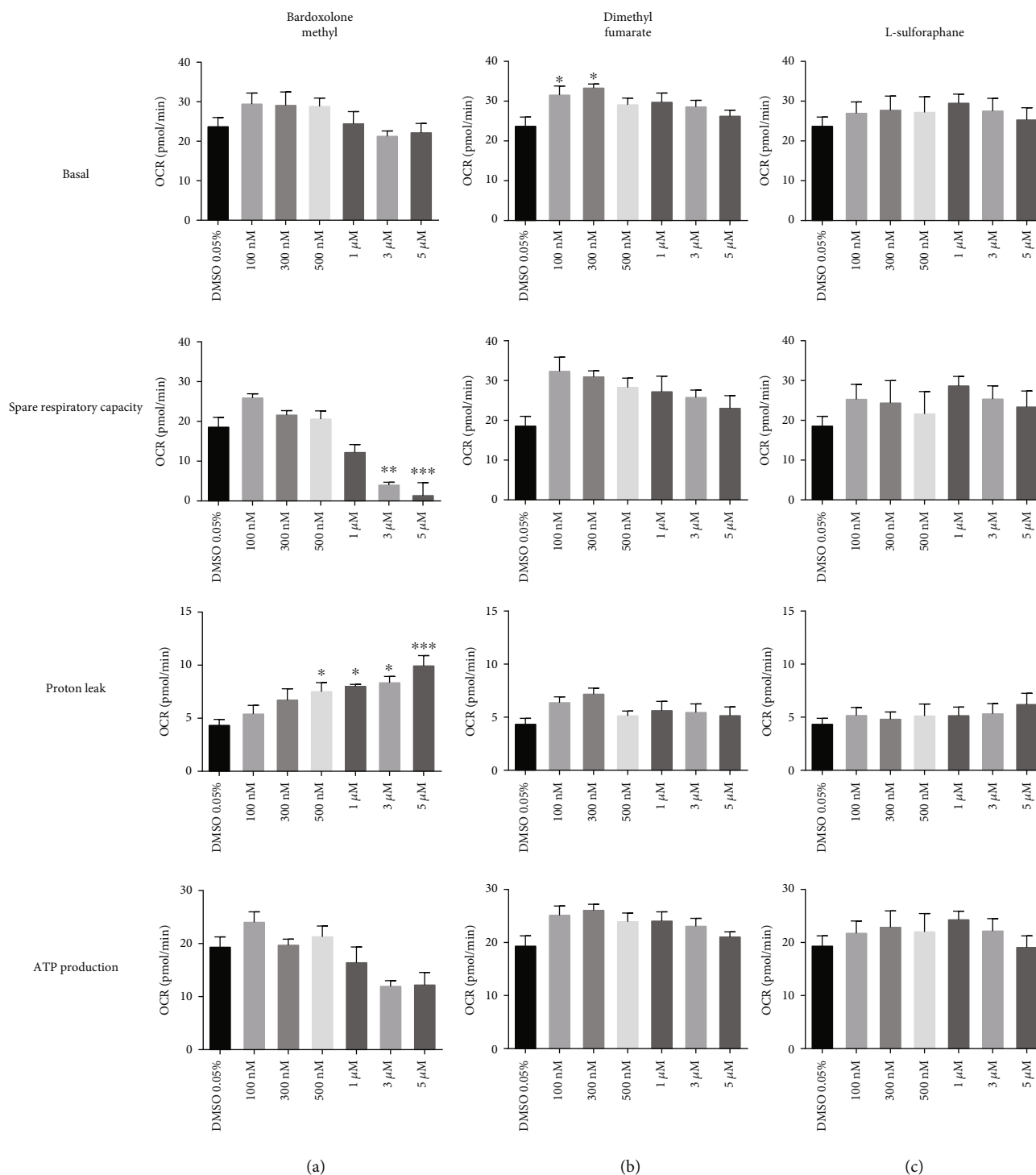


FIGURE 4: Effects of Nrf2 activators on mitochondrial function in endothelial cells. HMEC-1 cells were incubated for three hours with bardoxolone methyl (a), dimethyl fumarate (b), and L-sulforaphane (c) (100 nM–5 μM). Values are expressed as mean oxygen consumption rate (OCR, in pmol/min ± SEM, $n = 5$). The significance of the differences between the means was evaluated by one-way analysis of variance (ANOVA) with Dunnett's post hoc test if appropriate; * $p < 0.05$, ** $p < 0.01$, and *** $p < 0.001$ indicate significant difference vs. the control group (DMSO 0.05%). The results were obtained in five independent experiments.

and mitochondrial membrane potential. Interestingly, in cells treated with bardoxolone methyl, an increase in proton leak was observed even at the nontoxic concentration of 500 nM. The uncoupling effect could be beneficial for the cell [38–40]; however, the uncoupling effect of bardoxolone

methyl was severe and contributed to endothelial toxicity, in particular in the presence of higher concentrations of bardoxolone methyl. Other Nrf2 activators—dimethyl fumarate and L-sulforaphane—displayed neither endothelial toxicity nor detrimental effects on mitochondrial bioenergetics or

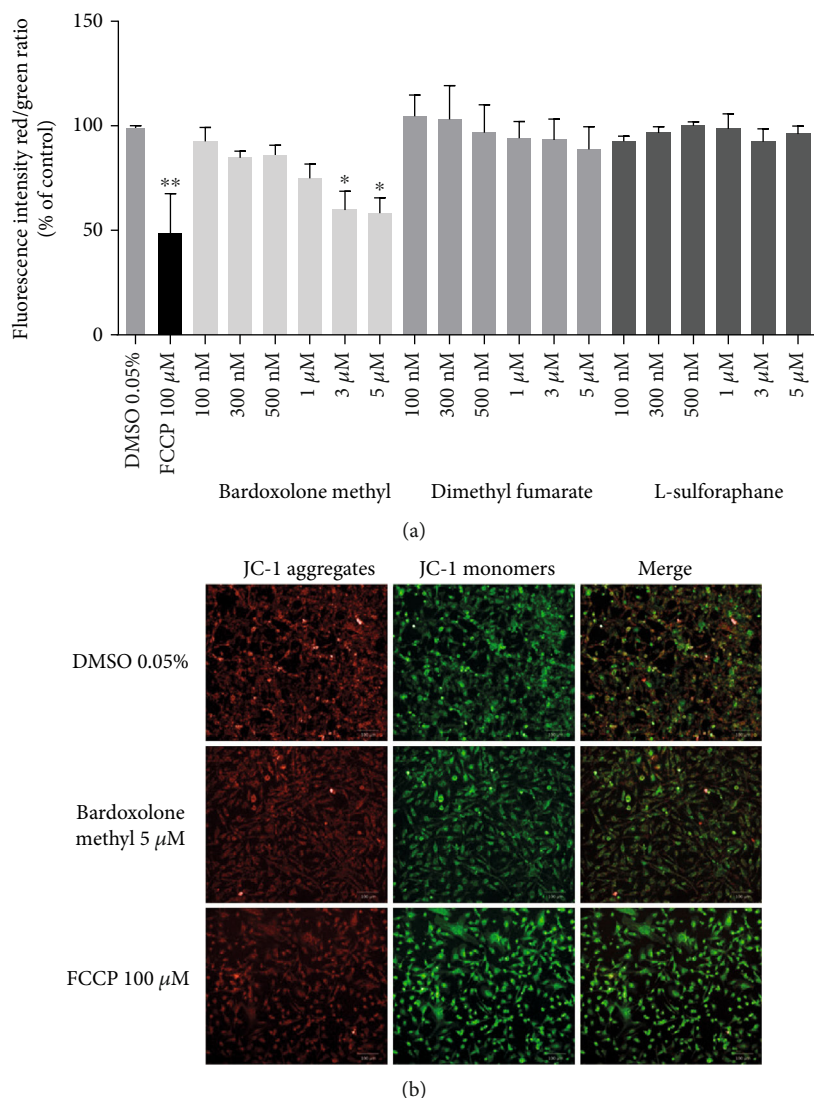


FIGURE 5: Effects of Nrf2 activators on mitochondrial membrane potential in endothelial cells. HMEC-1 cells were incubated for three hours with FCCP (100 μ M) or with bardoxolone methyl, dimethyl fumarate, and L-sulforaphane (100 nM–5 μ M) (a). Values are expressed as a ratio of red and green fluorescence intensity of JC-1 calculated as a % of control \pm SEM, $n = 3$. The significance of the differences between the means was evaluated by one-way analysis of variance (ANOVA) with Duncan's post hoc test if appropriate; * $p < 0.05$ and ** $p < 0.01$ indicate significant difference vs. the control group (DMSO 0.05%). (b) Representative images of HMEC-1 cells treated with 0.05% DMSO (upper panel), 5 μ M of bardoxolone methyl (middle panel), and 100 μ M of FCCCP (lower panel). Images were collected with the use of 20x magnification at 561/617 nm (red fluorescence, JC-1 aggregates), 488/525 nm (green fluorescence, JC-1 monomers), and merged. The results were obtained in three independent experiments.

mitochondrial membrane potential, even at the highest concentrations used. The endothelial toxicity of bardoxolone methyl was supposedly an Nrf-2-independent effect, since increased Nrf2 activity may modulate mitochondrial function and has a protective, rather than detrimental effect on mitochondrial integrity [41, 42]. On the other hand, the effects of dimethyl fumarate on respiration could be linked to the metabolism of dimethyl fumarate to fumarate, feeding the citric acid cycle [16].

Many Nrf2-activating chemicals including bardoxolone methyl are electrophilic, and their mechanisms of action are based on the modification of cysteine residues in Keap1, resulting in an impairment of Keap1 function, inhibition of

the ubiquitin E3 ligase activity of the Keap1-Cul3 complex, and subsequently leading to Nrf2 activation. Electrophiles are able to target distinct cysteine residues as well as lead to rapid and selective depletion of mitochondrial glutathione [43] implicating, at least partially, unspecific mechanisms of action of these types of compounds [44]. Proteomic analysis revealed that bardoxolone methyl interacts with 577 cellular proteins [45]. It was suggested that the side effects of bardoxolone methyl may be attributed to its highly reactive α -cyano- α , β -unsaturated ketone (CUK) moiety in ring A, which avidly reacts with other proteins besides Keap1. In fact, modification of the CUK moiety in ring A results in a marked decrease in cytotoxicity [45]. Thus, it may well be

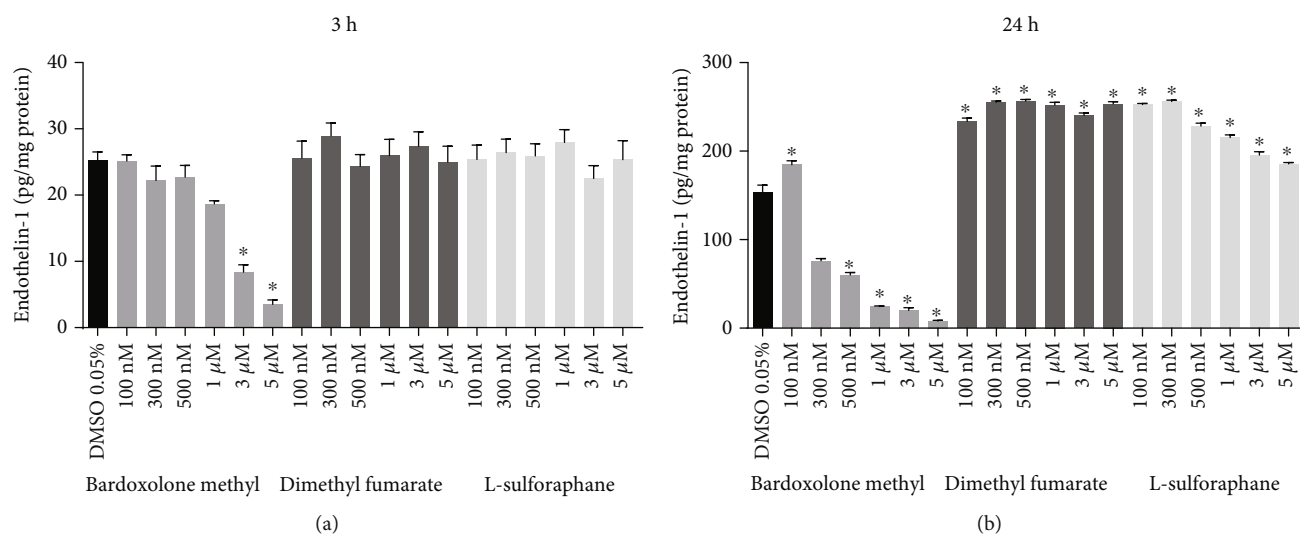


FIGURE 6: Effects of Nrf2 activators on secretion of endothelin-1 from endothelium to culture media. HMEC-1 cells were incubated for 3 (a) and 24 (b) hours with bardoxolone methyl, dimethyl fumarate, and L-sulforaphane (100 nM–5 μM). Values are expressed as mean ± SEM, $n = 3$. The significance of the differences between the means was evaluated by one-way analysis of variance (ANOVA) with Dunnett's post hoc test if appropriate; * $p < 0.0001$ indicates significant difference vs. the control group (DMSO 0.05%). The results were obtained in three independent experiments.

that the mitochondrial and cellular toxicity of bardoxolone methyl reported here was due to an unspecific modification of a thiol-containing mitochondrial protein, representing a known mechanism of cellular toxicity described for other agents [46]. Noteworthy, other mechanisms of bardoxolone methyl-induced cellular toxicity reported for cancer cells could also be involved in inducing endothelial toxicity by this compound [47]. Interestingly, it was demonstrated that dimethyl fumarate reduced cellular maximal respiratory and reserve capacity and these effects were completely inhibited by N-acetyl cysteine, again suggesting the involvement of thiols [48]. These experiments were conducted in retinal epithelial cells at a concentration of 10 μM and a longer incubation period compared to our study. Also, L-sulforaphane was shown to inhibit the proliferation of endothelial cells, although the concentrations used were higher than those investigated in our study [49]. These reports indicate that unspecific detrimental effects of Nrf2 activators on mitochondrial bioenergetics and cellular function may be seen not only with bardoxolone but also with other electrophilic activators of Nrf2 in higher concentrations and in a tissue-specific manner.

Increased risk of heart failure, hospitalization, or death from heart failure in bardoxolone methyl-treated patients in the BEACON trial was attributed to kidney-specific suppression of the endothelin pathway resulting in sodium and volume retention [19]. Given the fact that ET-1 directly decreases microvascular permeability, the inhibition of the ET-1-pathway in microvascular endothelium could increase endothelial permeability. Indeed, in a set of *ex vivo* experiments, ET-1 decreased permeability in rat mesenteric microvessels [50, 51]. Furthermore, decreased microvascular permeability caused by ET-1 was suggested to be mediated by the ET_B receptor [50, 51]. These reports uncovered, for the first time, an important role of ET-1 in the maintenance

and modulation of endothelial permeability. Recently, Kansanen et al. [52] demonstrated that in human aortic endothelial and human umbilical endothelial cells, nitrooleic acid, *via* an Nrf2-dependent pathway, leads to an increased expression of the ET_B receptor and a subsequent decrease in extracellular ET-1 secreted by endothelial cells. The authors postulated that this mechanism may limit the vasoconstrictive effects of ET-1 and could prove therapeutically useful, for example, in pulmonary artery hypertension [52]. Our results clearly indicate that ET-1 (in addition to its well-known vasoconstrictive, mitogenic, and proinflammatory effects via ET_A receptors, the NO- and PGI₂-releasing effect via the ET_B receptor), quite surprisingly, is also involved in maintaining the endothelial barrier function in human microvascular endothelial cells. In fact, exogenous ET-1 increased endothelial barrier function. Our experiments are not conclusive regarding the type of ET-1 receptor involved in the regulation of endothelial permeability by ET-1, especially given a possible heterodimerization of receptor A and B subunits [53]. However, the results presented in the present work fully support the notion of ET-1 as a local autocrine regulator of endothelial barrier function, as suggested previously [50, 51, 54]. Even though downregulation of ET-1 by laminar flow has vasoprotective effects and the suppression of ET-1-dependent mechanisms by Nrf2 activators may be efficacious in the treatment of pulmonary arterial hypertension (PAH) [33, 55], suppression of local ET-1 production in the microcirculation may lead to increased endothelial permeability.

In the present work, we demonstrate that bardoxolone methyl suppressed ET-1 release from HMECs and increased microvascular endothelial permeability. These effects were seen even after 3 hours of incubation with bardoxolone methyl, an experimental setting that was not associated with endothelial toxicity (Figure 3 and Table 1) but clearly

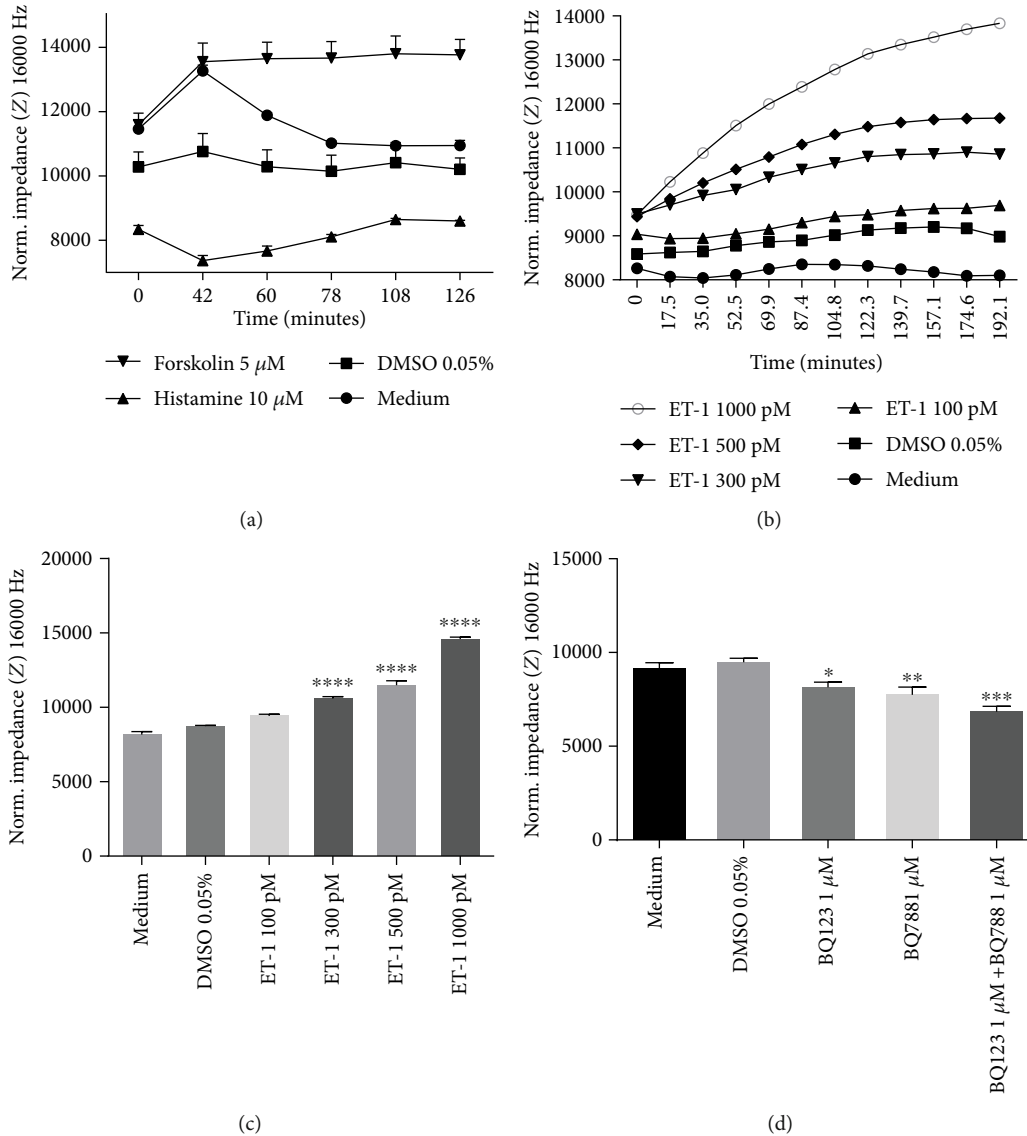


FIGURE 7: Effects of endothelin-1 and endothelin-1 receptor antagonists on endothelial permeability. The measurement of impedance was performed using an ECIS assay at a frequency of 16,000 Hz in HMEC-1 cells: (a) incubated for one hour with medium, DMSO 0.05%, histamine 10 μ M, and forskolin 5 μ M; (b and c) incubated for three hours with endothelin-1 (ET-1) (100 pM–1000 pM); (d) incubated for three hours with 1 μ M of BQ123 and/or BQ788. Values are expressed as mean normalized impedance \pm SEM, $n = 3$. The significance of the differences between the means was evaluated by one-way analysis of variance (ANOVA) with Dunnett's post hoc test if appropriate; * $p < 0.05$, ** $p < 0.01$, *** $p < 0.001$, and **** $p < 0.0001$ indicate significant difference vs. the control groups: medium (a) and DMSO 0.05% (b, c, and d). The results were obtained in three independent experiments.

lowered ET-1 production. Dimethyl fumarate did not disturb endothelial barrier function after 3 hours of incubation, and L-sulforaphane at the highest concentrations had only minor effects that were also present after 24 hours of incubation, but again they were weaker as compared with bardoxolone methyl.

Analysis of nuclear translocation of Nrf2 revealed that in the tested concentration range of Nrf2 activators, bardoxolone methyl was the most potent inducer of the Nrf2 pathway in HMECs, while L-sulforaphane was less potent. These results are compatible with the weaker effects of L-sulforaphane on ET-1 release and endothelial permeability. Lack of significant effects of dimethyl fumarate could

be attributed to the weakest effects of this compound on Nrf2 among all three Nrf2 activators in the tested concentration range. Indeed, L-sulforaphane was also shown by other authors to be a more potent inducer of Nrf2 compared with dimethyl fumarate [56]. It may also be that concomitant activation of other endothelial protective mechanisms by increasing mitochondrial respiration (as evidenced in our experiments) could play a role in a differential response of cells to dimethyl fumarate vs. L-sulforaphane [57]. Obviously, in order to identify whether the effects of bardoxolone methyl on ET-1 release and endothelial permeability are indeed mediated by Nrf2, further experiments are needed, e.g., with Nrf2 silencing.

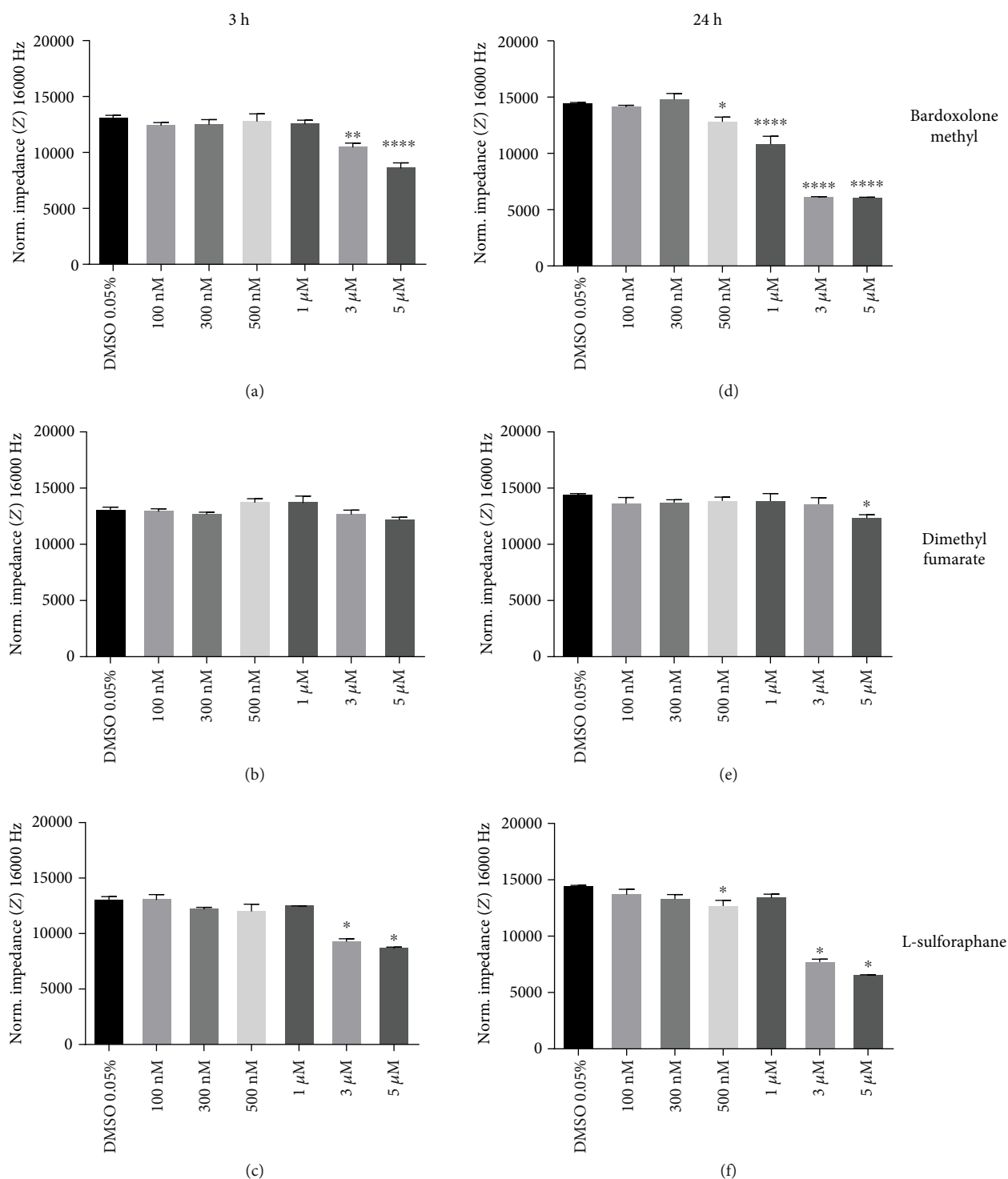


FIGURE 8: Effects of Nrf2 activators on endothelial permeability. The measurement of impedance was performed using an ECIS assay at a frequency of 16,000 Hz in HMEC-1 cells incubated for 3 and 24 hours with bardoxolone methyl (a and d), dimethyl fumarate (b and e), or L-sulforaphane (100 nM–5 μM) (c and f). Values are expressed as mean normalized impedance \pm SEM, $n = 3$. The significance of the differences between the means was evaluated by one-way analysis of variance (ANOVA) with Duncan's post hoc test if appropriate; * $p < 0.05$, ** $p < 0.01$, and **** $p < 0.0001$ indicate significant difference vs. the control group (DMSO 0.05%). The results were obtained in three independent experiments.

Altogether, our results provide a novel insight into a possible detrimental influence of bardoxolone methyl on microvascular endothelium that could have contributed to the side

effects of this compound reported in the BEACON study. However, the concentration range used here was higher than the therapeutic range of concentration for bardoxolone

methyl [8]; thus, this conclusion needs further verification in experimental studies, best to be performed in *in vivo* experimental conditions.

In clinical trials comprising bardoxolone methyl, dimethyl fumarate, or L-sulforaphane, C_{\max} plasma levels found in patients were 24.7 ± 13.3 ng/ml (49 nM), 1.87 mg/l (13 μ M), and 36.7 ng/ml (210 nM), respectively [8, 10, 58]. These results suggest that for bardoxolone methyl and L-sulforaphane, nanomolar ranges of concentrations are close to plasma concentration in patients, while it requires micromolar concentrations for dimethyl fumarate. Still, we cannot exclude that chronic treatment with bardoxolone methyl *in vivo*, in particular in patients with preexisting alterations of microvascular endothelial barrier function, e.g., due to diabetes, would result in the effects described *in vitro* using low micromolar concentrations of this compound.

In conclusion, despite the limitations described above, to the best of our knowledge, this study is the first to comprehensively evaluate the influence of three major Nrf2 activators on human microvascular endothelium to identify an endothelium-oriented explanation for the side effects of bardoxolone methyl reported in the BEACON clinical trial. We have demonstrated that bardoxolone methyl displays a distinct profile of activity in the endothelium, including detrimental effects on mitochondria and cellular viability and profound suppression of endothelial ET-1 release that could possibly interfere with ET-1-dependent autocrine regulation of endothelial permeability, safeguarding microvascular function.

Abbreviations

ROS:	Reactive oxygen species
CDDO-Me:	Bardoxolone methyl
CKD:	Chronic kidney disease
ET-1:	Endothelin 1
ET _A receptor:	Endothelin receptor type A
ET _B receptor:	Endothelin receptor type B
ESRD:	End-stage renal disease
HMEC-1:	Human microvascular endothelial cells
MTS:	3-(4,5-Dimethylthiazol-2-yl)-5-(3-carboxymethoxyphenyl)-2-(4-sulfophenyl)-2H-tetrazolium
Nrf2:	Nuclear factor (erythroid 2-related factor) 2
PGI ₂ :	Prostacyclin
PPAR- γ :	Peroxisome proliferator-activated receptor- γ .

Data Availability

Answer: yes. Comment: the data is being stored on the internal servers of the Jagiellonian Centre for Experimental Therapeutics JCET UJ in Jagiellonian University of Krakow. Any person interested in viewing the data is welcome to contact either the first or the corresponding author.

Conflicts of Interest

The authors declare that they have no conflicts of interest.

Authors' Contributions

ES-M and SC conceived and designed the research. Western blot experiments were performed by RC. ROS production experiments were performed by ES-M. Endothelial toxicity experiments were performed by ES-M, MS, and MG. Mitochondrial function experiments were performed by ES-M, MJ, and PK. Endothelin-1 release experiments were performed by ES-M. Permeability studies were performed by ES-M. Data analyses were performed by ES-M and PK. Interpretation of results was performed by ES-M, PK, and SC. Figure preparation was performed by ES-M. Manuscript drafting was performed by ES-M and SC. ES-M, MG, and SC edited and revised the manuscript. Preparation of the final manuscript was performed by ES-M and SC. All authors have corrected or have approved the final version of the manuscript.

Acknowledgments

This work was supported by the Foundation for Polish Science from the resources of the TEAM TECH-Core Facility program (application number 0016) financed by the European Regional Development Fund under the Intelligent Development Operational Program 2014-2020 (OP IR), Axis IV, Increasing the scientific and research potential, 4.4: Increasing the human resources potential of the R&D sector. ES-M would like to acknowledge financial support from the National Science Centre (grant no. 2019/03/X/NZ7/01601).

References


- [1] T. Suzuki, H. Motohashi, and M. Yamamoto, "Toward clinical application of the Keap 1-Nrf2 pathway," *Trends in Pharmacological Sciences*, vol. 34, no. 6, pp. 340–346, 2013.
- [2] D. Malhotra, E. Portales-Casamar, A. Singh et al., "Global mapping of binding sites for Nrf2 identifies novel targets in cell survival response through ChIP-Seq profiling and network analysis," *Nucleic Acids Research*, vol. 38, no. 17, pp. 5718–5734, 2010.
- [3] L. Baird and A. T. Dinkova-Kostova, "The cytoprotective role of the Keap1–Nrf2 pathway," *Archives of Toxicology*, vol. 85, no. 4, pp. 241–272, 2011.
- [4] I. M. Copple, "The Keap1–Nrf2 cell defense pathway—a promising therapeutic target?," in *Current Concepts in Drug Metabolism and Toxicology*, pp. 43–79, Elsevier, 2012.
- [5] A. Mandal and A. Bishayee, "*Trianthema portulacastrum* Linn. displays anti-inflammatory responses during chemically induced rat mammary tumorigenesis through simultaneous and differential regulation of NF- κ B and Nrf2 signaling pathways," *International Journal of Molecular Sciences*, vol. 16, no. 2, pp. 2426–2445, 2015.
- [6] S. K. Niture and A. K. Jaiswal, "Nrf2 protein up-regulates anti-apoptotic protein Bcl-2 and prevents cellular apoptosis," *The Journal of Biological Chemistry*, vol. 287, no. 13, pp. 9873–9886, 2012.
- [7] B. Chen, Y. Lu, Y. Chen, and J. Cheng, "The role of Nrf2 in oxidative stress-induced endothelial injuries," *The Journal of Endocrinology*, vol. 225, no. 3, pp. R83–R99, 2015.

- [8] D. S. Hong, R. Kurzrock, J. G. Supko et al., "A phase I first-in-human trial of bardoxolone methyl in patients with advanced solid tumors and lymphomas," *Clinical Cancer Research*, vol. 18, no. 12, pp. 3396–3406, 2012.
- [9] N. Esteras, A. T. Dinkova-Kostova, and A. Y. Abramov, "Nrf2 activation in the treatment of neurodegenerative diseases: a focus on its role in mitochondrial bioenergetics and function," *Biological Chemistry*, vol. 397, no. 5, pp. 383–400, 2016.
- [10] J. J. Alumkal, R. Slottke, J. Schwartzman et al., "A phase II study of sulforaphane-rich broccoli sprout extracts in men with recurrent prostate cancer," *Investigational New Drugs*, vol. 33, no. 2, pp. 480–489, 2015.
- [11] Z. Bahadoran, M. Tohidi, P. Nazari, M. Mehran, F. Azizi, and P. Mirmiran, "Effect of broccoli sprouts on insulin resistance in type 2 diabetic patients: a randomized double-blind clinical trial," *International Journal of Food Sciences and Nutrition*, vol. 63, no. 7, pp. 767–771, 2012.
- [12] P. Altmeyer, R. Hartwig, and U. Matthes, "Das wirkungs- und sicherheitsprofil von fumarsäureestern in der oralen langzeittherapie bei schwerer therapieresistenter psoriasis vulgaris," *Der Hautarzt*, vol. 47, no. 3, pp. 190–196, 1996.
- [13] A. Cuadrado, G. Manda, A. Hassan et al., "Transcription factor NRF2 as a therapeutic target for chronic diseases: a systems medicine approach," *Pharmacological Reviews*, vol. 70, no. 2, pp. 348–383, 2018.
- [14] R. A. Linker, D.-H. Lee, S. Ryan et al., "Fumaric acid esters exert neuroprotective effects in neuroinflammation via activation of the Nrf2 antioxidant pathway," *Brain*, vol. 134, no. 3, pp. 678–692, 2011.
- [15] R. Gold, L. Kappos, D. L. Arnold et al., "Placebo-controlled phase 3 study of oral BG-12 for relapsing multiple sclerosis," *The New England Journal of Medicine*, vol. 367, no. 12, pp. 1098–1107, 2012.
- [16] A. R. Gafson, C. Savva, T. Thorne et al., "Breaking the cycle," *Neurology - Neuroimmunology Neuroinflammation*, vol. 6, no. 3, 2019.
- [17] K. T. Liby and M. B. Sporn, "Synthetic oleanane triterpenoids: multifunctional drugs with a broad range of applications for prevention and treatment of chronic disease," *Pharmacological Reviews*, vol. 64, no. 4, pp. 972–1003, 2012.
- [18] D. de Zeeuw, T. Akizawa, P. Audhya et al., "Bardoxolone methyl in type 2 diabetes and stage 4 chronic kidney disease," *The New England Journal of Medicine*, vol. 369, no. 26, pp. 2492–2503, 2013.
- [19] M. P. Chin, S. A. Reisman, G. L. Bakris et al., "Mechanisms contributing to adverse cardiovascular events in patients with type 2 diabetes mellitus and stage 4 chronic kidney disease treated with bardoxolone methyl," *American Journal of Nephrology*, vol. 39, no. 6, pp. 499–508, 2014.
- [20] M. P. Chin, D. Wroldstad, G. L. Bakris et al., "Risk factors for heart failure in patients with type 2 diabetes mellitus and stage 4 chronic kidney disease treated with bardoxolone methyl," *Journal of Cardiac Failure*, vol. 20, no. 12, pp. 953–958, 2014.
- [21] M. P. Chin, G. L. Bakris, G. A. Block et al., "Bardoxolone methyl improves kidney function in patients with chronic kidney disease stage 4 and type 2 diabetes: post-hoc analyses from bardoxolone methyl evaluation in patients with chronic kidney disease and type 2 diabetes study," *American Journal of Nephrology*, vol. 47, no. 1, pp. 40–47, 2018.
- [22] D. E. Kohan, "The renal medullary endothelin system in control of sodium and water excretion and systemic blood pressure," *Current Opinion in Nephrology and Hypertension*, vol. 15, no. 1, pp. 34–40, 2006.
- [23] D. Camer and X.-F. Huang, "The endothelin pathway: a protective or detrimental target of bardoxolone methyl on cardiac function in patients with advanced chronic kidney disease?," *American Journal of Nephrology*, vol. 40, no. 3, pp. 288–290, 2014.
- [24] A. P. Davenport, K. A. Hyndman, N. Dhaun et al., "Endothelin," *Pharmacological Reviews*, vol. 68, no. 2, pp. 357–418, 2016.
- [25] J. J. Maguire and A. P. Davenport, "Endothelin receptors and their antagonists," *Seminars in Nephrology*, vol. 35, no. 2, pp. 125–136, 2015.
- [26] S. Tobe, D. E. Kohan, and R. Singarayer, "Endothelin receptor antagonists: new hope for renal protection?," *Current Hypertension Reports*, vol. 17, no. 7, p. 57, 2015.
- [27] D. Fischer, S. Rossa, U. Landmesser et al., "Endothelial dysfunction in patients with chronic heart failure is independently associated with increased incidence of hospitalization, cardiac transplantation, or death," *European Heart Journal*, vol. 26, no. 1, pp. 65–69, 2005.
- [28] Y. H. Ku, B.-J. Cho, M. J. Kim et al., "Rosiglitazone increases endothelial cell migration and vascular permeability through Akt phosphorylation," *BMC Pharmacology and Toxicology*, vol. 18, no. 1, p. 62, 2017.
- [29] D. Cheng, H. Gao, and W. Li, "Long-term risk of rosiglitazone on cardiovascular events: a systematic review and meta-analysis," *Endokrynologia Polska*, vol. 69, no. 4, pp. 381–394, 2018.
- [30] Z. Jiao, J. Chang, J. Li, D. Nie, H. Cui, and D. Guo, "Sulforaphane increases NRF2 expression and protects alveolar epithelial cells against injury caused by cigarette smoke extract," *Molecular Medicine Reports*, vol. 16, no. 2, pp. 1241–1247, 2017.
- [31] R. Szulcek, H. J. Bogaard, and G. P. van Nieuw Amerongen, "Electric cell-substrate impedance sensing for the quantification of endothelial proliferation, barrier function, and motility," *Journal of Visualized Experiments*, no. 85, article e51300, 2014.
- [32] J. Wegener, C. R. Keese, and I. Giaever, "Electric cell-substrate impedance sensing (ECIS) as a noninvasive means to monitor the kinetics of cell spreading to artificial surfaces," *Experimental Cell Research*, vol. 259, no. 1, pp. 158–166, 2000.
- [33] H. Morawietz, R. Talanow, M. Szibor et al., "Regulation of the endothelin system by shear stress in human endothelial cells," *The Journal of Physiology*, vol. 525, no. 3, pp. 761–770, 2000.
- [34] R. A. Lopes, K. B. Neves, R. C. Tostes, A. C. Montezano, and R. M. Touyz, "Downregulation of nuclear factor erythroid 2-related factor and associated antioxidant genes contributes to redox-sensitive vascular dysfunction in hypertension," *Hypertension*, vol. 66, no. 6, pp. 1240–1250, 2015.
- [35] A. Sharma, L. Rizky, N. Stefanovic et al., "The nuclear factor (erythroid-derived 2)-like 2 (Nrf2) activator dh 404 protects against diabetes-induced endothelial dysfunction," *Cardiovascular Diabetology*, vol. 16, no. 1, p. 33, 2017.
- [36] L. N. Groschner, M. Waldeck-Weiermair, R. Malli, and W. F. Graier, "Endothelial mitochondria-less respiration, more integration," *Pflügers Archiv - European Journal of Physiology*, vol. 464, no. 1, pp. 63–76, 2012.
- [37] L. M. Buja, "The pathobiology of acute coronary syndromes: clinical implications and central role of the mitochondria," *Texas Heart Institute Journal*, vol. 40, no. 3, pp. 221–228, 2013.

- [38] P. S. Brookes, "Mitochondrial H⁺ leak and ROS generation: an odd couple," *Free Radical Biology & Medicine*, vol. 38, no. 1, pp. 12–23, 2005.
- [39] A. B. J. F. Turrens, "Generation of superoxide anion by the NADH dehydrogenase of bovine heart mitochondria," *The Biochemical Journal*, vol. 191, no. 2, pp. 421–427, 1980.
- [40] A. Herrero and G. Barja, "ADP-regulation of mitochondrial free radical production is different with complex I- or complex II-linked substrates: implications for the exercise paradox and brain hypermetabolism," *Journal of Bioenergetics and Biomembranes*, vol. 29, no. 3, pp. 241–249, 1997.
- [41] M. J. Calkins, R. J. Jakel, D. A. Johnson, K. Chan, W. K. Yuen, and J. A. Johnson, "Protection from mitochondrial complex II inhibition in vitro and in vivo by Nrf2-mediated transcription," *Proceedings of the National Academy of Sciences of the United States of America*, vol. 102, no. 1, pp. 244–249, 2005.
- [42] J. M. Lee, A. Y. Shih, T. H. Murphy, and J. A. Johnson, "NF-E2-related factor-2 mediates neuroprotection against mitochondrial complex I inhibitors and increased concentrations of intracellular calcium in primary cortical neurons," *The Journal of Biological Chemistry*, vol. 278, no. 39, pp. 37948–37956, 2003.
- [43] I. Samudio, S. Kurinna, P. Ruvolo et al., "Inhibition of mitochondrial metabolism by methyl-2-cyano-3,12-dioxoolean-1,9-diene-28-oate induces apoptotic or autophagic cell death in chronic myeloid leukemia cells," *Molecular Cancer Therapeutics*, vol. 7, no. 5, pp. 1130–1139, 2008.
- [44] D. Del Prete, O. Tagliatalata-Scafati, A. Minassi et al., "Electrophilic triterpenoid enones: a comparative thiol-trapping and bioactivity study," *Journal of Natural Products*, vol. 80, no. 8, pp. 2276–2283, 2017.
- [45] Z. Huang, Y. Mou, X. Xu et al., "Novel derivative of bardoxolone methyl improves safety for the treatment of diabetic nephropathy," *Journal of Medicinal Chemistry*, vol. 60, no. 21, pp. 8847–8857, 2017.
- [46] A. Venkatraman, A. Landar, A. J. Davis et al., "Oxidative modification of hepatic mitochondria protein thiols: effect of chronic alcohol consumption," *American Journal of Physiology-Gastrointestinal and Liver Physiology*, vol. 286, no. 4, pp. G521–G527, 2004.
- [47] X.-Y. Wang, X.-H. Zhang, L. Peng et al., "Bardoxolone methyl (CDDO-Me or RTA402) induces cell cycle arrest, apoptosis and autophagy via PI3K/Akt/mTOR and p 38 MAPK/Erk 1/2 signaling pathways in K562 cells," *American Journal of Translational Research*, vol. 9, no. 10, pp. 4652–4672, 2017.
- [48] R. Foresti, C. Bucolo, C. M. B. Platania, F. Drago, J. L. Dubois-Randé, and R. Motterlini, "Nrf2 activators modulate oxidative stress responses and bioenergetic profiles of human retinal epithelial cells cultured in normal or high glucose conditions," *Pharmacological Research*, vol. 99, pp. 296–307, 2015.
- [49] M. Asakage, N. H. Tsuno, J. Kitayama et al., "Sulforaphane induces inhibition of human umbilical vein endothelial cells proliferation by apoptosis," *Angiogenesis*, vol. 9, no. 2, pp. 83–91, 2006.
- [50] G. P. Victorino, D. H. Wisner, and V. L. Tucker, "Basal release of endothelin-1 and the influence of the ETB receptor on single vessel hydraulic permeability," *The Journal of Trauma*, vol. 49, no. 2, pp. 314–319, 2000.
- [51] G. P. Victorino, C. R. Newton, and B. Curran, "Endothelin-1 decreases microvessel permeability after endothelial activation," *The Journal of Trauma: Injury, Infection, and Critical Care*, vol. 56, no. 4, pp. 832–836, 2004.
- [52] E. Kansanen, S. M. Kuosmanen, A.-K. Ruotsalainen, H. Hynynen, and A.-L. Levonen, "Nitro-oleic acid regulates endothelin signaling in human endothelial cells," *Molecular Pharmacology*, vol. 92, no. 4, pp. 481–490, 2017.
- [53] B. Gregan, M. Schaefer, W. Rosenthal, and A. Oksche, "Fluorescence resonance energy transfer analysis reveals the existence of endothelin-A and endothelin-B receptor homodimers," *Journal of Cardiovascular Pharmacology*, vol. 44, Supplement 1, pp. S30–S33, 2004.
- [54] G. P. Victorino, D. H. Wisner, and V. L. Tucker, "Direct actions of endothelin-1 on single vessel hydraulic permeability," *The Journal of Trauma*, vol. 47, no. 4, pp. 713–718, 1999.
- [55] S. Eba, Y. Hoshikawa, T. Moriguchi et al., "The nuclear factor erythroid 2-related factor 2 activator oltipraz attenuates chronic hypoxia-induced cardiopulmonary alterations in mice," *American Journal of Respiratory Cell and Molecular Biology*, vol. 49, no. 2, pp. 324–333, 2013.
- [56] S. Petrillo, E. Piermarini, A. Pastore et al., "Nrf2-inducers counteract neurodegeneration in frataxin-silenced motor neurons: disclosing new therapeutic targets for Friedreich's ataxia," *International Journal of Molecular Sciences*, vol. 18, no. 10, p. 2173, 2017.
- [57] H. Peng, H. Li, A. Sheehy, P. Cullen, N. Allaire, and R. H. Scannevin, "Dimethyl fumarate alters microglia phenotype and protects neurons against proinflammatory toxic microenvironments," *Journal of Neuroimmunology*, vol. 299, pp. 35–44, 2016.
- [58] D. Cada, T. Levien, and D. Baker, "dimethyl fumarate," *Hospital Pharmacy*, vol. 48, no. 8, pp. 668–679, 2013.

Research Article

Decoding Aging: Understanding the Complex Relationship among Aging, Free Radicals, and GSH

María E. López-Navarro ¹, **Mariana Jarquín-Martínez** ¹, **Luis A. Sánchez-Labastida** ¹,
Daniel Ramírez-Rosales,² **Marycarmen Godínez-Victoria** ¹,
Laura Itzel Quintas-Granados ³, and **José Guadalupe Trujillo-Ferrara** ¹

¹Departamento de Bioquímica y Sección de Estudios de Posgrado e Investigación, Escuela Superior de Medicina del Instituto Politécnico Nacional, Plan de San Luis y Salvador Díaz Mirón s/n, Casco de Santo Tomás, Ciudad de México 11340, Mexico

²Instituto Politécnico Nacional, ESFM, Av. Instituto Politécnico Nacional s/n, Edif. 9 U.P. Zacatenco, Col. San Pedro Zacatenco, Ciudad de México 07738, Mexico

³Universidad Mexiquense de Bicentenario, Unidad de Estudios Superiores de Tultitlán, Av. Ex Hacienda de Portales s/n, Villa Esmeralda, Tultitlán, Estado de México 54910, Mexico

Correspondence should be addressed to Laura Itzel Quintas-Granados; litqingra@gmail.com and José Guadalupe Trujillo-Ferrara; jtrujillo@ipn.mx

Received 30 January 2020; Revised 21 April 2020; Accepted 20 May 2020; Published 13 October 2020

Academic Editor: Luciano Saso

Copyright © 2020 María E. López-Navarro et al. This is an open access article distributed under the Creative Commons Attribution License, which permits unrestricted use, distribution, and reproduction in any medium, provided the original work is properly cited.

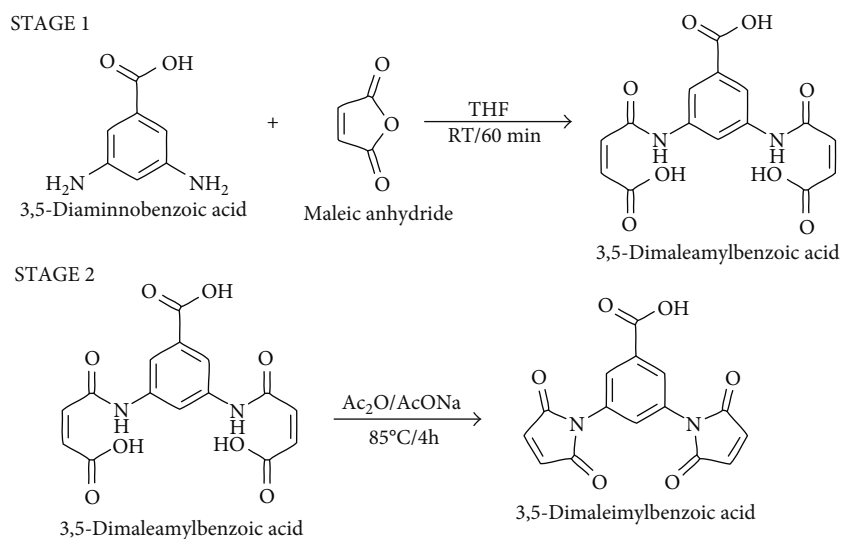
N-aryl maleimides can undergo a 1,4-Michael-type addition reaction with reduced glutathione (GSH), leading to a decreased concentration of GSH and an increased concentration of free radicals (FRs) in cells. GSH is a critical scavenging molecule responsible for protecting cells from oxidation and for maintaining redox homeostasis. N-aryl maleimides disturb redox homeostasis in cells because they scavenge thiol-containing molecules, especially GSH. This study aimed at measuring the concentrations of GSH and FRs by electronic paramagnetic resonance (EPR), in the brain and liver tissue of male Wistar rats (*ex vivo*) at different ages and after treatment with 3,5-dimaleimylbenzoic acid (3,5-DMB). Our results showed a relationship between age and the concentrations of GSH and FRs in cells. In young rats, the concentration of GSH was higher than in old rats, while the concentration of FRs was higher in adult rats than in young rats, suggesting an inverse relationship between GSH and FRs. On the other hand, the reaction of 3,5-DMB (an electrophilic maleimide) with cellular GSH increased the FR content. The results of this study contribute to the awareness that the process of aging implies not only a loss of tissue function but also essential changes in the molecular contents of cells, especially the concentrations of FRs and GSH.

1. Introduction

In the electron flow system, oxygen is the final single electron acceptor involved in the production of energy in the form of ATP. Cell respiration is balanced by the rates of free radical (FR) generation and elimination, which result from cell metabolism by single electron transfer. Some molecules lose or accept a single electron, leaving one or more unpaired electrons. Consequently, these molecules are highly reactive and unstable. The most abundant FRs in cells are reactive oxygen species (ROS) and reactive nitrogen species (RNS).

Reactive oxygen and nitrogen species (RONS) refer to reactive radical and nonradical derivatives of oxygen and nitrogen, respectively. Tobacco and alcohol consumption, air and water contamination, certain drugs, industrial solvents, radiation, and a diet particularly rich in carbohydrates can also give rise to RONS in biological systems [1].

To reduce oxidized targets and thus diminish or avoid oxidative stress (OS), cells have potent antioxidant enzymes and nonenzymatic antioxidant systems. These enzymes include superoxide dismutase (SOD), peroxiredoxin, glutathione peroxidase (GPx), and catalase (CAT) [2], each with



SCHEME 1: Synthesis of 3,5-dimaleimylbenzoic acid (3,5-DMB). Stage 1: 3,5-diaminobenzoic acid was reacted with maleic anhydride. Stage 2: cyclization of the precursor maleamide was achieved through dehydration with anhydrous sodium acetate to provide 3,5-DMB.

a distinct function. These enzymes may be sensors and transducers of oxidizing agents [3]. Other molecules participate in a nonenzymatic fashion in cells, such as ascorbic acid (vitamin C), α -tocopherol (vitamin E), glutathione (GSH), carotenoids, and flavonoids [2]. GSH is the major soluble antioxidant molecule in cells due to its abundance in the cytosol (1–11 mM), nucleus (3–15 mM), and mitochondrion (5–11 mM) of cells [2]. GSH, a reactive Cys residue containing tripeptide, is linked to glucose metabolism through the pentose phosphatase pathway. NADPH produced in this pathway maintains GSH in a reduced form [4].

The relationship between oxidants and the antioxidant system is the key to proper cell function, and the antioxidant system is triggered by signaling pathways in response to elevated levels of FRs and cell damage. OS occurs when oxidants and antioxidants are out of balance, provoking not only a disruption in redox signaling and control but also damage to molecules and cells [4, 5]. Hence, OS and FRs are linked to several age-related degenerative diseases, including cancer, stroke, and other cardiovascular and inflammatory diseases [6, 7]. According to the FR theory of aging, oxidants play an important role in the aging process. In childhood, the high level of thiols in cells creates a reducing environment that stimulates cell growth. In contrast, adult metabolism generates RONS, implying a considerable increase in the FR content in tissues.

A compound capable of selectively and covalently binding to thiols would inhibit increases in reducing environments, likely resulting in an increased level of FRs. In previous studies, our group found that GSH is scavenged by a series of aryl maleimides derived from benzoic acid, which are selective for thiol-containing compounds. Those aryl maleimides could be susceptible to nucleophilic attack at the carbonyl carbon and the olefinic carbons by a 1,2 addition reaction or a 1,4-Michael type addition reaction, respectively. Although both carbons are electrophiles, the highest value of local softness corresponds to olefinic carbons, indicating that they are more susceptible to a 1,4-Michael addi-

tion type reaction by thiol groups than are carbonyl carbons. This reactivity might be attributed to the soft base behavior of thiols [8]. The reaction of olefinic carbons with GSH leads to a significant decrease in the concentration of thiols in cells and the induction of apoptosis caused by a considerable increase in the level of FRs [8].

This study aimed at measuring the concentration of GSH and FRs in brain and liver tissues of male Wistar rats (*in vivo* and *ex vivo*) of different ages and after treatment with 3,5-dimaleimylbenzoic acid (3,5-DMB). The levels of FRs were determined with electronic paramagnetic resonance (EPR) which had been used to detect physiologic levels of specific species with a high specificity [9]. The reaction of 3,5-DMB (an electrophilic maleimide) with cellular GSH increased the FR content. A relationship was found between age and the concentration of GSH and FRs in cells. Young rats presented the highest levels of GSH and the lowest FRs levels. In contrast, old rats had the highest FR levels and the lower GSH amount, suggesting an inverse relationship between the GSH and FRs. The results of this study contribute to the awareness that the process of aging implies not only a loss of tissue function but also essential changes in the molecular contents of cells, especially the concentrations of FRs and GSH.

2. Materials and Methods

2.1. Synthesis of 3,5-Dimaleimylbenzoic Acid (3,5-DMB). The synthesis of 3,5-DMB involved two steps (Scheme 1). First, the precursor 3,5-dimaleamylbenzoic acid was obtained by mixing 3,5-diaminobenzoic acid (25 mmol) with maleic anhydride (50 mmol) at a 1 : 2 ratio in anhydrous tetrahydrofuran (THF). The solution was incubated at room temperature under vigorous shaking for 1 h. The precipitate that formed was separated by filtration, washed with ethanol at 4°C, and dried at 40°C under vacuum.

Subsequently, 72 mmol of the precursor amide (maleamide) was added to 14 mmol anhydrous sodium acetate

(AcONa) in 30 mL acetic anhydride (Ac_2O). The mixture was incubated at 85°C with vigorous stirring for 4 h. The precipitate was removed by filtration, and the supernatant was maintained under gentle agitation at 4°C . Then, 100 mL of acidic water (pH 3) was added to induce precipitation. Finally, the precipitate that formed was filtered, washed with distilled water, and dried at 40°C before being characterized.

2.2. Characterization of 3,5-DMB. Compound purity was analyzed by thin-layer chromatography with a mixture of 1:1 ethanol:acetone. The product was characterized by ^1H and ^{13}C NMR as 3,5-DMB following a previous report [10]. Briefly, ^1H - and ^{13}C -NMR spectra were recorded on a Jeol GSX-270 (JEOL USA, Inc.) and Bruker Ascend g750 Ultrashield. First-order analysis of the ^1H -NMR spin patterns was performed to obtain the chemical shifts (ppm) and coupling constants (Hz). ^1H -NMR spectra were acquired at a spectral width of 5.9 kHz with 16 K data points based on an acquisition time of 2.73 s, a recycle delay of 2 s, a flip angle of 45° and 8 scans. ^{13}C -NMR spectra were recorded with a spectral width of 25.1 kHz at 16 K data points, an acquisition time of 0.681 s, a flip angle of 45° , and 256 scans. 2D NMR spectra were captured on Jeol software at 295 K.

2.3. Characterization of the Reaction between 3,5-DMB and GSH. To determine whether a 1,4-Michael-type reaction occurred between 3,5-DMB and GSH, a solution of 3,5-DMB (1 mL of 0.1 M) in 0.01 M bicarbonate water (pH 8) was added to 1 mL of 0.2 M GSH or N-acetyl cysteine (NAC) at 5°C . Subsequently, thin layer chromatography was performed and revealed with 0.2% ninhydrin (2,2-dihydroxyindane-1,3-dione). The reaction was also monitored by VIS spectroscopy at 540 nm to distinguish among 3,5-DMB, GSH, and NAC. The reactions were characterized by ^1H and ^{13}C NMR at 270 MHz as mentioned above.

2.4. Global and Local Softness and Fukui Descriptors. Theoretical calculations were carried out as previously reported [8]. Briefly, the first potential ionization (I) and the electron affinity (A) were afforded by Gaussian 03 software and used to compute global parameters such as global hardness (η) (Equation (1)), chemical potential (μ) (Equation (2)), acceptor potential (μ^+) (Equation (3)), donating potential (μ^-) (Equation (4)), global softness (S) (Equation (5)), electrophilicity index (ω) (Equation (6)), electron-donating power (ω^-) (Equation (7)), and electron-accepting power (ω^+) (Equation (8)), according to the following equations:

$$\eta = \frac{I - A}{2}, \quad (1)$$

$$\mu = -\frac{I + A}{2}, \quad (2)$$

$$\mu^+ = -\frac{I + 3A}{4}, \quad (3)$$

$$\mu^- = -\frac{3I + A}{4}, \quad (4)$$

$$S = \frac{1}{\eta}, \quad (5)$$

$$\omega = \frac{\mu^2}{2\eta}, \quad (6)$$

$$\omega^- = \frac{(\mu^-)^2}{2\eta}, \quad (7)$$

$$\omega^+ = \frac{(\mu^+)^2}{2\eta^+}. \quad (8)$$

The condensed Fukui functions were ascertained with Equation (9) and Equation (10):

$$(f_x^+) = [q_x(N+1) - q_x(N)] \text{ for a reaction with a nucleophile} \quad (9)$$

$$(f_x^-) = [q_x(N) - q_x(N-1)] \text{ for a reaction with an electrophile} \quad (10)$$

Where q_x represents the electronic population of x atom in the molecule.

Furthermore, local softness was determined by multiplying the value of the condensed Fukui function ($f_x^{+/-}$) by the global softness (S). For each atom in the x position of the molecule, local softness $s_x^{+/-}$ is expressed as Equation (11) and Equation (12):

$$s_x^+ = (f_x^+) S \text{ for a nucleophilic local attack} \quad (11)$$

$$s_x^- = (f_x^-) S \text{ for an electrophilic local attack} \quad (12)$$

Theoretical calculations were performed for the electronic population by using Fukui descriptors, based on the quantum theory of atoms in molecules (QTAIM). The wave function for each of the neutral and ionic systems was computed using the optimized geometry for the neutral molecule. Finally, the electronic population was found using the AIM 2000 software, as previously described [8].

2.5. Biological Model and Experimental Design. Male Wistar rats served as the *in vivo* model. Rats were provided with a standard diet and water *ad libitum*. Animals were handled and maintained under the national guidelines on animal care, approved by the institutional Committee on Ethics in Research (registration # ESM-CICUAL-03/10-04-2019).

To study the 3,5-DMB effect on the GSH and FR, we selected to different organs, the brain, and the liver, because they have high mitochondrial amount, different metabolic requirements, both are FR producers and develop different complications and responses associated with redox homeostasis.

Control animals ($n = 21$) were monitored from 2-18 months of age. To examine the levels of GSH and FRs in liver and brain tissues, control subjects ($n = 3$) were analyzed at 2, 3, 5, 7, 8, 12, and 18 months of age.

Regarding the experimental group ($n = 48$), 3,5-DMB was intraperitoneally administered at 100 mg/kg body weight

to 2- and 15-month-old animals, to determine the 3,5-DMB effect on young and old individuals in which the levels of GSH and FR are different. Tissue samples were collected at 1, 2, 4, 6, 8, 12, and 16 h posttreatment. Three control animals were analyzed before injection (time zero). For the determination of FRs, 0.15 g of brain tissue was obtained by frontal lobe dissection in the direction of the corpus callosum, hypothalamus, and hippocampus. GSH was evaluated with 1 g of damp brain tissue. The determination of the same two parameters was performed on equal amounts of damp liver tissue.

2.6. Quantification of GSH. GSH content was assessed *ex vivo* in liver and brain tissues from rats treated with 3,5-DMB and control (untreated) animals at several time points (each time and condition were assayed in triplicate). Tissues were extracted by grinding in the presence of 5% trichloroacetic acid (0.2:1.5 $w(g)/v$) and centrifugation at 1500 g for 30 min at room temperature. The supernatant was collected and immediately used to measure the level of GSH by the 5,5'-dithio-(2-nitrobenzoic acid) method [11] and read at 412 nm.

2.7. EPR Spectroscopic Analysis. Tissue samples were cut into 50 mg pieces and with an external diameter of 1 mm and were immediately frozen at -70°C and characterized at the same temperature on an X-band (9.3 GHz) EPR spectrometer (RADIOPAN, Poznan, Poland) with modulation of the magnetic field at 100 kHz. A single EPR spectrum was determined at 10^{-4} sec. To decrease the signal/noise level, spectra were accumulated 200–300 times. EPR spectra were recorded at the first derivative at room temperature and 72°C .

The amplitude (A), integral intensity (I), and linewidth (ΔB_{pp}) values were determined from the EPR spectra using the ELF program of JAGMAR Firm (Kraków, Poland). The concentration of FRs in the samples is the value proportional to the integral of the intensity (I) of their EPR spectra. The g -factor was calculated from the resonance condition as follows (Equation (13)):

$$g = \frac{h\nu}{\mu_B Br}, \quad (13)$$

where h is the Planck constant, ν is the microwave frequency, μ_B is the Bohr magneton and Br is the resonance magnetic field [12]. The g -factor is related to a stable FR content.

2.8. Statistical Analysis. Data were analyzed with SAS/STAT® software and are expressed as the mean \pm SD. Data from EPR analysis and GSH quantification performed on tissue from three rats were used to calculate the mean and the standard deviation of FR and GSH levels, respectively. Normally distributed variables were examined with Student's t -test to determinate the possible correlation between FRs from the brain or liver and the age of rats.

3. Results

Synthesis of 3,5-DMB was achieved in 98% yield and 99% purity, in agreement with previously reported synthesis [8, 10, 13]. Structural analysis of the spectra indicated a close correspondence between the displacements and the composition/structure of 3,5-DMB.

Theoretical descriptors obtained from computational calculations of 3,5-DMB, NAC, cysteine, and GSH (Table 1) revealed that 3,5-DMB has the highest chemical potential (μ) and lowest global hardness (η). Accordingly, it was demonstrated in this study that 3,5-DMB selectively reacts with thiol groups from GSH.

Additionally, an *in vitro* reaction was carried out between 3,5-DMB and NAC. According to thin layer chromatography (data not shown), COSY H-H (^1H -H CORrelated Spectroscopy), COLOC (CORrelation through LONG-range Coupling) analysis, and ^1H and ^{13}C NMR at 270 MHz (Supplementary Figure S1), a 1,4-Michael type reaction takes place between 3,5-DMB and NAC, in which the α,β -unsaturated carbonyl structure in 3,5-DMB acts as an electrophilic compound (Figure 1). The reaction product is a 50–50% diastereoisomer mixture. Few changes occur in the imide moiety spectrum of 3,5-DMB due to reaction with NAC (compared to the spectrum reported for NAC alone). Moreover, aromatic moiety analysis of this reaction revealed a similar pattern as that found with the starting materials. However, there is a ^{13}C signal at 39.54 ppm corresponding to C-S bond formation and a double of doubles signal at 4.19 ppm for each of the protons in the methylene moiety (Supplementary Figure S1) due to the diastereotopic nature of the reaction product.

3.1. Effect of Age on the Levels of GSH and Free Radicals (FRs) in Liver and Brain Tissue. According to the EPR spectra, the samples did not contain paramagnetic impurities. The spectra of all the analyzed samples revealed the presence of FRs ($g = 2.003$, $\Delta H = 1.0$ mTl) (Supplementary Figure S2) that were stable (Table 2). The g -factor strongly indicates the presence of a high level of FRs.

An evaluation of the effect of age on the levels of GSH and FR in brain and liver tissues from rats is shown in Table 2 and Figure 2. Brain tissue displayed a 7-fold greater FR content in 18-month-old rats than that in 2-month-old rats (Table 2 and Figure 2(a)). Surprisingly, in liver tissue, the level of FRs was 23-fold higher in adult versus young rats (Table 2 and Figure 2(a)). In both liver and brain tissues, the concentration of FRs increased as a linear function of the age of rats. Experimental data were adjusted to a linear polynomial equation ($f(x) = ax + b$), where a is the slope and b is the intercept with the y -axis. Control experimental data fitted perfectly to a straight line (Figure 2) which allowed comparative analyzes. The r^2 value was 0.9232 for brain tissue and 0.9639 for liver tissue (Figure 2(a)). The slope of the data was 3-fold greater for liver tissue (69525.28) than for brain tissue (20640.47). Statistical analysis demonstrated a strong correlation between FRs from the brain or liver and the age of rats (brain, $r^2 = 0.8244$, $p = 0.0001$; liver, $r^2 = 0.9643$, $p = 0.0001$). Thus, the level of FRs significantly increased in both tissues as rats aged

TABLE 1: Theoretical global and local descriptors for 3,5-DMB, N-acetyl cysteine, cysteine, and GSH.

Compound										
			Global descriptors							
μ (eV)	μ^- (eV)	μ^+ (eV)	η (eV)	S (1/eV)	ω (eV)	ω^- (eV)	ω^+ (eV)			
3,5-DMB			-5.1062	-6.8024	-3.4100	3.0180	0.1657	3.4198	6.0687	1.5254
			Local softness s_x^+							
			C=C (C3-C4)			0.0066				
			C=O			0.0046				
Global descriptors										
μ (eV)	μ^- (eV)	μ^+ (eV)	η (eV)	S (1/eV)	ω (eV)	ω^- (eV)	ω^+ (eV)			
N-acetyl cysteine ¹			-3.8521	-6.2548	-1.4493	4.8055	0.1040	1.5439	4.0706	0.2186
			Local softness s_x^-							
			SH			0.0452				
Global descriptors										
μ (eV)	μ^- (eV)	μ^+ (eV)	η (eV)	S (1/eV)	ω (eV)	ω^- (eV)	ω^+ (eV)			
Cysteine			-3.3075	-6.0074	-0.6076	5.3998	0.0926	1.0129	3.3417	0.0342
			Local softness s_x^-							
			SH			0.0318				
Global descriptors										
μ (eV)	μ^- (eV)	μ^+ (eV)	η (eV)	S (1/eV)	ω (eV)	ω^- (eV)	ω^+ (eV)			
GSH			-3.6495	-5.8221	-1.4286	4.3936	0.1138	1.4957	3.8576	0.2322
			Local softness s_x^-							
			SH			0.0246				

3,5-DMB: 3,5-dimaleimylbenzoic acid, GSH: reduced Glutathione, μ : chemical potential, μ^- : donating potential, μ^+ : acceptor potential, η : global hardness value, S : global softness, ω : Electrophilicity index, ω^- : electron-donating power, ω^+ : electron-accepting power, eV: electronvolt. ¹Global local indexes of reactivity for N-acetyl cysteine were taken from published data [8, 13].

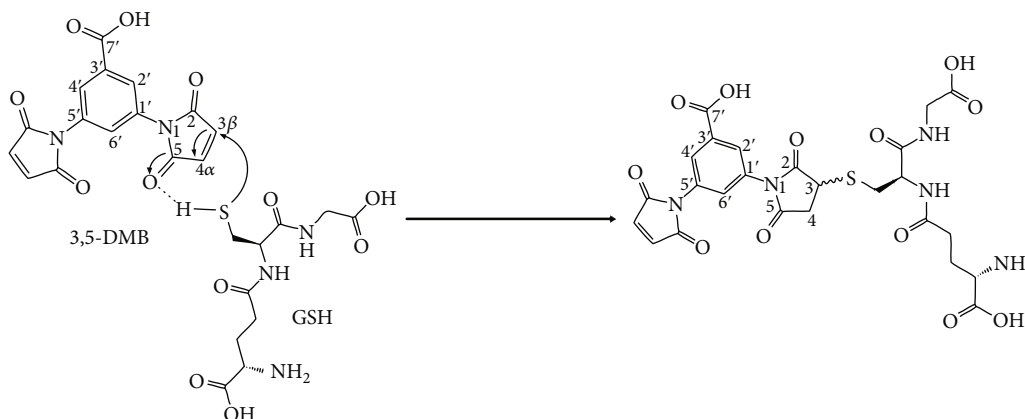


FIGURE 1: Proposed reaction mechanism for 3,5-dimaleimylbenzoic (3,5-DMB) acid with glutathione (GSH). The α,β -unsaturated carbonyl structure in 3,5-DMB acts as an electrophile, carrying out a 1,4-Michael-type reaction with the sulfur atom (S) from the thiol group of the cysteine residue in GSH (IUPAC-based numerical assignment). The β -carbon atom (C_3) is shown as the preferred site of attack due to its positive polarization, whereas GSH acts as a Michael acceptor because of its high reactivity toward soft electrophiles, such as α,β -unsaturated compounds.

and increased faster in the liver, probably due to the high metabolic rate in the liver and the importance of protecting the brain to allow several vital functions of the organism.

The concentration of GSH decreased in brain and liver tissues with age (Table 2 and Figure 2(b)). Young rats (2 months

old) showed 1.5-fold and 1.8-fold higher levels of GSH in brain and liver tissues, respectively, than those in brain and liver tissues in adults (18 months old) (Figure 2(b)). Adjusting the experimental values to a linear equation afforded r^2 values of 0.9522 for brain tissue and 0.9619 for liver tissue

TABLE 2: Quantification of free radicals and GSH in brain and liver tissue extracted from Wistar rats at various ages and treated with 3,5-DMB several times.

Age (months)	Tissue (1 g)	Relative number of FRs ¹	GSH content (mol/g) ²
2	Brain	$4.95 \times 10^4 \pm 1.36 \times 10^3$	$2.46 \times 10^{-5} \pm 1.30 \times 10^{-7}$
	Liver	$5.10 \times 10^4 \pm 0.88 \times 10^3$	$4.76 \times 10^{-5} \pm 1.12 \times 10^{-6}$
3	Brain	$6.24 \times 10^4 \pm 0.94 \times 10^3$	$2.33 \times 10^{-5} \pm 1.86 \times 10^{-7}$
	Liver	$14.93 \times 10^4 \pm 2.59 \times 10^3$	$4.32 \times 10^{-5} \pm 1.04 \times 10^{-7}$
5	Brain	$9.71 \times 10^4 \pm 1.08 \times 10^3$	$2.31 \times 10^{-5} \pm 8.30 \times 10^{-8}$
	Liver	$18.75 \times 10^4 \pm 4.10 \times 10^3$	$4.15 \times 10^{-5} \pm 2.51 \times 10^{-7}$
7	Brain	$12.92 \times 10^4 \pm 2.78 \times 10^3$	$2.22 \times 10^{-5} \pm 4.81 \times 10^{-7}$
	Liver	$36.90 \times 10^4 \pm 2.33 \times 10^3$	$4.03 \times 10^{-5} \pm 4.94 \times 10^{-7}$
8	Brain	$23.71 \times 10^4 \pm 13.90 \times 10^3$	$1.99 \times 10^{-5} \pm 1.36 \times 10^{-6}$
	Liver	$45.87 \times 10^4 \pm 2.82 \times 10^3$	$3.81 \times 10^{-5} \pm 1.00 \times 10^{-6}$
12	Brain	$29.10 \times 10^4 \pm 4.37 \times 10^3$	$1.93 \times 10^{-5} \pm 7.14 \times 10^{-7}$
	Liver	$57.77 \times 10^4 \pm 3.99 \times 10^3$	$3.59 \times 10^{-5} \pm 5.30 \times 10^{-7}$
18	Brain	$35.48 \times 10^4 \pm 5.59 \times 10^3$	$1.65 \times 10^{-5} \pm 7.40 \times 10^{-8}$
	Liver	$122.34 \times 10^4 \pm 14.75 \times 10^3$	$2.60 \times 10^{-5} \pm 1.33 \times 10^{-6}$
Posttreatment time (h)			
0	Brain	$32.88 \times 10^4 \pm 6.51 \times 10^3$	$1.73 \times 10^{-5} \pm 1.36 \times 10^{-7}$
	Liver	$62.67 \times 10^4 \pm 39.07 \times 10^3$	$3.47 \times 10^{-5} \pm 1.95 \times 10^{-6}$
1	Brain	$15.26 \times 10^4 \pm 11.84 \times 10^3$	$2.35 \times 10^{-5} \pm 4.35 \times 10^{-7}$
	Liver	$46.68 \times 10^4 \pm 7.44 \times 10^3$	$3.53 \times 10^{-5} \pm 1.03 \times 10^{-6}$
2	Brain	$28.42 \times 10^4 \pm 0.85 \times 10^3$	$1.77 \times 10^{-5} \pm 6.17 \times 10^{-7}$
	Liver	$72.66 \times 10^4 \pm 38.21 \times 10^3$	$1.94 \times 10^{-5} \pm 7.31 \times 10^{-7}$
4	Brain	$26.04 \times 10^4 \pm 1.32 \times 10^3$	$1.97 \times 10^{-5} \pm 5.26 \times 10^{-7}$
	Liver	$59.50 \times 10^4 \pm 6.71 \times 10^3$	$2.98 \times 10^{-5} \pm 1.23 \times 10^{-6}$
6	Brain	$60.57 \times 10^4 \pm 23.13 \times 10^3$	$1.62 \times 10^{-5} \pm 8.95 \times 10^{-7}$
	Liver	$72.05 \times 10^4 \pm 13.47 \times 10^3$	$1.91 \times 10^{-5} \pm 1.37 \times 10^{-6}$
8	Brain	$49.90 \times 10^4 \pm 15.28 \times 10^3$	$1.42 \times 10^{-5} \pm 9.51 \times 10^{-7}$
	Liver	$83.25 \times 10^4 \pm 12.16 \times 10^3$	$2.01 \times 10^{-5} \pm 1.98 \times 10^{-6}$
12	Brain	$47.00 \times 10^4 \pm 10.20 \times 10^3$	$1.12 \times 10^{-5} \pm 9.59 \times 10^{-7}$
	Liver	$81.68 \times 10^4 \pm 22.13 \times 10^3$	$2.29 \times 10^{-5} \pm 2.26 \times 10^{-6}$
16	Brain	$45.73 \times 10^4 \pm 14.99 \times 10^3$	$1.40 \times 10^{-5} \pm 2.84 \times 10^{-7}$
	Liver	$85.94 \times 10^4 \pm 49.69 \times 10^3$	$2.09 \times 10^{-5} \pm 1.01 \times 10^{-6}$

¹Data from EPR analysis performed on tissue from three rats (mean \pm standard deviation). ²Data were calculated from tissue from three rats and are expressed as the mean \pm standard deviation.

(Figure 2(b)). The slope of the data was 0.412-fold greater for liver tissue than for brain tissue, suggesting that the GSH content decreased faster in liver tissue.

To visualize the overall effect of age on the levels of GSH and FRs in brain and liver tissues, the adjusted experimental data were extrapolated from 0 to 36 months of age (Figure 2(c)), the average lifetime of a laboratory rat [14]. In very young individuals (<2 months old), the concentration of FRs was almost the same in brain and liver tissues, nearly zero (Figure 2(c)). Adult rats (>15 months old), on

the other hand, had a 3.4-fold higher level of FRs in the liver than in the brain.

The concentration of GSH was 2-fold greater in liver tissue than in brain tissue in young animals (2 months old). With the aging of rats, a decrease in the GSH content was observed in both tissues and was 0.41-fold lower in liver tissue than in brain tissue (Figure 2(c)). Statistical analysis revealed a strong and negative correlation between the GSH content in both tissues and the age of rats (brain, $r^2 = 0.8817$, $p = 0.0001$; liver, $r^2 = 0.9525$, $p = 0.0001$). During the process

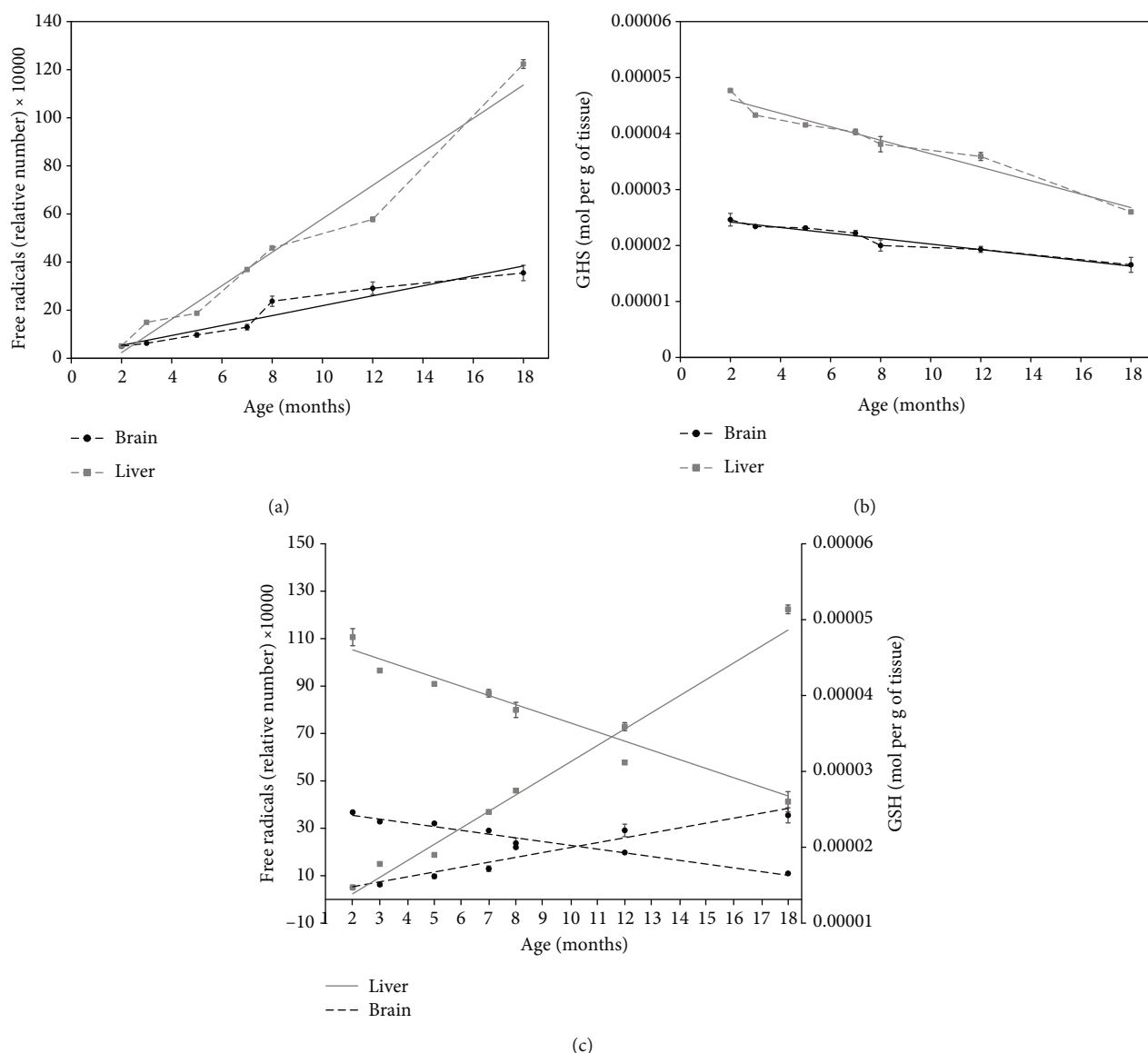


FIGURE 2: Effect of age on the levels of GSH and FRs. Male Wistar rats were used to obtain 1 g of brain (-●-) and liver (-■-) tissue at 2-18 months of age ($n = 3$ for each age and tissue) to quantify the relative concentrations of FRs (a) and GSH (b). Circles and squares represent the mean \pm standard deviation of three values from each sample extracted at a given measurement time. Experimental data were adjusted to a linear regression (solid lines). The statistical value (r^2) is denoted in each polynomial regression plot. The solid lines indicate the experimental values for the liver (-■-) tissue, and the dashed indicate the experimental values for the brain (-●-) tissue. Overall, the analysis indicates that with aging, the concentration of GSH decreases, and the FR content increases in both tissues (c).

of aging, the concentration of FRs increases, and that of GSH decreases in brain and liver tissues. The increase in FR content and the decrease in the concentration of GSH occur faster in liver tissue than in brain tissue (Figure 2(c)).

3.2. Treatment with 3,5-DMB Decreases the Level of GSH in Rats. 3,5-DMB treatment causes a loss of bright in the lens of treated rats but no weight loss was observed (data not shown). Brain tissue showed a significant increase (1.36-fold) in GSH content 1 h after treatment with 3,5-DMB, probably due to a specific cell reaction to maintain redox homeostasis. The level of GSH returned to the initial values by 2 h posttreatment and increases again (1.11-fold) at 4 h. From 4-12 h, the

GSH content steadily decreased but increased again at 16 h (1.25-fold) (Figure 3(a)).

The concentration of FRs in brain tissue (Figure 3(a)) decreased by 2.15-fold at 1 h posttreatment, followed by an increase at 2 h, and a significant increase (2.33-fold) at 6 h. From 6-16 h, a steady decrease occurred, although these values were still higher than the basal level.

In liver tissue, a slight increase in GSH content was detected (1.02-fold) 1 h after treatment, followed by a significant decrease (1.82-fold) at 2 h and an increase (1.54-fold) at 4 h, reaching the basal value. There was another decrease (1.56-fold) at 6 h, an increase at 12 h (1.20-fold), and a decrease (1.09-fold) at 16 h (Figure 3(b)).

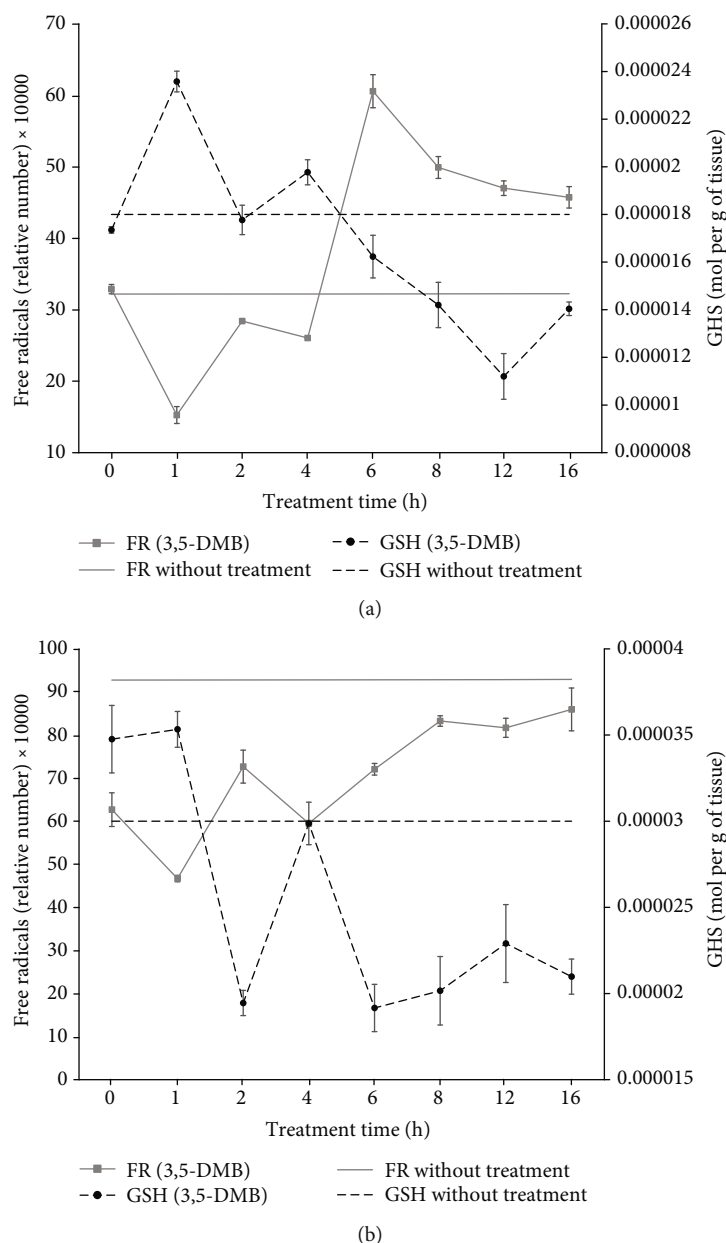


FIGURE 3: Effect of 3,5-DMB on the levels of GSH and FRs at 16 hours posttreatment in male Wistar rats. Evaluations were performed at 1, 2, 4, 6, 8, 12, and 16 h posttreatment with 3,5-DMB ($n = 3$). The relative number of FRs (\blacksquare) and concentration of GSH (\bullet) were determined in 1 g of brain tissue (a) and liver tissue (b). The standard deviation is shown. Linear regression plots for FRs (gray solid line) or GSH (black dashed line) in untreated samples from brain or liver tissue (Figure 2) are included for comparison.

Regarding FRs, their concentration in liver tissue decreased (1.34-fold) at 1 h, increased (1.56-fold) at 2 h, decreased (1.22-fold) at 4 h, and increased again (1.44-fold) at 16 h (Figure 3(b)).

4. Discussion

Based on theoretical calculations, 3,5-DMB is an electrophile with a partial positive charge (soft acid), while GSH is a nucleophile with a local negative charge (soft base). The local softness (S_x) values of α,β -unsaturated compounds suggest that they are more susceptible to nucleophilic attack.

The global and local reactivity indexes theoretically calculated from condensed Fukui functions (according to the published method) [8] point to the selectivity of 3,5-DMB for GSH. Since 3,5-DMB has greater chemical potential (μ) than GSH, the electron flow must go from the thiol group of GSH to the α,β -unsaturated carbonyl compound. Additionally, the fact that the lowest global hardness $\eta = 3.0180$ (Table 1) value was that of 3,5-DMB (versus that of GSH or NAC) reveals that it is most reactive as an electrophile among this group of compounds. According to its nucleophilicity, $\omega^- = 6.0687$ (Table 1), 3,5-DMB has a strong capacity to acquire electrons from the environment (until reaching saturation),

considering the electrophilicity index (ω). Thus, the α,β -unsaturated carbonyl of 3,5-DMB appears to have electrophilic behavior (Table 1), and GSH (a thiol-containing compound) has nucleophilic behavior.

When an electron is transferred from GSH to 3,5-DMB, the latter acquires greater stability, as evidenced by the higher ω value for 3,5-DMB than that for GSH (Table 1). The electron-donating ($\omega -$) and the electron-accepting ($\omega +$) power indexes indicate the electron acceptor capacity of the α,β -unsaturated carbonyl (which has a small positive charge) and the electron donor capacity of GSH (which has a small negative charge). The present findings are in agreement with previous reports on the selectivity of aryl maleimides for thiol-containing compounds (unlike their reaction with other nucleophile groups) due to the selectivity of their vinyl moiety (soft acid) for thiol groups (soft base) [8]. Hence, the $\alpha\text{-}\beta$ unsaturated moiety is apparently the preferred site of nucleophilic attack because of its polarizability. Moreover, GSH is a highly reactive compound toward soft electrophiles (e.g., α,β -unsaturated compounds) and acts as a Michael-type acceptor [15, 16]. According to the theoretical data, olefinic carbonyl carbons selectively react with thiol-containing compounds. The reaction is highly regioselective but not stereoselective, generating two asymmetric chiral centers in a 50-50% diastereomeric mixture. Furthermore, theoretical calculations point to the selectivity of the reaction of thiol species with the C-3 position of the α,β -unsaturated group (but not the carbonyl group) of 3,5-DMB [8].

FRs are commonly quantified by indirect methods through the evaluation of metabolic pathways, such as fatty acid double bond oxidation. The current study directly measured FRs in tissue using EPR. Moreover, the g -factor value obtained from EPR studies gives important information about the magnetic properties of the FR species. A g -factor of approximately 2 serves as an indicator of FRs. In our study, the g -factor value was 2.003, that agrees with the value reported in the literature for C-O species [17]. Although the specific radical species in the samples were not identified, the spectra strongly suggested that the EPR signals correspond to FRs. Furthermore, considering that the g -factor values were from 2.003–2.004, the radicals were probably a carbon-oxygen bonded combination [17].

It should be possible to predict the perinatal FR content by adjusting experimental values from 0 to 36 months of age (the average lifetime of a laboratory rat) [14] to obtain a proper perspective regarding the inverse relationship between GSH and FRs in brain and liver tissue. Regarding the level of FRs as a function of aging, a sharp increase was found in the liver and only a moderate increase was found in the brain. The rat central nervous system is relatively immature at birth, but after 7 to 21 days of postnatal development, there is a substantial increase in the activity of metabolic pathways [18, 19], which may contribute to the increase in the FR content and the decrease in the concentration of GSH in the liver. The accumulation of dysfunctional aged mitochondria leading to the alteration of redox homeostasis cannot be discounted [20].

On the other hand, more endogenous protective mechanisms exist against FRs in the brain than in the liver, such as

SOD (e.g., the catalytic activity of the isoforms Cu-Zn-SOD (SOD1) and Mn-SOD (SOD2)). These mechanisms are highly expressed in neurons [18] and possibly explain the lower increase in the level of FRs in the brain versus liver tissue. Since OS and cell damage occurs when the concentration of FRs exceeds the capacity of the scavenging system, the redox system is essential for the health of cells [18]. The only way to prevent cell damage or death is to strengthen the scavenging system, especially GSH. The current data reveal a rapid response of the antioxidant system to the imbalance between FR and GSH in brain tissue. This response likely involves a repair mechanism, physical defenses, and/or enzymatic antioxidant defenses (e.g., SOD, CAT, GPx, and GR) [2]. As observed with oxidation due to aging, treatment with 3,5-DMB (a thiol scavenger) produced a decrease in the level of GSH in a time-dependent manner after 3,5-DMB administration, resulting in a concomitant increase in the FR content of cells (Figure 3). Rapid response to a disturbance in redox homeostasis was anticipated for brain tissue because of its vital role in the organism. The significant decrease in the concentration of GSH in 15-month-old rats treated with 3,5-DMB led to a sharp and rapid increase in the FR content in both brain and liver tissues. Interestingly, a significant increase in the level of GSH was detected in brain tissue 1 h after 3,5-DMB treatment. At the same time, the level of FRs was lower in the brain tissue compared with liver tissue. Since 3,5-DMB decreased the level of thiols, the elevated GSH content at the early stages of treatment probably stemmed from an attempt by cells to maintain redox homeostasis. At 16 h posttreatment of adult rats, the concentration of GSH was 1.27-fold lower and the FR content was 1.42-fold higher than those in untreated samples, revealing that the imbalance in the adult rat brain was not completely repaired. According to a previous study, the immature brain of young rats is more vulnerable to OS in comparison to the mature adult brain [18]. The present finding of a 3,5-DMB-induced decrease in the level of GSH in young rats gives insight into how early-stage tissues face an elevated FR content, which is initially met with an increase of the concentration GSH (compared to that in untreated samples), similar to the response during the aging process. A daily dose of 3,5-DMB in young rats might cause that they age more quickly, generating “old juvenile-rats.” However, the 3,5-DMB effects on health, phenotype, and behavior need to be studied. On the other hand, it had been reported molecules that cause the opposite effect to 3,5-DMB treatment. One of these molecules is resveratrol that produces cell rejuvenation in the liver [21].

This initial 3,5-DMB-induced antioxidant response was more efficient in the brain than in the liver (Figure 3). Hence, the antioxidant response to a disturbance of redox homeostasis was more efficient in brain tissue than in liver tissue. It has been reported that GSH imbalance might cause diseases such as cancer, neurodegenerative diseases, cystic fibrosis, and HIV [22]. According to this, the systematic effect of 3,5-DMB on the organisms might cause a sustained GSH imbalance that may cause diseases.

It has been reported that there are approximately 1.1×10^{-9} mol GSH/embryo [23] or 1.91×10^{-5} mol GSH/g protein [24] in a Sprague-Dawley rat embryo (Wistar derived). Based

on extrapolation from the current data, 3.02×10^{-4} mol GSH/g brain tissue and 5.04×10^{-4} mol GSH/g liver tissue should be found in a Wistar rat embryo, suggesting that FRs are tightly regulated by rapid changes in the GSH/GSSG relation.

5. Conclusions

Finally, we concluded that the thiol compound selectively reacts with the olefinic carbons of 3,5-DMB due to their local softness, and the reaction of thiol species with 3,5-DMB shows selectivity for vinylic carbon from the α,β -unsaturated group but not for the carbonyl carbon group. The reaction is not stereoselective, as evidenced by the clear multiplicity of signals in the spectra, indicating a diastereomeric mixture.

The current study attempts to provide insights into the relationship among FRs, reducing agents such as GSH, and the aging process. There is a relationship between age, the concentration of GSH, and the level of FRs. Young rats had a higher level of GSH and a lower level of FRs, while the opposite results were found in adult rats. Given the lower concentration of GSH and abrupt changes in the FR content in adult rats, GSH appears to be a regulable variable, and FRs appear to be a regulator variable, meaning that GSH might modulate the FR production. Despite thiols and FR have an important contribution to the systemic metabolism, there is an inverse relation between these two molecular families, thiols, and FR which is apparently a mechanism to recover redox homeostasis. However, the expression of the enzymes involved in redox homeostasis before and after 3,5-DMB administration and the nature of FR needs to be investigated.

Data Availability

Data used to support the findings of this study have been deposited in the Mendeley Data V1 repository (doi:10.17632/9n8r8m5kk7.1).

Conflicts of Interest

The authors declare that there is no conflict of interest regarding the publication of this paper.

Acknowledgments

This research received financial support from CONACYT, SIP, COFAA, and the Instituto Politécnico Nacional (Mexico). J. G. Trujillo-Ferrara is EDI-IPN, COFAA, and SNI-CONACYT fellow.

Supplementary Materials

Herein, we investigate whether 3,5-DMB reacts with N-acetyl cysteine by NMR spectrometry, and according to our results, this reaction follows a 1,4-Michael type mechanism (Supplementary Materials). Furthermore, we measure the concentrations of reduced glutathione (GSH) and free radicals (FRs) in brain and liver tissue of male Wistar rats of different ages. The results showed that concentration of GSH was higher

in young rats than that in old rats, while the concentration of FRs, measurement by electronic paramagnetic resonance (Supplementary Materials) was higher in adult rats than that in young rats, suggesting an inverse relationship between GSH and FRs. Similar relationships were found when thiol scavenger maleimide was used. Supplementary Figure S1: analysis of the reaction of 3'5'-DMB with N-acetyl cysteine. A fragment of the NMR spectrum for 3'5'-DMB is shown. For COSY H-H and 1H and 406 13C NMR at 270 MHz, the spectra show displacements that indicate a 1,4-Michael type mechanism. Ha and Hb correspond to hydrogen atoms Supplementary Figure S2: EPR spectra used to determine the number of free radicals. (A) Brain control sample, (B) liver control sample, and (C) brain sample of an animal treated with 3'5'-DMB. (Supplementary Materials)

References

- [1] A. Phaniendra, D. B. Jestadi, and L. Periyasamy, "Free radicals: properties, sources, targets, and their implication in various diseases," *Indian Journal of Clinical Biochemistry*, vol. 30, no. 1, pp. 11–26, 2015.
- [2] M. Valko, D. Leibfritz, J. Moncol, M. T. D. Cronin, M. Mazur, and J. Telser, "Free radicals and antioxidants in normal physiological functions and human disease," *The International Journal of Biochemistry & Cell Biology*, vol. 39, no. 1, pp. 44–84, 2007.
- [3] S. G. Rhee, H. A. Woo, I. S. Kil, and S. H. Bae, "Peroxiredoxin functions as a peroxidase and a regulator and sensor of local peroxides," *Journal of Biological Chemistry*, vol. 287, no. 7, pp. 4403–4410, 2012.
- [4] K. M. Holmström and T. Finkel, "Cellular mechanisms and physiological consequences of redox-dependent signalling," *Nature Reviews Molecular Cell Biology*, vol. 15, no. 6, pp. 411–421, 2014.
- [5] H. Sies, "1 - Oxidative Stress: Introductory Remarks," in *Oxidative Stress*, H. Sies, Ed., pp. 1–8, Academic Press, London, 1985.
- [6] L. J. Machlin and A. Bendich, "Free radical tissue damage: protective role of antioxidant nutrients," *The FASEB Journal*, vol. 1, no. 6, pp. 441–445, 1987.
- [7] R. Hosseinzadeh, K. Khorsandi, and G. Hosseinzadeh, "Graphene oxide-methylene blue nanocomposite in photodynamic therapy of human breast cancer," *Journal of Biomolecular Structure and Dynamics*, vol. 36, no. 9, pp. 2216–2223, 2017.
- [8] E. Andrade-Jorge, M. Godínez-Victoria, E. S.-T. Luvia, L. Humberto Fabila-Castillo, and J. G. Trujillo-Ferrara, "Aryl maleimides as apoptosis inducers on L5178-Y murine leukemia cells (in silico, in vitro and ex vivo study)," *Anti-Cancer Agents in Medicinal Chemistry (Formerly Current Medicinal Chemistry-Anti-Cancer Agents)*, vol. 16, pp. 1615–1621, 2016.
- [9] H. B. Elajaili, L. Hernandez-Lagunas, K. Ranguelova, S. Dikalov, and E. Nozik-Grayck, "Use of electron paramagnetic resonance in biological samples at ambient temperature and 77 K," *Journal of Visualized Experiments*, vol. 143, no. 143, article e58461, 2019.
- [10] J. Trujillo-Ferrara, R. Santillan, H. I. Beltrán, N. Farfán, and H. Höpfl, "¹H and ¹³C NMR spectra for a series of arylmaleamic acids, arylmaleimides, arylsuccinamic acids and arylsuccinimides," *Magnetic Resonance in Chemistry*, vol. 37, no. 9, pp. 682–686, 1999.

- [11] G. L. Ellman, "Tissue sulfhydryl groups," *Archives of Biochemistry and Biophysics*, vol. 82, no. 1, pp. 70–77, 1959.
- [12] J. A. Weil, J. R. Bolton, and J. E. Wertz, *Electron paramagnetic resonance: elementary theory and practical applications*, Wiley, New York, NY, USA, 1994.
- [13] G. Carrasco-Torres, R. Baltiérrez-Hoyos, E. Andrade-Jorge, S. Villa-Treviño, J. G. Trujillo-Ferrara, and V. R. Vásquez-Garzón, "Cytotoxicity, oxidative stress, cell cycle arrest, and mitochondrial apoptosis after combined treatment of hepatocarcinoma cells with maleic anhydride derivatives and quercetin," *Oxidative Medicine and Cellular Longevity*, vol. 2017, Article ID 2734976, 16 pages, 2017.
- [14] P. Sengupta, "The laboratory rat: relating its age with human's," *International Journal of Preventive Medicine*, vol. 4, no. 6, pp. 624–630, 2013.
- [15] J. A. H. Schwöbel, D. Wondrousch, Y. K. Koleva, J. C. Madden, M. T. D. Cronin, and G. Schüürmann, "Prediction of Michael-type acceptor reactivity toward glutathione," *Chemical Research in Toxicology*, vol. 23, no. 10, pp. 1576–1585, 2010.
- [16] R. M. LoPachin, B. C. Geohagen, and L. U. Nordstroem, "Mechanisms of soft and hard electrophile toxicities," *Toxicology*, vol. 418, pp. 62–69, 2019.
- [17] M. Jiang, D. Bi, F. Huang, J. Wang, and B. Li, "Correlation between persistent free radicals of biochar and bio-oil yield at different pyrolysis temperatures," *BioResources*, vol. 15, no. 1, p. 13, 2020.
- [18] K. Blomgren and H. Hagberg, "Free radicals, mitochondria, and hypoxia-ischemia in the developing brain," *Free Radical Biology and Medicine*, vol. 40, no. 3, pp. 388–397, 2006.
- [19] M. Erecinska, S. Cherian, and I. A. Silver, "Energy metabolism in mammalian brain during development," *Progress in Neurobiology*, vol. 73, no. 6, pp. 397–445, 2004.
- [20] H. Shih, B. Lee, R. J. Lee, and A. J. Boyle, "The aging heart and post-infarction left ventricular remodeling," *Journal of the American College of Cardiology*, vol. 57, no. 1, pp. 9–17, 2011.
- [21] S. B. Baltaci, R. Mogulkoc, and A. K. Baltaci, "Resveratrol and exercise," *Biomedical Reports*, vol. 5, no. 5, pp. 525–530, 2016.
- [22] D. M. Townsend, K. D. Tew, and H. Tapiero, "The importance of glutathione in human disease," *Biomedicine & Pharmacotherapy*, vol. 57, no. 3-4, pp. 145–155, 2003.
- [23] T. L. McNutt and C. Harris, "Lindane embryotoxicity and differential alteration of cysteine and glutathione levels in rat embryos and visceral yolk sacs," *Reproductive Toxicology*, vol. 8, no. 4, pp. 351–362, 1994.
- [24] C. Harris, M. J. Namkung, and M. R. Juchau, "Regulation of intracellular glutathione in rat embryos and visceral yolk sacs and its effect on 2-nitrosofluorene-induced malformations in the whole embryo culture system," *Toxicology and Applied Pharmacology*, vol. 88, no. 1, pp. 141–152, 1987.

Research Article

Lupeol Counteracts the Proinflammatory Signalling Triggered in Macrophages by 7-Keto-Cholesterol: New Perspectives in the Therapy of Atherosclerosis

Sarmistha Saha,¹ Elisabetta Profumo,¹ Anna Rita Togna,² Rachele Riganò,¹ Luciano Saso ,² and Brigitta Buttari ¹

¹Department of Cardiovascular and Endocrine-Metabolic Diseases, and Aging, Italian National Institute of Health, Rome 00161, Italy

²Department of Physiology and Pharmacology “Vittorio Ersamer”, Sapienza University of Rome, Rome 00161, Italy

Correspondence should be addressed to Brigitta Buttari; brigitta.buttari@iss.it

Received 24 June 2020; Revised 6 August 2020; Accepted 26 August 2020; Published 27 September 2020

Academic Editor: Hassan Obied

Copyright © 2020 Sarmistha Saha et al. This is an open access article distributed under the Creative Commons Attribution License, which permits unrestricted use, distribution, and reproduction in any medium, provided the original work is properly cited.

Macrophage activation and polarization play a central role in atherosclerotic plaque fate. The M1/M2 activation phenotypes represent two profiles of the macrophage polarization state. During atherosclerosis regression or stabilization, macrophages switch from M1 proinflammatory phenotype to M2 anti-inflammatory reparative one. Here, we investigated whether the natural compound lupeol, a pentacyclic triterpene, induces phenotypical and functional changes in human M1 macrophages and counteracts the proinflammatory signalling triggered by 7-keto-cholesterol (7KC), a major product of oxidative stress-mediated cholesterol oxidation. Flow cytometric and immunochemical analysis showed that the treatment with lupeol of M1 monocyte-derived macrophages $M_{(IFN-\gamma/LPS)}$ specifically stimulated these cells to upregulate the expression of the anti-inflammatory cytokines interleukin- (IL-)10 and TGF- β , and of the scavenger receptor CD36, whereas downregulated the proinflammatory cytokine IL-12 and the M1 activation marker HLA-DR. Pretreatment of macrophages with lupeol prevented the release of IL-12, IL-1 β , and the upregulation of HLA-DR expression triggered by 7KC and increased the IL-10 production and CD36 expression. This treatment also prevented the impairment of endocytosis triggered by 7KC and prevented 7KC-induced foam cell formation by reducing the lipid droplet accumulation in M1-polarized THP-1 macrophages, whereas showed an additive effect in reactive oxygen species (ROS) production. Western blotting analysis of autophagy markers LC3-I/II and p62-SQSTM1 in M1-polarized THP-1 macrophages demonstrated that lupeol activated autophagy as indicated by increased LC3-II levels, and by marked inhibition of p62. These findings indicate that lupeol has a cytoprotective effect on 7KC-proinflammatory signalling by efficiently switching the macrophage polarization toward an anti-inflammatory phenotype, probably through the activation of the autophagy pathway by increasing ROS production, the reduction of cellular lipid accumulation, and an overall reduction of proinflammatory phenotype. Thus, our data demonstrating an anti-inflammatory and immunomodulatory activity of lupeol in human M1 macrophages suggest its usefulness as an adjunctive drug in the therapy of atherosclerosis.

1. Introduction

Atherosclerosis is a chronic inflammatory disease characterized by the accumulation of immune cells such as macrophages and foam cells in the intima of the vessel wall [1, 2]. Both cells contribute to the classical atherosclerotic plaque destabilization and rupture by secreting proinflammatory cytokines and matrix metalloproteinases. The fate of atherosclerotic plaques is highly

dependent on the balance between the recruitment and activation of monocyte-derived macrophages and their clearance from the vessel wall [3, 4]. A characteristic feature of macrophages is their plasticity due to the ability to reversibly change their phenotype and function in response to signals in the microenvironment. The so-called M1 and M2 activation phenotypes represent two profiles of the macrophage polarization state [5]. The predominant production of proinflammatory

cytokines and reactive oxygen species (ROS) by the M1 macrophage phenotype promotes atheroma formation, while the expression of immunosuppressive cytokines and growth factors by the M2 state resolves atheroma by stimulating angiogenesis and phagocytosis [4, 6, 7]. Thus, the M1/M2 phenotype balance is possibly responsible for cholesterol crystal formation or disappearance [8].

The molecular and cellular mechanisms involving macrophage polarization and activation play a central role in plaque progression and stability. Recent studies have shown that oxysterols, oxidative stress-mediated cholesterol oxidation products, which are abundant in atherosclerotic lesions, may switch macrophage phenotype towards a proinflammatory profile [9]. We recently demonstrated that 7-keto-cholesterol (7KC), the most abundant cholesterol oxidation product within atherosclerotic plaques [10, 11], is responsible for switching the macrophage phenotype towards a proinflammatory profile [9].

Few natural compounds such as apigenin, curcumin, and resveratrol have been shown to inhibit the proinflammatory functions of adipose tissue macrophages which were polarized to M1 cells by lipopolysaccharide [12–16]. A range of synthetic chemical entities and natural plant-derived compounds have been characterized for their ability to modulate inflammation and related signalling [12]. Moreover, preclinical as well as clinical studies have shown that the dietary phytochemicals lower the risk of developing coronary heart diseases [12]. Hence, this evidence prompted researchers to investigate the potential therapeutic interventions with plant-derived natural products.

Although their ability to modulate the M1/M2 phenotype is clear, it is still unclear whether these molecules could be practically effective as therapeutic agents for the treatment of atherosclerosis-related inflammation and the exact mechanisms behind their action. Therefore, it is worthwhile to add mechanistic insights into the effects of natural plant-derived compounds to modulate macrophage polarization.

In this regard, lupeol, a pentacyclic triterpene—widely available in fruits such as mango, red grapes, olives, and strawberry as well as in vegetables such as cucumber, white cabbage, and tomato—has been shown to exhibit potent anti-inflammatory activity by decreasing the release of proinflammatory cytokines such as TNF- α and IL- β in lipopolysaccharide-(LPS)-treated macrophages in rat and mouse models of inflammation [17–19]. Lupeol has also been shown to inhibit latent membrane protein 1-induced NF- κ B activation and consequently to switch proinflammatory macrophages into anti-inflammatory phenotype in experimental inflammatory bowel disease [20]. Furthermore, it has been also suggested that a derivative molecule of lupeol induces cell death in a cancer cell line by inducing autophagy rather than apoptosis and necrosis [21]. Growing evidence demonstrates that dysfunctional autophagy plays an important role in atherosclerotic plaque destabilization and the overall development of the disease [22–26]. Recently, it has also been revealed that the induction of autophagy in macrophages may have a plaque-stabilizing effect [24]. Therefore, the activation of the autophagy pathway could be a potential therapeutic strategy for atherosclerosis. This motivated us to investigate whether lupeol modulates the phenotype and function of human M1

macrophages by counteracting the 7KC-proinflammatory signalling. In particular, we investigated whether lupeol is able to induce autophagy in 7-KC-treated M1 macrophages.

In this work, we used immunochemical and flow cytometric analysis to investigate the endocytosis, ROS, cytokine production, surface marker expression, cellular lipid levels, and autophagy markers in human classically activated macrophages ($M_{(IFN-\gamma/LPS)}$), also known as M1 macrophages pretreated with lupeol and exposed to the proinflammatory stimulus 7KC.

2. Materials and Methods

2.1. Reagents. Recombinant human (rh) macrophage colony-stimulating factor (M-CSF) was purchased from R&D System (Minneapolis, MN). Fetal bovine serum (FBS) was purchased from Hyclone Laboratories (Logan, UT). Anti-CD14-coated microbeads, human IFN- γ 1b (IFN- γ), fluorescein isothiocyanate- (FITC-) conjugated mAbs to human leukocyte antigen-D region related (HLA-DR), and VioGreen-conjugated mAbs to CD36 were purchased from Miltenyi Biotec (Gladbach, Germany). Lupeol, 7KC, phorbol 12-myristate 13-acetate (PMA), lipopolysaccharides from *Escherichia coli* (LPS), FITC-dextran, and 2',7'-Dichlorofluorescein Diacetate (H2DCF-DA) were purchased from Sigma-Aldrich (Milan, Italy). Sytox Blue nucleic acid stain and 4',6-diamidino-2-phenylindole (DAPI) were purchased from Thermo Fisher Scientific (Waltham, Massachusetts, USA).

2.2. Preparation of Human $M_{(IFN-\gamma/LPS)}$ Macrophages. Peripheral blood mononuclear cells (PBMCs) were obtained from buffy coats of healthy blood donors collected from the Transfusion Center at the Sapienza University of Rome [27]. The study was conducted in accordance with the Helsinki Declaration of 1975 and 1983. Briefly, PBMCs were isolated by density gradient and CD14⁺ monocytes were purified by incubating PBMCs with anti-CD14-coated microbeads, followed by sorting with a magnetic device. Monocytes were then induced to differentiate in the presence of rhM-CSF to obtain monocyte-derived macrophages. Human leukemic cell line THP-1 (ATCC, Manassas, VA, USA) was grown in a complete medium (RPMI 1640 supplemented with 1% nonessential amino acids, sodium pyruvate (1%), Penicillin (50 units/mL), Streptomycin (50 μ g/mL), 2-mercaptoethanol (5×10^{-5} M) and 10% FBS) and prior to the experiments; THP-1 cells were differentiated to macrophages by incubating with 10 ng/mL PMA in culture medium for 48 hours, followed by a wash with phosphate-buffered saline (PBS) and finally grown in culture medium for 24 hours. Human monocyte-derived macrophages (primary macrophages) or THP-1 macrophages were then polarized towards the M1 phenotype using 10 ng/mL IFN- γ and 10 ng/mL toll-like receptor 4 ligand LPS $M_{(IFN-\gamma/LPS)}$ for an additional 24 h. All cells were cultured in complete medium, washed with warm PBS, and harvested using TrypLE™ Express Enzyme (Gibco, Grand Island, NY, USA).

2.3. Treatment of $M_{(IFN-\gamma/LPS)}$ Macrophages with Lupeol and/or 7-Keto-Cholesterol. Human primary $M_{(IFN-\gamma/LPS)}$

macrophages and THP-1 $M_{(\text{IFN-}\gamma/\text{LPS})}$ macrophages were treated or not with lupeol (10–50 μM) for 1 hour at 37°C and 5% CO_2 . The cells were then stimulated with 7KC dissolved in ethanol (15 μM) for 20 hours. The inflammatory stimuli LPS (200 ng/mL) and ethanol were used as controls. Cell viability was measured employing the Trypan blue exclusion assay, and cell morphology was checked by a light microscope.

2.4. Secretome Profile of Cytokines in Macrophage Culture Supernatants. Supernatants from human primary $M_{(\text{IFN-}\gamma/\text{LPS})}$ macrophages (7×10^5 cells per mL) pretreated with lupeol for 1 hour and then exposed to 7KC (20 nm/L) for a further 20 hours in 24-well plates were collected, centrifuged, and stored at -80°C. The levels of IL-12 p70, IL-1 β , IL-10, and TGF- β into the conditioned medium were determined by enzyme-linked immunosorbent assay (ELISA; OptEIA kits; BD Biosciences) following the manufacturer's instructions. The limits of detection were as follows: IL-10 and IL-1 β : 16 pg/mL; IL-12p70: 7.8 pg/mL; and TGF- β : 62.5 pg/mL.

2.5. Flow Cytometric Analysis of Macrophage Phenotype. To determine macrophage phenotypic surface markers, human primary $M_{(\text{IFN-}\gamma/\text{LPS})}$ macrophages were stained with anti-HLA-DR and anti-CD36 mAbs or with isotype-matched control mAbs for 30 minutes at 4°C and then analyzed by flow cytometry on a Gallios Flow Cytometer (Beckman Coulter) equipped with three lasers (488 nm, 638 nm, and 405 nm), and the results were further analyzed by the use of fluorescence-activated cell sorting (FACS) Kaluza analysis software (Beckman Coulter).

2.6. Flow Cytometric Analysis of Macrophage Endocytosis. Macrophage mannose receptor-mediated endocytosis was determined by the method as previously described [28]. In brief, human primary $M_{(\text{IFN-}\gamma/\text{LPS})}$ macrophages (1×10^6 cells/mL) were incubated with FITC-dextran (1 mg/mL) for 45 min at 37°C. Internalization ability was analyzed as the percentage and the mean fluorescence intensity (MFI) of FITC-positive cells by flow cytometry and then analyzed by flow cytometry on a Gallios Flow Cytometer (Beckman Coulter). The results were further analyzed by the use of fluorescence-activated cell sorting (FACS) Kaluza analysis software (Beckman Coulter). Dead cells were excluded by 1 μM Sytox Blue nucleic acid staining.

2.7. Flow Cytometric Analysis of Intracellular Lipid Levels. *In vitro* model of foam cell formation induced by the oxysterol mixture 7 β -hydroxycholesterol and 7KC was previously described by Yuan et al. [29]. Here, THP-1 $M_{(\text{IFN-}\gamma/\text{LPS})}$ macrophages were treated with only 7KC. In brief, THP-1 $M_{(\text{IFN-}\gamma/\text{LPS})}$ macrophages (1×10^6 cells/mL) were pretreated with lupeol for 1 hour and then exposed to 7KC (20 nm/L) for a further 20 hours in complete medium. Cells were stained with LipidSpot™ 488 Lipid Droplet Stains according to the manufacturer's instructions (Biotium, USA). LipidSpot™ dyes are fluorogenic neutral lipid stains that rapidly accumulate in lipid droplets, where they become brightly fluorescent (Abs/Em: 427/585 nm). After 30 min of incubation in the dark at 37°C, cells were centrifuged and the pellet

was washed twice with ice-cold PBS/FCS and stained with DAPI (4 $\mu\text{g}/\text{mL}$) to exclude dead cells. At least 5×10^3 cells/sample was analyzed by flow cytometry (Gallios Flow Cytometer; Beckman Coulter).

2.8. Flow Cytometric Analysis of Reactive Oxygen Species (ROS) Production. The production of ROS in human primary $M_{(\text{IFN-}\gamma/\text{LPS})}$ macrophages was measured through H2DCF-DA staining. In brief, macrophages (1×10^6 cells/mL) were incubated with H2DCF-DA at a final concentration of 2.5 μM . After 45 min of incubation in the dark at 37°C, cells were centrifuged, and the pellet was washed twice with ice-cold PBS/FCS, and then fixed with 1% formaldehyde. At least 5×10^3 cells/sample were analyzed by flow cytometry (Gallios Flow Cytometer; Beckman Coulter). DCFDA fluorescence intensity was measured in FL-1 with an excitation wavelength of 488 nm and an emission wavelength of 530 nm.

2.9. Western Blot Analysis of Macrophage Lysates for Autophagy Markers. $M_{(\text{IFN-}\gamma/\text{LPS})}$ polarized THP-1 macrophages and primary macrophages were lysed on ice in Cellytic buffer (Sigma Aldrich) plus protease and phosphatase inhibitors (protease inhibitor cocktail: 1 mM sodium fluoride, 1 mM sodium orthovanadate, and 1 mM sodium molybdate; 1 mM phenylmethylsulfonyl fluoride; and 1 mM phosphoinositidase C (Sigma Aldrich)). Other drugs used were chloroquine (ChQ; 50 μM), 3-metyladenine (3-MA; 5 mM), and rapamycin (Rapa; 2 μM), all purchased from Selleckchem (Verona, Italy). Lysates were incubated for 20 min at 4°C and centrifuged for 15 min at 16,000 \times g and 4°C to pellet the insoluble material. Samples were then stored at -20°C until use. At the time of analysis, the samples were denatured in 4 \times Laemmli Sample Buffer (Bio-Rad), added with 50 mM DTT, and then heated for 5 min at 95°C. Samples were then loaded per lane in equal volumes and separated by electrophoresis in 4-15% Mini-PROTEAN® TGX Stain-Free™ Precast Gels (Bio-Rad, Milan, Italy). Protein samples were then transferred electrophoretically in Towbin buffer (25 mM Tris, 192 mM glycine, pH 8.3, and 20% (v/v) methanol) to polyvinylidenedifluoride membranes (Millipore, Milan, Italy). After protein transfer, membranes were imaged for stain-free staining and total protein was quantified using Imagemag 6.0.1 (Bio-Rad) to correct for possible protein loading inaccuracy. The membranes were then blocked with 2% (wt/vol) low-fat milk in Tris-buffered saline (137 mM NaCl, 20 mM Tris-HCl, pH 7.6) containing 0.1% Tween 20 (TBS-T) for 1 h at room temperature. The membranes were further incubated overnight at 4°C with the primary antibodies rabbit anti-LC3B (at dilution 1:2000) and mouse anti-p62-SQSTM1 (1:1000). All the antibodies were procured from Novus Biologicals (Bio-Techne Ltd, Milan, Italy). After three washes with TBS-T, the membranes were incubated for 2 h, at room temperature, with an alkaline phosphatase-linked secondary antibody, specific to rabbit and mouse IgG (1:10000). Protein immunoreactive bands were visualized by chemifluorescence with the Clarity Western ECL Substrate (Bio-Rad) in a ChemiDoc Imaging System (Bio-Rad). Some membranes were reprobated with a monoclonal anti- β -actin Ab (1:5000; Sigma) for equal protein loading

control. The optical density of the bands was quantified with the Imagemab 6.0.1 (Bio-Rad). The results were normalized to total protein and expressed as the relative amount compared with control.

2.10. Statistical Analysis. Mean values and standard deviations (SD) were calculated for each variable under study. All the statistical analysis was performed by GraphPad Prism 8 software (San Diego, CA, USA). Normally distributed data were analyzed using one-way ANOVA with a Tukey post hoc test. Values of $P < 0.05$ were considered statistically significant.

3. Results

3.1. Lupeol Skews $M_{(IFN-\gamma/LPS)}$ towards Anti-Inflammatory Phenotype and Counteracts the Proinflammatory Signalling Triggered in Macrophages by 7-Keto-Cholesterol. Lupeol is a pentacyclic triterpene with potent anti-inflammatory activity [16]. Pentacyclic triterpenes have been found to exhibit anti-inflammatory activity although their role in macrophage polarization and the mechanism by which this process could take place has yet to be elucidated [20]. In order to confirm the hypothesis that lupeol could be able to exhibit antiatherosclerotic activity by inhibiting inflammatory changes, human CD14⁺ monocytes were differentiated into macrophages, polarized toward M1-like phenotype (primary $M_{(IFN-\gamma/LPS)}$ macrophages), and further treated with different concentrations of lupeol. Dose-response experiments demonstrated that 50 μM was the highest tolerated concentration of lupeol that did not affect macrophage viability in the Trypan blue exclusion assay and or cell morphology (see Figure S1 in the Supplementary Material for comprehensive result analysis). Therefore, we selected three different concentrations of 10, 25, and 50 μM of lupeol to investigate the total macrophage secretory capacity by determining the secretome profile of cytokines in the cell supernatants by ELISA. After incubation of the macrophages with 7KC or LPS, we observed a significant increase in the release of the proinflammatory cytokines IL-12, IL-1 β , whereas the release of the anti-inflammatory cytokines TGF- β and IL-10 was reduced as compared with unstimulated $M_{(IFN-\gamma/LPS)}$ cells (in Figure 1). Of note, the treatment of $M_{(IFN-\gamma/LPS)}$ macrophages with lupeol at 25 μM induced a significant increase of IL-10 and TGF- β production, whereas at 50 μM significantly decreased IL-12 (in Figure 1). The pretreatment with lupeol prevented the increase of IL-12 (at 25 μM) and IL-1 β (at 25 and 50 μM) in the cell supernatants induced by 7KC-treated macrophages. At 25 μM lupeol increased significantly the secretion of IL-10 in 7KC-treated macrophages (in Figure 1).

The flow cytometric analysis of the M1- or M2-related surface antigens HLA-DR and CD36 was conducted in primary $M_{(IFN-\gamma/LPS)}$ macrophages (in Figure 2). Analysis of surface antigen expressions of macrophages shows a reduction in the percentage of HLA-DR positive cells ($P < 0.024$) and an increase in the CD36 expression (MFI) ($P < 0.048$) after the treatment with 25 μM lupeol. As expected, 7KC induced an increase in the HLA-DR expression (MFI) ($P < 0.009$), but it did not alter the expression of the CD36.

The pretreatment with 25 μM lupeol prevented the increase of HLA-DR expression by 7KC ($P < 0.034$) and simultaneously increased the expression of CD36 ($P < 0.04$) on $M_{(IFN-\gamma/LPS)}$ macrophages. These results confirm that lupeol exerts anti-inflammatory activity by switching $M_{(IFN-\gamma/LPS)}$ macrophage phenotype toward an anti-inflammatory phenotype.

3.2. Lupeol Prevents the Impairment of Endocytosis in 7-Keto-Cholesterol-Treated $M_{(IFN-\gamma/LPS)}$ Macrophages. Endocytosis is a crucial factor in macrophage-mediated host defence, which involves the internalization and destruction of pathogens. Unlike anti-inflammatory, proinflammatory macrophages have shown less endocytic ability [27]. Flow cytometric analysis showed that the unstimulated primary $M_{(IFN-\gamma/LPS)}$ macrophages largely resulted positive for the FITC-dextran uptake. As expected, we found a significant decrease in the uptake of FITC-dextran due to the stimulation of $M_{(IFN-\gamma/LPS)}$ macrophages with the proinflammatory signalling triggered by 7KC (in Figure 3). Of note, the pretreatment of the cells with lupeol was able to prevent the reduction of endocytosis ability induced by 7KC, thus suggesting a less proinflammatory state of macrophages (in Figure 3).

3.3. Lupeol Prevents 7-Keto-Cholesterol-Induced Lipid Accumulation and Enhances Reactive Oxygen Species (ROS) Production in $M_{(IFN-\gamma/LPS)}$ Macrophages. To further confirm the ability of lupeol to counteract the atherosclerotic process, we used the 7KC to increase lipid accumulation in $M_{(IFN-\gamma/LPS)}$ polarized THP-1 macrophages. By flow cytometric analysis, we studied the ability of lupeol to reduce the accumulation of the LipidSpot™ dye induced by 7KC on THP-1 $M_{(IFN-\gamma/LPS)}$ macrophages. As expected, the mean fluorescence intensity for the LipidSpot™ significantly increased after the 20-hour exposure of $M_{(IFN-\gamma/LPS)}$ macrophages to 7KC (in Figure 4(a)). Of note, the 25 μM lupeol prevented 7KC-induced lipid accumulation in $M_{(IFN-\gamma/LPS)}$ macrophages (in Figure 4(a)). Previous studies showed that inflammatory macrophages release ROS, thus exacerbating oxidative stress in atherosclerosis [30, 31]. For this reason, we analyzed flow cytometry ROS production in primary $M_{(IFN-\gamma/LPS)}$ macrophages stimulated with 7KC after pretreatment or not with lupeol. As expected, we observed that the treatment of the $M_{(IFN-\gamma/LPS)}$ macrophages with 7KC (15 μM) induced a significant increase in ROS production ($P < 0.001$, in Figure 4(b)). Of note, lupeol pretreatment resulted in an additive effect in ROS production in macrophages stimulated with 7KC. The maximal effect of lupeol was observed at a concentration of 25 μM ($P < 0.001$; in Figure 4(b)).

3.4. Lupeol Counteracts Dysregulated Autophagy Induced by 7-Keto-Cholesterol in $M_{(IFN-\gamma/LPS)}$ Macrophages. A derivative molecule of lupeol has been shown to induce cell death in cancer cells by inducing autophagy rather than apoptosis and necrosis by accumulating ROS [21]. Adhering to this evidence, we next measured the effects of lupeol on the modulation of autophagy dysfunction in $M_{(IFN-\gamma/LPS)}$ macrophages induced by 7KC [29]. By using western blotting analysis, we evaluated the expression of the autophagic marker

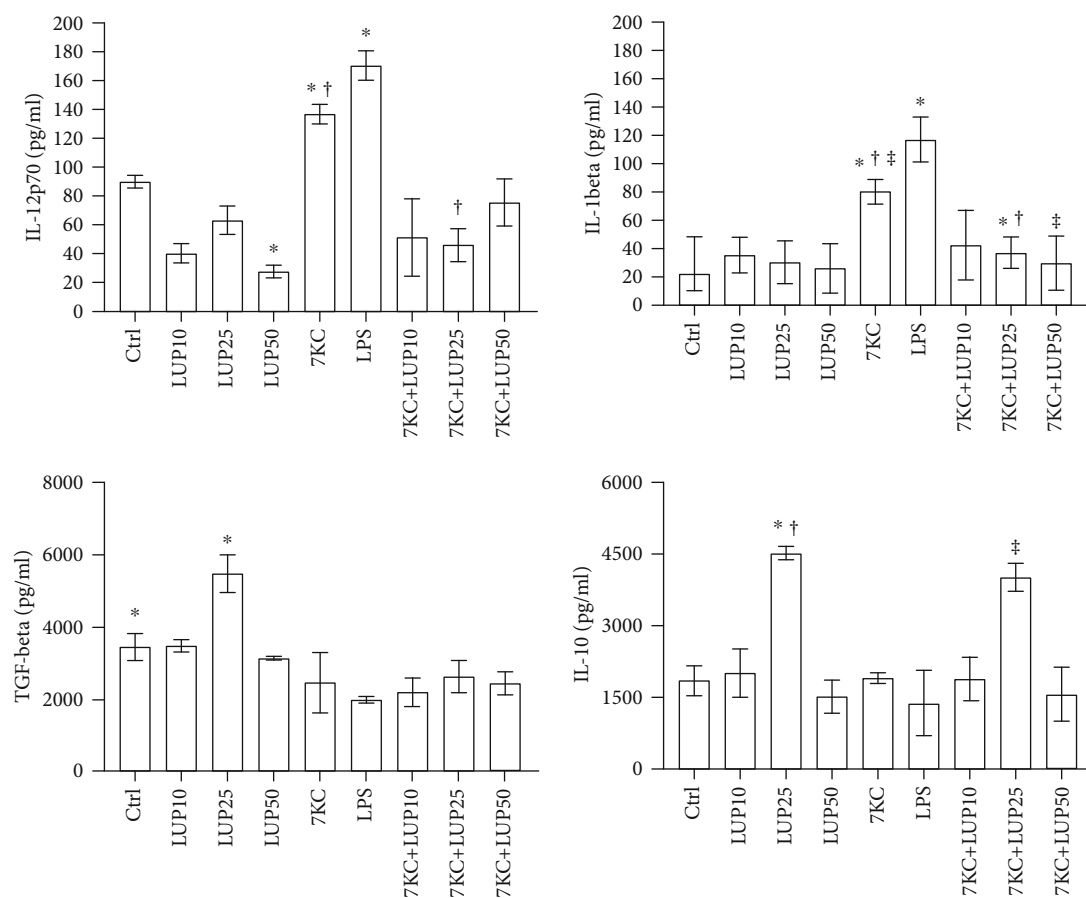
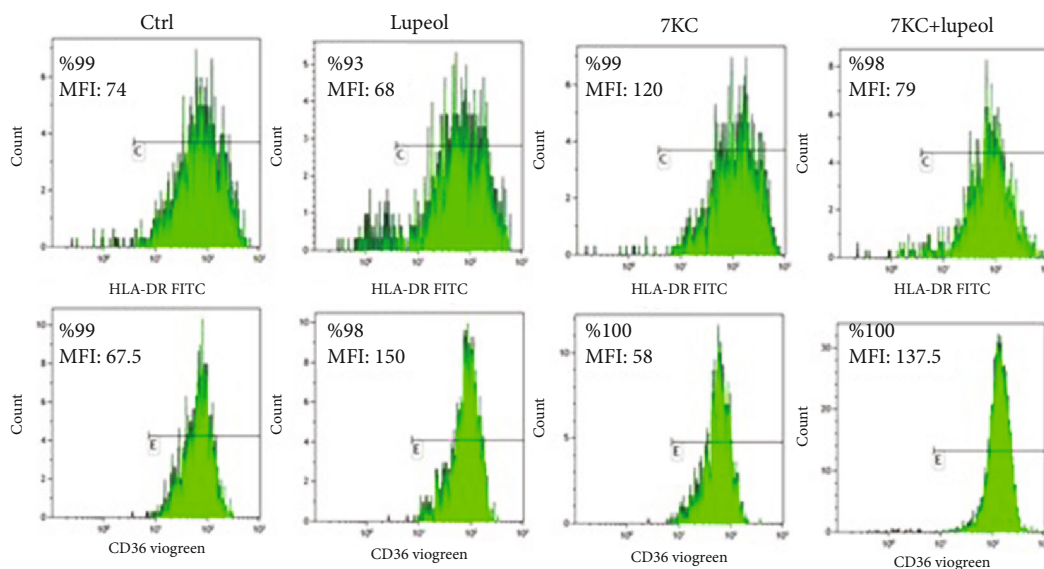


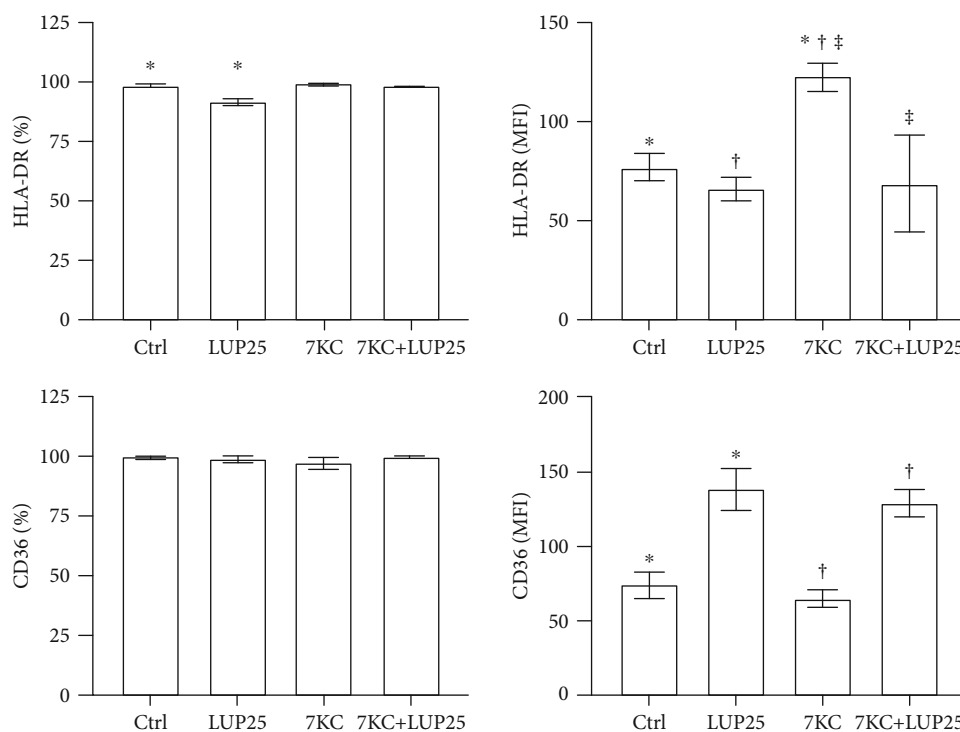
FIGURE 1: Cytokine production in $M_{(IFN-\gamma/LPS)}$ pretreated or not with lupeol before stimulation with 7-keto-cholesterol. Primary $M_{(IFN-\gamma/LPS)}$ macrophages (7×10^5 cells per mL) were stimulated or not with lupeol at the different concentrations for 1 hour and further stimulated with 7KC in complete medium. Supernatants were collected after 20 hours to measure cytokines by specific ELISA experiments. Results are expressed as mean value \pm SD of 3 independent experiments. P values were tested by one-way ANOVA. * \dagger lupeol 10 μ M vs. lupeol 25 μ M; * 7KC-treated group vs. 7KC+lupeol 25 μ M.

LC3-I/II, a widely used marker to monitor the autophagic process and the marker for autophagic clearance p62/sequestosome 1 (SQSTM1) on $M_{(IFN-\gamma/LPS)}$ -polarized THP-1 macrophages and on $M_{(IFN-\gamma/LPS)}$ -polarized primary macrophages pretreated with lupeol and further exposed or not to 7KC. In preliminary experiments, $M_{(IFN-\gamma/LPS)}$ macrophages derived from THP-1 and primary macrophages showed similar changes in the expression of autophagy markers when compared with respective unstimulated samples; in fact, both cells upregulated autophagy markers in response to 7KC (see Figure S2 in the Supplementary Material for comprehensive result analysis). As shown in Figure 5(a), the addition of lupeol or 7KC induced an increase in the transient autophagosomal membrane-bound form of LC3 (LC3-II) in $M_{(IFN-\gamma/LPS)}$ macrophages. It is already known that LC3-II could accumulate due to enhanced autophagosome formation or impaired autolysosomal degradation [32]. To rule out the possibility that the increase of LC3-II was due to inhibited autolysosomal degradation, rather than autophagy stimulation and the respective autophagosome formation, we further evaluated LC3-II flux. For this purpose, $M_{(IFN-\gamma/LPS)}$ -polarized THP-1 macrophages were incubated with lupeol

and 7KC in the presence of the lysosomal protein degradation inhibitor ChQ or of the autophagy inhibitor 3-MA. In these conditions, there was an increase in LC3-II induced by lupeol and 7KC in the presence of ChQ or 3MA, and this increase was significantly higher than in cells treated with inhibitor alone. LC3 has been proposed to function as a receptor for p62/SQSTM1. The LC3-p62 complex is preferentially degraded by autophagy and markedly accumulates in autophagy-deficient cells [33]. Since p62 accumulates when autophagy is inhibited and decreases when autophagy is induced, therefore, p62-SQSTM1 could be used as a marker to study autophagic flux [33]. In our experiments, lupeol inhibited the p62 protein levels, whereas an increase in the p62 protein levels was observed in 7KC, ChQ, and 3-MA treated cells (in Figure 5(b)), which suggests that p62/SQSTM1 autophagic degradation was inhibited by 7KC, similarly to ChQ and 3-MA, whereas lupeol increased the autophagic flux in macrophages. Of note, lupeol was able to significantly reduce the p62 accumulation in $M_{(IFN-\gamma/LPS)}$ -polarized THP-1 macrophages when these cells were treated with 7KC in the presence or absence of autophagy inhibitors (in Figure 5(b)).



(a)



(b)

FIGURE 2: Flow cytometric analysis of surface marker expressions on $M_{(IFN-\gamma/LPS)}$ macrophages. Lupeol skews primary $M_{(IFN-\gamma/LPS)}$ macrophage phenotype towards an anti-inflammatory phenotype and prevents 7-keto-cholesterol (7KC) induced changes in $M_{(IFN-\gamma/LPS)}$ macrophages. $M_{(IFN-\gamma/LPS)}$ primary macrophages were stimulated or not with lupeol at $25 \mu M$ for 1 hour and further stimulated with 7KC and then analyzed for HLA-DR and CD36 expressions by flow cytometry. (a) The results of one representative experiment of three are shown. The number in the histograms shows the percentages of positive cells (%) and the mean fluorescence intensity (MFI). (b) Flow cytometric analysis of surface marker expression on $M_{(IFN-\gamma/LPS)}$ macrophages. Results are expressed as % and MFI (mean \pm SD; $n = 3$). P values were calculated by one-way ANOVA with a Tukey post hoc test.

4. Discussion

The identification of the pathological role played by polarized macrophages has resulted in an increased focus on this paradigm for the identification of new therapeutic approaches

[16, 27]. Lupeol is a ubiquitously distributed pentacyclic triterpene of the edible vegetables, fruits, and many medicinal herbs [17]. Lupeol plays an anti-inflammatory role in several inflammatory disease models such as carrageenan-induced inflammation [34], A23187-stimulated macrophages [35], a

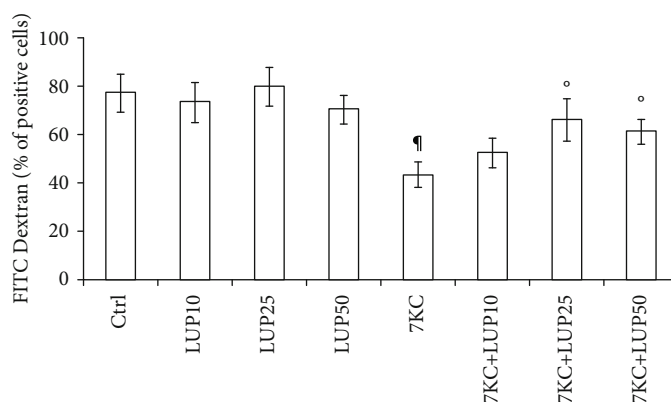


FIGURE 3: Analysis of $M_{(IFN-\gamma/LPS)}$ macrophage endocytosis. Lupeol prevents the impairment of endocytosis induced by 7-keto-cholesterol (7KC) in primary $M_{(IFN-\gamma/LPS)}$ macrophages. Human primary $M_{(IFN-\gamma/LPS)}$ macrophages were incubated with lupeol (10, 25, and 50 μM) followed by stimulation with 7KC (15 μM) and then added with FITC-dextran. The cellular uptake was then analyzed by flow cytometry. Results are expressed as a percentage of positive cells (%) and mean fluorescence intensity (MFI) (mean \pm SD; $n = 3$). P values were tested by one-way ANOVA. *Untreated vs. lupeol; [¶]Untreated control vs. 7KC-treated group; [°]7KC-treated group vs. 7KC+lupeol treated groups.

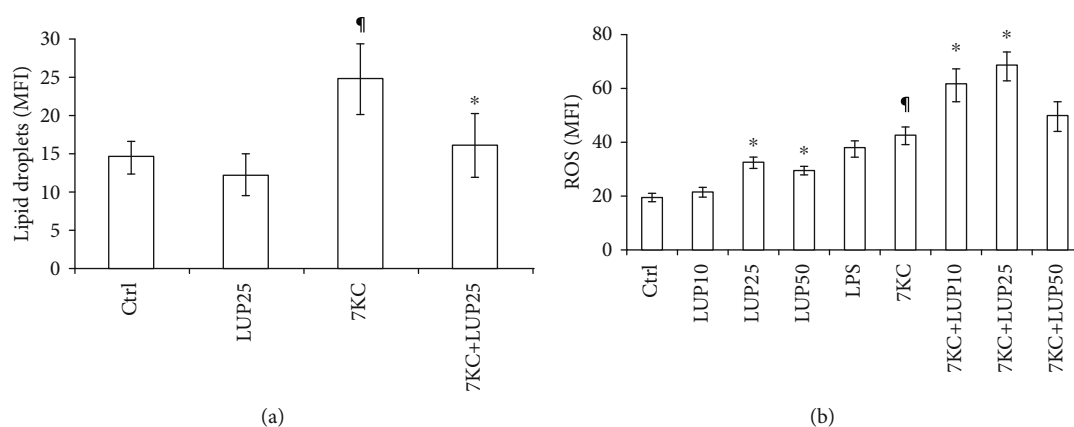


FIGURE 4: Effect of lupeol on intracellular lipid levels and reactive oxygen species (ROS) production. $M_{(IFN-\gamma/LPS)}$ macrophages pretreated with lupeol for 1 hour were stimulated with 7-keto-cholesterol (7KC) for 20 hours. THP-1 $M_{(IFN-\gamma/LPS)}$ macrophages were analyzed for lipid droplets (a) and primary $M_{(IFN-\gamma/LPS)}$ macrophages were analyzed for ROS generation (b) by flow cytometry. Results are expressed as mean \pm SD from three independent experiments. *Untreated vs. lupeol; [¶]Untreated control vs. 7KC-treated group; [°]7KC-treated group vs. 7KC+lupeol treated groups.

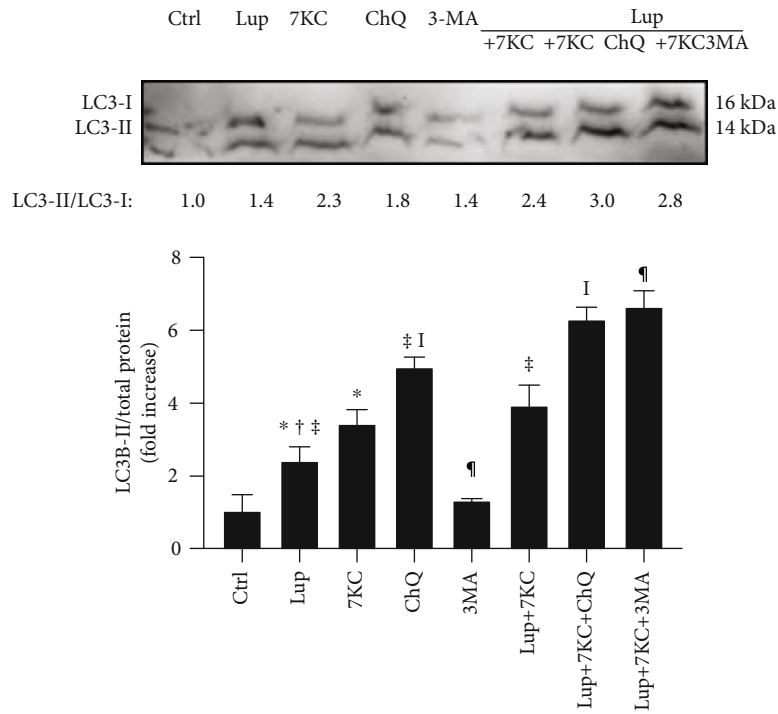
mouse model of arthritis [36], allergic airway inflammation [19], and LPS-treated macrophages [35].

In our previous study, we demonstrated that 7KC polarizes macrophages toward a proinflammatory state [9]; therefore, it is worthwhile to use this *in vitro* model to investigate the ability of a compound to switch human macrophages from a M1 proinflammatory phenotype (high IL-12 and IL-1 β production, high HLA-DR expression, and low endocytosis ability) to a M2 anti-inflammatory phenotype (high IL-10 and TGF- β production, high CD36 expression, and high endocytosis ability) [16, 27]. Thus, we have considered lupeol to meet the aims of our study.

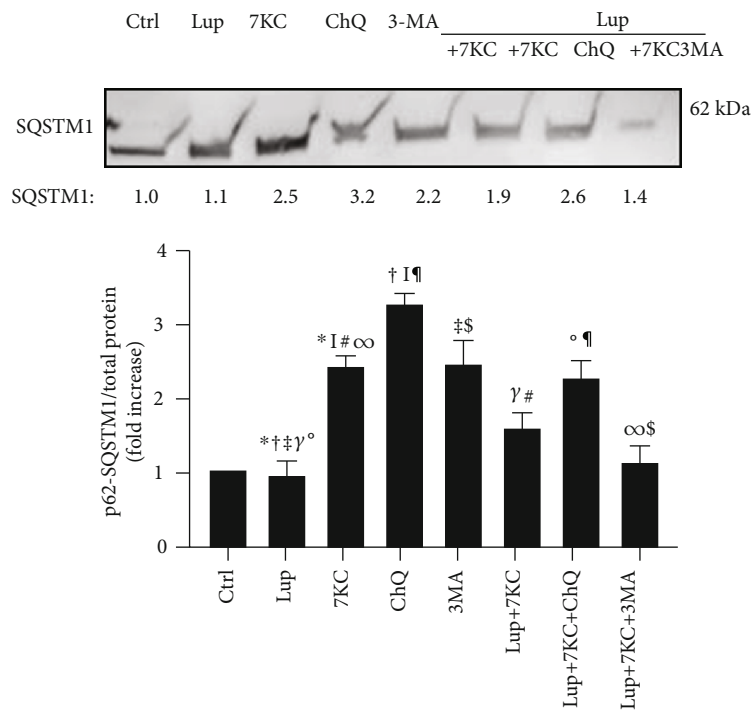
This study demonstrating an anti-inflammatory and immunomodulatory activity of lupeol in human $M_{(IFN-\gamma/LPS)}$ macrophages challenged with the inflammatory cholesterol oxidation product 7KC indicates lupeol as a promising therapeutic agent for atherosclerotic disease.

We first determined the effects of lupeol on the release of proinflammatory and anti-inflammatory cytokines in the

$M_{(IFN-\gamma/LPS)}$ macrophages and in 7KC-treated- $M_{(IFN-\gamma/LPS)}$ macrophages. Our study demonstrated the ability of lupeol to regulate macrophage polarization by reducing the release of the proinflammatory cytokine IL-12 and by increasing the release of the anti-inflammatory cytokines IL-10 and TGF- β , thus driving cells toward a M2 anti-inflammatory phenotype. Lupeol was also able to counteract the proinflammatory signalling triggered in macrophages by 7KC represented by the downregulation of IL-12 and IL-1 β production and upregulation of IL-10. Our results agree with a previous report showing that lupeol significantly inhibited proinflammatory cytokine production in macrophages and suppressed LPS-induced NF- κ B activity in inflammatory bowel disease [37]. While no cytotoxicity was observed upon lupeol treatment at the tested concentrations, the lack of cytokine production increase observed at the highest lupeol concentration suggests a possible interference of lupeol with immune cell regulation mechanisms as apoptosis pathway [38]. Furthermore, another natural compound, luteolin,



(a)



(b)

FIGURE 5: Western blotting analysis of autophagy markers in $M_{(IFN-\gamma/LPS)}$ macrophages. Lupeol enhances autophagy on $M_{(IFN-\gamma/LPS)}$ macrophages and counteracts dysregulated autophagy induced by 7-Keto-cholesterol (7KC). $M_{(IFN-\gamma/LPS)}$ -polarized THP-1 macrophages were stimulated or not with $25 \mu\text{M}$ lupeol for 1 hour and further stimulated with 7KC for 20 hours in the presence of the autophagy inhibitors ChQ or 3MA. Western blotting analysis of (a) LC3-I/II and (b) P62-SQSTM1 were performed in the whole-cell lysates of macrophages. Data are expressed relative to the control (fold increase) as mean \pm SD of 4 independent experiments. Values mentioned are the ratio of LC-3-II to LC3-I. Symbols indicate significant differences tested by one-way ANOVA.

inhibits inflammation by regulating the polarized phenotypes of macrophages and downregulates the release of proinflammatory cytokines [13].

Surface marker phenotyping confirmed that 7KC-treated- $M_{(IFN-\gamma/LPS)}$ macrophages showed an increased expression of the M1 activation marker HLA-DR [9], suggesting an upregulation of macrophage function as antigen-presenting cells that favor the activation of adaptive immune responses. In our experiments on primary macrophages, after 20 hours of exposure, 7KC did not alter the expression of the macrophage class B scavenger receptor CD36, a member of the scavenger receptor family involved in M2 polarization [39]. Hayden et al. [31] demonstrated that macrophages generated by 7KC treatment of THP-1 cells for 7 days increased CD36 expression about by 2-fold. A reason for this discrepancy between the effects of 7KC on primary macrophages and THP-1-macrophages may be due to the different intracellular lipid levels reached by the cells, which are the expression of both different culture conditions and cell differentiation state [40, 41]. The upregulation of CD36 observed in the $M_{(IFN-\gamma/LPS)}$ macrophages to lupeol is likely to positively influence the lipid uptake into cells, further increasing their anti-inflammatory clearance activity.

A further evidence of lupeol anti-inflammatory effects on $M_{(IFN-\gamma/LPS)}$ macrophages is its ability to increase the endocytic capacity of these cells. Similar results were observed in previous experiments with macrophage polarization in colorectal cancer cells [42].

Previous studies showed that excess-free cholesterol is stored as lipid droplets in macrophages and produces foam cell morphology [31, 43]. Since foam cell formation due to lipid droplets accumulation in macrophages is believed to play a crucial role in the progression of early atherosclerotic lesions and subsequent inflammation [44], we next evaluated the effects of lupeol pretreatment on 7KC-induced lipid droplets accumulation in $M_{(IFN-\gamma/LPS)}$ macrophages. The mean fluorescence intensity profiles reveal that lupeol reduces the accumulation of lipid droplets in macrophages treated with 7KC, thus further suggesting that the exposure of $M_{(IFN-\gamma/LPS)}$ macrophages with lupeol influences the polarization of proinflammatory macrophages toward a less proinflammatory phenotype through the influence on the lipid metabolism, similarly to what was observed in response to several other compounds modulating foam cell behaviour and inhibiting lipid accumulation [45]. Our results are in line with other studies on triterpenoids that have been shown to inhibit the accumulation of lipid droplets in macrophages [43]. Lupeol has been found to prevent the hypertrophic cardiac histopathology, the lipid abnormalities, and pathological biochemical changes induced by hypercholesterolemia [46]. Overall, available data on the potential benefit of lupeol as a natural lipid-lowering compound appear promising, thus further research on its beneficial effects needs to be performed.

Another crucial parameter in the pathogenesis of atherosclerosis is the ROS secretion. Our results on the increased ROS secretion due to 7KC stimulation are in agreement with previous studies showing the secretion of ROS by inflammatory macrophages that exacerbate oxidative stress in athero-

sclerosis [28, 30]. The finding that lupeol pretreatment significantly increased the ROS generation in our study is in line with the observation demonstrating that a derivative molecule of lupeol is able to induce the accumulation of ROS [20]. Notably, mitochondria and ROS are essential for autophagy stimulation [47–49].

Accumulating evidence shows that the dysfunctional autophagy plays a key role in atherosclerosis [24–26]. The impaired macrophage autophagy increases the immune response in obese mice by promoting proinflammatory M1 macrophage polarization [50]. Of note, a derivative molecule of lupeol induces cell death in a cancer cell line by inducing autophagy rather than apoptosis and necrosis [21]. Recently, a study showed that autophagy induction reduces 7KC-mediated cell death and reduces cellular lipid accumulation [29]. Our results suggest that lupeol is able to induce both autophagosome formation, as indicated by increased LC3 levels, and increased autophagy lysosomal degradation pathway, as marked by the lack of p62 accumulation [49].

Further studies on the characterization of ROS production induced by lupeol, over more extended time intervals, will establish whether this production simply regulates the autophagic pathway without leading to the collapse of the potential of the mitochondrial membrane or it can progress to autophagic cell death.

Taken together, our data provide evidence that lupeol has a cytoprotective effect toward 7-keto-cholesterol-induced proinflammatory signalling by efficiently switching the proinflammatory phenotype toward an anti-inflammatory one, which may be due to the activation of the autophagy pathway by increasing ROS production, to the modulation of cellular lipid accumulation and to an overall reduction of proinflammatory cytokines. Similar results have also been observed with urolithin A that shows high anti-inflammatory potential by inhibiting M1 polarization in macrophages and increasing the autophagic flux [51].

Extensive research so far on efficacy, safety, and pharmacokinetics profile of lupeol has shown that the oral administration of lupeol (<200 mg/kg) does not cause any systemic toxicity in animal models [52–54]. In a randomized controlled clinical trial (NCT02152865), the administration of lupeol was found to be safe and nontoxic for the treatment of oral malignant melanoma [55]. These findings suggest that lupeol should be studied further as anti-inflammatory therapeutics for future applications in humans. Lupeol has been shown to inhibit NF- κ B and to increase FGF-2, TGF- β 1, and collagen III levels, followed by the downregulation of IL-6 and subsequent upregulation of IL-10 levels in a wound healing model in diabetic patients [56]. Since our data confirm the anti-inflammatory activity of the lupeol against 7KC in $M_{(IFN-\gamma/LPS)}$ macrophages by suppressing inflammatory and activating autophagy, they suggest the possible usefulness of this molecule in the assessment of new potential therapeutic strategies for plaque regression.

5. Conclusions

Our results strengthen previous findings on the immunomodulatory effects of lupeol on innate immune cells and

depict the usefulness of lupeol as an adjunctive drug to counteract the proatherogenic oxysterol signalling within the atherosclerotic plaque through the activation of autophagy and inhibition of proinflammatory cytokines.

Data Availability

The data used to support the findings of this study are included within the article.

Conflicts of Interest

The authors do not have competing financial interests with this study.

Acknowledgments

The authors are thankful to the European Molecular Biology Organization for providing fellowship to S.S. The authors acknowledge the Flow Cytometry Facility at Istituto Superiore di Sanità Rome, for technical assistance in flow cytometry. This work was supported by the Italian Ministry of Health (ISS C.R. 2018) to B.B. and Sapienza Ateneo grant 2016 to L.A.

Supplementary Materials

Supplementary Figure 1: the effect of lupeol on cell vitality (measured by Trypan blue exclusion assay) and cell morphology (light microscope imaging) of 7-keto-cholesterol-treated $M_{(IFN-\gamma/LPS)}$ macrophages. Supplementary Figure 2: Western blotting analysis of LC3-I/II and p62-SQSTM1 in the whole-cell lysates of primary $M_{(IFN-\gamma/LPS)}$ macrophages and THP-1 $M_{(IFN-\gamma/LPS)}$ macrophages in response to 7-keto-cholesterol (a) or in response to lupeol plus 7KC (b). (*Supplementary Materials*)

References



- [1] P. Libby, P. M. Ridker, and G. K. Hansson, "Progress and challenges in translating the biology of atherosclerosis," *Nature*, vol. 473, no. 7347, pp. 317–325, 2011.
- [2] G. K. Hansson and A. Hermansson, "The immune system in atherosclerosis," *Nature Immunology*, vol. 12, no. 3, pp. 204–212, 2011.
- [3] T. Gui, A. Shimokado, Y. Sun, T. Akasaka, and Y. Muragaki, "Diverse roles of macrophages in atherosclerosis: from inflammatory biology to biomarker discovery," *Mediators of Inflammation*, vol. 2012, Article ID 693083, 14 pages, 2012.
- [4] K. J. Moore, F. J. Sheedy, and E. A. Fisher, "Macrophages in atherosclerosis: a dynamic balance," *Nature Reviews. Immunology*, vol. 13, no. 10, pp. 709–721, 2013.
- [5] D. M. Mosser and J. P. Edwards, "Exploring the full spectrum of macrophage activation," *Nature Reviews. Immunology*, vol. 8, no. 12, pp. 958–969, 2008.
- [6] S. Tavakoli and R. Asmis, "Reactive oxygen species and thiol redox signaling in the macrophage biology of atherosclerosis," *Antioxidants & Redox Signaling*, vol. 17, no. 12, pp. 1785–1795, 2012.
- [7] G. J. Randolph, "Mechanisms that regulate macrophage burden in atherosclerosis," *Circulation Research*, vol. 114, no. 11, pp. 1757–1771, 2014.
- [8] P. J. Murray, J. E. Allen, S. K. Biswas et al., "Macrophage activation and polarization: nomenclature and experimental guidelines," *Immunity*, vol. 41, no. 1, pp. 14–20, 2014.
- [9] B. Buttari, L. Segoni, E. Profumo et al., "7-Oxo-cholesterol potentiates pro-inflammatory signaling in human M1 and M2 macrophages," *Biochemical Pharmacology*, vol. 86, no. 1, pp. 130–137, 2013.
- [10] H. Larsson, Y. Böttiger, L. Iuliano, and U. Diczfalusy, "In vivo interconversion of 7 β -hydroxycholesterol and 7-ketocholesterol, potential surrogate markers for oxidative stress," *Free Radical Biology & Medicine*, vol. 43, no. 5, pp. 695–701, 2007.
- [11] A. Berthier, S. Lemaire-Ewing, C. Prunet et al., "7-Ketocholesterol-induced apoptosis," *The FEBS Journal*, vol. 272, no. 12, pp. 3093–3104, 2005.
- [12] U. Saqib, S. Sarkar, K. Suk, O. Mohammad, M. S. Baig, and R. Savai, "Phytochemicals as modulators of M1-M2 macrophages in inflammation," *Oncotarget*, vol. 9, no. 25, pp. 17937–17950, 2018.
- [13] J. Wang, Y. T. Liu, L. Xiao, L. Zhu, Q. Wang, and T. Yan, "Anti-inflammatory effects of apigenin in lipopolysaccharide-induced inflammatory in acute lung injury by suppressing COX-2 and NF-kB pathway," *Inflammation*, vol. 37, no. 6, pp. 2085–2090, 2014.
- [14] X. Feng, H. Qin, Q. Shi et al., "Chrysin attenuates inflammation by regulating M1/M2 status via activating PPAR γ ," *Biochemical Pharmacology*, vol. 89, no. 4, pp. 503–514, 2014.
- [15] Y. R. Li, D. Y. Chen, C. L. Chu et al., "Naringenin inhibits dendritic cell maturation and has therapeutic effects in a murine model of collagen-induced arthritis," *The Journal of Nutritional Biochemistry*, vol. 26, no. 12, pp. 1467–1478, 2015.
- [16] B. Buttari, E. Profumo, L. Segoni et al., "Resveratrol counteracts inflammation in human M1 and M2 macrophages upon challenge with 7-oxo-cholesterol: potential therapeutic implications in atherosclerosis," *Oxidative Medicine and Cellular Longevity*, vol. 2014, Article ID 257543, 12 pages, 2014.
- [17] A. A. M. T. Ramirez Apan, A. L. Pérez-Castorena, and A. R. de Vivar, "Anti-inflammatory constituents of *Mortonia greggii* Gray," *Zeitschrift für Naturforschung Section C*, vol. 59, no. 3-4, pp. 237–243, 2004.
- [18] V. Sudhakar, S. Ashok Kumar, P. Varalakshmi, and V. Sujatha, "Protective effect of lupeol and lupeol linoleate in hypercholesterolemia associated renal damage," *Molecular and Cellular Biochemistry*, vol. 317, no. 1-2, pp. 11–20, 2008.
- [19] J. F. Vasconcelos, M. M. Teixeira, J. M. Barbosa-Filho et al., "The triterpenoid lupeol attenuates allergic airway inflammation in a murine model," *International Immunopharmacology*, vol. 8, no. 9, pp. 1216–1221, 2008.
- [20] Y. Zhu, X. Li, J. Chen et al., "The pentacyclic triterpene Lupeol switches M1 macrophages to M2 and ameliorates experimental inflammatory bowel disease," *International Immunopharmacology*, vol. 30, pp. 74–84, 2016.
- [21] J. Hao, Y. Pei, G. Ji, W. Li, S. Feng, and S. Qiu, "Autophagy is induced by 3 β -O-succinyl-lupeol (LD9-4) in A549 cells via up-regulation of Beclin 1 and down-regulation mTOR pathway," *European Journal of Pharmacology*, vol. 670, no. 1, pp. 29–38, 2011.
- [22] J. Brown, H. Wang, J. Suttles, D. T. Graves, and M. Martin, "Mammalian target of rapamycin complex 2 (mTORC2)

- negatively regulates toll-like receptor 4-mediated inflammatory response via FoxO1," *The Journal of Biological Chemistry*, vol. 286, no. 52, pp. 44295–44305, 2011.
- [23] W. T. Festuccia, P. Pouliot, I. Bakan, D. M. Sabatini, and M. Laplante, "Myeloid-specific rictor deletion induces M1 macrophage polarization and potentiates in vivo pro-inflammatory response to lipopolysaccharide," *PLoS One*, vol. 9, no. 4, p. e95432, 2014.
- [24] W. Martinet and G. R. Y. De Meyer, "Autophagy in atherosclerosis: a cell survival and death phenomenon with therapeutic potential," *Circulation Research*, vol. 104, no. 3, pp. 304–317, 2009.
- [25] G. R. Y. de Meyer, M. O. J. Grootaert, C. F. Michiels, A. Kurdi, D. M. Schrijvers, and W. Martinet, "Autophagy in vascular disease," *Circulation Research*, vol. 116, no. 3, pp. 468–479, 2015.
- [26] M. O. J. Grootaert, P. A. da Costa Martins, N. Bitsch et al., "Defective autophagy in vascular smooth muscle cells accelerates senescence and promotes neointima formation and atherogenesis," *Autophagy*, vol. 11, no. 11, pp. 2014–2032, 2015.
- [27] A. A. Tarique, J. Logan, E. Thomas, P. G. Holt, P. D. Sly, and E. Fantino, "Phenotypic, functional, and plasticity features of classical and alternatively activated human macrophages," *American journal of respiratory cell and molecular biology*, vol. 53, no. 5, pp. 676–688, 2015.
- [28] S. Adamson and N. Leitinger, "Phenotypic modulation of macrophages in response to plaque lipids," *Current Opinion in Lipidology*, vol. 22, no. 5, pp. 335–342, 2011.
- [29] X.-M. Yuan, N. Sultana, N. Siraj, L. J. Ward, B. Ghafouri, and W. Li, "Autophagy induction protects against 7-oxysterol-induced cell death via lysosomal pathway and oxidative stress," *Journal of Cell Death*, vol. 9, 2016.
- [30] T. Wu, Y. Peng, S. Yan, N. Li, Y. Chen, and T. Lan, "Andrographolide ameliorates atherosclerosis by suppressing pro-inflammation and ROS generation-mediated foam cell formation," *Inflammation*, vol. 41, no. 5, pp. 1681–1689, 2018.
- [31] J. M. Hayden, L. Brachova, K. Higgins et al., "Induction of monocyte differentiation and foam cell formation in vitro by 7-ketocholesterol," *Journal of Lipid Research*, vol. 43, no. 1, pp. 26–35, 2002.
- [32] Y. Kabeya, N. Mizushima, T. Ueno et al., "LC3, a mammalian homologue of yeast Apg8p, is localized in autophagosomal membranes after processing," *The EMBO Journal*, vol. 19, no. 21, pp. 5720–5728, 2000.
- [33] N. Mizushima, "Autophagy: process and function," *Genes & Development*, vol. 21, no. 22, pp. 2861–2873, 2007.
- [34] E. L. Nguemfo, T. Dimo, A. B. Dongmo et al., "Anti-oxidative and anti-inflammatory activities of some isolated constituents from the stem bark of *Allanblackia monticola* Staner L.C (Guttiferae)," *Inflammopharmacology*, vol. 17, no. 1, pp. 37–41, 2009.
- [35] M. A. Fernández, B. de las Heras, M. D. García, M. T. Sáenz, and A. Villar, "New insights into the mechanism of action of the anti-inflammatory triterpene lupeol," *The Journal of Pharmacy and Pharmacology*, vol. 53, no. 11, pp. 1533–1539, 2001.
- [36] S. Bani, A. Kaul, B. Khan et al., "Suppression of T lymphocyte activity by lupeol isolated from *Crataeva religiosa*," *Phytotherapy Research*, vol. 20, no. 4, pp. 279–287, 2006.
- [37] C. Lee, J. W. Lee, J. Y. Seo, S. W. Hwang, J. P. Im, and J. S. Kim, "Lupeol inhibits LPS-induced NF-kappa B signaling in intestinal epithelial cells and macrophages, and attenuates acute and chronic murine colitis," *Life Sciences*, vol. 146, pp. 100–108, 2016.
- [38] W. He, X. Li, and S. Xia, "Lupeol triterpene exhibits potent antitumor effects in A427 human lung carcinoma cells via mitochondrial mediated apoptosis, ROS generation, loss of mitochondrial membrane potential and downregulation of m-TOR/PI3Ksol;AKT signalling pathway," *JBUON*, vol. 23, no. 3, pp. 635–640, 2018.
- [39] J. Oh, A. E. Riek, S. Weng et al., "Endoplasmic reticulum stress controls M2 macrophage differentiation and foam cell formation," *The Journal of Biological Chemistry*, vol. 287, no. 15, pp. 11629–11641, 2012.
- [40] J. Han, D. P. Hajjar, M. Febbraio, and A. C. Nicholson, "Native and modified low density lipoproteins increase the functional expression of the macrophage class B scavenger receptor, CD36," *The Journal of Biological Chemistry*, vol. 272, no. 34, pp. 21654–21659, 1997.
- [41] L. M. Yesner, H. Y. Huh, S. F. Pearce, and R. L. Silverstein, "Regulation of monocyte CD36 and thrombospondin-1 expression by soluble mediators," *Arteriosclerosis, Thrombosis, and Vascular Biology*, vol. 16, no. 8, pp. 1019–1025, 1996.
- [42] S. Edin, M. L. Wikberg, J. Rutegård, P. A. Oldenborg, and R. Palmqvist, "Phenotypic skewing of macrophages in vitro by secreted factors from colorectal cancer cells," *PLoS One*, vol. 8, no. 9, article e74982, 2013.
- [43] M. Ouimet and Y. L. Marcel, "Regulation of lipid droplet cholesterol efflux from macrophage foam cells," *Arteriosclerosis, Thrombosis, and Vascular Biology*, vol. 32, no. 3, pp. 575–581, 2012.
- [44] Y. Fujiwara, A. Hayashida, K. Tsurushima et al., "Triterpenoids isolated from *Zizyphus jujuba* inhibit foam cell formation in macrophages," *Journal of Agricultural and Food Chemistry*, vol. 59, no. 9, pp. 4544–4552, 2011.
- [45] L. T. H. Nguyen, A. Muktabar, J. Tang et al., "The potential of fluocinolone acetonide to mitigate inflammation and lipid accumulation in 2D and 3D foam cell cultures," *BioMed Research International*, vol. 2018, Article ID 3739251, 11 pages, 2018.
- [46] V. Sudhahar, S. A. Kumar, P. T. Sudharsan, and P. Varalakshmi, "Protective effect of lupeol and its ester on cardiac abnormalities in experimental hypercholesterolemia," *Vascular Pharmacology*, vol. 46, no. 6, pp. 412–418, 2007.
- [47] S. P. Elmore, T. Qian, S. F. Grissom, and J. J. Lemasters, "The mitochondrial permeability transition initiates autophagy in rat hepatocytes," *The FASEB Journal*, vol. 15, no. 12, pp. 1–17, 2001.
- [48] J. Huang, V. Canadien, G. Y. Lam et al., "Activation of antibacterial autophagy by NADPH oxidases," *Proceedings of the National Academy of Sciences of the United States of America*, vol. 106, no. 15, pp. 6226–6231, 2009.
- [49] R. Scherz-Shouval, E. Shvets, E. Fass, H. Shorer, L. Gil, and Z. Elazar, "Reactive oxygen species are essential for autophagy and specifically regulate the activity of Atg4," *The EMBO Journal*, vol. 26, no. 7, pp. 1749–1760, 2007.
- [50] K. Liu, E. Zhao, G. Ilyas et al., "Impaired macrophage autophagy increases the immune response in obese mice by promoting proinflammatory macrophage polarization," *Autophagy*, vol. 11, no. 2, pp. 271–284, 2015.
- [51] Y. D. Boakye, L. Groyer, and E. H. Heiss, "An increased autophagic flux contributes to the anti-inflammatory potential of urolithin A in macrophages," *Biochimica et Biophysica Acta (BBA) - General Subjects*, vol. 1862, no. 1, pp. 61–70, 2018.

- [52] M. Saleem, F. Afaq, V. M. Adhami, and H. Mukhtar, "Lupeol modulates NF- κ B and PI3K/Akt pathways and inhibits skin cancer in CD-1 mice," *Oncogene*, vol. 23, no. 30, pp. 5203–5214, 2004.
- [53] T. Geetha, P. Varalakshmi, and R. M. Latha, "Effect of triterpenes from *Crataeva nurvala* stem bark on lipid peroxidation in adjuvant induced arthritis in rats," *Pharmacological Research*, vol. 37, no. 3, pp. 191–195, 1998.
- [54] M. A. Ruiz-Rodríguez, A. Vedani, A. L. Flores-Mireles, M. H. Cháirez-Ramírez, J. A. Gallegos-Infante, and R. F. González-Laredo, "In silico prediction of the toxic potential of lupeol," *Chemical Research in Toxicology*, vol. 30, no. 8, pp. 1562–1571, 2017.
- [55] F. S. Tsai, L. W. Lin, and C. R. Wu, "Lupeol and its role in chronic diseases," in *Drug Discovery from Mother Nature*, S. Gupta, S. Prasad, and B. Aggarwal, Eds., vol. 929 of *Advances in Experimental Medicine and Biology*, pp. 145–175, Springer, Cham, 2016.
- [56] F. P. Beserra, A. J. Vieira, L. F. S. Gushiken et al., "Lupeol, a dietary triterpene, enhances wound healing in streptozotocin-induced hyperglycemic rats with modulatory effects on inflammation, oxidative stress, and angiogenesis," *Oxidative Medicine and Cellular Longevity*, vol. 2019, Article ID 3182627, 20 pages, 2019.

Research Article

New 2-Acetyl-3-aminophenyl-1,4-naphthoquinones: Synthesis and *In Vitro* Antiproliferative Activities on Breast and Prostate Human Cancer Cells

David Ríos ¹, Jaime A. Valderrama,¹ Miriam Cautin,¹ Milko Tapia,¹ Felipe Salas,¹ Angélica Guerrero-Castilla,¹ Giulio G. Muccioli,² Pedro Buc Calderón,^{1,3} and Julio Benites ¹

¹Química y Farmacia, Facultad de Ciencias de la Salud, Universidad Arturo Prat, Casilla 121, Iquique 1100000, Chile

²Bioanalysis and Pharmacology of Bioactive Lipids (BPBL), Louvain Drug Research Institute, Université Catholique de Louvain, 72 Avenue E. Mounier, BPBL 7201, 1200 Brussels, Belgium

³Research Group in Metabolism and Nutrition, Louvain Drug Research Institute, Université Catholique de Louvain, 73 Avenue E. Mounier, 1200 Brussels, Belgium

Correspondence should be addressed to David Ríos; darios@unap.cl and Julio Benites; juliob@unap.cl

Received 31 May 2020; Revised 27 July 2020; Accepted 28 August 2020; Published 26 September 2020

Academic Editor: Luciano Saso

Copyright © 2020 David Ríos et al. This is an open access article distributed under the Creative Commons Attribution License, which permits unrestricted use, distribution, and reproduction in any medium, provided the original work is properly cited.

The reaction of 2-acyl-1,4-naphthoquinones with *N,N*-dimethylaniline and 2,5-dimethoxyaniline, promoted by catalytic amounts of $\text{CeCl}_3 \cdot 7\text{H}_2\text{O}$ under “open-flask” conditions, produced a variety of 2-acyl-3-aminophenyl-1,4-naphthoquinones structurally related to the cytotoxic 2-acetyl-3-phenyl-1,4-naphthoquinone, an inhibitor of the heat shock chaperone protein Hsp90. The members of the 2-acyl-3-aminophenyl-1,4-naphthoquinone series were isolated in good yields (63-98%). The cyclic voltammograms of the 2-acyl-3-aminophenyl-1,4-naphthoquinone exhibit two one-electron reduction waves to the corresponding radical-anion and dianion and two quasireversible oxidation peaks. The first and second half-wave potential values ($E_{1/2}$) of the members of the series are sensitive to the push-pull electronic effects of the substituents in the naphthoquinone scaffold. Furthermore, the *in vitro* antiproliferative properties of these new quinones were evaluated on two human cancer cells DU-145 (prostate) and MCF-7 (mammary) and a nontumorigenic HEK-293 (kidney) cell line, using the MTT colorimetric method. Two members, within the series, exhibited interesting cytotoxic activities on human prostate and mammary cancer cells.

1. Introduction

The electroactive naphthoquinone core is a common structural constituent of a variety of biochemical systems involved in the human defense system [1]. Several biological active quinones as ubiquinone and vitamin K are known to be electron transporters and are essential for many enzymatic processes. They can act as anti- or prooxidants depending on the nature of the media: this chemical versatility gives them an important role in different biochemical processes that are essential to living organisms [2]. The oxidation state of naphthoquinones allows them to act by different mechanisms, such as free radical scavengers, metal ion chelators,

and also enzyme inhibitors for free radical production [3, 4]. This imbalance between the formation and removal of ROS (reactive oxygen species) causes damage to the cells at nucleic acids, proteins, and membrane lipids associated with ageing, carcinogenesis, cardiovascular, and coronary diseases [5]. In this context, the naturally occurring 2-hydroxy-1,4-naphthoquinone (lawsone) exhibits a number of interesting biological activities, such as antioxidant [6], antibacterial, antifungal [7], anti-inflammatory, antipyretic, analgesic [8], and anticancer cytotoxic [9]. Therefore, the quinones could play an important role in inhibiting or delaying oxidative stress that arises from an imbalance between free radical production and antioxidant and repair defenses [10].

Acylated 1,4-quinones such as 2-acyl-1,4-benzo- and 2-acyl-1,4-naphthoquinones are a valuable building block of several natural [1, 11–13] and synthetic compounds endowed with a wide range of biological activities [14–19]. Acylquinones are highly reactive towards nucleophiles due to the confluence of electrophilic centers at the quinone nucleus and the 2-carbonyl substituents. The relatively close location of these electrophilic centers in the acylquinone scaffold enables reactions with diverse mono- and binucleophiles such as arylamines [17], azaenamines [18], enamines [19], and 2-aminobenzothiazoles [20] to give a diversity of substances shown in Figure 1 such as 2,3-disubstituted 1,4-naphthoquinones (a, b) and heterocyclic fused 1,4-naphthoquinones (c–e).

High-throughput screening of a library of structurally diverse compounds has identified, among 120 active members, the 1,4-naphthoquinone derivatives, named HTS1 and HTS3, as a new class of inhibitors of the heat shock chaperone protein Hsp90 (Figure 2). The protein Hsp90, which ensures protein homeostasis in the presence and in the absence of cellular stress, is unique because most of its client proteins are conformationally labile signal transducers that play a crucial role in cell growth control, survival, and development processes [11]. Hsp90 represents 1–2% of the total protein cellular content, but its expression is enhanced by 2–10-fold in cancer cells [12], thus making it an attractive goal for the development of Hsp90 inhibitors [1, 13–15] and, consequently, a relevant target in cancer therapy [21]. Both HTS1 and HTS3 have been shown antiproliferative activity against human cancer mammary cells. For instance, HTS1 showed 4-fold greater antiproliferative activity against MCF-7 cells (an estrogen-dependent breast cancer cell line) compared to SKBr3 cells (an Her2-overexpressing breast cancer cell line), indicating that this scaffold may provide a useful probe to study estrogen-dependent cancers. On the other hand, HTS3 shows equal activity against both mammary cancer cells. In addition, the members I-III induced the degradation of oncogenic Hsp90 client proteins, a hallmark of Hsp90 inhibition [22].

Recently, we have reported the synthesis of a variety of 2-acyl-3-phenylamino-1,4-naphthoquinones (i.e., compound IV in Figure 2) prepared by oxidative amination of 2-acylnaphthoquinones with phenylamines. The members of this naphthoquinone series were designed as potential inhibitors of Hsp90 chaperoning function due to their close structural similarity to that of HTS1. The *in vitro* screening of the series demonstrated cytotoxic activity on cancer cells [23], and the congener IV (Figure 2) exhibited action as an inhibitor of Hsp90 chaperoning function [19].

Older studies reported by Pardo et al. [24] demonstrated that the reaction of 2-acetylnaphthohydroquinone with phenylamines, under oxidant conditions, takes place in a complex manner. Indeed, it yields four types of products depending upon the structure of the arylamine and the medium solvent: amination (C-N bond formation), arylation (C-C bond formation), arylation-cyclisation (C-C and C=N bond formations), and arylation-amination (C-C and N-C bond formations) [24, 25]. These reactions occur between the “nascent” 2-acetyl-1,4-naphthoquinone, *in situ* generated

by oxidation of acetylnaphthohydroquinone with sodium periodate, and the arylamines. Recent studies performed in our laboratory show that the reaction of diverse 2-acylnaphthoquinones with 3,4,5-trimethoxyaniline in methanol yields amination products (C-N bond formation) together with two types of arylation-cyclisation products (C-C and two alternative N=C or N-C bond formations). We have not detected arylation products in these assays probably due to the fact that they undergo fast cyclisation reactions to produce their respective arylation-cyclisation products [26].

Pardo et al. [24] reported the synthesis of arylation products, named as 2-acetyl-3-aminophenyl-1,4-naphthoquinones (Scheme 1), which are closely related to HTS1 (2-acetyl-3-phenyl-1,4-naphthoquinone) shown in Figure 2. Inspired by such structural similarities, we wanted to explore the acylquinone scope of this arylation reaction to the synthesis of 2-acyl-3-aminophenyl-1,4-naphthoquinones from a representative number of acylnaphthoquinones, *N,N*-dimethylaniline and 2,5-dimethoxyaniline.

In this paper, we report flexible access to 2-acyl-3-aminophenyl-1,4-naphthoquinones prepared from 2-acylnaphthohydroquinones, *N,N*-dimethylaniline and 2,5-dimethoxyaniline. The half-wave potentials of such new HTS1 analogues were calculated, and they were evaluated for their *in vitro* antiproliferative activities on two human-derived cancer cell lines DU-145 (prostate) and MCF-7 (breast) and nontumorigenic HEK-293 (kidney) cells using as endpoint the MTT colorimetric method.

2. Materials and Methods

2.1. General Information. All the solvents and reagents were purchased from different companies, such as Aldrich (St. Louis, MO, USA) and Merck (Darmstadt, Germany), and were used as supplied. Melting points (mp) were determined on a Stuart Scientific SMP3 (Staffordshire, UK) apparatus and are uncorrected. The record of IR, ^1H - and ^{13}C -NMR spectra, and chromatography procedures were done according to methods reported by Benites et al. [27]. Proton nuclear magnetic resonance (^1H NMR) spectra were measured at 300 MHz in a Bruker Ultrashield-300 spectrometer. Data for the ^1H NMR spectra are reported as follows: s = singlet, br s = broad singlet, d = doublet, and t = triplet, and the coupling constants (J) are in Hz. Carbon-13 nuclear magnetic resonance (^{13}C NMR) spectra were measured at 75 MHz in a Bruker Ultrashield-300 spectrometer. Bidimensional NMR techniques and distortion-less enhancement by polarization transfer (DEPT) were used for the signal assignment. Chemical shifts are expressed in ppm downfield relative to tetramethylsilane, and the coupling constants (J) are reported in Hertz. The high-resolution mass spectrometry (HRMS) data for all final compounds were obtained using a LTQ-Orbitrap mass spectrometer (Thermo-Fisher Scientific, Waltham, MA, USA) with the analysis performed using an atmospheric-pressure chemical ionization (APCI) source, operated in a positive mode. The acylnaphthohydroquinones (2–8) were prepared according to a previously reported procedure [28].

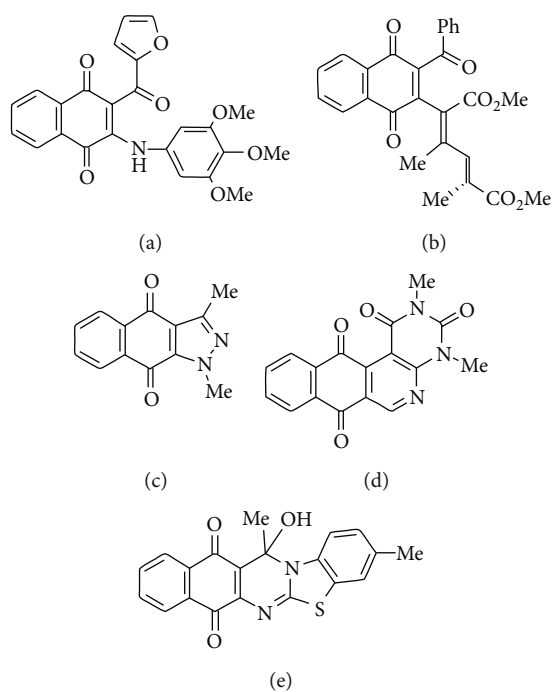


FIGURE 1: Examples of naphthoquinone-containing compounds prepared from acylquinones.

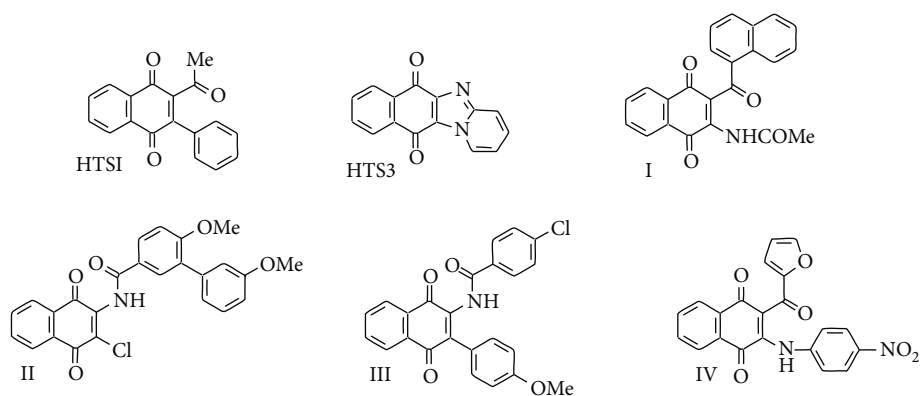
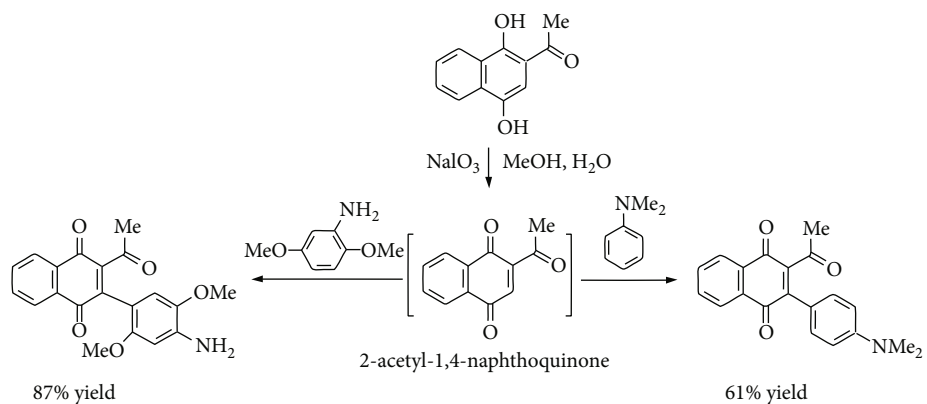
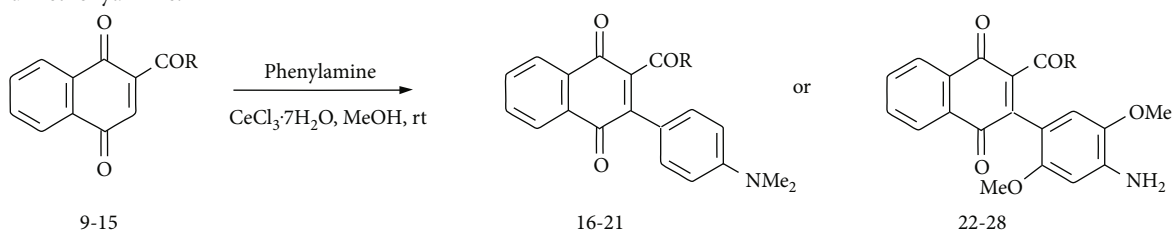


FIGURE 2: Structure of HTS1/HTS3 and quinone-analogue inhibitors of Hsp90.



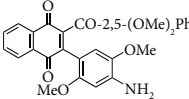
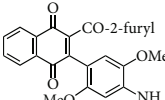
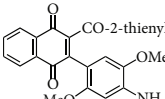
SCHEME 1: Formation of 2-acetyl-3-aminophenyl-1,4-naphthoquinones. Adapted from [24].

TABLE 1: Synthesis of 2-acyl-3-aminophenyl-naphthoquinones 16-28 from 2-acylnaphthoquinones 9-15, *N,N*-dimethylaniline and 2,5-dimethoxyaniline.



Acylquinone	Product	Structure	Time(hrs)	Yield(%)*
10	16		3	65
11	17		5	33
12	18		240	91
13	19		216	81
14	20		28	98
15	21		72	94
9	22		48	77
10	23		1.5	63
11	24		2	63
12	25		4	91

TABLE 1: Continued.

Acylquinone	Product	Structure	Time(hrs)	Yield(%)*
13	26		3	87
14	27		2.5	83
15	28		2	91

* Isolated by column chromatography. Yields are based on the corresponding acetylnaphthoquinones 2-8.

2.2. Chemistry

2.2.1. Preparation of 2-Acyl-3-aminophenyl-naphthoquinones (16-28): General Procedure. Suspensions of the acylnaphthoquinones 2-8 (1.0 mmol), Ag₂O (2.0 equiv.), and MgSO₄ anhydrous (300 mg) in dichloromethane (30 mL) were left with stirring for 30 min at room temperature (rt). The mixtures were filtered, the solids were washed with dichloromethane (3 × 15 mL), and the filtrates containing the respective 2-acyl-1,4-naphthoquinones were evaporated under reduced pressure. The residues were dissolved in methanol (15 mL), the phenylamines (2 equiv.) and CeCl₃·7H₂O (5% mmol) were added to the solutions, and the mixtures were left with stirring at rt according to the times collected in Table 1. The solvents were removed under reduced pressure, and the residues were column-chromatographed over silica gel (petroleum ether/EtOAc) to yield the corresponding pure 2-acyl-3-aminophenyl-naphthoquinones 16-28.

2.3. Biological Assays

2.3.1. Cell Lines and Cell Cultures. Human cancer cell lines MCF-7 (mammary) and DU-145 (prostate) and nontumor HEK-293 cells were obtained from the American Type Culture Collection (ATCC, Manassas, VA, USA). The cultures were maintained at a density of 1 × 10⁵ cells/mL, and the medium was changed at 48 to 72 h intervals. They were cultured in high-glucose Dulbecco's modified Eagle medium (Gibco, Grand Island, NY, USA) supplemented with 10% fetal calf serum, penicillin (100 U/mL), and streptomycin (100 μg/mL). All cultures were kept at 37°C in 95% air/5% CO₂ at 100% humidity. Phosphate-buffered saline (PBS) was purchased from Gibco. Cells were incubated at the indicated times at 37°C, with or without quinones at various concentrations.

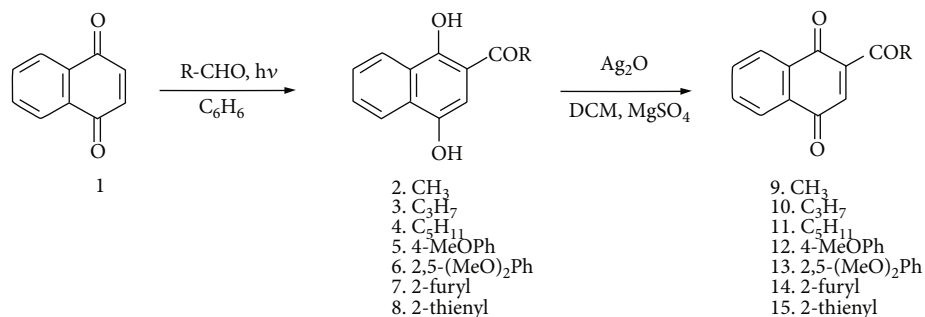
2.3.2. Cytotoxic Assays. The cytotoxicity of the quinones was assessed by the MTT (3-(4,5-dimethylthiazol-2-yl)-2,5-diphenyltetrazolium bromide) reduction assays [29], according to Valderrama et al. [30]. Briefly, adherent cells were detached by using trypsin/EDTA solution. The culture

medium was removed, and cells were washed with a free Ca-Mg salt solution to remove all traces of serum. After removing salt solution, trypsin/EDTA solution was added to completely cover the monolayer of cells for 2-3 min at 37°C. When the trypsinization process was completed, trypsin/EDTA was removed by aspiration and cells were resuspended, diluted in fresh medium, and seeded for 24 h into 96-well plates at a density of 10,000 cells/well. Then, they were further incubated for 48 h, with or without the quinone derivatives. Doxorubicin was used as the standard chemotherapeutic agent (positive control) in a dose range of 0.01 to 10 μM. Cells were then washed twice with warm PBS, and they were further incubated with MTT (0.5 mg/mL) for 2 hours at 37°C. Blue formazan crystals were solubilized by adding 100 μL DMSO/well, and the optical density of the colored solutions was subsequently read at 550 nm. Results are expressed as a percentage of MTT reduction, compared to untreated control conditions. The IC₅₀ values were calculated using the GraphPad Prism software (San Diego, CA, USA).

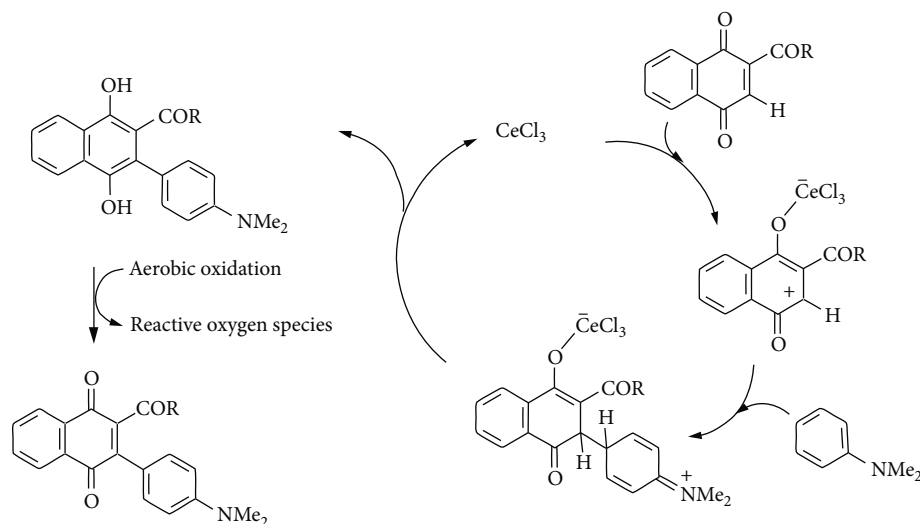
3. Results and Discussion

3.1. Chemistry. The 2-acylnaphthoquinones 9-15 selected for the study were prepared from the 2-acylnaphthoquinones 2-8 according to Scheme 2. The hydroquinone precursors 2-8 were synthesized by solar photo-Friedel-Crafts acylation of 1,4-naphthoquinone 1 with the following aldehydes: acetaldehyde, butyraldehyde, hexanal, 4-methoxybenzaldehyde, 2,5-dimethoxybenzaldehyde, 2-furancarbaldehyde, and 2-thiophencarbaldehyde, according to our previously reported procedure [28]. Access to the 2-acyl-1,4-naphthoquinones 9-15 was accomplished by oxidation of 2-acylnaphthoquinones 2-8 with silver (I) oxide in dichloromethane in the presence of dry magnesium sulphate [19]. The resulting acylnaphthoquinones isolated from the mixture reactions were dissolved in methanol and immediately reacted with the *N,N*-dimethylaniline and 2,5-dimethoxyaniline (Supplementary Materials (available here)).

Among the members of the acylnaphthoquinone series, compound 14 was selected to get preliminary insights into



SCHEME 2: Preparation of 2-acylnaphthoquinones 9-15 from 1 and diverse aldehydes.



SCHEME 3: Proposed reaction mechanism for the Ce(III)-promoted arylation reaction of acylnaphthoquinones with *N,N*-dimethylaniline.

its reactivity to undergo arylation reaction with *N,N*-dimethylaniline. In a preliminary assay, acylnaphthoquinone 14, prepared from acylnaphthohydroquinone 7, was reacted with *N,N*-dimethylaniline in methanol at rt. The reaction carried out under open-flask conditions to favor aerobic oxidation reactions takes place slowly to give, after 72 hours, the arylation product 20 in 73% yield, referred to precursor 7. Furthermore, it was observed that the reaction of 14 with *N,N*-dimethylaniline in refluxing ethanol takes place relatively faster (33 hours) than in methanol, but compound 20 is produced in moderate yield (51%).

The validity of the arylation mechanism of acylquinone 9 with arylamines proposed by Pardo et al. [24] was assumed to proceed through a sequence of a Michael addition reaction followed by aerobic oxidation of the adduct intermediate. Therefore, we envisaged to improve the arylation reaction of 14 (Table 1) with *N,N*-dimethylaniline by using a green Lewis acid catalyst such as CeCl₃·7H₂O [31] or IBr₃ [32]. Successful results on the use of the Ce(III) catalyst in the oxidative amination reaction of quinones with arylamines have been reported in literature [32–38]. These acid catalysts probably increase the electrophilic character of the enone system of the quinones, *via* coordination with the oxygen atom of the carbonyl group, thus promoting the Michael-type addition [35, 39, 40].

We examined the reactions of 14 with *N,N*-dimethylaniline in the presence of catalytic amounts of CeCl₃·7H₂O and IBr₃ (5%) in methanol, under open-flask conditions at room temperature. Both reactions occurred faster (28 h) than in the absence of these Lewis acids (72 h), and the arylation product 20 (Table 1) was isolated in 98 and 78% yield, respectively. The successful results obtained in the assay employing Ce(III) led us to evaluate the scope of the arylation reaction of the remaining members of the series with the selected arylamines, under the above optimized conditions. The results of the assays are summarized in Table 1.

The structures of compounds 16–28 were established by ¹H- and ¹³C-nuclear magnetic resonance (NMR), bidimensional nuclear magnetic resonance (2D-NMR), and high-resolution mass spectrometry (HRMS).

The data in Table 1 show that the arylation reaction of 2-acylnaphthoquinones 9-15 with the arylamines, catalyzed with Ce(III), yields the corresponding 2-acetyl-3-aminoaryl-1,4-naphthoquinones with good to excellent yields ranging from 63 to 98%, except in the case of product 17 (33%). Comparison of the reaction time formation of compounds 16-28 reveals two facts: the first one was linked to the lower reactivity of *N,N*-dimethylaniline compared to 2,5-dimethoxyaniline and secondly the strong influence of the stereoelectronic nature of the acyl substituents on the

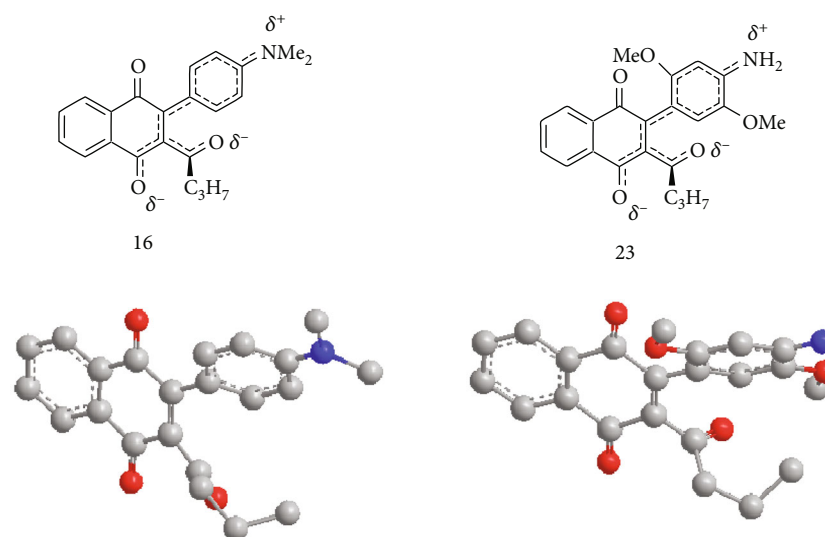
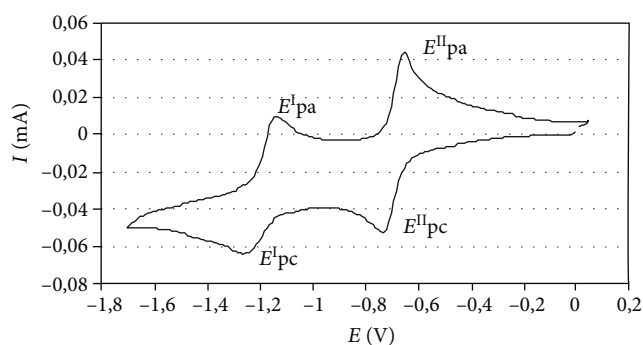
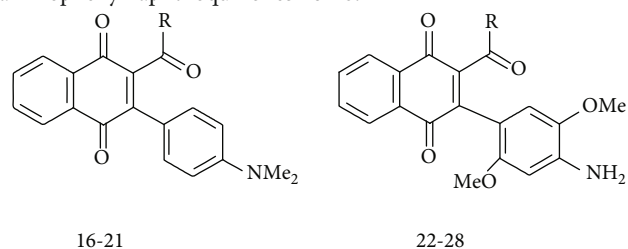


FIGURE 3: Hybrid and 3-D optimized structure of compounds 16 and 23.

FIGURE 4: Typical cyclic voltammogram of compound 23 in 0.1 M Et_4NBF_4 /acetonitrile obtained in Pt electrode, scan rate 100 mV/s. The cathodic (c) and anodic (a) peaks are indicated in the figure.

nucleophilic attack of the arylamines. It has to be mentioned that no attempts were made in order to decrease the reaction time formation of the arylation products. Based on our recent results [41] and that reported by Liu and Ji [42], on the arylation of quinones, we will attempt, in future researches, the use of ultrasound to accelerate the Ce(III)-promoted arylation reaction of acylnaphthoquinones with arenes in order to expand the 2-acetyl-3-aminoaryl-1,4-naphthoquinone series for further biological studies.

The acid-induced formation of the arylation compounds 16-28 from acylquinones 9-15 and their reaction with *N,N*-dimethylaniline are proposed to occur according to the mechanism of reaction depicted in Scheme 3. This approach is based on the reaction mechanism for the Ce(III)-promoted phenylation reaction of 1,4-naphthoquinone with 2-fluoro- and 2-methoxyanilines reported by Leyva et al. [35]. Initially, a selective conjugate Michael-type addition of the arylamine across the enone system $\text{C}_3=\text{C}_2-\text{C}_1=\text{O}$ seems plausible. This reaction, which involves the high electrophilic C-3 of the acylquinones, provides the respective C-C Michael adduct intermediates. Further enolization of these species, followed by aerobic oxidation, gives compounds 16-21. It

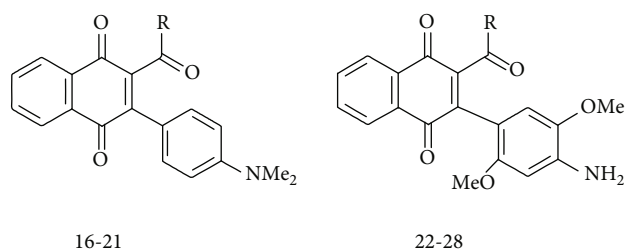
TABLE 2: Half-wave potential values $E^I_{1/2}$ and $E^{II}_{1/2}$ of 2-acyl-3-aminophenyl-naphthoquinones 16-28.

Product no.	R	$-E^I_{1/2}$ (mV)	$-E^{II}_{1/2}$ (mV)
16	C_3H_7	790	1180
17	C_5H_{11}	875	1295
18	4-MeOPh	815	1190
19	2,5-(OMe) ₂ Ph	845	1165
20	2-Furyl	620	1125
21	2-Thienyl	775	1165
22	CH_3	890	1410
23	C_3H_7	685	1180
24	C_5H_{11}	755	1230
25	4-MeOPh	720	1225
26	2,5-(OMe) ₂ Ph	760	1225
27	2-Furyl	710	1200
28	2-Thienyl	700	1205

should be noted that the electrophilicity of the C-3 in these acylquinones is mainly due to the electron-withdrawing effects of the acyl substituents attached to the 2-position. The coordination of Ce(III) to the oxygen atom of the enone system should contribute to increasing the electrophilicity of the C-3.

An interesting feature of the synthesized arylation products is their strong purple color of the chromophores that, according to Pardo et al. [24], is due to the strong donor-acceptor interactions between the quinoid and the electron-rich nitrogen substituents. Figure 3 shows the hybrid structures

TABLE 3: IC₅₀ ± SEM (μM) values of 16–28 on DU-145 (prostate cancer cells) and MCF-7 (mammary cancer cells) and nontumorigenic HEK-293 (embryonic kidney cells)*.



Compound no.	R	DU-145	MCF-7	Mean value	HEK-293
16	C ₃ H ₇	77.8 ± 1.1	>100	-	51.1 ± 0.8
17	C ₅ H ₁₁	>100	>100	-	77.4 ± 0.6
18	4-MeOPh	>100	>100	-	>100
19	2,5-(OMe) ₂ Ph	>100	>100	-	>100
20	2-Furyl	36.5 ± 0.2	>100	-	35.1 ± 1.4
21	2-Thienyl	53.1 ± 5.0	>100	-	67.6 ± 2.5
22	CH ₃	12.3 ± 0.4	21.2 ± 0.3	16.7	28.6 ± 1.9
23	C ₃ H ₇	22.5 ± 0.2	23.3 ± 0.5	22.9	21.5 ± 0.7
24	C ₅ H ₁₁	54.6 ± 1.5	>100	-	58.4 ± 0.6
25	4-MeOPh	>100	73.5 ± 1.6	-	71.3 ± 1.2
26	2,5-(OMe) ₂ Ph	28.7 ± 0.7	74.1 ± 2.4	51.4	53.3 ± 1.2
27	2-Furyl	13.2 ± 1.1	21.2 ± 1.4	17.2	11.2 ± 0.7
28	2-Thienyl	24.8 ± 0.3	33.1 ± 1.6	28.9	22.9 ± 0.7
DOX	-	0.70 ± 0.02	0.05 ± 0.003	-	4.27 ± 0.34

*Cells were incubated at 37°C for 48 h, with or without quinone derivatives. Afterwards, aliquots of cell suspensions were taken and the MTT test was performed, as described in Materials and Methods. Results are expressed as mean values ± SEM ($n = 3$). DOX = doxorubicin.

of compounds 16 and 23 where such interactions are clearly observable. Inspection of minimal energy conformation of compounds 16 and 23 performed by MM2 calculation (ChemBio3D 11.0, PerkinElmer, MA, USA) shows a noncoplanar orientation between the acyl-carbonyl groups and the naphthoquinone framework. This data agrees with the infrared absorption of the acyl-carbonyl groups of these compounds 16–28 that appeared within the range: ν_{\max} 1706–1735 cm⁻¹.

3.2. Voltammetric Measurements and Antioxidant Activities. In order to assess the redox properties of the members of the 2-acyl-3-aminoaryl-1,4-naphthoquinone series 16–28, their half-wave potentials $E^I_{1/2}$ and $E^{II}_{1/2}$ were measured by cyclic voltammetry. The measurement was conducted in acetonitrile at room temperature, using a platinum electrode and 0.1 M tetraethylammoniumtetrafluoroborate as the supporting electrolyte [19]. The voltammograms were recorded in the potential range from 0.0 to -2.0 V vs. nonaqueous Ag/Ag⁺. Figure 4 shows the typical electrochemical behavior of the arylation compound 23 that proceeded in two one-electron diffusion stages.

The cathodic peaks related to the reduction of quinone nucleus, and the anodic one due to its reoxidation, were observed for compound 23 as well-defined quasireversible waves. The $E_{1/2}$ values for the first one-electron correspond to the semiquinone radical anion formation and the second one-electron transfer to the dianion formation [17]. The

magnitude of these values falls within the ranges -875 to -620 mV/-1295 to -1125 mV for the members of the 2-acyl-3-(4-*N,N*-dimethylaminophenyl)naphthoquinones 16-21 and -890 to -685 mV/-1410 to -1180 mV for the members of the 2-acyl-3-(4-amino-2,5-dimethoxyphenyl)naphthoquinones 22-28 (Table 2).

The notable differences of the $E^I_{1/2}$ and $E^{II}_{1/2}$ values could be attributed to the stereoelectronic effects of the acyl substituents in the naphthoquinone scaffold (R = methyl, 1-propyl, 1-pentyl, 4-methoxyphenyl, 2,5-dimethoxyphenyl, 2-furyl, and 2-thienyl) in the 4-*N,N*-dimethylamino- and 4-amino-2,5-dimethoxyphenyl-1,4-naphthoquinone. Interestingly, the series 22-28 have lower $E^I_{1/2}$ values compared to 16-21, with the only exception of 20.

3.3. Antitumor Activity. The 2-acyl-3-aminophenyl-naphthoquinones 16-28 were evaluated for *in vitro* cytotoxic activities against nontumorigenic human embryonic kidney cells (HEK-293 cells) and two human cancer cell lines DU-145 (prostate) and MCF-7 (mammary) in 72 h drug exposure assays. The cytotoxic activities of the new compounds were measured using conventional microculture tetrazolium reduction assays [29]. Such activities are expressed in terms of IC₅₀. Doxorubicin, a well-known anticancer agent currently used in clinical practice, was taken as a positive control. The cytotoxic activity data are summarized in Table 3.

The data indicated that, in general, the DU-145 cells are more sensitive than MCF-7 cells to the compounds. In addition, the 2-acyl-3-(4-amino-2,5-dimethoxyphenyl)naphthoquinone members 22-28 exhibited higher activity than their corresponding analogues 16-21 but lower than those displayed by doxorubicin. Among the 2-acyl-3-(4-dimethylaminophenyl)naphthoquinone members, those containing the furan-2-carbonyl and thiophene-2-carbonyl groups, as compounds 20 and 21, are the most active on the DU-145 cancer cells. Inspection of the biological activity of 2-acyl-3-(4-amino-2,5-dimethoxyphenyl)naphthoquinone members reveals that those containing acetyl and furan-2-carbonyl groups, as 22 and 27, exhibited the higher activity on DU-145 and MCF-7 cancer cell lines. However, by taking the mean IC_{50} value and calculating a selectivity index (IC_{50} HEK-293 value/ IC_{50} cancer cell value), compound 22 displays a better index (1.71) than 27 (0.65), suggesting that this latter quinone did not discriminate between cancer and healthy cells. By increasing the number of the aliphatic chain within the acyl substituents, a decrease in the antiproliferative activity is observed: compounds 22 and 23 are more active than 24. The screening also shows that the members having 4-methoxy- and 2,5-dimethoxybenzoyl substituents, as compounds 18, 19, and 25 show weak or almost nonexistent cytotoxic activity. Finally, an additional element may be proposed to explain why compound 22 displays the best activity among the series: namely, its strong electronegative redox potential. In this regard, it is tempting to speculate that compound 22 has higher redox cycling ability, and therefore, it may generate the largest amount of ROS. Indeed, quinone redox cycling has been evoked as the main molecular mechanism explaining numerous deleterious effects by such molecules [43–46].

4. Conclusions

We have developed a simple and flexible route for the synthesis of novel 2-acyl-3-(aminophenylamino)-1,4-naphthoquinones whose structure is related to the HTS1, an inhibitor of the heat shock protein Hsp90. The members of the series were prepared in moderate to good yields (63–98%) by reaction of acynaphthoquinones with phenylamines, catalyzed by $CeCl_3 \cdot 7H_2O$. The new quinones were characterized by their spectral data and half-wave potentials. The first and second half-wave potential values ($E_{1/2}$) of the members of the series are sensitive to the acceptor and donor electronic effects of the substituents located in the quinone double bond. The *in vitro* cytotoxicities of the compounds on cancer cells were determined by using the MTT colorimetric method. The results of the biological evaluation of the 2-acyl-3-(aminophenyl)-1,4-naphthoquinone series show interesting *in vitro* cytotoxic activity on DU-145 and MCF-7 cancer cell lines for the member 22 making it a suitable new chemical entity to be further developed.

Data Availability

All data to be shared are included in the main text as well as in Supplementary Materials.

Conflicts of Interest

The authors declare no conflict of interest.

Acknowledgments

We thank Pilar Díaz from the Universidad Arturo Prat, Chile, for her excellent technical support and to Fondo Nacional de Ciencia y Tecnología (FONDECYT), grant numbers 11140544 and 1190577, and Proyecto Interno Universidad Arturo Prat VRIIP0030-17 for the financial support given to this study.

Supplementary Materials

Description of the spectral data of nuclear magnetic resonance (1H NMR and ^{13}C NMR) and high-resolution mass spectrometry (HRMS) of 2-acyl-3-aminophenyl-naphthoquinones. (*Supplementary Materials*)

References

- [1] R. H. Thompson, *Naturally Occurring Quinones IV: Recent Advances*, Blackie Academic & Professional, London, UK, 4th edition, 1997.
- [2] G. Lenaz, R. Fato, A. Baracca, and M. L. Genova, "Mitochondrial quinone reductases: complex I," in *Methods Enzymology*, vol. 382, pp. 3–20, Elsevier, 2004.
- [3] J. M. C. Gutteridge and B. Halliwell, "Free radicals and antioxidants in the year 2000. A historical look to the future," *The Annals of the New York Academy of Sciences*, vol. 899, no. 1, pp. 136–147, 2000.
- [4] B. Halliwell and J. M. C. Gutteridge, *Free Radicals in Biology and Medicine*, Oxford University Press, Oxford, 4th edition, 2006.
- [5] S. Y. Wang and H. Jiao, "Scavenging capacity of berry crops on superoxide radicals, hydrogen peroxide, hydroxyl radicals, and singlet oxygen," *Journal of Agricultural and Food Chemistry*, vol. 48, no. 11, pp. 5677–5684, 2000.
- [6] M. A. Omar, "Effect of 2-hydroxy-1, 4-naphthoquinone, a natural dye of Henna, on aldehyde oxidase activity in guinea pig liver," *Journal of Medical Sciences*, vol. 5, no. 3, pp. 163–168, 2005.
- [7] V. Ambrogi, D. Artini, I. Carneri et al., "Studies on the antibacterial and antifungal properties of 1, 4-naphthoquinones," *British Journal of Pharmacology*, vol. 40, no. 4, pp. 871–880, 1970.
- [8] B. H. Ali, A. K. Bashir, and M. O. Tanira, "Anti-inflammatory, antipyretic, and analgesic effects of *Lawsonia inermis* L.(Henna) in rats," *Pharmacology*, vol. 51, no. 6, pp. 356–363, 1995.
- [9] H. Kamei, T. Koide, T. Kojima, Y. Hashimoto, and M. Hasegawa, "Inhibition of cell growth in culture by quinones," *Cancer Biotherapy and Radiopharmaceuticals*, vol. 13, no. 3, pp. 185–188, 1998.
- [10] B. J. Day, "Antioxidant therapeutics: Pandora's box," *Free Radical Biology and Medicine*, vol. 66, pp. 58–64, 2014.
- [11] K. Maruyama and Y. Naruta, "Syntheses of α - and β -laphachones and their homologues by way of photochemical side chain introduction to quinone," *Chemistry Letters*, vol. 6, no. 8, pp. 847–850, 1977.

- [12] H. Uno, "Allylation of 2-alkanoyl 1,4-quinones with allylsilanes and allylstannanes. Efficient synthesis of pyranonaphthoquinone antibiotics," *The Journal of Organic Chemistry*, vol. 51, no. 3, pp. 350–358, 1986.
- [13] M. A. Brimble and S. M. Lynds, "A short synthesis of deoxyfrenolicin," *Journal of the Chemical Society, Perkin Transactions*, vol. 1, no. 5, pp. 493–496, 1994.
- [14] G. A. Kraus and H. Maeda, "A direct preparation of 1,4-benzodiazepines. The synthesis of medazepam and related compounds via a common intermediate," *Tetrahedron Letters*, vol. 35, no. 49, pp. 9189–9190, 1994.
- [15] P. A. Waske, J. Mattay, and M. Oelgemöller, "Photoacylations of 2-substituted 1,4-naphthoquinones: a concise access to biologically active quinonoid compounds," *Tetrahedron Letters*, vol. 47, no. 8, pp. 1329–1332, 2006.
- [16] J. A. Valderrama, J. Benites, M. Cortés, D. Pessoa-Mahana, E. Prina, and A. Fournet, "Studies on quinones. Part 35: access to antiprotazoal active euryfurylquinones and hydroquinones," *Tetrahedron*, vol. 58, no. 5, pp. 881–886, 2002.
- [17] D. R. Vásquez, J. Verrax, J. A. Valderrama, and P. B. Calderon, "Aminopyrimidoisoquinolinequinone (APIQ) redox cycling is potentiated by ascorbate and induces oxidative stress leading to necrotic-like cancer cell death," *Investigational New Drugs*, vol. 30, no. 3, pp. 1003–1011, 2012.
- [18] V. Delgado, A. Ibacache, C. Theoduloz, and J. A. Valderrama, "Synthesis and *in vitro* cytotoxic evaluation of aminoquinones structurally related to marine isoquinolinequinones," *Molecules*, vol. 17, no. 6, pp. 7042–7056, 2012.
- [19] D. Rios, J. Benites, J. A. Valderrama et al., "Biological evaluation of 3-acyl-2-arylamino-1,4-naphthoquinones as inhibitors of Hsp90 chaperoning function," *Current Topics in Medicinal Chemistry*, vol. 12, no. 19, pp. 2094–2102, 2012.
- [20] J. A. Valderrama, D. Rios, G. G. Muccioli, P. Buc Calderon, I. Brito, and J. Benites, "Hetero-annulation reaction between 2-acylnaphthoquinones and 2-aminobenzothiazoles. A new synthetic route to antiproliferative benzo[g]benzothiazolo[2,3-*b*]quinazoline-7,12-quinones," *Tetrahedron Letters*, vol. 56, no. 36, pp. 5103–5105, 2015.
- [21] J. Benites, J. A. Valderrama, M. Ramos, G. G. Muccioli, and P. Buc Calderon, "Targeting Akt as strategy to kill cancer cells using 3-substituted 5-anilinobenzo[c]isoxazolequinones: a preliminary study," *Biomedicine & Pharmacotherapy*, vol. 97, pp. 778–783, 2018.
- [22] M. K. Hadden, S. A. Hill, J. Davenport, R. L. Matts, and B. S. J. Blagg, "Synthesis and evaluation of Hsp90 inhibitors that contain the 1,4-naphthoquinone scaffold," *Bioorganic & Medicinal Chemistry*, vol. 17, no. 2, pp. 634–640, 2009.
- [23] R. Beck, R. C. Pedrosa, N. Dejeans et al., "Ascorbate/menadione-induced oxidative stress kills cancer cells that express normal or mutated forms of the oncogenic protein Bcr-Abl. An *in vitro* and *in vivo* mechanistic study," *Investigational New Drugs*, vol. 29, no. 5, pp. 891–900, 2011.
- [24] M. Pardo, K. Joos, and W. Schäfer, "Über die oxidative Aminierung von 1',4'-dihydroxy-2'-acetonaphthon," *Liebigs Annalen der Chemie*, vol. 1979, no. 4, pp. 503–521, 1979.
- [25] W. Schäfer and H. Schlude, "Über die chemie substituierter p-benzochinone IV synthese und eigenschaften substituierter aminochinone," *Tetrahedron Letters*, vol. 8, no. 44, pp. 4307–4312, 1967.
- [26] J. A. Valderrama, M. Cabrera, J. Benites et al., "Synthetic approaches and *in vitro* cytotoxic evaluation of 2-acyl-3-(3,4,5-trimethoxyanilino)-1,4-naphthoquinones," *RSC Advances*, vol. 7, no. 40, pp. 24813–24821, 2017.
- [27] J. Benites, H. Toledo, F. Salas et al., "In vitro inhibition of *Helicobacter pylori* growth by redox cycling phenylaminojuglones," *Oxidative Medicine and Cellular Longevity*, vol. 2018, Article ID 1618051, 8 pages, 2018.
- [28] J. Benites, D. Rios, P. Díaz, and J. A. Valderrama, "The solar-chemical photo-Friedel-Crafts heteroacylation of 1,4-quinones," *Tetrahedron Letters*, vol. 52, no. 5, pp. 609–611, 2011.
- [29] T. Mosmann, "Rapid colorimetric assay for cellular growth and survival: application to proliferation and cytotoxicity assays," *The Journal of Immunological Methods*, vol. 65, no. 1-2, pp. 55–63, 1983.
- [30] J. A. Valderrama, D. Rios, G. G. Muccioli, P. Buc Calderon, and J. Benites, "In vitro inhibition of Hsp90 protein by benzothiazoloquinazolinequinones is enhanced in the presence of ascorbate. A preliminary *in vivo* antiproliferative study," *Molecules*, vol. 25, no. 4, pp. 953–966, 2020.
- [31] G. Bartoli, E. Marcantoni, M. Marcolini, and L. Sambri, "Applications of CeCl₃ as an environmental friendly promoter in organic chemistry," *Chemical Reviews*, vol. 110, no. 10, pp. 6104–6143, 2010.
- [32] A. Corma and H. Garcia, "Lewis acids: from conventional homogeneous to green homogeneous and heterogeneous catalysis," *Chemical Reviews*, vol. 103, no. 11, pp. 4307–4366, 2003.
- [33] M. Kidwai and A. Jahan, "Cerium chloride (CeCl₃·7H₂O) as a highly efficient catalyst for one-pot three-component Mannich reaction," *Journal of the Brazilian Chemical Society*, vol. 21, no. 12, pp. 2175–2179, 2010.
- [34] J. M. Dos Santos Filho, "Mild, stereoselective, and highly efficient synthesis of N-acylhydrazones mediated by CeCl₃·7H₂O in a broad range of solvents," *European Journal of Organic Chemistry*, vol. 2014, no. 29, pp. 6411–6417, 2014.
- [35] E. Leyva, K. M. Baines, C. G. Espinosa-González et al., "2-(Fluoro-) and 2-(methoxyanilino)-1,4-naphthoquinones. Synthesis and mechanism and effect of fluorine substitution on redox reactivity and NMR," *Journal of Fluorine Chemistry*, vol. 180, pp. 152–160, 2015.
- [36] M. A. Brimble, O. Laita, and J. E. Robinson, "Addition of 2-tert-butylidimethylsilyloxythiophene to activated quinones: an approach to thia analogues of kalafungin," *Tetrahedron*, vol. 62, no. 13, pp. 3021–3027, 2006.
- [37] P. Ashok and A. Ilangoan, "Transition metal mediated selective C vs N arylation of 2-aminonaphthoquinone and its application toward the synthesis of benzocarbazoledione," *Tetrahedron Letters*, vol. 59, no. 5, pp. 438–441, 2018.
- [38] C. D. S. Lisboa, V. G. Santos, B. G. Vaz, N. C. de Lucas, M. N. Eberlin, and S. J. Garden, "C-H functionalization of 1,4-naphthoquinone by oxidative coupling with anilines in the presence of a catalytic quantity of copper(II) acetate," *The Journal of Organic Chemistry*, vol. 76, pp. 5264–5273, 2011.
- [39] Y. T. Pratt, "Quinolinequinones. VI. Reactions with aromatic amines¹," *The Journal of Organic Chemistry*, vol. 27, no. 11, pp. 3905–3910, 1962.
- [40] J. V. Schurman and E. I. Becker, "Synthesis of naphthylamino-naphthoquinones," *The Journal of Organic Chemistry*, vol. 18, no. 2, pp. 211–217, 1953.
- [41] J. A. Ibacache, J. A. Valderrama, J. Faúndes, A. Danimann, F. J. Recio, and C. A. Zúñiga, "Green synthesis and electrochemical

- properties of mono- and dimers derived from phenylaminoisoquinolinequinones,” *Molecules*, vol. 24, no. 23, pp. 4378–4390, 2019.
- [42] B. Liu and S.-J. Ji, “Facile synthesis of 2-amino-1,4-naphthoquinones catalyzed by molecular iodine under ultrasonic irradiation,” *Synthetic Communications*, vol. 38, no. 8, pp. 1201–1211, 2008.
- [43] P. Ravichandiran, S. Sheet, D. Premnath, A. R. Kim, and D. J. Yoo, “1,4-naphthoquinone analogues: potent antibacterial agents and mode of action evaluation,” *Molecules*, vol. 24, no. 7, pp. 1437–1451, 2019.
- [44] P. Ravichandiran, M. Maslyk, S. Sheet et al., “Synthesis and antimicrobial evaluation of 1,4-naphthoquinone derivatives as potential antibacterial agents,” *ChemistryOpen*, vol. 8, no. 5, pp. 589–600, 2019.
- [45] D. J. Yoo, P. Ravichandiran, S. A. Subramaniyan et al. et al., “Synthesis anticancer evaluation of novel 1,4-naphthoquinone derivatives containing a phenylamino-sulfanyl moiety,” *ChemMedChem*, vol. 14, no. 5, pp. 532–544, 2019.
- [46] C. Glorieux and P. Buc Calderon, “Cancer cell sensitivity to redox-cycling quinones is influenced by NAD(P)H: quinone oxidoreductase 1 polymorphism,” *Antioxidants*, vol. 8, no. 9, pp. 369–378, 2019.

Review Article

Mechanistic Insights into the Oxidized Low-Density Lipoprotein-Induced Atherosclerosis

Chainika Khatana,^{1,2} Neeraj K. Saini,^{3,4} Sasanka Chakrabarti,⁵ Vipin Saini,⁶ Anil Sharma,¹ Reena V. Saini ,¹ and Adesh K. Saini ¹

¹Department of Biotechnology and Central Research Cell, MMEC, Maharishi Markandeshwar (Deemed to be University), Mullana, 133207 Ambala, Haryana, India

²Faculty of Applied Sciences and Biotechnology, Shoolini University, Solan, 173212 Himachal Pradesh, India

³Department of Microbiology and Immunology, Albert Einstein College of Medicine, Bronx, NY 10461, USA

⁴Department of Biotechnology, Jawaharlal Nehru University, Delhi, India

⁵Department of Biochemistry and Central Research Cell, MM Institute of Medical Sciences & Research Maharishi Markandeshwar Deemed to be University, Mullana, 133207 Haryana, India

⁶Maharishi Markandeshwar University, Solan, 173212 Himachal Pradesh, India

Correspondence should be addressed to Reena V. Saini; reenavohra10@gmail.com and Adesh K. Saini; sainiade@gmail.com

Received 9 July 2020; Revised 30 August 2020; Accepted 1 September 2020; Published 15 September 2020

Academic Editor: Sander Bekeschus

Copyright © 2020 Chainika Khatana et al. This is an open access article distributed under the Creative Commons Attribution License, which permits unrestricted use, distribution, and reproduction in any medium, provided the original work is properly cited.

Dyslipidaemia has a prominent role in the onset of notorious atherosclerosis, a disease of medium to large arteries. Atherosclerosis is the prime root of cardiovascular events contributing to the most considerable number of morbidity and mortality worldwide. Factors like cellular senescence, genetics, clonal haematopoiesis, sedentary lifestyle-induced obesity, or diabetes mellitus upsurge the tendency of atherosclerosis and are foremost pioneers to definitive transience. Accumulation of oxidized low-density lipoproteins (Ox-LDLs) in the tunica intima triggers the onset of this disease. In the later period of progression, the build-up plaques rupture ensuing thrombosis (completely blocking the blood flow), causing myocardial infarction, stroke, and heart attack, all of which are common atherosclerotic cardiovascular events today. The underlying mechanism is very well elucidated in literature but the therapeutic measures remains to be unleashed. Researchers tussle to demonstrate a clear understanding of treating mechanisms. A century of research suggests that lowering LDL, statin-mediated treatment, HDL, and lipid-profile management should be of prime interest to retard atherosclerosis-induced deaths. We shall brief the Ox-LDL-induced atherogenic mechanism and the treating measures in line to impede the development and progression of atherosclerosis.

1. Introduction

World Health Organisation (WHO) has enumerated quite a few diseases responsible for the disability and deaths in the industrialized world, among which cardiovascular diseases (CVDs) are the most common, invoking about 17.9 million deaths annually (WHO fact sheet). In-depth mechanistic knowledge is anticipated to lessen the effects and consequences of critical risk factors involved in this disease. Epidemiological studies imply that elevated level of low-density lipoprotein (LDL) (cholesterol carrier through the blood of 20-25 nm size) is the chief contributor to atherosclerosis [1,

2]. Atherosclerosis refers to the disease of arteries which commonly manifests as coronary heart disease (CHD) leading to myocardial infarction and cerebrovascular disease leading to stroke and other complications. Atherosclerosis is a complex, progressive, inflammatory disease that mainly occurs in subendothelial space (tunica intima) of medium to large-sized arteries at regions of disturbed blood flow or bifurcates [3–5]. The progression of atherosclerotic disease depends on the presence, degree, and persistence of risk factors like high-fat diet, smoking, hypertension, history of heart diseases, or diabetes [6–8] (Table 1). Experimental observations have explicitly pinpointed oxidized low-density lipoprotein (Ox-

TABLE 1: Risk factors to atherosclerosis.

Hyperlipidemia
Homocysteine levels in plasma
Hypertension
Smoking
Low or impaired HDL
Family history of CVDs
Obesity
Aging
Male sex
Physical inactivity
Stress/depression
High cholesterol
Sedentary lifestyle
Unhealthy diet
Psychological and socioeconomic factors

LDL), endothelium dysfunction, and oxidative stress as the most prominent risk factors in atherosclerosis [9–11].

Under normal physiological condition cell maintains redox homeostasis which plays a significant role in signalling and, any imbalance in this homeostasis may instigate a chain of reactions generating free radicals (reactive oxygen species termed here as ROS or reactive nitrosative species termed here as RNS) [11, 12]. Disturbed redox balance or the imbalance between reactive species and antioxidant system leads to the oxidative stress that damages biomolecules like proteins, nucleic acids, and lipids. Exposure to exogenous chemical and physical agents (like environmental pollutants, radiation, UV exposure, or smoking) or endogenous enzymes (like NADPH oxidase, xanthine oxidase, cytochrome P450, or nitric oxide synthase (NOS) and metal ion catalysis (Fenton reaction)) generally results into increased ROS production [11, 13, 14]. Physical forces including oscillatory shear are also reported to have a share in vascular production of ROS [11, 15]. Lipids serve as primary targets of reactive species with important relevance to CVDs, and these lipids can be analyzed by several methods [13, 16, 17]. Lipid oxidation, commonly known as lipid peroxidation, is a process that involves peroxidation of phospholipids and cholesterol esters at the polyunsaturated fatty acid moieties (linoleate, arachidonate, etc.) by nonenzymatic mechanisms (ROS, RNS, or in presence of transition metals like Fe^{2+} and Cu^{2+}) [18–20]. Maintenance of plasma LDL levels is important for CVD (23, 24). Additionally, the polyunsaturated fatty acids may be oxidized by lipooxygenase, cyclooxygenase, and cytochrome P450-dependent oxygenases producing ROS in the process. Lipid peroxidation progresses through 3 stages: initiation, propagation, and termination [21]. The free radical chain oxidation mechanism initiates with a lipid radical formation (abstraction of hydrogen atom from the CH_2 group) leading to the propagation step where it reacts with oxygen generating lipid-peroxyl radicals that transform it into lipid hydroperoxides and finally, the reaction terminates once nonradical products are formed releasing oxygen [22]. It is

quite difficult to quantify the products of lipid peroxidation because of the complexity of lipid peroxidation pathway and its by-products. New techniques like mass spectroscopy tools are now being used to at least meet some challenges [17].

Under normal conditions, the plasma LDL is composed of triglycerides and cholesterol esters with an outer layer composed of phospholipids, free cholesterol, and apolipoprotein B (ApoB) that carry hydrophobic cholesterol through the blood [15]. Increase in the plasma LDL levels is generally associated with atherosclerosis [23]. Under oxidative stress, the oxidation of LDL occurs by the process of lipid peroxidation primarily involving the phospholipid molecules. In pathological conditions, ApoB-containing lipoproteins in the plasma penetrate through the damaged endothelium into vascular subendothelial intima getting oxidized by ROS [24, 25]. Under these conditions, the LDL is modified into Ox-LDL [26]. LDL retention in subendothelium confers monocyte recruitment to tunica intima, where they differentiate into macrophages. Ox-LDL serves as strong ligands for macrophage scavenger receptors (CD36, SR-AI/II, and SR-BI) that facilitate their entry into macrophages [27]. It is suggested that the oxidation of specific epitopes (OSEs) occur on Ox-LDL that are recognized by the cellular and humoral innate immune system and thus enhancing the internalization of Ox-LDL into macrophages [28]. Macrophages engulf Ox-LDL through its scavenger receptors and the accumulation of Ox-LDL into macrophages gives it a morphologic appearance of soap bubbles termed as foam cells which later result in atherosclerotic lesions leading to atherosclerotic plaque build-up, limiting the blood flow to the heart muscle (see Figure 1 for schematic diagram) [29, 30]. Very recently, a study was published providing insights into myeloid tribbles 1 that induces early atherosclerosis via extensive foam cell formation [31]. A native LDL cannot exert atherogenic mechanisms in vitro which implicate that to be pathogenic it must have been modified, explaining oxidative damage as a pro [32].

On the brighter side, high-density lipoproteins (HDLs), endogenous apolipoprotein E (ApoE), and ApoA-I proteins promote efflux of surplus cholesterol from the macrophage via specific transporters of the ATP binding cassette (ABC) gene family [33]. This efflux is the primary line of defence to protect against the progression of macrophage to foam cells. Further, antioxidants scavenge ROS combating atherosclerosis in the initiation period [34]. Efforts have been made to comprehend the mechanism of lipid peroxidation in developing effective therapeutic drugs and prevent its deleterious effects. Herein, we have discussed the role of distinct factors critical in the progression of atherosclerosis.

2. Oxidized Low-Density Lipoprotein as the Major Risk Factor in Atherosclerosis

Low-density lipoprotein is a chief carrier of cholesterol to the cells. High dietary fat adds to its abundance causing pathological complications above a threshold level [35]. It belongs to a heterogeneous group of particles having a mass of about 3000 kDa with a diameter of 220 nm [36]. The hydrophobic core of LDL is made of around 170 triglycerides, 1500 cholesterol esters, a hydrophilic coat composed of 700 molecules of

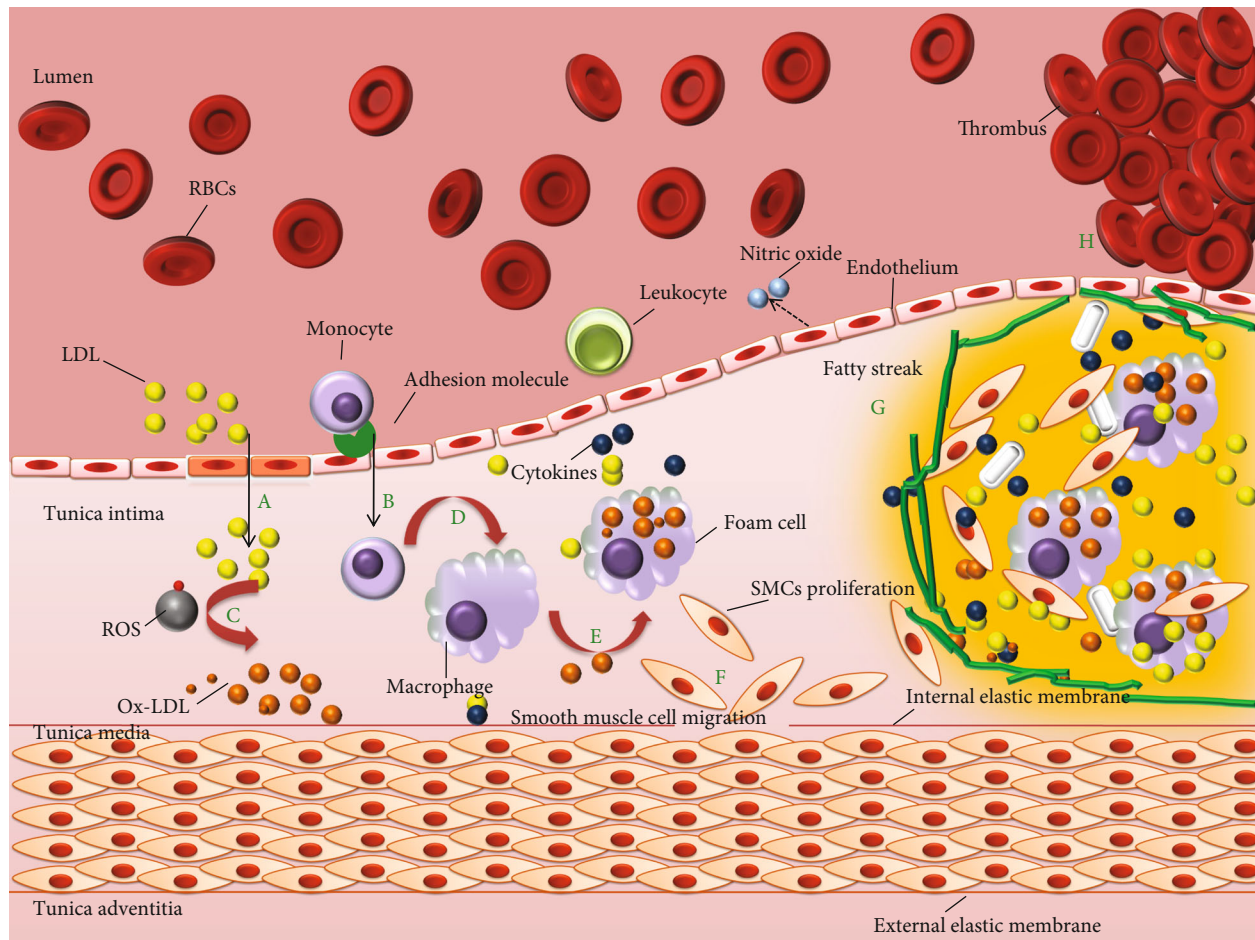


FIGURE 1: Schematic network of atherosclerosis process. The LDL in the blood stream passes through the damaged endothelium (caused by hypertension, high cholesterol, smoking, and hyperglycemia) gaining entry into tunica intima. Damaged endothelial cells being compromised express adhesion molecules that capture the monocytes. Monocytes enter into the intima producing free radicals which oxidizes the LDL. Oxidized LDL attracts more white blood cells (monocytes) and more immune cells to the site, macrophages engulf Ox-LDL particles becoming over laden and turning into foam cells. Foam cells die releasing its content outside that again is engulfed by other macrophages eventually building a large lesion area. Progression into this, lesion turns into plaque gradually accumulating calcium slats, smooth muscle cells (from tunica media), collagen, and the foam cells. The plaque is stable under the endothelium until the endothelium just above gets compromised. The damaged endothelium could no longer produce inhibitors for blood clotting making it more vulnerable to enter into the vessel lumen. The clot attached to the vessel wall would make a thrombus that may break causing stroke or myocardial infarction.

phospholipids, about 500 molecules of unesterified cholesterol, and a single large copy of the ApoB of 500 kDa [37]. Structure of LDL and Ox-LDL is shown in Figure 2.

During oxidative stress, the LDL is modified to Ox-LDL [38]. In addition to this, lipoxygenase and phospholipase A2 enzymes alter LDL in a manner of getting easily recognized and engulfed by macrophages [39]. Speaking specifically in terms of atherosclerosis, ROS induces lipid oxidation, instigating the disease. LDL oxidation brings about certain modifications to the LDL structure giving it a higher density, hydrolysing phosphatidylcholine, amending lysine residues of ApoB, and degrading ApoB [37]. Polyunsaturated fatty acids (PUFAs) in the LDL are more prone to oxidation as compared to monounsaturated fatty acids (MUFAs) [40]. PUFAs encountering oxidation (enzymatic and nonenzymatic) convert into hydroperoxides further breaking down to generate more reactive aldehyde products and metabolites such as malondialdehyde and 4-hydroxynoneal which build

adduct with Schiff-base lysine residue of ApoB, phosphatidylserine, and phosphatidylethanolamine [41]. ApoB in this context determines the generation and propagation of LDL oxidation. Additionally, the elevated temperature used while preparing meals increases the oxidation of cholesterol [42]. Nonetheless, oxysterols coming from the dietary sources into the bloodstream may implicate a fundamental role in the progression of this disease. Thereby, one cannot conclude the root embarking such progression and advanced studies need to be done.

Discoveries by Virchow and Windaus in the nineteenth century bring forth the crucial role of lipoproteins in atherosclerosis. Windaus discovered high cholesterol in human artery which thereafter confirmed by Nikolaj Anitschkow who produced atherosclerosis in cholesterol fed rabbits implicating dietary cholesterol as an important factor [43, 44]. Carl Muller revealed a compelling connection between heart attacks and plasma cholesterol giving the cholesterol research

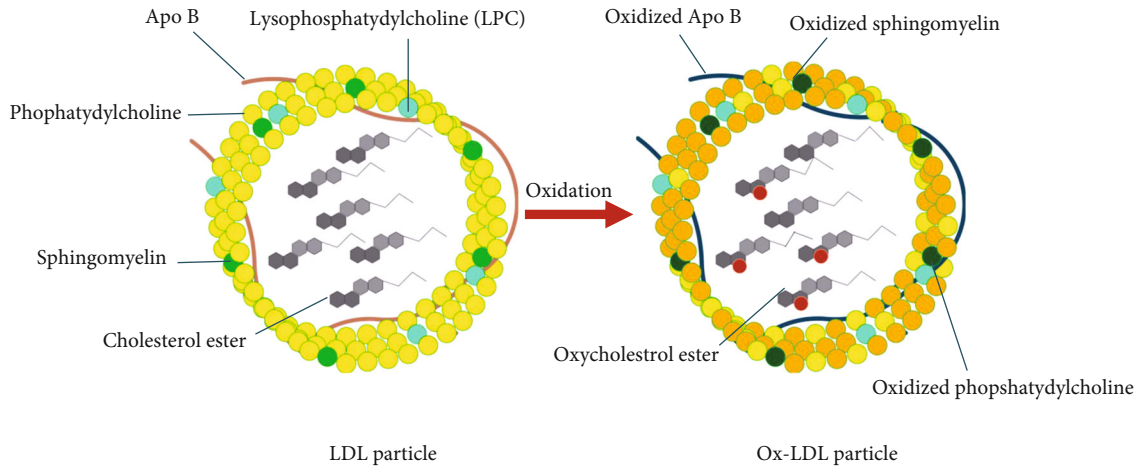


FIGURE 2: LDL and Ox-LDL Structure. The hydrophobic core of LDL is made of around 170 triglycerides, 1500 cholesterol esters, a hydrophilic coat composed of 700 molecules of phospholipids, about 500 molecules of unesterified cholesterol, and a single large copy of the apolipoprotein B (ApoB) of 500 kDa. Gaining entrance into the endothelium, LDL gets oxidatively modified by ROS.

a new turn introducing the hypercholesterolemia [45]. Widespread theories put forward LDL penetrating the dysfunctional endothelium and retaining in the subendothelium lining as the hallmark of atherosclerosis [46]. The higher the LDL the faster the plaque evolves. Surprisingly, native LDL is not atherogenic and needs to be oxidatively modified, particularly ApoB, to instigate the disease while it stays in the subendothelium bound to glycosaminoglycans [47, 48]. Macrophages with their surface receptors recognize the modified LDL and engulf them to become lipid laden foam cells which secrete cytokines making the site more vulnerable to inflammation and instigating smooth muscle cell (SMC) proliferation [49–51]. Today, many publications could be found on Ox-LDL to provide evidence for its role in atherosclerosis which makes it a relevant candidate and somewhat apparent therapeutic target. Though very few studies could robustly prove the definitive decrease of LDL with dietary antioxidant supplements, it is believed that a combination of antioxidants, therapeutics, and lipid management could work wonder (discussed later in this review).

2.1. Stages of Ox-LDL-Induced Atherosclerosis Mechanism: Initiation to Thrombosis. Atherosclerosis originates with the subendothelial retention of ApoB 100, containing lipoproteins. LDL penetration through dysfunctional endothelium brings many factors into the picture (summarized from the initiation to calcification in this review). Broadly, the process can be classified into three stages: initiation, progression, and thrombosis. A human artery is composed of three layers: the tunica intima, the tunica media, and the tunica adventitia, as shown in Figure 3. Intima is lined with a single layer of endothelial cells called the endothelium and subendothelial extracellular matrix (consisted of collagen and elastin). Endothelium aids in regulating vascular tone, coagulation, and maintaining vascular homeostasis via highly regulated mechanisms with the function of nitric oxide, prostacyclin, and endothelin-1 [52, 53]. Numerous smooth muscle cells (SMCs) are found in tunica media which are organised concentrically within an elastin-rich cellular matrix to store the

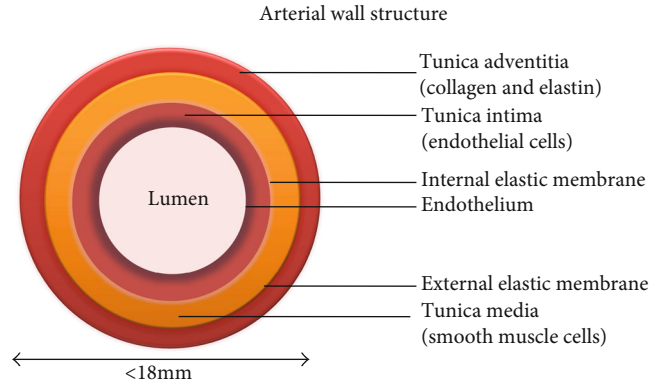


FIGURE 3: Artery is made of three layers: tunica intima, media, and adventitia.

required kinetic energy for transmission of pulsatile flow [54]. The adventitia contains mast cells, fibroblasts, and a matrix containing proteoglycans and collagen. Internal and external elastic lamina separates the intima, media, and adventitia, respectively [55]. Nevertheless, the artery gets compromised with the interplay of Ox-LDL and other risk factors making hard and narrowing the lumen for a disturbed blood flow. An atherosclerotic artery with plaque is shown in Figure 4 and a cross section of early and late atherosclerotic lesion is shown in Figure 5 [56].

Ox-LDL instigates atherosclerotic events throughout the disease progression, starting from endothelium dysfunction, white blood cell activation, foam cell formation, SMC migration and proliferation to platelet adhesion and aggregation (refer Figure 6).

2.2. Physiology of Endothelial Dysfunction: Initiation Stage. In normal body parameters, a healthy endothelium remains the primary regulator of vascular homeostasis [57–59]. It assists in keeping a balance between vasodilation and vasoconstriction, thrombogenesis and fibrinolysis, and inhibition and stimulation of SMC proliferation [60]. Nonetheless, it acts as

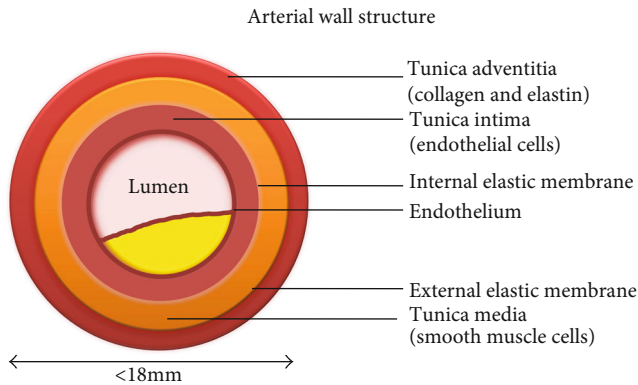


FIGURE 4: Atherosclerotic artery. Atherosclerotic artery has a plaque build-up in the subendothelium making the lumen too small for a smooth blood flow.

a barrier between the circulating blood (in lumen) and the artery lining (endothelium) [61]. An intact endothelium experiencing laminar shear stress elicits signalling pathways to maintain glycocalyx layer, proliferation, and endothelial cell coaxial alignment [10, 62]. Nitric oxide synthase (NOS) is expressed via MEK5 signalling which promotes the nitric oxide (NO) production and further helping in the endothelium survival. The antiatherogenic role of NO is supported by numerous studies on knockout mice for ApoE and other animal models of atherosclerosis [63]. In these models, inhibition of endothelial NO production accelerates the formation of lesions in the aorta and the coronary arteries, and treatment with L-arginine preserves vessel morphology. Superoxide dismutase (SOD), catalase, glutathione peroxidase (GPx), and peroxiredoxins (Prxs) are expressed to counter cellular ROS [64]. Arteries experiencing disturbed blood flow and low shear stress at the curves and branches are susceptible to atherosclerotic lesions [5]. These regions contain a sensitive glycocalyx layer with an irregular alignment. Consequently, the low production of NOS and antioxidant enzymes compromise endothelium integrity. In exposure to certain predisposing risk factors such as hypertension, hyperglycemia, diabetes, ageing, hypercholesterolemia, and the mechanical stimuli owing to low shear stress, endothelium undergoes certain modifications which are characteristics for atherosclerotic initiation process [9, 65]. Morphological modification of endothelial cells and increased permeability to LDL particles thus allows penetration (transcytosis) and accumulation of ApoB, chylomicrons, and remnants of very-low-density lipoproteins (VLDLs) in the subendothelial space where they experience oxidative modifications by cytokines (monocyte chemoattractant protein-1 (MCP-1)) [48]. The antithrombotic factors are compromised along with elevated vasoconstrictor and prothrombotic products via cell surface adhesion molecules such as intercellular adhesion molecule 1 (ICAM-1) and vascular cell adhesion molecule 1 (VCAM-1), hence elevating risk for inflammatory actions owing to Ox-LDL [66, 67]. These changes increase the adhesion of monocytes and penetration through the vascular wall which is modulated by cytokines and is augmented by interferon gamma and tumour necrosis factor-alpha [68, 69]. Studies report Ox-

LDL as a key into the above-mentioned mechanism. In fact, Ox-LDL is chief in activating endothelium to secrete MCPs recruiting monocytes and T cells into endothelium.

NO plays a crucial part in protecting endothelium with its vasodilator property. It is also seen to reduce monocyte adhesion to the endothelium. Ox-LDL-induced reduction in the NO derived from the endothelium NOS is suggested as one of the causes of endothelial phenotypic changes [70]. Most of its activity is proposed to lectin-like oxidized LDL receptor 1 (LOX 1). LOX 1 is an Ox-LDL receptor found on endothelial cells and is likely to be overexpressed in atherosclerotic conditions.

There have been debates among chronology of events that lead to plaque formation. Since few scientists consider subendothelial retention of ApoB lipoproteins as the initiating factor in atherosclerosis, contradictory to which some authors suggest that everything starts with endothelial dysfunction [53]. High LDL level also marks its strong part in the argument. A plethora of research suggests that all these phenomena are more or less equally indispensable factors in the progression of atherosclerosis [71].

2.3. LDL Retention in the Subendothelium Elicits an Immune Response: Progression Stage. The entry of LDL particles in the subendothelium (tunica intima) followed by their retention through ApoB 100 binding to proteoglycans of the extracellular matrix is a key initiating factor in early atherogenesis. Oxidative modifications of LDL induce expression of cell adhesion molecules on the endothelial cells recruiting mainly monocytes and T lymphocytes into the inflamed arterial wall. Differentiation of monocytes into macrophage expresses scavenger receptors (CD36, SR-AI/II, and SR-BI) and LOX 1 (lectin-like Ox-LDL receptor 1) on the surface to recognize Ox-LDL [58, 59]. Various studies have established that to be recognized by a scavenger or oxidized receptors, the native LDL must be converted to Ox-LDL as discussed in previous section (due to its high affinity to scavenger receptors, SR) [72]. As soon as macrophages engulf massive Ox-LDL particles, foam cells are generated and a number of proinflammatory events take place: lipid retention, more oxidation of native LDL, release of proinflammatory cytokines, ROS, metalloproteases, and monocyte and Ox-LDL recruitment. Cytokines released by T lymphocytes and foam cells promote inflammation and ROS generation. Unsurprisingly, Ox-LDL along with these cells releases growth factors promoting SMC migration (via platelet derived growth factor and basic fibroblast growth factor) from tunica media into site region and abnormal proliferation (via insulin-like growth factor 1 and epidermal growth factor) that involves secretion of extracellular matrix proteins [73]. It is also seen that Ox-LDL drives SMCs to produce collagen and elastin which forms a necrotic core around the plaque increasing the lesion size at some point. It is important to mention that a lot of these events are more or less LOX 1 mediated [74]. Atherosclerotic plaque is a large necrotic core of foam cells, SMCs, collagen, calcium, and a thin fibrous cap preventing plaque from the bloodstream [75]. Hence, Ox-LDL plays a significant role in these events and moreover it is believed to induce apoptosis or at some point necrosis, favouring cellular debris deposits in

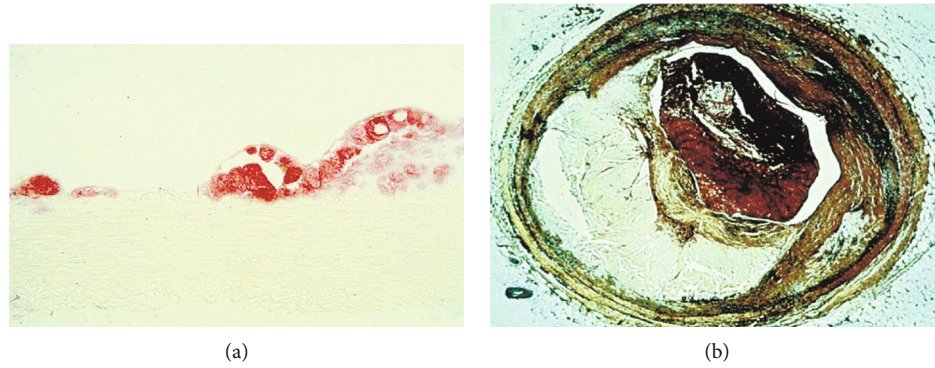


FIGURE 5: Early and late atherosclerotic lesions. The figure is reproduced from Glass and Witztum [56] (under the Creative Commons Attribution License/public domain) “(Reprinted (Atherosclerosis: The Road Ahead) with permission from Elsevier (License number 4825741069515)).”(a) Cross section of a fatty streak lesion from the aorta of a cholesterol-fed rabbit immune stained for a macrophage-specific marker (micrograph courtesy of Wulf Palinski). (b) Cross section through a human coronary artery at the level of a thrombotic atherosclerotic lesion causing fatal myocardial infarction.

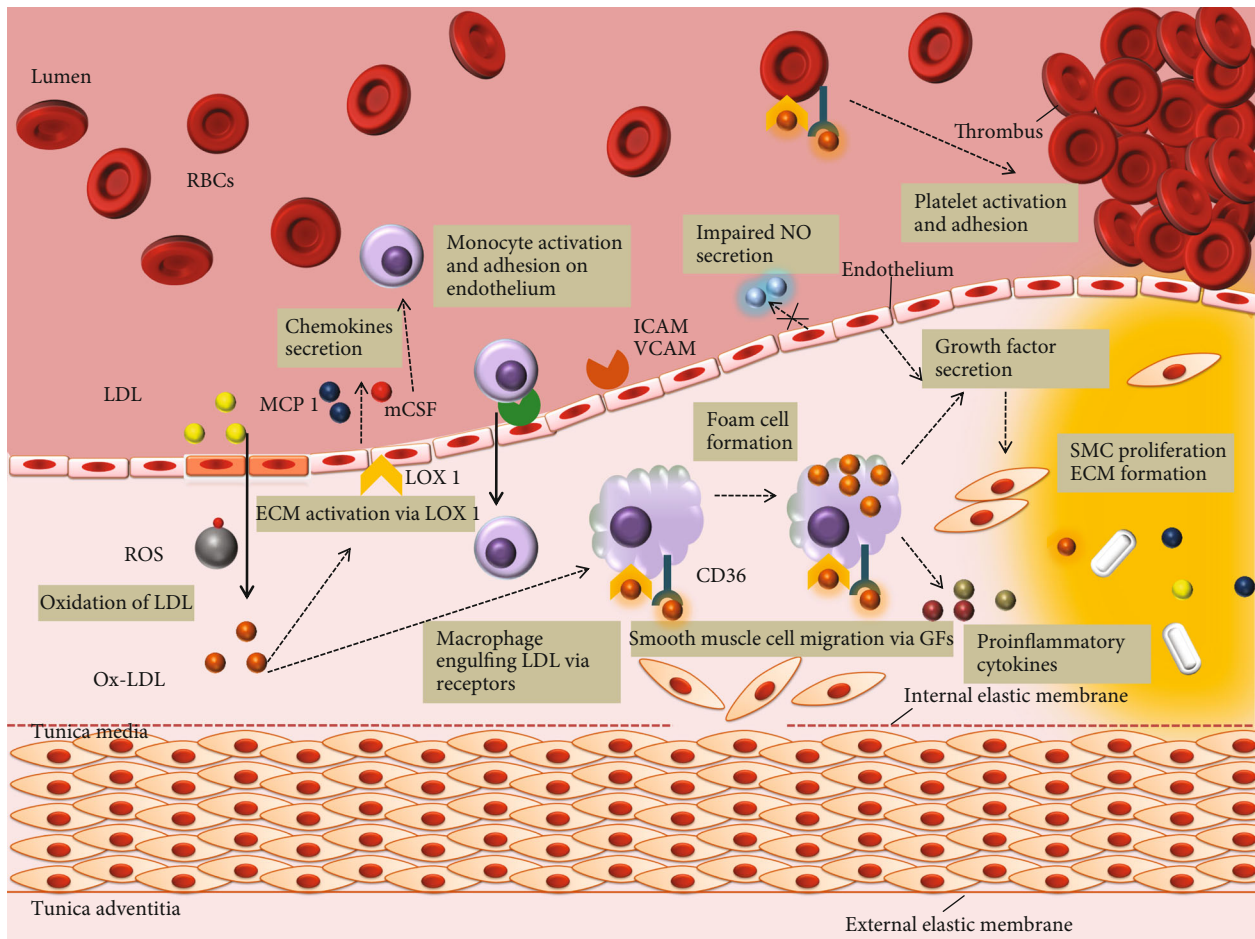


FIGURE 6: Schematic illustration of the role of Ox-LDL in atherosclerosis progression. Ox-LDL elicits atherosclerotic events right from their production in the subendothelium. Due to downregulated LDL receptors, the native LDL cannot be internalized by macrophages. Ox-LDL, via LOX 1 and other factors, activates endothelium for a number of events: adherence of LDL, monocytes, and platelets; secretion of chemokines and growth factors; production of ROS; impairing NO secretion; and so on. SRs, CD36, and LOX 1 help in the uptake of OX-LDL by monocyte-derived macrophages in the subendothelium. Growth factors mediate SMC proliferation and extracellular matrix formation. Platelet adherence and accumulation is also, in part elicited by Ox-LDL which results into a rupture prone thrombus.

the lesion area. Moreover, the ROS present in the plaque tends to induce cell death making the plaque unstable and rupture, which is the worst part of the progression.

2.4. Rupturing of Plaque: Thrombosis. A vulnerable plaque is subject to rupture. ROS degrades the fibrous wall of plaque via the release of matrix metalloproteinases (MMPs) [76] causing thrombus formation. Recent studies suggest a major difference in the lipid profiles of stable and unstable plaque considering former to be more susceptible to oxidation (due to increased PUFAs) and enhanced oxidation in the latter due to increased 18:0 containing lysophosphatidylcholine [77]. Rupturing of this plaque causes sudden expansion of the lesions leading to thrombus formation accounting for myocardial infarction, stroke, or sudden death [63, 64]. Looking more into the mechanism; Ox-LDL induces CD36 and P-selectin expression in the platelets activating them to further express LOX 1 for their adhesion on endothelium. Chemokines released from activated platelets mediate endothelium dysfunction, foam cell formation, and ROS production favouring progression of the plaque. Ox-LDL again makes the plaque scenario complex by platelet activation and adhesion on the endothelium which in turn blocks the NO production, which is said to be dysfunctional, yet again the cycle goes on [78].

3. Therapeutics to Block or Retard the Process: Endothelium Dysfunction to Thrombosis

The level and persistence of disease is the deciding factor for its treatment measures [79]. Some patients only require a lifestyle amendment and some have to undergo surgical procedures. HDL, antioxidant enzymes, diet, statins, and lipid lowering are foreseen as potent factors in preventing atherosclerosis. An illustration of effects of such parameters on CVDs is shown in Figure 7 [35]. Pharmacological interventions like angiotensin converting enzyme (ACE) inhibitors, statin insulin sensitizers and L-arginine, folates, and tetrahydrobiopterin are suggested to improve damaged endothelium which would resist LDL entry into subendothelium.

3.1. Lipid Management Is the Primary Prevention. As reviewed by Michos et al. [80] very recently, lipid management remains the primary prevention to atherosclerosis. If we look back into this review and perhaps in literature, the story always begins with high LDL cholesterol (LDL-C) which makes it the hallmark and a potent treatment target. Additionally, the CVD prevention guidelines published by the American College of Cardiology-America Heart Association recommends cholesterol management as a primary prevention by opting a healthy lifestyle [81]. Keeping in view the sedentary lifestyle and family history of CVDs as important risk factors, improvement in lifestyle and diet has been seen to reduce CVDs by about 50%. A healthy lifestyle here involves maintaining an ideal weight, keeping check on the blood sugar levels, regular exercise, and looking after calories intake. The notion “lower is better” goes exactly with the diet intake for a healthy lifestyle. Though merely management of lipids cannot completely prevent the disease, it does lower the

risk to an extent. According to US Cholesterol Clinical practice guidelines (2018), statins should be the primary choice of pharmacological treatments for LDL-C considering the latter being critical in the therapeutics [82]. Statins tend to reduce about 50% LDL cholesterol via inhibiting 3-hydroxy-3-methylglutaryl-CoA reductase (HMG CoA), a rate limiting inhibitor of LDL-C. In atherosclerosis, there is an aberrant increase in the expression of MHC-II and thus, it is also considered as a chronic inflammatory disease. A study suggested that statins could function as immune suppressors by repressing the MHC-II expression and thereby, reducing the MHC-II-dependent T-lymphocyte activation and thus, statins could modulate the adaptive immunity [83]. Statins are seen to block the cholesterol synthesis by the activation of SREBP-2, a mechanism illustrated by Goldstein and Brown given in Figure 8 [35]. Compelling results from meta-analysis trials have revealed a lowering of about 22% risk of cardiovascular events with the reduction of a significant amount of LDL level [84]. Additionally, cardiac events like myocardial infarction and stroke can be prevented by lipid lowering with the use of high-intensity statins [85, 86].

3.2. HDL Retards the Atherosclerotic Process. HDL along with its major lipid poor apolipoprotein A-I (ApoA-I) aids in removing cholesterol from foam cells for clearance by the liver. The efflux from macrophage foam cells is the first step towards reverse cholesterol transport that lowers further inflammation preventing atherosclerosis burden [73, 74]. A line of epidemiological trails has revealed that HDL accounts for douching lipid oxidation via antioxidant enzymes like Lp-PLA2, LCAT, and PON1 along with ApoA-I which helps in removing hydroperoxides from cells and LDL [87]. HDL signalling via endothelial cell receptors like SR-BI helps in enhancing NO production, thus maintaining endothelium homeostasis [88]. Additionally, it prompts cholesterol efflux from platelets preventing platelet aggregation and eventually thrombosis [89]. Accumulation and retention of Ox-LDL is the key initiating factor in chemotaxis and monocytes invasion. This LDL modification primarily by endothelium, SMCs, and macrophages in the lesion area would suggest that cells actively modify LDL. LDL is either oxidized nonenzymatically by transition metal ions, hemin, and many other catalysts or by enzymes within the artery wall. HDL obviates the oxidative modification of LDL employing proteins circulating on HDL itself. The most important protein is paraoxonase 1 (PON1) that confers an ability to prevent LDL oxidation by enhancing the antioxidative function of HDL [87]. Additionally, ApoA-I aids in reducing lipid hydroperoxides to lipid hydroxides owing to oxidation in its methionine residues [90]. LCAT and lipoprotein-associated phospholipase A2 (Lp-PLA2) have also been reported to douche oxidative mechanisms as suggested in mice experiments [91]. Nevertheless, HDL could absorb oxidizing lipids to prevent the further process of LDL oxidative modification. Figure 9 gives illustrations of key events where HDL comes in to play. Hence, antioxidative capacity conferred by HDL proteins ensures protective measures to retard the atherosclerotic lesion and more extensive research is required to better understand it to use it as a therapeutic target.

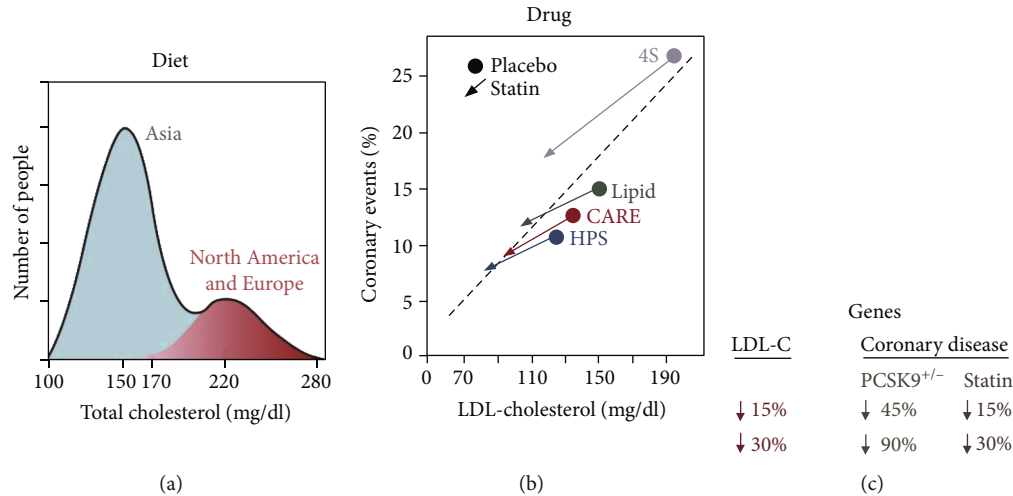


FIGURE 7: Diagram illustrating the effects of diet, drugs, and genes on plasma LDL and coronary disease. The figure is reproduced from Goldstein and Brown [35] (under the Creative Commons Attribution License/public domain) “(Reprinted (A Century of Cholesterol and Coronaries: From Plaques to Genes to Statins) with permission from Elsevier (License number 4825791117921)).” (a) Diet. Idealized depiction of the frequency distribution of plasma cholesterol levels in the human species as extrapolated from surveys of middle-aged people in major populations of the world. The higher the cholesterol level, higher the risk for coronary disease, as denoted by graded red shading. (b) Drugs. Frequency of coronary events plotted against plasma level of LDL cholesterol in four double-blind, placebo-controlled trials in which middle-aged people at risk for heart attacks were treated for 5 years with a statin or placebo. The number of subjects in each study was as follows: 4S Study, 4,444; LIPID, 9,014; CARE, 4,159; and HPS, 20,536. (c) Genes. Difference in risk for coronary disease in middle-aged people depending on whether plasma LDL cholesterol level is reduced over a lifetime (heterozygous loss of function of PCSK9) or for only 5 years (statin therapy).

3.3. Role of Dietary Antioxidants in Treating Atherosclerosis.

Antioxidants scavenge free radicals (reactive oxygen/nitrogen species) and reduce the probability of oxidative stress [92]. Antioxidants can be synthesized by a cell itself or can be taken exogenously. Antioxidants synthesized by a cell include glutathione, uric acid, caeruloplasmin, ferritin, transferrin, or lactoferrin, whereas vitamin E, vitamin C, flavonoids, and carotenoids come from the diet [93–95]. The endogenous nonenzymatic antioxidants like GSH, uric acid, bilirubin, coenzyme Q, and lipoic acid can be present intracellularly or extracellularly and serve as the primary defence system against imbalanced redox stress [96, 97]. Glutathione, a cofactor for glutathione peroxidase (GPx) scavenges hydroxide, hypochlorous acid, and peroxynitrite, thus modulates size of the atherosclerotic lesion [98]. Coenzyme Q improves endothelial function by scavenging peroxy radicals [99]. Bilirubin, uric acid, and lipoic acid have shown remarkable scavenging properties towards oxidants, hence improving endothelium and decreasing inflammatory actions [100–102].

The secondary defence mechanism involves exogenous antioxidants like vitamin C, vitamin E, vitamin A, vitamin B, carotenoids, or polyphenols [100, 103–105]. As mentioned above, the native LDL, when turned into Ox-LDL becomes atherogenic and this oxidative modification in LDL is due to imbalanced ROS. Vitamin E, a lipid soluble antioxidant, aids in neutralizing free radicals hence retarding LDL oxidation. Moreover, vitamin E inhibits the expression of CD36, SR-BI, and protein kinase C to reverse foam cell formation and SMC proliferation along with further associated complications of the CVD [106, 107]. It is also observed that vitamin E modulates the expression of connective tissue growth factors and adhesion molecules (VCAM 1, ICAM 1) on

endothelial cells and helps in the prevention endothelium dysfunction and internalization of LDL molecules into the intima. In contrast, some clinical trials have given completely opposite outcomes where studies showed almost no effect of vitamin E doses (50 mg–300 mg/day) in the CVD patients [103, 106]. No decrease of stroke and myocardial infarction was observed in population with CVDs. While the outcomes of the trails remain contradictory, more studies are anticipated to build a strong conclusion. Vitamin C (ascorbate) helps to stabilize cell membranes by scavenging peroxy radicals, ROS, and superoxide radicals. It enhances NO bioavailability, thus improving endothelium and vasodilation. In vitro experiments have shown lowered Ox-LDL generation on treating with ascorbate (vitamin C), while depletion of the same is related to atherosclerosis in vivo [100]. Ascorbate has also been seen to reduce endothelium dysfunction which again is a key initiation factor of the CVD [94]. But several other clinical trials have shown contradictory results where no significant relationship between vitamin C and the reversal of atherosclerosis was found. A study group of 29,133 men (50–69 yrs) was given synthetic α -tocopherol (50 mg/day) and β -carotene (20 mg/day) for ~6 years, and no effect was seen in improving heart condition. In fact, the risk of lung carcinoma and ischemic heart disease was increased [108]. Similar study on people without any CVD was carried out for 4 years in which incidences of angina pectoris slightly increased as an adverse effect of the supplementation [109]. In another study on group of smokers and nonsmokers (45–74 yrs), even including the vitamin A in a combination with above two had no effect. In an additional study, β -carotene (50 mg/day) could not show any positive effect on patients supplemented for 4–8 years (27–84 yrs)

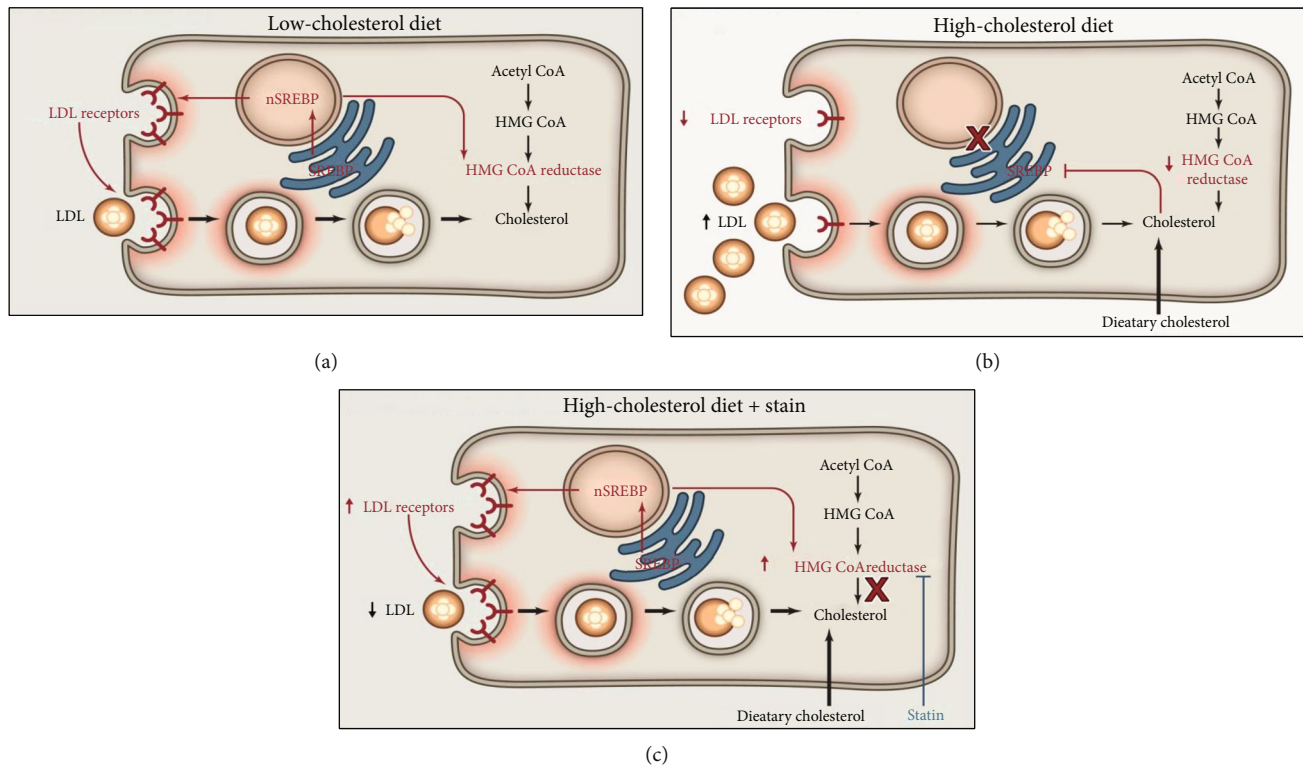


FIGURE 8: Hepatic responses to diet and statins mediated by the SREBP pathway. The figure is reproduced from Goldstein and Brown [35] [under the Creative Commons Attribution License/public domain] “(Reprinted (A Century of Cholesterol and Coronaries: From Plaques to Genes to Statins) with permission from Elsevier (License number 4825791117921)).” (a) Low-cholesterol diet. Proteolytic cleavage of SREBP is increased. The cleaved SREBP enters the nucleus to activate genes controlling cholesterol synthesis (including HMG CoA reductase) and uptake (LDL receptor). nSREBP, nuclear portion of cleaved SREBP. (b) High-cholesterol diet. Proteolytic cleavage of SREBPs is decreased, resulting in decreased nuclear SREBP and decreased activation of target genes. The decrease in LDL receptors produces an increase in plasma LDL. (c) High-cholesterol diet plus statin therapy. Statins inhibit HMG CoA reductase, causing a transient decrease in ER cholesterol. In response, SREBP cleavage is increased, and the resulting nuclear SREBP activates the genes for HMG CoA reductase and LDL receptor. The increased HMG CoA reductase is inhibited by the statin, and the increased LDL receptors lower plasma LDL.

[110]. Combination of vitamin E (30 mg/day), vitamin C (120 mg/day), β -carotene (6 mg/day), selenium (100 μ g/day), and zinc (20 mg/day) was given to 13,017 middle-aged people for 7.5 years, and it was found that combined supplementation had very slight effect on men in improving cardiovascular health and no effect at all was seen on women participants [111]. Although dietary supplements have some role in preventing atherosclerosis in mice and human trails [112], yet a very little is known to conclude exactly how much, when, and what should be included in the diet to have the best effect.

3.4. Antioxidant Enzymes Are Critical in Atherosclerosis Prevention. In addition to the above-mentioned antioxidants, the cells also express antioxidant enzymes like catalase, superoxide dismutase (SOD), thioredoxin reductase (TrxR), peroxiredoxins (Prxs), glutathione peroxidase (GPx), glutathione reductase, and glutathione-S-transferase which maintain redox homeostasis [113–115]. The most crucial enzymes in such mechanisms include peroxiredoxins (Prxs) and glutathione peroxidase 4 (Gpx4). Peroxiredoxins (Prxs; 1-6) are proteins that have cysteine residues that reduce peroxides, in turn, getting oxidized into sulfenic acid [116, 117]. Prx1 and Prx2 exacerbate atherosclerosis on deletion in ApoE mice [118]. While Prx4 inhibits the disease from being

overexpressed in ApoE mice, Prx6 has no such effect [119]. Glutathione peroxidases convert glutathione to glutathione disulfide and reduce lipid peroxides to water [120]. The most crucial role is played by Gpx4. Loss of GPx4 activity in the cellular membranes leads to ferroptosis, which is a regulated nonapoptotic cell death process and it is enhanced by the accumulation of ROS in a lipid-rich environment [121]. As mentioned above, PUFAs with labile bis-allylic hydrogen atoms are prone to lipid peroxidation and it is also the hallmark of ferroptosis [122]. According to Yang et al., there are two key drivers in ferroptosis induced by PUFA peroxidation: lipoxygenase and phosphorylase kinase G2 (PHKG2). The study suggested that PUFA peroxidation is caused by lipoxygenases via PHKG2 and consequently the inhibition of catalytic selenocysteine in GPx4 causes the accumulation of the hydroperoxides leading to cell death [123]. Ferroptosis is linked to several diseases like cancer and atherosclerosis and needs clear mechanistic insights for therapeutic interventions [124, 125].

4. Outlook

Endothelium under oxidative stress primes to the formation of oxidized cholesterol (oxysterols) as a result of low-

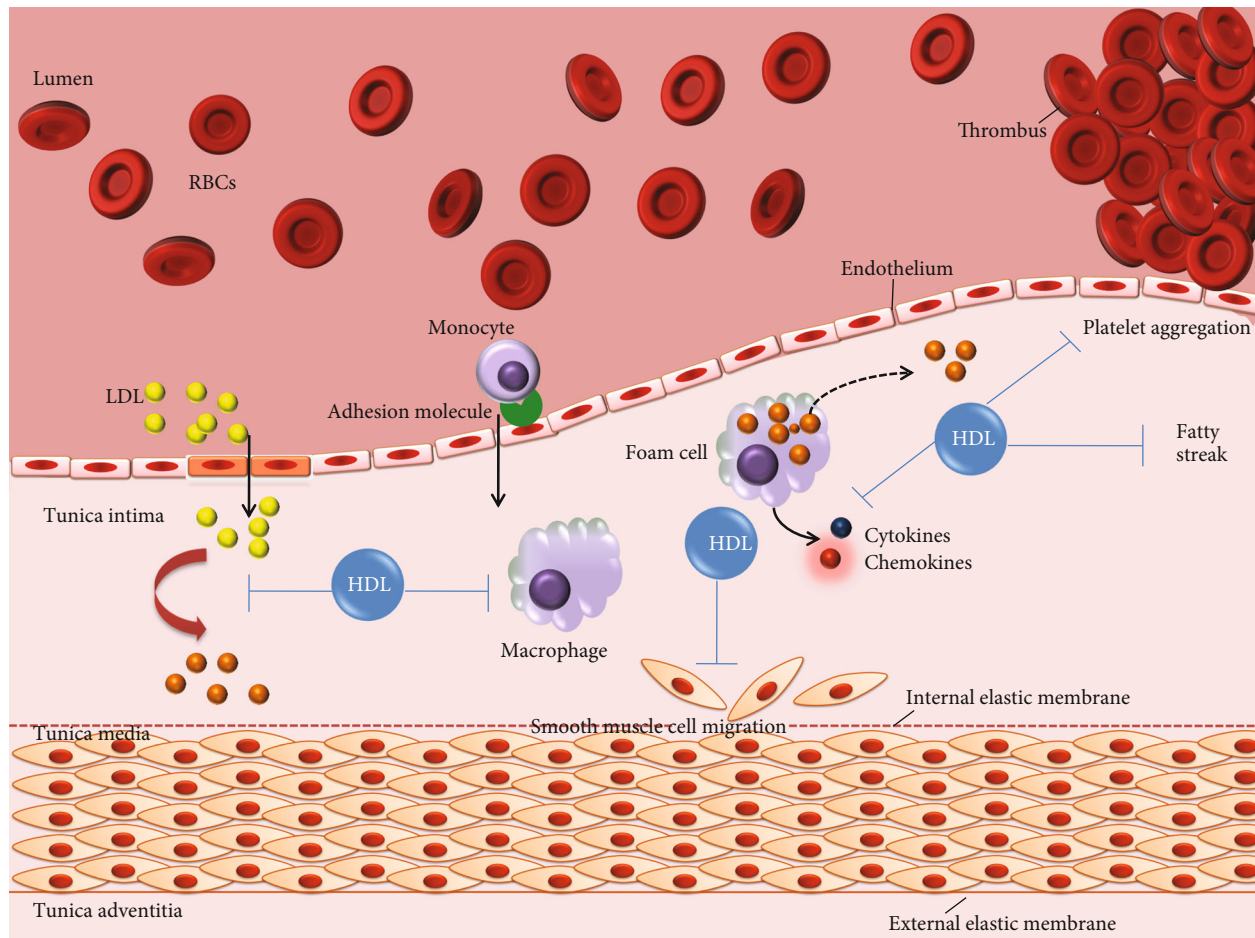


FIGURE 9: Schematic representation of HDL countering major atherosclerotic stages. HDL counters significant stages of atherosclerosis. First, HDL retards the oxidation process of LDL and helps in the efflux of cholesterol from macrophages, preventing it from becoming foam cells. Cytokines and growth factors released by T lymphocytes and foam cells induce SMC migration and proliferation that is again countered by HDL. Additionally, platelet migration and aggregation is prevented to the site of plaque. Hence, high HDL is antiatherosclerotic and comes into play as soon as the LDL penetrates the dysfunctional endothelium.

density lipoprotein (cholesterol carrier through the blood) oxidation. The oxidation is driven by oxygen, nitrogen, or other reactive species which brings up the oxidative or nitrosative stress in uncontrolled measures. Certain irritants like toxins from smoking (nicotine and carbon monoxide), high blood pressure due to hypertension, high level of low-density lipoproteins, HDL dysfunction, obesity, and diabetes mellitus alter the endothelium lining causing permeation and accumulation of LDL particles into the subendothelial space. Retention of LDL particles brings about a lot of factors into play which upsurges the risk for fatty streak development and further complication into atherosclerosis progression. What come to the rescue are monocytes but turns out to be exaggerating the process. Hence, the immune system more likely induces inflammation making things more complicated. Antioxidant enzymes and genes, however, are potent measures to counter ROS to prevent lipid peroxidation. Since dietary antioxidants and statins have also shown effective activity in vivo, these can be effectively prescribed for treatment and cholesterol lowering. Additionally, maintaining a healthy lifestyle is a key to homeostasis and a healthy cardio-

vascular system. Although, an enormous amount of research has been conducted on the above events, yet a clear understanding of therapeutic measures is required.

Conflicts of Interest

The authors declare that there are no conflicts of interest.

Acknowledgments

CK would like to thank the Department of Science and Technology, Government of India, Grant No. DST/IN-SPIRE Fellowship (IF180523) for the support in the ongoing research on the similar topic. NKS is supported by the Ramanuja Fellowship (SB/S2/RJN-107/2018). RVS and AKS are supported by the Central Research Cell, MMIMSR, MM(DU).

References

- [1] J. L. Goldstein and M. S. Brown, "The LDL receptor and the regulation of cellular cholesterol metabolism," *Journal of Cell*

- Science. Supplement*, vol. 1985, Supplement 3, pp. 131–137, 1985.
- [2] T. Matsumoto, H. Takashima, N. Ohira et al., “Plasma level of oxidized low-density lipoprotein is an independent determinant of coronary macrovasomotor and microvasomotor responses induced by bradykinin,” *Journal of the American College of Cardiology*, vol. 44, no. 2, pp. 451–457, 2004.
- [3] I. Tabas, “Cholesterol and phospholipid metabolism in macrophages,” *Biochim. Biophys. Acta-Mol. Cell Biol. Lipids.*, vol. 1529, no. 1-3, pp. 164–174, 2000.
- [4] G. Wick, M. Knoflach, and Q. Xu, “Autoimmune and inflammatory mechanisms in atherosclerosis,” *Annual Review of Immunology*, vol. 22, no. 1, pp. 361–403, 2004.
- [5] G. Siasos, J. D. Sara, M. Zaromytidou et al., “Local low shear stress and endothelial dysfunction in patients with nonobstructive coronary atherosclerosis,” *Journal of the American College of Cardiology*, vol. 71, no. 19, pp. 2092–2102, 2018.
- [6] W. G. Nayler, “Atherosclerosis and endothelial damage: a brief overview,” *Cardiovascular Drugs and Therapy*, vol. 9, no. S1, pp. 25–30, 1995.
- [7] J. Lee and J. P. Cooke, “The role of nicotine in the pathogenesis of atherosclerosis,” *Atherosclerosis*, vol. 215, no. 2, pp. 281–283, 2011.
- [8] M. D. Ashen and R. S. Blumenthal, “Low HDL Cholesterol Levels,” *New England Journal of Medicine*, vol. 353, no. 12, pp. 1252–1260, 2005.
- [9] P. Libby, P. M. Ridker, and A. Maseri, “Inflammation and atherosclerosis,” *Circulation*, vol. 105, no. 9, pp. 1135–1143, 2002.
- [10] R. Ross, “The pathogenesis of atherosclerosis — an update,” *The New England Journal of Medicine*, vol. 314, no. 8, pp. 488–500, 1986.
- [11] C. C. Winterbourn, “Reconciling the chemistry and biology of reactive oxygen species,” *Nature Chemical Biology*, vol. 4, no. 5, pp. 278–286, 2008.
- [12] B. D’Autréaux and M. B. Toledano, “ROS as signalling molecules: mechanisms that generate specificity in ROS homeostasis,” *Nature Reviews Molecular Cell Biology*, vol. 8, no. 10, pp. 813–824, 2007.
- [13] H. Sies, C. Berndt, and D. P. Jones, “Oxidative Stress,” *Annual Review of Biochemistry*, vol. 86, no. 1, pp. 715–748, 2017.
- [14] B. C. Dickinson and C. J. Chang, “Chemistry and biology of reactive oxygen species in signaling or stress responses,” *Nature Chemical Biology*, vol. 7, no. 8, pp. 504–511, 2011.
- [15] N. Duerrschmidt, C. Stielow, G. Muller, P. J. Pagano, and H. Morawietz, “NO-mediated regulation of NAD (P) H oxidase by laminar shear stress in human endothelial cells,” *The Journal of Physiology*, vol. 576, no. 2, pp. 557–567, 2006.
- [16] T. Münzel, G. G. Camici, C. Maack, N. R. Bonetti, V. Fuster, and J. C. Kovacic, “Impact of oxidative stress on the heart and vasculature: part 2 of a 3-part series,” *Journal of the American College of Cardiology*, vol. 70, no. 2, pp. 212–229, 2017.
- [17] H. Yin, L. Xu, and N. A. Porter, “Free radical lipid peroxidation: mechanisms and analysis,” *Chemical Reviews*, vol. 111, no. 10, pp. 5944–5972, 2011.
- [18] S. N. Desai, F. F. Farris, and S. D. Ray, “Lipid Peroxidation,” in *Encyclopedia of Toxicology*, Elsevier, Third edition, 2014.
- [19] S. Hill, K. Hirano, V. V. Shmanai et al., “Isotope-reinforced polyunsaturated fatty acids protect yeast cells from oxidative stress,” *Free Radical Biology & Medicine*, vol. 50, no. 1, pp. 130–138, 2011.
- [20] M. Johansson, X. Chen, S. Milanova, C. Santos, and D. Petranovic, “PUFA-induced cell death is mediated by Yca1p-dependent and -independent pathways, and is reduced by vitamin C in yeast,” *FEMS Yeast Research*, vol. 16, no. 2, pp. fow007–fow009, 2016.
- [21] J. Semprine and A. B. M. Repetto, “Lipid Peroxidation: Chemical Mechanism,” in *Biological Implications and Analytical Determination*, p. 13, Intech, 2013.
- [22] A. K. Hauck and D. A. Bernlohr, “Oxidative stress and lipotoxicity,” *Journal of Lipid Research*, vol. 57, no. 11, pp. 1976–1986, 2016.
- [23] S. Marventano, P. Kolacz, S. Castellano et al., “A review of recent evidence in human studies of n-3 and n-6 PUFA intake on cardiovascular disease, cancer, and depressive disorders: does the ratio really matter?,” *International Journal of Food Sciences and Nutrition*, vol. 66, no. 6, pp. 611–622, 2015.
- [24] H. S. Kruth, W. Huang, I. Ishii, and W. Y. Zhang, “Macrophage foam cell formation with native low density lipoprotein,” *The Journal of Biological Chemistry*, vol. 277, no. 37, pp. 34573–34580, 2002.
- [25] D. Harrison, K. K. Griendling, U. Landmesser, B. Hornig, and H. Drexler, “Role of oxidative stress in atherosclerosis,” *The American Journal of Cardiology*, vol. 91, no. 3, pp. 7–11, 2003.
- [26] R. Carnevale, S. Bartimoccia, C. Nocella et al., “LDL oxidation by platelets propagates platelet activation via an oxidative stress-mediated mechanism,” *Atherosclerosis*, vol. 237, no. 1, pp. 108–116, 2014.
- [27] A. Hofmann, C. Brunssen, and H. Morawietz, “Contribution of lectin-like oxidized low-density lipoprotein receptor-1 and LOX-1 modulating compounds to vascular diseases,” *Vascular Pharmacology*, vol. 107, pp. 1–11, 2018.
- [28] C. J. Binder, N. Papac-Milicevic, and J. L. Witztum, “Innate sensing of oxidation-specific epitopes in health and disease,” *Nature Reviews. Immunology*, vol. 16, no. 8, pp. 485–497, 2016.
- [29] M. E. Haberland, G. Mottino, M. Le, and J. S. Frank, “Sequestration of aggregated LDL by macrophages studied with freeze-etch electron microscopy,” *Journal of Lipid Research*, vol. 42, no. 4, pp. 605–619, 2001.
- [30] W. Palinski, M. E. Rosenfeld, S. Yla-Herttuala et al., “Low density lipoprotein undergoes oxidative modification in vivo,” *Proceedings of the National Academy of Sciences of the United States of America*, vol. 86, no. 4, pp. 1372–1376, 1989.
- [31] J. M. Johnston, A. Angyal, R. C. Bauer et al., “Myeloid Tribbles 1 induces early atherosclerosis via enhanced foam cell expansion,” *Science Advances*, vol. 5, no. 10, p. eaax9183, 2019.
- [32] M. T. Quinn, S. Parthasarathy, and D. Steinberg, “Endothelial cell-derived chemotactic activity for mouse peritoneal macrophages and the effects of modified forms of low density lipoprotein,” *Proceedings of the National Academy of Sciences of the United States of America*, vol. 82, no. 17, pp. 5949–5953, 1985.
- [33] N. Wang and A. R. Tall, “Regulation and mechanisms of ATP-binding cassette transporter A1-mediated cellular cholesterol efflux,” *Arteriosclerosis, Thrombosis, and Vascular Biology*, vol. 23, no. 7, pp. 1178–1184, 2003.
- [34] E. R. Miller, L. J. Appel, and T. H. Risby, “Effect of dietary patterns on measures of lipid Peroxidation,” *Circulation*, vol. 98, no. 22, pp. 2390–2395, 1998.

- [35] J. L. Goldstein and M. S. Brown, "A century of cholesterol and coronaries: from plaques to genes to statins," *Cell*, vol. 161, no. 1, pp. 161–172, 2015.
- [36] A. Zmyslowski and A. Szterk, "Current knowledge on the mechanism of atherosclerosis and pro-atherosclerotic properties of oxysterols," *Lipids in Health and Disease*, vol. 16, no. 1, p. 188, 2017.
- [37] H. Esterbauer, J. Gebicki, H. Puhl, and G. Jürgens, "The role of lipid peroxidation and antioxidants in oxidative modification of LDL," *Free Radical Biology & Medicine*, vol. 13, no. 4, pp. 341–390, 1992.
- [38] X. Yang, Y. Li, Y. Li et al., "Oxidative Stress-Mediated Atherosclerosis: Mechanisms and Therapies," *Frontiers in Physiology*, vol. 8, 2017.
- [39] C. P. Sparrow, S. Parthasarathy, and D. Steinberg, "Enzymatic modification of low density lipoprotein by purified lipoxygenase plus phospholipase A2 mimics cell-mediated oxidative modification," *Journal of Lipid Research*, vol. 29, no. 6, pp. 745–753, 1988.
- [40] J. F. P. Berbée, I. M. Mol, G. L. Milne et al., "Deuterium-reinforced polyunsaturated fatty acids protect against atherosclerosis by lowering lipid peroxidation and hypercholesterolemia," *Atherosclerosis*, vol. 264, pp. 100–107, 2017.
- [41] P. Friedman, S. Hörkkö, D. Steinberg, J. L. Witztum, and E. A. Dennis, "Correlation of Antiphospholipid Antibody Recognition with the Structure of Synthetic Oxidized Phospholipids," *Journal of Biological Chemistry*, vol. 277, no. 9, pp. 7010–7020, 2002.
- [42] L. Tao and Department of Animal Science, Cornell University, Ithaca, NY, USA, "Oxidation of Polyunsaturated Fatty Acids and its Impact on Food Quality and Human Health," *Advances in Food Technology and Nutritional Sciences - Open Journal*, vol. 1, no. 6, pp. 135–142, 2015.
- [43] G. Finking and H. Hanke, "Nikolaj Nikolajewitsch Anitschkow (1885-1964) established the cholesterol-fed rabbit as a model for atherosclerosis research," *Atherosclerosis*, vol. 135, no. 1, pp. 1–7, 1997.
- [44] D. Steinberg, "An interpretive history of the cholesterol controversy: part II: the early evidence linking hypercholesterolemia to coronary disease in humans," *Journal of Lipid Research*, vol. 46, no. 2, pp. 179–190, 2005.
- [45] C. Müller, "Xanthomata, Hypercholesterolemia, Angina Pectoris," *Acta Medica Scandinavica*, vol. 95, no. S89, pp. 75–84, 2009.
- [46] P. O. Bonetti, L. O. Lerman, and A. Lerman, "Endothelial dysfunction: a marker of atherosclerotic risk," *Arteriosclerosis, Thrombosis, and Vascular Biology*, vol. 23, no. 2, pp. 168–175, 2003.
- [47] D. Steinberg and J. L. Witztum, "Oxidized low-density lipoprotein and atherosclerosis," *Arteriosclerosis, Thrombosis, and Vascular Biology*, vol. 30, no. 12, pp. 2311–2316, 2010.
- [48] J. L. Witztum and D. Steinberg, "Role of oxidized low density lipoprotein in atherogenesis," *The Journal of Clinical Investigation*, vol. 88, no. 6, pp. 1785–1792, 1991.
- [49] M. S. Brown and J. L. Goldstein, "Lipoprotein metabolism in the macrophage: implications for cholesterol deposition in atherosclerosis," *Annual Review of Biochemistry*, vol. 52, no. 1, pp. 223–261, 1983.
- [50] A. Gisterå and G. K. Hansson, "The immunology of atherosclerosis," *Nature Reviews. Nephrology*, vol. 13, no. 6, pp. 368–380, 2017.
- [51] D. Steinberg, "The LDL modification hypothesis of atherogenesis: an update," *Journal of Lipid Research*, vol. 50, Supplement, pp. S376–S381, 2009.
- [52] G. Lima, D. M. Ghisi, A. Durieux, R. Pinho, and M. Benetti, "Clinical update physical exercise and endothelial dysfunction," *Arquivos Brasileiros de Cardiologia*, vol. 95, no. 5, pp. 130–137, 2010.
- [53] H. A. R. Hadi, C. S. Carr, and J. Al Suwaidi, "Endothelial dysfunction: cardiovascular risk factors, therapy, and outcome," *Vascular Health and Risk Management*, vol. 1, no. 3, pp. 183–198, 2005.
- [54] G. Maiolino, G. Rossitto, P. Caielli, V. Bisogni, G. P. Rossi, and L. A. Calò, "The role of oxidized low-density lipoproteins in atherosclerosis: the myths and the facts," *Mediators of Inflammation*, vol. 2013, Article ID 714653, 13 pages, 2013.
- [55] E. C. Boyle, D. G. Sedding, and A. Haverich, "Targeting vasa vasorum dysfunction to prevent atherosclerosis," *Vascular Pharmacology*, vol. 96–98, pp. 5–10, 2017.
- [56] C. K. Glass and J. L. Witztum, "Atherosclerosis," *Cell*, vol. 104, no. 4, pp. 503–516, 2001.
- [57] R. F. Furchgott and P. M. Vanhoutte, "Endothelium-derived relaxing and contracting factors," *The FASEB Journal*, vol. 3, no. 9, pp. 2007–2018, 1989.
- [58] A. C. Santos, M. J. N. N. Alves, M. U. P. B. Rondon, A. C. P. Barretto, H. R. Middlekauff, and C. E. Negrão, "Sympathetic activation restrains endothelium-mediated muscle vasodilatation in heart failure patients," *American Journal of Physiology-Heart and Circulatory Physiology*, vol. 289, no. 2, pp. H593–H599, 2005.
- [59] R. J. Esper, R. A. Nordaby, J. O. Vilariño, A. Paragano, J. L. Cacharrón, and R. A. Machado, "Endothelial dysfunction: a comprehensive appraisal," *Cardiovascular Diabetology*, vol. 5, no. 1, pp. 4–18, 2006.
- [60] M. A. Gimbrone, "Endothelial Dysfunction, Hemodynamic Forces, and Atherosclerosis," *Thrombosis and Haemostasis*, vol. 82, no. 8, pp. 722–726, 2017.
- [61] M. A. Gimbrone and G. García-Cardena, "Vascular endothelium, hemodynamics, and the pathobiology of atherosclerosis," *Cardiovascular Pathology*, vol. 22, no. 1, pp. 9–15, 2013.
- [62] M. Nieuwdorp, T. W. van Haeften, M. C. L. G. Gouverneur et al., "Loss of Endothelial Glycocalyx During Acute Hyperglycemia Coincides With Endothelial Dysfunction and Coagulation Activation In Vivo," *Diabetes*, vol. 55, no. 2, pp. 480–486, 2006.
- [63] M. Khazaei, F. Moien-afshari, and I. Laher, "Vascular endothelial function in health and diseases," *Pathophysiology*, vol. 15, no. 1, pp. 49–67, 2008.
- [64] A. Negre-Salvayre, P. Guerby, S. Gayral, M. Laffargue, and R. Salvayre, "Role of reactive oxygen species in atherosclerosis: Lessons from murine genetic models," *Free Radical Biology and Medicine*, vol. 149, pp. 8–22, 2020.
- [65] K. E. Sorensen, D. S. Celmaj, D. Georgakopoulos, G. Hatcher, D. J. Betteridge, and J. E. Deanfield, "Impairment of endothelium-dependent dilation is an early event in children with familial hypercholesterolemia and is related to the lipoprotein (a) level," *The Journal of Clinical Investigation*, vol. 93, no. 1, pp. 50–55, 1994.
- [66] C. D. A. Goonasekera, "Vascular Endothelial Cell Activation Associated with Increased Plasma Asymmetric Dimethyl Arginine in Children and Young Adults with Hypertension: A Basis for Atheroma?," *Blood Pressure*, vol. 9, no. 1, pp. 16–21, 2009.

- [67] U. Landmesser and H. Drexler, "Oxidative stress, the renin-angiotensin system, and atherosclerosis," *European heart journal supplements*, vol. 5, pp. A3–A7, 2003.
- [68] J. W. Petersen and G. M. Felker, "Inflammatory biomarkers in heart failure," *Congestive Heart Failure*, vol. 12, no. 6, pp. 324–328, 2006.
- [69] Y. Seta and K. H. Shan, "Symposium basic mechanisms in heart failure : the cytokine hypothesis," *Journal of Cardiac Failure*, vol. 2, 2002.
- [70] L. Cominacini, A. Rigoni, A. F. Pasini et al., "The binding of oxidized low density lipoprotein (ox-LDL) to ox-LDL receptor-1 reduces the intracellular concentration of nitric oxide in endothelial cells through an increased production of superoxide," *The Journal of Biological Chemistry*, vol. 276, no. 17, pp. 13750–13755, 2001.
- [71] P. L. da Luz, A. C. P. Chagas, P. M. M. Dourado, and F. R. M. Laurindo, "Endothelium in Atherosclerosis: Plaque Formation and Its Complications," in *Endothelium and Cardiovascular Diseases*, pp. 493–512, 2018.
- [72] K. Sakakura, M. Nakano, F. Otsuka, E. Ladich, F. D. Kolodgie, and R. Virmani, "Pathophysiology of Atherosclerosis Plaque Progression," *Heart, Lung and Circulation*, vol. 22, no. 6, pp. 399–411, 2013.
- [73] P. Rajendran, T. Rengarajan, J. Thangavel et al., "The vascular endothelium and human diseases," *International Journal of Biological Sciences*, vol. 9, no. 10, pp. 1057–1069, 2013.
- [74] A. J. Kattoor, N. V. K. Pothineni, D. Palagiri, and J. L. Mehta, "Oxidative Stress in Atherosclerosis," *Current Atherosclerosis Reports*, vol. 19, no. 11, 2017.
- [75] D. R. J. Owen, A. C. Lindsay, R. P. Choudhury, and Z. A. Fayad, "Imaging of atherosclerosis," *Annual Review of Medicine*, vol. 62, no. 1, pp. 25–40, 2011.
- [76] G. Virella, K. Wilson, J. Elkes et al., "Immune complexes containing malondialdehyde (MDA) LDL induce apoptosis in human macrophages," *Clinical Immunology*, vol. 187, pp. 1–9, 2018.
- [77] D. Tsikas, "Assessment of lipid peroxidation by measuring malondialdehyde (MDA) and relatives in biological samples: analytical and biological challenges," *Analytical Biochemistry*, vol. 524, pp. 13–30, 2017.
- [78] E. Leiva, S. Wehinger, L. Guzmán, and R. Orrego, "Role of oxidized LDL in atherosclerosis," *Hypercholesterolemia*, pp. 55–78, 2015.
- [79] T. Wang and J. Butany, "Pathogenesis of atherosclerosis," *Diagnostic Histopathol.*, vol. 23, no. 11, pp. 473–478, 2017.
- [80] E. D. Michos, J. W. McEvoy, and R. S. Blumenthal, "Lipid management for the prevention of atherosclerotic cardiovascular disease," *The New England Journal of Medicine*, vol. 381, no. 16, pp. 1557–1567, 2019.
- [81] M. Aggarwal, B. Bozkurt, G. Panjra et al., "Lifestyle modifications for preventing and treating heart failure," *Journal of the American College of Cardiology*, vol. 72, no. 19, pp. 2391–2405, 2018.
- [82] C. Aluganti Narasimhulu, K. Y. Burge, M. Doomra, A. Riad, and S. Parthasarathy, "Primary prevention of atherosclerosis by pretreatment of low-density lipoprotein receptor knockout mice with sesame oil and its aqueous components," *Scientific Reports*, vol. 8, no. 1, p. 12270, 2018.
- [83] B. Kwak, F. Mulhaupt, S. Myit, and F. Mach, "Statins as a newly recognized type of immunomodulator," *Nature Medicine*, vol. 6, no. 12, pp. 1399–1402, 2000.
- [84] P. Libby, J. E. Buring, L. Badimon et al., "Atherosclerosis," *Nature Reviews Disease Primers*, vol. 5, no. 1, 2019.
- [85] M. Mahmoudi, "The pathogenesis of atherosclerosis," *Medicine*, vol. 46, no. 9, pp. 505–508, 2018.
- [86] M. K. Jensen, M. L. Bertoia, L. E. Cahill, I. Agarwal, E. B. Rimm, and K. J. Mukamal, "Novel metabolic biomarkers of cardiovascular disease," *Nature Reviews. Endocrinology*, vol. 10, no. 11, pp. 659–672, 2014.
- [87] A. Tward, Y. R. Xia, X. P. Wang et al., "Decreased atherosclerotic lesion formation in human serum paraoxonase transgenic mice," *Circulation*, vol. 106, no. 4, pp. 484–490, 2002.
- [88] G. Valacchi, C. Sticozzi, Y. Lim, and A. Pecorelli, "Scavenger receptor class B type I: a multifunctional receptor," *Annals of the New York Academy of Sciences*, vol. 1229, no. 1, pp. E1–E7, 2011.
- [89] G. Assmann and J.-R. Nofer, "Atheroprotective effects of high-density lipoproteins," *Annual Review of Medicine*, vol. 54, no. 1, pp. 321–341, 2003.
- [90] M. Navab, S. Y. Hama, G. M. Anantharamaiah et al., "Normal high density lipoprotein inhibits three steps in the formation of mildly oxidized low density lipoprotein: steps 2 and 3," *Journal of Lipid Research*, vol. 41, no. 9, pp. 1495–1508, 2000.
- [91] M. E. Brousseau and J. M. Hoeg, "Transgenic rabbits as models for atherosclerosis research," *Journal of Lipid Research*, vol. 40, pp. 365–375, 1999.
- [92] K. Goszcz, S. J. Deakin, G. G. Duthie, D. Stewart, S. J. Leslie, and I. L. Megson, "Antioxidants in Cardiovascular Therapy: Panacea or False Hope?," *Frontiers in Cardiovascular Medicine*, vol. 2, 2015.
- [93] A. K. Chahal, G. Chandan, R. Kumar, A. K. Chhillar, A. K. Saini, and R. V. Saini, "Bioactive constituents of *Embllica officinalis* overcome oxidative stress in mammalian cells by inhibiting hyperoxidation of peroxiredoxins," *Journal of Food Biochemistry*, vol. 44, no. 2, 2020.
- [94] I. JIALAL and S. M. GRUNDY, "Influence of antioxidant vitamins on LDL oxidation," *Annals of the New York Academy of Sciences*, vol. 669, no. 1, pp. 237–247, 1992.
- [95] H. Esterbauer, G. Jürgens, O. Quehenberger, and E. Koller, "Autoxidation of human low density lipoprotein: loss of polyunsaturated fatty acids and vitamin E and generation of aldehydes," *Journal of Lipid Research*, vol. 28, no. 5, pp. 495–509, 1987.
- [96] R. Siekmeier, C. Steffen, and W. März, "Role of Oxidants and Antioxidants in Atherosclerosis: Results of In Vitro and In Vivo Investigations," *Journal of Cardiovascular Pharmacology and Therapeutics*, vol. 12, no. 4, pp. 265–282, 2016.
- [97] G. Vogiatzi, D. Tousoulis, and C. Stefanadis, "The role of oxidative stress in atherosclerosis," *Hellenic Journal of Cardiology*, vol. 1, pp. 402–409, 2009.
- [98] A. Pastore and F. Piemonte, "Protein glutathionylation in cardiovascular diseases," *International Journal of Molecular Sciences*, vol. 14, no. 10, pp. 20845–20876, 2013.
- [99] J. W. E. Moss and D. P. Ramji, "Nutraceutical therapies for atherosclerosis," *Nature Reviews. Cardiology*, vol. 13, no. 9, pp. 513–532, 2016.
- [100] B. Frei, "Ascorbic acid protects lipids in human plasma and low-density lipoprotein against oxidative damage," *The*

- American Journal of Clinical Nutrition*, vol. 54, no. 6, pp. 1113S–1118S, 1991.
- [101] B. Feng, X. F. Yan, J. L. Xue, L. Xu, and H. Wang, “The protective effects of α -lipoic acid on kidneys in type 2 diabetic Goto-Kakizaki rats via reducing oxidative stress,” *International Journal of Molecular Sciences*, vol. 14, no. 4, pp. 6746–6756, 2013.
- [102] M. G. Battelli, L. Polito, and A. Bolognesi, “Xanthine oxidoreductase in atherosclerosis pathogenesis: not only oxidative stress,” *Atherosclerosis*, vol. 237, no. 2, pp. 562–567, 2014.
- [103] H. Esterbauer, M. Dieber-Rotheneder, G. Striegl, and G. Waeg, “Role of vitamin E in preventing the oxidation of low-density lipoprotein,” *The American Journal of Clinical Nutrition*, vol. 53, no. 1, pp. 314S–321S, 1991.
- [104] P. D. Reaven, “Oxidized low density lipoproteins in atherogenesis: role of dietary modification,” *Annual Review of Nutrition*, vol. 16, no. 1, pp. 51–71, 1996.
- [105] A. Costa-Mugica, A. E. Batista-Gonzalez, D. Mondejar et al., “Inhibition of LDL-oxidation and antioxidant properties related to polyphenol content of hydrophilic fractions from seaweed *Halimeda Incrassata* (Ellis) Lamouroux,” *Brazilian Journal of Pharmaceutical Sciences*, vol. 48, no. 1, pp. 31–37, 2012.
- [106] U. Singh, S. Devaraj, and I. Jialal, “Vitamin E, oxidative stress, and inflammation,” *Annual Review of Nutrition*, vol. 25, no. 1, pp. 151–174, 2005.
- [107] Y. M. Park, “CD36, a scavenger receptor implicated in atherosclerosis,” *Experimental & Molecular Medicine*, vol. 46, no. 6, pp. e99–e99, 2014.
- [108] S. A. Brenner, *The Effect of Vitamin E and Beta Carotene on the Incidence of Lung Cancer and Other Cancers in Male Smokers*, 1994.
- [109] J. M. Rapola, J. Virtamo, S. Ripatti et al., “Randomised trial of α -tocopherol and β -carotene supplements on incidence of major coronary events in men with previous myocardial infarction,” *Lancet*, vol. 349, no. 9067, pp. 1715–1720, 1997.
- [110] G. S. Omenn, G. E. Goodman, M. D. Thornquist et al., “Effects of a Combination of Beta Carotene and Vitamin A on Lung Cancer and Cardiovascular Disease,” *New England Journal of Medicine*, vol. 334, no. 18, pp. 1150–1155, 1996.
- [111] M. E. Törnwall, J. Virtamo, P. A. Korhonen et al., “Effect of α -tocopherol and β -carotene supplementation on coronary heart disease during the 6-year post-trial follow-up in the ATBC study,” *European Heart Journal*, vol. 25, no. 13, pp. 1171–1178, 2004.
- [112] P. Morales, I. C. F. R. Ferreira, A. M. Carvalho et al., “Wild edible fruits as a potential source of phytochemicals with capacity to inhibit lipid peroxidation,” *European Journal of Lipid Science and Technology*, vol. 115, no. 2, pp. 176–185, 2013.
- [113] S. Boukhenouna, H. Mazon, G. Branlant et al., “Evidence that glutathione and the glutathione system efficiently recycle 1-cys sulfiredoxin in vivo,” *Antioxidants & Redox Signaling*, vol. 22, no. 9, pp. 731–743, 2015.
- [114] U. Förstermann, “Oxidative stress in vascular disease: causes, defense mechanisms and potential therapies,” *Nature Clinical Practice. Cardiovascular Medicine*, vol. 5, no. 6, pp. 338–349, 2008.
- [115] C. Ding, X. Fan, and G. Wu, “Peroxiredoxin 1 – an antioxidant enzyme in cancer,” *Journal of Cellular and Molecular Medicine*, vol. 21, no. 1, pp. 193–202, 2017.
- [116] R. Kumar, A. Mohammad, R. V. Saini et al., “Deciphering the in vivo redox behavior of human peroxiredoxins I and II by expressing in budding yeast,” *Free Radical Biology and Medicine*, vol. 145, pp. 321–329, 2019.
- [117] R. Rezzani, F. Bonomini, S. Tengattini, A. Fabiano, and R. Bianchi, “Atherosclerosis and oxidative stress,” *Histology and Histopathology*, vol. 23, pp. 381–390, 2008.
- [118] J. Kisucka, A. K. Chauhan, I. S. Patten et al., “Peroxiredoxin 1 prevents excessive endothelial activation and early atherosclerosis,” *Circulation Research*, vol. 103, no. 6, pp. 598–605, 2008.
- [119] X. Wang, S. A. Phelan, C. Petros et al., “Peroxiredoxin 6 deficiency and atherosclerosis susceptibility in mice: significance of genetic background for assessing atherosclerosis,” *Atherosclerosis*, vol. 177, no. 1, pp. 61–70, 2004.
- [120] M. Conrad, V. E. Kagan, H. Bayir et al., “Regulation of lipid peroxidation and ferroptosis in diverse species,” *Genes & Development*, vol. 32, no. 9-10, pp. 602–619, 2018.
- [121] M. Lovatt, K. Adnan, V. Kocaba, M. Dirisamer, G. S. L. Peh, and J. S. Mehta, “Peroxiredoxin-1 regulates lipid peroxidation in corneal endothelial cells,” *Redox Biology*, vol. 30, p. 101417, 2020.
- [122] L. Galluzzi, I. Vitale, S. A. Aaronson et al., “Molecular mechanisms of cell death: recommendations of the Nomenclature Committee on Cell Death 2018,” *Cell Death & Differentiation*, vol. 25, no. 3, pp. 486–541, 2018.
- [123] W. S. Yang, K. J. Kim, M. M. Gaschler, M. Patel, M. S. Shchepinov, and B. R. Stockwell, “Peroxidation of polyunsaturated fatty acids by lipoxygenases drives ferroptosis,” *Proceedings of the National Academy of Sciences*, vol. 113, 2016no. 34, pp. E4966–E4975, 2016.
- [124] W. S. Yang, R. Sriramaratnam, M. E. Welsch et al., “Regulation of ferroptotic cancer cell death by GPX4,” *Cell*, vol. 156, no. 1-2, pp. 317–331, 2014.
- [125] H. Feng and B. R. Stockwell, “Unsolved mysteries: how does lipid peroxidation cause ferroptosis?,” *PLoS Biology*, vol. 16, no. 5, pp. e2006203–e2006215, 2018.

Review Article

Hydrogen: A Novel Option in Human Disease Treatment

Mengling Yang ¹, Yinmiao Dong ¹, Qingnan He ¹, Ping Zhu ², Quan Zhuang ³,
Jie Shen ¹, Xueyan Zhang ⁴, and Mingyi Zhao ¹

¹Department of Pediatrics, The Third Xiangya Hospital, Central South University, Hunan Province, Changsha 410013, China

²Guangdong Cardiovascular Institute, Guangdong Provincial People's Hospital, Guangdong Academy of Medical Sciences, Guangzhou, Guangdong 510100, China

³Transplantation Center of the 3rd Xiangya Hospital, Central South University, Hunan Province, Changsha 410013, China

⁴Xiangya School of Medicine, Central South University, Hunan Province, Changsha 410013, China

Correspondence should be addressed to Mingyi Zhao; 36163773@qq.com

Received 21 March 2020; Revised 6 June 2020; Accepted 13 July 2020; Published 8 September 2020

Academic Editor: Luciano Saso

Copyright © 2020 Mengling Yang et al. This is an open access article distributed under the Creative Commons Attribution License, which permits unrestricted use, distribution, and reproduction in any medium, provided the original work is properly cited.

H₂ has shown anti-inflammatory and antioxidant ability in many clinical trials, and its application is recommended in the latest Chinese novel coronavirus pneumonia (NCP) treatment guidelines. Clinical experiments have revealed the surprising finding that H₂ gas may protect the lungs and extrapulmonary organs from pathological stimuli in NCP patients. The potential mechanisms underlying the action of H₂ gas are not clear. H₂ gas may regulate the anti-inflammatory and antioxidant activity, mitochondrial energy metabolism, endoplasmic reticulum stress, the immune system, and cell death (apoptosis, autophagy, pyroptosis, ferroptosis, and circadian clock, among others) and has therapeutic potential for many systemic diseases. This paper reviews the basic research and the latest clinical applications of H₂ gas in multiorgan system diseases to establish strategies for the clinical treatment for various diseases.

1. Introduction

Molecular hydrogen (H₂) is the lightest chemical element in the earth's atmosphere. H₂ is often mixed in gas cylinders for deep-sea divers to breathe, to prevent decompression and nitrogen sickness [1]. In mammals, H₂ is spontaneously produced by intestinal bacteria in the process of anaerobic metabolism to produce energy and is enzymatically catabolized by hydrogenases to provide electrons.

Therapeutic applications of H₂ were first described in 1975. Dole et al. reported that hyperbaric hydrogen caused marked regression of tumors in mice with skin squamous carcinoma [2]. However, hyperbaric H₂ is not a clinically feasible option, and H₂ is a physiologically inert gas that seems not to react with any active substances, including oxygen gas, in mammalian cells. Thus, H₂ was perceived as being nonfunctional and was disregarded clinically.

In 2007, the potential therapeutic benefits of H₂ were described. Ohsawa et al. discovered that H₂ has selective antioxidant properties that protect the brain against ischemia/reperfusion (I/R) injury and stroke by specifically neutralizing hydroxyl radicals ($\cdot\text{OH}$) and peroxynitrite (ONOO⁻) but not superoxide anion radical ($\text{O}_2^{\cdot-}$), hydrogen peroxide (H₂O₂), and nitric oxide (NO) [3]. The report generated worldwide attention and thrust H₂ into the spotlight of therapeutic medical gas research. Many studies using cellular, animal, and clinical experiments in a variety of biomedical fields have explored the therapeutic and preventive effects of H₂. The collective data have indicated that H₂ is an important pathophysiological regulatory factor with antioxidative, anti-inflammatory, and antiapoptotic effects on cells and organs [4–6]. It is so convenient to use that H₂ can be easily administered in various ways, including inhalation, injection of H₂-rich saline (HRS), drinking H₂-rich

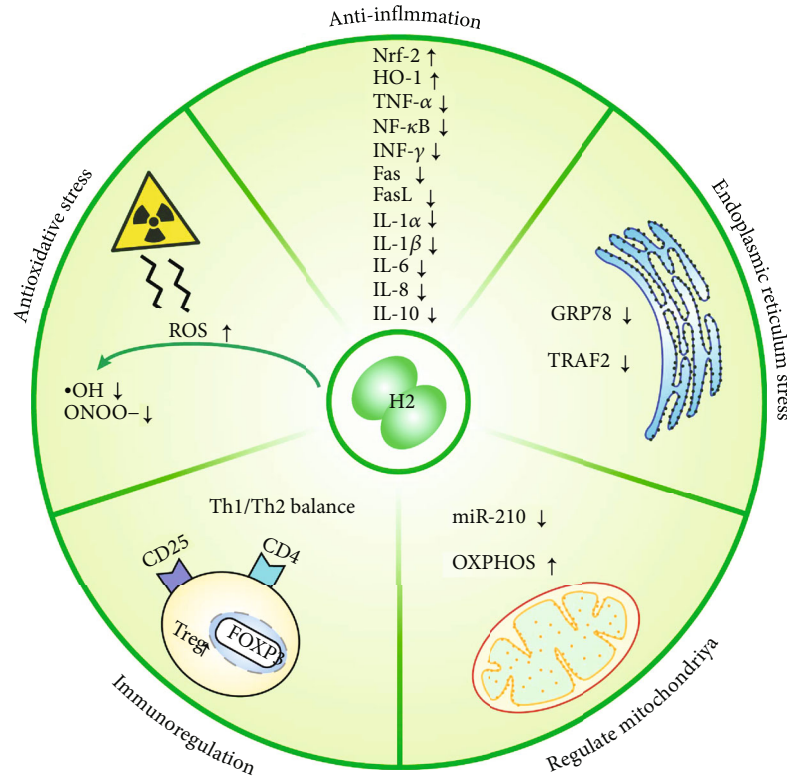


FIGURE 1: Biological effects of H_2 . H_2 exhibits selective antioxidative and anti-inflammatory activities and can regulate ER stress, mitochondria, and immune function. H_2 selectively scavenges $\cdot OH$ and $ONOO^-$, upregulates Nrf-2 and HO-1, and downregulates the expression of proinflammatory and inflammatory cytokines that include TNF- α , NF- κ B, INF- γ , Fas, FasL, IL-1 α , IL-1 β , IL-6, IL-8, and IL-10, as well as downregulates ER stress-related factors that include GRP78 and TRAF2. H_2 also reduces miR-210 and activates OXPHOS in mitochondria. Finally, H_2 increases CD4+CD25+Foxp3+Treg cells and maintains the Th1/Th2 balance.

water (HW), bathing in HW, and using HRS eyedrops. As well, the production of intestinal H_2 by bacteria can be increased via oral administration of acarbose and lactulose. Liu and his colleagues demonstrated that the hydrogen concentration reached a peak of 5 min after oral and intraperitoneal administration, and in only 1 min following intravenous administration [7].

Beginning on 31 December 2019 in Wuhan, China, illness and pneumonia named coronavirus disease-2019 (COVID-19) caused by severe acute respiratory syndrome coronavirus 2 (SARS-CoV-2) has spread to become a pandemic. The seventh edition of *Chinese Clinical Guidance for COVID-19 Pneumonia Diagnosis and Treatment (7th edition)* issued by China National Health Commission recommended the inhalation of oxygen mixed with hydrogen gas (33.3% O_2 and 66.6% H_2), bringing H_2 to the forefront of contemporary therapeutic medical gas research.

The preventive and therapeutic effects of H_2 have been intensively investigated for various pathological processes. In this review, we summarize the most recently published literature concerning the use of H_2 in respiratory, cardiovascular, nervous, digestive, reproductive, urinary, motor, and sensory system diseases, as well as for the treatment of metabolic syndrome and cancer. We also briefly discuss some known mechanisms underlying the action of H_2 . We hope that this information will increase the understanding of the therapeutic activities of H_2 and inform future H_2 -based therapies.

2. Mechanisms of the Action of H_2

To fully explain the preventive and therapeutic effects of H_2 , biological effects and possible mechanisms are summarized in Figures 1 and 2.

2.1. Anti-Inflammatory Effect of H_2 . The anti-inflammatory effect of H_2 has already been reported in many studies. In the early stage of inflammation, H_2 can reduce the infiltration of neutrophils and M1 macrophages, and the release of proinflammatory factors by downregulating the expression of intercellular cell adhesion molecule-1 (ICAM-1), granulocyte-macrophage colony-stimulating factor (GM-CSF), and granulocyte colony-stimulating factor (G-CSF) [4]. H_2 can also inhibit the expression of proinflammatory cytokines during the progress of inflammation and has been revealed in many animal models to decrease the overexpression of early proinflammatory cytokines, such as interleukin-(IL-) 1 β , IL-6, IL-8, IL-10, tumor necrosis factor-alpha (TNF- α) [8], interferon-gamma (INF- γ), and late proinflammatory cytokines, such as high-mobility group box-1 protein (HMGB1) [9]. Tanaka and colleagues [10] conducted a gene array analysis of lung grafts from donor rats pretreated with hydrogen ventilation. The authors described that pretreatment with H_2 obviously elevated the expression of two stress-response proteins: heat shock protein A5 (HSPA5) and dual-specificity phosphatase 1 (DUSP1). HSP70 protein

and α -tocopherol, H_2 can easily penetrate biofilms and does not affect the normal metabolic redox reaction due to its small molecular weight and antioxidative activity which selectively affects only the strongest oxidant [17]. H_2 can enhance the expression of the heme oxygenase-1 (HO-1) antioxidant by activating nuclear factor erythroid 2-related factor 2 (Nrf-2), an upstream regulating molecule of HO-1. H_2 can also downregulate ROS directly or as a regulator of a gas-mediated signal. Further, by upregulating the expression of SOD and glutathione (GSH), and downregulating the expression of NADPH oxidase (NOX2) [18], H_2 can significantly reduce ROS. Another study [19] showed that H_2 mainly blocks the phosphorylation of ASK1 and its downstream signal molecules p38 MAPK or c-Jun N-terminal kinase (JNK), but not the production of ROS by NADPH oxidase.

The effects on the free radical chain reaction of lipid peroxidation may be another important mechanism of hydrogen antioxidation. Since Otha et al. reported at the 5th Symposium of Medical Molecular Hydrogen at Nagoya, Japan, in 2015 that exposure to a low concentration of hydrogen causes abnormal oxidation of phospholipids [20], many studies have established that H_2 can protect cells from lipid and fatty acid peroxidation [21, 22]. Additionally, H_2 can also reduce the expression of myeloperoxidase (MPO) [23] or decrease mitochondrial oxidoreductase activity [21] and stabilize mitochondrial membrane potential [24], so as to improve the tissue damage caused by oxidative stress.

2.3. Regulation of Endoplasmic Reticulum Stress. The accumulation of unfolded protein in the endoplasmic reticulum (ER) caused by pathological stress can trigger ER stress. Zhao et al. [18] observed that hydrogen inhalation significantly reduced the ER stress-related protein and alleviated tissue damage in myocardial I/R injury and later found that a mixture of H_2 and O_2 can block endoplasmic reticulum stress via the PKR-like ER-localized eIF2 α kinase-eukaryotic initiation factor 2 alpha-activating transcription factor 4 (PERK-eIF2 α -ATF 4), inositol-requiring enzyme 1-X-box binding protein 1 (IRE 1-XBP1), and ATF 6 pathways. A study of the relationship between H_2 and ER stress in rats with I/R injury found that H_2 induced the decrease of GRP78 and TNF receptor-associated factor 2 (TRAF2) expression [25], suggesting that the protective effects of H_2 on myocardial I/R injury are related to decreased ER stress.

2.4. Regulation of Mitochondria. The accumulation of ROS can trigger the release of calcium from the ER, which results in the depolarization of mitochondria and the loss of the mitochondrial membrane potential [26]. The negative regulation of ROS and the inhibition of programmed cell death by H_2 help maintain the structure and function of mitochondria. It was reported [27] that hydrogen treatment can block the opening of mitochondrial permeability transition pores in neurons during neurodegenerative disease. However, whether H_2 can indirectly block these pores by reducing the production of ROS or acts directly is unclear. Early studies [28] showed that HRS moderated mitochondrial structural damage and simultaneously reduced microRNA- (miR)-

210 in hypoxic-reperfusion nerve tissue. However, recent studies have shown that the increase of miR-210 in injured tissues may be a compensatory action to maintain cell function and reduce ROS production [29, 30]. Whether H_2 can directly inhibit miR-210 or indirectly reduce it by alleviating inflammation also remains unclear.

Mitochondrial damage caused by oxidative stress is an important cause of many neurodegenerative diseases. Early clinical experiments on Parkinson's disease [31] showed that H_2 can significantly improve neurodegenerative symptoms with a therapeutic effect comparable to that of nonergot dopamine therapy. This cannot be explained by the antioxidative effect of H_2 , and thus, it was suggested that H_2 may target mitochondria to improve the energy metabolism of cells. The observation that H_2 treatment significantly improved the level of SH-SY5Y ATP and $\Delta\psi_m$ in neuroblastoma [32] is an indication that H_2 treatment can elevate energy metabolism in mitochondria by activating oxidative phosphorylation.

The observations of the conserved structural features shared between hydrogenases and the energy-converting complex I prompted the suggestion that H_2 might serve as both a reductant and oxidant [24]. The hypothetical function of H_2 in rectifying mitochondrial electron flow can explain the scavenging effect on ROS and the ability to slightly improve oxidative stress.

2.5. The Effects of Hydrogen on the Immune System. The main effect of H_2 on the immune system is to reduce the production of immune active substances. Evidence suggests that H_2 relieves inflammation in some autoimmune disorders, including rheumatoid arthritis (RA) [33, 34], dermatomyositis [35], and psoriasis [36]. However, whether H_2 directly influences immune cells or organs remains unclear. Recent studies have found that H_2 can relieve the dysregulated Th1/Th2 balance and can influence the number of T-regulatory cells (Tregs). H_2 was first reported to restore Treg loss in a rat model of chronic pancreatitis [15] and was later proven to increase CD4+CD25+Foxp3+Treg cells and significantly reduce nasal mucosa damage in animals with allergic rhinitis, which may be secondary to the restoration of Th1/Th2 balance [37]. Upregulation of Tregs has been reported in cerebral I/R models [28]. This may be caused by the upregulation of tumor necrosis factor-beta 1 (TNF- β 1) and downregulation of miR-21 or miR-210. H_2 can also activate peroxisome proliferator-activated receptor-gamma coactivator-1 alpha (PGC-1 α) to influence some kinds of T cells [38]. The specific mechanisms underlying the effects of H_2 on immune cells remain to be defined.

2.6. Effects of H_2 on Cell Death

2.6.1. Prevention of Apoptosis. Apoptosis is a form of programmed cell death characterized by cell shrinkage, apoptotic body formation, karyorrhexis, and chromatin condensation. Apoptosis can be induced by both intrinsic and extrinsic signals. H_2 exhibits antiapoptotic effects by up- or downregulating apoptosis-related factors. H_2 inhibits the expression of the proapoptotic factors B-cell lymphoma-2-associated X-protein (Bax), caspase-3, caspase-8, and caspase-12 and

upregulates the antiapoptotic factors B-cell lymphoma-2 (Bcl-2) and B-cell lymphoma-extra-large (Bcl-xl) [6]. Additionally, Terasaki and colleagues reported that H₂ can downregulate the gene expression of proapoptotic Bax and inhibit its translocation to mitochondria by an unknown mechanism [39]. H₂ can also inhibit apoptosis by activating the phosphatidylinositol-3-kinase/protein kinase B (PI3K/AKT) and the Janus kinase 2/signal transducer and activator of transcription 3 (JAK2-STAT3) signaling pathways in rats with myocardial ischemia-reperfusion injury (MIRI) [40, 41], as well as downregulating the p38 MAPK signaling pathway in rat models with lipopolysaccharide- (LPS-) induced acute lung dysfunction [42] and cerebral ischemia-reperfusion injury (CIRI) [43]. Interestingly, Wang et al. recently discovered that H₂ inhibited the growth, migration, and invasion of the A549 and H1975 lung cancer cell lines and promoted cell apoptosis, suggesting that H₂ might play crucial roles in the treatment of lung cancer [44]. Li et al. also revealed the apoptosis-inducing effect of H₂ on KYSE-70 human esophageal squamous cell carcinoma cells [45]. Thus, H₂ may protect normal cells from damage and suppressing cancer cells.

2.6.2. Autophagy. Although the activation of autophagy can maintain the energy balance of cells through the degradation of macromolecular substances, excessive autophagy or autophagy-related stress triggered by stress stimuli will aggravate the inflammatory damage in tissues and organs. H₂ plays a dual role in the regulation of autophagy. Under the regulation of H₂, autophagy can be activated when protein aggregation becomes toxic and blocked once excessive autophagy causes damage to tissues. Zhuang et al. [46] showed that H₂ treatment downregulated the expression of phosphomammalian target of rapamycin (p-mTOR)/mTOR and p62 in LPS-treated neuroglial cells and increased the expression of phospho-AMP-activated protein kinase (p-AMPK)/AMPK, light chain 3 (LC3) II/LC3 I, triggering receptor expressed on myeloid cells 2 (TREM-2), and Beclin-1 to activate autophagy and attenuate neuroinflammation in sepsis. Guan et al. [47] revealed that H₂ can ameliorate chronic intermittent hypoxia-induced kidney injury by decreasing ER stress and inducing autophagy by inactivating oxidative stress-dependent p38 and JNK MAPKs. H₂ can also inhibit autophagy by downregulating NF- κ B, Beclin-1, and MAPK and upregulating the HO-1, mTOR, and LC3B signaling pathways. Zhang et al. [42] found that saturated hydrogen saline alleviated LPS-treated lung injury and significantly reduced the expression of autophagy-related proteins, including LC3 and Beclin-1 ($P < 0.05$), suggesting that hydrogen saline can protect lung tissue against excessive autophagy. Saturated hydrogen saline can prevent excessive autophagy by eliminating excessive free radicals, reducing the concentration of free radicals in lung tissue, and promoting the expression of mTOR. HO-1 can function as an endogenous cytoprotective protein to assist in the prevention of oxidative stress and excessive cell autophagy. H₂ can increase the tissue expression of HO-1 by promoting the expression of nuclear erythroid 2-related factor 2 (Nrf2) [48].

Toll-like receptors (TLRs) could be a potential target for H₂ in autophagy regulation. TLR4, a key factor in the recog-

nition of viral and bacterial factors, can be activated by LPS to induce autophagy of macrophages [49]. The inhibition of an LPS-induced inflammatory response by H₂ supports the speculation that TLR may be a potential pathway of hydrogen-induced autophagy.

2.6.3. Pyroptosis. Pyroptosis is an inflammatory programmed cell death pathway that protects multicellular hosts from invasive pathogens, including microbial infections [50]. Human and mouse caspase-1, human caspase-4 and caspase-5, and mouse caspase-11 act as essential activators of pyroptosis. While pyroptosis is normally beneficial for the host, excessive pyroptosis can result in sepsis and septic shock. Although there is no experimental data to explain the relationship between H₂ and the pyroptosis pathway, it is conceivable that the regulation of some inflammatory factors and nuclear factors by H₂ will interfere with the triggering of pyroptosis, or at least reduce pyroptosis-related inflammation. In one study [51], inhalation of 2% H₂ reduced the expression of caspase-1, a key factor for pyroptosis activation. Physical rupture of cells caused by pyroptosis leads to the release of the proinflammatory cytokines IL-1 β and IL-18, while hydrogen pretreatment can significantly reduce the level of these cytokines [52]. H₂ has also been shown to regulate the expression of Atg7, which inhibits pyroptosis [53]. It has been proposed that HMGB1 [54] and IFN- γ [50] are necessary for caspase-11-dependent pyroptosis activation. The negative effect of H₂ on the expression of these two factors may protect cells from pyroptosis. H₂ is able to block the expression of caspase-3 [55], which serves both as the activator of apoptosis, and also blocks pyroptosis by cleaving gasdermin D [56]. Bidirectional crosstalk exists between the caspase-3 produced in apoptosis and the caspase in pyroptosis. The mechanism of this crosstalk remains unclear.

Human immunodeficiency virus (HIV) can accelerate the depletion of CD4+ T cells via interferon-gamma inducible protein 16- (IFI16-) triggered pyroptosis [50]. Thus, the regulation of pyroptosis by H₂ may be a potential mechanism to treat HIV affection.

2.6.4. Ferroptosis. Ferroptosis is a form of regulated cell death proposed by Dixon et al. [57] in 2012. Ferroptosis is accompanied by a lethal iron-dependent accumulation of lipid hydroperoxides. Although laboratory verification has not been forthcoming, we can still speculate that hydrogen can interfere with ferroptosis to alleviate inflammatory necrosis of tissues and organs in the pathological state, given the great deal of overlap between hydrogen regulation and ferroptosis pathways. It has been well-established that hydrogen has a negative regulatory effect on ROS. We speculate that the most critical redox imbalance in the process of ferroptosis will be eliminated by hydrogen; thus, ferroptosis will be blocked. In addition, H₂ is able to block MAPK pathways, which are to prevent the depletion of reducing substances caused by iron ions and ROS [58]. A recent study [59] showed that HMGB1, which can be downregulated by hydrogen [9], can act as a positive regulator of ferroptosis via the RAS-JNK/p38 pathway.

HO-1 activity can be increased by hydrogen. HO-1 is a potential source of intracellular iron, and a recent study [60] demonstrated that HO-1-deficient renal epithelial cells were more sensitive to ferroptosis, indicating that free iron produced by HO-1 does not promote ferroptosis itself, and that HO-1 has an anti-ferroptotic effect. However, the effects of hydrogen on ferroptosis may not always be inhibitory. For example, miR-9, an inflammatory miRNA that is down-regulated by hydrogen, can reduce the occurrence of ferroptosis [16]. The mechanism underlying the action of hydrogen on ferroptosis is yet to be fully clarified.

Some of the anti-inflammatory and antioxidation mechanisms of hydrogen are similar to those of GPX4 [61]. Both molecules have negative effects on the formation of lipid peroxide and NF- κ B. The combination of hydrogen and GPX4 activator may provide a new solution for the treatment of inflammation and other lipid peroxidation-mediated diseases.

2.6.5. Circadian Clock. The circadian clock refers to an endogenous oscillator that controls 24 h physiological, metabolic, and behavioral processes. This clock is particularly crucial in maintaining homeostasis [62]. Intestinal microbiota, which regularly produce hydrogen gas in the process of the energy-producing anaerobic fermentation [63], undergo diurnal oscillations in composition and function [64]. In humans, the amount of hydrogen produced varies depending on the individual and the time of the day. Wilking et al. suggested that the circadian regulation of protein expression plays an important role in the cellular response to oxidative stress; they concluded that levels of byproducts of oxidative stress, such as protein damage, or lipid peroxidation, also oscillate with circadian rhythmicity, indicating circadian oscillations of oxidative stress responses. Thus, this rhythmicity of antioxidant levels can be exploited for a more precise targeting of ROS to offer better protection for the cells [65]. As the antioxidant activity of H₂ has been widely verified, we suggest that H₂ may exert a negative regulatory effect on ROS by regulating circadian rhythm, but there is yet no evidence regarding how H₂ is involved in the regulation of circadian rhythm.

3. Preventive and Therapeutic Applications of H₂

H₂ has preventive and therapeutic effects on different system diseases (Table 1).

3.1. Effects of Hydrogen on the Respiratory System. The seventh edition of *Chinese Clinical Guidance for COVID-19 Pneumonia Diagnosis and Treatment (7th edition)* issued by China National Health Commission recommends the inhalation of O₂ mixed with H₂. The recommendation recognized the efficacy of hydrogen in the treatment of respiratory diseases. A recent review summarized several researches on SARS-CoV-2 and pointed out that the possibility that H₂ could alleviate SARS-CoV-2 infection through affecting cellular responses [66]. Antiviral efficacy and safety of H₂ in treating NCP patients have attracted the attention of

researchers in completed or ongoing multicenter clinical trials. Guan et al. [67] evidenced that inhalation of H₂/O₂ mixed gas efficiently improved respiratory symptoms especially dyspnea as well as disease severity without observed side effects. Another multi-centre RTC (ChiCTR2000030258) aims verifying the efficacy and safety of H₂/O₂ mixed gas is ongoing. Due to its small molecular weight, hydrogen in the inhaled gas mixture can reduce airway resistance, increase oxygen dispersion, and increase oxygen flow. COVID-19 can provoke an inflammatory storm by excessively activating the immune system, causing severe inflammatory damage to the lungs and extrapulmonary tissue, which is also the main cause of death [68].

A study involving 41 patients with NCP showed that patients in the intensive care unit displayed a significantly higher level of inflammatory factors that included IL-2, IL-7, IL-10, and TNF- α and that most of these factors could be downregulated by hydrogen [69]. We speculate that the application of hydrogen may reduce the risk of inflammatory storm and thus prevent severe effects. Many NCP patients need ventilator-assisted therapy. Inflammatory changes in the respiratory system make lung tissue prone to ventilator-induced lung injury (VILI), even with low tidal volume [70]. Ventilation with 2% H₂ was proved to be able to down-regulate the mRNAs for proinflammatory mediators such as TNF- α , IL-1 β , Egr-1, and CCL2 and induced antiapoptotic genes including Bcl-2 and Bcl-xL. It is consistent with the histopathological results which showed that inflammatory cell infiltration and bronchial epithelial apoptosis were improved in VILI mice after H₂ treatment. H₂ has a potential to protect human lung tissues from VILI as well via its anti-inflammatory, antioxidant, and antiapoptotic effects [11]. Moreover, hydrogen can also increase surfactant proteins to prevent further lung injury [11]. One study reported that chest computed tomography scans performed at the early stage in patients that ultimately developed in severe infection revealed multiple small flake shadows and interstitial changes, suggesting that pulmonary fibrosis affects the prognosis of the disease. HRS has been reported to reverse epithelial-mesenchymal transition (EMT) and prevent pulmonary fibrosis by inhibiting oxidative stress and increasing the expression of E-cadherin [71].

Hydrogen also has the potential to protect lung tissues from pulmonary hypertension [72], sepsis [73], smoke inhalation injury [74], hemorrhagic shock and resuscitation [75], and other toxic substances/events. In animal models, hydrogen also affects asthma and chronic obstructive pulmonary disease [76].

3.2. Effects of Hydrogen on the Nervous System. Myriad forms of irreversible damage that occur in nervous system diseases are often caused by neuroinflammation, excessive oxidative stress, mitochondrial dysfunction, and cell death. The therapeutic effects of hydrogen on the nervous system have been verified in animal models and clinical trials. Hydrogen can reportedly reduce the loss of dopaminergic neurons and can improve nigrostriatal degeneration a mouse model of Parkinson's disease (PD) following treatment with 6-hydroxydopamine [77] and 1-methyl-4-phenyl-1,2,3,6-tetrahydropyridine [78]. A recent

TABLE 1: Mechanisms of H₂ in multiple systemic diseases.

Diseases	Effects of H ₂	Reference
Respiratory system	Regulates IL-2, IL-7, IL-10, and TNF- α	[66]
	Increases surfactant proteins	[11]
	Reverses EMT and increases E-cadherin	[68]
Cardiovascular system	Suppresses macrophage infiltration, TNF- α expression, and vascular aging	[88]
	Inhibits cardiomyocyte apoptosis	[39, 40]
	Decreases MDA, 8-OHdG, and IL-1 β	[92, 93]
Nervous system	Reduces loss of dopaminergic neurons and improves nigrostriatal degeneration	[74, 75]
	Reduces neurological deficits and endothelial cell injury	[83, 84]
Digestive system	Induces HO-1 and Sirt1 expression	[98]
	Activates the A2A receptor-mediated PI3K-Akt pathway	[99]
Reproductive system	Inhibits bile acid oxidation	[114]
	Inhibits cell proliferation and improves SOD	[130]
	Improves serum levels of anti-Müllerian hormone	[133]
	Improves serum testosterone level	[135]
Urinary system	Increases Il-4 and Il-13 and promotes macrophage polarization to the M2 type	[140]
	Activates the Keap1/Nrf2 signaling pathway	[145]
Motor system	Prevents HK-2 cells from undergoing EMT	
	Reduces blood lactate levels	[47]
Sensory system	Suppresses serum 8-OHdG levels	[154]
	Reduces wound area and levels of proinflammatory cytokines	[159]
Metabolic syndrome	Improves auditory brainstem response	[161]
	Decreases LDL and increases high-density lipoprotein	[148]
	Decreases glucose and insulin levels	[149]
Cancer	Stimulates energy metabolism	[152]
	Controls cancer progression and improves quality-of-life	[140]
	Reduces proportion of terminal PD-1+ CD8+ T cells	[37]

clinical trial showed that HW can improve the total Unified Parkinson's Disease Rating Scale score of PD [31]. Early clinical trials revealed that hydrogen improves PD through antioxidation. More recent research found that hydrogen may slightly increase oxidative stress or act as the rectifier of the mitochondrial electron flow and improve PD by regulating mitochondrial energy [24] or via hormetic mechanisms. By hormetic mechanisms, H₂ will simulate strenuous exercise to generate a mild increase of ROS which will evoke hormesis and then activate the Nrf2, NF- κ B pathways, and heat shock responses to protect neurons and other tissues [16]. Hydrogen also improved cognitive function in Alzheimer's patients in a clinical trial [79]. The collective findings indicate the safety and effectiveness of hydrogen in the treatment of neurodegenerative diseases.

Hydrogen has also been shown to protect the nervous system of a fetus or newborn. In two case studies, pregnant women who had become infected with COVID-19 displayed a high delivery rate of fetuses with intrauterine distress leading to a higher incidence of perinatal hypoxic-ischemic brain damage [77, 78]. The findings indicate the necessity of measures to prevent neonatal encephalopathy or reduce neonatal neurological deficit for pregnant women infected with COVID-19. H₂ can inhibit the activation of proinflammatory cytokines, microglia [79], and 8-hydroxy dehydrogenase (8-OHdG) [80] to reduce oxidative damage and neuroinflam-

mation in the fetal brain in animal models. The protective effects have been verified by clinical trials. Hippocampal damage caused by I/R injury in the uterus on day 7 after birth was reportedly improved for pregnant women who had been treated with HW and was associated with reductions of 4-hydroxy ketone and 8-OHdG [81]. The available data support the possibility that hydrogen therapy could protect fetuses of pregnant women infected with COVID-19. In addition, hydrogen can also protect against spinal cord injury and a variety of brain injuries caused by ischemia, hypoxia, trauma, and hemorrhage. A clinical study of patients suffering from cerebral infarction reported that hydrogen inhalation improved imaging results, National Institutes of Health Stroke Scale scores used to quantify the severity of stroke, and physical therapy evaluations based on the Barthel Index [82]. A rat model of subarachnoid hemorrhage revealed the influence of hydrogen in lessening neurological deficits [83] and endothelial cell injury [84]. In rats, hydrogen can also relieve neuropathic pain [85] after spinal cord injury and can ameliorate neurotoxicity [69].

3.3. Effects of Hydrogen on Cardiovascular Diseases. With the acceleration of urbanization and aging of global societies, the risk of cardiovascular diseases (CVD) has increased. The World Health Organization ranks CVD as the leading cause

of death globally, accounting for 17.5 million deaths annually. Two of every five deaths in China are attributed to CVD, which exceeds the death rate due to cancer or other diseases [86]. However, most clinical trials to date have failed to effectively prevent and treat CVD. Thus, novel therapies are urgently required.

During the past decade, many basic and clinical studies have provided evidence supporting the view that H₂ treatment protects against CVD and improves cardiac function. Ohsawa et al. discovered that consumption of HW for 6 months reduced the oxidative stress level and the volume of atherosclerotic lesions derived from macrophage accumulation in apolipoprotein E knockout mice (ApoE^{-/-} mice) [87]. Iketani et al. recently revealed that continuous administration of HW in low-density lipoprotein (LDL) receptor-deficient mice decreased the numbers of endothelial cells in the atheroma expressing the senescence factors p16INK4a and p21, as well as suppressing macrophage infiltration and TNF- α expression in the atheroma, suggesting that vascular aging can be suppressed by HW [88]. Another study demonstrated increased flow-mediated dilation in the high-H₂ group in which eight males and females drank HW containing 7 ppm H₂, indicating that H₂ may protect the vasculature from shear stress-derived ROS that is detrimental [89].

In addition to treating atherosclerosis, H₂ reduces MIRI, which refers to a heart lesion that develops upon the resumption of the flow of oxygen-rich blood after a period of ischemia and which usually occurs during acute myocardial infarction or open-heart surgery [40, 90]. A recent series of studies by Li et al. found that HW inhibited cardiomyocyte apoptosis by activating the PI3K/AKT and JAK2-STAT3 signaling pathways and can also reduce the level of oxidative stress in myocardial tissue by upregulating the expression of the nuclear erythroid 2-related factor 2/antioxidant response element (Nrf2/ARE) signaling pathway, which alleviated I/R injury in isolated rat hearts [39, 40, 91]. Other studies demonstrated that intraperitoneal injection of HW before reperfusion significantly decreased the concentration of malondialdehyde (MDA) and infarct size, as well as reducing myocardial 8-OHdG and the levels of TNF- α and IL-1 β in an area at risk zones [92, 93]. Moreover, Qian et al. described the hydrogen-mediated protection of myocardium degeneration due to radiation-induced injury in rats [94]. Treatment with HRS was shown to ameliorate vascular dysfunction, including aortic hypertrophy and endothelial function, in spontaneously hypertensive rats by abating oxidative stress, restoring baroreflex function, preserving mitochondrial function, and enhancing nitric oxide bioavailability [95]. In another study, the intraperitoneal administration of HRS improved hemodynamics and reversed right ventricular hypertrophy in male Sprague-Dawley rats with pulmonary hypertension induced by monocrotaline [96]. H₂ inhalation is also a favorable strategy to mitigate mortality and functional outcome of postcardiac arrest syndrome in a rat model [97]. These collective findings indicate the potential of H₂ in novel therapeutic approaches for the clinical treatment of CVD.

3.4. Effects of Hydrogen on Digestive System Diseases. Hepatic ischemia-reperfusion injury (HIRI) is common in liver sur-

gery and liver transplantation. H₂ treatment ameliorated HIRI in a mouse fatty liver model by reducing hepatocyte apoptosis, inhibiting macrophage activation and inflammatory cytokines, and inducing HO-1 and Sirt1 expression [98]. Inhalation of high concentrations of hydrogen significantly improved liver function in a mouse HIRI model by activating the A2A receptor-mediated PI3K-Akt pathway [99]. A recent series of studies also discovered that portal vein injection of HRS in miniature pigs with laparoscopic HIRI promoted liver function recovery and liver regeneration by reducing hepatocyte autophagy and apoptosis and inhibited ER stress, with significant hepatoprotective effects observed [100–103]. Hydrogen flush after cold storage refers to an end-ischemic H₂ flush directly to donor organs *ex vivo*. This approach can significantly protect liver grafts from IRI [104], providing a potentially effective strategy for organ preservation. Other studies demonstrated the protective effects of H₂ in liver damage induced by parasites [105], obstructive jaundice [106], shock and resuscitation [107], sepsis [108], doxorubicin [6], and aflatoxin B1 [109]. In a mouse model of nonalcoholic fatty liver disease (NAFLD), HW downregulated Nrf2-mediated miR-136 expression by targeting the maternally expressed 3 long noncoding RNA gene [110], providing a rationale for further clinical trials. In a human study, HW also significantly reduced liver fat accumulation in twelve overweight outpatients with NAFLD [111]. Another *in vivo* study revealed that oral HW significantly attenuated oxidative stress in patients with chronic hepatitis B [112]. In recent years, it has become widely accepted that bile acids are a nutrient signaling hormone [113]. Molecular hydrogen was recently demonstrated to participate in the regulation of bile acid metabolism, particularly in the inhibition of bile acid oxidation, in some gut bacteria [114].

Intestinal I/R injury is a multifactorial pathophysiological process with high morbidity and mortality. I/R injury occurs in a variety of clinical settings that include major cardiovascular surgery, trauma, shock, and small intestinal transplantation [115]. Yao et al. recently observed that intraperitoneal injection of H₂ attenuated I/R-induced mucosal injury and apoptosis of epithelial cells in mice by regulating miRNAs, in particular by regulating miR-199a-3p [116]. Furthermore, HW reportedly inhibited intestinal I/R-induced oxidative stress, apoptosis, and inflammation and promoted epithelial cell proliferation in rats, which protected against intestinal contractile dysfunction and damage induced by intestinal I/R [117–119]. Most gastrointestinal microbial species encode the genetic capacity to metabolize H₂, meaning that H₂ might affect the gut bacterial composition [120], and bacterial translocation is an important cause of multiple organ dysfunction syndromes in critical illness. Ikeda et al. described that the luminal administration of HW prevented intestinal dysbiosis, hyperpermeability, and bacterial translocation in a murine model of sepsis [121]. In another study, the inhalation of 2% H₂ also attenuated intestinal injuries caused by severe sepsis in male Nrf2 KO mice by regulating HO-1 and HMGB1 release [122]. Moreover, an *in vivo* study revealed that H₂ inhalation improved the prognosis in patients with stage IV colorectal cancer by activating PGC-1 α and restoring exhausted CD8⁺ T cells [123].

Wang et al. interestingly discovered that cytotoxin-associated gene A cytotoxin, a virulence factor of *Helicobacter pylori* that augments the risk of gastric cancer, can be delivered into host cells by the H₂-utilizing respiratory chain of the bacterium, extending the roles of H₂ oxidation to include transport of a carcinogenic toxin [124]. Although this study indicated that H₂ may play a role in increasing gastric cancer risk, abundant studies also demonstrated that H₂ is protective in gastric damage induced by oxidative stress [125] and aspirin [126]. Franceschelli et al. found that electrolyzed reduced water, which is rich in molecular hydrogen, rapidly improved symptoms in patients with gastroesophageal reflux disease [127]. H₂ treatment also controlled the severity of chronic pancreatitis [15] and acute necrotizing pancreatitis [128].

3.5. Effects of Hydrogen on Reproductive System Diseases.

Yang et al. recently demonstrated using a mouse model of human endometrial tumor xenograft that HW has an antitumor effect that was sufficient to inhibit xenograft volume and weight of endometrial tumors via the ROS/NLRP3/caspase-1/GSDMD-mediated pyroptotic pathway, indicating a biphasic effect of H₂ on cancer that involves the promotion of tumor cell death and protection of normal cells [129]. Other authors reported that H₂ inhalation reduced the size of the endometrial explants, inhibited cell proliferation, improved SOD, and regulated the expression of matrix metalloproteinase 9 and cyclooxygenase 2 in an endometriosis rat model [130]. HRS is effective in attenuating ovary injury induced by I/R [131] and cisplatin [132]. HW improved serum anti-Müllerian hormone levels and reduced ovarian granulosa cell apoptosis in a mouse immune premature ovarian failure model induced by zona pellucida glycoprotein 3 [133]. In a hemisectioned spinal cord injury rat model, HRS inhibited the injury-induced ultrastructural changes in gonadotrophs, ameliorated the abnormal regulation of the hypothalamic-pituitary-testis axis, and thereby promoted the recovery of testicular injury [134]. In irradiated rats, HRS improved testis weight, testis dimensions, sperm count, sperm motility, and serum testosterone levels [135]. HW stimulated spermatogenesis as well as increased sperm production and sperm motility in mice of different ages [136]. Based on previous studies, Begum et al. hypothesized that H₂ may modulate intracellular MAPK cAMP and Ca²⁺ signals involved in testosterone hormone production to improve male fertility caused by redox imbalance [137]. Finally, H₂ decreased the percentage of sperm abnormalities and improved sperm morphology following the prolonged exposure of mouse low doses of radiation [138]. The collective data indicate that hydrogen can protect both female and male fertility.

3.6. Effects of Hydrogen on Urinary System Diseases.

Acute kidney injury (AKI) is an important risk factor for the development of chronic kidney disease. Wu et al. recently found that saturated hydrogen alleviates CCL4-induced AKI via JAK2/STAT3/p65 signaling [139]. Inhalation of a hydrogen-rich aerosol appears to be very useful for renal protection and inflammation reduction in septic AKI, based on the observations of increased anti-inflammatory cytokine (IL-4 and IL-13) mRNA levels in renal tissues and

increased macrophage polarization to the M2 type, which generates additional anti-inflammatory cytokines (IL-10 and transforming growth factor-beta, TGF- β) [140]. Additionally, H₂ can alleviate AKI induced by I/R [141], liver transplantation [142], burns [143], and sodium taurocholate-induced acute pancreatitis [144]. Recently, Lu et al. demonstrated that HW can restore a balanced redox status and alleviate cyclosporine A-induced nephrotoxicity by activating the Keap1/Nrf2 signaling pathway [145]. H₂ can ameliorate kidney injury induced by chronic intermittent hypoxia by decreasing ER stress and activating autophagy through the inhibition of oxidative stress-dependent p38 and JNK MAPK activation [46]. HW also reportedly can inhibit the development of renal fibrosis and prevent HK-2 cells from undergoing EMT mediated through Sirt1, a downstream molecule of TGF- β 1. HRS markedly reduced interstitial congestion, edema, and hemorrhage in renal tissue, prevented renal injury, and promoted renal function recovery after I/R injury in rats through antiapoptotic and anti-inflammatory actions in kidney cells [146]. Other authors described that HW significantly reduced the increased post-void residual volume in obstructed rats and ameliorated bladder dysfunction secondary to bladder outlet obstruction by attenuating oxidative stress [147].

3.7. Effects of Hydrogen on Metabolic Syndrome.

Metabolic syndrome is associated with excess calorie intake and encompasses a range of medical conditions that include obesity, insulin resistance, and dyslipidemia. Many studies have demonstrated the protective effects of H₂ in metabolic syndrome. Qiu et al. reported that saturated hydrogen decreased total cholesterol, total glyceride, and LDL, increased high-density lipoprotein in the peripheral blood, and alleviated the activity of isocitrate lyase, suggesting that H₂ could improve lipid metabolism disorders by inhibiting the glyoxylic acid cycle [148]. Glucose and insulin levels in the serum were also significantly lower in H₂-treated mice, which markedly improved type 2 diabetes mellitus and diabetic nephropathy-related outcomes [149]. Moreover, gut-derived hydrogen production induced by L-arabinose reportedly had beneficial effects on metabolic syndrome in C57BL/6J mice fed a high-fat diet [150] and reduced oxidative stress and the peripheral blood IL-1 β mRNA level in sixteen type 2 diabetic patients [151]. H₂ treatment has also shown positive effects on energy metabolism. In 2011, Kamimura et al. reported that prolonged consumption of HW significantly controlled fat and body weights in db/db obese mice by stimulating energy metabolism [152]. A recent study revealed that H₂ attenuated allergic inflammation in a mouse model of allergic airway inflammation by reversing an energy metabolic pathway switch from oxidative phosphorylation to aerobic glycolysis [153].

3.8. Effects of Hydrogen on Motor System Diseases.

Although many studies have investigated the effectiveness of H₂ on various diseases related to oxidative stress, little is known about the influence of H₂ on exercise-induced oxidative stress. In 2012, Aoki et al. found that HW reduced blood lactate levels and improved exercise-induced decline of muscle function in ten male soccer players [47]. Yamazaki et al. discovered that

the serum 8-OHdG levels in H₂-treated race horses were significantly suppressed, strongly suggesting a protective effect of H₂ in exercise-induced, ROS-mediated detrimental tissue damage [154]. Additionally, hydrogen bathing attenuated exercise-induced muscle damage and delayed-onset muscle soreness but had no effects on the peripheral neutrophil count and both dynamics and functions of neutrophils [155]. These findings highlight that further studies are needed to clarify the mechanisms of H₂. Inhalation of H₂ significantly decreased infarct zone and area with loss of tissue structure, attenuated muscle damage, and enhanced functional recovery in a mouse hindlimb I/R injury model [156]. Finally, Hasegawa et al. revealed that H₂ improved muscular dystrophy in the mdx mouse model for Duchenne muscular dystrophy [157].

3.9. Effects of Hydrogen on Sensory System Diseases. Hydrogen has a therapeutic role in alleviating the damage to some sensory organs, mainly through antioxidation. Hydrogen promotes wound healing in tissue or protective barriers including skin and mucosa. For example, preinhalation of hydrogen-containing gas decreased wound healing time in a rat model of radiation-induced skin injury [158]. Other authors reported that H₂ inhalation reduced the wound area and levels of proinflammatory cytokines in pressure ulcers [159]. Moreover, hydrogen can improve skin lesions in some immune disorders by interfering with the immune system or ROS removal [160]. HW also benefits the wound healing process of the oral palate. Hydrogen also may protect hearing and vision. Kurioka et al. [161] demonstrated that hydrogen inhalation significantly reduced outer hair cell loss and improved auditory brainstem response after noise exposure, indicating a protective effect for noise-induced hearing loss. Hydrogen has been shown to be effective in treating cornea injury caused by alkali [162], fluoride, chloropicrin [163], and ultraviolet B radiation [164].

3.10. Effects of Hydrogen on Cancer. Many animal models have established the efficacy of hydrogen against cancers. The attributes of hydrogen include blocking of the regulator for chromosome condensation [43], some crucial molecules in stemness [165], proliferation [123], and angiogenesis [165], and the alleviation of oxidative stress. The combination therapy of hydrogen and other novel antineoplastic drugs, such as LY294002 [166], which is an inhibitor of PI3K, has demonstrated great potential and efficacy. An increasing number of clinical trials are being carried out. A recent survey [140] on 82 advanced cancer patients exemplified that hydrogen can control cancer progression and improve the quality-of-life. Akagi [37] treated 55 stage IV colorectal carcinoma patients using hydrogen inhalation and documented enhanced mitochondrial activity due to the activation of PGC-1 α to reduce the proportion of terminal PD-1+ CD8+ T cells. The depletion of these cells is associated with improved cancer prognosis [37, 123]. This therapeutic effect has also been confirmed in another trial conducted in one patient with metastatic gallbladder cancer [167]. In a case report in 2019, hydrogen gas therapy resulted in the disappearance of the metastatic brain tumors in a

woman diagnosed with lung cancer [168]. Finally, hydrogen can also reduce the side effects of cisplatin [169] and radiotherapy [170]. Though growing evidences have shown the effects of H₂ on alleviating both cancer progression and side effects of chemotherapeutics, the H₂ therapy applied in cancer is just in a nascent stage. At present, the published researches on the anticancer effects of H₂ mainly focus on lung cancer [168], colorectal cancer [37], and glioma [165]. It remains unclear how many cancers can effectively be alleviated by H₂ and how many can not be.

At present, patients with COVID-19 pneumonia are usually treated with high flow pure oxygen (without adding H₂), although the effect of O₂ when associated with H₂ may give better results [171]. The production of mucus in these patients reduces the absorption of O₂, while with a mixture of O₂ and H₂, the bronchioles and the alveoli of lungs are further expanded, optimizing the absorption of O₂ [172]. H₂ is used as a catalyst to accelerate the binding of hemoglobin with O₂ and the release of hemoglobin with carbon dioxide [173].

4. Conclusions

Hydrogen has great potential in the regulation of oxidative stress, inflammation, energy metabolism of organelles, and programmed cell death. Many animal experiments and clinical trials have established the protective effects of hydrogen on many organs and systems.

Research in this area has increased over the past 15 years. However, the details of the specific molecular mechanisms of the therapeutic effects of hydrogen remain unclear. For example, whether hydrogen can truly be used to regulate ferroptosis, pyroptosis, or the circadian clock is not known. Since H₂ is not something like rapamycin or leucine only going to have one direction (opposite) effects on autophagy, is it possible to regulate autophagy or apoptosis in a specific direction? Previous studies have clearly explained the antioxidative stress effect of hydrogen. However, some recent clinical trials have shown that H₂ can induce oxidative stress in some cases as well. Ventilation with H₂ can induce a mild increase of ROS to activate the Nrf2, NF- κ B pathways, and heat shock responses. H₂-induced ROS production can also be observed in cancer cells. The specific mechanism underlying the hydrogen-induced increase of oxidative stress should be explained by more experiments. These and other questions concerning the mechanism of hydrogen should be further explored.

There are many factors that limit the clinical use of hydrogen. Firstly, hydrogen is considered unsafe at concentrations above 4% because such a high level of H₂ is explosive and might bring cytotoxic effects. Previous studies have indicated that the concentration of hydrogen should be stabilized beyond 2% to enable protection from acute oxidative stress. However, even 2% of hydrogen is not absolutely safe. Most clinical ventilators are equipped with platinum hot manometers, because H₂ and O₂ can overheat the platinum surface at room temperature. Secondly, there is a lack of specialized devices that enable the administration of effective hydrogen concentrations, while ensuring that they are safe. Thirdly,

there have been few large-scale controlled human studies on the effects of hydrogen. Fourthly, Liu and his colleagues demonstrated that the inhalation of H₂ resulted in a slower elevation of the H₂ concentration than that achieved with intraperitoneal, intravenous, or oral administration. However, the elevated H₂ concentrations were maintained for at least 60 minutes after inhalation. Thus, it should be deliberated to choose the administration of H₂ [7]. As a result, the dose-specific effects or side effects of hydrogen in humans remain unclear.

The data regarding the known mechanisms underlying the action of hydrogen indicate that hydrogen can alleviate the damage in multiple organs in NCP patients. The comparisons of the different modalities of hydrogen indicate the value of HW in the effective treatment of such patients.

Hydrogen is inexpensive and safe and can be administered through many ways. We anticipate that as large-scale clinical trials confirm the therapeutic efficacy and safety of hydrogen, its full clinical potential will be realized.

Abbreviation

NCP:	Novel coronavirus pneumonia
H ₂ :	Hydrogen
I/R:	Ischemia/reperfusion
HRS:	H ₂ -rich saline
HW:	H ₂ -rich water
ROS:	Reactive oxygen species
ER:	Endoplasmic reticulum
EMT:	Epithelial-mesenchymal transition
CVD:	Cardiovascular diseases
NAFLD:	Nonalcoholic fatty liver disease
AKI:	Acute kidney injury
MDA:	Malondialdehyde
Nrf2:	Nuclear erythroid 2-related factor 2
PGC-1 α :	Peroxisome proliferator-activated receptor-gamma coactivator-1 alpha.

Conflicts of Interest

The authors declare no conflict of interest.

Authors' Contributions

Mengling Yang and Yinmiao Dong collected the literature and drafted the initial manuscript. Yinmiao Dong, Jie Shen, and Xueyan Zhang assisted in the preparation of the figures and table. Qingnan He, Quan Zhuang, and Ping Zhu revised the manuscript and edited the language. Mingyi Zhao was the lead investigator. All authors approved the final manuscript as submitted and are accountable for all aspects of the work. Mengling Yang, Yinmiao Dong, and Qingnan He contributed equally to this article.

Acknowledgments

This research was funded by the National Key Research and Development Program of China (2018YFA0108700 and 2017YFA0105602), the NSFC Projects of International

Cooperation and Exchanges (81720108004), the National Natural Science Foundation of China (81570279, 81974019, and 81970248), the Research Team Project of Natural Science Foundation of Guangdong Province of China (2017A030312007), the key program of Guangzhou science research plan (805212639211), and the Special Project of Dengfeng Program of Guangdong Provincial People's Hospital (DFJH201812 and KJ012019119).

References

- [1] J. H. Abraini, M. C. Gardette-Chauffour, E. Martinez, J. C. Rostain, and C. Lemaire, "Psychophysiological reactions in humans during an open sea dive to 500 m with a hydrogen-helium-oxygen mixture," *Journal of Applied Physiology*, vol. 76, no. 3, pp. 1113–1118, 1994.
- [2] M. Dole, F. Wilson, and W. Fife, "Hyperbaric hydrogen therapy: a possible treatment for cancer," *Science*, vol. 190, no. 4210, pp. 152–154, 1975.
- [3] I. Ohsawa, M. Ishikawa, K. Takahashi et al., "Hydrogen acts as a therapeutic antioxidant by selectively reducing cytotoxic oxygen radicals," *Nature Medicine*, vol. 13, no. 6, pp. 688–694, 2007.
- [4] M. Chen, J. Zhang, Y. Chen et al., "Hydrogen protects lung from hypoxia/re-oxygenation injury by reducing hydroxyl radical production and inhibiting inflammatory responses," *Scientific Reports*, vol. 8, no. 1, p. 8004, 2018.
- [5] Y. Bi, Y. Zhu, M. Zhang et al., "Effect of shikonin on spinal cord injury in rats via regulation of HMGB1/TLR4/NF- κ B signaling pathway," *Cellular Physiology and Biochemistry*, vol. 43, no. 2, pp. 481–491, 2017.
- [6] Y. Gao, H. Yang, Y. Fan, L. Li, J. Fang, and W. Yang, "Hydrogen-rich saline attenuates cardiac and hepatic injury in doxorubicin rat model by inhibiting inflammation and apoptosis," *Mediators of Inflammation*, vol. 2016, Article ID 1320365, 10 pages, 2016.
- [7] C. Liu, R. Kurokawa, M. Fujino, S. Hirano, B. Sato, and X. K. Li, "Estimation of the hydrogen concentration in rat tissue using an airtight tube following the administration of hydrogen via various routes," *Scientific Reports*, vol. 4, no. 1, article 5485, 2015.
- [8] W. Liu, L. P. Shan, X. S. Dong, X. W. Liu, T. Ma, and Z. Liu, "Combined early fluid resuscitation and hydrogen inhalation attenuates lung and intestine injury," *World Journal of Gastroenterology*, vol. 19, no. 4, pp. 492–502, 2013.
- [9] Y. Yu, Y. Yang, M. Yang, C. Wang, K. Xie, and Y. Yu, "Hydrogen gas reduces HMGB1 release in lung tissues of septic mice in an Nrf2/HO-1-dependent pathway," *International Immunopharmacology*, vol. 69, pp. 11–18, 2019.
- [10] Y. Tanaka, N. Shigemura, T. Kawamura et al., "Profiling molecular changes induced by hydrogen treatment of lung allografts prior to procurement," *Biochemical and Biophysical Research Communications*, vol. 425, no. 4, pp. 873–879, 2012.
- [11] C. S. Huang, T. Kawamura, S. Lee et al., "Hydrogen inhalation ameliorates ventilator-induced lung injury," *Critical Care*, vol. 14, no. 6, article R234, 2010.
- [12] A. Manaenko, T. Lekic, Q. Ma, J. H. Zhang, and J. Tang, "Hydrogen inhalation ameliorated mast cell-mediated brain injury after intracerebral hemorrhage in mice," *Critical Care Medicine*, vol. 41, no. 5, pp. 1266–1275, 2013.

- [13] D. Schmit, D. D. le, S. Heck et al., "Allergic airway inflammation induces migration of mast cell populations into the mouse airway," *Cell and Tissue Research*, vol. 369, no. 2, pp. 331–340, 2017.
- [14] T. Kajisa, T. Yamaguchi, A. Hu, N. Suetake, and H. Kobayashi, "Hydrogen water ameliorates the severity of atopic dermatitis-like lesions and decreases interleukin-1 β , interleukin-33, and mast cell infiltration in NC/Nga mice," *Saudi Medical Journal*, vol. 38, no. 9, pp. 928–933, 2017.
- [15] L. Chen, C. Ma, Y. Bian et al., "Hydrogen treatment protects mice against chronic pancreatitis by restoring regulatory T cells loss," *Cellular Physiology and Biochemistry*, vol. 44, no. 5, pp. 2005–2016, 2017.
- [16] M. Hirayama, M. Ito, T. Minato, A. Yoritaka, T. W. LeBaron, and K. Ohno, "Inhalation of hydrogen gas elevates urinary 8-hydroxy-2'-deoxyguanine in Parkinson's disease," *Medical Gas Research*, vol. 8, no. 4, pp. 144–149, 2018.
- [17] S. Liu, K. Liu, Q. Sun et al., "Consumption of hydrogen water reduces paraquat-induced acute lung injury in rats," *Journal of Biomedicine & Biotechnology*, vol. 2011, Article ID 305086, 7 pages, 2011.
- [18] Y.-S. Zhao, J. R. An, S. Yang et al., "Hydrogen and oxygen mixture to improve cardiac dysfunction and myocardial pathological changes induced by intermittent hypoxia in rats," *Oxidative Medicine and Cellular Longevity*, vol. 2019, Article ID 7415212, 12 pages, 2019.
- [19] K. Ohno, M. Ito, M. Ichihara, and M. Ito, "Molecular hydrogen as an emerging therapeutic medical gas for neurodegenerative and other diseases," *Oxidative Medicine and Cellular Longevity*, vol. 2012, Article ID 353152, 11 pages, 2012.
- [20] M. Ichihara, S. Sobue, M. Ito, M. Ito, M. Hirayama, and K. Ohno, "Beneficial biological effects and the underlying mechanisms of molecular hydrogen - comprehensive review of 321 original articles," *Medical Gas Research*, vol. 5, no. 1, p. 12, 2015.
- [21] K. Iuchi, K. Nishimaki, N. Kamimura, and S. Ohta, "Molecular hydrogen suppresses free-radical-induced cell death by mitigating fatty acid peroxidation and mitochondrial dysfunction," *Canadian Journal of Physiology and Pharmacology*, vol. 97, no. 10, pp. 999–1005, 2019.
- [22] K. Kohama, H. Yamashita, M. Aoyama-Ishikawa et al., "Hydrogen inhalation protects against acute lung injury induced by hemorrhagic shock and resuscitation," *Surgery*, vol. 158, no. 2, pp. 399–407, 2015.
- [23] M. Diao, S. Zhang, L. Wu et al., "Hydrogen gas inhalation attenuates seawater instillation-induced acute lung injury via the Nrf2 pathway in rabbits," *Inflammation*, vol. 39, no. 6, pp. 2029–2039, 2016.
- [24] T. Ishibashi, "Therapeutic efficacy of molecular hydrogen: a new mechanistic insight," *Current Pharmaceutical Design*, vol. 25, no. 9, pp. 946–955, 2019.
- [25] Y. Gao, H. Yang, J. Chi et al., "Hydrogen gas attenuates myocardial ischemia reperfusion injury independent of postconditioning in rats by attenuating endoplasmic reticulum stress-induced autophagy," *Cellular Physiology and Biochemistry*, vol. 43, no. 4, pp. 1503–1514, 2017.
- [26] H. Zhong, R. Song, Q. Pang et al., "Propofol inhibits parthanatos via ROS-ER-calcium-mitochondria signal pathway in vivo and vitro," *Cell Death & Disease*, vol. 9, no. 10, pp. 932–932, 2018.
- [27] X. Chen, J. Cui, X. Zhai et al., "Inhalation of hydrogen of different concentrations ameliorates spinal cord injury in mice by protecting spinal cord neurons from apoptosis, oxidative injury and mitochondrial structure damages," *Cellular Physiology and Biochemistry*, vol. 47, no. 1, pp. 176–190, 2018.
- [28] Q. Li, P. Yu, Q. Zeng et al., "Neuroprotective effect of hydrogen-rich saline in global cerebral ischemia/reperfusion rats: up-regulated Tregs and down-regulated miR-21, miR-210 and NF- κ B expression," *Neurochemical Research*, vol. 41, no. 10, pp. 2655–2665, 2016.
- [29] X. Ma, J. Wang, J. Li et al., "Loading MiR-210 in endothelial progenitor cells derived exosomes boosts their beneficial effects on hypoxia/reoxygenation-injured human endothelial cells via protecting mitochondrial function," *Cellular Physiology and Biochemistry*, vol. 46, no. 2, pp. 664–675, 2018.
- [30] R. K. Mutharasan, V. Nagpal, Y. Ichikawa, and H. Ardehali, "MicroRNA-210 is upregulated in hypoxic cardiomyocytes through Akt- and p53-dependent pathways and exerts cytoprotective effects," *Heart and Circulatory Physiology*, vol. 301, no. 4, pp. H1519–H1530, 2011.
- [31] A. Yoritaka, M. Takanashi, M. Hirayama, T. Nakahara, S. Ohta, and N. Hattori, "Pilot study of H₂ therapy in Parkinson's disease: a randomized double-blind placebo-controlled trial," *Movement Disorders*, vol. 28, no. 6, pp. 836–839, 2013.
- [32] Y. Murakami, M. Ito, and I. Ohsawa, "Molecular hydrogen protects against oxidative stress-induced SH-SY5Y neuroblastoma cell death through the process of mitohormesis," *PLoS One*, vol. 12, no. 5, article e0176992, 2017.
- [33] J. Meng, P. Yu, H. Jiang et al., "Molecular hydrogen decelerates rheumatoid arthritis progression through inhibition of oxidative stress," *American Journal of Translational Research*, vol. 8, no. 10, pp. 4472–4477, 2016.
- [34] T. Ishibashi, "Molecular hydrogen: new antioxidant and anti-inflammatory therapy for rheumatoid arthritis and related diseases," *Current Pharmaceutical Design*, vol. 19, no. 35, pp. 6375–6381, 2013.
- [35] M. Ito, T. Ibi, K. Sahashi, M. Ichihara, M. Ito, and K. Ohno, "Open-label trial and randomized, double-blind, placebo-controlled, crossover trial of hydrogen-enriched water for mitochondrial and inflammatory myopathies," *Medical Gas Research*, vol. 1, no. 1, p. 24, 2011.
- [36] Q. Zhu, Y. Wu, Y. Li et al., "Positive effects of hydrogen-water bathing in patients of psoriasis and parapsoriasis en plaques," *Scientific Reports*, vol. 8, no. 1, pp. 8051–8051, 2018.
- [37] F. Xu, S. Yu, M. Qin et al., "Hydrogen-rich saline ameliorates allergic rhinitis by reversing the imbalance of Th1/Th2 and up-regulation of CD4+CD25+Foxp3+regulatory T cells, interleukin-10, and membrane-bound transforming growth factor- β in guinea pigs," *Inflammation*, vol. 41, no. 1, pp. 81–92, 2018.
- [38] J. Akagi, "Immunological effect of hydrogen gas-hydrogen gas improves clinical outcomes of cancer patients," *Gan to Kagaku Ryoho*, vol. 45, no. 10, pp. 1475–1478, 2018.
- [39] Y. Terasaki, I. Ohsawa, M. Terasaki et al., "Hydrogen therapy attenuates irradiation-induced lung damage by reducing oxidative stress," *American Journal of Physiology Lung Cellular and Molecular Physiology*, vol. 301, no. 4, pp. L415–L426, 2011.
- [40] L. Li, X. Li, Z. Zhang et al., "Effects of hydrogen-rich water on the PI3K/AKT signaling pathway in rats with myocardial

- ischemia-reperfusion injury,” *Current Molecular Medicine*, vol. 20, no. 5, pp. 396–406, 2020.
- [41] X. Li, L. Li, X. Liu et al., “Attenuation of cardiac ischaemia-reperfusion injury by treatment with hydrogen-rich water,” *Current Molecular Medicine*, vol. 19, no. 4, pp. 294–302, 2019.
- [42] Y. Zhang, Y. Liu, and J. Zhang, “Saturated hydrogen saline attenuates endotoxin-induced lung dysfunction,” *The Journal of Surgical Research*, vol. 198, no. 1, pp. 41–49, 2015.
- [43] D. Li and Y. Ai, “Hydrogen saline suppresses neuronal cell apoptosis and inhibits the p38 mitogen-activated protein kinase-caspase-3 signaling pathway following cerebral ischemia-reperfusion injury,” *Molecular Medicine Reports*, vol. 16, no. 4, pp. 5321–5325, 2017.
- [44] D. Wang, L. Wang, Y. Zhang, Y. Zhao, and G. Chen, “Hydrogen gas inhibits lung cancer progression through targeting SMC3,” *Biomedicine & Pharmacotherapy*, vol. 104, pp. 788–797, 2018.
- [45] Q. Li, Y. Tanaka, and N. Miwa, “Influence of hydrogen-occluding-silica on migration and apoptosis in human esophageal cells *in vitro*,” *Medical Gas Research*, vol. 7, no. 2, pp. 76–85, 2017.
- [46] X. Zhuang, Y. Yu, Y. Jiang et al., “Molecular hydrogen attenuates sepsis-induced neuroinflammation through regulation of microglia polarization through an mTOR-autophagy-dependent pathway,” *International Immunopharmacology*, vol. 81, article 106287, 2020.
- [47] P. Guan, Z. M. Sun, L. F. Luo et al., “Hydrogen protects against chronic intermittent hypoxia induced renal dysfunction by promoting autophagy and alleviating apoptosis,” *Life Sciences*, vol. 225, pp. 46–54, 2019.
- [48] J. Yuan, D. Wang, Y. Liu, X. Chen, and H. Zhang, “Effects of hydrogen rich water on the expression of Nrf 2 and the oxidative stress in rats with traumatic brain injury,” *Zhonghua wei zhong bing ji jiu yi xue*, vol. 27, no. 11, pp. 911–915, 2015.
- [49] A. Pla, M. Pascual, J. Renau-Piqueras, and C. Guerri, “TLR4 mediates the impairment of ubiquitin-proteasome and autophagy-lysosome pathways induced by ethanol treatment in brain,” *Cell Death & Disease*, vol. 5, no. 2, article e1066, 2014.
- [50] S. M. Man, R. Karki, and T.-D. Kanneganti, “Molecular mechanisms and functions of pyroptosis, inflammatory caspases and inflammasomes in infectious diseases,” *Immunological Reviews*, vol. 277, no. 1, pp. 61–75, 2017.
- [51] M. Yan, Y. Yu, X. Mao et al., “Hydrogen gas inhalation attenuates sepsis-induced liver injury in a FUNDC1-dependent manner,” *International Immunopharmacology*, vol. 71, pp. 61–67, 2019.
- [52] S. Tan, Z. Long, X. Hou et al., “H₂ protects against lipopolysaccharide-induced cardiac dysfunction via blocking TLR4-mediated cytokines expression,” *Frontiers in Pharmacology*, vol. 10, pp. 865–865, 2019.
- [53] Q. Pu, C. Gan, R. Li et al., “Atg7 deficiency intensifies inflammasome activation and pyroptosis in *Pseudomonas Sepsis*,” *Journal of immunology*, vol. 198, no. 8, pp. 3205–3213, 2017.
- [54] M. Deng, Y. Tang, W. Li et al., “The endotoxin delivery protein HMGB1 mediates caspase-11-dependent lethality in sepsis,” *Immunity*, vol. 49, no. 4, pp. 740–753.e7, 2018.
- [55] C. Li, L. Hou, D. Chen et al., “Hydrogen-rich saline attenuates isoflurane-induced caspase-3 activation and cognitive impairment via inhibition of isoflurane-induced oxidative stress, mitochondrial dysfunction, and reduction in ATP levels,” *American Journal of Translational Research*, vol. 9, no. 3, pp. 1162–1172, 2017.
- [56] C. Y. Taabazuing, M. C. Okondo, and D. A. Bachovchin, “Pyroptosis and apoptosis pathways engage in bidirectional crosstalk in monocytes and macrophages,” *Cell chemical biology*, vol. 24, no. 4, pp. 507–514.e4, 2017.
- [57] S. J. Dixon, K. M. Lemberg, M. R. Lamprecht et al., “Ferroptosis: an iron-dependent form of nonapoptotic cell death,” *Cell*, vol. 149, no. 5, pp. 1060–1072, 2012.
- [58] Y. Li, F. Chen, J. Chen et al., “Disulfiram/copper induces anti-tumor activity against both nasopharyngeal cancer cells and cancer-associated fibroblasts through ROS/MAPK and ferroptosis pathways,” *Cancers*, vol. 12, no. 1, p. 138, 2020.
- [59] F. Ye, W. Chai, M. Xie et al., “HMGB1 regulates erastin-induced ferroptosis via RAS-JNK/p38 signaling in HL-60/NRAS^{Q61L} cells,” *American Journal of Cancer Research*, vol. 9, no. 4, pp. 730–739, 2019.
- [60] O. Adedoyin, R. Boddu, A. Traylor et al., “Heme oxygenase-1 mitigates ferroptosis in renal proximal tubule cells,” *Renal Physiology*, vol. 314, no. 5, pp. F702–F714, 2018.
- [61] C. Li, X. Deng, X. Xie, Y. Liu, J. P. Friedmann Angeli, and L. Lai, “Activation of glutathione peroxidase 4 as a novel anti-inflammatory strategy,” *Frontiers in Pharmacology*, vol. 9, pp. 1120–1120, 2018.
- [62] F. A.-O. X. Rijo-Ferreira and J. S. Takahashi, “Genomics of circadian rhythms in health and disease,” *Genome Medicine*, vol. 11, no. 1, p. 82, 2019.
- [63] C. A. Thaiss, M. Levy, T. Korem et al., “Microbiota diurnal rhythmicity programs host transcriptome oscillations,” *Cell*, vol. 167, no. 6, pp. 1495–1510.e12, 2016.
- [64] A. Iida, N. Nosaka, T. Yumoto et al., “The clinical application of hydrogen as a medical treatment,” *Acta Medica Okayama*, vol. 70, no. 5, pp. 331–337, 2016.
- [65] M. Wilking, M. Ndiaye, H. Mukhtar, and N. Ahmad, “Circadian rhythm connections to oxidative stress: implications for human health,” *Antioxidants & Redox Signaling*, vol. 19, no. 2, pp. 192–208, 2013.
- [66] G. Russell, M. Rehman, L. B. TW, D. Veal, E. Adukwu, and J. Hancock, “An overview of SARS-CoV-2 (COVID-19) infection and the importance of molecular hydrogen as an adjunctive therapy,” *Reactive Oxygen Species*<https://uwe-repository.worktribe.com/output/6050001>.
- [67] W.-J. Guan, C. H. Wei, A. L. Chen et al., “Hydrogen/oxygen mixed gas inhalation improves disease severity and dyspnea in patients with Coronavirus disease 2019 in a recent multicenter, open-label clinical trial,” *Journal of Thoracic Disease*, vol. 12, no. 6, pp. 3448–3452, 2020.
- [68] F. Zhou, T. Yu, R. du et al., “Clinical course and risk factors for mortality of adult inpatients with COVID-19 in Wuhan, China: a retrospective cohort study,” *The Lancet*, vol. 395, no. 10229, pp. 1054–1062, 2020.
- [69] C. Huang, Y. Wang, X. Li et al., “Clinical features of patients infected with 2019 novel coronavirus in Wuhan, China,” *The Lancet*, vol. 395, no. 10223, pp. 497–506, 2020.
- [70] L. Gattinoni, T. Tonetti, and M. Quintel, “Regional physiology of ARDS,” *Critical Care*, vol. 21, Supplement 3, p. 312, 2017.
- [71] W. W. Dong, Y. Q. Zhang, X. Y. Zhu et al., “Protective effects of hydrogen-rich saline against lipopolysaccharide-induced alveolar epithelial-to-mesenchymal transition and pulmonary fibrosis,” *Medical Science Monitor*, vol. 23, pp. 2357–2364, 2017.

- [72] T. Wang, L. Zhao, M. Liu et al., "Oral intake of hydrogen-rich water ameliorated chlorpyrifos-induced neurotoxicity in rats," *Toxicology and Applied Pharmacology*, vol. 280, no. 1, pp. 169–176, 2014.
- [73] Y. Liu and J. Zhang, "Saturated hydrogen saline ameliorates lipopolysaccharide-induced acute lung injury by reducing excessive autophagy," *Experimental and Therapeutic Medicine*, vol. 13, no. 6, pp. 2609–2615, 2017.
- [74] X. Chen, Q. Liu, D. Wang et al., "Protective effects of hydrogen-rich saline on rats with smoke inhalation injury," *Oxidative Medicine and Cellular Longevity*, vol. 2015, Article ID 106836, 8 pages, 2015.
- [75] D. H. Moon, D. Y. Kang, S. J. Haam et al., "Hydrogen gas inhalation ameliorates lung injury after hemorrhagic shock and resuscitation," *Journal of Thoracic Disease*, vol. 11, no. 4, pp. 1519–1527, 2019.
- [76] Z. Liu, W. Geng, C. Jiang et al., "Hydrogen-rich saline inhibits tobacco smoke-induced chronic obstructive pulmonary disease by alleviating airway inflammation and mucus hypersecretion in rats," *Experimental Biology and Medicine*, vol. 242, no. 15, pp. 1534–1541, 2017.
- [77] Y. Fu, M. Ito, Y. Fujita et al., "Molecular hydrogen is protective against 6-hydroxydopamine-induced nigrostriatal degeneration in a rat model of Parkinson's disease," *Neuroscience Letters*, vol. 453, no. 2, pp. 81–85, 2009.
- [78] K. Fujita, T. Seike, N. Yutsudo et al., "Hydrogen in drinking water reduces dopaminergic neuronal loss in the 1-methyl-4-phenyl-1,2,3,6-tetrahydropyridine mouse model of Parkinson's disease," *PLoS One*, vol. 4, no. 9, p. e7247, 2009.
- [79] K. Nishimaki, T. Asada, I. Ohsawa et al., "Effects of molecular hydrogen assessed by an animal model and a randomized clinical study on mild cognitive impairment," *Current Alzheimer Research*, vol. 15, no. 5, pp. 482–492, 2018.
- [80] H. Chen, J. Guo, C. Wang et al., "Clinical characteristics and intrauterine vertical transmission potential of COVID-19 infection in nine pregnant women: a retrospective review of medical records," *The Lancet*, vol. 395, no. 10226, pp. 809–815, 2020.
- [81] H. Zhu, L. Wang, C. Fang et al., "Clinical analysis of 10 neonates born to mothers with 2019-nCoV pneumonia," *Translational Pediatrics*, vol. 9, no. 1, pp. 51–60, 2020.
- [82] K. Imai, T. Kotani, H. Tsuda et al., "Administration of molecular hydrogen during pregnancy improves behavioral abnormalities of offspring in a maternal immune activation model," *Scientific Reports*, vol. 8, no. 1, article 9221, 2018.
- [83] J. Nemeth, V. Toth-Szuki, V. Varga, V. Kovacs, G. Remzso, and F. Domoki, "Molecular hydrogen affords neuroprotection in a translational piglet model of hypoxic-ischemic encephalopathy," *Journal of Physiology and Pharmacology*, vol. 67, no. 5, pp. 677–689, 2016.
- [84] Y. Mano, T. Kotani, M. Ito et al., "Maternal molecular hydrogen administration ameliorates rat fetal hippocampal damage caused by in utero ischemia-reperfusion," *Free Radical Biology and Medicine*, vol. 69, pp. 324–330, 2014.
- [85] H. Ono, Y. Nishijima, S. Ohta et al., "Hydrogen gas inhalation treatment in acute cerebral infarction: a randomized controlled clinical study on safety and neuroprotection," *Journal of Stroke and Cerebrovascular Diseases*, vol. 26, no. 11, pp. 2587–2594, 2017.
- [86] R. Camara, N. Matei, J. Camara, B. Enkhjargal, J. Tang, and J. H. Zhang, "Hydrogen gas therapy improves survival rate and neurological deficits in subarachnoid hemorrhage rats: a pilot study," *Medical Gas Research*, vol. 9, no. 2, pp. 74–79, 2019.
- [87] K. Zhuang, Y. C. Zuo, P. Sherchan, J. K. Wang, X. X. Yan, and F. Liu, "Hydrogen inhalation attenuates oxidative stress related endothelial cells injury after subarachnoid hemorrhage in rats," *Frontiers in Neuroscience*, vol. 13, article 1441, 2020.
- [88] H. Chen, C. Zhou, K. Xie, X. Meng, Y. Wang, and Y. Yu, "Hydrogen-rich saline alleviated the hyperpathia and microglia activation via autophagy mediated inflammasome inactivation in neuropathic pain rats," *Neuroscience*, vol. 421, pp. 17–30, 2019.
- [89] L. Y. Ma, W. W. Chen, R. L. Gao et al., "China cardiovascular diseases report 2018: an updated summary," *Journal of Geriatric Cardiology*, vol. 17, no. 1, pp. 1–8, 2020.
- [90] I. Ohsawa, K. Nishimaki, K. Yamagata, M. Ishikawa, and S. Ohta, "Consumption of hydrogen water prevents atherosclerosis in apolipoprotein E knockout mice," *Biochemical and Biophysical Research Communications*, vol. 377, no. 4, pp. 1195–1198, 2008.
- [91] M. Iketani, K. Sekimoto, T. Igarashi et al., "Administration of hydrogen-rich water prevents vascular aging of the aorta in LDL receptor-deficient mice," *Scientific Reports*, vol. 8, no. 1, article 16822, 2018.
- [92] T. Sakai, B. Sato, K. Hara et al., "Consumption of water containing over 3.5 mg of dissolved hydrogen could improve vascular endothelial function," *Vascular Health and Risk Management*, vol. 10, pp. 591–597, 2014.
- [93] J. Ding, Z. Yang, H. Ma, and H. Zhang, "Mitochondrial aldehyde dehydrogenase in myocardial ischemic and ischemia-reperfusion injury," in *Aldehyde Dehydrogenases*, vol. 1193 of *Advances in Experimental Medicine and Biology*, Springer, Singapore.
- [94] L. Li, T. Liu, L. Liu et al., "Effect of hydrogen-rich water on the Nrf2/ARE signaling pathway in rats with myocardial ischemia-reperfusion injury," *Journal of Bioenergetics and Biomembranes*, vol. 51, no. 6, pp. 393–402, 2019.
- [95] Y. Zhang, Q. Sun, B. He, J. Xiao, Z. Wang, and X. Sun, "Anti-inflammatory effect of hydrogen-rich saline in a rat model of regional myocardial ischemia and reperfusion," *International Journal of Cardiology*, vol. 48, no. 1, pp. 91–95, 2011.
- [96] Q. Sun, Z. Kang, J. Cai et al., "Hydrogen-rich saline protects myocardium against ischemia/reperfusion injury in rats," *Experimental Biology and Medicine*, vol. 234, no. 10, pp. 1212–1219, 2009.
- [97] L. Qian, F. Cao, J. Cui et al., "The potential cardioprotective effects of hydrogen in irradiated mice," *Journal of Radiation Research*, vol. 51, no. 6, pp. 741–747, 2010.
- [98] H. Zheng and Y. S. Yu, "Chronic hydrogen-rich saline treatment attenuates vascular dysfunction in spontaneous hypertensive rats," *Biochemical Pharmacology*, vol. 83, no. 9, pp. 1269–1277, 2012.
- [99] Y. Wang, L. Jing, X. M. Zhao et al., "Protective effects of hydrogen-rich saline on monocrotaline-induced pulmonary hypertension in a rat model," *Respiratory Research*, vol. 12, no. 1, 2011.
- [100] K. Hayashida, M. Sano, N. Kamimura et al., "H₂Gas improves functional outcome after cardiac arrest to an extent comparable to therapeutic hypothermia in a rat model," *Journal of the American Heart Association*, vol. 1, no. 5, article e003459, 2012.

- [101] Y. Ding, H. Wang, H. Shen et al., "The clinical pathology of severe acute respiratory syndrome (SARS): a report from China," *The Journal of Pathology*, vol. 200, no. 3, pp. 282–289, 2003.
- [102] A. Badawi and S. G. Ryoo, "Prevalence of comorbidities in the Middle East respiratory syndrome coronavirus (MERS-CoV): a systematic review and meta-analysis," *International Journal of Infectious Diseases*, vol. 49, pp. 129–133, 2016.
- [103] K. J. Clerkin, J. A. Fried, J. Raikhelkar et al., "COVID-19 and Cardiovascular Disease," *Circulation*, vol. 141, no. 20, pp. 1648–1655, 2020.
- [104] E. Driggin, M. V. Madhavan, B. Bikdeli et al., "Cardiovascular Considerations for Patients, Health Care Workers, and Health Systems During the COVID-19 Pandemic," *Journal of the American College of Cardiology*, vol. 75, no. 18, pp. 2352–2371, 2020.
- [105] B. Li, J. Yang, F. Zhao et al., "Prevalence and impact of cardiovascular metabolic diseases on COVID-19 in China," *Clinical Research in Cardiology*, vol. 109, no. 5, pp. 531–538, 2020.
- [106] S. Li, M. Fujino, N. Ichimaru et al., "Molecular hydrogen protects against ischemia-reperfusion injury in a mouse fatty liver model via regulating HO-1 and Sirt1 expression," *Scientific Reports*, vol. 8, no. 1, article 14019, 2018.
- [107] H. Li, O. Chen, Z. Ye et al., "Inhalation of high concentrations of hydrogen ameliorates liver ischemia/reperfusion injury through A2A receptor mediated PI3K-Akt pathway," *Biochemical Pharmacology*, vol. 130, no. 83, pp. 83–92, 2017.
- [108] Q. Zhang, C. Piao, J. Xu et al., "Comparative study on protective effect of hydrogen rich saline and adipose-derived stem cells on hepatic ischemia-reperfusion and hepatectomy injury in swine," *Biomedicine & Pharmacotherapy*, vol. 120, article 109453, 2019.
- [109] Q. Zhang, Y. Ge, H. Li et al., "Corrigendum to "Effect of hydrogen-rich saline on apoptosis induced by hepatic ischemia reperfusion upon laparoscopic hepatectomy in miniature pigs" [Research in Veterinary Science, Volume 119, August 2018, Pages 285–291]," *Research in Veterinary Science*, vol. 126, p. 37, 2019.
- [110] G. Bai, H. Li, Y. Ge et al., "Influence of hydrogen-rich saline on hepatocyte autophagy during laparoscopic liver ischemia-reperfusion combined resection injury in miniature pigs," *Journal of Veterinary Research*, vol. 62, no. 3, pp. 395–403, 2018.
- [111] H. Li, G. Bai, Y. Ge et al., "Hydrogen-rich saline protects against small-scale liver ischemia-reperfusion injury by inhibiting endoplasmic reticulum stress," *Life Sciences*, vol. 194, pp. 7–14, 2018.
- [112] I. Tamaki, K. Hata, Y. Okamura et al., "Hydrogen flush after cold storage as a new end-ischemic ex vivo treatment for liver grafts against ischemia/reperfusion injury," *Liver Transplantation*, vol. 24, no. 11, pp. 1589–1602, 2018.
- [113] B. Gharib, S. Hanna, O. M. S. Abdallahi, H. Lepidi, B. Gardette, and M. de Reggi, "Anti-inflammatory properties of molecular hydrogen: investigation on parasite-induced liver inflammation," *Comptes Rendus de l'Académie des Sciences - Series III - Sciences de la Vie*, vol. 324, no. 8, pp. 719–724, 2001.
- [114] Q. Liu, W. F. Shen, H. Y. Sun et al., "Hydrogen-rich saline protects against liver injury in rats with obstructive jaundice," *Liver International*, vol. 30, no. 7, pp. 958–968, 2010.
- [115] Y. Dang, T. Liu, X. Mei et al., "Hyperoxygenated hydrogen-rich solution suppresses shock- and resuscitation-induced liver injury," *Journal of Surgical Research*, vol. 220, pp. 363–371, 2017.
- [116] M. Iketani, J. Ohshiro, T. Urushibara et al., "Preadministration of hydrogen-rich water protects against lipopolysaccharide-induced sepsis and attenuates liver injury," *Shock*, vol. 48, no. 1, pp. 85–93, 2017.
- [117] H. L. Hu, J. Gao, W. J. Guo, F. H. Zhou, H. Y. Liu, and C. C. Su, "Anti-injury effect of hydrogen-enriched water in a rat model of liver injury induced by aflatoxin B₁," *Acta Physiologica Sinica*, vol. 71, no. 5, pp. 725–731, 2019.
- [118] X. Wang and J. Wang, "High-content hydrogen water-induced downregulation of miR-136 alleviates non-alcoholic fatty liver disease by regulating Nrf2 via targeting MEG3," *Biological Chemistry*, vol. 399, no. 4, pp. 397–406, 2018.
- [119] D. Korovljević, V. Stajer, J. Ostojic, T. W. LeBaron, and S. M. Ostojic, "Hydrogen-rich water reduces liver fat accumulation and improves liver enzyme profiles in patients with non-alcoholic fatty liver disease: a randomized controlled pilot trial," *Clinics and Research in Hepatology and Gastroenterology*, vol. 43, no. 6, pp. 688–693, 2019.
- [120] C. Xia, W. Liu, D. Zeng, L. Zhu, X. Sun, and X. Sun, "Effect of hydrogen-rich water on oxidative stress, liver function, and viral load in patients with chronic hepatitis B," *Clinical and Translational Science*, vol. 6, no. 5, pp. 372–375, 2013.
- [121] T. Li and J. Y. L. Chiang, "Bile acid signaling in metabolic disease and drug therapy," *Pharmacological Reviews*, vol. 66, no. 4, pp. 948–983, 2014.
- [122] S. C. Harris, S. Devendran, C. Méndez-García et al., "Bile acid oxidation by Eggerthella lenta strains C592 and DSM 2243^T," *Gut Microbes*, vol. 9, no. 6, pp. 523–539, 2018.
- [123] K. Katada, T. Takagi, K. Uchiyama, and Y. Naito, "Therapeutic roles of carbon monoxide in intestinal ischemia-reperfusion injury," *Journal of Gastroenterology and Hepatology*, vol. 30, pp. 46–52, 2015.
- [124] W. Yao, X. Lin, X. Han et al., "MicroRNA files in the prevention of intestinal ischemia/reperfusion injury by hydrogen rich saline," *Bioscience Reports*, vol. 40, no. 1, 2020.
- [125] H. Chen, Y. P. Sun, P. F. Hu et al., "The effects of hydrogen-rich saline on the contractile and structural changes of intestine induced by ischemia-reperfusion in rats," *Journal of Surgical Research*, vol. 167, no. 2, pp. 316–322, 2011.
- [126] T. Shigeta, S. Sakamoto, X. K. Li et al., "Luminal injection of hydrogen-rich solution attenuates intestinal ischemia-reperfusion injury in rats," *Transplantation*, vol. 99, no. 3, pp. 500–507, 2015.
- [127] S. Eryilmaz, Z. Turkyilmaz, R. Karabulut et al., "The effects of hydrogen-rich saline solution on intestinal anastomosis performed after intestinal ischemia reperfusion injury," *Journal of Pediatric Surgery*, 2020.
- [128] Y. Higashimura, Y. Baba, R. Inoue et al., "Effects of molecular hydrogen-dissolved alkaline electrolyzed water on intestinal environment in mice," *Medical Gas Research*, vol. 8, no. 1, pp. 6–11, 2018.
- [129] M. Ikeda, K. Shimizu, H. Ogura et al., "Hydrogen-rich saline regulates intestinal barrier dysfunction, dysbiosis, and bacterial translocation in a murine model of sepsis," *Shock*, vol. 50, no. 6, pp. 640–647, 2018.
- [130] Y. Yu, Y. Yang, Y. Bian et al., "Hydrogen gas protects against intestinal injury in wild type but not NRF2 knockout mice

- with severe sepsis by regulating HO-1 and HMGB1 release," *Shock*, vol. 48, no. 3, pp. 364–370, 2017.
- [131] J. Akagi and H. Baba, "Hydrogen gas restores exhausted CD8 + T cells in patients with advanced colorectal cancer to improve prognosis," *Oncology Reports*, vol. 41, no. 1, pp. 301–311, 2019.
- [132] G. Wang, J. Romero-Gallo, S. L. Benoit et al., "Hydrogen metabolism in *Helicobacter pylori* Plays a role in gastric carcinogenesis through facilitating CagA translocation," *mBio*, vol. 7, no. 4, 2016.
- [133] X. Liu, Z. Chen, N. Mao, and Y. Xie, "The protective of hydrogen on stress-induced gastric ulceration," *International Immunopharmacology*, vol. 13, no. 2, pp. 197–203, 2012.
- [134] J.-Y. Zhang, Q. F. Wu, Y. Wan et al., "Protective role of hydrogen-rich water on aspirin-induced gastric mucosal damage in rats," *World Journal of Gastroenterology*, vol. 20, no. 6, pp. 1614–1622, 2014.
- [135] S. Franceschelli, D. M. P. Gatta, M. Pesce et al., "Modulation of the oxidative plasmatic state in gastroesophageal reflux disease with the addition of rich water molecular hydrogen: a new biological vision," *Journal of Cellular and Molecular Medicine*, vol. 22, no. 5, pp. 2750–2759, 2018.
- [136] Q. Shi, C. Chen, W. H. Deng et al., "Hydrogen-rich saline attenuates acute hepatic injury in acute necrotizing pancreatitis by inhibiting inflammation and apoptosis, involving JNK and p38 mitogen-activated protein kinase-dependent reactive oxygen species," *Pancreas*, vol. 45, no. 10, pp. 1424–1431, 2016.
- [137] Y. Yang, P. Y. Liu, W. Bao, S. J. Chen, F. S. Wu, and P. Y. Zhu, "Hydrogen inhibits endometrial cancer growth via a ROS/NLRP3/caspase-1/GSDMD-mediated pyroptotic pathway," *BMC Cancer*, vol. 20, no. 1, p. 28, 2020.
- [138] Y. He, J. Z. Shi, R. J. Zhang et al., "Effects of hydrogen gas inhalation on endometriosis in rats," *Reproductive Sciences*, vol. 24, no. 2, pp. 324–331, 2016.
- [139] N. Gokalp, A. C. Basaklar, K. Sonmez et al., "Protective effect of hydrogen rich saline solution on experimental ovarian ischemia reperfusion model in rats," *Journal of Pediatric Surgery*, vol. 52, no. 3, pp. 492–497, 2017.
- [140] X. Meng, H. Chen, G. Wang, Y. Yu, and K. Xie, "Hydrogen-rich saline attenuates chemotherapy-induced ovarian injury via regulation of oxidative stress," *Experimental and Therapeutic Medicine*, vol. 10, no. 6, pp. 2277–2282, 2015.
- [141] X. He, S. Y. Wang, C. H. Yin, T. Wang, C. W. Jia, and Y. M. Ma, "Hydrogen-rich water exerting a protective effect on ovarian reserve function in a mouse model of immune premature ovarian failure induced by zona pellucida 3," *Chinese Medical Journal*, vol. 129, no. 19, pp. 2331–2337, 2016.
- [142] L. Ge, L. H. Wei, C. Q. du et al., "Hydrogen-rich saline attenuates spinal cord hemisection-induced testicular injury in rats," *Oncotarget*, vol. 8, no. 26, pp. 42314–42331, 2017.
- [143] Z. Jiang, B. Xu, M. Yang, Z. Li, Y. Zhang, and D. Jiang, "Protection by hydrogen against gamma ray-induced testicular damage in rats," *Basic & Clinical Pharmacology & Toxicology*, vol. 112, no. 3, pp. 186–191, 2013.
- [144] J. Y. Ku, M. J. Park, H. J. Park, N. C. Park, and B. S. Joo, "Combination of Korean red ginseng extract and hydrogen-rich water improves spermatogenesis and sperm motility in male mice," *Chinese Journal of Integrative Medicine*, vol. 26, no. 5, pp. 361–369, 2020.
- [145] R. Begum, J. Bajgai, A. Fadriquel, C. S. Kim, S. K. Kim, and K. J. Lee, "Molecular hydrogen may enhance the production of testosterone hormone in male infertility through hormone signal modulation and redox balance," *Medical Hypotheses*, vol. 121, pp. 6–9, 2018.
- [146] J. Guo, D. Zhao, X. Lei et al., "Protective effects of hydrogen against low-dose long-term radiation-induced damage to the behavioral performances, hematopoietic system, genital system, and splenic lymphocytes in mice," *Oxidative Medicine and Cellular Longevity*, vol. 2016, Article ID 1947819, 15 pages, 2016.
- [147] S. Wu, Z. Fang, and S. Zhou, "Saturated hydrogen alleviates CCl4-induced acute kidney injury via JAK2/STAT3/p65 signaling," *The Journal of International Medical Research*, vol. 48, no. 1, 2020.
- [148] W. Yao, A. Guo, X. Han et al., "Aerosol inhalation of a hydrogen-rich solution restored septic renal function," *Aging*, vol. 11, no. 24, pp. 12097–12113, 2019.
- [149] J. Chen, H. Zhang, J. Hu et al., "Hydrogen-rich saline alleviates kidney fibrosis following AKI and retains klotho expression," *Frontiers in Pharmacology*, vol. 8, p. 499, 2017.
- [150] H. Du, M. Sheng, L. Wu et al., "Hydrogen-rich saline attenuates acute kidney injury after liver transplantation via activating p53-mediated autophagy," *Transplantation*, vol. 100, no. 3, pp. 563–570, 2016.
- [151] S. X. Guo, Q. Fang, C. G. You et al., "Effects of hydrogen-rich saline on early acute kidney injury in severely burned rats by suppressing oxidative stress induced apoptosis and inflammation," *Journal of Translational Medicine*, vol. 13, no. 1, p. 183, 2015.
- [152] Q. Shi, K. S. Liao, K. L. Zhao et al., "Hydrogen-Rich Saline Attenuates Acute Renal Injury in Sodium Taurocholate-Induced Severe Acute Pancreatitis by Inhibiting ROS and NF- κ B Pathway," *Mediators of Inflammation*, vol. 2015, Article ID 685043, 13 pages, 2015.
- [153] Y. Lu, C.-F. Li, N.-N. Ping et al., "Hydrogen-rich water alleviates cyclosporine A-induced nephrotoxicity via the Keap1/Nrf2 signaling pathway," *Journal of Biochemical and Molecular Toxicology*, vol. 34, no. 5, article e22467, 2020.
- [154] Z. Xing, W. Pan, J. Zhang et al., "Hydrogen rich water attenuates renal injury and fibrosis by regulation transforming growth factor- β induced Sirt1," *Biological & Pharmaceutical Bulletin*, vol. 40, no. 5, pp. 610–615, 2017.
- [155] J. Li, Z. Hong, H. Liu et al., "Hydrogen-rich saline promotes the recovery of renal function after ischemia/reperfusion injury in rats via anti-apoptosis and anti-inflammation," *Frontiers in Pharmacology*, vol. 7, p. 106, 2016.
- [156] N. Miyazaki, O. Yamaguchi, M. Nomiya, K. Aikawa, and J. Kimura, "Preventive effect of hydrogen water on the development of detrusor overactivity in a rat model of bladder outlet obstruction," *The Journal of Urology*, vol. 195, no. 3, pp. 780–787, 2016.
- [157] X. Qiu, Q. Ye, M. Sun, L. Wang, Y. Tan, and G. Wu, "Saturated hydrogen improves lipid metabolism disorders and dysbacteriosis induced by a high-fat diet," *Experimental Biology and Medicine*, vol. 245, no. 6, pp. 512–521, 2020.
- [158] X. Zhang, J. Liu, K. Jin et al., "Subcutaneous injection of hydrogen gas is a novel effective treatment for type 2 diabetes," *Journal of Diabetes Investigation*, vol. 9, no. 1, pp. 83–90, 2018.
- [159] L. Zhao, Y. Wang, G. Zhang, T. Zhang, J. Lou, and J. Liu, "L-Arabinose elicits gut-derived hydrogen production and

- ameliorates metabolic syndrome in C57BL/6J mice on high-fat-diet,” *Nutrients*, vol. 11, no. 12, p. 3054, 2019.
- [160] A. Tamasawa, K. Mochizuki, N. Hariya et al., “Hydrogen gas production is associated with reduced interleukin-1 β mRNA in peripheral blood after a single dose of acarbose in Japanese type 2 diabetic patients,” *European Journal of Pharmacology*, vol. 762, pp. 96–101, 2015.
- [161] N. Kamimura, K. Nishimaki, I. Ohsawa, and S. Ohta, “Molecular hydrogen improves obesity and diabetes by inducing hepatic FGF21 and stimulating energy metabolism in db/db mice,” *Obesity*, vol. 19, no. 7, pp. 1396–1403, 2011.
- [162] Y. Niu, Q. Nie, L. Dong et al., “Hydrogen attenuates allergic inflammation by reversing energy metabolic pathway switch,” *Scientific Reports*, vol. 10, no. 1, article 1962, 2020.
- [163] K. Aoki, A. Nakao, T. Adachi, Y. Matsui, and S. Miyakawa, “Pilot study: effects of drinking hydrogen-rich water on muscle fatigue caused by acute exercise in elite athletes,” *Medical Gas Research*, vol. 2, no. 1, p. 12, 2012.
- [164] M. Yamazaki, K. Kusano, T. Ishibashi, M. Kiuchi, and K. Koyama, “Intravenous infusion of H₂-saline suppresses oxidative stress and elevates antioxidant potential in thoroughbred horses after racing exercise,” *Scientific Reports*, vol. 5, no. 1, article 15514, 2015.
- [165] T. Kawamura, K. Suzuki, M. Takahashi et al., “Involvement of neutrophil dynamics and function in exercise-induced muscle damage and delayed-onset muscle soreness: effect of hydrogen bath,” *Antioxidants*, vol. 7, no. 10, p. 127, 2018.
- [166] M. Watanabe, N. Kamimura, K. Iuchi et al., “Protective effect of hydrogen gas inhalation on muscular damage using a mouse hindlimb ischemia-reperfusion injury model,” *Plastic and Reconstructive Surgery*, vol. 140, no. 6, pp. 1195–1206, 2017.
- [167] S. Hasegawa, M. Ito, M. Fukami, M. Hashimoto, M. Hirayama, and K. Ohno, “Molecular hydrogen alleviates motor deficits and muscle degeneration in mdx mice,” *Redox Report*, vol. 22, no. 1, pp. 26–34, 2016.
- [168] S. Watanabe, M. Fujita, M. Ishihara et al., “Protective effect of inhalation of hydrogen gas on radiation-induced dermatitis and skin injury in rats,” *Journal of Radiation Research*, vol. 55, no. 6, pp. 1107–1113, 2014.
- [169] W. Fang, G. Wang, L. Tang et al., “Hydrogen gas inhalation protects against cutaneous ischaemia/reperfusion injury in a mouse model of pressure ulcer,” *Journal of Cellular and Molecular Medicine*, vol. 22, no. 9, pp. 4243–4252, 2018.
- [170] T. Ishibashi, M. Ichikawa, B. Sato et al., “Improvement of psoriasis-associated arthritis and skin lesions by treatment with molecular hydrogen: a report of three cases,” *Molecular Medicine Reports*, vol. 12, no. 2, pp. 2757–2764, 2015.
- [171] T. Kurioka, T. Matsunobu, Y. Satoh, K. Niwa, and A. Shiotani, “Inhaled hydrogen gas therapy for prevention of noise-induced hearing loss through reducing reactive oxygen species,” *Neuroscience Research*, vol. 89, pp. 69–74, 2014.
- [172] C. Cejka, J. Kossl, B. Hermankova, V. Holan, and J. Cejkova, “Molecular hydrogen effectively heals alkali-injured cornea via suppression of oxidative stress,” *Oxidative Medicine and Cellular Longevity*, vol. 2017, Article ID 8906027, 12 pages, 2017.
- [173] J. G. Lehman, R. D. Causey, C. V. LaGrasta, and A. L. Ruff, “High throughput siRNA screening for chloropicrin and hydrogen fluoride-induced cornea epithelial cell injury,” *Journal of Visualized Experiments*, no. 136, 2018.
- [174] C. Cejka, J. Kossl, B. Hermankova et al., “Therapeutic effect of molecular hydrogen in corneal UVB-induced oxidative stress and corneal photodamage,” *Scientific Reports*, vol. 7, no. 1, article 18017, 2017.
- [175] M. Y. Liu, F. Xie, Y. Zhang et al., “Molecular hydrogen suppresses glioblastoma growth via inducing the glioma stem-like cell differentiation,” *Stem Cell Research & Therapy*, vol. 10, no. 1, p. 145, 2019.
- [176] Y. Jiang, G. Liu, L. Zhang et al., “Therapeutic efficacy of hydrogen-rich saline alone and in combination with PI3K inhibitor in non-small cell lung cancer,” *Molecular Medicine Reports*, vol. 18, no. 2, pp. 2182–2190, 2018.
- [177] J. Chen, F. Mu, T. Lu, Y. Ma, D. du, and K. Xu, “A gallbladder carcinoma patient with pseudo-progressive remission after hydrogen inhalation,” *Oncotargets and Therapy*, vol. 12, pp. 8645–8651, 2019.
- [178] J. Chen, F. Mu, T. Lu, D. du, and K. Xu, “Brain metastases completely disappear in non-small cell lung cancer using hydrogen gas inhalation: a case report,” *Oncotargets and Therapy*, vol. 12, pp. 11145–11151, 2019.
- [179] N. Nakashima-Kamimura, T. Mori, I. Ohsawa, S. Asoh, and S. Ohta, “Molecular hydrogen alleviates nephrotoxicity induced by an anti-cancer drug cisplatin without compromising anti-tumor activity in mice,” *Cancer Chemotherapy and Pharmacology*, vol. 64, no. 4, pp. 753–761, 2009.
- [180] K. Mei, S. Zhao, L. Qian, B. Li, J. Ni, and J. Cai, “Hydrogen protects rats from dermatitis caused by local radiation,” *The Journal of Dermatological Treatment*, vol. 25, no. 2, pp. 182–188, 2013.
- [181] Z. Xu, L. Shi, Y. Wang et al., “Pathological findings of COVID-19 associated with acute respiratory distress syndrome,” *The Lancet Respiratory Medicine*, vol. 8, no. 4, pp. 420–422, 2020.
- [182] W. J. Guan, R. C. Chen, and N. S. Zhong, “Strategies for the prevention and management of coronavirus disease 2019,” *European Respiratory Journal*, vol. 55, no. 4, article 2000597, 2020.

Research Article

Blueberry Extracts as a Novel Approach to Prevent Ozone-Induced Cutaneous Inflammasome Activation

Erika Pambianchi,¹ Francesca Ferrara,^{1,2} Alessandra Pecorelli,¹ Brittany Woodby,¹ Mary Grace,³ Jean-Philippe Therrien,⁴ Mary Ann Lila ,³ and Giuseppe Valacchi ^{1,2,5}

¹Plants for Human Health Institute, Animal Sciences Dept., NC Research Campus Kannapolis, NC State University, 28081, NC, USA

²Department of Biomedical and Specialist Surgical Sciences, University of Ferrara, Ferrara, Italy

³Plants for Human Health Institute, Food Bioprocessing & Nutrition Sciences Dept., NC Research Campus Kannapolis, NC State University, 28081, NC, USA

⁴JP Therrien Consulting LLC, NC, USA

⁵Department of Food and Nutrition, Kyung Hee University, Seoul, Republic of Korea

Correspondence should be addressed to Giuseppe Valacchi; giuseppe.valacchi@unife.it

Received 8 April 2020; Revised 24 June 2020; Accepted 21 July 2020; Published 14 August 2020

Academic Editor: Luciano Saso

Copyright © 2020 Erika Pambianchi et al. This is an open access article distributed under the Creative Commons Attribution License, which permits unrestricted use, distribution, and reproduction in any medium, provided the original work is properly cited.

The World Health Organization estimates that 7 million people die every year due to pollution exposure. Among the different pollutants to which living organisms are exposed, ozone (O₃) represents one of the most toxic, because its location which is the skin is one of the direct tissues exposed to the outdoor environment. Chronic exposure to outdoor stressors can alter cutaneous redox state resulting in the activation of inflammatory pathways. Recently, a new player in the inflammation mechanism was discovered: the multiprotein complex NLRP1 inflammasome, which has been shown to be also expressed in the skin. The topical application of natural compounds has been studied for the last 40 years as a possible approach to prevent and eventually cure skin conditions. Recently, the possibility to use blueberry (BB) extract to prevent pollution-induced skin toxicity has been of great interest in the cosmeceutical industry. In the present study, we analyzed the cutaneous protective effect of BB extract in several skin models (2D, 3D, and human skin explants). Specifically, we observed that in the different skin models used, BB extracts were able to enhance keratinocyte wound closure and normalize proliferation and migration responses previously altered by O₃. In addition, pretreatment with BB extracts was able to prevent ozone-induced ROS production and inflammasome activation measured as NLRP1-ASC scaffold formation and also prevent the transcripts of key inflammasome players such as CASP1 and IL-18, suggesting that this approach as a possible new technology to prevent cutaneous pollution damage. Our data support the hypothesis that BB extracts can effectively reduce skin inflammation and be a possible new technology against cutaneous pollution-induced damage.

1. Introduction

The last estimates of the World Health Organization (WHO) state that 9 out of 10 people living in urban areas are exposed to pollution levels above the healthy recommendations, leading to around 7 million deaths per year [1].

Pollution is a term used to describe a wide array of pollutants (ozone, diesel fuel exhaust, cigarette smoke, and heavy metals) to which living organisms are exposed, and among them, tropospheric ozone (O₃) is one of the most toxic [2].

O₃ concentrations can vary depending on altitude, seasonality, and the geographical location of the area (rural or urban); in some of the most polluted cities, O₃ concentration can reach concentration between 0.5 ppm and 0.8 ppm [2–4].

O₃ is a secondary pollutant because its formation is due to the interaction between the hydrocarbons and oxides of nitrogen released from car exhaust and sunlight (UV), leading to photochemical smog [2]. The effects of O₃ exposure on target organs such as the respiratory tract have been investigated over the last 3 decades, and a strong correlation was

clearly revealed between the development of respiratory conditions and ozone exposure. On the other hand, the effects that O₃ has on the skin have been studied only recently [5–8] suggesting a link between the development of skin conditions and ozone exposure [2, 9–11]. Although O₃ is not a radical per se, it is very reactive and its ability to induce tissue damage is mainly associated with its interaction with the cutaneous lipids present in the stratum corneum (SC), generating molecules such as hydrogen peroxide (H₂O₂) and lipid peroxidation products (4-hydroxynonenal (4HNE)) that can trigger an inflammatory response [12–16].

Recently, a new protein complex, the inflammasome, has been shown to be involved in several inflammatory tissue responses. It can be activated by a wide array of stimuli, such as pathogen and danger-associated molecular patterns (PAMPs and DAMPs), ionic flux, lysosomal damage, mitochondrial dysfunction, and the production of reactive oxygen species (ROS) [17].

Different inflammasomes have been so far identified (NLRP1, NLRP3, NLRC4, and AIM2); they are all multimeric protein complex part of the innate immune system and which rely on pattern recognition receptors (PPRs) to sense extracellular stimuli and a variety of stress factors [17, 18]. In particular, stimulation of inflammasomes NLRP1 and NLRP3 leads to the assembly of the components of this receptor (NOD-like sensor receptor (NLRs), apoptosis-associated speck-like adaptor protein (ASC), and procaspase 1) yielding to caspase 1-mediated activation which induces the secretion of proinflammatory cytokines such as IL-18 and IL-1 β [17]. Chronic activation of the inflammasome has been correlated with the development of different conditions: atherosclerosis, autoinflammatory disease, Parkinson's and Alzheimer's disease [19–24], and recently also with skin diseases such as vitiligo, atopic dermatitis, acne, melanoma, pigmentation, and psoriasis [25–27].

Previous studies provided evidences that the NLRP1 (rather than the NLRP3) inflammasome is involved in epidermis inflammation [28, 29]. Canonical activation of the inflammasome requires the oligomerization of 3 different proteins: sensor receptor NLRP1, the speck-like receptor ASC, and procaspase 1. Once these interactions are established, the autocatalysis of the procaspase 1 in active caspase 1 induces the cleavage of the inactive zymogens pro-IL-18 and pro-IL-1 β into their active forms [17]. Our previous work unveiled the ability of ozone (ranging from 0.4 to 0.5 ppm) to activate cutaneous NLRP1 inflammasome [30].

Cells are able to quench, to a certain extent, the production of ROS via endogenous antioxidant enzymes (glutathione peroxidase, catalase, and superoxide dismutase, including the thioredoxin and peroxiredoxin systems) [31–33]; nevertheless, this defensive system can be insufficient when the exposure to oxidative stimuli is particularly intense or long lasting, as can be the case when living in polluted environments [31, 34].

The use of topical interventions to improve skin defense against the outdoor environment has been studied for many years [15, 16, 35, 36]. Interventional studies indicate that it is possible to delay extrinsic skin aging and cutaneous damage and to improve skin conditions through the administration of specific natural compounds [37, 38] such as vitamin C

and vitamin E (tocopherols) [14–16, 39–41], but more research needs to be done in providing more efficient compounds or even possibly mixture combining several natural extracts to be used against pollution-induced skin damage.

In the last few years, research on health benefits associated with blueberry (BB) dietary intake has risen sharply, due to evidence supporting blueberry's beneficial properties in reducing the risk of cardiovascular disease and type 2 diabetes, improving weight maintenance, and neuroprotection and most of all due to their significant antioxidant and anti-inflammatory properties thanks to their abundant polyphenolic compounds [42–44].

Blueberries are rich in polyphenolic compounds, which are widely distributed in nature and are important for plant survival since they attract pollinators and protect the fruit itself against various abiotic and biotic stress sources [45]. The main phytochemicals present in blueberry fruit are polyphenol compounds, including anthocyanins, proanthocyanidin, flavonols, and phenolic acids. Anthocyanins represent the major group of polyphenols in BB, including monoglycosides of delphinidin, cyanidin, petunidin, peonidin, and malvidin [46]. For cultivated blueberries, anthocyanins are mostly concentrated in the blueberry skin, giving the characteristic indigo color; therefore, a small-sized blueberry would have a relatively higher skin surface (with respect to the berry volume) and consequently higher anthocyanin content compared to another bigger blueberry [47]. Wild lowbush blueberry (*Vaccinium angustifolium* Aiton), typically smaller than most cultivated blueberries, contains anthocyanins in both the skin and the flesh of the berry fruit [48, 49].

The topical application of various blueberries has been studied to reduce telangiectasias, wrinkle formation, and skin aging [50–52], and its topical and medicinal use has been recorded in the Traditional Ecological Knowledge of Native American pharmacopoeia [53]; but the potential advantageous mechanisms of topical application against pollution-induced damage have never been evaluated, especially for *Vaccinium* species.

Since ozone exposure has already been associated with the development and exacerbation of inflammatory skin diseases ([2, 54, 55]), we hypothesized that the use of blueberry (BB) extracts would be able to quench the ozone-induced activation of cutaneous inflammasome through the prevention of redox imbalance.

In the present study, we have observed that BB extract was able to prevent ozone-induced inflammasome-related genes and proteins levels and also the oligomerization of the inflammasome components. In addition, BB extract pretreatment was efficient in improving epithelial wound healing and decreasing oxidative markers related to ozone exposure.

2. Materials and Methods

2.1. Ozone Generator. O₃ was generated via electrical corona arc discharge from O₂ and combined with ambient air to flow into a plexiglass box (ECO3 model CUV-01, Italy, Model 306 Ozone Calibration Source, 2B Technologies, Ozone Solution), as previously described [56] and constantly

monitored by an ozone detector. The dose was based on our previous studies [15].

2.2. Plant Material. A uniform composite of ripe wild low-bush blueberries (*V. angustifolium*, Aiton) grown in maritime provinces of Canada (Quebec, Nova Scotia, Prince Edward Island, and New Brunswick) and the State of Maine (USA) was provided by the Wild Blueberry Association of North America (Old Town, ME, USA). Blueberries (BB) were individually quick-frozen (IQF) within hours of harvest and then stored at -70°C until they were shipped to North Carolina on dry ice, where they were then stored at -80°C . Frozen BB samples were lyophilized before extraction.

2.3. Extraction. Extraction of lyophilized BB was conducted according to our published procedures with minor modifications [57]. Ground freeze-dried BB (5 g) were placed in 50 ml centrifuge tubes embedded in ice and homogenized in 30 ml of cold extraction solvent (70% aqueous methanol, 0.5% acetic acid) using a Pro 250 homogenizer (Pro Scientific Inc. Oxford, CT, USA) for 4 min. The obtained slurry was centrifuged (Sorvall RC-6 Plus, Asheville, NC, USA) for 10 min at $3452 \times g$ force at 4°C . The supernatant was collected in a 100 ml volumetric flask. The residue was then extracted twice with same solvent, and supernatants were collected all together and brought to a final volume of 100 ml with the extraction solvent. An aliquot was evaporated to an aqueous solution and lyophilized [58].

2.4. Blueberry Extract Preparation. BB frozen extract powder was solubilized in a volume of dimethylsulfoxide (DMSO) (Thermo Fisher Scientific, USA, cat no. 20688 99.5%) needed to reach a primary concentration of 100 mg/ml (stock), aliquoted, and stored at -80°C . For each experiment, a new freshly made BB treatment was prepared in complete media from the stock, via serial dilutions: ranging from 0.1 $\mu\text{g}/\text{ml}$ to 100 $\mu\text{g}/\text{ml}$ based on the skin model utilized. The specific volumes utilized to prepare the serial dilutions of BB extract were also utilized to make the negative controls of DMSO (final concentration 0.01%) in complete media.

2.5. Keratinocytes Culture, BB Pretreatment, and Ozone Exposure. HaCaT cells (AddexBio, USA) were cultured in high-glucose (4.5%) Dulbecco's modified Eagle's medium (Corning, USA) supplemented with 10% FBS (Sigma, USA), 100 U/ml penicillin, and 100 $\mu\text{g}/\text{ml}$ streptomycin (Gibco, USA) (complete media) and grown at 37°C in 5% CO_2 and 95% air. For LDH, BrdU, and DCFDH, 10,000 cells were seeded in 96-well plate dishes (Corning, USA); 250,000 cells were seeded into 12-well plates (Corning, USA) to perform the scratch-wound assay; and 1 million cells were instead seeded in 6 cm^2 petri dishes (Corning, USA) for RT-PCRs. After 8 hours from the seeding, HaCaT were starved with high-glucose Dulbecco's modifies Eagle's medium supplemented with 1% FBS (Sigma, USA), 100 U/ml penicillin, and 100 $\mu\text{g}/\text{ml}$ streptomycin (Gibco, USA). On the second day, in the morning, the media were removed and either control medium containing the preestablished volume of DMSO (0.01%) or BB extracts were added at a dose of 10 $\mu\text{g}/\text{ml}$ and left for 24 h while cells were incubated at

37°C in 5% CO_2 and 95% air. In the third morning, the BB pretreatment media and the control media were discarded and complete media were added; then, cells were placed in a plexiglass box connected to the ozone generator and exposed to ozone for 1 h at the dose of 0.5 ppm. After the ozone exposure, samples were harvested for the biochemical and immunochemical assays.

2.6. 3D Skin Model Treatment and Ozone Exposure. 3D skin model "EpiDerm" (reconstructed human epidermis (RHE)) was purchased from MatTek corporation (EpiDerm, EPI-200). Upon arrival, the 24 inserts containing 3D skin tissues were transferred into 6-well plates prefilled with 1 ml of MatTek Assay medium (provided by MatTek corporation, USA), according to the manufacturer's instructions as previously described [59]. The plates were placed in the incubator overnight (5% CO_2 , 37°C) for recovery. On the day after, either control medium containing the preestablished volume of DMSO or BB extracts were added at the dose 100 $\mu\text{g}/\text{ml}$ and left for 24 h. On day 3, the media were discarded and complete media were added to the tissues and exposed to O_3 for 5 h at the dose 0.5 ppm. Protein and RNA were collected right after exposure (T0), 6 h (T6), and 24 h (T24) postexposure.

2.7. Human Skin Explant Treatment and Ozone Exposure. Healthy human skin was purchased from Hunstad/Kortesis/Bharti Cosmetic Surgery clinic. 12 mm punch biopsies were taken from the skin and excised using sterile scissors; subcutaneous tissue was removed with a scalpel, and the biopsies were rinsed with Phosphate-Buffered Saline (PBS) containing antibiotics/antimycotic using a sterile technique [30]. Then, the skin explants were transferred to 6-well plates and cultured in complete media, at 37°C in 5% CO_2 and 95% air. The morning after, either control medium containing the preestablished volume of DMSO or BB extracts were added at the dose of 100 $\mu\text{g}/\text{ml}$ and incubated for 24 h. On day 3, the tissues were placed in a plexiglass box connected to the ozone generator and exposed for 5 h at the dose of 0.5 ppm. Skin samples were collected, dehydrated, and embedded in paraffin to perform immunohistochemistry at 0 h, 6 h, and 24 h upon ozone exposure.

2.8. Lactate Dehydrogenase (LDH) Cytotoxicity Assay. After 24 h of BB pretreatment at the doses of 0.1, 0.5, 1, 5, and 10 $\mu\text{g}/\text{ml}$ for HaCaT and 10, 50, and 100 $\mu\text{g}/\text{ml}$ for RHE, supernatants from both the 2D and 3D models were collected, and cytotoxicity was calculated by measuring the amount of the enzyme lactate dehydrogenase (LDH) released in the cytosol, according to manufacturer's instructions (Roche, USA, cat no. 11644793001). Levels of LDH released into the media from keratinocytes and RHE were normalized to the positive control Triton X100, considered 100% LDH release [60].

2.9. Scratch Wound Healing Assay. After seeding (250,000 HaCaT cells per 12-well plate), BB pretreatment, and ozone exposure, the adherent monolayer of human keratinocytes was mechanically scratched with a sterile p200 pipette tip and cellular debris were washed off with PBS (Corning, USA). Pictures of the wound area were taken at different time

points (0 h, 18 h, and 36 h upon ozone exposure) in three different places, using AxioVision software (40x magnification). Quantification of the wound width was determined by analysis with ImageJ software (National Institutes of Health, Bethesda, MD, USA) and compared to the wound area at 0 h, arbitrarily set at 100 [61, 62].

2.10. In Vitro Cell Migration Assay. HaCaT cells were seeded in 10 cm² petri dishes and pretreated with BB at the dose 10 µg/ml for 24 h; then, the cells were detached and 50,000 cells were resuspended in serum-free media and seeded in 8 µm pore size transwells (QCMTM 24-well Colorimetric Cell Migration Assay kit, Millipore, USA) coated with 0.15 mg/ml bovine collagen IV. After 30 min, 650 µl of complete media was added at the bottom of each well, acting as a chemoattractant. Following ozone exposure (0.5 ppm for 1 h) the transwell inserts were fixed for 10 min with 70% ethanol, stained with 0.02% of Coomassie Blue for 15 min, and rinsed with double-distilled water. HaCaT cells left unmigrated in the upper part of the transwell were gently removed with a cotton swab, and pictures of 3 randomly selected fields were captured using AxioVision software (20x magnification). Automated quantification of the migrated cells was performed using ImageJ program as follows: conversion to grayscale of the image, removal of noise, and adjustment of brightness and contrast (min = 87, max = 167); then, a Phansalkar threshold and watershed were applied [62].

2.11. In Vitro Cell Proliferation Assay. Cellular proliferation in HaCaT cells was evaluated by bromodeoxyuridine (BrdU) incorporation assay (Roche, USA, cat no. 11647229001). After seeding (10,000 cells/well in 96-well plate) and upon BB pretreatment and ozone exposure, 20 µl of BrdU labeling solution/well was added to the cells and incubated for 24 h (5% CO₂, 37°C); following, the cells were dried and fixed and the cellular DNA was denatured allowing a better detection by the antibody of the already incorporated BrdU [63]. Then, as indicated by the manufacturer, the monoclonal anti-BrdU peroxidase-conjugated antibody was added to each well and incubated at room temperature for 90 min. The cells were then rinsed with PBS, and the bound peroxidase was photometrically detected after 30 min via substrate reaction and quantified by measuring the absorbance produced at 370 nm (reference wavelength 492 nm).

2.12. Dichlorofluorescein (DCF) Assay. 10,000 cells were seeded in a 96-well plate, starved overnight, and pretreated with BB 10 µg/ml for 24 h. Prior to ozone exposure, the BB pretreatment was removed and cells were washed with warm PBS. Then, 2',7' acetylated dichlorofluorescein (DCF) (Invitrogen, Thermo Fisher Scientific, USA, cat no. C2938) was resuspended in PBS to reach the concentration 10 µM and incubated with the cells, in the dark, for 30 min at 37°C, to allow the internalization of the fluorescent probe in the cells. Following, the DCF was removed and 100 µl/well of Dulbecco's modified Eagle's medium without Red Phenol (Corning) supplemented with 1% of FBS (Sigma), 100 U/ml penicillin, and 100 µg/ml streptomycin (Gibco) was added. The cells were then exposed to ozone (1 h at 0.5 ppm), and the fluores-

cence of oxidized DCF dye was evaluated 1 hour after ozone exposure as previously described [64].

2.13. ASC Oligomerization Assay. HaCaT cells (1 × 10⁶) were grown in 6 cm² petri dishes, starved overnight, and pretreated with BB 10 µg/ml for 24 h. Just prior to ozone exposure, the BB pretreatment was removed, and cells were exposed to ozone for 1 h at 0.5 ppm and collected after 0 h, 1 h, and 3 h. Cells were washed in cold PBS, gently detached with a scraper, and centrifuged for 5 min at 1500 × g. The cell pellet was resuspended in 500 µl of cold lysis buffer (containing Hepes, KOH 20 mM (pH 7.5), KCl 150 mM, NP-40 1%, 1% protease inhibitor cocktails (Sigma), and PMSF 0.1 mM). Following, cell lysates were centrifuged at 1800 × g at 4°C for 8 min, and 30 µl of the lysates was collected as input for Western blot analysis (later resuspended in 2X Laemmli buffer, 20% beta-mercaptoethanol), while the remaining volume was centrifuged again for 10 min at 5000 × g at 4°C. Upon centrifugation, to induce crosslinking of the oligomers, the lysates were resuspended in 500 µl of cold PBS containing disuccinimidyl suberate (DSS) (Thermo Fisher Scientific, USA, CAS 68528-80-3 Alfa Aesar) and incubated at RT for 30 min on a rotator. Following, the cellular samples were centrifuged for 10 min at 2500 rpm at 4°C, and the crosslinked pellets were then resuspended in 1X Laemmli buffer and 10% beta-mercaptoethanol. The input and crosslinked samples were boiled for 10 min at 95°C and then analyzed by running samples on a 4–12% SDS-PAGE gel. Bands were digitized, and densitometric analysis was performed using ImageJ software.

2.14. Immunocytochemistry. HaCaT cells were grown on coverslips (10,000 cells), starved overnight, and pretreated with BB 10 µg/ml for 24 h. Right before ozone exposure, the BB pretreatment was removed, and cells were exposed to ozone for 1 h, at 0.5 ppm, collected at the different time points, and fixed in 4% paraformaldehyde (PFA) in PBS for 30 min at 4°C. Permeabilization was performed with 0.25% Triton X100 in PBS and then blocked in PBS-BSA (Bovine Serum Albumin, Sigma) 1% at room temperature for 1 h. ASC and NLRP1 primary antibodies were then incubated overnight (ASC, cat NBP1-78977 NovusBio, USA 1:100 in 0.25% BSA/PBS and NLRP1 sc-166368 Santa Cruz, USA 1:50 in 0.25% BSA/PBS) at 4°C. The following day, the coverslips were incubated with the fluorochrome-conjugated secondary antibodies (A11004 Alexa Fluor 568, A11008 Alexa Fluor 488) for 1 h at room temperature. DAPI (D1306 Invitrogen, USA) was utilized to stain the nuclei (1 min at room temperature). Then, coverslips were mounted onto glass slides using PermaFluor Aqueous Mounting Medium (TA-006-FM Thermo Fisher Scientific) and examined using a Zeiss Z1 AxioObserver LSM10 confocal microscope equipped at 40x magnification. ASC specks were analyzed via ImageJ, and ASC speck number was correlated with the number of nuclei present in the correspondent picture.

As for the skin explants, 4 µm sections were punched and deparaffinized with the use of xylene and rehydrated in decreasing alcohol gradients. 10 mM sodium citrate buffer (AP-9003-500, Thermo Fisher Scientific) (pH 6.0) was utilized at a subboiling temperature (microwave settings

500 W, 10 min) to induce antigen retrieval and then cooled off for 20 min. Following, 2 washes \times 5 min with PBS were performed and then sections were blocked with 5% BSA in PBS at room temperature for 45 min, then incubated overnight at 4°C with primary antibodies for ASC (cat NBP1-78977 NovusBio, USA) dil. 1:100 in PBS with 2% BSA, NLRP1 (sc-166368 Santa Cruz, USA) at 1:50 dilution in 2% BSA in PBS, and 4HNE (AB5605 Millipore Corp., USA) at 1:400 dilution in 2% BSA in PBS. The following day, 3 washes with PBS of 5 min each were performed, followed by the incubation in the dark with fluorochrome-conjugated secondary antibodies (A11004 Alexa Fluor 568, A11008 Alexa Fluor 488 and A11055 Alexa Fluor 488) at 1:500 dilutions in PBS with 2% BSA for 1 h at room temperature. After 3 washes (5 min each) with PBS, the sections were mounted onto glass slides using PermaFluor mounting media (Thermo Fisher Scientific) and images were collected by a Zeiss LSM10 microscope equipped with 40x magnification.

2.15. Protein Extraction. Cell lysates were extracted in ice-cold lysis buffer containing 50 mM Tris (pH 7.5), 150 mM NaCl, 10% glycerol, 1% Nonidet P-40, 1 mM EDTA, 0.1% SDS, 5 mM nethylmaleamide (Sigma), and protease and phosphatase inhibitor cocktails (Sigma). Lysates were then centrifuged for 15 min at 4°C and 12700 rpm, supernatants were collected, and soluble protein concentration was measured via Quick Start Bradford protein method (Bio-Rad, USA). RHE were collected and harvested in Tissue Protein Extraction Reagent (T-PERTM) (Thermo Fisher Scientific) supplemented with 1% of protease and phosphatase inhibitor cocktails (Sigma, USA). Three cycles of freezing/thawing by moving from liquid nitrogen to 37°C were performed, and following, centrifugation at 12700 rpm for 15 min at 40°C was assessed. Protein content was evaluated on the RHE lysates via Bradford assay (Bio-Rad).

2.16. Western Blot Assay. 4–12% polyacrylamide SDS gels were loaded with equivalent amounts of protein (previously denatured for 10 min at 95°C), which were then separated by molecular size. The gel was electroblotted onto nitrocellulose membranes, and blocking was performed with Tris-buffered saline, pH 7.5, containing 0.5% Tween 20 and 5% nonfat milk, for 1 h at room temperature. After overnight incubation with the antibody caspase 1 (2225S cell signaling, USA) diluted 1:1000 in TBS-T with 1% nonfat milk (Bio-Rad, USA), the membranes were incubated for 1 h with the secondary antibody conjugated with horseradish peroxidase and the signal was detected by chemiluminescence (Bio-Rad, USA). Beta-actin (A3854 Sigma, USA) was used for loading control. Bands were digitalized, and densitometry analysis was evaluated via ImageJ software.

2.17. RNA Extraction and Quantitative Real-Time PCR (q-rtPCR). For HaCaT cells and RHE, total RNA extraction was performed via the Aurum Total RNA Mini Kit with DNase digestion (Bio-Rad), according to the manufacturer's protocol. Specifically, for the RHE, 700 μ l of lysis buffer provided by the kit was added and the tissues were homogenized with Precellys tissue homogenizer (9 cycles of 30 s with a 30 s

break at 8000 rpm at 4°C). The same kit was utilized to extract total RNA from HaCaT samples. cDNA was then generated from 1 μ g of total RNA, using the iScript cDNA Synthesis Kit (Bio-Rad). Evaluation of the mRNA levels of ASC, Caspase 1, and IL-18 genes was assessed via quantitative real-time PCR using SYBR® Green Master Mix (Bio-Rad) on a LightCycler® 480 Real-Time PCR System (Roche), according to the manufacturer's protocol. Gene expression was quantified via the number of cycles obtained to reach a predetermined threshold value in the intensity of the PCR signal (CT value). Beta-actin was employed as the reference gene, and the samples were compared using the relative cycle threshold (CT). After normalization, the fold change was determined using the $2^{-\Delta\Delta CT}$ method. The primers used are listed here: (β -actin forward ATTGCCGAC AGGATGCAGA/reverse AGTACTTGCCTCAGGAGGA, ASC forward ATGCGCTGGAGAACCCTGA/reverse TCT CCAGGTAGAAGCTGACCA, Caspase 1 forward CCGTTC CATGGGTGAAGGTA/reverse TGCCCCTTTCGGAATAA CGG, and IL-18 forward TGCAGTCTACACAGCTTCG/reverse ACTGGTTCAGCAGCCATCTT).

2.18. Statistical Analysis. Each of the variables tested is expressed as mean \pm standard deviation (SD) of three independent experiments.

Statistical analysis was performed via GraphPad Prism 6 software (GraphPad Software Inc., La Jolla, CA, USA). Differences between groups were evaluated by analysis of variance (ANOVA) for single time point or by two-way ANOVA when different time points were included, followed by Tukey's post hoc test. A *p* value < 0.05 was considered statistically significant.

3. Results

3.1. Cytotoxic Evaluation of Blueberry (BB) Extract in 2D and 3D Cutaneous Models. The first step of our study was the evaluation of the cytotoxicity of the BB extracts in our 2D and 3D cell culture models. Human keratinocytes and skin 3D models (RHE) were pretreated for 24 hours with different doses of BB extracts (0.1, 0.5, 1, 5, and 10 μ g/ml for the HaCaT and 10, 50, and 100 μ g/ml for the RHE), and cytosolic LDH released was evaluated in the supernatant. Our results showed that BB treatment did not affect cellular viability at all the doses tested in both the models. The average release of LDH for HaCaT cells was around 20% (Figure 1(a)) and 18% for the RHE (Figure 1(b)) with respect to the 100% cell death (Triton X100). Based on these results, we have decided to use the following doses of BB: 10 μ g/ml for HaCaT and 100 μ g/ml for RHE models.

3.2. Effect of Blueberry (BB) Extract on Ozone Modulation of Keratinocyte Migration, Proliferation, and H₂O₂ Production. In our previous study, we demonstrated that O₃ and other pollutants are able to impair the skin repair abilities [65, 66]; therefore, next, we wanted to evaluate the potential properties of BB extract in improving the wound closure impairment induced by O₃.

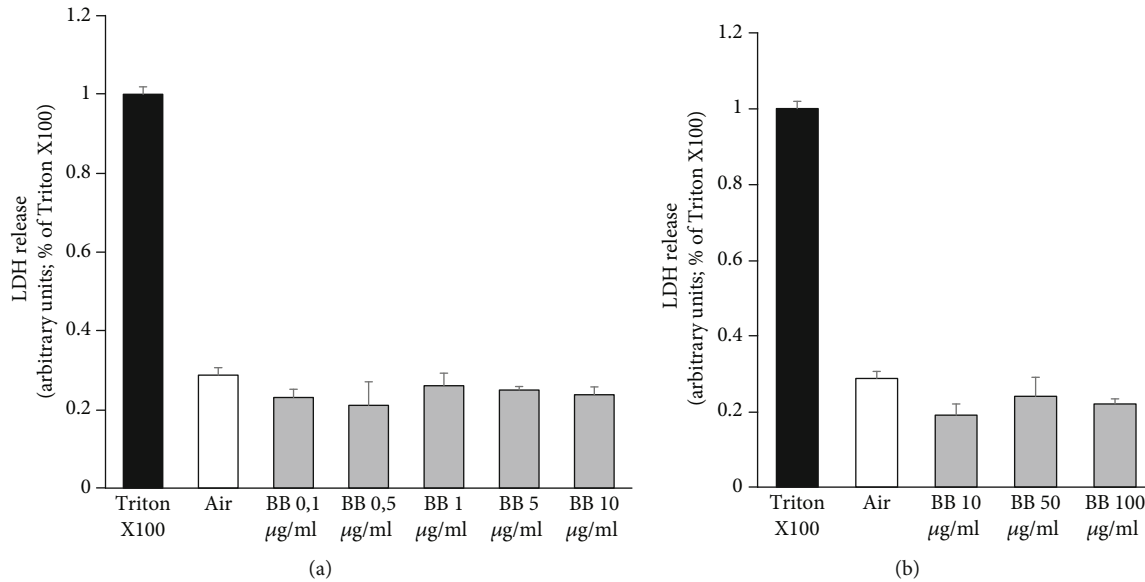


FIGURE 1: Cytotoxic evaluation of blueberry (BB) extract in 2D and 3D cutaneous models. (a) Keratinocytes cells were pretreated with different doses of BB (0.1, 0.5, 1, 5, and 10 $\mu\text{g/ml}$) for 24 h. (b) 3D models were pretreated with BB doses ranging from 10 to 100 $\mu\text{g/ml}$. Cytotoxicity was calculated into the supernatant of pretreated 2D and 3D models, by measuring the amount of LDH released from the cytosol. Data are the average \pm SD of three independent experiments.

As shown in Figure 2(a), exposure to O_3 (0.5 ppm for 1 h) significantly impairs the ability of the keratinocytes to recover the scratch wound. Indeed, after ozone exposure, at 18 h time point, the wound was still 75% open with respect to the 30% of the control. This difference was still evident after 36 h of ozone exposure, where the wound was still 35% open while the control was completely recovered. Of notice, 24 h pretreatment with BB extracts significantly improved the keratinocyte wound closure ability with 50% and 15% open wound at 18 h and 36 h, respectively.

Because the scratch-wound assay is not able to discriminate between a proliferative and migratory effect, we decided to further evaluate both of these cellular responses in our experimental conditions.

As depicted in Figure 2(b), O_3 exposure decreased by 50% the migratory property of the cells after 3 h of exposure and over 50% at 6 h time point. Also, in this case, BB extract pretreatment was able to completely abolish the effect of O_3 exposure at 3 h time point and to improve the migratory efficiency of about 50% at 6 h.

Similar response was observed also for the proliferative assay as depicted in Figure 2(c). O_3 exposure reduced HaCaT proliferation by 15%, and BB pretreatment was able to rescue this effect.

Considering the antioxidant properties of BB, we have tested whether BB were able to prevent O_3 -induced H_2O_2 formation. As shown in Figure 2(d), keratinocyte ROS production after 1 h post- O_3 exposure was 5-fold higher compared to the control, and the pretreatment with BB extracts significantly suppressed this increase (circa 25%).

3.3. Blueberry (BB) Extract Prevents O_3 -Induced Activation of Inflammasome in 2D Skin Models. Cellular proliferative and migratory alterations are phenomena that are present in sev-

eral inflammatory skin conditions [67, 68]. We have recently showed the ability of O_3 to induce inflammasome activation and oligomerization [30]; now, we wanted to assess whether BB pretreatment could prevent this effect.

As showed in Figures 3, 24 h after O_3 exposure, there was a significant increase in the transcript levels of key players in the inflammasome activation in HaCaT cells. As depicted in Figure 3(c), IL-18, which is an end product of the inflammasome activation, increased around 5-fold at 24 h time point; while Caspase 1 (Figure 3(b)) and ASC (Figure 3(a)) were already induced right after the O_3 exposure (T0) and further increased at the later time point (T24). Of note, pretreatment with BB extracts was able to prevent the induction of ASC (Figure 3(a)), Caspase 1 (Figure 3(b)), and IL-18 (Figure 3(c)) in keratinocytes.

3.4. Blueberry (BB) Extract Prevents O_3 -Induced Activation of Inflammasome in 3D Skin Models. Since Caspase 1 is the cardinal player of the inflammasome, which actively cleaved the cytokine proforms, we evaluated its transcripts and protein levels also in the 3D model (RHE) [69].

As expected, the RHE confirmed the keratinocyte results. Indeed, O_3 exposure clearly induced a remarkable increase in Caspase 1 transcripts and protein levels at the different time points analyzed (6 h for mRNA and 0 h, 6 h, and 24 h for proteins). Also, in this case, BB extract pretreatment clearly decreased the O_3 effect, especially after 24 h, with a 4.5-fold decrease in caspase 1 protein levels (Figure 4(a) and 4(b)).

3.5. Blueberry (BB) Extract Prevents O_3 -Induced Inflammasome Oligomerization in HaCaT Cells. The activation of the NLRP1 inflammasome occurs only following the oligomerization of the scaffold-forming components. To evaluate the effect of BB extract on the oligomerization and

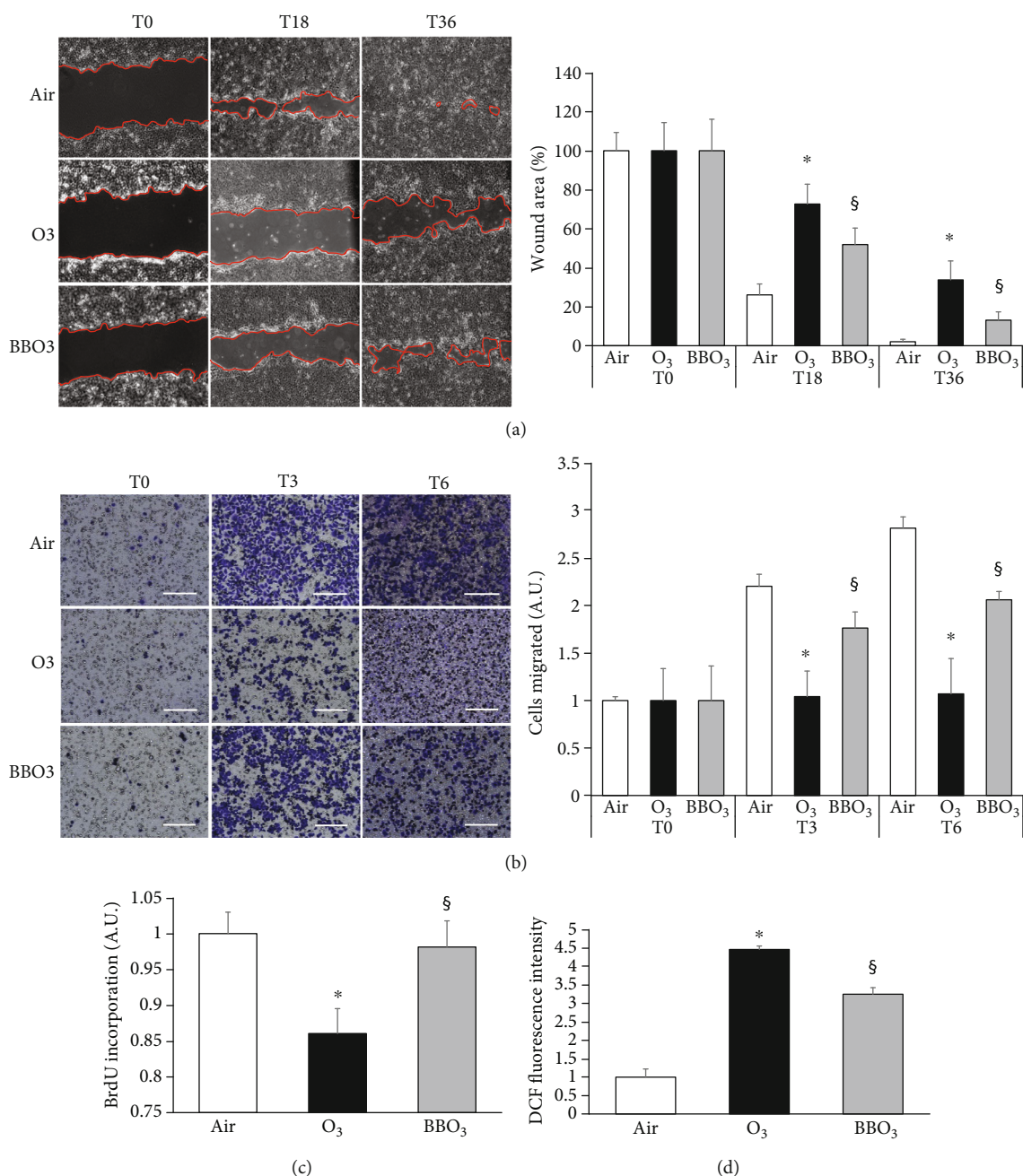


FIGURE 2: Effect of blueberry (BB) extract on ozone modulation of keratinocytes migration, proliferation, and ROS production. (a) Scratch was performed on confluent monolayer of HaCaT cells, and pictures were taken to measure wound area at different time points (0-18-36 h). On the left, depiction of the wound after 0, 18, and 36 h. On the right, quantification of the wound area at each time point via ImageJ. Data are shown as percent of 0 h. (b) Representative depiction of migration experiment performed on HaCaT cells, scale bar 200 μ m. Cells were seeded in 8 μ m pore size transwells, exposed to O₃, and incubated for 0, 3, and 6 h. After fixation, migrated cells were stained with 0.02% Coomassie Blue. On the right, ImageJ quantification of the migrated cells after 0, 3, and 6 h from O₃ exposure. Data are shown as average of 6 picture fields (20x magnification). (c) The growth response of HaCaT cells pretreated with BB was assessed after 24 h after O₃ exposure by BrdU incorporation. (d) H₂O₂ production was evaluated via DCF after 1 h upon O₃ exposure (1 h at 0.5 ppm) in HaCaT cells pretreated with BB. Data are the results of three independent experiments. * $p < 0.05$ air vs. O₃, § $p < 0.05$ O₃ vs. BBO₃ by one-way or two-way ANOVA.

inflammasome activation in keratinocytes upon O₃ exposure, we performed immunofluorescence using different dyes (green for ASC, red for NLRP1).

We observed increased perinuclear colocalization of ASC and NLRP1 upon O₃ exposure at 0 h, 3 h, and 6 h,

and the BB extract pretreatment significantly decreased the oligomerization of the scaffold (Figure 5(a)). Therefore, it is possible to hypothesize that BB extracts somehow are able to prevent the formation of ASC oligomers which is the first step for the inflammasome activation [70].

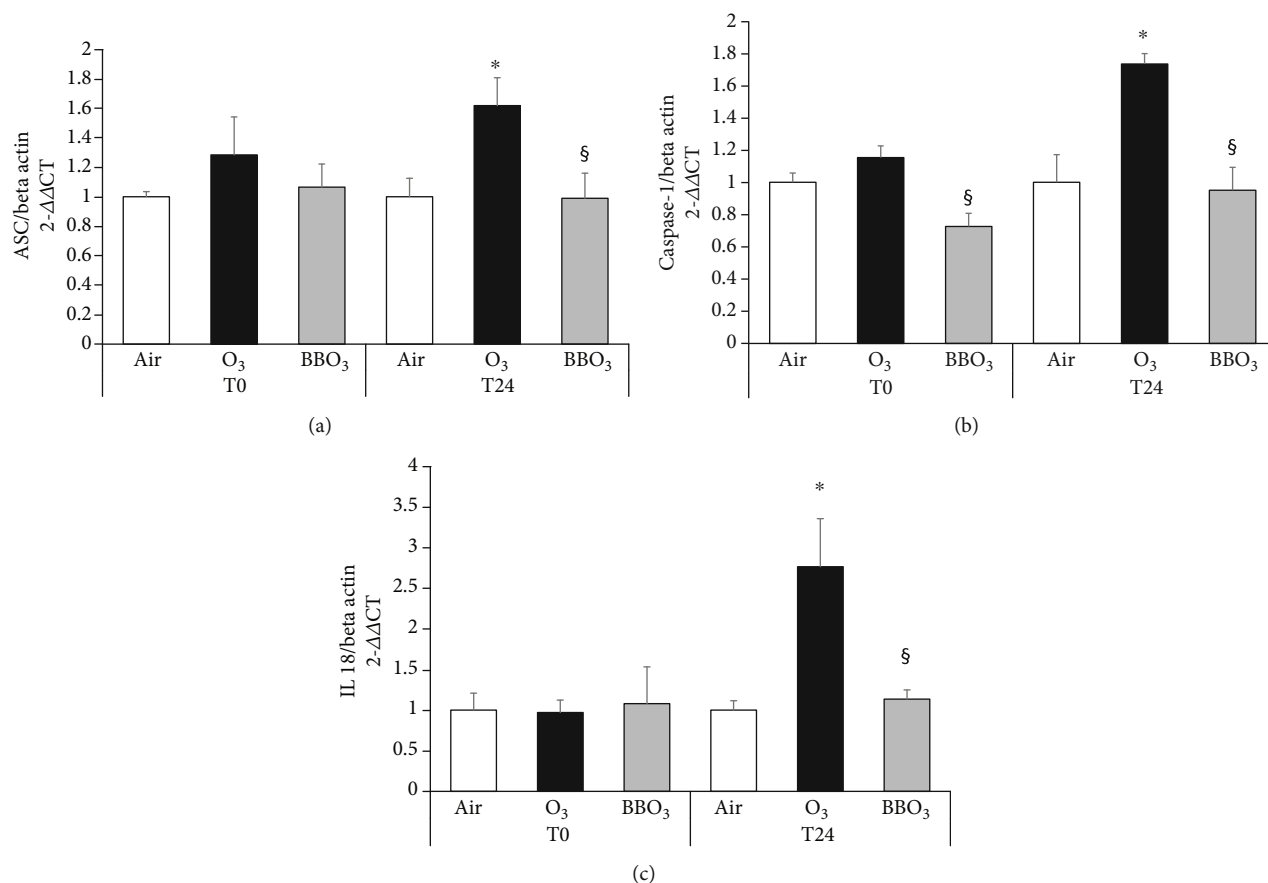


FIGURE 3: Blueberry (BB) extract prevents O₃-induced activation of inflammasome in 2D skin models. HaCaT transcript levels for (a) ASC, (b) Caspase 1, and (c) IL-18 at 0 and 24 h. Data are the results of three independent experiments. * $p < 0.05$ air vs. O₃, § $p < 0.05$ O₃ vs BBO₃ by two-way ANOVA.

ASC oligomerization assay confirmed these results as shown in Figure 5, where it is possible to appreciate an increase in ASC oligomer and dimer formation (15%) after O₃ exposure while this effect was almost completely rescued by BB extracts (Figure 5(b)).

3.6. Blueberry (BB) Extract Prevents O₃-Induced Inflammasome Activation and Oxidative Stress in Ex Vivo Human Skin Biopsies. To further validate our previous data on 2D and 3D skin models, we decided to perform our experiments on a more complete cutaneous model represented by the *ex vivo* human skin explants.

The biopsies were pretreated with 100 μg/ml of BB extracts for 24 h and exposed to 0.5 ppm of O₃ for 5 hours. As depicted in Figure 6(a); BB extract topical application was able to quench the increased protein levels of both ASC (green) and NLRP1 (red) and their nuclear colocalization 6 h after O₃ exposure.

Since redox signaling is an important part of the inflammatory pathway [71], we also evaluated the level of 4-hydroxynonenal (4HNE) as a reliable marker of oxidative damage and lipid peroxidation. As depicted in Figure 6(b), O₃ significantly increases the 4HNE levels immediately after the exposure and this effect was still visible at the later time

points. BB extract pretreatment was able to prevent the 4HNE formation.

4. Discussion

It is now well accepted and documented that exposure to environmental pollution affects our health and this phenomenon is not localized to few urban centers, but it is a global emergency that has been estimated to decrease human life span by 10-15 years [72]. There are several pollutants to which living organisms are daily exposed, and among them, O₃ has been shown to be one of the most toxic. It should be mentioned that the O₃ derived from the stratospheric-tropospheric exchanges accounts for 20% of its tropospheric level. Nowadays, ozone is mainly produced by complex photochemical reactions involving solar radiation and anthropogenic pollutants [73, 74]. Photochemical ozone is formed by reactions involving solar radiation and anthropogenic pollutants (methane, non-methane volatile organic compounds, and carbon monoxide) in the presence of nitrogen oxides while in less polluted environments, ozone is produced in the presence of sunlight (at wavelengths < 424 nm), through the photolysis of NO₂ [73].

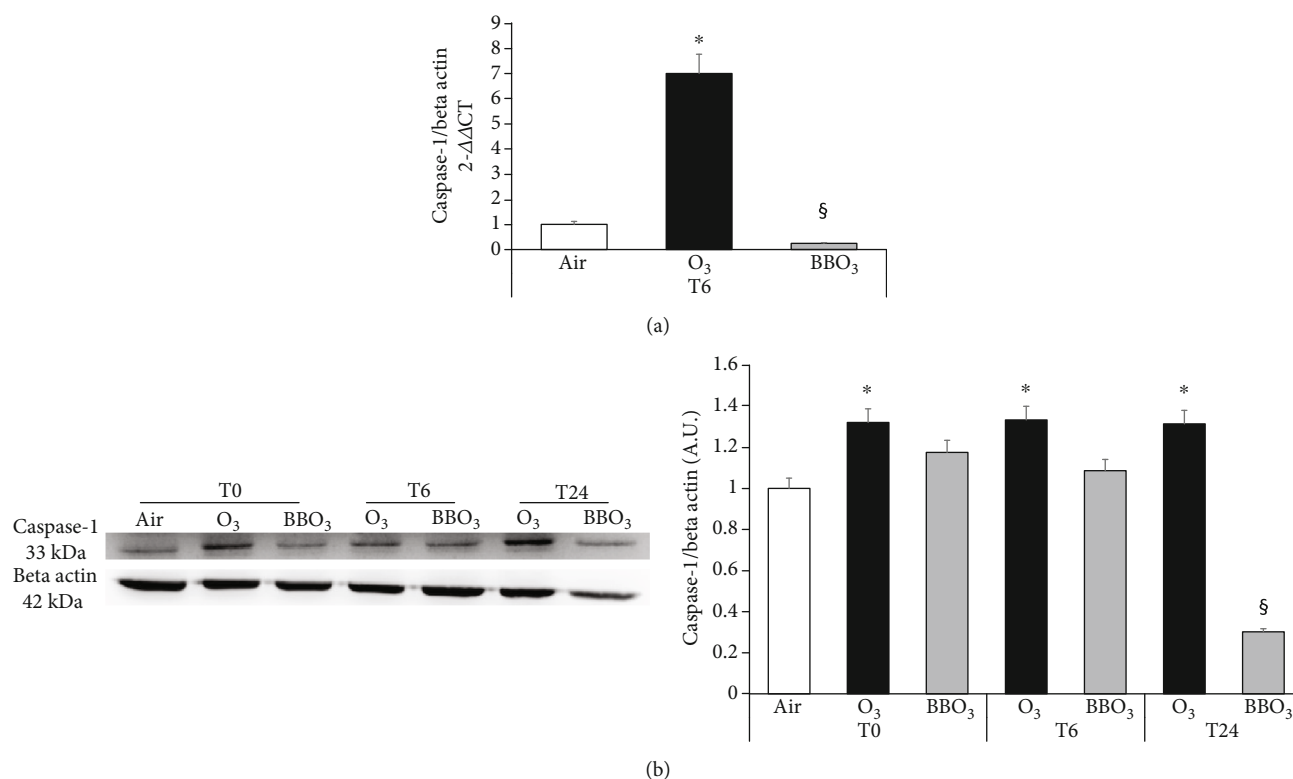


FIGURE 4: Blueberry (BB) extract prevents O₃-induced activation of inflammasome in 3D skin models. RHE transcript levels for Caspase 1 (a). Protein levels of Caspase 1 in RHE at 0, 6, and 24 h after O₃ exposure (b), on the right, relative quantification via ImageJ analysis. Data are the results of two independent experiments. * $p < 0.05$ air vs. O₃, § $p < 0.05$ O₃ vs. BBO₃ by two-way ANOVA.

In addition, as recently reported, the levels of O₃ are still increasing making the effect of this pollutant to our health a real concern not only for the present but even more for the future [75].

Being a gas, the toxicity of O₃ has been well documented in the respiratory tract [76–78] and in the last 2 decades, its effect on cutaneous tissues has been also investigated since the skin is another organ directly exposed to this agent [2, 5–8].

O₃ is a small molecule with strong oxidizing properties, with a redox potential of +2.07, able to oxidize a wide range of compounds including rubber. Indeed, it is too reactive to penetrate the tissues and as shown first for the lungs and more recently even for the skin [3], its ability to affect the tissues is mainly due to the generation of bioactive compounds that are formed by its interaction with the biological systems. Several studies have confirmed the ability of O₃ to oxidize cell membrane, generating radical species that can damage the tissues. The generation of redox-mediated molecules in the stratum corneum can eventually affect the deeper layers of the skin, modulating important physiopathological skin pathways [12].

The cutaneous proinflammatory effect of O₃ is mainly driven by its ability to activate nuclear factor kappa-light-chain enhancer (NF- κ B) which is a master regulator of proinflammatory responses. In the last few years, different players of inflammation have been studied and in particular, the inflammasome machinery has been recognized to play a key role in inflammatory skin conditions [25–27]. The activation

of the inflammasome occurs in response to different stimuli including cell damage and pathogen-associated molecular patterns (DAMPs and PAMPs) as well as prooxidant stimuli such as O₃ [17, 18], and also, in this case, NF- κ B activation plays an important role.

In our previous work, we have shown the inflammatory and oxidative effect of O₃ on the skin and its ability to activate NF- κ B and increase oxidative damage [30]. The aim of the present study was to evaluate the eventual protective effect of BB extracts against O₃-induced skin damage. Indeed, the exponential increase of pollution levels has aroused the need to find effective molecules that can be used as defensive agents against pollution-induced skin damage and premature cutaneous aging.

The antiaging research has been focused on an enormous range of products (natural or synthetic) with the aim to prevent, postpone, or reverse cutaneous aging signs. In general, those molecules can act in 2 ways, either quenching directly the radicals or by activating the cellular endogenous defensive system nuclear factor (erythroid-derived 2)-like 2 (NRF2) [79–81].

BB has been shown to be able to activate the nuclear factor erythroid-2-related factor 2 (NRF2) [82] and also quench radical formation [83] in several tissues, and it is now a general belief that BB beneficial effects are not limited to the “chemical” antioxidant properties, but mainly to its ability to induce an active cellular defense [84]. Therefore, as a follow-up of our recent study [30], in the present work, we were interested in evaluating the ability of BB extracts to

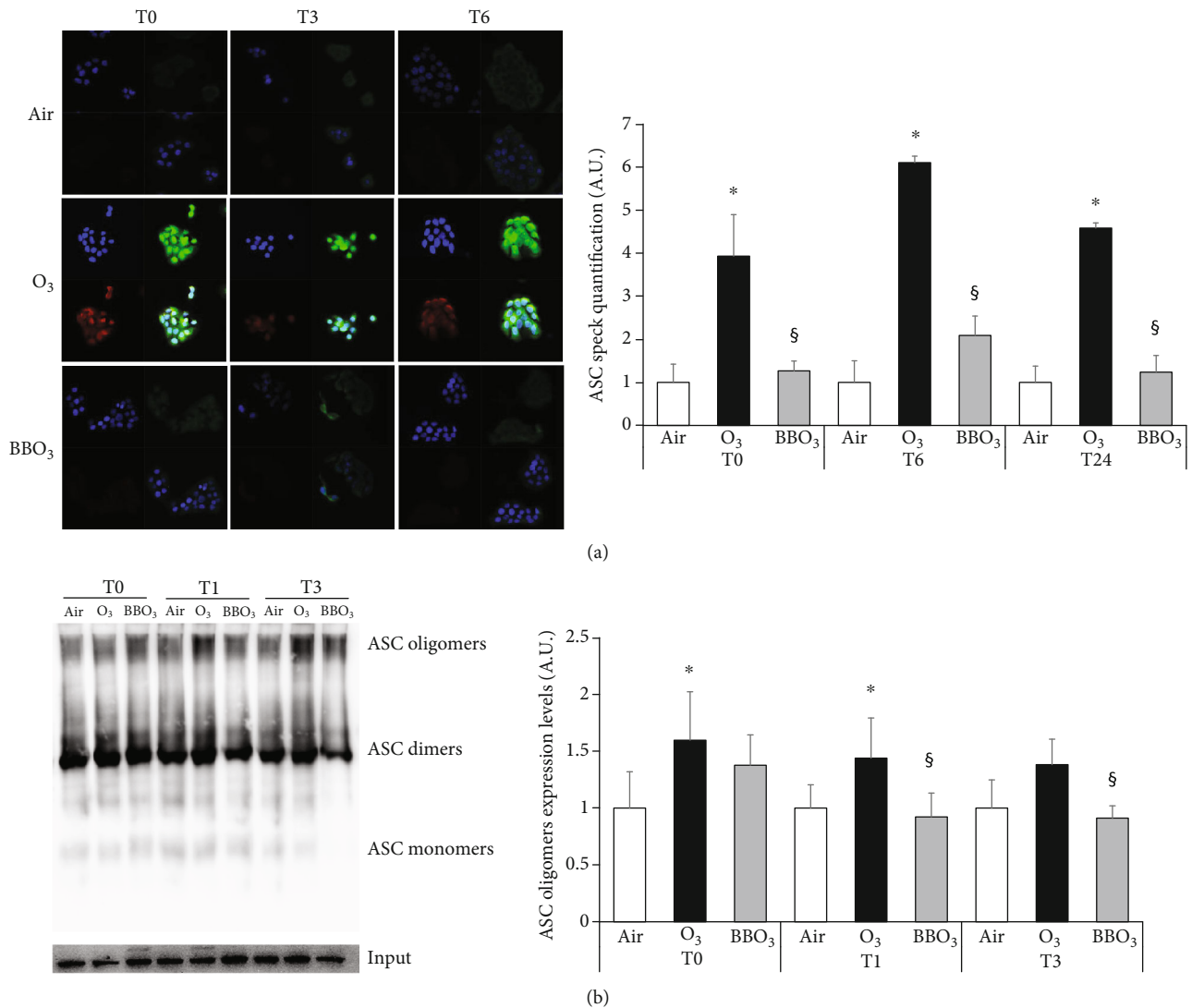


FIGURE 5: Blueberry (BB) extract prevents O₃-induced inflammasome oligomerization in HaCaT cells. (a) Immunofluorescence staining of ASC (green), NLRP1 (red), DAPI (blue), and merge in HaCaT cells pretreated with 10 $\mu\text{g}/\text{ml}$ of BB for 24 h then exposed to 0.5 ppm of O₃ for 1 h at 0, 3, and 6 h postexposure (40x magnification). On the right, ASC speck formation was quantified using ImageJ. (b) ASC oligomers, dimers, monomers, and input protein levels in keratinocytes at 0, 1, and 3 h after O₃ exposure (1 h, 0.5 ppm). On the right, depiction of ASC oligomers and dimer quantification using ImageJ. Data are the results of three independent experiments. * $p < 0.05$ air vs. O₃, § $p < 0.05$ O₃ vs. BBO₃ by two-way ANOVA.

prevent O₃-induced skin inflammasome activation. In addition, BB topical application has been shown to stimulate collagen synthesis and prevent chronological skin aging [50–52, 85]. Among the wide array of natural antioxidant substances, we decided to focus our attention on blueberries because of their complex phytochemical profiles that have already shown to quench free radicals [42, 43]. The ability of BB to activate the NRF2 pathway could also indirectly affect the inflammasome activation as altered redox homeostasis can be also a trigger for this inflammatory pathway [18, 86]. We should also mention that the crosstalk between NRF2 and NF- κ B is crucial for maintaining the cellular responses and to resolve an inflammatory status. An imbalance between NRF2 and NF- κ B pathways can lead to chronic inflammation; therefore, the activation of NRF2 by BB

extracts can prevent NF- κ B activation and modulate the tissue inflammatory status [87].

We were able to show that BB extracts were not toxic in the tested *in vitro* and *ex vivo* models. We found that BB extracts improved the recovery of scratch wound closure in O₃-treated cells. The impairment of O₃ on cutaneous wound healing has also been described previously by Lim et al., in aged mice [66], showing that the combination of aging and O₃ exposure is able to reduce the levels of TGF β , a key player in tissue wound healing [66, 88]. Considering that *in vitro* wound healing is mainly a test to evaluate the proliferative and migratory properties of the cells, we assessed whether O₃ could affect any of those pathways and the eventual role of BB extracts. Our data showed that O₃ was able to decrease both proliferation and migration of the cells while the BB

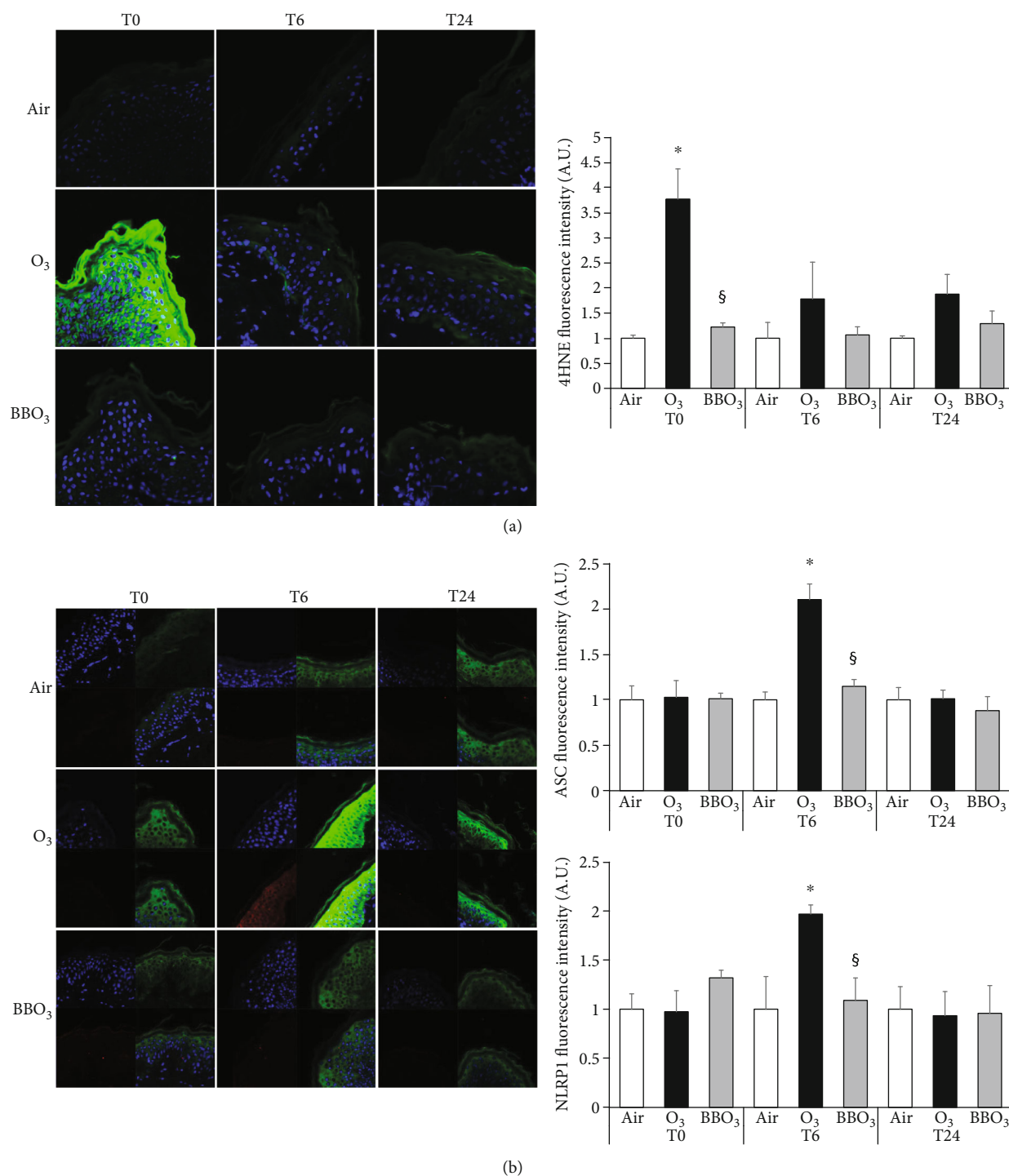


FIGURE 6: Blueberry (BB) extract prevents O₃-induced inflammasome activation and oxidative stress in *ex vivo* human skin biopsies. (a) Immunofluorescence staining for 4HNE (green), DAPI (blue), and merge in *ex vivo* human skin biopsies exposed to O₃ for 5 hours, 0.5 ppm, directly after exposure, 6 h and 24 h postexposure (40x magnification). Quantification of the fluorescence is depicted in the right panel. (b) Immunofluorescence staining of ASC (green), NLRP1 (red), DAPI (blue), and merge in *ex vivo* human skin explants pretreated with 100 μg/ml of BB for 24 h then exposed to 0.5 ppm of O₃ for 5 h at 0, 6, and 24 h postexposure (40x magnification). On the right panels, semiquantifications of the intensities of the signals of 4HNE (a) and ASC and NLRP1 (b) using ImageJ. Data are the results of three independent experiments. **p* < 0.05 air vs. O₃, [§]*p* < 0.05 O₃ vs. BBO₃ by two-way ANOVA.

pretreatment prevented these effects probably either via the activation of a cellular defensive system or less probably, by a direct interaction with the free radicals generated by O₃.

It is possible that the inhibition of proliferation is a consequence of their ability to activate NRF2 which has an inhibitory influence on NF-κB that is one of the regulators of cyclin

D1 expression, a key protein for cellular proliferation [61, 85, 89]. Although we did not evaluate the effect of BB on NFR2 activation, we showed a significant decrease in H_2O_2 by BB after O_3 exposure, although the use of the probe DCF to measure H_2O_2 is controversial [90].

The overproduction of ROS and NF- κ B activation has often been linked to the development of inflammatory responses related to skin and other tissues. Recently, the involvement of the inflammasome machinery has been studied in relation of several skin conditions. The activation of the inflammasome requires two steps: a “priming” step that induces transcriptional upregulation of NLRP1, pro-IL-18, and pro-IL-1 β , via NF- κ B and AP-1 signaling and post-translational modifications of NLRP1 (phosphorylation, ubiquitination), followed by a second signal that yields to conformational changes in the NOD-like receptor structure which allows for the binding with the adaptor ASC and assembly of the whole complex [17].

To better understand the molecular mechanisms responsible for the BB effect on O_3 -induced inflammasome activation and oligomerization, we pretreated the keratinocytes with BB extracts, before exposing them to O_3 and then, we evaluated transcript levels of IL-18, ASC, and Caspase 1 as well as ASC specks and oligomers. Our data evidenced the remarkable activity of BB in preventing the increased aforementioned mRNA levels and the oligomerization of the proteins NLRP1 and ASC, upon O_3 exposure. These data confirmed the study by Wang et al. which demonstrated reduced gene expression levels of NLRP, Caspase 1, ASC, and proinflammatory cytokines IL-1 β , TNF- α , IL-6, and iNOS in macrophages pretreated with BB extracts and then challenged with lipopolysaccharide [91].

As keratinocytes grown in monolayer culture do not undergo terminal differentiation, which results in the formation of the outermost layer of the skin, the stratum corneum (SC), and since this layer is the main target of O_3 [92], we have performed our experiments also in RHE (reconstructed human epidermis). The use of RHE is strongly recommended to study *in vitro* cutaneous protection, since is not only represented by all the living epidermis layers but it also includes the SC [69], and our data confirmed the ability of BB extracts to prevent O_3 -induced Caspase 1 increase at both transcripts and protein levels. Although, RHE is a very reliable *in vitro* model, it still does not present all the SC layers making it more accessible to outdoor stressors. In addition, the lack of other skin cells such as melanocytes, immunity cells, might compromise skin responses [69].

For this reason, we further confirm our data in an *ex vivo* human skin explant which presents a normal skin barrier, functional basal layer, a mature SC, and all the cell types and cutaneous appendages present in *in vivo* human skin [93].

As demonstrated in 2D and 3D models, O_3 was able to activate the inflammasome machinery also in the human skin explants, and BB extracts prevented this induction. In the specific, O_3 exposure not only induced the oligomerization of the inflammasome components but also increased the levels of lipid peroxidation as detected by 4HNE protein adduct formation (as previously reported [16]) while the pre-

treatment with BB extract was able to prevent the O_3 -induced increase of 4HNE, ASC, and NLRP1 and their oligomerization. These data are in line not only with the theory that O_3 is able to affect skin via the formation of lipid peroxidation products but also with the theory that this mechanism is redox mediated.

In conclusion, we have demonstrated, by the use of three different skin models, that BB extracts are able to prevent the inflammatory and oxidative skin damage induced by O_3 , making blueberries a possible innovative natural ingredient for new technologies against cutaneous pollution-induced damage.

Data Availability

All data will be available upon request to the corresponding author.

Conflicts of Interest

The authors declare that they have no conflicts of interest.

Authors' Contributions

Mary Ann Lila and Giuseppe Valacchi equally supervised the manuscript.

Supplementary Materials

The cutaneous interaction with tropospheric O_3 induced an increase in oxidative stress mediators (ROS) and a consequent induction of the inflammasome-related proteins NLRP1 and Caspase 1 that will lead to the assemble of the inflammasome scaffold and the activations of the inflammasome machinery. Blueberry extract (BB) treatment is able to prevent the inflammasome activation by O_3 . (*Supplementary materials*)

References

- [1] World Health Organization (WHO), Who, 2016.
- [2] K. B. Fuks, B. Woodby, G. Valacchi, and D. Hautarzt, 2019.
- [3] C. E. Cross, G. Valacchi, B. Schock et al., “Environmental Oxidant Pollutant Effects on Biologic Systems,” *American Journal of Respiratory and Critical Care Medicine*, vol. 166, supplement_1, pp. S44–S50, 2002.
- [4] M. G. Mustafa, “Biochemical basis of ozone toxicity,” in *Free Radical Biology and Medicine*, pp. 245–265, Elsevier, 1990.
- [5] G. Valacchi, E. Pagnin, A. M. Corbacho et al., “In vivo ozone exposure induces antioxidant/stress-related responses in murine lung and skin,” *Free Radical Biology and Medicine*, vol. 36, no. 5, pp. 673–681, 2004.
- [6] G. Valacchi, C. Sticozzi, A. Pecorelli, F. Cervellati, C. Cervellati, and E. Maioli, “Cutaneous responses to environmental stressors,” *Annals of the New York Academy of Sciences*, vol. 1271, no. 1, pp. 75–81, 2012.
- [7] J. Krutmann, A. Bouloc, G. Sore, B. A. Bernard, and T. Passeron, “The skin aging exposome,” *Journal of Dermatological Science*, vol. 85, no. 3, pp. 152–161, 2017.

- [8] G. Valacchi, A. van der Vliet, B. C. Schock et al., "Ozone exposure activates oxidative stress responses in murine skin," *Toxicology*, vol. 179, no. 1-2, pp. 163–170, 2002.
- [9] E. Lavigne, P. J. Villeneuve, and S. Cakmak, "Air Pollution and Emergency Department Visits for Asthma in Windsor, Canada," *Canadian Journal of Public Health*, vol. 103, no. 1, pp. 4–8, 2012.
- [10] G. G. Kaplan, E. Dixon, R. Panaccione et al., "Effect of ambient air pollution on the incidence of appendicitis," *Canadian Medical Association Journal*, vol. 181, no. 9, pp. 591–597, 2009.
- [11] S. H. Lee, S. K. Jeong, and S. K. Ahn, "An Update of the Defensive Barrier Function of Skin," *Yonsei Medical Journal*, vol. 47, no. 3, pp. 293–306, 2006.
- [12] A. Pecorelli, B. Woodby, R. Prieux, and G. Valacchi, "Involvement of 4-hydroxy-2-nonenal in pollution-induced skin damage," *BioFactors*, vol. 45, 2019.
- [13] C. De Luca and G. Valacchi, "Surface lipids as multifunctional mediators of skin responses to environmental stimuli," *Mediators of Inflammation*, vol. 2010, Article ID 321494, 11 pages, 2010.
- [14] G. Valacchi, X. M. Muresan, C. Sticozzi et al., "Ozone-induced damage in 3D-Skin Model is prevented by topical vitamin C and vitamin E compound mixtures application," *Journal of Dermatological Science*, vol. 82, no. 3, pp. 209–212, 2016.
- [15] G. Valacchi, C. Sticozzi, G. Belmonte et al., "Vitamin C Compound Mixtures Prevent Ozone-Induced Oxidative Damage in Human Keratinocytes as Initial Assessment of Pollution Protection," *PLOS ONE*, vol. 10, no. 8, p. e0131097, 2015.
- [16] G. Valacchi, A. Pecorelli, G. Belmonte et al., "Protective Effects of Topical Vitamin C Compound Mixtures against Ozone-Induced Damage in Human Skin," *Journal of Investigative Dermatology*, vol. 137, no. 6, pp. 1373–1375, 2017.
- [17] N. Kelley, D. Jeltema, Y. Duan, and Y. He, "The NLRP3 Inflammasome: An Overview of Mechanisms of Activation and Regulation," *International Journal of Molecular Sciences*, vol. 20, no. 13, p. 3328, 2019.
- [18] J. M. Abais, M. Xia, Y. Zhang, K. M. Boini, and P. L. Li, "Redox Regulation of NLRP3 Inflammasomes: ROS as Trigger or Effector?," *Antioxidants & Redox Signaling*, vol. 22, no. 13, pp. 1111–1129, 2015.
- [19] L. C. Freeman and J. P.-Y. Ting, "The pathogenic role of the inflammasome in neurodegenerative diseases," *Journal of Neurochemistry*, vol. 136, pp. 29–38, 2016.
- [20] M. T. Heneka, M. P. Kummer, and E. Latz, "Innate immune activation in neurodegenerative disease," *Nature Reviews Immunology*, vol. 14, no. 7, pp. 463–477, 2014.
- [21] M. T. Heneka, "Inflammasome activation and innate immunity in Alzheimer's disease," *Brain Pathology*, vol. 27, no. 2, pp. 220–222, 2017.
- [22] H. Guo, J. B. Callaway, and J. P. Y. Ting, "Inflammasomes: mechanism of action, role in disease, and therapeutics," *Nature Medicine*, vol. 21, no. 7, pp. 677–687, 2015.
- [23] S. L. Masters, E. Latz, and L. A. J. O'Neill, "The Inflammasome in Atherosclerosis and Type 2 Diabetes," *Science Translational Medicine*, vol. 3, no. 81, p. 81ps17, 2011.
- [24] P. Duedwell, H. Kono, K. J. Rayner et al., "NLRP3 inflammasomes are required for atherogenesis and activated by cholesterol crystals," *Nature*, vol. 464, no. 7293, pp. 1357–1361, 2010.
- [25] Y. Dombrowski, M. Peric, S. Koglin et al., "Cytosolic DNA Triggers Inflammasome Activation in Keratinocytes in Psoriatic Lesions," *Science Translational Medicine*, vol. 3, no. 82, p. 82ra38, 2011.
- [26] D. C. de Sá and C. F. Neto, "Inflammasomes and dermatology," *Anais Brasileiros de Dermatologia*, vol. 91, no. 5, pp. 566–578, 2016.
- [27] H.-D. Beer, E. Contassot, and L. E. French, "The Inflammasomes in Autoinflammatory Diseases with Skin Involvement," *Journal of Investigative Dermatology*, vol. 134, no. 7, pp. 1805–1810, 2014.
- [28] M. Burian, A. S. Yazdi, and J. Invest, "NLRP1 Is the Key Inflammasome in Primary Human Keratinocytes," *Journal of Investigative Dermatology*, vol. 138, no. 12, pp. 2507–2510, 2018.
- [29] G. Fenini, S. Grossi, E. Contassot et al., "Genome Editing of Human Primary Keratinocytes by CRISPR/Cas9 Reveals an Essential Role of the NLRP1 Inflammasome in UVB Sensing," *The Journal of Investigative Dermatology*, vol. 138, no. 12, pp. 2644–2652, 2018.
- [30] F. Ferrara, E. Pambianchi, A. Pecorelli et al., "Redox regulation of cutaneous inflammasome by ozone exposure," *Free Radical Biology and Medicine*, vol. 152, pp. 561–570, 2020.
- [31] E. Birben, U. M. Sahiner, C. Sackesen, S. Erzurum, and O. Kalayci, "Oxidative Stress and Antioxidant Defense," *World Allergy Organization Journal*, vol. 5, no. 1, pp. 9–19, 2012.
- [32] M. L. Circu and T. Y. Aw, "Reactive oxygen species, cellular redox systems, and apoptosis," *Free Radical Biology and Medicine*, vol. 48, no. 6, pp. 749–762, 2010.
- [33] E. M. Hanschmann, J. R. Godoy, C. Berndt, C. Hudemann, and C. H. Lillig, "Thioredoxins, Glutaredoxins, and Peroxiredoxins—Molecular Mechanisms and Health Significance: from Cofactors to Antioxidants to Redox Signaling," *Antioxidants & Redox Signaling*, vol. 19, no. 13, pp. 1539–1605, 2013.
- [34] B. Poljsak, D. Šuput, and I. Milisav, "Achieving the Balance between ROS and Antioxidants: When to Use the Synthetic Antioxidants," *Oxidative Medicine and Cellular Longevity*, vol. 2013, Article ID 956792, 11 pages, 2013.
- [35] E. S. Krol, K. A. Kramer-Stickland, and D. C. Liebler, "Photoprotective Actions of Topically Applied Vitamin E*," *Drug Metabolism Reviews*, vol. 32, no. 3-4, pp. 413–420, 2000.
- [36] K. E. Burke, J. Clive, G. F. Combs, J. Commisso, C. L. Keen, and R. M. Nakamura, "Effects of Topical and Oral Vitamin E on Pigmentation and Skin Cancer Induced by Ultraviolet Irradiation in Skh:2 Hairless Mice," *Nutrition and Cancer*, vol. 38, no. 1, pp. 87–97, 2000.
- [37] M. Działo, J. Mierziak, U. Korzun, M. Preisner, J. Szopa, and A. Kulma, "The Potential of Plant Phenolics in Prevention and Therapy of Skin Disorders," *International Journal of Molecular Sciences*, vol. 17, no. 2, p. 160, 2016.
- [38] S. A. Souyoul, K. P. Saussy, and M. P. Lupo, "Nutraceuticals: A Review," *Dermatology and Therapy*, vol. 8, no. 1, pp. 5–16, 2018.
- [39] J.-Y. Lin, M. A. Selim, C. R. Shea et al., "UV photoprotection by combination topical antioxidants vitamin C and vitamin E," *Journal of the American Academy of Dermatology*, vol. 48, no. 6, pp. 866–874, 2003.
- [40] J. J. Thiele and S. Ekanayake-Mudiyanselage, "Vitamin E in human skin: Organ-specific physiology and considerations for its use in dermatology," *Molecular Aspects of Medicine*, vol. 28, no. 5-6, pp. 646–667, 2007.
- [41] N. Mistry, "Guidelines for Formulating Anti-Pollution Products," *Cosmetics*, vol. 4, no. 4, p. 57, 2017.

- [42] W. Kalt, A. Cassidy, L. R. Howard et al., "Recent Research on the Health Benefits of Blueberries and Their Anthocyanins," *Advances in Nutrition*, vol. 11, 2019.
- [43] T. Tsuda, "Dietary anthocyanin-rich plants: biochemical basis and recent progress in health benefits studies," *Molecular Nutrition & Food Research*, vol. 56, no. 1, pp. 159–170, 2012.
- [44] S. Lee, K. I. Keirse, R. Kirkland, Z. I. Grunewald, J. G. Fischer, and C. B. de la Serre, "Blueberry Supplementation Influences the Gut Microbiota, Inflammation, and Insulin Resistance in High-Fat-Diet-Fed Rats," *The Journal of Nutrition*, vol. 148, no. 2, pp. 209–219, 2018.
- [45] Y. Liu, Y. Tikunov, R. E. Schouten, L. F. M. Marcelis, R. G. F. Visser, and A. Bovy, "Anthocyanin Biosynthesis and Degradation Mechanisms in Solanaceous Vegetables: A Review," *Frontiers in Chemistry*, vol. 6, 2018.
- [46] K. L. Wolfe, X. Kang, X. He, M. Dong, Q. Zhang, and R. H. Liu, "Cellular Antioxidant Activity of Common Fruits," *Journal of Agricultural and Food Chemistry*, vol. 56, no. 18, pp. 8418–8426, 2008.
- [47] D. Stevenson and J. Scalzo, "Anthocyanin composition and content of blueberries from around the world," *Journal of Berry Research*, vol. 2, no. 4, pp. 179–189, 2012.
- [48] W. Kalt, D. A. J. Ryan, J. C. Duy, R. L. Prior, M. K. Ehlenfeldt, and S. P. Vander Kloet, "Interspecific Variation in Anthocyanins, Phenolics, and Antioxidant Capacity among Genotypes of Highbush and Lowbush Blueberries (*Vaccinium* Section *cyanococcusspp.*)," *Journal of Agricultural and Food Chemistry*, vol. 49, no. 10, pp. 4761–4767, 2001.
- [49] M. H. Grace, D. M. Ribnicky, P. Kuhn et al., "Hypoglycemic activity of a novel anthocyanin-rich formulation from lowbush blueberry, *Vaccinium angustifolium* Aiton," *Phytomedicine*, vol. 16, no. 5, pp. 406–415, 2009.
- [50] S. Grether-Beck, J. Krutmann, K. Wilkens, and K. D'Amato, "Effect of a Blueberry-Derived Antioxidant Matrix on Infrared-A Induced Gene Expression in Human Dermal Fibroblasts," *Journal of Drugs in Dermatology*, vol. 6, pp. s125–s128, 2017.
- [51] F. C. Lau, M. Bagchi, S. Zafra-Stone, and D. Bagchi, "The Benefits of Antioxidant-Rich Fruits on Skin Health," in *Nutritional Cosmetics*, William Andrew Publishing, 2009.
- [52] M. Bagchi, S. Zafra-Stone, J. N. Losso et al., "Anti-angiogenic functional and medicinal foods," in *Anti-angiogenic functional and medicinal foods*, CRC Press, 2007.
- [53] M. A. Lila and K. D. Lila, *Recent Advances in Polyphenol Research Volume 7, Chapter 3*, E. S. Quideau, V. Freitas, and J. Reed, Eds., Wiley and Sons Ltd, 2020.
- [54] F. Xu, S. Yan, M. Wu et al., "Ambient ozone pollution as a risk factor for skin disorders," *British Journal of Dermatology*, vol. 165, no. 1, pp. 224–225, 2011.
- [55] T. Kousha, G. Valacchi, and J. Toxicol, "The air quality health index and emergency department visits for urticaria in Windsor, Canada," *Journal of Toxicology and Environmental Health*, vol. 78, no. 8, pp. 524–533, 2015.
- [56] M. Benedusi, E. Frigato, M. Beltramello, C. Bertolucci, and G. Valacchi, "Circadian clock as possible protective mechanism to pollution induced keratinocytes damage," *Mechanisms of Ageing and Development*, vol. 172, pp. 13–20, 2018.
- [57] M. H. Grace, C. W. Warlick, S. A. Neff, and M. A. Lila, "Efficient preparative isolation and identification of walnut bioactive components using high-speed counter-current chromatography and LC-ESI-IT-TOF-MS," *Food Chemistry*, vol. 158, pp. 229–238, 2014.
- [58] M. H. Grace, D. Esposito, K. L. Dunlap, and M. A. Lila, "Comparative Analysis of Phenolic Content and Profile, Antioxidant Capacity, and Anti-inflammatory Bioactivity in Wild Alaskan and Commercial *Vaccinium* Berries," *Journal of Agricultural and Food Chemistry*, vol. 62, no. 18, pp. 4007–4017, 2014.
- [59] N. D. Magnani, X. M. Muresan, G. Belmonte et al., "Skin Damage Mechanisms Related to Airborne Particulate Matter Exposure," *Toxicological Sciences*, vol. 149, no. 1, pp. 227–236, 2016.
- [60] F. Cervellati, X. M. Muresan, C. Sticozzi et al., "Comparative effects between electronic and cigarette smoke in human keratinocytes and epithelial lung cells," *Toxicology in Vitro*, vol. 28, no. 5, pp. 999–1005, 2014.
- [61] G. Valacchi, A. Pecorelli, M. Mencarelli et al., "Rottlerin: a multifaceted regulator of keratinocyte cell cycle," *Experimental Dermatology*, vol. 18, no. 6, pp. 516–521, 2009.
- [62] M. X. Maria, S. Claudia, B. Giuseppe et al., *Archives of Biochemistry and Biophysics*, 2018.
- [63] G. Valacchi, C. Sticozzi, I. Zanardi et al., "Ozone mediators effect on "in vitro" scratch wound closure," *Free Radical Research*, vol. 50, no. 9, pp. 1022–1031, 2016.
- [64] C. Sticozzi, A. Pecorelli, A. Romani et al., "Tropospheric ozone affects SRB1 levels via oxidative post-translational modifications in lung cells," *Free Radical Biology and Medicine*, vol. 126, pp. 287–295, 2018.
- [65] X. M. Muresan, C. Sticozzi, G. Belmonte, V. Savelli, P. Evelson, and G. Valacchi, "Modulation of cutaneous scavenger receptor B1 levels by exogenous stressors impairs "in vitro" wound closure," *Mechanisms of Ageing and Development*, vol. 172, pp. 78–85, 2018.
- [66] Y. Lim, A. D. Phung, A. M. Corbacho et al., "Modulation of cutaneous wound healing by ozone: differences between young and aged mice," *Toxicology letters*, 2006.
- [67] M. Leibold, "Psoriasis," *Annals of Internal Medicine*, vol. 168, no. 7, pp. ITC49–ITC64, 2018.
- [68] N. K. Haass, K. S. M. Smalley, L. Li, and M. Herlyn, "Adhesion, migration and communication in melanocytes and melanoma," *Pigment Cell Research*, vol. 18, no. 3, pp. 150–159, 2005.
- [69] A. Rossi, A. Appelt-Menzel, S. Kurdyn, H. Walles, and F. Groeber, "Generation of a Three-dimensional Full Thickness Skin Equivalent and Automated Wounding," *Journal of Visualized Experiments*, no. 96, 2015.
- [70] M. S. Dick, L. Sborgi, S. Rühl, S. Hiller, and P. Broz, "ASC filament formation serves as a signal amplification mechanism for inflammasomes," *Nature Communications*, vol. 7, no. 1, 2016.
- [71] G. Valacchi, F. Virgili, C. Cervellati, and A. Pecorelli, "OxInflammation: From Subclinical Condition to Pathological Biomarker," *Frontiers in Physiology*, vol. 9, 2018.
- [72] J. Lelieveld, A. Pozzer, U. Pöschl, M. Fnais, A. Haines, and T. Münzel, "Inappropriate evaluation of methodology and biases by P. Morfeld and T.C. Erren.," *Cardiovascular Research*, vol. 116, no. 8, p. e102, 2020.
- [73] M. C. M. Alvim-Ferraz, S. I. V. Sousa, M. C. Pereira, and F. G. Martins, "Contribution of anthropogenic pollutants to the increase of tropospheric ozone levels in the Oporto Metropolitan Area, Portugal since the 19th century," *Environmental Pollution*, vol. 140, no. 3, pp. 516–524, 2006.

- [74] A. Marengo, H. Gouget, P. Nedelec, J. P. Pages, and F. Karcher, "Evidence of a long-term increase in tropospheric ozone from Pic du Midi data series: Consequences: Positive radiative forcing," *Journal of Geophysical Research*, vol. 99, no. D8, p. 16617, 1994.
- [75] M. Lin, L. W. Horowitz, Y. Xie et al., "Vegetation feedbacks during drought exacerbate ozone air pollution extremes in Europe," *Nature Climate Change*, vol. 10, no. 5, pp. 444–451, 2020.
- [76] F. J. Kelly and I. S. Mudway, "Protein oxidation at the air-lung interface," *Amino Acids*, vol. 25, no. 3-4, pp. 375–396, 2003.
- [77] F. Kazemiparkouhi, K.-D. Eum, B. Wang, J. Manjourides, and H. H. Suh, "Long-term ozone exposures and cause-specific mortality in a US Medicare cohort," *Journal of Exposure Science and Environmental Epidemiology*, vol. 30, no. 4, pp. 650–658, 2020.
- [78] L. M. T. Luong, D. Phung, T. N. Dang, P. D. Sly, L. Morawska, and P. K. Thai, "Seasonal association between ambient ozone and hospital admission for respiratory diseases in Hanoi, Vietnam," *PLoS One*, vol. 13, no. 9, p. e0203751, 2018.
- [79] H. Si and D. Liu, "Dietary antiaging phytochemicals and mechanisms associated with prolonged survival," *Journal of Nutritional Biochemistry*, vol. 25, no. 6, pp. 581–591, 2014.
- [80] H. O. M. E. R. S. BLACK and M. I. C. H. E. L. I. N. E. M. MATHEWS-ROTH, "PROTECTIVE ROLE OF BUTYLATED HYDROXYTOLUENE AND CERTAIN CAROTENOIDS IN PHOTOCARCINOGENESIS," *Photochemistry and Photobiology*, vol. 53, no. 5, pp. 707–716, 1991.
- [81] M. R. de la Vega, A. Krajisnik, D. Zhang, and G. Wondrak, "Targeting NRF2 for Improved Skin Barrier Function and Photoprotection: Focus on the Achiote-Derived Apocarotenoid Bixin," *Nutrients*, vol. 9, no. 12, p. 1371, 2017.
- [82] J. S. Tang, M. C. M. Vissers, R. F. Anderson et al., "Bioavailable Blueberry-Derived Phenolic Acids at Physiological Concentrations Enhance Nrf2-Regulated Antioxidant Responses in Human Vascular Endothelial Cells," *Molecular Nutrition & Food Research*, vol. 62, 2018.
- [83] P. Drózdź, V. Šežienė, and K. Pyrzynska, "Phytochemical Properties and Antioxidant Activities of Extracts from Wild Blueberries and Lingonberries," *Plant Foods for Human Nutrition*, vol. 72, no. 4, pp. 360–364, 2017.
- [84] Y. Song, L. Huang, and J. Yu, "Effects of blueberry anthocyanins on retinal oxidative stress and inflammation in diabetes through Nrf2/HO-1 signaling," *Journal of Neuroimmunology*, vol. 301, pp. 1–6, 2016.
- [85] S. Shin, S. H. Cho, D. Park, and E. Jung, "Anti-skin aging properties of protocatechuic acid in vitro and in vivo," *Journal of Cosmetic Dermatology*, vol. 19, no. 4, pp. 977–984, 2020.
- [86] A. Rubartelli, M. Gattorno, M. G. Netea, and C. A. Dinarello, "Interplay between redox status and inflammasome activation," *Trends in Immunology*, vol. 32, no. 12, pp. 559–566, 2011.
- [87] J. D. Wardyn, A. H. Ponsford, and C. M. Sanderson, "Dissecting molecular cross-talk between Nrf2 and NF- κ B response pathways," *Biochemical Society Transactions*, vol. 43, no. 4, pp. 621–626, 2015.
- [88] L. Lu, S. S. Chen, J. Q. Zhang, F. J. Ramires, and Y. Sun, "Activation of nuclear factor- κ B and its proinflammatory mediator cascade in the infarcted rat heart," *Biochemical and Biophysical Research Communications*, vol. 321, no. 4, pp. 879–885, 2004.
- [89] W. Y. Huang, Y. M. Liu, J. Wang, X. N. Wang, and C. Y. Li, "Anti-Inflammatory Effect of the Blueberry Anthocyanins Malvidin-3-Glucoside and Malvidin-3-Galactoside in Endothelial Cells," *Molecules*, vol. 19, no. 8, pp. 12827–12841, 2014.
- [90] H. J. Forman, O. Augusto, R. Brigelius-Flohe et al., "Even free radicals should follow some rules: a guide to free radical research terminology and methodology," *Free Radical Biology and Medicine*, vol. 78, pp. 233–235, 2015.
- [91] H. Wang, X. Guo, J. Liu, T. Li, X. Fu, and R. H. Liu, "Comparative suppression of NLRP3 inflammasome activation with LPS-induced inflammation by blueberry extracts (*Vaccinium* spp.)," *RSC Advances*, vol. 7, no. 46, pp. 28931–28939, 2017.
- [92] L. Packer and G. Valacchi, "Antioxidants and the Response of Skin to Oxidative Stress: Vitamin E as a Key Indicator," *Skin Pharmacology and Physiology*, vol. 15, no. 5, pp. 282–290, 2002.
- [93] G. P. Sidgwick, D. McGeorge, and A. Bayat, "Functional testing of topical skin formulations using an optimised ex vivo skin organ culture model," *Archives of Dermatological Research*, vol. 308, no. 5, pp. 297–308, 2016.

Research Article

Increased Serum Levels of IFN- γ , IL-1 β , and IL-6 in Patients with Alopecia Areata and Nonsegmental Vitiligo

Katarzyna Tomaszewska ¹, Magdalena Kozłowska,² Andrzej Kaszuba,² Aleksandra Lesiak,² Joanna Narbutt,² and Anna Zalewska-Janowska¹

¹Psychodermatology Department, Clinical Immunology and Rheumatology, Medical University of Lodz, Pomorska 251, 92-213 Lodz, Poland

²Department of Dermatology, Pediatric Dermatology and Oncology, Medical University of Lodz, Kniaziewiczza 1/5, 91-347 Lodz, Poland

Correspondence should be addressed to Katarzyna Tomaszewska; katarzyna.tomaszewska@umed.lodz.pl

Received 9 April 2020; Revised 16 June 2020; Accepted 24 July 2020; Published 3 August 2020

Academic Editor: Luciano Saso

Copyright © 2020 Katarzyna Tomaszewska et al. This is an open access article distributed under the Creative Commons Attribution License, which permits unrestricted use, distribution, and reproduction in any medium, provided the original work is properly cited.

Alopecia areata (AA) and vitiligo are both common skin diseases of autoimmune origin. Both alopecia areata and vitiligo have shown to be affected by oxidative stress. The present work is aimed at evaluating and comparing the serum proinflammatory cytokine levels in AA and nonsegmental vitiligo (NSV). A cross-sectional study was conducted of 33 patients with AA, 30 patients with NSV, and 30 healthy controls. Serum levels of interferon γ (IFN- γ), interleukin- (IL-) 1 β , and IL-6 were determined quantitatively by ELISA method. Our analysis identified a *signature of oxidative stress* associated with AA and NSV, characterized by elevated levels of IFN- γ (AA: $p = 0.007283$; NSV: $p = 0.038467$), IL-1 β (AA; NSV: $p \leq 0.001$), and IL-6 (AA; NSV: $p \leq 0.001$). IL-6 was also significantly increased in NSV patients in comparison with AA patients ($p = 0.004485$). Our results supported the hypothesis that oxidative stress may play a significant role in promoting and amplifying the inflammatory process both in AA and vitiligo. The complex understanding of both disease etiopathogenesis involves interrelationships between oxidative stress and autoimmunity. The clinical study registration number is RNN/266/16/KE.

1. Introduction

Alopecia areata (AA) and vitiligo are both autoimmune diseases, and striking similarities in pathogenesis have been identified at the level of both the innate and adaptive immune systems. Increased reactive oxygen species and high cellular stress levels have been suggested as the initiating trigger of the innate immune system in both diseases, and genome-wide association studies have implicated risk alleles that influence both innate and adaptive immunity [1–3]. Both conditions are known to carry a considerable impact on health-related quality of life [4, 5].

AA is a nonscarring hair loss with an unpredictable course and a wide spectrum of manifestations. It affects both genders equally with a cumulative lifetime incidence of about two percent and no significant racial predominance [6]. The

most frequent clinical presentation of AA is in single or multiple patches. Occasionally, AA may progress to complete baldness, which is referred to as alopecia (areata) totalis (AT). When the entire body suffers from complete hair loss, it is referred to as alopecia (areata) universalis (AU). Ophiasis is a form of AA characterized by the loss of hair in the shape of a wave at the circumference of the head [7].

Vitiligo is an acquired disorder of the skin and mucous membranes that is characterized by well-circumscribed, depigmented macules and patches that occur secondary to selective destruction of melanocytes [8]. Vitiligo itself has been classified based on clinical grounds into two major forms, namely, segmental vitiligo (SV) and nonsegmental vitiligo (NSV), the latter including several variants (generalized vitiligo, acrofacial vitiligo, and universal vitiligo) [9]. NSV is the most common form of the disease (accounting

for 85 to 90% of cases overall) and is associated with an increased risk of autoimmune diseases, especially Hashimoto's thyroiditis [10].

Due to limited knowledge regarding the role of systemic cytokine profiles associated with oxidative stress in AA and vitiligo, we aimed to determine and compare the serum levels of interferon γ (IFN- γ), interleukin- (IL-) 1β , and IL-6 in AA and NSV patients. Whether the pattern of serum cytokines could be associated with clinical details and disease activity in patients was also investigated. Previous studies had shown that both Th1 and Th17 cells are involved in the development of AA and NSV. Proinflammatory cytokines of innate immunity such as IL- 1β and IL-6 with transforming growth factor β (TGF- β) are essential for Th1 and Th17 differentiation [11, 12]. IFN- γ is crucial for potentiating the activity of CD8+ T cells and natural killer cells in AA and NSV [13]. IL-15 stimulates the proliferation and activation of T cells, macrophages, CD5 memory lymphocytes, and cytotoxic CD8 lymphocytes [14]. IFN- γ , IL- 1β , and IL-6 are also known as oxidative stress triggers.

2. Materials and Methods

2.1. Materials/Study Subjects. The study included 33 patients with AA and 30 patients with NSV. The control group consisted of 30 healthy individuals. All patients were of caucasian ethnicity. The diagnosis of AA and NSV was based on a detailed medical history and clinical and dermoscopic/trichoscopic examination. Clinically ambiguous cases, patients with a sign of infection, and patients with a history of using topical treatment within the past 2 weeks or systemic treatment within the past 4 weeks were excluded from the study. A detailed history and clinical examination were recorded for each patient. Controls consisted of healthy individuals of similar age who do not have alopecia areata or vitiligo and other comorbidities.

The group of patients with AA included 21 females (63.6%) and 12 males (36.4%), and the group of patients with vitiligo included 18 females (60%) and 12 males (40%). The control group contained 23 females (76.7%) and 7 males (23.3%) subjects. The mean ages of AA patients, NSV patients, and healthy controls were 18.64 ± 8.56 years, 28.55 ± 19.23 years, and 19.95 ± 13.08 years, respectively. There were no statistical differences in sex (c2 test) and age (*t*-test) between the patients and the normal controls.

To assess the clinical extent of AA and NSV, we calculated the Severity of Alopecia Tool (SALT) [15] and Vitiligo Area Severity Index (VASI) [16] scores, respectively. The activity of both AA and NSV was assessed at the Vitiligo Disease Activity (VIDA) Score [17].

The study was approved by the Bioethics Committee of the Medical University of Lodz (RNN/266/16/KE) and was conducted following the Declaration of Helsinki. All subjects gave informed consent to participate in the study.

2.2. Methods. Peripheral venous blood samples were collected from all patients and healthy controls. Sera were isolated by centrifugation and stored at -70°C before analysis and the concentrations of cytokines (pg/ml), namely, IFN- γ , IL- 1β

(Diaclone, Besancon Cedex, France), and IL-6 (Gen-Probe Inc., San Diego, California, USA) were determined quantitatively in collected serum samples by the enzyme-linked immunosorbent assay (ELISA) method in both patients and controls. ELISA tests were performed according to the manufacturer's instructions. The serum cytokine levels were compared between groups. The correlation of serum cytokine levels with sex, extent, activity, and duration of disease was studied.

2.3. Statistical Analysis. Statistical analysis was carried out with the Statistica software version 12 (StatSoft, Tulsa, OK, USA). To determine the distribution of quantitative variables, the Shapiro-Wilk test was used. The Mann-Whitney test was used to compare the median serum cytokine levels between the groups. Correlation analysis was determined using the Spearman rank correlation test. Data were considered to be statistically significant at a value of $p < 0.05$.

3. Results and Discussion

3.1. Results

3.1.1. Demographic and Clinical Characteristics. The demographic and clinical characteristics of study participants are described in Table 1. Of the 33 enrolled patients with AA, 26 had patchy AA (SALT: $S1 \geq S4a$) and 7 had severe disease (SALT: $S4b \geq S5$). All of the 30 enrolled patients with vitiligo had NSV.

3.1.2. Serum Concentrations of IFN- γ , IL- 1β , and IL-6 among Patients with AA, NSV, and Healthy Controls. IFN- γ , IL- 1β , and IL-6 serum levels were significantly elevated in AA patients and in NSV patients compared to healthy controls. Only IL-6 level was also significantly higher in NSV compared to AA patients (see Table 2). We found no significant sex difference in cytokines level of female and male patients with AA and NSV.

3.1.3. Correlations between Serum Levels of IFN- γ , IL- 1β , and IL-6 and Extent, Activity, and Duration of the Disease. The correlation between increased IL-6 serum levels and duration of the AA was confirmed in the Spearman test ($q = 0.453$; $p = 0.010474$). In AA patients, there were no correlations found between serum cytokine levels and extent (SALT)/activity of disease (VIDA) (see Table 3).

In NSV patients, the correlations between increased IL- 1β serum levels and extent of vitiligo (VASI) ($q = 0.383$; $p = 0.040441$), duration of disease ($q = 0.458$; $p = 0.012573$) were revealed in the Spearman test. IL- 1β serum level was negatively correlated with the activity of disease (VIDA) in NSV patients ($q = -0.435$; $p = 0.018387$), which may indicate that IL- 1β in the initial stages of the disease has a local pathogenic effect on melanocytes (see Table 3).

4. Discussion

Oxidative stress and autoimmunity with genetic susceptibility have been associated with the pathogenesis of AA and vitiligo [2, 18–20]. The correlation between those two pathways

TABLE 1: Demographic and clinical characteristics of patients with alopecia areata (AA), patients with nonsegmental vitiligo (NSV), and healthy controls.

	AA patients	NSV patients	Controls
Total	33	30	30
Female/male, <i>n</i> (%)	21/12, 63.6/36.4	18/12, 60/40	23/7, 76.7/23.3
Average age \pm SD (years)	18.64 \pm 8.56	28.55 \pm 19.23	19.95 \pm 13.08
Female	18.76 \pm 6.33	28.65 \pm 19.58	18.40 \pm 10.72
Male	18.44 \pm 11.85	28.41 \pm 19.54	15.05 \pm 19.13
Mean SALT (AA)/VASI (NSV) \pm SD	42.09% \pm 33.81%	7.49 \pm 8.28	n/a
Mean VIDA \pm SD	3.06 \pm 0.65	2.96 \pm 0.33	n/a
Duration of disease \pm SD	4.33 \pm 5.075	7.63 \pm 12.036	n/a
Age of onset	7.97 \pm 8.17	14.59 \pm 8.25	n/a

Data are expressed in *n*, percentage (%) or mean and standard deviation (SD). SALT: Severity of Alopecia Tool; VASI: Vitiligo Area Scoring Index; VIDA: Vitiligo Disease Activity Score; n/a: not applicable.

TABLE 2: Serum concentrations of IFN- γ , IL-1 β , and IL-6 (pg/ml) among patients with alopecia areata (AA), patients with nonsegmental vitiligo (NSV), and healthy controls and a comparison of *p* values in the Mann-Whitney test among AA patients, NSV patients, and healthy controls. Data were considered to be statistically significant at a value of *p* < 0.05.

	AA patients (<i>n</i> = 33)	NSV patients (<i>n</i> = 30)	Controls (<i>n</i> = 30)	<i>p</i> value (AA patients vs. control)	<i>p</i> value (NSV patients vs. control)	<i>p</i> value (AA patients vs. NSV patients)
IFN- γ , mean \pm SD (pg/ml)	237.68 \pm 55.05	226.10 \pm 50.18	199.59 \pm 41.27	<i>p</i> = 0.007283	<i>p</i> = 0.038467	<i>p</i> > 0.05
IL-1 β , mean \pm SD (pg/ml)	300.09 \pm 87.97	329.72 \pm 85.24	219.61 \pm 60.89	<i>p</i> \leq 0.001	<i>p</i> \leq 0.001	<i>p</i> > 0.05
IL-6, mean \pm SD (pg/ml)	121.38 \pm 31.01	144.95 \pm 33.46	75.26 \pm 21.15	<i>p</i> \leq 0.001	<i>p</i> \leq 0.001	<i>p</i> = 0.004485

Data are expressed in *n*, mean and standard deviation (SD). IL: interleukin; IFN: interferon.

TABLE 3: The correlation between serum levels of interferon γ (IFN- γ), interleukin- (IL-) 1 β , and IL-6 (pg/ml) and extent, activity, and duration of the disease among patients with alopecia areata (AA) and patients with nonsegmental vitiligo (NSV).

Correlation between serum cytokine levels and	Alopecia areata (AA)			Nonsegmental vitiligo (NSV)		
	Extent of AA (SALT)	Activity of AA (VIDA)	Duration of AA	Extent of NSV (VASI)	Activity of NSV (VIDA)	Duration of NSV
IFN- γ (<i>q</i> in the Spearman test/ <i>p</i> value)	-0.055/0.759218	-0.206/0.250208	-0.150/0.421353	-0.055/0.778851	-0.148/0.444011	-0.137/0.478715
IL-1 β (<i>q</i> in the Spearman test/ <i>p</i> value)	0.038/0.833562	0.181/0.314325	-0.073/0.694889	0.383/0.040441	-0.435/0.018387	0.458/0.012573
IL-6 (<i>q</i> in the Spearman test/ <i>p</i> value)	0.116/0.520565	-0.050/0.784260	0.453/0.010474	-0.054/0.779845	-0.190/0.323085	0.222/0.247687

SALT: Severity of Alopecia Tool score; VIDA: Vitiligo Disease Activity Score; VASI: Vitiligo Area Severity Index; IL: interleukin; IFN: interferon.

is not fully understood. Heat-shock proteins, including Hsp60, Hsp70, and gp96, have been shown to exert cytokine-like effects on antigen-presenting cell (APC) maturation. These activities include the ability to enhance tumor necrosis factor- α (TNF- α), IL-1 β , IL-6, and IL-12 secretion from monocytes, macrophages, and dendritic cells (DCs), to enhance surface expression of B7 and major histocompatibility complex (MHC) class II on DCs, to stimulate maturation and migration of DCs to draining lymph nodes, and to induce chemokine secretion by macrophages and DCs [21]. Enhanced Hsp70 is upregulated by IFN- γ from perilesional cytotoxic T lymphocytes (CTLs). Additionally, Hsp70 enhances IFN- γ release from CTLs through a positive feedback mechanism.

The loop amplifies the process and exacerbates the destruction of vitiligo melanocytes [22]. Human genetic studies and functional studies have identified pathways critical for AA development, implicating a role for CD8+ T cells and IFN- γ in mediating hair follicle (HF) damage [23]. The study by Jacquemin et al. revealed that Hsp70 potentiated DNA-induced IFN- α production by plasmacytoid dendritic cells (pDCs) and subsequently IFN- α -induced expression of s and CXCL10 by keratinocytes [24]. Damaged cells upregulate stress ligands and IFN production. IFNs induce CXCL10 secretion from keratinocytes, which then attracts CXCR3-positive T cells [25]. Besides, TNF- α , IL-1 β , and IFN- γ can induce another cytotoxic effector molecule, inducible nitric oxide synthase

(iNOS) [26]. The inflammatory nature of AA/vitiligo and significant psychological stress associated with those diseases may further increase the levels of oxidative parameters.

In this study, we showed that the levels of IFN- γ , IL-1 β , and IL-6 were higher in sera of AA and NSV patients compared to healthy controls. This may imply the role of these cytokines in both disease development and biology. The study has demonstrated the correlations between increased IL-1 β serum levels and the extent of vitiligo (VASI) and also the duration of disease in NSV patients. IL-1 β serum level was negatively correlated with the activity of disease (VIDA). These data may indicate that IL-1 β at the initial stages of development of vitiligo is expressed mainly in the tissue.

We also demonstrated significantly increased IL-6 levels in NSV patients compared to AA patients. As established in previous studies serum IL-6 level increases in chronic diseases depending on the disease severity and location [27]. In our study, IL-6 levels were also positively correlated with the duration of the AA. Singh et al. have revealed similar findings, but in patients with vitiligo in whom the duration of disease was more than 15 years [28].

The studies show that IFN- γ is the key player in xanthine oxidase- (XO-) mediated oxidative stress. The role of xanthine oxidase (XO) in oxidative stress and its association with nitric oxide (NO)/NO synthase (NOS) have been widely reported [29]. Proinflammatory IL-1 β can also induce rapid expression of iNOS and generate a large amount of NO in tissues [30]. Moreover, oxidative stress increases intercellular adhesion molecule-1 (ICAM-1) expression in epithelial cells through the IL-6/AKT/STAT3/NF- κ B-dependent pathway. Several studies indicate that the upregulation of ICAM-1 expression on epithelial cells is closely associated with proinflammatory cytokines, such as IL-6, IL-1 β , and tumor necrosis factor- α (TNF- α) [31]. All those facts suggest an interesting link between oxidative stress and the serum cytokine profile in patients with AA and NSV. It indicates similar pathogenesis of both diseases.

As for the limitations of the study, we would like to mention that the number of subjects in the respective groups is quite small, but we employed suitable statistic methods for such groups. Furthermore, we did not measure direct stress markers such as superoxide dismutase, catalase, glutathione peroxidase, malondialdehyde, superoxide dismutase, catalase, hydrogen peroxide, nitric oxide, or total antioxidant capacity but could be the next step of our further studies in the future.

5. Conclusions

Our results supported the hypothesis that the elevated cytokines identified in this study could be the cause of oxidative stress observed in patients with AA and vitiligo, which can contribute to the onset of autoimmunity in genetically predisposed individuals. It suggests new perspectives in the advances in the understanding of both disease etiopathogenesis which involve interrelationships between oxidative stress and autoimmunity. Further studies exploring the effect of different oxidative stress markers and triggers in AA and vitiligo may be required to develop potential therapeutic

strategies for those diseases. The JAK inhibitors that also suppress the response to oxidative stress have demonstrated promising results in promoting hair regrowth and repigmentation.

Data Availability

The data used to support the findings of this study are available from the corresponding author upon request.

Conflicts of Interest

The authors declare no conflict of interest regarding the publication of this article.

Acknowledgments

This work was supported by the Medical University of Lodz, Poland (grant numbers 502-03/1-137-04/502-14-392-18, 503/1-137-04/503-11-001-18, and 503/5-064-01/503-01).

References

- [1] Q. Deng, J. Wei, P. Zou et al., "Transcriptome analysis and emerging driver identification of CD8+ T cells in patients with vitiligo," *Oxidative Medicine and Cellular Longevity*, vol. 2019, Article ID 2503924, 15 pages, 2019.
- [2] T. Simakou, J. P. Butcher, S. Reid, and F. L. Henriquez, "Alopecia areata: A multifactorial autoimmune condition," *Journal of Autoimmunity*, vol. 98, pp. 74–85, 2019.
- [3] R. Speeckaert and N. van Geel, "Vitiligo: an update on pathophysiology and treatment options," *American Journal of Clinical Dermatology*, vol. 18, no. 6, pp. 733–744, 2017.
- [4] J. C. Boza, N. Giongo, P. MacHado, R. Horn, A. Fabbrin, and T. Cestari, "Quality of Life Impairment in Children and Adults with Vitiligo: A Cross-Sectional Study Based on Dermatology-Specific and Disease-Specific Quality of Life Instruments," *Dermatology*, vol. 232, no. 5, pp. 619–625, 2016.
- [5] L. Y. Liu, B. A. King, and B. G. Craiglow, "Health-related quality of life (HRQoL) among patients with alopecia areata (AA): a systematic review," *Journal of the American Academy of Dermatology*, vol. 75, no. 4, pp. 806–812.e3, 2016.
- [6] F. Rajabi, L. A. Drake, M. M. Senna, and N. Rezaei, "Alopecia areata: a review of disease pathogenesis," *British Journal of Dermatology*, vol. 179, no. 5, pp. 1033–1048, 2018.
- [7] R. M. Trüeb and M. F. R. G. Dias, "Alopecia areata: a comprehensive review of pathogenesis and management," *Clinical Reviews in Allergy and Immunology*, vol. 54, no. 1, pp. 68–87, 2018.
- [8] A. Alikhan, L. M. Felsten, M. Daly, and V. Petronic-Rosic, "Vitiligo: a comprehensive overview," *Journal of the American Academy of Dermatology*, vol. 65, no. 3, pp. 473–491, 2011.
- [9] K. Ezzedine, H. W. Lim, T. Suzuki et al., "Revised classification/nomenclature of vitiligo and related issues: the Vitiligo Global Issues Consensus Conference," *Pigment Cell & Melanoma Research*, vol. 25, no. 3, pp. E1–13, 2012.
- [10] A. Taïeb and M. Picardo, "Vitiligo," *The New England Journal of Medicine*, vol. 360, no. 2, pp. 160–169, 2009.
- [11] V. Dardalhon, T. Korn, V. K. Kuchroo, and A. C. Anderson, "Role of Th1 and Th17 cells in organ-specific autoimmunity," *Journal of Autoimmunity*, vol. 31, no. 3, pp. 252–256, 2008.

- [12] C. Q. F. Wang, A. E. Cruz-Inigo, J. Fuentes-Duculan et al., "Th17 cells and activated dendritic cells are increased in vitiligo lesions," *PLoS One*, vol. 6, no. 4, article e18907, 2011.
- [13] L. Zhou, I. I. Ivanov, R. Spolski et al., "IL-6 programs T_H-17 cell differentiation by promoting sequential engagement of the IL-21 and IL-23 pathways," *Nature Immunology*, vol. 8, no. 9, pp. 967–974, 2007.
- [14] B. Jabri and V. Abadie, "IL-15 functions as a danger signal to regulate tissue-resident T cells and tissue destruction," *Nature Reviews Immunology*, vol. 15, no. 12, pp. 771–783, 2015.
- [15] E. A. Olsen, M. K. Hordinsky, V. H. Price et al., "Alopecia areata investigational assessment guidelines—Part II," *Journal of the American Academy of Dermatology*, vol. 51, no. 3, pp. 440–447, 2004.
- [16] I. Hamzavi, H. Jain, D. McLean, J. Shapiro, H. Zeng, and H. Lui, "Parametric modeling of narrowband UV-B phototherapy for vitiligo using a novel quantitative tool: the Vitiligo Area Scoring Index," *Archives of Dermatology*, vol. 140, no. 6, pp. 677–683, 2004.
- [17] M. D. Njoo, P. K. Das, J. D. Bos, and W. Westerhof, "Association of the Köbner phenomenon with disease activity and therapeutic responsiveness in vitiligo vulgaris," *Archives of Dermatology*, vol. 135, no. 4, pp. 407–413, 1999.
- [18] Y. Wang, S. Li, and C. Li, "Perspectives of new advances in the pathogenesis of vitiligo: from oxidative stress to autoimmunity," *Medical Science Monitor*, vol. 25, pp. 1017–1023, 2019.
- [19] K. Jimbow, H. Chen, J. S. Park, and P. D. Thomas, "Increased sensitivity of melanocytes to oxidative stress and abnormal expression of tyrosinase-related protein in vitiligo," *The British Journal of Dermatology*, vol. 144, no. 1, pp. 55–65, 2001.
- [20] H. A. Al-Shobaili and Z. Rasheed, "Oxidized tyrosinase: a possible antigenic stimulus for non-segmental vitiligo autoantibodies," *Journal of Dermatological Science*, vol. 79, no. 3, pp. 203–213, 2015.
- [21] D. G. Millar, K. M. Garza, B. Odermatt et al., "Hsp70 promotes antigen-presenting cell function and converts T-cell tolerance to autoimmunity *in vivo*," *Nature Medicine*, vol. 9, no. 12, pp. 1469–1476, 2003.
- [22] H. Xie, F. Zhou, L. Liu et al., "Vitiligo: how do oxidative stress-induced autoantigens trigger autoimmunity?," *Journal of Dermatological Science*, vol. 81, no. 1, pp. 3–9, 2016.
- [23] J. E. Harris, "Vitiligo and alopecia areata: apples and oranges?," *Experimental Dermatology*, vol. 22, no. 12, pp. 785–789, 2013.
- [24] C. Jacquemin, J. Rambert, S. Guillet et al., "Heat shock protein 70 potentiates interferon alpha production by plasmacytoid dendritic cells: relevance for cutaneous lupus and vitiligo pathogenesis," *The British Journal of Dermatology*, vol. 177, no. 5, pp. 1367–1375, 2017.
- [25] L. Raam, E. Kaleviste, M. Šunina et al., "Lymphoid stress surveillance response contributes to vitiligo pathogenesis," *Frontiers in Immunology*, vol. 9, 2018.
- [26] V. Ramirez-Ramirez, M. A. Macias-Islas, G. G. Ortiz et al., "Efficacy of fish oil on serum of TNF α , IL-1 β , and IL-6 oxidative stress markers in multiple sclerosis treated with interferon beta-1b," *Oxidative Medicine and Cellular Longevity*, vol. 2013, Article ID 709493, 8 pages, 2013.
- [27] M. Narazaki and T. Kishimoto, "The two-faced cytokine IL-6 in host defense and diseases," *International journal of molecular sciences*, vol. 19, no. 11, 2018.
- [28] S. Singh, U. Singh, and S. S. Pandey, "Serum concentration of IL-6, IL-2, TNF- α , and IFN γ in Vitiligo patients," *Indian Journal of Dermatology*, vol. 57, no. 1, pp. 12–14, 2012.
- [29] D. Singh, V. Kumar, and C. Singh, "IFN- γ regulates xanthine oxidase-mediated iNOS-independent oxidative stress in maneb- and paraquat-treated rat polymorphonuclear leukocytes," *Molecular and Cellular Biochemistry*, vol. 427, no. 1–2, pp. 133–143, 2017.
- [30] R. Gu, Y. Shi, W. Huang et al., "Theobromine mitigates IL-1 β -induced oxidative stress, inflammatory response, and degradation of type II collagen in human chondrocytes," *International Immunopharmacology*, vol. 82, article 106226, 2020.
- [31] C. W. Liu, T. L. Lee, Y. C. Chen et al., "PM2.5-induced oxidative stress increases intercellular adhesion molecule-1 expression in lung epithelial cells through the IL-6/AKT/STAT3/NF-KB-dependent pathway," *Particle and Fibre Toxicology*, vol. 15, no. 1, 2018.

Review Article

Ellagic Acid-Derived Urolithins as Modulators of Oxidative Stress

Jasmina Djedjibegovic ¹, Aleksandra Marjanovic,¹ Emiliano Panieri ²,
and Luciano Saso ²

¹Faculty of Pharmacy, University of Sarajevo, Zmaja od Bosne 8, 71000 Sarajevo, Bosnia and Herzegovina

²Department of Physiology and Pharmacology “Vittorio Erspamer”, Sapienza University, P.le Aldo Moro 5, 00185 Rome, Italy

Correspondence should be addressed to Jasmina Djedjibegovic; djedjibegovic@gmail.com

Received 29 April 2020; Accepted 6 July 2020; Published 28 July 2020

Academic Editor: Fabiana Morroni

Copyright © 2020 Jasmina Djedjibegovic et al. This is an open access article distributed under the Creative Commons Attribution License, which permits unrestricted use, distribution, and reproduction in any medium, provided the original work is properly cited.

Oxidative stress is a state of excess of prooxidative species relative to the antioxidant defenses (enzymatic and nonenzymatic) in a living organism. The consequence of this imbalance is damage of the major cellular macromolecules (carbohydrates, lipids, proteins, and DNA), which further leads to a gradual loss of tissue and organ function. It has been shown that oxidative stress plays an important role in the pathogenesis of many chronic diseases (cardiovascular, metabolic, and neurodegenerative diseases and cancer) and in the process of aging. Thus, many strategies to combat oxidative stress have been proposed and tested. In this context, food rich in antioxidants has received great attention. Pomegranate, berries, and walnuts have been recognized as “superfood” particularly for their cardioprotective effects. The common characteristic of these foods is the high content of ellagitannins. Since tannins are not bioavailable, they have been neglected in nutrition science and even considered antinutrients for a long time. However, this view has changed dramatically once it was recognized that ellagic acid, released from ellagitannins in the gastrointestinal system, is further metabolized by colonic microbiota to bioavailable compounds—known as urolithins. Thus, urolithins (3,4-benzocoumarin derivatives) have emerged as novel natural bioactive compounds and are now the focus of extensive investigations. So far, urolithins were shown to be powerful modulators of oxidative stress and agents with potential anti-inflammatory, antiproliferative, and antiaging properties. Furthermore, a few synthetic derivatives of urolithins were recognized as lead compounds for new drug development. Available data on urolithin synthesis, physicochemical and pharmacokinetic characteristics, biological activity, and safety will be presented in this review.

1. Introduction

Urolithins are a subgroup of dibenzo[b,d]pyran-6-ones (also named 3,4-benzocoumarins or dibenzo- α -pyrones) which were first isolated from natural sources (beaver scent glands) in 1949 [1]. Thereafter, their presence has been confirmed in many microorganisms, plants, human feces, and animal waste [2, 3]. Dibenzo[b,d]pyran-6-ones are biosynthesized by microorganisms, mostly by fungi through the polyketide pathway. Their presence in plants and animal and human intestines is probably a result of bacterial metabolism of ellagic acid [3]. Various dibenzo[b,d]pyran-6-ones detected in extracts of medicinal plants were described by Y. L. Garazd and M. M. Garazd [4], while those produced by fungi were

described by Mao et al. [3]. Some of these compounds are toxic to humans and animals (mycotoxins), while the others show a number of beneficial health effects (antioxidant, anti-allergic, antimicrobial, anti-inflammatory, antiproliferative, etc.) [3, 4].

In contrast to their structural homolog coumarin, the research on urolithins (and their natural precursor ellagic acid) has only started in the previous decade (Figure 1). Yet, the data collected so far are promising and support further research in this field. The focus of this review is ellagic acid-derived urolithins as bioactive compounds. Urolithins are attractive both as nutraceuticals and as intermediates in the development of novel pharmacological compounds (drugs). Data on their (bio) synthesis, pharmacokinetics,

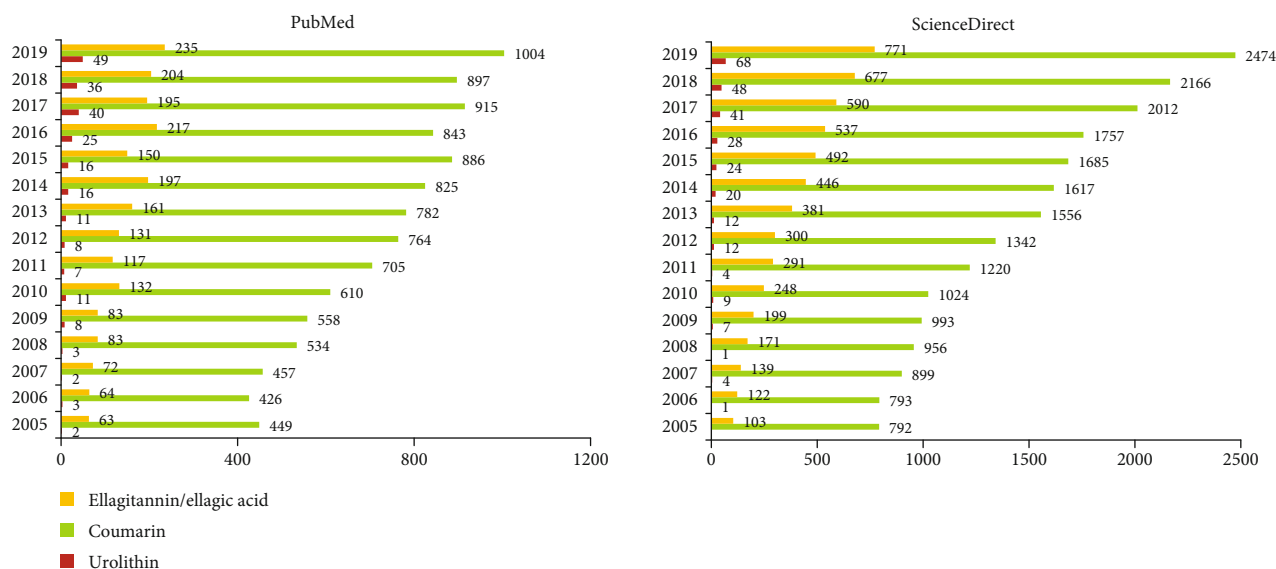


FIGURE 1: Timeline of published papers (number per year) corresponding to the keywords “uroolithin”, “ellagitannins OR ‘ellagic acid’”, and “coumarin”.

biological activity in the modulation of oxidative stress, and safety will be presented in the present review.

2. Urolithin Production by the Gut Microbiome

Ellagic acid, mainly in the form of ellagitannins, is present in various medicinal and edible plants. High concentrations found in berries, pomegranate, and nuts make these foods good dietary sources [5]. During digestion, ellagitannins are converted to ellagic acid which is further metabolized by the gut microbiota to various dibenzo[b,d]pyran-6-one derivatives, named urolithins [6]. After cleavage and decarboxylation of one lactone ring in the molecule of ellagic acid, further metabolism occurs through a series of dehydroxylation reactions (Figure 2).

Contrary to poorly bioavailable ellagic acid, urolithins are more easily absorbed and have been detected in the circulation (mainly as glucuronide, sulfate, or methyl derivatives) at high nM to low μ M concentrations [7]. It is believed that urolithins are responsible for the many health effects of ellagic acid, ellagitannins, and food rich in these compounds. Urolithin presence in plasma and urine persists for a couple of days after oral intake, probably due to enterohepatic recirculation [8, 9]. The main isomers found in human biological fluids and tissues after ingestion of ellagitannin-rich food are urolithin A and urolithin B. A novel metabolite was recently identified in human feces, although the study was conducted on a limited number of participants [10].

Urolithin production in the intestine is dependent on the host microbiome, and three distinct metabotypes have been identified: A (producing only urolithin A), B (producing urolithin A, urolithin B, and isourolithin A), and 0 (only negligible urolithin production). These metabotypes seem to be quite stable and independent of food source, age, and health status [11]. The recognition of metabotype is essential in dietary intervention studies, but it also suggests that the exact

amount of urolithins produced and absorbed from various dietary sources might be hardly estimated, especially when considering the effect of a dietary matrix, ellagitannin structures, and its variable food concentrations. In this regard, direct urolithin consumption as a dietary supplement might be a promising approach.

3. Urolithin Synthesis and Physicochemical Characteristics

Besides their biological activities, urolithins are also important intermediates in the synthesis of various dibenzopyrone derivatives with potential pharmaceutical use. For example, 4-bromo urolithin A was recently shown to be a very potent casein kinase 2 inhibitor [12]. On the other hand, urolithin B derivatives showed remarkable cholinesterase inhibitory activity which was comparable to that of galantamine and higher than that of rivastigmine [13]. Therefore, methods for efficient synthesis of these compounds are intensively developing.

Different strategies for urolithin synthesis were reported in the literature (e.g., copper-catalyzed Hurdley reaction, ellagic acid decarboxylative hydrolysis, inverse electron demand Diels–Alder reaction, and 2-bromobenzoic acid esterification followed by the Heck coupling) [14, 15]. Examples of urolithin synthesis are shown in Figure 3.

Urolithins have a molecular mass of less than 300 g/mol (e.g., 276.2 g/mol for urolithin M5 and 212.2 for urolithin B). The log *p* value is 2.7 for monohydroxy urolithin B, 1.1 for urolithin B glucuronide, and 1.3 for pentahydroxy urolithin M5. The number of hydrogen bond acceptors is typically less than 10 (e.g., 3 in urolithin B and 9 in its glucuronide), and the number of hydrogen bond donors is ≤ 5 (1 in urolithin B, 4 in urolithin B glucuronide, and 5 in urolithin M). Thus, these molecules do not show violations of Lipinski’s “rule of five” [22, 23]. Furthermore, urolithins have 0

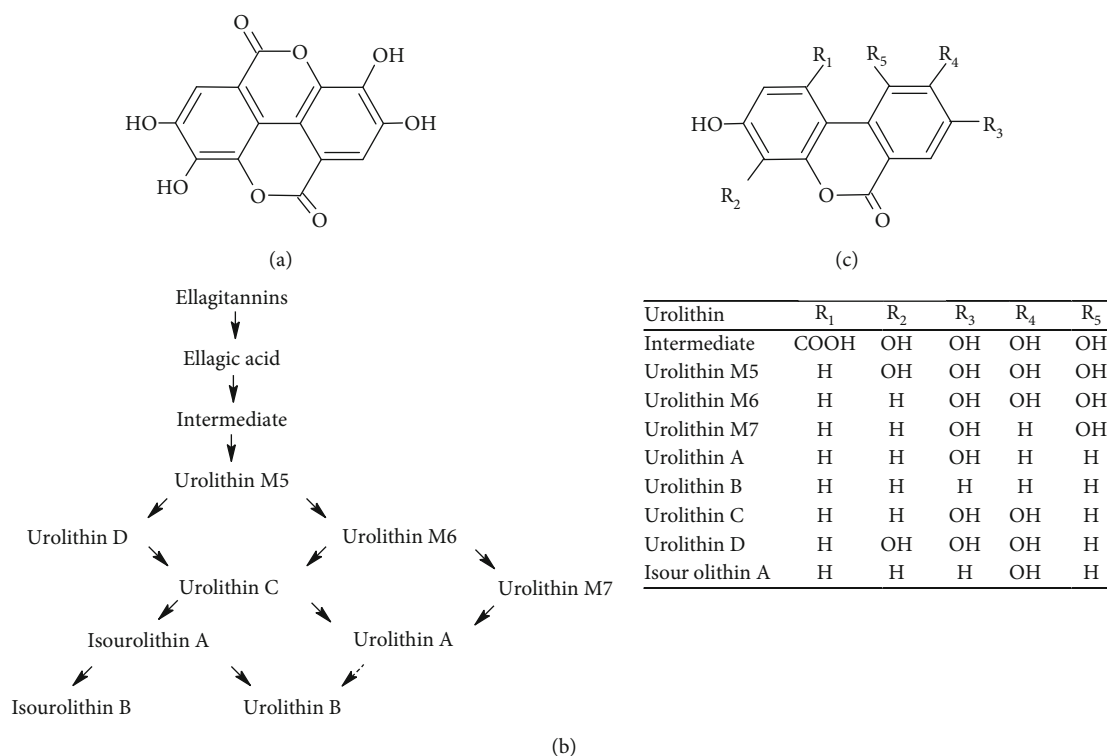


FIGURE 2: (a) Structure of ellagic acid, (b) diagram of its metabolism by the gut microbiota, and (c) structures of various urolithins.

rotatable bonds (up to 3 when glucuronidated), and the polar surface area is typically $<130 \text{ \AA}^2$ (143 \AA^2 for urolithin B glucuronide). Veber's rule states that a compound with ≤ 10 rotatable bonds and polar surface area $\leq 140 \text{ \AA}^2$ (or 12 or fewer hydrogen bond donors and acceptors) most likely will have a good oral bioavailability [24]. Another set of rules to be used in assessing "drug-likeness" of a certain compound were described by Ghose and coworkers and thus are commonly known as the Ghose filter. This filter defines the following "drug-likeness" constraints: $\log p$ is between -0.4 and 5.6 , molecular weight ranges from 160 to 480 , molar refractivity ranges from 40 to 130 , and the total number of atoms is 20 to 70 [25]. The molar refractivity values of urolithin B, urolithin B glucuronide, and urolithin M5 are 58.3 , 94.75 , and 64.9 , respectively. The total number of atoms in a molecule is between 20 and 70 for both urolithins and their glucuronides. Urolithins were recently assessed through the SwissADME web tool which provides researchers with a pool of predictive models for physicochemical properties, as well as pharmacokinetics, and drug-likeness [26]. The analysis showed high gastrointestinal absorption for urolithin B, but low absorption for urolithin M and urolithin B glucuronide. The software also predicted that urolithin B can cross the blood-brain barrier and act as the CYP1A2 inhibitor, in contrast with the urolithin B glucuronide or the highly hydroxylated urolithin M5. Moreover, none of these three substances appeared to be a substrate for P-glycoprotein (P-gp) which is normally responsible for the extrusion of the intracellular xenobiotics and thereby a factor limiting the efficacy of some drugs and other bioactive compounds. Still, it must be noted

that some *in vitro* results suggest that P-gp and other ABC transporters (MRP, ABCG2/BCRP) might play a role in the urolithin transport and metabolism in certain cell lines (HT-29, MDCKII) [27]. In a quite recent study, urolithin B was detected in the brain of rats upon intravenous administration, confirming that this compound can cross the blood brain barrier, consistently with the software prediction [28].

4. Urolithin Pharmacokinetic Characteristics and Safety

Considering direct urolithin consumption, the first issue that has to be addressed is their stability in the gastrointestinal system. Using an *in vitro* digestion model (a sequence of oral, gastric, and pancreatic digestion, followed by a 24 h fecal fermentation), Mena et al. showed that urolithin B was more stable than urolithin B glucuronide and urolithin A. The recovery (% of the initial quantity) at the end of the last (colonic) step was $47 \pm 8\%$ for urolithin B, $30 \pm 4\%$ for urolithin B glucuronide (recovered as urolithin B, indicating a complete deglucuronidation during colonic fermentation), and $16 \pm 5\%$ for urolithin A [29]. However, this study proved the bioaccessibility of orally administered urolithin isomers. Bioavailability (i.e., the actual absorption in the circulation) after direct urolithin administration was tested only for urolithin A in healthy elderly subjects. Dose-dependent increase in maximum plasma concentration (C_{\max}) and total exposure (AUC) was observed (dose range of 250 - 1000 mg). The highest plasma concentration was found for urolithin A glucuronide, followed by urolithin A sulfate, and the parent

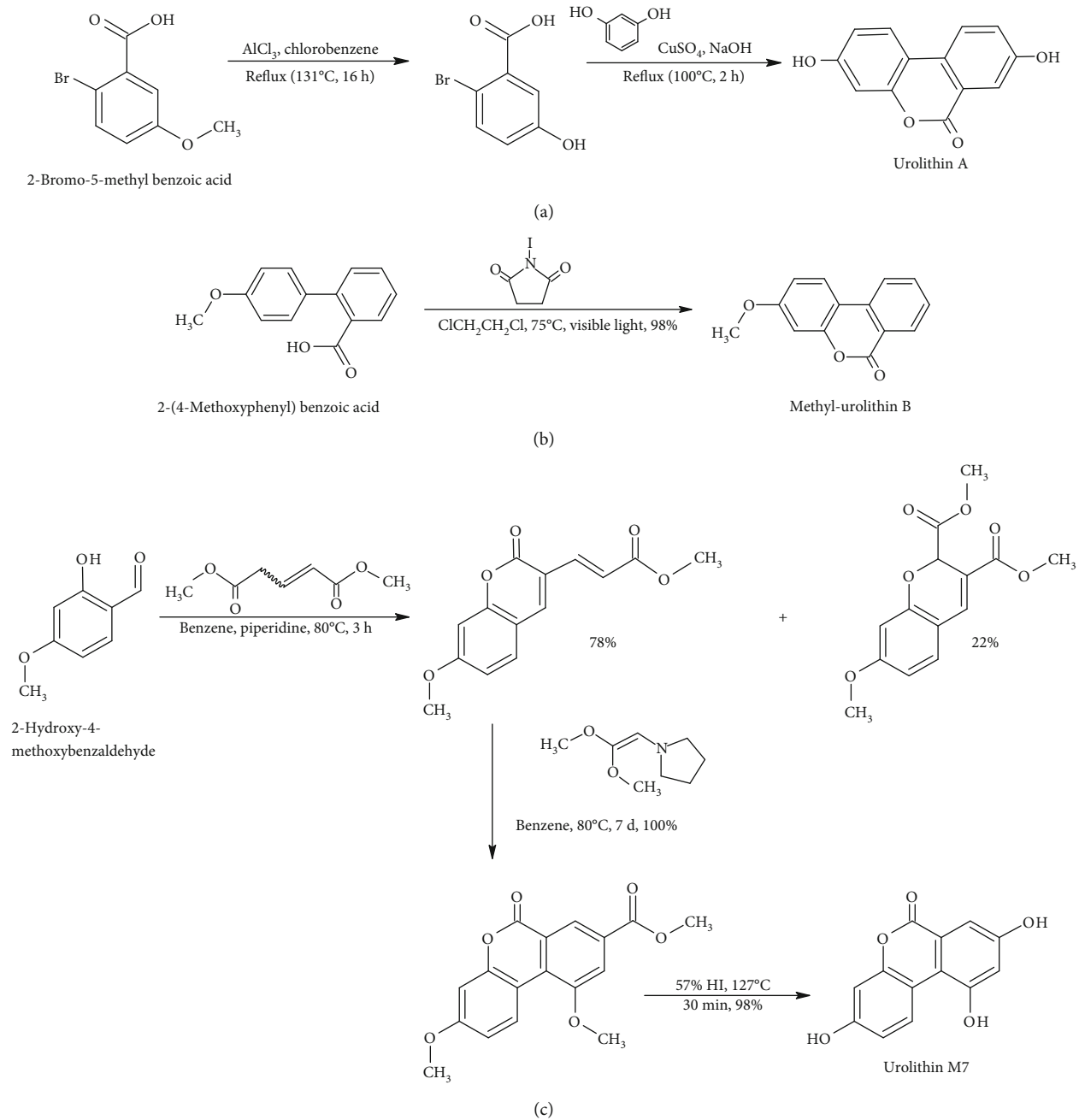


FIGURE 3: Continued.

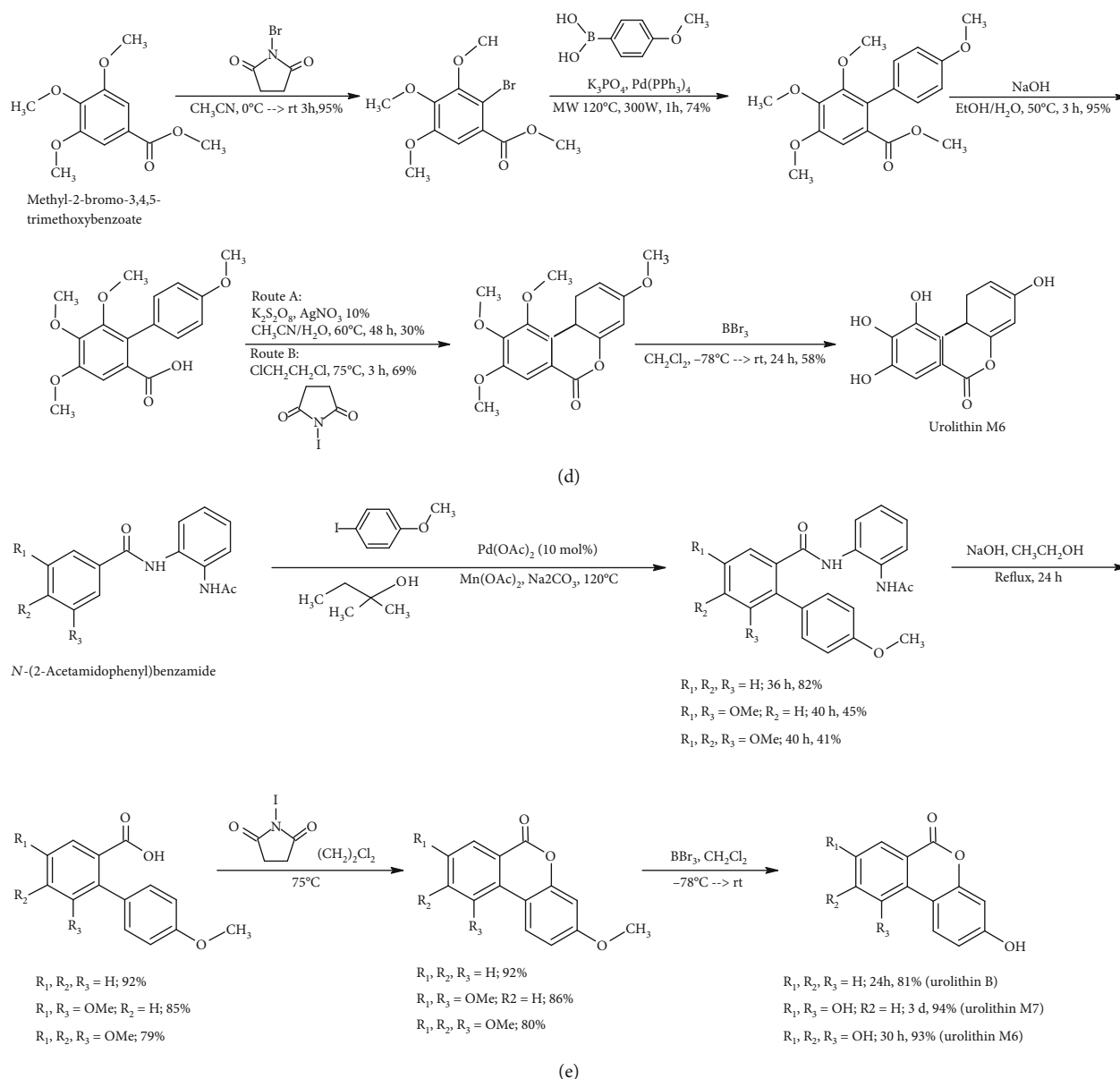


FIGURE 3: Strategies in urolithin synthesis: (a) from References [16, 17], (b) from Reference [18], (c) from Reference [19], (d) from Reference [20], and (e) from Reference [21].

compound with the dose-dependent corresponding C_{\max} in ranges 1500–3000 nM, 200–400 nM, and 4–7 nM, respectively. The time to maximum concentration (T_{\max}) was 6 hours for all three compounds after administration of two lower doses (250 and 500 mg), while it was somewhat longer for the highest dose (1000 mg). The biphasic kinetics was shown for metabolites, probably due to enterohepatic circulation. The half-life ($t_{1/2}$) ranged from 17 to 22 hours for the parent compound and urolithin glucuronide, while it was slightly longer (25–58 hours) for urolithin A sulfate. All the three compounds were eliminated from circulation in 72–96 hours. During 4 weeks of administration, a dose-dependent increase was also observed in total urolithin A (parent compound + metabolites) steady-state concentrations ranging from about 400 ng/mL for the lowest dose to about 600 ng/mL for the

highest dose. The authors reported no accumulation in plasma after multiple-dose as compared to single-dose pharmacokinetics. Urolithin A was detected in muscle tissue in a concentration of about 6 ng/g tissue 8 hours after an oral dose of 2000 mg, mostly as a parent compound with only traces of urolithin A glucuronide found in two out of six participants [30]. This is an important finding since tissue distribution and cell availability of many natural compounds are often an issue. As already mentioned, urolithin glucuronides (the main form in the circulation) are quite large molecules with a lot of polar groups and their transmembrane transport is expected to be low. Moreover, according to some authors, it is possible that phase II metabolism could hamper urolithin activity. However, novel findings indicate that tissue availability of urolithins could actually be higher than expected

due to the *in situ* deglucuronidation process. Ávila-Gálvez et al. described tissue deglucuronidation of urolithin A glucuronide in response to lipopolysaccharide-induced systemic inflammation in male Sprague-Dawley rats [31]. The authors observed a dramatic and statistically significant decrease in the urolithin A glucuronide/urolithin A ratio in all the tested organs of treated rats vs. controls, including the small intestine, liver, kidney, bladder, spleen, and lung as well as the urine. However, further research is needed to elucidate the precise mechanisms underlying this process. Piwowarski et al. also tested the effect of the inflammation on urolithin glucuronides. Here, the glucuronides of urolithin A, isourolithin A, and urolithin B isolated from the urine of a volunteer after ingestion of ellagitannin-rich food were shown to be cleaved by β -glucuronidase released from human neutrophils (upon *N*-formylmethionine-leucyl-phenylalanine stimulation), *Escherichia coli* standard strains, and clinical samples from patients with urinary tract infections [32]. Since β -glucuronidase is present at high concentrations in the sites of inflammation as well as in a tumor microenvironment, this could be one of the biologically relevant mechanisms underlying the protective effects of urolithins reported from many *in vitro* tests and suggested by epidemiological studies. Of note, some of the protective effects were also shown for glucuronide metabolites and not only for urolithin aglycone forms [14, 33]. On the other hand, it appears that urolithin metabolism could be cell-specific. A remarkable difference was reported from a study on the effects of urolithin aglycones (urolithin A, urolithin B, and isourolithin A) and their metabolites (sulfates and glucuronides) in two types of human breast carcinoma, MDA-MB-231 and MCF-7. In contrast to MDA-MB-231 cells, in MCF-7 cells, urolithins were metabolized much faster and mainly to sulfate, which did not exert any antiproliferative or estrogenic/antiestrogenic activity [34].

Regarding urolithins' safety upon direct consumption, we were able to identify only one toxicological study for urolithin A and none for the other isomers. The battery of genotoxicity assays (Ames test and *in vivo* and *in vitro* micronucleus assay, both with and without S9 metabolic activation) demonstrated that urolithin A is not genotoxic. After both oral and intravenous administrations to Wistar rats, the predominant metabolites were glucuronide and sulfate. After oral administration (1000 mg/kg bw), wide tissue distribution was found, although with the highest recovery in the gastrointestinal tract. The authors reported negative results for overall and organ toxicity after 28- and 90-day studies. The NOAEL was the highest dose applied (3451 mg/kg bw/day in males and 3826 mg/kg bw/day in females), corresponding to a human equivalent dose of approximately 557 mg/kg bw/day in males and 617 mg/kg bw/day in females [35].

In the urolithin A study in the elderly healthy volunteers, six adverse events were recorded in a single dose testing (2 in a placebo group of 6 participants and 4 in a test group of 18 participants). In a 28-day multiple ascending dose trial, 31 adverse effects were recorded in total (7 in a placebo group of 9 participants and 24 in a treatment group of 27 participants). All the adverse effects were mild to moderate and with

one single exception were assessed to be unrelated or unlikely to be related to the product tested. There were no dropouts during the study and no reports of any clinical or laboratory abnormalities up to a dose of 2000 mg of urolithin A (the highest dose tested) [30].

Based mostly on the above presented findings, urolithin A already received a favorable review by the US FDA (Food and Drug Administration) under their generally recognized as safe (GRAS) notification program and can be used as a food ingredient at levels up to 1000 mg/serving, which is estimated to result in (applicant-reported) mean dietary exposure to urolithin A of 1183 mg/day in the consumers [36]. For comparison, the mean estimated dietary exposure to urolithin A (from ellagic acid in food) based on food consumption data from the 2013–2014 National Health and Nutrition Examination Survey reported by an applicant was 3.0 to 15.9 mg/day. The application for approval of urolithin A as a novel food was also submitted to EFSA (European Food Safety Authority) and is currently being processed. Although it is clear that urolithins are produced from ellagic acid in the human intestine, they are not known to be present in food and need to get approval before being used as nutritive additives or dietary supplements.

5. Urolithin Activity in the Modulation of Oxidative Stress

Oxidative stress is a state of excess of prooxidative species (primarily reactive oxygen species (ROS) and reactive nitrogen species (NOS)) relative to the antioxidant defenses (enzymatic and nonenzymatic) in a living cell or an organism. The consequence of this imbalance is damage to a variable extent to the major cellular macromolecules (carbohydrates, lipids, proteins, and DNA), which further leads to a gradual loss of tissue and organ function. It has been shown that oxidative stress plays an important role in the pathogenesis of many chronic diseases (cardiovascular, metabolic, and neurodegenerative diseases and cancer) and in the process of aging [37, 38]. Thus, various natural sources (food and medicinal plants) are tested for their ability to combat oxidative stress. In that respect, the identification of bioactive compounds and their mechanism of action is crucially important. Besides a direct antioxidative effect via radical scavenging, which can be easily measured *in vitro* but often fails to be clinically relevant, oxidative stress modulators can also modulate the activity of different cellular pathways that control the redox homeostasis *in vivo* [39, 40]. Of note, ellagic acid-derived urolithins were recently recognized as emerging oxidative stress modulators.

In order to comprehensively evaluate the antioxidative potency of seven different urolithins, Bialonska et al. applied a cellular assay which allows estimation of the cellular bioavailability of the test compounds and enables the detection of their antioxidative activity. Antioxidant activity in myelomonocytic HL-60 cells treated with phorbol-12-myristate-13 acetate (PMA) was determined by the DCFH-DA (2',7'-dichlorodihydrofluorescein diacetate) method. The test measures the ability of the investigated compounds (urolithin A; urolithin B; urolithin C; urolithin D; 8-O-methylurolithin A;

8,9-di-O-methyluroolithin C; and 8,9-di-O-methyluroolithin D) to inhibit the DCFH oxidation by the generated ROS. The results of this study revealed that the antioxidative activity of urolithins was correlated with the number of OH groups and lipophilicity of the molecules. The highest antioxidant activity was detected for urolithin C ($IC_{50} = 0.16 \mu M$) and urolithin D ($IC_{50} = 0.33 \mu M$). Urolithin A showed less significant antioxidant activity ($IC_{50} = 13.6 \mu M$), while urolithin B and all the methylated urolithins did not show antioxidant activity at all. The overall conclusion of this study was that urolithins may account for systemic antioxidant effects [17].

So far, dual redox nature of plant-derived polyphenols is widely known, making it necessary to investigate not only the antioxidant but also the prooxidant capacities of these compounds, since their physiological actions may depend upon their behavior as either an antioxidant or a prooxidant. Kallio et al. conducted for the first time a study to investigate the prooxidant properties of urolithins. Besides that, the aim was also to characterize the antioxidant properties of urolithins A and B using the *in vitro* ORAC assay, cell-based assays, and electrochemistry. In addition to redox properties, potential antiproliferative effects on HepG2 cells were also investigated. The ORAC values for ellagic acid (4.35 Trolox equivalent), urolithin A (6.67 Trolox equivalent), and urolithin B (5.77 Trolox equivalent) were two times lower than ORAC values for quercetin. The ratios between the ORAC values for urolithins and ellagic acid were 1.53 for urolithin A and 1.33 for urolithin B, so these ellagic acid metabolites can be described as relatively strong antioxidants. In a cell-based antioxidant activity assay on the promyelocytic cell line HL-60, wherein a reporter dye is oxidized by peroxy radicals, urolithin A showed antioxidative action, while urolithin B did not show any obvious concentration-dependent antioxidant or prooxidant activity in the cell cultured medium. However, when the intracellular antioxidant activity was assessed, urolithins A and B showed no antioxidant properties, while instead they acted as prooxidants. In a copper-initiated prooxidant activity (CIPA) assay, both urolithins A and B were prooxidants, whereas urolithin A showed a stronger prooxidant activity. The authors further investigated the electrochemical oxidation of urolithins with cyclic voltammetry (CV) employing screen-printed carbon electrodes. The cyclic voltammograms of urolithin A showed both anodic and cathodic peaks at each scan rate. The cyclic voltammogram of urolithin B revealed an irreversible redox reaction as no cathodic peak was observed. Moreover, urolithins A and B caused significant decrease in the proliferation of HepG2 cells after 48 h incubation, while ellagic acid did not induce any changes in cell proliferation [41].

Mazumder et al. made an *in silico* investigation on the inhibitory potential of the constituents of pomegranate juice on the antioxidant defense mechanism. They hypothesized that although polyphenols present in pomegranate juice may scavenge free radicals and exert antioxidant activity, different compounds may interfere with enzymes involved in the antioxidant defense mechanisms and thereby paradoxically contribute to oxidative stress. This study was conducted to elucidate the potential of different constituents of pomegranate juice and their metabolites in affecting the cellular

antioxidant defense system, using computational modeling analysis. Results showed that among others, urolithin A, urolithin A glucuronide, and urolithin B have the potential to inhibit catalase, SOD (superoxide dismutase), GR (glutathione reductase), GPx (glutathione peroxidase), and GST (glutathione-S-transferase), by interfering with their active catalytic sites. These findings suggest that these compounds can act both as prooxidants and as antioxidants [42].

The phosphatidylinositol-3-kinase (PI3K)/Akt pathway is responsible for many important cellular processes, including protein synthesis, proliferation, apoptosis, autophagy, glucose uptake, and metabolism. This pathway, among the other functions, mediates the metabolic effects of insulin at the cellular level. ROS at the same time activate PI3K and inactivate phosphatase and tensin homolog (PTEN), which is a negative regulator of Akt. Akt is activated through the phosphorylation at serine (Ser473) or threonine (Thr308) sites. Previously, it was reported that this activation is dependent on oxidative stress levels. Endothelial Akt-kinase plays a key role in the pathogenesis of cardiovascular complications in type 2 diabetes mellitus (T2DM), and therefore, the modulation of its activity would be of great physiopathological importance. Dirimanov and Högger conducted a study to identify subclasses of polyphenols, including urolithins, that can modulate the PI3K/Akt signaling pathway and thus be effective in the prevention and management of late T2DM complications. Here, the quantitative effects of the investigated compounds in endothelial cells *in vitro* were determined by ELISA and confirmed by Western blot analysis. Urolithin A showed significant and reproducible inhibition of Akt phosphorylation ($35 \pm 12\%$, $n = 6$, $p = 0.001$). Other urolithins (urolithins B, C, and D) did not show statistically significant inhibitory effects. Among urolithins, differences in inhibitory effects were recorded, most likely related to the different structures. Indeed, the presence of two OH groups at the C₃ and C₈ positions in urolithin A appeared to be important for the inhibitory effects [43]. Similar results were reported in two other studies of Komatsu et al. [44] and Piwowarski et al. [45] that were aimed at evaluating the anti-inflammatory potential of urolithins and their underlying mechanisms in lipopolysaccharide- (LPS-) stimulated murine RAW264 macrophages.

ROS are known proinflammatory mediators which can activate microglia and cause chronic neuroinflammation resulting in the onset of neurodegenerative diseases. Lee et al. investigated the antioxidant and anti-inflammatory effects of urolithin B in activated microglia. According to the results of Western blot analyses, urolithin B increased AMPK phosphorylation and decreased Akt, JNK, and ERK phosphorylation without affecting phospho-p38. These findings suggest a possible mechanism of anti-inflammatory activity. Urolithin B also showed antioxidant effects by inhibiting intracellular ROS production in LPS- (lipopolysaccharides from *Escherichia coli* serotype 055:B5) stimulated BV2 microglial cells. The probable mechanism of antioxidative action appears to be the inhibition of NADPH oxidase subunits along with the upregulation of heme oxygenase-1 (HO-1) [46]. Similarly, Xu et al. in their study concluded that urolithins A and B inhibit LPS-induced inflammation of

microglia through the inhibition of the NF- κ B, MAPK, and PI3K/Akt signaling pathways [47].

At both cellular and molecular levels, inflammation has an important role in initiating and accelerating osteoarthritis development. Ding et al. conducted a study to investigate the possible anti-inflammatory action of urolithin A related to the attenuation of IL-1 β -induced degradation of collagen II and aggrecan and the decreased production of inflammatory mediators via the ERK, JNK, p38, and NF- κ B pathways in rat chondrocytes. Results showed that the MAPK and NF- κ B pathways were involved in the protective effects of urolithin A since this metabolite inhibited the phosphorylation of MAPK pathway members thus protecting chondrocytes against IL- β -induced inflammation injury. The overall conclusion of this study was that urolithin A is a promising possible therapeutic agent for the treatment of osteoarthritis [48]. Importantly, the results of this study confirmed those previously reported by Fu et al. [49].

In another study, González-Sarriás et al. showed that urolithins (Uro-A, Uro-B, Uro-C, and Uro-D) and urolithin glucuronide conjugates in blood exerted potent protection against H₂O₂-induced cell injury. Results of the study revealed that neither the different hydroxylation patterns of urolithins nor the phase II metabolism was critical for their neuroprotective effects. No differences were observed among all the urolithins' aglycone and glucuronide conjugates, except for the Uro-B. Pretreatment with Uro-A significantly decreased the percentage of late apoptosis (12%, $p < 0.05$) in human neuroblastoma SH-SY5Y cells, compared to H₂O₂ treatment alone. Urolithins reduced intracellular ROS levels, increased mitochondrial oxidation-reduction activity, and decreased apoptosis induced by oxidative stress, by preventing the caspase-3 activation. The authors also noted that these neuroprotective effects of urolithins were less pronounced than those obtained with ellagic acid under the same conditions [50]. However, in consideration of the already discussed issues regarding ellagic acid metabolism and absorption, it seems to be at least questionable that ellagic acid might reach the effective concentration in the brain tissue.

Similar findings on LPS-BV-2 microglial cells and human neuroblastoma SH-SY5Y cells were reported in another study by DaSilva et al. [51].

It is well known that redox status has a great impact on the development of neurodegenerative diseases. Therefore, Cásedas et al. investigated whether urolithin A could have antioxidative and neuroprotective effects on the murine Neuro-2a neuroblastoma cell line. Results showed that urolithin A had a great antioxidant capacity, as measured in the ORAC test (13.1 μ mol TE/mg) and exerted a number of cytoprotective effects. Indeed, this metabolite improved mitochondrial activity in cells exposed to H₂O₂, decreased lipid peroxidation in cells subjected to oxidative stress, enhanced the activity of superoxide dismutase (SOD), catalase (CAT), glutathione reductase (GR), and glutathione peroxidase (GPx), and dose-dependently increased the expression of peroxiredoxins 1 and 3 (Prx1 and Prx3) compared to control [52].

A study of Chen et al. tested the neuroprotective effect of urolithin A on H₂O₂-induced oxidative injury in PC12

(pheochromocytoma) cells. Results showed that urolithin A effectively prevented H₂O₂-induced apoptosis in PC12 cells by markedly regulating in the opposite ways the protein levels of caspase-3 and Bcl-2 (both $p < 0.01$). The *in vivo* D-galactose-induced brain aging model showed that urolithin A significantly suppressed the upregulation of miR-34a induced by D-galactose. The overall conclusion was that urolithin A may have neuroprotective effects, especially in preventing D-gal-induced brain aging through the activation of the miR-34a-mediated SIRT1/mTOR signaling pathway [53].

Later on, Zheng et al. conducted a study on possible protective effects and molecular mechanisms of urolithin B on myocardial ischemia/reperfusion (IR) injury. Here, treatment with urolithin B significantly decreased the levels of superoxide anion radicals and lipid peroxidation products in H9c2 cells, restoring also the SOD expression. To examine the potential role of autophagy in the protective effects of urolithin B, levels of LC3 and p62 were determined. IR increased the ratio of LC3II/I and conversely decreased p62 levels, which were significantly reversed by urolithin B treatment. Accumulation of p62 and its interaction with KEAP1 had an important role in the antioxidative effects mediated by urolithin B, promoting Nrf2 nuclear translocation and subsequent expression of antioxidant enzymes such as HO-1, GSTP1, and NQO1. Results suggested that protective effects of urolithin B could be partially due to the modulation of autophagy [54]. Additionally, Tang et al. revealed that urolithin A could reduce myocardial apoptosis following ischemia/reperfusion. The authors concluded that the protective effect of urolithin on cardiomyocyte apoptosis during hypoxia/reoxygenation injury was at least partially mediated by the activation of the PI3K/Akt signaling pathway [55].

Nonenzymatic protein glycation reactions are usually observed in conditions related to oxidative stress. As a result, advanced glycation end products (AGEs) are formed and can be accumulated mainly in proteins with a long half-life, altering their structural and functional properties. It seems that AGEs have a significant role in the progression of cardiovascular complications associated with diabetes and also Alzheimer's disease and neuropathy. In this regard, Verzeloni et al. investigated the inhibitory activity of urolithins A and B against AGE formation, using concentrations that can be reached *in vivo* and assessing their ability to counteract mild oxidative stress in cultured human neuron cells. They also evaluated iron chelation ability with a ferrozine assay and radical scavenging activity, which was measured with the ABTS (2,2'-azino-bis(3-ethylbenzothiazoline-6-sulfonic acid)) assay. The results showed that urolithins A and B at the lowest concentrations of 0.5 μ mol/L had weak antiglycative activity, while their activity was much stronger when higher concentrations (1 μ mol/L) were used. Urolithin A had substantial antiglycative activity at the highest concentration (10 μ mol/L). The antiglycative activity of urolithin B at the highest concentration (10 μ mol/L) was only slightly higher than that observed at 1 μ mol/L. Both urolithins showed much higher activity than all the other colonic polyphenol metabolites tested, including pyrogallol (raspberry/pomegranate "ellagitannin group"), colonic

metabolites of “coffee group” polyphenols (dihydrocaffeic acid, dihydroferulic acid, and feruloylglycine), and “berry/red wine anthocyanin group” polyphenols (3-hydroxyphenylacetic acid, 3,4-dihydroxyphenylacetic acid, and 3-methoxy-4-hydroxyphenylacetic acid). In the ABTS assay, both of urolithins showed low activity, therefore suggesting that the antiglycative effect was not exclusively related to their antioxidant capacity. Neither of the urolithins was able to bind iron at 50 $\mu\text{mol/L}$. Urolithin B showed stronger neuroprotective effects compared to urolithin A and all the other tested metabolites *in vitro*. Both urolithins showed protective effects with an increase in cellular viability after induction of oxidative stress with 2,3-dimethoxy-1,4-naphthoquinone (DMNQ) [56]. Kim et al. examined possible mechanisms of neuroprotective action of urolithin A against H_2O_2 -induced oxidative stress *in vitro*. Here, after treatment with urolithin A, the expressions of cytochrome c, cleaved caspase-9, cleaved caspase-3, and cleaved poly (ADP-ribose) polymerase (PARP) were suppressed, confirming that urolithin A attenuated apoptotic cell death in H_2O_2 -exposed SK-N-MC cells. In brief, urolithin A decreased ROS production in cells, inhibited the mitochondrial-related apoptosis pathway, and modulated the p-38 MAPK pathway [57].

Both of these studies were conducted in human neuroblastoma SK-N-MC cells, as reported by the authors. Although the SK-N-MC cell line is often used as a model for testing neuroprotective effects [58–61], it must be noted that this cell line is now widely regarded as having originated from Askin’s tumor related to Ewing’s sarcoma and not neuroblastoma as originally described [62].

Apart from reducing sugars, advanced glycation end products (AGEs) can also be formed in the reaction of nucleophilic groups of macromolecules with reactive carbonyl species (RCS). RCS such as glyoxal (GO), methylglyoxal (MGO), and 3-deoxyglucosone (3-DG) can be formed as side products of several enzymatic pathways involving carbohydrates. Biological effects caused by RCS seem somewhat similar to those induced by ROS. Methylglyoxal is one of the most reactive glycation agents, so it is a relevant target so its inhibition might be useful to prevent or at least attenuate the formation of AGEs. Liu et al. investigated the *in vitro* antiglycation effects of a standardized pomegranate fruit extract (PE) along with its major phenolic constituents, punicalagin (PA), ellagic acid (EA), and gallic acid (GA) as minor phenolic constituents as well as urolithins A and B. Inhibitory effects of the tested samples were evaluated with BSA-fructose and G.K. peptide-ribose assays, MALDI-TOF mass spectrometry, and circular dichroism (CD). Additionally, the dicarbonyl-scavenging properties of the samples were also examined by HPLC-DAD methods. Results showed that PA and EA were the major contributors to the antiglycation effects of PE, but urolithins A and B also showed promising antiglycation activity which was similar to that of the positive control. All the tested compounds showed dicarbonyl-scavenging capacity, but in the case of urolithins, it was weaker than that of the positive control [63].

Enhanced production of ROS is connected with peripheral inflammatory responses. In the study conducted by Ishimoto et al., *in vivo* anti-inflammatory and antioxidant

activities of urolithin A were evaluated in the carrageenan-induced paw edema mouse model with an ORAC assay. The association between plasma ORAC scores and levels of urolithin A in plasma after oral administration in mice was investigated. Results indicated a strong correlation of plasma urolithin A levels and the plasma ORAC scores after oral administration of urolithin A. These findings can explain the profound anti-inflammatory effects exerted by urolithin A [64].

Subsequently, the study conducted by Saha et al. revealed that urolithin A potentially inhibits heme peroxidases, namely, myeloperoxidase (MPO) and lactoperoxidase (LPO), compared to ellagic acid. Urolithin A significantly reduced the MPO and LPO activities in both dose- and time-dependent manners. Also, inhibition of MPO and LPO by urolithin A could be prevented by neutrophil gelatinase-associated lipocalin (NGAL), which is expressed in neutrophils and is involved in innate immunity by sequestering iron, thus limiting bacterial growth. The Chrome Azurol S assay suggested that ellagic acid was capable of binding iron, whereas urolithin A failed to chelate iron. However, this allows urolithin A to retain its ability to inhibit peroxidase in the presence of ferric ion. As a consequence, urolithin A significantly reduced superoxide generation induced by phorbol myristate acetate (PMA) in neutrophils. These findings pointed out that urolithin A does inhibit not only MPO and LPO but also other prooxidant enzymes. To confirm these findings *in vitro*, urolithin A and ellagic acid were tested for their efficacy against PMA-induced ear edema in mice. Here, treatment with urolithin A was almost comparable to a positive control (indomethacin), which markedly reduced ear edema by 47.5%. Urolithin A also inhibited MPO activity, which suggests the potential role of urolithin A as an anti-inflammatory agent [16].

Singh et al. showed that urolithin A not only exerts the anti-inflammatory activity but also upregulates epithelial tight junction proteins through activation of AhR-Nrf2-dependent pathways. The anti-inflammatory activity was evidenced by a significant decrease in LPS-induced IL-6 and TNF- α both *in vitro* (mouse bone marrow-derived macrophages) and *in vivo* (LPS-induced peritonitis mouse model). While the anti-inflammatory effect was partially preserved in Nrf2^{-/-} cells, it seems to be strongly AhR-dependent. AhR-Nrf2 pathways are essential for urolithin A-induced upregulation of tight junction proteins. Urolithin A was shown to attenuate colitis in preclinical models as both prophylactic and therapeutic agents and could be an even better therapeutic option than anti-TNF- α antibodies currently used in the treatment of irritable bowel disease [65].

Endothelium-derived NO has a critical role in regulating vascular homeostasis, and its bioactivity is impaired in atherosclerosis and related diseases. Loss of bioactivity under these conditions is related to increased oxidative stress, especially caused by enhanced production of superoxide anion and accumulation of lipid peroxidation products. Therefore, antioxidant supplementation can restore endothelial vasomotor function. In this respect, Spigoni et al. assessed *in vitro* effects of urolithin A, urolithin B, and urolithin B glucuronide on endothelial function in primary human aortic

endothelial cells (HAECs). The study was aimed at investigating effects of urolithins on the activation of endothelial nitric oxide synthase (eNOS) and the release of NO. Urolithins were tested both individually and as a mixture. This study was the first in assessing the effects of a mixture of urolithins at physiologically attainable concentrations on endothelial cell function. Results revealed that the mixture was more potent in releasing NO compared to individual urolithins. These findings suggest that benefits related to the ellagitannin-rich diet could be due to the combined activity of different metabolites [66].

Oxidized low-density lipoprotein (ox-LDL) can cause changes in various endothelial functions, impairing NO synthesis and stimulating endothelial cell expression of proinflammatory cytokines. This can lead to further inflammation, endothelial dysfunction, and atherogenesis. Han et al. investigated the effects of urolithin A on ox-LDL-induced endothelial dysfunction. Results showed that urolithin A in probable physiological concentrations could dose-dependently attenuate the ox-LDL-induced increase in LDH levels in human artery endothelial cells (HAECs). Moreover, urolithin A increased also the production of NO in a dose-dependent manner, suggesting that it might promote the NO synthesis by modulating the expression of endothelial nitric oxide synthase (eNOS) [67]. This is in agreement with the results obtained by Rosenblat et al. showing that both urolithins A and B significantly and dose-dependently inhibited copper ion-induced LDL oxidation, as measured by the TBARS or by the lipid peroxide assays [68].

Also, Larrosa et al. conducted a study to evaluate the effects of diet supplementation with a pomegranate extract (PE) and urolithin A on a dextran sodium sulfate- (DSS-) induced colon inflammation rat model to also assess whether the effects might be related to urolithins. Here, the antioxidant status of plasma was assessed with the ferric-reducing antioxidant power (FRAP) assay, while lipid peroxidation levels in colon tissue were evaluated by thiobarbituric acid-reactive substances (TBARS) measurement. Results showed that only the administration of PE ameliorated the antioxidant status in plasma, while urolithin A showed low antioxidative capacity in the FRAP assay. Peroxidation levels in rats supplemented with PE were significantly lower compared to control, while urolithin A administration did not produce any effect. Results also showed that both PE and urolithin A supplementations were able to abrogate the NO production by suppressing iNOS induction triggered by DSS treatment in rats. Overall, supplementation with urolithin A was more effective than that with PE in ameliorating the inflammation. The authors also noted that colonic inflammation could lower ellagic acid conversion to urolithins [69], while other work from Zhao et al. also suggested protective effects of urolithin A in high-fat diet-induced metabolic inflammation, based on the recovery of tissue damage in the colon and the regulation of the gut microbiota [70].

Olennikov et al. analyzed the commercial formulation known as Padma Liver regulator, which contains chebulic ellagitannins indicated for weak liver function and also recommended for preventing liver damage. One aim of the

study was to estimate the hepatoprotective potentials of urolithins against tert-butyl hydroperoxide-induced experimental hepatocyte injury. The results suggested that urolithins in the presence of t-BHP protected the hepatocytes against the oxidative injury in a dose-dependent manner, acting as antioxidants. Indeed, the level of malondialdehyde (MDA) production in urolithin C-treated cells was lower than those in urolithin A and B groups demonstrating its good antioxidant properties. This is explained by the fact that urolithin C has the highest number of hydroxyl groups, while the least active was urolithin B having only one monohydroxy-substituted phenolic ring [71].

An early key step in the development of hepatocellular carcinoma is characterized by overexpression of proinflammatory molecules and the release of different growth factors. This is a result of ROS overproduction and metabolic alterations in the liver cancer cells. By using HepG2 cells as a model, Wang et al. explored the effects of urolithin A on the expression of NF- κ B-related inflammatory factor and ROS formation in H₂O₂-induced oxidative stress. The effects of urolithin A on ROS production and superoxide dismutase (SOD), malondialdehyde (MDA), and glutathione peroxidase (GSH-Px) levels were evaluated in response to H₂O₂ treatment. Here, the incubation of HepG2 cells with urolithin A led to the inhibition of ROS generation by nearly 50%, reinforcing the levels of SOD and GSH-Px, while in untreated cells, a significant increase in MDA was observed. The authors proposed that one potential mechanism of urolithin A action in HepG2 cells might derive from the decreased release of proinflammatory mediators caused by the suppression of the NF- κ B signaling pathway, followed by inhibition of oxidative stress [72].

ROS have the potential to cause cellular damage, especially to DNA, RNA, lipids, and proteins, that can eventually promote carcinogenesis. Kojadinovic et al. tried to characterize the intracellular response to oxidative stress after treatment of the human adenocarcinoma Caco-2 cell line with physiological amounts of urolithins mixture (urolithins A, B, C, and D). To determine the protective effect of urolithins, two types of treatments were used: a long-term preincubation condition and a short-term incubation treatment. For all the measurements in tested cells, oxidative stress was induced with H₂O₂ and cells were pretreated with urolithin mixture in a concentration of 30 μ M. The mixture of urolithins reduced the generation of ROS in both the experimental conditions (short term and long term), despite that a more pronounced effect was observed in the short term. Effects of urolithins were also evaluated by measuring the activity of specific antioxidant enzymes, such as superoxide dismutase (SOD), catalase (CAT), and glutathione peroxidase (GSH-Px) in Caco-2 cells. The addition of urolithins in growth medium significantly decreased the activity of CAT ($p < 0.05$), while SOD and GSH-Px activity was unaffected. These data indicate that the mixture of urolithins can attenuate the induced oxidative stress in the Caco-2 cells. Even short-term treatment can cause a decrease in ROS formation in cells, preventing the oxidative damage. Additionally, urolithins can modulate the activity of antioxidative enzymes [73].

The mitogen-activated protein kinase (MAPK) cascades, consisting of the extracellular signal-related kinases (ERK1/2), the c-Jun N-terminal kinases (JNK), the p38 kinase (p38), and the big MAP kinase 1 (BMK1/ERK5) pathway, play an important role in various cellular processes such as cell growth, differentiation, development, cell cycle, survival, and cell death. The p38 kinase is involved in malignant invasion and metastasis of bladder cancer. Qiu et al. conducted a study aimed at investigating the antiproliferative properties of urolithin A, urolithin B, 8-OMe-urolithin A, and ellagic acid in T24 human bladder cancer cells. They also evaluated the antioxidative activity of these compounds and their effects on caspase-3 activation and mRNA and/or protein of p38-MAPK (mRNA, phosphorylated protein), MEKK1 (mRNA, protein), c-Jun (mRNA, phosphorylated and nonphosphorylated protein), p53 (mRNA), cleaved caspase-3 (protein), and peroxisome proliferator-activated receptors gamma (PPAR- γ , protein). Oxidative stress induced by H₂O₂ in T24 human bladder cancer cells was estimated by measuring the intracellular content of ROS and MDA as well as the SOD activity. After incubation with different urolithins and ellagic acid, both the ROS and MDA levels were significantly decreased, whereas SOD activity markedly increased compared to the negative control. Results also suggested that urolithins and ellagic acid modulated both the transcription and protein content of p38-MAPK, MEKK1, and c-Jun in T24 cells, confirming possible antiproliferative effects on T24 cells [74].

One of the most widely diffused alterations across several types of malignant cancers is related to the functional inactivation of the oncosuppressor p53 that largely contributes to the acquirement of a chemoresistant phenotype [75, 76]. Thus, the reactivation of p53 represents an attractive therapeutic option in oncology that has been shown to promote tumor regression due to the induction of senescence in sarcomas and carcinomas or the activation of apoptosis in lymphomas [75, 77]. In case of p53 mutation or deletion (present in more than 50% of cancers), this reactivation could be achieved through gene therapy or targeted therapy aimed at substituting the p53 mutant form with the corresponding wild-type form. Of note, in tumors expressing the p53 wild-type form, its activity is often diminished by the overexpression of p53 inhibitors, namely, the E3 ubiquitin-protein ligase MDM2 (or MDM4) [75, 78]. In such tumors, the therapeutic strategy is aimed at disrupting the binding of p53 inhibitors to its target. Although still in its early phase, research on p53 reactivation in the context of cancer therapy is rapidly emerging. Besides some small molecules acting as MDM2 inhibitors already in the clinical trials, many natural compounds are currently tested for their p53 restoration activity in cancer cells. Several studies demonstrated such activity for urolithins. For instance, Giménez-Bastida et al. [79] reported that urolithin A applied in physiologically relevant noncytotoxic concentrations (0.5, 1, and/or 10 μ M) dose-dependently induced cellular senescence in p53 wild-type human colon cancer HCT-116 cells. This effect was not observed in two other cancer cell lines, namely, Caco-2 (p53-null) and HT-29 (mutant p53), as well as nontumorigenic CCD18-Co (wild-type p53) cells. On the other hand,

urolithin B, urolithin C, isourolithin A, and ellagic acid did not exert this effect in the tested cell lines. In contrast to apoptosis, which can be induced at much higher concentrations, the induction of cellular senescence suggests the potential chemopreventive role of a regular dietary intake of urolithin precursors, at least for urolithin A-producing metabolites. Another important point is the lack of effect resulting from testing with urolithin A metabolites (glucuronide or sulfate). This can also explain the absence of effect in Caco-2 and HT-29 cells, which metabolize urolithins at a much higher rate in comparison to HCT-116 cells.

Norden and Heiss also reported that urolithin A-induced p53 stabilization in HCT-116 cells not only exerted antiproliferative effects (IC₅₀ = 19 μ M) but also synergized with the anticancer drug oxaliplatin. In the absence of p53, a significant decrease in urolithin A antiproliferative activity was however noted (IC₅₀ = 38 μ M) [80].

Both p53-dependent and p53-independent antiproliferative effects of urolithin A were demonstrated in the three human prostate cancer lines with different p53 activities, namely, LNCaP (p53^{+/+}), 22RV1 (p53^{-/+}), and PC3 (p53^{-/-}) cells. Here, an increased expression in both p53 and MDM2 was observed in LNCaP and 22RV1 cells, but this was paralleled by a strong inhibition of their reciprocal interaction. In contrast, in PC3 cells, urolithin A downregulated MDM2 and upregulated p21 and p14ARF expression in a p53-independent manner [78].

The role of p53 in cancer formation and progression involves the regulation of oxidative stress by controlling the expression of various antioxidant and metabolic genes. The final effect can be either antioxidant or prooxidant, depending on the extent of stress signals. Under the physiological conditions of low stress, p53 lowers ROS levels via induction of antioxidant genes (sestrins, TIGAR, GPX1, ALDH4, GLS2, and Parkin) and the stabilization of Nrf2. This antioxidant activity protects cells from oxidative stress-induced DNA damage and promotes cell survival. Under the conditions of severe stress, p53 induces prooxidant genes (PIG3, PIG6, FDRX, Bax, and Puma) thus increasing ROS levels in the cells. This increase in ROS levels further activates p53, leading to a high accumulation of ROS. The resulting state of oxidative stress leads to apoptosis and senescence, preventing the propagation of mutated cells. In p53-null cells, the elevation of intracellular ROS levels increases DNA oxidation and the rate of mutagenesis, and the use of antioxidants can reverse this effect [81]. In contrast to the wild-type p53, mutant p53 isoforms are not functional and support tumor progression. ROS formation is also enhanced by the Warburg effect, which was shown to be sustained in cells with mutant p53 proteins. However, mutant p53-driven ROS accumulation was also shown to enhance cell sensitivity to H₂O₂ treatment. It was then speculated that mutant p53-bearing cancer cells could be significantly more sensitive to prooxidant drugs [82]. In conclusion, the final effect of p53 activation seems to be dependent on the cell type, p53 isoform, level of p53 activity, and its location within the cell and can promote cell proliferation, migration, further genotoxic damage, senescence, or cell death.

Urolithin A was also shown to regulate mitochondrial function. The decline in mitochondrial function, characterized by changes in organelle morphology, insufficient ATP production, accumulation of mitochondrial DNA mutations, increased production of mitochondrial ROS, and oxidative damage to macromolecules, is one of the hallmarks of aging and age-related diseases. Since mitophagy enables the degradation of damaged mitochondria and it is significantly impaired in several human pathologies (neurodegenerative disorders, cardiovascular pathologies, and cancer), there is a rising interest in therapeutic interventions aimed at the induction of mitophagy. Ryu et al. found that urolithin A potently induces mitophagy and through this mechanism it extended lifespan and improved fitness during aging in *Caenorhabditis elegans* as well as muscle function and exercise capacity in rodents [83]. This corroborates the finding of Boakye et al. who demonstrated that urolithin A increased autophagic flux in murine J774.1 macrophages in a concentration-dependent manner, thereby contributing to anti-inflammatory action. An elevated autophagic flux could be attributed to suppression of LPS-induced phosphorylation of AKT and its downstream targets TSC2, mTOR, and p70S6K. The increased autophagic flux further contributed to the alleviation of LPS-stimulated proinflammatory M1 polarization in J774.1 macrophages (inhibition of iNOS/Cox2/pro-IL-1 β expression and NO and ROS release). Finally, the urolithin A-induced increase in autophagic flux contributed to the reduced nuclear abundance of NF- κ B, presumably by interfering between the NF- κ B release from its complex with the inhibitor and its transport into the nucleus [84].

Elevated autophagy, augmented mitochondrial biogenesis, and attenuated NF- κ B activation were also recorded in the livers of C57BL/6 male mice fed a high-fat diet after intraperitoneal application of urolithin A in physiologically relevant concentrations (20 μ g/mice). Augmented mitochondrial mass and activity were demonstrated to contribute to the triglyceride- (TG-) lowering effect of urolithin A. This effect was probably due to a significant increase in the expression of mitochondrial genes related to beta-oxidation, namely, carnitine palmitoyltransferase 1 (Cpt1) and sirtuin 1 (Sirt1). Simultaneously, levels of the lipogenic gene and protein expression (e.g., fatty acid synthase and stearoyl-CoA desaturase 1) were decreased. Moreover, livers from urolithin A-treated mice had augmented expression of ROS-scavenging enzymes, such as SOD1 and SOD2. Furthermore, urolithin A decreases macrophage infiltration into adipose tissue and favors M2 over M1 polarization of macrophages. The overall observed systemic effects were reduced hepatic and adipose inflammation and improved insulin sensitivity in the dietary challenge with a high-fat diet [85].

The beneficial effects of urolithin A on mitochondrial health were also reported in the first human randomized, double-blind, placebo-controlled clinical study in sedentary elderly subjects. Although the study duration (4 weeks) did not allow the assessment of physiological effects (muscle function), it showed a global impact on the biomarkers of mitochondrial health following urolithin A oral administration at doses of 500 and 1000 mg. A dose-dependent decrease

in acylcarnitine levels (C8 to C14 and >C20) was observed in plasma, without change in free carnitine levels, indicating that UA improves fatty acid oxidation at the level of the whole body. Mitochondrial abundance was evaluated by measuring the ratio of mitochondrial DNA to nuclear DNA, which tended to increase, albeit not significantly. Treatment with UA was seen to upregulate the transcription of mitochondrial genes. Taken together, these data demonstrate that urolithin A stimulated mitochondrial biogenesis in the skeletal muscle of the participants. Further studies of longer duration are needed to evaluate urolithin A effects on muscle strength as well as possible variations in a dose-effect relationship from chronic exposure [30].

6. Conclusions

Ellagic acid-derived urolithins are produced by the gut microbiome, absorbed, and regarded to be responsible for the systemic beneficial health effects associated with the consumption of ellagitannin-rich food. The research interest in urolithins has considerably grown in the past decade. Efficient methods for urolithin synthesis have been developed, many tests on their activity were performed, their bioaccessibility was proven in an *in vitro* digestive simulation test, and toxicological studies have shown a good safety profile for urolithin A. The results obtained so far confirm that urolithins can potentially be used to modulate oxidative stress and ameliorate tissue damage through different mechanisms. The first functional food containing urolithin A is already on the horizon. The evidence also indicates that urolithin metabolism could be cell-specific, which in turn alters their activity *in vitro*, a phenomenon that warrants further investigation. On the other hand, a couple of synthetic urolithin derivatives were shown to be potent and selective inhibitors of certain enzymes (CK, cholinesterase) which makes them novel drug candidates. In conclusion, urolithins are promising molecules with many potential therapeutic activities that are yet to be validated in clinical trials. It is anticipated that these compounds will be the focus of extensive research in the near future, hopefully providing new and exciting results in different physiopathological settings.

Conflicts of Interest

The authors declare that they have no conflicts of interest.

References

- [1] E. Lederer, "Chemistry and biochemistry of some mammalian secretions and excretions," *Journal of the Chemical Society*, pp. 2115–2125, 1949.
- [2] R. González-Barrio, P. Truchado, H. Ito, J. C. Espín, and F. A. Tomás-Barberán, "UV and MS identification of urolithins and nasutins, the bioavailable metabolites of ellagitannins and ellagic acid in different mammals," *Journal of Agricultural and Food Chemistry*, vol. 59, no. 4, pp. 1152–1162, 2011.
- [3] Z. Mao, W. Sun, L. Fu, H. Luo, D. Lai, and L. Zhou, "Natural dibenzo- α -pyrones and their bioactivities," *Molecules*, vol. 19, no. 4, pp. 5088–5108, 2014.

- [4] Y. L. Garazd and M. M. Garazd, "Natural dibenzo[*b,d*]pyran-6-ones: structural diversity and biological activity," *Chemistry of Natural Compounds*, vol. 52, no. 1, pp. 1–18, 2016.
- [5] A. Smeriglio, D. Barreca, E. Bellocco, and D. Trombetta, "Proanthocyanidins and hydrolysable tannins: occurrence, dietary intake and pharmacological effects," *British Journal of Pharmacology*, vol. 174, no. 11, pp. 1244–1262, 2017.
- [6] J. C. Espín, M. Larrosa, M. T. García-Conesa, and F. Tomás-Barberán, "Biological significance of urolithins, the gut microbial ellagic acid-derived metabolites: the evidence so far," *Evidence-Based Complementary and Alternative Medicine*, vol. 2013, Article ID 270418, 15 pages, 2013.
- [7] M. Savi, L. Bocchi, P. Mena et al., "In vivo administration of urolithin A and B prevents the occurrence of cardiac dysfunction in streptozotocin-induced diabetic rats," *Cardiovascular Diabetology*, vol. 16, no. 1, p. 80, 2017.
- [8] P. Truchado, M. Larrosa, M. T. García-Conesa et al., "Strawberry processing does not affect the production and urinary excretion of urolithins, ellagic acid metabolites, in humans," *Journal of Agricultural and Food Chemistry*, vol. 60, no. 23, pp. 5749–5754, 2011.
- [9] I. A. Ludwig, P. Mena, L. Calani et al., "New insights into the bioavailability of red raspberry anthocyanins and ellagitannins," *Free Radical Biology & Medicine*, vol. 89, pp. 758–769, 2015.
- [10] R. García-Villalba, M. V. Selma, J. C. Espín, and F. A. Tomás-Barberán, "Identification of novel urolithin metabolites in human feces and urine after the intake of a pomegranate extract," *Journal of Agricultural and Food Chemistry*, vol. 67, no. 40, pp. 11099–11107, 2019.
- [11] F. A. Tomás-Barberán, R. García-Villalba, A. González-Sarrías, M. V. Selma, and J. C. Espín, "Ellagic acid metabolism by human gut microbiota: consistent observation of three urolithin phenotypes in intervention trials, independent of food source, age, and health status," *Journal of Agricultural and Food Chemistry*, vol. 62, no. 28, pp. 6535–6538, 2014.
- [12] G. Cozza, A. Gianoncelli, P. Bonvini et al., "Urolithin as a converging scaffold linking ellagic acid and coumarin analogues: design of potent protein kinase CK2 inhibitors," *ChemMedChem*, vol. 6, no. 12, pp. 2273–2286, 2011.
- [13] M. Norouzbahari, E. V. Burgaz, T. Ercetin et al., "Design, synthesis and characterization of novel urolithin derivatives as cholinesterase inhibitor agents," *Letters in Drug Design & Discovery*, vol. 15, no. 11, pp. 1131–1140, 2018.
- [14] J. A. Giménez-Bastida, A. González-Sarrías, M. Larrosa, F. Tomás-Barberán, J. C. Espín, and M. T. García-Conesa, "Ellagitannin metabolites, urolithin A glucuronide and its aglycone urolithin A, ameliorate TNF- α -induced inflammation and associated molecular markers in human aortic endothelial cells," *Molecular Nutrition & Food Research*, vol. 56, no. 5, pp. 784–796, 2012.
- [15] J. Zhang, D. Shi, H. Zhang et al., "Synthesis of dibenzopyranones and pyrazolobenzopyranones through copper(0)/selectfluor system-catalyzed double CH activation/oxygen insertion of 2-arylbenzaldehydes and 5-arylpyrazole-4-carbaldehydes," *Tetrahedron*, vol. 73, no. 2, pp. 154–163, 2017.
- [16] P. Saha, B. S. Yeoh, R. Singh et al., "Gut microbiota conversion of dietary ellagic acid into bioactive phytochemical urolithin A inhibits heme peroxidases," *PLoS One*, vol. 11, no. 6, article e0156811, 2016.
- [17] D. Bialonska, S. G. Kasimsetty, S. I. Khan, and D. Ferreira, "Urolithins, intestinal microbial metabolites of pomegranate ellagitannins, exhibit potent antioxidant activity in a cell-based assay," *Journal of Agricultural and Food Chemistry*, vol. 57, no. 21, pp. 10181–10186, 2009.
- [18] P. Gao and Y. Wei, "NIS-mediated oxidative lactonization of 2-arylbenzoic acids for the synthesis of dibenzopyranones under metal-free conditions," *Synthesis*, vol. 46, no. 3, pp. 343–347, 2014.
- [19] I. R. Pottie, P. R. Nandaluru, and G. J. Bodwell, "An Inverse Electron-Demand Diels-Alder-Based Total Synthesis of Urolithin M7," *Synlett*, vol. 2011, no. 15, pp. 2245–2247, 2011.
- [20] S. Rupiani, L. Guidotti, M. Manerba et al., "Synthesis of natural urolithin M6, a galloflavin mimetic, as a potential inhibitor of lactate dehydrogenase A," *Organic & Biomolecular Chemistry*, vol. 14, no. 46, pp. 10981–10987, 2016.
- [21] M. D. Reddy, A. N. Blanton, and E. B. Watkins, "Palladium-catalyzed, *N*-(2-aminophenyl)acetamide-assisted *ortho*-arylation of substituted benzamides: application to the synthesis of urolithins B, M6, and M7," *The Journal of Organic Chemistry*, vol. 82, no. 10, pp. 5080–5095, 2017.
- [22] C. A. Lipinski, F. Lombardo, B. W. Dominy, and P. J. Feeney, "Experimental and computational approaches to estimate solubility and permeability in drug discovery and development settings," *Advanced Drug Delivery Reviews*, vol. 46, no. 1–3, pp. 3–26, 2001.
- [23] C. A. Lipinski, "Lead- and drug-like compounds: the rule-of-five revolution," *Drug Discovery Today: Technologies*, vol. 1, no. 4, pp. 337–341, 2004.
- [24] D. F. Veber, S. R. Johnson, H. Y. Cheng, B. R. Smith, K. W. Ward, and K. D. Kopple, "Molecular properties that influence the oral bioavailability of drug candidates," *Journal of Medicinal Chemistry*, vol. 45, no. 12, pp. 2615–2623, 2002.
- [25] A. K. Ghose, V. N. Viswanadhan, and J. J. Wendoloski, "A knowledge-based approach in designing combinatorial or medicinal chemistry libraries for drug discovery. 1. A qualitative and quantitative characterization of known drug databases," *Journal of Combinatorial Chemistry*, vol. 1, no. 1, pp. 55–68, 1999.
- [26] A. Daina, O. Michielin, and V. Zoete, "SwissADME: a free web tool to evaluate pharmacokinetics, drug-likeness and medicinal chemistry friendliness of small molecules," *Scientific Reports*, vol. 7, no. 1, 2017.
- [27] A. González-Sarrías, J. A. Giménez-Bastida, M. Á. Núñez-Sánchez et al., "Phase-II metabolism limits the antiproliferative activity of urolithins in human colon cancer cells," *European Journal of Nutrition*, vol. 53, no. 3, pp. 853–864, 2014.
- [28] M. Gasperotti, S. Passamonti, F. Tramer et al., "Fate of microbial metabolites of dietary polyphenols in rats: is the brain their target destination?," *ACS Chemical Neuroscience*, vol. 6, no. 8, pp. 1341–1352, 2015.
- [29] P. Mena, M. Dall'Asta, L. Calani, F. Brighenti, and D. Del Rio, "Gastrointestinal stability of urolithins: an in vitro approach," *European Journal of Nutrition*, vol. 56, no. 1, pp. 99–106, 2017.
- [30] P. A. Andreux, W. Blanco-Bose, D. Ryu et al., "The mitophagy activator urolithin A is safe and induces a molecular signature of improved mitochondrial and cellular health in humans," *Nature Metabolism*, vol. 1, no. 6, pp. 595–603, 2019.
- [31] M. A. Ávila-Gálvez, J. A. Giménez-Bastida, A. González-Sarrías, and J. C. Espín, "Tissue deconjugation of urolithin A glucuronide to free urolithin A in systemic inflammation," *Food & Function*, vol. 10, no. 6, pp. 3135–3141, 2019.

- [32] J. P. Piwowarski, I. Stanisławska, S. Granica, J. Stefańska, and A. K. Kiss, "Phase II conjugates of urolithins isolated from human urine and potential role of β -glucuronidases in their disposition," *Drug Metabolism and Disposition*, vol. 45, no. 6, pp. 657–665, 2017.
- [33] M. Savi, L. Bocchi, L. Bresciani et al., "Trimethylamine-N-oxide (TMAO)-induced impairment of cardiomyocyte function and the protective role of urolithin B-glucuronide," *Molecules*, vol. 23, no. 3, p. 549, 2018.
- [34] M. Á. Ávila-Gálvez, J. C. Espín, and A. González-Sarriás, "Physiological relevance of the antiproliferative and estrogenic effects of dietary polyphenol aglycones versus their phase-II metabolites on breast cancer cells: a call of caution," *Journal of Agricultural and Food Chemistry*, vol. 66, no. 32, pp. 8547–8555, 2018.
- [35] J. Heilman, P. Andreux, N. Tran, C. Rinsch, and W. Blanco-Bose, "Safety assessment of urolithin A, a metabolite produced by the human gut microbiota upon dietary intake of plant derived ellagitannins and ellagic acid," *Food and Chemical Toxicology*, vol. 108, no. Part A, pp. 289–297, 2017.
- [36] D. M. Keefe, "GRAS Notice No. GRN 000791," Food and Drug Administration, 2018.
- [37] I. Liguori, G. Russo, F. Curcio et al., "Oxidative stress, aging, and diseases," *Clinical Interventions in Aging*, vol. 13, pp. 757–772, 2018.
- [38] L. He, T. He, S. Farrar, L. Ji, T. Liu, and X. Ma, "Antioxidants maintain cellular redox homeostasis by elimination of reactive oxygen species," *Cellular Physiology and Biochemistry*, vol. 44, no. 2, pp. 532–553, 2017.
- [39] M. Sova and L. Saso, "Design and development of Nrf2 modulators for cancer chemoprevention and therapy: a review," *Drug Design, Development and Therapy*, vol. Volume 12, pp. 3181–3197, 2018.
- [40] B. Marengo, M. Nitti, A. L. Furfaro et al., "Redox homeostasis and cellular antioxidant systems: crucial players in cancer growth and therapy," *Oxidative Medicine and Cellular Longevity*, vol. 2016, Article ID 6235641, 16 pages, 2016.
- [41] T. Kallio, J. Kallio, M. Jaakkola, M. Mäki, P. Kilpeläinen, and V. Virtanen, "Urolithins display both antioxidant and pro-oxidant activities depending on assay system and conditions," *Journal of Agricultural and Food Chemistry*, vol. 61, no. 45, pp. 10720–10729, 2013.
- [42] M. K. Mazumder, S. Choudhury, and A. Borah, "An in silico investigation on the inhibitory potential of the constituents of pomegranate juice on antioxidant defense mechanism: relevance to neurodegenerative diseases," *IBRO Reports*, vol. 6, pp. 153–159, 2019.
- [43] S. Dirimanov and P. Högger, "Screening of inhibitory effects of polyphenols on akt-phosphorylation in endothelial cells and determination of structure-activity features," *Biomolecules*, vol. 9, no. 6, p. 219, 2019.
- [44] W. Komatsu, H. Kishi, K. Yagasaki, and S. Ohhira, "Urolithin A attenuates pro-inflammatory mediator production by suppressing PI3-K/Akt/NF- κ B and JNK/AP-1 signaling pathways in lipopolysaccharide-stimulated RAW264 macrophages: possible involvement of NADPH oxidase-derived reactive oxygen species," *European Journal of Pharmacology*, vol. 833, pp. 411–424, 2018.
- [45] J. P. Piwowarski, A. K. Kiss, S. Granica, and T. Moeslinger, "Urolithins, gut microbiota-derived metabolites of ellagitannins, inhibit LPS-induced inflammation in RAW 264.7 murine macrophages," *Molecular Nutrition & Food Research*, vol. 59, no. 11, pp. 2168–2177, 2015.
- [46] G. Lee, J. S. Park, E. J. Lee, J. H. Ahn, and H. S. Kim, "Anti-inflammatory and antioxidant mechanisms of urolithin B in activated microglia," *Phytomedicine*, vol. 55, pp. 50–57, 2019.
- [47] J. Xu, C. Yuan, G. Wang et al., "Urolithins attenuate LPS-induced neuroinflammation in BV2 Microglia via MAPK, Akt, and NF- κ B signaling pathways," *Journal of Agricultural and Food Chemistry*, vol. 66, no. 3, pp. 571–580, 2018.
- [48] S. L. Ding, Z. Y. Pang, X. M. Chen et al., "Urolithin A attenuates IL-1 β -induced inflammatory responses and cartilage degradation via inhibiting the MAPK/NF- κ B signaling pathways in rat articular chondrocytes," *Journal of Inflammation*, vol. 17, no. 1, 2020.
- [49] X. Fu, L. F. Gong, Y. F. Wu et al., "Urolithin A targets the PI3K/Akt/NF- κ B pathways and prevents IL-1 β -induced inflammatory response in human osteoarthritis: *in vitro* and *in vivo* studies," *Food & Function*, vol. 10, no. 9, pp. 6135–6146, 2019.
- [50] A. González-Sarriás, M. Á. Núñez-Sánchez, F. A. Tomás-Barberán, and J. C. Espín, "Neuroprotective effects of bioavailable polyphenol-derived metabolites against oxidative stress-induced cytotoxicity in human neuroblastoma SH-SY5Y cells," *Journal of Agricultural and Food Chemistry*, vol. 65, no. 4, pp. 752–758, 2017.
- [51] N. A. DaSilva, P. P. Nahar, H. Ma et al., "Pomegranate ellagitannin-gut microbial-derived metabolites, urolithins, inhibit neuroinflammation *in vitro*," *Nutritional Neuroscience*, vol. 22, no. 3, pp. 185–195, 2017.
- [52] G. Cásedas, F. Les, C. Choya-Foces, M. Hugo, and V. López, "The metabolite urolithin-A ameliorates oxidative stress in Neuro-2a cells, becoming a potential neuroprotective agent," *Antioxidants*, vol. 9, no. 2, p. 177, 2020.
- [53] P. Chen, F. Chen, J. Lei, Q. Li, and B. Zhou, "Activation of the miR-34a-mediated SIRT1/mTOR signaling pathway by urolithin A attenuates D-galactose-induced brain aging in mice," *Neurotherapeutics*, vol. 16, no. 4, pp. 1269–1282, 2019.
- [54] D. Zheng, Z. Liu, Y. Zhou et al., "Urolithin B, a gut microbiota metabolite, protects against myocardial ischemia/reperfusion injury via p62/Keap1/Nrf2 signaling pathway," *Pharmacological Research*, vol. 153, article 104655, 2020.
- [55] L. Tang, Y. Mo, Y. Li et al., "Urolithin A alleviates myocardial ischemia/reperfusion injury via PI3K/Akt pathway," *Biochemical and Biophysical Research Communications*, vol. 486, no. 3, pp. 774–780, 2017.
- [56] E. Verzelloni, C. Pellacani, D. Tagliacuzzi et al., "Antiglycative and neuroprotective activity of colon-derived polyphenol catabolites," *Molecular Nutrition & Food Research*, vol. 55, Suppl 1, pp. S35–S43, 2011.
- [57] K. B. Kim, S. Lee, and J. H. Kim, "Neuroprotective effects of urolithin A on H₂O₂-induced oxidative stress-mediated apoptosis in SK-N-MC cells," *Nutrition Research and Practice*, vol. 14, no. 1, pp. 3–11, 2020.
- [58] S. Y. Kim, C. W. Chae, H. J. Lee et al., "Sodium butyrate inhibits high cholesterol-induced neuronal amyloidogenesis by modulating NRF2 stabilization-mediated ROS levels: involvement of NOX2 and SOD1," *Cell Death & Disease*, vol. 11, no. 6, p. 469, 2020.
- [59] Y. C. Kuo and C. W. Tsao, "Neuroprotection against apoptosis of SK-N-MC cells using RMP-7- and lactoferrin-grafted liposomes carrying quercetin," *International Journal of Nanomedicine*, vol. 12, pp. 2857–2869, 2017.

- [60] X. Gao, D. Deeb, H. Jiang, Y. Liu, S. A. Dulchavsky, and S. C. Gautam, "Synthetic triterpenoids inhibit growth and induce apoptosis in human glioblastoma and neuroblastoma cells through inhibition of prosurvival Akt, NF- κ B and Notch₁ signaling," *Journal of Neuro-Oncology*, vol. 84, no. 2, pp. 147–157, 2007.
- [61] H. Lee, J. Ryu, Y. Jung et al., "High glucose upregulates BACE1-mediated A β production through ROS-dependent HIF-1 α and LXR α /ABCA1-regulated lipid raft reorganization in SK-N-MC cells," *Scientific Reports*, vol. 6, no. 1, 2016.
- [62] M. S. Staeger, C. Hutter, I. Neumann et al., "DNA microarrays reveal relationship of Ewing family tumors to both endothelial and fetal neural crest-derived cells and define novel targets," *Cancer Research*, vol. 64, no. 22, pp. 8213–8221, 2004.
- [63] W. Liu, H. Ma, L. Frost, T. Yuan, J. A. Dain, and N. P. Seeram, "Pomegranate phenolics inhibit formation of advanced glycation endproducts by scavenging reactive carbonyl species," *Food & Function*, vol. 5, no. 11, pp. 2996–3004, 2014.
- [64] H. Ishimoto, M. Shibata, Y. Myojin et al., "In vivo anti-inflammatory and antioxidant properties of ellagitannin metabolite urolithin A," *Bioorganic & Medicinal Chemistry Letters*, vol. 21, no. 19, pp. 5901–5904, 2011.
- [65] R. Singh, S. Chandrashekhara, S. R. Bodduluri et al., "Enhancement of the gut barrier integrity by a microbial metabolite through the Nrf2 pathway," *Nature Communications*, vol. 10, no. 1, p. 89, 2019.
- [66] V. Spigoni, P. Mena, M. Cito et al., "Effects on nitric oxide production of urolithins, gut-derived ellagitannin metabolites, in human aortic endothelial cells," *Molecules*, vol. 21, no. 8, p. 1009, 2016.
- [67] Q. A. Han, C. Yan, L. Wang, G. Li, Y. Xu, and X. Xia, "Urolithin A attenuates ox-LDL-induced endothelial dysfunction partly by modulating microRNA-27 and ERK/PPAR- γ pathway," *Molecular Nutrition & Food Research*, vol. 60, no. 9, pp. 1933–1943, 2016.
- [68] M. Rosenblat, N. Volkova, H. Borochoy-Neori, S. Judeinstein, and M. Aviram, "Anti-atherogenic properties of date vs. pomegranate polyphenols: the benefits of the combination," *Food & Function*, vol. 6, no. 5, pp. 1496–1509, 2015.
- [69] M. Larrosa, A. González-Sarriás, M. J. Yáñez-Gascón et al., "Anti-inflammatory properties of a pomegranate extract and its metabolite urolithin-A in a colitis rat model and the effect of colon inflammation on phenolic metabolism," *The Journal of Nutritional Biochemistry*, vol. 21, no. 8, pp. 717–725, 2010.
- [70] R. Zhao, X. Long, J. Yang et al., "Pomegranate peel polyphenols reduce chronic low-grade inflammatory responses by modulating gut microbiota and decreasing colonic tissue damage in rats fed a high-fat diet," *Food & Function*, vol. 10, no. 12, pp. 8273–8285, 2019.
- [71] D. N. Olennikov, N. I. Kashchenko, and N. K. Chirikova, "In vitro bioaccessibility, human gut microbiota metabolites and hepatoprotective potential of chebulic ellagitannins: a case of Padma Hepaten formulation," *Nutrients*, vol. 7, no. 10, pp. 8456–8477, 2015.
- [72] Y. Wang, Z. Qiu, B. Zhou et al., "In vitro antiproliferative and antioxidant effects of urolithin A, the colonic metabolite of ellagic acid, on hepatocellular carcinomas HepG2 cells," *Toxicology In Vitro*, vol. 29, no. 5, pp. 1107–1115, 2015.
- [73] M. Kojadinovic, A. Arsic, G. Petovic-Oggiano, M. Gavrovic-Jankulovic, M. Glibetic, and M. Popovic, "Effect of urolithins on oxidative stress of colorectal adenocarcinoma cells-Caco-2," *International Journal of Food Sciences and Nutrition*, vol. 68, no. 8, pp. 952–959, 2017.
- [74] Z. Qiu, B. Zhou, L. Jin et al., "In vitro antioxidant and antiproliferative effects of ellagic acid and its colonic metabolite, urolithins, on human bladder cancer T24 cells," *Food and Chemical Toxicology*, vol. 59, pp. 428–437, 2013.
- [75] G. Lozano, "Restoring p53 in cancer: the promises and the challenges," *Journal of Molecular Cell Biology*, vol. 11, no. 7, pp. 615–619, 2019.
- [76] G. Blandino and S. Di Agostino, "New therapeutic strategies to treat human cancers expressing mutant p53 proteins," *Journal of Experimental & Clinical Cancer Research*, vol. 37, no. 1, p. 30, 2018.
- [77] A. Rufini, P. Tucci, I. Celardo, and G. Melino, "Senescence and aging: the critical roles of p53," *Oncogene*, vol. 32, no. 43, pp. 5129–5143, 2013.
- [78] Y. I. Mohammed Saleem, H. Albassam, and M. Selim, "Urolithin A induces prostate cancer cell death in p53-dependent and in p53-independent manner," *European Journal of Nutrition*, vol. 59, no. 4, pp. 1607–1618, 2020.
- [79] J. A. Giménez-Bastida, M. Á. Ávila-Gálvez, J. C. Espín, and A. González-Sarriás, "The gut microbiota metabolite urolithin A, but not other relevant urolithins, induces p53-dependent cellular senescence in human colon cancer cells," *Food and Chemical Toxicology*, vol. 139, article 111260, 2020.
- [80] E. Norden and E. H. Heiss, "Urolithin A gains in antiproliferative capacity by reducing the glycolytic potential via the p53/TIGAR axis in colon cancer cells," *Carcinogenesis*, vol. 40, no. 1, pp. 93–101, 2019.
- [81] Y. Liang, J. Liu, and Z. Feng, "The regulation of cellular metabolism by tumor suppressor p53," *Cell & Bioscience*, vol. 3, no. 1, p. 9, 2013.
- [82] M. Cordani, G. Butera, R. Pacchiana et al., "Mutant p53-associated molecular mechanisms of ROS regulation in cancer cells," *Biomolecules*, vol. 10, no. 3, p. 361, 2020.
- [83] D. Ryu, L. Mouchiroud, P. A. Andreux et al., "Urolithin A induces mitophagy and prolongs lifespan in *C. elegans* and increases muscle function in rodents," *Nature Medicine*, vol. 22, no. 8, pp. 879–888, 2016.
- [84] Y. D. Boakye, L. Groyer, and E. H. Heiss, "An increased autophagic flux contributes to the antiinflammatory potential of urolithin A in macrophages," *Biochimica et Biophysica Acta*, vol. 1862, no. 1, pp. 61–70, 2018.
- [85] A. M. Toney, R. Fan, Y. Xian, V. Chaidez, A. E. Ramer-Tait, and S. Chung, "Urolithin A, a gut metabolite, improves insulin sensitivity through augmentation of mitochondrial function and biogenesis," *Obesity*, vol. 27, no. 4, pp. 612–620, 2019.

Research Article

Sitagliptin Mitigates Total Body Irradiation-Induced Hematopoietic Injury in Mice

Meifang Wang ¹, Yinping Dong, ¹ Jing Wu ¹, Hongyan Li, ¹ Junling Zhang, ¹ Lu Lu, ¹ Yuanyang Zhang ¹, Zewei Zhou, ¹ Saijun Fan ¹, Deguan Li ¹, and Aimin Meng ^{1,2}

¹Tianjin Key Laboratory of Radiation Medicine and Molecular Nuclear Medicine, Institute of Radiation Medicine, Chinese Academy of Medical Sciences & Peking Union Medical College, Tianjin 300192, China

²NHC Key Laboratory of Human Disease Comparative Medicine (The Institute of Laboratory Animal Science, CAMS&PUMC); Beijing Key Laboratory for Animal Models of Emerging and Reemerging Infectious Diseases; Beijing Engineering Research Center for Laboratory Animal Models of Human Critical Diseases, Beijing 100021, China

Correspondence should be addressed to Deguan Li; lidgeuan@irm-cams.ac.cn and Aimin Meng; aiminmeng@cnilas.org

Received 24 February 2020; Revised 7 May 2020; Accepted 2 June 2020; Published 25 July 2020

Academic Editor: Luciano Saso

Copyright © 2020 Meifang Wang et al. This is an open access article distributed under the Creative Commons Attribution License, which permits unrestricted use, distribution, and reproduction in any medium, provided the original work is properly cited.

Sitagliptin, an inhibitor of the dipeptidyl peptidase IV (DPP4), has been implicated in the regulation of type 2 diabetes. However, the role and mechanism of sitagliptin administration in total body irradiation (TBI)-induced hematopoietic cells injury are unclear. In this study, we demonstrated that sitagliptin had therapeutic effects on hematopoietic damage, which protected mice from 7.5 Gy TBI-induced death, increased the numbers and colony formation ability of hematopoietic cells. These therapeutic effects might be attributed to the inhibition of NOX4-mediated oxidative stress in hematopoietic cells, and the alleviation of inflammation was also helpful. Therefore, sitagliptin has potential as an effective radiotherapeutic agent for ameliorating TBI-induced hematopoietic injury.

1. Introduction

Ionizing radiation (IR) has been widely used in industry, agriculture, and medical therapy, such as nuclear power generation, agricultural breeding, cancer treatment, and so on [1, 2]. However, the risks of accidental nuclear accidents, radiotherapy sequelae, and even nuclear war and nuclear terrorism are gradually rising, which makes the demand for radiation protection and treatment increasing. Exposure to a high dose of IR within a relatively short period of time may induce acute radiation syndromes (ARS), including effects experienced in the hematopoietic system, gastrointestinal system and brain [2–4], and hematopoietic radiation injury is the most common ARS.

The hematopoietic system has a hierarchical structure, in which hematopoietic stem cells (HSCs) is located at the top, which can proliferate downwards into multipotential progenitor cells (MPPs) and hematopoietic progenitor cells (HPCs), and further differentiate into mature blood cells

[5, 6]. HPCs show high sensitivity to radiation due to their fast proliferation rate. Middle or high doses of IR can deplete MPPs and HPCs and lead to acute myelosuppression. Then, HSCs proliferate and differentiate to supplement MPPs and HPCs, but persistent myelosuppression occurs with HSCs injury [7, 8]. Radiation-induced myelosuppression is one of the important pathological basis of clinical manifestations of ARS, including infection, hemorrhage, and anemia, so recovery of the hematopoietic system plays an important role in the treatment of radiation damage. The hematopoietic growth factors (HGFs) such as granulocyte colony-stimulating factor (G-CSF) filgrastim and pegfilgrastim and the granulocyte-macrophage colony-stimulating factor (GM-CSF) sargramostim have currently been approved by the US Food and Drug Administration to mitigate hematopoietic abnormalities in ARS in order to improve patients survival [9]. However, the application of HGFs not only may lead to fever, pain, vomiting, and so on, but also destroys the self-renewal

ability of HSCs, which accelerates the depletion of HSCs and further affects the long-term recovery of hematopoietic system [10–13]. Therefore, studying the mechanism of regulation of the hematopoietic system and exploring strategies to mitigate hematopoietic radiation damage are urgent problems to be solved.

As an oral hypoglycemic agent approved by FDA, sitagliptin increases the activity of glucagon-like peptide-1 (GLP-1) and glucose-dependent insulinotropic polypeptide by highly selective inactivation of DPP4, thereby promoting insulin secretion from β -cells and inhibiting glucagon secretion from α -cells, so sitagliptin is widely used in the treatment of type 2 diabetes [14–17]. Studies have shown that sitagliptin can suppress oxidative stress in severe acute pancreatitis-associated intestinal inflammation, diabetic cardiomyopathy, chronic cerebral hypoperfusion, heart failure, liver ischemia-reperfusion, and so on [18–22]. Broxmeyer et al. [23] found that radiation increased the activity of DPP4 in bone marrow (BM) cells, and DPP4 knockout or inhibition before IR prevented the hematopoietic radiation injury. Sitagliptin's target DPP4 exists on the surfaces of a variety of cells including HSCs and HPCs, and partially presents in the circulating blood in soluble form [24, 25]. DPP4 is able to combine with chemokines, colony-stimulating factors (CSFs), and interleukins involved in the regulation of hematopoietic system [26], inhibiting its activity is beneficial to homing and implantation of hematopoietic cells [27]. However, the therapeutic effects and the mechanism of sitagliptin in the treatment of hematopoietic radiation damage remain to be studied.

In this article, we investigated the therapeutic role of sitagliptin in hematopoietic radiation injury and its underlying mechanisms. Our results demonstrated that the administration of sitagliptin had therapeutic effects on TBI-induced hematopoietic damage, which protected mice from TBI-induced death, increased the numbers of hematopoietic cells and the proliferation ability of HPCs. In addition, sitagliptin not only inhibited NOX4-mediated oxidative stress response in hematopoietic cells, but also might mitigate inflammation.

2. Materials and Methods

2.1. Reagents. Biotin conjugated anti-mouse-CD4 (clone 34 GK1.5), anti-mouse-CD8 (clone 53-6.7), anti-mouse-CD11b (clone M1/70), anti-mouse-CD45R/B220 (clone RA3-6B2), anti-mouse-Ly6G/Gr-1 (clone RB68C5), anti-mouse-Ter119 (clone Ter119), anti-mouse-CD117 (c-kit)-APC (clone 2B8), anti-mouse -Ly-6A/EA (Sca-1)-PE (clone D7), and PERCP-conjugated streptavidin were purchased from eBioscience (San Diego, CA, USA). In addition, 2,7-dichlorodihydrofluorescein diacetate (DCFDA) was purchased from Sigma (St. Louis, MO, USA). MethoCult GF M3534 medium was purchased from Stem Cell Technologies (Vancouver, Canada). MitSox red mitochondrial superoxide indicator was obtained from Life Technologies (Grand Island, NY, USA). Rabbit anti- γ H2AX was obtained from Cell Signaling Technology (Danvers, MA, USA). Rabbit anti-NOX4 was obtained from Proteintech (Wuhan, China). FITC-conjugated goat anti-rabbit antibodies were obtained from Abcam Biotechnology (Cambridge,

MA, USA). Cytofix/Cytoperm buffer (554722), Perm/Wash buffer (554723), and Cytoperm Permeabilization Buffer Plus (561651) were obtained from BD Pharmingen (San Diego, CA, USA). Sitagliptin was obtained from Merck Sharp & Dohme (South Granville, NSW, Australia).

2.2. Animals. Male C57BL/6J mice weighing 20–22 g were purchased from Beijing HFK Bioscience Co, Ltd. (Beijing, China) and housed in the certified animal facility at the Institute of Radiation Medicine of the Chinese Academy of Medical Sciences (CAMS). All mice were randomly divided into different groups one week prior to the study to allow for acclimatization. All procedures involving animal experiments were conducted in accordance with a protocol approved by the Institutional Animal Care and Use Committee of CAMS.

2.3. Irradiation and Treatment. Mice were randomly assigned to 4 groups: control, sitagliptin, TBI, and TBI+sitagliptin in survival experiment and assigned to 3 groups: control, TBI, and TBI+sitagliptin in other experiments. Mice were exposed to a LD50 dose (7.5 Gy) TBI for the survival study or sublethal dose (4 Gy) TBI for experiments using a ^{137}Cs source housed in an Exposure Instrument Gammacell-40 (Atomic Energy of Canada Lim) at a dose rate of 1.0 Gy per min. For sitagliptin treatment, mice were treated with 10 mg/kg sitagliptin via oral administration once daily for 7 d; the first dose was administered 2 hours after TBI. The determination of the dose for mice was based on the conversion of the recommended dose for humans (100 mg/kg). Mice in the control and TBI groups were given PBS in the same protocol. In the 7.5 Gy irradiation experiment, 10 mice were used in each group, while in the 4 Gy irradiation experiment, 5 mice per group. 10 days after 4 Gy TBI, the mice were sacrificed and samples were collected [13].

2.4. Analysis of the Numbers of Bone Marrow Mononuclear Cells (BMMNCs), HPCs, and HSCs. BM cells were flushed from mouse femurs with PBS, and the numbers of BMMNCs were counted using a MEK-7222k hemocytometer (NIHON KOHDEN, Tokyo, Japan) and expressed as $\times 10^6$ /femur. BM cells were incubated with biotin-conjugated lineage antibodies specific for murine CD4, CD8, Ter119, CD11b, CD45R/B220, and Gr-1, and stained with streptavidin-PerCp, Sca1-PE, and c-kit-APC. The numbers of HPCs ($\text{lin}^- \text{c-kit}^+ \text{Sca-1}^-$) and HSCs ($\text{lin}^- \text{c-kit}^+ \text{Sca-1}^+$, LSK) were calculated using the following equation: percentage \times BMMNCs/femur [13].

2.5. Colony Forming Unit-Granulocyte Macrophages (CFU-GM) Assay. The CFU-GM assays were conducted by culturing BM cells in MethoCult GF M3534 methylcellulose medium (Stemcell Technologies, Vancouver, BC). The colonies of CFU-GM were counted on day 7 according to the manufacturer's protocol. The results were presented as the numbers of CFU-GMs per 2×10^4 cells [28].

2.6. Competitive Repopulation Assay (CRA). In the present study, donor cells (1×10^6 BMMNCs) were collected from C57BL/6-Ly-5.1 (CD45.1) mice after they received various treatments and mixed with 1×10^6 competitive BMMNCs

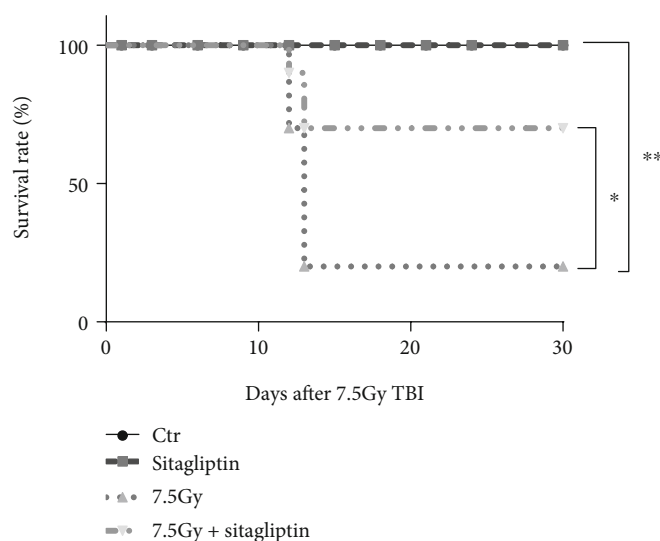


FIGURE 1: Effects of sitagliptin on the survival of mice exposed to 7.5 Gy TBI. Mice were divided into 4 groups: the control group and 7.5 Gy group were intragastrically administrated with PBS, and the sitagliptin group and 7.5 Gy+sitagliptin group were intragastrically administrated with sitagliptin. The drugs were given for the first time 2 hours after the 7.5 Gy TBI, followed by continuous administration for 7 days, and the survival of the mice was observed for 30 days. Kaplan-Meier survival analysis of mice after TBI, $n = 10$, * $p < 0.05$, ** $p < 0.01$.

from C57BL/6J (CD45.2) mice. The mixed cells were transplanted into lethally irradiated (9.0 Gy TBI) C57BL/6J (CD45.2) recipient mice through lateral canthus vein injection. The percentage of donor-derived (CD45.1 positive) cells in the recipients' peripheral blood was examined 2 months after transplantation. The red blood cells (RBCs) were lysed using RBC lysis solution (eBioscience), and then the blood samples were stained with the following antibodies: anti-CD45.1-FITC, anti-CD45.2-PE. The cells were analyzed with an Accuri C6 flow cytometer (BD Bioscience) [28, 29].

2.7. Analysis of the Levels of Intracellular Reactive Oxygen Species (ROS). After the BM cells were stained with the LSK antibodies as described above, the cells were incubated with 10 μ M DCFDA or 5 μ M MitSox for 20 min at 37°C. The intracellular ROS levels in hematopoietic cells were analyzed by measuring the mean fluorescence intensity (MFI) of DCF and MitSox by flow cytometry. For each sample, a minimum of 100,000 Lin⁺ cells were acquired [30].

2.8. Analysis of γ H2AX Phosphorylation and NOX4 Expression. After the BM cells were stained with the LSK antibodies as described above, the cells were fixed and permeabilized by BD Cytotfix/Cytoperm buffer according to the manufacturer's protocol and then stained with antibodies against γ H2AX phosphorylation or NOX4 and FITC-conjugated secondary antibodies. The expression of γ H2AX and NOX4 in the hematopoietic cells was determined by analyzing the MFI of FITC by flow cytometry [30].

2.9. Measurement of Inflammatory Cytokines in Serum. 10 days after irradiation, the peripheral blood of mice was collected, and the serum was taken after standing overnight. Then, the serum was analyzed using the BD Cytometric Bead Array Mouse Inflammation Kit (San Diego, CA, USA) as the manufacturer's protocol. In brief, the samples were incubated

with mixed capture beads and detection antibodies. After incubation for two hours at room temperature, the samples were washed and detected by flow cytometry. The results were analyzed by the company.

2.10. Statistical Analysis. Data were presented as the mean \pm standard error of the mean. Significant differences between experimental groups were evaluated by using a one-way analysis of variance (ANOVA) with repeated measures followed by post hoc comparisons with Tukey's multiple paired comparison test except result 2. Significant differences between groups of the numbers of hematopoietic cells were evaluated by unpaired two-tailed Student's t test. Mice survival curves were analyzed by the Kaplan-Meier method and log-rank tests. Differences were considered significant at $p < 0.05$. Statistical analyses were performed using GraphPad Prism 8 software (San Diego, CA, USA).

3. Results

3.1. Sitagliptin Increased the Survival Rate of Mice after TBI. In order to test whether sitagliptin affected the survival of mice after TBI, we treated mice with 10 mg/kg sitagliptin daily for 7 days after 7.5 Gy TBI and observed their 30-day survival rate. As shown in Figure 1, the Kaplan-Meier analysis of survival indicated that the survival rate of irradiated mice treated with sitagliptin was significantly higher than that of 7.5 Gy irradiated mice.

3.2. Sitagliptin Increased the Numbers of Hematopoietic Cells after TBI. The survival of mice exposed to sublethal dose radiation can partly attribute to the recovery of the hematopoietic system [13, 28]. In the present study, the numbers of BMMNCs and HSPCs in BM were also analyzed. 4 Gy TBI caused a decrease in the numbers of BMMNCs and HSPCs compared with that from control mice. However,

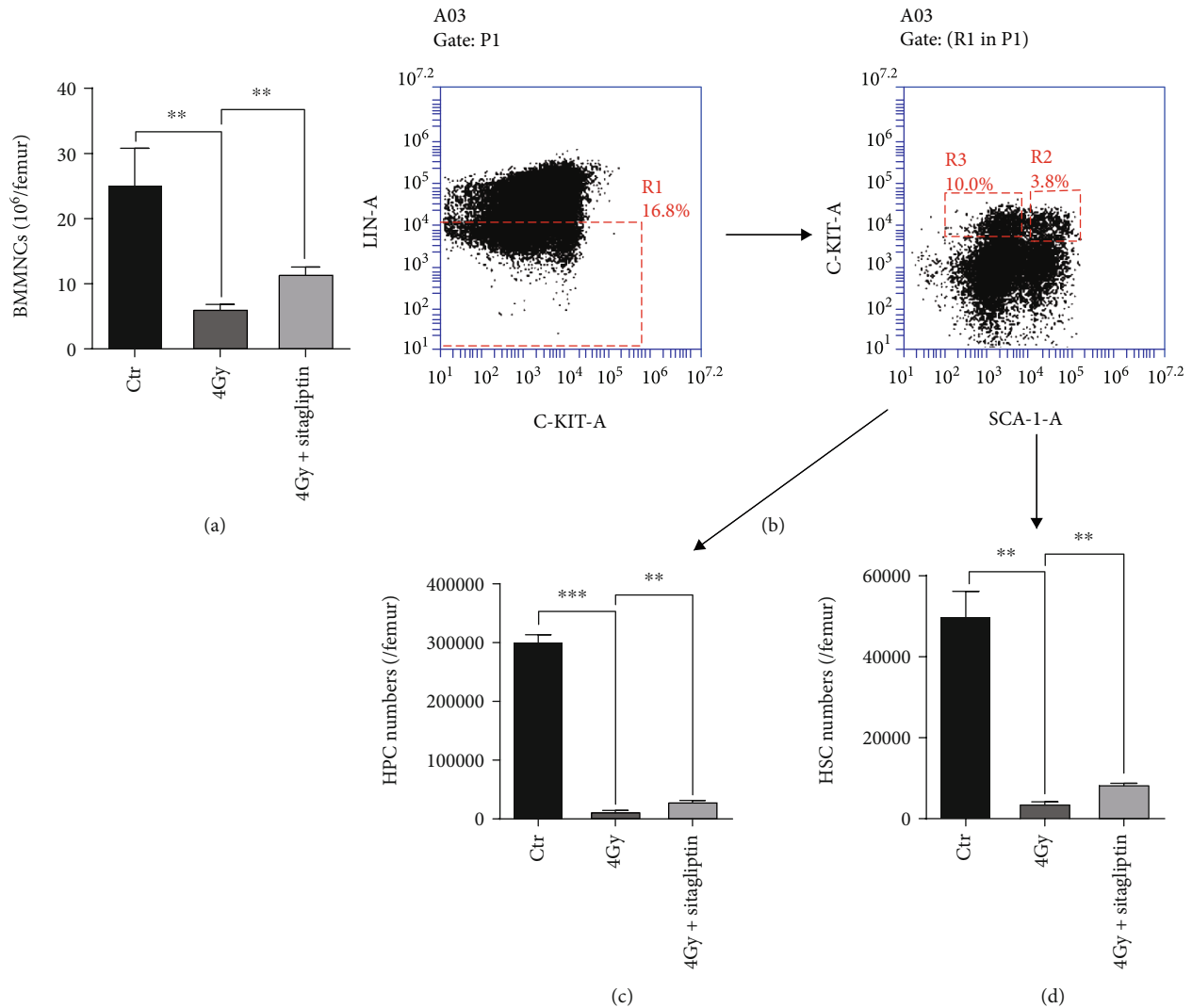


FIGURE 2: Effects of sitagliptin on the numbers of hematopoietic cells. Mice were divided into 3 groups: sham irradiation, 4 Gy group, and 4 Gy+sitagliptin group. The dosage regimen was the same as above. BM cells were collected from mice 10 days after TBI. (a) Numbers of BMMNCs; (b) Representative flow cytometry gate graph of lineage negative and HSPCs; (c) Numbers of HPCs; (d) Numbers of HSCs. Data were expressed as the mean \pm SEM ($n = 5$). ** $p < 0.01$, *** $p < 0.001$.

sitagliptin mitigated the impaired BMMNCs and HSPCs in BM (Figure 2). These data suggested that sitagliptin effectively relieved 4 Gy TBI-induced hematopoietic cell injury.

3.3. Sitagliptin Influenced the Functions of HSPCs after TBI. BM exposed to moderate or high-dose TBI may have long-term hematopoietic residual damage, mainly due to defects in the self-renewal and differentiation ability of HSCs [7]. Thus, we analyzed the effects of sitagliptin on the clonogenic function of HPCs in mice exposed to 4 Gy via CFU assays and the engraftment capability via CRA. As shown in Figure 3(a), 4 Gy TBI caused a significant suppression of HPCs clonogenic function, and sitagliptin increased the formation of CFU-GMs. Since long-term and repeated transplantation are the gold standard for measuring HSCs functions [31], we performed a CRA to determine whether sitagliptin improved HSC self-renewal function. Our results showed that the engraftment capability of irradiated HSCs

did not improve after sitagliptin treatment (Figures 3(b) and 3(c)). These results suggested that sitagliptin had no obvious protective effect on the self-renewal of HSCs.

3.4. Sitagliptin Reduced TBI-Induced DNA Double-Strand Breaks (DSBs). As reported previously, TBI caused sustained DNA damage and oxidative DNA damage [32]. To evaluate whether sitagliptin regulated DNA damage of hematopoietic cells, we used flow cytometry to analyze histone H2AX phosphorylation. As shown in Figure 4, compared with the control group, the expression of histone H2AX phosphorylation was higher in BMMNCs, HPCs, and HSCs when the mice exposed 4 Gy TBI, consistent with our previous finding [13, 33]. These data suggested that sitagliptin effectively decreased TBI-induced persistent DNA damage.

3.5. Sitagliptin Decreased TBI-Induced Oxidative Stress Levels in Hematopoietic Cells. In our previous studies, we have

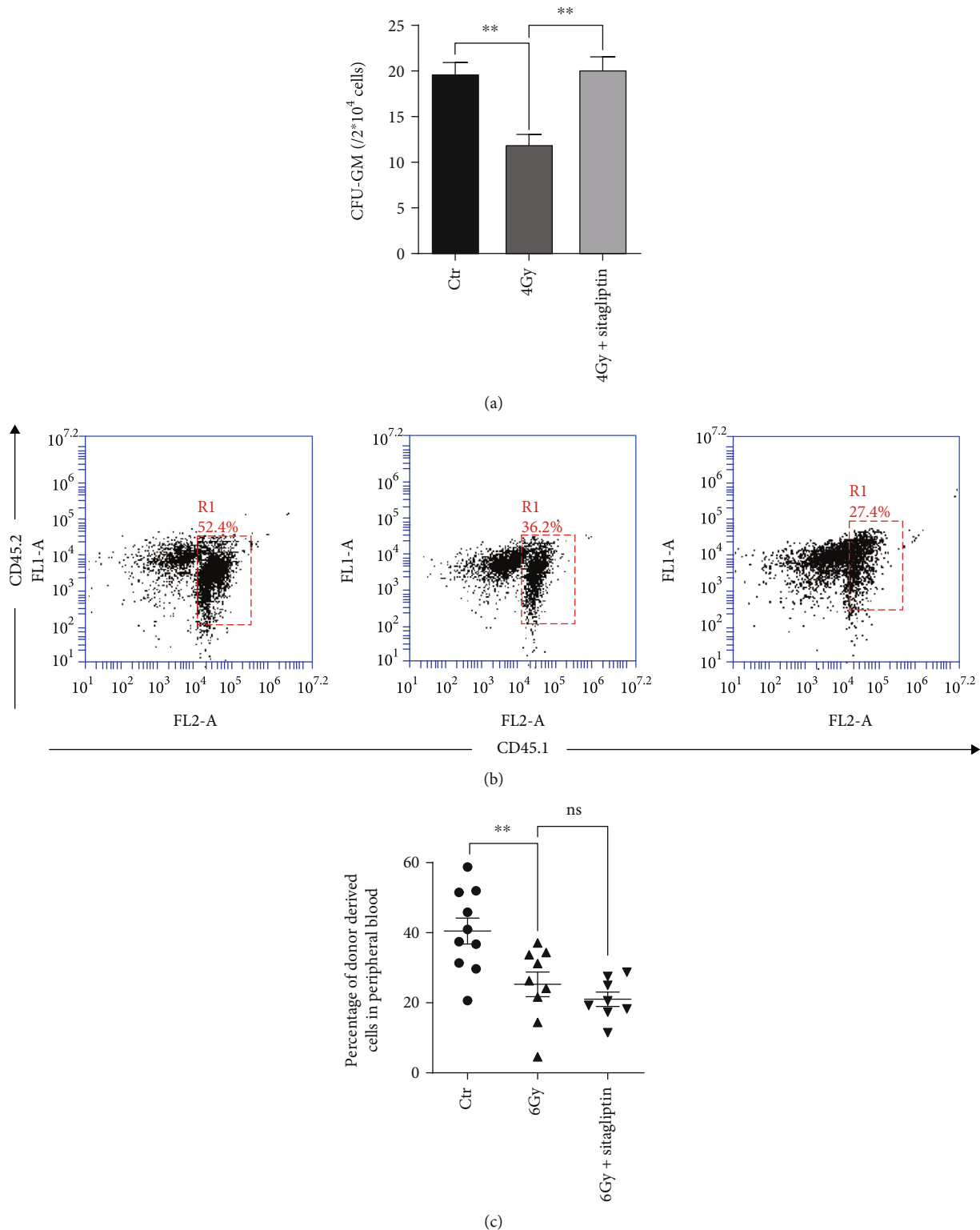


FIGURE 3: Effects of sitagliptin on the functions of HSPCs. The grouping and administration methods are the same as above. BM cells were collected from mice 10 days after TBI. (a) BM cells were cultured in MethoCult GF M3534 methyl ligand medium, and the numbers of CFU-GMs were counted after 7 days. The proportion of donor cells in the recipient mice was measured 2 months after the donor cells were transplanted to the recipient mice; (b) Representative FACS analysis of the CRA; (c) The percentage of donor-derived cells in peripheral blood cells. Data were expressed as the mean \pm SEM ($n = 5$), ** $p < 0.01$.

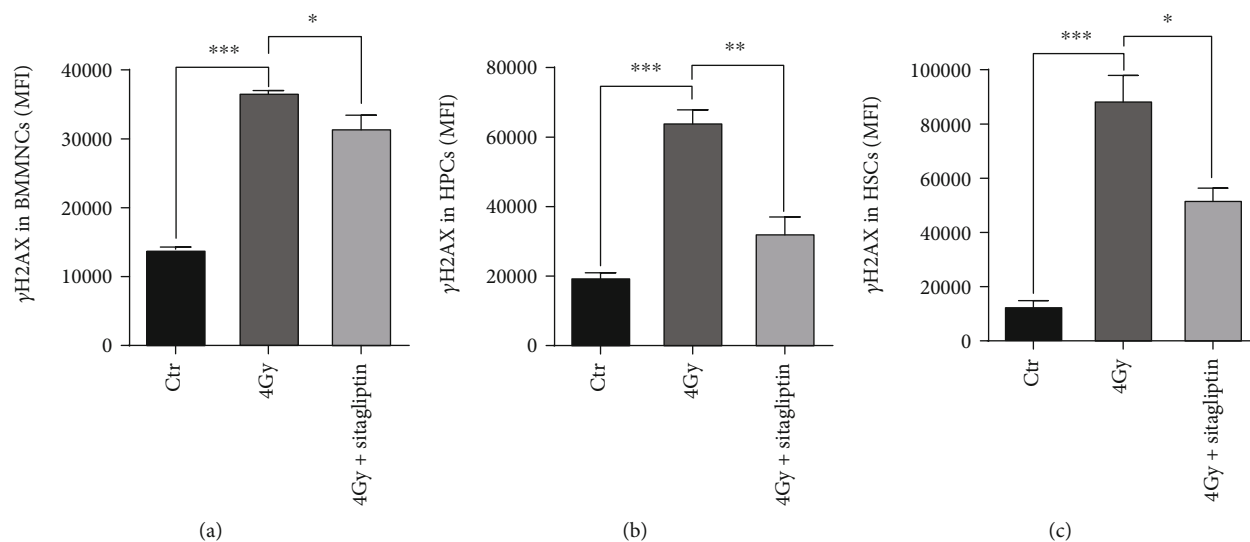


FIGURE 4: Effects of sitagliptin on the IR induced DNA injury of the hematopoietic cells. Grouping and administration methods as described above. Fixed and permeabilized BM cells after LSK antibodies incubation, then stained with γ H2AX phosphorylation antibody. (a) γ H2AX formation in BMMNCs; (b) γ H2AX formation in HPCs; (c) γ H2AX formation in HSCs. Data were expressed as the mean \pm SEM ($n = 5$), * $p < 0.05$, ** $p < 0.01$, *** $p < 0.001$.

demonstrated that the mice exposed to sublethal doses develop long-term myelosuppression through chronic oxidative stress [34, 35], thus we examined whether sitagliptin ameliorated TBI-induced BM suppression via decreasing ROS levels. In our study, we detected ROS and mitochondrial superoxide radicals by using DCFH-DA and MitSox, respectively. As shown in Figures 5(a)–5(c), compared with those in the control mice, the levels of ROS in mice receiving 4 Gy TBI elevated significantly. When treated with sitagliptin, the ROS levels in BMMNCs and HSPCs decreased obviously. In addition, sitagliptin also decreased the levels of MitSox in hematopoietic cells especially in HPCs (Figures 5(d)–5(f)). These results indicated that sitagliptin decreased oxidative stress in hematopoietic cells.

3.6. Sitagliptin Reduced the Expression of NOX4 after TBI. NOX4 is a prooxidase that has been shown to mediate IR-induced increases in ROS production in HSCs [28]. Therefore, we examined the effects of DPP4's inhibition on the expression of NOX4. As shown in Figure 6, an increase in NOX4 expression was detected in BMMNCs, HPCs, and HSCs in the irradiation group compared with the control group, respectively. Sitagliptin decreased the expression of NOX4 in hematopoietic cells. These findings suggested that sitagliptin decreased the levels of ROS in hematopoietic cells in part via a downregulation of NOX4 expression.

3.7. Sitagliptin Relieved TBI-Induced Inflammatory Response. DPP4 cleaves the N-terminus of GM-CSF, G-CSF, IL-3, and erythropoietin, and the inhibition of DPP4 enhances their activity [23], so we examined the effect of sitagliptin on the expression of inflammatory cytokines in serum. In our study, we found that sublethal dose irradiation increased the expression of IL-6, IL-12, and γ -IFN in mice, while sitagliptin significantly reduced the expression of cytokines (Figure 7).

These results suggested that sitagliptin might influence the level of inflammation in the BM microenvironment.

4. Discussion

Sitagliptin is a type 2 diabetes treatment drug, which acts by inhibiting the activity of DPP4. In recent years, sitagliptin was found to have antioxidant and anti-inflammatory effects, which plays a role in atherosclerosis, inflammatory bowel disease, heart failure, vascular inflammation, and other diseases [18, 36, 37]. Metformin as another kind of type 2 diabetes drug approved by FDA, our previous study has shown that it alleviates HSCs aging by inhibiting NOX4-mediated oxidative stress, thus improving long-term HSCs injury induced by IR in mice [13]. In addition, metformin improves ARS symptoms such as pulmonary fibrosis and skin collagen deposition [37, 38]. Therefore, we speculate that sitagliptin may also have therapeutic effects on IR-induced tissue damage. In this study, we observed the effect of sitagliptin on the survival rate of irradiated mice and showed that sitagliptin significantly increased the 30-day survival rate, which indicated that sitagliptin had a therapeutic effect on radiation injury in mice.

Then, the therapeutic effects of sitagliptin on hematopoietic radiation injury were explored. Firstly, the changes in the numbers of hematopoietic cells were observed. The results showed that the numbers of BMMNCs, HPCs, and HSCs in mice exposed to IR increased after the administration of sitagliptin, which indicated that sitagliptin could decrease hematopoietic radiation damage. Secondly, the effects of sitagliptin on the function of HPCs and HSCs were evaluated by CFU-GM and CRA experiments. The CFU-GM results showed that sitagliptin could restore the proliferation ability of HPCs, but the CRA results suggested that sitagliptin had no obvious direct effect on the self-renewal of HSCs. It may

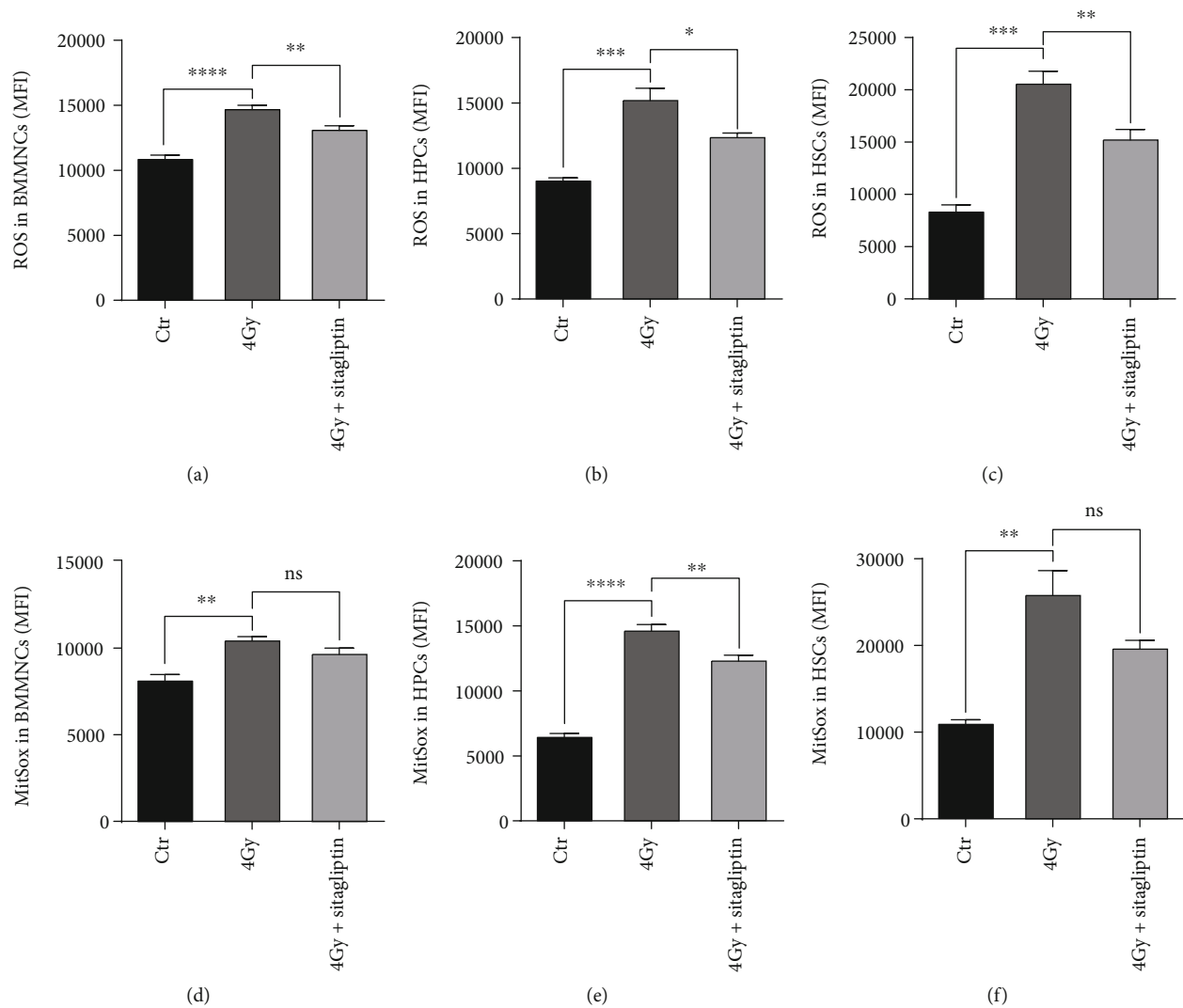


FIGURE 5: Effects of sitagliptin on the oxidative stress levels of hematopoietic cells. Grouping and administration methods as described above. After 10 days of TBI, BM cells were collected and labeled with LSK antibodies, then incubated with DCFDA or MitSox. (a) ROS of BMMNCs; (b) ROS of HPCs; (c) ROS of HSCs; (d) MitSox of BMMNCs; (e) MitSox of HPCs; (f) MitSox of HSCs. Data were expressed as the mean \pm SEM ($n = 3$), * $p < 0.05$, ** $p < 0.01$, *** $p < 0.001$, **** $p < 0.0001$.

be due to part of DPP4 is soluble and exists in the microenvironment [25, 39]. Sitagliptin may play a protective role in the hematopoietic injury by direct regulation of hematopoietic cells and indirect action on the hematopoietic microenvironment, which is partly proved by our following serum cytokines results (Figure 7). The oxidative stress induced by IR is an important reason of hematopoietic injury. At the instant of irradiation, IR will cause radiation decomposition of intracellular water and stimulate nitrogen oxide synthase to produce ROS and reactive nitrogen species (RNS), respectively [39]. Radiation also leads to electron leakage of mitochondria, increases expression of cyclooxygenase and lipoxygenase, and changes in NOXs expression [40, 41], resulting in the production of a large numbers of cell-derived free radicals, giving rise to long-term damage to cells. Radiation-induced DNA damage and oxidative stress lead to an increase in the numbers of apoptotic, necrotic, autophagic, and senescent cells [42]. The products of dead cells can trigger inflam-

mation of immune cells and activate the expression of TGF- β [43], which in turn lead to the upregulation of NOXs expression; NOXs further amplifies reactions such as oxidative stress in the positive feedback loop and aggravates radiation damage. There are several isoforms of NOXs in nonphagocytic cells, including NOX1, NOX2, NOX3, NOX4, NOX5, DUOX1, and DUOX2 [44]. Previous studies have shown that NOXs, especially NOX4, might be the main reason for TBI-induced ROS production in HSCs [45]. In our previous studies, we have demonstrated that many compounds such as metformin, resveratrol, and 3,3'-diindolylmethane protect hematopoietic radiation injury by inhibiting NOX4 [13, 35, 45]. Recent studies also showed that melatonin alleviated the injury of the radiation-induced hematopoietic system by inhibiting the expression of NOX2 and NOX4 [46]. In this study, we observed that sitagliptin significantly decreased the oxidation level in BMMNCs, HPCs, and HSCs by inhibiting the expression of NOX4. Therefore, NOX4 is a promising

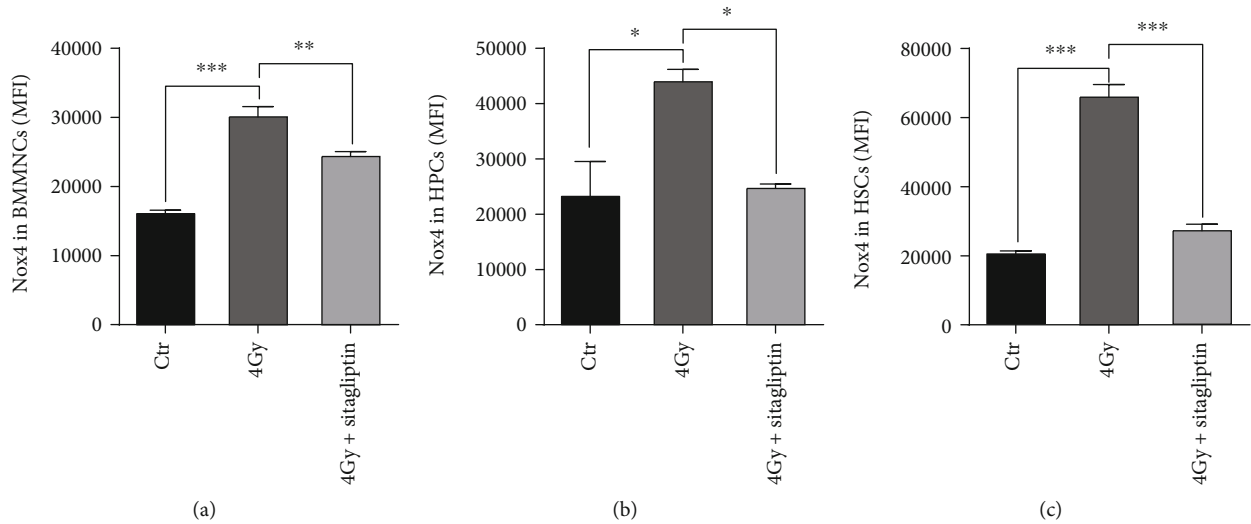


FIGURE 6: Effects of sitagliptin on the NOX4 expression of hematopoietic cells. Grouping and administration methods as described above. Fixed and permeabilized BM cells after LSK antibodies incubation as mentioned above, then, stained with NOX4 antibody. (a) NOX4 expression in BMMNCs; (b) NOX4 expression in HPCs; (c) NOX4 expression in HSCs. Data were expressed as the mean \pm SEM ($n = 3$), * $p < 0.05$, ** $p < 0.01$, *** $p < 0.001$.

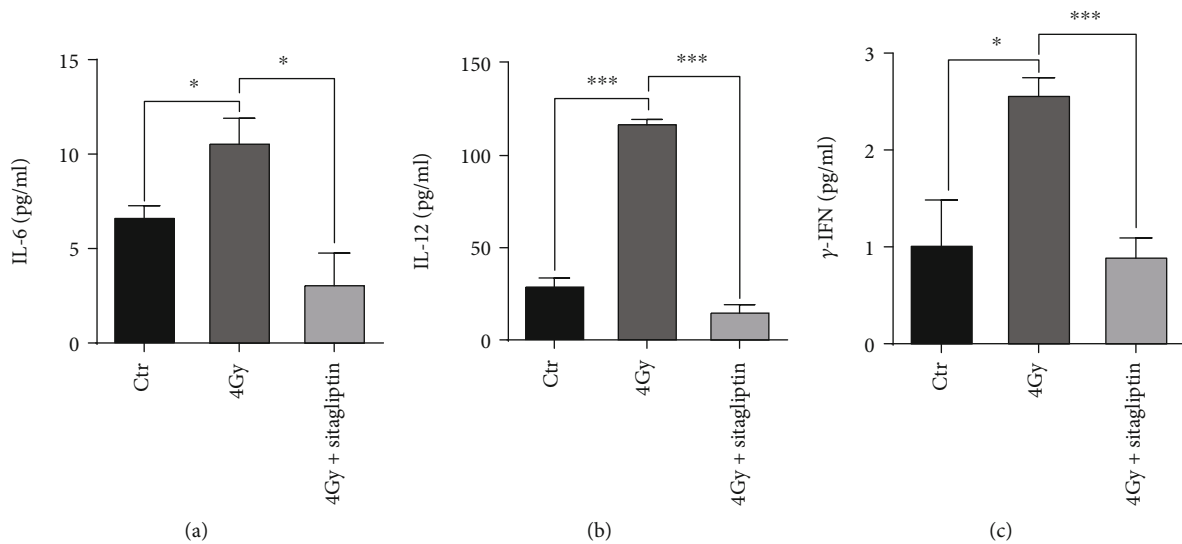


FIGURE 7: Effects of sitagliptin on the expression of cytokines in the serum. The peripheral blood of mice was collected 10 days after TBI, then left to stand overnight to separate serum and detected by an inflammatory factor kit. (a) IL-6 cytokine; (b) IL-12 cytokine; (c) γ -IFN cytokine. Data were expressed as the mean \pm SEM ($n = 3 - 5$), * $p < 0.05$, *** $p < 0.001$.

target for the treatment of IR-induced hematopoietic injury, and targeting the promotion or inhibition of this enzyme family may mitigate radiation damage to certain organs, such as hematopoietic system, gastrointestinal system, central nervous system, and skin system.

IR not only induces DNA structural damage directly through the ionizing photons, but also destroys DNA structure caused by the increase of ROS [47]. The destruction of DNA structure will lead to metabolic and functional changes and eventually lead to cell damage or death. In this study, we observed the relationship between sitagliptin and DNA damage and found that sitagliptin decreased the expression of γ H2AX, consistent with the research in chronic cerebral

hypoperfusion mice [48]. These results indicated that sitagliptin alleviated cellular DNA damage and exerted hematopoietic radiation therapy.

Medium or high doses of IR not only damages the hematopoietic system, but also causes injury to the gastrointestinal tract, resulting in intestinal microorganisms to enter the systemic circulation through penetrating mucous membrane [49]. Endotoxins in bacteria will directly interact with cells including endothelial cells in the bone marrow microenvironment, changing the release ability of inflammatory factors, thus inducing myelosuppression and HSCs failure [50]. Studies have shown that rBPI21 reduces the injury and death of HSCs by reducing the level of inflammation

and promoting the expression of CSFs in plasma and bone marrow [51]. Sitagliptin exerts a comprehensive and effective anti-inflammatory action on humans, which reduces the concentrations of CRP and IL-6 in plasma [17]. In addition, previous studies have shown that DPP4 may be involved in the expression of IL-6 and other cytokines in the JAK-STAT signaling pathway, while the JAK-STAT signaling pathway is involved in the differentiation, activation, and proliferation of Th cells, and the expression of Th1 cytokines (γ -IFN, IL-2, TNF- α , etc.) or Th2 cytokines (IL-4, IL-6, IL-10, etc.) is decreased after blocking the JAK-STAT pathway; therefore, the inflammatory response is alleviated [52, 53]. In our study, we observed the relationship between sitagliptin and the expression of inflammatory cytokines IL-6, IL-12, and γ -IFN in serum. It was found that sublethal dose irradiation increased the expression of IL-6, IL-12, and γ -IFN in mice, while sitagliptin significantly reduced the expression of cytokines (Figure 7). These suggested that sitagliptin might treat hematopoietic injury from IR by influencing cytokines in the BM microenvironment.

5. Conclusions

In conclusion, our study showed that the administration of sitagliptin had therapeutic effects on hematopoietic injury. The therapeutic effect might be mainly achieved by reducing the level of NOX4-mediated oxidative stress in hematopoietic cells, and the alleviation of inflammatory was also helpful. Therefore, sitagliptin might be a potential therapeutic agent for the treatment of radiation-induced hematopoietic injury.

Data Availability

The data used to support the findings of this study are available from the corresponding author upon request.

Conflicts of Interest

The authors declare that they have no conflicts of interest.

Acknowledgments

This study was supported by the National Natural Science Foundation of China [grant numbers 81573094 and 81972975]; CAMS Medicine and Health Technology Innovation Project [grant numbers 2017-I2M-3-019].

References





- [1] N. M. Gandhi, "Baicalein protects mice against radiation-induced DNA damages and genotoxicity," *Molecular and Cellular Biochemistry*, vol. 379, no. 1-2, pp. 277–281, 2013.
- [2] Y. Dong, Y. Cheng, Q. Hou, J. Wu, D. Li, and H. Tian, "The protective effect of new compound XH-103 on radiation-induced GI syndrome," *Oxidative Medicine and Cellular Longevity*, vol. 2018, Article ID 3920147, 9 pages, 2018.
- [3] J. G. Kiang and A. O. Olabisi, "Radiation: a poly-traumatic hit leading to multi-organ injury," *Cell Biosci*, vol. 9, no. 1, 2019.
- [4] S. Banerjee, Q. Fu, S. K. Shah et al., "C/EBP δ protects from radiation-induced intestinal injury and sepsis by suppression of inflammatory and nitrosative stress," *Scientific Reports*, vol. 9, no. 1, p. 13953, 2019.
- [5] T. Reya, "Regulation of hematopoietic stem cell self-renewal," *Recent Progress in Hormone Research*, vol. 58, no. 1, pp. 283–295, 2003.
- [6] S. Pinho and P. S. Frenette, "Haematopoietic stem cell activity and interactions with the niche," *Nature Reviews Molecular Cell Biology*, vol. 20, no. 5, pp. 303–320, 2019.
- [7] L. Shao, Y. Luo, and D. Zhou, "Hematopoietic stem cell injury induced by ionizing radiation," *Antioxidants & Redox Signaling*, vol. 20, no. 9, pp. 1447–1462, 2014.
- [8] Y. Wang, B. A. Schulte, and D. Zhou, "Hematopoietic stem cell senescence and long-term bone marrow injury," *Cell Cycle*, vol. 5, no. 1, pp. 35–38, 2005.
- [9] D. I. Bunin, J. Bakke, C. E. Green, H. S. Javitz, M. Fielden, and P. Y. Chang, "Romiplostim (Nplate[®]) as an effective radiation countermeasure to improve survival and platelet recovery in mice," *International Journal of Radiation Biology*, vol. 96, no. 1, pp. 145–154, 2020.
- [10] R. V. Gardner, R. Begue, and E. McKinnon, "The effect of granulocyte-macrophage colony-stimulating factor (GM-CSF) on primitive hematopoietic stem cell (PHSC) function and numbers, after chemotherapy," *Experimental Hematology*, vol. 29, no. 9, pp. 1053–1059, 2001.
- [11] R. van Os, S. Robinson, T. Sheridan, J. M. Mislow, D. Dawes, and P. M. Mauch, "Granulocyte colony-stimulating factor enhances bone marrow stem cell damage caused by repeated administration of cytotoxic agents," *Blood*, vol. 92, no. 6, pp. 1950–1956, 1998.
- [12] R. van Os, S. Robinson, T. Sheridan, and P. M. Mauch, "Granulocyte-colony stimulating factor impedes recovery from damage caused by cytotoxic agents through increased differentiation at the expense of self-renewal," *Stem Cells*, vol. 18, no. 2, pp. 120–127, 2000.
- [13] G. Xu, H. Wu, J. Zhang et al., "Metformin ameliorates ionizing irradiation-induced long-term hematopoietic stem cell injury in mice," *Free Radical Biology and Medicine*, vol. 87, pp. 15–25, 2015.
- [14] T. J. Kieffer, C. H. McIntosh, and R. A. Pederson, "Degradation of glucose-dependent insulintropic polypeptide and truncated glucagon-like peptide 1 in vitro and in vivo by dipeptidyl peptidase IV," *Endocrinology*, vol. 136, no. 8, pp. 3585–3596, 1995.
- [15] P. E. MacDonald, W. El-kholy, M. J. Riedel, A. M. F. Salapatek, P. E. Light, and M. B. Wheeler, "The multiple actions of GLP-1 on the process of glucose-stimulated insulin secretion," *Diabetes*, vol. 51, Supplement 3, pp. S434–S442, 2002.
- [16] G. Holz and O. Chepurny, "Glucagon-like peptide-1 synthetic analogs: new therapeutic agents for use in the treatment of diabetes mellitus," *Current Medicinal Chemistry*, vol. 10, no. 22, pp. 2471–2483, 2003.
- [17] A. Makdissi, H. Ghanim, M. Vora et al., "Sitagliptin exerts an anti-inflammatory action," *The Journal of Clinical Endocrinology and Metabolism*, vol. 97, no. 9, pp. 3333–3341, 2012.
- [18] X. Zhou, W. Wang, C. Wang et al., "DPP4 Inhibitor attenuates severe acute pancreatitis-associated intestinal inflammation via Nrf2 signaling," *Oxidative Medicine and Cellular Longevity*, vol. 2019, Article ID 6181754, 11 pages, 2019.
- [19] Y. Wu, M. Xu, H. Bao, and J.-H. Zhang, "Sitagliptin inhibits EndMT in vitro and improves cardiac function of diabetic rats

- through the SDF-1 α /PKA pathway,” *European Review for Medical and Pharmacological Sciences*, vol. 23, no. 2, pp. 841–848, 2019.
- [20] G. Pujadas, V. de Nigris, F. Prattichizzo, L. la Sala, R. Testa, and A. Ceriello, “The dipeptidyl peptidase-4 (DPP-4) inhibitor teneligliptin functions as antioxidant on human endothelial cells exposed to chronic hyperglycemia and metabolic high-glucose memory,” *Endocrine*, vol. 56, no. 3, pp. 509–520, 2017.
- [21] G. Esposito, D. Cappetta, R. Russo et al., “Sitagliptin reduces inflammation, fibrosis and preserves diastolic function in a rat model of heart failure with preserved ejection fraction,” *British Journal of Pharmacology*, vol. 174, no. 22, pp. 4070–4086, 2017.
- [22] S. A. Abdel-Gaber, A. Gedday, and R. A. Moussa, “The hepatoprotective effect of sitagliptin against hepatic ischemia reperfusion-induced injury in rats involves Nrf-2/HO-1 pathway,” *Pharmacological Reports*, vol. 71, no. 6, pp. 1044–1049, 2019.
- [23] H. E. Broxmeyer, J. Hoggatt, H. A. O’Leary et al., “Dipeptidyl-peptidase 4 negatively regulates colony-stimulating factor activity and stress hematopoiesis,” *Nature Medicine*, vol. 18, no. 12, pp. 1786–1796, 2012.
- [24] C. Klemann, L. Wagner, M. Stephan, and S. von Hörsten, “Cut to the chase: a review of CD26/dipeptidyl peptidase-4’s (DPP4) entanglement in the immune system,” *Clinical and Experimental Immunology*, vol. 185, no. 1, pp. 1–21, 2016.
- [25] H. E. Broxmeyer, M. Capitano, T. B. Campbell, G. Hangoc, and S. Cooper, “Modulation of hematopoietic chemokine effects in vitro and in vivo by DPP-4/CD26,” *Stem Cells and Development*, vol. 25, no. 8, pp. 575–585, 2016.
- [26] X. Ou, H. A. O’Leary, and H. E. Broxmeyer, “Implications of DPP4 modification of proteins that regulate stem/progenitor and more mature cell types,” *Blood*, vol. 122, no. 2, pp. 161–169, 2013.
- [27] E. Yoo, L. A. Paganessi, W. A. Alikhan et al., “Loss of CD26 protease activity in recipient mice during hematopoietic stem cell transplantation results in improved transplant efficiency,” *Transfusion*, vol. 53, no. 4, pp. 878–887, 2013.
- [28] L. Lu, J. Dong, D. Li, J. Zhang, and S. Fan, “3,3’-diindolyl-methane mitigates total body irradiation-induced hematopoietic injury in mice,” *Free Radical Biology and Medicine*, vol. 99, pp. 463–471, 2016.
- [29] C. Li, L. Lu, J. Zhang et al., “Granulocyte colony-stimulating factor exacerbates hematopoietic stem cell injury after irradiation,” *Cell & Bioscience*, vol. 5, no. 1, 2015.
- [30] W. Long, G. Zhang, Y. Dong, and D. Li, “Dark tea extract mitigates hematopoietic radiation injury with antioxidative activity,” *Journal of Radiation Research*, vol. 59, no. 4, pp. 387–394, 2018.
- [31] Y. Wang, J. Kellner, L. Liu, and D. Zhou, “Inhibition of p38 mitogen-activated protein kinase promotes ex vivo hematopoietic stem cell expansion,” *Stem Cells and Development*, vol. 20, no. 7, pp. 1143–1152, 2011.
- [32] J. Zhang, X. Xue, X. Han et al., “Hydrogen-rich water ameliorates total body irradiation-induced hematopoietic stem cell injury by reducing hydroxyl radical,” *Oxidative Medicine and Cellular Longevity*, vol. 2017, Article ID 8241678, 16 pages, 2017.
- [33] J. Zhang, X. Xue, X. Han et al., “Vam3 ameliorates total body irradiation-induced hematopoietic system injury partly by regulating the expression of Nrf2 -targeted genes,” *Free Radical Biology and Medicine*, vol. 101, pp. 455–464, 2016.
- [34] J. Zhang, X. Han, Y. Zhao, X. Xue, and S. Fan, “Mouse serum protects against total body irradiation-induced hematopoietic system injury by improving the systemic environment after radiation,” *Free Radical Biology and Medicine*, vol. 131, pp. 382–392, 2019.
- [35] H. Zhang, Z. Zhai, Y. Wang et al., “Resveratrol ameliorates ionizing irradiation-induced long-term hematopoietic stem cell injury in mice,” *Free Radical Biology and Medicine*, vol. 54, pp. 40–50, 2013.
- [36] Y. He, G. Yang, F. Yao et al., “Sitagliptin inhibits vascular inflammation via the SIRT6-dependent signaling pathway,” *International Immunopharmacology*, vol. 75, p. 105805, 2019.
- [37] N. Sato, N. Takasaka, M. Yoshida et al., “Metformin attenuates lung fibrosis development via NOX4 suppression,” *Respiratory Research*, vol. 17, no. 1, p. 107, 2016.
- [38] J.-M. Kim, H. Yoo, J. Y. Kim et al., “Metformin alleviates radiation-induced skin fibrosis via the downregulation of FOXO3,” *Cellular Physiology and Biochemistry*, vol. 48, no. 3, pp. 959–970, 2018.
- [39] T. Kumagai, F. Rahman, and A. M. Smith, “The microbiome and radiation induced-bowel injury: evidence for potential mechanistic role in disease pathogenesis,” *Nutrients*, vol. 10, no. 10, p. 1405, 2018.
- [40] K. Bedard and K.-H. Krause, “The NOX family of ROS-generating NADPH oxidases: physiology and pathophysiology,” *Physiological Reviews*, vol. 87, no. 1, pp. 245–313, 2007.
- [41] J. Chang, W. Feng, Y. Wang et al., “Whole-body proton irradiation causes long-term damage to hematopoietic stem cells in mice,” *Radiation Research*, vol. 183, no. 2, pp. 240–248, 2015.
- [42] G. C. Barnett, C. M. L. West, A. M. Dunning et al., “Normal tissue reactions to radiotherapy: towards tailoring treatment dose by genotype,” *Nature Reviews Cancer*, vol. 9, no. 2, pp. 134–142, 2009.
- [43] M. Najafi, N. Hashemi Goradel, B. Farhood et al., “Macrophage polarity in cancer: a review,” *Journal of Cellular Biochemistry*, vol. 120, no. 3, pp. 2756–2765, 2018.
- [44] A. Daiber, S. Steven, K. Vujacic-Mirski et al., “Regulation of vascular function and inflammation via cross talk of reactive oxygen and nitrogen species from mitochondria or NADPH oxidase-implications for diabetes progression,” *International Journal of Molecular Sciences*, vol. 21, no. 10, p. 3405, 2020.
- [45] Y. Wang, L. Liu, S. K. Pazhanisamy, H. Li, A. Meng, and D. Zhou, “Total body irradiation causes residual bone marrow injury by induction of persistent oxidative stress in murine hematopoietic stem cells,” *Free Radical Biology and Medicine*, vol. 48, no. 2, pp. 348–356, 2010.
- [46] P. Amini, M. Ashrafzadeh, E. Motevaseli, M. Najafi, and A. Shirazi, “Mitigation of radiation-induced hematopoietic system injury by melatonin,” *Environmental Toxicology*, pp. 1–7, 2020.
- [47] K. Mortezaee, D. Shabeeb, A. E. Musa, M. Najafi, and B. Farhood, “Metformin as a radiation modifier; implications to normal tissue protection and tumor sensitization,” *Current Clinical Pharmacology*, vol. 14, no. 1, pp. 41–53, 2019.
- [48] T.-H. Tsai, C. K. Sun, C. H. Su et al., “Sitagliptin attenuated brain damage and cognitive impairment in mice with chronic cerebral hypo-perfusion through suppressing oxidative stress and inflammatory reaction,” *Journal of Hypertension*, vol. 33, no. 5, pp. 1001–1013, 2015.

- [49] C. Booth, G. Tudor, J. Tudor, B. P. Katz, and T. J. MacVittie, "Acute gastrointestinal syndrome in high-dose irradiated mice," *Health Physics*, vol. 103, no. 4, pp. 383–399, 2012.
- [50] R. I. Walker, G. D. Ledney, and C. B. Galley, "Aseptic endotoxemia in radiation injury and graft-vs-host disease," *Radiation Research*, vol. 62, no. 2, pp. 242–249, 1975.
- [51] K. J. Janec, H. Yuan, J. E. Norton Jr et al., "rBPI21(opebacan) promotes rapid trilineage hematopoietic recovery in a murine model of high-dose total body irradiation," *American Journal of Hematology*, vol. 93, no. 8, pp. 1002–1013, 2018.
- [52] M. Jargosch, S. Kröger, E. Gralinska et al., "Data integration for identification of important transcription factors of STAT6-mediated cell fate decisions," *Genetics and Molecular Research*, vol. 15, no. 2, 2016.
- [53] Y. Jamilloux, T. el Jammal, L. Vuitton, M. Gerfaud-Valentin, S. Kerever, and P. Sève, "JAK inhibitors for the treatment of autoimmune and inflammatory diseases," *Autoimmunity Reviews*, vol. 18, no. 11, 2019.

Research Article

Hexachloronaphthalene Induces Mitochondrial-Dependent Neurotoxicity via a Mechanism of Enhanced Production of Reactive Oxygen Species

Malwina Lisek ¹, Joanna Stragierowicz ², Feng Guo,³ Philipp P. Prosseda,⁴ Magdalena Wiktorska,⁵ Bozena Ferenc,¹ Anna Kilanowicz,² Ludmila Zylinska ¹, and Tomasz Boczek ¹

¹Department of Molecular Neurochemistry, Medical University of Lodz, 92215 Lodz, Poland

²Department of Toxicology, Medical University of Lodz, 90151 Lodz, Poland

³Department of Pharmaceutical Toxicology, China Medical University, Shenyang 110122, China

⁴Department of Patho Biochemistry, Goethe Universitätsklinikum, 60590 Frankfurt am Main, Germany

⁵Department of Molecular Cell Mechanisms, Medical University of Lodz, 92215 Lodz, Poland

Correspondence should be addressed to Tomasz Boczek; tomasz.boczek@umed.lodz.pl

Received 14 April 2020; Accepted 9 June 2020; Published 26 June 2020

Guest Editor: Sasanka Chakrabarti

Copyright © 2020 Malwina Lisek et al. This is an open access article distributed under the Creative Commons Attribution License, which permits unrestricted use, distribution, and reproduction in any medium, provided the original work is properly cited.

Hexachloronaphthalene (PCN67) is one of the most toxic among polychlorinated naphthalenes. Despite the known high bioaccumulation and persistence of PCN67 in the environment, it is still unclear to what extent exposure to these substances may interfere with normal neuronal physiology and lead to neurotoxicity. Therefore, the primary goal of this study was to assess the effect of PCN67 in neuronal *in vitro* models. Neuronal death was assessed upon PCN67 treatment using differentiated PC12 cells and primary hippocampal neurons. At 72 h postexposure, cell viability assays showed an IC_{50} value of $0.35 \mu\text{g/ml}$ and dose-dependent damage of neurites and concomitant downregulation of neurofilaments L and M. Moreover, we found that younger primary neurons (DIV4) were much more sensitive to PCN67 toxicity than mature cultures (DIV14). Our comprehensive analysis indicated that the application of PCN67 at the IC_{50} concentration caused necrosis, which was reflected by an increase in LDH release, HMGB1 protein export to the cytosol, nuclear swelling, and loss of homeostatic control of energy balance. The blockage of mitochondrial calcium uniporter partially rescued the cell viability, loss of mitochondrial membrane potential ($\Delta\Psi_m$), and the overproduction of reactive oxygen species, suggesting that the underlying mechanism of neurotoxicity involved mitochondrial calcium accumulation. Increased lipid peroxidation as a consequence of oxidative stress was additionally seen for $0.1 \mu\text{g/ml}$ of PCN67, while this concentration did not affect $\Delta\Psi_m$ and plasma membrane permeability. Our results show for the first time that neuronal mitochondria act as a target for PCN67 and indicate that exposure to this drug may result in neuron loss via mitochondrial-dependent mechanisms.

1. Introduction

Polychlorinated naphthalenes (PCNs) were included in 2015 into the Stockholm Convention on Persistent Organic Pollutants to protect human health and the environment from highly dangerous, long-lasting chemicals by the elimination of their production and reduction of their unintentional release [1]. Despite these restrictions and no commercial use for over 30 years, the general population is constantly

exposed to PCNs due to their main accumulation in foods of animal origin, especially those rich in fat (oil from fish, meat, and milk) [2–5]. Currently, the main sources of PCNs are not old technical formulations used previously (e.g., Halowax) but high-temperature industrial processes that contribute to global environmental contamination [6–10]. The evidence of their ubiquity in the environment is their detection in sediments, soil, water, and air [11–18]. In addition, high lipophilicity and resistance to degradation have

led to their bioconcentration and bioaccumulation in the food chain [19]. This is confirmed by their persistent presence in various biological materials collected from the general population such as serum [20, 21], liver [22], adipose tissue [23], human milk [24, 25], and umbilical cord blood [26].

PCNs are often labelled as dioxin-like compounds (DLCs) not only because their mechanism of action (through the aryl hydrocarbon receptor (AhR)) is similar to polychlorinated dibenzo-*p*-dioxins (PCDDs), polychlorinated dibenzo-*p*-furans (PCDFs), and polychlorinated biphenyls (PCBs) [27, 28] but also primarily because of the toxic effects observed in occupationally exposed humans and experimental animals [29, 30]. Primarily, chloracne and hepatotoxic effects have been demonstrated in workers exposed by inhalation and dermal route to PCNs [31, 32]. In animal studies, orally administered PCNs have also shown hepatotoxicity [33, 34] and additionally hematological disorders [35, 36], thyroid and sex hormone disturbances [37], and prenatal toxicity [38–41]. Some nonspecific symptoms such as weight loss due to reduced appetite (anorexia), headaches, vertigo, and insomnia [42] have also been reported suggesting a potential neurotoxic effect of PCNs and the mechanism of action similar to DLCs. The hypothesis that PCNs can also target the central nervous system (CNS) is further supported by several studies showing their affinity for sciatic nerve as well as a spectrum of anorectic and behavioral effects in response to *in vivo* drug administration [34, 43–45]. While the mechanism by which PCNs can modify the behavioral pattern of animals is not known, studies performed both *in vivo* and *in vitro* suggest the action through GABAergic and/or glutamatergic systems [37, 46].

It has been estimated that one of the most toxic among all 75 known PCNs are hexachloronaphthalenes, mainly congeners 1,2,3,4,6,7-hexachloronaphthalene (PCN66), 1,2,3,5,6,7-hexachloronaphthalene (PCN67), and 1,2,3,6,7,8-hexachloronaphthalene (PCN70) [47, 48]. Besides, pentachloronaphthalenes, PCN66/67, are considered to be characteristic for combustion processes [12, 49, 50] and are most frequently detected in food [4, 51]. Hexachloronaphthalenes are also characterized by their highest bioaccumulation (especially in the liver, adipose tissue, and milk during lactation) as revealed in both humans and experimental animals [25, 52].

Despite widely documented harmful and adverse effects of PCN67, it is still unknown whether it may disturb neuronal function and produce subsequent neurotoxicity. To investigate the role of this substance in neurological processes, we employed *in vitro* models of primary hippocampal neurons and differentiated PC12. Here, we demonstrate that PCN67 disrupts neuronal sprouting and the formation of neurites. Moreover, our studies show the induction of mitochondrial-related necrotic death in a dose- and time-dependent manner. Our report is the first study, showing that mitochondria may be a primary intracellular target for PCN67 in neuronal cells.

2. Materials and Methods

2.1. Reagents. All reagents, if not separately mentioned, were purchased from Sigma-Aldrich. The PC12 rat pheochromo-

cytoma cell line was obtained from the American Type Culture Collection (ATCC). Maxima SYBR Green Master Mix, M-MLV Reverse Transcriptase, Trizol[®], Alexa Fluor 488, Lipofectamine LTX reagent, B27, and Neurobasal were from Thermo Fisher Scientific. Protein Assay Kit was from Bio-Rad. Anti-GAPDH (Cat. No. sc-32233) and anti-histone H3 (Cat. No. sc-517576) were from Santa Cruz Biotechnology. HMGB1 antibody (Cat. No. 3935) was from Cell Signaling Technology. LDH Cytotoxicity Assay Kit was from Cayman Chemical. GcAMP3 calcium sensor was a gift from Loren Looger (Addgene plasmid #22692). Primers were synthesized in the Institute of Biochemistry and Biophysics (Poland).

2.2. The Compound. The mixture of hexachloronaphthalene congeners (94.14% purity) used in this study contained 81.17% of PCN67 as a dominant congener and additionally congeners 1,2,3,4,6,7-; 2,3,4,5,6,7-; and 1,2,4,5,6,7-hexachloronaphthalene comprising together up to 12.98% and 5.85% of 1,2,3,4,5,6,7-heptachloronaphthalene. The synthesis, characteristic, and purity were described previously [33, 36, 37, 40, 45]. The analysis using the HRGC/HRMS method showed that the content of PCDDs and PCDFs was below 0.1 pg/mg.

2.3. PC12 Cell Culture, Differentiation, and PCN67 Treatment. PC12 cells derived from pheochromocytoma were routinely grown in collagen-coated (type I from rat tail) plastic dishes in RPMI 1640 medium supplemented with 10% horse serum, 5% fetal bovine serum, 25 mM HEPES, pH 7.4, 2 mM L-glutamine, 1 mM sodium pyruvate, and the mix of penicillin/streptomycin in a humidified incubator at 37°C with 5% CO₂. Cells were plated at the density of 1–2 × 10⁵ /ml and cultured for 2 days before PCN67 administration. PCN67 was dissolved in DMSO and was added together with 1 mM dibutyryl-cAMP (differentiating agent). Cells were cultured with both agents for up to 72 h. No more than 20 cell passages were used for all experiments. Cells simultaneously cultured in the presence of 0.1% DMSO were used as a control. The black/white pictures of cell morphology were taken using an Olympus CK-40 inverted microscope equipped with a CCD camera.

2.4. Quantification of PC12 Cell Differentiation. We used two parameters to score the potency of PC12 cell to differentiate into neuronal phenotype: the length of the longest neurite (any protrusion longer than the diameter of the cell body) and the number of cells possessing at least one neurite. Cells were chosen randomly. The images were captured at 400x magnification, and the neurites were measured using Image J software (NIH, USA).

2.5. Viability Assays. 5 × 10³ cells were plated in each well of a 96-well plate. For WST-1 assay, plates were incubated with WST-1 solution in a 1 : 10 ratio for 4 h at 37°C. The absorbance was measured at 450 nm using a Victor X3 multiwell plate reader (PerkinElmer). The IC₅₀ value was determined by nonlinear regression analysis in Prism 8.0 software (GraphPad Software, San Diego, CA). When indicated, cells were pretreated for 4 h with 5 μM BAPTA A/M added 48 h

following PCN67 administration and the viability was assessed on the next day. Membrane permeability was determined in the presence of 7.5 μ M propidium iodide. Ru360 or cyclosporine A (CsA) was added 30 min before PCN67 treatment, and the viability was measured after 72 h. For experiments with 0 mM extracellular Ca^{2+} , following 48 h of incubation with PCN67, the growing medium was changed to Hank's balanced salt solution with or without calcium for 4 h and cells were imaged 24 h after using a Leica DM4000 microscope. For some experiments, cells were cultures in the presence of galactose (10 mM) in RPMI medium for 5 days following treatment with PCN67 for another 24 h.

2.6. Primary Hippocampal Neurons. Hippocampal cultures were prepared from Sprague Dawley rat embryonic day 18 embryos. Briefly, the rat hippocampal CA1-CA3 region was dissected in PBS medium with 10 mM D-glucose and digested with 0.05% trypsin-EDTA in PBS for 20 min at 37°C. The dissociated tissues were centrifuged at 200g for 2 min and then triturated in the presence of DNase (100 U/ml) with a fire-polished glass pipet in Hank's balanced salt solution (HBSS) containing calcium and magnesium. Dissociated neurons were plated on nitric acid-treated 25 mm cover glass coated with poly-L-lysine in a plating medium. Four hours after plating, the medium was replaced with Neurobasal medium supplemented with 2% B27, 1 mM sodium pyruvate, and 2 mM L-glutamine. After four days, 4 μ M cytosine arabinoside was added to inhibit glial proliferation, and the neurons were transfected with the pEGFP-N3 vector using Lipofectamine LTX.

2.7. Axon Outgrowth Assay. The primary hippocampal neurons were grown until they reached either DIV4 or DIV14, and they were next treated with indicated PCN67 concentration. These stages were chosen because they correspond to distinct neuronal developmental processes such as axon formation and dendrite outgrowth in immature neurons (DIV4) or synaptogenesis associated with maturation (DIV14) as described previously [53]. 40 mM KCl was added to some cultures together with PCN67 as indicated. After two days, the neurons were imaged with Zeiss inverted scope and the photographs were processed using Corel Draw 11. The length of the longest neuron for approximately 20 neurons average per condition was measured for each experiment with Image J Simple Neurite Tracker plugin (NIH, USA).

2.8. Total RNA Isolation and Real-Time PCR. Total cellular RNA was isolated from PC12 cells using Trizol reagent based on the protocol provided by the manufacturer. Single-stranded cDNA was synthesized using M-MLV reverse transcriptase and oligo(dT) primers using 1 μ g of RNA. The gene expression was quantified using Maxima SYBR Green Master Mix in the conditions: 15 min at 95°C followed by 40 cycles at 95°C for 15 s, 60°C for 30 s, and 72°C for 30 s using the Abi Prism 7000 sequence detection system (Applied Biosciences). The specificity of primers was checked by running a melting curve. Each time, the expression level of the gene of interest was normalized to the endogenous expression of *Gapdh* and the relative fold change was calculated using the $2^{-\Delta\Delta\text{Ct}}$

method [54]. Either the primers were designed using the GenScript Primer Design Tool (USA) or their sequence was previously published elsewhere, as specified in Table 1.

2.9. Visualization of Necrotic Death with Flow Cytometry. 1×10^6 PC12 cells were double stained with Annexin V (to visualize apoptotic cells) and propidium iodide (sensitive to necrotic cells) for 15 min at 25°C in the dark using the Annexin V-FITC Apoptosis Detection Kit based on the information provided by the manufacturer and analyzed using the FACScan Becton Dickinson flow cytometer. The fluorescence was collected from 10^4 cells, and the data were plotted with CellQuest Becton Dickinson software.

2.10. Lactate Dehydrogenase Release Assay. Lactate dehydrogenase (LDH) release from PC12 cells after drug treatment was measured with the LDH Cytotoxicity Assay Kit per manufacturer's protocol.

2.11. Cell Fractionation and Western Blot. PC12 cells were lysed on ice with RIPA buffer supplemented with 1 mM PMSF, 2 mM Na_3VO_4 , and protein inhibitor cocktail for 30 min. The lysates were next centrifuged at 800 x g for 15 min at 4°C; the supernatant was boiled for 5 min in the Laemmli buffer and stored at -80°C for further use. Protein concentration was measured using Bradford reagent according to the manufacturer's instruction. Postnuclear fraction referred here as cytosolic was obtained based on the method of Blobel and Potter [57]. The purity was checked by using glyceraldehyde3-phosphate dehydrogenase (GAPDH) as a marker of cytosolic fraction and histone H3 for nuclear fraction. For Western blot, approximately 40 μ g of cytosolic proteins were separated using 10% SDS-PAGE and transferred to a nitrocellulose membrane with a semidry method. Membranes were blocked with 5% bovine serum albumin in TBST buffer (10 mM Tris-HCl, pH 7.4, 150 mM NaCl, and 0.05% Tween-20) for 1 h at room temperature and then incubated overnight at 4°C with primary antibodies: anti-HMGB1 (1:1000), anti-GAPDH (1:2500), or antihistone H3 (1:1000), followed by 4 h incubation with secondary antibodies (1:10000) coupled with alkaline phosphatase. BCIP/NBT, an artificial alkaline phosphatase substrate, was used to visualize immunoreactive bands. Membranes were densitometrically quantified using Image J software (NIH, USA). The results are presented as arbitrary units obtained after normalization of the marker protein.

2.12. Cellular ATP Content Measurement. ATP concentration in PC12 cells was determined using adenosine 5'-triphosphate (ATP) Bioluminescent Assay Kit on GloMax 20/20 luminometer and normalized to the protein content. For each set of measurements, a second negative control (no cells) was included, and background fluorescence was further subtracted from all other values. The results are presented as nmoles ATP/mg protein.

2.13. Live Cell Imaging. Simultaneous Ca^{2+} and membrane permeability live cell images were acquired using an inverted Zeiss Axio Observer 7 Marianas™ Microscope equipped with a X-Cite 120LED Boost White Light LED System and a high-

TABLE 1: The list of primers used for gene expression quantification. The sequence for *Nefl* and *Gapdh* was taken from [55, 56], respectively. The primers for *Nefm* were designed as described in Section 2.8.

Gene name	Sequence 5'-3'	NCBI number
<i>Nefm</i> (<i>neurofilament M, NF-M</i>)	F: ATCACTTGGAGGAAGACATCCACCGG R: TTCCTCTGCAATGACTGTAGGGC	NM_017029
<i>Nefl</i> (<i>neurofilament L, NF-L</i>)	F: AGACATCAGCGCCATGCA R: TTCGTGCTTCGCAGCTCAT	NM_031783.1
<i>Gapdh</i>	F: GGTTACCAGGGCTGCCTTCT R: CTTCCATTCTCAGCCTTGACT	NG_028301.1

resolution Prime™ Scientific CMOS digital camera that is controlled by a workstation loaded with SlideBook imaging and microscope control software (Intelligent Imaging Innovations, USA). Differentiated PC12 cells were transfected with a GcAMP3 calcium sensor using Lipofectamine LTX and treated with PCN67 as described in *Drug Treatment* subsection in the presence of 7.5 μ M propidium iodide. The images were acquired at 63x with the excitation time of 100 ms and one-hour interval time using the following filter set: GFP Exciter FF01-474/27, GFP Emitter FF01-525/45, and for propidium iodide: Exciter FF01-578/21 and Emitter FF02-641/75. The environmental control system (Okolab, USA) was used to keep constant experimental conditions (37°C, 5% CO₂). The focus was automatically controlled by Definite Focus.2 (Zeiss, Germany). Regions of interest (ROIs) after background subtraction were normalized as $\Delta F/F_0$ and processed using Microsoft Excel software. ROIs were averaged over each condition. At least 10 cells were imaged per experimental condition, and all experiments were performed in triplicate.

2.14. Measurement of Mitochondrial and Plasma Membrane Potential. Mitochondrial membrane potential ($\Delta\Psi_m$) was measured with TMRE (tetra-methyl-rhodamine-ethyl ester) whereas plasma membrane potential ($\Delta\Psi_p$) was measured with DiSBAC₂ (Bis-(1,3-diethylthiobarbituric acid) trimethine oxonol). Following 72 h of incubation with PCN67, PC12 cells were loaded with 25 nM TMRE or 1 μ M DiSBAC₂ for 30 min at 25°C in the dark in a buffer containing 20 mM HEPES, pH 7.4, 2 mM CaCl₂, 150 mM NaCl, 5 mM KCl, 1 mM MgCl₂, and 10 mM glucose and the fluorescence of 10⁴ cells was recorded by a FACScan Becton Dickinson flow cytometer. The accompanying software analyzed the data. Cells incubated with 0.1% DMSO, used as a solvent for TMRE and PCN67, were monitored to record background fluorescence, which was later subtracted from the recordings.

2.15. Detection of ROS Level. The ROS level was measured with DCFH-DA (2',7'-dichlorofluorescein diacetate) following 72 h treatment with PCN67. Briefly, at the end of the treatment, PC12 cells were washed with PBS and incubated with DCFH-DA at a final concentration of 10 μ M for 30 min at 37°C in the dark. After three washes with PBS to remove the excess of the dye, the fluorescence intensity was measured with a flow cytometer (Becton Dickinson) with 488 nm excitation wavelength and emission at 525 nm. Dur-

ing each experiment, 10⁴ cells were recorded. The background fluorescence was obtained with 0.1% DMSO.

2.16. Quantification of Lipid Peroxidation. The level of thiobarbituric acid reactive substances (TBARS) in PC12 cells was determined according to the method described previously [58]. The results were normalized to the protein content and are expressed as OD/mg.

2.17. Nitric Oxide Assay. Nitric oxide generation in PC12 cells following 72 h of PCN67 treatment was determined in phenol red-free media according to the method described previously [59]. Briefly, at the end of 72 h treatment, 100 μ l of culturing medium was transferred into a 96-well plate and mixed in a 1:1 ratio with Griess reagent (1% sulfanilamide/0.1% NED in 5% phosphoric acid) followed by 10 min incubation in the dark. The absorbance at 540 nm was measured using a Victor X3 multiwell plate reader (PerkinElmer). DMSO-treated cells were used as control.

2.18. Statistical Analysis. All data are expressed as mean \pm S.E.M from at least 3 experiments unless otherwise stated. One-way or two-way ANOVA was performed with matching as appropriate. *P* values for experiments involving multiple comparisons were obtained by the Tukey post hoc testing, albeit *P* values for not all comparisons are indicated on the graphs. *P* < 0.05 was considered statistically significant. **P* < 0.05, ***P* < 0.01, and ****P* < 0.001.

3. Results

3.1. The Dose-Dependent Effect of PCN67 on Differentiated PC12 Cell Survival. To assess *in vitro* neurotoxicity of PCN67, differentiated PC12 cells were exposed to a concentration ranging from 0.001 μ g/ml to 25 μ g/ml (Figures 1(a)–1(c)). A significant rise in cell mortality was visible after 72 h of incubation. The lowest tested concentration that caused a reduction in the number of viable cells was 0.5 μ g/ml (*F*(3,24), *P* < 0.05). Increasing PCN67 concentration only potentiated the prodeath effect. Based on the dose-response curve presented in Figure 1(d), the calculated IC₅₀ value was 0.35 μ g/ml while the IC₁₀ was 0.039 μ g/ml. In this context, we decided to employ the IC₅₀ concentration and the highest concentration that did not produce significant cell death (0.1 μ g/ml) for the following experiments done 72 h after PCN67 treatment.

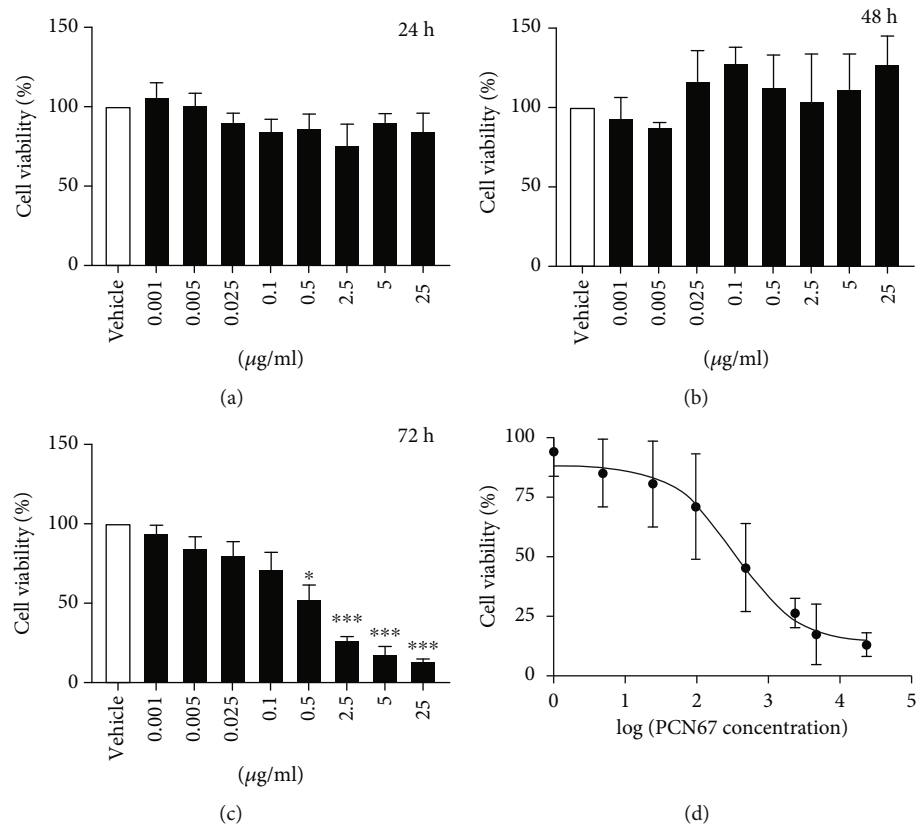


FIGURE 1: Dose- and time-dependent effect of PCN67 on differentiated PC12 cells. The cells were treated with PCN67 concentration ranging from 0.001 $\mu\text{g/ml}$ to 25 $\mu\text{g/ml}$ for 24 h (a), 48 h (b), and 72 h (c). The half-maximal inhibitory concentration (IC_{50}) was determined based on viability data obtained following 72 h treatment using nonlinear regression analysis (d). Cell viability in vehicle-treated cells was taken as 100%. * $P < 0.05$ and *** $P < 0.001$.

3.2. PCN67 Interferes with the Differentiation of PC12 Cells.

PC12 cells exposed to 1 mM dibutyryl-cAMP showed de novo outgrowth of bi- or tripolar neurites, which appeared mostly straight, occasionally forming branches in some areas. The body of the cell was mostly polygonal. We scored two parameters: the length of the neurites and the percentage of the cell bearing neurites, to evaluate the effect of PCN67 on the differentiation potential of PC12 cells. As shown in Figure 2(a), treatment with 0.1 $\mu\text{g/ml}$ of PCN67 for 72 h did not affect the general morphology, in contrast to the IC_{50} concentration, which led to some cell detachment, floating and losing the characteristic neuronal-like shape. Moreover, treatment with this concentration resulted in the formation of neurites shorter by 15% (77.1 μm vs. 90.7 μm in control, $F(2,145)$, $P < 0.05$) but did not affect the number of cells bearing neuronal protrusions (Figures 2(b) and 2(c)). We subsequently analyzed the expression of neurofilament M (NF-M) and neurofilament L (NF-L) which are major components of the neuronal cytoskeleton and are frequently used as differentiation markers. No emphasis was given to neurofilament H, as it is expressed later during PC12 and sympathetic neuron differentiation, and its role in the early stages of this process is not defined [60]. Real-time PCR analysis showed a 77% reduction of the NF-M mRNA level ($F(2,6)$, $P < 0.001$) after treatment with IC_{50} concentration of PCN67 when compared to the vehicle-treated control

(Figure 2(d)). The expression level of NF-L measured at the same time point (Figure 2(e)) was reduced by 72% ($F(2,6)$, $P < 0.01$). These results demonstrate that PCN67 in a dose-dependent manner may interfere with the gene expression of NF-L and NF-M associated with the differentiation of PC12 cells into neuronal phenotype.

3.3. Susceptibility of Primary Neurons to PCN67 Depends on the Maturation Stage.

Because differentiated PC12 cells acquire and retain several core features of primary neurons, we next checked whether the PCN67 effect observed in PC12 cells could be reproduced in hippocampal neurons *in vitro*. To search for any developmental-dependent effect, we used neurons at DIV4 and DIV14 that were susceptible to chronic KCl stimulation. It has been shown that KCl protects neurons from death resulting from overinhibition and from neurotrophic factor deprivation [61, 62]. Morphological observation showed significant disintegration on the neuronal network of DIV4 neurons treated with PCN67 at the IC_{50} concentration (Figure 3(a)). Moreover, measurement of the longest neurite at DIV4 showed a 43% reduction of the baseline length ($F(5,94)$, $P < 0.01$) and no prosurvival effect of KCl (Figures 3(b) and 3(c)). Such effect was not observed for 0.1 $\mu\text{g/ml}$ PCN67 suggesting a dose-dependent action. The reduction of neurite outgrowth by 20% ($F(5,102)$, $P < 0.05$) upon treatment with IC_{50}

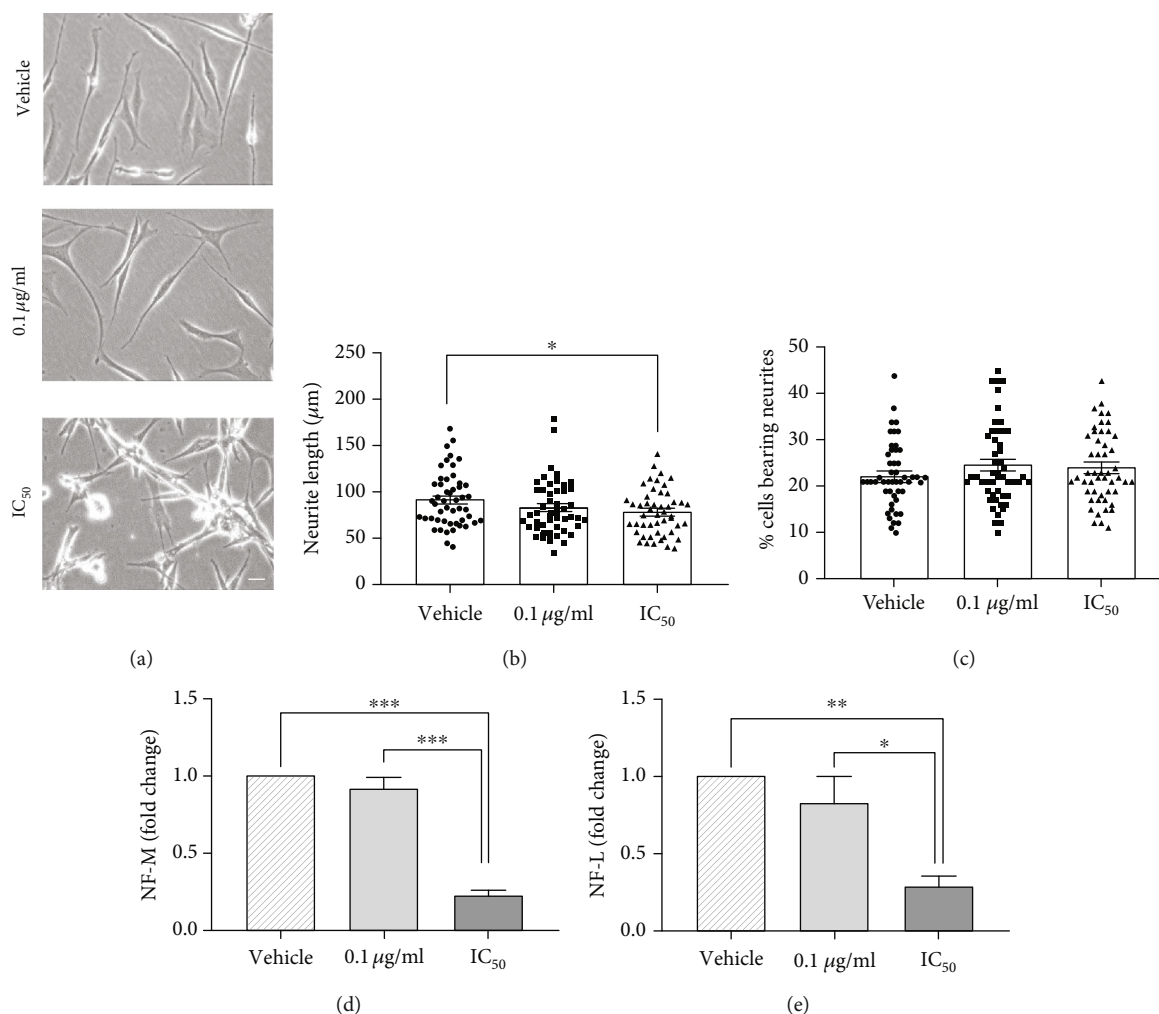


FIGURE 2: The effect of PCN67 on PC12 cell differentiation. (a) Morphology of control and PCN67-treated differentiated PC12 cells photographed under an inverted phase microscope with a CCD camera. Scale bar 10 μm . (b) Quantification of an average length of neurites. The cell protrusion was counted as neurite when its length was at least twice of cell diameter. (c) Quantification of an average number of neurite-forming cells. Cells with at least one visible neurite were considered. (d) The expression of neurofilament M (NF-M) and (e) neurofilament L (NF-L) was assessed by real-time PCR 72 h after PCN67 treatment. The expression level in vehicle-treated cells was taken as 1. * $P < 0.05$, ** $P < 0.01$, and *** $P < 0.001$.

concentration of PCN67 was also demonstrated at DIV14; however, KCl was able to abolish the prodeath effect of PCN67 and rescue the axonal length (Figure 3(d)).

3.4. Induction of Necrosis by PCN67 Is Dose-Dependent. To investigate the nature of cell death, we next quantified Annexin V/propidium iodide (Ax-V/PI) staining (Figure 4(a)). The percentage of necrotic cells (Ax-V/PI⁺) in the total cell population was increased to 45% ($F(2,9)$, $P < 0.001$) only in PC12 cells treated with PCN67 at the concentration of IC₅₀ (Figure 4(b)). In addition, virtually no early apoptotic cells (Ax-V⁺/PI⁻) were detected and the population of late apoptotic cells (Ax-V⁺/PI⁺) was of minor importance (less than 3%). To study this further, we measured the necrosis-associated membrane changes by detecting the release of lactate dehydrogenase (LDH) [63]. After treatment with the concentration corresponding to IC₅₀ (Figure 4(c)), LDH presence in the extracellular

media was significantly increased ($F(2,36)$, $P < 0.001$). In parallel, we observed the accumulation of HMGB1 protein (high-mobility group protein B1) in the cytosol (Figure 4(d)), which is normally sequestered in the nucleus but upon induction of necrosis, it is exported to the cytosol to induce an inflammatory response [64]. Another feature of necrosis is nuclear swelling. The nuclear diameter following PCN67 treatment was significantly increased (Figure 4(e)) compared to vehicle-treated control ($F(2,79)$, $P < 0.001$). In contrast to apoptosis, which is an ATP-dependent process, necrosis is energy-independent but results in ATP depletion [65]. In this context, upon treatment with PCN67 at IC₅₀, we detected a cellular ATP level decrease by 55% ($F(2,6)$, $P < 0.05$) (Figure 4(f)). Interestingly, exposure to 0.1 $\mu\text{g/ml}$ of PCN67 did not induce any necrotic features, pointing to a dose-dependent effect. Apoptotic markers were subsequently evaluated to eliminate the possibility of apoptotic death. However, neither PARP cleavage nor caspase 3/7

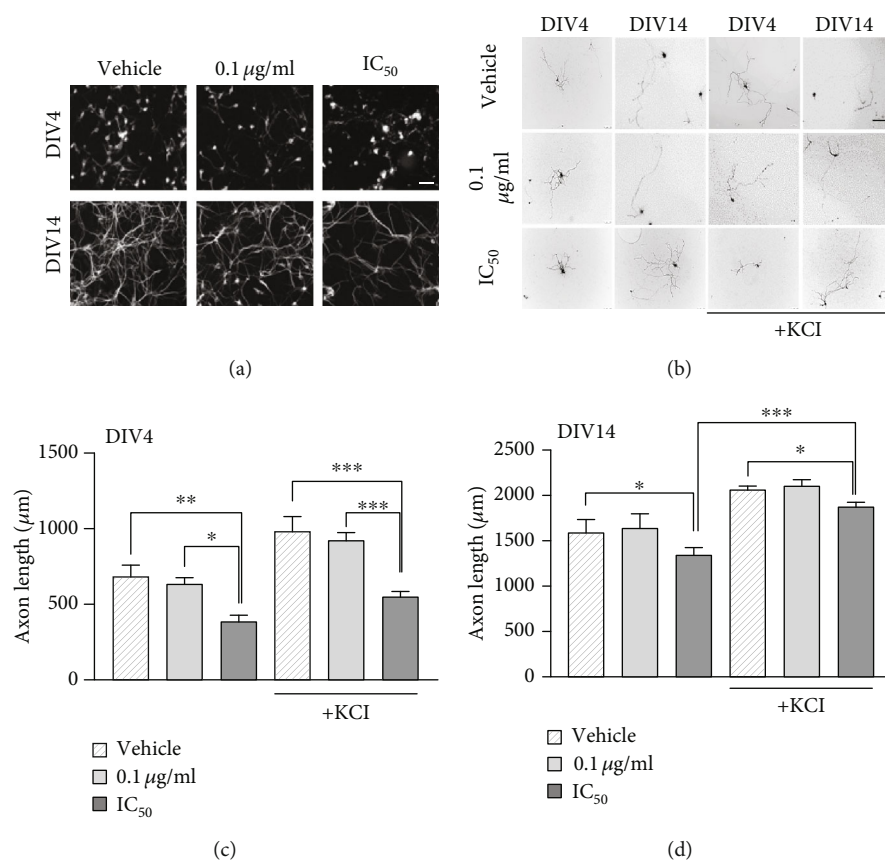


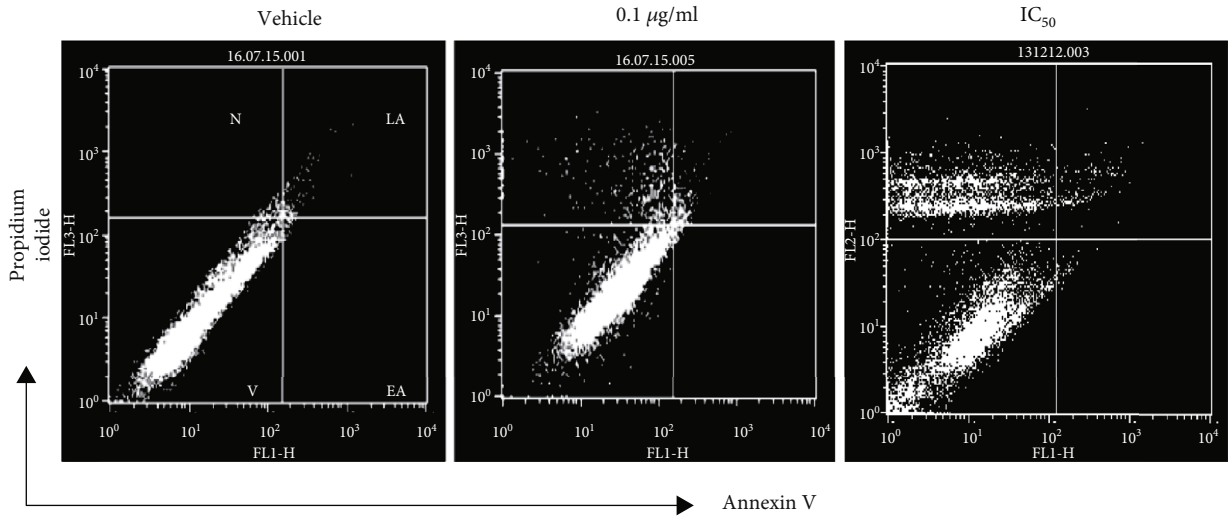
FIGURE 3: Toxicity of PCN67 depends on the maturation stage of primary hippocampal neurons. (a) The grayscale images of neuronal network photographed using an inverted phase microscope with a CCD camera. Scale bar 10 µm. (b) Neurons transfected with GFP plasmid cultured in defined media in the presence or absence of KCl (40 mM). KCl was added together with PCN67, and the images were taken 2 days later. (c) Quantification of axon length at DIV4 and (d) at DIV14. The longest neurite was measured. * $P < 0.05$, ** $P < 0.01$, and *** $P < 0.001$.

activation was observed (not shown). Collectively, our data suggests that PCN67 dose equivalent to IC₅₀ induces the necrotic death of differentiated PC12 cells.

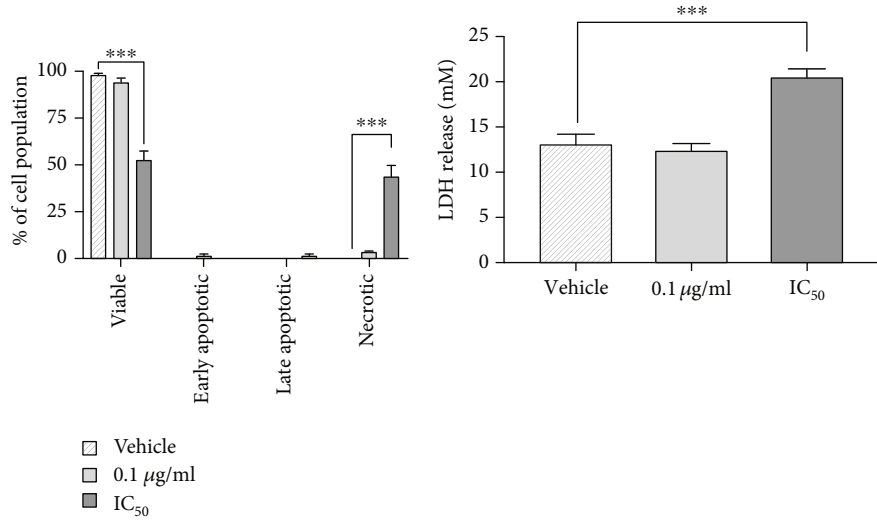
3.5. Increased $[Ca^{2+}]_c$ Does Not Contribute to PCN67-Induced Cell Death. Another hallmark of necrosis is increased intracellular calcium concentration [65]. To verify whether the PCN67 mechanism of cell death involves disruption of calcium homeostasis, we used genetically encoded sensor GcAMP3 for a long-lasting recording of intracellular calcium changes. As shown in Figure 5(a), PCN67 applied at the concentration of IC₅₀ but not 0.1 µg/ml, resulted in a gradual increase in calcium level starting within the first 24 h and reaching significance at approximately 48 h and onward. After 2 days of treatment, a significant increase in propidium iodide uptake was visible, indicating plasma membrane hyperpermeability (Figure 5(b)). Further accumulation of propidium iodide was almost parallel to increasing GcAMP3 fluorescence. Next, we checked the requirement of extracellular calcium for PCN67-induced necrotic death. Replacing the regular calcium-containing growth media with Hank's balanced salt solution (calcium-free media) did not protect from compromised membrane permeability (Figure 5(c)), suggesting that extracellular calcium does not play a significant role.

Pretreatment with intracellular calcium chelator—BAPTA A/M—after 48 h of PCN67 incubation, when a significant increase in calcium and membrane permeability started to be detectable, significantly, but only slightly preserved cell viability (Figure 5(d)). However, this effect was observed only at a higher dose of PCN67. These data illustrate that, although time-dependent calcium rise is noticeable after continuous treatment with IC₅₀ concentration of PCN67, it does not have a noticeable effect on PCN67-induced necrotic death.

3.6. PCN67 Induces Necrosis-Associated Plasma Membrane Depolarization. Changes in plasma membrane potential can be monitored by using fluorescent dye—DiBAC4(3). Its uptake to the cell is driven by electrochemical gradient which results in increased fluorescence [66]. The measurements following 72 h of exposure showed elevated DiBAC4(3) fluorescence in cells treated with PCN67 concentration corresponding to IC₅₀ value (2.5 times higher than that of control, $F(2,9)$, $P < 0.001$) indicating plasma membrane depolarization (Figure 5(e)). This correlates closely with the increased membrane permeability to propidium iodide (Figure 5(b), 72 h). Lower doses of PCN67 did not provoke depolarization events or increased propidium iodide uptake.

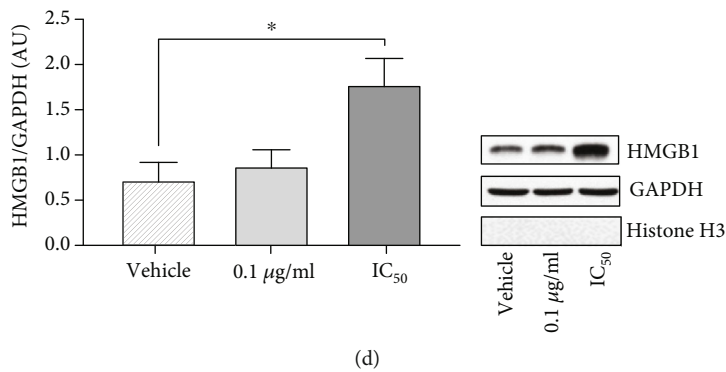


(a)



(b)

(c)



(d)

(e)

FIGURE 4: Continued.

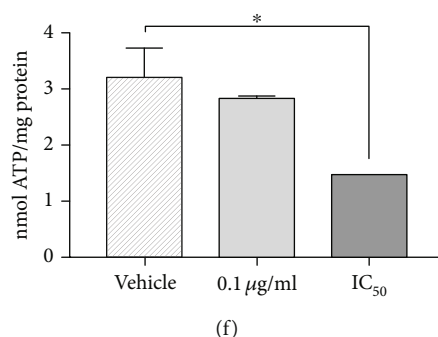


FIGURE 4: PCN67 treatment induces characteristics of necrotic death in differentiated PC12 cells. (a) Representative dot plots of necrotic/apoptotic cell distribution following 72 h of PCN67 treatment. Cells were stained with Annexin V and propidium iodide and analyzed with flow cytometry. (b) Quantification of viable (V), early apoptotic (EA), late apoptotic (LA), and necrotic (N) cells in a population. (c) Determination of plasma membrane integrity measured by the release of lactate dehydrogenase (LDH) 72 h following PCN67 treatment. (d) Western blot-based quantification of HMGB1 protein in cytosolic fraction collected from 72 h-treated cells. The results are presented as arbitrary units following normalization to the GAPDH level used as a marker of a cytosolic fraction. Histone H3, a protein marker of a nuclear fraction, was used to determine the purity of fractionation. (e) Average measurement of the nuclear diameter of differentiated PC12 cells after 72 h of PCN67 treatment. (f) The changes in the ATP level following 72 h of PCN67 treatment. The results were normalized to the protein level and are expressed as nmoles/mg. * $P < 0.05$ and *** $P < 0.001$.

These data indicate that PCN67 may perturb the plasma membrane in a dose-dependent manner leading to membrane hyperpermeability, calcium overload, and necrotic death.

3.7. PCN67 Promotes Mitochondrial Dysfunction. To evaluate the contribution of mitochondria to cell death, the fluctuations in mitochondrial membrane potential ($\Delta\Psi_m$) were monitored using TMRE (tetra-methyl-rhodamine-ethyl ester), which accumulates in the mitochondrial matrix according to the Nernst equation [67]. Treatment with IC₅₀ concentration resulted in massive mitochondrial depolarization after 72 h ($F(2,15)$, $P < 0.05$) which was reflected by a decrease in TMRE fluorescence (Figure 6(a)). To further elucidate the role of mitochondria in PCN67-induced cell death, an inhibitor of mitochondrial calcium uniporter—Ru360—was used. Pretreatment with Ru360 increased cell survival in a concentration-dependent manner ($F(4,20)$, $P < 0.05$) when measured 72 h after exposure to PCN67 (Figure 6(b)). The presence of galactose in the medium, which is expected to upregulate mitochondrial oxidative phosphorylation and produce drug-induced mitochondrial failure [68, 69], sensitized cells to PCN67 (Figure 6(c)) as indicated by reduced viability detected already after 24 h. Interestingly, the same effect was also observed at a dose of 0.1 µg/ml ($F(1,24)$, $P < 0.05$). We next tested whether observed necrotic death involved mitochondrial permeability transition pore (mPTP) opening. Pretreatment with cyclosporin A, a potent mPTP inhibitor, failed to protect from PCN67-induced cell death (Figure 6(d)). These results collectively suggest that mitochondrial calcium may drive the PCN67-mediated necrotic process, which is however independent from mPTP.

3.8. The Role of Cellular Stress in HxCN-Induced Cell Death. Based on the above results, we speculated that an increased ROS level could underlie compromised cell viability due to its interaction with mitochondria. Therefore, following 72 h of incubation with PCN67, cells were stained with DCFH-

DA (2',7'-dichlorofluorescein diacetate) to measure ROS. Significantly elevated ROS level ($F(2,15)$, $P < 0.001$) was detected at IC₅₀ concentration (Figure 7(a)). This corresponds to compromised membrane integrity measured by the release of LDH to the media (compare with Figure 5(c)). Interestingly, the average increase in ROS by (\pm SEM) $309 \pm 10\%$ was also noticeable at the lower concentration used when compared to vehicle-treated cells (100%). Because ROS can react with the polyunsaturated lipids, we next measured malondialdehyde levels to quantify membrane lipid peroxidation using TBARS assay. Exposure of PC12 cells to PCN67 resulted in marked increases in TBARS fluorescence for both concentrations (Figure 7(b)).

In order to dissect whether reactive nitrogen species could also contribute to observed necrotic death, we treated cells with PCN67 for 72 h and assessed the formation of a nitrile as a stable product of NO reaction with air using Greiss reagent. During the treatment, the cells were not challenged with lipopolysaccharide or γ interferon as differentiated PC12 cells have nNOS [70, 71]. Here, our aim was to assess if PCN67 is able to induce excessive NO generation. The data clearly indicate that neither PCN67 concentration stimulated or inhibited NO generation in relation to the vehicle-treated cells (Figure 7(c)).

4. Discussion

Neurons are a highly specialized type of cells required for cell-to-cell communication through axons and dendrites and information processing in the brain and spinal cord of the central nervous system. Under *in vitro* conditions, PC12 cells are a widely used model system to study neuronal processes, such as sprouting, excitability, and neurotransmitter release [72–74]. The PC12 line was originally derived from pheochromocytoma [73], a tumor arising from chromaffin cells of the adrenal medulla. Because chromaffin cells and sympathetic neurons originate from the neural crest, differentiated PC12 cells acquire both neuronal phenotype and

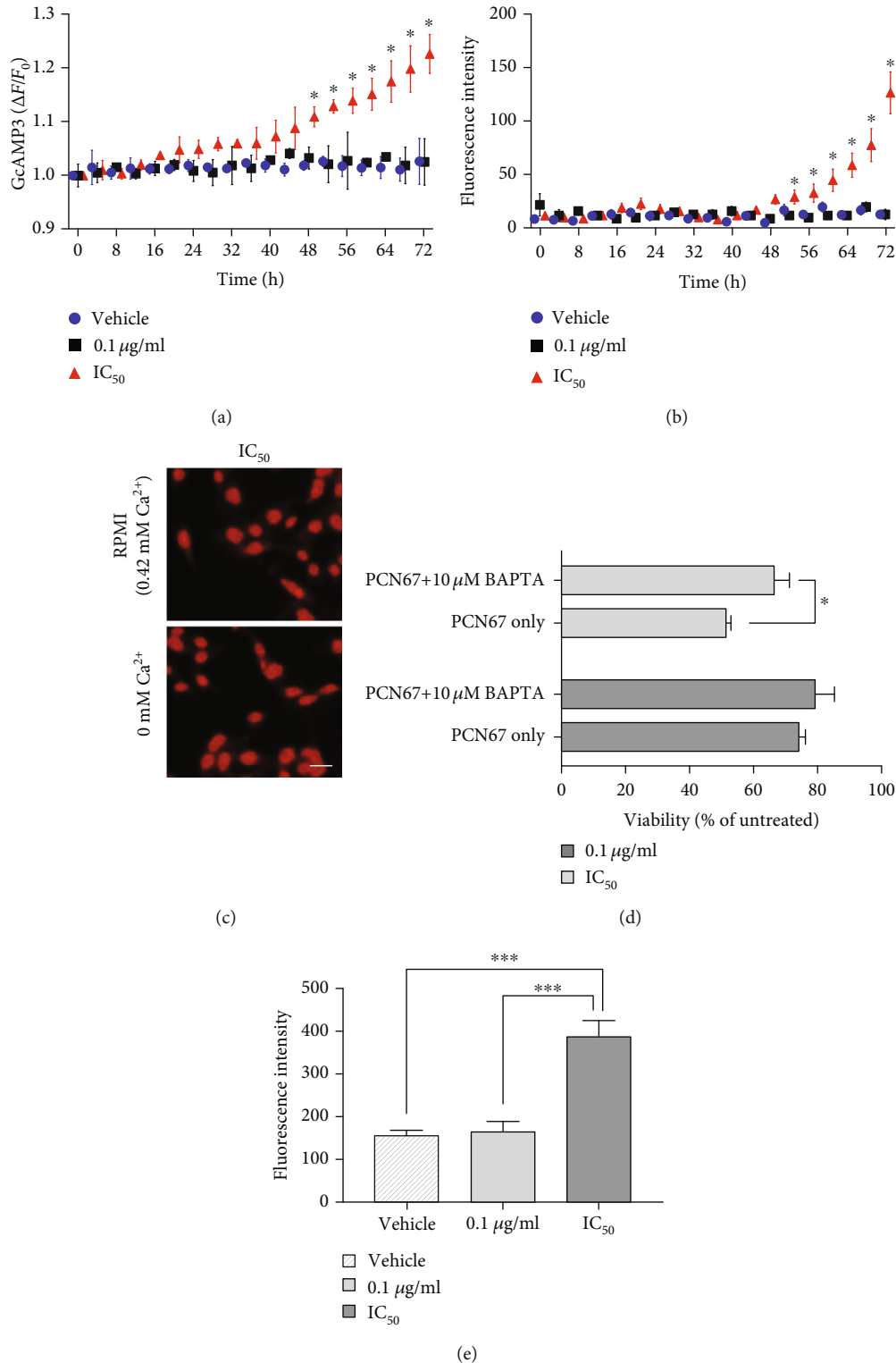


FIGURE 5: PCN67 induces intracellular calcium rise and plasma membrane depolarization. (a) Differentiated PC12 cells were treated with PCN67 for 72 h in the presence of intracellular calcium indicator—GcAMP3 and (b) propidium iodide (7.5 μM). The cells were placed into an environmental chamber with controlled temperature and CO₂ concentration, and the fluorescence changes were recorded every 4 h using an Axio Observer 7 Marianas™ Microscope equipped with 63x objective. The fluorescence of single cells was processed as $\Delta F/F_0$ after background subtraction. (c) Representative images of cells stained with propidium iodide (7.5 μM) following treatment with PCN67 (IC₅₀) for 72 h in the presence or absence of calcium in the culture media. Scale bar 10 μm . (d) Chelation of intracellular calcium partially protected from cell death. BAPTA-AM (5 μM) was added to the culture 48 h after PCN67 treatment, and the viability was determined the day after. Vehicle-treated cells were taken as 100%. (e) Plasma membrane potential was measured 72 h following PCN67 treatment using DiSBAC₂ (1 μM). Cells were loaded with a dye for 30 min, and the fluorescence was analyzed using flow cytometry. * $P < 0.05$ and *** $P < 0.001$.

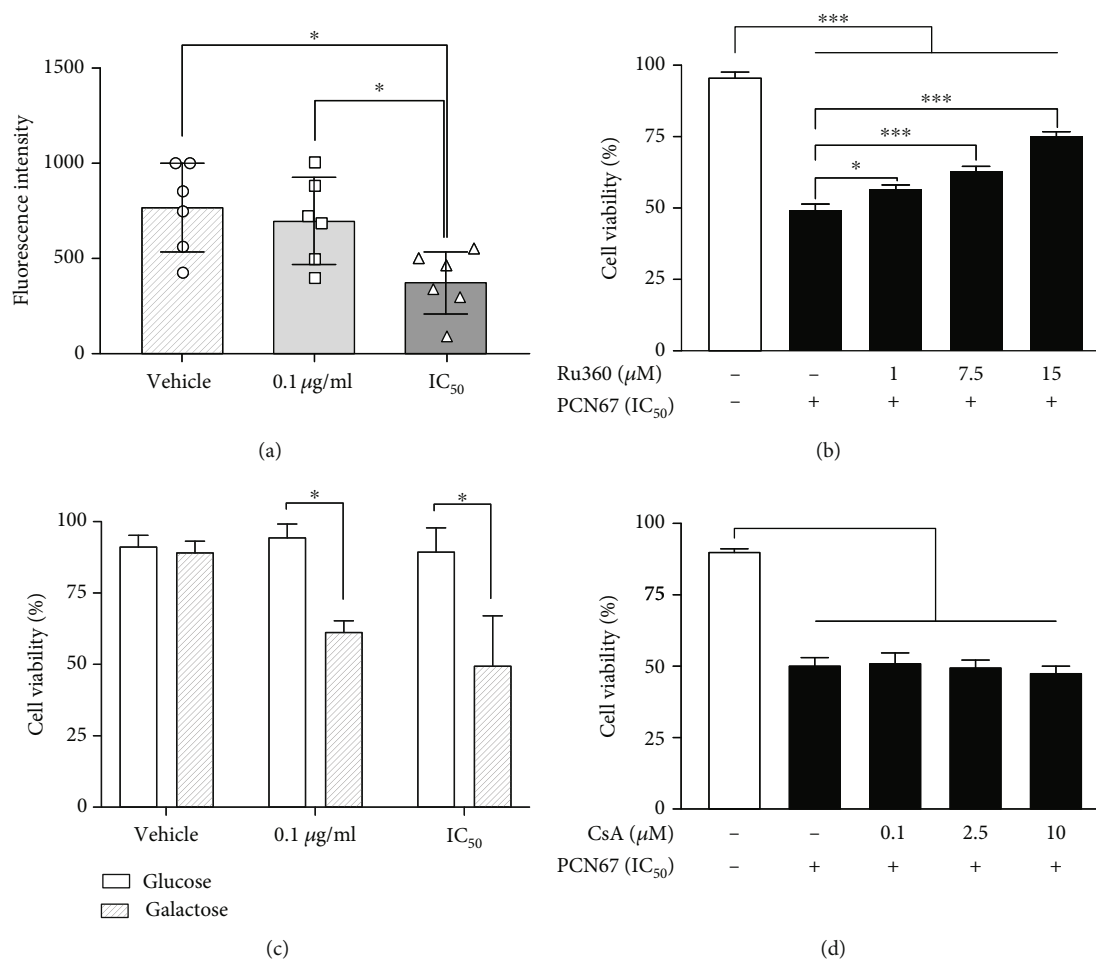


FIGURE 6: The role of mitochondria in PCN67-induced toxicity. (a) For measuring mitochondrial membrane potential, differentiated PC12 cells were cultured in the presence of PCN67 for 72 h and then loaded with TMRE (25 nM) for 30 min. TMRE-loaded cells were analyzed for fluorescence intensity using flow cytometry. Individual data points are shown. (b) Partial prevention of PCN67-induced death by Ru360. Ru360 was added 30 min before PCN67 treatment, and the viability was measured 72 h after. (c) Viability assessment of cells cultured in the presence of glucose (25 mM) or galactose (10 mM) supplemented RPMI for 5 days and then treated with PCN67 for 24 h. (d) PCN67-induced cell death is not inhibited by cyclosporine A (CsA). Differentiated PC12 cells were cotreated with PCN67 and CsA, and the viability was assessed 72 h later. * $P < 0.05$ and *** $P < 0.001$.

several key features of functional neurons. These cells have also been employed to determine neuronal toxicity of a wide variety of environmental pollutants [75–78].

Polychlorinated naphthalenes, a group of substances widely used up to the 1980s, are still considered as a serious environmental threat as they have been found in practically all ecosystems, and their accumulation has also been confirmed in humans [22]. Despite some reports suggesting an interaction of these compounds with the neuronal physiology [45, 46], the underlying mechanisms and potential neurotoxic effects have not been studied so far. Therefore, in order to establish the model for PCN67 neurotoxicity and calculate the IC₅₀, we performed a dose-dependent analysis (concentration ranging from 1 ng/ml to 25 µg/ml) based on viability assay. The IC₅₀ (0.35 µg/ml) was additionally used to evaluate the nature of cell death. We employed the lowest PCN67 concentration (0.1 µg/ml) that did not alter the viability of PC12 cells as compared to the control. Surprisingly, we found that already low PCN67 concentration of 0.1 µg/ml

which did not alter the viability of PC12 cells as compared to control induced cellular stress. Previous studies have shown that higher chlorinated polychlorinated naphthalenes, including PCN67, did not affect the viability of MCF-7 cells, when treated with the concentration of 100–10,000 pg/ml for 72 h [79]. However, at 1000 pg/ml, they increased caspase-8 activity and PCN67 additionally stimulated caspase-9, suggesting that the early molecular stages of death cascades may be initiated at much lower doses. Furthermore, it was demonstrated that the mixture of polychlorinated naphthalenes commercially available as Halowax 1051 downregulated aryl hydrocarbon receptor (AhR) when applied at 1 ng/ml and 10 ng/ml [80]. The disruption in AhR signaling has been shown to impair neuronal growth and development in *C. elegans* [81], affect arborization of sensory neurons in *Drosophila* [82], and diminish neuronal differentiation in dentate gyrus of the hippocampus [83]. Polychlorinated naphthalenes are potent agonists of AhR [84]; therefore, we cannot exclude that the effect of PCN67 on *in vitro*

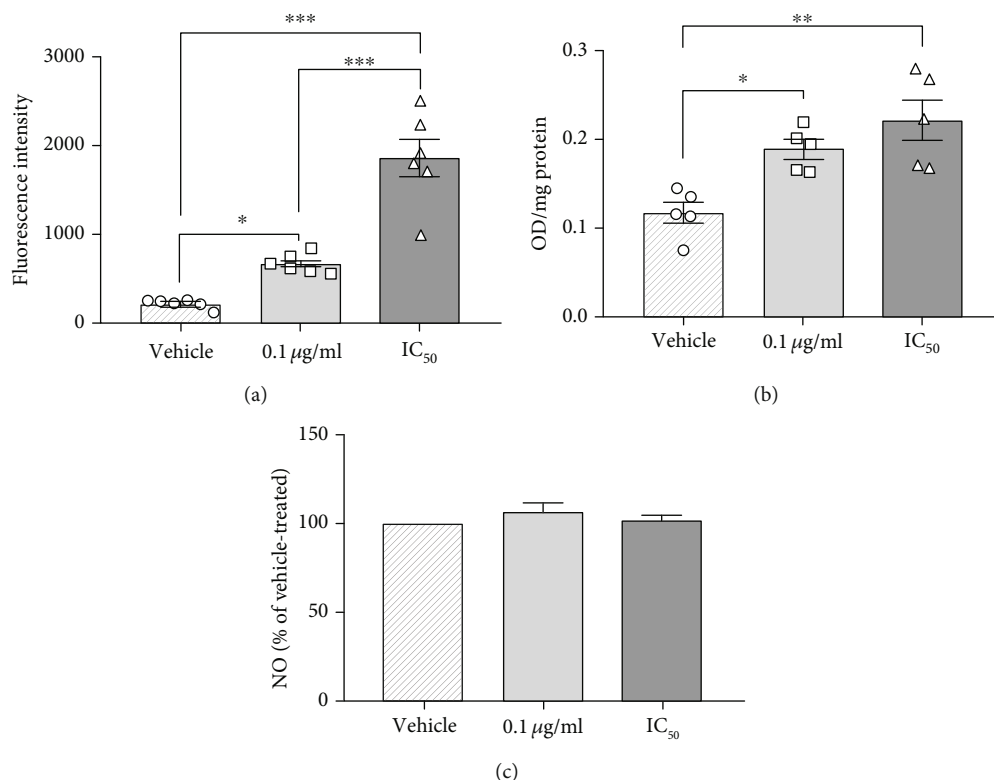


FIGURE 7: The effect of PCN67 on oxidative and nitritive stress. (a) Differentiated PC12 cells were treated with vehicle and PCN67 for 72 h. ROS generation was assessed with DCFH-DA (10 μM) using the excitation and emission filters set at 488 nm and 525 nm. Individual data points are shown. (b) The oxidative damage of lipids by reactive oxygen species was assessed by measuring thiobarbituric acid reactive substances (TBARS), and the results are normalized to the protein level. Individual data points are shown. (c) The level of NO was determined using Griess reagent, and the absorbance readings at 540 nm were measured by a microplate reader. * $P < 0.05$, ** $P < 0.01$, and *** $P < 0.001$.

differentiation observed in our study can be, at least in part, mediated by AhR signaling. We demonstrated here that PCN67 treatment at IC_{50} concentration significantly decreased the number of neurite-forming cells and the average length of neurite in PC12 cells. A similar effect on axon length was also observed in primary hippocampal neurons, although more advanced culture stages (DIV14) seemed to be more resistant to PCN67 toxicity than the younger one (DIV4). Although no *in vitro* studies explored the effect of PCN67 on primary neurons so far, the finding of developmental-dependent sensitivity appears to be in line with our earlier work, showing the fetotoxic and embryotoxic effect of PCN67 at the doses that did not cause maternal toxicity [33]. Moreover, our results are supported by earlier reports, showing the effect of 2,3,7,8-tetrachlorodibenzo-*p*-dioxin (TCDD) on viability and neuronal outgrowth in different *in vitro* models [85–87]. However, some studies also showed enhanced binding of nerve growth factor to its receptor in PC12 cells in the presence of PCBs [88]. Thus, the neurotoxic effect of PCNs, which may be expected in analogy to TCDD and PCBs, would be determined by the biochemical and neurochemical properties of individual congeners.

One of the main characteristics of PCNs is high lipophilicity which allows to anticipate high penetration through biological membranes and rapid modification of membrane homeostasis and permeability. In our study, the earliest

molecular change observed following PCN67 treatment at the IC_{50} concentration was mitochondrial membrane depolarization and significant depletion of ATP. In parallel to increased permeability of the plasma membrane to small molecules (e.g., propidium iodide), that started to be detectable 2 days following the treatment, we observed a gradual increase in cytosolic calcium concentration. Calcium is immediately taken up by mitochondrial calcium uniporter (MCU) which has been linked to H_2O_2 production, electron transport chain alteration, and disruption of $\Delta\Psi_m$ homeostasis [89]. A significant drop in the ATP level and thus the increase in AMP to ATP ratio observed for instance in Caco-2 cells treated with environmental pollutant TCDD [90], may activate AMP kinase that regulates mitochondrial homeostasis through the PGC1 α pathway. AMP kinase-PGC1 α -dependent control of mitochondrial metabolism is expected to limit ROS production [91], which in concert with mitochondrial calcium overload could promote mPTP-driven cell death. Although we excluded the contribution of mPTP, our findings that (1) PCN67 is more effective in glucose-free media and (2) inhibition of MCU partially reversed the neurotoxic effect of PCN67, suggest a key functional role of mitochondria in PCN67-induced necrotic death.

Compounds that target mitochondrial metabolism usually induce cellular stress [92, 93]. Since PCN67 interfere with mitochondria and affect energy metabolism, its neurotoxicity

could be associated with the production of free radical species. A dose-dependent elevation in ROS production revealed in this study not only confirmed PCN67 action on mitochondria but also suggested its detrimental effect on plasma membrane integrity as determined by increased lipid peroxidation and permeability to LDH. Generation of ROS and associated peroxidation of lipids were reported earlier in rat hepatocytes following PCN67 [33, 40] and PCN mixture treatment [43, 44] or neuronal cells exposed TCDD and PCBs [94, 95] suggesting a common mechanism. Interestingly, the cellular effects of oxidative stress were also detected for PCN67 concentration of 0.1 $\mu\text{g}/\text{ml}$, which did not affect $\Delta\psi_m$ and plasma membrane permeability. We hypothesize that the observed dose-dependent effect can be attributed to the potency of PCN67 to influence cellular antioxidant defense, in particular GSH/GSSG redox potential. Indeed, it has been demonstrated that prolonged administration of PCNs *in vivo* decreased GSH concentration [43]. Therefore, lack of morphological and biochemical symptoms of cell death in the presence of increased ROS level at the concentration of 0.1 $\mu\text{g}/\text{ml}$ may imply that cellular defense systems are still sufficiently enough, to counteract oxidative damage. Moreover, the lack of damage to neurites could suggest that neuronal viability and function are preserved during short time exposure (72 h in this study) to lower PCN67 concentrations. However, since PCNs are highly bioaccumulative, it is plausible that exposure to even lower doses during a long-time period and concomitant gradual accumulation may ultimately lead to neurophysiological dysfunction. To support that, a variety of neurobehavioral tests performed on rats exposed to PCN67 showed dose-dependent impaired long-term memory, reduced pain threshold, and stress-induced analgesia [45]. However, the molecular targets for PCN67 in the brain have not been revealed so far.

Neuronal injury may activate other nonneuronal cells in the CNS-like astrocytes and microglia to trigger a neuroinflammatory response. Therefore, we investigated whether PCN67-induced damage and necrotic death could also involve excessive production of NO, one of the main mediators of inflammation. We found no significant changes between vehicle- and PCN67-treated groups. Although no studies demonstrated the effect of PCNs on NO production, data derived from persistent organic pollutants with a similar mechanism of action indicated no evidence of nitrate stress in cerebellar neurons and in rat hypothalamus [96, 97]. Since excessive production of NO and consecutive active inflammatory processes are usually associated with cytotoxicity, lack of enhanced NO production in response to PCN67 indicates that NO did not contribute to PCN67-induced neurotoxicity.

5. Conclusion

It has been documented that dysfunctional mitochondria or altered synaptic transmission due to changes in the neuronal network could be associated with several neurobehavioral disorders such as anorexia [98], depression [99], or memory loss [100]. The findings of neurite damage and impaired physiological function of mitochondria revealed in our study

suggest that these phenomena may be one of the contributing factors for cognitive defects during long-term exposure to PCN67. On the other hand, since profoundly altered homeostatic control of energy balance and neuronal loss is frequently observed in schizophrenia [101] and Alzheimer's disease [102], the dose-dependent neurotoxicity and changes in the ATP level and lactate production could highlight a potential higher susceptibility for specific individuals exposed to PCNs to some neurodegenerative disorders. In this regard, further studies are vital to shed light on the possible implication of PCN in neurological disorders.

Data Availability

The raw data used to support the findings of this study have been deposited in the 4TU.ResearchData repository (DOI: 10.4121/uuid:5eb7226e-7546-4960-91bd-8b806c09668a).

Conflicts of Interest

The authors declare that there is no conflict of interest regarding the publication of this paper.

Authors' Contributions

Malwina Lisek and Joanna Stragierowicz contributed equally to this work.

Acknowledgments

This work was supported by the grant No. 503/6-086-02/503-61-001 from the Medical University of Lodz, Poland, and No. 2019/33/B/NZ4/00587 from the National Science Centre, Poland.

References

- [1] UNEP, *United Nations Environmental Programme (UNEP), The Stockholm Convention on persistent organic pollutants*, Secretariat of the Stockholm Convention on Persistent Organic Pollutants United Nations Environment Programme (UNEP) International Environment House, Geneva, Switzerland, 2015.
- [2] Y. Han, W. Liu, H. Li et al., "Distribution of polychlorinated naphthalenes (PCNs) in the whole blood of typical meat animals," *Journal of Environmental Sciences*, vol. 72, pp. 208–212, 2018.
- [3] A. Fernandes, M. Rose, and J. Falandysz, "Polychlorinated naphthalenes (PCNs) in food and humans," *Environment International*, vol. 104, no. 7, pp. 1–13, 2017.
- [4] A. R. Fernandes, D. Mortimer, M. Rose, F. Smith, Z. Steel, and S. Panton, "Recently listed Stockholm convention POPs: analytical methodology, occurrence in food and dietary exposure," *Science of the Total Environment*, vol. 678, pp. 793–800, 2019.
- [5] J. Falandysz, F. Smith, S. Panton, and A. R. Fernandes, "A retrospective investigation into the occurrence and human exposure to polychlorinated naphthalenes (PCNs), dibenzo-p-dioxins and furans (PCDD/Fs) and PCBs through cod liver products (1972-2017)," *Chemosphere*, vol. 231, pp. 240–248, 2019.

- [6] J. Falandysz, "Polychlorinated naphthalenes: an environmental update," *Environmental Pollution*, vol. 101, no. 1, pp. 77–90, 1998.
- [7] G. Liu, Z. Cai, and M. Zheng, "Sources of unintentionally produced polychlorinated naphthalenes," *Chemosphere*, vol. 94, pp. 1–12, 2014.
- [8] M. Odabasi, Y. Dumanoglu, M. Kara, H. Altiok, T. Elbir, and A. Bayram, "Polychlorinated naphthalene (PCN) emissions from scrap processing steel plants with electric-arc furnaces," *Science of The Total Environment*, vol. 574, pp. 1305–1312, 2017.
- [9] L. Yang, M. Zheng, Y. Zhao, Y. Yang, C. Li, and G. Liu, "Unintentional persistent organic pollutants in cement kilns co-processing solid wastes," *Ecotoxicology and Environmental Safety*, vol. 182, article 109373, 2019.
- [10] S. Waheed, M. U. Khan, A. J. Sweetman, K. C. Jones, H. B. Moon, and R. N. Malik, "Exposure of polychlorinated naphthalenes (PCNs) to Pakistani populations via non-dietary sources from neglected e-waste hubs: a problem of high health concern," *Environmental Pollution*, vol. 259, article 113838, 2020.
- [11] A. Mahmood, R. N. Malik, J. Li, and G. Zhang, "Congener specific analysis, spatial distribution and screening-level risk assessment of polychlorinated naphthalenes in water and sediments from two tributaries of the river Chenab, Pakistan," *Science of The Total Environment*, vol. 485–486, pp. 693–700, 2014.
- [12] N. D. Dat, K. S. Chang, and M. B. Chang, "Characteristics of atmospheric polychlorinated naphthalenes (PCNs) collected at different sites in northern Taiwan," *Environmental Pollution*, vol. 237, pp. 186–195, 2018.
- [13] A. Orlikowska, N. Hanari, B. Wyrzykowska et al., "Airborne chloronaphthalenes in Scots pine needles of Poland," *Chemosphere*, vol. 75, no. 9, pp. 1196–1205, 2009.
- [14] F. Li, J. Jin, Y. Gao et al., "Occurrence, distribution and source apportionment of polychlorinated naphthalenes (PCNs) in sediments and soils from the Liaohe River Basin, China," *Environmental Pollution*, vol. 211, pp. 226–232, 2016.
- [15] J. Pan, Y. Yang, X. Zhu et al., "Altitudinal distributions of PCDD/Fs, dioxin-like PCBs and PCNs in soil and yak samples from Wolong high mountain area, eastern Tibet-Qinghai Plateau, China," *Science of The Total Environment*, vol. 444, pp. 102–109, 2013.
- [16] B. Wyrzykowska, N. Hanari, A. Orlikowska et al., "Polychlorinated biphenyls and -naphthalenes in pine needles and soil from Poland - Concentrations and patterns in view of long-term environmental monitoring," *Chemosphere*, vol. 67, no. 9, pp. 1877–1886, 2007.
- [17] B. Wyrzykowska, N. Hanari, A. Orlikowska, N. Yamashita, and J. Falandysz, "Dioxin-like compound compositional profiles of furnace bottom ashes from household combustion in Poland and their possible associations with contamination status of agricultural soil and pine needles," *Chemosphere*, vol. 76, no. 2, pp. 255–263, 2009.
- [18] Y. Horii, J. Falandysz, N. Hanari et al., "Concentrations and fluxes of chloronaphthalenes in sediment from Lake Kitaura in Japan in past 15 centuries," *Journal of Environmental Science and Health. Part A, Toxic/Hazardous Substances & Environmental Engineering*, vol. 39, no. 3, pp. 587–609, 2004.
- [19] L. Cui, S. Wang, L. Gao et al., "Concentrations and trophic magnification of polychlorinated naphthalenes (PCNs) in marine fish from the Bohai coastal area, China," *Environmental Pollution*, vol. 234, pp. 876–884, 2018.
- [20] J. Jin, S. Wang, J. Hu et al., "Polychlorinated naphthalenes in human serum samples from an industrial city in eastern China: levels, sources, and sex differences," *Ecotoxicology and Environmental Safety*, vol. 177, pp. 86–92, 2019.
- [21] H. Park, J. H. Kang, S. Y. Baek, and Y. S. Chang, "Relative importance of polychlorinated naphthalenes compared to dioxins, and polychlorinated biphenyls in human serum from Korea: contribution to TEQs and potential sources," *Environmental Pollution*, vol. 158, no. 5, pp. 1420–1427, 2010.
- [22] C. Weistrand and K. Noren, "Polychlorinated naphthalenes and other organochlorine contaminants in human adipose and liver tissue," *Journal of Toxicology and Environmental Health. Part A*, vol. 53, no. 4, pp. 293–311, 2010.
- [23] A. Schiavone, K. Kannan, Y. Horii, S. Focardi, and S. Corsolini, "Polybrominated diphenyl ethers, polychlorinated naphthalenes and polycyclic musks in human fat from Italy: comparison to polychlorinated biphenyls and organochlorine pesticides," *Environmental Pollution*, vol. 158, no. 2, pp. 599–606, 2010.
- [24] A. Lundén and K. Norén, "Polychlorinated naphthalenes and other organochlorine contaminants in Swedish human milk, 1972–1992," *Archives of Environmental Contamination and Toxicology*, vol. 34, no. 4, pp. 414–423, 1998.
- [25] C. Li, L. Zhang, J. Li et al., "Polychlorinated naphthalenes in human milk: health risk assessment to nursing infants and source analysis," *Environment International*, vol. 136, article 105436, 2020.
- [26] J. T. Kim, M. H. Son, D. H. Lee, W. J. Seong, S. Han, and Y. S. Chang, "Partitioning behavior of heavy metals and persistent organic pollutants among fetomaternal bloods and tissues," *Environmental Science & Technology*, vol. 49, no. 12, pp. 7411–7422, 2015.
- [27] D. L. Villeneuve, K. Kannan, and J. S. Khi, "Relative potencies of individual polychlorinated naphthalenes to induce dioxin-like responses in fish and mammalian in vitro bioassays," *Archives of Environmental Contamination and Toxicology*, vol. 39, no. 3, pp. 273–281, 2000.
- [28] J. Falandysz, A. Fernandes, E. Gregoraszczyk, and M. Rose, "The toxicological effects of halogenated naphthalenes: a review of aryl hydrocarbon receptor-mediated (dioxin-like) relative potency factors," *Journal of Environmental Science and Health. Part C, Environmental Carcinogenesis & Ecotoxicology Reviews*, vol. 32, no. 3, pp. 239–272, 2014.
- [29] IPCS, "International Programme on Chemical Safety (IPCS), Concise International Chemical Assessment Document (CICAD)," in *Chlorinated naphthalenes*, vol. 34, World Health Organization, Geneva, 2001.
- [30] I. Całkosiński, J. Rosińczuk-Tonderys, J. Bazan, M. Dobrzyński, A. Bronowicka-Szydełko, and K. Dzierżba, "Influence of dioxin intoxication on the human system and possibilities of limiting its negative effects on the environment and living organisms," *Annals of Agricultural and Environmental Medicine*, vol. 21, no. 3, pp. 518–524, 2014.
- [31] W. Popp, K. Norpoth, C. Vahrenholz, S. Hamm, E. Balfanz, and J. Theisen, "Polychlorinated naphthalene exposures and liver function changes," *American Journal of Industrial Medicine*, vol. 32, no. 4, pp. 413–416, 1997.
- [32] E. M. Ward, A. M. Ruder, A. Suruda, A. B. Smith, C. A. Fessler-Flesch, and S. H. Zahm, "Acute and chronic liver toxicity resulting from exposure to chlorinated naphthalenes at a

- cable manufacturing plant during World War II,” *American Journal of Industrial Medicine*, vol. 30, no. 2, pp. 225–233, 1996.
- [33] A. Kilanowicz and M. Skrzypinska-Gawrysiak, “Toxicity of hexachloronaphthalene (HxCN) and induction of CYP 1A in rats,” *Ecotoxicology and Environmental Safety*, vol. 73, no. 2, pp. 196–205, 2010.
- [34] M. J. Hooth, A. Nyska, L. M. Fomby et al., “Repeated dose toxicity and relative potency of 1,2,3,4,6,7-hexachloronaphthalene (PCN 66) 1,2,3,5,6,7-hexachloronaphthalene (PCN 67) compared to 2,3,7,8-tetrachlorodibenzo-p-dioxin (TCDD) for induction of CYP1A1, CYP1A2 and thymic atrophy in female Harlan Sprague-Dawley rats,” *Toxicology*, vol. 301, no. 1-3, pp. 85–93, 2012.
- [35] M. Klimczak, A. Darago, E. Bruchajzer et al., “The effects of hexachloronaphthalene on selected parameters of heme biosynthesis and systemic toxicity in female wistar rats after 90-day oral exposure,” *Environmental Toxicology*, vol. 33, no. 6, pp. 695–705, 2018.
- [36] A. Kilanowicz, M. Markowicz-Piasecka, M. Klimczak, J. Stragierowicz, and J. Sikora, “Hexachloronaphthalene as a hemostasis disturbing factor in female Wistar rats - a pilot study,” *Chemosphere*, vol. 228, pp. 577–585, 2019.
- [37] J. Stragierowicz, E. Bruchajzer, A. Daragó, M. Nasiadek, and A. Kilanowicz, “Hexachloronaphthalene (HxCN) as a potential endocrine disruptor in female rats,” *Environmental Pollution*, vol. 243, Part B, pp. 1026–1035, 2018.
- [38] A. Kilanowicz, K. Sitarek, M. Skrzypinska-Gawrysiak, and A. Sapota, “Prenatal developmental toxicity of polychlorinated naphthalenes (PCNs) in the rat,” *Ecotoxicology and Environmental Safety*, vol. 74, no. 3, pp. 504–512, 2011.
- [39] A. Kilanowicz, K. Sitarek, J. Stragierowicz, M. Klimczak, and E. Bruchajzer, “Prenatal toxicity and maternal-fetal distribution of 1,3,5,8-tetrachloronaphthalene (1,3,5,8-TeCN) in Wistar rats,” *Chemosphere*, vol. 226, pp. 75–84, 2019.
- [40] A. Kilanowicz, P. Czekaj, A. Sapota et al., “Developmental toxicity of hexachloronaphthalene in Wistar rats. A role of CYP1A1 expression,” *Reproductive Toxicology*, vol. 58, pp. 93–103, 2015.
- [41] M. Omura, Y. Masuda, M. Hirata et al., “Onset of spermatogenesis is accelerated by gestational administration of 1,2,3,4,6,7-hexachlorinated naphthalene in male rat offspring,” *Environmental Health Perspectives*, vol. 108, no. 6, pp. 539–544, 2000.
- [42] D. Hayward, “Identification of bioaccumulating polychlorinated naphthalenes and their toxicological significance,” *Environmental Research*, vol. 76, no. 1, pp. 1–18, 1998.
- [43] A. Kilanowicz, M. Skrzypinska-Gawrysiak, A. Sapota, A. Galoch, and A. Daragó, “Subacute toxicity of polychlorinated naphthalenes and their effect on cytochrome P-450,” *Ecotoxicology and Environmental Safety*, vol. 72, no. 2, pp. 650–657, 2009.
- [44] A. Galoch, A. Sapota, M. Skrzypinska-Gawrysiak, and A. Kilanowicz, “Acute toxicity of polychlorinated naphthalenes and their effect on cytochrome P450,” *Human & Experimental Toxicology*, vol. 25, no. 2, pp. 85–92, 2016.
- [45] A. Kilanowicz, D. Wiaderna, P. Lutz, and W. Szymczak, “Behavioral effects following repeated exposure to hexachloronaphthalene in rats,” *Neurotoxicology*, vol. 33, no. 3, pp. 361–369, 2012.
- [46] H. Vinitskaya, A. Lachowicz, A. Kilanowicz, J. Bartkowiak, and L. Zylinska, “Exposure to polychlorinated naphthalenes affects GABA-metabolizing enzymes in rat brain,” *Environmental Toxicology and Pharmacology*, vol. 20, no. 3, pp. 450–455, 2005.
- [47] G. Suzuki, C. Michinaka, H. Matsukami, Y. Noma, and N. Kajiwara, “Validity of using a relative potency factor approach for the risk management of dioxin-like polychlorinated naphthalenes,” *Chemosphere*, vol. 244, article 125448, 2020.
- [48] E. J. van de Plassche and A. M. Schwegler, *Polychlorinated naphthalenes. Dossier prepared for the third meeting of the UN-ECE Ad hoc Expert Group on POPs. Royal Haskoning Report L0002.A01 R0010/EVDP/TLA.M.G.R.2002*, Ministry of Housing, Spatial Planning and the Environment, Directorate-General for Environmental Protection, Nijmegen, The Netherlands, 2002.
- [49] S. C. Lee, T. Harner, K. Pozo et al., “Polychlorinated naphthalenes in the Global Atmospheric Passive Sampling (GAPS) study,” *Environmental Science & Technology*, vol. 41, no. 8, pp. 2680–2687, 2007.
- [50] K. Vorkamp, K. Falk, S. Møller, R. Bossi, F. F. Rigét, and P. B. Sørensen, “Perfluoroalkyl substances (PFASs) and polychlorinated naphthalenes (PCNs) add to the chemical cocktail in peregrine falcon eggs,” *Science of The Total Environment*, vol. 648, pp. 894–901, 2019.
- [51] J. Falandysz and A. R. Fernandes, “Compositional profiles, persistency and toxicity of polychlorinated naphthalene (PCN) congeners in edible cod liver products from 1972 to 2017,” *Environmental Pollution*, vol. 260, article 114035, 2020.
- [52] A. Kilanowicz, A. Galoch, and A. Sapota, “Tissue distribution and elimination of selected chlorinated naphthalenes,” *International Journal of Occupational Medicine and Environmental Health*, vol. 17, no. 3, pp. 355–360, 2004.
- [53] M. van Spronsen, E. Y. van Battum, M. Kuijpers et al., “Developmental and activity-dependent miRNA expression profiling in primary hippocampal neuron cultures,” *PLoS One*, vol. 8, no. 10, article e74907, 2013.
- [54] K. J. Livak and T. D. Schmittgen, “Analysis of Relative Gene Expression Data Using Real-Time Quantitative PCR and the $2^{-\Delta\Delta C_T}$ Method,” *Methods*, vol. 25, no. 4, pp. 402–408, 2001.
- [55] J. Chung, H. Kubota, Y. Ozaki, S. Uda, and S. Kuroda, “Timing-dependent actions of NGF required for cell differentiation,” *PLoS One*, vol. 5, no. 2, article e9011, 2010.
- [56] M. Sobczak, T. Boczek, B. Ferenc et al., “Functional characteristic of PC12 cells with reduced microsomal glutathione transferase 1,” *Acta Biochimica Polonica*, vol. 57, no. 4, pp. 589–596, 2010.
- [57] G. Blobel and V. R. Potter, “Nuclei from rat liver: isolation method that combines purity with high yield,” *Science*, vol. 154, no. 3757, pp. 1662–1665, 1966.
- [58] Y. Goodman, A. J. Bruce, B. Cheng, and M. P. Mattson, “Estrogens attenuate and corticosterone exacerbates excitotoxicity, oxidative injury, and amyloid beta-peptide toxicity in hippocampal neurons,” *Journal of Neurochemistry*, vol. 66, no. 5, pp. 1836–1844, 1996.
- [59] R. B. Badisa and C. B. Goodman, “Effects of chronic cocaine in rat C6 astroglial cells,” *International Journal of Molecular Medicine*, vol. 30, no. 3, pp. 687–692, 2012.
- [60] V. M. Lee, “Neurofilament protein abnormalities in PC12 cells: comparison with neurofilament proteins of normal

- cultured rat sympathetic neurons," *The Journal of Neuroscience*, vol. 5, no. 11, pp. 3039–3046, 1985.
- [61] N. Heck, A. Golbs, T. Riedemann, J. J. Sun, V. Lessmann, and H. J. Luhmann, "Activity-dependent regulation of neuronal apoptosis in neonatal mouse cerebral cortex," *Cerebral Cortex*, vol. 18, no. 6, pp. 1335–1349, 2008.
- [62] C. P. Turner, R. Miller, C. Smith et al., "Widespread neonatal brain damage following calcium channel blockade," *Developmental Neuroscience*, vol. 29, no. 3, pp. 213–231, 2007.
- [63] F. K. M. Chan, K. Moriwaki, and M. J. de Rosa, "Detection of necrosis by release of lactate dehydrogenase activity," *Methods in Molecular Biology*, vol. 979, pp. 65–70, 2013.
- [64] P. Scaffidi, T. Misteli, and M. E. Bianchi, "Release of chromatin protein HMGB1 by necrotic cells triggers inflammation," *Nature*, vol. 418, no. 6894, pp. 191–195, 2002.
- [65] P. Golstein and G. Kroemer, "Cell death by necrosis: towards a molecular definition," *Trends in Biochemical Sciences*, vol. 32, no. 1, pp. 37–43, 2007.
- [66] D. E. Epps, M. L. Wolfe, and V. Groppi, "Characterization of the steady-state and dynamic fluorescence properties of the potential-sensitive dye bis-(1,3-dibutylbarbituric acid)trimethine oxonol (Dibac₄(3)) in model systems and cells," *Chemistry and Physics of Lipids*, vol. 69, no. 2, pp. 137–150, 1994.
- [67] B. Ehrenberg, V. Montana, M. D. Wei, J. P. Wuskell, and L. M. Loew, "Membrane potential can be determined in individual cells from the nernstian distribution of cationic dyes," *Biophysical Journal*, vol. 53, no. 5, pp. 785–794, 1988.
- [68] C. Aguer, D. Gambarotta, R. J. Mailloux et al., "Galactose enhances oxidative metabolism and reveals mitochondrial dysfunction in human primary muscle cells," *PLoS One*, vol. 6, no. 12, article e28536, 2011.
- [69] J. A. Dykens, J. Jamieson, L. Marroquin, S. Nadanaciva, P. A. Billis, and Y. Will, "Biguanide-induced mitochondrial dysfunction yields increased lactate production and cytotoxicity of aerobically-poised HepG2 cells and human hepatocytes *in vitro*," *Toxicology and Applied Pharmacology*, vol. 233, no. 2, pp. 203–210, 2008.
- [70] H. Kawasaki, A. Shigenaga, M. Uda et al., "Nitration of tryptophan in ribosomal proteins is a novel post-translational modification of differentiated and naive PC12 cells," *Nitric Oxide*, vol. 25, no. 2, pp. 176–182, 2011.
- [71] N. Peunova and G. Enikolopov, "Nitric oxide triggers a switch to growth arrest during differentiation of neuronal cells," *Nature*, vol. 375, no. 6526, pp. 68–73, 1995.
- [72] T. Boczek, M. Lisek, A. Kowalski et al., "Downregulation of PMCA2 or PMCA3 reorganizes Ca²⁺ handling systems in differentiating PC12 cells," *Cell Calcium*, vol. 52, no. 6, pp. 433–444, 2012.
- [73] L. A. Greene and A. S. Tischler, "Establishment of a noradrenergic clonal line of rat adrenal pheochromocytoma cells which respond to nerve growth factor," *Proceedings of the National Academy of Sciences of the United States of America*, vol. 73, no. 7, pp. 2424–2428, 1976.
- [74] M. O. Frégeau, M. Carrier, and G. Guillemette, "Mechanism of dopamine D2 receptor-induced Ca²⁺ release in PC-12 cells," *Cellular Signalling*, vol. 25, no. 12, pp. 2871–2877, 2013.
- [75] K. Yang, X. Jiang, S. Cheng et al., "Synaptic dopamine release is positively regulated by SNAP-25 that involves in benzo[a]pyrene-induced neurotoxicity," *Chemosphere*, vol. 237, article 124378, 2019.
- [76] S. H. Enayah, B. C. Vanle, L. J. Fuortes, J. A. Doorn, and G. Ludewig, "PCB95 and PCB153 change dopamine levels and turn-over in PC12 cells," *Toxicology*, vol. 394, no. 2, pp. 93–101, 2018.
- [77] S. Mizukami-Murata, K. Fujita, and T. Nakano, "Effect of lower chlorinated hydroxylated-polychlorobiphenyls on development of PC12 cells," *Environmental Science and Pollution Research International*, vol. 25, no. 17, pp. 16434–16445, 2018.
- [78] F. Fonnum and E. Mariussen, "Mechanisms involved in the neurotoxic effects of environmental toxicants such as polychlorinated biphenyls and brominated flame retardants," *Journal of Neurochemistry*, vol. 111, no. 6, pp. 1327–1347, 2009.
- [79] E. L. Gregoraszczyk, J. Barć, and J. Falandysz, "Differences in the action of lower and higher chlorinated polychlorinated naphthalene (PCN) congeners on estrogen dependent breast cancer cell line viability and apoptosis, and its correlation with Ahr and CYP1A1 expression.," *Toxicology*, vol. 366–367, no. 7, pp. 53–59, 2016.
- [80] J. Barć and E. L. Gregoraszczyk, "Halowax 1051 affects steroidogenesis by down-regulation of aryl hydrocarbon and estrogen receptors and up-regulation of androgen receptor in porcine ovarian follicles," *Chemosphere*, vol. 144, pp. 467–474, 2016.
- [81] H. Qin and J. A. Powell-Coffman, "The *Caenorhabditis elegans* aryl hydrocarbon receptor, AHR-1, regulates neuronal development," *Developmental Biology*, vol. 270, no. 1, pp. 64–75, 2004.
- [82] M. D. Kim, L. Y. Jan, and Y. N. Jan, "The bHLH-PAS protein spineless is necessary for the diversification of dendrite morphology of *Drosophila* dendritic arborization neurons," *Genes & Development*, vol. 20, no. 20, pp. 2806–2819, 2006.
- [83] S. E. Latchney, A. M. Hein, M. K. O'Banion, E. DiCiccobloom, and L. A. Opanashuk, "Deletion or activation of the aryl hydrocarbon receptor alters adult hippocampal neurogenesis and contextual fear memory," *Journal of Neurochemistry*, vol. 125, no. 3, pp. 430–445, 2013.
- [84] A. L. Blankenship, K. Kannan, S. A. Villalobos et al., "Relative potencies of individual polychlorinated naphthalenes and Halowax mixtures to induce Ah receptor-mediated responses," *Environmental Science & Technology*, vol. 34, no. 15, pp. 3153–3158, 2000.
- [85] J. E. Jung, J. Y. Moon, S. H. Ghil, and B. S. Yoo, "2,3,7,8-Tetrachlorodibenzo-*p*-dioxin (TCDD) inhibits neurite outgrowth in differentiating human SH-SY5Y neuroblastoma cells," *Toxicology Letters*, vol. 188, no. 2, pp. 153–156, 2009.
- [86] H. Q. Xie, H. M. Xu, H. L. Fu et al., "AhR-mediated effects of dioxin on neuronal acetylcholinesterase expression *in vitro*," *Environmental Health Perspectives*, vol. 121, no. 5, pp. 613–618, 2013.
- [87] G. Xu, Q. Zhou, C. Wan et al., "2,3,7,8-TCDD induces neurotoxicity and neuronal apoptosis in the rat brain cortex and PC12 cell line through the down-regulation of the Wnt/ β -catenin signaling pathway," *Neurotoxicology*, vol. 37, pp. 63–73, 2013.
- [88] W. G. R. Angus and M. L. Contreras, "Aroclor 1254 alters the binding of ¹²⁵I-labeled nerve growth factor in PC12 cells," *Neuroscience Letters*, vol. 191, no. 1–2, pp. 23–26, 1995.
- [89] A. A. Starkov, B. M. Polster, and G. Fiskum, "Regulation of hydrogen peroxide production by brain mitochondria by

- calcium and Bax,” *Journal of Neurochemistry*, vol. 83, no. 1, pp. 220–228, 2002.
- [90] N. E. Rainey, A. Saric, A. Leberre et al., “Synergistic cellular effects including mitochondrial destabilization, autophagy and apoptosis following low-level exposure to a mixture of lipophilic persistent organic pollutants,” *Scientific Reports*, vol. 7, no. 1, article 4728, 2017.
- [91] R. C. Rabinovitch, B. Samborska, B. Faubert et al., “AMPK maintains cellular metabolic homeostasis through regulation of mitochondrial reactive oxygen species,” *Cell Reports*, vol. 21, no. 1, pp. 1–9, 2017.
- [92] H. P. Glauert, J. C. Tharappel, Z. Lu et al., “Role of oxidative stress in the promoting activities of pcbs,” *Environmental Toxicology and Pharmacology*, vol. 25, no. 2, pp. 247–250, 2008.
- [93] D. Bagchi, J. Balmoori, M. Bagchi, X. Ye, C. B. Williams, and S. J. Stohs, “Comparative effects of TCDD, endrin, naphthalene and chromium (VI) on oxidative stress and tissue damage in the liver and brain tissues of mice,” *Toxicology*, vol. 175, no. 1-3, pp. 73–82, 2002.
- [94] J. F. Reichard, T. P. Dalton, H. G. Shertzer, and A. Puga, “Induction of oxidative stress responses by dioxin and other ligands of the aryl hydrocarbon receptor,” *Dose-Response*, vol. 3, no. 3, pp. 306–331, 2005.
- [95] K. Selvakumar, S. Bavithra, G. Krishnamoorthy, P. Venkataraman, and J. Arunakaran, “Polychlorinated biphenyls-induced oxidative stress on rat hippocampus: a neuroprotective role of quercetin,” *Scientific World Journal*, vol. 2012, article 980314, 10 pages, 2012.
- [96] S. B. Cheng, S. Kuchiiwa, X. Q. Ren, H. Z. Gao, T. Kuchiiwa, and S. Nakagawa, “Dioxin exposure down-regulates nitric oxide synthase and NADPH-diaphorase activities in the hypothalamus of Long-Evans rat,” *Neuroscience Letters*, vol. 345, no. 1, pp. 5–8, 2003.
- [97] M. Llansola, C. Montoliu, J. Boix, and V. Felipo, “Polychlorinated biphenyls PCB 52, PCB 180, and PCB 138 impair the glutamate-nitric oxide-cGMP pathway in cerebellar neurons in culture by different mechanisms,” *Chemical Research in Toxicology*, vol. 23, no. 4, pp. 813–820, 2010.
- [98] V. M. Victor, S. Rovira-Llopis, V. Saiz-Alarcon et al., “Altered mitochondrial function and oxidative stress in leukocytes of anorexia nervosa patients,” *PLoS One*, vol. 9, no. 9, article e106463, 2014.
- [99] Y. Bansal and A. Kuhad, “Mitochondrial dysfunction in depression,” *Current Neuropharmacology*, vol. 14, no. 6, pp. 610–618, 2016.
- [100] M. Mancuso, V. Calsolaro, D. Orsucci et al., “Mitochondria, cognitive impairment, and Alzheimer’s disease,” *International Journal of Alzheimer’s Disease*, vol. 2009, article 951548, 8 pages, 2009.
- [101] D. Ma, P. C. Guest, and S. Bahn, “Metabonomic studies of schizophrenia and psychotropic medications: focus on alterations in CNS energy homeostasis,” *Bioanalysis*, vol. 1, no. 9, pp. 1615–1626, 2009.
- [102] A. Loehfelm, A. Boucsein, D. Pretz, and A. Tups, “Timing matters: circadian effects on energy homeostasis and Alzheimer’s disease,” *Trends in Endocrinology and Metabolism*, vol. 30, no. 2, pp. 132–143, 2019.

Research Article

A Stereological Study of the Toxic Effects of Cerium Oxide during Pregnancy on Kidney Tissues in Neonatal NMRI Mice

Afsaneh Nemati,¹ Vahideh Assadollahi,² Ilaria Peluso ,³ Abolfazl Abbaszadeh,⁴ Mandana Beigi-boroujeni,¹ Zahra Khanipur,¹ and Mohammadreza Gholami ⁵

¹Razi Herbal Medicines Research Center, Lorestan University of Medical Sciences, Khorramabad, Iran

²Cancer and Immunology Research Center, Research Institute for Health Development, Kurdistan University of Medical Sciences, Sanandaj, Iran

³Council for Agricultural Research and Economics, Research Center for Food and Nutrition (CREA-AN), Via Ardeatina 546, 00178 Rome, Italy

⁴Hazrat Fatemeh Hospital, School of Medicine, Burn Research Center, Iran University of Medical Sciences, Tehran, Iran

⁵Department of Anatomy, Kermanshah University of Medical Sciences, Kermanshah, Iran

Correspondence should be addressed to Mohammadreza Gholami; rezagholami57@gmail.com

Received 23 February 2020; Revised 27 April 2020; Accepted 2 June 2020; Published 23 June 2020

Academic Editor: Luciano Saso

Copyright © 2020 Afsaneh Nemati et al. This is an open access article distributed under the Creative Commons Attribution License, which permits unrestricted use, distribution, and reproduction in any medium, provided the original work is properly cited.

Background. Both antioxidant and prooxidant activities have been previously reported for cerium oxide (CeO₂). The aim of this study was to investigate the effects of CeO₂ at different doses on changes in kidney tissues and markers in neonatal mice. **Methods.** We randomly divided 30 pregnant NMRI mice into five groups ($n = 6$ per group)—a control group and four groups treated with intraperitoneal (i.p.) administration of different doses of CeO₂ (10, 25, 80, or 250 mg/kg body weight (bw)) on gestation days (GD) 7 and GD14. At the end of the treatment period, we analyzed the kidney tissues and serum samples. The levels of two serum redox markers, malondialdehyde (MDA) and ferric reducing/antioxidant power (FRAP), were determined. Data were analyzed using one-way ANOVA and Tukey's test, and a P value of <0.05 was considered significant. **Results.** The mean total volumes of the renal corpuscle, glomeruli, and Bowman's capsule membranes significantly increased, and there was a significant decrease in the mean total volume of Bowman's space in the high-dose CeO₂ group compared to that in the control group. No statistically significant differences existed in the serum levels of MDA and FRAP in the treated and control groups. **Conclusion.** Our results suggest that high doses of CeO₂ impair fetal renal development in pregnant mice, which results in kidney damage. Therefore, CeO₂ administration during pregnancy could have dose-dependent adverse effects on the developing kidneys in neonates.

1. Introduction

Cerium is the most abundant rare-earth metal and most active element in the lanthanide group. Cerium is a soft, ductile, and malleable metal with a color that ranges from iron-gray (commercial grade) to silver (pure form). Cerium compounds have the highest environmental activity compared to other members of the lanthanide group [1].

Cerium oxide (CeO₂) is the most commonly used commercial compound of cerium [2]. Cerium oxide lanthanides are widely used as catalysts, oxygen sensors, in the manufacture of solar/fuel cells, and polishing agents

in various fields [3–6]. The unique properties of CeO₂, especially its low toxicity and high reducibility, have increased the use of micro- and nanosized CeO₂ in various medical fields and led to significant advances in these fields [1]. The medical applications of CeO₂ are due to its antioxidant, anti-inflammatory, and antibacterial properties and its high angiogenic potential. Cerium oxide is used to assist with the healing of various tissues such as the bones, skin, cardiac, and nerves. Recently, the transfer of drugs and genes by CeO₂ nanoparticles and the use of CeO₂ as treatments for cancer and other diseases has received much attention [7, 8].

Cerium, itself, has no properties and is not physiologically important for living organisms; however, soluble Ce^{3+} salts (sulfate, nitrate, chloride, phosphate, and hydroxide) contain various properties that are of medical importance. Cerium oxide is a pale yellow-white powder with the chemical formula CeO_2 [9]. The autoregenerative cycle nature of CeO_2 is due to the presence of an enormous number of surface defects and its ability to switch between Ce^{3+} and Ce^{4+} oxidation states. The formation of an oxygen vacancy in CeO_2 is associated with reduced Ce^{4+} and Ce^{3+} oxidation. This property allows Ce to absorb or give off an electron from the active oxygen species, making them inactive and neutral, and indicates a key role in the ratio of the $\text{Ce}^{3+}/\text{Ce}^{4+}$ oxide in the antioxidant activity of CeO_2 [9–11]. Cerium oxide is believed to function as a superoxide dismutase (SOD)/catalase mimetic [9, 12–15]. In an experiment on mice, the antioxidant properties of CeO_2 nanoparticles inhibited active oxygen species and its potential for the treatment of oxidative stress was reported [16]. Oxidative stress is an imbalance between reactive oxygen species (ROS) and antioxidants in the body [17]. Researchers propose that CeO_2 could be used to treat diseases associated with oxidative stress and inflammation [9, 10, 18, 19]. This ability of the nanoscale to neutralize ROS from a pool of high concentration polymer ligands suggests that nanoscale activity may not decrease in the physiological environment, even when coated with a protein corona. A study on the distribution of inhaled CeO_2 nanoparticles in mice showed that the cells phagocytosed the nanoparticles [20, 21].

Previous studies on the effects of CeO_2 in living organisms reported contradictory results. Some researchers reported that CeO_2 caused oxidative stress in mitochondria and hepatocellular damage [22], inflammation in tissues such as the kidneys and liver [23], and DNA damage in peripheral blood leukocytes (PBL) and liver cells [24]. Cerium oxide can also cause lung fibrosis [25] and angiogenesis [26].

In contrast, other researchers reported that CeO_2 could act as an antioxidant and be used for cancer prevention and treatment [27, 28]. In another study, the optimum concentration (10^{-3} – 10^{-9} M) of CeO_2 increased cell division of primary fetal fibroblasts *in vitro* [29]. The results of a study showed that CeO_2 nanoparticles reduced oxidative stress and inflammation in mice treated with diethylnitrosamine [30]. The protective effect of CeO_2 nanoparticles in preventing tissue damage and oxidative stress induced by diabetes in pregnant mice has been reported [31]. Existing synthetic protocols have the ability to obtain CeO_2 nanoparticles with different physical and chemical properties (shape, size, zeta potential, and cerium valence state). The synthesis method directly affects their biological activity [32]. The impact of these characteristics on toxicity, especially fetal toxicity, has not been elucidated.

The impact of a wide range of cerium nanoparticles stabilized by citrate on the growth of two-cell embryos was investigated. The results showed that the cerium nanoparticle concentrations had no toxic effects on fetal development [33].

Cerium oxide can cross the placenta and make its way to the liver, spleen, and lung tissues of adult, neonatal, and fetal mice, inducing tissue destruction and necrosis [34]. In addition, the results from our previous study have shown that

high-dose CeO_2 can have a devastating effect on testicular tissue development in neonatal mice [35].

The kidneys play a key role in regulating the body's homeostasis and excreting waste products [36]. Metanephric development begins in humans during week five of gestation and in mice at embryonic day (E) 10.5 [37]. There is an enhanced chance for exposure to CeO_2 because of the increase in its various uses in daily life. Pregnant women are exposed to CeO_2 via the skin, inhalation, foods, and medicines.

Congenital anomalies of the kidneys are among the most important anomalies [38]. When pregnant mice are exposed to CeO_2 , these particles can cross the placenta and accumulate in the fetal organs [22–24, 34]. CeO_2 may hinder embryonic development and may have possible demographic impacts [34]. Given the importance of kidney development during pregnancy and the postpartum period, the present study is aimed at comparing histological changes in neonatal kidneys after their mothers were exposed to different doses of a CeO_2 suspension during the gestational day (GD) 7 and GD14 of pregnancy.

2. Materials and Methods

2.1. Materials. Cerium (IV) oxide (CeO_2) powder that had a diameter $< 5 \mu\text{m}$, assay of 99.9% trace metal basis, and density of 7.13 g/ml at 25°C (lit.) was purchased from Sigma-Aldrich Corporation (St. Louis, MO, USA). We prepared the different doses of CeO_2 in double-distilled (dd) water. Ultrasonic vibration (100 W, 30 kHz) was performed for 15 min before administration.

In this study, the selected doses were based on previous studies and doses lower than the lethal dose; 50% (LD50) were used for the animals [34, 39]. Based on the contradictory results of previous studies, we selected various doses that ranged from low to high to detect dose-dependent effects in the laboratory animals. We performed our experiment based on the characteristics reported by the manufacturer of CeO_2 and previous experiments [1, 34, 40–42].

The different doses of CeO_2 were prepared in double-distilled (dd) water. Ultrasonic vibration (100 W, 30 kHz) was performed for 15 min before administration.

Trichloroacetic acid ACS reagent, $\geq 99.0\%$ (TCA); 2,4,6-tripyridyl-s-triazine (TPTZ); 2-thiobarbituric acid $\geq 98\%$ (TBA); ferric chloride (FeCl_3); sodium acetate; and hydrochloric acid-ACS reagent, 37% (HCl), were also purchased from Sigma-Aldrich Corporation.

2.2. Animals and Experimental Groups. We obtained adult NMRI mice (male:female ratio of 1:2) that had an average weight of 25–30 g from Pasteur Institute of Iran (Tehran, Iran). The animals were allowed to acclimate for one week under standard conditions that included a 12:12 h light/dark cycle with ad libitum access to food and water. Once acclimated to their new environment, the male and female mice were kept in a cage at a 1:2 ratio. The pregnant mice were placed in separate cages. The detection of a vaginal plug was considered to be gestation day (GD) 0. The pregnant mice were randomly divided into five groups ($n=6$ per group): a control and four treatment groups. Mice in the

treatment groups received intraperitoneal (i.p.) injections of different doses of CeO₂ (10, 25, 80, or 250 mg/kg body weight (bw)) on GD7 and GD14.

In this experiment, 15-day-old neonates were used for histological evaluation of kidney tissues and serum biochemical parameters. Changes in body weights and kidney tissue in 2- and 6-day-old neonates were evaluated.

2.3. Histological Examinations of the Kidneys. The 15-day-old postpartum (dpp) offspring were weighed and anesthetized by chloroform. After dissection, blood samples were collected from the heart using a 1 cc syringe. The left kidneys from the mice were excised and rinsed with distilled water, weighed, and fixed for one week in a 10% formaldehyde solution. After tissue passage and paraffin block preparation, the paraffin blocks were sectioned into 5 μm sections with a microtome and subsequently stained with Heidenhain's Azan stain [43]. We randomly selected nine sections from each kidney to evaluate the histological parameters.

2.4. Kidney Volume. We used the Cavalieri method to assess kidney volume [44]. First, we systematically selected 15 random tissue sections from all of the 5 μm sections at the same interval. The predesigned point probe was randomly uniform on the image of each of the sections, and the points encountered with the whole kidney image were counted.

The kidney volume was calculated in all the slices by using the following formula:

$$V_{(\text{total})} = \sum_{i=1}^n P \times a(p) \times t, \quad (1)$$

where $\sum_{i=1}^n P$ is the sum of the total points, "t" represents the thickness between selected sections, and "a(p)" is the level of the point probe.

Next, we calculated the cortex and medullary volumes. Tissues were chosen by regular, random sampling, and the average of 15 fields of view from each 5 μm section was assessed at 100x magnification by placing the point probe on each field.

2.5. Volumes of the Cortex, Medulla, and Cortex Components. The total number of points that hit the probe with the entire field was $\sum_{i=1}^n P_{\text{total}}$; the whole number of the points that hit the probe in the cortex was $\sum_{i=1}^n P_{\text{cortex}}$; and the whole number of points that hit the probe in the medulla was $\sum_{i=1}^n P_{\text{medulla}}$.

Volumetric density was calculated using the following formulas for the cortex and medulla:

$$V_{v \text{ cortex}} = \frac{\sum_{i=1}^n P_{\text{cortex}}}{\sum_{i=1}^n P_{\text{total}}}, \quad (2)$$

$$V_{v \text{ medulla}} = \frac{\sum_{i=1}^n P_{\text{medulla}}}{\sum_{i=1}^n P_{\text{total}}}.$$

We separately estimated the volumes of the cortex and medulla by multiplying the volume density of each by the kidney volume in each neonatal mouse.

$$V_{\text{cortex}} = V_{v \text{ cortex}} \times V_{\text{total}}, \quad (3)$$

$$V_{\text{medulla}} = V_{v \text{ medulla}} \times V_{\text{total}}.$$

We estimated the volume of the components of the cortex, proximal tubule (PT), and distal tubule (DT), with the lumen and their epithelium, glomeruli, and interstitial tissue by systematic random sampling. An average of 15 fields of view from each 5 μm slide was assessed by placing a counting frame on each field. The total number of the points that hit the frame with the entire field of view was selected ($\sum_{i=1}^n P_{\text{total}}$), and the whole number of points that hit each component ($\sum_{i=1}^n P_x$) was shown. The volume density was calculated using the following formula:

$$V_{vx} = \frac{\sum_{i=1}^n P_{(x)}}{\sum_{i=1}^n P_{\text{total}}}, \quad (4)$$

where "x" represents the PT and DT, lumen, epithelium, interstitial tissue, and glomeruli.

Then, using the following formula, we separately calculated the volumes of the PT and DT, lumen, epithelium, interstitial tissue, or glomeruli by multiplying the volume density of each in the cortical volume:

$$V_x = V_{\text{cortex}} \times V_{vx}. \quad (5)$$

In the above formula, "x" represents the PT, DT, lumen, epithelium, interstitial tissue, and glomeruli.

2.6. Volume of Bowman's Capsule and Space. In order to obtain the volume of the glomeruli components, we first compared the whole number of the points that hit the frame with these components ($\sum_{i=1}^n P_x$) and the whole number of the points that hit the frame with each glomerulus ($\sum_{i=1}^n P_{\text{glomerulus}}$). The volumetric density of the glomerulus was calculated using the following formula:

$$V_{vx} = \frac{\sum_{i=1}^n P_{(x)}}{\sum_{i=1}^n P_{\text{glomerulus}}}, \quad (6)$$

where "x" represents each of the components of the glomerulus (Bowman's capsule and space).

Then, the volume of Bowman's capsule and space were calculated by multiplying the volume density of each component in the volume of the glomerulus as follows:

$$V_x = V_{\text{glomerulus}} \times V_{vx}, \quad (7)$$

where "x" represented any of the glomerulus components, namely, Bowman's capsule and space.

2.7. Length of Proximal Tubules (PT) and Distal Tubules (DT). In order to calculate the length of the PT and DT from the 5 μm slides of kidney tissue at 400x magnification, we used systematic random sampling to select 15 fields of view. The counting probe was randomly placed on each of the microscopic fields of view, and the number of tubules

counted within the frame or those that collided with the reception lines was counted. The number of tubules that contacted the banned lines was not counted. Then, the longitudinal densities of the PT and DT were calculated from the following equation:

$$L_{V=2} = 2 \times \frac{\sum_{i=1}^n Q_i}{alf \sum_{i=1}^n P_i}, \quad (8)$$

where $\sum Q_i$ is the sum of selected tubules, alf is the desired frame level at the texture scale, and $\sum P_i$ is the sum of the points of contact with the kidney tissue.

2.8. Serum Redox Markers. Blood samples were collected from 15-day-old neonatal hearts to estimate the serum redox markers, malondialdehyde (MDA) and ferric reducing/antioxidant power (FRAP).

2.9. Malondialdehyde (MDA) Levels. Buege and Aust's procedure was used to evaluate serum MDA levels. In this method, a solution that contained trichloroacetic acid (TCA; 15% g/ml), TBA (0.375%, g/ml), and hydrochloric acid (HCl, 25% normal) was prepared and the sera were combined in a 2:1 ratio and placed in a bain-marie for 15 min. The solution was placed in cold water and then centrifuged for 10 min. The absorbance of the solution was read using a spectrophotometer at a wavelength of 532 nm [45, 46].

2.10. Ferric Reducing/Antioxidant Power (FRAP) Assay. The FRAP assay was used to estimate the antioxidants. We combined 0.5 ml of serum with 1.5 ml of the reaction mixture. The degree of plasma regeneration is proportional to the concentration of this complex. At low pH, the reduction of the TPTZ- Fe^{3+} complex in the form of ferrous (Fe^{2+}) creates a blue complex that has a maximum absorption of 593 nm. The degree of the regenerative capacity of the serum was measured by increasing the concentration of the above complex using a spectrophotometer. The FRAP assay directly evaluates the whole antioxidant power [47].

2.11. Statistical Analysis. Data were analyzed with SPSS 16 (Statistical Package for the Social Sciences), ANOVA, and Tukey's test. P values < 0.05 were considered statistically significant.

3. Results

3.1. Histological Evaluation of the Kidney Tissues. In the control group, we observed that the kidney tissues had a normal structure with regular tubules, cylindrical epithelial cells based on the basement membrane, lumen space, and normal glomeruli. In the group that received less than 250 mg/kg bw CeO_2 , the glomeruli were inflamed, and there was a significant increase in the volumes of the glomeruli and the membrane of the Bowman's capsule, along with a significant decrease in volume of Bowman's capsule space compared to the control group ($P < 0.02$). There were no statistically significant differences in the other groups treated with CeO_2 compared to the control group (Figure 1).

3.2. Body and Kidney Weights. There were no statistically significant differences in body and kidney weights in the treatment and control groups (Table 1).

3.3. Volume of the Kidney, Cortex, Medulla, and Cortex Components. A comparison of kidney volumes in the treatment and control groups showed a significant decrease in the group that received the 250 mg/kg bw CeO_2 dose ($P < 0.02$) (Table 2).

The cortex volume was significantly reduced in the group that received 250 mg/kg bw CeO_2 ($P < 0.03$) compared to that in the control group. There was no statistically significant difference in the other groups treated with CeO_2 compared to that in the control group. We also observed no statistically significant difference in medulla volume in the treatment groups compared to that in the control group.

There were significant increases in volume in the interstitial tissue ($P < 0.01$), renal corpuscle ($P < 0.02$), glomerulus ($P < 0.02$), and Bowman's capsule ($P < 0.02$) tissues in the 250 mg/kg bw CeO_2 group compared with those in the control group. The other treatment groups showed no significant volume changes in these tissues when compared with the control group (Table 3).

A significant decrease was observed in the volume of Bowman's space in the 250 mg/kg bw CeO_2 ($P < 0.05$) group compared with that in the control group; however, the other treatment groups did not significantly differ with the control group (Table 3).

The volume of the PT and its epithelium ($P < 0.04$) and the PT lumen ($P < 0.05$) decreased significantly in the group that received 250 mg/kg bw CeO_2 compared to that in the control group ($P < 0.05$).

There was no significant difference between the volume of the DT and the epithelium and its lumen in the group that received 250 mg/kg bw of CeO_2 compared with that in the control group (Table 4).

3.4. Lengths of Proximal Tubules (PT) and Distal Tubules (DT). There was no significant difference between the DT and PT lengths in the treatment groups compared to that in the control group (Table 5).

3.5. Biochemical Evaluations. Statistical analysis of blood serum MDA showed no significant difference between treatment groups compared to the control group (Figure 2). In addition, statistical analysis of blood serum total antioxidant capacity (TAC) showed no significant difference between treatment groups compared to the control group (Figure 3).

4. Discussion

In this study, we administered i.p. injections of different doses of a CeO_2 microparticle suspension to pregnant mice on GD7 and GD14 and examined their effects on neonatal mice kidney tissues by light microscopy. The selection of the CeO_2 micropowder for this experiment was based on previous studies in which the toxic effects of CeO_2 microparticles and their faster accumulation in the tissues of living organisms were confirmed [34, 48]. Exposure of pregnant

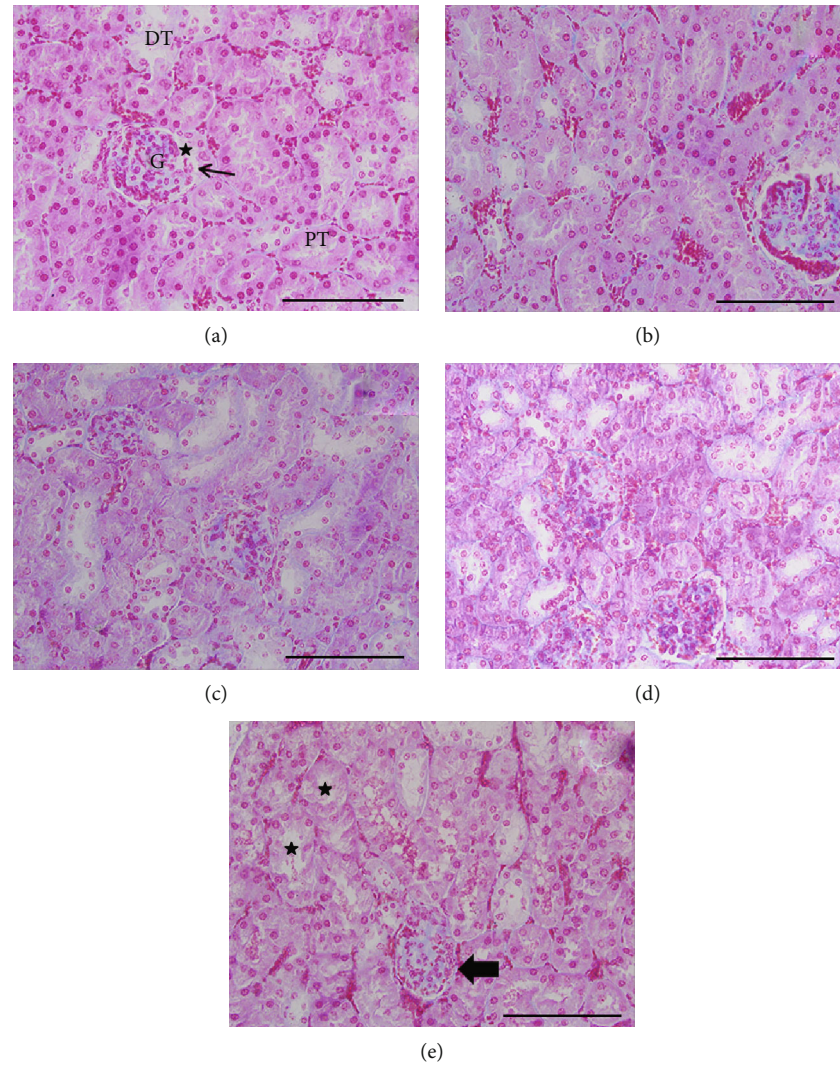


FIGURE 1: Microscopic images of kidney tissue from 15-day-old mice. The $5\mu\text{m}$ sections stained with Heidenhain's Azan show histopathologic changes in the kidney tissue. Magnification: 400x (scale bars= $100\mu\text{m}$). Control (a): renal tubules with a regular arrangement of epithelial cells and glomerulus with natural size components and structure (arrow: Bowman's capsule membrane; star: Bowman's capsule space). PT: proximal convoluted tubule; DT: distal convoluted tubule; G: glomerulus in the control group. Cerium oxide (CeO_2); 10 mg/kg body weight (bw) (b), CeO_2 ; 25 mg/kg bw (c): renal tubules with a regular arrangement of epithelial cells and glomeruli with natural size components and structure in the groups treated with 10 and 25 mg/kg bw CeO_2 . CeO_2 ; 80 mg/kg bw (d): histological changes are not significant compared to the control group. CeO_2 ; 250 mg/kg bw (e): vacuolization in the renal tubules, along with disruption, injury, and degeneration in PTs, vascularization in the interstitial kidney tissue, hypertrophy in the glomerulus, and reduced Bowman's capsule space in the 250 mg/kg bw CeO_2 treatment group.

TABLE 1: Comparison of body weight (bw) and kidney weight in the study groups.

Group	bw (D_2)	bw (D_6)	bw (D_{15})	Kidney W (D_2)	Kidney W (D_6)	Kidney W (D_{15})
Control	$1.87 \pm 0.18^{\text{ab}}$	$3.77 \pm 0.18^{\text{ab}}$	$7.13 \pm 0.87^{\text{a}}$	$0.015 \pm 0.001^{\text{ab}}$	$0.029 \pm 0.002^{\text{ab}}$	$0.042 \pm 0.002^{\text{ab}}$
CeO_2 (10 mg/kg bw)	$1.86 \pm 0.24^{\text{ab}}$	$3.94 \pm 0.34^{\text{a}}$	$7.54 \pm 0.8^{\text{8a}}$	$0.016 \pm 0.002^{\text{a}}$	$0.030 \pm 0.003^{\text{a}}$	$0.044 \pm 0.002^{\text{a}}$
CeO_2 (25 mg/kg bw)	$1.96 \pm 0.11^{\text{b}}$	$3.59 \pm 0.2^{\text{ab}}$	$6.87 \pm 0.38^{\text{a}}$	$0.013 \pm 0.002^{\text{ab}}$	$0.027 \pm 0.003^{\text{ab}}$	$0.040 \pm 0.004^{\text{ab}}$
CeO_2 (80 mg/kg bw)	$1.76 \pm 0.12^{\text{ab}}$	$3.64 \pm 0.27^{\text{ab}}$	$6.82 \pm 0.31^{\text{a}}$	$0.013 \pm 0.003^{\text{ab}}$	$0.026 \pm 0.002^{\text{ab}}$	$0.038 \pm 0.003^{\text{b}}$
CeO_2 (250 mg/kg bw)	$1.68 \pm 0.09^{\text{b}}$	$3.45 \pm 0.2^{\text{b}}$	$6.68 \pm 0.47^{\text{a}}$	$0.011 \pm 0.001^{\text{b}}$	$0.025 \pm 0.001^{\text{b}}$	$0.037 \pm 0.002^{\text{b}}$

bw (D_2): 2-day-old newborn body weight; bw (D_6): 6-day-old newborn body weight; bw (D_{15}): 15-day-old newborn body weight. Kidney W (D_2): 2-day-old newborn kidney weight; Kidney W (D_6): 6-day-old newborn kidney; Kidney W (D_{15}): 15-day-old newborn kidney. Values are means \pm SD. The means with different letter codes are significantly different from each other (ANOVA, Tukey's test, $P < 0.05$).

TABLE 2: Comparison of total kidney volume, cortex, and medulla in the study groups.

Group	Kidney V (mm ³)	Cortex V (mm ³)	Medulla (mm ³)
Control	106 ± 8.21 ^{ab}	86.4 ± 7.43 ^{ab}	19.6 ± 1.14 ^{ab}
CeO ₂ (10 mg/kg bw)	111.17 ± 10.14 ^a	91.16 ± 8.84 ^a	20 ± 1.78 ^a
CeO ₂ (25 mg/kg bw)	102.5 ± 2.51 ^{abc}	83.83 ± 2.13 ^{abc}	19 ± 1.09 ^{ab}
CeO ₂ (80 mg/kg bw)	99.17 ± 2.22 ^{bc}	80.50 ± 2.16 ^{bc}	18.66 ± 0.81 ^{ab}
CeO ₂ (250 mg/kg bw)	93.67 ± 3.44 ^c	75.83 ± 3.6 ^c	17.83 ± 0.75 ^b

Values are means ± SD. The means with different letter codes are significantly different from each other (ANOVA, Tukey's test, and $P < 0.05$).

TABLE 3: Comparison of interstitial tissue, glomerulus, and Bowman's capsule and space volumes in the study groups.

Group	InT (mm ³)	Renal corpuscle (mm ³)	Glomerulus (mm ³)	Bowman's capsule (mm ³)	Bowman's space (mm ³)
Control	6.25 ± 0.42 ^a	4.12 ± 0.35 ^a	2.49 ± 0.46 ^a	0.65 ± 0.12 ^{ab}	0.97 ± 0.04 ^a
CeO ₂ (10 mg/kg bw)	6.31 ± 1.08 ^a	4.04 ± 0.5 ^a	2.49 ± 0.56 ^a	0.51 ± 0.11 ^a	1.03 ± 0.12 ^a
CeO ₂ (25 mg/kg bw)	6.23 ± 1.11 ^a	4.13 ± 0.36 ^a	2.62 ± 0.38 ^{ab}	0.60 ± 0.05 ^a	0.89 ± 0.11 ^{ab}
CeO ₂ (80 mg/kg bw)	7.29 ± 0.82 ^{ab}	4.33 ± 0.56 ^{ab}	2.64 ± 0.58 ^{ab}	0.81 ± 0.8 ^{bc}	0.87 ± 0.10 ^{ab}
CeO ₂ (250 mg/kg bw)	8.03 ± 0.40 ^b	5.06 ± 0.49 ^b	3.47 ± 0.47 ^b	0.84 ± 0.08 ^c	0.74 ± 0.07 ^b

Values are means ± SD. The means with different letter codes are significantly different from each other (ANOVA, Tukey's test, $P < 0.05$).

TABLE 4: Comparison of the volumes of the renal structures in the study groups.

Group	PT (mm ³)	PT (E) (mm ³)	PT (L) (mm ³)	DT (mm ³)	DT (E) (mm ³)	DT (L) (mm ³)
Control	64 ± 5.33 ^{ab}	48 ± 4 ^{ab}	16 ± 1.33 ^a	17.2 ± 0.83 ^{ab}	11.62 ± 0.91 ^{ab}	5.57 ± 0.38 ^b
CeO ₂ (10 mg/kg bw)	68.16 ± 7.13 ^a	51.12 ± 5.35 ^a	17.04 ± 1.78 ^a	19 ± 2.19 ^a	12.39 ± 1.12 ^a	6.61 ± 1.12 ^a
CeO ₂ (25 mg/kg bw)	62.16 ± 1.94 ^{abc}	46 ± 45 ± 1.39 ^{abc}	15.54 ± 0.48 ^{ab}	17.33 ± 0.51 ^{ab}	11.7 ± 0.32 ^{ab}	5.63 ± 0.36 ^{ab}
CeO ₂ (80 mg/kg bw)	59.16 ± 1.32 ^{bc}	44.37 ± 0.99 ^{bc}	15.12 ± 0.73 ^{ab}	16.5 ± 0.54 ^b	11.19 ± 0.51 ^{ab}	5.31 ± 0.26 ^b
CeO ₂ (250 mg/kg bw)	56.08 ± 3.47 ^c	42.08 ± 2.59 ^c	14 ± 0.88 ^b	15.75 ± 0.75 ^b	10.53 ± 0.55 ^b	5.21 ± 0.24 ^b

PT: proximal convoluted tubule; DT: distal convoluted tubule; lumen: L; epithelium: E. Values are means ± SD. The means with different letter codes are significantly different from each other (ANOVA, Tukey's test, $P < 0.05$).

TABLE 5: Lengths of the proximal tubules (PT) and distal tubules (DT) in the study groups.

Group	PT (m)	DT (m)
Control	37.81 ± 1.59 ^a	22.46 ± 4.86 ^a
CeO ₂ (10 mg/kg bw)	38.69 ± 1.22 ^a	25.33 ± 1.3 ^a
CeO ₂ (25 mg/kg bw)	37.47 ± 1.19 ^a	25.26 ± 1.12 ^a
CeO ₂ (80 mg/kg bw)	35.53 ± 3.65 ^a	22.70 ± 3.9 ^a
CeO ₂ (250 mg/kg bw)	35.04 ± 3.81 ^a	19.92 ± 5.21 ^a

Values are means ± SD. The means with different letter codes are significantly different from each other (ANOVA, Tukey's test, $P < 0.05$).

mice to CeO₂, according to the administered dose, caused changes in the neonatal kidney tissue.

Determining the average tissue and body weights is an important indicator for assessing the toxic effects of a substance on the body. In this study, body and kidney weight changes in offspring were measured at 2, 6, and 15 dpp. The results indicated that there were no significant differences in body and kidney weights between the experimental and control groups (Table 1).

Previous findings have indicated that CeO₂ passes through the placenta [34]. In mice, the development of the

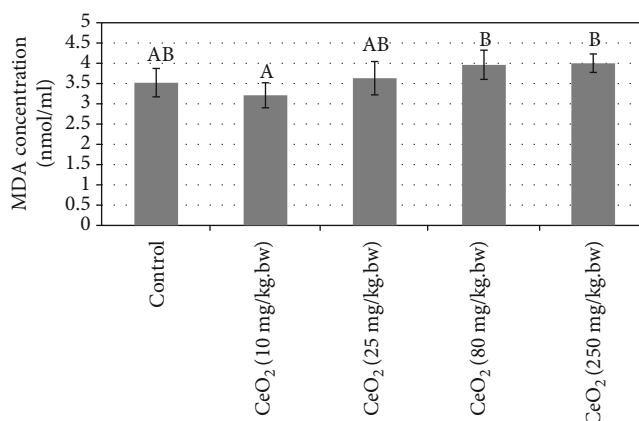


FIGURE 2: Comparison of the mean levels of serum malondialdehyde (MDA; nmol/ml) in the different groups of 15-day-old neonatal mice. Values are means ± SD. The means with different letter codes are significantly different from each other (ANOVA, Tukey's test, $P < 0.05$).

metanephros is considered to begin at E10.5–11 and ends at 7–10 days after birth [49, 50]. The kidney, like all other major organs of the body, is susceptible to exposure to a

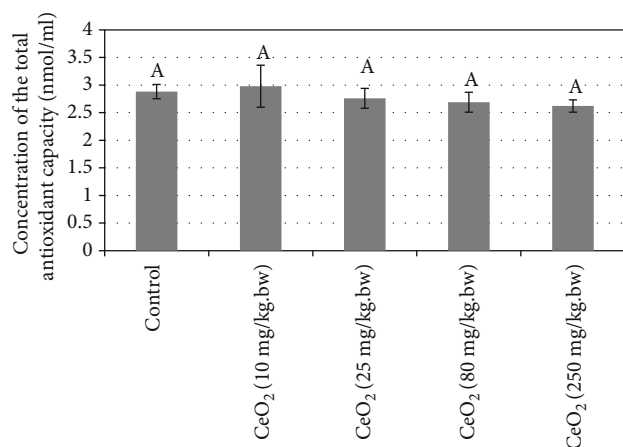


FIGURE 3: Comparison of the mean levels of serum total antioxidant capacity (TAC; nmol/ml) in the different groups of 15-day-old neonatal mice. Values are means \pm SD. The means with different letter codes are significantly different from each other (ANOVA, Tukey's test, $P < 0.05$).

wide range of chemicals during developmental periods. Regulated differentiation and proliferation of mesenchymal cells and urinary epidermal primordial cells cause nephrogenesis in the embryonic period [50]. Kidney development in mice is completed two weeks after birth [51]. Accordingly, we decided to investigate changes in kidney tissue 15 days after birth.

Studies have also shown that CeO₂ can accumulate and cause inflammation in tissues such as the lungs, liver, and kidneys [23]. Cerium is capable of switching between the Ce³⁺ and Ce⁴⁺ states, which may aid the antioxidant property of CeO₂. On the other hand, another investigation has shown that CeO₂ causes ROS formation, inflammation, and DNA loss [19]. The result of one study indicated that CeO₂ increased ROS formation and, consequently, induced oxidative damage in mitochondria [22].

Increased CeO₂-induced ROS levels may be the cause of observed cellular damage and apoptosis. ROS production and oxidative stress might be due to the catalytic properties of CeO₂, impaired mitochondrial function, or a combination of both mechanisms [24, 42].

ROS is capable of reacting with proteins, lipids, and nucleic acids, leading to lipid oxidation in biological membranes and the effects of enzymatic processes such as ion pump activity and DNA damage, thereby inhibiting transcription, repair, and apoptosis [52, 53]. As a result, lipid peroxidation destroys unsaturated fatty acids in the membranes [54]. This can be one reason for the decrease in cell volume and, ultimately, the decrease in kidney volume in the group that received 250 mg/kg bw CeO₂ compared to that in the control group (Table 2).

Increased glomeruli volume, as representative of the renal and functional units of the kidney, can compensate for lost glomeruli function, adapt to new conditions, and remove toxins from the body [55, 56]. Glomeruli undergo hyperfiltration to control the conditions and maintain filtration, resulting in an increase in glomerular volume [57].

Oxidative stress contributes to kidney damage through several mechanisms. This primarily occurs through increased expression of the vascular endothelial growth factor (VEGF) gene in podocytes, endothelial cells, and renal mesangial cells that increase glomerular permeability and protein excretion through urine [58]. Growth factors increase the expression of collagen types I, III, IV, V, and VI, and the laminin and fibronectin proteins, which increases the extracellular matrix and thickening of the glomerular basement membrane [58, 59].

It has been shown that oxygen free radicals play a major role in inflammation in kidney interstitial tissue [60, 61]. Therefore, an increase in interstitial tissue volume in the group that received CeO₂ at a dose of 250 mg/kg bw compared to that in the control group (Table 3) might indicate inflammation caused by CeO₂.

In the present study, the lumen space of the PT in the group that received 250 mg/kg bw CeO₂ was decreased compared to that in the control group (Table 4). This could be due to the destructive dose-dependent effect of CeO₂ on tubules and the presence of necrosis, an apoptotic margin of the PT epithelial cells, and swelling of the epithelial cells of the wall of the tubule. It can be concluded that the swelling of PT wall cells reduces the lumen spaces of tubules [23].

The data of this study showed no statistically significant difference between serum MDA and FRAP levels in the treatment groups compared with the control group (Figure 3). Oxidative stress is due to reduced body resistance to oxidants and lower antioxidant levels in the blood. [22, 62]. According to other studies, antioxidant capacity *in vivo* depends on many factors such as environmental conditions (diet, etc.) [63, 64].

Studies of CeO₂ in different animals showed that the level of CeO₂ toxicity depended on the duration of exposure, tissue environment, and type of cell [19, 65].

Previous research has suggested that the effect and toxicity of CeO₂ are closely related to the types of tissues and cells, as well as the type of animal and the duration of exposure [66–68].

Studies of the dose-dependent relationship of CeO₂ effects on living organisms are complex. In one study, ICR mice were treated by oral gavage with one of three doses (10, 20, or 40 mg/kg bw/day) for six weeks. The accumulation of Ce particles in the nuclei of liver cells and mitochondria had a direct relationship to the increased dose [22]. The inflammatory effects of CeO₂ nanoparticles were studied at different doses (2000, 3000, and 5000 mg/kg bw) administered daily for 14 days in CD-1 mice. The results did not show any relationship between the concentration used and toxic effects [23].

In the present study, animals exposed to the highest doses of CeO₂ (250 mg/kg bw) showed significantly different histological parameters from their control counterparts. Animals exposed to the lowest doses (10, 25, and 80 mg/kg bw) did not show significant differences in histological parameters compared to the control group. Studies on the effect of CeO₂ on living organisms *in vivo* and *in vitro* confirm our findings. Previous studies have shown that low-dose CeO₂ can be used to treat cancer and eye diseases and is a powerful

antioxidant [69, 70]. Therefore, according to review data, low-dose CeO₂ may have beneficial and possibly protective effects.

According to histological data, the high dose of CeO₂ in this experiment (250 mg/kg bw) was not tolerable for the animals. This dose could lead to toxic effects and oxidative stress, as well as disruption in the development of kidney tissues in mice. The present study results indicated that the dose of CeO₂ could determine the presence of positive and negative effects from its various applications. However, additional research should be conducted to confirm these findings.

5. Conclusion

We observed significant increases in the mean total volume of the kidney, cortex, renal corpuscle, glomerulus, and membrane of Bowman's capsule and a significant decrease in the mean total volume of Bowman's space in the group that received 250 mg/kg bw of CeO₂ compared to that in the control group. Our data showed no statistically significant differences between serum MDA and TAC levels in the treatment and control groups. According to our experiment, the efficacy of CeO₂ on kidney development in neonatal mice was dose dependent. More studies should be conducted to investigate CeO₂-induced renal damage in offspring exposed to CeO₂ in utero.

Abbreviation

Bw:	Body weight
Ce:	Cerium
CeO ₂ :	Cerium (IV) oxide
CTGF:	Connective tissue growth factor
DD:	Double distilled
DPP:	Days postpartum
D2:	2-day-old infant
D6:	6-day-old infant
DT:	Distal tubules
°C:	Degree centigrade
Fig:	Figure
g:	Gram
GD:	Gestational day
G:	Glomerulus
HCL:	Hydrochloric acid
H:	Hour
i.p.:	Intraperitoneal
μL:	Microliter
MDA:	Malondialdehyde concentration
μm:	Micrometer
min:	Minute
mm ³ :	Cubic millimeters
mg/kg bw:	Milligrams per kilogram of body weight
ml:	Milliliter
Nm:	Nanometer
Nmol:	Nanomolar
PBL:	Peripheral blood leukocytes
PT:	Proximal tubules
PDGF:	Platelet-derived growth factor
KCL:	Potassium chloride

LDH:	Lactate dehydrogenase
REEs:	Rare earth elements
TAC:	Total antioxidant capacity
TCA:	Trichloroacetic acid
TPTZ:	2,4,6-Tripyridyl-s-triazine
TBA:	Thiobarbituric acid
TGF-1:	Transforming growth factor-1
VEGF:	Vascular endothelial growth factor
V:	Volume
W:	Weight.

Data Availability

No data were used to support this study.

Ethical Approval

All stages of this experiment are in accordance with the ethical standards of the Ethics Committee of Kermanshah University of Medical Sciences, Kermanshah, Iran (Approval ID: IR.KUMS.REC.1398.874).

Conflicts of Interest

There is no conflict of interest related to this research.

Acknowledgments

This study was supported by the Razi Herbal Medicines Research Center, Lorestan University of Medical Sciences and Kermanshah University of Medical Sciences, Kermanshah, Iran.

References

- [1] S. Scirè and L. Palmisano, *Cerium and cerium oxide: a brief introduction, in Cerium Oxide (CeO₂): Synthesis, Properties and Applications*, Elsevier, 2020.
- [2] M. Gehlhaus, M. Osier, F. Lladós et al., "Toxicological review of cerium oxide and cerium compounds (CAS No. 1306-38-3) in support of summary information on the integrated risk information system (IRIS)," US Environmental Protection Agency, 2009, <http://www.epa.gov/iris/toxreviews/1018tr.pdf>.
- [3] F. R. Cassee, E. C. van Balen, C. Singh et al., "Exposure, health and ecological effects review of engineered nanoscale cerium and cerium oxide associated with its use as a fuel additive," *Critical Reviews in Toxicology*, vol. 41, no. 3, pp. 213–229, 2011.
- [4] Z. Zhang, P. Gao, Y. Qiu, G. Liu, Y. Feng, and M. Wiesner, "Transport of cerium oxide nanoparticles in saturated silica media: influences of operational parameters and aqueous chemical conditions," *Scientific Reports*, vol. 6, no. 1, article 34135, 2016.
- [5] S. Rajeshkumar and P. Naik, "Synthesis and biomedical applications of cerium oxide nanoparticles—a review," *Biotechnology Reports*, vol. 17, pp. 1–5, 2018.
- [6] F. E. Adzo, *Cerium levels in fine and coarse airborne particulate matter in El Paso, Texas—a geospatial and temporal Investigation*, The University of Texas at El Paso, 2018.









- [7] S. Kargozar, F. Bains, S. J. Hoseini et al., "Biomedical applications of nanoceria: new roles for an old player," *Nanomedicine*, vol. 13, no. 23, pp. 3051–3069, 2018.
- [8] J. Kailashiya and D. Dash, "Nanoceria and its biomedical relevance," *Annals of the National Academy of Medical Sciences (India)*, vol. 55, no. 1, pp. 014–017, 2019.
- [9] B. Nelson, M. Johnson, M. Walker, K. Riley, and C. Sims, "Antioxidant cerium oxide nanoparticles in biology and medicine," *Antioxidants*, vol. 5, no. 2, p. 15, 2016.
- [10] E.-J. Park, W. S. Cho, J. Jeong et al., "Induction of inflammatory responses in mice treated with cerium oxide nanoparticles by intratracheal instillation," *Journal of Health Science*, vol. 56, no. 4, pp. 387–396, 2010.
- [11] C. Li, X. Shi, Q. Shen, C. Guo, Z. Hou, and J. Zhang, "Hot topics and challenges of regenerative nanoceria in application of antioxidant therapy," *Journal of Nanomaterials*, vol. 2018, Article ID 4857461, 12 pages, 2018.
- [12] A. Dhall and W. Self, "Cerium oxide nanoparticles: a brief review of their synthesis methods and biomedical applications," *Antioxidants*, vol. 7, no. 8, p. 97, 2018.
- [13] E. G. Heckert, A. S. Karakoti, S. Seal, and W. T. Self, "The role of cerium redox state in the SOD mimetic activity of nanoceria," *Biomaterials*, vol. 29, no. 18, pp. 2705–2709, 2008.
- [14] V. Baldim, F. Bedioui, N. Mignet, I. Margail, and J. F. Berret, "The enzyme-like catalytic activity of cerium oxide nanoparticles and its dependency on Ce 3+ surface area concentration," *Nanoscale*, vol. 10, no. 15, pp. 6971–6980, 2018.
- [15] A. Y. Estevez, B. Stadler, and J. S. Erlichman, "In-vitro analysis of catalase-, oxidase-and SOD-mimetic activity of commercially available and custom-synthesized cerium oxide nanoparticles and assessment of neuroprotective effects in a hippocampal brain slice model of ischemia," *The FASEB Journal*, vol. 31, article 693.5, 1_supplement, 2017.
- [16] S. M. Hirst, A. Karakoti, S. Singh et al., "Bio-distribution and in vivo antioxidant effects of cerium oxide nanoparticles in mice," *Environmental Toxicology*, vol. 28, no. 2, pp. 107–118, 2013.
- [17] E. Birben, U. M. Sahiner, C. Sackesen, S. Erzurum, and O. Kalayci, "Oxidative stress and antioxidant defense," *World Allergy Organization Journal*, vol. 5, no. 1, pp. 9–19, 2012.
- [18] A. Ramesh, N. N. Ratla, R. Indukuri, K. Venkatesh, and S. T. Rao, "Acute and sub-acute oral toxicity assessment of the cerium oxide nanoparticles in Wistar rats," *International Journal of Phytopharmacology*, vol. 5, no. 1, pp. 46–50, 2014.
- [19] S. N. Rogers, *Toxicological effects of cerium oxide nanoparticle aggregates on Caenorhabditis elegans*, Marshall University, 2013.
- [20] D. Li, M. Morishita, J. G. Wagner et al., "In vivo biodistribution and physiologically based pharmacokinetic modeling of inhaled fresh and aged cerium oxide nanoparticles in rats," *Particle and Fibre Toxicology*, vol. 13, no. 1, article 45, 2015.
- [21] C. Portioli, D. Benati, Y. Pii et al., "Short-term biodistribution of cerium oxide nanoparticles in mice: focus on brain parenchyma," *Nanoscience and Nanotechnology Letters*, vol. 5, no. 11, pp. 1174–1181, 2013.
- [22] P. Huang, J. Li, S. Zhang et al., "Effects of lanthanum, cerium, and neodymium on the nuclei and mitochondria of hepatocytes: accumulation and oxidative damage," *Environmental Toxicology and Pharmacology*, vol. 31, no. 1, pp. 25–32, 2011.
- [23] A. Poma, A. M. Ragnelli, J. de Lapuente et al., "In vivo inflammatory effects of ceria nanoparticles on CD-1 mouse: evaluation by hematological, histological, and TEM analysis," *Journal of Immunology Research*, vol. 2014, Article ID 361419, 14 pages, 2014.
- [24] M. Kumari, S. I. Kumari, S. S. K. Kamal, and P. Grover, "Genotoxicity assessment of cerium oxide nanoparticles in female Wistar rats after acute oral exposure," *Mutation Research/Genetic Toxicology and Environmental Mutagenesis*, vol. 775–776, pp. 7–19, 2014.
- [25] J. Y. Ma, R. R. Mercer, M. Barger et al., "Induction of pulmonary fibrosis by cerium oxide nanoparticles," *Toxicology and Applied Pharmacology*, vol. 262, no. 3, pp. 255–264, 2012.
- [26] S. Das, S. Singh, J. M. Dowding et al., "The induction of angiogenesis by cerium oxide nanoparticles through the modulation of oxygen in intracellular environments," *Biomaterials*, vol. 33, no. 31, pp. 7746–7755, 2012.
- [27] F. Corsi, F. Caputo, E. Traversa, and L. Ghibelli, "Not only redox: the multifaceted activity of cerium oxide nanoparticles in cancer prevention and therapy," *Frontiers in Oncology*, vol. 8, 2018.
- [28] J. Das, Y. J. Choi, J. W. Han, A. M. M. T. Reza, and J. H. Kim, "Nanoceria-mediated delivery of doxorubicin enhances the anti-tumour efficiency in ovarian cancer cells via apoptosis," *Scientific Reports*, vol. 7, no. 1, p. 9513, 2017.
- [29] A. L. Popov, N. R. Popova, I. I. Selezneva, A. Y. Akkizov, and V. K. Ivanov, "Cerium oxide nanoparticles stimulate proliferation of primary mouse embryonic fibroblasts in vitro," *Materials Science and Engineering: C*, vol. 68, pp. 406–413, 2016.
- [30] O. A. Adebayo, O. Akinloye, and O. A. Adaramoye, "Cerium oxide nanoparticles attenuate oxidative stress and inflammation in the liver of diethylnitrosamine-treated mice," *Biological Trace Element Research*, vol. 193, no. 1, pp. 214–225, 2020.
- [31] Z. Vafaei-Pour, M. Shokrzadeh, M. Jahani, and F. Shaki, "Embryo-protective effects of cerium oxide nanoparticles against gestational diabetes in mice," *Iranian Journal of Pharmaceutical Research: IJPR*, vol. 17, no. 3, pp. 964–975, 2018.
- [32] M. Nyoka, Y. E. Choonara, P. Kumar, P. P. D. Kondiah, and V. Pillay, "Synthesis of cerium oxide nanoparticles using various methods: implications for biomedical applications," *Nanomaterials*, vol. 10, no. 2, p. 242, 2020.
- [33] A. S. Chernov, D. A. Reshetnikov, A. L. Popov, N. R. Popova, I. V. Savintseva, and V. K. Ivanov, "Cerium oxide nanoparticles are nontoxic for mouse embryogenesis *In Vitro* and *In Vivo*," *Nano Hybrids and Composites*, vol. 13, pp. 248–254, 2017.
- [34] M. Kawagoe, K. Ishikawa, S. C. Wang et al., "Acute effects on the lung and the liver of oral administration of cerium chloride on adult, neonatal and fetal mice," *Journal of Trace Elements in Medicine and Biology*, vol. 22, no. 1, pp. 59–65, 2008.
- [35] A. Nemati, A. Farhadi, C. Jalili, and M. Gholami, "The effect of cerium oxide during pregnancy on the development of the testicular tissue of newborn NMRI mice," *Biological Trace Element Research*, vol. 195, no. 1, pp. 196–204, 2020.
- [36] A. J. Davidson, "Mouse kidney development," *African Scientist*, vol. 16, no. 3, pp. 171–204, 2019.
- [37] K. A. Walker and J. F. Bertram, "Kidney development: core curriculum 2011," *American Journal of Kidney Diseases*, vol. 57, no. 6, pp. 948–958, 2011.
- [38] S. Rosenblum, A. Pal, and K. Reidy, "Renal development in the fetus and premature infant," *Seminars in Fetal and Neonatal Medicine*, vol. 22, no. 2, pp. 58–66, 2017.

- [39] C. H. Baker, "Harnessing cerium oxide nanoparticles to protect normal tissue from radiation damage," *Translational Cancer Research*, vol. 2, no. 4, pp. 343–358, 2013.
- [40] K. M. Dunnick, R. Pillai, K. L. Pisane, A. B. Stefaniak, E. M. Sabolsky, and S. S. Leonard, "The effect of cerium oxide nanoparticle valence state on reactive oxygen species and toxicity," *Biological Trace Element Research*, vol. 166, no. 1, pp. 96–107, 2015.
- [41] G. Cepriá, W. R. Córdova, O. Céspedes et al., "Physical and chemical characterization of cerium (IV) oxide nanoparticles," *Analytical and Bioanalytical Chemistry*, vol. 408, no. 24, pp. 6589–6598, 2016.
- [42] R. A. Yokel, T. C. Au, R. MacPhail et al., "Distribution, elimination, and biopersistence to 90 days of a systemically introduced 30 nm ceria-engineered nanomaterial in rats," *Toxicological Sciences*, vol. 127, no. 1, pp. 256–268, 2012.
- [43] S. Karbalay-Doust, A. Noorafshan, and S.-M. Pourshahid, "Taxol and taurine protect the renal tissue of rats after unilateral ureteral obstruction: a stereological survey," *Korean Journal of Urology*, vol. 53, no. 5, pp. 360–367, 2012.
- [44] V. Howard and M. Reed, *Unbiased stereology: three-dimensional measurement in microscopy*, Garland Science, 2004.
- [45] J. A. Buege and S. D. Aust, "[30] Microsomal lipid peroxidation," in *Methods in enzymology*, pp. 302–310, Elsevier, 1978.
- [46] H. Esterbauer and K. H. Cheeseman, "[42] Determination of aldehydic lipid peroxidation products: malonaldehyde and 4-hydroxynonenal," in *Methods in enzymology*, pp. 407–421, Elsevier, 1990.
- [47] I. F. F. Benzie and J. J. Strain, "The Ferric Reducing Ability of Plasma (FRAP) as a Measure of "Antioxidant Power": The FRAP Assay," *Analytical Biochemistry*, vol. 239, no. 1, pp. 70–76, 1996.
- [48] I. Gosens, L. E. A. M. Mathijssen, B. G. H. Bokkers, H. Muijsers, and F. R. Cassee, "Comparative hazard identification of nano- and micro-sized cerium oxide particles based on 28-day inhalation studies in rats," *Nanotoxicology*, vol. 8, no. 6, pp. 643–653, 2013.
- [49] M. Krause, A. Rak-Raszewska, I. Pietilä, S. Quaggin, and S. Vainio, "Signaling during kidney development," *Cell*, vol. 4, no. 2, pp. 112–132, 2015.
- [50] P. Nuñez, T. Fernandez, M. García-Arévalo et al., "Effects of bisphenol A treatment during pregnancy on kidney development in mice: a stereological and histopathological study," *Journal of Developmental Origins of Health and Disease*, vol. 9, no. 2, pp. 208–214, 2018.
- [51] S. L. Clark Jr., "Cellular differentiation in the kidneys of newborn mice studied with the electron microscope," *The Journal of Cell Biology*, vol. 3, no. 3, pp. 349–362, 1957.
- [52] B. Seyedalipour, N. Barimani, A. A. D. Jooybari, S. M. Hosseini, and M. Oshrieh, "Histopathological evaluation of kidney and heart tissues after exposure to copper oxide nanoparticles in *Mus musculus*," *Journal of Babol University of Medical Sciences*, vol. 17, no. 7, pp. 44–50, 2015.
- [53] A. Hasanvand, A. Abbaszadeh, S. Darabi, A. Nazari, M. Gholami, and A. Kharazmkia, "Evaluation of selenium on kidney function following ischemic injury in rats; protective effects and antioxidant activity," *Journal of Renal Injury Prevention*, vol. 6, no. 2, pp. 93–98, 2017.
- [54] S. V. Shah, R. Baliga, M. Rajapurkar, and V. A. Fonseca, "Oxidants in chronic kidney disease," *Journal of the American Society of Nephrology*, vol. 18, no. 1, pp. 16–28, 2006.
- [55] I. J. Murawski, R. W. Maina, and I. R. Gupta, "The relationship between nephron number, kidney size and body weight in two inbred mouse strains," *Organogenesis*, vol. 6, no. 3, pp. 189–194, 2014.
- [56] L. Xie, G. Koukos, K. Barck et al., "Micro-CT imaging and structural analysis of glomeruli in a model of Adriamycin-induced nephropathy," *American Journal of Physiology-Renal Physiology*, vol. 316, no. 1, pp. F76–F89, 2019.
- [57] G. Pazvant, B. Sahin, K. O. Kahvecioglu, H. Gunes, N. Gezer, and D. Bacinoglu, "The volume fraction method for the evaluation of kidney: a stereological study," *Ankara Üniversitesi Veteriner Fakültesi Dergisi*, vol. 50, no. 1, pp. 233–239, 2003.
- [58] S. Karam Sichani, N. Naghsh, and N. Razm, "Effects of alcoholic extract of *Peganumharmala* L. on malondialdehyde concentration and catalase and glutathione peroxidase activity in mice treated with nanosilver particles," *Journal of Mazandaran University of Medical Sciences*, vol. 22, no. 95, pp. 10–17, 2012.
- [59] S. Rana, *Protective effect of ascorbic acid against oxidative stress induced by inorganic arsenic in liver and kidney of rat*, 2007.
- [60] B. B. Ratliff, W. Abdulmahdi, R. Pawar, and M. S. Wolin, "Oxidant mechanisms in renal injury and disease," *Antioxidants & Redox Signaling*, vol. 25, no. 3, pp. 119–146, 2016.
- [61] L. V. Stebounova, A. Adamcakova-Dodd, J. Kim et al., "Nanosilver induces minimal lung toxicity or inflammation in a subacute murine inhalation model," *Particle and Fibre Toxicology*, vol. 8, no. 1, p. 5, 2011.
- [62] A. Ghiselli, M. Serafini, F. Natella, and C. Scaccini, "Total antioxidant capacity as a tool to assess redox status: critical view and experimental data," *Free Radical Biology and Medicine*, vol. 29, no. 11, pp. 1106–1114, 2000.
- [63] O. Erel, "A novel automated method to measure total antioxidant response against potent free radical reactions," *Clinical Biochemistry*, vol. 37, no. 2, pp. 112–119, 2004.
- [64] A. Floegel, D. O. Kim, S. J. Chung, S. I. Koo, and O. K. Chun, "Comparison of ABTS/DPPH assays to measure antioxidant capacity in popular antioxidant-rich US foods," *Journal of Food Composition and Analysis*, vol. 24, no. 7, pp. 1043–1048, 2011.
- [65] A. Ranjbar, H. Ghasemi, A. Abedian, and N. Kheiripour, "Cerium oxide nanoparticle modulates hepatic damage, inflammatory and oxidative stress biomarkers in a dose-dependent manner: an in vivo study of rat liver," *Nanomedicine Journal*, vol. 5, no. 4, pp. 245–250, 2018.
- [66] J. Chen, H. J. Xiao, T. Qi, D. L. Chen, H. M. Long, and S. H. Liu, "Rare earths exposure and male infertility: the injury mechanism study of rare earths on male mice and human sperm," *Environmental Science and Pollution Research*, vol. 22, no. 3, pp. 2076–2086, 2015.
- [67] M. A. E. Hegazy, H. M. Maklad, D. A. Abd Elmonsif et al., "The possible role of cerium oxide (CeO₂) nanoparticles in prevention of neurobehavioral and neurochemical changes in 6-hydroxydopamine-induced parkinsonian disease," *Alexandria Journal of Medicine*, vol. 53, no. 4, pp. 351–360, 2017.
- [68] O. A. Adua, I. W. Akinmuyisitana, and F. A. Gbore, "Growth performance and blood profile of female rabbits fed dietary cerium oxide," *Journal of Bio-Science*, vol. 21, pp. 69–75, 2015.

- [69] X. Cai, S. Seal, and J. McGinnis, "Non-toxic retention of nanoceria in murine eyes," *Molecular Vision*, vol. 22, pp. 1176–1187, 2016.
- [70] M. S. Wason and J. Zhao, "Cerium oxide nanoparticles: potential applications for cancer and other diseases," *American Journal of Translational Research*, vol. 5, no. 2, pp. 126–131, 2013.

Research Article

Oxidative Damage of Blood Platelets Correlates with the Degree of Psychophysical Disability in Secondary Progressive Multiple Sclerosis

Angela Dziedzic ¹, Agnieszka Morel ¹, Elzbieta Miller ², Michal Bijak ³,
Tomasz Sliwinski ⁴, Ewelina Synowiec ⁴, Michal Ceremuga ⁵,
and Joanna Saluk-Bijak ¹

¹Department of General Biochemistry, Faculty of Biology and Environmental Protection, University of Lodz, Pomorska 41/143, 90-236 Lodz, Poland

²Department of Neurological Rehabilitation, Medical University of Lodz, Milionowa 14, 93-113 Lodz, Poland

³Biohazard Prevention Centre, Faculty of Biology and Environmental Protection, University of Lodz, Pomorska 141/143, 90-236 Lodz, Poland

⁴Department of Molecular Genetics, Laboratory of Medical Genetics, Faculty of Biology and Environmental Protection, University of Lodz, Pomorska 141/143, Lodz, Poland

⁵Military Institute of Armament Technology, Prymasa Stefana Wyszyńskiego 7, 05-220 Zielonka, Poland

Correspondence should be addressed to Angela Dziedzic; angela.dziedzic@unilodz.eu

Received 22 April 2020; Revised 22 May 2020; Accepted 30 May 2020; Published 17 June 2020

Academic Editor: Francisco J. Romero

Copyright © 2020 Angela Dziedzic et al. This is an open access article distributed under the Creative Commons Attribution License, which permits unrestricted use, distribution, and reproduction in any medium, provided the original work is properly cited.

The results of past research studies show that platelets are one of the main sources of reactive oxygen species (ROS) and reactive nitrogen species (RNS) to be found in the course of many pathological states. The aim of this study was to determine the level of oxidative/nitrative stress biomarkers in blood platelets obtained from multiple sclerosis (MS) patients ($n = 110$) and to verify their correlation with the clinical parameters of the psychophysical disability of patients. The mitochondrial metabolism of platelets was assessed by measuring the intracellular production of ROS using the fluorescence method with DCFH-DA dye and by identification of changes in the mitochondrial membrane potential of platelets using the JC-1 dye. Moreover, we measured the mRNA expression for the gene encoding the cytochrome c oxidase subunit I (*MTCO-1*) and glyceraldehyde 3-phosphate dehydrogenase (*GAPDH*) in platelets and megakaryocytes using the RT-qPCR method, as well as the concentration of NADPH oxidase (NOX-1) by the ELISA method. Our results proved an increased level of oxidative/nitrative damage of proteins (carbonyl groups, 3-nitrotyrosine) ($p < 0.0001$) and decreased level of -SH in MS ($p < 0.0001$) and also a pronounced correlation between these biomarkers and parameters assessed by the Expanded Disability Status Scale and the Beck's Depression Inventory. The application of fluorescence methods showed mitochondrial membrane potential disruption ($p < 0.001$) and higher production of ROS in platelets from MS compared to control ($p < 0.0001$). Our research has also confirmed the impairment of red-ox metabolism in MS, which was achieved by increasing the relative mRNA expression in platelets for the genes studied (2-fold increase for the *MTCO-1* gene and 1.5-fold increase in *GAPDH* gene, $p < 0.05$), as well as the augmented concentration of NOX-1 compared to control ($p < 0.0001$). Our results indicate that the oxidative/nitrative damage of platelets is implicated in the pathophysiology of MS, which reflects the status of the disease.

1. Introduction

Oxidative stress plays an important role in regulating brain plasticity, and the intensive production of reactive oxygen

species (ROS) and reactive nitrogen species (RNS) significantly affect the disorder of neuronal neurotransmission, which is the main cause of physical and mental disability [1, 2]. Brain structures are prone to oxidative stress due to

their extensive oxygen metabolism [3]. Despite the existence of natural antioxidant mechanisms, the cells of the central nervous system (CNS), especially neurons, are poorly protected against the harmful effects of ROS/RNS [4]. ROS and RNS are extremely reactive molecules that damage various cellular structures in the brain (neurons, oligodendrocytes, astrocytes, and microglia) and lead to cell death [5].

Multiple sclerosis (MS) is a multifactorial disease that consists of several pathological processes occurring in the CNS and peripheral nervous system (PNS). MS is an inflammatory demyelinating disease of CNS, nonetheless, tightly related to the injury of blood vessels, mainly as a result of augmented permeability of the blood-brain barrier (BBB) [6, 7]. Autoimmune development, inflammation, and the permanent oxidative stress contribute to demyelination and in consequence to axonal and neuronal loss [8, 9].

The interactions of platelets with leukocytes and endothelial cells are considered to be the first essential step in the initiation of the pathogenesis of MS, leading to the massive infiltration of lymphocytes and further to the creation of demyelinating lesions in CNS [10]. The chronic activation of platelets in MS is proven [11–13], even though their role in this pathology still needs to be clarified. The latest clinical reports confirm an increased risk of cardiovascular disease in MS, especially ischemic stroke and myocardial infarction, directly associated with abnormal platelet function redirected to their prothrombotic activity [14–20]. Chronic inflammation and massive ROS/RNS production may be the main cause of excessive platelet activation in MS [21]. Platelet functioning strictly depends on the activity of prooxidative processes and their current red-ox state. Platelet aggregation could be induced by H_2O_2 (a source of hydroxyl radicals), which suggests that ROS may act as “second messengers” during the initial phase of the platelet activation process [22]. Blood platelets have an inherent ability to produce ROS by various pathways, including as a by-product of the respiratory pathway [23]. Despite the lack of a cell nucleus, platelets contain basic cellular organelles, including numerous mitochondria (from 5 to 8), and maintain an active metabolism [24]. These tiny size cells arrive first at sites of vascular injury and can be seen as substantial players in neurodegenerative diseases. The aim of the present study was to assess the oxidative/nitrative modifications of blood platelet proteins in the course of SP MS and correlation of their levels with the degree of psychophysical disability of patients.

2. Materials and Methods

2.1. Demographic and Clinical Characteristics. The 110 patients with SP MS and 110 healthy volunteers were included in the study. All patients with SP MS were diagnosed according to the revised McDonald criteria [25]. Patients were observed for one year prior to the commencement of the study, and the clinical parameters of patients with SP MS are included: mean age 48.2 ± 15.2 years, mean disease duration 14.3 ± 8.3 years, EDSS 5.5 ± 1.8 , and BDI 9.6 ± 4.6 . The healthy volunteers did not take any medica-

tions and had never been diagnosed with MS or other neurodegenerative disease and any chronic inflammation. The mean platelet counts in SP MS patients and controls were within the reference range ($150 - 450 \times 10^3/\mu\text{l}$). The control group and SP MS patients were matched by the number, age, and sex in Table 1.

The EDSS scale is a method for quantifying the degree of disability in the course of MS. The scale range of EDSS is from 0 (no disability) to 10 (death due to MS) [26, 27]. BDI is a psychometric test for measuring the severity of depression. The presence of depression is observed when the BDI score is above 13, and major depression when the score is ≥ 30 [28].

Blood samples from SP MS patients were delivered from Neurological Rehabilitation Division III General Hospital in Lodz, Poland, and those from healthy volunteers were collected at Laboratory Diagnostics Center in Lodz, Poland. The protocol and all procedures were conducted according to the Helsinki declaration and were approved by the Ethics Committee of the Faculty of Biology and Environmental Protection of University of Lodz, Poland No.5/KBBN-UŁ/II/2013.

2.2. Isolation of Blood Platelets. The human blood samples, which were taken from a peripheral vein between 8 and 9 a.m., were kept in CPDA-1 (citrate phosphate dextrose adenine-1). Blood platelets were isolated from freshly collected blood by using a modified method of BSA-Sepharose 2B gel-filtration described by Walkowiak et al. [29], and resuspended in modified Tyrode's (Ca^{+2}/Mg^{+2}) free buffer (127 mM NaCl, 2.7 mM KCl, 0.5 mM NaH_2PO_4 , 12 mM $NaHCO_3$, 5 mM HEPES, 5.6 mM glucose, pH 7.4). The number of platelets was determined based on the photometric method according to Walkowiak et al. [30] and were routinely diluted to obtain 2×10^8 platelets/ml. Platelet suspensions for the determination of 3-NT and carbonyl group were diluted in lysis buffer 1:1 (2% Triton X-100, 100 mM EDTA, 0.1 M Tris-HCl, pH 7.4) and stored in -80°C until analysis.

2.3. Measurement of the Level of Carbonyl Groups by the ELISA Method. The detection of carbonyl groups, estimated as adducts of 2,4-dinitrophenylhydrazine (DNPH), was carried out according to the ELISA method described by Buss et al. [31] and modified by Almadari et al. [32]. The microplates were incubated with a blocking buffer, overnight at 4°C , to block any nonspecific binding. Following three washes with $300 \mu\text{l}$ PBS, the frozen blood platelet proteins (-80°C) were reacted with substrate DNPH. After incubation for 45 minutes at room temperature in the dark, all wells were washed 5 times with $300 \mu\text{l}$ PBS: ethanol (1:1, v/v) and with $300 \mu\text{l}$ PBS. The carbonyl groups were detected by the first anti-DNP antibodies and then by the second antibody conjugated with horseradish peroxidase. The level of carbonyl groups was determined spectrophotometrically (at $\lambda = 316 \text{ nm}$) according to the Levine et al. [33]. To confirm the linearity of the ELISA method, the standard curve was prepared using oxidized albumin, which expressed nmol carbonyl groups/mg of albumin.

TABLE 1: The characteristics of control and study group (SP MS).

	Control group (n = 110)	SP MS (n = 110)
Mean age (years)	48.7 ± 12.21	48.2 ± 15.2
Gender:		
Male	43	43
Female	67	67
BMI (kg/m ²)	21.9 ± 4.85	21.1 ± 9.7
EDSS	NA	5.5 ± 1.8
BDI	NA	9.6 ± 4.6
Mean disease duration (years)	NA	14.3 ± 8.3

Abbreviations: EDSS: Expanded Disability Status Scale; BDI: Beck's Depression Inventory; SP MS: secondary progressive multiple sclerosis; NA: not applicable; BMI: body mass index.

2.4. Determination of 3-Nitrotyrosine Level by the Competitive ELISA Method. The detection of 3-NT in the frozen human blood platelet proteins (-80°C) was performed according to the Khan et al. [34] using the competitive ELISA test. The concentration of 3-NT was assessed based on the standard curve, drawn up of the 3-NT containing fibrinogen (3-NT-Fg). The human fibrinogen was treated with the peroxynitrite at the final concentration of 1 mM to obtain the 3-NT-Fg. The amount of 3-NT-Fg was spectrophotometrically determined at the $\lambda = 430$ nm ($\epsilon = 4,400$ M⁻¹ cm⁻¹) with a plate reader. After the spectrophotometric measurement, the nitro-fibrinogen was used to prepare the standard curve, ranging from 10 to 1000 nM/l of 3-NT-Fg equivalent.

2.5. The Sulfhydryl Group (-SH) Measurement. The total concentration of protein -SH groups was denoted by the spectrophotometric method originally described by Ando and Steiner [35]. According to this method, free thiol groups react with the 5,5'-dithiobis-2-nitrobenzoic acid (DTNB) and the colored thiols are formed. To the frozen blood platelet samples (-80°C), 500 μ l of protein precipitating solution buffer was added (0.85% H₃PO₄, 0.2% EDTA, 30% NaCl). Acid-insoluble (proteins) platelet fractions were separated according to Ando and Steiner [35]. All samples were double frozen and thawed and then centrifuged (3000 g, 20 min.). To the pellet (acid-precipitable fraction), 3 ml of 10% SDS was added. To the obtained pellet, 3.2 ml of 0.32 M Na₂HPO₄, 250 μ l of 4 mM DNTB in 1% sodium citrate was added. All samples were incubated for 30 minutes at room temperature. The concentration of free sulfhydryl groups was spectrophotometrically estimated at $\lambda = 412$ nm and was expressed as nmol/mg platelet proteins.

2.6. Measurement of NADPH Oxidase 1 Concentration. The concentration of NOX-1 in a frozen suspension of blood platelets (-80°C) obtained from patients with SP MS and healthy volunteers was determined using Human NOX-1 ELISA Kit (Fine Test, Wuhan, China). In this kit, the biotin conjugated anti-Human NOX-1 antibody was used to detect antibodies. HRP- (horseradish peroxidase-) streptavidin was added, and then, 3,3',5,5'-tetramethylbenzidine (TMB) sub-

strate was used to visualize the HRP enzymatic reaction producing a blue color product that changed yellow after adding an acidic stop solution. The level of NOX-1 was determined spectrophotometrically at $\lambda = 450$ nm. The results are presented in ng/ml of platelet suspension, based on a standard calibration curve.

2.7. Analysis of MMP in Blood Platelets. MMP was determined by the fluorescent dye JC-1 (Molecular Probes, Eugene, OR, USA) [36]. In undamaged mitochondria, JC-1 dye accumulates in large amounts in a hyperpolarized membrane, where it forms aggregates that emit red fluorescence ($\lambda_{ex} = 530$ nm, $\lambda_{em} = 590$ nm). During depolarization and permeation of the mitochondrial membrane, there is the breakdown of aggregates into monomers emitting green fluorescence, similar to that of fluorescein ($\lambda_{ex} = 485$ nm, $\lambda_{em} = 538$ nm). The red to green fluorescence intensity ratio (reflecting the level of mitochondrial membrane damage) is only dependent on the membrane potential, and there are no other factors such as shape, mitochondrial size, or density that can influence the single-component fluorescence signals. The human blood platelets freshly isolated by BSA-Sepharose 2B gel-filtration were suspended in modified Tyrode's Ca²⁺/Mg²⁺ free buffer (2 × 10⁸ platelets/ml). A stock solution of JC-1 of 1500 μ M was prepared in dimethyl sulfoxide (DMSO) and added into the platelet suspension to a final concentration of 5 μ M. The platelet suspension with JC-1 and without a dye (control) was preincubated on black 96-well plates with a transparent bottom (Greiner Bio-One, Monroe, NC, US) and incubated at 37°C for 30 min. The fluorescence was measured immediately after incubation using the Bio-Tek Synergy HT Microplate Reader (Bio-Tek Instruments, Winooski, VT, US).

2.8. Measurement of Intracellular ROS Levels. The level of intracellular ROS in blood platelets was measured using the red-ox-sensitive fluorescent dye-DCFH-DA (Molecular Probes, Eugene, OR, USA) [37]. The freshly isolated blood platelet samples were preincubated with 5 μ M of DCFH-DA (prepared in Tyrode's Ca²⁺/Mg²⁺ free buffer), at 37°C for 30 min. Fluorescence was measured at an excitation wavelength of 480 nm and an emission wavelength of 510 nm, using a Bio-Tek Synergy HT Microplate Reader (Bio-Tek Instruments, Winooski, VT, USA). Results are expressed as the level of DCF-DA fluorescence ± SD, which corresponds to the amount of ROS produced in platelets in both SP MS and control groups.

2.9. Isolation of RNA and Reverse Transcription (RT-PCR). Total RNA was isolated from frozen (-80°C) blood platelets suspended in RNAlater solution (Invitrogen, Carlsbad, CA, USA) using the Isolate II RNA Mini Kit (Biolone, London, GB) following the manufacturer's instructions. RNA concentration was determined by spectrophotometric measurement of absorbance at 260 nm, and purity was calculated at a ratio of A260/A280 with a Bio-Tek Synergy HT Microplate Reader (Bio-Tek Instruments, Inc., Winooski, VT, USA). Total RNA (1 μ g) was reverse transcribed into cDNA with a Maxima First Strand cDNA Synthesis Kit for RT-qPCR (Thermo

Fisher Scientific Waltham, MA, USA). All steps were performed according to the manufacturer's recommendations.

2.10. Expression of mRNA by RT-qPCR Method. Quantitative Real-Time PCR (RT-qPCR) was performed to determine relative expression of mRNA using the following TaqMan probes: Hs02596864_g1 for the *MTCO-1* gene (mitochondrial encoded cytochrome C oxidase I), Hs02786624_g1 for the *GAPDH* gene (glyceraldehyde-3-phosphate dehydrogenase), and Hs99999901_s1 as an endogenous control (the human 18S rRNA gene), sourced from Life Technologies, Carlsbad, CA, USA. RT-qPCR analyses were performed using a CFX96 Real-Time PCR system (Bio-Rad Laboratories, Hercules, CA, USA), with a TaqMan Universal Master Mix II without UNG (Life Technologies, Carlsbad, CA, USA). All procedures were performed according to the manufacturers' protocols. The Ct values were calculated automatically, and the analyses performed using CFX Manager™ Software (version 3.1). Relative expressions of mRNA for the studied genes were calculated using the $2^{-\Delta Ct}$ method, where $\Delta Ct = Ct_{\text{target gene}} - Ct_{18\text{SrRNA}}$.

2.11. Statistical Analysis. StatsDirect statistical software V.2.7.2. was used to perform the statistical analysis. All values were expressed as a mean \pm SD. The Shapiro-Wilk test was used to analyze the normality of the distribution of results. The significance of the differences was analyzed depending on their normality by using the unpaired Student-*t* test (for data with normal distribution) or Mann-Whitney *U* test (for data with abnormal distribution). Spearman's rank correlation was used for correlation analysis between oxidative stress biomarkers and clinical parameters: EDSS and BDI. A level of $p < 0.05$ was accepted as statistically significant.

3. Results

3.1. The Level of Oxidative Stress Markers and Their Correlation with BDI and EDSS Scales. Our data demonstrate the high level of oxidative/nitrative damages in platelet proteins obtained from SP MS patients. In our studies on SP MS patients, we have shown the statistically significant increased level of carbonyl groups (6.1 nmol/mg in SP MS vs. 3.99 nmol/mg in control, $p < 0.0001$) (Figure 1), 3-NT (16.06 nmol/mg in SP MS vs. 8.09 nmol/mg in control, $p < 0.0001$) (Figure 2), and the statistically significant decreased level of thiol groups (117.66 nmol/mg in SP MS vs. 158.61 nmol/mg in control, $p < 0.0001$) (Figure 3) compared to the control group. Moreover, we established the positive correlation between the level of carbonyl groups (Figures 4(a) and 4(b); Table 2), 3-NT (Figures 5(a) and 5(b); Table 2) and EDSS or BDI scales.

3.2. Measurement of Intracellular ROS Level. The next step in our studies was a measurement of intracellular concentration of ROS generated in blood platelets. The results obtained showed that the level of ROS in untreated platelets from SP MS patients was 2.5-fold higher compared to that of control (DCF-DA fluorescence was 4.689 in SP MS vs. 1.816 in control, $p < 0.0001$) (Figure 6).

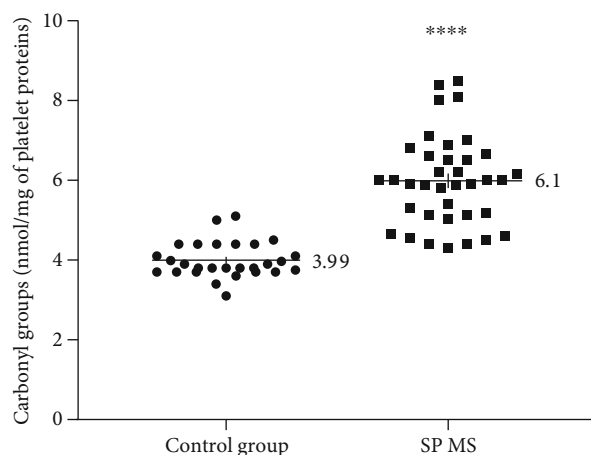


FIGURE 1: The concentration of carbonyl groups in blood platelets, determined immediately after isolation from whole, untreated blood in SP MS patients ($n = 40$) and the control group ($n = 40$). The results are expressed as values obtained for individual subjects (nmol/mg of platelet proteins) with the mean value \pm SD. Statistical analysis was performed using the unpaired Student-*t*, **** $p < 0.0001$.

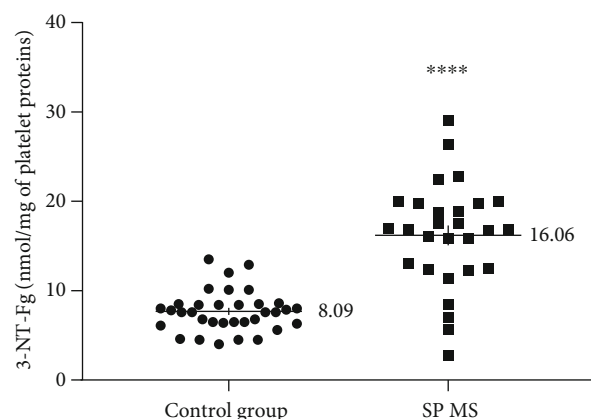


FIGURE 2: The concentration of 3-NT in blood platelets, determined immediately after isolation from whole, untreated blood in SP MS patients ($n = 40$) and control group ($n = 40$). The results are expressed as values obtained for individual subjects (nmol/mg of platelet proteins) with the mean value \pm SD. Statistical analysis was performed using the unpaired Student-*t*, **** $p < 0.0001$.

3.3. Analysis of Changes in the MMP in Blood Platelets Using the JC-1 Method. JC-1 dye can be used both as qualitative (considering the shift from green to red fluorescence emission) and quantitative (considering only the pure fluorescence intensity) measure of MMP. The ratio of the fluorescence of JC-1 aggregates to JC-1 monomers (590 nm/538 nm) reflects the level of membrane damage to cell mitochondria. The results we obtained indicate an over 1.5-fold lower ($p < 0.001$) ratio of aggregates to monomers of the JC-1 dye in platelets from people with SP MS compared to the control group (8.1 vs. 3.8, respectively) (Figure 7). The decrease in the aggregated form of the JC-1 dye indicates the depolarization and permeability of the platelet mitochondrial membrane in SP MS relative to normal platelets.

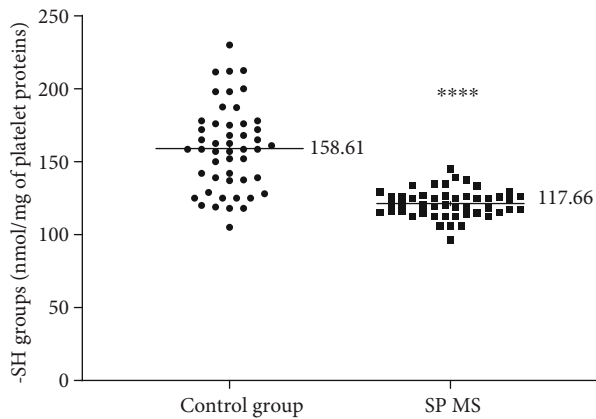


FIGURE 3: The concentration of $-SH$ groups in blood platelets, determined immediately after isolation from whole, untreated blood in SP MS patients ($n = 50$) and the control group ($n = 50$). The results are expressed as values obtained for individual subjects (nmol/mg of platelet proteins) with the mean value \pm SD. Statistical analysis was performed using the unpaired Student- t , **** $p < 0.0001$.

3.4. The Expression of Enzymes Involved in the Red-Ox Status. In another set of experiments, we found that the level of NOX-1 was significantly higher by about 30% $p < 0.0001$ in platelets from SP MS patients than in the control group (0.49 ng/ml vs. 0.39 ng/ml, respectively) (Figure 8).

Analysis of the relative expression of mRNA for the *MTCO-1* gene in blood platelets showed a more than 2-fold statistically significant ($p < 0.05$) increase in the level of transcripts for the *MTCO-1* gene in SP MS, compared to the control group ($2^{-\Delta Ct}$ was 0.057 in SP MS vs. 0.027 in control). Analogous analysis for megakaryocytes presented no statistically significant differences between the compared groups ($2^{-\Delta Ct}$ was 0.017 in SP MS vs. 0.011 in control, $p > 0.05$) (Figure 9).

Measurement of the relative mRNA expression of *GAPDH* gene in platelets showed an approximately 2.5-fold statistically significant ($p < 0.05$) increase in the level of transcripts for *GAPDH* gene in SP MS, in comparison to the control group ($2^{-\Delta Ct}$ was 0.0011 in SP MS vs. 0.0004 in control). However, in the case of megakaryocytes, also for these transcripts, no statistically significant differences were found between the compared groups ($2^{-\Delta Ct}$ was 0.00028 in SP MS vs. 0.00021 in control, $p > 0.05$) (Figure 10).

4. Discussion

Oxidative stress in patients with MS is associated with an increase damage of myelin and axonal that may lead to the appearance of clinical symptoms [11, 38–40]. ROS/RNS generation in the course of MS alters brain plasticity and through oxidative damage causes disturbances in neurotransmission and formation of new cells [41]. In chronic inflammatory diseases, such as MS, antioxidant defenses are eclipsed, which leads to oxidative stress [42]. The latest research conducted by Siotto et al. has shown that in relapsing-remitting multiple sclerosis (RR MS) patients with low disability (EDSS near

1.0) and short duration of the disease (approximately 2 years), the oxidative stress status is elevated. It is revealed by low levels of total antioxidant status (TAS) and high levels of total plasma hydroperoxides. In RR MS, the neurodegeneration rate is usually relatively low, but there is a strong oxidative imbalance associated with the development of the inflammatory process and autoimmunity [43].

Demyelination and axonal destruction, which are both the pathological hallmarks of MS, are mainly caused by overproduction of ROS and RNS generated by invading inflammatory cells, as well as resident CNS cells. Generation of ROS/RNS ($O_2^{\cdot-}$, OH^{\cdot} , H_2O_2 , NO, and ONOO $^{\cdot-}$) contributes to several mechanisms underlying the pathogenesis of MS lesions (oxidation/nitration of proteins, lipid peroxidation, damage to nucleic acids, enzyme inhibition, and activation of programmed cell death pathway) [44]. High levels of NO, ONOO $^{\cdot-}$, and $O_2^{\cdot-}$ have all been demonstrated in spinal fluid from patients with MS [45]. Myelin, which surrounds the axons, consists of 30% proteins and 70% lipids and is the major target of a ROS/RNS attack in MS [46].

ROS/RNS generation is responsible for demyelination and neurodegeneration in MS, but it is also likely to cause cardiovascular disorders in MS associated with the impaired response of blood platelets [47]. Currently, there is relatively little information about the functioning of blood platelets during neurodegeneration and knowledge about their participation in these diseases is still neglected and poorly understood. However, available clinical data have confirmed the elevated activation of circulating platelets in MS [48]. Our previous study revealed an increase in the prothrombotic and proinflammatory properties of platelets [11, 49, 50]. In neurobiological studies, blood platelets are regarded as a cellular model for the analysis of metabolic pathways related to the pathogenesis of MS and the regulation of oxidative stress [49, 51]. Oxidative/nitrative species are implicated in the regulation of platelet function, and during platelet activation, in the receptor-mediated signalling pathways, they may be produced as the “second messengers” [52]. In the following years, the participation of several platelet-derived ROS in MS, including $O_2^{\cdot-}$, OH^{\cdot} , and H_2O_2 , after stimulation with typical agonists was reported [53]. ROS production in activated blood platelets is mainly dependent on the activity of NOX and xanthine oxidase, an enzymatic cascade of arachidonic acid metabolized via COX, glutathione (GSH) cycle, and metabolism of phosphoinositides [54].

Two independent research groups, Begonja et al. [55] and Krötz et al. [56] have proven that during platelet activation, mainly $O_2^{\cdot-}$ is produced. They have shown that NOX-dependent platelet $O_2^{\cdot-}$ formation increases platelet aggregation by stimulation of the phospholipase A2-dependent arachidonic acid released from the platelet membrane. Our previous studies indicated a positive correlation between the level of $O_2^{\cdot-}$ in platelets and their amplified activation expressed as elevated adhesion and aggregation in SP MS [11]. Since the presence of NOX-1 in the cell membrane of blood platelets is one of the major regulators of ROS production, our current studies were designed to demonstrate the difference in the expression level of NOX-1 between platelets from SP MS patients and healthy controls. Our findings have

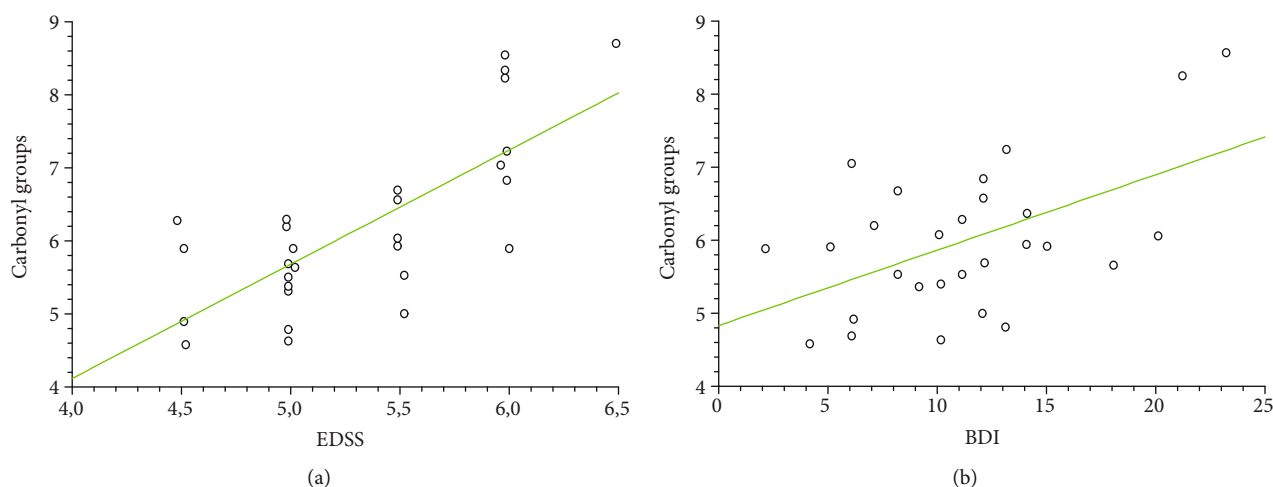


FIGURE 4: Regression plots of carbonyl group levels in platelet proteins obtained from SP MS patients and EDSS (a), BDI (b) scales.

TABLE 2: Correlation coefficient values obtained for oxidative stress biomarkers and EDSS and BDI scales. Correlation was analyzed using Spearman's rank correlation method. Table consists of Spearman's rank correlation coefficient (Rho) and probability of correlation (p).

EDSS	Carbonyl groups	3-NT
Spearman's rank correlation (ρ)	0.706381	0.723329
Probability of correlation	$p = 0.0001$	$p = 0.0001$
BDI	Carbonyl groups	3-NT
Spearman's rank correlation (ρ)	0.357093	0.417139
Probability of correlation	$p = 0.02$	$p = 0.01$

confirmed that the platelet expression of NOX-1 in SP MS patients is significantly elevated (by approximately 30%) compared to its level in platelets from healthy subjects (Figure 8). The elevated level of ROS generated within platelets in SP MS has been demonstrated by us using a fluorescent method with DCFH-DA dye, which enters through the cell membrane and is enzymatically hydrolyzed with intracellular esterases to nonfluorescent DCFH, which is then oxidized to highly fluorescent dichlorofluorescein (DCF) in the presence of intracellular ROS [54]. That analysis showed that the level of intracellular ROS in blood platelets from SP MS patients is much higher than in the control group ($p < 0.0001$) (Figure 6).

In blood platelets devoid of the nucleus, the proteins are the main target of ROS/RNS [8]. Exposure of proteins to ROS/RNS can cause major physical changes in protein structure [47]. The oxidative/nitrative damage of proteins leads to the peptide backbone cleavage, cross-linking and/or modifications of the side chain of every amino acid [57]. The great number of protein injuries is irreparable, and oxidative/nitrative changes of protein structure have functional consequences, such as inhibition of enzymatic activities, a misfolding, the increased ability of proteins to aggregation and proteolysis, and altered immunogenicity [58]. In our

studies, the oxidative damage of platelet proteins has been demonstrated as a significantly increased level of carbonyl groups in SP MS patients (Figure 1). The results obtained are in line with other reports indicating an elevated level of carbonyl proteins in neurodegenerative disease. Bizzozero et al. found an increased amount of protein carbonyls in the brain white and grey matter of patients with MS [59]. Rommer et al. also showed a raised level of carbonyl groups in cerebrospinal fluid in MS patients compared to the control group [60].

Certain studies have suggested that there is a link between depression severity and the progression of the disease. Major Depressive Disorder (MDD) is extraordinarily common in MS (prevalence of depression 15-30%). MDD lifetime prevalence rates in patients with MS are close to 50%, i.e., three times higher than in the general population. Depression is more common among patients with MS than other chronic illnesses, including other coexisting neurologic disorders [61, 62]. In our study, we have shown the positive correlation between the intensity of carbonyl group formation in blood platelet proteins obtained from SP MS patients and clinical parameters EDSS (Figure 4(a)) or BDI (Figure 4(b)). Our findings indicate that the level of carbonyl groups might be a useful biomarker expressing the progression of neurodegenerative processes caused by ROS/RNS.

NO is a chemical compound that contributes to the regulation of blood flow and participates in some synaptic transmissions. High levels of NO, ONOO⁻ and O₂^{-•} have all been demonstrated in spinal fluid from patients with MS [45, 63]. The studies of Bö et al. indicate that NO has a role in the pathogenesis of demyelinating MS lesions because of the markedly elevated human inducible nitric oxide synthase (iNOS) present in tissue sections from MS [64]. In the fast reaction between NO and O₂^{-•}, short survival ROS and RNS capable of inducing oxidative/nitrative changes in a wide variety of biomolecules are produced. Among them, the highest activity exhibits ONOO⁻ [65]. ONOO⁻ is a highly reactive compound that modifies tyrosine residues resulting in protein nitration, expressed as the 3-NT [66, 67]. It is known that 3-NT is a strong NO-derived oxidant and

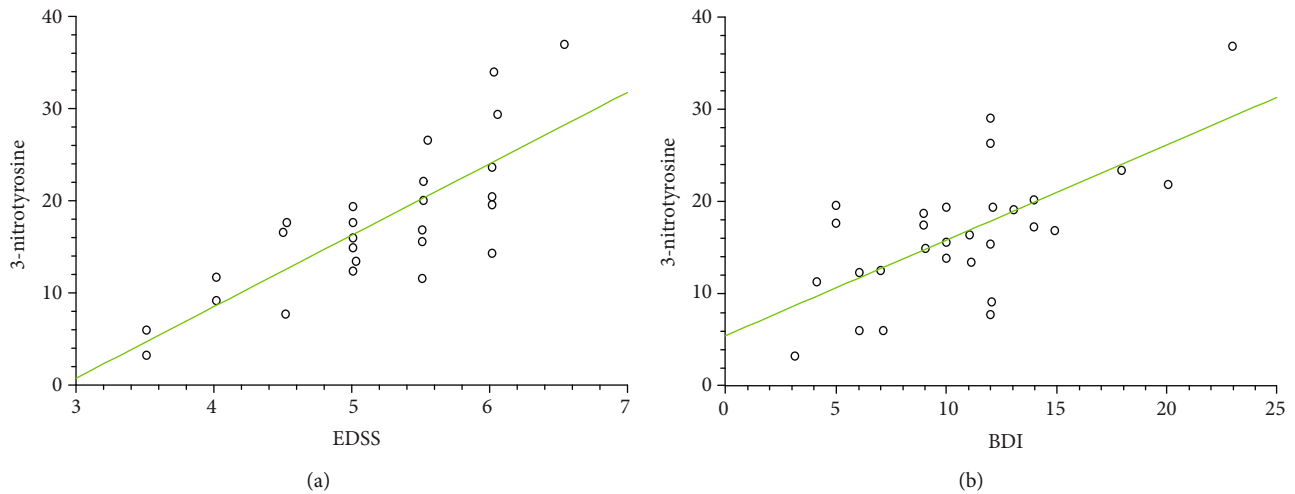


FIGURE 5: Regression plots of 3-NT levels in platelet proteins obtained from SP MS patients and EDSS (a), BDI (b) scales.

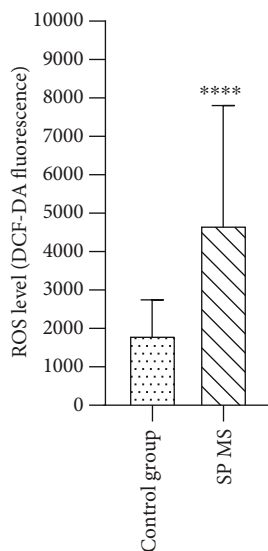


FIGURE 6: The level of intracellular ROS generated in blood platelets. ROS production measured as intensity of DCF fluorescence in SP MS patients ($n = 30$) and control group ($n = 30$). Statistical analysis was performed using the Mann-Whitney U test. The results are expressed as the mean value of DCF-DA fluorescence \pm SD, **** $p < 0.0001$.

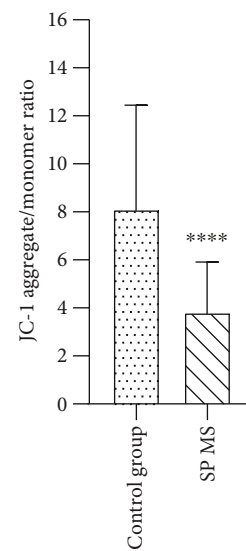


FIGURE 7: Changes in MMP ($\Delta\Psi_m$) in blood platelets. MMP is expressed as a ratio of JC-1 aggregates (530 nm/590 nm) to JC-1 monomers (485 nm/538 nm), as quantified with a fluorescent plate reader after JC-1 staining in blood platelets obtained from SP MS patients ($n = 30$) and the control group ($n = 30$). Statistical analysis was performed using the Mann-Whitney U test. The results are shown as the mean value of fluorescence ratio (590 nm/538 nm) \pm SD, **** $p < 0.0001$.

the earliest detectable biomarker found in the plaques of the brain from patients suffering from MS and other neurodegenerative disorders [68, 69]. In our studies, the elevated level of 3-NT in platelet proteins obtained from SP MS patients, compared to the control group, was observed (Figure 2). We also revealed the positive correlation between the increased level of 3-NT and EDSS or BDI in SP MS patients (Figures 5(a) and 5(b), respectively). Our findings are consistent with the report of Jack et al., who detected the raised level of 3-NT in active demyelinated lesions in MS [70]. Thus, we emphasize the importance of platelets in the pathogenesis of MS, in inflammatory lesions, where red-ox balance is disturbed.

Individual proteins can display different susceptibilities to an oxidative attack, which is linked to the distribution of -SH groups. The thiol-disulphide homeostasis is important in antioxidant defense, detoxification, apoptosis, signal transduction, regulation of enzymatic activity, and transcription and intracellular signalling mechanisms [71]. Mitosek-Szewczyk et al. showed a reduced level of protein -SH groups in cerebrospinal fluid and serum delivered from MS patients [72]. Our blood platelet studies also confirm the strong oxidation of protein thiol groups in SP MS patients (Figure 3). However, the correlations between the level of -SH groups and EDSS as well as BDI scale have not been observed.

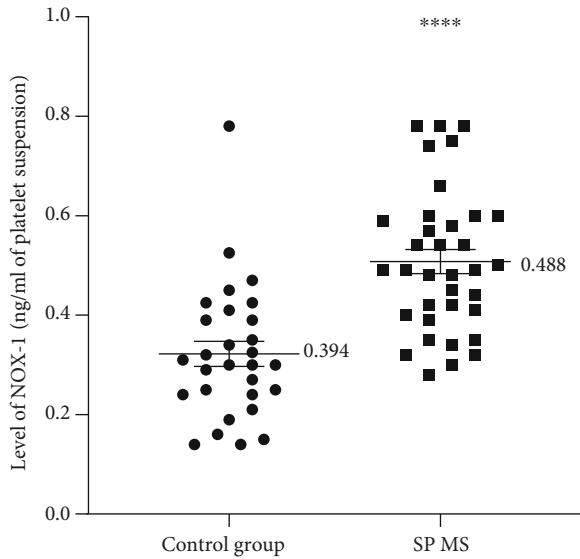


FIGURE 8: The concentration of NOX-1 in blood platelets, determined immediately after isolation from whole blood untreated. The comparison of NOX-1 expression level (ng/ml) measured in blood platelets in SP MS patients ($n = 30$) and control group ($n = 30$). The results are expressed as values obtained for individual subjects with the mean value \pm SD. Statistical analysis was performed using the Mann-Whitney U test, **** $p < 0.0001$.

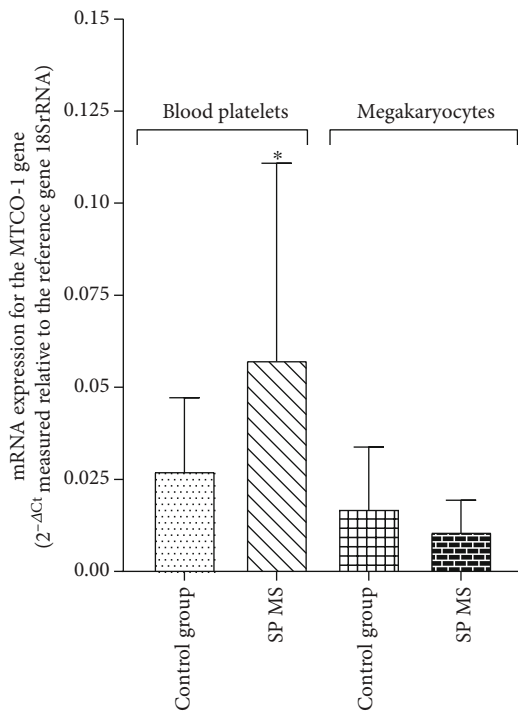


FIGURE 9: The mRNA level of *MTCO-1* gene in blood platelets and megakaryocytes. Relative expression of mRNA for the *MTCO-1* gene in platelets and megakaryocytes from patients with SP MS ($n = 45$) and control group ($n = 45$). Statistical analysis was performed using the Mann-Whitney U test. The results are expressed as the mean value of $2^{-\Delta C_t} \pm$ SD (according to the reference gene-18SrRNA), * $p < 0.05$.

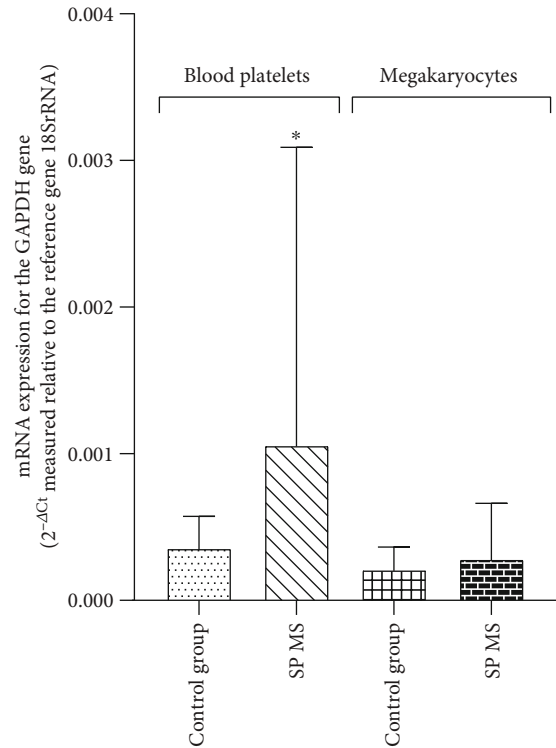


FIGURE 10: The mRNA level of *GAPDH* gene in blood platelets and megakaryocytes. The relative expression of mRNA for the *GAPDH* gene in platelets and megakaryocytes from patients with SP MS ($n = 45$) and control group ($n = 45$). Statistical analysis was performed using the Mann-Whitney U test. The results are expressed as the mean value of $2^{-\Delta C_t} \pm$ SD (according to the reference gene-18SrRNA), * $p < 0.05$.

The rate of ADP turnover in blood platelets is even greater than in resting mammalian muscle, suggesting an essential role for mitochondria (and red-ox signalling) in platelet function. Furthermore, energy demand escalates during the platelet activation and the complex signalling cascade that regulates adhesion, aggregation, and secretion processes [73]. This incremental energy consumption is one of the main determinants of platelet function. Mitochondria encode functionally important subunits of the mitochondrial respiratory chain complexes, located in the inner mitochondrial membrane that consists of four complexes (complexes I-IV) and complex V (ATP synthase) [74]. Cytochrome c oxidase (complex IV) is the last and key enzyme of the electron transport chain in the oxidative phosphorylation process, encoded by the mitochondrial *MTCO-1* gene. This terminal complex is where over 90% of cell oxygen is consumed. Cytochrome c oxidase is the component of the respiratory chain that catalyzes the reduction of O_2 to H_2O . [75]. The MMP ($\Delta\psi_m$) generated by proton pumps is an essential component in the process of energy storage during oxidative phosphorylation [76]. The decrease of $\Delta\psi_m$ may be a signal of loss of cell viability leading to various pathologies. GAPDH is a multifunctional protein that also mediates cell death under oxidative stress. In the largest amounts, the enzyme is present in the cytoplasm, but part of the enzyme is also found in mitochondria [77]. Recent studies have

shown that GAPDH has a significant role in ATP production and autoimmune response-induced neuroaxonal pathological changes in MS. GAPDH as a membrane protein is involved in energy generation, polymerization of tubulin into microtubules, and the control of protein synthesis in the endoplasmic reticulum [78]. GAPDH is extremely sensitive to oxidative stress modifications and damage, and, it is even considered to be one of the main cellular targets for ROS and RNS [79]. However, there are a lot of studies in which GAPDH was used as housekeeping gene (reference gene) and is shown to be the most stable gene in platelets used in mRNA expression studies [80, 81]. Surprisingly, in our studies, we showed that the amount of mRNA transcripts for the GAPDH gene in SP MS patients is pathologically increased in comparison to the control group (Figure 10). Our findings have suggested the presence of spontaneous mitochondrial damage in SP MS, which is also confirmed by the decrease in the expression of transcripts for the *MTCO-1* gene in SP MS (Figure 9) and the significant depolarization of platelet mitochondrial membrane in SP MS patients (Figure 7), compared to the control group.

5. Conclusion

We suggest that oxidative/nitrative damage of platelet proteins is implicated in the pathophysiology of MS, reflecting disease status expressed as a degree on the EDSS and BDI scales. The use of biomarkers such as 3-NT or carbonyl groups may improve the sensitivity and specificity of the measurement of the risk factor, namely, oxidative stress. We strongly recommend the introduction of antiplatelet and antioxidative therapy in the future treatment of MS.

Data Availability

The datasets used and analyzed during the current study are available from the corresponding author on request.

Conflicts of Interest

The authors declare that there is no conflict of interest regarding the publication of this article.

Authors' Contributions

All authors conceived the idea, designed the work, and contributed to the acquisition of data.

Acknowledgments

This work was supported with funding from scientific research grant from the Polish National Science Centre (No. UMO-2016/21/B/NZ4/00543) as well as with University of Lodz grant (No. 506/1136).

References

- [1] C. A. Cobb and M. P. Cole, "Oxidative and nitrative stress in neurodegeneration," *Neurobiology of Disease*, vol. 84, pp. 4–21, 2015.
- [2] T. F. Beckhauser, J. Francis-Oliveira, and R. De Pasquale, "Reactive oxygen species: physiological and physiopathological effects on synaptic plasticity," *Journal of Experimental Neuroscience*, vol. 10s1, 2016.
- [3] S. Salim, "Oxidative stress and the central nervous system," *Journal of Pharmacology and Experimental Therapeutics*, vol. 360, no. 1, pp. 201–205, 2016.
- [4] A. Singh, R. Kukreti, L. Saso, and S. Kukreti, "Oxidative stress: a key modulator in neurodegenerative diseases," *Molecules*, vol. 24, no. 8, p. 1583, 2019.
- [5] A. I. Rojo, G. McBean, M. Cindric et al., "Redox control of microglial function: molecular mechanisms and functional significance," *Antioxidants & Redox Signaling*, vol. 21, no. 12, pp. 1766–1801, 2014.
- [6] S. P. Cramer, H. Simonsen, J. L. Frederiksen, E. Rostrup, and H. B. W. Larsson, "Abnormal blood-brain barrier permeability in normal appearing white matter in multiple sclerosis investigated by MRI," *NeuroImage: Clinical*, vol. 4, pp. 182–189, 2014.
- [7] N. Ghasemi, S. Razavi, and E. Nikzad, "Multiple sclerosis: pathogenesis, symptoms, diagnoses and cell-based therapy," *Cell Journal*, vol. 19, no. 1, pp. 1–10, 2017.
- [8] L. Haider, "Inflammation, iron, energy failure, and oxidative stress in the pathogenesis of multiple sclerosis," *Oxidative Medicine and Cellular Longevity*, vol. 2015, Article ID 725370, 10 pages, 2015.
- [9] E. Miller and J. Kędziora, "Effect of whole body cryotherapy on uric acid concentration in plasma of multiple sclerosis patients," *International Review of Allergology and Clinical Immunology*, vol. 17, pp. 20–23, 2011.
- [10] H. Hamzeh-Cognasse, F. Cognasse, S. Palle et al., "Direct contact of platelets and their released products exert different effects on human dendritic cell maturation," *BMC Immunology*, vol. 9, no. 1, p. 54, 2008.
- [11] A. Morel, M. Bijak, E. Miller, J. Rywaniak, S. Miller, and J. Saluk, "Relationship between the increased haemostatic properties of blood platelets and oxidative stress level in multiple sclerosis patients with the secondary progressive stage," *Oxidative Medicine and Cellular Longevity*, vol. 2015, Article ID 240918, 10 pages, 2015.
- [12] A. Morel, E. Miller, M. Bijak, and J. Saluk, "The increased level of COX-dependent arachidonic acid metabolism in blood platelets from secondary progressive multiple sclerosis patients," *Molecular and Cellular Biochemistry*, vol. 420, no. 1–2, pp. 85–94, 2016.
- [13] A. Morel, J. Rywaniak, M. Bijak, E. Miller, M. Niwald, and J. Saluk, "Flow cytometric analysis reveals the high levels of platelet activation parameters in circulation of multiple sclerosis patients," *Molecular and Cellular Biochemistry*, vol. 430, no. 1–2, pp. 69–80, 2017.
- [14] S. Christensen, D. K. Farkas, L. Pedersen, M. Miret, C. F. Christiansen, and H. T. Sorensen, "Multiple sclerosis and risk of venous thromboembolism: a population-based cohort study," *Neuroepidemiology*, vol. 38, no. 2, pp. 76–83, 2012.
- [15] C. F. Christiansen, S. Christensen, D. K. Farkas, M. Miret, H. T. Sorensen, and L. Pedersen, "Risk of arterial cardiovascular diseases in patients with multiple sclerosis: a population-based cohort study," *Neuroepidemiology*, vol. 35, no. 4, pp. 267–274, 2010.
- [16] E. Jadidi, M. Mohammadi, and T. Moradi, "High risk of cardiovascular diseases after diagnosis of multiple sclerosis,"

- Multiple Sclerosis Journal*, vol. 19, no. 10, pp. 1336–1340, 2013.
- [17] S. V. Ramagopalan, C. J. Wotton, A. E. Handel, D. Yeates, and M. J. Goldacre, “Risk of venous thromboembolism in people admitted to hospital with selected immune-mediated diseases: Record-linkage study,” *BMC Medicine*, vol. 9, no. 1, 2011.
- [18] B. Zoller, X. Li, J. Sundquist, and K. Sundquist, “Risk of pulmonary embolism in patients with autoimmune disorders: a nationwide follow-up study from Sweden,” *The Lancet*, vol. 379, no. 9812, pp. 244–249, 2012.
- [19] P. J. H. L. Peeters, M. T. Bazelier, B. M. J. Uitdehaag, H. G. M. Leufkens, M. L. De Bruin, and F. de Vries, “The risk of venous thromboembolism in patients with multiple sclerosis: the Clinical Practice Research Datalink,” *Journal of Thrombosis and Haemostasis*, vol. 12, no. 4, pp. 444–451, 2014.
- [20] H. Brønnum-Hansen, N. Koch-Henriksen, and E. Stenager, “Trends in survival and cause of death in Danish patients with multiple sclerosis,” *Brain*, vol. 127, no. 4, pp. 844–850, 2004.
- [21] N. Sumi, T. Nishioku, F. Takata et al., “Lipopolysaccharide-activated microglia induce dysfunction of the blood-brain barrier in rat microvascular endothelial cells co-cultured with microglia,” *Cellular and Molecular Neurobiology*, vol. 30, no. 2, pp. 247–253, 2010.
- [22] G. Sonego, M. Abonnenc, J. D. Tissot, M. Prudent, and N. Lion, “Redox proteomics and platelet activation: understanding the redox proteome to improve platelet quality for transfusion,” *International Journal of Molecular Sciences*, vol. 18, no. 2, p. 387, 2017.
- [23] S. J. Forrester, D. S. Kikuchi, M. S. Hernandez, Q. Xu, and K. K. Griendling, “Reactive oxygen species in metabolic and inflammatory signaling,” *Circulation Research*, vol. 122, no. 6, pp. 877–902, 2018.
- [24] H. Melchinger, K. Jain, T. Tyagi, and J. Hwa, “Role of platelet mitochondria: life in a nucleus-free Zone,” *Frontiers in Cardiovascular Medicine*, vol. 6, pp. 153–153, 2019.
- [25] C. H. Polman, S. C. Reingold, B. Banwell et al., “Diagnostic criteria for multiple sclerosis: 2010 revisions to the McDonald criteria,” *Annals of Neurology*, vol. 69, no. 2, pp. 292–302, 2011.
- [26] J. F. Kurtzke, “Rating neurologic impairment in multiple sclerosis: an expanded disability status scale (EDSS),” *Neurology*, vol. 33, no. 11, pp. 1444–1452, 1983.
- [27] B. G. Weinshenker, B. Bass, G. P. A. Rice et al., “The natural history of multiple sclerosis: a geographically based STUDY,” *Brain*, vol. 112, Part 1, pp. 133–146, 1989.
- [28] A. T. Beck, C. H. Ward, M. Mendelson, J. Mock, and J. Erbaugh, “An inventory for measuring depression,” *Archives of General Psychiatry*, vol. 4, no. 6, pp. 561–571, 1961.
- [29] B. Walkowiak, U. Kralisz, L. Michalec et al., “Comparison of platelet aggregability and P-selectin surface expression on platelets isolated by different methods,” *Thrombosis Research*, vol. 99, no. 5, pp. 495–502, 2000.
- [30] B. Walkowiak, E. Michalak, W. Koziolkiewicz, and C. S. Cierniewski, “Rapid photometric method for estimation of platelet count in blood plasma or platelet suspension,” *Thrombosis Research*, vol. 56, no. 6, pp. 763–766, 1989.
- [31] H. Buss, T. P. Chan, K. B. Sluis, N. M. Domigan, and C. C. Winterbourn, “Protein carbonyl measurement by a sensitive ELISA method,” *Free Radical Biology and Medicine*, vol. 23, no. 3, pp. 361–366, 1997.
- [32] D. Alamdari, E. Kostidou, K. Paletas et al., “High sensitivity enzyme-linked immunosorbent assay (ELISA) method for measuring protein carbonyl in samples with low amounts of protein,” *Free Radical Biology and Medicine*, vol. 39, no. 10, pp. 1362–1367, 2005.
- [33] R. L. Levine, D. Garland, C. N. Oliver et al., “[49] Determination of carbonyl content in oxidatively modified proteins,” *Methods in Enzymology*, vol. 186, pp. 464–478, 1990.
- [34] J. Khan, D. M. Brennand, N. Bradley, B. Gao, R. Bruckdorfer, and M. Jacobs, “3-Nitrotyrosine in the proteins of human plasma determined by an ELISA method,” *Biochemical Journal*, vol. 330, no. 2, Part 2, pp. 795–801, 1998.
- [35] Y. Ando and M. Steiner, “Sulfhydryl and disulfide groups of platelet membranes. II. Determination of disulfide groups,” *Biochimica et Biophysica Acta (BBA) - Biomembranes*, vol. 311, no. 1, pp. 38–44, 1973.
- [36] M. Reers, S. T. Smiley, C. Mottola-Hartshorn, A. Chen, M. Lin, and L. B. Chen, “[29] Mitochondrial membrane potential monitored by JC-1 dye,” *Methods in Enzymology*, vol. 260, pp. 406–417, 1995.
- [37] C. P. LeBel, H. Ischiropoulos, and S. C. Bondy, “Evaluation of the probe 2',7'-dichlorofluorescein as an indicator of reactive oxygen species formation and oxidative stress,” *Chemical Research in Toxicology*, vol. 5, no. 2, pp. 227–231, 1992.
- [38] J. van Horssen, G. Schreiberl, J. Drexhage et al., “Severe oxidative damage in multiple sclerosis lesions coincides with enhanced antioxidant enzyme expression,” *Free Radical Biology and Medicine*, vol. 45, no. 12, pp. 1729–1737, 2008.
- [39] L. Haider, M. T. Fischer, J. M. Frischer et al., “Oxidative damage in multiple sclerosis lesions,” *Brain*, vol. 134, no. 7, pp. 1914–1924, 2011.
- [40] R. Ibitoye, K. Kemp, C. Rice, K. Hares, N. Scolding, and A. Wilkins, “Oxidative stress-related biomarkers in multiple sclerosis: a review,” *Biomarkers in Medicine*, vol. 10, no. 8, pp. 889–902, 2016.
- [41] B. Adamczyk and M. Adamczyk-Sowa, “New insights into the role of oxidative stress mechanisms in the pathophysiology and treatment of multiple Sclerosis,” *Oxidative Medicine and Cellular Longevity*, vol. 2016, Article ID 1973834, 18 pages, 2016.
- [42] B. Uttara, A. V. Singh, P. Zamboni, and R. T. Mahajan, “Oxidative stress and neurodegenerative diseases: a review of upstream and downstream antioxidant therapeutic options,” *Current Neuropharmacology*, vol. 7, no. 1, pp. 65–74, 2009.
- [43] M. Siotto, M. M. Filippi, I. Simonelli et al., “Oxidative stress related to Iron metabolism in relapsing remitting multiple sclerosis patients with low disability,” *Frontiers in Neuroscience*, vol. 13, pp. 86–86, 2019.
- [44] K. K. Griendling, R. M. Touyz, J. L. Zweier et al., “Measurement of reactive oxygen species, reactive nitrogen species, and redox-dependent signaling in the cardiovascular system: a scientific statement From the American Heart Association,” *Circulation Research*, vol. 119, no. 5, pp. e39–e75, 2016.
- [45] V. Calabrese, G. Scapagnini, A. Ravagna et al., “Nitric oxide synthase is present in the cerebrospinal fluid of patients with active multiple sclerosis and is associated with increases in cerebrospinal fluid protein nitrotyrosine and S-nitrosothiols and with changes in glutathione levels,” *Journal of Neuroscience Research*, vol. 70, no. 4, pp. 580–587, 2002.

- [46] A. Jana and K. Pahan, "Oxidative stress kills human primary oligodendrocytes via neutral sphingomyelinase: implications for multiple sclerosis," *Journal of Neuroimmune Pharmacology*, vol. 2, no. 2, pp. 184–193, 2007.
- [47] E. Miller, "Multiple sclerosis," *Advances in Experimental Medicine and Biology*, vol. 724, pp. 222–238, 2012.
- [48] J. Saluk-Bijak, A. Dziedzic, and M. Bijak, "Pro-thrombotic activity of blood platelets in multiple sclerosis," *Cells*, vol. 8, no. 2, p. 110, 2019.
- [49] A. Morel, M. Bijak, M. Niwald, E. Miller, and J. Saluk, "Markers of oxidative/nitrative damage of plasma proteins correlated with EDSS and BDI scores in patients with secondary progressive multiple sclerosis," *Redox Report*, vol. 22, no. 6, pp. 547–555, 2016.
- [50] M. Bijak, A. Olejnik, B. Rokita et al., "Increased level of fibrinogen chains in the proteome of blood platelets in secondary progressive multiple sclerosis patients," *Journal of Cellular and Molecular Medicine*, vol. 23, no. 5, pp. 3476–3482, 2019.
- [51] B. Wachowicz, A. Morel, E. Miller, and J. Saluk, "The physiology of blood platelets and changes of their biological activities in multiple sclerosis," *Acta Neurobiologiae Experimentalis*, vol. 76, no. 4, pp. 269–281, 2016.
- [52] B. Wachowicz, "Blood platelet as a peripheral cell in oxidative stress in psychiatric disorders," in *Studies on Psychiatric Disorders*, pp. 327–353, Springer, 2015.
- [53] D. Caccese, D. Praticò, A. Ghiselli et al., "Superoxide anion and hydroxyl radical release by collagen-induced platelet aggregation—role of arachidonic acid metabolism," *Thrombosis and Haemostasis*, vol. 83, no. 3, pp. 485–490, 2017.
- [54] X. Chen, Z. Zhong, Z. Xu, L. Chen, and Y. Wang, "2',7'-Dichlorodihydrofluorescein as a fluorescent probe for reactive oxygen species measurement: forty years of application and controversy," *Free Radical Research*, vol. 44, no. 6, pp. 587–604, 2010.
- [55] A. J. Begonja, S. Gambaryan, J. Geiger et al., "Platelet NAD(P)H-oxidase-generated ROS production regulates α IIb β 3-integrin activation independent of the NO/cGMP pathway," *Blood*, vol. 106, no. 8, pp. 2757–2760, 2005.
- [56] F. Krötz, H. Y. Sohn, T. Gloe et al., "NAD(P)H oxidase-dependent platelet superoxide anion release increases platelet recruitment," *Blood*, vol. 100, no. 3, pp. 917–924, 2002.
- [57] K. Wirdefeldt, H. O. Adami, P. Cole, D. Trichopoulos, and J. Mandel, "Epidemiology and etiology of Parkinson's disease: a review of the evidence," *European Journal of Epidemiology*, vol. 26, Supplement 1, pp. 1–58, 2011.
- [58] M. Takalo, A. Salminen, H. Soininen, M. Hiltunen, and A. Haapasalo, "Protein aggregation and degradation mechanisms in neurodegenerative diseases," *American Journal of Neurodegenerative Disease*, vol. 2, no. 1, pp. 1–14, 2013.
- [59] O. A. Bizzozero, G. DeJesus, K. Callahan, and A. Pastuszyn, "Elevated protein carbonylation in the brain white matter and gray matter of patients with multiple sclerosis," *Journal of Neuroscience Research*, vol. 81, no. 5, pp. 687–695, 2005.
- [60] P. S. Rommer, J. Greilberger, S. Salhofer-Polanyi, E. Auff, F. Leutmezer, and R. Herwig, "Elevated levels of carbonyl proteins in cerebrospinal fluid of patients with neurodegenerative diseases," *The Tohoku Journal of Experimental Medicine*, vol. 234, no. 4, pp. 313–317, 2014.
- [61] M. L. Pucak, K. A. L. Carroll, D. A. Kerr, and A. L. Kaplin, "Neuropsychiatric manifestations of depression in multiple sclerosis: neuroinflammatory, neuroendocrine, and neurotrophic mechanisms in the pathogenesis of immune-mediated depression," *Dialogues in Clinical Neuroscience*, vol. 9, no. 2, pp. 125–139, 2007.
- [62] T. Paparrigopoulos, C. Tzavara, C. Theleritis, C. Psarros, C. Soldatos, and Y. Tountas, "Insomnia and its correlates in a representative sample of the Greek population," *BMC Public Health*, vol. 10, no. 1, p. 531, 2010.
- [63] K. J. Smith and H. Lassmann, "The role of nitric oxide in multiple sclerosis," *Lancet Neurology*, vol. 1, no. 4, pp. 232–241, 2002.
- [64] L. Bö, T. M. Dawson, S. Wesselingh et al., "Induction of nitric oxide synthase in demyelinating regions of multiple sclerosis brains," *Annals of Neurology*, vol. 36, no. 5, pp. 778–786, 1994.
- [65] L. L. Horstman, W. Jy, Y. S. Ahn et al., "Role of platelets in neuroinflammation: a wide-angle perspective," *Journal of Neuroinflammation*, vol. 7, no. 1, pp. 10–10, 2010.
- [66] P. Pacher, J. S. Beckman, and L. Liaudet, "Nitric oxide and peroxynitrite in health and disease," *Physiological Reviews*, vol. 87, no. 1, pp. 315–424, 2007.
- [67] F. Krötz, H.-Y. Sohn, and U. Pohl, "Reactive oxygen species," *Arteriosclerosis, Thrombosis, and Vascular Biology*, vol. 24, no. 11, pp. 1988–1996, 2004.
- [68] B. Olas and B. Wachowicz, "Role of reactive nitrogen species in blood platelet functions," *Platelets*, vol. 18, no. 8, pp. 555–565, 2009.
- [69] M. Gutowicz, "The influence of reactive oxygen species on the central nervous system," *Postępy Higieny i Medycyny Doświadczalnej*, vol. 65, pp. 104–113, 2011.
- [70] C. Jack, J. Antel, W. Bruck, and T. Kuhlmann, "Contrasting potential of nitric oxide and peroxynitrite to mediate oligodendrocyte injury in multiple sclerosis," *Glia*, vol. 55, no. 9, pp. 926–934, 2007.
- [71] A. T. Nurden, "Platelets, inflammation and tissue regeneration," *Thrombosis and Haemostasis*, vol. 105, Supplement 1, pp. S13–S33, 2017.
- [72] K. Mitosek-Szewczyk, W. Gordon-Krajcer, P. Walendzik, and Z. Stelmasiak, "Free radical peroxidation products in cerebrospinal fluid and serum of patients with multiple sclerosis after glucocorticoid therapy," *Folia Neuropathologica*, vol. 48, no. 2, pp. 116–122, 2010.
- [73] S. Zharikov and S. Shiva, "Platelet mitochondrial function: from regulation of thrombosis to biomarker of disease," *Biochemical Society Transactions*, vol. 41, no. 1, pp. 118–123, 2013.
- [74] L. K. Sharma, J. Lu, and Y. Bai, "Mitochondrial respiratory complex I: structure, function and implication in human diseases," *Current Medicinal Chemistry*, vol. 16, no. 10, pp. 1266–1277, 2009.
- [75] D. Mahad, H. Lassmann, and D. Turnbull, "Review: mitochondria and disease progression in multiple sclerosis," *Neuropathology and Applied Neurobiology*, vol. 34, no. 6, pp. 577–589, 2008.
- [76] L. D. Zorova, V. A. Popkov, E. Y. Plotnikov et al., "Mitochondrial membrane potential," *Analytical Biochemistry*, vol. 552, pp. 50–59, 2018.
- [77] B. McDonald, B. Reep, E. G. Lapetina, and L. Molina y Vedia, "Glyceraldehyde-3-phosphate dehydrogenase is required for the transport of nitric oxide in platelets," *Proceedings of the National Academy of Sciences of the United States of America*, vol. 90, no. 23, pp. 11122–11126, 1993.

- [78] H. Nakajima, M. Itakura, T. Kubo et al., "Glyceraldehyde-3-phosphate dehydrogenase (GAPDH) aggregation causes mitochondrial dysfunction during oxidative stress-induced cell death," *Journal of Biological Chemistry*, vol. 292, no. 11, pp. 4727–4742, 2017.
- [79] N. R. Hwang, S. H. Yim, Y. M. Kim et al., "Oxidative modifications of glyceraldehyde-3-phosphate dehydrogenase play a key role in its multiple cellular functions," *Biochemical Journal*, vol. 423, no. 2, pp. 253–264, 2009.
- [80] K. Zsóri, L. Muszbek, Z. Csiki, and A. Shemirani, "Validation of reference genes for the determination of platelet transcript level in healthy individuals and in patients with the history of myocardial infarction," *International Journal of Molecular Sciences*, vol. 14, no. 2, pp. 3456–3466, 2013.
- [81] K. Mossberg, P. A. Svensson, O. Gidlof, D. Erlinge, S. Jern, and H. Brogren, "Normalization of qPCR in platelets - YWHAE a potential generic reference gene," *Platelets*, vol. 27, no. 8, pp. 729–734, 2016.

Research Article

Proteome and Transcriptome Analysis of the Antioxidant Mechanism in Chicken Regulated by Eucalyptus Leaf Polyphenols Extract

Wei Li,¹ Ze-qi He,¹ Xiao-Ying Zhang,¹ Yun-Jiao Chen ¹, Jian-Jun Zuo,² and Yong Cao ¹

¹College of Food Science, South China Agricultural University, Guangdong Provincial Key Laboratory of Nutraceuticals and Functional Foods, Guangdong Research Center for Engineering Technology in Bioactive Natural Products, Guangzhou 510642, China

²College of Animal Science, South China Agriculture University, Guangzhou 510642, China

Correspondence should be addressed to Yong Cao; caoyong2181@scau.edu.cn

Received 25 February 2020; Revised 23 April 2020; Accepted 13 May 2020; Published 15 June 2020

Academic Editor: Luciano Saso

Copyright © 2020 Wei Li et al. This is an open access article distributed under the Creative Commons Attribution License, which permits unrestricted use, distribution, and reproduction in any medium, provided the original work is properly cited.

Eucalyptus leaf polyphenols extract (EPE) has been proved to have various bioactivities, but few reports focus on its antioxidant mechanism *in vivo*. The purpose of this study was to elucidate the effect and mechanism of EPE dietary supplements on antioxidant capacity in chicken. A total of 216 chickens were randomly selected for a 40-day experiment. Four treatment groups received diets including the control diet only, the control diet + low EPE (0.6 g/kg), the control diet + moderate EPE (0.9 g/kg), and the control diet + high EPE (1.2 g/kg). Compared with control group, the glutathione peroxidase (GSH-Px) activity and glutathione (GSH) content in the breast muscle of the moderate EPE treatment group was significantly higher ($p < 0.05$), while the malonaldehyde (MDA) content in the moderate EPE group was reduced ($p < 0.05$). Moreover, proteomic and transcriptomic analyses of the breast muscle revealed that glutathione metabolism and the peroxisome were the two crucial metabolic pathways responsible for increased antioxidant capacity of the muscle. Accordingly, nine candidate genes and two candidate proteins were identified related to improved antioxidant status induced by EPE supplements. This research provides new insights into the molecular mechanism of antioxidant capacity in chickens treated with EPE dietary supplements.

1. Introduction

The genus *Eucalyptus* comprises over 900 species of economically valuable plants endemic to Australia [1, 2]. In China, the eucalyptus plantation area reached 4.5 million hm^2 by the end of 2016 [3]. There is a growing need to develop alternative uses for eucalyptus products, and eucalyptus plants have attracted broad interest among researchers to investigate their functionality and potential applications [4–6]. Eucalyptus leaves are known to contain numerous bioactive substances including, but not limited to, terpenoids, tannins, flavonoids, and phloroglucinol derivatives, and eucalyptus has also been shown to function as antioxidants [7, 8]. Accordingly, bioactive components derived from eucalyptus leaves and their functions for use in the food industry are widely researched, with many studies focused on their antioxidant capacity [9–11].

Recent technological advances in proteomics and transcriptomics have substantially improved the understanding of how variation in proteins and genes impact living organisms [12–15]. In particular, these methods may be used to elucidate the molecular mechanism of antioxidant capacity. Using proteomic techniques, Wang et al. [16] discovered that broiler chickens given albusin B supplements could upregulate the expression of GST, Prdx6, PPIA, alfatoin aldehyde reductase, and superoxide dismutase to improve antioxidant defense.

Our previous study revealed that EPE exhibited a strong antioxidant activity in chemical-based and cellular-based assay [7]. Moreover, EPE treatment could protect acute-induced oxidative damage by improving antioxidant enzymes (GSH-Px, T-SOD) in chicken [7]. Several researches also reported that diet with eucalyptus leaves extract

TABLE 1: Ingredients and nutrient composition of the experimental diets.

Ingredients (%)	Content	Nutrient level	Content
Corn	64	Metabolic energy (mcal/kg)	2.96
Wheat shorts	2	Crude protein (%)	15.5
Rice bran	3	Lysine (%)	0.65
Bean pulp	9.7	Calcium (%)	1.19
Peanut bran	4	Phosphorus (%)	0.57
Corn gluten meal	2	Sodium (%)	0.206
Refined three worm powder CP45%	6	Chlorine (%)	0.196
Rock flour	1.5	Potassium (%)	0.47
Calcium hydrophosphate	1.3	Methionine (%)	0.25
Soybean oil	2.5	Arginine (%)	0.83
338 gunk	4		
Total	100		

Note: the vitamin/mineral premix includes (per kg feed): vitamin A, 15750 IU; vitamin D, 3500 IU; vitamin E 35 mg; Menadione, 4.4 mg; Thiamine, 3.5 mg; Riboflavin, 10.5 mg; vitamin B₆, 7 mg; vitamin B₁₂, 35 mg; Nicotinic acid, 70 mg; Pantothenic acid, 21 mg; Folic acid, 1.75 mg; Biotin, 0.175 mg.

significantly improves antioxidant status [17, 18]. Eucalyptus leaves extracts with immense biomass and great antioxidant potential benefited to improve growth performance and health status of broilers, which could be useful for the poultry industry [19, 20]. However, few studies have investigated the antioxidant mechanism of EPE in chicken. Therefore, this study was performed to reveal EPE dietary supplements on the antioxidant mechanism of chicken using proteomic and transcriptomic analysis.

2. Materials and Methods

2.1. Experimental Material. All the Huiyang beard chickens used in this study were provided by Xingtai Modern Agricultural Limited Company of Huizhou in Guangdong, China.

EPE: Eucalyptus leaves (*Eucalyptus grandis* × *Eucalyptus urophylla* GL9) were picked in October in Zhanjiang and air-dried naturally (7~9 d, 28 ± 2°C, moisture content 15.53 ± 2.11%). The eucalyptus leaves were extracted by 70% ethanol solvent (v/v) at 75°C. And then the extraction solution was vacuum-concentrated and spray-dried (the yield of EPE was 25.78 ± 2.03%), the EPE was stored at 4°C for the subsequent experiment.

The total polyphenol content in EPE was determined using the Folin-phenol method [21]. Additionally, the EPE was analyzed using high-performance liquid chromatography (HPLC) with a Diamonsil C18 column (250 × 4.6 mm, 5 μm, Diamonsil, China). EPE was reconstituted in buffer A (H₂O) and loaded onto the column. It was then eluted using gradient buffer B (Methanol) in the following order: 10% at 0 min and 10~90% at 60 min. The flow rate was 1 mL/min and the injection volume was 10 μL. The column temperature was 37°C and a detection wavelength of 270 nm.

2.2. Animal Experimental Design. A total of 216 chickens (90 days old) were randomly assigned to one of four treatments (6 pens/treatment and 6 chicken/pen), and the duration of the trial was 40 days (from 90 to 130 days). Four treatment groups received diets including control diet only (Table 1),

low EPE (control diet+0.6 g/kg EPE), moderate EPE (control diet+0.9 g/kg EPE), and high EPE (control diet+1.2 g/kg EPE). The experimental design and procedures were approved by following the requirements of the Regulations for the Administration of Affairs Concerning Experimental Animals of China.

2.3. Experimental Basic Fodder and Management. Ingredients and nutrient compositions of the diets are shown in Table 1, and the diets were used throughout the whole experimental period. The chickens were raised in cages in a controlled environment and had free access to food and drinking water. The temperature in the house was 24~29°C, and the relative humidity was 60~78%. Pens were routinely disinfected to maintain appropriate standards of cleanliness. All animal procedures were conducted under the protocol (SCAU-AEC-2010-0416) approved by the Animal Ethics Committee of South China Agricultural University.

2.4. Sample Collection. After 40 days, 12 chickens were randomly selected from each treatment group (2 broiler chickens from each replication), and blood samples were drawn from the neck vein with a sterile syringe. The blood was centrifuged at 3000 × g for 15 min to obtain serum samples, and they were stored at -80°C until analysis. Chickens were then euthanized, and the whole breast muscle tissues were preserved in liquid nitrogen.

2.5. Antioxidant Activity in Serum and Muscle Tissue. About 0.25 g muscle tissue was mixed with 9 times (m/v) 0.9% physiological saline, and then, homogenized with a tissue grinder (Lawson, Japan) at 4°C. After being centrifuged for 10 min at 4000 r/min (Eppendorf, Germany), the supernatant was used for subsequent analysis. The activities of total superoxide dismutase (T-SOD, A001-1-2), GSH-Px (A005-1-2), total antioxidant capacity (T-AOC, A015-1-2), the contents of malondialdehyde (MDA, A003-1-2), and GSH (A061-1-1) in serum and breast muscle were determined spectrophotometrically using the commercial kits obtained from Nanjing

Jiancheng Institute of Bioengineering (Nanjing, Jiangsu, China) [22]. The quantities of T-SOD, GSH-Px, and T-AOC are expressed as units (U) per milligram of protein. The MDA and GSH content are expressed as nanomoles per milligram of protein and milligram per gram of protein, respectively.

2.6. Screening and Annotation of Differentially Expressed Genes (DEGs) in Muscle Induced by EPE Dietary Supplements in Chicken Based on RNA-Seq Techniques. Based on the evaluation of antioxidant activity in this study and a previous study [23], the moderate EPE treatment group tended to exhibit higher antioxidant effects compared with the other group. Therefore, breast muscles were obtained from the control group and the moderate EPE treatment group (0.9 g/kg) for transcriptome sequencing, with two replicates per group [24].

2.6.1. Total RNA Isolation, Labeling, and Sequencing. Total RNA was extracted from muscle samples. RNA concentration and purity were evaluated by Nanodrop 2000 (Thermo, USA), and RNA integrity was determined by 1% agarose gel electrophoresis. Then, mRNA was isolated from the total RNA using Oligo (dT) beads. Fragmentation buffer was used to randomly shear mRNA into 200 bp fragments. Using reverse transcriptase, random hexamers were added to synthesize a strand of cDNA from the mRNA template, followed by two-strand synthesis to form a stable double-stranded structure. The viscous end of the double-stranded cDNA structure was repaired using End Repair Mix (Enzymatics, USA), followed by the addition of an A base at the 3' end to form the Y-form linker. The final library was sequenced on an Illumina Hiseq (Hokkaido System Science, Sapporo, Japan) [25, 26].

2.6.2. Data Analysis and Bioinformatics of Genes. Chicken transcriptome sequencing was carried out using an Illumina sequencing platform (2 × 150 bp, 375 bp insert size). Quality control of the sequenced data was completed, and the transcriptome data were analyzed using an established bioinformatics method [27]. DEGs were calculated based on gene read count data by the edgeR software, and the screening criteria for DEGs were False discovery rate (FDR) < 0.05, *p* value < 0.05 and fold change (FC) > 2. Gene Ontology (GO) and Kyoto Encyclopedia of Genes and Genomes (KEGG) were used to annotate and enrich the DEGs.

2.7. Screening and Annotation of Differentially Expressed Proteins (DEPs) in Muscle Induced by EPE Dietary Supplements in Chicken Based on iTRAQ Techniques. The breast muscle was obtained from the control group and the moderate (0.9 g/kg) EPE group for proteomic analysis, with two replicates per group [28].

2.7.1. Two-Dimensional Fluorescence Difference Gel Electrophoresis. About 15 mg of breast muscle was manually ground with liquid nitrogen, and then, 8 M urea containing 1% sodium dodecyl sulfate (Sinopharm Chemical Reagent Co., Ltd, China) and protease inhibitor were added in a 1:5 ratio. The solution was placed on ice in an ultrasound wave

for 2 min and then centrifuged at 4°C for 20 min. The supernatant was taken to determine the protein concentration via gel electrophoresis. A 100 microgram aliquot of protein sample was dissolved with 100 μl 8 M urea containing 1% sodium dodecyl sulfate, and then, 10 mM TCEP solution (Thermo, USA) was added to the sample and incubated at 37°C for 60 min. 40 mM iodoacetamide (Sigma, USA) was then added, and the solution was incubated at room temperature for 40 min. Precooled acetone (Sinopharm Chemical Reagent Co., Ltd, China) was added in a 6:1 ratio (acetone:sample). Samples were precipitated at -20°C for 4 h, followed by centrifugation at 10000 g for 20 min. Then, samples were digested overnight at 37°C with 100 μL 100 mM triethylammonium bicarbonate buffer (TEAB, Sigma, USA), and trypsin was added according to a mass ratio of 1:25 (enzyme:protein) [29].

2.7.2. Identification of DEPs. Muscle was digested with trypsin, and the peptide was dried with a vacuum pump and redissolved with a 0.4 M TEAB solution. The iTRAQ reagent (AB Sciex, USA) was added per 100 μg of peptide, and samples were incubated for 2 h, followed by adding 50 μL ultrapure water and incubating for 30 min. Each group of labeled product was mixed and dried. The peptide samples were reconstituted with UPLC loading buffer and separated by C18 column during the pH liquid phase.

The first-dimensional separation was performed using Waters' ACQUITY UPLC BEH C18 column (3 mm × 150 mm, 1.7 μm, Waters, USA) with a flow rate of 400 μL/min. The detection wavelength was 214 nm. The labeled peptides were reconstituted in buffer A (2% acetonitrile, pH 10.0) and loaded onto the column. The peptides were then eluted at 37°C using gradient buffer B (80% acetonitrile, pH 10.0) in the following order: 0% in 2 min, 0~3.8% in 15 min, 3.8~24% in 18 min, 24~30% in 3 min, 30~43% in 1 min, 43~100% in 1 min, 100~0% in 6 min, and 0% keeping for 20 min.

The second-dimensional separation was performed using Liquid-mass spectrometry. The chromatographic instrument was EASY-nLC 1200 (75 μm × 25 cm, Thermo, USA), the mass spectrometer was Q-Exactive (Thermo, USA), and the data acquisition software was Thermo Xcalibur 4.0 (Thermo, USA). The samples were reconstituted in buffer A (2% acetonitrile with 0.1% formic acid) and loaded onto the column. The peptides were then eluted at 37°C using gradient buffer B (80% acetonitrile with 0.1% formic acid) in the following order: 0~5% in 1 min, 5~23% in 62 min, 23~48% in 25 min, 48~100% in 1 min, 100% keeping for 6 min, 100~0% in 5 min, and 0% keeping for 20 min. Mass spectrometry conditions were as follows: MS scan range (*m/z*) 350-1300, acquisition mode DDA; Top 20 (select the strongest signal in the parent ion 20 for secondary fragmentation); first-order mass spectrometry resolution of 70000, fragmentation HCD; Resolution 17500, dynamic exclusion time 18 s.

2.7.3. Bioinformatic Analysis of Proteins. The GO analysis and the KEGG pathways analysis were implemented in

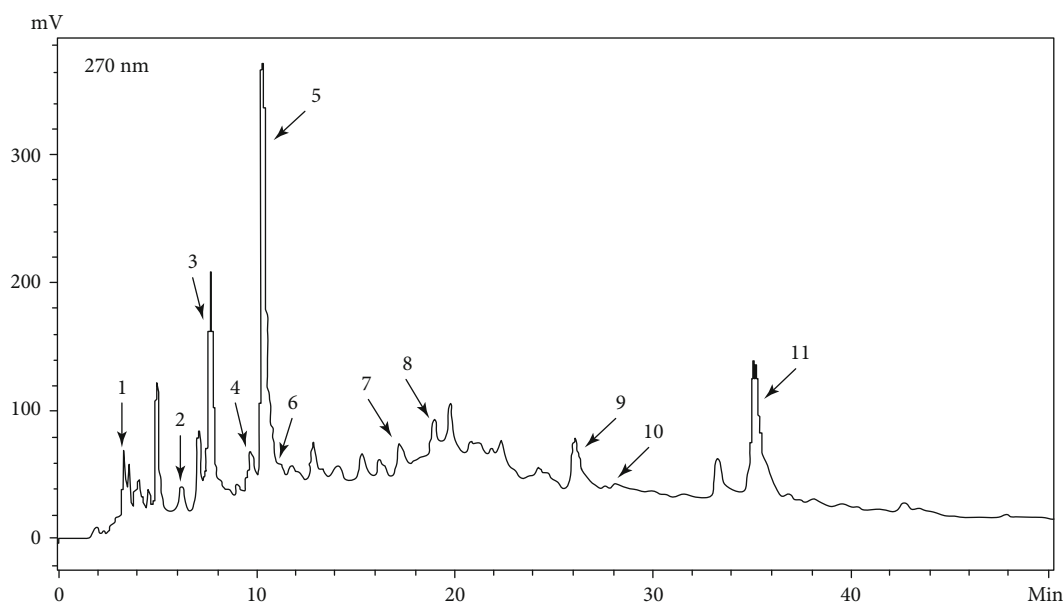


FIGURE 1: High-performance liquid chromatography of EPE. Note: 1 Gemin D; 2, 4 Pedunculagin; 3 Gallic acid; 5 Oenothlein B; 6,7 TellimagrandinI; 8 Chlorogenic acid; 9 Ethyl gallate; 10 1,2,3,4,6-*O*-pentagalloylglucose; 11 Hyperoside.

TABLE 2: Effect of EPE dietary supplements on antioxidant capacity of serum ($n = 12$).

Item	Control group	0.6 g/kg EPE group	0.9 g/kg EPE group	1.2 g/kg EPE group
T-SOD (U/mgprot)	69.03 ± 1.43	69.23 ± 1.63	70.99 ± 1.96	69.48 ± 1.70
T-AOC (U/mgprot)	11.43 ± 0.66	11.44 ± 0.57	11.56 ± 0.46	11.81 ± 0.63
GSH-Px (U/mgprot)	775.61 ± 45.28	803.12 ± 38.08	815.64 ± 25.76	882.27 ± 57.32
MDA (nmol/mL)	2.45 ± 0.20	2.13 ± 0.28	1.96 ± 0.25	2.12 ± 0.21

TABLE 3: Effect of EPE dietary supplements on antioxidant capacity of breast muscle ($n = 12$).

Item	Control group	0.6 g/kg EPE group	0.9 g/kg EPE group	1.2 g/kg EPE group
T-SOD (U/mgprot)	28.31 ± 5.60	27.48 ± 5.63	33.39 ± 7.82	30.12 ± 4.41
T-AOC (U/mgprot)	7.43 ± 0.81	7.42 ± 1.45	8.39 ± 0.98	8.96 ± 1.75
GSH-Px (U/mgprot)	127.77 ± 24.61 ^b	133.64 ± 30.06 ^{ab}	184.63 ± 38.69 ^a	159.26 ± 33.58 ^{ab}
GSH (mg/gprot)	3.47 ± 0.25 ^b	3.73 ± 0.21 ^{ab}	4.28 ± 0.31 ^a	4.19 ± 0.13 ^a
MDA (nmol/mgprot)	13.74 ± 1.79 ^b	11.26 ± 0.93 ^{ab}	10.25 ± 1.81 ^a	11.65 ± 1.50 ^{ab}

^{a-b}Means within a row with different superscripts differ significantly ($p < 0.05$).

KOBAS [30], and significance was evaluated using Fisher's exact test.

2.8. Statistical Analysis. Data were analyzed by one-way ANOVA (SPSS, 2010). Differences among treatment groups were evaluated using Duncan's multiple range tests, with a significance threshold of $p < 0.05$.

3. Results

3.1. Quality of EPE. According to the Folin-reagent method described by Wang et al. (Gallic acid as the equivalent polyphenol) [21], the total polyphenols content in EPE was 317.08 ± 16.49 mg/g. Further, HPLC of EPE (Figure 1) indicated that the main active substance was of comparable qual-

ity to the EPE reported in our previous research, based on the standard substance retention time [23].

3.2. Variation of Antioxidant Capacity in Serum. As shown in Table 2, the concentrations of GSH-Px, T-SOD, T-AOC, and MDA in serum were not significantly different among the treatment groups ($p > 0.05$). Compared with the control group, the T-SOD activity and T-AOC increased in the EPE treatment groups, and the GSH-Px activity in the moderate EPE group increased (0.9 g/kg) by 13.8% ($p > 0.05$).

3.3. Variation of Antioxidant Capacity in Muscle Tissue. As shown in Table 3, the T-SOD activity and T-AOC of the breast muscle in the moderate EPE (0.9 g/kg) and high EPE (1.2 g/kg) groups showed an increasing trend compared to

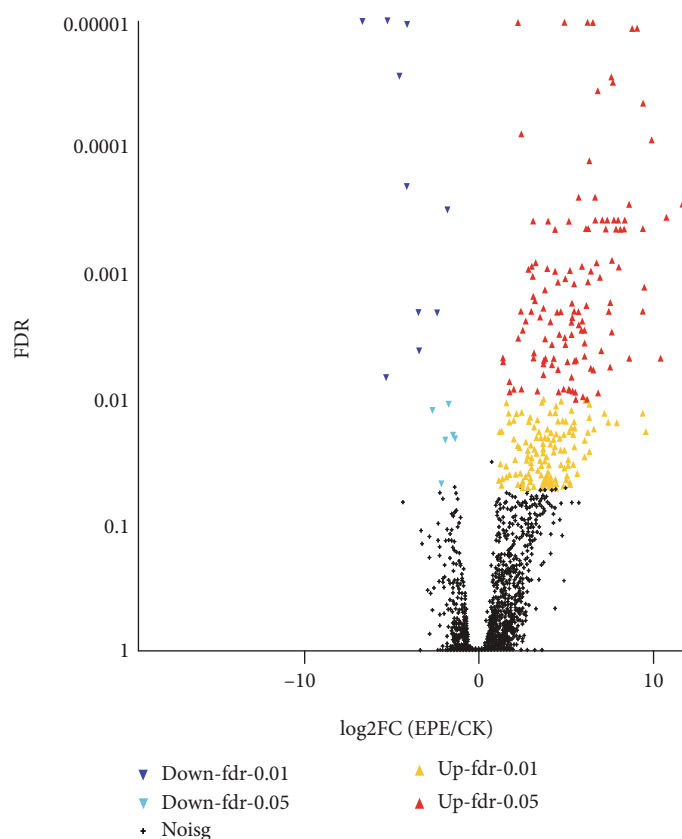


FIGURE 2: Volcano plots of DEGs. Note: differentially expressed genes (DEGs). The abscissa is the fold change of the gene's expression difference. The ordinate is the statistical test value of the difference in the amount of gene arrival, and the higher the p value, the more significant the difference in expression. Red dots indicate significantly upregulated genes, blue dots indicate significantly down-regulated genes, and black dots are nonsignificant differentially expressed genes.

the control group ($p > 0.05$). The GSH-Px activity of the breast muscle tissue in the moderate (0.9 g/kg) EPE group was 44.5%, higher than that of the control group ($p < 0.05$), and there was an upward trend in the low (0.6 g/kg) and high (1.2 g/kg) EPE groups ($p > 0.05$). The GSH content of breast muscle in the moderate and high EPE groups increased by 23.3% and 20.7% compared with the control group ($p < 0.05$). Additionally, MDA content in the breast muscle of the moderate (0.9 g/kg) EPE group was reduced by 25.4% ($p < 0.05$), though the other two groups did not show a significant change ($p > 0.05$).

3.4. Screening and Annotation of DEGs in Muscle Induced by EPE Dietary Supplements in Chicken Based on RNA-Seq Techniques. To ensure high quality data, raw sequencing reads were filtered based on coverage, sequence saturation, the redundant distribution frequency map, and the distribution of sequencing reads across the chromosomes. A total of 14621 genes were identified as differentially regulated, of which 289 were significantly different between the EPE treatment group and the control group. The overall distribution of gene expression differences was visualized by a volcanic map (Figure 2).

3.4.1. Gene Ontology Enrichment Analysis of the DEGs. Gene Ontology (GO) enrichment analysis was used to annotate

these DEGs by biological process, cellular component, and molecular function (Figure 3). Overall, 47 different biological processes were enriched, including oxygen transport, oxidation-reduction, aminophospholipid transport, phospholipid translocation, and lipid translocation. Cellular component analysis revealed that the apical plasma membrane, membrane region, membrane part, cellular component, integral component of membrane, plasma membrane region, brush border, hemoglobin complex, and substrate-specific transporter activity were significantly enriched. Additionally, oxygen binding, oxygen transporter activity, phospholipid-translocating ATPase activity, and other 22 molecular function items were identified by the molecular function analysis.

Based on the above GO enrichment analysis, glutathione metabolic process (biological process), glutathione transferase activity (molecular function), and peroxisome (cellular component) were the enriched GO terms most clearly associated with antioxidant capacity (Table 4). Overall, 4 antioxidant genes (gamma-glutamyltransferase 1, GGT1; microsomal glutathione S-transferase 1, MGST1; glutathione S-transferase alpha 4, GSTA4L; and glutathione S-transferase class-alpha, GSTAL1) in the EPE group were substantially enhanced in glutathione metabolic process relative to the control group. Similarly, three of these genes (MGST1, GSTA4L, and GSTAL1) were also associated with glutathione metabolic process and glutathione transferase activity, which play an

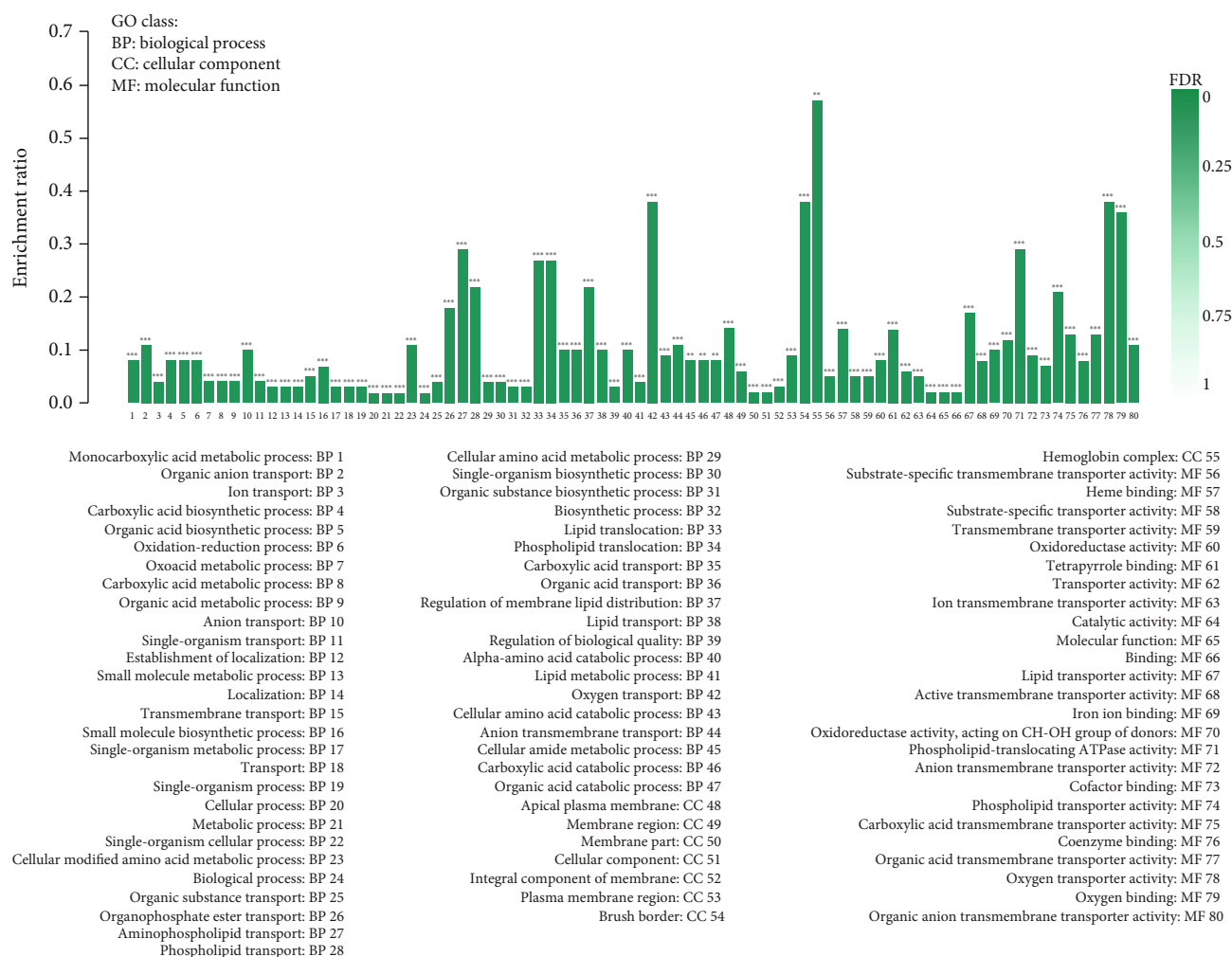


FIGURE 3: GO enrichment histogram for DEGs. Note: differentially expressed genes (DEGs). Each column in the figure is a GO term, and the abscissa text indicates the name and classification of the GO term. The height of the column, that is, the ordinate, indicates the enrichment rate. The color indicates the significance of enrichment, that is, FDR. The darker the color, the more significant the enrichment of the GO term, wherein the mark with FDR < 0.001 is ***, the mark with FDR < 0.01 is **, and the mark with FDR < 0.05 is *, the right color gradient indicates the FDR size.

important role in muscle antioxidant activity. Additionally, hydroxyacid oxidase 1 (HAO1), hydroxyacid oxidase 2 (HAO2), and bile acid-CoA: amino acid N-acyltransferase (BAAT) are peroxisome genes known to be involved in the oxidation of fatty acids, regulation of oxygen concentration, and decomposition of hydrogen peroxide to improve the antioxidant status in breast muscle.

3.4.2. Kyoto Encyclopedia of Genes and Genomes (KEGG) Analysis of the DEGs. DEGs were enriched in 148 pathways in the KEGG enrichment analysis, and 38 KEGG pathways were identified to have significant changes. Based on the previous analysis of physiological indicators, the peroxisomes and the glutathione metabolism pathway were selected for further evaluation of the antioxidant capacity of the muscle by KEGG enrichment metabolic pathway analysis. Significant DEGs that were enriched in the peroxisomes and glutathione metabolism pathway showed some overlap with the genes related to antioxidant status identified by the GO

enrichment analysis, including HAO1, HAO2, and GGT1 (Table 5).

3.5. Screening and Annotation of DEPs in Muscle Induced by EPE Dietary Supplements in Chicken Based on iTRAQ Techniques

3.5.1. Identification and GO Analysis of DEPs Induced by EPE. The total number of tested proteins was 1430, and there were 149 protein differences between the EPE group and the control group. According to the standard of differential protein screening, there were 14 significant differences in protein concentration (>1.2-fold change, $p < 0.05$), 10 of which were upregulated and 4 were downregulated (Table 6). These proteins were annotated (cellular components, molecular functions, and biological processes) by GO enrichment analysis (Figure 4). Biological process analysis revealed that most proteins were associated with 31 different GO terms, including p53 class mediator, threonyl-tRNA aminoacylation, and

TABLE 4: GO enrichment analysis for DEGs related antioxidant capacity.

GO id	Description of GO enrichment	Seq id	<i>p</i> value	Regulate	Description	Symbol name
GO:0006749	Glutathione metabolic process	ENSGALG00000006565	<0.01	Up	Gamma-glutamyltransferase 1	GGT1
		ENSGALG00000013098	<0.01	Up	Microsomal glutathione S-transferase 1	MGST1
GO:0006749/GO:0016705	Glutathione metabolic process/glutathione transferase activity	ENSGALG00000016324	<0.01	Up	Glutathione S-transferase alpha 4-like	GSTA4L
		ENSGALG00000038652	<0.01	Up	Glutathione S-transferase class-alpha-like 1	GSTAL1
		ENSGALG00000008845	<0.01	Up	Hydroxyacid oxidase 1	HAO1
GO:0005777	Peroxisome	ENSGALG00000014766	<0.01	Up	Hydroxyacid oxidase 2	HAO2
		ENSGALG00000040619	<0.01	Up	Bile acid-CoA: amino acid N-acyltransferase	BAAT

Note: differentially expressed genes (DEGs). The screening criteria for significantly GO enrichment analysis were $p < 0.05$.

TABLE 5: KEGG enrichment pathways for DEGs associated with antioxidant capacity.

Name of KEGG pathway	KEGG ID	Number of different gene	<i>p</i> value	Description	Symbol name
Peroxisome	ko04146	6	<0.01	Solute carrier family 27 member 5, alanine-glyoxylate and serine-pyruvate aminotransferase, Peroxisomal sarcosine oxidase, hydroxyacid oxidase 1, hydroxyacid oxidase 2, bile acid-CoA: amino acid N-acyltransferase	SLC27A5, AGXT, PIPOX, HAO1, HAO2, BAAT
Glutathione metabolism	ko00480	4	<0.05	Gamma-glutamyltranspeptidase 1, microsomal glutathione S-transferase 1, glutathione S-transferase class-alpha, glutathione S-transferase alpha 4	GGT1, MGST1, GSTAL1, GSTA4L

Note: differentially expressed genes (DEGs). The screening criteria for significantly KEGG enrichment pathways were $p < 0.05$. Hydroxyacid oxidase 1 (HAO1); hydroxyacid oxidase 2 (HAO2); bile acid-CoA: amino acid N-acyltransferase (BAAT); microsomal glutathione S-transferase 1 (MGST1); glutathione S-transferase class-alpha (GSTAL1); glutathione S-transferase alpha 4 (GSTA4L).

regulation of DNA damage checkpoint. When DEPs were annotated by the cell components, significantly enriched terms included chylomicron, plasma lipoprotein particle, very-lower-density lipoprotein particle, triglyceride-rich lipoprotein particle, protein-lipid complex, and five other cellular components terms. A total of five DEPs were annotated by molecular function, and there was significant enrichment of nineteen GO terms, including threonine-tRNA ligase activity, nutrient reservoir activity, p53 binding, and glutathione transferase activity.

3.5.2. KEGG Pathway Analysis of the DEPs. DEPs were analyzed by KEGG pathway analysis and the results indicated that cytochrome b-c1 complex subunit Rieske (Q5ZLR5), A0A0A0MQ61, and F1P372 were main proteins associated with oxidative phosphorylation, glutathione metabolism, aminoacyl-tRNA biosynthesis, metabolism of xenobiotics by cytochrome P450, etc. (Table 7).

3.6. Combined Analysis of Transcriptomics and Proteomics. All proteins and their associated transcripts in both the transcriptomic and proteomic analyses were classified into nine categories (Figure 5). Of the 61 proteins and genes that were upregulated in the EPE group, the A0A0A0MQ61 protein

and the glutathione S-transferase alpha-like 2 gene (GSTAL2) played a crucial role in enhancing antioxidant status. The glutathione metabolism in the transcriptomic analysis indicated that GGT1, MGST1, and GSTA4L were downstream genes regulated by glutathione, which correspond to the observed increase in GSH-Px activity in muscle tissue induced by EPE supplements. Accordingly, A0A0A0MQ61, the protein product of the glutathione S-transferase gene, was substantially upregulated in glutathione metabolism, which was in line with the expression of GGT1, MGST1, and GSTA4L (Figure 6). Therefore, EPE may enhance the antioxidant status of chicken by improving the activity of specific antioxidant proteins.

4. Discussion

Phylogenetic feed additives have been gaining attention in improving the health status of the flocks [31, 32]. Our previous study revealed that diet with polyphenols obtained from eucalyptus leaves exhibited a positive effect on growth performance in laying hens [23]. In the present study, different concentrations of EPE in chicken diet did not exhibit significant positive or negative effect on chicken performance, including average daily gain, average daily feed take, and feed conversion rate

TABLE 6: Significantly DEPs in the proteomics analysis.

Proteins	Description	Fold change	p value	Regulate
Q7LZS1	12K serum protein, beta-2-m cross-reactive (fragment)	0.71	0.04	Down
A0A1D5NXR4	Uncharacterized protein	0.34	0.003	Down
F1P372	Uncharacterized protein	1.24	0.03	Up
F1NG89	Ubiquitin carboxyl-terminal hydrolase 10	1.20	0.02	Up
A0A1D5PFH3	Uncharacterized protein	1.28	0.02	Up
F1NHM9	Phosphoglycerate mutase	0.82	0.02	Down
E1C4V1	ATP synthase-coupling factor 6, mitochondrial	1.20	0.02	Up
A0A0A0MQ61	Uncharacterized protein	1.48	0.03	Up
A7UEB0	Alpha-1-acid glycoprotein	0.69	0.01	Down
Q5ZLR5	Cytochrome b-c1 complex subunit Rieske, mitochondrial	1.25	0.01	Up
P02659	Apovitellenin-1	1.41	0.002	Up
Q5ZHZ0	Spliceosome RNA helicase DDX39B	1.21	0.05	Up
Q91968	Alpha-tropomyosin	1.49	0.04	Up
A0A1D5NZ55	Uncharacterized protein	1.30	0.05	Up

Note: differentially expressed proteins (DEPs). The screening criteria for significantly differentially expressed proteins were $p < 0.05$ and ($FC < 0.83$ or $FC > 1.20$).

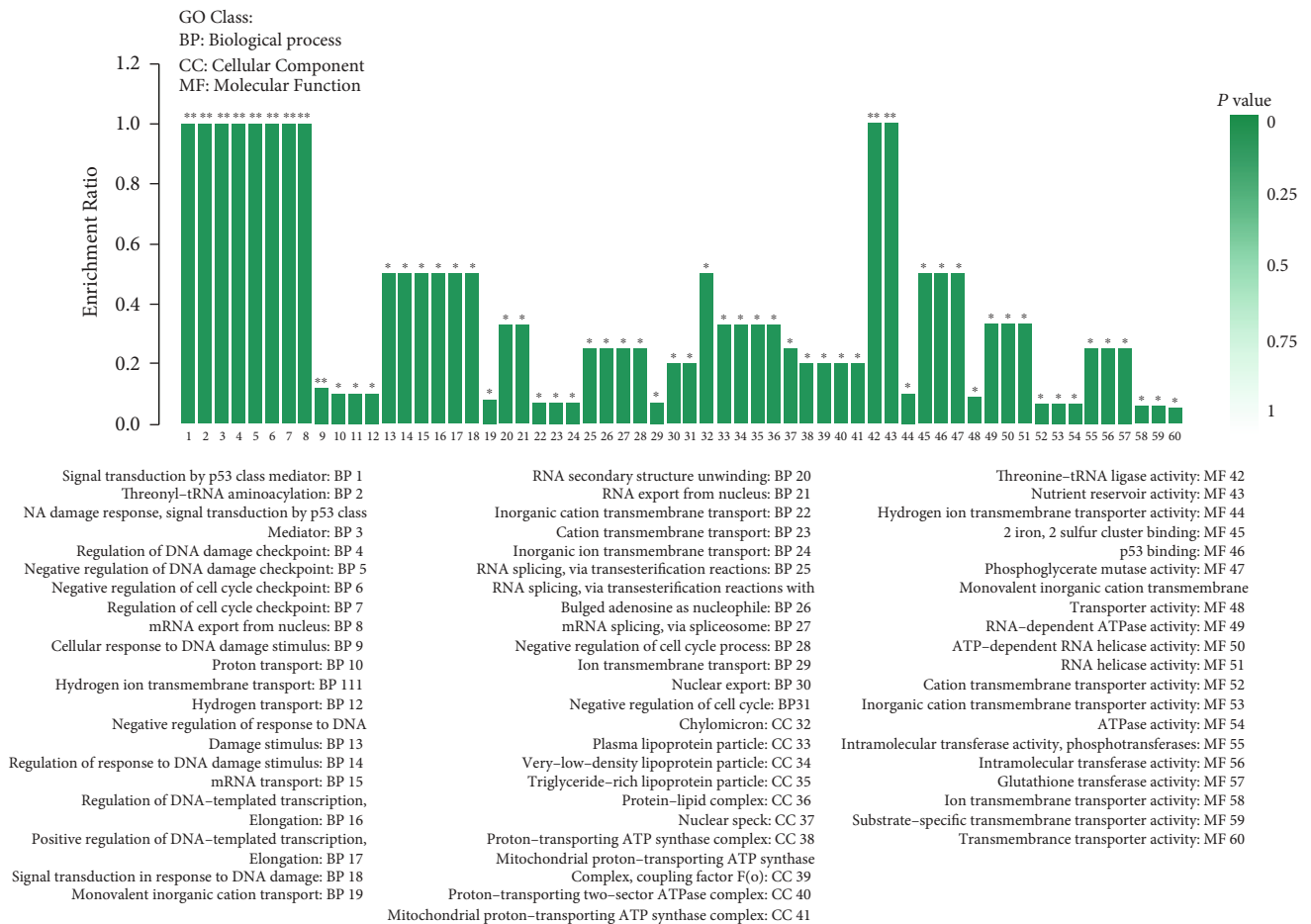


FIGURE 4: GO enrichment histogram for DEPs. Note: differentially expressed proteins (DEPs). Each column in the figure is a GO term, and the abscissa text indicates the name and classification of the GO. The height of the column, that is, the ordinate, indicates the enrichment rate. The color indicates the significance of enrichment, that is, FDR. The darker the color, the more significant the enrichment of the GO term, wherein the mark with $FDR < 0.001$ is ***, the mark with $FDR < 0.01$ is **, and the mark with $FDR < 0.05$ is *, the right color gradient indicates the FDR size.

TABLE 7: KEGG enrichment pathways for DEPs.

Pathway	Pathway definition	Number of proteins	Proteins
ko00190	Oxidative phosphorylation	1	
ko01100	Metabolic pathways	1	
ko04260	Cardiac muscle contraction	1	
ko04932	Nonalcoholic fatty liver disease (NAFLD)	1	Q5ZLR5 (connectin/fragment)
ko05010	Alzheimer's disease	1	
ko05012	Parkinson's disease	1	
ko05016	Huntington's disease	1	
ko00480	Glutathione metabolism	1	
ko05204	Chemical carcinogenesis	1	
ko00980	Metabolism of xenobiotics by cytochrome P450	1	A0A0A0MQ61 (uncharacterized protein)
ko00982	Drug metabolism-cytochrome P450	1	
ko00970	Aminoacyl-tRNA biosynthesis	1	F1P372 (uncharacterized protein)

Note: differentially expressed proteins (DEPs). Q5ZLR5 (cytochrome b-c1 complex subunit Rieske, mitochondrial), A0A0A0MQ61 (uncharacterized protein), F1P372 (uncharacterized protein).

(data not shown), which is in agreement with the report of Sedaghat and Torshizi [33], and might be due to that the chickens were in the adulthood.

Recently, natural polyphenols used in animal diets have been reported to build an integrated antioxidant system to prevent from damage led by free radicals [34–37]. This antioxidant capacity is assumed to result from the free radical-scavenging properties of phenolic compounds [38–40]. Our previous study reported that EPE effectively scavenged DPPH• and ABTS• free radicals *in vitro* [21]. In the present study, the antioxidant effects in serum were not obviously affected by the EPE supplement. However, an increasing trend in GSH-Px was observed with a higher concentration of the EPE diet, whereas the MDA content showed the opposite effects. This result was supported by the previous report that diet with 0.8 g/kg polyphenols from eucalyptus leaves increased the GSH-Px activity in serum of laying hen and an insignificant decrease in MDA was observed in quails supplement with eucalyptus leaves [23, 31]. Interestingly, our study revealed that EPE dietary supplements significantly improved GSH-Px activity and GSH content and decreased MDA content in breast muscle tissues. Higher concentration of the EPE diet led to higher GSH-Px activity, which is consistent with the report by Fathi et al. [31]. Similarly, MDA content can reflect the degree of lipid peroxidation; thereby, indirectly reflect cell damage and freshness of meat [41]. In agreement with our results, a diet with green tea extract led to a remarkably decreasing MDA content in meat tissue [42]. Polyphenols might be accumulated to exhibit antioxidant effects in meat tissues [35]. To explain the antioxidant capacity of polyphenols, it is crucial to understand how they are absorbed, metabolized, and eliminated from the body. It is stated that the intestinal utilization of polyphenols depended on their degree of polymerization and galloylation [43]. Monomeric and some oligomeric polyphenols tended to be easily absorbed at small intestine compared with the polymeric forms of polyphenols [44]. This suggested that monomeric and some oligomeric polyphenols in EPE, such as gallic acid, pedunculagin, hyperoside, and other com-

pounds, could be absorbed and functioned as an antioxidant in chickens. This hypothesis was supported by Chamorro et al. that monomeric (catechin, epicatechin, gallic acid, and epicatechin-O-gallate) and dimeric (procyanidin B1 and procyanidin B2) catechins in grape pomace were easily digested and absorbed in chickens [45]. Overall, EPE dietary supplements are able to improve the antioxidant capacity of chicken.

The results of the transcriptomic analysis indicated that glutathione transferase activity, glutathione metabolic process, and the peroxisome were the three GO enrichment terms related to antioxidant activity. That is, several significantly upregulated antioxidant genes, such as GGT1, MGST1, GSTA4L, HAO1, and HAO2, are all believed to improve antioxidant status. Moreover, previous research indicated that GGT1 and PGDS play an important role in the synthesis of glutathione, and its upregulation exerts a prooxidant action [46]. Shinno et al. [47] reported that microsomal glutathione S-transferase 1 (MGST1) could be activated by gallic acid to protect the membrane against damage caused by oxidative stress. These results suggested that these antioxidant genes were vital to improve antioxidant status in chicken. Likewise, the KEGG pathway enrichment analysis also indicated that the peroxisomes and the glutathione metabolism pathway were the two crucial antioxidant pathways. Peroxisomes are rich in enzymes, mainly including oxidases, catalase, and peroxidase. Catalase, in particular, is known to protect cells by hydrolyzing the hydrogen peroxide generated in redox reactions [48, 49]. Additionally, several differentially expressed antioxidant-related genes were significantly enriched in the glutathione metabolism pathway, and the content of glutathione may be altered in cells as a result of EPE supplements. Glutathione is known to effectively scavenge free radicals and other reactive oxygen species, and it can be oxidized to form GSSG [50, 51]. In this study, significantly improved GSH-Px converted GSSG into GSH to enhance antioxidant status. In addition, SOD and APOA4 genes were notably identified to be upregulated in this study, though the protein products

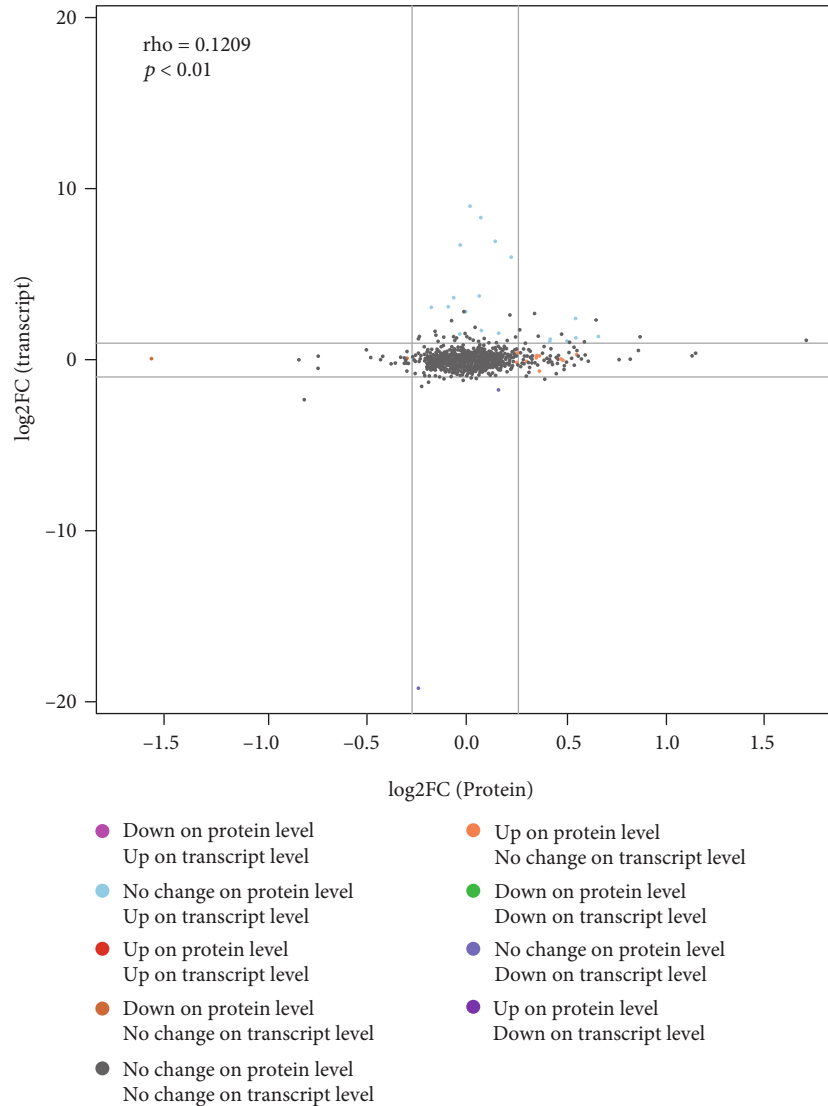


FIGURE 5: A scatter plots of the expression levels of all proteins and their associated transcripts in both groups. Note: the abscissa in the figure indicates the difference in the expression of the protein in the EPE treatment group and the control group, and the ordinate indicates the difference in the FPKM value of the corresponding transcript in the experimental group and the control group. Each point represents a protein and its associated transcript; in the upper left corner, rho represents the Pearson's correlation coefficient between the two omics, p represents the correlation test p value; when $\rho > 0$, it is called positive correlation; When $\rho < 0$, it is called negative correlation; when $\rho = 0$, it is called zero correlation, that is, there is no correlation; the larger the $|\rho|$, the greater the correlation between the two omics.

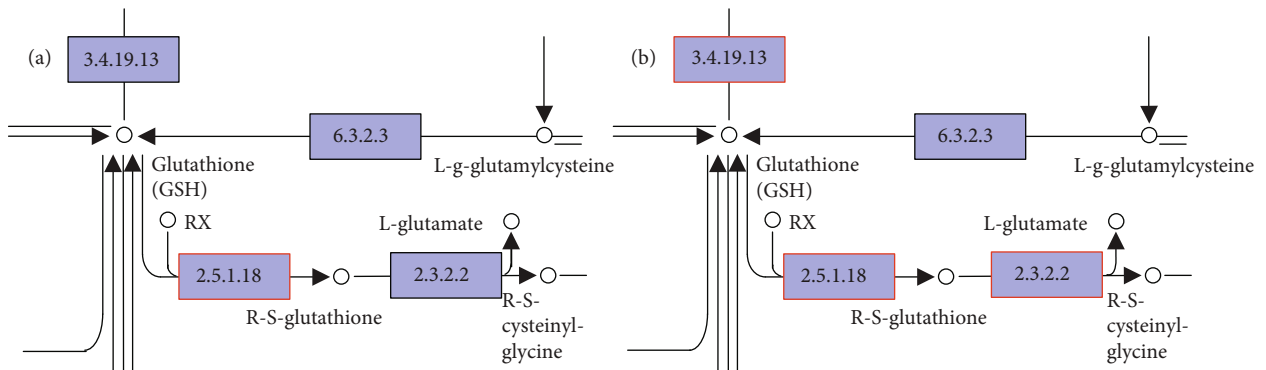


FIGURE 6: Upregulated protein in the proteome (a) and genes in the transcriptome (b) in glutathione metabolism. Note: the genes with red borders in the figure belong to the DEGs or DEPs detected by this sequencing, in which red represents the upregulated gene.

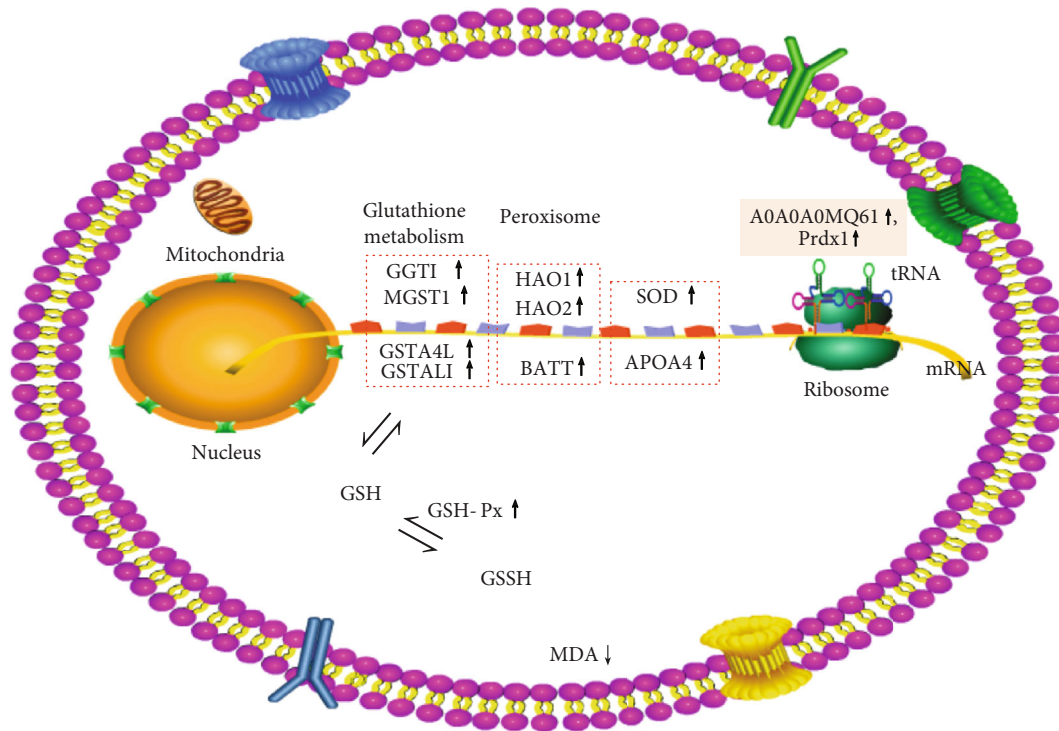


FIGURE 7: Potential antioxidant mechanism in muscle regulated by EPE.

remained unchanged. They may also contribute to the antioxidation of muscle, given the known functions of SOD and the known APOA4 [52]. In the present study, the gene expression variation of superoxide dismutase was consistent with the increasing trend of SOD enzyme activity in the breast muscle in the moderate (0.9 g/kg) EPE treatment groups compared to the control group. This result suggests that EPE improved the activity of SOD, but supplementation with EPE over a long period of time or an increased dose of EPE in chicken feed also substantially impacted the animal's antioxidant capacity. Previous research indicated that the expressions of GST, Prdx6, PPIA, alfatoin aldehyde reductase, and SOD regulated by albumin B were enhanced to activate the systemic antioxidant defense [16], and SOD, catalase (CAT), GST, and GSH-Px were considered as AOE to protect against oxidative stress [53]. Overall, the functions of these upregulated genes were highly correlated with antioxidant status and could be linked to the improvement of antioxidant capacity induced by EPE supplements.

Many previous studies reported that glutathione is associated with glutathione metabolism pathways and that it likely functions as a reducing milieu to improve antioxidant function in cells [54]. As such, the results of the proteomic analysis indicated that antioxidant-related glutathione transferase activity was significantly increased in response to EPE supplements. The corresponding protein was a kind of glutathione S-transferase (A0A0A0MQ61, EC2.5.1.18) that is known to function in glutathione metabolism in *Gallus gallus*. Additionally, A0A0A0MQ61, an antioxidant protein, was significantly increased as a result of EPE dietary supple-

ments. Further, the upregulated peroxiredoxin-1 protein in the peroxisome metabolic pathway is a known redox-regulating protein and is considered to be an antioxidant enzyme to eliminate various ROS [55]. Based on the above analyses, the antioxidant mechanism of muscle tissue in chicken treated with EPE dietary supplements is inferred and given in Figure 7. As shown, EPE treatments significantly improved GSH-Px activity and decreased MDA content of the breast muscle. Transcriptomic and proteomic analyses revealed that nine candidate genes and two candidate proteins were identified, which are responsible for improving antioxidant status induced by EPE supplements. Overall, this study promotes the understanding of the antioxidant mechanism in chicken regulated by EPE treatment.

5. Conclusion

Overall, EPE dietary supplements appeared to improve the antioxidant status of chicken by enhancing GSH-Px activity and reducing MDA content in muscle tissues. Glutathione metabolism and the peroxisome were considered the key metabolic pathways underlying the upregulation of AOE. Furthermore, all of the changes induced by EPE supplements may contribute to the systemic antioxidant defense of chicken, and these altered proteins and genes should be further explored in the future.

Abbreviations

EPE: Eucalyptus leaf polyphenols extract
GSH-Px: Glutathione peroxidase

MDA: Malonaldehyde
 T-SOD: Total superoxide dismutase
 T-AOC: Total antioxidant capacity
 DEGs: Differentially expressed genes
 DEPs: Differentially expressed proteins
 GO: Gene Ontology
 KEGG: Kyoto Encyclopedia of Genes and Genomes
 GGT1: Gamma-glutamyltransferase 1
 MGST1: Microsomal glutathione S-transferase 1
 GSTA4L: Glutathione S-transferase alpha 4
 GSTAL1: Glutathione S-transferase class-alpha
 HAO1: Hydroxyacid oxidase 1
 HAO2: Hydroxyacid oxidase 2
 BAAT: Bile acid-CoA: amino acid N-acyltransferase
 SLC27A5: Solute carrier family 27 member 5
 AGXT: Alanine-glyoxylate and serine-pyruvate aminotransferase
 PIPOX: Peroxisomal sarcosine oxidase
 GGT1: Gamma-glutamyltranspeptidase 1
 ROS: Reactive oxygen species
 GSH: Glutathione
 CAT: Catalase
 GST: Glutathione-S-transferase
 GPX: Glutathione peroxidase
 AOE: Antioxidant enzymes.

Data Availability

The data used to support the findings of this study are included within the article and the supplementary information file.

Conflicts of Interest

The authors declare no conflicts of interest.

Authors' Contributions

Wei Li conceptualized, did the methodology, and wrote the original draft. Ze-Qi He did the methodology and resources. Xiao-Ying Zhang conceptualized and did the methodology. Yun-Jiao Chen did the resources, wrote the review, and edited. Jian-Jun Zuo wrote the review and edited. Yong Cao supervised, wrote the review, and edited.

Acknowledgments

This work was supported by the National Key R&D Program of China (2016YFD0600806), the Guangdong Modern Agricultural Industry Technology System Innovation Team Project (2019KJ117), and the National Natural Science Foundation of China (31700501) for their financial support.

References



- [1] L. Harkat-Madouri, B. Asma, K. Madani et al., "Chemical composition, antibacterial and antioxidant activities of essential oil of Eucalyptus globulus from Algeria," *Industrial Crops and Products*, vol. 78, pp. 148–153, 2015.
- [2] N. L. Poersch, L. R. T. F. Filho, E. P. Miguel, G. H. M. d. Cruz, K. L. Francisquette, and S. B. Cavalheiro, "Influence of climate variables in the initial growth of *Corymbia citriodora* and different species of *Eucalyptus*," *Bioscience Journal*, vol. 33, no. 6, pp. 1452–1464, 2017.
- [3] B. Engler, G. Becker, and S. Hoffmann, "Process mechanization models for improved *Eucalyptus* plantation management in Southern China based on the analysis of currently applied semi-mechanized harvesting operations," *Biomass and Bioenergy*, vol. 87, pp. 96–106, 2016.
- [4] H. Tolba, H. Moghrani, A. Benelmouffok, D. Kellou, and R. Maachi, "Essential oil of Algerian *Eucalyptus citriodora*: chemical composition, antifungal activity," *Journal de Mycologie Médicale/Journal of Medical Mycology*, vol. 25, no. 4, pp. e128–e133, 2015.
- [5] L. W. Zhu, P. Zhao, Q. Wang et al., "Stomatal and hydraulic conductance and water use in a eucalypt plantation in Guangxi, Southern China," *Agricultural and Forest Meteorology*, vol. 202, pp. 61–68, 2015.
- [6] A. A. Anigboro, O. J. Avwioroko, and C. O. Cholu, "Phytochemical constituents, antimalarial efficacy, and protective effect of *Eucalyptus camaldulensis* aqueous leaf extract in *Plasmodium berghei*-infected mice," *Preventive Nutrition and Food Science*, vol. 25, no. 1, pp. 58–64, 2020.
- [7] Y. Chen, J. Wang, Y. Ou et al., "Cellular antioxidant activities of polyphenols isolated from *Eucalyptus* leaves (*Eucalyptus grandis* × *Eucalyptus urophylla* GL9)," *Journal of Functional Foods*, vol. 7, pp. 737–745, 2014.
- [8] K. Sebei, F. Sakouhi, W. Herchi, M. L. Khouja, and S. Boukhchina, "Chemical composition and antibacterial activities of seven *Eucalyptus* species essential oils leaves," *Biological Research*, vol. 48, no. 1, p. 7, 2015.
- [9] B. Gullón, A. Muñiz-Mouro, T. A. Lú-Chau, M. T. Moreira, J. M. Lema, and G. Eibes, "Green approaches for the extraction of antioxidants from eucalyptus leaves," *Industrial Crops and Products*, vol. 138, p. 111473, 2019.
- [10] E. González-Burgos, M. Liaudanskas, J. Viškelis, V. Žvikas, V. Janulis, and M. P. Gómez-Serranillos, "Antioxidant activity, neuroprotective properties and bioactive constituents analysis of varying polarity extracts from *Eucalyptus globulus* leaves," *Journal of Food and Drug Analysis*, vol. 26, no. 4, pp. 1293–1302, 2018.
- [11] Y. Vitta, M. Figueroa, M. Calderon, and C. Ciangherotti, "Synthesis of iron nanoparticles from aqueous extract of *Eucalyptus robusta* Sm and evaluation of antioxidant and antimicrobial activity," *Materials Science for Energy Technologies*, vol. 3, pp. 97–103, 2020.
- [12] Z. Pan, Y. Zeng, J. An, J. Ye, Q. Xu, and X. Deng, "An integrative analysis of transcriptome and proteome provides new insights into carotenoid biosynthesis and regulation in sweet orange fruits," *Journal of Proteomics*, vol. 75, no. 9, pp. 2670–2684, 2012.
- [13] C. Zhang, Y. Wei, D. Xiao et al., "Transcriptomic and proteomic analyses provide new insights into the regulation mechanism of low-temperature-induced leafy head formation in Chinese cabbage," *Journal of proteomics*, vol. 144, pp. 1–10, 2016.
- [14] J. Zhang, S. Wang, S. Song, F. Xu, Y. Pan, and H. Wang, "Transcriptomic and proteomic analyses reveal new insight into chlorophyll synthesis and chloroplast structure of maize leaves under zinc deficiency stress," *Journal of Proteomics*, vol. 199, pp. 123–134, 2019.

- [15] J. Soewarto, C. Hamelin, S. Bocs et al., "Transcriptome data from three endemic Myrtaceae species from New Caledonia displaying contrasting responses to myrtle rust (*Austropuccinia psidii*)," *Data in Brief*, vol. 22, pp. 794–811, 2019.
- [16] H.-T. Wang, Y.-H. Li, I.-P. Chou, Y.-H. Hsieh, B.-J. Chen, and C.-Y. Chen, "Albusin B modulates lipid metabolism and increases antioxidant defense in broiler chickens by a proteomic approach," *Journal of the Science of Food and Agriculture*, vol. 93, no. 2, pp. 284–292, 2013.
- [17] W. Li, X. Zhang, Z. He et al., "In vitro and in vivo antioxidant activity of eucalyptus leaf polyphenols extract and its effect on chicken meat quality and cecum microbiota," *Food Research International*, vol. 136, p. 109302, 2020.
- [18] M. Fathi, M. Abdelsalam, I. Al-Homidan et al., "Supplemental effects of eucalyptus (*Eucalyptus camaldulensis*) leaves on growth performance, carcass characteristics, blood biochemistry and immune response of growing rabbits," *Annals of Animal Science*, vol. 19, no. 3, pp. 779–791, 2019.
- [19] H. Mashayekhi, M. Mazhari, and O. Esmaeilipour, "Eucalyptus leaves powder, antibiotic and probiotic addition to broiler diets: effect on growth performance, immune response, blood components and carcass traits," *Animal*, vol. 12, no. 10, pp. 2049–2055, 2018.
- [20] N. T. S. A. Salman and J. K. M. Al-Gharawi, "Effect of eucalyptus of leaves water extract on some productive trait of broilers," *Plant archives*, vol. 19, pp. 920–923, 2019.
- [21] J. L. Wang, S. Y. Xiao, Y. J. Chen, X. X. Chen, J. Tang, and Y. Cao, "Antioxidant activity of polyphenol extracts from leaves of *E. grandis* × *E. urophylla* Guanglin No. 9," *Food Science*, vol. 33, no. 1, pp. 20–24, 2012.
- [22] F. L. Cao, X. H. Zhang, W. W. Yu, L. G. Zhao, and T. Wang, "Effect of feeding fermented Ginkgo biloba leaves on growth performance, meat quality, and lipid metabolism in broilers," *Poultry Science*, vol. 91, no. 5, pp. 1210–1221, 2012.
- [23] Y. Chen, H. Chen, W. Li et al., "Polyphenols in eucalyptus leaves improved the egg and meat qualities and protected against ethanol-induced oxidative damage in laying hens," *Journal of Animal Physiology and Animal Nutrition*, vol. 102, no. 1, pp. 214–223, 2018.
- [24] L. U. Gleason and R. S. Burton, "RNA-seq reveals regional differences in transcriptome response to heat stress in the marine snail *Chlorostoma funebris*," *Molecular ecology*, vol. 24, no. 3, pp. 610–627, 2016.
- [25] H. Watson, E. Videvall, M. N. Andersson, and C. Isaksson, "Transcriptome analysis of a wild bird reveals physiological responses to the urban environment," *Scientific Reports*, vol. 7, no. 1, p. 44180, 2017.
- [26] H. Sun, R. Jiang, S. Xu et al., "Transcriptome responses to heat stress in hypothalamus of a meat-type chicken," *Journal of Animal Science and Biotechnology*, vol. 6, no. 1, p. 6, 2015.
- [27] N. Sevane, F. Bialade, S. Velasco et al., "Dietary inulin supplementation modifies significantly the liver transcriptomic profile of broiler chickens," *Plos One*, vol. 9, no. 6, article e989426, 2014.
- [28] L.-B. Yan, Y.-J. Yu, Q.-B. Zhang et al., "Identification of p 90 ribosomal S6 kinase 2 as a novel host protein in HBx augmenting HBV replication by iTRAQ-based quantitative comparative proteomics," *Proteomics-Clinical Applications*, vol. 12, no. 3, p. e1700090, 2018.
- [29] X. Xu, J. Yang, Z. Ning, and X. Zhang, "Proteomic analysis of intestinal tissues from mice fed with Lentinula edodes-derived polysaccharides," *Food & Function*, vol. 7, no. 1, pp. 250–261, 2016.
- [30] C. Xie, X. Mao, J. Huang et al., "KOBAS 2.0: a web server for annotation and identification of enriched pathways and diseases," *Nucleic acids research*, vol. 39, suppl_2, pp. W316–W322, 2011.
- [31] M. M. Fathi, I. Al-Homidan, T. A. Ebeid, O. K. Abou-Emera, and M. M. Mostafa, "Dietary supplementation of Eucalyptus leaves enhances eggshell quality and immune response in two varieties of Japanese quails under tropical condition," *Poultry Science*, vol. 99, no. 1, pp. 879–885, 2019.
- [32] S. R. Hashemi and H. Davoodi, "Phytogenics as new class of feed additive in poultry industry," *Journal of Animal and Veterinary Advances*, vol. 9, no. 17, pp. 2295–2304, 2010.
- [33] A. Sedaghat and M. A. Karimi Torshizi, "Immune responses, intestinal microbiota, performance and blood characteristics of Japanese quail fed on diets containing camphor," *Animal*, vol. 11, no. 12, pp. 2139–2146, 2017.
- [34] M. S. Ramay and S. Yalçın, "Effects of supplemental pine needles powder (*Pinus brutia*) on growth performance, breast meat composition, and antioxidant status in broilers fed linseed oil-based diets," *Poultry Science*, vol. 99, no. 1, pp. 479–486, 2020.
- [35] P. F. Surai, "Polyphenol compounds in the chicken/animal diet: from the past to the future," *Journal of Animal Physiology and Animal Nutrition*, vol. 98, no. 1, pp. 19–31, 2014.
- [36] M. Alagawany, M. E. A. El-Hack, M. R. Farag et al., "Dietary supplementation of *Yucca schidigera* extract enhances productive and reproductive performances, blood profile, immune function, and antioxidant status in laying Japanese quails exposed to lead in the diet," *Poultry science*, vol. 97, no. 9, pp. 3126–3137, 2018.
- [37] J. Xiang, F. B. Apea-Bah, V. U. Ndolo, M. C. Katundu, and T. Beta, "Profile of phenolic compounds and antioxidant activity of finger millet varieties," *Food Chemistry*, vol. 275, pp. 361–368, 2019.
- [38] A. T. Kishawy, S. A. Amer, M. E. A. El-Hack, I. M. Saadeldin, and A. A. Swelum, "The impact of dietary linseed oil and pomegranate peel extract on broiler growth, carcass traits, serum lipid profile, and meat fatty acid, phenol, and flavonoid contents," *Asian-Australasian journal of animal sciences*, vol. 32, no. 8, pp. 1161–1171, 2019.
- [39] N. Acero, A. Gradillas, M. Beltran, A. García, and D. Muñoz Mingarro, "Comparison of phenolic compounds profile and antioxidant properties of different sweet cherry (*Prunus avium* L.) varieties," *Food Chemistry*, vol. 279, pp. 260–271, 2019.
- [40] J. Wang, R. Jia, P. Celi et al., "Green tea polyphenol epigallocatechin-3-gallate improves the antioxidant capacity of eggs," *Food & Function*, vol. 11, no. 1, pp. 534–543, 2020.
- [41] D. Tsikas, "Assessment of lipid peroxidation by measuring malondialdehyde (MDA) and relatives in biological samples: analytical and biological challenges," *Analytical Biochemistry*, vol. 524, pp. 13–30, 2017.
- [42] X. Chi, Y. Zhang, X. Ma et al., "Antioxidative stress of oral administration of tea extract granule in chickens," *Poultry Science*, vol. 99, no. 4, pp. 1956–1966, 2020.
- [43] S. M. Henning, J. J. Choo, and D. Heber, "Nongallated compared with gallated flavan-3-ols in green and black tea are more bioavailable," *Journal of Nutrition*, vol. 138, no. 8, pp. 1529S–1534S, 2008.

- [44] K. Ou and L. Gu, "Absorption and metabolism of proanthocyanidins," *Journal of Functional Foods*, vol. 7, pp. 43–53, 2014.
- [45] S. Chamorro, A. Viveros, A. Rebolé et al., "Addition of exogenous enzymes to diets containing grape pomace: effects on intestinal utilization of catechins and antioxidant status of chickens," *Food Research International*, vol. 96, pp. 226–234, 2017.
- [46] R. Laskaj, D. Slavica, I. Cepelak, and I. Kuzman, "Gamma-glutamyltransferase activity and total antioxidant status in serum and platelets of patients with community-acquired pneumonia," *Archives of Medical Research*, vol. 38, no. 4, pp. 424–431, 2007.
- [47] E. Shinno, M. Shimoji, N. Imaizumi, S. Kinoshita, H. Sunakawa, and Y. Aniya, "Activation of rat liver microsomal glutathione S-transferase by gallic acid," *Life Science*, vol. 78, no. 1, pp. 99–106, 2005.
- [48] S. Sahay and M. Gupta, "An update on nitric oxide and its benign role in plant responses under metal stress," *Nitric Oxide*, vol. 67, pp. 39–52, 2017.
- [49] L. A. Del Río and E. López-Huertas, "ROS generation in peroxisomes and its role in cell signaling," *Plant and Cell Physiology*, vol. 57, no. 7, pp. 1364–1376, 2016.
- [50] G. Y. Wu, Y. Z. Fang, S. Yang, J. R. Lupton, and N. D. Turner, "Glutathione metabolism and its implications for health," *Journal of Nutrition*, vol. 134, no. 3, pp. 489–492, 2004.
- [51] S. M. Liu and S. J. Eady, "Glutathione: its implications for animal health, meat quality, and health benefits of consumers," *Australian of Agricultural Research*, vol. 56, no. 8, pp. 775–780, 2005.
- [52] F. Wang, A. B. Kohan, C.-M. Lo, M. Liu, P. Howles, and P. Tso, "Apolipoprotein A-IV: a protein intimately involved in metabolism," *Journal of Lipid Research*, vol. 56, no. 8, pp. 1403–1418, 2015.
- [53] R. Hu, Y. He, M. A. Arowolo, S. Wu, and J. He, "Polyphenols as potential attenuators of heat stress in poultry production," *Antioxidants*, vol. 8, no. 3, p. 67, 2019.
- [54] K. Aquilano, S. Baldelli, and M. R. Ciriolo, "Glutathione: new roles in redox signaling for an old antioxidant," *Frontiers in pharmacology*, vol. 5, no. 196, 2014.
- [55] C. Ding, X. Fan, and G. Wu, "Peroxiredoxin 1- an antioxidant enzyme in cancer," *Journal of Cellular and Molecular Medicine*, vol. 21, no. 1, pp. 193–202, 2017.

Research Article

Enhanced Efficacy of Direct-Acting Antivirals in Hepatitis C Patients by Coadministration of Black Cumin and Ascorbate as Antioxidant Adjuvants

Sarfraz Ahmed,¹ Adeela Zahoor,² Muhammad Ibrahim,² Muhammad Younus ³,
Sadia Nawaz,⁴ Rahat Naseer,⁴ Qaiser Akram,³ Cun-Liang Deng,⁵
and Suvash Chandra Ojha ⁵

¹Department of Basic Sciences, University of Veterinary and Animal Sciences, Lahore, 51600, Narowal Campus, Pakistan

²Department of Biochemistry, Bahauddin Zakariya University, Multan 60800, Pakistan

³Department of Pathobiology, University of Veterinary and Animal Sciences, Lahore, 51600, Narowal Campus, Pakistan

⁴Institute of Biochemistry & Biotechnology, University of Veterinary and Animal Sciences, Lahore, 54000 Lahore, Pakistan

⁵Department of Infectious Diseases, The Affiliated Hospital of Southwest Medical University, Luzhou 646000, China

Correspondence should be addressed to Suvash Chandra Ojha; suvash_ojha@swmu.edu.cn

Received 19 February 2020; Revised 11 April 2020; Accepted 8 May 2020; Published 3 June 2020

Academic Editor: Luciano Saso

Copyright © 2020 Sarfraz Ahmed et al. This is an open access article distributed under the Creative Commons Attribution License, which permits unrestricted use, distribution, and reproduction in any medium, provided the original work is properly cited.

The widespread adaptation of a new generation of direct-acting antiviral agents (DAAs) unveils a superlative effect in the eradication of the hepatitis C virus (HCV). However, this therapy has been reported to exhibit vigorous side effects that pose a risk in fleet recovery. This study was conducted to investigate the efficacy of DAAs: sofosbuvir (SOF) and ribavirin (RBV), along with black cumin (BLC) and ascorbate (ASC), as adjuvants on hematological parameters; oxidative stress markers such as total antioxidant status (TAS), superoxide dismutase (SOD), reduced (GSH) and oxidized (GSSG) glutathione (GSH), gamma-glutamyl transferase (GGT), and malondialdehyde (MDA); liver function markers such as aspartate transaminase (AST), alanine aminotransferase (ALT), bilirubin, and alkaline phosphatase (ALP); and viral load with determined genotypes. HCV-infected patients ($n = 30$) were randomly divided into two equal groups: control group ($n = 15$) and treatment group ($n = 15$). The control group was subjected only to SOF and RBV (400 mg each/day). Synergistically, the treatment group was administered with adjuvant therapy of BLC (250 mg/day) and ASC (1000 mg/day) along with DAAs (400 mg each/day) for 8 weeks. All selected patients were subjected to sampling at pre- and posttreatment stages for the assessment of defined parameters. The data revealed that the BLC/ASC adjuvant therapy boosted the efficacy of DAAs by reducing the elevated levels of liver markers such as AST, ALT, ALP, and bilirubin in the treatment group compared with those in the control group ($P > 0.05$). The adjuvant therapy synchronously showed an ameliorating effect on hematological parameters. The SOF/RBV with adjuvant therapy also demonstrated an increasing effect in the activity of SOD, TAS, and GSH and a decreasing effect for GSSG, GGT, and malondialdehyde (MDA; $P > 0.05$) followed by curtailing a RT-PCR-quantified viral load. Our findings provide evidence that systemic administration of BLC/ASC efficiently alleviates hematological, serological, and antioxidant markers as well as the viral load in hepatitis C patients. This highlights a potentially novel role of BLC and ASC in palliating hepatitis C.

1. Introduction

Hepatitis C is a major health issue with a massive health care burden worldwide [1]. Globally, 200 million individuals are currently infected with hepatitis C virus (HCV), which char-

ters about 2–3% of the world's total population [2]. Yearly, an estimated 3–4 million people are newly diagnosed with HCV worldwide [3]. In Pakistan, 10 million individuals are reported to be infected with HCV every year with a prevalence rate of 5% in the general population [4]. Persistent

HCV infection induces liver fibrosis and cirrhosis. It also leads to several metabolic alterations such as insulin and interferon resistance, excess of iron, steatosis, and development of hepatocellular carcinomas with a high mortality rate [5].

In the past few decades, the recommended treatment for hepatitis C infection was a combination therapy of PEGylated interferon (PEG-IFN) and ribavirin (RBV) for 48 weeks. This combination was not effective enough for the eradication of HCV infection and was reported to suppress the infection by only 45–50% with vigorous side effects [6]. Currently, HCV treatment has evolved rapidly, which has led to the development of direct-acting antiviral agents (DAAs) for PEG-IFN-free antiviral regimens. This has navigated to a remarkable increase in sustained virological response (SVR) rates (<90%) opening therapeutic options for patients with contraindications or low SVR rates using PEG-IFN-based antiviral therapy regimens [7].

Sofosbuvir (SOF) is a direct-acting antiviral agent developed as an oral treatment for hepatitis C infection. It is a nucleotide analog that inhibits the polymerase enzyme that plays a key role in RNA replication. Because of its structural resemblance to a nucleotide, it competes with characteristic nucleotides, and thus by blocking the target site, it ultimately terminates viral replication within the host cell [8]. RBV is also a guanosine-nucleoside analog and flaunts antiviral activity against both RNA and DNA viruses. It is the main part of HCV regimens for hepatitis C infection over the last two decades. In the IFN-free period of hepatitis C treatment, ribavirin still exhibits a significant position in the most favorable treatment of various difficult-to-cure subgroups of HCV-infected patients. It escalates the SVR rate and enhances the efficacy of PEG-IFN when used in combination with other DAAs [9]. The combination of SOF and RBV is used in Pakistan as a standard antiviral combination against chronic hepatitis C infection.

The molecular mechanism to probe HCV pathogenesis and progression of liver disease to severe liver injuries is still poorly understood. Oxidative stress acts as a key player in the development and pathogenesis of chronic HCV [10–12]. In addition to their high SVR rates, SOF and RBV exhibit adverse side effects, including oxidative stress, which urge us to explore new therapeutics and/or adjunct therapies with a safer and more efficacious profile. Several options are available to manage the adverse effects of antiviral drugs and to maintain liver protection, which may include natural agents and or organic synthetic agents [13–19]. A combination of ASC and BLC was used as an adjunct therapy in this study. ASC (vitamin C analog) is abundant in a number of natural products. It stipulates remarkable antiviral, anticancer, anti-inflammatory, major antioxidant, and immune-regulatory effects [20]. ASC has been reported to enhance constituents of the human immune system such as lymphocyte proliferation, natural-killer cell activity, chemotaxis, and hypersensitivity. It plays an important role in maintaining the balance between the human body's oxidant and antioxidant systems. ASC has a direct antioxidant potential and is involved in the protection of reactive nitrogen species and antioxidant oxygen radicals during immune activation. It may defend neu-

trophils from reactive oxygen species (ROS) generation during phagocytosis [21] to avoid endogenous oxidative injury to lymphocytes and DNA [22–24]. ASC has also shown antiviral activity against influenza infection [25].

In common English, BLC is popularly known as black seeds and small fennel. It is scientifically known as *Nigella sativa* and belongs to the family *Ranunculaceae*. It is widely cultivated as a medicinal plant in southwest Asia and in Middle Eastern countries [13]. It marks its usage in ancient complementary medicines in conventional systems of medication such as Ayurveda and those of other old civilizations [26, 27]. Its novel medicinal potential is attributed to the presence of a phytochemical thymoquinone, which is considered its major bioactive component [13]. The literature explains that BLC contains fat, proteins, carbohydrates, crude fiber, and ash with a small amount of vitamins and minerals such as P, Cu, Fe, and Zn. The seeds exhibit carotenes and unsaturated fatty acids: mainly oleic acid, linoleic acid, dihomolinoleic acid, and eicosadienoic acid [28, 29]. The most important active compounds are thymoquinone, dithymoquinone, thymohydroquinone, and thymol. The black seeds also contain other classes of compounds such as alkaloids (isoquinoline alkaloids; e.g., nigellicimine-N-oxide and nigellicimine), pyrazole alkaloids (nigellidine and nigellicine), tannins, terpenoids, flavonoids, phenols, steroids, saponins, and a wide range of several other organic compounds [28, 29]. The literature shows that BLC exhibits antioxidant, antihypertensive, hepatoprotective, analgesics, anticancer, antiviral, diuretics, antidiarrheal, antiparasitic, and antibacterial effects. It is also used as a liver tonic, emmenagogue, appetite stimulant, and immune-stimulating agent [13, 27, 30–34]. This study was designed to probe the efficacy of BLC and ASC as adjuncts along with DAAs in hepatitis C patients. The potential therapeutic effects of BLC and ASC in our study were to investigate the antiviral effects. The study also highlights the potential role of BLC and ASC in ameliorating hematological parameters and serological and antioxidant markers.

2. Materials and Methods

2.1. Study Design. This clinical study was conducted in collaboration with the Department of Pathology and Department of Medicine, Bakhtawar Amin Medical College and Hospital, Multan, Pakistan. All experiments for this study have been approved by the Ethics Committee of the Biochemistry Department, Bahauddin Zakariya University Multan and Bakhtawar Amin Medical College (medical trial approval/2017/203). All selected patients gave consent to participate. The study was prospective and was randomized with a meticulous follow-up to the study's end that conformed to the ethics guidelines of the 1975 Declaration of Helsinki.

2.2. Patients. All HCV patients presenting to the department were scaled for eligibility. Patients were screened for human immunodeficiency virus (HIV), hepatitis B virus (HBV), and hepatitis C virus (HCV) viral antibodies to diagnose the infections. The patients' detailed history was taken, and their previous test reports were examined thoroughly. The

inclusion criteria included only HCV-RNA-infected patients of both sexes from 18 to 50 years of age. The exclusion criteria included patients with a history of anti-HCV treatment with PEG-IFN and ribavirin (RBV) less than 6 months earlier to enrolment, coinfection with hepatitis B virus (HBV) and human immunodeficiency virus (HIV), and a history of anti-cancer treatment 6 months before registration. Excluded from the present study were patients addicted to cigarettes or alcohol or who were taking any other antiviral drugs during the examination; pregnant and lactating women; patients diagnosed with hepatocellular carcinoma (HCC) or other malignancies; patients suffering a major illness such as congestive heart failure, renal failure, respiratory failure, or autoimmune disease; or patients exhibiting noncompliance to treatment. The recruited HCV-positive subjects ($n = 30$) were divided into two equal groups: control ($n = 15$, receiving standard drugs) and treated ($n = 15$, receiving standard drugs along with adjuvant therapy). The control group ($n = 15$) was administered only the standard antiviral treatment SOF (400 mg/day) and RBV (1000 mg/day), whereas the treatment group ($n = 15$) was treated with SOF (400 mg/day) and RBV (1000 mg/day) with supplementation of the BLC (250 mg/day) and ASC (1 000 mg/day) for a period of 8 weeks.

2.3. Drugs and Adjuvant Therapy Administration. SOF and RBV were supplied to the patients from the department (Getz pharma and Hilton pharma, Pakistan). ASC tablets and BLC capsules supplied were purchased (Abbott Pakistan and Qarshi Pharma). Standard antiviral drugs SOF (400 mg) [35] and RBV (1 000 or 1 200 mg, in accordance with patients' weight; 1 000 mg b.i.d. for patients with a body weight < 75 kg; and 1 200 mg b.i.d. for patients with a body weight \geq 75 kg) [36, 37] were administered for the treatment of HCV, whereas treatment supplements BLC 250 mg [38, 39] and ASC 1000 mg [40, 41] were administered daily for 8 weeks. Patients were followed up every 2 weeks to assess treatment adherence, tolerability, and incidence of adverse reactions. All selected patients were subjected to sampling at enrollment and after 8 weeks of therapy for the assessment of defined parameters. The patients for HCV confirmation were tested with both enzyme immunoassay (EIA) and RT-PCR.

2.4. Laboratory Investigations

2.4.1. Blood Sample Collection. Blood samples (4–5 mL) from all patients were taken in the EDTA vials (Atlas Labovac, K3 EDTA) with the help of 10 mL syringes (Becton Dickinson Company, Singapore) for total blood count (TBC). Approximately 3–4 mL blood samples were also taken in the gel vials (Imu Med gel & clot activator) for a liver function test (LFT), antioxidant markers, and quantitative viral detection. For a fasting blood glucose (FBG) determination, the patients included in the study were on overnight fasting (~8 hrs). Blood sampling of the patients was performed at baseline and after the treatment period.

2.4.2. Serum Sample Preparation. Blood samples taken in gel vials were left to clot for 10 minutes before centrifugation for

6 minutes at 60 000 rpm using a centrifugation machine (EBA 20, Hettich Zentrifugen, Germany). Approximately 2–3 mL of serum was collected and stored at -20°C until assayed for a LFT, antioxidant markers, and quantitative viral detection.

2.4.3. Determination of Hematological Parameters and FBG Level. TBC was carried out using an automated cell count analyzer (Sysmex KX, Japan) by noncyanide hemoglobin analysis. The autoanalyzer was capable of running several parameters for each sample such as hemoglobin (Hb), packed cell volume (PCV), red blood cells (RBC), mean cell volume (MCV), mean corpuscular hemoglobin concentration (MCHC), mean corpuscular hemoglobin (MCH), platelets, and white blood cell (WBC) counts. The equipment sampling probe aspirated 20 μL well-mixed blood samples, and the analysis result was obtained accordingly. Similarly, fasting blood sugar was measured using a blood sugar automated analyzer (Architect Ci8200 integrated system, USA) by the hexokinase method.

2.4.4. Determination of Liver Function Markers. LFT was performed using the Beckman Coulter, USA (Au480), capable of autoanalyzing several serological markers such as aspartate aminotransferase (AST), alanine aminotransferase (ALT), alkaline phosphatase (ALP), and bilirubin levels.

2.4.5. Total Antioxidant Status (TAS). TAS at the serum level was measured using an autoanalyzer (Hitachi) with a Randox reagent kit (Cayman Chemicals, USA). Control samples were run in parallel. The assay involved the reaction of ABTS (2,2-azinodi-[3-ethylbenzthiazoline sulfonate]) with a peroxidase (metmyoglobin) and H_2O_2 to produce the radical cation (ABTS⁺). Serum antioxidants suppress cations (ABTS⁺) to a degree proportional to their concentrations. The mentioned cation gives a fairly stable blue-green color measured at 600 nm.

2.4.6. Reduced and Oxidized Glutathione (GSH). Serum GSH concentration was measured using an assay kit (Cayman Chemicals, USA) and a microplate reader (Molecular Devices, Sunnyvale, CA). The assay involved the reaction of GSH with Ellman's reagent (5,5'-dithiobis-2 nitrobenzoic acid (DTNB)), which gives rise to a product quantified through a spectrophotometer at 412 nm. This reaction measures the reduction of GSSG to GSH, predicting the rate of reaction proportional to GSH and GSSG concentrations.

2.4.7. Gamma-Glutamyl Transferase (GGT). GGT at the serum level was measured through an autoanalyzer (Thermo Fisher Scientific, USA) using a reaction-specific kit (Cayman Chemicals, USA). Control serum samples were run in parallel to impose accuracy. The GGT promotes catalysis via the transfer of γ -glutamyl moiety of L- γ -glutamyl-3-carboxy-4-nitranilide to glycylglycine, leading to products of L- γ -glutamyl glycylglycine+5-amino-2-nitrobenzoate. The formation of the 5-amino-2-nitrobenzoate product serves as a measure of GGT activity analyzed through spectrophotometry at 405 nm.

2.4.8. Superoxide Dismutase (SOD) and Malondialdehyde (MDA). The SOD activity was investigated using the McCord and Fridovich method [42]. MDA activity was evaluated by modified thiobarbituric acid using TBA/TCA reagents as described by Janero [43]. The antioxidant assay principle depended on the determination of the antioxidative activity by the reaction of antioxidants in the sample with a defined amount of H_2O_2 provided exogenously. The antioxidants eliminated a quite certain amount of the H_2O_2 provided. The residual H_2O_2 was determined colorimetrically by an enzymatic reaction that involved the conversion of 3,5-dichloro-2-hydroxy benzene sulfonate to a colored product. Total antioxidant activity was assessed using a TAC kit from Bio-diagnostic and was measured spectrophotometrically (Thermo Fisher Scientific, USA).

2.4.9. Viral Load Evaluation. HCV RNA was extracted using an extraction kit (GF-1 viral nucleic acid extraction kit, Vivantis, Malaysia). RT-PCR was performed on the ABI 7500 RT-PCR system using the ROBO GENE- HCV RNA Quantification Kit (polymerase chain reaction (PCR) for HCV (lower detection limit, <50 copies)). The results of the PCR were also run on agarose gel.

2.4.10. Genotyping. The amplicons obtained were first hybridized with oligonucleotide sequences specific for variant HCV genotypes using nitrocellulose strips (GEN-C, Reverse Hybridization Strip Assay, NLM, Italy). The bands specific to variant HCV genotypes gained through labeling the hybridizing sequences with specific probes were analyzed to define genotypes.

2.5. Data Statistical Analysis. Statistical software (SPSS, version 23.0; SPSS) was used for statistical analysis. A P value was determined by a one-way ANOVA test, results were expressed as the mean and standard deviation, and $P < 0.05$ was considered the level of significance.

3. Results

3.1. Hematological Parameters. Hematological functions varied significantly after the adjuvant therapy. Our study's results showed that adjuvant therapy of BLC/ASC had an ameliorating effect on the hematological parameters of hepatitis C patients. In the treated group, SOF/RBV, along with BLC/ASC therapy, showed an increase in RBCs ($P = 0.32$), WBCs ($P = 0.67$), platelet count ($P = 0.84$), hemoglobin ($P = 0.79$), and neutrophils ($P = 0.18$) compared with the control group ($P > 0.05$), which received only SOF/RBV. Fasting blood glucose decreased significantly after treatment in the treated group ($P = 0.001$; Table 1).

3.2. Oxidative Markers. No significant ($P > 0.05$) difference was observed on the level of oxidative markers in both the control and treatment groups at baseline (Table 2).

3.3. Total Antioxidant Status (TAS). Our results obtained reveal that TAS increased after treatment in both the control (SOF+RBV) and treatment (SOF+RBV+BLC+ASC) groups.

However, TAS was slightly higher in the treated group when compared with the control ($P > 0.05$; Table 2).

3.4. Reduced Glutathione (GSH). Our findings show that GSH increased slightly after treatment in both the control and treated groups. However, the GSH level was slightly higher in the group receiving adjuvant therapy than in the control group ($P > 0.05$; Table 2).

3.5. Oxidized Glutathione (GSSG). Our findings demonstrate that the GSSG level decreased after treatment in both the control and treated groups but that the GSSG level was slightly more decreased in the treated group than in the control ($P > 0.05$; Table 2).

3.6. Gamma-Glutamyl Transferase (GGT). The serum-level GGT level was found to have decreased after treatment in both the control and treated groups. However, adjuvant therapy in the treated group showed better results in decreasing the GGT level than in the control group ($P > 0.05$; Table 2).

3.7. Superoxide Dismutase (SOD) and Malondialdehyde (MDA). Our results indicated an increasing effect on SOD and a decreasing effect on MDA levels after treatment in both the control and treated groups. However, BLC/ASC therapy in the treated group showed slightly better results for the increasing effect on SOD and a decreasing effect on MDA than did the control ($P > 0.05$; Table 2).

3.8. Liver Function Markers. Our study findings revealed that the administration of BLC/ASC in the treated group had a decreasing effect on the elevated levels of liver function markers AST, ALT, ALP, and T. bilirubin compared with the control group ($P > 0.05$; Figure 1).

3.9. Quantitative RT-PCR. Findings of RT-PCR indicated that during the 8 weeks, the therapy of SOF/RBV along with BLC/ASC in the treated group and the solo therapy of SOF/RBV in the control group had a maximum illustrious effect on the inhibition of HCV replication and consequently on the reduction in viral load. Thus, in both the control and the treated groups, SOF/RBV alone and SOF/RBV in combination with BLC/ASC eradicated the viral load in all the HCV patients. Figure 2 represents the PCR response at baseline and after 8 weeks of treatment. Gel electrophoresis results for the samples run are shown in Figure 3.

3.10. Genotyping. Genotyping results revealed a major trend of genotype 3a in both the control and treated groups with a minute frequency of 2b. Table 3 presents the genotyping results.

3.11. Persistence of Side Effects. The side effects observed decreased regarding the platelet level in the control group after the treatment of SOF/RBV. However, this effect was found to be ameliorated in the treated group receiving BLC/ASC adjuvant therapy. A slight decrease in fasting blood glucose levels was observed in both the control and treated groups after treatment, but the treated group showed a slightly lower decreasing effect on fasting blood glucose levels compared to the control (Table 1).

TABLE 1: Effect of BLC/ASC along with SOF/RBV on hematological parameters.

Parameters	Pretreatment (group)		P value	Posttreatment (group)		P value
	Control	Treatment		Control	Treatment	
RBC ($10^{12}/L$)	5.98 ± 8.98	5.34 ± 12.08	0.264	4.48 ± 0.43	6.65 ± 0.57	0.325
WBC ($10^9/L$)	8.13 ± 1.70	8.23 ± 1.64	0.154	7.63 ± 2.12	8.98 ± 2.02	0.67
Hb (g/dL)	12.93 ± 1.44	13.1 ± 1.52	0.750	11.67 ± 1.40	13.53 ± 1.55	0.794
PCV (%)	42.11 ± 4.13	41.72 ± 3.82	0.792	41.47 ± 3.14	44.31 ± 4.21	0.359
MCV (fL)	80.44 ± 17.64	100.15 ± 8.65	0.320	76.48 ± 20.33	99.09 ± 6.14	0.128
MCH (pg)	28.71 ± 6.13	26.61 ± 2.38	0.226	27.58 ± 2.88	27.69 ± 3.66	0.926
MCHC (g/L)	32.23 ± 0.66	31.91 ± 0.51	0.704	31.57 ± 1.38	31.99 ± 1.44	0.701
Lymphocytes (%)	30.98 ± 1.43	30.41 ± 2.27	0.927	30.0 ± 10.14	30.7 ± 9.69	0.234
Monocytes (%)	2.2 ± 0.2	2.59 ± 0.46	0.125	2.3 ± 0.68	2.93 ± 0.74	0.125
Eosinophils (%)	3.0 ± 0.32	3.63 ± 0.59	0.365	3.6 ± 1.06	4.13 ± 0.99	0.165
Platelets ($10^9/L$)	271.67 ± 14.23	270.13 ± 22.35	0.956	256.0 ± 29.66	292.0 ± 45.49	0.842
Neutrophils (%)	63.81 ± 1.56	62.29 ± 2.09	0.574	60.43 ± 9.51	62.13 ± 9.21	0.183
FBG	103.03 ± 13.4	105.03 ± 37.2	0.23	99.03 ± 3.2	103.23 ± 23.3	0.001

Data were expressed as the mean ± S.D. and compared using a one-way ANOVA test. RBC: red blood cells; WBC: white blood cells; Hb: hemoglobin; PCV: packed cell volume; MCV: mean corpuscular volume; MCH: mean corpuscular hemoglobin; MCHC: mean corpuscular hemoglobin concentration; FBG: fasting blood glucose.

TABLE 2: Level of oxidative stress markers in before and after treatment groups.

Parameters	Pretreatment group		P value	Posttreatment group		P value
	Control	Treatment		Control	Treatment	
TAS (mmol/L)	1.68 ± 0.72	1.71 ± 0.64	0.14	1.98 ± 0.02	2.01 ± 0.52	0.52
GSH ($\mu\text{mol}/L$)	1.82 ± 0.58	1.79 ± 0.48	0.41	2.20 ± 0.18	2.84 ± 0.38	0.44
GSSG ($\mu\text{mol}/L$)	0.18 ± 0.03	0.17 ± 0.08	0.11	0.16 ± 0.27	0.12 ± 0.43	0.31
GGT (U/L)	18.99 ± 4.15	19.09 ± 4.16	0.24	13.19 ± 0.15	12.89 ± 3.05	0.18
SOD (U/mL)	296.25 ± 10.28	295.97 ± 14.13	0.34	327.34 ± 8.19	343.79 ± 9.18	0.12
MDA (nmol/mL)	7.93 ± 12.38	7.80 ± 11.88	0.64	5.52 ± 13.02	4.24 ± 12.785	0.42

Values represent the mean ± S.D. and compared using a one-way ANOVA test. TAS: total antioxidant status; GSH: reduced glutathione; GSSG: oxidized glutathione; GGT: gamma-glutamyl transferase; SOD: superoxide dismutase; MDA: malondialdehyde.

4. Discussion

Hepatitis C is a complicated infectious disease of the liver. This infection has attracted attention because of its contagious, pervasive nature, large-scale burden, and novel therapies [44]. Hepatitis C is a common source of chronic liver disease (CLD), which is considered the main cause of morbidity and mortality worldwide [45]. The antineoplastic, antiviral, and anti-inflammatory effects of BLC and ASC have been previously documented through *in vitro* and *in vivo* studies [20, 46]. The present study explored whether BLC/ASC in combination with SOF/RBV increased the efficacy of antiviral agents in hepatitis C patients and showed a rising trend in hematological parameters, oxidative stress, liver markers, and viral load. Our results showed that BLC/ASC as an adjuvant therapy increased the level of RBC, WBC, PCV, Hb, and platelet count in the treated group compared with the control group. A solo treatment of direct antiviral therapy did not show a noteworthy effect on hema-

tological parameters. A study reported that BLC seeds are proficient in improving RBC, Hb, and PCV in the rabbit model [47]. Our results are also in line with a study reporting that BLC boosts the hematological parameters in hepatitis C patients in a dosage of 450 mg three times a day when taken as a sole antiviral treatment [48]. Another study showed that ASC had an ameliorating effect on the hematological parameters with a dose of 200 mg/kg per day in the rat model against deltamethrin toxicity and malathion-induced hepatotoxicity [49, 50]. Thus, our findings show that BLC/ASC may tend to ameliorate the hematological parameters in hepatitis C patients. The results of our study also suggest that BLC/ASC may modify Hb, RBC, and PCV to alleviate anemia. Similarly, BLC/ASC therapy seems to reinstate fasting blood glucose in a resting mode compared with the control group.

Our study's serological findings revealed that BLC/ASC adjuvant therapy had a remodeling effect on the levels of ALT, AST, and ALP (U/L), which declined considerably

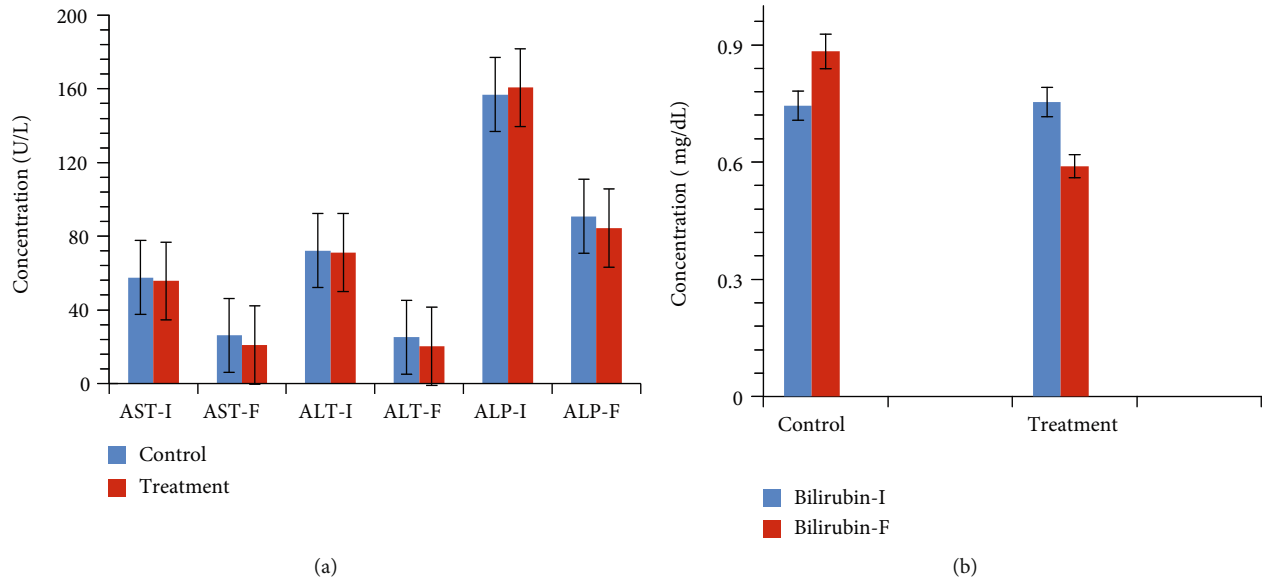


FIGURE 1: Bar graph showing levels of liver function markers in the (a) control and (b) treatment groups at baseline and after the treatment. Data was expressed as the mean and standard deviation by using a one-way ANOVA test. Abbreviations: AST-I = aspartate transaminase initial; AST-F = aspartate transaminase final; ALT-I = alanine aminotransferase initial; ALT-F = alanine aminotransferase final; ALP-I = alkaline phosphatase initial; ALP-F = alkaline phosphatase final; Bilirubin-I = bilirubin initial; Bilirubin-F = bilirubin final.

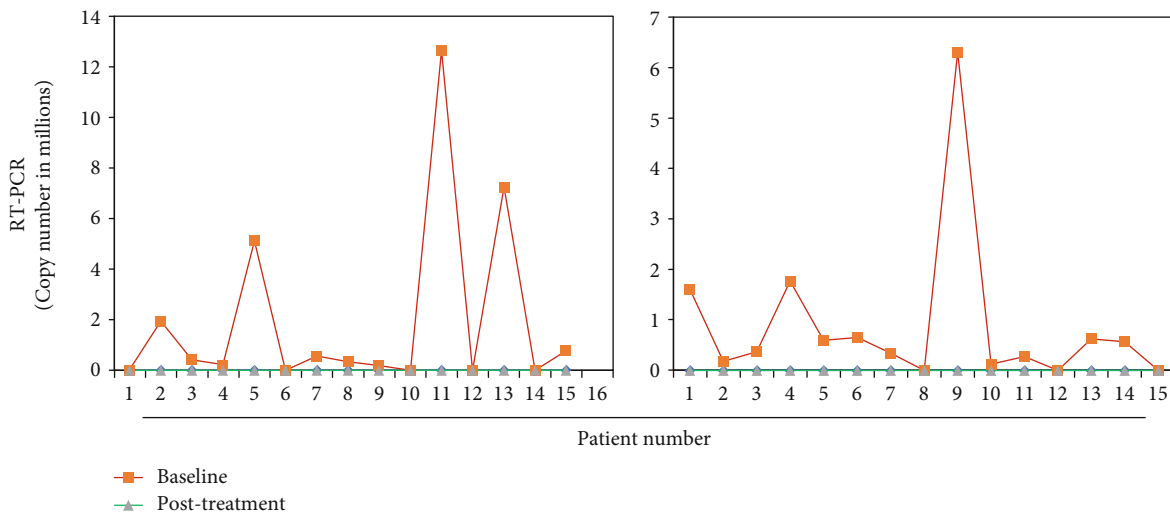


FIGURE 2: Line plot showing viral copy number at baseline and posttreatment as determined by quantitative RT-PCR in the (a) control and (b) treated groups.

toward normal in the treated group compared with the control group (Figure 1(a)). The level of total bilirubin decreased in the treated group to a normal level compared with that in the control group, which was shown to be chronic (Figure 1(b)). The literature showed the alleviating effects of BLC on AST and ALT in ethanol-induced liver injury in the rat model [51]. However, a study showed that BLC had no protective effects on liver enzymes but showed an ameliorating effect on the level of total bilirubin in hepatitis C patients. Our findings are supported by previous studies conducted in rat models that demonstrate that BLC seems to be sufficiently efficient to normalize the level of liver markers

against deltamethrin and malathion toxicity [49, 50, 52]. Our study provides evidence that BLC and ASC may act as novel immune potentiators at the hematological and serological levels.

Oxidative stress has been proposed as a key regulatory step in the development and progression of liver damage [10]. A decreased antioxidant and an increased level of oxidative stress in chronic hepatitis C patients have been reported in the literature [53, 54]. The pathogenic mechanism through which HCV may cause cell damage remains obscure; however, it has been demonstrated clearly that the oxidative stress may play a pathogenic role in this chronic infection [55].

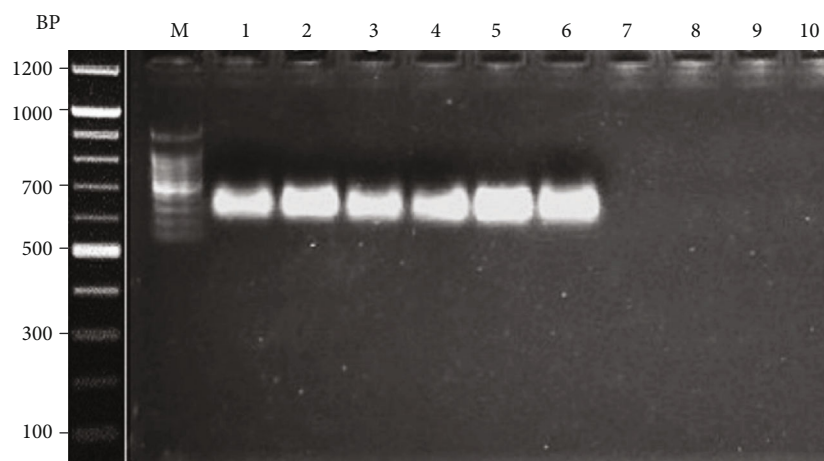


FIGURE 3: Gel electrophoresis showing detection of HCV by PCR. Abbreviations: BP: base pairs; M: DNA marker; lanes 1-3: HCV samples from the control group at baseline; lanes 4-6: HCV samples of the treatment group at baseline; lanes 7 and 8: HCV samples of the control group following treatment; lanes 9 and 10: HCV samples from the treated group. Random sample selection was carried out to validate the PCR results.

TABLE 3: Genotyping frequencies of HCV positive patients in control and treatment groups.

Groups	HCV genotype	Frequency (%)
Control	3a	14 (93.33)
Control	2b	1 (0.066)
Treatment	3a	13 (86.66)
Treatment	2b	2 (1.33)

Glutathione, or GSH, a nonenzymatic antioxidant present in the cell, plays a key role in the defense against oxidative stress in cell injury. Glutathione is present mainly in its reduced form in cells, which can be converted to oxidized glutathione (GSSG) with glutathione peroxidase (GSH-Px), which reverts to a reduced form after reacting with glutathione reductase. Cells also exhibit the enzymatic antioxidant mechanisms that play an essential role in eliminating free radicals [56]. The enzymatic antioxidant defense system of the humans may include CAT, SOD, and GSH-Px. SOD has been reported to protect a cell from toxic effects of superoxide radicals [56]. GSH-Px decomposes H_2O_2 and converts lipid peroxides to harmless molecules, protecting cells from the adverse effects of lipid peroxidation [57]. Our data report that direct antivirals and BLC/ASC adjuvant therapy may boost the level of TAS, GSH, and SOD, and these treatments also reduce the level of GSSG, GGT, and MDA. However, BLC/ASC therapy showed a slightly increasing effect on TAS, GSH, and SOD with a decreasing effect on GSSG, GGT, and MDA in the treated group compared with the control group. Research has shown that anti-HCV therapy in CHC patients increases the effect on TAS, GSH, and SOD with a decreasing effect on GSSG, GGT, and MDA [55]. Our results are also in line with previous reports that ASC and BLC balanced the oxidative stress and boosted the human antioxidant system in HCV patients and in ethanol-induced oxidative stress rat models [51, 58, 59]. Our findings suggest that BLC and ASC may be used as potential antioxidant supplements to abate hepati-

tis C. It has been shown that levels of oxidative markers such as MDA are correlated with the severity of chronic hepatitis C [60]. Thus, our results suggest that antioxidants such as BLC and ASC may be proposed as adjuvants along with standard antiviral regimens to ameliorate HCV pathogenesis. The pattern of differences in the pathogenicity of genotypes remains unclear, but the genotype has been proven one of the key predictors of HCV with regard to antiviral therapy. Because of genotypic-specific variations in response to the new generation of antiviral drugs, HCV genotype examination may assist in the management of appropriate strategies, particularly during treatment [61]. It can be hypothesized that antioxidant supplements in patients with resistant genotypes may bring more favorable outcomes, as our study shows. Research has shown that supplementation with ascorbate, vitamin E, and selenium enhanced the antioxidant status with no profound effect on the viral load [62]. Thus, the effect of antioxidants on the viral load could be the subject of future studies. Intriguingly, our data show that SOF and ribavirin improved oxidative markers, but these are not antioxidants. Their antiviral potential might reduce the viral load and inflammation, and perhaps, this mechanism may reduce virus-induced oxidative stress, a possible mechanism as observed in our study in the amelioration of oxidative stress. The statistical P value was found insignificant that could be potentially due to smaller sample size in our study. The hypothesis for smaller sample size has been well explained by Lee [63], which entails that a statistically insignificant difference between two observed groups (the sample) does not indicate that this effect does not exist in the population from which the sample is taken. But it signifies nothing more than the fact that the observed sample is too small to detect a population effect [63].

Hepatitis C patients can achieve SVR12 at week 4 of treatment with the oral DAA-based therapy [64]. BLC has shown a decline in the HCV-RNA after 12 weeks of treatment in hepatitis C patients [48]. ASC with vitamin E has been proven to exert antiviral effects against HIV [65]. Our

study shows that HCV-RNA was out of the detection limit after 8 weeks of treatment in all 30 patients treated as well as in the control group. Thus, our results suggest that new-generation antiviral SOF, along with RBV, is absolutely enough to eradicate HCV-RNA in HCV patients (Figure 3). Though this study could not determine the effect of adjuvant therapy on the viral load, we may postulate that BLC and ASC may assist in demolishing the HCV-RNA load, which has been well supported by other studies [48, 65]. Furthermore, the effect of BLC and ASC on the viral load removal should be addressed in a shorter span to probe their actual role for rectification. Overall, BLC and ASC, if tested for antiviral potency, may be akin to drugs that manage the disease by modulating different markers or parameters involved at the hematological and serological levels through a bridge of antioxidant activity, as was reported in our results. We may hypothesize that the administration of BLC and ASC has a potentially useful effect in hepatitis C progression, which can be attributed to their antioxidant, anti-inflammatory, and immunomodulatory effects.

5. Conclusion

This study concludes that the systemic administration of BLC and ASC as an adjuvant therapy considerably ameliorates hematological parameters, thus indirectly revamping the immune-regulatory system through antioxidant activity. It tends to normalize liver function markers efficiently and thus may restrain the adverse effects of SOF and RBV. The study also elaborates that SOF and RBV are quite effective in diminishing the viral load. We believe that the current findings should facilitate further research to explore whether BLC and ASC could synergize with or substitute for immune-regulatory drugs given at suboptimal doses for antiviral therapy. Further studies with larger sample size are highly desirable for greater statistical power that could pave the way toward initiating and adhering to BLC and ASC as an adjuvant therapy.

Data Availability

The datasets generated during and/or analyzed during the present study are available from the corresponding author on reasonable request.

Ethical Approval

The ethical clearance of the proposed study was obtained from the institutional ethical committee of the Department of Biochemistry, Bahauddin Zakariya University, Multan, Pakistan. Informed written consent was obtained from the volunteers who participated in this study.

Conflicts of Interest

The authors declare no conflicts of interest regarding this study.

Authors' Contributions

S.C.O., S.A., and C.-L.D. conceived the idea and contributed to the experimental design. S.A., A.Z., and M.I. collected the samples and performed the experiments. M.Y., A.R., S.N., R.N., and Q.A. analyzed and interpreted the data and wrote the main manuscript. All authors read and approved the final manuscript.

Acknowledgments

This research was supported by the Department of Biochemistry, Bahauddin Zakariya University, Multan, and Higher Education Commission, Pakistan. The authors would like to thank the patients who participated in this study and are grateful to Dr. Muhammad Tayyab and his technical team from Bakhtawar Amin Medical College and Hospital for providing technical assistance with conducting trial and data collection.

References

- [1] K. M. Hanafiah, J. Groeger, A. D. Flaxman, and S. T. Wiersma, "Global epidemiology of hepatitis C virus infection: new estimates of age-specific antibody to HCV seroprevalence," *Hepatology*, vol. 57, no. 4, pp. 1333–1342, 2013.
- [2] H. Zaheer, U. Saeed, Y. Waheed, S. Karimi, and U. Waheed, "Prevalence and trends of hepatitis B, hepatitis C and human immunodeficiency viruses among blood donors in Islamabad, Pakistan 2005–2013," *Journal of Blood Disorders and Transfusion*, vol. 5, no. 217, 2014.
- [3] D. Lavanchy, "Evolving epidemiology of hepatitis C virus," *Clinical Microbiology and Infection*, vol. 17, no. 2, pp. 107–115, 2011.
- [4] Y. Waheed, T. Shaf, S. Z. Saf, and I. Qadri, "Hepatitis C virus in Pakistan: a systematic review of prevalence, genotypes and risk factors," *World Journal of Gastroenterology*, vol. 15, no. 45, pp. 5647–5653, 2009.
- [5] A. Ivanov, B. Bartosch, O. Smirnova, M. Isagulians, and S. Kochetkov, "HCV and oxidative stress in the liver," *Viruses*, vol. 5, no. 2, pp. 439–469, 2013.
- [6] M. Issur and M. Götte, "Resistance patterns associated with HCV NS5A inhibitors provide limited insight into drug binding," *Viruses*, vol. 6, no. 11, pp. 4227–4241, 2014.
- [7] T. M. Welzel, G. Dultz, and S. Zeuzem, "Interferon-free antiviral combination therapies without nucleosidic polymerase inhibitors," *Journal of Hepatology*, vol. 61, no. 1, pp. S98–S107, 2014.
- [8] E. J. Gane, C. A. Stedman, R. H. Hyland et al., "Nucleotide polymerase inhibitor sofosbuvir plus ribavirin for hepatitis C," *New England Journal of Medicine*, vol. 368, no. 1, pp. 34–44, 2013.
- [9] J. J. Feld, I. M. Jacobson, M. S. Sulkowski, F. Poordad, F. Tatch, and J. M. Pawlotsky, "Ribavirin revisited in the era of direct-acting antiviral therapy for hepatitis C virus infection," *Liver International*, vol. 37, no. 1, pp. 5–18, 2017.
- [10] M. P. Simula and V. De Re, "Hepatitis C virus-induced oxidative stress and mitochondrial dysfunction: a focus on recent advances in proteomics," *Proteomics – Clinical Applications*, vol. 4, no. 10–11, pp. 782–793, 2010.

- [11] J. Choi and J.-H. James Ou, "Mechanisms of liver injury. III. Oxidative stress in the pathogenesis of hepatitis C virus," *American Journal of Physiology-Gastrointestinal and Liver Physiology*, vol. 290, no. 5, pp. G847–G851, 2006.
- [12] M. Vidali, M.-F. Tripodi, A. Ivaldi et al., "Interplay between oxidative stress and hepatic steatosis in the progression of chronic hepatitis C," *Journal of Hepatology*, vol. 48, no. 3, pp. 399–406, 2008.
- [13] A. Ahmad, A. Husain, M. Mujeeb et al., "A review on therapeutic potential of *Nigella sativa*: a miracle herb," *Asian Pacific Journal of Tropical Biomedicine*, vol. 3, no. 5, pp. 337–352, 2013.
- [14] Z. Selamoglu and I. Yilmaz, "The investigation of the antioxidative properties of the synthetic organoselenium compounds in liver tissue of rat with histological and biochemical analyses," *Journal of Pharmaceutical Care*, vol. 2, no. 4, pp. 162–169, 2014.
- [15] M. E. Erdemli, H. Akgul, B. Ege, Z. Aksungur, H. G. Bag, and Z. Selamoglu, "The effects of grapeseed extract and low level laser therapy administration on the liver in experimentally fractured mandible," *Journal of Turgut Ozal medical Center*, vol. 24, no. 2, pp. 127–133, 2017.
- [16] M. E. Erdemli, R. Ekhteiari Salmas, S. Durdagi et al., "Biochemical changes induced by grape seed extract and low level laser therapy administration during intraoral wound healing in rat liver: an experimental and in silico study," *Journal of Biomolecular Structure and Dynamics*, vol. 36, no. 4, pp. 993–1008, 2017.
- [17] Z. Talas, I. Ozdemir, O. Ciftci, M. Gulhan, and A. Savci, "Antioxidant effect of ethanolic extract of propolis in liver of L-NAME treated rats," *Advances in Clinical and Experimental Medicine*, vol. 24, no. 2, article 52031, pp. 227–232, 2015.
- [18] G. Badr, E. A. Sayed, H. Waly, K. Hassan, M. H. Mahmoud, and Z. Selamoglu, "The therapeutic mechanisms of propolis against CCl₄-mediated liver injury by mediating apoptosis of activated hepatic stellate cells and improving the hepatic architecture through PI3K/AKT/mTOR, TGF- β /Smad2, Bcl2/BAX/P53 and iNOS signaling pathways," *Cellular Physiology and Biochemistry*, vol. 53, no. 2, pp. 301–322, 2019.
- [19] M. E. Erdemli, University of Inonu, Department of Medical Biochemistry, T. Malatya, H. Akgul, and Z. Selamoglu, "The Effects on Oxidative Systems in Liver Tissues of Systemic Ozone Application after Critical Size Bone Defect Surgery in Rat Mandibles," *Romanian Biotechnological Letters*, vol. 24, no. 3, pp. 538–544, 2019.
- [20] R. Bei, "Effects of vitamin C on health: a review of evidence," *Frontiers in Bioscience*, vol. 18, no. 3, pp. 1017–1029, 2013.
- [21] A. C. Carr and B. Frei, "Toward a new recommended dietary allowance for vitamin C based on antioxidant and health effects in humans," *The American Journal of Clinical Nutrition*, vol. 69, no. 6, pp. 1086–1107, 1999.
- [22] L. A. Brennan, G. M. Morris, G. R. Wasson, B. M. Hannigan, and Y. A. Barnett, "The effect of vitamin C or vitamin E supplementation on basal and H₂O₂-induced DNA damage in human lymphocytes," *British Journal of Nutrition*, vol. 84, no. 2, pp. 195–202, 2000.
- [23] C. G. Fraga, P. A. Motchnik, M. K. Shigenaga, H. J. Helbock, R. A. Jacob, and B. N. Ames, "Ascorbic acid protects against endogenous oxidative DNA damage in human sperm," *Proceedings of the National Academy of Sciences*, vol. 88, no. 24, pp. 11003–11006, 1991.
- [24] S. J. Duthie, A. Ma, M. A. Ross, and A. R. Collins, "Antioxidant Supplementation Decreases Oxidative DNA Damage in Human Lymphocytes," *Cancer Research*, vol. 56, no. 6, pp. 1291–1295, 1996.
- [25] Y. Kim, H. Kim, S. Bae et al., "Vitamin C is an essential factor on the anti-viral immune responses through the production of interferon- α/β at the initial stage of influenza A virus (H3N2) infection," *Immune Network*, vol. 13, no. 2, pp. 70–74, 2013.
- [26] P. M. Paarakh, "*Nigella sativa* Linn.—a comprehensive review," *Indian Journal of Natural Products and Resources*, vol. 1, no. 4, pp. 409–429, 2010.
- [27] W. Goreja, *Black seed: nature's miracle remedy*, Karger Publishers, 2003.
- [28] Y. H. Mohammed, J. M. Ghaidaa, and H. H. Imad, "Analysis of bioactive chemical compounds of *Nigella sativa* using gas chromatography-mass spectrometry," *Journal of Pharmacognosy and Phytotherapy*, vol. 8, no. 2, pp. 8–24, 2016.
- [29] A. M. Yessuf, "Phytochemical extraction and screening of bio active compounds from black cumin (*Nigella sativa*) seeds extract," *American Journal of Life Sciences*, vol. 3, no. 5, pp. 358–364, 2015.
- [30] B. K. A. Abel-Salam, "Immunomodulatory effects of black seeds and garlic on alloxan-induced diabetes in albino rat," *Allergologia et Immunopathologia*, vol. 40, no. 6, pp. 336–340, 2012.
- [31] K. A. Abdel-Sater, "Gastroprotective effects of *Nigella sativa* oil on the formation of stress gastritis in hypothyroidal rats," *International Journal of Physiology, Pathophysiology and Pharmacology*, vol. 1, no. 2, pp. 143–149, 2009.
- [32] M. E. Assayed, "Radioprotective effects of black seed (*Nigella sativa*) oil against hemopoietic damage and immunosuppression in gamma-irradiated rats," *Immunopharmacology and Immunotoxicology*, vol. 32, no. 2, pp. 284–296, 2010.
- [33] A. O. Abdel-Zaher, M. S. Abdel-Rahman, and F. M. ELwasei, "Protective effect of *Nigella sativa* oil against tramadol-induced tolerance and dependence in mice: role of nitric oxide and oxidative stress," *Neurotoxicology*, vol. 32, no. 6, pp. 725–733, 2011.
- [34] M. H. Boskabady, N. Mohsenpoor, and L. Takaloo, "Antiasthmatic effect of *Nigella sativa* in airways of asthmatic patients," *Phytomedicine*, vol. 17, no. 10, pp. 707–713, 2010.
- [35] G. Shiha, R. Soliman, M. ElBasiony, A. A. Hassan, and N. N. H. Mikhail, "Sofosbuvir plus Daclatasvir with or without ribavirin for treatment of chronic HCV genotype 4 patients: real-life experience," *Hepatology International*, vol. 12, no. 4, pp. 339–347, 2018.
- [36] F. Andersohn, A.-K. Claes, W. Kulp, J. Mahlich, and J. K. Rockstroh, "Simeprevir with pegylated interferon alfa 2a plus ribavirin for treatment of hepatitis C virus genotype 1 in patients with HIV: a meta-analysis and historical comparison," *BMC Infectious Diseases*, vol. 16, no. 1, 2015.
- [37] Q.-L. Zeng, G.-H. Xu, J.-Y. Zhang et al., "Generic ledipasvir-sofosbuvir for patients with chronic hepatitis C: A real-life observational study," *Journal of Hepatology*, vol. 66, no. 6, pp. 1123–1129, 2017.
- [38] F. R. Dehkordi and A. F. Kamkhah, "Antihypertensive effect of *Nigella sativa* seed extract in patients with mild hypertension," *Fundamental and Clinical Pharmacology*, vol. 22, no. 4, pp. 447–452, 2008.
- [39] M. A. Ansari, N. A. Ansari, and S. A. Junejo, "Montelukast versus *nigella sativa* for management of seasonal allergic rhinitis:

- a single blind comparative clinical trial," *Pakistan Journal of Medical Sciences*, vol. 26, no. 2, pp. 249–254, 2010.
- [40] C. Pacier and D. M. Martirosyan, "Vitamin C: optimal dosages, supplementation and use in disease prevention," *Functional Foods in Health and Disease*, vol. 5, no. 3, pp. 89–107, 2015.
- [41] C. Lux-Battistelli and D. Battistelli, "Latent scurvy with tiredness and leg pain in alcoholics," *Medicine (Baltimore)*, vol. 96, no. 47, pp. e8861–e8861, 2017.
- [42] J. M. McCord and I. Fridovich, "Superoxide dismutase. An enzymic function for erythrocyte protein (hemocuprein)," *The Journal of Biological Chemistry*, vol. 244, no. 22, pp. 6049–6055, 1969.
- [43] D. R. Janero, "Malondialdehyde and thiobarbituric acid-reactivity as diagnostic indices of lipid peroxidation and peroxidative tissue injury," *Free Radical Biology and Medicine*, vol. 9, no. 6, pp. 515–540, 1990.
- [44] A. Nawaz, S. F. Zaidi, K. Usmanghani, and I. Ahmad, "Concise review on the insight of hepatitis C," *Journal of Taibah University Medical Sciences*, vol. 10, no. 2, pp. 132–139, 2015.
- [45] S. Bernuth, E. Yagmur, D. Schuppan et al., "Early changes in dynamic biomarkers of liver fibrosis in hepatitis C virus-infected patients treated with sofosbuvir," *Digestive and Liver Disease*, vol. 48, no. 3, pp. 291–297, 2016.
- [46] K. S. Zaher, W. Ahmed, and S. N. Zerizer, "Observations on the biological effects of black cumin seed (*Nigella sativa*) and green tea (*Camellia sinensis*)," *Global Veterinaria*, vol. 2, no. 4, pp. 198–204, 2008.
- [47] S. Asgary, S. Najafi, A. Ghannadi, G. Dashti, and A. Helalat, "Efficiency of black cumin seeds on hematological factors in normal and hypercholesterolemic rabbits," *ARYA Atherosclerosis*, vol. 7, no. 4, pp. 146–150, 2012.
- [48] E. M. F. Barakat, L. M. El Wakeel, and R. S. Hagag, "Effects of *Nigella sativa* on outcome of hepatitis C in Egypt," *World Journal of Gastroenterology*, vol. 19, no. 16, pp. 2529–2536, 2013.
- [49] S. Kalender, F. G. Uzun, D. Durak, F. Demir, and Y. Kalender, "Malathion-induced hepatotoxicity in rats: the effects of vitamins C and E," *Food and Chemical Toxicology*, vol. 48, no. 2, pp. 633–638, 2010.
- [50] S. Mongi, M. Mahfoud, B. Amel, J. Kamel, and E. F. Abdelfattah, "Protective effects of vitamin C against haematological and biochemical toxicity induced by deltamethrin in male Wistar rats," *Ecotoxicology and Environmental Safety*, vol. 74, no. 6, pp. 1765–1769, 2011.
- [51] S. Develi, B. Evran, E. Betül Kalaz, N. Koçak-Toker, and G. Ö. Erata, "Protective effect of *Nigella sativa* oil against binge ethanol-induced oxidative stress and liver injury in rats," *Chinese Journal of Natural Medicines*, vol. 12, no. 7, pp. 495–499, 2014.
- [52] M. Ismail, "Protective effects of vitamin C against biochemical toxicity induced by malathion pesticides in male albino rat," *Journal of Evolutionary Biology Research*, vol. 5, no. 1, pp. 1–5, 2013.
- [53] F. Duygu, S. T. Koruk, H. Karsen, N. Aksoy, A. Taskin, and M. Hamidanoglu, "Prolidase and oxidative stress in chronic hepatitis C," *Journal of Clinical Laboratory Analysis*, vol. 26, no. 4, pp. 232–237, 2012.
- [54] D. Venturini, A. N. C. Simão, D. S. Barbosa et al., "Increased oxidative stress, decreased total antioxidant capacity, and iron overload in untreated patients with chronic hepatitis C," *Digestive Diseases and Sciences*, vol. 55, no. 4, pp. 1120–1127, 2010.
- [55] G. Levent, A. Ali, A. Ahmet et al., "Oxidative stress and antioxidant defense in patients with chronic hepatitis C patients before and after pegylated interferon alfa-2b plus ribavirin therapy," *Journal of Translational Medicine*, vol. 4, no. 1, 2006.
- [56] P. Boya, A. . . Peña, O. Belouqui et al., "Antioxidant status and glutathione metabolism in peripheral blood mononuclear cells from patients with chronic hepatitis C," *Journal of Hepatology*, vol. 31, no. 5, pp. 808–814, 1999.
- [57] A. M. Chrobot, A. Szaflarska-Szczepanik, and G. Drewa, "Antioxidant defense in children with chronic viral hepatitis B and C," *Medical Science Monitor*, vol. 6, no. 4, pp. 713–718, 2000.
- [58] P. C. Badgujar, N. N. Pawar, G. A. Chandratre, A. G. Telang, and A. K. Sharma, "Fipronil induced oxidative stress in kidney and brain of mice: protective effect of vitamin E and vitamin C," *Pesticide Biochemistry and Physiology*, vol. 118, pp. 10–18, 2015.
- [59] K. Tanbek, E. Ozerol, S. Bilgic, M. Iraz, N. Sahin, and C. Colak, "Protective effect of *Nigella sativa* oil against thioacetamide-induced liver injury in rats," *Medicine*, vol. 6, no. 1, pp. 96–103, 2017.
- [60] S. Cunningham-Rundles, S. Ahrn, R. Abuav-Nussbaum, and A. Dnistrian, "Development of immunocompetence: role of micronutrients and microorganisms," *Nutrition Reviews*, vol. 60, suppl_5, pp. S68–S72, 2002.
- [61] D. S. Bowden and M. D. Berzsenyi, "Chronic hepatitis C virus infection: genotyping and its clinical role," *Future Microbiology*, vol. 1, no. 1, pp. 103–112, 2006.
- [62] K. Groenbaek, H. Friis, M. Hansen, H. Ring-Larsen, and H. B. Krarup, "The effect of antioxidant supplementation on hepatitis C viral load, transaminases and oxidative status: a randomized trial among chronic hepatitis C virus-infected patients," *European Journal of Gastroenterology and Hepatology*, vol. 18, no. 9, pp. 985–989, 2006.
- [63] D. K. Lee, "Alternatives to P value: confidence interval and effect size," *Korean Journal of Anesthesiology*, vol. 69, no. 6, pp. 555–562, 2016.
- [64] J. Pineda, L. Morano-Amado, R. Granados et al., "Week 4 response predicts sustained virological response to all-oral direct-acting antiviral-based therapy in cirrhotic patients with hepatitis C virus genotype 3 infection," *Clinical Microbiology and Infection*, vol. 23, no. 6, pp. 409.e5–409.e8, 2017.
- [65] J. P. Allard, E. Aghdassi, J. Chau et al., "Effects of vitamin E and C supplementation on oxidative stress and viral load in HIV-infected subjects," *AIDS*, vol. 12, no. 13, pp. 1653–1659, 1998.

Research Article

Zinc Oxide Nanoparticle Synergizes Sorafenib Anticancer Efficacy with Minimizing Its Cytotoxicity

Ahmed Nabil ^{1,2} Mohamed M. Elshemy,³ Medhat Asem,³ Marwa Abdel-Motaal,^{4,5} Heba F. Gooma,⁶ Faten Zahran,⁷ Koichiro Uto,¹ and Mitsuhiro Ebara ^{1,8,9}

¹Research Center for Functional Materials, National Institute for Materials Science (NIMS), 1-1 Namiki, Tsukuba, Ibaraki 305-0044, Japan

²Biotechnology and Life Sciences Department, Faculty of Postgraduate Studies for Advanced Sciences (PSAS), Beni-Suef University, Beni-Suef, Egypt

³Faculty of Science, Menoufia University, Menoufia, Egypt

⁴Department of Chemistry, Faculty of Science, Mansoura University, Mansoura, Egypt

⁵Chemistry Department, College of Science, Qassim University, Qassim, Saudi Arabia

⁶Zoology Department, Faculty of Science, Ain-Shams University, Biology Department, Faculty of Sciences and Arts-Scientific Departments, Qassim University, Saudi Arabia

⁷Biochemistry Department, Faculty of Science, Zagazig University, Egypt

⁸Graduate School of Pure and Applied Sciences, University of Tsukuba, 1-1-1 Tennodai, Tsukuba, Ibaraki 305-8577, Japan

⁹Graduate School of Industrial Science and Technology, Tokyo University of Science, 6-3-1 Niijuku, Katsushika-ku, Tokyo 125-8585, Japan

Correspondence should be addressed to Ahmed Nabil; drnabil_100@psas.bsu.edu.eg

Received 26 February 2020; Revised 15 April 2020; Accepted 15 May 2020; Published 29 May 2020

Academic Editor: Luciano Saso

Copyright © 2020 Ahmed Nabil et al. This is an open access article distributed under the Creative Commons Attribution License, which permits unrestricted use, distribution, and reproduction in any medium, provided the original work is properly cited.

Cancer, as a group, represents the most important cause of death worldwide. Unfortunately, the available therapeutic approaches of cancer including surgery, chemotherapy, radiotherapy, and immunotherapy are unsatisfactory and represent a great challenge as many patients have cancer recurrence and severe side effects. Methotrexate (MTX) is a well-established (antineoplastic or cytotoxic) chemotherapy and immunosuppressant drug used to treat different types of cancer, but its usage requires high doses causing severe side effects. Therefore, we need a novel drug with high antitumor efficacy in addition to safety. The aim of this study was the evaluation of the antitumor efficacy of zinc oxide nanoparticle (ZnO-NPs) and sorafenib alone or in combination on solid Ehrlich carcinoma (SEC) in mice. Sixty adult female Swiss-albino mice were divided equally into 6 groups as follows: control, SEC, MTX, ZnO-NPs, sorafenib, and ZnO-NPs+sorafenib; all treatments continued for 4 weeks. ZnO-NPs were characterized by TEM, zeta potential, and SEM mapping. Data showed that ZnO-NPs synergized with sorafenib as a combination therapy to execute more effective and safer anticancer activity compared to monotherapy as showed by a significant reduction ($P < 0.001$) in tumor weight, tumor cell viability, and cancer tissue glutathione amount as well as by significant increase ($P < 0.001$) in tumor growth inhibition rate, DNA fragmentation, reactive oxygen species generation, the release of cytochrome c, and expression of the apoptotic gene caspase-3 in the tumor tissues with minimal changes in the liver, renal, and hematological parameters. Therefore, we suggest that ZnO-NPs might be a safe candidate in combination with sorafenib as a more potent anticancer. The safety of this combined treatment may allow its use in clinical trials.

1. Introduction

Each year, tens of millions of people are diagnosed with cancer around the world. As concerns mortality, cancer is con-

sidered the second cause of death throughout the world and will soon become the first cause of death in many parts of the globe ([1, 2]. Unfortunately, the available therapeutic and diagnostic approaches of cancer are unsatisfactory and

represent a great challenge as many patients have cancer recurrence and severe side effects [3]. So, there are increasing demands for investigation and identification of new drugs as antitumor therapy with low side effects [4].

SEC is an undifferentiated solid carcinoma derived from mammary adenocarcinoma in mice (Sakai et al., 2010) which has a high transplantable capacity, rapidly growing tumor, short life span, and 100% malignancy [5] and is used as an experimental model to investigate the anticancer activity of drugs or natural compounds [6].

Chemotherapy is one of the most common and effective treatments for cancer which kills tumor cells using genotoxicity. However, it also harms normal cells that cause diverse dose-dependent side effects such as fatigue, loss of appetite, nausea, bowel issues, hair loss, skin discoloration, and even death in extreme cases [7]. MTX is a chemotherapeutic agent that was firstly used in the treatment of solid cancers by (Pierce and Dixon, 1958). Also, it is used in the treatment of various types of tumors and autoimmune diseases [8] due to its ability to hinder cell proliferation and synthesis of nucleotide and proteins by suppression of dihydrofolate reductase of folate metabolic pathway that plays a key role in nucleotide biosynthesis pathway [9]. Moreover, MTX derivatives like pemetrexed suppress enzymes involved in purine and pyrimidine metabolism, impairing RNA and DNA synthesis in tumors [10]. Previous studies proposed that coassembly of hydroxycamptothecin and MTX followed by surface covering through acidity-responsive polyethylene glycol might be a promising strategy for synergistically enhancing chemotherapy efficiency with minimized side effect synergistic therapeutic function [11].

Tyrosine kinase inhibitors (TKIs) are a pharmaceutical drug including three generations (first, second, and third generation) that inhibits tyrosine kinase enzymes that compete with ATP for the ATP binding site of protein tyrosine kinase and reduce tyrosine kinase phosphorylation inhibiting tumor cell proliferation. Sorafenib, a systematic multikinase inhibitor with antiproliferative properties, has been used as the first-line drug for advanced hepatocellular carcinoma patients as it suppresses tumor cells' growth and proliferation by inhibition of serine/threonine kinase and other tyrosine kinase signalling pathways [12].

ZnO-NPs have received considerable attention in various fields due to their excellent physicochemical properties, safety, biodegradability [13], and their fast delivery to different tissues and organs in addition to various biological purposes including drug delivery and immune-modulatory agent (Kalpana et al., 2018; [14]). ZnO-NPs have shown a promising anticancer behaviour besides its therapeutic activity against diabetes, microbial infections, inflammations, and wound healing [15]. Regarding cancer treatment, ZnO-NPs were approved to have a potential molecular effect including a reduction in cellular viability, loss of membrane integrity, and activation of the programmed cell death (apoptosis) [16]. It is now clear that ZnO-NPs possess a kind of cytotoxicity against tumor cells with a minimum injury to healthy cells [17]. Therefore, in the present study, we aimed to evaluate the anticarcinogenic potency of sorafenib and ZnO-NPs alone and in combination against solid Ehrlich carci-

noma compared with FDA-approved chemotherapeutic agent MTX.

2. Materials and Methods

2.1. Drugs and Chemicals. MTX was obtained from Sandoz Limited, a Novartis division, UK. Sorafenib (formerly Nexavar®) was generously supplied by Bayer AG of Germany, while zinc acetate dihydrate, ethane-1, 2-diol, and triglycol were obtained from Sigma-Aldrich Chemical Co. (St. Louis, MO, USA). Other chemicals and reagents used were of the highest purity grade.

2.2. Induction of Solid Ehrlich Carcinoma (SEC) Tumor in Mice. A model of SEC used, for Ehrlich carcinoma cells (ECC), was obtained from the National Cancer Institute, Cairo University (Giza, Egypt). Mice were implanted subcutaneously with 2×10^6 Ehrlich carcinoma cells into the right thigh of the hind limb [18]. A solid tumor mass developed within 12 days after implantation.

2.3. Animals and Experimental Design. This study was carried out on sixty adult female Swiss-albino mice weighting approximately 22-29 g, which were purchased from Medical Experimental Research Centre, Faculty of Medicine, Mansoura University (MERC), Mansoura, Egypt. Mice were kept in an air-conditioned animal house with specific pathogen-free conditions with a 12:12 h daylight/darkness and provided food and water ad libitum. All the procedures relating to animal care and treatments strictly adhered to the Guide for the Care and Use of Laboratory Animals published by the US National Institutes of Health (Publication No. 85-23, revised 1996). Mice were divided equally into 6 groups as follows:

Group I: 10 mice were injected with saline and kept as healthy control.

Group II: 10 mice were implanted subcutaneously with 2×10^6 Ehrlich carcinoma cells into the right thigh of the hind limb, injected with saline instead of treatment, and kept as the untreated control.

Group III: 10 mice were implanted subcutaneously with 2×10^6 Ehrlich carcinoma cells into the right thigh of the hind limb then treated with MTX (2.5 mg/kg/I.P.) every day [19].

Group IV: 10 mice were implanted subcutaneously with 2×10^6 Ehrlich carcinoma cells into the right thigh of the hind limb then treated with 5 mg/kg of ZnO-NPs I.P. every day [20].

Group V: 10 mice were implanted subcutaneously with 2×10^6 Ehrlich carcinoma cells into the right thigh of the hind limb then treated with 30 mg/kg sorafenib orally every day [21].

Group VI: 10 mice were implanted subcutaneously with 2×10^6 Ehrlich carcinoma cells into the right thigh of the hind limb then treated with 5 mg/kg of ZnO-NPs I.P. plus 30 mg/kg sorafenib orally every day.

2.4. Collection and Preparation of Samples. At the end of the experiment (4 weeks), all animals were euthanized by

decapitation, and blood samples collected for biochemical and tumor markers investigations. The tumor was excised, weighed, then homogenized/decellularized for cell viability assay, DNA content, flow cytometry apoptotic markers, oxidation assay, and tumor growth inhibition (% TGI) calculation.

2.5. Hematological and Biochemical Analysis. Blood samples were used for determining haemoglobin (Hb), red blood cells (RBCs), and leucocytes using the Sysmex XT 2000 Haematology Autoanalyzer (Sysmex, Kobe, Japan) according to the manufacturer's recommendation. The levels of aspartate aminotransferase (AST) and alanine aminotransferase (ALT) were measured as liver injury markers; urea and creatinine levels were measured as renal injury markers using assay kits supplied by Spinreact Diagnostics, Girona, Spain.

2.6. Synthesis and Characterization of the ZnO-NPs. ZnO-NPs were synthesized by refluxing its precursor zinc acetate dihydrate (0.1 M) in ethane-1,2-diol and triglycol at 180 and 220°C, respectively. The time of the reaction varied for 2 or 3 h in the presence and absence of sodium acetate (0.01 M). The solution was put on a magnetic stirrer at 80°C (1.5 h) then centrifuged at 8000 rpm (15 min) and rinsed with deionized water and ethyl alcohol 3 times. Finally, it was dried overnight at 80°C. ZnO-NP dose was dissolved in deionized water till the complete dissolution. Size, morphology, and elemental composition were observed and measured by a transmission and scanning electron microscope (TEM and SEM) (JEOL, Japan), while the surface zeta potential measurements were also measured by a zeta potential analyzer (Malvern Device, UK) [22].

2.7. Cell Viability Assay. Cell viability was determined in all groups using the 3-(4,5-dimethylthiazol-2-yl)-2,5-diphenyltetrazolium bromide (MTT) assay [23]. In brief, the solid tumor was decellularized; then, the cell suspension was seeded in 96-well plates (Greiner, Frickenhausen, Germany) at a density of 1×10^4 cells/well, incubated for 24 h at 37°C (5% CO₂). After incubation, 100 µL/well of 0.5 mg/mL MTT was added to each well then incubated for 4 h, and the absorbance was measured at 570 nm using an enzyme-linked immunosorbent assay (ELISA) reader [24].

2.8. DNA Damage. The solid tumor was homogenized in chilled homogenization buffer (Ultra-Turrax, IKA T25, Germany) (pH 7.5) to obtain a tissue suspension; then, a centrifugation step was done with the generation of two fractions (corresponding to intact and fragmented DNA, respectively), precipitation of DNA, hydrolysis, and colorimetric quantitation upon staining with diphenylamine (DPA), which binds to deoxyribose. Optical density was measured at 600 nm with a multiwell spectrophotometer reader.

2.9. Caspase-3 and Cytochrome c Analysis. Caspase-3 used for evaluation of apoptosis induction in tumor cells using Cell-Event Caspase-3 detection reagent (5 µM in PBS with 5% FBS) for 30 min at 37°C was purchased from Thermo Fisher Scientific (USA). Tumor cells (1×10^6) from different groups were incubated with the primary anti-mouse antibodies for 1 h; then, the secondary antibodies FITC-conjugated goat-

anti-rabbit antibodies were added for 30 min at 37°C and analyzed by flow cytometry (FACSCalibur, BD Biosciences) using CellQuest software. The activity of cytochrome c was measured in the homogenized tumor tissues using the Human ELISA kit (Abcam, Cambridge, UK). Specific cytochrome c antibodies were precoated onto 96-well plates incubated at room temperature. Washed with wash buffer, a streptavidin-HRP conjugate was added to each well and incubated at room temperature, and unbound conjugates were washed away and TMB was added and catalyzed by HRP to produce a yellow color. The density of yellow color was directly proportional to the concentration of cytochrome c.

2.10. Oxidative Stress Assessment. Tumor was homogenized using a Branson Sonifier (250, VWR Scientific, Danbury, CT) in potassium phosphate buffer (pH 6.5, 1:10) then centrifuged at $10,000 \times g$ at 4°C for 20 min for the determination of antioxidant enzymes, tissue-reduced glutathione (GSH) [25], tissue malondialdehyde (MDA) [26], and nitric oxide (NO) [27]. The level of reactive oxygen species (ROS) was measured in the homogenized tumor tissues depending on using the cell-permeant reagent 2',7'-dichlorofluorescein diacetate (DCFDA), a fluorogenic dye that measures hydroxyl, peroxy, and another ROS activity within the cell. After diffusion into the cell, DCFDA is deacetylated by cellular esterases to a nonfluorescent compound, which is later oxidized by ROS into 2',7'-dichlorofluorescein (DCF). DCF is a highly fluorescent compound. Briefly, homogenized tissues were stained by adding 100 µL of DCFDA to each well and incubated for 45 min at 37°C in the dark. Blank wells (with nonstained cells) were also used as a control. The fluorescence intensity was measured using an Infinite® 200 PRO plate reader at Ex/Em = 488/525 nm, and the values were expressed as fluorescence intensity (FU)/protein content (mg).

Moreover, catalase (CAT) and superoxide dismutase (SOD) enzyme activity in the homogenate was assayed using colorimetric diagnostic kits (Biodiagnostic, Cairo, Egypt) according to the manufacturer's instructions. Serum total antioxidant capacity (TAC) was determined according to the methods reported by Koracevic et al. [28].

2.11. Statistical Analyses. Data were analyzed using SPSS software version 22 for Windows (IBM, Armonk, NY, USA). Descriptive statistics were calculated in the form of mean \pm standard deviation (SD). ANOVA and Tukey's post hoc tests were used for comparison between groups. A level of $P < 0.05$ was defined as statistically significant.

3. Results

3.1. ZnO-NP Characterization. ZnO-NP actual size and surface charge were confirmed by TEM, SEM, and a zeta potential analyzer. TEM micrographs revealed that ZnO-NPs were spheroid in shape (Figure 1(a)) and showed an average particle size = 37 nm; the zeta potential of ZnO-NPs was -22 mV, zeta deviation = 3.3 mV, and conductivity = 0.1 mS/cm (Figure 1(c)). SEM analysis of the synthesized ZnO-NPs shown in (Figure 1(b)) indicated the uniform grain appearance and the unique morphology without impurities.

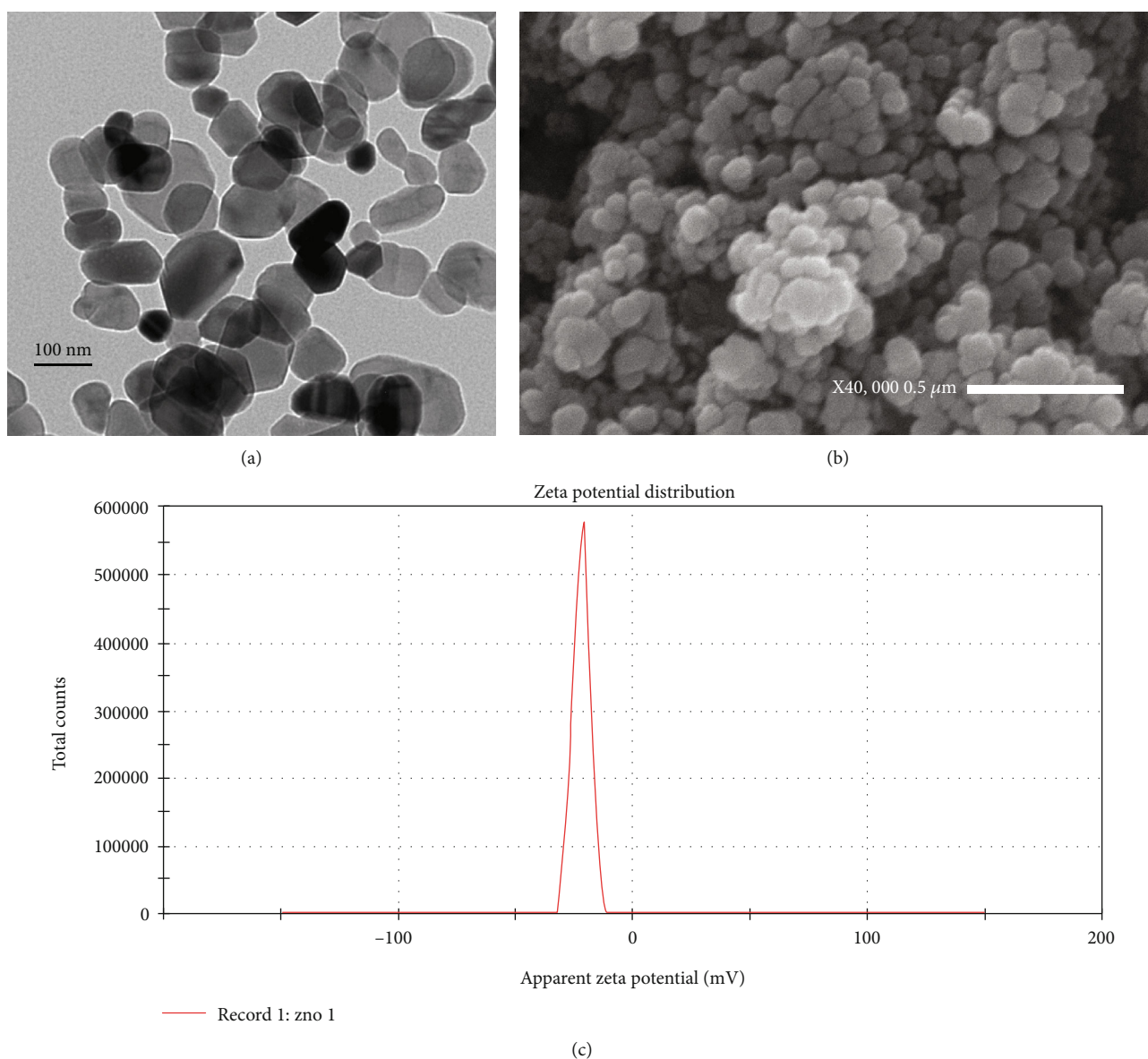


FIGURE 1: Characterization of ZnO-NPs: (a) TEM image of ZnO-NP average particle size = 37 nm; (b) SEM image of the synthesized ZnO-NPs; (c) zeta potential of ZnO-NPs.

3.2. Tumor Growth Inhibition Rate and the Difference in Tumor Weight. The administration of monotherapy MTX, ZnO-NPs, sorafenib, and ZnO-NPs+sorafenib combination showed significant reductions ($P < 0.001$) in tumor weight compared to the nontreated SEC group (G2). Moreover, G6 that received combination therapy (ZnO-NPs+sorafenib) showed the best reduction in tumor (1.07 ± 0.21 g) weight (Table 1, Figure 2). On the other hand, tumor growth inhibition % in different groups was 43.12%, 17.09%, 34.17%, and 47.23% for G3, G4, G5, and G6, respectively, which indicates that the combination treatment of ZnO-NPs+sorafenib significantly inhibits the tumor growth rate ($P < 0.001$) compared with the other monotherapy (Table 1).

3.3. Hematological and Biochemical Parameters. Table 2 showed a slight improvement in hematological parameters

including Hb% and RBCs and significant improvement ($P < 0.001$) in leucocyte count towards normal observed with the different treatment regimens used in this experiment to antagonise the alterations induced by SEC in mice. Moreover, some liver and renal biomarker alterations induced by the tumor including AST and ALT as well as urea and creatinine significantly indicated liver and renal injury in the nontreated SEC group compared to the normal group. Conversely, different treatment regimens showed significant ($P < 0.001$) modulation in all liver and renal biochemical parameters while the combination therapy (ZnO-NPs+sorafenib) showed the most apparent improvement towards normal.

3.4. DNA Content. All treated groups showed a statistically significant decrease ($P < 0.05$) in DNA content compared

TABLE 1: Tumor growth inhibition rate and difference in tumor weights. Values are expressed as $M \pm SD$ of 10 animals in each group.

Parameters	SEC	MTX	ZnO-NPs	Sorafenib	ZnO-NPs+sorafenib	<i>P</i>
Tumor weight (g)	2.62 ± 0.20	1.22 ± 0.13 ^a	1.41 ± 0.28 ^a	1.32 ± 0.14 ^a	1.07 ± 0.21 ^a	<0.001**
Tumor growth inhibition (%)	—	43.72	19.09 ^b	35.17 ^c	46.23 ^c	<0.001**

SD: standard deviation; *P*: probability; *significance < 0.05; **high significance. The test used one-way ANOVA followed by post hoc Tukey. ^aSignificant compared to the control SEC group. ^bSignificant compared to the MTX group. ^cSignificant compared to the ZnO-NP group. ^dSignificant compared to the sorafenib group.

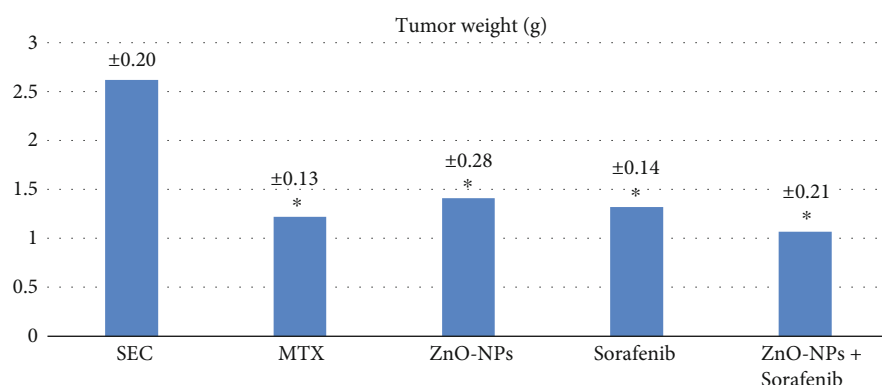


FIGURE 2: Effect of the treatment with MTX (2.5 mg/kg/I.P.), ZnO-NPs (5 mg/kg/I.P.), sorafenib (30 mg/kg/orally), and the combination of ZnO-NPs+sorafenib on SEC weight for 4 weeks. Results showed significant reductions ($P < 0.001$) in tumor weight in all treated groups compared to nontreated SEC group, and the best reduction in tumor (1.07 ± 0.21 g) weight was observed in the group that received combination therapy as ZnO-NPs synergized with sorafenib to execute the antitumor activity.

TABLE 2: Hematological and biochemical parameters. Values are expressed as $M \pm SD$ of 10 animals in each group.

Parameters	Control	SEC	MTX	ZnO-NPs	Sorafenib	ZnO-NPs+sorafenib	<i>P</i>
Hematological parameters							
HB (g/L)	103.1 ± 7	78.3 ± 13.5 ^a	94.6 ± 2.9	88 ± 13	83 ± 2.6	87.6 ± 8.1	<0.001**
Leucocytes (cells × 10 ³ /mm ³)	5.1 ± 0.4	13.5 ± 0.9 ^a	5.4 ± 0.58 ^b	6.6 ± 2.72 ^b	6.33 ± 1.5 ^b	4.8 ± 0.83 ^{b,d}	<0.001**
RBCs (cells × 10 ⁶ /mm ³)	4.1 ± 0.3	3.13 ± 0.62	3.71 ± 0.15	3.66 ± 0.46	3.86 ± 0.61	3.53 ± 0.57	<0.001**
Renal parameters							
Urea (mmol/L)	7.3 ± 0.41	11.2 ± 1.7 ^a	5.8 ± 0.5 ^b	9.9 ± 1.3 ^c	8.9 ± 1.3	6.3 ± 0.9 ^{b,d}	<0.001**
Creatinine (mmol/L)	0.07 ± 0.002	0.21 ± 0.02 ^a	0.09 ± 0.04 ^b	0.09 ± 0.04 ^b	0.12 ± 0.01 ^{a,b}	0.08 ± 0.02 ^{b,e}	<0.001**
Hepatic parameters							
ALT (U/L)	45.6 ± 5.8	76.96 ± 9.1 ^a	36.2 ± 4.05 ^b	54.23 ± 12.8 ^{b,c}	63.9 ± 12.62 ^{a,c}	41.8 ± 14.4 ^{b,e}	<0.001**
AST (U/L)	64.8 ± 10.6	192.9 ± 8.3 ^a	121 ± 7.76 ^{a,b}	111.63 ± 17.1 ^{a,b}	96.2 ± 7.96 ^{a,b}	87.36 ± 4.37 ^{a,b,c}	<0.001**

SD: standard deviation; *P*: probability; *significance < 0.05; **high significance. The test used one-way ANOVA followed by post hoc Tukey. ^aSignificant compared to the control group. ^bSignificant compared to the control SEC group. ^cSignificant compared to the MTX group. ^dSignificant compared to the ZnO-NP group. ^eSignificant compared to the sorafenib group.

with the untreated SEC group as shown in Table 3, especially with the combination therapy which decreases DNA content compared with other monotherapy.

3.5. Cell Viability Assay. Significant ($P < 0.001$) reduction in cell viability with different treatments compared to the SEC group was observed (Table 3). Also, the best cell viability reduction was observed with combined therapy.

3.6. Caspase-3 and Cytochrome c. As shown in Table 3 and Figure 3, MTX, ZnO-NPs, sorafenib, and the combination significantly release ($P < 0.001$) cytochrome c into the cyto-

plasm. Additionally, flow cytometry reported a marked increase in the expression of active caspase-3 with the different treatment regimens used in this experiment in comparison with the SEC group ($P < 0.001$). Furthermore, the combination therapy revealed a slight increase in the tissue expression of active caspase-3 and apoptotic cell population % compared to monotherapy (Figure 3(f)).

3.7. Oxidative Stress Assessment. The current study revealed a significant elevation in MDA level and ROS generation in the tumor tissues ($P < 0.001$) as well as a marked reduction in GSH content, CAT, and SOD enzyme activity in all

TABLE 3: Parameters of oxidative stress, cell viability assay, DNA fragmentation, and cytochrome c. Values are expressed as $M \pm SD$ of 10 animals in each group.

Parameters	SEC	MTX	ZnO-NPs	Sorafenib	ZnO-NPs+sorafenib	P
Tumor tissue						
MTT	0.49 \pm 0.06	0.32 \pm 0.05 ^a	0.38 \pm 0.08 ^a	0.34 \pm 0.05 ^a	0.26 \pm 0.10 ^{a,c}	<0.001**
DNA content ($\mu\text{g}/100\text{ mg}$)	744.5 \pm 62.9	421.9 \pm 32.7 ^a	532.5 \pm 52.5 ^a	621.5 \pm 130.4 ^b	365.6 \pm 41.9 ^{a,c,d}	<0.001**
Cytochrome c (ng/mL)	0.32 \pm 0.05	0.87 \pm 0.15 ^a	0.76 \pm 0.10 ^a	0.74 \pm 0.14 ^a	0.92 \pm 0.18 ^a	<0.001**
ROS (FU/mg)	380 \pm 60	730 \pm 31 ^a	530 \pm 63 ^{a,b}	650 \pm 72 ^a	790 \pm 12 ^{a,c}	<0.001**
NO (nmol/100 mg tumor)	82.03 \pm 16.6	66.23 \pm 14.47	83.10 \pm 14.90	72.76 \pm 4.32	75.8 \pm 15.01	<0.001**
GSH (nmol/100 mg tumor)	328.4 \pm 28.9	240.5 \pm 30.6 ^a	202.5 \pm 72.3 ^a	194.9 \pm 33.1 ^{a,b}	175.1 \pm 31 ^{a,b}	<0.001**
MDA (nmol/100 mg tumor)	10.86 \pm 1.20	18.73 \pm 1.87 ^a	19.3 \pm 1.03 ^a	14.26 \pm 1.26 ^a	22.40 \pm 1.53 ^{a,d}	<0.001**
CAT (U/g tumor)	170.3 \pm 11.2	97.4 \pm 9.8 ^a	84.6 \pm 5.8 ^a	110.5 \pm 8.7 ^a	77.9 \pm 5.3 ^{a,d}	<0.001**
SOD (U/g tumor)	8.9 \pm 1.5	4.2 \pm 1.37 ^a	3.9 \pm 1.04 ^a	5.4 \pm 1.13 ^a	3.2 \pm 1.2 ^{a,d}	<0.001**
Serum TAC ($\mu\text{mol}/\text{L}$)	0.5 \pm 0.05	0.91 \pm 0.05 ^a	0.8 \pm 0.14 ^a	0.54 \pm 0.07 ^{a,b,c}	0.72 \pm 0.08 ^{a,b,d}	<0.001**

SD: standard deviation; P: probability; *significance < 0.05; **high significance. The test used one-way ANOVA followed by post hoc Tukey. ^aSignificant compared to the control SEC group. ^bSignificant compared to the MTX group. ^cSignificant compared to the ZnO-NP group. ^dSignificant compared to the sorafenib group.

treated groups compared to the nontreated SEC group tissues as shown in (Table 3). No significant difference was observed in the NO level between different study groups. Serum TAC of the SEC group significantly decreased as compared to that of all treated groups. Moreover, animals treated by ZnO-NPs combined with sorafenib reversed the antioxidant enzymes, MDA level, and serum TAC alterations towards the normal ranges compared with different monotherapy and SEC groups.

3.8. The Probable Anticancer Synergistic Mechanism between ZnO-NPs and Sorafenib. Figure 4 shows the possible mechanism by which ZnO-NPs synergized with sorafenib to execute a more effective and safer anticancer activity.

4. Discussion

Tumor treatment represents a challenging goal to find selective, effective, and safe therapy [29]. Ehrlich carcinoma has many advantages including the affordable cost, easily reproducible, and accessible to evaluate the efficacy and safety of anticancer therapies [30].

MTX is one of the most successful anticancer (antineoplastic or cytotoxic) chemotherapeutic drugs (used in high doses), but these doses had severe side effects. Therefore, we need new drugs with the same efficacy and high safety [31].

In this study, we evaluated the cytotoxic activity of sorafenib and ZnO-NPs alone and in combination against solid Ehrlich carcinoma compared with FDA-approved chemotherapeutic agent MTX.

Sorafenib, an oral multiple kinase inhibitor, significantly induces apoptosis in cancer model process, as well as inhibits tumor angiogenesis and cell proliferation to exert its anticancer activity, but it has severe cytotoxicity, leading to adverse events [32]. It was approved by the FDA as an effective therapy for advanced renal cell carcinoma in 2006 and advanced hepatocellular carcinoma in 2007 [33]. Being a multitarget

kinase inhibitor, sorafenib blocks tyrosine kinase signalling receptors (VEGFR, PDGFR, and RET) and inhibits downstream Raf serine/threonine kinase activity to prevent tumor growth by antiangiogenic, antiproliferative, or proapoptotic effects that promote tumor cell apoptosis [34].

The previous studies found that ZnO-NPs have the potential to be used as anticancer therapy by targeting cancerous cells, enhancing cytotoxicity and cell death, which could be used as a foundation for developing new antitumor therapies [35]. ZnO-NPs did not show any kind of cytotoxicity in the liver and renal tissues when used as an anticancer agent [36].

It is generally admitted that positively charged nanoparticles have more affinity to be engulfed by cells than neutral or negative nanoparticles. It is supposedly due to favourable electrostatic interactions with the negatively charged cell membrane [37].

ZnO-NP surface has neutral hydroxyl groups which play an important role in the NP charging behaviour [38]. In alkaline pH, protons moved away from the metal surface inducing a negatively charged surface partly bonded oxygen atom (ZnO^-); in acidic pH, H^+ from the environment are likely moved to the NP surface, causing a positively charged surface (ZnOH_2^+). Under physiological state (acidic pH of tumor cells), the isoelectric point from 9 to 10 shows that ZnO-NPs will possess a strongly positive-charged surface [39]. On the other hand, cancer cell outer layer membranes are characterized by the presence of a large number of anionic phospholipids [40]. Therefore, ZnO-NPs may be electrostatically attracted to the tumor tissues increasing cellular uptake of the nanoparticles [35]. In contrast, the normal healthy cells are either charge-neutral or slightly positive which show insignificant binding to the NPs [41].

Another important feature is that nanoparticles with size ≤ 100 nm remain in the circulation for a longer time and are able to avoid clearance by the reticuloendothelial system, also increasing intratumor concentrations [42]. Our

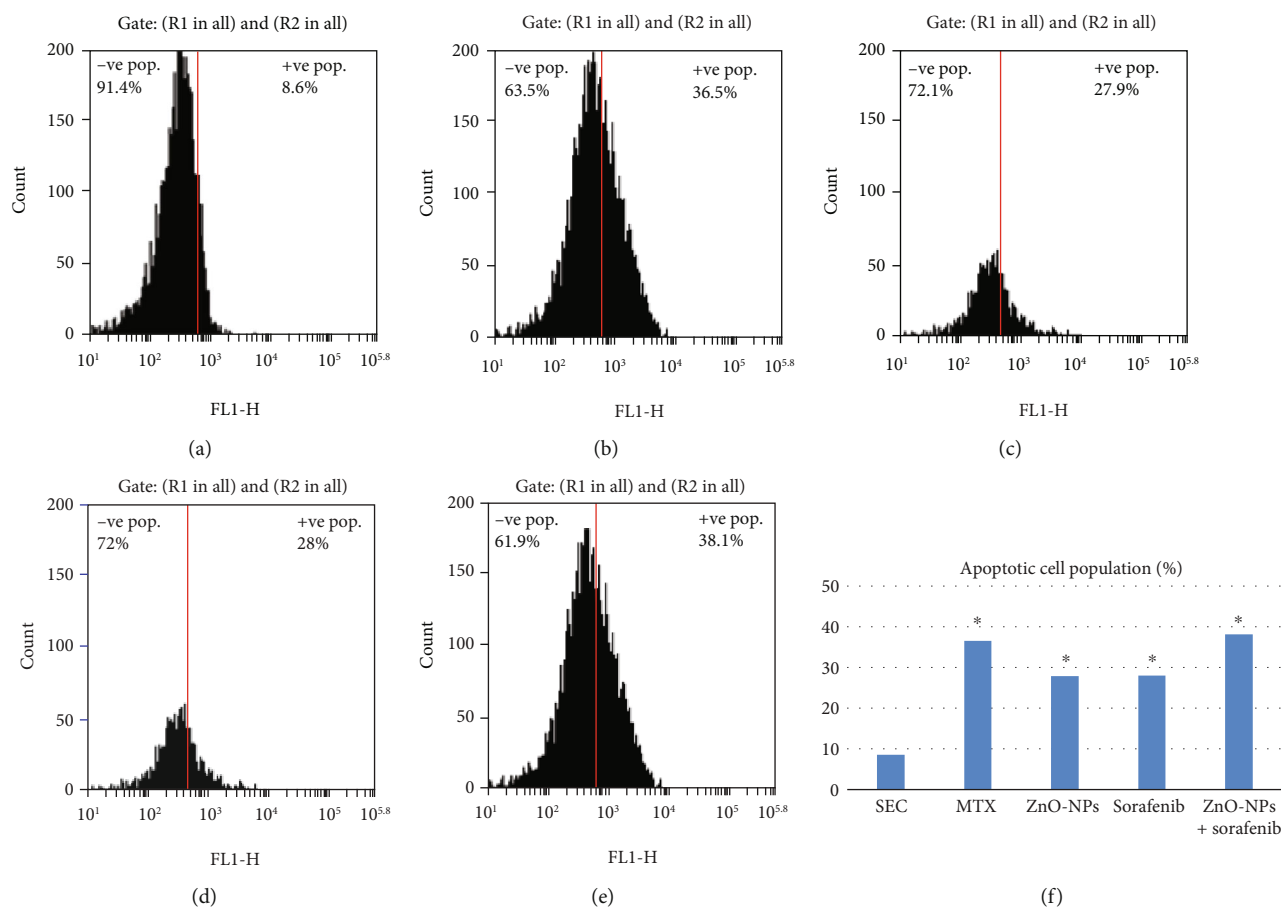


FIGURE 3: Caspase-3 flow cytometry analysis indicates apoptotic cell population % in all groups. (a) SEC group. (b) MTX group. (c) ZnO-NP group. (d) Sorafenib group. (e) ZnO-NPs+sorafenib group. (f) Apoptotic cell population (%).

data showed that the prepared ZnO-NP particle size average is equal to 37 nm and the zeta potential of ZnO-NPs was -22 mV; this stability and small particle size uniformity revealed the ability to target cancerous cells, enhancing cytotoxicity and cell death.

Our results are parallel to Xia et al. [43] who reported that ZnO-NPs induce ROS generation, enhancing cancer cytotoxicity and cell death. In agreement with other studies, different used treatment regimens especially the combination therapy significantly increase ROS levels which leads to oxidative damage to cellular structures and decreases antioxidant enzymes SOD and CAT activity in tumor tissue compared with the SEC group [44] as SOD catalyzes the dismutation of superoxide anion (O_2^-) to H_2O_2 and O_2 [45]; also, CAT enzyme reduces H_2O_2 to H_2O [43]. Treatment with ZnO-NPs showed a marked increase in MDA level which indicates lipid peroxidation and depletion of GSH in ESC tissues; these findings are in agreement with El-Shorbagy et al. [46].

Measuring the serum TAC may help to identify conditions affecting the oxidative status and the evaluation of physiological factors. TAC considers the cumulative action of all the antioxidants present in serum and body fluids, thus giving an insight into the delicate balance in vivo between oxidants and antioxidants [47]. Our data showed a significant reduction of serum TAC in the SEC and sorafenib

groups due to oxidative stress and which is returning nearly to the basic state with MTX, ZnO-NPs, and the combined therapy (ZnO-NPs+sorafenib) with the best result observed with the combination. Previous parallel studies found that serum TAC decreased insignificantly in all groups when the concentration of zinc oxide nanoparticles was increased up to 200 mg/kg compared to the control group [48]. Another study [49] reported that there was no statistically significant alteration in serum levels of TAC, after 8 weeks of MTX dose up to 7.5 mg/kg therapy. Furthermore, Eisa et al. [50] reported that serum TAC of the Ehrlich carcinoma group significantly decreased as compared to that of the normal control group.

Consistent with our results, Diab et al. [51] revealed that oral administration of sorafenib in a dose of 10 mg/kg.b.wt. of rats daily for 2 weeks causes a significant decrease ($P < 0.05$) in total antioxidant capacity compared to the control healthy group. Moreover, Coriat et al. [52] reported that the sera of sorafenib-treated hepatocellular carcinoma patients contain increased levels of advanced oxidation protein products as sorafenib inhibits the MEK/ERK pathway that controls ROS production which exerts cytotoxic effects. Conversely, in animals treated by ZnO-NPs combined with sorafenib, the serum TAC level returning nearly to the basic state indicated that the combination had a less cytotoxic effect.

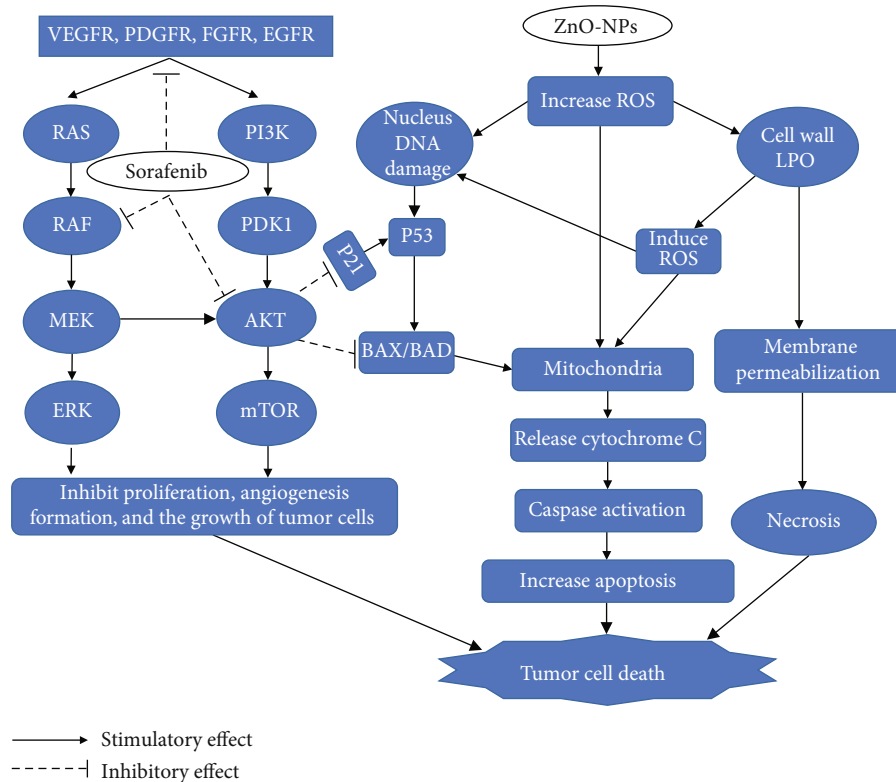


FIGURE 4: Schematic diagram of the probable mechanism of synergy between ZnO-NPs and sorafenib. Sorafenib has antagonist effect on vascular endothelial growth factor receptor (VEGFR- β), platelet-derived growth factor receptor (PDGFR), fibroblast growth factor receptor (FGFR), epidermal growth factor receptor (EGFR), protooncogene B-Raf, and protein kinase B-1 (AKT-1). However, ZnO-NPs are involved in reactive oxygen species (ROS) generation and increased cell wall lipid peroxidation (LPO) leading to cytotoxic and genotoxic effects. MEK: mitogen-activated protein kinase; ERK: extracellular signal-regulated kinase; PI3K: phosphatidylinositol-3-kinase; PDK1: pyruvate dehydrogenase lipoamide kinase isozyme 1; mTOR: mammalian target of rapamycin; p53: tumor protein p53; BAD: BCL-2-associated death promoter.

ROS including H_2O_2 , $\cdot OH$, and $\cdot O_2^-$ may react with nucleophilic centres leading to DNA fragmentation and apoptosis upregulation, ultimately leading to carcinoma cell death [53]. Our findings agree with Bai et al. [54] who reported a significant increase in the DNA damage in the ZnO-NP-treated group compared with the nontreated SEC group.

The combined therapy of two or more therapeutic agents is a cornerstone of cancer treatment as it increases efficacy compared with monotherapy and may decrease the toxic effects on normal cells [55]. To the best of our knowledge, the current study was the first to evaluate the antitumor activity of sorafenib and ZnO-NP combined treatment. Our results showed that the tumor weight and growth inhibition rate significantly decreased with the different monotherapy treatment regimens compared to the nontreated SEC group as reported in previous studies [19, 56]; moreover, the best significant reduction in tumor weight (1.07 ± 0.21 g) and growth inhibition rate (47.23%) was observed in the combined therapy (ZnO-NPs+sorafenib) compared to monotherapy which demonstrates that the combined therapy had the best antitumor activity against SEC.

In the present study, Ehrlich tumor causes alterations in hematological parameters (Hb%, RBCs, and leucocytes) mainly due to iron deficiency as reported in previous studies [57]. Furthermore, our results were consistent with Boren-

tain et al. [58] and Mutar et al. [59] who reported that SEC has led to liver and renal injury and marked changes in the liver and renal function in mice through an elevation in the levels of ALT, AST, urea, and creatinine. Conversely, animals treated by ZnO-NPs combined with sorafenib reversed the hematological and biochemical parameter alterations towards the normal ranges compared with different monotherapy and SEC groups which indicates a protective action on the liver, kidney, and the hematopoietic system against tumor cells in SEC mice.

The antiproliferative effect was determined using the MTT assay, which links directly to the mitochondrial enzymes [60]. Our results showed a significant reduction in cancer cell viability in the treated groups compared with the nontreated SEC group. Moreover, the highest reduction in cell viability was observed in the group treated with the combined therapy compared to monotherapy as ZnO-NPs synergized with sorafenib to execute the best antitumor activity.

ZnO-NPs induce oxidative damage of the plasma membrane which causes the loss of mitochondrial membrane potential, increased intracellular Ca_2+ level, and release of cytochrome c which leads to the activation of caspases that enter the mitochondrial matrix to cleave key substrates in the electron transport chain [61]. Furthermore, sorafenib initiated apoptosis by cleavage of caspases

and the mitochondrial release of cytochrome c [62]. Our data showed a marked increase in cytochrome c level and caspase-3 in the SEC tissues with both monotherapy and combination compared with the nontreated SEC group with the highest expression in the combined therapy group, as ZnO-NPs synergized with sorafenib inducing upregulation of cytochrome c and caspase-3 gene expression causing tumor cell death.

5. Conclusion

Finally, we conclude that ZnO-NPs synergized sorafenib to execute safer and effective antitumor activity leading to SEC growth reduction as shown in Figure 4 with a low cytotoxic effect on normal cells. Therefore, new therapeutic strategies for cancer treatment including ZnO-NPs combined with sorafenib could be developed. Moreover, long-term toxicity studies are required to rule out any long-term side effects regarding the combination.

Data Availability

Data used to support the findings of this study are available from the corresponding author upon request.

Conflicts of Interest

The authors declare that they have no conflict of interest.

References

- [1] X. Ma and H. Yu, "global burden of cancer," *The Yale journal of Biology And Medicine*, vol. 79, no. 3-4, pp. 85-94, 2006.
- [2] C. Mattiuzzi and G. Lippi, "Current cancer epidemiology," *Journal of Epidemiology and Global Health*, vol. 9, no. 4, pp. 217-222, 2019.
- [3] P. K. Chaudhuri, B. C. Low, and C. T. Lim, "Mechanobiology of tumor growth," *Chemical Reviews*, vol. 118, no. 14, pp. 6499-6515, 2018.
- [4] A. D. Kinghorn, E. J. C. De Blanco, H.-B. Chai et al., "Discovery of anticancer agents of diverse natural origin," *Anticancer Research*, vol. 81, pp. 1051-1063, 2009.
- [5] M. Ozaslan, I. D. Karagoz, I. H. Kilic, and M. E. Guldur, "Ehrlich ascites carcinoma," *African Journal of Biotechnology*, vol. 10, pp. 2375-2378, 2011.
- [6] M. Al Abdan, "Alfa-lipoic acid controls tumor growth and modulates hepatic redox state in Ehrlich-ascites-carcinoma-bearing mice," *The Scientific World Journal*, vol. 2012, Article ID 509838, 6 pages, 2012.
- [7] V. T. DeVita and E. Chu, "A history of cancer chemotherapy," *Cancer Research*, vol. 68, no. 21, pp. 8643-8653, 2008.
- [8] D. Zhang, Y. Li, and P. Sun, "miR-770-5p modulates resistance to methotrexate in human colorectal adenocarcinoma cells by downregulating HIPK1," *Experimental and Therapeutic Medicine*, vol. 19, pp. 339-346, 2020.
- [9] A. D. Robinson, M.-L. Eich, and S. J. C. L. Varambally, "Dysregulation of de novo nucleotide biosynthetic pathway enzymes in cancer and targeting opportunities," *Cancer letters*, vol. 470, no. 1, pp. 134-140, 2020.
- [10] Y. Li, J. Lin, P. Wang et al., "Tumor microenvironment responsive shape-reversal self-targeting virus-inspired nano-drug for imaging-guided near-infrared-II photothermal chemotherapy," *ACS Nano*, vol. 13, no. 11, pp. 12912-12928, 2019.
- [11] Y. Li, J. Lin, Z. Cai et al., "Tumor microenvironment-activated self-recognizing nanodrug through directly tailored assembly of small-molecules for targeted synergistic chemotherapy," *Journal of Controlled Release*, vol. 321, pp. 222-235, 2020.
- [12] S. M. Rida, S. A. M. el-Hawash, H. T. Y. Fahmy, A. A. Hazzaa, and M. M. M. el-Meligy, "Synthesis of novel benzofuran and related benzimidazole derivatives for evaluation of in vitro anti-HIV-1, anticancer and antimicrobial activities," *Archives of Pharmacological Research*, vol. 29, no. 10, pp. 826-833, 2006.
- [13] J. Zhou, N. S. Xu, and Z. L. Wang, "Dissolving behavior and stability of ZnO wires in biofluids: a study on biodegradability and biocompatibility of ZnO nanostructures," *Advanced Materials*, vol. 18, no. 18, pp. 2432-2435, 2006.
- [14] P. Kielbik, J. Kaszewski, B. Dominiak et al., "Preliminary studies on biodegradable zinc oxide nanoparticles doped with Fe as a potential form of iron delivery to the living organism," *Nanoscale Research Letters*, vol. 14, no. 1, p. 373, 2019.
- [15] S.-E. Jin and H. E. Jin, "Synthesis, characterization, and three-dimensional structure generation of zinc oxide-based nanomedicine for biomedical applications," *Pharmaceutics*, vol. 11, no. 11, p. 575, 2019.
- [16] J. Brooking, S. S. Davis, and L. Illum, "Transport of nanoparticles across the rat nasal mucosa," *Journal of Drug Targeting*, vol. 9, no. 4, pp. 267-279, 2001.
- [17] H. F. H. Hassan, A. M. Mansour, A. M. H. Abo-Youssef, B. E. M. Elsadek, and B. A. S. Messiha, "Zinc oxide nanoparticles as a novel anticancer approach; in vitro and in vivo evidence," *Clinical and Experimental Pharmacology and Physiology*, vol. 44, no. 2, pp. 235-243, 2017.
- [18] A. E. M. M. Osman, M. M. S. Ahmed, M. T. E. D. Khayyal, and M. M. El-Merzabani, "Hyperthermic potentiation of cisplatin cytotoxicity on solid Ehrlich carcinoma," *Tumori Journal*, vol. 79, no. 4, pp. 268-272, 1993.
- [19] C. R. Corso, M. C. Stipp, E. R. Adami et al., "Salvia lachnostachys Benth has antitumor and chemopreventive effects against solid Ehrlich carcinoma," *Molecular Biology Reports*, vol. 46, no. 5, pp. 4827-4841, 2019.
- [20] M. F. A. El Fatoh, M. R. Farag, A. E. Shafika, M. A. Hussein, M. A. Kamel, and G. A. Salem, "Cytotoxic impact of zinc oxide nanoparticles against Ehrlich ascites carcinoma cells in mice," *International Journal of Pharma Sciences*, vol. 4, pp. 560-564, 2014.
- [21] H. Huynh, J. W. J. Lee, P. K. H. Chow et al., "Sorafenib induces growth suppression in mouse models of gastrointestinal stromal tumor," *Molecular Cancer Therapeutics*, vol. 8, no. 1, pp. 152-159, 2009.
- [22] R. Sharma and Technique, "Kinetic measurements from in situ TEM observations," *Microscopy Research and Technique*, vol. 72, no. 3, pp. 144-152, 2009.
- [23] S. Bhattacharya, A. Prasanna, and P. K. Haldar, "Evaluation of antiproliferative activity of Trichosanthes dioica root against Ehrlich ascites carcinoma cells," *Academic Journal of Cancer Research*, vol. 4, pp. 38-42, 2011.
- [24] M. Abdel-Motaal and A. Nabil, "Biological activity of some newly synthesized hydrazone derivatives derived from (dicyclopropylmethylene) hydrazone," *European Chemical Bulletin*, vol. 7, no. 10, pp. 280-287, 2018.

- [25] J. Sedlak and R. H. Lindsay, "Estimation of total, protein-bound, and nonprotein sulfhydryl groups in tissue with Ellman's reagent," *Analytical Biochemistry*, vol. 25, no. 1, pp. 192–205, 1968.
- [26] M. Uchiyama and M. Mihara, "Determination of malonaldehyde precursor in tissues by thiobarbituric acid test," *Analytical Biochemistry*, vol. 86, no. 1, pp. 271–278, 1978.
- [27] L. C. Green, D. A. Wagner, J. Glogowski, P. L. Skipper, J. S. Wishnok, and S. R. Tannenbaum, "Analysis of nitrate, nitrite, and [15N]nitrate in biological fluids," *Analytical Biochemistry*, vol. 126, no. 1, pp. 131–138, 1982.
- [28] D. Koracevic, G. Koracevic, V. Djordjevic, S. Andrejevic, and V. Cosic, "Method for the measurement of antioxidant activity in human fluids," *Journal of Clinical Pathology*, vol. 54, no. 5, pp. 356–361, 2001.
- [29] L. Astolfi, S. Ghiselli, V. Guarani et al., "Correlation of adverse effects of cisplatin administration in patients affected by solid tumours: a retrospective evaluation," *Oncology Reports*, vol. 29, no. 4, pp. 1285–1292, 2013.
- [30] M. V. Céspedes, I. Casanova, M. Parreño, and R. Mangués, "Mouse models in oncogenesis and cancer therapy," *Clinical and Translational Oncology*, vol. 8, no. 5, pp. 318–329, 2006.
- [31] M. Ekenel, F. M. Iwamoto, L. S. Ben-Porat et al., "Primary central nervous system lymphoma: the role of consolidation treatment after a complete response to high-dose methotrexate-based chemotherapy," *Cancer Research*, vol. 113, no. 5, pp. 1025–1031, 2008.
- [32] C.-Y. Liu, L. M. Tseng, J. C. Su et al., "Novel sorafenib analogues induce apoptosis through SHP-1 dependent STAT3 inactivation in human breast cancer cells," *Breast Cancer Research*, vol. 15, no. 4, 2013.
- [33] Y.-J. Zhu, B. Zheng, H. Y. Wang, and L. Chen, "New knowledge of the mechanisms of sorafenib resistance in liver cancer," *Acta Pharmacologica Sinica*, vol. 38, no. 5, pp. 614–622, 2017.
- [34] S. Wilhelm, C. Carter, M. Lynch et al., "Discovery and development of sorafenib: a multikinase inhibitor for treating cancer," *Nature Reviews Drug Discovery*, vol. 5, no. 10, pp. 835–844, 2006.
- [35] J. W. Rasmussen, E. Martinez, P. Louka, and D. G. Wingett, "Zinc oxide nanoparticles for selective destruction of tumor cells and potential for drug delivery applications," *Expert Opinion on Drug Delivery*, vol. 7, no. 9, pp. 1063–1077, 2010.
- [36] M. Kundu, P. Sadhukhan, N. Ghosh et al., "pH-responsive and targeted delivery of curcumin via phenylboronic acid-functionalized ZnO nanoparticles for breast cancer therapy," *Journal of Advanced Research*, vol. 18, pp. 161–172, 2019.
- [37] V. Forest and J. Pourchez, "Preferential binding of positive nanoparticles on cell membranes is due to electrostatic interactions: a too simplistic explanation that does not take into account the nanoparticle protein corona," *Materials Science and Engineering*, vol. 70, pp. 889–896, 2017.
- [38] F. Qu and P. C. Morais, "The pH dependence of the surface charge density in oxide-based semiconductor nanoparticles immersed in aqueous solution," *IEEE Transactions on Magnetics*, vol. 37, pp. 2654–2656, 2001.
- [39] A. Degen and M. Kosec, "Effect of pH and impurities on the surface charge of zinc oxide in aqueous solution," *Journal of the European Ceramic Society*, vol. 20, no. 6, pp. 667–673, 2000.
- [40] C. Peetla, S. Vijayaraghavalu, and V. Labhasetwar, "Biophysics of cell membrane lipids in cancer drug resistance: implications for drug transport and drug delivery with nanoparticles," *Advanced Drug Delivery Reviews*, vol. 65, no. 13–14, pp. 1686–1698, 2013.
- [41] W. Le, B. Chen, Z. Cui, Z. Liu, and D. Shi, "Detection of cancer cells based on glycolytic-regulated surface electrical charges," *Biophysics Reports*, vol. 5, no. 1, pp. 10–18, 2019.
- [42] L. Brannon-Peppas and J. O. Blanchette, "Nanoparticle and targeted systems for cancer therapy," *Advanced Drug Delivery Reviews*, vol. 56, no. 11, pp. 1649–1659, 2004.
- [43] T. Xia, M. Kovochich, J. Brant et al., "Comparison of the abilities of ambient and manufactured nanoparticles to induce cellular toxicity according to an oxidative stress paradigm," *Nano Letters*, vol. 6, no. 8, pp. 1794–1807, 2006.
- [44] R. J. Carmody and T. G. Cotter, "Signalling apoptosis: a radical approach," *Redox Report*, vol. 6, no. 2, pp. 77–90, 2001.
- [45] T. Siddique, H. X. Deng, and S. Ajroud-Driss, "Chapter 132 - motor neuron disease," in *Emery and Rimoin's Principles and Practice of Medical Genetics*, D. Rimoin, R. Pyeritz, and B. Korf, Eds., Academic Press, Oxford, 2013.
- [46] H. M. El-Shorbagy, S. M. Eissa, S. Sabet, and A. A. El-Ghor, "Apoptosis and oxidative stress as relevant mechanisms of antitumor activity and genotoxicity of ZnO-NPs alone and in combination with N-acetyl cysteine in tumor-bearing mice," *International Journal of Nanomedicine*, vol. Volume 14, pp. 3911–3928, 2019.
- [47] A. Ghiselli, M. Serafini, F. Natella, and C. Scaccini, "Total antioxidant capacity as a tool to assess redox status: critical view and experimental data," *Free Radical Biology and Medicine*, vol. 29, no. 11, pp. 1106–1114, 2000.
- [48] R. Abbasalipourkabir, H. Moradi, S. Zarei et al., "Toxicity of zinc oxide nanoparticles on adult male Wistar rats," *Food and Chemical Toxicology*, vol. 84, pp. 154–160, 2015.
- [49] S. Kilic, S. Emre, A. Metin, S. Isikoglu, and O. Erel, "Effect of the systemic use of methotrexate on the oxidative stress and paraoxonase enzyme in psoriasis patients," *Archives of Dermatological Research*, vol. 305, no. 6, pp. 495–500, 2013.
- [50] N. H. Eisa, H. S. Said, N. ElSherbiny, L. A. Eissa, and M. M. el-Shishtawy, "Phenethyl isothiocyanate triggers apoptosis, combats oxidative stress and inhibits growth of Ehrlich ascites carcinoma mouse model," *Iranian journal of pharmaceutical research*, vol. 17, no. 4, pp. 1328–1338, 2018.
- [51] A. Diab, S. El-Aziz, A. Hendawy, R. Hamza, and D. Salim, "Protective effect of antioxidants combinations (Vit A, C, E and selenium) (Antox drug) against oxidative stress and cellular toxicity induced by sorafenib in male albino rats," *Journal of Chemical and Pharmaceutical Research*, vol. 10, pp. 43–50, 2018.
- [52] R. Coriat, C. Nicco, C. Chereau et al., "Sorafenib-induced hepatocellular carcinoma cell death depends on reactive oxygen species production in vitro and in vivo," *Molecular Cancer Therapeutics*, vol. 11, no. 10, pp. 2284–2293, 2012.
- [53] K. Unfried, C. Albrecht, L. O. Klotz, A. Von Mikecz, S. Grether-Beck, and R. P. Schins, "Cellular responses to nanoparticles: target structures and mechanisms," *Nanotechnology*, vol. 1, pp. 52–71, 2007.
- [54] D.-P. Bai, X. F. Zhang, G. L. Zhang, Y. F. Huang, and S. Gurunathan, "Zinc oxide nanoparticles induce apoptosis and autophagy in human ovarian cancer cells," *International Journal of Nanomedicine*, vol. Volume 12, pp. 6521–6535, 2017.
- [55] R. B. Mokhtari, T. S. Homayouni, N. Baluch et al., "Combination therapy in combating cancer," *Oncotarget*, vol. 8, no. 23, pp. 38022–38043, 2017.

- [56] M. M. Abd-Alhaseeb, S. A. Zaitone, S. H. Abou-el-Ela, and Y. M. Moustafa, "Olmesartan potentiates the anti-angiogenic effect of sorafenib in mice bearing Ehrlich's ascites carcinoma: role of angiotensin (1-7)," *PLoS One*, vol. 9, no. 1, p. e85891, 2014.
- [57] S. Sreelatha, P. R. Padma, and E. Umasankari, "Evaluation of anticancer activity of ethanol extract of *Sesbania grandiflora* (Agati Sesban) against Ehrlich ascites carcinoma in Swiss albino mice," *Journal of Ethnopharmacology*, vol. 134, no. 3, pp. 984-987, 2011.
- [58] P. Borentain, R. Gérolami, F. Dodero et al., "Un adénome hépatique révélé par une élévation isolée des phosphatases alcalines," *Gastroentérologie Clinique et Biologique*, vol. 30, no. 2, pp. 304-306, 2006.
- [59] T. F. Mutar, E. Tousson, E. Hafez, M. A. Gazia, and S. Salem, "Ameliorative effects of vitamin B17 on the kidney against Ehrlich ascites carcinoma induced renal toxicity in mice," *Environmental Toxicology*, vol. 35, no. 4, pp. 528-537, 2019.
- [60] P. Price and T. McMillan, "Use of the tetrazolium assay in measuring the response of human tumor cells to ionizing radiation," *Cancer Research*, vol. 50, no. 5, pp. 1392-1396, 1990.
- [61] E. Gottlieb, S. M. Armour, M. H. Harris, and C. B. Thompson, "Mitochondrial membrane potential regulates matrix configuration and cytochrome *c* release during apoptosis," *Cell Death & Differentiation*, vol. 10, no. 6, pp. 709-717, 2003.
- [62] C. Schult, M. Dahlhaus, S. Ruck et al., "The multikinase inhibitor sorafenib displays significant antiproliferative effects and induces apoptosis via caspase 3, 7 and PARP in B- and T-lymphoblastic cells," *BMC Cancer*, vol. 10, no. 1, 2010.

Research Article

Metformin Ameliorates A β Pathology by Insulin-Degrading Enzyme in a Transgenic Mouse Model of Alzheimer's Disease

Xin-Yi Lu ^{1,2}, Shun Huang ³, Qu-Bo Chen,¹ Dapeng Zhang,⁴ Wanyan Li,⁴ Ran Ao,⁴ Feona Chung-Yin Leung,⁵ Zhimin Zhang,⁴ Jisheng Huang ^{6,7,8}, Ying Tang ⁹, and Shi-Jie Zhang ²

¹Biological Resource Center, The Second Affiliated Hospital of Guangzhou University of Chinese Medicine, Guangzhou, China

²Department of Neurology, The Second Affiliated Hospital of Guangzhou University of Chinese Medicine, Guangzhou, China

³Nanfang PET Center, Nanfang Hospital, Southern Medical University, Guangzhou, China

⁴The First Affiliated Hospital of Guangzhou Medical University, Guangzhou, China

⁵School of Chinese Medicine, LKS Faculty of Medicine, The University of Hong Kong, Hong Kong

⁶Drug Non-Clinical Evaluation Center of Guangzhou Institute of Pharmaceutical Industry, Guangzhou General Pharmaceutical Research Institute Co. Ltd., Guangzhou, China

⁷School of Basic Medical Sciences, Center for Post-Doctoral Studies of Southern Medical University, Guangzhou, China

⁸Post-Doctoral Research Center of Guangzhou Pharmaceutical Holdings Ltd., Guangzhou, China

⁹The First Affiliated Hospital of Guangzhou University of Chinese Medicine, Guangzhou University of Chinese Medicine, Guangzhou, China

Correspondence should be addressed to Jisheng Huang; ziyuanhuang@163.com, Ying Tang; 18825144748@163.com, and Shi-Jie Zhang; zsj19891122@gmail.com

Received 29 January 2020; Revised 5 March 2020; Accepted 25 March 2020; Published 21 April 2020

Academic Editor: Luciano Saso

Copyright © 2020 Xin-Yi Lu et al. This is an open access article distributed under the Creative Commons Attribution License, which permits unrestricted use, distribution, and reproduction in any medium, provided the original work is properly cited.

Alzheimer's disease (AD) is the most common neurodegenerative disease. The accumulation of amyloid beta (A β) is the main pathology of AD. Metformin, a well-known antidiabetic drug, has been reported to have AD-protective effect. However, the mechanism is still unclear. In this study, we tried to figure out whether metformin could activate insulin-degrading enzyme (IDE) to ameliorate A β -induced pathology. Morris water maze and Y-maze results indicated that metformin could improve the learning and memory ability in APP^{swe}/PS1^{dE9} (APP/PS1) transgenic mice. ¹⁸F-FDG PET-CT result showed that metformin could ameliorate the neural dysfunction in APP/PS1 transgenic mice. PCR analysis showed that metformin could effectively improve the mRNA expression level of nerve and synapse-related genes (*Syp*, *Ngf*, and *Bdnf*) in the brain. Metformin decreased oxidative stress (malondialdehyde and superoxide dismutase) and neuroinflammation (IL-1 β and IL-6) in APP/PS1 mice. In addition, metformin obviously reduced the A β level in the brain of APP/PS1 mice. Metformin did not affect the enzyme activities and mRNA expression levels of A β -related secretases (*ADAM10*, *BACE1*, and *PS1*). Meanwhile, metformin also did not affect the mRNA expression levels of A β -related transporters (*LRP1* and *RAGE*). Metformin increased the protein levels of p-AMPK and IDE in the brain of APP/PS1 mice, which might be the key mechanism of metformin on AD. In conclusion, the well-known antidiabetic drug, metformin, could be a promising drug for AD treatment.

1. Introduction

Alzheimer's disease (AD), a progressive neurodegenerative disease with a high incidence rate in this century, has cognitive and functional ability decline with the disease progress. AD is mainly characterized by the accumulation of amyloid

beta (A β) plaques and neurofibrillary tangles (NFTs) in the brain [1–3]. Accumulation of A β , which is generated from the amyloid precursor protein (APP), is the main hallmark of AD [4]. Thus, targeting A β is leading to a potential therapeutic strategy [5]. However, a series of clinical trials, such as inhibitors of β -secretase (BACE1) or γ -secretase (PS1), have

failed [6, 7]. Promoting the degradation or clearance of A β is considered as an alternative therapeutic strategy [8].

Diabetes mellitus (DM) is also associated with a higher risk of AD [9, 10], in which insulin deficiency or insulin resistance may be responsible. Metformin, as a major antidiabetic drug, has been demonstrated to reduce β -secretase activity, promote phospho-thr-231-tau degradation, and influence mitochondrial function [10–14]. Recently, some molecules, which are widely studied in diabetes, have been proved to affect A β clearance, including insulin-degrading enzyme (IDE), neprilysin (NEP), receptor for advanced glycation end products (RAGE), and matrix metalloproteinases (MMPs) [15–19]. Among these molecules, IDE plays an important role in both diabetes and AD. Loss-of-function mutation in the IDE gene can lead to impaired degradation of A β [20]. Colocalization and codeposition of IDE with A β plaques can be found in the AD brain. Inhibition of IDE in the brain is identified as one of the major factors involved in the crosstalk between DM and AD [21]. However, whether metformin could protect against AD through the IDE pathway is still unknown.

APP^{swe}/PS1^{dE9} (APP/PS1) double transgenic mice were used for the study. The APP/PS1 mouse exhibits the A β plaque formation and memory impairment, which is similar to clinical phenotype [22], including memory deficits, anxiety, hyperactivity, and social interaction impairment. Metformin, an experimental therapy, was used to explore the hypothesis that metformin protects against AD via IDE signaling in APP/PS1 mice.

2. Material and Methods

2.1. Materials. Metformin and Thioflavin T (ThT) reagent were purchased from Sigma-Aldrich (Saint Louis, MO, USA). A BCA protein assay kit and superoxide dismutase (SOD) assay kit were obtained from Beyotime Biotechnology. The malondialdehyde (MDA) Assay Kit (TBA method) was purchased from Nanjing Jiancheng Bioengineering Institute (Nanjing, China). qPCR reagents and ECL kit were purchased from Invitrogen. All the antibodies were obtained from Cell Signaling Technology, Inc. (Danvers, MA, USA).

2.2. Animals and Treatments. The 7-month-old male APP/PS1 double transgenic mice and wild-type mice (C57BL/6) were obtained from the Model Animal Research Institute of Nanjing University (Nanjing, China) and maintained at the laboratory animal center of Guangzhou Medical University under the standard housing conditions with free access to food and water. The animal management was approved by the Institutional Animal Care and Use Committee of Guangzhou Medical University (SCXK2019-0013). All mice were randomly divided into three groups: wild type (WT, $n = 15$), APP/PS1 ($n = 15$), and APP/PS1 + metformin (200 mg/kg/day, $n = 15$) [23, 24]. After oral drug administration for 8 weeks, mice were performed behavioral tests and subsequently sacrificed for the collection of brains.

2.3. Morris Water Maze Test. The Morris water maze test was performed to evaluate the spatial memory performance. The

opaque platform with a diameter of 10 cm was positioned 1 cm beneath the water surface. The duration of training and testing session was 60 s. In the training session, mice completed four trials daily with at least 20 minutes of interval between two trials for six consecutive days. Each mouse was released into the water by facing the wall in one of the four quadrants. If the mouse failed to reach the platform within 60 s, it would be directed to the platform and stay there for 15 s. In the testing session, the platform was removed from the pool and the mice were allowed to search for the platform for 60 s. A computerized video imaging analysis system (Feidi, Guangzhou) was used to record and analyze the swimming paths in the maze.

2.4. Y-Maze Test. The Y-maze test was performed to evaluate the working memory performance. The apparatus consisted of three arms (one start arm and two goal arms) of 30 \times 10 \times 20 cm connected by an intersection. The duration of training and testing session was 2 min. Before the training and testing sessions, the body weight of mice would reduce to 90% by food restriction. In the training session, mice completed 10 trials daily with at least 20 min interval between two trials for four consecutive days. Prior to the reward alternation testing session, each mouse would consume the food which was filled at the end of the arm for 4–6 times to habituate to the maze. The choice for each goal arm should be given equally, and the percentage of correct choices would be calculated to analysis.

2.5. ¹⁸F-FDG PET Imaging. After 8 weeks of metformin administration, the microPET-CT was used to evaluate brain glucose uptake. ¹⁸F-Fluorodeoxyglucose (¹⁸F-FDG) was intraperitoneally injected into animals. The mice were scanned by using a Focus 220 microPET scanner (Siemens Medical Solutions USA, Inc., Knoxville, TN, USA). Dynamic scans were conducted for 1 h. PET images were reconstructed using the microPET-CT manager (Siemens Medical Solutions USA, Inc.). To evaluate relative glucose metabolism, the ratio of the SUV standardized uptake value was obtained by dividing the SUV of each region with the SUV of the whole brain.

2.6. ELISA. Brain tissues were homogenized with saline, containing a cocktail of protease inhibitors. Samples were centrifuged by 12000 $\times g$ for 15 min. The supernatants were measured for IL-1 β , IL-6 (Thermo Fisher Scientific), A β 1-40, A β 1-42 (Invitrogen), and α -, β -, and γ -secretases (R&D Systems, USA) by using the ELISA kits according to the manufacturer's proposals.

2.7. ThT Staining. The sections were washed three times in PBS at room temperature and then incubated with a ThT reagent (50 μ M) for 30 min. After washing three times in PBS, the sections were captured by a fluorescence microscope (Leica).

2.8. Measurement of SOD and MDA. The brain tissues were homogenized and centrifuged by 12000 $\times g$ for 15 min. The supernatants were used to test SOD activity and MDA level according to the kit instructions (Nanjing Jiancheng Bioengineering Institute).

2.9. qPCR. Total RNA from brain tissues were extracted using a TRIzol reagent. Reverse transcription was treated with an ExScript RT Reagent Kit (Invitrogen). Real-time PCR analysis was undertaken using SYBR Premix Ex Taq (Invitrogen). The transcriptions were investigated for several target genes, including *synaptophysin* (*Syp*): For 5'-GTGCTGCAATGGTCTTCG-3' and Rev 5'-CCGTGGCCAGAAAGTCAG-3'; *nerve growth factor* (*Ngf*): For 5'-CAAGGACGCAGCTTTCTATACTG-3' and Rev 5'-CTTCAGGGACAGAGTCTCCTTCT-3'; *brain-derived neurotrophic factor* (*Bdnf*): For 5'-TACTTCGGTTGCATGAAGGCG-3' and Rev 5'-GTCAGACCTCTCGAACCTGCC-3'; *a disintegrin and metalloproteinase domain-containing protein 10* (*ADAM10*): For 5'-TTCTCCCTCCGGATCGATGT-3' and Rev 5'-ATACTGACCTCCCATCCCCG-3'; *beta-secretase 1* (*BACE1*): For 5'-ACTTTACACTCTGTTCTGGGTGG-3' and Rev 5'-ACCACAAAGCCTGGCAATCTC-3'; *presenilin 1* (*PS1*): For 5'-AATGACGACAACGGTGAGGG-3' and Rev 5'-CCAGATTAGGTGCTTCCCCG-3'; *low-density lipoprotein receptor-related protein 1* (*LRP1*): For 5'-GGACCACCATCGTGGA-3' and Rev 5'-TCCCAGCCACGGTGATAG-3'; *receptor for advanced glycation end products* (*RAGE*): For 5'-GGACCCTTAGCTGGCACTTAGA-3' and Rev 5'-GAGTCCCGTCTCAGGGTGTCT-3'; and β -actin: For 5'-AGAGCTACGAGCTGCCTGAC-3' and Rev 5'-AGCACTGTGTTGGCGTACAG-3'.

2.10. Western Blotting. The fresh brain tissues were homogenated with RIPA buffer containing 1% phenylmethanesulfonyl fluoride and phosphatase inhibitors. The samples were separated by sodium dodecyl sulfate polyacrylamide gel electrophoresis (SDS-PAGE) and transferred onto PVDF membranes. The blotting membranes were blocked with 5% BSA. The membranes were incubated at 4°C overnight with the following primary antibodies: anti-p-AMP-activated protein kinase (AMPK), anti-AMPK, anti-IDE, anti-NEP, and anti- β -actin. All the antibodies were purchased from CST. The membranes were incubated with a secondary antibody at room temperature. The membranes were covered with mixed liquid from the ECL Chemiluminescent Substrate Reagent Kit. The bands were scanned by a luminescent image analyzer (Invitrogen).

2.11. Statistical Analysis. All statistical analyses were conducted by SPSS 20.0 software. One-way analysis of variance (ANOVA) and Student *t*-test were used to analyze. Data were expressed as means \pm SEM. *p* < 0.05 was considered significant.

3. Results

3.1. Metformin Ameliorates Learning and Memory Dysfunctions in APP/PS1 Mice. To prove the therapeutic effect of metformin on APP/PS1 mice, the Morris water maze and Y-maze tests were used to assess the cognitive function. Results showed that APP/PS1 mice suffered an obvious decline in cognitive function. Metformin could significantly

improve escape latency, increase the crossing times, and shorten the time of finding the platform (Figures 1(a)–1(c)). Swimming speed differences among the three groups did not have any statistical significance (Figure 1(d)). In the Y-maze test, APP/PS1 mice showed a significant downward trend in spontaneous alternation, compared to the WT group. After metformin treatment, the mice exhibited better performance than the APP/PS1 group (Figure 1(e)).

3.2. Metformin Improves Brain Function in APP/PS1 Mice. Decreased glucose metabolism is the characteristic symptom of AD. ^{18}F -FDG-PET was used to evaluate the cerebral metabolism. As shown in Figure 2, microPET-CT imaging suggested that ^{18}F -FDG uptake intensity was sharply decreased in the brain of APP/PS1 mice. Metformin remarkably increased ^{18}F -FDG uptake in the brain of APP/PS1 mice. In addition, the mRNA expression levels of neurotrophic factors (*Bdnf* and *Ngf*) and synaptic factor (*Syp*) were significantly reduced in APP/PS1 mice (Figures 3(a)–3(c)). Metformin significantly improved the mRNA expression levels of neurotrophic factors and synapse-related proteins.

3.3. Metformin Reduces Oxidative Stress and Inflammation in the Brain of APP/PS1 Mice. Neural oxidative stress and inflammation are the key pathologies of AD [25]. In the brain of APP/PS1 mice, the level of MDA was increased, and the activity of SOD was reduced (Figures 4(a) and 4(b)). Metformin significantly relieved the oxidative stress status. In addition, the levels of inflammatory markers, IL-1 β and IL-6, were significantly increased in the brain of APP/PS1 mice (Figures 4(c) and 4(d)). Metformin reduced the levels of IL-1 β and IL-6. These data suggested that metformin could inhibit oxidative stress and inflammation in APP/PS1 mice.

3.4. Metformin Reduces A β Accumulation in the Brain of APP/PS1 Mice. The accumulation of A β is the main pathological feature of AD. The brain of APP/PS1 mice is overloaded with A β . Thus, A β levels were further studied. ELISA results indicated that metformin effectively reduced the levels of A β 1-40 and A β 1-42 in the brain of APP/PS1 mice (Figures 5(a) and 5(b)). ThT staining results further confirmed that metformin ameliorated A β accumulation in the brain of APP/PS1 mice (Figure 5(c)). These were strong evidences that metformin could reduce A β accumulation in APP/PS1 mice.

3.5. Metformin Activates AMPK and Increases IDE in the Brain of APP/PS1 Mice. We next studied how metformin influences A β metabolism. Sequential cleavage of the APP by β - and γ -secretases can produce A β [26]. Thus, we firstly detected these secretases. ELISA results showed that metformin had no effect on α -, β -, or γ -secretase (Figures 6(a)–6(c)). The mRNA expression levels of *ADAM10*, *BACE1*, and *PS1* were also tested. Metformin did not affect these gene expression levels except for a slight decrease of *BACE1* (Figures 6(d)–6(f)). We next detected the A β transportation-related gene. Results showed that metformin also had no effect on the mRNA expression levels of *LRP1* and *RAGE* (Figures 6(g) and 6(h)). In addition, IDE and NEP, as the degrading enzymes of A β , are other key aspects of the process

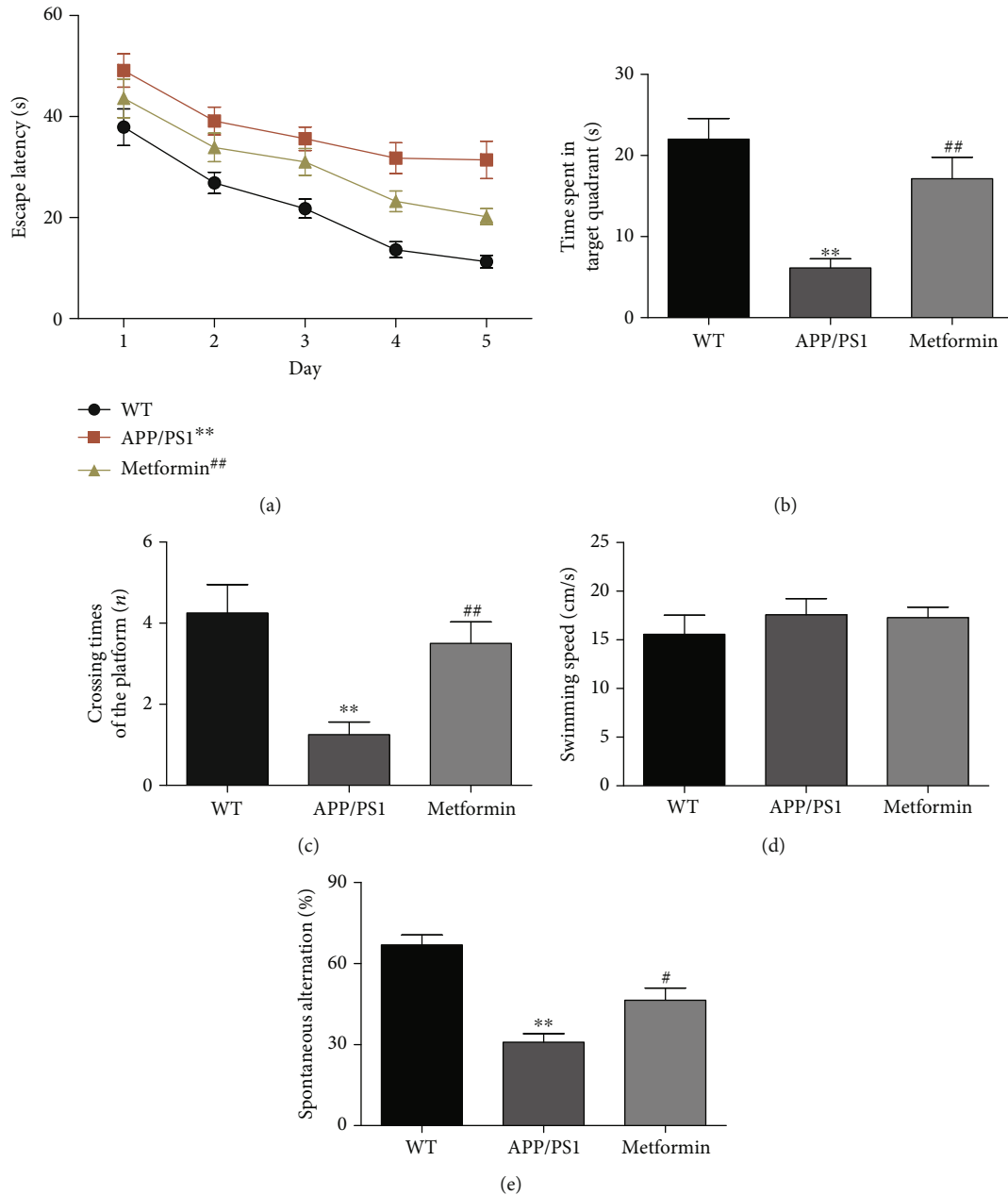


FIGURE 1: Metformin improves learning and memory impairment in APP/PS1 mice. (a) Escape latency of the five-day Morris water maze. (b) Time spent in the target quadrant in the Morris water maze. (c) Crossing times of the target platform in the Morris water maze. (d) Swimming speed in the Morris water maze. (e) Percentage of spontaneous alternation of Y-maze. Data represent the mean \pm SEM ($n = 15$ per group). * $p < 0.05$, ** $p < 0.01$, and *** $p < 0.001$ vs. WT; # $p < 0.05$, ## $p < 0.01$, and ### $p < 0.001$ vs. APP/PS1.

of $A\beta$ clearance. We assessed the protein expression levels of IDE and NEP in the brain of APP/PS1 mice (Figure 7). The IDE and NEP expression levels were significantly decreased in APP/PS1 mice compared to wild-type mice. Metformin significantly increased the expression level of IDE, but not NEP, in the APP/PS1 mice. Previous studies have reported that the AMPK pathway is involved in metformin effect [24, 27–30]. Our results verified this phenomenon. Metformin significantly increased the protein expression level of p-AMPK. These data suggested that the IDE signaling pathway might participate in the neuroprotective effect of metformin.

4. Discussion

In this study, we verified that the antidiabetic drug, metformin, could effectively ameliorate AD symptom in APP/PS1 double transgenic mice. After 8 weeks' treatment, we found that metformin could relieve learning and memory dysfunction and improve brain function. Meanwhile, metformin significantly inhibited oxidative stress and neuroinflammation. Furthermore, metformin activates AMPK and increases IDE in the brain of APP/PS1 mice, which might be the key neuroprotective mechanism of metformin.

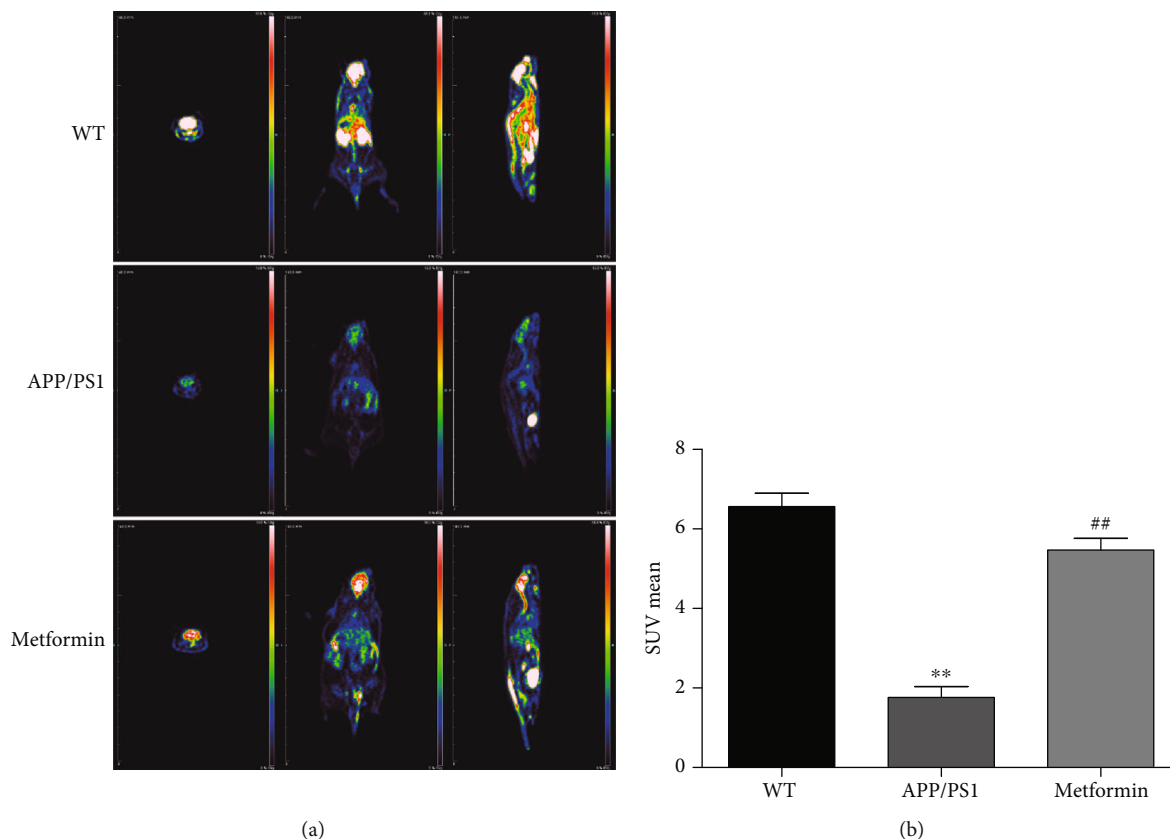


FIGURE 2: Metformin improves glucose metabolism in APP/PS1 mice. (a) PET-CT images. (b) ^{18}F -FDG uptake of mice brains. Data represent the mean \pm SEM ($n = 3$ per group). * $p < 0.05$, ** $p < 0.01$, and *** $p < 0.001$ vs. WT; # $p < 0.05$, ## $p < 0.01$, and ### $p < 0.001$ vs. APP/PS1.

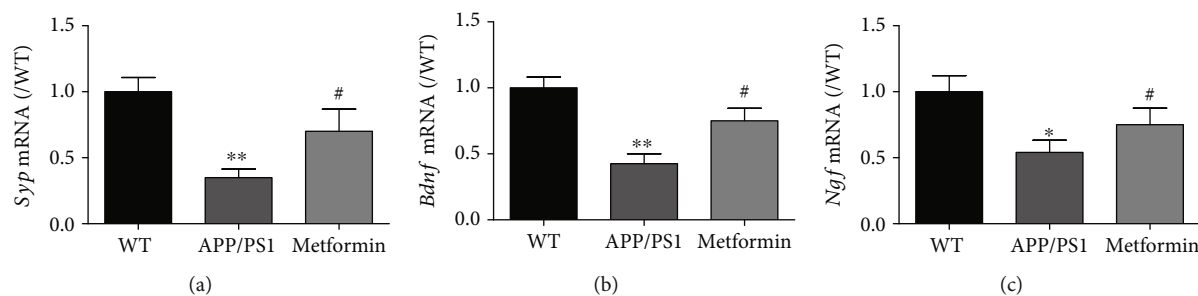


FIGURE 3: Metformin improves neurotrophic factors in APP/PS1 mice. The mRNA levels of (a) *Syp*, (b) *Bdnf*, and (c) *Ngf* in the APP/PS1 mice. Data represent the mean \pm SEM ($n = 6$ per group). * $p < 0.05$, ** $p < 0.01$, and *** $p < 0.001$ vs. WT; # $p < 0.05$, ## $p < 0.01$, and ### $p < 0.001$ vs. APP/PS1.

$A\beta$ accumulation is the main pathology of AD, which can cause the cascade reaction and induce neural apoptosis [31]. Studies have shown that metformin is beneficial for AD patients [10–12]. In this experiment, we further investigated the neuroprotective mechanism of metformin on APP/PS1 mice. We did the preliminary experiments: different dosages of metformin (25, 50, 100, and 200 mg/kg/day) were given to APP/PS1 mice. Morris water maze test results indicated that metformin (200 mg/kg/day) was the best dosage (data not shown), which was consistent with previous studies [23, 24]. Behavioral studies (Morris water maze and Y-maze) con-

firmed that metformin could significantly improve learning and memory in APP/PS1 mice, which was consistent with previous studies. In addition, metformin improved cerebral metabolism and brain function and reduced the level of $A\beta$.

$A\beta$ accumulation exacerbates oxidative damage and inflammation. $A\beta$ can increase the synthesis of the superoxide anion, reduce the activity of catalase and SOD, activate MDA production, and finally produce reactive oxygen species [30]. In our findings, we found that the contents of MDA were significantly increased and SOD activity was significantly decreased in APP/PS1 mice. After metformin

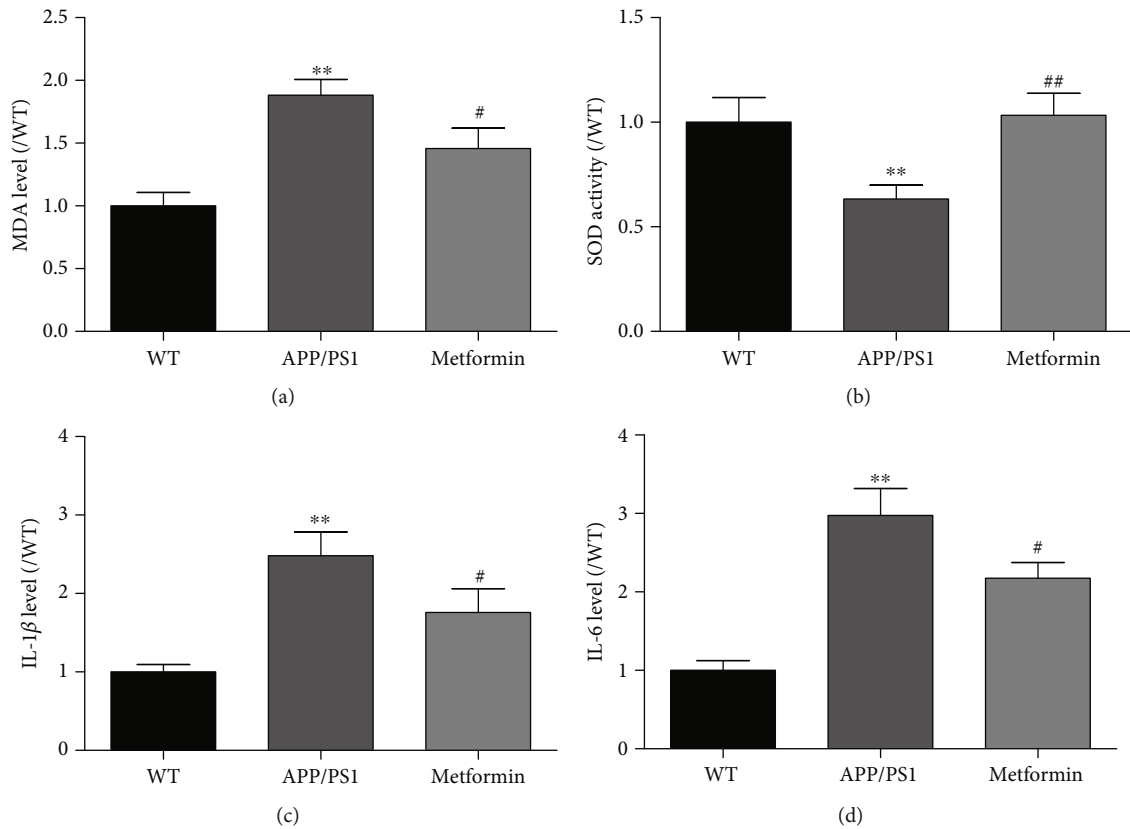


FIGURE 4: Metformin ameliorates oxidative stress and neuroinflammation in APP/PS1 mice. The level of (a) MDA and the activity of (b) SOD in the brain of APP/PS1 mice. The levels of (a) IL-1 β and (b) IL-6 in the brain of APP/PS1 mice. Experimental values were expressed as the mean \pm SEM ($n = 6$ per group). * $p < 0.05$, ** $p < 0.01$, and *** $p < 0.001$ vs. WT; # $p < 0.05$, ## $p < 0.01$, and ### $p < 0.001$ vs. APP/PS1.

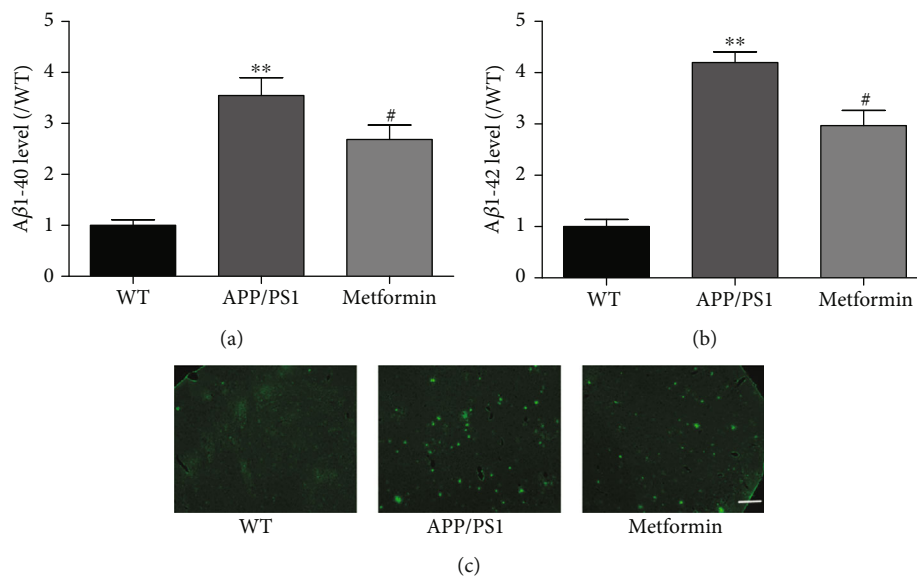


FIGURE 5: Metformin decreases A β levels in APP/PS1 mice. The levels of (a) A β 1-40 and (b) A β 1-42 in the brain of APP/PS1 mice. ThT staining of the brain slides in APP/PS1 mice. Experimental values were expressed as the mean \pm SEM ($n = 6$ per group). * $p < 0.05$, ** $p < 0.01$, and *** $p < 0.001$ vs. WT; # $p < 0.05$, ## $p < 0.01$, and ### $p < 0.001$ vs. APP/PS1. Bar: 100 μ m.

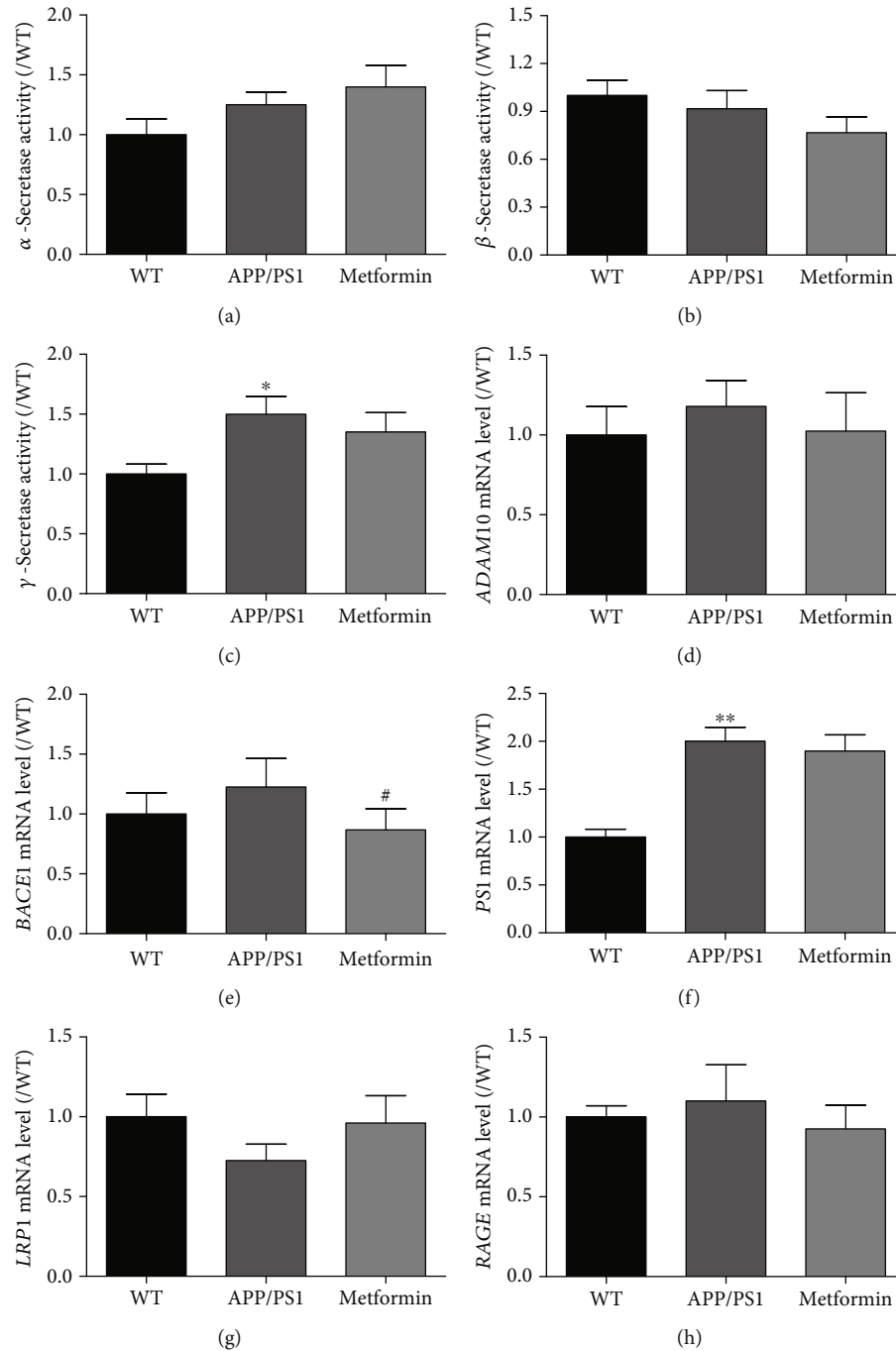


FIGURE 6: Metformin has no effect on $A\beta$ production and transportation-related genes in APP/PS1 mice. The activities of (a) α -, (b) β -, and (c) γ -secretases. The mRNA expressions of (d) *ADAM10*, (e) *BACE1*, (f) *PS1*, (g) *LRP1*, and (h) *RAGE*. Experimental values were expressed as the mean \pm SEM ($n = 6$ per group). * $p < 0.05$, ** $p < 0.01$, and *** $p < 0.001$ vs. WT; # $p < 0.05$, ## $p < 0.01$, and ### $p < 0.001$ vs. APP/PS1.

treatment, oxidative stress was relieved. $A\beta$ accumulation can increase the levels of IL-1 β and IL-6, the proinflammatory factors, in APP/PS1 mice [32, 33]. Neuroinflammation can also exacerbate AD pathology [25]. In this study, metformin reduced the levels of IL-1 β and IL-6 in APP/PS1 mice.

$A\beta$ production is strongly linked with α -, β -, and γ -secretases [26]. When APP is proteolytically processed by β - and γ -secretases, $A\beta$ production is increased. When the activity of α -secretase is increased, $A\beta$ production is inhibited. $A\beta$

transportation is another way of $A\beta$ metabolism. RAGE and LRP1 are the two main molecules, which participate in $A\beta$ transportation [34]. In this study, both ELISA and qPCR results showed that metformin had little influence on α -, β -, and γ -secretases and RAGE and LRP1, except for a small reduction in *BACE1* expression, which was consistent with a previous study [11]. These results indicated that except $A\beta$ production and transportation, other signaling pathways might also be involved in the effect of metformin.

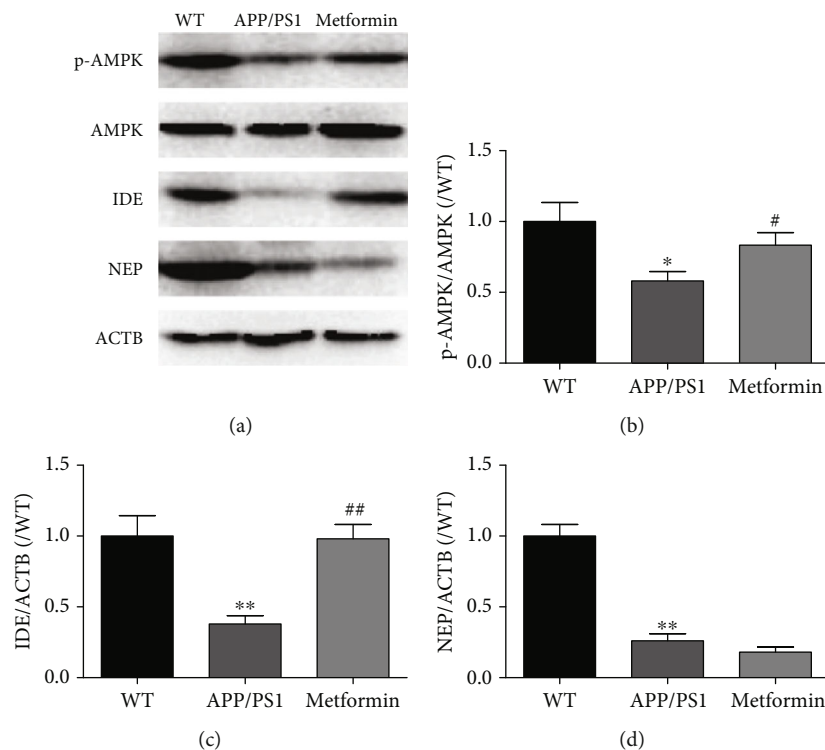


FIGURE 7: Metformin activates AMPK and increases IDE in the brain of APP/PS1 mice. (a) The representative bands of p-AMPK, AMPK, IDE, NEP, and ACTB. Western blot analysis: (b) p-AMPK/AMPK, (c) IDE/ACTB, and (d) NEP/ACTB. Experimental values were expressed as the mean \pm SEM ($n = 3$ per group). * $p < 0.05$, ** $p < 0.01$, and *** $p < 0.001$ vs. WT; # $p < 0.05$, ## $p < 0.01$, and ### $p < 0.001$ vs. APP/PS1.

AMPK is a crucial factor in the regulation of intracellular systems [30]. AMPK activation can enhance anti-inflammatory effect, which might be regulated by AMPK/mTOR and AMPK/NF- κ B signaling pathways [24, 27–30]. Metformin was supposed to have a potential pharmacological effect, due to AMPK activation [35]. In some studies, AMPK/SIRT1 takes part in the nonamyloidogenic pathway to improve AD [36]. In this study, metformin obviously activated AMPK in the brain of APP/PS1 mice. In regard to $A\beta$ clearance, IDE and NEP are the main cellular degrading enzymes of $A\beta$. Early findings showed that IDE could regulate $A\beta$ and insulin levels in vivo [37]. The major locations of IDE are the cytosol, mitochondria, and peroxisomes [38]. IDE is specific toward β -structure-forming substrates of toxic oligomers ($A\beta$) [39]. The activity of IDE in the brain decreases with age and during early stages of AD. Overexpression of IDE in transgenic mice can prevent amyloid plaque formation [40]. Inhibition of IDE is identified as one of the crosstalk between T2D and AD [21]. In our findings, the protein expression levels of IDE and NEP were significantly decreased in APP/PS1 mice. Metformin effectively increased the protein level of IDE. These data indicated that the IDE pathway might also participate in the neuroprotective effect of metformin.

In conclusion, we provided the evidence that metformin had beneficial effects by reducing the $A\beta$ level through the IDE pathway in APP/PS1 mice. In addition, metformin could decrease inflammation and oxidative stress. However, further studies are still needed. Metformin might offer a new promising avenue in AD treatment.

Data Availability

The data used to support the findings of this study are available from the corresponding author upon request.

Conflicts of Interest

The authors declare that they have no conflicts of interest.

Authors' Contributions

Xin-Yi Lu, Shun Huang, and Qu-Bo Chen finished most of the experiments; Dapeng Zhang, Wanyan Li, Ran Ao, Feona Chung-Yin Leung, and Zhimin Zhang helped with data organization. Ying Tang and Shi-Jie Zhang helped to revise the manuscript. Jisheng Huang, Ying Tang, and Shi-Jie Zhang designed the experiments and modified the manuscript. Xin-Yi Lu, Shun Huang, and Qu-Bo Chen contributed equally to this work.

Acknowledgments

This work was supported by the Project of Administration of Traditional Chinese Medicine of Guangdong Province of China (Project No. 20190408212815).

References

- [1] D. J. Selkoe and M. B. Podlisny, "Deciphering the genetic basis of Alzheimer's disease," *Annual Review of Genomics and Human Genetics*, vol. 3, pp. 67–99, 2002.

- [2] D. M. Walsh and D. J. Selkoe, "Deciphering the molecular basis of memory failure in Alzheimer's disease," *Neuron*, vol. 44, no. 1, pp. 181–193, 2004.
- [3] Y. Yang and W. Song, "Molecular links between Alzheimer's disease and diabetes mellitus," *Neuroscience*, vol. 250, pp. 140–150, 2013.
- [4] S. Sinha, J. P. Anderson, R. Barbour et al., "Purification and cloning of amyloid precursor protein β -secretase from human brain," *Nature*, vol. 402, no. 6761, pp. 537–540, 1999.
- [5] P. Picone, D. Nuzzo, D. Giacomazza, and M. Di Carlo, " β -Amyloid peptide: the cell compartment multi-faceted interaction in Alzheimer's disease," *Neurotoxicity Research*, vol. 37, no. 2, pp. 250–263, 2020.
- [6] J. Zhang, Y. Guo, Y. Wang, L. Song, R. Zhang, and Y. Du, "Long-term treadmill exercise attenuates $A\beta$ burdens and astrocyte activation in APP/PS1 mouse model of Alzheimer's disease," *Neuroscience Letters*, vol. 666, pp. 70–77, 2018.
- [7] K. Yin, J. Jin, X. Zhu et al., "CART modulates beta-amyloid metabolism-associated enzymes and attenuates memory deficits in APP/PS1 mice," *Neurological Research*, vol. 39, no. 10, pp. 885–894, 2017.
- [8] N. L. Sikanyika, H. C. Parkinson, A. I. Smith, and S. Kuruppu, "Powering amyloid beta degrading enzymes: a possible therapy for Alzheimer's disease," *Neurochemical Research*, vol. 44, no. 6, pp. 1289–1296, 2019.
- [9] I. Kazkayasi, M.-A.-M. Ismail, C. Parrado-Fernandez et al., "Lack of insulin results in reduced seladin-1 expression in primary cultured neurons and in cerebral cortex of STZ-induced diabetic rats," *Neuroscience Letters*, vol. 633, pp. 174–181, 2016.
- [10] P. Picone, S. Vilasi, F. Librizzi et al., "Biological and biophysics aspects of metformin-induced effects: cortex mitochondrial dysfunction and promotion of toxic amyloid pre-fibrillar aggregates," *Aging*, vol. 8, no. 8, pp. 1718–1734, 2016.
- [11] Y. Chen, K. Zhou, R. Wang et al., "Antidiabetic drug metformin (Glucophage^R) increases biogenesis of Alzheimer's amyloid peptides via up-regulating *BACE1* transcription," *Proceedings of the National Academy of Sciences of the United States of America*, vol. 106, no. 10, pp. 3907–3912, 2009.
- [12] M. P. Sajan, B. C. Hansen, M. G. Higgs et al., "Atypical PKC, PKC λ /1, activates β -secretase and increases $A\beta_{1-40/42}$ and phospho-tau in mouse brain and isolated neuronal cells, and may link hyperinsulinemia and other aPKC activators to development of pathological and memory abnormalities in Alzheimer's disease," *Neurobiology of Aging*, vol. 61, pp. 225–237, 2018.
- [13] P. Imfeld, M. Bodmer, S. S. Jick, and C. R. Meier, "Metformin, other antidiabetic drugs, and risk of Alzheimer's disease: a population-based case-control study," *Journal of the American Geriatrics Society*, vol. 60, no. 5, pp. 916–921, 2012.
- [14] P. Picone, D. Nuzzo, L. Caruana et al., "Metformin increases APP expression and processing via oxidative stress, mitochondrial dysfunction and NF- κ B activation: use of insulin to attenuate metformin's effect," *Biochimica et Biophysica Acta (BBA) - Molecular Cell Research*, vol. 1853, no. 5, pp. 1046–1059, 2015.
- [15] J.-M. Paumier, N. A. Py, L. García-González et al., "Proamyloidogenic effects of membrane type 1 matrix metalloproteinase involve MMP-2 and BACE-1 activities, and the modulation of APP trafficking," *The FASEB Journal*, vol. 33, no. 2, pp. 2910–2927, 2019.
- [16] K. J. Yin, J. R. Cirrito, P. Yan et al., "Matrix metalloproteinases expressed by astrocytes mediate extracellular amyloid- β peptide catabolism," *The Journal of Neuroscience*, vol. 26, no. 43, pp. 10939–10948, 2006.
- [17] P. Yan, X. Hu, H. Song et al., "Matrix metalloproteinase-9 degrades amyloid- β fibrils *in vitro* and compact plaques *in situ*," *Journal of Biological Chemistry*, vol. 281, no. 34, pp. 24566–24574, 2006.
- [18] A. Fragkouli, E. C. Tsilibary, and A. K. Tzinia, "Neuroprotective role of MMP-9 overexpression in the brain of Alzheimer's 5xFAD mice," *Neurobiology of Disease*, vol. 70, pp. 179–189, 2014.
- [19] K. Baranger, Y. Marchalant, A. E. Bonnet et al., "MT5-MMP is a new pro-amyloidogenic proteinase that promotes amyloid pathology and cognitive decline in a transgenic mouse model of Alzheimer's disease," *Cellular and Molecular Life Sciences*, vol. 73, no. 1, pp. 217–236, 2016.
- [20] W. Farris, S. Mansourian, M. A. Leissring et al., "Partial loss-of-function mutations in insulin-degrading enzyme that induce diabetes also impair degradation of amyloid β -protein," *The American Journal of Pathology*, vol. 164, no. 4, pp. 1425–1434, 2004.
- [21] M. W. Akhtar, S. Sanz-Blasco, N. Dolatabadi et al., "Elevated glucose and oligomeric β -amyloid disrupt synapses via a common pathway of aberrant protein S -nitrosylation," *Nature Communications*, vol. 7, no. 1, article 10242, 2016.
- [22] H. Huang, S. Nie, M. Cao et al., "Characterization of AD-like phenotype in aged APPSwe/PS1dE9 mice," *Age*, vol. 38, no. 4, pp. 303–322, 2016.
- [23] S. A. Farr, E. Roesler, M. L. Niehoff, D. A. Roby, A. McKee, and J. E. Morley, "Metformin improves learning and memory in the SAMP8 mouse model of Alzheimer's disease," *Journal of Alzheimer's Disease*, vol. 68, no. 4, pp. 1699–1710, 2019.
- [24] Z. Ou, X. Kong, X. Sun et al., "Metformin treatment prevents amyloid plaque deposition and memory impairment in APP/PS1 mice," *Brain, Behavior, and Immunity*, vol. 69, pp. 351–363, 2018.
- [25] S. Kyrkanides, R. H. Tallents, J.-n. H. Miller et al., "Osteoarthritis accelerates and exacerbates Alzheimer's disease pathology in mice," *Journal of Neuroinflammation*, vol. 8, no. 1, article 112, 2011.
- [26] F. Song, T. Liu, S. Meng, F. Li, Y. Zhang, and L. Jiang, "Insulin-like growth factor-1 alleviates expression of $A\beta_{1-40}$ and α -, β -, and γ -secretases in the cortex and hippocampus of APP/PS1 double transgenic mice," *Journal of Molecular Neuroscience*, vol. 66, no. 4, pp. 595–603, 2018.
- [27] Z. Gong, J. Huang, B. Xu et al., "Urolithin A attenuates memory impairment and neuroinflammation in APP/PS1 mice," *Journal of Neuroinflammation*, vol. 16, no. 1, p. 62, 2019.
- [28] R. Corpas, C. Grinan-Ferre, E. Rodriguez-Farre, M. Pallas, and C. Sanfeliu, "Resveratrol induces brain resilience against Alzheimer neurodegeneration through proteostasis enhancement," *Molecular Neurobiology*, vol. 56, no. 2, pp. 1502–1516, 2019.
- [29] H. Zhang, C. Zhao, G. Cao et al., "Berberine modulates amyloid- β peptide generation by activating AMP-activated protein kinase," *Neuropharmacology*, vol. 125, pp. 408–417, 2017.
- [30] M. Markowicz-Piasecka, J. Sikora, A. Szydłowska, A. Skupien, E. Mikiciuk-Olasik, and K. M. Huttunen, "Metformin - a future therapy for neurodegenerative diseases : theme: drug discovery, development and delivery in Alzheimer's disease

- guest editor: Davide Brambilla,” *Pharmaceutical Research*, vol. 34, no. 12, pp. 2614–2627, 2017.
- [31] Y. M. Li, M. Xu, M. T. Lai et al., “Photoactivated gamma-secretase inhibitors directed to the active site covalently label presenilin 1,” *Nature*, vol. 405, no. 6787, pp. 689–694, 2000.
- [32] L. Hoeijmakers, S. R. Ruigrok, A. Amelanchik et al., “Early-life stress lastingly alters the neuroinflammatory response to amyloid pathology in an Alzheimer’s disease mouse model,” *Brain, Behavior, and Immunity*, vol. 63, pp. 160–175, 2017.
- [33] M. L. de Lemos, A. V. de la Torre, D. Petrov et al., “Evaluation of hypoxia inducible factor expression in inflammatory and neurodegenerative brain models,” *The International Journal of Biochemistry & Cell Biology*, vol. 45, no. 7, pp. 1377–1388, 2013.
- [34] Q. Liu, J. Zhang, H. Tran et al., “LRP1 shedding in human brain: roles of ADAM10 and ADAM17,” *Molecular Neurodegeneration*, vol. 4, no. 1, p. 17, 2009.
- [35] R. D. Yudhani, I. Astuti, M. Mustofa, D. Indarto, and M. Muthmainah, “Metformin modulates cyclin D1 and P53 expression to inhibit cell proliferation and to induce apoptosis in cervical cancer cell lines,” *Asian Pacific Journal of Cancer Prevention*, vol. 20, no. 6, pp. 1667–1673, 2019.
- [36] S. A. Shah, G. H. Yoon, S. S. Chung et al., “Novel osmotin inhibits SREBP2 via the AdipoR1/AMPK/SIRT1 pathway to improve Alzheimer’s disease neuropathological deficits,” *Molecular Psychiatry*, vol. 22, no. 3, pp. 407–416, 2017.
- [37] W. Farris, S. Mansourian, Y. Chang et al., “Insulin-degrading enzyme regulates the levels of insulin, amyloid β -protein, and the β -amyloid precursor protein intracellular domain *in vivo*,” *Proceedings of the National Academy of Sciences of the United States of America*, vol. 100, no. 7, pp. 4162–4167, 2003.
- [38] G. R. Tundo, D. Sbardella, C. Ciaccio et al., “Multiple functions of insulin-degrading enzyme: a metabolic crosslight?,” *Critical Reviews in Biochemistry and Molecular Biology*, vol. 52, no. 5, pp. 554–582, 2017.
- [39] I. V. Kurochkin, E. Guarnera, and I. N. Berezovsky, “Insulin-Degrading Enzyme in the Fight against Alzheimer’s Disease,” *Trends in Pharmacological Sciences*, vol. 39, no. 1, pp. 49–58, 2018.
- [40] A. Stargardt, J. Gillis, W. Kamphuis et al., “Reduced amyloid- β degradation in early Alzheimer’s disease but not in the APPs-wePS1dE9 and 3xTg-AD mouse models,” *Aging Cell*, vol. 12, no. 3, pp. 499–507, 2013.

Research Article

TBHQ Attenuates Neurotoxicity Induced by Methamphetamine in the VTA through the Nrf2/HO-1 and PI3K/AKT Signaling Pathways

Xianyi Meng , Chenghong Zhang , Yu Guo, Ying Han, Chunyang Wang, Haiying Chu , Li Kong, and Haiying Ma 

Department of Histology and Embryology, College of Basic Medical Sciences, Dalian Medical University, Dalian 116044, China

Correspondence should be addressed to Haiying Ma; hyma20060602@aliyun.com

Received 30 January 2020; Revised 3 March 2020; Accepted 17 March 2020; Published 13 April 2020

Academic Editor: Luciano Saso

Copyright © 2020 Xianyi Meng et al. This is an open access article distributed under the Creative Commons Attribution License, which permits unrestricted use, distribution, and reproduction in any medium, provided the original work is properly cited.

Methamphetamine (METH) leads to nervous system toxicity. Long-term exposure to METH results in damage to dopamine neurons in the ventral tegmental area (VTA), and depression-like behavior is a clinical symptom of this toxicity. The current study was designed to investigate whether the antioxidant tertiary butylhydroquinone (TBHQ) can alleviate neurotoxicity through both antioxidative stress and antiapoptotic signaling pathways in the VTA. Rats were randomly divided into a control group, a METH-treated group (METH group), and a METH+TBHQ-treated group (METH+TBHQ group). Intraperitoneal injections of METH at a dose of 10 mg/kg were administered to the rats in the METH and METH+TBHQ groups for one week, and METH was then administered at a dose that increased by 1 mg/kg per week until the sixth week, when the daily dosage reached 15 mg/kg. The rats in the METH+TBHQ group received 12.5 mg/kg TBHQ intragastrically. Chronic exposure to METH resulted in increased immobility times in the forced swimming test (FST) and tail suspension test (TST) and led to depression-like behavior. The production of reactive oxygen species (ROS) and apoptosis levels were increased in the VTA of animals in the METH-treated group. METH downregulated Nrf2, HO-1, PI3K, and AKT, key factors of oxidative stress, and the apoptosis signaling pathway. Moreover, METH increased the caspase-3 immunocent. These changes were reversed by treatment with the antioxidant TBHQ. The results indicate that TBHQ can enhance Nrf2-induced antioxidative stress and PI3K-induced antiapoptotic effects, which can alleviate METH-induced ROS and apoptosis, and that the crosstalk between Nrf2 and PI3K/AKT is likely the key factor involved in the protective effect of TBHQ against METH-induced chronic nervous system toxicity.

1. Introduction

Methamphetamine (METH) is a highly addictive drug that adversely impacts physical functions, brain functions, cognition, and social support. Dependence on this drug is difficult to treat [1, 2] because of the severity of METH withdrawal symptoms. In contrast to METH withdrawal, which is characterized by sedation and depression, chronic METH exposure is well correlated with increased depression and hyperactivity [3] due to the stimulant actions of the drug. However, stress can trigger paradoxical depression during METH withdrawal despite the fact that the stimulant effect of the drug is no longer present [4, 5]. Current evidence indi-

cates that this neurotoxic effect of METH is due to the damage it induces in the dopaminergic (DAergic) nervous system. METH competes with dopamine (DA) uptake, stimulates DA efflux via the dopamine transporter (DAT) [6], and decreases tyrosine hydroxylase (TH) activity [7]. When administered in chronic doses, METH induces long-term deficits in striatal DAergic markers, including the DAT, TH, DA, and DA metabolites [8–11]. To some extent, the loss of DAT, TH, DA, and its metabolites is due to DAergic neuron damage and the physical loss of axons [12], which is a cause of several mental diseases and plays central roles in the predisposition of chronic METH users to the development of depression-like behavior. DA neurons project from

the ventral tegmental area (VTA), which is an important part of the mesolimbic DA system [13] and a key modulator of motivated behaviors, reinforcement learning, and reward processing [14, 15]. Dysfunction of this system has been implicated in neuropsychiatric disorders such as substance abuse disorders [16, 17] and depression [18]. While METH addiction has led to intense study of the influence of VTA DA neuron damage on abuse behaviors, much less is known about the relationship between METH-induced depression-like behavior and VTA DA neuron injury.

METH-induced neurotoxicity may be related to apoptosis [18], oxidative stress (OS) [19, 20], and inflammatory changes [21]. The oxidative damage-inducing action of METH may be mediated in part by reactive oxygen species (ROS) [22]. Others have shown that exposure to METH increases the content of malondialdehyde, a product of lipid peroxidation by ROS, in brain regions of METH-exposed rats [23] and METH users [24]. Additionally, some studies have shown that METH dependence and the administration of large doses of METH [25] induce long-term changes in the brain structure, function, synaptic plasticity [26], and cell death via apoptotic and neurotoxic effects [27].

Nuclear factor erythroid 2-related factor-2 (Nrf2) is a fundamental regulator of antioxidant response element-dependent transcription and plays a significant role in the cellular adaptive response to OS [28]. Under unstressed conditions, a low level of Nrf2 is maintained by Kelch-like ECH-associated protein 1, while under OS conditions, Nrf2 is released to activate antioxidant response elements, e.g., heme oxygenase-1 (HO-1), in the nucleus [29].

Phosphatidylinositol 3-kinase (PI3K) is involved in various cellular functions, such as cell growth, proliferation, differentiation, motility, and survival, by activating protein kinase B (also known as AKT) [30]. Various reports have demonstrated that the activation of the AKT signaling pathway in different cell types is sufficient to prevent cell death induced by various apoptotic stimuli or to inhibit growth factor-induced cell survival by significantly inhibiting AKT signaling. Studies have reported that activated nuclear Nrf2, in addition to having antiapoptotic effects, further regulates several endogenous redox-regulated enzymes, such as HO-1 and glutathione cysteine ligase modulatory subunit (GCLM), via phosphorylated PI3K and phosphorylated AKT [31, 32]. Based on these findings, we hypothesize that Nrf2-PI3K is likely the key crosstalk factor linked to OS and apoptosis induced by METH.

Tertiary butylhydroquinone (TBHQ), a commonly used food antioxidant permitted by China (Health Standard GB2760.2011), is widely found in oils, biscuits, and other foods. The bodily oxidation of TBHQ can provide H⁺ radicals, which can stop the reaction and thus play an antioxidant role [33]. Furthermore, TBHQ induces phase II enzymes and the Nrf2 signaling pathway and shows remarkable antioxidant activity in various cell types and tissues. TBHQ was reported to reduce OS-induced injury in mice with diabetes by activating the Nrf2/ARE pathway [34] and to reduce the apoptosis of human neural stem cells and other cell types [35]. TBHQ also demonstrated the ability to repair nerve cells in the brains of mice with brain injury [36]. Therefore, in the current study, a model of chronic METH exposure

was established, and TBHQ was administered. Our hypothesis was tested, and the findings indicated that chronic METH exposure can induce DA neuron damage, probably via increasing OS and apoptosis, and that these changes can be alleviated by TBHQ.

2. Materials and Methods

2.1. Chronic Methamphetamine Exposure. Thirty male Wistar rats (200 ± 10 g) were purchased from the Animal Resource Center of China Medical University (certificate number: Liaoning SCSK 2012-0005). All 30 rats were randomly divided into a control group, a METH-treated group (METH group), and a TBHQ administration group (METH+TBHQ group). During the first week, intraperitoneal injections of methamphetamine at a dose of 10 mg/kg were administered to the rats in the METH and METH+TBHQ groups, and METH was then administered twice per day for 6 weeks at a dose that increased by 1 mg/kg per week until the sixth week, when the daily dose reached 15 mg/kg [37, 38]. Furthermore, the rats in the control group were injected with an equal volume of a 0.9% physiological saline solution. After the administration of METH, the rats in the METH+TBHQ group then received 12.5 mg/kg TBHQ intragastrically. The rats in the control and METH groups were intragastrically administered an equal volume of 0.5% gum tragacanth. All animals were housed in a room with controlled temperature (18–22°C) and humidity (50%–70%) on an alternating 12 h light/12 h dark cycle and provided solid food and water ad libitum. All procedures were performed in accordance with the *Guide for the Care and Use of Laboratory Animals* of the National Institutes of Health (NIH), and all protocols were approved by the Institutional Animal Care and Use Committee of Dalian Medical University. A schematic representation of protocols, treatments, behavioral tests, and biochemical analysis is presented in Figure 1.

2.2. Forced Swimming Test (FST). The FST was performed according to previous reports [39, 40]. The behavioral apparatus consisted of a cylindrical tank with water, and the mice could not touch the bottom of the tank or escape. The tank was made of transparent Plexiglas that was 30 cm high and 20 cm in diameter and filled with water at 22 ± 2°C to a depth of 19 cm. The mice were placed in the cylinder for 5 min, and the session was recorded. The water was replaced with clean water after each test. Three predominant behaviors were observed in the FST: immobility (when a mouse floated in the water without struggling and moved only enough to keep its head above the water), swimming (when a mouse moved horizontally in the swim cylinder, including crossing into another quadrant), and climbing (upward-directed movement of the forepaws, usually against the side of the swim cylinder) [39, 41]. Scoring was performed by an independent observer who was blinded to the treatment conditions. The total time spent engaged in each activity was analyzed.

2.3. Tail Suspension Test (TST). The TST was performed according to previous reports [42]. Each mouse was individually suspended by the tail to a vertical bar. The animals were

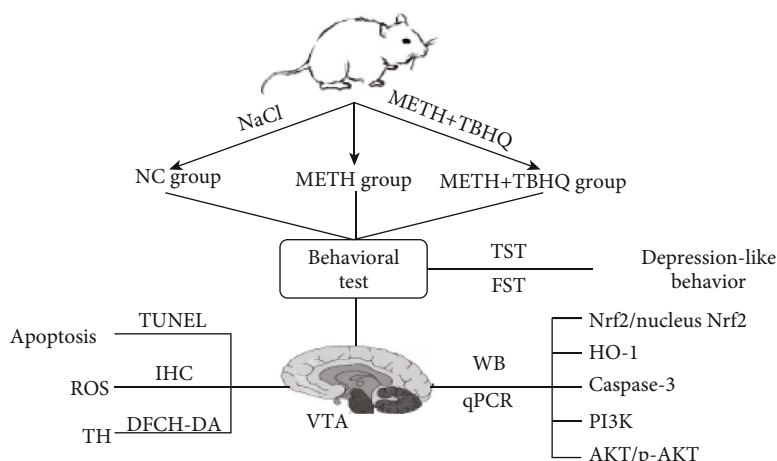


FIGURE 1: A schematic representation of protocols, treatments, behavioral tests, and biochemical analysis.

fastened by the tail for 6 min. The total duration of immobility was recorded during the last 4 min of the 6 min long testing period. The mouse was judged to be immobile when it ceased moving its limbs and body, making only those movements necessary to breathe. The immobility time was scored in real time by an independent observer who was blinded to the treatments.

2.4. Immunohistochemistry (IHC). Rats were overdosed with sodium pentobarbital and transcardially perfused with 0.9% saline followed by 4% paraformaldehyde. Their brains were then extracted and postfixed in 4% paraformaldehyde in deionized water before being transferred to gradient alcohol solutions for dehydration. After dehydration, the brains were embedded in paraffin and cut into 10 μm thick coronal paraffin sections. The sections were placed in an oven to dry for 2 h and stored at room temperature until IHC was performed [43].

Paraffin sections were hydrated in gradient alcohol solutions before being transferred to ethylenediaminetetraacetic acid (EDTA) for antigen repair and washed 3 times with phosphate-buffered saline (PBS). The sections were blocked with goat serum solution for 15 min at room temperature, incubated overnight at 4°C with rabbit anti-TH (1:200, Proteintech, USA), and washed 3 times with PBS. Then, the sections were incubated with appropriate amounts of biotin-labeled goat anti-mouse/rabbit IgG at room temperature for 20 min and washed 3 times with PBS. Subsequently, the sections were incubated with the appropriate amount of horseradish peroxidase-labeled streptavidin at room temperature for 20 min and washed 3 times with PBS. Diaminobenzidine (DAB) solution was applied to the sections for 10 s–5 min, and the sections were washed 3 times with PBS. Hematoxylin was used to stain the cell nuclei. Five random slices were selected from each group, and five randomly selected visual fields in the VTA region from each slice were observed. The mean optical density was quantified by Image-Pro Plus 5.1 software.

2.5. In Situ TdT-Mediated dUTP Nick End Labeling (TUNEL) Assay. The TUNEL assay was performed on tissues according

to the manufacturer's instructions (TransGen Biotech, China). Briefly, deparaffinized tissue sections were washed with PBS 3 times. One hundred microliters of immunostaining permeate (0.1% Triton X-100) was added and incubated for 8–10 min at ambient temperature followed by washing with PBS for 5 min. Tissues were incubated with 50 μl of a well-mixed labeling solution and 2 μl of terminal deoxynucleotidyl transferase (TdT) at 37°C for 60 min in the dark to allow the tailing reaction to occur and then washed with PBS for 5 min 3 times. Then, 100 μl of immunostaining permeate (0.1% Triton X-100) was added and incubated for 5 min at ambient temperature 3 times. One drop of antifade solution was added to the area containing the treated section, and the slices were mounted using glass coverslips and left to dry for 5–10 min [44]. Fluorescent cells were quantified by Image-Pro Plus 5.1 software.

2.6. ROS Staining and Fluorescence Microscopy Imaging. Rats were overdosed with sodium pentobarbital and transcardially perfused with 0.9% saline followed by 4% paraformaldehyde. Their brains were then extracted and postfixed for 3 h in 4% paraformaldehyde in deionized water before being transferred to 30% sucrose in deionized water. The brains were allowed to sink in the sucrose solution and were then cut on a Leica cryostat into four series of 15 μm coronal sections. Frozen sections were fixed with cold acetone for 15 min at 4°C, and the serial sections were stored at -20°C until immunofluorescence (IF) analysis was performed [45].

ROS staining was performed according to the following specifications: frozen sections were washed with PBS three times for 10 min each, incubated in the probe solution (DCFH-DA) at 37°C for 30 min, washed with PBS, stained with DAPI, and sealed. The sections were then observed, and images were taken with a fluorescence microscope. The fluorescence intensity was quantified by Image-Pro Plus 5.1 software.

2.7. Western Blot Analysis. Nrf2, HO-1, PI3K, AKT, p-AKT, and caspase-3 were analyzed by Western blotting. Rats were anesthetized with isoflurane and immediately decapitated. The brains were quickly dissected, and sagittal sections were

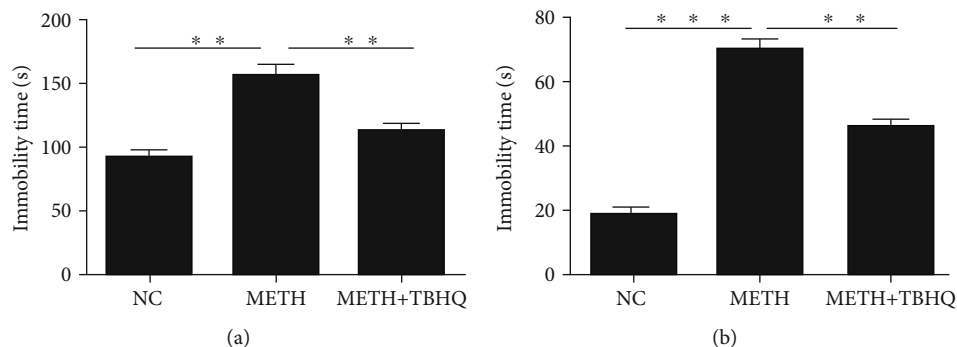


FIGURE 2: The antidepressant-like effects of TBHQ in rats treated with METH: (a) forced swimming test; (b) tail suspension test. The values represent the means \pm SEMs ($n = 5$). ** $p < 0.01$, *** $p < 0.001$.

cut at a thickness of 30 μm and stored at -80°C for Western blot experiments and reverse transcription-polymerase chain reaction (real-time PCR).

The samples were thawed, washed in ice-cold PBS, and sonicated in KeyGen lysis assay buffer (KeyGen Biotech, China). The samples were then sonicated, incubated on ice for 30 min, and centrifuged at $10,000 \times g$ for 20 min at 4°C . The protein concentration in the supernatant was determined by a Pierce BCA Protein Assay Kit (Life Technologies). Equal amounts of protein (20 μg) were combined with loading buffer, boiled for 5 min, and loaded onto 8–12% SDS-PAGE minigels. The separated proteins were transferred onto PVDF membranes (Merck Millipore, Darmstadt, Germany). The membranes were blocked with 5% nonfat milk in TBST (0.1% Tween 20 in 20 mM Tris-HCl, pH 7.4, and 410 mM NaCl) for 2 h at room temperature and then incubated overnight at 4°C with Nrf2 (1:2000, Proteintech, USA), HO-1 (1:2000, Proteintech), PI3K (1:2000, Proteintech), AKT (1:2000, Proteintech), p-AKT (1:2000, Proteintech), caspase-3 (1:2000, Proteintech), and β -actin (1:200, Abcam, UK). The blots were washed with TBST three times for 10 min each, incubated for 1 h with horseradish peroxidase-conjugated goat anti-rabbit or goat anti-mouse IgG (1:5000; ZSGB-Bio, China), and washed with TBST three times for 10 min each. The bound antibodies were detected by chemiluminescence using an ECL Western blotting detection system kit (GE Amersham Biosciences, Buckinghamshire, UK) and exposed to ChemiDOC™ XRS+ Image Lab™ Software (Bio-Rad Laboratories, Inc., Hercules, CA, USA) [46].

2.8. Quantitative Real-Time PCR. Total RNA was isolated from tissues using a TRIzol reagent (TaKaRa, China) according to the manufacturer's instructions and treated with RNase-free DNase (TaKaRa). Single-stranded cDNA synthesis was performed using AMV Reverse Transcriptase (TaKaRa). PCR was performed using Taq DNAzyme (TaKaRa) under standard conditions (10 μl of 5x PCR Buffer, 28.75 μl of ddH_2O , 0.25 μl of TaKaRa Ex Taq HS, 0.5 μl of each specific primer, and 10 μl of cDNA) using a hot start at 94°C for 4 min; 30 cycles at 94°C for 30 s, 55°C for 30 s, and 72°C for 1 min; and a final extension at 72°C for 10 min. Glyceraldehyde 3-phosphate dehydrogenase (GAPDH) was

coamplified as an internal control in each reaction. The primers for the target genes were as follows: Nrf2, forward primer 5'-GTCCAAGGAGCAATTCA-3' and reverse primer 5'-TCGTCTTTAAGTGGCC-3'; PI3K, forward primer 5'-CCACGACGATTGCTCAA-3' and reverse primer 5'-AGCCTGCACAGGAGTAA-3'; and caspase-3, forward primer 5'-CAATGGTACCGATGTCGATG-3' and reverse primer 5'-GACCCGTCCCTTGAATTTCT-3'.

2.9. Statistical Analysis. Independent sample t -tests were performed to detect differences between the mean values of the groups. Data are expressed as the means \pm SEMs for three independent experiments and were analyzed by GraphPad Prism 5.0 software (GraphPad Software, Inc., La Jolla, CA, USA). Differences were considered significant at $p < 0.05$.

3. Results

3.1. The Antidepressant-Like Effects of TBHQ on a Model of Chronic METH Exposure. The depressive-like behaviors of METH-treated rats and METH+TBHQ-treated rats were evaluated using the FST and TST. The analysis showed that immobility times in both the FST and TST were significantly increased in the METH-treated rats compared to the control rats ($p < 0.01$ and $p < 0.001$, respectively). However, compared with the METH-treated rats, the METH+TBHQ-treated rats showed a decreased immobility time ($p < 0.01$ and $p < 0.01$, respectively) (see Figures 2(a) and 2(b)).

3.2. The Administration of TBHQ Rescued Neuronal Morphology in the VTA. To verify the damage to DA neurons in the VTA induced by METH, we detected the TH protein immunoccontent by immunohistochemistry. The number of TH-immunolabeled neurons was decreased in METH-treated rats compared to that in control rats (see Figure 3(a)). Quantitative analysis showed that the average optical density was significantly decreased in METH-treated rats compared with control rats ($p < 0.001$). Compared with the METH-treated rats, the METH+TBHQ-treated rats showed an increased average optical density ($p < 0.05$) (see Figure 3(b)).

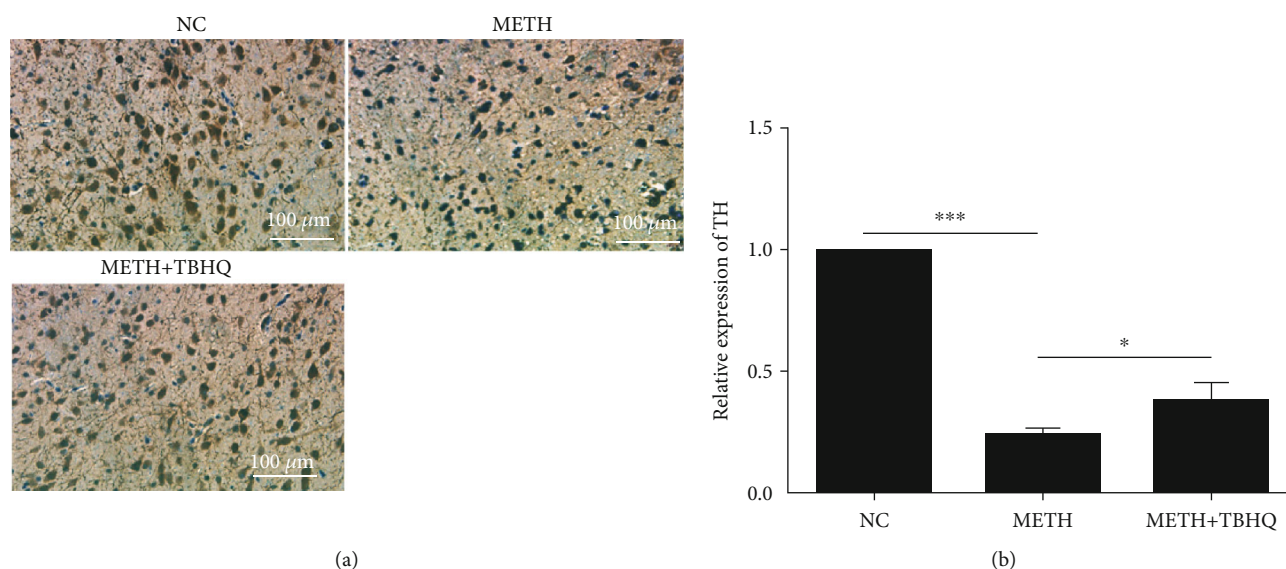


FIGURE 3: The administration of TBHQ increased the immunocontent of TH during treatment with METH. (a) Representative immunohistochemical staining for TH in the VTA. (b) TH-positive cells were quantified by the mean optical density values. The data are expressed as the means \pm SEMs of three independent experiments. $n = 5$. * $p < 0.05$, *** $p < 0.001$.

3.3. The Antiapoptotic Effect of TBHQ in the VTA Induced by METH. We detected the apoptosis of neurons by the TUNEL assay to further verify the damage to neurons in the VTA induced by METH. The number of positive cells with red fluorescence signals was much higher in the METH group than in the control group (see Figure 4(a)). Quantitative analysis showed that the number of positive cells was significantly increased in METH-treated rats compared with control rats ($p < 0.05$) but decreased in the VTA of METH+TBHQ-treated rats compared with METH-treated rats ($p < 0.05$) (see Figure 4(b)).

3.4. The Administration of TBHQ Decreased the Production of ROS in the VTA. Increased ROS levels are an important indicator of OS [47]. Figure 5(a) shows ROS staining in the VTA. The METH-treated rats showed stronger green fluorescence signals than the control rats. Compared to the METH-treated group, the METH+TBHQ-treated group showed distinctly less green fluorescence ($p < 0.05$) (see Figure 5(b)).

3.5. Effects of TBHQ on the Gene and Protein Levels of Nrf2, a Key Factor in the Antioxidant Stress Signaling Pathway, in the VTA of METH-Treated Rats. Changes in the immunocontent of Nrf2 partly reflected the degree of induction and development of antioxidant stress. Real-time PCR was used to detect Nrf2. The results showed that the Nrf2 gene was downregulated in the METH-treated group compared with the control group ($p < 0.05$). The Nrf2 gene in the METH+TBHQ group was upregulated compared with that in the control group and the METH-treated group ($p < 0.05$ and $p < 0.05$, respectively) (see Figure 6(a)). Western blotting was used to detect the Nrf2 protein inside and outside the nucleus. Consistent with the gene level, both the intra- and extranuclear levels of the Nrf2 protein in the VTA were sig-

nificantly downregulated in the METH-treated group compared with the control group ($p < 0.01$, $p < 0.05$). In the METH+TBHQ-treated group, these levels were upregulated compared with those in the control group and METH-treated group ($p < 0.05$, $p < 0.01$, $p < 0.05$, and $p < 0.01$, respectively) (see Figure 6(c) and 6(d)).

3.6. TBHQ Increased the Immunocontent of HO-1 in the VTA of METH-Treated Rats. HO-1, as a downstream factor regulated by Nrf2 in the Nrf2/HO-1 signaling pathway, was detected. Compared with that in the control group, the HO-1 immunocontent in the METH-treated group was downregulated ($p < 0.01$), while in the METH+TBHQ-treated group, the HO-1 immunocontent was upregulated compared with that in the control group and METH-treated group ($p < 0.05$ and $p < 0.01$, respectively) (see Figure 6(b)).

3.7. Effects of TBHQ Treatment on PI3K and Caspase-3 Gene and Protein Immunocontent. The mRNA levels of PI3K (see Figure 7(a)) and caspase-3 (see Figure 7(b)) were detected, revealing that PI3K was significantly decreased in METH-treated rats compared with control rats ($p < 0.05$). However, PI3K immunocontent was increased in METH+TBHQ-treated rats compared with METH-treated and control rats ($p < 0.05$ and $p < 0.05$, respectively). To further illuminate the increase in apoptosis, we assessed the mRNA levels of caspase-3, revealing that they were upregulated in METH-treated and METH+TBHQ-treated rats compared with control rats ($p < 0.05$ and $p < 0.05$, respectively). Compared with those in METH-treated rats, the mRNA levels of caspase-3 were obviously reduced in METH+TBHQ-treated rats ($p < 0.05$).

Similarly, caspase-3 protein levels were significantly increased in METH-treated rats compared with control rats, and PI3K protein levels were decreased ($p < 0.01$ and $p <$

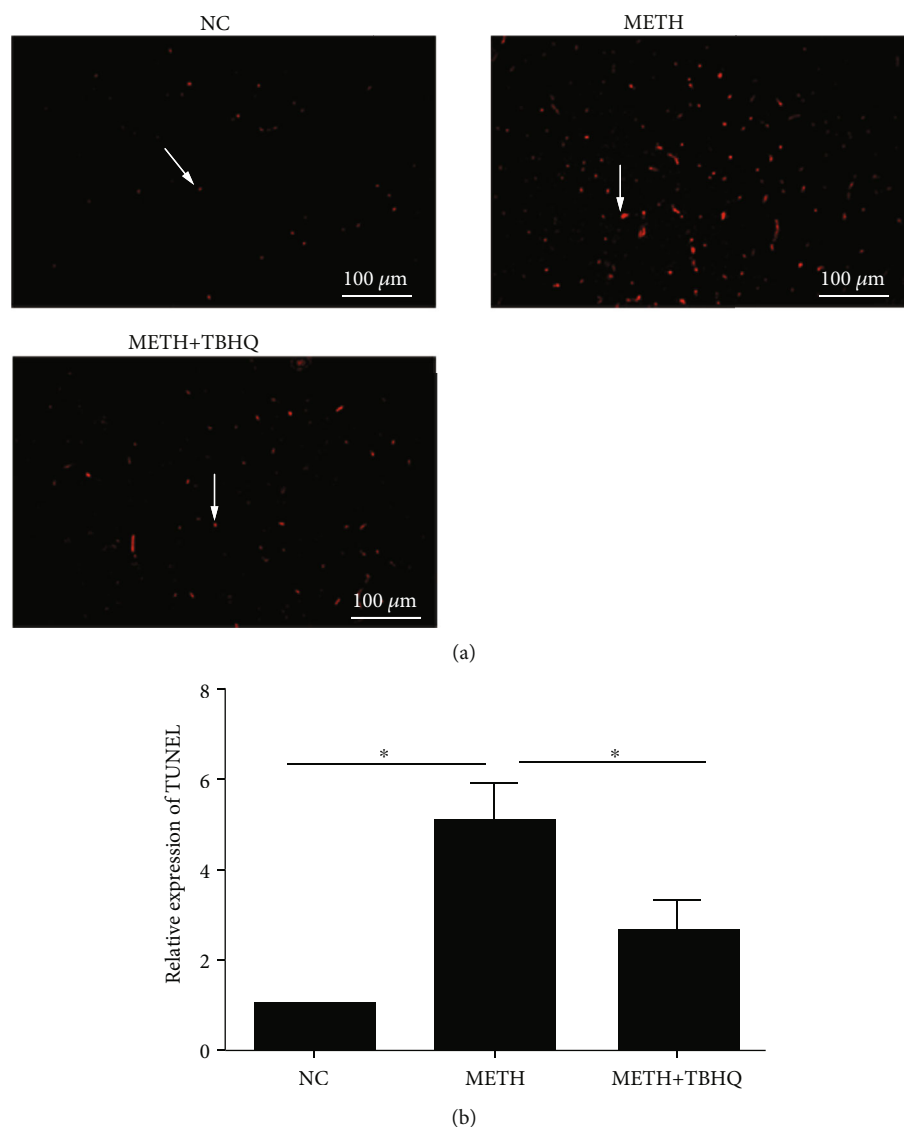


FIGURE 4: TBHQ alleviated the apoptosis induced by METH in the VTA. (a) Positive cells with a red fluorescence signal (arrows) were present in the VTA as determined by the TUNEL assay. (b) Quantitative statistical analysis of TUNEL-positive cells. A minimum of three random fields per group were used to count and calculate the percentage of positively labeled cells. The data are expressed as the means \pm SEMs of three independent experiments. $n = 5$. * $p < 0.05$.

0.05). Compared with the METH-treated rats, the METH+TBHQ-treated rats showed decreased caspase-3 protein immunocentent and increased PI3K protein immunocentent ($p < 0.01$) (see Figures 7(c) and 7(d)).

3.8. Effects of METH and TBHQ Treatment on AKT and p-AKT in the PI3K/AKT Signaling Pathway. To further investigate the mechanism by which the antiapoptotic signaling pathway is involved in the effects of TBHQ, Western blot analysis was performed to detect the immunocentent of AKT and p-AKT. The results showed that the AKT (see Figure 8(a)) and p-AKT (see Figure 8(b)) immunocentent levels were significantly decreased in METH-treated rats compared with control rats ($p < 0.05$ and $p < 0.05$, respectively). However, AKT and p-AKT immunocentent was increased in METH+TBHQ-treated rats compared with

METH-treated rats and control rats ($p < 0.01$, $p < 0.05$, $p < 0.05$, and $p < 0.05$, respectively).

4. Discussion

As a powerfully addictive drug, METH damages multiple organs, such as the brain, heart, and lungs [48–50]. This study showed that chronic exposure of Wistar rats to METH increased their immobility times in the FST and TST, which have good predictive validity and allow the rapid and economical detection of substances with potential antidepressant-like activity [51]. METH induced neurotoxicity in the VTA of rats by increasing ROS and apoptosis, thus promoting changes in the structure and function of DA neurons. METH inhibited Nrf2-mediated antioxidative stress by downregulating Nrf2 and HO-1 and further

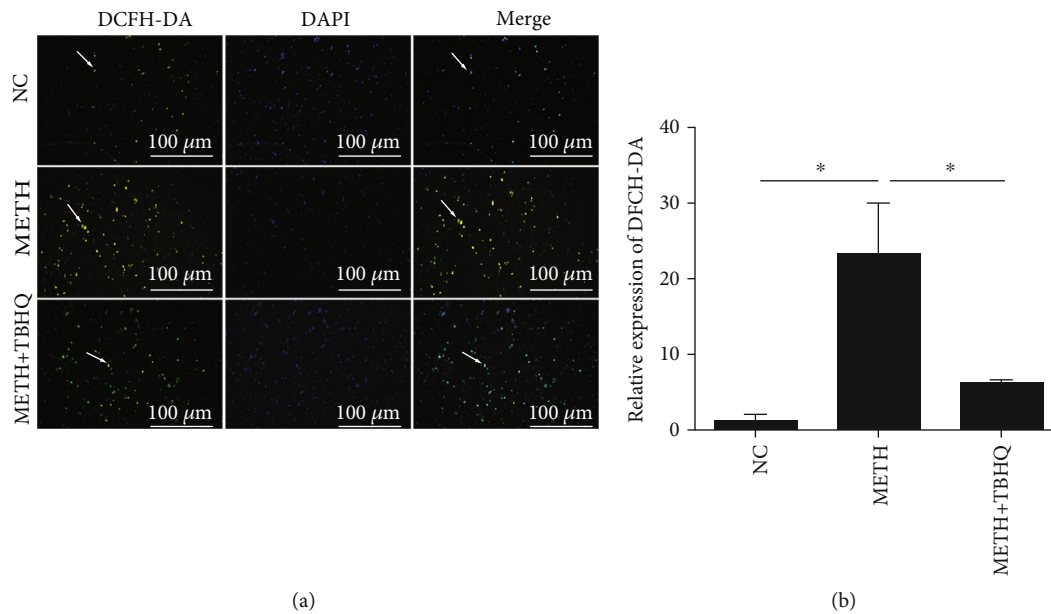


FIGURE 5: Effects of METH and TBHQ on ROS in rat VTA cells. (a) ROS production in the VTA was detected by the DCFH-DA assay. Green indicates a typical positive cell, and blue indicates a nucleus. (b) Statistical analysis of the ROS average optical density; the average optical density values were used to quantify ROS-positive cells. The data are expressed as the means \pm SEMs of three independent experiments. $n = 5$. * $p < 0.05$.

induced apoptosis by decreasing PI3K, AKT, and p-AKT expression and increasing caspase-3 immunopositive content. These changes were reversed by treatment with the antioxidant TBHQ through the upregulation of the Nrf2 immunopositive content. TBHQ alleviated METH-induced OS and apoptosis, possibly through the interaction between Nrf2/HO-1 and PI3K/AKT. PI3K/Nrf2 is likely the key crosstalk factor between OS and apoptosis in METH-induced chronic neurotoxicity.

In this study, we found that in the VTA, the ROS levels in Wistar rats were increased by chronic exposure to METH but reversed by TBHQ, which is in accordance with previous reports showing that OS damage in the nervous system caused by METH can be attenuated by antioxidants [52]. Redox imbalance and the generation of free radicals can lead to OS [53]. ROS include ozone (O_3), singlet oxygen (1O_2), hydrogen peroxide (H_2O_2), the superoxide anion radical ($O_2^{\cdot-}$), and the hydroxyl radical (OH^{\cdot}) [54]. Many normal cellular activities produce ROS, and physiologically, cells eliminate ROS by upregulating antioxidant proteins such as superoxide dismutase, catalase (CAT), and glutathione peroxidase (GPx) to prevent cell damage [55]. A variety of exogenous factors, such as environmental toxicants, hypoxia, hyperoxia, and stress stretching, can stimulate the body to produce excessive ROS. When ROS are not effectively removed by antioxidant enzymes, OS is induced and damages cells. Therefore, the neurotoxicity of METH may be due to excessive ROS production caused by chronic exposure. TBHQ plays an antioxidant role in METH-induced OS.

To further investigate the antioxidant mechanism of TBHQ, a novel Nrf2 activator, intra- and extranuclear Nrf2, in the VTA was detected in the model because it is proved that TBHQ possesses an oxidizable 1,4-diphenolic structure

that confers its potent ability to dissociate the Keap1-Nrf2 complex [56]. Under normal conditions, Nrf2 is posttranslationally and constitutively regulated in the cytoplasm by its antagonist Keap1 through targeted ubiquitination [57]. However, upon OS, the activation of Nrf2 results in the modification of Keap1 cysteine 151 and allows Nrf2 to translocate into the cell nucleus and recruit small Maf proteins to form a heterodimer [58]. The heterodimer can bind to the antioxidant response element (ARE) and eventually transactivate a battery of antioxidant enzymes, such as NQO1 and HO-1 [59]. We found that METH significantly decreased the gene and protein immunopositive levels of Nrf2 and prevented its translocation to the nucleus, which subsequently decreased the immunopositive content of HO-1. However, the decrease in Nrf2 induced by METH was markedly reversed by TBHQ treatment. It was also reported that Nrf2 deficiency exacerbates METH-induced damage to DA neurons in Nrf2 knockout (Nrf2 $^{-/-}$) mice, indicating the involvement of Nrf2 in the pathogenesis of METH-induced neurotoxicity [60]. TBHQ showed the ability to activate Nrf2-dependent HO-1 gene during inflammation-induced oxidative stress, which probably restores the cellular redox homeostasis thereby rendering protection against oxidative stress-mediated cell death [61]. Combining these previous studies, our results demonstrate that TBHQ may ultimately reduce the production of METH-induced ROS by activating the Nrf2/HO-1 pathway, thus playing an antioxidant role in the mouse model of METH chronic exposure.

Furthermore, we found high levels of apoptosis in the VTA of rats treated with METH. Compared with those in control rats, the number of DA neurons was reduced and morphological changes were obvious in the DA neurons of METH-treated rats. METH significantly increased the

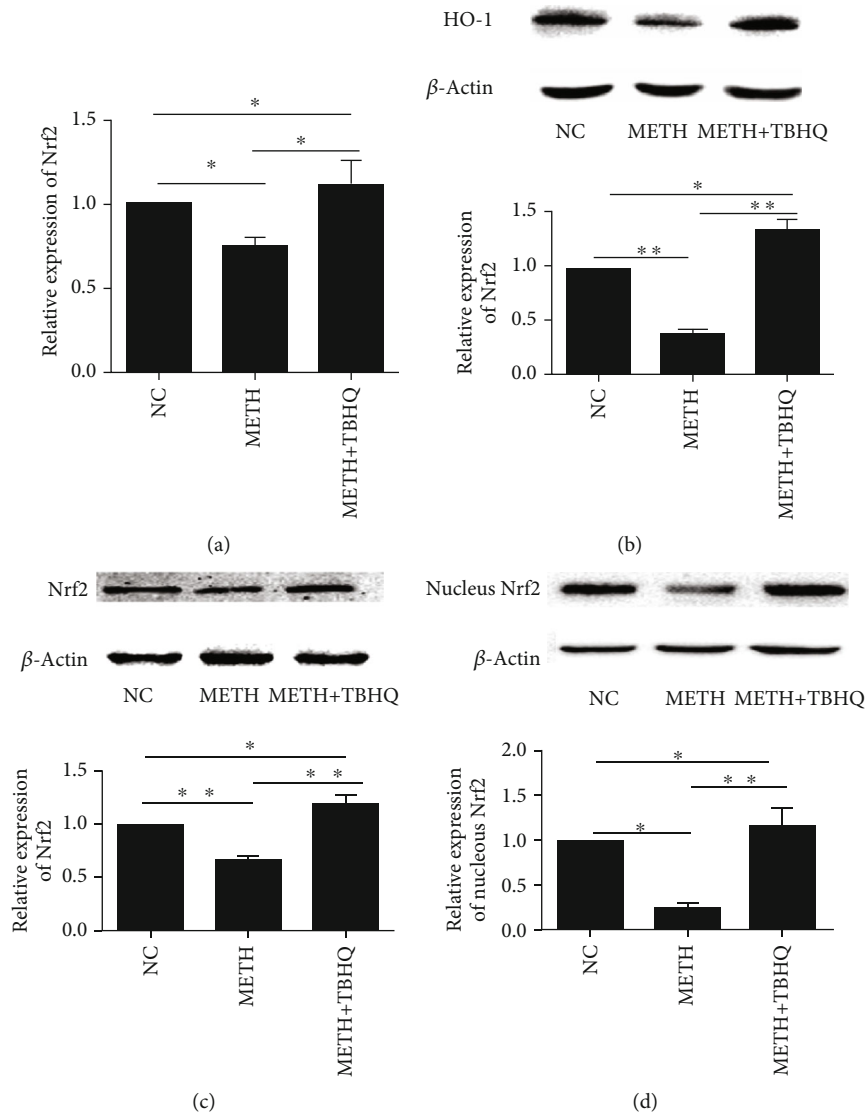


FIGURE 6: TBHQ increased the Nrf2 gene and protein immunocent in the VAT of METH-induced rats. (a) Quantitative PCR analysis of VTA Nrf2 mRNA levels. (b) Representative Western blot images and analysis of HO-1. (c, d) Representative Western blot images and analysis of extranuclear and intranuclear Nrf2. The data are expressed as the means \pm SEMs of three independent experiments. $n = 5$. * $p < 0.05$, ** $p < 0.01$.

immunocontent of caspase-3. However, the changes were reversed by TBHQ treatment. The caspase family is a major player in the apoptotic process. Caspase-3 is located downstream of the caspase family cascade and is the apoptotic executive protein; it can amplify the apoptotic response and play an important role in the apoptosis family. Caspase-3 activation and high immunocontent can cause apoptosis [62]. Therefore, these results indicated that TBHQ can participate in the protection of DA neurons by inhibiting apoptosis. Based on these results together with those of the behavioral tests, we deduced that chronic METH stimulation can cause depression-like behavior in rats by increasing OS- and apoptosis-induced damage of DA neurons in the VTA. However, TBHQ attenuated METH-induced neurotoxicity in DA neurons by increasing and activating antioxidative stress and antiapoptotic abilities.

PI3K/AKT signaling is crucial for neuronal survival through the inhibition of apoptosis. PI3K is a Ser/Thr kinase and phosphatidylinositol kinase [63]. The Ser/Thr kinase activity of PI3K activates the downstream target AKT. Once AKT is activated, the biological response of AKT that controls apoptosis is simultaneously activated [64]. Research has shown that caspase-3 immunocontent can be decreased by activating the PI3K/AKT pathway to exert an antiapoptotic effect and improve neuronal damage in damaged brain regions [65]. Our data presented herein revealed that METH decreased the immunocontent of PI3K, AKT, and p-AKT and that this decrease was markedly reversed by TBHQ treatment. These results further indicate that the activation of the PI3K/AKT pathway may participate in TBHQ-mediated protection to reduce caspase-3 activation and alleviate apoptosis.

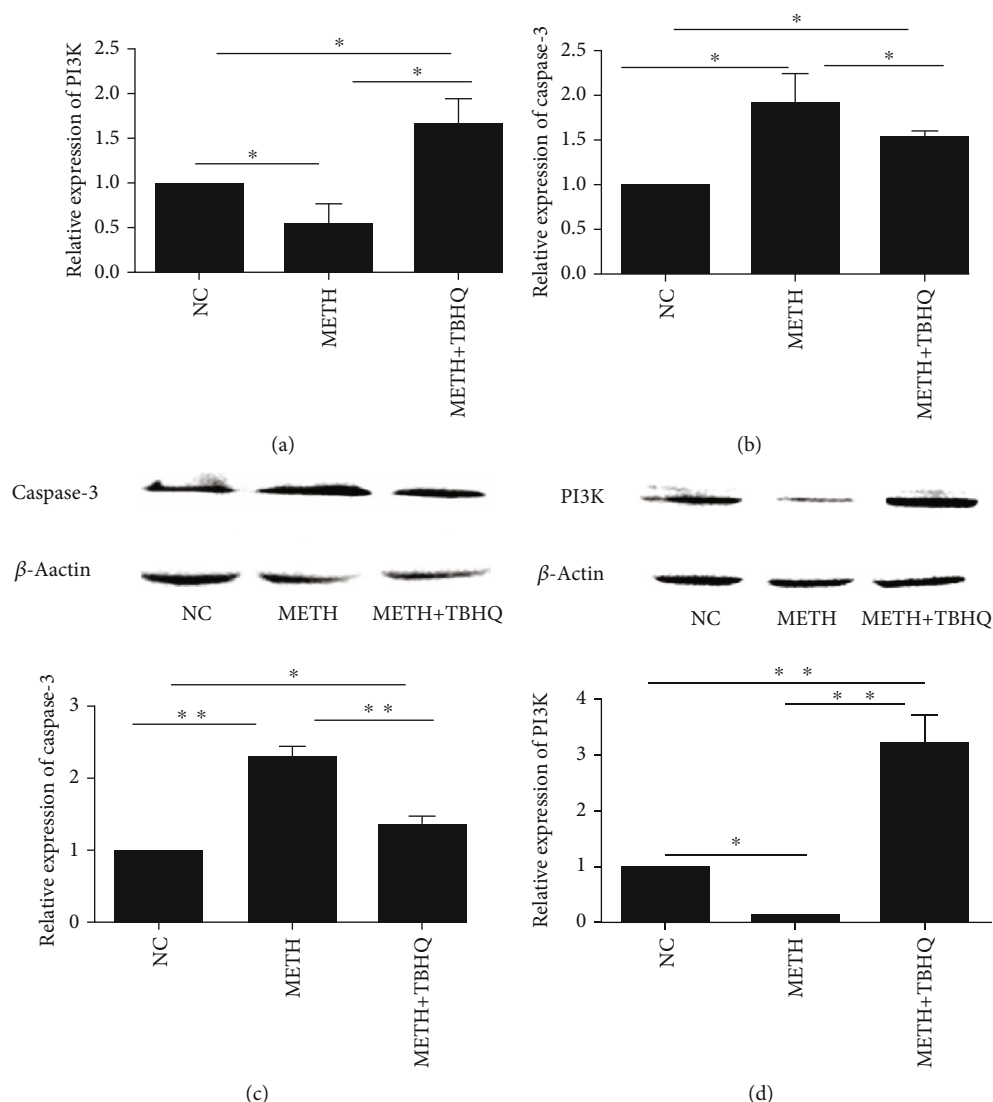


FIGURE 7: Effects of METH and TBHQ on the gene and protein immunocontent of PI3K and caspase-3. (a) Quantitative PCR analysis of VTA PI3K mRNA levels. (b) Quantitative PCR analysis of VTA caspase-3 mRNA levels. (c, d) Representative Western blot images and analysis of PI3K and caspase-3. The data are expressed as the means \pm SEMs of three independent experiments. $n = 5$. * $p < 0.05$, ** $p < 0.01$.

It has been reported that PI3K/AKT signaling is an upstream pathway that regulates the nuclear translocation of Nrf2 [66]. When the body is damaged by OS caused by ROS, the phosphorylation of Ser/Thr residues is a key for Nrf2 activation, and PI3K/AKT can phosphorylate these residues [67]. Lee et al. reported that activation of the hNQO1-ARE by TBHQ is mediated by PI3K [68]. In the absence of an inducer, constitutively activated PI3K can also increase the activity of the Nrf2 target gene NQO1 and the level of glutathione [69]. In Nrf2 knockout cells, AKT shows a decreased trend of responsiveness to platelet-derived growth factor (PDGF) and/or insulin [70]. All of these studies suggest that the PI3K/AKT pathway increases the antioxidative effect of Nrf2. Therefore, we deduced that TBHQ exerts antioxidative stress and antiapoptotic effects in METH-induced DA neurons through activating Nrf2/HO-1 and regulating the PI3K-AKT pathway. Inhibitors of

Nrf2 or PI3K need to be used to further verify this conclusion (see Figure 9).

5. Conclusions

Chronic exposure to METH causes significant damage to DA neurons in the VTA of experimental rats. The administration of TBHQ has significant protective effects against METH-induced damage based on both morphological and behavioral assessments. Our study implies that Nrf2/PI3K is likely the key crosstalk factor between OS and apoptosis in METH-induced chronic neurotoxicity. Potentially, TBHQ successfully protects DA neurons from METH-induced neurotoxicity via exerting an amplified effect on the Nrf2/HO-1 pathway, thereby reducing OS and protecting the normal signal transduction of the PI3K/AKT pathway and the antiapoptotic ability of PI3K/AKT. Concurrently, the PI3K/AKT

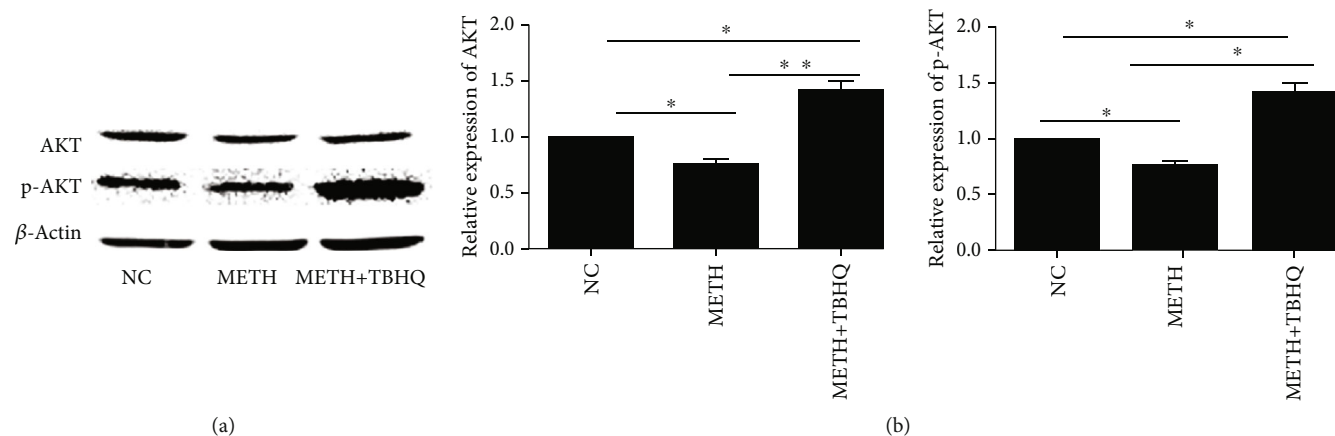


FIGURE 8: Changes in the immunocontent levels of AKT and p-AKT in the PI3K/AKT signaling pathway of METH+TBHQ-treated rats. (a) Representative Western blot images and analysis of AKT. (b) Representative Western blot images and analysis of p-AKT. Data are expressed as the means \pm SEMs for three independent experiments. $n = 5$. * $p < 0.05$, ** $p < 0.01$.

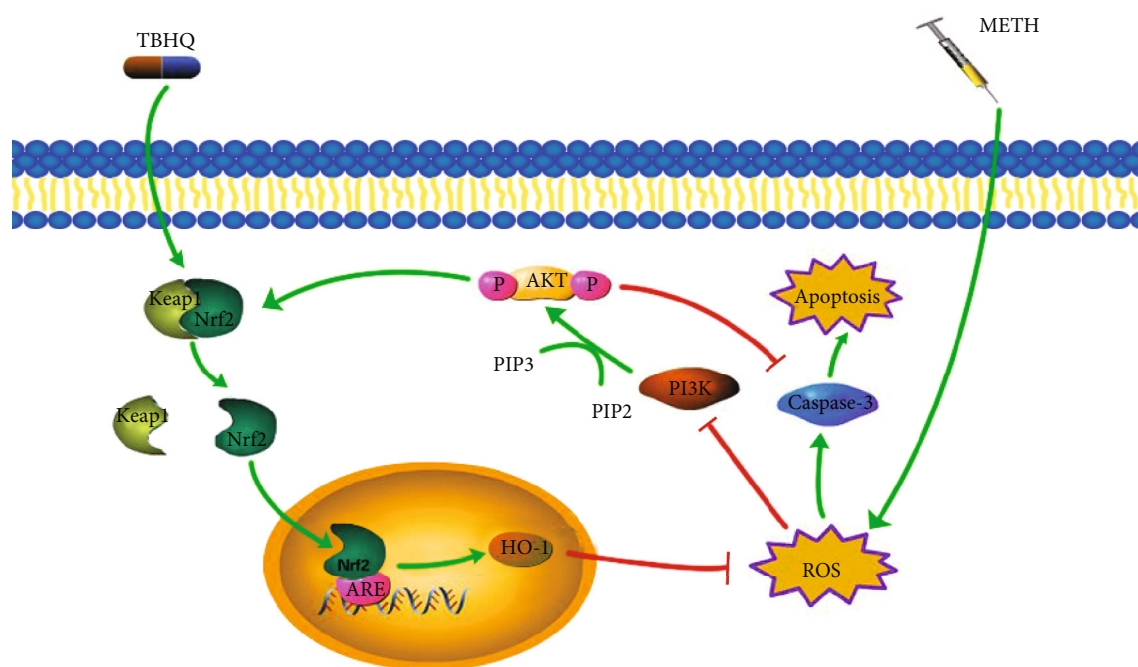


FIGURE 9: The protective role of TBHQ related to Nrf2/HO-1 and PI3K/AKT. METH chronic exposure induced the body to produce excessive ROS. On the one hand, it leads to OS disorder by reducing immunocontent of PI3K, AKT, and p-AKT; on the other hand, it promotes apoptosis through increasing caspase-3. However, TBHQ activates the Nrf2/HO-1 pathway, thereby reducing OS and protecting the normal signal transduction of the PI3K/AKT pathway to exert antioxidative stress and antiapoptotic effects.

pathway increases Nrf2 protein immunocontent and further enhances the antioxidative capacity via the Nrf2/HO-1 pathway.

Data Availability

The data used to support the findings of this study are available from the corresponding author upon request.

Conflicts of Interest

The authors have no conflicts of interest to declare.

Authors' Contributions

Xianyi Meng and Chenghong Zhang contributed equally to this work.

Acknowledgments

This work was supported by the National Natural Science Foundation of China (grant number 31300812), the Natural Science Foundation of Liaoning Province (grant number 20180550468), and the Liaoning Provincial Program for Top Discipline of Basic Medical Sciences.

References

- [1] M. Cretzmeyer, M. V. Sarrazin, D. L. Huber, R. I. Block, and J. A. Hall, "Treatment of methamphetamine abuse: research findings and clinical directions," *Journal of Substance Abuse Treatment*, vol. 24, no. 3, pp. 267–277, 2003.
- [2] S. J. Shoptaw, U. Kao, K. Heinzerling, and W. Ling, "Treatment for amphetamine withdrawal," *Cochrane Database of Systematic Reviews*, vol. 28, no. 2, article CD003021, 2009.
- [3] A. M. Barr, W. J. Panenka, G. MacEwan et al., "The need for speed: an update on methamphetamine addiction," *Journal of Psychiatry & Neuroscience*, vol. 31, no. 5, pp. 301–313, 2006.
- [4] E. D. London, S. L. Simon, S. M. Berman et al., "Mood disturbances and regional cerebral metabolic abnormalities in recently abstinent methamphetamine abusers," *Archives of General Psychiatry*, vol. 61, no. 1, pp. 73–84, 2004.
- [5] M. J. Mancino, B. W. Gentry, Z. Feldman, J. Mendelson, and A. Oliveto, "Characterizing methamphetamine withdrawal in recently abstinent methamphetamine users: a pilot field study," *American Journal of Drug & Alcohol Abuse*, vol. 37, no. 2, pp. 131–136, 2011.
- [6] B. A. Bennett, C. K. Hollingsworth, R. S. Martin, and J. J. Harp, "Methamphetamine-induced alterations in dopamine transporter function," *Brain Research*, vol. 782, no. 1-2, pp. 219–227, 1998.
- [7] H. M. Haughey, A. E. Fleckenstein, and G. R. Hanson, "Differential regional effects of methamphetamine on the activities of tryptophan and tyrosine hydroxylase," *Journal of Neurochemistry*, vol. 72, no. 2, pp. 661–668, 1999.
- [8] G. C. Wagner, G. A. Ricaurte, L. S. Seiden, C. R. Schuster, R. J. Miller, and J. Westley, "Long-lasting depletions of striatal dopamine and loss of dopamine uptake sites following repeated administration of methamphetamine," *Brain Research*, vol. 181, no. 1, pp. 151–160, 1980.
- [9] K. L. Preston, G. C. Wagner, C. R. Schuster, and L. S. Seiden, "Long-term effects of repeated methylamphetamine administration on monoamine neurons in the rhesus monkey brain," *Brain Research*, vol. 338, no. 2, pp. 243–248, 1985.
- [10] D. C. Harvey, G. Lacan, S. P. Tanious, and W. P. Melega, "Recovery from methamphetamine induced long-term nigrostriatal dopaminergic deficits without substantia nigra cell loss," *Brain Research*, vol. 871, no. 2, pp. 259–270, 2000.
- [11] D. J. Mooney, L. K. Hansen, R. Langer, J. P. Vacanti, and D. E. Ingber, "Extracellular matrix controls tubulin monomer levels in hepatocytes by regulating protein turnover," *Molecular Biology of the Cell*, vol. 5, no. 12, pp. 1281–1288, 1994.
- [12] J. F. Bowyer and L. C. Schmued, "Fluoro-Ruby labeling prior to an amphetamine neurotoxic insult shows a definitive massive loss of dopaminergic terminals and axons in the caudate-putamen," *Brain Research*, vol. 1075, no. 1, pp. 236–239, 2006.
- [13] M. Morales and E. B. Margolis, "Ventral tegmental area: cellular heterogeneity, connectivity and behaviour," *Nature Reviews. Neuroscience*, vol. 18, no. 2, pp. 73–85, 2017.
- [14] A. A. Hamid, J. R. Pettibone, O. S. Mabrouk et al., "Mesolimbic dopamine signals the value of work," *Nature Neuroscience*, vol. 19, no. 1, pp. 117–126, 2016.
- [15] J. D. Salamone and M. Correa, "The mysterious motivational functions of mesolimbic dopamine," *Neuron*, vol. 76, no. 3, pp. 470–485, 2012.
- [16] S. Ikemoto and A. Bonci, "Neurocircuitry of drug reward," *Neuropharmacology*, vol. 76, pp. 329–341, 2014.
- [17] C. Luscher, "The emergence of a circuit model for addiction," *Annual Review of Neuroscience*, vol. 39, no. 1, pp. 257–276, 2016.
- [18] P. Jumnonprakhon, P. Govitrapong, C. Tocharus, W. Tungkum, and J. Tocharus, "Protective effect of melatonin on methamphetamine-induced apoptosis in glioma cell line," *Neurotoxicity Research*, vol. 25, no. 3, pp. 286–294, 2014.
- [19] X.-K. Thi Nguyen, J. Lee, E.-J. Shin et al., "Liposomal melatonin rescues methamphetamine-elicited mitochondrial burdens, pro-apoptosis, and dopaminergic degeneration through the inhibition PKC δ gene," *Journal of Pineal Research*, vol. 58, no. 1, pp. 86–106, 2015.
- [20] D. Wen, M. An, H. Gou et al., "Cholecystokinin-8 inhibits methamphetamine-induced neurotoxicity via an anti-oxidative stress pathway," *Neurotoxicology*, vol. 57, pp. 31–38, 2016.
- [21] J. H. Park, Y. H. Seo, J. H. Jang, C. H. Jeong, S. Lee, and B. Park, "Asiatic acid attenuates methamphetamine-induced neuroinflammation and neurotoxicity through blocking of NF- κ B/STAT3/ERK and mitochondria-mediated apoptosis pathway," *Journal of Neuroinflammation*, vol. 14, no. 1, p. 240, 2017.
- [22] M. R. Gluck, L. Y. Moy, E. Jayatilleke, K. A. Hogan, L. Manzino, and P. K. Sonsalla, "Parallel increases in lipid and protein oxidative markers in several mouse brain regions after methamphetamine treatment," *Journal of Neurochemistry*, vol. 79, no. 1, pp. 152–160, 2001.
- [23] K. A. Horner, Y. E. Gilbert, and S. D. Cline, "Widespread increases in malondialdehyde immunoreactivity in dopamine-rich and dopamine-poor regions of rat brain following multiple, high doses of methamphetamine," *Frontiers in Systems Neuroscience*, vol. 5, p. 27, 2011.
- [24] P. S. Fitzmaurice, J. Tong, M. Yazdanpanah, P. P. Liu, K. S. Kalasinsky, and S. J. Kish, "Levels of 4-hydroxynonenal and malondialdehyde are increased in brain of human chronic users of methamphetamine," *Journal of Pharmacology and Experimental Therapeutics*, vol. 319, no. 2, pp. 703–709, 2006.
- [25] X. Deng and J. L. Cadet, "Methamphetamine-induced apoptosis is attenuated in the striata of copper-zinc superoxide dismutase transgenic mice," *Brain Research. Molecular Brain Research*, vol. 83, no. 1-2, pp. 121–124, 2000.
- [26] J. Swant, S. Chirwa, G. Stanwood, and H. Khoshbouei, "Methamphetamine reduces LTP and increases baseline synaptic transmission in the CA1 region of mouse hippocampus," *PLoS One*, vol. 5, no. 6, article e11382, 2010.
- [27] L. C. Schmued and J. F. Bowyer, "Methamphetamine exposure can produce neuronal degeneration in mouse hippocampal remnants," *Brain Research*, vol. 759, no. 1, pp. 135–140, 1997.
- [28] B. Yang, H. Cheng, L. Wang et al., "Protective roles of NRF2 signaling pathway in cobalt chloride-induced hypoxic cytotoxicity in human HaCaT keratinocytes," *Toxicology and Applied Pharmacology*, vol. 355, pp. 189–197, 2018.
- [29] T. Suzuki, H. Motohashi, and M. Yamamoto, "Toward clinical application of the Keap1–Nrf2 pathway," *Trends in Pharmacological Sciences*, vol. 34, no. 6, pp. 340–346, 2013.
- [30] A. Saudemont and F. Colucci, "PI3K signalling in lymphocyte migration," *Cell Cycle*, vol. 8, no. 20, pp. 3307–3310, 2009.
- [31] K. Nakaso, H. Yano, Y. Fukuhara, T. Takeshima, K. Wada-Isoe, and K. Nakashima, "PI3K is a key molecule in the Nrf2-mediated regulation of antioxidative proteins by hemin in

- human neuroblastoma cells," *FEBS Letters*, vol. 546, no. 2-3, pp. 181–184, 2003.
- [32] L. Wang, Y. Chen, P. Sternberg, and J. Cai, "Essential roles of the PI3 kinase/Akt pathway in regulating Nrf2-dependent antioxidant functions in the RPE," *Investigative Ophthalmology & Visual Science*, vol. 49, no. 4, pp. 1671–1678, 2008.
- [33] Y. Wang, Y. H. Gu, M. Liu, Y. Bai, L. Y. Liang, and H. L. Wang, "TBHQ alleviated endoplasmic reticulum stress-apoptosis and oxidative stress by PERK-Nrf2 crosstalk in methamphetamine-induced chronic pulmonary toxicity," *Oxidative Medicine and Cellular Longevity*, vol. 2017, Article ID 4310475, 12 pages, 2017.
- [34] J. P. Hansen, "Ten keys to successful NCQA accreditation: a health plan perspective," *Journal for Healthcare Quality*, vol. 24, no. 5, pp. 39–42, 2002.
- [35] X. Shi, Y. Li, J. Hu, and B. Yu, "Tert-butylhydroquinone attenuates the ethanol-induced apoptosis of and activates the Nrf2 antioxidant defense pathway in H9c2 cardiomyocytes," *International Journal of Molecular Medicine*, vol. 38, no. 1, pp. 123–130, 2016.
- [36] T. E. Nordahl, R. Salo, and M. Leamon, "Neuropsychological effects of chronic methamphetamine use on neurotransmitters and cognition: a review," *The Journal of Neuropsychiatry and Clinical Neurosciences*, vol. 15, no. 3, pp. 317–325, 2003.
- [37] Y. Wang, M. Liu, H. M. Wang et al., "Involvement of serotonin mechanism in methamphetamine-induced chronic pulmonary toxicity in rats," *Human & Experimental Toxicology*, vol. 32, no. 7, pp. 736–746, 2013.
- [38] J. Lan, X. Deng, and H. Wang, "Research of nitration modification in chronic methamphetamine treated rats and human serum and the neurotoxicity," *Chinese Journal of Drug Dependence*, vol. 20, no. 3, pp. 177–181, 2011.
- [39] G. Masi and P. Bovedani, "The hippocampus, neurotrophic factors and depression: possible implications for the pharmacotherapy of depression," *CNS Drugs*, vol. 25, no. 11, pp. 913–931, 2011.
- [40] J. F. Cryan and A. Holmes, "The ascent of mouse: advances in modelling human depression and anxiety," *Nature Reviews. Drug Discovery*, vol. 4, no. 9, pp. 775–790, 2005.
- [41] A. Tamburella, G. M. Leggio, V. Micale et al., "Behavioural and neurochemical changes induced by stress-related conditions are counteracted by the neurokinin-2 receptor antagonist saredutant," *International Journal of Neuropsychopharmacology*, vol. 16, no. 4, pp. 813–823, 2013.
- [42] L. Steru, R. Chermat, B. Thierry, and P. Simon, "The tail suspension test: a new method for screening antidepressants in mice," *Psychopharmacology*, vol. 85, no. 3, pp. 367–370, 1985.
- [43] J. B. Cook, *Ethanol Alters the GABAergic Neuroactive Steroid (3alpha,5alpha)-3-Hydroxypregnan-20-One (3alpha,5alpha-THP or Allopregnanolone) at Local Brain Sites: Significance of Local 3alpha,5alpha-THP Increases in the Ventral Tegmental Area*, The University of North Carolina at Chapel Hill, ProQuest Dissertations Publishing, 2013.
- [44] K. Kyrylkova, S. Kyryachenko, M. Leid, and C. Kioussi, "Detection of apoptosis by TUNEL assay," *Methods in Molecular Biology*, vol. 887, pp. 41–47, 2012.
- [45] L. Chen, C. Zhang, Y. Han et al., "Gingko biloba extract (EGb) inhibits oxidative stress in neuro 2A cells overexpressing APPsw," *BioMed Research International*, vol. 2019, Article ID 7034983, 9 pages, 2019.
- [46] T. Chen, Y. Wu, Y. Wang et al., "Brain-derived neurotrophic factor increases synaptic protein levels via the MAPK/Erk signaling pathway and Nrf2/Trx axis following the transplantation of neural stem cells in a rat model of traumatic brain injury," *Neurochemical Research*, vol. 42, no. 11, pp. 3073–3083, 2017.
- [47] J. Pi, Q. Zhang, J. Fu et al., "ROS signaling, oxidative stress and Nrf2 in pancreatic beta-cell function," *Toxicology and Applied Pharmacology*, vol. 244, no. 1, pp. 77–83, 2010.
- [48] S. M. Wells, M. C. Buford, S. N. Braseth, J. D. Hutchison, and A. Holian, "Acute inhalation exposure to vaporized methamphetamine causes lung injury in mice," *Inhalation Toxicology*, vol. 20, no. 9, pp. 829–838, 2008.
- [49] S. J. Kish, I. Boileau, R. C. Callaghan, and J. Tong, "Brain dopamine neurone 'damage': methamphetamine users vs. Parkinson's disease - a critical assessment of the evidence," *The European Journal of Neuroscience*, vol. 45, no. 1, pp. 58–66, 2017.
- [50] S. Sliman, J. Waalen, and D. Shaw, "Methamphetamine-associated congestive heart failure: increasing prevalence and relationship of clinical outcomes to continued use or abstinence," *Cardiovascular Toxicology*, vol. 16, no. 4, pp. 381–389, 2016.
- [51] V. Castagné, P. Moser, S. Roux, and R. D. Porsolt, "Rodent models of depression: forced swim and tail suspension behavioral despair tests in rats and mice," *Current Protocols in Neuroscience*, vol. 55, 2011.
- [52] M. Shen, L. Wang, B. Wang et al., "Activation of volume-sensitive outwardly rectifying chloride channel by ROS contributes to ER stress and cardiac contractile dysfunction: involvement of CHOP through Wnt," *Cell Death & Disease*, vol. 5, no. 11, article e1528, 2014.
- [53] M. A. Birch-Machin and A. Bowman, "Oxidative stress and ageing," *The British Journal of Dermatology*, vol. 175, no. S2, pp. 26–29, 2016.
- [54] D. B. Zorov, M. Juhaszova, and S. J. Sollott, "Mitochondrial reactive oxygen species (Ros) and Ros-induced Ros release," *Physiological Reviews*, vol. 94, no. 3, pp. 909–950, 2014.
- [55] D. Wu and P. Yotnda, "Production and detection of reactive oxygen species (ROS) in cancers," *Journal of Visualized Experiments*, no. 57, article e3357, 2011.
- [56] A. Y. Shih, P. Li, and T. H. Murphy, "A small-molecule-inducible Nrf2-mediated antioxidant response provides effective prophylaxis against cerebral ischemia in vivo," *The Journal of Neuroscience*, vol. 25, no. 44, pp. 10321–10335, 2005.
- [57] A. Alfieri, S. Srivastava, R. C. Siow, M. Mudo, P. A. Fraser, and G. E. Mann, "Targeting the Nrf2-Keap1 antioxidant defence pathway for neurovascular protection in stroke," *Journal of Physiology*, vol. 589, no. 17, pp. 4125–4136, 2011.
- [58] Z. Jian, K. Li, L. Liu et al., "Heme oxygenase-1 protects human melanocytes from H2O2-induced oxidative stress via the Nrf2-ARE pathway," *Journal of Investigative Dermatology*, vol. 131, no. 7, pp. 1420–1427, 2011.
- [59] G. P. Sykiotis and D. Bohmann, "Stress-activated cap'n'collar transcription factors in aging and human disease," *Science Signaling*, vol. 3, no. 112, article re3, 2010.
- [60] N. Granado, I. Lastres-Becker, S. Ares-Santos et al., "Nrf2 deficiency potentiates methamphetamine-induced dopaminergic axonal damage and gliosis in the striatum," *Glia*, vol. 59, no. 12, pp. 1850–1863, 2011.
- [61] S. Ghosh, S. Choudhury, O. Chowdhury et al., "Inflammation-induced behavioral changes is driven by alterations in Nrf2-

- dependent apoptosis and autophagy in mouse hippocampus: role of fluoxetine,” *Cellular Signalling*, vol. 68, article 109521, 2020.
- [62] D. R. Green, “Apoptotic pathways: paper wraps stone blunts scissors,” *Cell*, vol. 102, no. 1, pp. 1–4, 2000.
- [63] P. Voigt, C. Brock, B. Nürnberg, and M. Schaefer, “Assigning functional domains within the p101 regulatory subunit of phosphoinositide 3-kinase gamma,” *The Journal of Biological Chemistry*, vol. 280, no. 6, pp. 5121–5127, 2005.
- [64] R. J. Shaw and L. C. Cantley, “Ras, PI(3)K and mTOR signaling controls tumour cell growth,” *Nature*, vol. 441, no. 7092, pp. 424–430, 2006.
- [65] T. Jover-Mengual, T. Miyawaki, A. Latuszek, E. Alborch, R. S. Zukin, and A. M. Etgen, “Acute estradiol protects CA1 neurons from ischemia-induced apoptotic cell death via the PI3K/Akt pathway,” *Brain Research*, vol. 1321, pp. 1–12, 2010.
- [66] N. M. Reddy, H. R. Potteti, S. Vegiraju, H. J. Chen, C. M. Tamam, and S. P. Reddy, “PI3K-AKT signaling via Nrf2 protects against hyperoxia-induced acute lung injury, but promotes inflammation post-injury independent of Nrf2 in mice,” *PLoS One*, vol. 10, no. 6, article e0129676, 2015.
- [67] L. Baird and A. T. Dinkova-Kostova, “The cytoprotective role of the Keap1-Nrf2 pathway,” *Archives of Toxicology*, vol. 85, no. 4, pp. 241–272, 2011.
- [68] J. M. Lee, J. M. Hanson, W. A. Chu, and J. A. Johnson, “Phosphatidylinositol 3-kinase, not extracellular signal-regulated kinase, regulates activation of the antioxidant-responsive element in IMR-32 human neuroblastoma cells,” *The Journal of Biological Chemistry*, vol. 276, no. 23, pp. 20011–20016, 2001.
- [69] Z. R. Healy, N. H. Lee, X. Gao et al., “Divergent responses of chondrocytes and endothelial cells to shear stress: cross-talk among COX-2, the phase 2 response, and apoptosis,” *Proceedings of the National Academy of Sciences of the United States of America*, vol. 102, no. 39, pp. 14010–14015, 2005.
- [70] G. Rachakonda, Y. Xiong, K. R. Sekhar, S. L. Stamer, D. C. Liebler, and M. L. Freeman, “Covalent modification at Cys151 dissociates the electrophile sensor Keap1 from the ubiquitin ligase CUL3,” *Chemical Research in Toxicology*, vol. 21, no. 3, pp. 705–710, 2008.